

MICROWAVE TRANSMISSION CIRCUITS

Edited by

GEORGE L. RAGAN

GENERAL ELECTRIC RESEARCH LABORATORY

OFFICE OF SCIENTIFIC RESEARCH AND DEVELOPMENT
NATIONAL DEFENSE RESEARCH COMMITTEE

FIRST EDITION
THIRD IMPRESSION



NEW YORK · TORONTO · LONDON
McGRAW-HILL BOOK COMPANY, INC.

1948

MASSACHUSETTS INSTITUTE OF TECHNOLOGY
RADIATION LABORATORY SERIES

Board of Editors

LOUIS N. RIDENOUR, *Editor-in-Chief*

GEORGE B. COLLINS, *Deputy Editor-in-Chief*

BRITTON CHANCE, S. A. GOUDSMIT, R. G. HERB, HUBERT M. JAMES, JULIAN K. KNIPP,
JAMES L. LAWSON, LEON B. LINFORD, CAROL G. MONTGOMERY, C. NEWTON, ALBERT
M. STONE, LOUIS A. TURNER, GEORGE E. VALLEY, JR., HERBERT H. WHEATON

1. RADAR SYSTEM ENGINEERING—*Ridenour*
2. RADAR AIDS TO NAVIGATION—*Hall*
3. RADAR BEACONS—*Roberts*
4. LORAN—*Pierce, McKenzie, and Woodward*
5. PULSE GENERATORS—*Glasoe and Lebacyz*
6. MICROWAVE MAGNETRONS—*Collins*
7. KLYSTRONS AND MICROWAVE TRIODES—*Hamilton, Knipp, and Kuper*
8. PRINCIPLES OF MICROWAVE CIRCUITS—*Montgomery, Dicke, and Purcell*
9. MICROWAVE TRANSMISSION CIRCUITS—*Ragan*
10. WAVEGUIDE HANDBOOK—*Marcwitz*
11. TECHNIQUE OF MICROWAVE MEASUREMENTS—*Montgomery*
12. MICROWAVE ANTENNA THEORY AND DESIGN—*Silver*
13. PROPAGATION OF SHORT RADIO WAVES—*Kerr*
14. MICROWAVE DUPLEXERS—*Smullin and Montgomery*
15. CRYSTAL RECTIFIERS—*Torrey and Whitmer*
16. MICROWAVE MIXERS—*Pound*
17. COMPONENTS HANDBOOK—*Blackburn*
18. VACUUM TUBE AMPLIFIERS—*Valley and Wallman*
19. WAVEFORMS—*Chance, Hughes, MacNichol, Sayre, and Williams*
20. ELECTRONIC TIME MEASUREMENTS—*Chance, Hulsizer, MacNichol, and Williams*
21. ELECTRONIC INSTRUMENTS—*Greenwood, Holdam, and MacRae*
22. CATHODE RAY TUBE DISPLAYS—*Soller, Starr, and Valley*
23. MICROWAVE RECEIVERS—*Van Voorhis*
24. THRESHOLD SIGNALS—*Lawson and Uhlenbeck*
25. THEORY OF SERVOMECHANISMS—*James, Nichols, and Phillips*
26. RADAR SCANNERS AND RADOMES—*Cady, Karelitz, and Turner*
27. COMPUTING MECHANISMS AND LINKAGES—*Svoboda*
28. INDEX—*Henney*

MICROWAVE TRANSMISSION CIRCUITS

EDITORIAL STAFF

C. G. MONTGOMERY
GEORGE L. RAGAN
D. D. MONTGOMERY
MARY E. PALMER

CONTRIBUTING AUTHORS

F. EDWARD EHLERS
ROBERT M. FANO
A. W. LAWSON
F. L. NIEMANN
GEORGE L. RAGAN
RICHARD M. WALKER
F. T. WORRELL

MICROWAVE TRANSMISSION CIRCUITS

Edited by

GEORGE L. RAGAN

GENERAL ELECTRIC RESEARCH LABORATORY

OFFICE OF SCIENTIFIC RESEARCH AND DEVELOPMENT
NATIONAL DEFENSE RESEARCH COMMITTEE

FIRST EDITION
THIRD IMPRESSION



NEW YORK · TORONTO · LONDON
McGRAW-HILL BOOK COMPANY, INC.

1948

TR 6573

M41

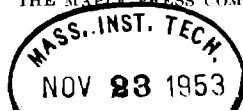
MICROWAVE TRANSMISSION CIRCUITS

COPYRIGHT, 1948, BY THE
MCGRAW-HILL BOOK COMPANY, INC.
PRINTED IN THE UNITED STATES OF AMERICA

*All rights reserved. This book, or
parts thereof, may not be reproduced
in any form without permission of
the publishers.*

SCIENCE LIBRARY

THE MAPLE PRESS COMPANY, YORK, PA.



Contents

PREFACE	ix
CHAP. 1. INTRODUCTION	1
CHAP. 2. ELEMENTARY LINE THEORY.	9
CONVENTIONAL TRANSMISSION-LINE THEORY.	9
2-1. The Telegraphers' Equation.	9
2-2. Interpretation of the Solution	11
2-3. Impedance Relations, Reflection Coefficients, and Standing Waves	13
2-4. Propagation Factor and Characteristic Impedance	19
2-5. Application to Coaxial Line Characteristics	23
2-6. Some Useful Relations in Transmission Lines	29
TRANSMISSION LINES AS GUIDES FOR ELECTROMAGNETIC WAVES.	36
2-7. The Guided-wave Concept	36
2-8. Transmission Characteristics of a Simple Parallel-plate Waveguide	40
2-9. Rectangular Waveguide, TE_{10} -mode	46
2-10. Characteristics of some Common Waveguides	54
TRANSMISSION-LINE CHARTS AND IMPEDANCE-MATCHING.	59
2-11. Reflection-coefficient Chart with Impedance Contours, Smith Chart.	60
2-12. Other Types of Transmission-line Charts	67
2-13. The Choice of a Transmission-line Chart	75
IMPEDANCE-MATCHING AND DESIGN PROCEDURE	82
2-14. The Design of Matched Circuit Elements.	82
2-15. Impedance-matching Transformers.	90
2-16. Other Design Factors.	95
2-17. Series Branches and Choke or Capacity Coupling	100
CHAP. 3. MATERIALS AND CONSTRUCTION TECHNIQUES.	115
METALLIC MATERIALS.	115
3-1. Tubing for Coaxial Lines and Waveguides.	115
3-2. Dimensional Tolerances.	117

CONTENTS

3-3. Miscellaneous Metallic Parts	119
3-4. Construction Techniques	121
FINISHES AND ELECTROPLATING	124
3-5. Nonmetallic Finishes.	124
3-6. Electroplating.	125
3-7. Corrosion Tests and Measurements.	130
DIELECTRIC MATERIALS.	132
3-8. Uses and General Requirements	132
3-9. Characteristics of Dielectric Materials	133
3-10. Construction of Dielectric Parts	137
PRESSURIZATION PROBLEMS.	139
3-11. Sealing of Transmission Lines and Couplings	140
3-12. Rotary-joint Pressure Seals	141
CHAP. 4. RIGID TRANSMISSION LINES	144
COAXIAL LINES.	144
4-1. Factors Governing Choice of Dimensions	144
4-2. Couplings for Coaxial Lines.	150
4-3. Bead Supports.	155
4-4. Stub Supports and Angles.	170
4-5. Coaxial Impedance Transformers.	182
4-6. Coaxial-line Discontinuities	184
WAVEGUIDES.	188
4-7. Factors Governing Choice of Dimensions	188
Waveguide Couplings	193
4-8. Contact Couplings.	193
4-9. Circular-groove Choke-flange Couplings.	193
4-10. Other Choke Couplings.	200
4-11. Summary of Choke-coupling Designs.	202
Corners, Circular Bends, and Twists.	203
4-12. Waveguide Corners.	203
4-13. Waveguide Bends and Twists	207
Impedance-matching	209
4-14. Inductive Matching Diaphragms	211
4-15. Capacitive Matching Diaphragms	214
4-16. Capacitive Buttons and Dents.	215
4-17. Quarter-wavelength Transformer.	217
Pressurizing Windows	218

CONTENTS

4-18. Thin Sheets, Nonresonant.	218
4-19. Thin Sheets in Resonant Mount.	220
4-20. Half-wavelength Dielectric Plugs.	222
4-21. T-shaped Plugs Three-quarters Wavelength Long	223
4-22. Summary of Pressurizing-window Designs.	226
Voltage Breakdown at Microwave Frequencies	227
4-23. Apparatus and Methods	227
4-24. Preliminary Considerations	231
4-25. Effect of Duration and Repetition Rate of Pulses	235
4-26. Effect of Pressure, Gap, and Wavelength	237
4-27. Summary and Discussion of Breakdown Results.	240
CHAP. 5. FLEXIBLE COUPLING UNITS AND LINES.	243
FLEXIBLE COAXIAL CABLES	243
5-1. Attenuation in Flexible Cables.	245
5-2. Jacketing Materials	247
5-3. Cables for Low-power Levels	248
5-4. High-power Cables.	252
5-5. Resonances in Coaxial Cables	253
5-6. Flexibility and Durability of Coaxial Cables.	254
5-7. Connectors for Cables for Low Power.	256
5-8. HN Connectors	260
5-9. High-power Connectors to Rigid Lines	260
5-10. Polyglas Connectors	267
5-11. Summary.	268
WAVEGUIDE UNITS	273
Nonresonant Flexible Waveguide	274
5-12. Wound Metal Hose	274
5-13. Wound Metal Hose, Rubber-covered.	277
5-14. Titeflex.	279
5-15. Titeflex, Rubber-covered	281
5-16. Seamless Corrugated Waveguide.	282
5-17. Plastic and Plastic-filled Waveguides.	285
5-18. Wire-screen Flexible Waveguides	287
Resonant Flexible Waveguide and Coupling Units.	288
5-19. Flexible Bellows	288
5-20. Open Choke-flange Junctions	291
5-21. Vertebrae.	294
5-22. Summary.	303
CHAP. 6. TRANSITION UNITS	305
TRANSITIONS FROM ONE COAXIAL LINE TO ANOTHER.	305
6-1. Tapers in Coaxial Lines.	305
6-2. Transformer Sections between Coaxial Lines.	311

CONTENTS

TRANSITIONS FROM COAXIAL LINE TO WAVEGUIDE.	314
6-3. The Transition Problem	314
6-4. Matching Techniques	317
6-5. Narrowband Matching	318
6-6. Broadband Matching with Waveguide Irises.	322
6-7. Broadband Matching with Coaxial Stubs	332
6-8. Tuning Adjustments	336
6-9. Examples of Transition Construction.	338
6-10. Crossed Transitions from Coaxial Line to Waveguide.	339
6-11. Probe Transitions	341
6-12. Crossbar Transitions.	346
6-13. "Doorknob" Transitions	349
6-14. Magnetic and Resonant-slot Couplings	354
6-15. Applications and Special Transitions	355
LOWEST MODE IN THE WAVEGUIDE TRANSITIONS.	361
6-16. The Transition between Rectangular Waveguides of Different Sizes.	361
6-17. Transition from Rectangular to Cylindrical Waveguide.	364
6-18. Circular Polarization of the TE_{11} -mode.	369
6-19. Circular Polarization in Square Waveguide	378
TRANSITIONS INVOLVING A CHANGE IN WAVEGUIDE MODE	379
6-20. Transitions to the TM_{01} -mode.	379
6-21. Determining Percentage of TE_{11} -mode in Cylindrical Waveguide	381
6-22. TE_{11} -mode Filters	388
6-23. Straight-on TM_{01} -mode Transitions	400
6-24. High-power Capacity.	403
6-25. Summary.	404
CHAP. 7. MOTIONAL JOINTS.	406
MOTIONAL JOINTS IN COAXIAL LINE	407
7-1. General Design Considerations for Coaxial Rotary Joints	407
7-2. Examples of Rotary Joint Construction.	409
7-3. Other Coaxial Motional Joints.	413
WAVEGUIDE ROTARY JOINTS.	416
7-4. Resonances in Rotary Joints.	416
7-5. Rotary Joints Using Transitions with the Compound TE - TM - stub	420
7-6. Resonances in the High-power Rotary Joint.	422
7-7. Resonances in the TE_{11} -mode for the Filter-ring Type of Rotary Joint.	423
7-8. Rotary Joint Using TE_{11} -mode Filter-ring Type of Transitions with TE_{11} -absorbers	425
7-9. Rotary Joints for 1.25-cm Wavelength	427
7-10. Analysis of the Resonances in Rotary Joints Composed of Transi- tions with Diametric Fins in the Round Waveguide	427

CONTENTS

7-11. Rotary Joint Using Circular Polarization	428
7-12. Resonance in a Circular-polarization Rotary Joint	429
7-13. Rotary Joints Using a TE_{11} -mode Polarization Rotator.	430
MISCELLANEOUS WAVEGUIDE MOTIONAL JOINTS	433
7-14. Swivel Joints	433
7-15. Hinge Joints.	438
7-16. Universal Joints.	442
MOTIONAL JOINTS COMBINING COAXIAL LINE AND WAVEGUIDE	446
7-17. General Considerations.	446
7-18. Rotary Joints with Cross-transition from Coaxial Line to Waveguide.	446
7-19. Rotary Joints with Probe Transitions.	447
7-20. Rotary Joints with Combinations of Transitions.	448
7-21. High-power Rotary Joints with Doorknob Transitions	451
CHAP. 8. TUNERS, POWER DIVIDERS, AND SWITCHES.	456
TUNERS (VARIABLE IMPEDANCE TRANSFORMERS)	456
<i>Applications and General Principles</i>	456
8-1. Applications.	456
8-2. General Principles; Use of Impedance Charts	457
<i>Coaxial Line Tuners.</i>	460
8-3. Short-circuiting Plungers	460
8-4. The Sliding Series Stub Tuner.	464
8-5. Slug Tuners.	466
8-6. Stub Tuners.	472
8-7. Phase Shifter	478
<i>Waveguide Tuners.</i>	481
8-8. Short-circuiting Plungers	481
8-9. Waveguide Stub Tuners	483
8-10. Variable-position, Single-screw Tuner.	485
8-11. Single-slug Tuner	489
8-12. Waveguide Double-slug Tuners	494
8-13. Fixed-position, Capacitive-screw Tuners	498
8-14. General-susceptance Screws.	499
8-15. A Waveguide Double-screw Tuner.	507
8-16. Phase Shifters.	513
POWER DIVIDERS.	516
<i>Coaxial Power Dividers</i>	516
8-17. Fixed Coaxial Power Dividers.	516
8-18. Variable Power Divider.	519

CONTENTS

<i>Waveguide Power Dividers</i>	522
8-19. Fixed Power Divider.	522
8-20. Variable Power Dividers	525
SWITCHES	528
8-21. Coaxial-line Switches.	528
8-22. Waveguide Switches	533
CHAP. 9. THE THEORY OF MICROWAVE FILTERS	540
MATHEMATICAL REPRESENTATION OF TWO-TERMINAL-PAIR NETWORKS	541
9-1. Parameters Specifying Two-terminal-pair Networks	541
9-2. The Use of Matrices in Circuit Analysis.	544
9-3. Determination of Input Impedance and Insertion Loss.	547
9-4. Wave Matrices and Accumulative Mismatches.	551
IMAGE PARAMETERS.	554
9-5. Image Impedance and Propagation Functions.	554
9-6. Behavior of Image Parameters of Reactive Networks.	557
NORMALIZATION OF FILTER DESIGNS	560
9-7. Impedance Normalization.	561
9-8. Pass-band Normalization	562
REACTIVE NETWORKS WITH SPECIFIED IMAGE PARAMETERS	566
9-9. Designs Based on Lattice Structures	566
9-10. Constant- k Filters	569
9-11. m -derived Filters.	572
9-12. Limitations on the Use of Image Parameters.	576
REACTIVE NETWORKS WITH SPECIFIED INSERTION LOSS.	580
9-13. Physical Realizability of Insertion-loss Functions.	580
9-14. Determination of Input Impedance from a Prescribed Insertion Loss	583
9-15. Specification of a Network with a Prescribed Input Impedance.	586
9-16. Summary of the Method of Designing Reactive Networks with Specified Insertion Loss.	589
SELECTION OF POWER-LOSS RATIOS.	589
9-17. Selection of Polynomials $P(\omega^2)$ and $Q^2(\omega)$	589
9-18. Tchebysheff Pass-band Behavior.	590
9-19. Tchebysheff Behavior in the Attenuation Band	593
PHYSICAL REALIZATION OF SPECIFIED REACTIVE NETWORKS.	597
9-20. Properties of Ladder Networks.	597
9-21. Determination of Ladder Elements.	598

CONTENTS

EFFECT OF INCIDENTAL DISSIPATION ON FILTER CHARACTERISTICS	601
9-22. Analysis of Uniformly Dissipative Networks	601
9-23. Effect of Dissipation on Pass-band Characteristics	603
9-24. Effect of Dissipation on Rejection-band Characteristics	604
9-25. Correction for Uniform Dissipation	607
EFFECT OF MISMATCHED TERMINATIONS ON FILTER CHARACTERISTICS	609
9-26. Superposition of Mismatches	609
9-27. Accumulative Effect of Mismatches	611
CHAP. 10. THE DESIGN OF MICROWAVE FILTERS	613
FILTERS EMPLOYING TRANSMISSION LINES	614
10-1. The Frequency Behavior of Lines	614
10-2. Practical Limitations on the Use of Lines	623
10-3. Filters Employing Lines as Two-terminal Elements	625
10-4. Filters Employing Lines as Four-terminal Elements	634
10-5. Waveguide Filters	643
FILTERS EMPLOYING DIRECT-COUPLED CAVITY RESONATORS	645
10-6. Cavity Resonators as Circuit Elements	646
10-7. Design of Cavity Resonators	653
10-8. Theory of Direct-coupled Cavities	661
10-9. Filters Employing Direct-coupled Cavities	666
10-10. Cavities Excited in More Than One Mode	673
FILTERS EMPLOYING QUARTER-WAVELENGTH COUPLINGS	677
10-11. Theory of Quarter-wavelength Coupling	677
10-12. Filters Employing $\lambda_g/4$ -coupled Cavities	683
10-13. Filters Employing Quarter-wavelength-coupled Resonant Irises	688
10-14. Refined Theory of Quarter-wavelength Coupling	690
10-15. Quarter-wavelength-coupled Filters with Tchebysheff Characteristics	696
MISCELLANEOUS FILTERS	706
10-16. Lattice Networks	706
10-17. Mode Filters	707
10-18. Absorption Filters	707
10-19. Multiplexers	708
ASSEMBLY AND TEST PROCEDURES	709
10-20. Broadband Filters	709
10-21. Narrow-band Filters	710
10-22. Quarter-wavelength-coupled Filters	714
INDEX	717

CHAPTER 1

INTRODUCTION

BY GEORGE L. RAGAN

The course of the development of techniques and applications of radio frequencies has been one of progression from low frequencies to higher and higher frequencies. Most recently this progression has seen the development, at a greatly accelerated rate, of techniques and applications of the extremely high frequencies of the microwave region. The rapidity with which this region of the radio-frequency spectrum has been developed is a result of the expenditure of an enormous effort in the design and manufacture of devices using these waves to advantage in military applications. Radar apparatus, used to detect objects and to determine their location, is of course the most familiar of these devices. Applications such as those of navigation and communication, however, are also very important and should not be overlooked. Although the impetus resulting in the accelerated development of the microwave region came from the pressure of military needs, the techniques and apparatus developed have many peacetime applications.

It is impossible to give an exact definition of the limits of frequency or wavelength implied by the term "microwave." The microwave circuits to be described in this volume were developed for operation within the region of wavelengths extending from about 12 cm down to about 1.2 cm, the corresponding frequencies being 2500 to 25,000 Mc/sec. The term "microwave" is usually considered to embrace a somewhat broader region of the radio-frequency spectrum, perhaps including all wavelengths shorter than about 30 cm or frequencies exceeding about 1000 Mc/sec.

Microwaves are unique among electromagnetic waves in that their wavelength is of the same order of magnitude as the dimensions of the apparatus in which they are used. The closest analogy to microwave phenomena is to be found in sound waves, which have wavelengths of the same order of magnitude. Like sound waves, microwaves may be propagated along hollow tubes and focused into a sharp beam by means of horns or parabolic reflectors of moderate size. Another analogy that is sometimes useful in the understanding of microwave phenomena is to be found in a study of the diffraction of light waves in passing through holes or slits the dimensions of which are comparable with the wavelengths of the light waves.

Among the properties of microwaves which are useful are the following:

1. Microwaves may be directed into sharp beams of radiation by means of relatively small horns or reflectors. This property makes them especially valuable in applications requiring antennas of high gain or high angular resolution. Radar makes use of this property in order to obtain precise information concerning the direction of a reflecting object.
2. An enormous number of bands, each broad in terms of cycles per second, may be contained within a region covering a range in frequency of only a few per cent. For example, 500 bands, each 1 Mc/sec wide, may be used in the region from 2500 to 3000 Mc/sec (12 to 10 cm) or in the region from 29,500 to 30,000 Mc/sec (1.02 to 1.00 cm).
3. Pulses of extremely short duration may be used, since the sidebands introduced by the pulse modulation represent a relatively small percentage spread in frequency.

The circuits used at microwave frequencies are radically different from those used at lower frequencies. During the previous stages in the evolution toward higher frequencies, little fundamental change had been necessary. The process had been one of improvement and refinement of the older techniques and circuits along well-defined and clear-cut lines. As the wavelength decreased to the point where it became comparable with the dimensions of the apparatus, the older circuits became impractical. For example, lumped circuits became prohibitively small and entailed excessively large losses, and two-wire lines suffered from increasingly serious radiation effects. The smallness of the wavelength, which led to the downfall of the conventional circuits, made practical the use of circuits of a new type to replace them. Thus, the use of hollow-pipe waveguides became practical as a substitute for the failing two-wire line, and the cavity resonator emerged as a replacement for the older resonant circuit composed of lumped elements. Coaxial lines and coaxial-line circuits, useful at long wavelengths and down well into the microwave region, serve as transitional circuits, helping to bridge the gap. The "skin effect," already important at high radio frequencies, becomes increasingly important in microwave work.

Concurrent with the marked change in the form of the circuits, changed points of view involving various concepts are required. It is found necessary to relinquish, or at least to relegate to a minor role, the idea that currents and voltages are the fundamental entities in the transmission of radio-frequency power. Instead, the concept of the transmission of power by means of electromagnetic waves traveling in

the dielectric medium associated with the transmission line or hollow pipe is found to be more significant. This concept is far from new, since it was used by Lord Rayleigh as early as 1897, in working out the theory of hollow-pipe waveguides. Furthermore, electromagnetic-field theory has always formed the basis for the understanding of the radiation from antennas and the propagation of radio-frequency energy through space.

Electromagnetic-field theory is embodied, in concise mathematical form, in the set of relations known as Maxwell's equations. Anyone who plans to design microwave circuits will find it advisable to gain an understanding of the basic principles underlying these equations, even though he may rarely, if ever, find it necessary to apply the equations themselves to any specific problem of circuit design. He should develop a feeling for such fundamental things as: (1) the relation between current in a conductor and the magnetic field in the medium adjacent to the conductor, (2) the fact that in any electromagnetic wave the electric field and the magnetic field are always orthogonal, and (3) boundary conditions, such as those forbidding a tangential component of electric field or a normal component of magnetic field in the electromagnetic wave at the surface of a perfect conductor. It is hoped that the material of Chap. 2, which presents a brief semiquantitative explanation of the behavior of waveguides on the basis of reflected plane waves, will assist those who do not have such a feeling for the fundamentals of the wave point of view to obtain it.

It is thus evident that a different point of view, involving concepts that are not particularly helpful in the design of circuits for low frequencies, is needed in the design of microwave circuits. Nevertheless, many of the older concepts, in somewhat modified form, continue to be useful in microwave work. One of the most important of these concepts is that of impedance. To be sure, it is necessary, when working with waveguides, to redefine impedance in terms of electric and magnetic fields; but the concepts of impedance and impedance transformations along the waveguide, carried over from conventional transmission-line theory, are extremely useful. For this reason, Chap. 2 begins with a brief exposition of this conventional theory, and a considerable amount of emphasis is placed, in later sections, on the use of transmission-line calculators or impedance charts based on the equations resulting from this theory.

Since the circuits used in microwave transmission differ so greatly from those used at lower frequencies, the design problems are naturally different. In addition, a greater emphasis is placed on impedance-matching, with the result that a great deal of the designer's effort goes into the measurement of impedance and the elimination of mismatch. Each separate microwave circuit should match the characteristic imped-

ance of the line within close tolerances. When the line leading from the circuit toward the load is free of reflected waves, no reflected wave should be generated in the input line by the circuit itself. The principal reasons for the stringent requirements for well-matched circuits are the following:

1. Stable operation of microwave magnetron transmitters is dependent on well-matched circuits. This requirement is associated with the fact that microwave magnetrons are efficient self-excited oscillators tightly coupled to a line that is many microwavelengths long.
2. The line suffers voltage breakdown more readily if a standing wave exists on it. This situation becomes very serious at the high power levels attained in the short pulses frequently used in microwave applications.
3. An impedance mismatch implies a partial reflection of the power in the incident wave. This reflected power may be wasted, as by reradiation of a received signal, or it may cause an unfavorable loading of the magnetron, thereby lowering its efficiency.
4. Even though the input impedance of a transmission line may be matched by means of an impedance transformer, extra dissipative losses occur in the line because of the standing waves caused by a mismatch.

In addition to the emphasis on impedance matching, it is usually desired to design circuits in such a way that they maintain the matched condition over a broad band of frequencies. It is usually felt to be worth while to take great pains in design work in order to achieve this broadband performance without resorting to the use of circuit parameters that require adjustment as the frequency is changed. Indeed, the tendency has been to establish, in the course of the design work, dimensions and tolerances for all details of the circuit which will ensure proper performance of the finished product without further adjustment. This procedure has been adopted in order to relieve the manufacturer and the user of the equipment of the task of making adjustments that are frequently difficult and time-consuming.

It seems pertinent, at this point, to introduce a few remarks about the manufacture of the novel circuits used for microwave transmission. These circuits amply justify, by their outward appearance, the term "plumbing" that is frequently applied to them. Unfortunately, the precision and skill required in their manufacture are not in the same class with those of ordinary plumbing. They should be made with care by skilled workmen, a fact that is sometimes hard to impress upon shops not familiar with the manufacture of precision radio equipment. The accuracy of the workmanship required may easily be underestimated,

even by those familiar with the requirements of low-frequency circuits. The allowable departures from design dimensions tend to decrease in proportion to the decrease of wavelength, if the same reflection or mismatch may be tolerated. This consideration, added to that of the increased importance of matched circuits already referred to, affords some idea as to the quality of workmanship needed.

The user of microwave equipment frequently finds it extremely difficult, because of a lack of experience with microwave equipment or because of adverse operating conditions, to make even the minimum number of required adjustments on his equipment. Both difficulties were particularly prevalent in the use of microwave equipment for military purposes. The elimination of nonessential adjustments is therefore a very material contribution to the quality of the performance of the equipment.

Although the microwave transmission circuits to be described in this volume were designed principally for use in radar apparatus, most of them will doubtless be found useful in communication and navigation equipment. A schematic diagram of the radio-frequency components of a simple radar set is presented in Fig. 1-1. It is found convenient to subdivide the r-f components into several groups, each group forming a more or less complete unit with its special techniques and problems. Each specialized group of components is discussed separately in the appropriate volume or volumes of the Radiation Laboratory Series. The components¹ indicated within the dotted squares are: (1) transmitter components, (2) duplexer components, (3) mixer and receiver components, and (4) antenna components. The remaining components fall into the group frequently termed "transmission-line components." These last components constitute the microwave transmission circuits to be described in this volume.

The function of these transmission circuits is to transmit r-f power and signals from one of the specialized components to another. Among other things, the circuits must provide for the necessary bends and twists in the line, and must permit the required relative motions of the components. The transmission lines used to carry microwave power or signals are almost always either hollow-pipe waveguide, as indicated schematically in Fig. 1-1, or coaxial lines.

A number of materials and techniques that may be found useful in designing microwave transmission circuits is presented in Chap. 3. In this presentation are described materials and techniques that are felt to be particularly applicable to the fabrication of microwave transmission

¹ *Microwave Magnetrons*, Vol. 6; *Microwave Duplexers*, Vol. 14; *Microwave Mixers*, Vol. 16; *Crystal Rectifiers*, Vol. 15; *Klystrons and Microwave Triodes*, Vol. 7; *Microwave Receivers*, Vol. 23; *Microwave Antenna Theory and Design*, Vol. 12, Radiation Laboratory Series.

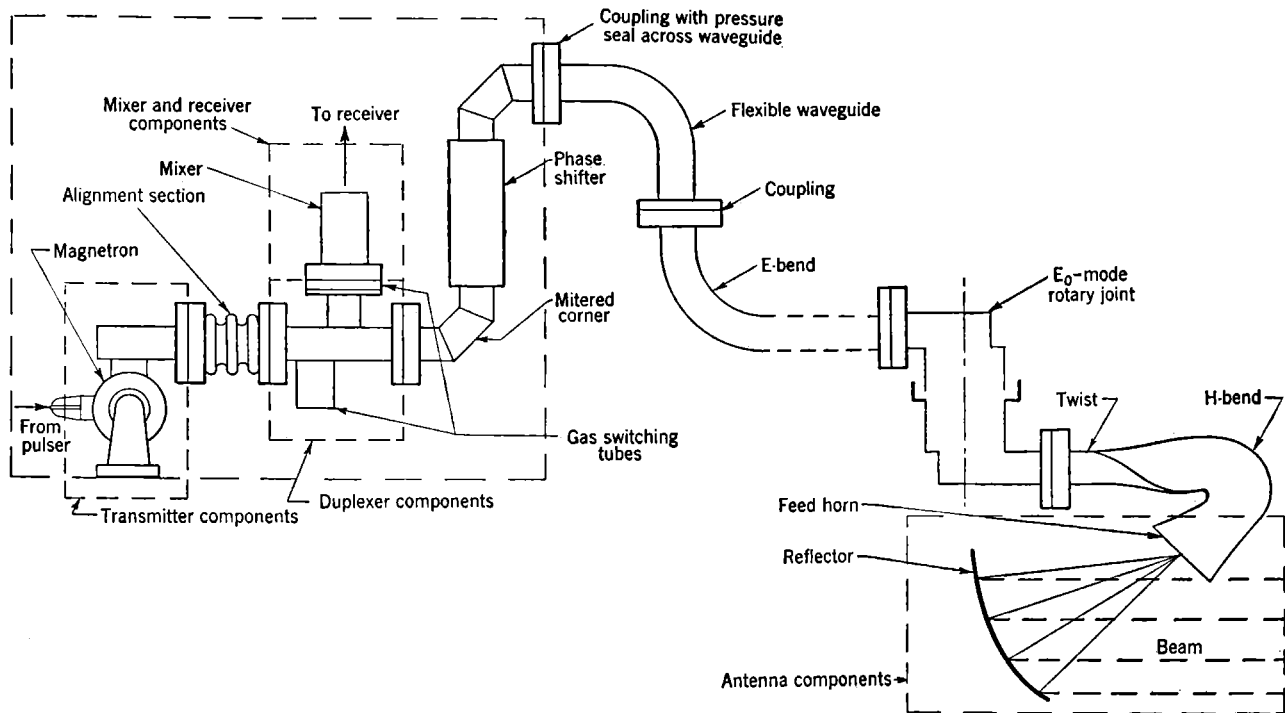


FIG. 1-1.—Schematic diagram of the r-f components of a sample radar set. Several transmission line components are shown in relation to other types of r-f components.

circuits, with emphasis on the more recent developments. This material is presented early in the volume because the capabilities and limitations of the manufacturing processes must be considered when designing the circuits described in the succeeding chapters.

Before passing on to a consideration of specific transmission line components, it seems desirable to point out the fact that no material on test equipment or on testing techniques is included in this volume. This material is omitted, not because it is unimportant, but because it merits a more thorough and more lengthy treatment than could profitably be included in the present volume. For a comprehensive and authoritative treatment of this important subject the reader is referred to another volume¹ of the Radiation Laboratory Series.

In Chap. 4, the basic problem of connecting sections of transmission lines by means of suitable couplings is treated. Consideration is given also to such problems, intimately associated with transmission lines, as coaxial line supports, waveguide pressure seals, and phenomena of high-power breakdown. The choice between coaxial lines and waveguides is dictated by considerations of physical size, attenuation, high-power limitations, and bandwidth. At the shortest wavelengths, waveguides have a clear superiority, whereas at the longest wavelengths their large size makes them unsuitable for many applications. Some properties of coaxial lines and waveguides are discussed in Chap. 4. These properties should be carefully considered in choosing the type of transmission line to be used for any given purpose.

It is frequently desirable to be able to transfer r-f energy from a coaxial line to a waveguide or from one waveguide mode to another. This is accomplished by circuits known as transitions, examples of which are presented in Chap. 6. The rotary joint indicated in Fig. 1-1 employs transition units to pass from the lowest mode in rectangular waveguide to the second mode in round waveguide, which is a symmetrical mode suitable for use in rotary joints. Rotary joints of this type as well as others, are discussed in Chap. 7. Other motional joints that permit various relative motions are also described.

Certain large motions, such as those occurring between r-f units that are separately shock-mounted, are best permitted by the use of the flexible sections of coaxial line or waveguide presented in Chap. 5. In addition, these flexible lines are useful in temporary installations and in experimental or test apparatus.

Variable impedance transformers of a number of types are discussed in Chap. 8. The transformer most frequently used in r-f transmission lines is the phase shifter indicated schematically in Fig. 1-1. The use in r-f systems of variable impedance transformers, commonly referred to as

¹ *Technique of Microwave Measurements*, Vol. 11, Radiation Laboratory Series.

"tuners," is, in general, discouraged. Tuners are, nevertheless, discussed extensively in Chap. 8, since they are required in some system applications and are very useful in experimental work in the laboratory.

Information concerning r-f power dividers and r-f switches is also included in Chap. 8. These devices have been used to some extent in radar systems, but few sets require them. Variable power dividers are more useful in experimental laboratory work, as variable attenuators operating at high power levels.

The concluding chapters, Chaps. 9 and 10, contain an extensive treatment of the theory and design of microwave filters. For a long time, certain filter circuits have been used in radar sets, particularly in connection with gas-filled switching tubes and mixers. There was, however, no well-formed theoretical groundwork to guide the designer of microwave filters. Toward the end of the war period, it began to appear that the growing number of microwave sets in use made it advisable to investigate the use of filters as a means of reducing troublesome interference between equipments. Consequently, a broad program for the study of principles to serve as a guide in the design of microwave filters was undertaken. The theory and techniques described in these two chapters came too late to play any significant role in the war, but they should prove extremely useful in peacetime developments. The principles described are not merely extensions to microwave frequencies of principles already in use at low frequencies. They represent, rather, a significant contribution to filter theory along lines that had not previously been exploited. The results of this work should find many useful applications in the design of filters for use at low frequencies as well as at microwave frequencies.

Throughout this volume, as in others of the Radiation Laboratory Series, rationalized mks units are used except where alternative units are specifically indicated.

CHAPTER 2

ELEMENTARY LINE THEORY

BY GEORGE L. RAGAN

CONVENTIONAL TRANSMISSION-LINE THEORY

A great deal of interesting and useful information may be obtained by applying low-frequency circuit theory to the problem of a long transmission line with distributed constants. In this treatment it is convenient to focus attention on the current flowing in the conductors and the voltage between conductors, rather than on the electromagnetic fields in the dielectric medium. Although the former point of view may be less accurate than the latter, it leads more simply to the same result.

2.1. The Telegraphers' Equation.—Proceeding in the usual way,¹ let us consider the two-wire transmission line of Fig. 2-1. The series impedance and the shunt admittance per unit length of line are, respectively, Z and Y . Fixing our attention on the infinitesimal element of line whose length is dz , we write expressions for dI , the current flowing from one conductor to the other through the conductance $Y dz$, and dV , the change in potential difference between conductors caused by the current I flowing in the impedance $Z dz$, as

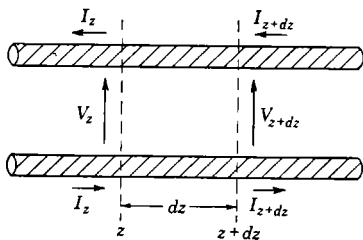


FIG. 2-1.—Voltage and currents in a transmission line.

$$\left. \begin{aligned} dI &= -VY dz, \\ dV &= -IZ dz. \end{aligned} \right\} \quad (1)$$

Or, expressed as derivatives,

$$\left. \begin{aligned} \frac{dI}{dz} &= -VY, \\ \frac{dV}{dz} &= -IZ. \end{aligned} \right\} \quad (2)$$

Here V and I are the complex voltage and current associated with a

¹ Sarbacher and Edson, *Hyper and Ultra-High-Frequency Engineering*, 1st ed., Wiley, New York, 1943, Chap. 9; J. C. Slater, *Microwave Transmission*, McGraw-Hill, New York, 1942, Chap. 4; S. A. Schelkunoff, *Electromagnetic Waves*, Van Nostrand, New York, 1943, Chap. 7.

steady-state condition¹ characterized by sinusoidal time variation. In general, both Z and Y will be complex:

$$\left. \begin{aligned} Z &= R + jX, \\ Y &= G + jB. \end{aligned} \right\} \quad (3)$$

Taking the second derivatives of Eqs. (2), we obtain

$$\left. \begin{aligned} \frac{d^2 I}{dz^2} &= -Y \frac{dV}{dz} = YZI, \\ \frac{d^2 V}{dz^2} &= -\frac{dI}{dz} = ZYV. \end{aligned} \right\} \quad (4)$$

Let us solve the second of these equations by assuming the solution to have the form

$$V = Ae^{-\gamma z}, \quad (5)$$

where A and γ are constants which will be evaluated presently. Using the solution assumed in Eq. (5),

$$\frac{d^2 V}{dz^2} = \gamma^2 Ae^{-\gamma z} = \gamma^2 V = YZV, \quad (6)$$

which enables us to write

$$\left. \begin{aligned} \gamma^2 &= YZ, \\ \gamma &= \pm \sqrt{YZ}. \end{aligned} \right\} \quad (7)$$

We shall let γ represent the positive root and use $-\gamma$ where the negative root is required. The general solution will be of the same form as Eq. (5); but, since we are dealing with a differential equation of the second order, the solution will contain two constants of integration, A and B , which, in general, will be complex,

$$V = Ae^{-\gamma z} + Be^{\gamma z}. \quad (8)$$

The expression for the current is easily obtained by substituting Eq. (8) in the second of Eqs. (1),

$$\begin{aligned} \frac{dV}{dz} &= -\gamma(Ae^{-\gamma z} - Be^{\gamma z}) = -IZ, \\ I &= \frac{\gamma}{Z} (Ae^{-\gamma z} - Be^{\gamma z}), \\ &= \frac{1}{Z_0} (Ae^{-\gamma z} - Be^{\gamma z}). \end{aligned} \quad (9)$$

¹ For a discussion of the more general problem of transients or nonsinusoidal waveforms, see Brainerd, Kohler, Reich, and Woodruff, *Ultra-High-Frequency Techniques*, Van Nostrand, New York, 1942, Chap. 11; or E. A. Guillemin, *Communication Networks*, Vol. II, Wiley, New York, 1935, Chap. 11.

For convenience a new quantity has been defined

$$Z_0 = \frac{Z}{\gamma} = \sqrt{\frac{Z}{Y}}, \quad (10)$$

whose significance will appear presently.

2.2. Interpretation of the Solution.—Since γ is defined in terms of the complex quantities Z and Y , it is itself complex and may be written as

$$\gamma = \alpha + j\beta. \quad (11)$$

Writing the solution, Eq. (8), in full including the time factor gives

$$V e^{j\omega t} = A e^{-\alpha z} e^{j(\omega t - \beta z)} + B e^{\alpha z} e^{j(\omega t + \beta z)}. \quad (12)$$

The factor $e^{j(\omega t - \beta z)}$ indicates that this term varies sinusoidally with both t and z . The significance of ω is easily recalled by remembering that the phase angle ωt increases by 2π radians, when t increases by the periodic time $1/\nu$. That is,

$$\begin{aligned} \omega \left(t + \frac{1}{\nu} \right) &= \omega t + 2\pi, \\ \omega &= 2\pi\nu. \end{aligned} \quad (13)$$

Similarly, the phase angle must increase by 2π between the successive inphase points z and $z + \lambda$

$$\begin{aligned} \beta(z + \lambda) &= \beta z + 2\pi, \\ \beta &= \frac{2\pi}{\lambda}. \end{aligned} \quad (14)$$

It must be borne in mind that λ is the wavelength in the transmission line, not the associated free-space wavelength.

This factor $e^{j(\omega t - \beta z)}$ represents the phase of a wave traveling in the positive z direction. This fact is easily demonstrated by noting that the factor has the same value, and hence the same phase, at the points z and $z + dz$ at successive instants of time t and $t + dt$, provided that

$$\begin{aligned} \omega t - \beta z &= \omega(t + dt) - \beta(z + dz), \\ \omega dt &= \beta dz, \\ v_p &= \frac{dz}{dt} = \frac{\omega}{\beta}. \end{aligned} \quad (15)$$

Now ω is obviously positive, and it will be shown in Sec. 2.4 that β is positive for ordinary lines, since γ was defined as the positive root of Eq. (7). Hence the phase velocity v_p of the wave represented by this term is positive; that is, this wave travels in the positive z direction. Similarly, it may be shown that the other imaginary exponential term for negative γ represents the phase of a wave traveling in the negative z direction with an equal phase velocity.

Phase velocity, as used above, is a simple concept, and its value is easily calculated. Unfortunately, the group and signal velocities, which are equally important, are rather obscure. For the type of line to which the present discussion, based on the telegraphers' equation, applies, the three velocities¹ are equal. This follows from the fact that such lines are nondispersive; that is, the phase velocity is independent of frequency. Substitution of Eqs. (13) and (14) in Eq. (15) yields the fundamental relation

$$v_p = \nu\lambda, \quad (16)$$

which may be solved for λ , giving

$$\lambda = \frac{v_p}{\nu}. \quad (17)$$

The real exponential factors of Eq. (12) represent attenuation of the waves. In each case, the wave is attenuated in the direction in which it is propagated. This agrees with our experience that in actual lines there is such an attenuation; and the concept of energy conservation demands that the wave become weaker, rather than stronger, as it advances. The constants A and B are in general complex; they represent the magnitude and phase of the waves traveling to right and left, respectively, at the point $z = 0$ at the time $t = 0$.

The expression for the current, Eq. (9), is interpreted similarly as representing waves whose complex amplitudes are A/Z_0 and $-B/Z_0$, traveling to right and left, respectively. The amplitude of each current wave is related to that of the corresponding voltage wave by the factor Z_0 . In the special case in which Z_0 is a pure real number, each current wave is in phase with the associated voltage wave. In general, Z_0 is complex so that a shift in phase occurs between the associated current and voltage waves. The quantity Z_0 , called the "characteristic impedance" of the line, may be thought of as representing, for that particular line, the complex ratio of voltage to current in a traveling wave.

The significance of the negative sign in the amplitude of the current wave traveling to the left is not immediately obvious. It arises mathematically, because the derivatives of $e^{-\gamma z}$ and $e^{\gamma z}$ have opposite signs. To understand this physically, let us consider what happens if a d-c generator is connected to the left-hand terminals in Fig. 2-1. If the upper terminal is made negative, the voltage (integral of electric field) and current (conventional or positive) will be in the directions indicated, and power will flow to the resistive load which, it is assumed, is connected to the right-hand terminals. If the generator and load are interchanged, and the upper wire is kept negative, the voltage will

¹ For a good discussion of these three velocities, see Sarbacher and Edson, *loc. cit.*, Sec. 5-8.

remain in the direction shown, but the current will be reversed and the power will now be flowing to the left. Thus we see the origin of the negative sign on the current of the wave traveling to the left. A rigorous demonstration involving electromagnetic fields and Poynting's vector is easily given, but will not be carried out here.

Reviewing our general procedure in setting up and solving the line equations, it should be pointed out that first the line was described in terms of differential equations involving the two quantities Z and Y . In the solution of these differential equations, Z and Y were found occurring only in the combinations \sqrt{ZY} and $\sqrt{Z/Y}$. For the sake of convenience, new symbols γ and Z_0 were then introduced for these two combinations. These new symbols were given a simple physical interpretation and christened, respectively, "propagation factor" and "characteristic impedance." It should be clearly understood that a knowledge of either the original quantities Z and Y , or the derived ones γ and Z_0 , enables us to calculate the other pair through the relations

$$\begin{aligned} \gamma &= \sqrt{ZY}, & Z &= \gamma Z_0, \\ Z_0 &= \sqrt{\frac{Z}{Y}}, & Y &= \frac{\gamma}{Z_0}. \end{aligned} \quad (18)$$

2.3. Impedance Relations, Reflection Coefficients, and Standing Waves.

—It will be seen later, as practical problems of design and performance are approached, that the concept of impedance in lines and a knowledge of impedance transformations are extremely useful tools. The results obtained in Sec. 2.1 may be used as a starting point in the development of these indispensable aids. Just as in low-frequency circuit theory, the complex impedance Z_z at a point z may be defined as the ratio of the complex voltage to the complex current at that point.

Using Eqs. (8) and (9), we may write

$$Z_z = \frac{V}{I} = Z_0 \frac{Ae^{-\gamma z} + Be^{\gamma z}}{Ae^{-\gamma z} - Be^{\gamma z}} \quad (19)$$

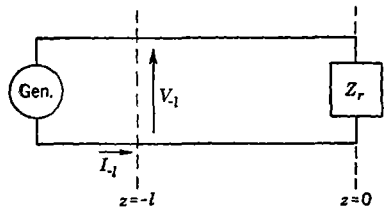


FIG. 2.2.—Transmission line with generator and load.

Up to the present point in this development, the origin of the two waves traveling in opposite directions has not been discussed. Two generators of exactly the same frequency may be assumed to be connected to the opposite ends of a very long line, a line so long that the attenuation in the line prevents appreciable interaction between the generators. A much more practical case is that shown in Fig. 2.2.

At the point $z = 0$, a receiving-end impedance Z_r is placed. Equation (19) must be satisfied for any value of z , including $z = 0$, so we may write

$$Z_r = Z_0 \frac{A + B}{A - B} = Z_0 \frac{1 + \frac{B}{A}}{1 - \frac{B}{A}} \quad (20)$$

This equation may be solved for the complex ratio

$$\frac{B}{A} = \frac{Z_r - Z_0}{Z_r + Z_0} \quad (21)$$

which represents, at the point $z = 0$, the amplitude and phase of the volt-

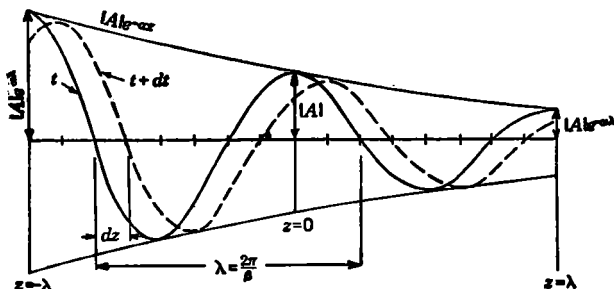


FIG. 2-3.—A voltage wave propagated to the right.

age wave traveling to the left relative to that traveling to the right (see Fig. 2-3).

Several important inferences may now be pointed out.

1. We have discovered that when we terminate a line with an impedance, a wave will be set up, which travels back toward the source.
2. It is natural to call the voltage wave of amplitude A traveling toward the load the "incident wave," and the voltage wave of amplitude B traveling back toward the generator the "reflected wave." The complex ratio B/A is then referred to as the "voltage reflection coefficient," for which we shall use the symbol Γ .
3. In the special case where $Z_r = Z_0$, B/A is zero; that is, no reflected wave is set up. To our previous interpretation of Z_0 (see Sec. 2-2) may now be added the remark that, if a line be terminated in its characteristic impedance, no reflected wave will be generated.

Having evaluated the voltage reflection coefficient Γ_r , arising at a terminal impedance Z_r , it is interesting to discover the relation between reflected and incident waves at other points along the line. To do this, the total voltage V , given by Eq. (8), is evaluated, at the point $z = -l$,

$$V_{-l} = Ae^{\gamma l} + Be^{-\gamma l}. \quad (22)$$

This equation has been interpreted as signifying that the total voltage is the sum of an incident voltage

$$V_{\text{inc}} = Ae^{\gamma l}, \quad (23)$$

and a reflected voltage

$$V_{\text{ref}} = Be^{-\gamma l}. \quad (24)$$

The ratio of these two complex voltages

$$\frac{V_{\text{ref}}}{V_{\text{inc}}} = \frac{B}{A} e^{-2\gamma l} \quad (25)$$

shall be called the "voltage reflection coefficient" at the point $z = -l$. The relation between this quantity, which will be designated, as Γ_{-l} , and the voltage reflection coefficient at $z = 0$, designated as Γ_0 , is

$$\Gamma_{-l} = \Gamma_0 e^{-2\gamma l} = \Gamma_0 e^{-2\alpha l} e^{-2j\beta l}. \quad (26)$$

This equation indicates that the complex reflection coefficient at any distance l from the load behaves as a vector (see Fig. 2-4), whose value varies from Γ_0 at the load to zero as l approaches infinity. The amplitude decreases because of the factor $e^{-2\alpha l}$, and the phase angle varies cyclically because of the factor $e^{-2j\beta l}$. Thus, for very long lines, the reflected wave disappears at large distances from the load and only the incident wave remains. If the incident voltage should be taken as a reference vector (see Fig. 2-5), the relative voltage V'_l may be written as

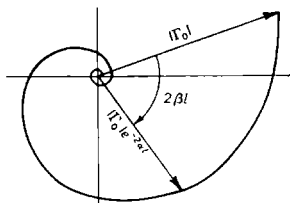


FIG. 2-4.—Transformation of the voltage-reflection coefficient along the line.

$$V'_l = \frac{V_{-l}}{V_{\text{inc}}} = 1 + \Gamma_0 e^{-2\gamma l}. \quad (27)$$

Similarly, we could proceed from Eqs. (9) to write

$$\frac{I_{\text{ref}}}{I_{\text{inc}}} = -\frac{B}{A} e^{-2\gamma l} = -\Gamma_0 e^{-2\gamma l}. \quad (28)$$

The current reflection coefficient here is the negative of the voltage reflection coefficient; the significance of the negative sign was discussed in the previous section. The total current relative to the incident current vector is

$$I'_{-l} = \frac{I_{-l}}{I_{\text{inc}}} = 1 - \Gamma_0 e^{-2\gamma l}. \quad (29)$$

One reason for dealing at length with the subject of reflection coefficients and their variation along the line lies in the fact that the concept of reflected waves set up by an improper termination or by discontinuities in the line is an indispensable aid to visualizing what takes place in a line. Another reason is that these ideas will be used to advantage later on in connection with reflection-coefficient charts based on Eqs. (27) and (29).

The way in which the incident and reflected waves combine is illustrated by Fig. 2-6. In *a* the two waves are in phase, and the resultant voltage has its maximum amplitude $|A| + |B|$ at certain positions. In *b*, a quarter cycle later in time, each wave has traveled a quarter wave-

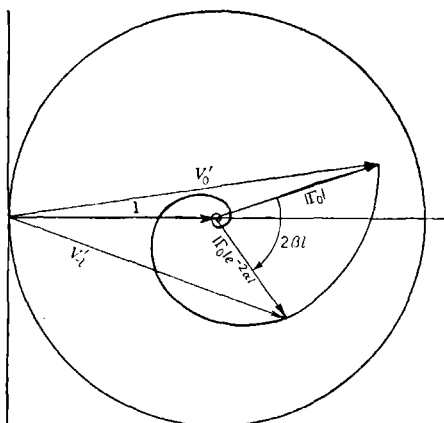


FIG. 2-5.—Transformation of relative voltage along the line.

length in its direction of propagation, so that the two waves are now out of phase. They may be subtracted to give a voltage amplitude $|A| - |B|$ at positions midway between those at which the maximum amplitudes of *a* occurred. In successive quarter cycles, the resultants have the same amplitudes as in *a* and *b* but reversed in sign. In *c* is shown the maximum amplitude occurring at each position along the line. This corresponds to V_{-l} of Eq. (22).

To examine this case mathematically, Eq. (22) is rewritten, replacing γ by $j\beta$ and neglecting α ,

$$V_{-l} = |A|e^{j(\phi+\beta l)} + |B|e^{j(\theta-\beta l)},$$

where the complex nature of the amplitudes A and B , written as $|A|e^{j\phi}$ and $|B|e^{j\theta}$, is brought into evidence (see Fig. 2-7). For certain positions l_1 , the voltage amplitudes have the same phase angle; that is

$$\begin{aligned}
 (\phi + \beta l_1) &= (\theta - \beta l_1) \pm 2\pi n, \\
 l_1 &= \frac{\theta - \phi \pm 2\pi n}{2\beta}.
 \end{aligned}$$

Remembering that $\beta = 2\pi/\lambda$, we may write

$$l_1 = \left(\frac{\theta - \phi}{4\pi} \pm \frac{n}{2} \right) \lambda. \quad (30)$$

Similarly it may be shown that the positions l_2 at which the two amplitudes have phase angles differing by π are

$$l_2 = \left(\frac{\theta - \phi}{4\pi} \pm \frac{2n + 1}{4} \right) \lambda. \quad (31)$$

At the positions l_1 the voltage amplitude is

$$V_{\max} = |A| + |B|. \quad (32)$$

Furthermore, Eq. (30) shows that these voltage maxima occur at half-wavelength intervals. At the positions l_2 the voltage amplitude is

$$V_{\min} = |A| - |B|.$$

That such voltage minima occur at points midway between maxima is revealed by comparing Eqs. (30) and (31). The ratio of maximum to minimum voltage is

$$r = \frac{V_{\max}}{V_{\min}} = \frac{|A| + |B|}{|A| - |B|} = \frac{1 + \frac{|B|}{|A|}}{1 - \frac{|B|}{|A|}}. \quad (33)$$

It is common practice to refer to r as the "standing-wave ratio," or more precisely as the "voltage standing-wave ratio," frequently abbreviated as VSWR. This ratio is rather easily determined experimentally. Equation (33) may be solved for the magnitude of the reflection coefficient

$$\left| \frac{B}{A} \right| = |\Gamma| = \frac{r - 1}{r + 1}. \quad (34)$$

The groundwork has now been laid for a commonly used method of

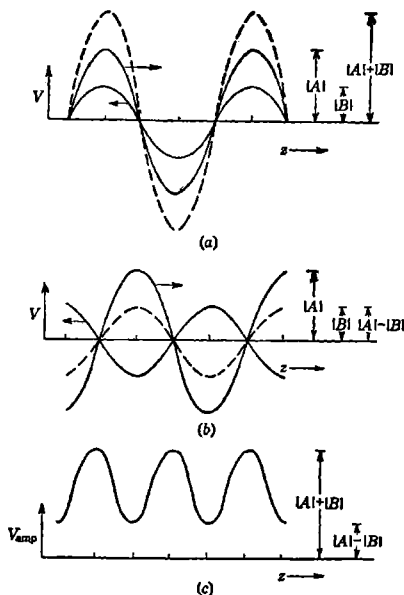


FIG. 2-6.—Combination of incident and reflected waves to form a standing wave. (a) Incident and reflected waves adding in phase. (b) Waves in opposition a quarter cycle later. (c) Standing wave voltage amplitude pattern.

impedance measurement. By measuring r and l_2 and by applying Eqs. (34) and (31), both magnitude and phase of the ratio B/A may be determined. The load impedance Z_r may then be calculated by Eq. (20). Equation (19) for the point $z = -l$ may be written in the form

$$Z_{-l} = Z_0 \frac{e^{\gamma l} + \frac{B}{A e^{-\gamma l}}}{e^{\gamma l} - \frac{B}{A e^{-\gamma l}}}. \quad (35)$$

If the value of B/A as given by Eq. (21) is substituted in Eq. (35) and the result rearranged, we obtain

$$Z_{-l} = Z_0 \frac{Z_r(e^{\gamma l} + e^{-\gamma l}) + Z_0(e^{\gamma l} - e^{-\gamma l})}{Z_0(e^{\gamma l} + e^{-\gamma l}) + Z_r(e^{\gamma l} - e^{-\gamma l})}. \quad (36)$$

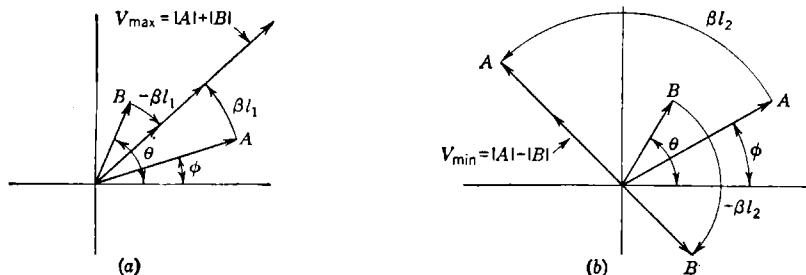


FIG. 2.7.—Vector relations for combining incident and reflected voltages.

This may be written, in terms of hyperbolic functions, as

$$Z_{-l} = Z_0 \frac{Z_r \cosh \gamma l + Z_0 \sinh \gamma l}{Z_0 \cosh \gamma l + Z_r \sinh \gamma l}, \quad (37)$$

or alternatively as

$$Z_{-l} = Z_0 \frac{Z_r + Z_0 \tanh \gamma l}{Z_0 + Z_r \tanh \gamma l}. \quad (38)$$

This result is extremely useful. If we know the load impedance Z_r and the line characteristics Z_0 and γ , we may calculate the impedance Z_l at any point a distance l from the load, toward the input end of the line. It is frequently convenient to express all impedances in terms of Z_0 . We shall denote such "normalized" impedances by a prime; thus

$$Z'_{-l} = \frac{Z_{-l}}{Z_0},$$

$$Z'_r = \frac{Z_r}{Z_0}.$$

Equation (38) may then be written

$$Z'_{-l} = \frac{Z'_r + \tanh \gamma l}{1 + Z'_r \tanh \gamma l}. \quad (39)$$

In many practical problems the attenuation of the line is small enough to give the impedance transformations with sufficient accuracy by a simplified formula. If

$$\begin{aligned} \alpha &= 0 \\ \gamma &= j\beta, \end{aligned}$$

then $\tanh \gamma l$ becomes

$$\tanh j\beta l = j \tan \beta l.$$

Equation (38) then simplifies to

$$Z_{-l} = Z_0 \frac{Z_r + jZ_0 \tan \beta l}{Z_0 + jZ_r \tan \beta l}, \quad (40)$$

and Eq. (39) to

$$Z'_{-l} = \frac{Z'_r + j \tan \beta l}{1 + jZ'_r \tan \beta l}. \quad (41)$$

It will be seen later on that this equation is the basis for the common rectangular impedance chart.

2-4. Propagation Factor and Characteristic Impedance.—The significance of these two line constants was discussed, in a general way, in Sec. 2-2. There are two special cases that are deserving of further elaboration. In each case it will be assumed that Z and Y of Eqs. (3) may be expressed simply as

$$\left. \begin{aligned} Z &= R + j\omega L, \\ Y &= G + j\omega C. \end{aligned} \right\} \quad (42)$$

It will be noted that any possible series-capacitance or shunt-inductance effects have been neglected; a little reflection will show that this is justifiable in ordinary types of line. Equations (7) and (10) then become

$$\gamma = \sqrt{ZY} = (\sqrt{R + j\omega L})(G + j\omega C), \quad (43)$$

$$Z_0 = \sqrt{\frac{Z}{Y}} = \sqrt{\frac{R + j\omega L}{G + j\omega C}}. \quad (44)$$

Ideal (Lossless) Line.—Many practical problems are solved accurately enough, and a great deal more easily, if Eqs. (43) and (44) are simplified by assuming ideal conductors and dielectric mediums for which

$$R = G = 0.$$

Those equations then become

$$\gamma = j\omega \sqrt{LC}, \quad (45)$$

$$Z_0 = \sqrt{\frac{L}{C}}. \quad (46)$$

The real and imaginary parts of γ are

$$\left. \begin{aligned} \alpha &= 0, \\ \beta &= \omega \sqrt{LC}. \end{aligned} \right\} \quad (47)$$

It is worth noting that the phase velocity, given by Eq. (15), may now be evaluated as

$$v_p = \frac{\omega}{\beta} = \frac{1}{\sqrt{LC}}. \quad (48)$$

From Eqs. (13) and (14) it is noted that

$$\frac{\omega}{\beta} = v\lambda. \quad (49)$$

Equations (48) and (49) may be combined to yield the following expression for the wavelength:

$$\lambda = \frac{v_p}{\nu} = \frac{1}{\nu \sqrt{LC}}. \quad (50)$$

It may be seen from Eq. (46) that Z_0 is real, that is, it is purely resistive. This means that a resistance having this particular value will properly terminate the line. It means also that the current and voltage in a traveling wave are in phase. This may be seen by writing Eqs. (8) and (9) for a pure traveling wave, that is, $B = 0$,

$$\left. \begin{aligned} V &= Ae^{-\gamma z}, \\ I &= \frac{A}{Z_0} e^{-\gamma z} = \frac{V}{Z_0}. \end{aligned} \right\} \quad (51)$$

Since these expressions represent the amplitudes of quantities varying sinusoidally with time, the power flowing in the traveling wave is the time average of their product; namely,

$$P = \frac{1}{2} VI = \frac{1}{2} \frac{V^2}{Z_0} = \frac{1}{2} I^2 Z_0. \quad (52)$$

Line with Small Losses.—In problems involving long lines, or lines with appreciable attenuation, the foregoing simplifying assumptions are no longer valid. In many such cases it will be true that $R \ll \omega L$ and $G \ll \omega C$. It then becomes possible to simplify Eqs. (43) and (44) by performing a binomial expansion. If Eq. (43) is written as

$$\gamma = j\omega \sqrt{LC} \left(1 + \frac{R}{j\omega L}\right)^{1/2} \left(1 + \frac{G}{j\omega C}\right)^{1/2},$$

and expanded by the binomial expansion, the solution becomes

$$\gamma = j\omega \sqrt{LC} \left(1 + \frac{R}{2j\omega L} - \frac{R^2}{8j^2\omega^2 L^2} + \dots \right) \left(1 + \frac{G}{2j\omega C} - \frac{G^2}{8j^2\omega^2 C^2} + \dots \right).$$

Neglecting terms of order higher than the second, the result is

$$\gamma = \alpha + j\beta = j\omega \sqrt{LC} \left[1 + \left(\frac{R}{2j\omega L} + \frac{G}{2j\omega C} \right) + \left(\frac{R^2}{8\omega^2 L^2} - \frac{RG}{4\omega^2 LC} + \frac{G^2}{8\omega^2 C^2} \right) \right]. \quad (53)$$

Equating real parts of this expression, one obtains

$$\alpha = \frac{R}{2} \sqrt{\frac{C}{L}} + \frac{G}{2} \sqrt{\frac{L}{C}} \quad \text{neper/m} \quad (53a)$$

Using the ideal-line characteristic impedance,

$$Z'_0 = \sqrt{\frac{L}{C}},$$

and the corresponding characteristic admittance, defined as

$$Y'_0 = \frac{1}{Z'_0} = \sqrt{\frac{C}{L}},$$

Eq. (53a) may be written as

$$\alpha = \frac{R}{2Z'_0} + \frac{G}{2Y'_0} \quad \text{nepers/m.} \quad (54)$$

It is easily recognized that the first term on the right is due to conductor loss, the second to dielectric loss. This equation may be expressed as

$$\alpha = \alpha_c + \alpha_d, \quad (55)$$

where

$$\alpha_c = \frac{R}{2Z'_0} \quad (56)$$

and

$$\alpha_d = \frac{G}{2Y'_0}. \quad (57)$$

If the imaginary parts of Eq. (53) are equated

$$\beta = \omega \sqrt{LC} \left(1 + \frac{R^2}{8\omega^2 L^2} - \frac{RG}{4\omega^2 LC} + \frac{G^2}{8\omega^2 C^2} \right),$$

or

$$\beta = \omega \sqrt{LC} \left[1 + \frac{1}{2} \left(\frac{R}{2\omega L} - \frac{G}{2\omega C} \right)^2 \right]. \quad (58)$$

If primed symbols are used to indicate quantities for the same line but with $R = G = 0$, Eq. (14) may be written as

$$\beta' = \omega \sqrt{LC} = \frac{2\pi}{\lambda'}$$

Then it is easily verified that Eq. (58) is equivalent to

$$\beta = \beta' \left[1 + \frac{1}{2} \left(\frac{\alpha_c}{\beta'} - \frac{\alpha_d}{\beta'} \right)^2 \right]; \quad (59)$$

the wavelength relation which follows is

$$\lambda = \lambda' \left[1 - \frac{1}{2} \left(\frac{\alpha_c}{\beta'} - \frac{\alpha_d}{\beta'} \right)^2 \right]. \quad (60)$$

Equations (59) and (60) contain terms which are readily interpreted. The conductor loss enters these expressions in the form

$$\frac{\alpha_c}{\beta'} = \frac{\alpha_c \lambda'}{2\pi},$$

which has the dimensions of nepers per radian of line length. Similarly, the term α_d/β' represents the dielectric loss in nepers per radian. It will be noted that, when these two losses are equal, β has the same value as in the case of an ideal line; referring to Eq. (58) this statement is equivalent to specifying that

$$\frac{R}{\omega L} = \frac{G}{\omega C}.$$

The greatest change in β obviously occurs when one type of attenuation is much larger than the other. Even in this case, however, the fact that this small term is squared means that a rather large attenuation per radian is required to affect β or λ appreciably.

Now that the discussion of Eq. (43) has been completed for the case of small R and G , the same procedure is applied to Eq. (44), which may be rewritten as

$$Z_0 = \sqrt{\frac{L}{C}} \left(1 + \frac{R}{j\omega L} \right)^{1/2} \left(1 + \frac{G}{j\omega C} \right)^{-1/2}.$$

Application of the binomial expansion yields

$$Z_0 = \sqrt{\frac{L}{C}} \left(1 + \frac{R}{2j\omega L} - \frac{R^2}{8j^2\omega^2 L^2} + \dots \right) \left(1 - \frac{G}{2j\omega C} + \frac{3G^2}{8j^2\omega^2 C^2} - \dots \right).$$

If terms of higher order than the second are dropped from the result, this becomes

$$Z_0 = \sqrt{\frac{L}{C}} \left[1 + \frac{1}{2} \left(\frac{R^2}{4\omega^2 L^2} + \frac{RG}{2\omega^2 LC} - \frac{3G^2}{4\omega^2 C^2} \right) + j \left(\frac{G}{2\omega C} - \frac{R}{2\omega L} \right) \right]. \quad (61)$$

Simplifying in the same manner as in Eq. (58), we obtain finally

$$Z_0 = Z'_0 \left[1 + \frac{1}{2} \left(\frac{\alpha_c}{\beta'} + 3 \frac{\alpha_d}{\beta'} \right) \left(\frac{\alpha_c}{\beta'} - \frac{\alpha_d}{\beta'} \right) - j \left(\frac{\alpha_c}{\beta'} - \frac{\alpha_d}{\beta'} \right) \right]. \quad (62)$$

The real part of the characteristic impedance may be compared to the phase constant β , Eq. (59); and the imaginary part to the attenuation constant α , Eqs. (54) and (55). The conductor attenuation and the dielectric attenuation add in the case of α ; but both β and Z_0 remain equal to their ideal-line values β' and Z'_0 so long as the conductor losses are equal to the dielectric losses. When these losses are not balanced, it will be noted that, in all cases, the attenuation in nepers per radian of line length enters, in a rather simple way, into the perturbation of each quantity from its ideal-line value. In β and in the real part of Z_0 , the attenuation enters squared and is, hence, relatively unimportant. In the imaginary part of Z_0 it enters to the first power and may be appreciable. It must be remembered, however, that these approximations are valid only for

$$\frac{R}{\omega L} \ll 1,$$

$$\frac{G}{\omega C} \ll 1.$$

In terms of the corresponding attenuations in nepers per radian this means that

$$\frac{\alpha_c}{\beta'} \ll \frac{1}{2}$$

and

$$\frac{\alpha_d}{\beta'} \ll \frac{1}{2}.$$

If these restrictions are not fulfilled, recourse should be had to the original expressions, Eqs. (43) and (44).

2-5. Application to Coaxial Line Characteristics. *The Ideal or Lossless Line.*—The appropriate equations from Sec. 2-4 which are needed in the present discussion are

$$\left. \begin{aligned} \alpha &= 0, \\ \beta &= \omega \sqrt{LC}, \end{aligned} \right\} \quad (2-47)$$

$$Z_0 = \sqrt{\frac{L}{C}}. \quad (2-46)$$

The basic assumption that the conductor has infinite conductivity leads, through the "skin effect" to be discussed presently, to a current flowing

entirely on the surface of the conductors. Referring to Fig. 2-8, the inductance and capacitance for a unit length of ideal coaxial line may be written as

$$L = \frac{\mu_1}{2\pi} \ln \frac{b}{a} \quad (63)$$

$$C = \frac{2\pi\epsilon_1}{\ln \frac{b}{a}} \quad (64)$$

Here μ_1 and ϵ_1 apply to the dielectric medium between conductors; the expression for C is easily obtained by simple electrostatic theory; that for L is derived on the assumption that all current is confined to the surface of the conductors so that it is accurate only at relatively high frequencies.

Equation (47) may now be

written, using Eqs. (63) and (64),

$$\beta = \omega \sqrt{\mu_1 \epsilon_1} \quad (65)$$

Introducing relative inductive capacities and remembering that $\sqrt{\mu_0 \epsilon_0} = 1/c$, the following result is obtained

$$\beta = \omega \sqrt{\mu_0 \epsilon_0} \sqrt{k_{m_1} k_{e_1}} = \frac{\omega}{c} \sqrt{k_{m_1} k_{e_1}} \quad (66)$$

Recalling Eq. (48), note the phase velocity is found to be

$$v_p = \frac{\omega}{\beta} = \frac{c}{\sqrt{k_{m_1} k_{e_1}}} \quad (67)$$

By use of the fundamental relation $\lambda = v_p/\nu$, Eq. (16),

$$\lambda = \frac{c}{\nu \sqrt{k_{m_1} k_{e_1}}} = \frac{\lambda_0}{\sqrt{k_{m_1} k_{e_1}}} \quad (68)$$

where $\lambda_0 = c/\nu$ is the associated free-space wavelength. Usually k_{m_1} has the value unity for ordinary dielectrics; consequently Eqs. (66), (67), and (68) may be written as

$$\beta = \frac{2\pi}{\lambda_0} \sqrt{k_{e_1}} = \frac{2\pi}{\lambda} \quad (69)$$

$$v_p = \frac{c}{\sqrt{k_{e_1}}} \quad (70)$$

$$\lambda = \frac{\lambda_0}{\sqrt{k_{e_1}}} \quad (71)$$

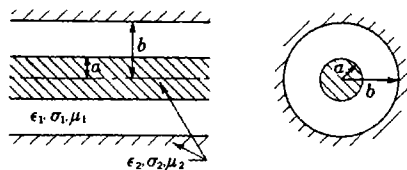


FIG. 2-8.—Coaxial line dimensions.

It will be noted that the phase velocity is independent of frequency; that is, an ideal coaxial line is a nondispersive transmission line. Consequently, the group and signal velocities are equal to the phase velocity (see Footnote 1, p. 12).

Similarly, substituting Eqs. (63) and (64) in Eq. (46) gives

$$\begin{aligned} Z_0 &= \frac{1}{2\pi} \sqrt{\frac{\mu_1}{\epsilon_1}} \ln \frac{b}{a}, \\ &= \frac{1}{2\pi} \sqrt{\frac{\mu_0}{\epsilon_0}} \sqrt{\frac{k_{m_1}}{k_{e_1}}} \ln \frac{b}{a}. \end{aligned} \quad (72)$$

Let us again restrict our consideration to dielectrics for which $k_{m_1} = 1$. Inserting the numerical value 376.7 ohms for the quantity $\sqrt{\mu_0/\epsilon_0}$, the so-called "impedance of free space," we obtain

$$Z_0 = \frac{60.0}{\sqrt{k_{e_1}}} \ln \frac{b}{a}, \quad (73)$$

$$Z_0 = \frac{138.0}{\sqrt{k_{e_1}}} \log_{10} \frac{b}{a}. \quad (74)$$

The power in a running wave may be written, using Eq. 52,

$$P = \frac{1}{2} \frac{V^2}{Z_0} = \frac{\sqrt{k_{e_1}} V^2}{120 \ln b/a}. \quad (75)$$

If the electric field intensity at the center conductor is denoted by E_a , the voltage may be shown to be

$$V = \int_a^b \frac{E_a a}{r} dr = E_a a \ln \frac{b}{a}. \quad (76)$$

Using this relation, Eq. (75) may be written

$$P = \frac{1}{2Z_0} E_a^2 a^2 \left(\ln \frac{b}{a} \right)^2 = \frac{E_a^2 a^2 \sqrt{k_{e_1}}}{120} \ln \frac{b}{a}. \quad (77)$$

The Actual or Low-loss Line.—The attenuation in actual coaxial lines is usually low enough to permit the use of the equations developed in the latter part of Sec. 2-4. These equations contain all the general relations needed for calculating α , β , and Z_0 . The line characteristics requiring specific evaluation for coaxial lines are α_c , α_d , β' , and Z'_0 . The last two are the values of β and Z_0 for an ideal line and have been evaluated in the first part of this section; the first two are the attenuation constants for conductor and dielectric losses which may now be calculated.

Equation (56) gives the attenuation due to the conductors:

$$\alpha_c = \frac{R}{2Z'_0}.$$

Here Z'_0 is the characteristic impedance, neglecting losses, given by Eq. (72), and R is the effective resistance per unit length of line. Since the current flows mostly near the surface of the conductors, a calculation of this effective resistance requires consideration of the "skin effect." The current density has its maximum value at the surface of the conductor and falls off exponentially to $1/e$ of this maximum value in a distance

$$\delta = \frac{1}{\sqrt{\pi \nu \mu_2 \sigma_2}}. \quad (78)$$

Subscripts 2 refer to the conductor material. This quantity δ is usually called the "skin depth." The losses in a conductor in which the current density is distributed according to this exponential law may be calculated. They are found to be exactly the same as those which would result from the same total current of uniform distribution flowing in the walls of a tubular conductor of wall thickness δ . The effective resistance per unit length of center conductor is then

$$R_a = \frac{1}{2\pi a \delta \sigma_2} = \frac{1}{2\pi a} \sqrt{\frac{\pi \nu \mu_2}{\sigma_2}}.$$

A similar expression may be written for the outer conductor, replacing a by b . The total resistance is the sum

$$R_a + R_b = R = \frac{1}{2\pi} \sqrt{\frac{\pi \nu \mu_2}{\sigma_2}} \left(\frac{1}{a} + \frac{1}{b} \right). \quad (79)$$

Substitution in Eq. (56) gives the alternative forms

$$\begin{aligned} \alpha_c &= \frac{1}{4\pi Z'_0} \sqrt{\frac{\pi \nu \mu_2}{\sigma_2}} \left(\frac{1}{a} + \frac{1}{b} \right) \quad \text{nepers/m} \\ &= \frac{1.581 \times 10^{-4}}{Z'_0} \sqrt{\frac{\nu k_m}{\sigma_2}} \left(\frac{1}{a} + \frac{1}{b} \right) \quad \text{nepers/m.} \end{aligned} \quad (79a)$$

If we let subscripts 1 refer to the characteristics of the dielectric medium, Eq. (72) becomes, for the present case,

$$Z'_0 = \frac{1}{2\pi} \sqrt{\frac{\mu_1}{\epsilon_1}} \ln \frac{b}{a}. \quad (80)$$

Substitution of Eq. (80) in Eq. (79a) yields the conductor loss

$$\alpha_c = \frac{1}{2} \sqrt{\frac{\pi \nu \mu_2 \epsilon_1}{\sigma_2 \epsilon_1}} \left(\frac{1}{a} + \frac{1}{b} \right) \frac{1}{\ln \frac{b}{a}} \quad \text{nepers/m.} \quad (81)$$

Introducing relative inductive capacities and inserting numerical values for the constants, one obtains as the final form

$$\alpha_c = \frac{2.63 \times 10^{-5}}{\ln \frac{b}{a}} \sqrt{\frac{\nu k_e k_{m_2}}{\sigma_2 k_{m_1}}} \left(\frac{1}{a} + \frac{1}{b} \right) \quad \text{nepers/m.} \quad (82)$$

The attenuation due to the dielectric is given by Eq. (57);

$$\alpha_d = \frac{G}{2Y'_0} \quad (2.57)$$

A simple integration gives, for a dielectric whose effective conductivity is σ_1 ,

$$G = \frac{2\pi\sigma_1}{\ln \frac{b}{a}} \quad (83)$$

In Eq. (57), substitute this for G and the reciprocal of Z'_0 , Eq. (80), for Y'_0 :

$$\alpha_d = \frac{\sigma_1}{2} \sqrt{\frac{\mu_1}{\epsilon_1}} \quad (84)$$

It is noted at once that this loss is independent of the dimensions of the line. The effective conductivity may be a true conductivity which could be measured with a d-c ohmmeter; or it may be due, wholly or in part, to a hysteresis loss which occurs in the molecules of the dielectric as they are subjected to polarization by the high frequency fields. In any case, the dielectric may be described by a dielectric constant ϵ_1 and an effective conductivity σ_1 .

The current density in the dielectric medium is

$$J = \sigma_1 E + \epsilon_1 \frac{\partial E}{\partial t} \quad (85)$$

By Ohm's law, $\sigma_1 E$ is the "conduction" current, including both true conduction current and current supplying hysteresis losses; the term $\epsilon_1 \frac{\partial E}{\partial t}$ is the displacement current. For a harmonic voltage,

$$E = E_0 e^{j\omega t};$$

and

$$\frac{\partial E}{\partial t} = j\omega E.$$

Equation (85) may now be written

$$J = (\sigma_1 + j\omega\epsilon_1)E. \quad (86)$$

The conduction current is in phase with the electric field and therefore represents a power loss. The displacement current is out of phase and therefore does not. Since the conduction current is usually small compared with the displacement current, it is convenient to rewrite Eq. (86) as

$$J = j\omega\epsilon_1 \left(1 - j \frac{\sigma_1}{\omega\epsilon_1} \right) E. \quad (87)$$

it is convenient to define a complex dielectric constant,

$$\epsilon_{c1} = \epsilon_1 \left(1 - j \frac{\sigma_1}{\omega\epsilon_1} \right), \quad (88)$$

in order to simplify Eq. (87); thus

$$J = j\omega\epsilon_{c1}E. \quad (89)$$

The conductivity no longer appears explicitly but is contained in the complex dielectric constant. If ϵ_{c1} is substituted for ϵ_1 in equations derived on the basis of an ideal dielectric with a simple dielectric constant ϵ_1 , the resulting equations will take into account the non-ideal character of the dielectric. The complex dielectric constant is usually expressed as

$$\epsilon_{c1} = \epsilon'_1 - j\epsilon''_1. \quad (90)$$

Comparison with Eq. (88) shows that

$$\epsilon'_1 = \epsilon_1 \quad (91)$$

$$\epsilon''_1 = \frac{\sigma_1}{\omega} \quad (92)$$

is the imaginary part of the complex dielectric constant. These relations are presented diagrammatically in Fig. 2-9. The power lost per unit volume is

$$P_1 = JE \cos \theta = JE \sin \delta.$$

Therefore, the power factor, in the usual sense, is

$$p = \cos \theta = \sin \delta. \quad (93)$$

The ratio

$$\frac{\epsilon''_1}{\epsilon'_1} = \tan \delta \quad (94)$$

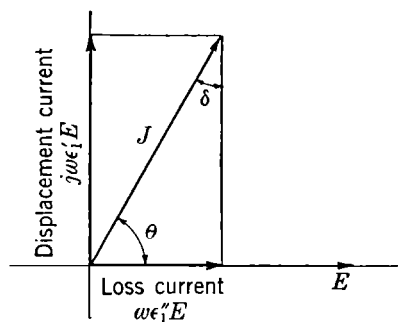


FIG. 2-9.—Current-voltage relations in imperfect dielectric.

is called the "loss tangent" and is, for small angles, almost identical with the power factor.

The dielectric attenuation given by Eq. (84) may be rewritten, using Eq. (92),

$$\alpha_d = \frac{\omega \epsilon_1''}{2} \sqrt{\frac{\mu_1}{\epsilon_1}} = \pi \nu \frac{\epsilon_1''}{\epsilon_1} \sqrt{\epsilon_1 \mu_1} \quad \text{nepers/m.} \quad (95)$$

By use of Eq. (94) and the introduction of relative inductive capacities, one obtains

$$\alpha_d = \pi \nu \sqrt{k_{e1} k_{m1}} \sqrt{\epsilon_0 \mu_0} \tan \delta \quad \text{nepers/m} \quad (96)$$

$$= \frac{\pi \nu}{c} \sqrt{k_{m1} k_{e1}} \tan \delta \quad \text{nepers/m.} \quad (97)$$

In view of Eq. (68), this may be written

$$\alpha_d = \frac{\pi}{\lambda_1} \tan \delta \quad \text{nepers/m,} \quad (98)$$

where λ_1 is the wavelength in the line. Other forms for this equation are

$$\begin{aligned} \alpha_d &= \pi \tan \delta \quad \text{nepers/line wavelength} \\ &= \frac{1}{2} \tan \delta \quad \text{nepers/radian.} \end{aligned} \quad (99)$$

2.6. Some Useful Relations in Transmission Lines.—A number of the frequently used transmission-line equations developed earlier in the present chapter have been collected, for easy reference, in Table 2.1. The equation numbers given in the table correspond to the earlier appearance of those equations in the text. Where no such number is given, the corresponding equation does not appear explicitly in the text but is a simple extension or special case of one of the numbered equations.

Aside from these transmission-line equations, a number of relations of miscellaneous character are frequently useful. Several such relations, valid for ideal or low-loss lines, are tabulated in Table 2.2. Figures 2.10, 2.11, and 2.12 present some of these relations in graphical form.

Most of the relations should be clear from the table, but Items 4, 5, and 6 of Table 2.2 may require additional explanation. Item 4 is likely to prove confusing unless one notes particularly that it is the *net* power trans-

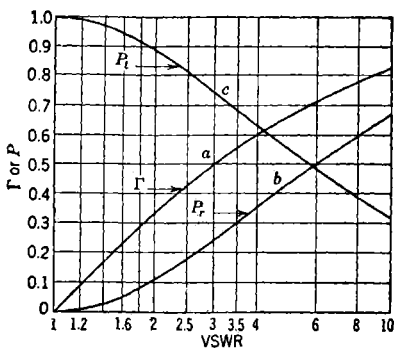


FIG. 2.10.—Relation between VSWR and (a) reflection coefficient Γ , (b) power reflected P_r , (c) power transmitted P_t .

mitted to the load which is being considered. This power may be calculated by considering the conditions at a voltage maximum, Item 2*b*, when the voltage there has the breakdown value V_b . The net power transferred into the impedance R by this breakdown voltage is

$$P_b = \frac{1}{2} \frac{V_b^2}{R} = \frac{1}{2} \frac{V_b^2}{r Z_0} \quad (100)$$

For a matched line $r = 1$, the power is

$$P_m = \frac{1}{2} \frac{V_b^2}{Z_0} \quad (101)$$

and Item 4 follows:

$$\frac{P_b}{P_m} = \frac{1}{r} \quad (102)$$

Item 5 may be clarified by noting that, in a section of line in which a reflected wave exists, the mean-square current in the walls is larger, for a given net power transfer to the load, than if a pure traveling wave were in the line. This means that the actual ohmic loss in the walls is increased because of the presence of standing waves. Similarly, the ohmic loss in the dielectric of the line is higher because of an increase in the mean-square voltage across the line. If we consider a half wavelength of line, both current and voltage go through a complete cycle of variation; therefore, the averaging will be unique, irrespective of the phase

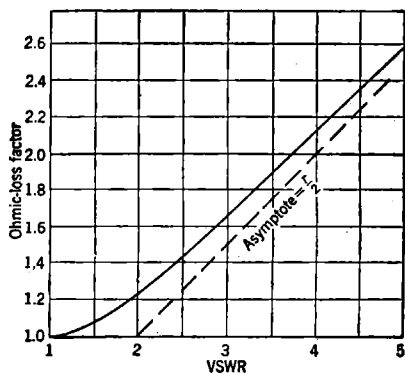


Fig. 2-11.—Increase in ohmic loss due to standing waves.

of the standing wave along the line section chosen. Item 5 is valid, strictly speaking, only for an integral number of half wavelengths or for those lengths containing a sufficient number of half wavelengths to make phase effects negligible. In the latter case, however, the total loss must be so low that the value of r is essentially constant. If this is not the case, the actual loss-increase factor will lie somewhere between those factors calculated on the basis of the values of r at input and output ends of the line section considered.

It is true here, as it is in general, that the power lost per unit length P_L must correspond to the decrease, per unit length, of the net power P being transmitted toward the load. Since the power decreases exponentially, $P = P_0 e^{-2\alpha z}$, we have

It is true here, as it is in general, that the power lost per unit length P_L must correspond to the decrease, per unit length, of the net power P being transmitted toward the load. Since the power decreases exponentially, $P = P_0 e^{-2\alpha z}$, we have

$$P_L = -\frac{dP}{dZ} = -\frac{d}{dZ}(P_0 e^{-2\alpha z}) = 2\alpha P. \tag{103}$$

Consequently we obtain the general relation

$$\alpha = \frac{P_L}{2P}. \tag{104}$$

In the present instance, the power loss is the sum of that loss caused by incident and reflected waves. If the conductors have a resistance R per unit length, this is

$$P_L = \frac{1}{2}(I_i^2 R + I_r^2 R) = \frac{1}{2} I_i^2 R (1 + \Gamma^2). \tag{105}$$

By Eq. (52), the net power transmitted is

$$P = \frac{1}{2}(I_i^2 Z_0 - I_r^2 Z_0) = \frac{1}{2} I_i^2 Z_0 (1 - \Gamma^2). \tag{106}$$

By Eq. (104), the attenuation is

$$\alpha_r = \frac{R}{2Z_0} \frac{(1 + \Gamma^2)}{(1 - \Gamma^2)}. \tag{107}$$

For matched lines $\Gamma = 0$, we obtain from Eq. (107)

$$\alpha_m = \frac{R}{2Z_0}. \tag{108}$$

After division, Item 5 is

$$\frac{\alpha_r}{\alpha_m} = \frac{1 + \Gamma^2}{1 - \Gamma^2} = \frac{r^2 + 1}{2r}, \tag{109}$$

where Item 1b has been used to obtain the final term.

It must be recognized that this effect is quite distinct from that of Item 3, which must be considered in addition to the ohmic loss factor. By using a suitable impedance transformer at the input end of a section of line on which standing waves exist, all the power available at that point may be caused to enter the line section; but if its output end is mismatched instead of matched, a greater percentage of power will be used to supply losses in the line section.

Item 6 of Table 2.2 is offered without proof, since proof is rather difficult to obtain on the basis of the transmission-line theory developed in the present chapter; it may, however, be proved by the use of network theory (see Chap. 10). It has been assumed that the line losses are small; hence, each value of r remains substantially constant in passing from the dis-

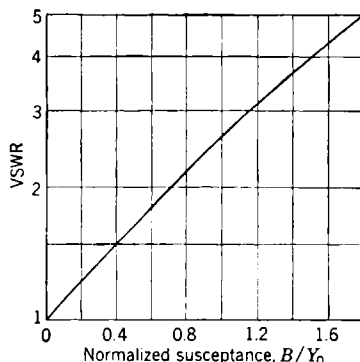


Fig. 2.12.—Voltage standing-wave ratio for susceptance-shunting matched line.

TABLE 2-1.—SUMMARY OF TRANSMISSION LINE EQUATIONS

No.	Quantity	General line		Ideal line		Approximation, low-loss line	
		Expression	Eq. No.	Expression	Eq. No.	Expression	Eq. No.
1	Propagation constant $\gamma = \alpha + j\beta$	$\sqrt{(R + j\omega L)(G + j\omega C)}$	43	$j\omega \sqrt{LC}$	45	See α and β below	..
2	Phase constant β	$\text{Im } \gamma$..	$\omega \sqrt{LC} = \frac{\omega}{v_p} = \frac{2\pi}{\lambda}$	47 ff.	$\beta' \left[1 + \frac{1}{2} \left(\frac{\alpha_c}{\beta'} - \frac{\alpha_d}{\beta'} \right)^2 \right]$	59
3	Attenuation constant α	$\text{Re } \gamma = \frac{-1}{2} \frac{dP}{P dl}$..	0	..	$\alpha_c + \alpha_d = \frac{R}{2Z_0'} + \frac{G}{2Y_0'}$	54
4	Characteristic Impedance Z_0	$\sqrt{\frac{R + j\omega L}{G + j\omega C}}$	44	$\sqrt{\frac{L}{C}}$	46	$Z_0' \left[1 + \frac{1}{2} \left(\frac{\alpha_c}{\beta'} - \frac{\alpha_d}{\beta'} \right) \left(\frac{\alpha_c}{\beta'} + \frac{3\alpha_d}{\beta'} \right) \right]$ $- jZ_0' \left(\frac{\alpha_c}{\beta'} - \frac{\alpha_d}{\beta'} \right)$	62
5	Input Impedance Z_{-l}	$Z_0 \frac{Z_r + Z_0 \tanh \gamma l}{Z_0 + Z_r \tanh \gamma l}$	38	$Z_0 \frac{Z_r + jZ_0 \tan \beta l}{Z_0 + jZ_r \tan \beta l}$	40
6	Impedance of short-circuited line	$Z_0 \tanh \gamma l$..	$jZ_0 \tan \beta l$..	$Z_0 \frac{\alpha l + j \tan \beta l}{1 + j\alpha l \tan \beta l}$..
7	Impedance of open-circuited line	$Z_0 \coth \gamma l$..	$-jZ_0 \cot \beta l$..	$Z_0 \frac{1 + j\alpha l \tan \beta l}{\alpha l + j \tan \beta l}$..
8	Impedance of a line an odd number of quarter wavelengths long	$Z_0 \frac{Z_r + Z_0 \coth \alpha l}{Z_0 + Z_r \coth \alpha l}$..	$\frac{Z_0^2}{Z_r}$..	$Z_0 \frac{Z_0 + Z_r \alpha l}{Z_r + Z_0 \alpha l}$..
9	Impedance of a line an integral number of half wavelengths long	$Z_0 \frac{Z_r + Z_0 \tanh \alpha l}{Z_0 + Z_r \tanh \alpha l}$..	Z_r	..	$Z_0 \frac{Z_r + Z_0 \alpha l}{Z_0 + Z_r \alpha l}$..

TABLE 2-1.—SUMMARY OF TRANSMISSION LINE EQUATIONS.—(Continued)

No.	Quantity	General line		Ideal line		Approximation, low-loss line	
		Expression	Eq. No.	Expression	Eq. No.	Expression	Eq. No.
10	Voltage V_{-l} along line	$V_i(1 + \Gamma_0 e^{-2\gamma l})$	27	$V_i(1 + \Gamma_0 e^{-2j\beta l})$
11	Current I_{-l} along line	$I_i(1 - \Gamma_0 e^{-2\gamma l})$	29	$I_i(1 - \Gamma_0 e^{-2j\beta l})$
12	Voltage reflection coefficient	$\frac{Z_r - Z_0}{Z_r + Z_0}$	21	$\frac{Z_r - Z_0}{Z_r + Z_0}$

R, L, G, C = distributed resistance, inductance, conductance, capacitance per unit length.

β' = \sqrt{LC} = phase constant, neglecting losses.

$Z_0 = \sqrt{\frac{L}{C}}$ = characteristic impedance, neglecting loss; $Y_0 = \frac{1}{Z_0}$.

λ = wavelength measured along line.

v_p = phase velocity of line, equals velocity of light in dielectric of line for an ideal line.

Γ_0 = reflection coefficient at $z = 0$.

l = distance along line, from load end.

Subscript r denotes receiving end, (load) quantities at $z = 0$.

Subscript $-l$ denotes input end, quantities at $z = -l$.

Subscript i denotes incident wave quantities.

TABLE 2-2.—SOME MISCELLANEOUS RELATIONS IN LOW-LOSS TRANSMISSION LINES

Item	Equation	Fig.	Explanation
1a	$r = \frac{1 + \Gamma }{1 - \Gamma }$	1	r = voltage standing-wave ratio
1b	$ \Gamma = \frac{r - 1}{r + 1}$	1	$ \Gamma $ = magnitude of reflection coefficient
2a	$\Gamma = \frac{R - Z_0}{R + Z_0}$..	Γ = reflection coefficient (real) at a point in a line where the impedance is real (R). Point may be at an actual resistive load or at a voltage max. or min. in standing-wave pattern
2b	$r = \frac{R}{Z_0}$; $R = rZ_0$..	Conditions for $R > Z_0$, i.e., at voltage maximum
2c	$r = \frac{Z_0}{R}$; $R = \frac{1}{r} Z_0$..	Conditions for $R < Z_0$, i.e., at voltage minimum
3a	$\frac{P_r}{P_i} = \Gamma ^2 = \left(\frac{r - 1}{r + 1}\right)^2$	1	P_r = power in wave reflected by discontinuity or mismatched load P_i = power in incident wave
3b	$\frac{P_t}{P_i} = 1 - \Gamma ^2 = \frac{4r}{(r + 1)^2}$..	P_t = power in transmitted (or absorbed) wave
4	$\frac{P_b}{P_m} = \frac{1}{r}$..	P_b = net power transmitted to load at onset of breakdown in a line in which a VSWR = r exists P_m = same when line is matched, $r = 1$
5	$\frac{\alpha_r}{\alpha_m} = \frac{1 + \Gamma^2}{1 - \Gamma^2} = \frac{r^2 + 1}{2r}$	2	α_m = ordinary attenuation constant; matched line, $r = 1$ α_r = attenuation constant allowing for increased ohmic loss caused by standing waves (VSWR = r)

TABLE 2-2.—SOME MISCELLANEOUS RELATIONS IN LOW-LOSS TRANSMISSION LINES.—(Continued)

Item	Equation	Fig.	Explanation
6a	$r_{\max} = r_1 r_2$..	Resultant VSWR when two separate mismatches combine in worst phase
6b	$r_{\min} = \frac{r_2}{r_1}; r_1 < r_2$..	Resultant when they combine in best phase
6c	$r_{\max} = r_1 r_2 r_3 \cdots r_n$..	Resultant for n mismatches, worst phase
6d	$r_{\min} = \frac{r_n}{r_1 r_2 \cdots r_{n-1}}$ $r_1 < r_2 < r_3 < \cdots < r_n$..	Resultant for n mismatches, best phase. If this gives $r_{\min} < 1$, then $r_{\min} = 1$
7a	$ \Gamma = \frac{ X }{\sqrt{X^2 + 4}}$..	Relations for the case of a normalized reactance X in series with resistance Z_0
7b	$r = \frac{\sqrt{X^2 + 4} + X }{\sqrt{X^2 + 4} - X }$	3	
7c	$ X = \frac{r - 1}{\sqrt{r}}$..	
8a	$ \Gamma = \frac{ B }{\sqrt{B^2 + 4}}$..	Relations for the case of a normalized susceptance B shunting conductance Y_0
8b	$r = \frac{\sqrt{B^2 + 4} + B }{\sqrt{B^2 + 4} - B }$	3	
8c	$ B = \frac{r - 1}{\sqrt{r}}$	3	

continuity giving rise to it to the next discontinuity. For mathematical convenience, the standing-wave ratios have been numbered with subscripts assigned in the order of increasing values. Since r is, by definition, equal to or greater than unity, whenever the formulas give values less than unity, the true minimum is unity. By proper phasing of the various discontinuities, any value of resultant VSWR between the minimum and maximum values indicated is attainable.

TRANSMISSION LINES AS GUIDES FOR ELECTROMAGNETIC WAVES

2-7. The Guided-wave Concept—Unfortunately, the conventional transmission-line theory outlined above is limited in its application to lines with two or more conductors, such as coaxial or parallel-wire lines. Even these simple lines may propagate waves in which the distribution

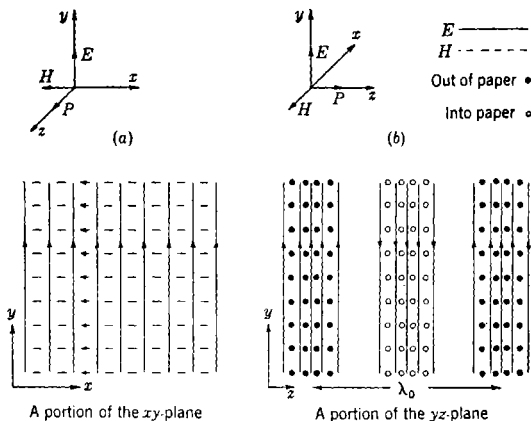


FIG. 2-13. —Fields in a plane wave in free space.

of currents and electric fields is more complicated than the assumptions of the conventional theory permit. To study these so-called “higher modes,” a more comprehensive approach must be made. This is afforded by the application of electromagnetic theory to the problem. Whereas the conventional theory chiefly considers currents and voltages, the electromagnetic theory is primarily concerned with the electric and magnetic fields associated with these currents and voltages. The concept of the propagation of energy through space in the form of an electromagnetic wave is one which is familiar in connection with radio and light waves. The electric and magnetic fields for a portion of an infinitely large wavefront are shown in Fig. 2-13. The wave is being propagated (vector \mathbf{P}) in the positive z -direction, toward the reader; in Fig. 2-13 a small portion of the yz -plane is shown. The wave is being propagated to the right and the distance λ_0 , between points of identical phase, is

indicated. The only electric field present is E_y , and the only magnetic field is H_x . Both are uniform over the xy -plane, and vary, with time and z -coordinate, as $e^{j\omega t - \gamma z}$. For free space, α is 0, so $\gamma = j\beta = j2\pi/\lambda_0$. The velocity of propagation is identical with the phase velocity,

$$c = 1/\sqrt{\mu_0\epsilon_0} = 2.99776 \times 10^8 \text{ m/sec.}$$

There is a unique relation between \mathbf{E} and \mathbf{H} in such a plane wave.

$$\mathbf{E} = \sqrt{\mu_0/\epsilon_0} \mathbf{H};$$

the quantity $\sqrt{\mu_0/\epsilon_0}$ is called the "wave impedance of free space" and has the value 376.7 ohms.

A transmission line may be regarded as a guide which confines the electromagnetic energy to the dielectric medium that comprises part of the line, thereby permitting its propagation with relatively high efficiency along the line. In a coaxial line, for example, the electric and magnetic fields are confined to the space between the outer and inner cylinders. At the boundary between dielectric medium and metallic conductor, a sharp discontinuity in electrical properties occurs. The high conductivity of the metal wall gives rise to boundary conditions which impose certain restrictions on the form of the electric and magnetic fields which may exist within the dielectric. A consequence of the good conductivity of the metallic walls is this: electrical currents are induced in the walls by the magnetic fields, thus providing a connecting link between the conventional viewpoint and the electromagnetic-wave approach. For simple transmission lines, the voltage between conductors is simply the integral of the electric field; this provides another connecting link.

The electromagnetic-wave concept is based on the fundamental set of equations known as Maxwell's Equations. These equations draw on experimental and theoretical contributions of Gauss, Ampere, and Faraday as well as on those of Maxwell, who incorporated their various theories into one comprehensive electromagnetic theory. These equations may be expressed in compact vector form as

$$\text{div } \mathbf{D} = \rho, \quad (110a)$$

$$\text{div } \mathbf{B} = 0, \quad (110b)$$

$$\text{curl } \mathbf{H} = \mathbf{J} + \frac{\partial \mathbf{D}}{\partial t}, \quad (110c)$$

$$\text{curl } \mathbf{E} = -\frac{\partial \mathbf{B}}{\partial t}, \quad (110d)$$

where

$$\mathbf{D} = \epsilon \mathbf{E}, \quad (111a)$$

and

$$\mathbf{B} = \mu \mathbf{H}, \quad (111b)$$

are the electric and magnetic inductions. The conduction current density \mathbf{J} is related to the electric field by Ohm's law,

$$\mathbf{J} = \sigma \mathbf{E}. \quad (112)$$

These equations are given here chiefly for reference. It is beyond the scope of this volume to carry through a detailed development of transmission-line problems based on these equations. Rather, the general procedure for such a development will be outlined briefly and the results for specific types of waveguide written.¹

Let us consider a waveguide which is formed by one or more metallic conductors of unspecified cross-sectional form, but which has a uniform cross section throughout its length. The most common types of waveguide are coaxial cylinders, parallel wires, hollow tubes of rectangular cross section, and hollow tubes of circular cross section. The present discussion applies to any one of these as well as to other less common shapes. For the sake of concreteness, let us think of the discussion as applying to the rectangular waveguide of Fig. 2-14, although the discussion itself will be kept perfectly general. It is customary to simplify the problem

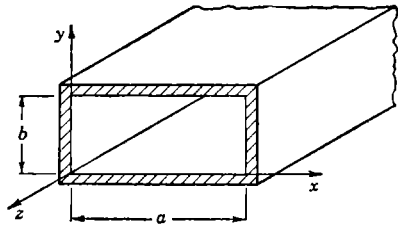


FIG. 2-14.—Rectangular-waveguide coordinates.

by considering first the case of an ideal waveguide with perfectly conducting walls. This consideration immediately imposes the boundary condition that the tangential component of the electric field must vanish on all conducting surfaces. The compact vector equations, Eqs. (110b) and (110d), are then expanded into expressions involving field components. This expansion is written in that system of coordinates in which the boundary conditions are most easily expressed. Thus, for rectangular waveguide the expansion is written in rectangular coordinates, while for cylindrical waveguide and for coaxial cylinders the cylindrical coordinate system is used. These equations are simplified by assuming all the fields to vary sinusoidally in time and to be propagated in the axial coordinate direction with a propagation constant γ ; that is,

$$\begin{aligned} \mathbf{E} &= \mathbf{E}' e^{j\omega t - \gamma z}, \\ \mathbf{H} &= \mathbf{H}' e^{j\omega t - \gamma z} \end{aligned} \quad (113)$$

The problem, then, becomes one of finding expressions for the variation of

¹ The same notation and equations to be found in *Principles of Microwave Circuits*, Vol. 8 of the Radiation Laboratories Series, will be used. The reader is referred to this volume for an excellent treatment of the subject.

the field components in the other two coordinates consistent with the field equations and satisfying the boundary conditions. Simple field distributions which meet these requirements in three common waveguide types are sketched in Fig. 2-15. The mode designations will be explained below.

To recapitulate, the dependence on time and on the axial coordinate is assumed to be given by Eq. (113). If equations for the cross-sectional

dependence of the fields can be found which satisfy the field equations, Eqs. (110c) and (110d), and which require no tangential electric field on the metallic walls, a solution of the waveguide problem will have been found. Although one might fear that no such solution can be found by this method, it actually turns out that an infinite number of solutions results. This arises from the fact that there are more variables and parameters than connecting equations. As a matter of fact, the usual practice is to choose one field component (usually E_z or H_z) equal to zero and solve for the remaining field components. Even when this is done, an infinite set of solutions exists which satisfies the connecting equations and the boundary conditions.

If $E_z = 0$, then the vector \mathbf{E} clearly lies in the plane transverse to the propagational axis z . The resulting set of solutions, commonly termed "modes," are designated as transverse electric or TE -modes. If $H_z = 0$, the resulting solutions are termed transverse magnetic, or TM -modes. In some special cases (for example, coaxial line or two-wire line operating in the simplest manner) both E_z and H_z are zero, and the solution is termed transverse electromagnetic, or TEM -mode. It is only to these simple cases that the conventional transmission-line theory applies.

In these simple cases, there is no lower limit on the frequencies that may be propagated along the line; nor is the phase velocity dependent on the frequency. That is, such a line is nondispersive, and the group and

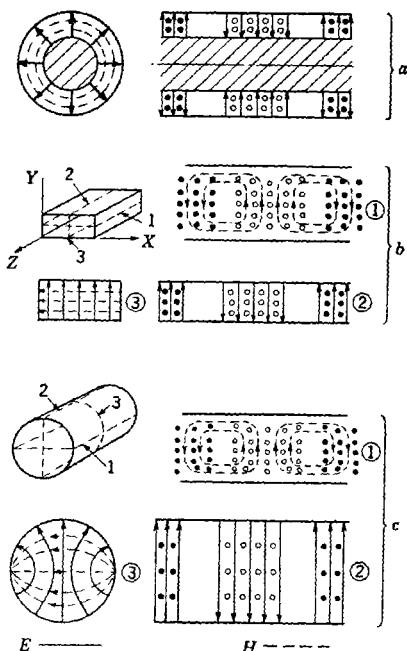


FIG. 2-15.—Fields in waveguides. The modes are (a) TEM in coaxial line, (b) TE_{10} in rectangular tube, (c) TE_{11} in round tube.

signal velocities are identical with the phase velocity. In the general case for a given waveguide, each separate mode of the TE - or TM -series is characterized by a frequency below which propagation does not occur. This is called the "cutoff frequency" for the particular mode, and the associated free-space wavelength is called the "cutoff wavelength." At the cutoff frequency the phase velocity for that mode is infinite and drops rapidly as the frequency is increased. Consequently, such modes are dispersive, and the group and signal velocities are not equal to the phase velocity. Similarly, the guide wavelength, the distance between equiphase points in the waveguide, is infinite at the cutoff frequency and drops rapidly as the frequency is increased.

2-8. Transmission Characteristics of a Simple Parallel-plate Waveguide.—In order to visualize better the physical situation that exists in a waveguide transmitting an electromagnetic wave, it may be found

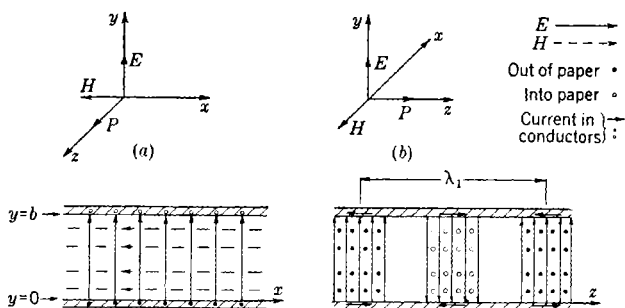


FIG. 2-16.—Portion of a plane wave confined between infinite conducting planes.

helpful to consider in some detail the fields in a simple waveguide. Although a purely mathematical development based on Maxwell's equations gives expressions for all the field components and enables one to map the fields, an aid to physical understanding is afforded by a consideration of the problem from the standpoint of plane waves.

Lossless Waveguide.—The type of waveguide easiest to visualize is that composed of two parallel planes, Fig. 2-16, infinite in extent and having perfect conductivity. The electric field has only a y -component; hence the boundary condition requiring zero electric field tangential to the conductor planes is satisfied. The magnetic field, being tangential to the conducting planes, induces currents on them as indicated. The direction of propagation of the energy is given by the right-hand-screw rule: it is the direction of advance of such a screw when turning the vector \mathbf{E} into the vector \mathbf{H} , the axis of the screw being perpendicular to the plane containing \mathbf{E} and \mathbf{H} . The wave of Fig. 2-16 is being propagated in the positive z -direction, as indicated by the vector \mathbf{P} . The direction of propagation, as well as the instantaneous rate of transfer of electro-

magnetic energy across unit area in this direction, is given by the Poynting vector,

$$\mathbf{S} = \mathbf{E} \times \mathbf{H},$$

\mathbf{E} and \mathbf{H} being instantaneous values at the point considered. The time average of \mathbf{S} , taken over a cycle, gives the average power per unit area flowing through an infinitesimal element of surface chosen perpendicular to the vector \mathbf{S} . If we have, at a certain point, only the fields E_y and H_x , where the symbols stand for the amplitude of fields varying sinusoidally with time, the average power per unit area will be

$$p_z = \frac{1}{2} E_y H_x. \quad (114)$$

The factor $\frac{1}{2}$ arises, of course, from the averaging process. If we consider a width a , in the x dimension of Fig. 2-16, the power transferred is the product of power per unit area p_z and the area ab ;

$$P = \frac{1}{2} E_y H_x ab. \quad (115)$$

Since the amplitude of the current for unit width of either conducting plane is equal to the amplitude of the magnetic field,

$$I_l = H_x;$$

therefore the total current in width a is

$$I = aH_x, \quad (116)$$

and the amplitude of the voltage between planes is

$$V = bE_y. \quad (117)$$

Substituting Eqs. (116) and (117) in Eq. (115), we obtain

$$P = \frac{1}{2} VI, \quad (118)$$

which is in agreement with the result obtained by ordinary low-frequency or conventional transmission-line theory. The equivalent characteristic impedance for a section of width a is

$$Z_e = \frac{V}{I} = \frac{b}{a} \frac{E_y}{H_x}. \quad (119)$$

By suitable mathematical manipulation of Maxwell's equations, it can be shown that for a plane wave in a medium whose magnetic permeability is μ_1 , and whose dielectric constant is ϵ_1 , the ratio between electric and magnetic fields is the wave impedance,

$$Z_w = \frac{E_y}{H_x} = \sqrt{\frac{\mu_1}{\epsilon_1}}. \quad (120)$$

The relation between the fields in our simple waveguide is not altered if we change the plane separation b . If we increase b indefinitely, we obtain in the limit an infinite plane wave. Therefore, these fields have the same form as those of a plane wave, and Eq. (120) is applicable to the simple waveguide. Equation (119) may then be written

$$Z_e = \frac{b}{a} Z_w. \quad (121)$$

Similarly, the phase velocity for a plane wave, propagated in a medium whose characteristic constants are μ_1 and ϵ_1 , may be shown, by use of Maxwell's equations, to be

$$v_p = \frac{1}{\sqrt{\mu_1 \epsilon_1}} = \frac{c}{\sqrt{k_{e_1} k_{m_1}}}. \quad (122)$$

The intrinsic wavelength in the medium is

$$\lambda_1 = \frac{v_p}{\nu} = \frac{1}{\nu \sqrt{\mu_1 \epsilon_1}} = \frac{\lambda_0}{\sqrt{k_{e_1} k_{m_1}}}. \quad (123)$$

These same relations apply to the simple waveguide that we are discussing. Since the conduction planes are assumed to be perfectly conducting, no conductor loss is present. Similarly, the dielectric medium is assumed to be ideal; therefore there is no dielectric loss. Hence, for the simple case we have been considering, the transmission characteristics are

$$\left. \begin{aligned} \alpha &= 0, \\ \beta &= \frac{2\pi}{\lambda_1} = \omega \sqrt{\mu_1 \epsilon_1}, \\ Z_w &= \sqrt{\frac{\mu_1}{\epsilon_1}}, \\ Z_e &= \frac{b}{a} Z_w. \end{aligned} \right\} \quad (124)$$

Waveguide with Losses.—If the dielectric is not ideal but possesses an effective conductivity σ_1 , the power dissipated per unit volume is $\frac{1}{2} E_y^2 \sigma_1$; and the power lost per unit length for a section of waveguide of width a is

$$P_l = ab \frac{1}{2} E_y^2 \sigma_1. \quad (125)$$

It is true here, as it is in general, that the power lost per unit length P_l must correspond to the decrease per unit length of the power P being transmitted. Since $P = P_0 e^{-2\alpha z}$, we have

$$P_l = -\frac{dP}{dz} = -\frac{d}{dz} P_0 e^{-2\alpha z} = 2\alpha P.$$

Therefore, we obtain the general relation

$$\alpha = \frac{P_1}{2P}. \quad (126)$$

The value of P in this case is found, using Eqs. (115) and (120), to be

$$P = \frac{1}{2} ab E_y^2 \sqrt{\frac{\epsilon_1}{\mu_1}}. \quad (127)$$

Substituting in Eq. (126) we obtain the dielectric loss factor,

$$\alpha_d = \frac{\frac{1}{2} ab E_y^2 \sigma_1}{ab E_y^2 \sqrt{\frac{\epsilon_1}{\mu_1}}} = \frac{\sigma_1}{2} \sqrt{\frac{\mu_1}{\epsilon_1}}. \quad (128)$$

Although this relation was derived for a certain size of guide, it is clear that it holds for any size. Since, in Eq. (126), both P_1 and P are directly proportional to the cross-sectional area, their ratio is independent of the guide dimensions. Conventional transmission-line theory, Eq. (57), gives

$$\alpha_d = \frac{G}{2Y_0'}. \quad (2-57)$$

The conductance G , per unit length of a waveguide strip of width a , is

$$G = \frac{a\sigma_1}{b}. \quad (129)$$

The equivalent characteristic admittance Y_e plays the part of Y_0' in the previous section. For such a strip Y_e is the reciprocal of Z_e ;

$$Y_e = \frac{1}{Z_e} = \frac{a}{b \sqrt{\frac{\mu_1}{\epsilon_1}}}. \quad (130)$$

Hence, we obtain the dielectric loss by substituting in Eq. (57),

$$\alpha_d = \frac{a\sigma_1}{b} \frac{b}{2a} \sqrt{\frac{\mu_1}{\epsilon_1}} = \frac{\sigma_1}{2} \sqrt{\frac{\mu_1}{\epsilon_1}}. \quad (131)$$

Again, the conventional transmission-line theory agrees with electromagnetic-wave theory.

To obtain an accurate expression for the conductor loss, one would have to solve the electromagnetic field equations, taking into account the finite conductivity σ_2 and the constants μ_2 and ϵ_2 , characteristic of the conductor material. This would lead to nonvanishing tangential components of \mathbf{E} on conductor surfaces, which may be thought of as arising from an ohmic relation between the currents induced in the conductor by

the magnetic field and the finite resistivity of the conductor. For any ordinary metallic conductor, and for frequencies up to those approaching the optical region, this tangential field is very much smaller than the normal component of electric field; hence, the following approximate method of obtaining the attenuation is good. The relation between the complex magnetic field H'_z and the complex tangential electric field E'_z , at the surface of the conductor, is found to be the so-called "surface impedance";

$$\left. \begin{aligned} Z_s &= \frac{E'_z}{H'_z} = \sqrt{\frac{\pi\nu\mu_2}{\sigma_2}} (1 + j) \\ Z_s &= R_s + jX_s \end{aligned} \right\} \quad (132)$$

The factor $(1 + j)$ indicates that the fields E'_z and H'_z are 45° out of phase in time. As a matter of fact, this impedance is merely the intrinsic impedance, the ratio of E' to H' , for plane-wave propagation in a metal. The power flowing into a unit area of each conductor to supply the conductor loss is given by the time average of the y component of the Poynting vector. Taking H'_z as a reference, E'_z has a component

$$E_{z1} = R_s H_z = \sqrt{\frac{\pi\nu\mu_2}{\sigma_1}} H_z,$$

in phase with H'_z , and an equal component out of phase. The time average of the Poynting vector is the same as the time average of the product of these in-phase fields; thus,

$$P_2 = \frac{1}{2} \sqrt{\frac{\pi\nu\mu_2}{\sigma_2}} H_z^2. \quad (133)$$

This relation gives the power dissipated per unit area of each conductor in terms of the amplitude of the magnetic field H_x . It is assumed that H_z is, to a good approximation, the same as that given by the simple theory in which the conductors are assumed to be perfectly conducting. As previously noted, this assumption is good for ordinary metals at radio frequencies. The total loss in both conductors per unit length of a strip of waveguide of width a is

$$P_l = 2aP_2 = a \sqrt{\frac{\pi\nu\mu_2}{\sigma_2}} H_z^2. \quad (134)$$

The power transmitted is, using Eqs. (115) and (120),

$$P = \frac{1}{2} ab E_y H_x = \frac{1}{2} ab \sqrt{\frac{\mu_1}{\epsilon_1}} H_z^2. \quad (135)$$

Substitution of these expressions in Eq. (126) gives the conductor loss factor

$$\begin{aligned}\alpha_c &= \frac{a \sqrt{\frac{\pi \nu \mu_2}{\sigma_2}} H_x^2}{ab \sqrt{\frac{\mu_1}{\epsilon_1}} H_x^2} \\ &= \frac{1}{b} \sqrt{\frac{\pi \nu \mu_2 \epsilon_1}{\sigma_2 \mu_1}}.\end{aligned}\quad (136)$$

It might seem odd that the strip width a does not appear in this expression. This is easily understood, however, when it is recalled that both power transmitted and power lost are directly proportional to a ; hence the attenuation, their ratio, is independent of a . As an interesting application of this result, let us see what thickness of conducting plane, carrying the same total current uniformly distributed, would give the same loss. Since the current per unit width is equal to H_x , the loss per unit area in a sheet of thickness d , which has a conductivity σ_2 , is

$$P_2 = \frac{1}{2} I^2 R = \frac{1}{2} H_x^2 \frac{1}{\sigma_2 d}.\quad (137)$$

Equating Eqs. (133) and (137) gives

$$\frac{1}{2} \sqrt{\frac{\pi \nu \mu_2}{\sigma_2}} H_x^2 = \frac{H_x^2}{2 \sigma_2 d},$$

so that

$$d = \frac{1}{\sqrt{\pi \nu \mu_2 \sigma_2}}.\quad (138)$$

It will be noticed that this expression for d is precisely that given by Eq. (78) as the "skin depth" or "depth of penetration," denoted by δ . The magnetic field H_x , electric field E_z , and associated current density J_z all decrease in amplitude as one passes from the surface $y = b$ into the metal of the top plate. Each of the three expressions contains the factor $e^{-(y-b)/\delta}$, so δ may be interpreted as the distance into the metal required for fields and current density to decrease to $1/e$ of their values on the surface of the metal.

In this waveguide with losses, the phase constant β , the characteristic impedance Z_0 , and the wave impedance Z_w are all practically the same as those for the lossless waveguide already discussed. Small correction terms such as those developed in the latter part of Sec. 2.4 would apply here as well. The attenuation factor for this simple parallel-plate waveguide is, for a strip of width a ,

$$\alpha = \alpha_c + \alpha_d,$$

where

$$\left. \begin{aligned} \alpha_e &= \frac{1}{b} \sqrt{\frac{\pi \nu \mu_2 \epsilon_1}{\sigma_2 \mu_1}} \\ \alpha_d &= \frac{\sigma_1}{2} \sqrt{\frac{\mu_1}{\epsilon_1}} \end{aligned} \right\} \quad (139)$$

2.9. Rectangular Waveguide, TE_{10} -mode.—Although the simple parallel-plate waveguide just discussed is easy to analyze, it is not a practical type of waveguide. By a fairly simple extension of the plane-wave approach, the TE_{10} -mode in a rectangular waveguide may be visualized. Let us take the parallel-plane waveguide of Fig. 2-16 and

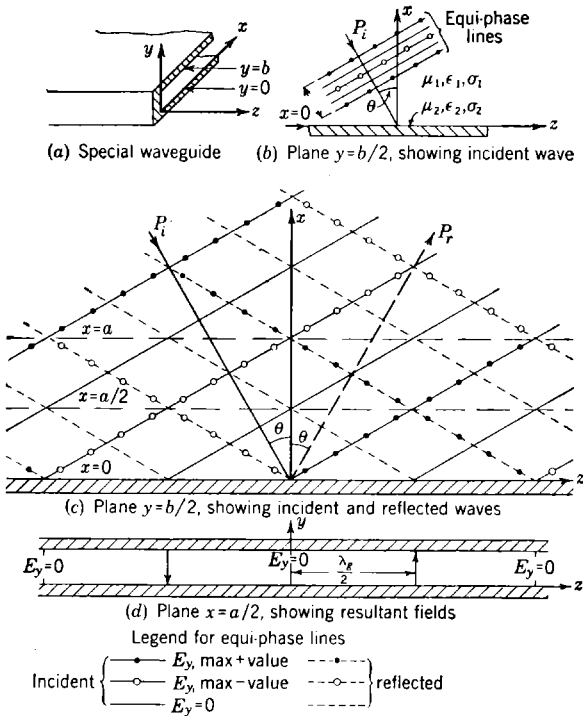


FIG. 2-17.—Development of TE_{10} -mode.

add a conducting wall in the $(x = 0)$ -plane as shown in Fig. 2-17. Let a plane wave of the type discussed in Sec. 2-8 approach the plane $x = 0$ as shown in Fig. 2-17. The intrinsic wavelength in the medium, as given in Eq. (123), is indicated. The direction of propagation P_i makes an angle θ with the x -axis, the normal to the $(x = 0)$ -plane. When this incident wave strikes the $(x = 0)$ -plane, it will be reflected in the direc-

tion P_r in such a way as to satisfy the boundary condition $E_y = 0$ on the conducting ($x = 0$)-plane. The resulting interference pattern is indicated in Fig. 2-17. It will be noted that each positive equiphase line of the incident wave intersects a negative equiphase line (its own reflection) at the conducting plane $x = 0$. Similarly, the amplitude of the field E_y at each point along the conducting plane $x = 0$ may be shown to be zero, as required. A similar situation exists on the ($x = a$)-plane, where each positive equiphase line intersects a negative equiphase line of the reflected wave (not its own reflection, but that of the positive equiphase line which preceded it by one wavelength). Similarly, at each point of the ($x = a$)-plane the field E_y is zero. If we should place a conducting sheet in the ($x = a$)-plane, there would be no tangential electric field there, and therefore it would not disturb the electric field pattern. We could then consider the reflected wave P_r as being incident on this conductor and as being reflected from it as the wave P_r' of Fig. 2-18. This

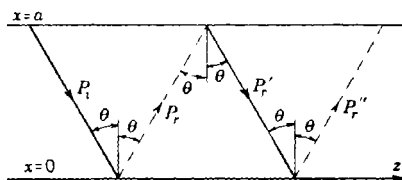


FIG. 2-18.—Successive reflections.

wave is in turn reflected in the ($x = 0$)-plane as P_r'' , and so on down the waveguide in the z direction. The resulting waveguide is shown in Fig. 2-19.

We are now ready for some more quantitative discussions of the propagation characteristics. Figure 2-20 represents a section of the waveguide just developed, with a minimum number of phase lines drawn in and some pertinent dimensions indicated. Some simple trigonometric relations enable us to write

$$\cos \theta = \frac{\lambda_1/2}{a} = \frac{\lambda_1}{2a} \quad (140)$$

$$\cot \theta = \frac{\lambda_g/4}{a/2} = \frac{\lambda_g}{2a} \quad (141)$$

Division of Eq. (141) by Eq. (140) gives

$$\frac{\lambda_g}{\lambda_1} = \frac{\cot \theta}{\cos \theta} = \frac{1}{\sin \theta} \quad (142)$$

Using Eq. (140), $\sin \theta$ may be expressed

$$\sin \theta = \sqrt{1 - \cos^2 \theta} = \sqrt{1 - \left(\frac{\lambda_1}{2a}\right)^2} \quad (143)$$

substituting in Eq. (142), we obtain the desired relation

$$\lambda_g = \frac{\lambda_1}{\sqrt{1 - \left(\frac{\lambda_1}{2a}\right)^2}} \quad (144)$$

Since the cosine function never exceeds unity, Eq. (140) cannot be satisfied if λ_1 is greater than $2a$; but it can be satisfied for any λ_1 smaller

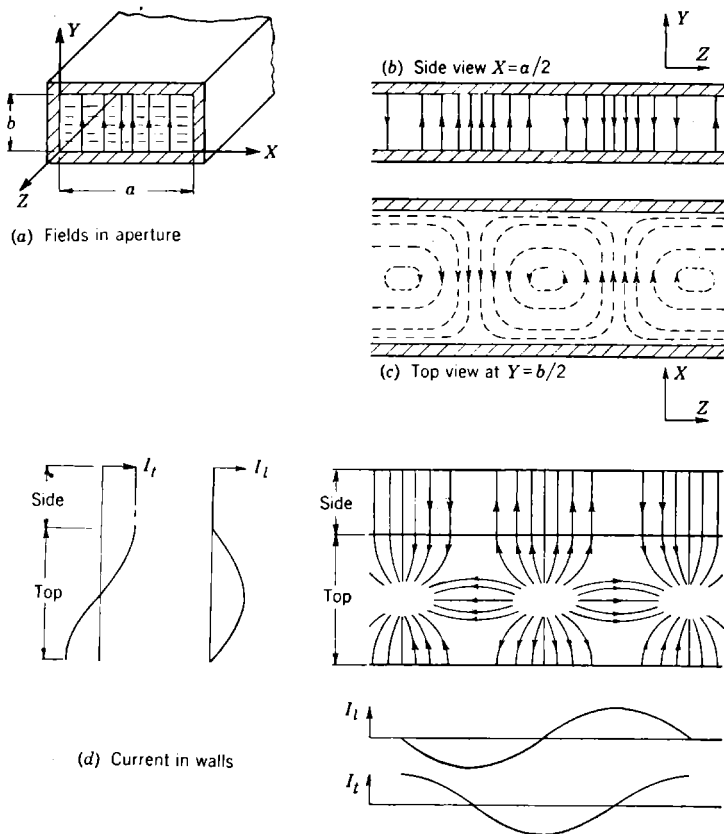


FIG. 2-19.—Fields and currents in rectangular waveguide, TE_{10} -mode.

than $2a$. Similarly, the guide wavelength must equal or exceed λ_1 , the intrinsic wavelength in the medium, in order to satisfy Eq. (142). Both of these conclusions are indicated also by Eq. (144), since if λ_1 exceeds $2a$, λ_g become imaginary; and if λ_1 is less than $2a$, λ_g equals or exceeds λ_1 . The "critical" or "cutoff" wavelength is the free-space wavelength λ_0

associated with $\lambda_1 = 2a$. Using Eq. (123), $\lambda_1 = \lambda_0/\sqrt{k_{e_1}k_{m_1}}$, we may write

$$\lambda_c = 2a \sqrt{k_{e_1}k_{m_1}}. \quad (145)$$

This is the longest wavelength that will propagate down this waveguide in this mode. The corresponding frequency,

$$\nu_c = \frac{c}{\lambda_c} = \frac{c}{2a \sqrt{k_{e_1}k_{m_1}}}, \quad (146)$$

is the cutoff frequency which is approached as the angle θ approaches zero; that is, the wave bounces back and forth across the guide, making

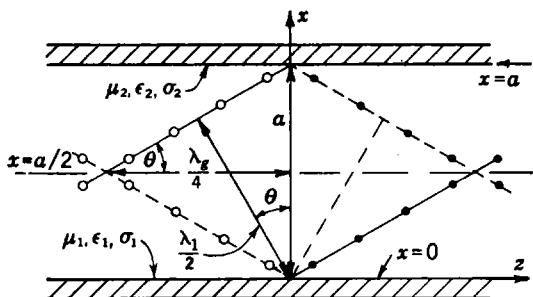


FIG. 2-20.—Relations in TE_{10} -mode.

little progress along it. In the limit, at cutoff, the wave bounces back and forth across the guide at perpendicular incidence to the walls.

Applying Eq. (145), we may write Eq. (144) as

$$\lambda_g = \frac{\lambda_0/\sqrt{k_{e_1}k_{m_1}}}{\sqrt{1 - \left(\frac{\lambda_0}{\lambda_c}\right)^2}}. \quad (147)$$

Although this result was derived for a special waveguide and mode, it is characteristic of all types of waveguide and of all modes. For each case, there is a cutoff wavelength λ_c which is the longest free-space wavelength that may be propagated. The expression for this cutoff wavelength, in terms of the dimensions and materials of the waveguide being considered, may be obtained for any desired mode by setting up and solving the appropriate field equations. The value thus obtained may then be used in Eq. (147) to obtain the guide wavelength.

We now turn our attention to the constants α , β , and Z_0 . The phase constant is

$$\beta = \frac{2\pi}{\lambda_g} = \frac{2\pi}{\lambda_0} \sqrt{1 - \left(\frac{\lambda_0}{\lambda_c}\right)^2} \sqrt{k_{e_1}k_{m_1}}. \quad (148)$$

The phase velocity, $v_p = \omega/\beta$, is

$$v_p = \frac{\nu\lambda_0}{\sqrt{k_{e_1}k_{m_1}}\sqrt{1 - \left(\frac{\lambda_0}{\lambda_c}\right)^2}} = \frac{c}{\sqrt{k_{e_1}k_{m_1}}\sqrt{1 - \left(\frac{\lambda_0}{\lambda_c}\right)^2}}. \quad (149)$$

Since the phase velocity depends on the frequency, the guide is dispersive, and the signal and group velocities are not equal to v_p . The attenuation constant α may be calculated in the same way as that of the parallel-plate waveguide of Sec. 2-7, but to do so the magnetic fields should be known. In the simple plane-wave treatment of the TE_{10} -wave the magnetic fields have not been considered, and it does not seem profitable to do so since a complicated analysis would be necessary. Both magnetic and electric fields are indicated in Fig. 2-15; expressions for them may be found elsewhere.¹ When the calculations are made, the resulting dielectric attenuation factor is

$$\begin{aligned} \alpha_d &= \frac{\sigma_1}{2} \sqrt{\frac{\mu_1}{\epsilon_1}} \frac{1}{\sqrt{1 - \left(\frac{\lambda_1}{2a}\right)^2}} \\ &= \alpha'_d \frac{\lambda_g}{\lambda_1}, \end{aligned} \quad (150)$$

where the prime denotes the corresponding attenuation factor of the parallel-plate waveguide, Eq. (139). Similarly, the conductor attenuation is

$$\begin{aligned} \alpha_c &= \frac{1}{b} \sqrt{\frac{\pi\nu\mu_2\epsilon_1}{\sigma_2\mu_1}} \frac{1 + \frac{2b}{a} \left(\frac{\lambda_1}{2a}\right)^2}{\sqrt{1 - \left(\frac{\lambda_1}{2a}\right)^2}} \\ &= \alpha'_c \frac{\lambda_g}{\lambda_1} \left[1 + \frac{2b}{a} \left(\frac{\lambda_1}{2a}\right)^2 \right]. \end{aligned} \quad (151)$$

The last term in the bracket is associated with the losses in the side walls at $x = 0$ and at $x = a$, and the first one is associated with losses on the walls at $y = 0$ and $y = b$. Both attenuation factors contain the factor λ_g/λ_1 , which becomes infinite at the cutoff wavelength; this seems reasonable because near cutoff the wave bounces back and forth across the guide, suffering attenuation with each crossing but making little progress down the guide. When operating far from cutoff, on the other hand, λ_g/λ_1 approaches unity and $\lambda_1/2a$ approaches zero, so that both attenuations approach the values for the simple parallel-plate waveguide; this also seems quite reasonable, since by our reflected-wave concept the

¹ See *Waveguide Handbook*, Vol. 10, Radiation Laboratory Series.

wave is now essentially a plane wave traveling parallel to the walls of the guide.

Since α and β have been discussed, the consideration of characteristic impedance may now be studied. For the parallel-plate waveguide there was no difficulty in defining the potential difference V between the two plates. In the present instance, however, there is only one conductor; hence, this definition of V becomes meaningless. Similarly in the previous discussion, the current I flowing in unit width of each plate of the waveguide was calculated. Now, there are no separate conductors carrying current; moreover, some currents flow transverse to the direction of propagation, as indicated in Fig. 2-19. These transverse currents, however, are not associated with the magnetic field component H_x which enters into the Poynting-vector expression for power propagated in the z direction. The top and bottom walls of the waveguide of Fig. 2-19 may be considered as forming a sort of parallel-strip transmission line and carrying currents in opposite directions. Let us calculate the total longitudinal current in the lower strip, in the ($y = 0$)-plane, and its negative in the top strip. This gives for the total longitudinal current,

$$I_t = \frac{2}{\pi} a H_x. \quad (152)$$

Here H_x , the amplitude of the magnetic field, is equal to the current per unit width at the center, and the factor $2/\pi$ arises from averaging the sinusoidally varying magnetic field across the width a . The definition of a reasonable voltage between top and bottom walls is a still more difficult matter. The voltage is zero at the side walls, at $x = 0$ and at $x = a$, and has the amplitude bE_y at the center. Some sort of averaging appears to be in order. Let us choose, if possible, an averaging factor so that an effective voltage V_e results which is defined by the equation

$$P = \frac{1}{2} V_e I_t. \quad (153)$$

When the Poynting vector is integrated over the cross section and averaged in time, the power is found to be

$$P = \frac{ab}{4} E_y H_x. \quad (154)$$

Equating Eqs. (153) and (154), and using Eq. (152), we obtain

$$\begin{aligned} V_e &= \frac{abE_y H_x}{2I_t}, \\ &= \frac{\pi}{4} bE_y. \end{aligned} \quad (155)$$

The effective voltage so defined is lower than the integrated voltage across the center of the waveguide by the factor $\pi/4$. However, this factor is somewhat higher than the factor $2/\pi$ which would be obtained

by a simple averaging across the a dimension. This seems reasonable, since the longitudinal current associated with the voltage is strongest at the center; and, consequently, the higher voltages at the center should be given greater weight in the averaging process than the lower voltages nearer the side walls.

In the procedure outlined above the transverse currents were ignored and the total longitudinal current flowing in the top and bottom walls was calculated. Then an effective voltage was defined as that voltage which, when used in conjunction with the longitudinal current just calculated, would give the power being transmitted. There can be no doubt that the current and voltage so defined are appropriate for the purpose of calculating power transmission. They are not the only definitions which could be used, of course. One might begin by choosing the maximum voltage bE_y to be the voltage V , though this does not seem particularly logical. An effective current could then be defined in such a way that it could be used to calculate transmitted power. Although this combination of V and I would give the proper value for power, it does not seem nearly so logical as the method which was originally used. In fact, the original method seems so plausible that one is tempted to use the current and voltage so defined to calculate an effective characteristic impedance;

$$Z_c = \frac{V_e}{I_l} = \frac{\pi^2 b}{8 a} \frac{E_y}{H_x} \quad (156)$$

In attempting to define any such equivalent characteristic impedance one enters into a very controversial subject. There can be no denying that this is the proper definition on the basis of power transmission and total longitudinal current, for that is the basis on which it was derived. Thus it is certainly true that

$$P = \frac{1}{2} I_l^2 Z_c \quad (157)$$

It is when one begins to extend an impedance defined on a certain basis to other uses that trouble and controversy arise. A number of different definitions, each useful for certain purposes, have been proposed. Three of these, based on the maximum voltage V , total longitudinal current I , and power P , are given by Schelkunoff;¹

$$\left. \begin{aligned} Z_{V,I} &= \frac{V}{I} = \frac{\pi}{2} \frac{bE_y}{aH_x} \\ Z_{V,P} &= \frac{V^2}{2P} = 2 \frac{bE_y}{aH_x} \\ Z_{P,I} &= \frac{2P}{I^2} = \frac{\pi^2}{8} \frac{bE_y}{aH_x} \end{aligned} \right\} \quad (158)$$

¹ S. A. Schelkunoff, *Electromagnetic Waves*, Van Nostrand, New York, 1943, Chap. 8, p. 319.

The last of these is the one which we obtained above. It will be noted that all these impedances involve the dimensions of the waveguide in the same way and differ only by numerical constants. They are all proportional to the wave impedance $Z_w = E_y/H_x$, which may be shown to be

$$Z_w = \frac{E_y}{H_x} = \sqrt{\frac{\mu_1}{\epsilon_1}} \frac{1}{\sqrt{1 - \left(\frac{\lambda_1}{2a}\right)^2}} \quad (159)$$

Slater¹ proposes the evaluation of the numerical factor of Eq. (158) by requiring that, as a approaches infinity, the expression be asymptotic to that for a parallel-plane waveguide, Eq. (119).

In any case, there is little need for an actual numerical value in ohms which may be quoted as the characteristic impedance of a waveguide. In most cases what is really important is the impedance, on whatever basis one wishes to conceive it, at a given position z along a waveguide relative to the characteristic impedance, on the same basis, of the waveguide. This relative impedance will be independent of whether one (a) thinks of impedance as maximum voltage over total longitudinal current and uses $Z_{v,I}$, or (b) thinks of impedance as our effective voltage V_e divided by the total longitudinal current and uses Z_e .

Perhaps the most satisfactory procedure of all, from the point of view of valid concepts, is to consider impedance as the ratio of transverse E to transverse H and use the wave impedance Z_w . This concept gives exactly the same relative impedance as those involving currents and voltages, since the maximum voltage and total longitudinal current are directly proportional to the maximum transverse electric and magnetic fields, respectively.

It is only when one wishes to predict what will happen, when two different waveguides are joined, that the way in which the dimensions enter into an expression for characteristic impedance must be considered. Even in this case, the numerical constant involved need not be specified, since it will cancel out when the expression for the impedance of one waveguide relative to the other is written. Thus, let us join two waveguides whose dimensions are, respectively, a_1, b_1 , and a_2, b_2 . Assume the dielectrics filling them to have constants μ_1, ϵ_1 , and μ_2, ϵ_2 , and intrinsic wavelengths λ_1 and λ_2 . By any of the relations given above, the impedance ratio will be

$$\frac{Z_1}{Z_2} = \frac{b_1 a_2}{b_2 a_1} \sqrt{\frac{\mu_1 \epsilon_2}{\mu_2 \epsilon_1}} \frac{\sqrt{1 - \left(\frac{\lambda_2}{2a_2}\right)^2}}{\sqrt{1 - \left(\frac{\lambda_1}{2a_1}\right)^2}} \quad (160)$$

¹ J. C. Slater, *Microwave Transmission*, 1st ed., McGraw-Hill, New York, 1942, Chap. 4, p. 185.

The assumption that the reflection from the junction will behave in the manner implied by Eq. (160) is unjustified. All the equivalent characteristic impedances are defined on the basis of a single uniform waveguide, and there is no reason to expect them to be particularly significant in predicting what will happen when two different waveguides are joined. In order to solve this problem theoretically, one must treat it as a boundary-value problem in electromagnetic theory. After laborious calculation, one finds¹ that, for small changes in dimensions, Eq. (160) does indeed represent the situation rather accurately. For small changes in a and b , the reflections introduced are those which would be expected to result from the joining of two ideal transmission lines whose relative impedance is given by this equation. For large changes in dimensions, the real part of the impedance mismatch at the junction is still given by Eq. (160); but, in addition, a shunt susceptance appears in the equivalent circuit. This introduction of a shunt susceptance at a step discontinuity in a transmission line is characteristic of the behavior of sudden discontinuities.

2-10. Characteristics of Some Common Waveguides.—The three types of waveguide most commonly used in microwave transmission are: (1) coaxial lines, (2) round tubing, and (3) rectangular tubing. The electric and magnetic field distributions in the “lowest mode” that may be propagated in each type are indicated in Columns 1, 2, and 4 of Fig. 2-21. By “lowest mode” is meant the field pattern characterized by the lowest cutoff frequency (or longest cutoff wavelength). A coaxial line may propagate any frequency, including, of course, zero frequency, but the other two types of waveguide have a definite lower limit of frequency (or upper limit of wavelength), as indicated in Columns 2 and 4.

Round waveguide is seldom used as a transmission line because of difficulties arising from the fact that there is no unique direction of polarization of the fields. That is to say, the field pattern of Column 2 of Fig. 2-21 may be rotated through any angle about the axis of the tube. Imperfections in the tubing and bends required in installing it tend to introduce other components of polarization which then get out of phase, resulting in elliptical polarization of the waves.

As a matter of fact, the second or TM_{01} -mode, Column 3 of Fig. 2-21, in round waveguide is more frequently used than the lowest mode. The fields in the TM_{01} -mode possess symmetry about the axis of the tube; this mode is suitable for rotary joints (see Secs. 6-20 and 7-4), and is frequently used in this way.

In Fig. 2-22 the next higher modes are presented. The cutoff wavelength given for the coaxial-line mode is only approximate, but it is a very good approximation for lines whose diameter ratio b/a is low. For a

¹ See *Waveguide Handbook*, Vol. 10, Radiation Laboratory Series.

	Coaxial	Round		Rectangular
	TEM	TE ₁₁	TM ₀₁	TE ₁₀
<p>Cross-section</p> <p> — E - - - H • Out of paper ○ Into paper </p>				
<p>Longitudinal section at A-A</p>				
<p>Field components present</p>	E_r, H_ϕ	$H_z, H_r, H_\phi, E_r, E_\phi$	E_z, E_r, H_ϕ	H_z, H_x, E_y
<p>λ_c</p>	None	$3.41a$	$2.61a$	$2a$
<p>Attenuation in air-filled copper waveguide</p>	$\lambda^{-\frac{1}{2}}(2.27 \times 10^{-5}) \frac{1 + \frac{b}{a}}{b \log_{10} \frac{b}{a}}$	$\lambda^{-\frac{3}{2}}(35.5 \times 10^{-5}) \left(\frac{\lambda}{\lambda_c}\right) \frac{0.420 + \left(\frac{\lambda}{\lambda_c}\right)^2}{\sqrt{1 - \left(\frac{\lambda}{\lambda_c}\right)^2}}$	$\lambda^{-\frac{3}{2}}(27.2 \times 10^{-5}) \left(\frac{\lambda}{\lambda_c}\right) \frac{1}{\sqrt{1 - \left(\frac{\lambda}{\lambda_c}\right)^2}}$	$\lambda^{-\frac{3}{2}}(41.64 \times 10^{-5}) \left(\frac{\lambda}{\lambda_c}\right) \frac{\frac{a}{\lambda} + \left(\frac{\lambda}{\lambda_c}\right)^2}{\sqrt{1 - \left(\frac{\lambda}{\lambda_c}\right)^2}}$
<p>$\frac{P}{\Sigma_{\max}^2}$</p>	$1.92 \times 10^{-2} a^2 \log_{10} \left(\frac{b}{a}\right)$	$19.9 \times 10^{-4} a^2 \sqrt{1 - \left(\frac{\lambda}{\lambda_c}\right)^2}$	$11.3 \times 10^{-4} a^2 \left(\frac{\lambda_c}{\lambda}\right)^2 \sqrt{1 - \left(\frac{\lambda}{\lambda_c}\right)^2}$ if $\left(\frac{a}{\lambda}\right) < 0.761$	$6.63 \times 10^{-4} ab \sqrt{1 - \left(\frac{\lambda}{\lambda_c}\right)^2}$

FIG. 2-21.—Modes commonly used in waveguide.

	Coaxial	Round		Rectangular
	TE ₁₀	TE ₀₁	TE ₂₁	TE ₂₀
Cross-section — E - - - H • Out of paper ◦ Into paper				
Longitudinal section at A-A				
Field components present	$H_z, H_r, H_\phi, E_r, E_\phi$	H_z, H_r, E_ϕ	$H_z, H_r, H_\phi, E_r, E_\phi$	H_z, H_x, E_y
λ_c	$\approx \pi(a+b)$	$1.64a$	$2.06a$	a

FIG. 2-22.—Higher modes in waveguide.

diameter ratio of 2.3 (50-ohm air-filled line) the approximation gives a result which is 3.2 per cent above the correct cutoff wavelength.

The TE_{20} -mode given for rectangular waveguide is the second mode if $b < a/2$, but if $b > a/2$ the second mode is the TE_{01} -mode. The TE_{01} -mode may be considered to be the TE_{10} -mode polarized at 90° to that shown in Fig. 2-21, and the cutoff wavelength is merely $2b$. Rectangular waveguides are commonly chosen with the dimensions $a = 2b$; consequently both TE_{20} - and TE_{01} -modes have half the cutoff wavelength of the TE_{10} -mode. This choice permits propagation of the TE_{10} -mode alone between $\lambda = 2a$ and $\lambda = a$. This twofold factor is to be compared with the factor 1.31 within which the TE_{11} -mode in round waveguide has exclusive rights and with the infinite factor (though limited wavelength range) for which the TEM -mode in coaxial line holds exclusive rights.

The first two diagrams¹ of Fig. 2-23 illustrate waveguides that are essentially compact versions of the basic TE_{10} -mode of rectangular

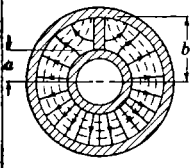
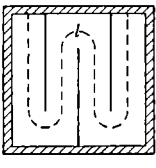
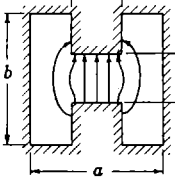
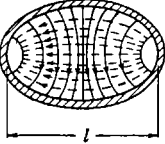
Septate coaxial	Baffle type	H-shaped	Elliptical
			
$\lambda_c \approx 2\pi(a+b)$ See ref. 1 in text	$\lambda_c \approx 2l$ See ref. 1 in text	$\lambda_c \approx \pi \sqrt{(a-a')a'(\frac{b}{b'})}$ See ref. 2 in text	$\lambda_c \approx 1.68l$ See ref. 3 in text

FIG. 2-23.—Miscellaneous types of waveguides.

waveguide. The third² may be thought of as a TE_{10} -mode in rectangular waveguide with capacity loading introduced by the ridge. The approximate cutoff wavelength given in the figure is taken from Ramo and Whinnery.

The mode shown in the elliptical pipe is the lowest mode, termed by Chu³ the ${}_oH_1$ wave. It corresponds to the TE_{11} -mode in round waveguide and to the TE_{10} -mode in rectangular waveguide. The next higher mode in elliptical pipe will, in general, be the ${}_oH_1$ wave, which is like the mode

¹ W. L. Barrow and H. Schaevitz, "Hollow Pipes of Relatively Small Dimensions," *Trans. A.I.E.E.*, **60**, (Mar. 22, 1943).

² S. B. Cohn, "Properties of Ridge Waveguide," RRL Report No. 411-211, Aug. 1945; S. Ramo and J. R. Whinnery, *Fields and Waves in Modern Radio*, Wiley, 1944, p. 364.

³ L. J. Chu, "Electromagnetic Waves in Hollow Elliptic Pipes of Metal," *J. Applied Phys.*, **IX**, No. 9 (Sept. 1938).

shown but polarized at 90° from that shown. It has a higher cutoff frequency (shorter λ_c) and may thus be eliminated in a certain wavelength interval, leaving the mode shown in complete possession. In this respect it partakes of the advantage of the rectangular waveguide, still retaining some of the advantages of round waveguide.

The attenuation formulas of Fig. 2-21 give only the attenuation caused by the finite conductivity of the walls of an air-filled copper waveguide. The attenuation due to the walls will be altered if a wall of different conductivity is used or if a dielectric whose properties differ from that of air is used. If we let the characteristics of copper be denoted by subscript c , and those of an alternative material by subscript 2, the attenuation of an air-filled waveguide of the new material may be found by multiplying the formulas by the factor

$$\frac{\alpha_2}{\alpha_c} = \sqrt{\frac{\sigma_c}{\sigma_2}} \quad (161)$$

If a waveguide be filled with a dielectric whose relative inductive capacity is k_r , the cutoff wavelength is increased by the factor

$$\frac{\lambda_c(1)}{\lambda_c(\text{air})} = \sqrt{k_r} \quad (162)$$

At the same time, the attenuation and guide wavelengths are altered.¹

Two quantities which are frequently of interest but which have been omitted from the figures are: (a) specific wave impedance, and (b) loss in the dielectric. These have been omitted because it is possible to give them in terms which are generally applicable to all waveguides.

The specific wave impedance is defined as the ratio of transverse components of electric and magnetic fields,

$$Z_w = \frac{E_T}{H_T} \quad (163)$$

This ratio is constant over the guide cross section for any waveguide mode. For air-filled waveguides transmitting *TEM*-modes, it is simply the so-called "impedance of free space,"

$$Z_{TEM} = \zeta_0 = \sqrt{\frac{\mu_0}{\epsilon_0}} \approx 377 \quad \text{ohms.} \quad (164)$$

For all modes the wave impedance approaches this value for wavelengths much shorter than the cutoff wavelength of the mode. Usually it differs from this value by a factor depending on the ratio λ_0/λ_c . For all

¹See, for instance, R. I. Sarbacher and W. A. Edson, *Hyper and Ultrahigh Frequency Engineering*, 1st ed., Wiley, New York, 1943, Chapters 6 and 7.

TE- and *TM*-modes the wave impedance for air-filled guides is given respectively by

$$Z_{TE} = \zeta_0 \frac{1}{\sqrt{1 - \left(\frac{\lambda_0}{\lambda_c}\right)^2}} = \zeta_0 \frac{\lambda_g}{\lambda_0}, \quad (165)$$

$$Z_{TM} = \zeta_0 \sqrt{1 - \left(\frac{\lambda_0}{\lambda_c}\right)^2} = \zeta_0 \left(\frac{\lambda_0}{\lambda_g}\right). \quad (166)$$

If the waveguide is filled with a dielectric characterized by μ_1 and ϵ_1 , these relations become

$$Z_{TEM} = \zeta_1 = \sqrt{\frac{\mu_1}{\epsilon_1}} = 377 \sqrt{\frac{k_{m_1}}{k_{\epsilon_1}}} \quad \text{ohms}, \quad (167)$$

$$Z_{TE} = \zeta_1 \frac{1}{\sqrt{1 - \left(\frac{\lambda_0}{\lambda_c}\right)^2}} = \zeta_1 \left(\frac{\lambda_g}{\lambda_1}\right), \quad (168)$$

$$Z_{TM} = \zeta_1 \sqrt{1 - \left(\frac{\lambda_0}{\lambda_c}\right)^2} = \zeta_1 \left(\frac{\lambda_1}{\lambda_g}\right), \quad (169)$$

where ζ_1 is the intrinsic impedance of the medium, λ_1 is the intrinsic wavelength in the medium, and λ_g is the actual guide wavelength in the dielectric-filled waveguide.

The dielectric attenuation constant for *TEM*-modes is independent of the dimensions or form of the waveguide, and it has been shown¹ to be

$$\alpha_{dTEM} = \frac{\sigma_1}{2} \sqrt{\frac{\mu_1}{\epsilon_1}} = \frac{\sigma_1 \zeta_1}{2}. \quad (170)$$

A more useful form is derived from Eq. (98),

$$\alpha_1 = 27.3 \frac{\sqrt{k_{m_1} k_{\epsilon_1}}}{\lambda} \tan \delta \quad \text{db/m}. \quad (171)$$

For both *TE*- and *TM*-modes the dielectric attenuation factors are increased to

$$\alpha_d = \alpha_1 \frac{1}{\sqrt{1 - \left(\frac{\lambda}{\lambda_c}\right)^2}} = \alpha_1 \left(\frac{\lambda_g}{\lambda_1}\right). \quad (172)$$

TRANSMISSION-LINE CHARTS AND IMPEDANCE-MATCHING

The way in which voltage and current vary along a transmission line has been discussed in Secs. 2-1 and 2-2. In later sections it has been

¹ See Eq. (84) for coaxial line, and Eq. (131) for parallel-plate waveguide.

shown that the electric and magnetic fields in waveguides vary in a similar way and may be described in terms of analogous line constants α , β , and Z_0 or Z_w . In Sec. 2-3 the concept of impedance was introduced, the complex impedance at any position along the line being defined as the ratio of the complex voltage at that position to the complex current there. An analogous quantity for waveguides was later seen to be the ratio of complex electric field to complex magnetic field. The concepts of reflection coefficient and standing waves also were introduced in Sec. 2-3, and later these were extended to waveguides. A clear understanding of these concepts and of the way in which the various quantities vary along the line or guide is a valuable aid in the design of microwave transmission circuits and in the understanding of their behavior. The equations developed in Sec. 2-3 enable one to calculate the relations between these quantities and the way they vary along the line. A clearer insight into the meaning of these relationships is afforded, and a valuable aid in the rapid solution of practical problems is gained by the graphical representations of the equations which will be presented in the following sections.

2-11. Reflection-coefficient Chart with Impedance Contours, Smith Chart.—One of the most instructive and convenient charts is that based on a polar plot of the reflection coefficient, Eq. (26) and Fig. 2-4. The

chart might equally well be considered as based on the relative voltage diagram of Fig. 2-5. Let us consider the transmission line of Fig. 2-24, which is assumed for simplicity to have no loss (that is, $\alpha = 0$) but to have a phase constant β and a real characteristic impedance Z_0 . If we terminate this line at the point $z = 0$ in a pure resistance R_1 , which is larger than Z_0 , we calculate the reflection coefficient at $z = 0$ from Eq. (21) as

$$\Gamma_0 = \frac{B}{A} = \frac{R_1 - Z_0}{R_1 + Z_0} \quad (173)$$

This is real, positive, and less than unity, as indicated in Fig. 2-25a. The relative voltage, taking the incident voltage as unity, is $V'_0 = 1 + \Gamma_0$, as indicated in Fig. 2-25b. Equation (173) shows that the reflected voltage is in phase with the incident voltage, which is reasonable, since the load is real and lies between Z_0 and infinity or open-circuit impedance. Similarly, the relative current, considering the incident current as unity, is $I'_0 = 1 - \Gamma_0$, as shown in Fig. 2-25c. At the point $z = -l$, the vector Γ_0 has rotated through an angle $-\beta l$ with the resulting changes to Γ , V' , and I' . It should be recalled from Sec. 2-3 that

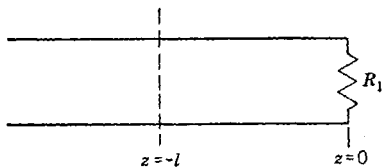


FIG. 2-24.—Terminated transmission line.

$$\left. \begin{aligned} \Gamma &= \Gamma_0 e^{-j2\beta l}, \\ \mathbf{V} &= (1 + \Gamma)\mathbf{V}_{inc} = \mathbf{V}'\mathbf{V}_{inc}, \\ \mathbf{I} &= (1 - \Gamma)\mathbf{I}_{inc} = \mathbf{I}'\mathbf{I}_{inc} = \mathbf{I}'\mathbf{V}_{inc}/Z_0. \end{aligned} \right\} \quad (174)$$

It is clear from Fig. 2-25 that the relative voltage has its maximum value $1 + |\Gamma_0|$ at the load and its minimum value of $1 - |\Gamma_0|$ a quarter wavelength away. The separate quantities of Fig. 2-25 have been combined

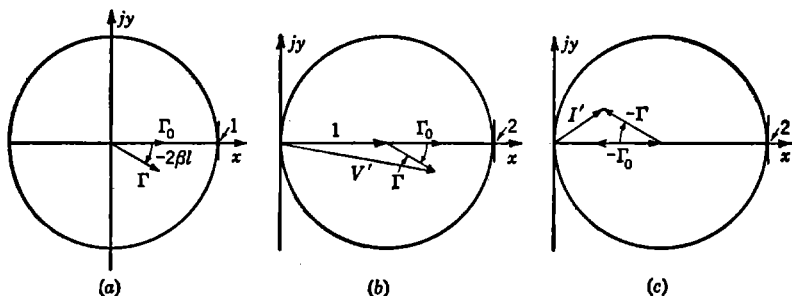


FIG. 2-25.—Vector diagrams of (a) reflection coefficient, (b) relative voltage, and (c) relative current.

into one diagram in Fig. 2-26; the relative voltage has been resolved into components V'_1 in phase with the current and V'_2 out of phase with it. A simple theorem in plane geometry requires that the intersection point Q lie on the circle. The impedance is found from Eq. (174) to be

$$\mathbf{Z} = \frac{\mathbf{V}}{\mathbf{I}} = \frac{\mathbf{V}'\mathbf{V}_{inc}}{\mathbf{I}'\frac{\mathbf{V}_{inc}}{Z_0}} = \frac{\mathbf{V}'}{\mathbf{I}'} Z_0. \quad (175)$$

The impedance relative to Z_0 expressed in terms of the components of \mathbf{V}' , is

$$\frac{\mathbf{Z}}{Z_0} = \frac{\mathbf{V}'}{\mathbf{I}'} = \frac{\mathbf{V}'_1}{\mathbf{I}'} + \frac{\mathbf{V}'_2}{\mathbf{I}'}. \quad (176)$$

In terms of the angle a , the complex vectors are

$$\begin{aligned} \mathbf{I}' &= |\mathbf{I}'|e^{ja}, \\ \mathbf{V}'_1 &= |\mathbf{V}'_1|e^{ja}, \\ \mathbf{V}'_2 &= |\mathbf{V}'_2|e^{j(\pi/2-a)}. \end{aligned}$$

Substitution in Eq. (176) gives

$$\begin{aligned} \frac{\mathbf{Z}}{Z_0} &= \frac{|\mathbf{V}'_1|e^{ja}}{|\mathbf{I}'|e^{ja}} + \frac{|\mathbf{V}'_2|e^{-j(\pi/2-a)}}{|\mathbf{I}'|e^{ja}}, \\ &= \frac{|\mathbf{V}'_1|}{|\mathbf{I}'|} - \frac{j|\mathbf{V}'_2|}{|\mathbf{I}'|}. \end{aligned} \quad (177)$$

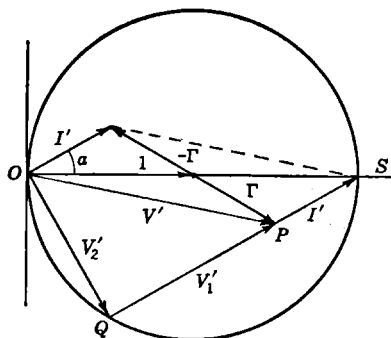


FIG. 2-26.—Basic diagram for reflection-coefficient impedance chart.

This may be written

$$\mathbf{Z}' = R' + jX', \quad (178)$$

where we have defined

$$\left. \begin{aligned} \mathbf{Z}' &= \frac{\mathbf{Z}}{\mathbf{Z}_0}, \\ R' &= \frac{R}{Z_0} = \frac{|\mathbf{V}'_1|}{|\mathbf{I}'|}, \\ X' &= \frac{X}{Z_0} = -\frac{|\mathbf{V}'_2|}{|\mathbf{I}'|}. \end{aligned} \right\} \quad (179)$$

It should be obvious that whenever P lies in the lower half of the diagram the ratio $\mathbf{V}'_2/\mathbf{I}'$ will have a phase angle $-j\pi/2$, resulting in a negative sign for the reactance X' . On the other hand, when it lies in the upper half, X' will be positive.

The position of the point P within the circle of Fig. 2-26 is seen to determine Γ , \mathbf{V}' , \mathbf{I}' , and through them the components R' and X' of the

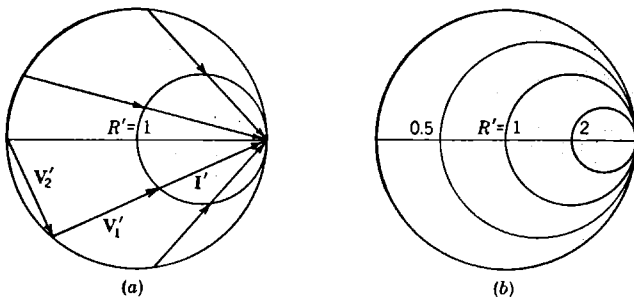


FIG. 2-27.—Circles of constant resistance.

impedance \mathbf{Z}' . In Fig. 2-27a the circle marked $R' = 1$ is the locus traced by the point P moving in such a way that $R' = \frac{|\mathbf{V}'_1|}{|\mathbf{I}'|}$ remains constant and equal to unity. Other circles, each representing a different value of R' , are shown in Fig. 2-27b. The fact that these loci are circles is not obvious at first but may be shown by simple analytic geometry. Similarly, the locus of points P such that $X' = |\mathbf{V}'_2|/|\mathbf{I}'|$ has the value ± 1 is shown in Fig. 2-28a. Other curves of constant reactance are shown in Fig. 2-28b. These curves are arcs of circles whose centers lie on the vertical line through the point S , as may be shown by analytic geometry.

When the two sets of circles of Figs. 2-27 and 2-28 are superposed as in Fig. 2-29, they form a gridwork of orthogonal circles. Using this gridwork as a coordinate system, one may read the related impedance components R' and X' by plotting on this chart the point P corresponding to any given reflection coefficient Γ . This type of chart was developed by

P. H. Smith¹ of the Bell Telephone Laboratories and is frequently referred to as the "Smith chart." To avoid confusing the diagram, the actual lines of the polar coordinates needed for plotting Γ are omitted. Instead, the arm shown is pivoted at the center; and its radial scale together with the phase scale around the circumference of the chart enables one to plot the points. The phase scale is calibrated directly in wavelengths; when l varies through $\lambda/2$, the phase angle $2\beta l = 4\pi l/\lambda$ varies through a complete cycle, 2π radians. On a purely logical basis one would choose the positive direction as the reference or zero-phase direction, since this corresponds to zero-phase angle for the vector Γ of Fig. 2-25. It is common practice, however, to refer phase measurements in transmission lines

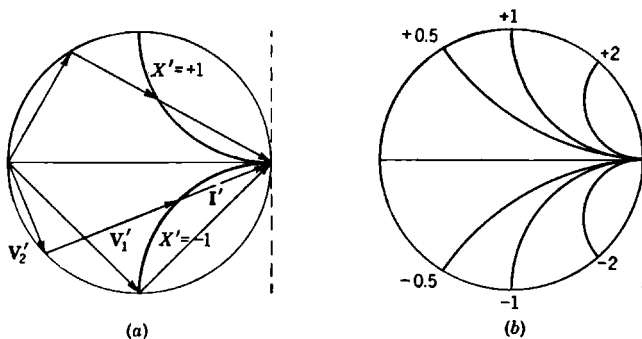


FIG. 2-28.—Circles of constant reactance.

to the voltage minimum since it can be located more precisely than the maximum, particularly in the case of large standing-wave ratios. This practice is followed in the Smith chart, as it is in most transmission-line impedance charts; hence, the zero-phase line is the line from $Z' = 1$ to $Z' = 0$, and refers to the voltage minimum. The radial scale is calibrated in terms of the standing-wave ratio rather than directly in terms of reflection coefficient. The simple connecting relations were given by Eqs. (33) and (34)

$$\left. \begin{aligned} r &= \frac{1 + |\Gamma|}{1 - |\Gamma|} \\ |\Gamma| &= \frac{r - 1}{r + 1} \end{aligned} \right\} \quad (180)$$

A number of ways of expressing standing-wave ratios have been used. Some people use "voltage standing-wave ratio," while others prefer to use the square of this which is sometimes called "power standing-wave ratio." In both cases, there have been those who expressed the ratio as maximum

¹P. H. Smith, "Transmission Line Calculator," *Electronics* (Jan. 1939); "An Improved Transmission Line Calculator," *Electronics* (Jan. 1944).

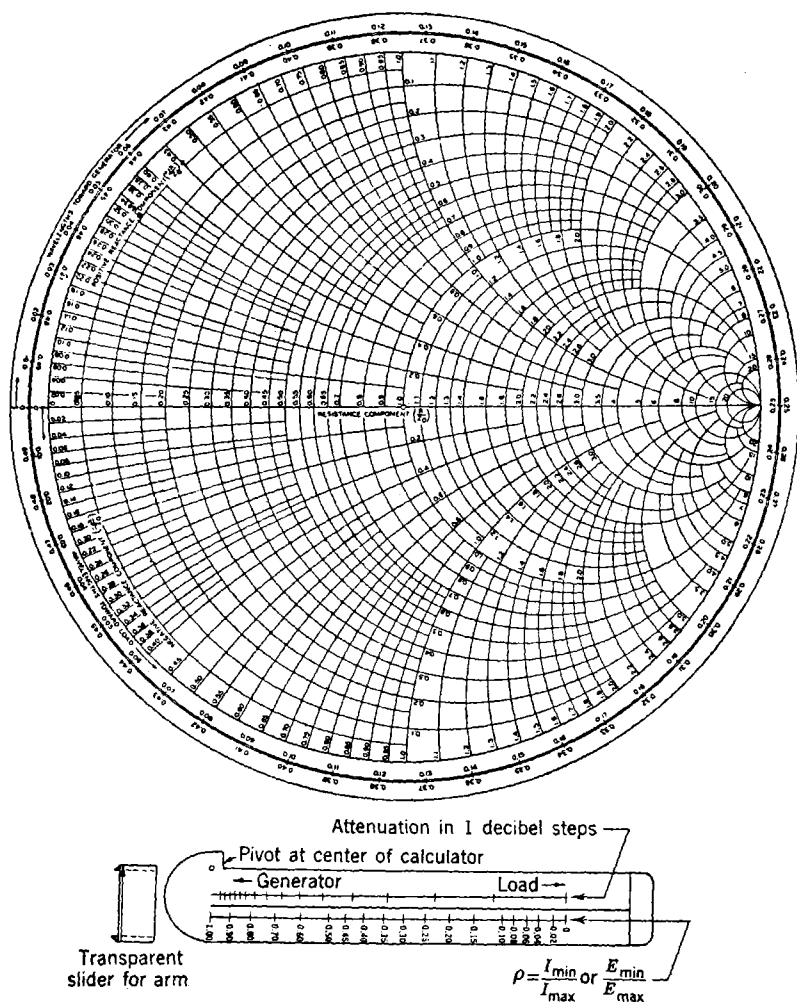


FIG. 2-29.—Circular form of transmission-line calculator. (P. H. Smüh, "Electronics," January 1939.)

over minimum, giving a number in the range unity to infinity; others used the minimum over maximum and obtained numbers in the range unity to zero. There seems to be emerging a general preference in favor of using the voltage standing-wave ratio exceeding unity,

$$r = \frac{V_{\max}}{V_{\min}} \quad (181)$$

which is abbreviated to VSWR. This is, of course, the same in value as

I_{\max}/I_{\min} , the only difference being a shift of a quarter wavelength in position of the maxima and minima. The scale marked on the arm of the Smith chart shown is the reciprocal of this, that is, $1/r$. In the later version of his chart, in the 1944 article, Smith adopts the ratio r . Another definition of standing-wave ratio which is sometimes convenient is in terms of decibels,

$$\text{SWR (db)} = 20 \log_{10} r. \quad (182)$$

If one is accustomed to thinking in terms of the so-called "power standing-wave ratio," Eq. (182) would be written as $10 \log_{10} r^2$, which would give the same db standing-wave ratio.

In any case, the conversion is made from the linear radial scale of reflection coefficient to a scale reading directly in whatever standing-wave ratio one prefers to use. In addition, a number of other useful scales which are related directly to the reflection coefficient may be included on the arm. The scale marked "attenuation in 1-decibel steps" is useful in calculating impedance transformations when the line loss is not negligible. It is used to introduce the factor $e^{-2\alpha l}$, by which the reflection coefficient decreases going a distance l toward the generator clockwise, or $e^{2\alpha l}$, by which it increases going in the reverse direction. The power transmitted by a running wave contains the same factor $e^{-2\alpha l}$, though it decreases toward the load rather than increasing as does the reflection coefficient. Another method of using this type of chart has been found very useful, especially when transforming a number of plotted points simultaneously through a specified distance along the line is desired. A sheet of tracing paper is laid over the chart and the points P are plotted on it rather than on the chart. To transform the points along the line, the tracing paper is pivoted at the center and rotated through the desired number of wavelengths in the proper direction, as indicated on the wavelength scales. The new impedance values may then be read from the chart.

An especially good example of the usefulness of the tracing-paper technique is offered by its application to the discussion of the impedance-tuning characteristics of variable transformers (see Chap. 8). It has been found convenient to mount the chart on a plywood board and to pivot the tracing paper by sticking a glass-headed thumbtack into the center. In plotting experimental data, marks are first made on the tracing paper at 0 and 0.25λ of the phase scale and labeled accordingly. If the load is a real impedance $R_1 > Z_0$, the point P may be plotted at the proper place along the real axis to the right of center, as in Fig. 2-30. The load is, in this case, at a voltage maximum, and the voltage standing-wave ratio is, using Eq. (183),

$$r_1 = \frac{1 + |\Gamma_1|}{1 - |\Gamma_1|} = \frac{1 + \left(\frac{R_1 - Z_0}{R_1 + Z_0} \right)}{1 - \left(\frac{R_1 - Z_0}{R_1 + Z_0} \right)} = \frac{R_1}{Z_0} = R'_1. \quad (183)$$

This fact, that r is equal to the relative impedance R' for real loads $R > Z_0$, is very useful in the tracing-paper method of plotting experimental data. It makes easily available a scale of the same type furnished by the arm of the Smith chart, converting $|\Gamma|$ to r . As a corollary to this observation, it is useful to remember that, at any voltage maximum, the impedance in the line is real and greater than Z_0 by the factor r . If it is desirable to find the impedance a distance l toward the load from such a voltage maximum, one may simply describe an arc in the counter-clockwise direction about the center of the chart, as in Fig. 2-30a. The

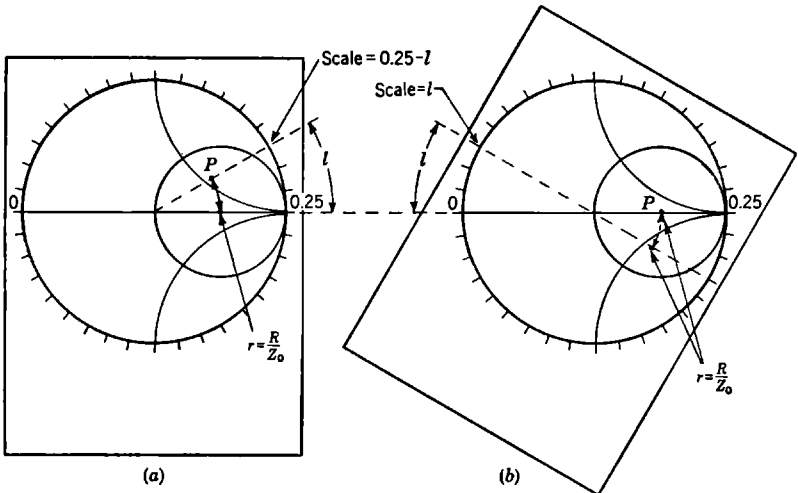


FIG. 2-30.—Tracing-paper method of plotting data over reflection coefficient chart. (a) Compass and straight-edge method. $(R/Z_0) = r$ is impedance at V_{\max} , P is that a distance l toward load. (b) Alternative method, rotating paper. Paper is returned to original position as in *a* after plotting P .

radius of the arc is determined by the value of r , and the angle of the arc is indicated by the outer wavelength scale. An alternative method of plotting the point P which does not require compass or straightedge is indicated in Fig. 2-30b. The outer scale of the Smith chart gives directly the distance l below the index mark labeled 0λ . When the tracing paper is returned to the original position as in Fig. 2-30a, the point P represents the impedance at a distance l toward the load from a voltage maximum. If the distance from the reference point in the load to the closest voltage maximum is l_{\max} , the impedance of the load is plotted by applying the above procedure using the value l_{\max} for the length l . Frequently, the distance l_{\min} to the nearest voltage minimum, rather than the distance l_{\max} , is obtained in taking data. Since these two distances differ by exactly a quarter wavelength or one-half turn on the chart, it is necessary merely

to turn the tracing paper through 180° and use the index labeled 0.25 λ in conjunction with the outer wavelength scale to read l_{\min} .

The method of deriving the impedance components R and X by current and voltage vectors, as in Eq. (179), gives a certain insight into the current and voltage relations existing. However, it is more direct to calculate the components of Z by the use of Eq. (21),

$$\Gamma = \frac{Z - Z_0}{Z + Z_0} \quad (184)$$

Introducing relative impedance and its components, we obtain

$$\Gamma = \frac{Z' - 1}{Z' + 1} = \frac{R' + jX' - 1}{R' + jX' + 1} \quad (185)$$

The real and imaginary components of Γ are then

$$\Gamma = \frac{R' + X'^2 - 1}{(R' + 1)^2 + X'^2} + \frac{j2X'}{(R' + 1)^2 + X'^2} \quad (186)$$

2-12. Other Types of Transmission-line Charts.—The chart based on the reflection coefficient has thus far been correlated with a gridwork of impedance contours. In certain problems other types of contour lines, such as $Y = G + jB$, $Z = |Z|/\theta$, or $Y = |Y|/\phi$, are much more useful. It is sometimes desired to base the chart on a rectangular impedance or admittance plane rather than on the reflection-coefficient circle.

Smith Admittance Chart.—In the previous section the point P was plotted, Fig. 2-26, at the terminus of the relative voltage vector $V' = 1 + \Gamma$, and the related gridwork of R and X circles, Fig. 2-29, was derived, thus enabling us to read the corresponding components of impedance. In a similar way, we now plot the point P' , Fig. 2-31, at the terminus of the relative current vector $I' = 1 - \Gamma$ and derive the related gridwork of admittance circles. We define $Y = 1/Z$, $Y_0 = 1/Z_0$, $Y' = 1/Z'$, and write

$$Y' = \frac{I'}{V'} = \frac{I'}{V'} + \frac{I'_2}{V'_2} \quad (187)$$

corresponding to Eq. (176). By taking steps exactly analogous to those

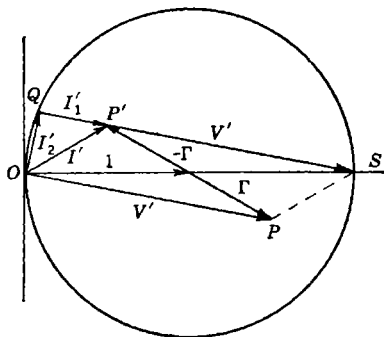


FIG. 2-31.—Basic diagram for reflection-coefficient admittance chart (cf. Fig. 2-26).

leading to Eq. (179), we may define the admittance components by

$$\left. \begin{aligned} \mathbf{Y}' &= G' + jB', \\ G' &= \frac{G}{Y_0} = \frac{|\mathbf{I}'_1|}{|\mathbf{V}'|}, \\ B' &= \frac{B}{Y_0} = \frac{|\mathbf{I}'_2|}{|\mathbf{V}'|}. \end{aligned} \right\} \quad (188)$$

Since P' in this example lies in the upper half of the diagram, B' has the positive sign.

Whether a gridwork applying to the impedance case or to admittance is being derived, the generalized diagram of Fig. 2-32 may be used. The

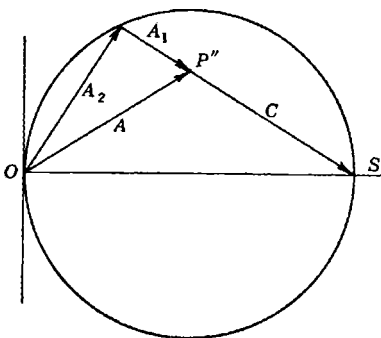


FIG. 2-32.—Generalized diagram for deriving either impedance or admittance chart.

point P'' represents the appropriate point P or P' , and the vectors \mathbf{A}_2 , \mathbf{A}_1 , and \mathbf{C} represent the appropriate current or voltage vectors. The real and imaginary components of the coordinates being derived are these.

$$\text{Real part} = \frac{|\mathbf{A}_1|}{|\mathbf{C}|},$$

$$\text{Imaginary part} = \pm \frac{|\mathbf{A}_2|}{|\mathbf{C}|}. \quad (189)$$

If P'' lies in the upper half of the diagram, the imaginary part is positive; if in the lower half, it is negative. It should therefore be evident that the

admittance components G' and B' corresponding to a given position of P' are the same as the impedance components R' and X' corresponding to the same position of P . That is, the gridwork developed for reading the components of impedance for a point P plotted at position $1 + \Gamma$ may be used also for reading the components of admittance for a point P' plotted at position $1 - \Gamma$.

A useful property of the Smith chart is now evident. Since points P and P' of Fig. 2-31 have as their respective coordinates on the Smith chart the impedance and the admittance corresponding to each, this chart provides an easy method of converting from admittance to impedance and vice versa. This is particularly useful in the tracing-paper method of using the chart, since any plotted impedance point or points may be converted readily to the equivalent admittance plot by a simple rotation of one-half turn of the tracing paper. Obviously the inverse conversion is also accomplished by a half-turn rotation. It may be noticed that the half-turn operation performed on an impedance plot may equally well

be thought of as giving the impedance plot a quarter wavelength down the line. This brings out clearly the well-known inversion of impedance by a quarter-wavelength section of line. That is, it gives a complex impedance equal to the original admittance which is the reciprocal of the original impedance. In more general terms, the chart affords a simple means of finding the reciprocal of any complex number.

A word should be said regarding the plotting of data as an admittance plot. One obvious method is to plot the data on tracing paper as an impedance plot, as outlined in the preceding section, and then to convert this impedance plot to an admittance plot by rotating the tracing paper half a turn. If one prefers, the admittance may be plotted directly, making use of the fact that the normalized admittance at the current maximum (voltage minimum) is real, greater than Y_0 , and numerically equal to r . For admittances (see Fig. 2-30), $G/Y_0 = r$ is the admittance at V_{\min} , P is at a distance l toward the load from V_{\min} . If the data are taken by measuring the distance l from a voltage minimum, the method of Fig. 2-30 plots admittance directly, but if l is measured from a voltage maximum it plots impedance directly. It is perhaps simplest to bear this in mind and make the direct plot by this method using the data for l in whatever form they are taken. The resulting plot may then be converted from impedance to admittance or vice versa by a half-turn rotation.

Charts Expressing Impedance or Admittance in Polar Form.—It is sometimes convenient to express the impedance in terms of its magnitude $|Z|$ and its phase angle θ , rather than in terms of its components R and X ; thus,

$$Z = |Z|e^{i\theta}. \quad (190)$$

The process of deriving this chart is quite similar to the previous derivations, and therefore it will not be carried through in detail. Referring to Fig. 2-31, the magnitude and phase angle of the impedance are

$$\begin{aligned} |Z| &= \frac{|V|}{|I|} = \frac{\overline{OP}}{\overline{PS}} \\ \theta &= \angle P'OP. \end{aligned} \quad (191)$$

The position of the point P is accordingly represented by the coordinates $|Z|$ and θ . The angle θ is positive when P is above the real axis OS , negative when it is below. The resulting gridwork of coordinates is shown in Fig. 2-33.

There is naturally a 1-to-1 correspondence between a given impedance point P on the Smith chart and the point P in the same position in the $|Z|/\theta$ chart. Each is basically a plot of the relative voltage V' . Using this fact, the latter chart may be derived directly from the former simply by converting from given rectangular coordinates (R, X) to the polar

coordinates $(|Z|, \theta)$ which define the same impedance. Another consequence of this fact is that the same method of plotting data is used; the right half of the diameter OS is marked in terms of $R' = r$, just as was the Smith chart.

Just as in the case of the Smith chart, the same gridwork of impedance coordinates may be used for admittance coordinates provided that the

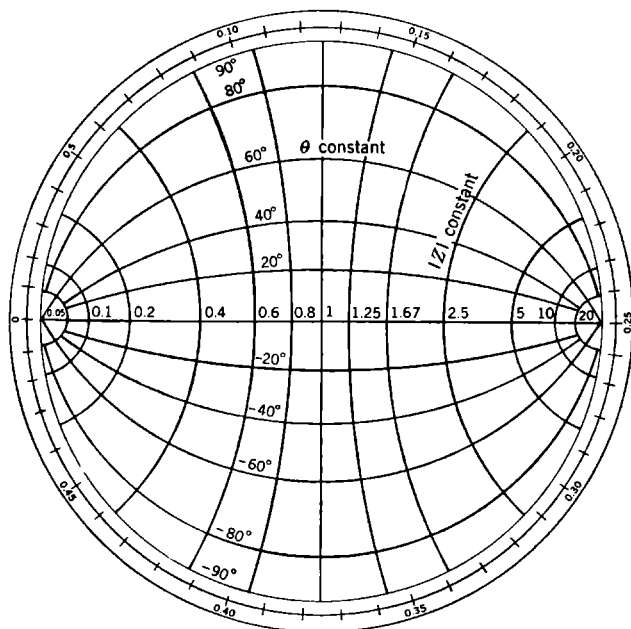


FIG. 2-33.—Reflection coefficient chart with $|Z|$ and θ coordinates.

proper change in the method of plotting the data is observed. The chart is, when used for admittances, a plot of relative current just as the Smith chart was when used as an admittance chart. The data-plotting technique is likewise identical with that for the Smith admittance chart. If we let the admittance be expressed as

$$Y' = |Y'|e^{j\theta} = \frac{1}{Z'}, \quad (192)$$

the magnitude and angle are

$$\left. \begin{aligned} |Y'| &= \frac{1}{|Z'|} = \frac{|I'|}{|V'|} = \frac{PS}{OP'} \\ \phi &= -\theta = \angle POP'. \end{aligned} \right\} \quad (193)$$

Magnified Center Portion of Reflection-coefficient Charts.—When it is desirable to plot data or calculations precisely, the reflection-coefficient chart may be drawn to a large scale. In many cases where such precise work is being done the data or calculations involve only small reflection coefficients; therefore only the central portion of this large-scale chart is needed. One extremely precise version of the central portion of the Smith chart is reproduced¹ in Fig. 2-34. It is limited to $r \leq 2$, which is equiva-

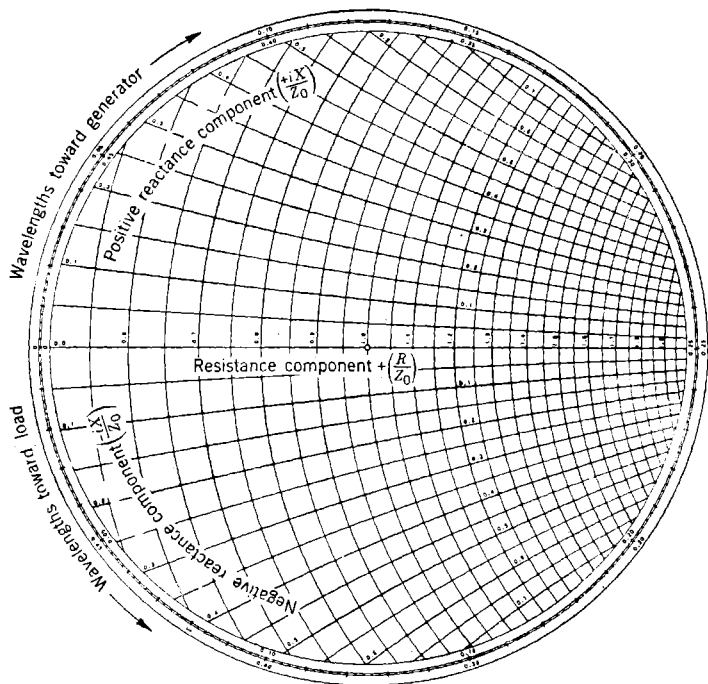


Fig. 2-34.—Enlargement of portion of Smith chart. (This chart prepared by L. F. Woodruff for 2nd. ed. of *Ultra-High-Frequency Techniques*, D. Van Nostrand Co., J. G. Brainerd, editor.)

lent to $|\Gamma| \leq \frac{1}{3}$. This chart has been found very useful in the design of microwave transmission circuits because it gives a scale which is about as large as the data would justify; and plotting any points for which r exceeds 2 is seldom necessary. Further magnification is occasionally useful, especially in aiding calculations.

The $|Z|/\theta$ type chart may be similarly magnified. One version of this chart, drawn to a large scale and including the whole chart, has been printed by the Radio Corporation of America.² It includes also the

¹ Reproduced by courtesy of L. F. Woodruff of the Elec. Eng. Dept., M.I.T.

² P. S. Carter, *R.C.A. Rev.*, III, No. 3 (Jan. 1939).

polar coordinate lines, radii, and circles concentric about the center for plotting Γ . Although these lines have a certain usefulness, they tend to confuse the diagram for the average person.

Rectangular Impedance or Admittance Chart.—In the previous discussions we used the reflection coefficient as the basis for a transmission-line chart because it transforms in a simple manner along the line. The corresponding resistance and reactance coordinates were then derived; they were rather unusual in form. In the present instance we shall begin by choosing rectangular coordinates for the resistance and reactance, and proceed to plot contour lines on this coordinate system to enable us to follow the transformation of impedance along the line. This transformation is given by Eq. (41),

$$Z'_{-l} = \frac{Z'_r + j \tan \beta l}{1 + j Z'_r \tan \beta l} \quad (194)$$

Let us consider again the line of Fig. 2-24. For this line Eq. (194) becomes

$$Z' = \frac{R'_1 + j \tan \beta l}{1 + j R'_1 \tan \beta l} \quad (195)$$

By choosing a particular value for R_1 and allowing βl to vary from 0 to 2π , a circle with its center on the real axis as in Fig. 2-35, will be plotted. Remembering that R'_1 is equal to the VSWR, this circle may be considered characteristic of the value r_1 . If a number of values for R'_1 are chosen, a complete set of such circles for various values of r will be mapped. Similarly, the angle βl may be assigned a value and R_1 varied from unity to infinity. This will map one of the semicircles centered on the imaginary axis, as in Fig. 2-35. This semicircle is characteristic of the value βl , or of the length l measured in wavelengths, and may be so marked. When this is repeated for a number of values of βl , a set of these semicircles will be drawn in. As in the Smith chart, it is the usual practice to consider the reference or zero phase to be the real axis from $Z' = 1$ to $Z' = 0$, which is the position of the voltage minimum.

In this type of chart it is necessary to include both the (R,X) -coordinates and the (r,l) -coordinates. The use of tracing paper has no special advantage, since transformations along the line are not effected by a simple rotation. Data are plotted directly in terms of the measured r and l values, l measured from the voltage minimum. If it is desired, a section of the chart in the neighborhood of $Z' = 1$ may be enlarged just as in the case of the chart based on the reflection coefficient.

In order to use this chart to plot admittances, it is only necessary to consider the reference phase line from $Z' = 1$ to $Z' = 0$ as being the voltage maximum. To convert from Z' to the corresponding Y' one

follows around the standing-wave-ratio circle from the point Z' to a point a quarter wavelength away as denoted by the markings on the phase circles.

The transformation of the Smith chart into the rectangular (R - X)-plot may be seen qualitatively by inspection and quantitatively by use of the mathematical connecting equations. Qualitatively, one sees that the upper-half circumference of the Smith chart has been pivoted at the

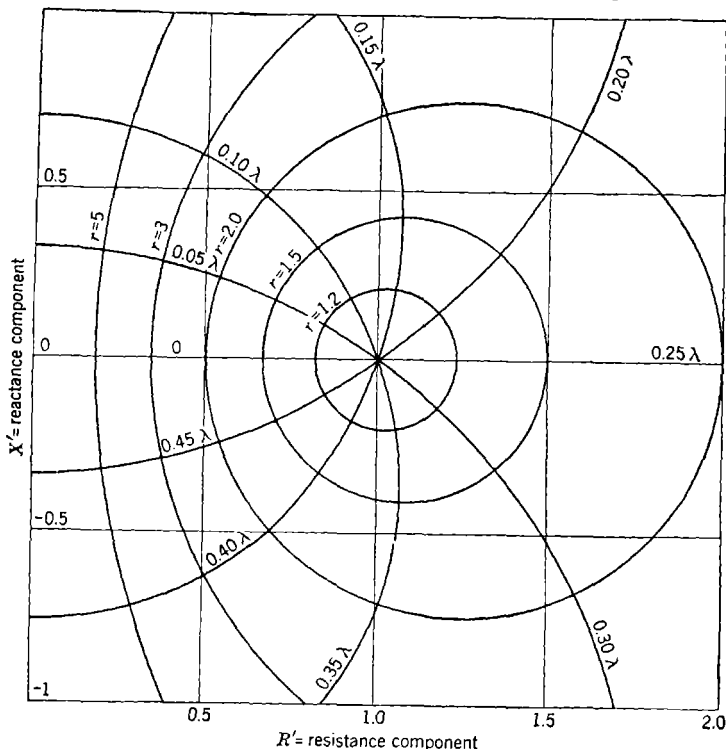


FIG. 2-35.—Rectangular impedance chart.

($R = X = 0$)-point and bent upward and left and stretched out to form the positive imaginary axis of the (R - X)-plot. In the same way the lower-half circumference is bent downward and left to form the negative imaginary axis. At the same time, the real axis is stretched out to infinite length. The R - and X -circles of the Smith chart are thereby straightened out into a rectangular coordinate system. The radial constant-phase lines of the Smith chart (not drawn in) are bent into circular arcs passing through $R' = 1$, $X' = 0$. The set of circles, for constant VSWR or $|\Gamma|$, which were concentric in the Smith chart, have been shifted so that

each has a different center in the $(R-X)$ -chart. Mathematically, the transformation of coordinates is of the conformal mapping type. The complex Z' -plane is transformed into the complex Γ -plane through the relation of Eq. (185),

$$\Gamma = \frac{Z' - 1}{Z' + 1}, \quad (196)$$

and the inverse transformation is obtained through the inverse form of Eq. (196),

$$Z' = \frac{1 + \Gamma}{1 - \Gamma}. \quad (197)$$

Previously the circular impedance chart was based on a diagram in which the voltage vectors V' , V_1' , and V_2' , of Fig. 2-26, were drawn relative to the incident voltage vector, which appears as the unit vector in the positive real direction. Since this unit vector also represents the incident current, Fig. 2-26 may be thought

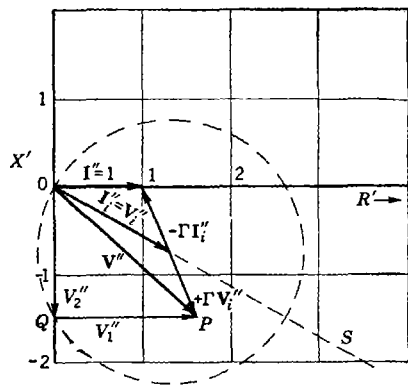


FIG. 2-36.—Vector relations for rectangular impedance chart, derived from Fig. 2-26.

of as a voltage vector diagram based on the incident current vector with the factor Z_0 relating the scales of current and voltage; that is, since $V_i = Z_0 I_i$, we may express the voltage vector V' as

$$V' = \frac{V}{V_i} = \frac{V}{Z_0 I_i} = \frac{(V/Z_0)}{I_i}. \quad (198)$$

Now let us rotate the vector diagram so that the vector I' , the total current, lies along the positive real axis, and let us also change the scale so that it becomes the unit vector; that is, the vector diagram is now transformed as in

Fig. 2-36, so that the vector currents and voltages are all expressed relative to the total current at the given point in the line. Equation (198) now becomes, using $V/I = Z$,

$$V'' = \frac{V/Z_0}{I} = \frac{Z}{Z_0}; \quad (199)$$

and the components of V become

$$\left. \begin{aligned} V_1'' &= \frac{R}{Z_0} \\ V_2'' &= j \frac{X}{Z_0} \end{aligned} \right\} \quad (200)$$

It is, in this way, easy to establish the relations between magnitudes and phases of the various currents and voltages by simple construction, using a rectangular impedance chart. Although the present procedure necessarily yields results in agreement with the related construction of Fig. 2-26, transformations of vectors along the line are much more complicated than in the earlier case. This is due to the fact that the diagram is now based on total current, which changes from point to point; the earlier diagram was based on incident current, which remains constant.

In a similar way, Fig. 2-31 may be transformed into a diagram showing the vector relations for a rectangular admittance chart, Fig. 2-37. While the original diagrams, Figs. 2-26 and 2-31, are drawn to the same scale, based on incident voltage and current, the resulting rectangular diagrams, Figs. 2-36 and 2-37, have different scales. This is easily adjusted by change of scale, of course, but is mentioned as one consequence of the transformation.

2.13. The Choice of a Transmission-line Chart.—

In the preceding sections two different forms of chart, a circular one based on Γ and a rectangular one based on the components of Z or Y , have been described, and in either case the chart may be used to represent either Z or Y . Moreover, the circular chart may be used to give either rectangular

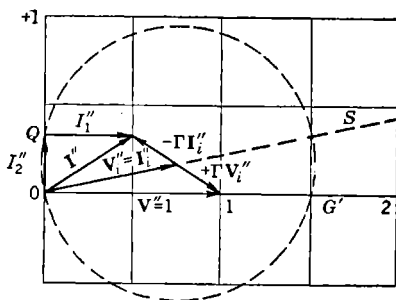


FIG. 2-37.—Vector relations for rectangular admittance chart, derived from Fig. 2-31.

components of Z or Y or the corresponding magnitude and phase angle. There are numerous other charts in use, but the ones described are the most common, and they are adequate to treat any transmission line in a clear and convenient manner. The problem of choosing from among them the proper chart to represent most clearly the solution to a given problem deserves some consideration. In some cases the choice is largely a matter of personal preference, but more often a clear choice is indicated.

Circular vs. Rectangular.—When data are to be plotted simply for record purposes or to read R and X components, this choice is largely a matter of personal taste. In the following cases, however, the circular chart has certain advantages. Frequently the choice of a reference point for which the impedance is plotted is rather arbitrary, and it may be desired to shift the reference point after plotting the data. If the data are plotted on tracing paper over a circular chart, this is easily achieved by a simple rotation of the paper. In this way it is frequently possible to discover a position for which the variation of a certain parameter leads to a

variation in reactance alone or of susceptance, resistance, or conductance alone. In the case of the rectangular chart such simple rotations of the plotted points are never valid. For the circular chart, rotation is accurate for data taken at constant wavelength, in error in phase angle only if not at constant wavelength. For slight rotations and small wavelength variations, the phase error is not serious. In the rectangular chart, the size and shape of the plot of a given set of data at constant wavelength depend on the choice of a reference point, while in the circular chart they do not. Since the choice is so frequently arbitrary, this variability in size and shape does not seem physically significant, and the circular chart seems the more desirable. Even in cases in which the reference point is not wholly arbitrary, it may turn out to be desirable to transform an impedance plot into an admittance plot. This is easily accomplished by a half-turn rotation of the circular chart, and the plot is not distorted in size and shape as it would be on the rectangular plot.

One may suspect from the foregoing that it is the author's judgment that in most cases the circular chart is to be preferred. This is, indeed, the case where the plotting and transforming of data are concerned. The rectangular chart seems better suited, however, to the task of showing the vector relations existing between the various voltages and currents *at a point* where an equivalent series- or shunt-circuit representation is valid. Figure 2-39 illustrates such an application. Another problem which is treated better by the rectangular chart is that of representing qualitatively, as in a discussion, a multiple transformation in which two or more characteristic impedances are involved. The diagram of Fig. 4-16 is an example of this. In such cases the R and X (or G and B) coordinates are in terms of absolute values rather than relative, and the constant-phase and constant-VSWR circles are omitted. A set of such circles, based on the appropriate characteristic impedance, is implied for each characteristic impedance involved. In actual numerical calculations it is impractical to work with other than normalized impedances, relative to the particular characteristic impedance being considered; therefore the rectangular chart loses its advantage for quantitative work.

Admittance vs. Impedance.—In low-frequency circuits it is usually quite obvious, from the form of the circuit connections, when to use impedance and when to use admittance. The over-all performance of a combination of circuit elements is then easily predicted by adding series impedances or shunt admittances. In microwave transmission circuits it is rarely possible to combine either impedances or admittances in this simple way. This is because circuit elements—for example, junctions between transmission lines or waveguides, physical discontinuities such as dielectric supports in coaxial lines, and so forth—are not small compared with a wavelength as they are in low-frequency circuits. This means

that the phase of current or of voltage is not constant over any one circuit element or combination of elements.

For example, consider a T-junction formed by joining three coaxial lines of equal characteristic impedance. With two of the lines terminated in their characteristic impedances, let us inquire as to the input impedance presented to the third line. At low frequencies, one reasons simply that the current is shared between the two branches while the voltage across the two branches is the same; and one draws the valid conclusions that the two branches form a parallel circuit shunting the third and that the admittances of the two branches are simply added to get the admittance of the combination as seen from the third line. If the frequency is so high that the wavelength is comparable to the dimensions of the junction, the first question to be answered is: At what point in the junction should the impedance be expressed? Before answering this, let us consider the manner in which this impedance is to be measured. The standing-wave ratio and position of a voltage minimum will be determined in the input line by moving a voltage-measuring probe along a slotted section of line some little distance from the T-junction. By use of a transmission-line chart, the impedance or admittance may be extrapolated to any desired point in the junction. Actually, the fields and currents in the immediate neighborhood of the junction are so complicated that a measurement of impedance in this region is, from the practical standpoint, impossible and, from the theoretical standpoint, meaningless. It is only by correlating the effects observed a little distance away from the junction with an effective impedance at the junction, which would have produced, in a simple uniform line, the same effects at the same distance away, that meaning is attached to the "impedance at the junction." We have not yet answered the question regarding the choice of a reference point in the junction, but it should be fairly clear that the choice is rather arbitrary since it is only the effect produced a little distance down the line which is significant. The natural choice would seem to be the point at which the axes of the three coaxial lines coincide. When the impedance or admittance is extrapolated to this point, it will probably be found that the admittance is approximately the sum of the characteristic admittances of the two branch lines. At low frequencies this approximation will be very good indeed. As the frequency approaches that for which the second coaxial mode may be propagated, it will very likely become an extremely poor approximation.

The method of treating junctions in terms of an equivalent circuit in network theory is described thoroughly in other volumes¹ of this series, and briefly, in Sec. 2-14. The point to be made here is that, although

¹ *Waveguide Handbook*, Vol. 10, and *Principles of Microwave Circuits*, Vol. 8, Radiation Laboratory Series.

simple addition of impedances or admittances is valid for low frequencies, the situation is usually much more complicated at high frequencies. There are, nevertheless, instances of particularly simple discontinuities or junctions for which the simple concepts of addition of admittance or impedance are valid, even in waveguide or relatively large coaxial lines. In all such cases, the validity is limited to discontinuities for which the dimensions in the direction of propagation are negligible compared to a wavelength.

The most commonly used discontinuity of this type is the thin inductive flap in rectangular waveguide, Fig. 2-38. The equivalent circuit shown is strictly valid only for an extremely thin flap of perfectly conducting material; but it is adequate for cases of practical interest. The flap is usually of 0.020-in. to 0.064-in. brass for wavelengths of 1 to 10 cm, and

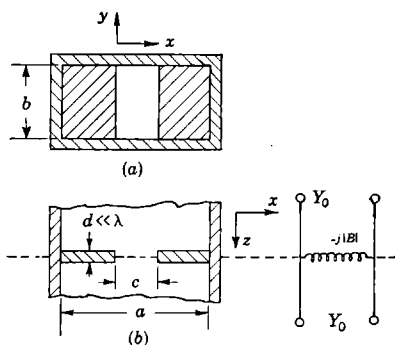


FIG. 2-38.—Inductive iris in waveguide.

and therefore d is not more than about 0.03-guide wavelengths. For thicknesses of this magnitude, it is found that a correction must be applied to the value of B calculated for very thin flaps, but that the equivalent circuit need not, for practical purposes, be modified. These flaps are extensively used as waveguide impedance transformers and are discussed in more detail in Chap. 4. At the present moment we are particularly interested in their relation to imped-

ance and admittance charts. Flaps made of reasonably good conductors may be considered as lossless without serious error. If the output waveguide is terminated in such a way that the normalized admittance at the reference plane of this termination is Y_1 , then the input admittance Y_3 is the sum of Y_1 and the inductive flap susceptance jB_2 ; that is, $Y_3 = Y_1 + jB_2$. This is the familiar addition of admittances which is used in low-frequency circuits. The way in which this addition is shown on a rectangular admittance chart is illustrated in Fig. 2-39. The admittance chart may be thought of as representing a current diagram at the reference plane when unit voltage, common to Y_1 , B_2 , and Y_3 , is applied there. We may take $B_2 = j0.5$ and show, Figs. 2-39 and 2-40, how this combines with (a) a general admittance such as $Y_1 = 0.5 - j0.5$ to give $Y_3 = 0.5 - j1.0$, and (b) the special admittance $Y_1 = 1 + j0.5$ to give the special value $Y_3 = 1 + j0$, or matched-line condition. This latter procedure will be discussed in greater detail later when we come to the use of the inductive flap as a waveguide matching

element. For Case *a*, the principles of Fig. 2-37 are used to show the voltage and current vectors, Fig. 2-39, each relative to the positive real unit vector which represents the voltage common to Y_1 , B_2 , and Y_3 . The voltage in the "incident," or positively traveling wave to the right of the discontinuity is V_{i1} . This is seen to lead the incident wave V_{i3} , to the left of the discontinuity, by a slight phase angle. The magnitude of the incident wave is seen to be lower on the right, though this is not always the case. If the discontinuity is lossless, conservation of energy demands only that

$$V_{i1}^2(1 - \Gamma_1^2) = V_{i3}^2(1 - \Gamma_3^2),$$

since each side of the equality is proportional to the net power flowing to the right. Thus if $\Gamma_3 = 0$, as in Case *b*, V_{i1} will equal or exceed V_{i3} .

The admittance transformations for these two cases are shown on the circular chart in Fig. 2-40. If one is not interested in the relations between the various currents and voltages, and this is so more often than not, then the circular chart serves equally as well as the rectangular.

The inductive flap in waveguide has been cited as an example in which the use of an admittance diagram is indicated. A similar type of equivalent circuit holds for the coaxial-line discontinuity of Fig. 2-41, although the shunt susceptance is capacitive in this case. It is apparent that in this problem, too, an admittance diagram is required. It is characteristic of radial discontinuities in coaxial lines, where one or the other or both conductors abruptly change diameter, that the equivalent circuit contains a pure shunt element, and in all such problems the use of admittance diagrams is indicated.

In Figs. 2-42 and 2-43, discontinuities which yield a series-type equivalent circuit are shown for waveguide and coaxial lines. Just as in Fig. 2-38, the discontinuity must have small extent d in the longitudinal direction. In either circuit, the reactance X may have any value, either positive or negative, depending on the dimension c . Discontinuities of this type naturally call for the use of impedance charts to represent them. The principles of Fig. 2-36 may be used to obtain the relations between voltages and currents in terms of the total complex current which is common to the elements of a series circuit.

($R-X$) vs. ($Z-\theta$); ($G-B$) vs. ($Y-\theta$).—This choice is usually clear in any

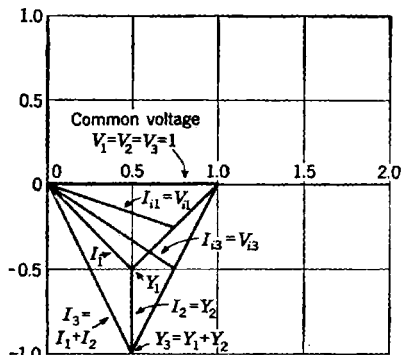


FIG. 2-39.—Admittance diagram for inductive iris.

given problem. The problems discussed in the preceding paragraphs clearly required the expression of Z or Y in rectangular form rather than in polar form. In the majority of cases, this will be the choice. There is one particular type of problem, however, in which the use of the polar form for Z or Y is useful. This is the problem in which neither series-impedance elements nor shunt-admittance elements are needed, but in which a change of characteristic impedance occurs.

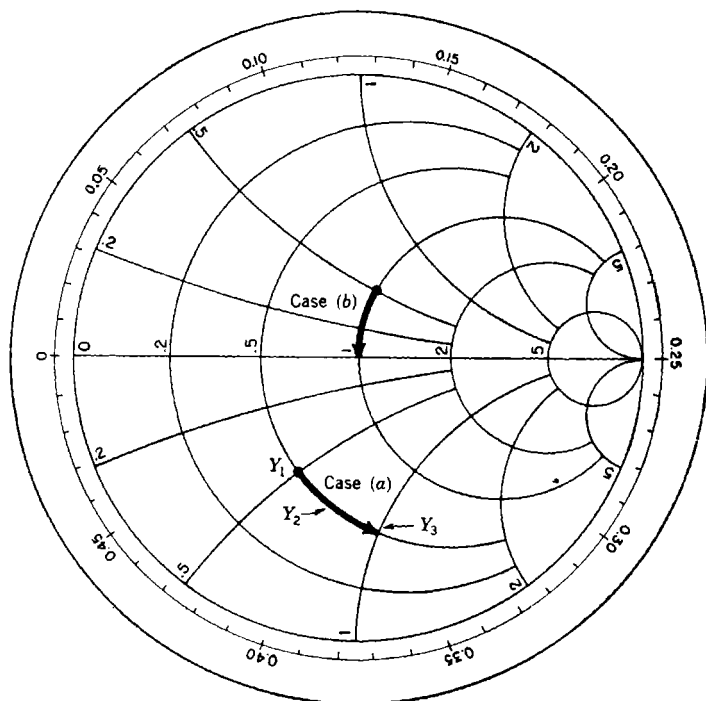


FIG. 2-40.—Admittance diagram (a) corresponding to Fig. 2-39, and (b) illustrating match ing by inductive iris.

An example of this problem arises in connection with the prediction of impedance transformations along a coaxial line supported by dielectric beads. This problem is discussed in detail in Chap. 4, but Fig. 2-44 gives an illustrative example. The impedance at a is $Z_0 = 1.6 Z'_0$; hence it is entered at $Z = 1.6$, $\theta = 0$. The arc of length 0.05 represents passage through the bead, leading to the impedance $Z_b/Z'_0 = 1.45/-18^\circ$. This impedance is expressed in terms of the air-filled line merely by reducing the magnitude of impedance by the factor 1.6, leaving the phase angle unaltered.

The ordinary (R - X)-chart could be used, in which case both R and X would be reduced by the factor 1.6. The positions of all the plotted points are naturally the same for the two charts, the only advantage of the

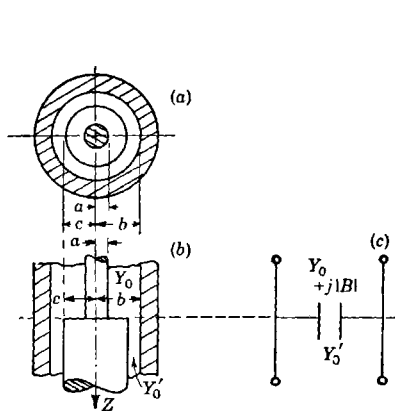


FIG. 2-41.—Capacitive step in coaxial line.

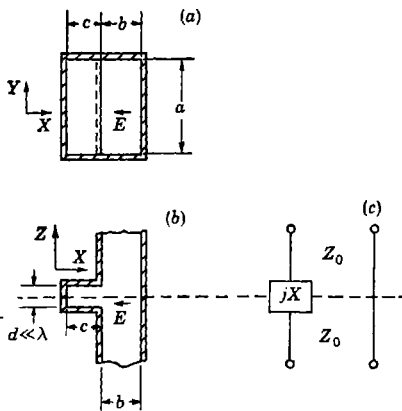


FIG. 2-42.—Series waveguide stub.

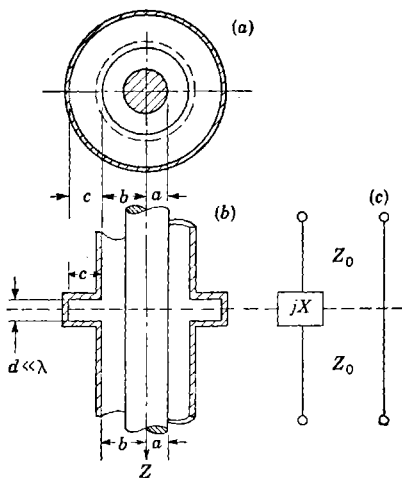


FIG. 2-43.—Series coaxial-line choke.

(Z - θ)- over the (R - X)-chart being the simpler conversion from one characteristic impedance to another. Of course, if steps of the type shown in Fig. 2-41 occur, a (G - B)-chart is needed in order to add a shunt B . Transfer of characteristic-admittance level involves changing G and B by the factor 1.6, just as in the case of R and X , but in the opposite direction.

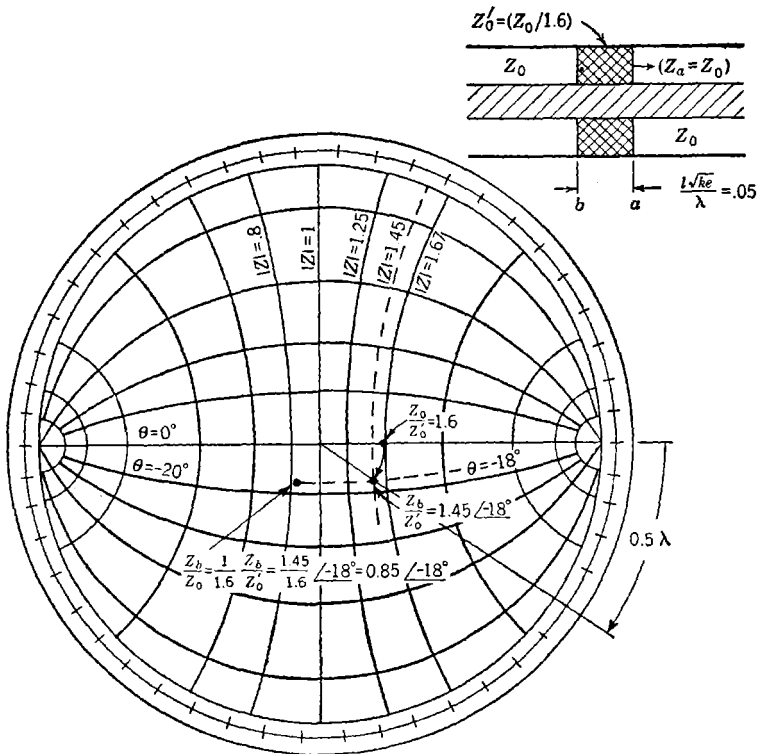


FIG. 2-44.—Use of $(Z-\theta)$ -chart for beads in a coaxial line.

The $(Y-\phi)$ -chart might have been used in place of the $(Z-\theta)$ -chart in solving the problem of Fig. 2-44. Clearly, the whole diagram would have been rotated 180° . There is no special rule for choosing between the two alternatives; it is merely a matter of personal preference. As indicated above, the $(R-X)$ - and $(G-B)$ -charts may be used for this type of problem with only slightly more work in converting characteristic impedance or admittance. It is seldom that the polar-type chart is really necessary; it is usually preferable to use the usual $(R-X)$ - or $(G-B)$ -chart rather than change to a different one.

IMPEDANCE-MATCHING AND DESIGN PROCEDURE

2-14. The Design of Matched Circuit Elements.—*Reason for Matching.*—It was stated in Chap. 1 that one of the most important, and one of the most difficult, problems in the design of microwave transmission circuits is that of maintaining a “matched” condition in all circuit ele-

ments. If the line on the output side of a given element is terminated in such a way that no standing wave exists in it, then it is desired that no standing wave be excited in the input line by the element itself. Now, using the theory developed in the present chapter, it can be shown that under these circumstances the transmission line and the associated circuits introduce a minimum of ohmic attenuation, transmit maximum power without breakdown, and present a minimum rate of change, with change of frequency, of the impedance presented to the transmitter output terminals. If the transmitter is designed to work into the characteristic impedance of the line and the antenna presents a reflectionless termination, then such a continuously matched line provides optimum coupling between antenna and transmitter.

Although the other factors mentioned are important enough to suggest the desirability of the continuously matched operation, by far the

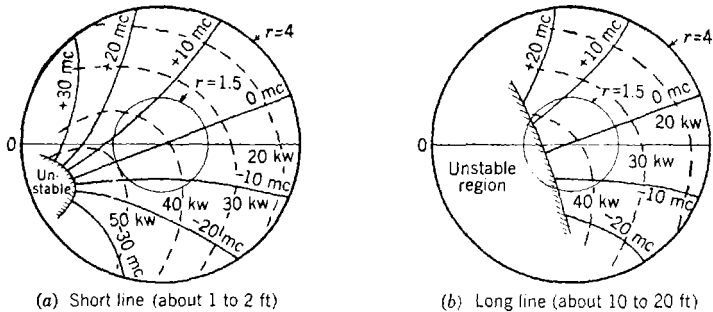


FIG. 2-45.—Typical Rieke diagram for magnetron.

most important factors are those involving the load characteristics of the transmitter. Power output, operating frequency, and frequency stability of microwave oscillators are all rather critically dependent on the character of the load into which they operate. This is particularly true of high-efficiency tubes such as magnetrons, but it is true to some extent of other tubes such as klystrons or triodes. To indicate the magnitude of these effects a detailed study is necessary. Those who are interested in studying them further will want to refer to Vol. 6 of this series.

The way in which the output power and operating frequency depend on the load presented to a typical magnetron is illustrated in the so-called "Rieke diagram" of Fig. 2-45. The polar coordinates which form the basis of this chart give the phase and magnitude of the reflection coefficient at a chosen reference point in the magnetron. This coordinate plane is identical with that which we used in earlier impedance charts, and the radial scale has again been marked in terms of voltage standing-wave ratio rather than of voltage reflection coefficient. Diagrams of this type are obtained in this manner: first, by coupling the magnetron to a matched

load and noting the power delivered and the operating frequency; then by introducing a mismatch and varying the reflection coefficient in a systematic way by means of a variable impedance transformer, and noting, for each point on the reflection-coefficient diagram, the power and frequency. When a sufficiently good coverage of the chart has been obtained, lines indicating constant-power and constant-frequency contours are drawn in.

With such a diagram available, the effect of an impedance mismatch on the magnetron may be determined. Let us take, for example, a VSWR of 1.5 and note its effect for various phases. Maximum power, 50 kw, occurs for the phase marked 0.46 wavelengths on the circumferential scale, and the minimum power, 34 kw, occurs for a phase of 0.20 wavelengths. The maximum frequency, 13 Mc/sec above that for matched line, occurs for a phase of 0.07λ , and minimum frequency, 13 Mc/sec below, occurs for 0.38λ phase. The frequency sensitivity of an oscillator to its load impedance is popularly known as "pulling," and the total frequency difference between maximum and minimum for a VSWR of 1.5, a common measure of this sensitivity, is known as the "pulling figure." In the example above, the pulling figure is 26 Mc/sec.

Large standing-wave ratios in the phase region 0.47λ lead to unstable operation of the magnetron, indicated by shading in Fig. 2-45. This instability is associated with the convergence of the frequency contours and is aggravated by interposing an additional length of line between magnetron and mismatch, Fig. 2-45b.

Let us summarize by recapitulating the effect on this typical magnetron of allowing the reflection coefficient to vary in magnitude from 0 ($r = 1.0$) to 0.2 ($r = 1.5$) and to vary through all phases. The extremes of power are 50 kw, or a variation of about ± 20 per cent from the mean. The extremes of frequency are ± 13 Mc/sec from the mean. And for long lines, unstable operation occurs over part of the impedance region under consideration. These variations are usually the most important considerations in judging the degree of impedance-matching to be attained in designing components.

The next most important consideration is, in many cases, that involving voltage breakdown. It was shown in Sec. 2-6 that the *net* power which may be transmitted through a transmission line to a load is decreased, compared with the net power transferred in a matched line, by a factor exactly equal to the value of the VSWR in the line. Thus, in our example above, the power-handling capacity of the transmission line is reduced to two-thirds of that of the matched condition by the assumed VSWR of 1.5. For high-power apparatus, operating close to the limit of the power-handling capacity of the transmission line and components, this may be a very serious limitation.

The remaining factors, increased ohmic losses and reflection of power from the incident wave, are relatively minor ones. Using the relations of Sec. 2-6, these are evaluated for a VSWR of 1.5 to compare with the previous factors. The ohmic attenuation is increased by only about 8 per cent. The power reflected by the mismatch whose VSWR is 1.5 is only 4 per cent.

Measurement of Mismatch.—The direct approach to the problem of achieving this matched-line condition is simply to terminate the output line in a reflectionless load and to examine the standing waves introduced in the input line by the component being designed. The experimental procedure involved is described in detail in Vol. 11 of this series. The data consist of the value of the VSWR and the position of a voltage minimum in the standing wave. These data enable one to plot the impedance or admittance at a chosen reference point in the component being tested. The magnitude of the VSWR is, of course, sufficient to indicate the extent of the mismatch, but the phase information and impedance plot are frequently helpful in analyzing defects in the design and in effecting an improvement.

Still further information, leading to more complete knowledge of the characteristics of the component, may be obtained by an indirect approach. Briefly, this method consists of terminating the output line in a movable short-circuiting plunger, rather than in a perfect match, and determining merely the position of the voltage minimum of the complete standing wave resulting in the input line. If the component under test is perfectly matched, any motion of the plunger in the output line will cause an exactly equal shift of phase in the standing-wave pattern in the input line. If the component introduces a mismatch, the phase of the standing wave in the input line will not follow linearly the position of the short-circuiting plunger as it moves along the output line. Although we cannot go into the details of the interpretation here, suffice it to say that the extent of this departure from linearity is a direct measure of the VSWR introduced by the component when under normal operating conditions. In addition, the positions of the output plunger and of the voltage minimum in the input line, when maximum departure from linearity occurs, constitute useful information. From the nonlinearity and phase data one may deduce the input impedance at any chosen point in the input line when the output line is matched. Moreover, one may predict exactly how the input impedance varies with the output impedance, and one may even predict the same characteristics for operation in the reverse direction, interchanging input and output ends. This wealth of information is usually expressed as an "equivalent circuit" in any one of several different forms familiar to those versed in network theory.

In general, the direct approach already described will be used rather

than the indirect one, since it requires fewer measurements and leads directly to an impedance plot. Occasionally the indirect method is desirable because of the additional information which it furnishes; there are still other instances in which the indirect method is preferable because of instrumental reasons. This is particularly true when either input or output line is too small to be conveniently handled by the usual slotted-line technique. In such cases the small line is made the output line and terminated in a movable short circuit. Since the indirect method provides a complete equivalent circuit, the line used as the output line in the measurement is immaterial. Even when both input and output lines are too small to enable accurate measurements of VSWR by the use of slotted section, the location of the phase of a voltage null (the only use of a slotted section needed in the indirect method) is quite reliable.

Methods of Achieving a Match.—If the measurement of the mismatch of a circuit being designed indicates that the mismatch is too large to be acceptable, there are, in general, two courses of action which may be followed. The simplest one is to design, on the basis of the impedance measurement, an impedance transformer to be built into the unit in the appropriate manner. Although this may be satisfactory in some instances, it will not in general produce a desirable design, especially if the VSWR matched out by the transformer is large. Such a procedure ordinarily leads to a device which requires very accurate machining in order to give the transformer the proper transformation characteristics, and which is rather frequency-sensitive and subject to voltage breakdown.

The second method, and the one frequently used, is the attempt to effect an improvement in the match by a systematic variation of one or more design parameters. In initiating the design of a circuit to accomplish a given requirement it is well to bear this in mind and to provide one or more conveniently adjustable parameters, such as a variable-length coaxial-line stub, waveguide short-circuiting plate position, and so forth. Usually such elements will present themselves rather naturally in each design.

In the case of a T-stub support for coaxial line we have at our disposal, as an adjustable parameter, the stub length. By trying a series of different lengths it will be found possible to choose a length which will give a perfect match past the stub. This is an example of the simplest type of matching, achieved by adjusting a single parameter. If the admittance point were plotted for successive increments of stub length, a series of points would be obtained falling on a smooth curve and passing through the perfect-match point at the center of the chart.

An example of a slightly more complicated nature is afforded by the problem of the design of a transition from coaxial line to waveguide, Fig. 6-9. Here we have two parameters, the probe length P and the end-plate

distance D . One parameter is first fixed at some arbitrary value, and the other is then varied. The procedure is repeated for other values of the first parameter. The corresponding admittance points are shown in Fig. 6-10, in which contour lines corresponding to constant P and constant D are drawn. This gridwork of admittance contours may be used to estimate, by interpolation, the values of the two parameters which would give the matched condition. It is also useful in estimating how much departure from optimum value may be tolerated in either parameter in order not to exceed a maximum allowable VSWR. It also enables one to establish such mechanical tolerances for variation of the two parameters occurring simultaneously.

Sometimes it will be found that it is impossible to obtain perfect match with the parameters available, but that a reasonably low VSWR may be obtained. An example of this is found in the design of a stub angle, Sec. 4-4. It is then common practice to supplement the parameter-adjustment method of matching with the addition of a suitable transformer. Other situations calling for a combination of the two methods will be discussed in the next section.

The Principle of Scaling or Similitude.—It is possible, by taking advantage of certain principles of similarity, to make use of the details of an existing circuit in the design of a new one to operate at a different frequency. This process is quite analogous to the design of full-size aircraft and ships on the basis of experiments conducted on scale models. In the scaling of mechanical models, the scaling of dimensions must be accompanied by appropriate changes in the properties of the fluid medium and in the velocity of motion. Similarly, in the scaling of electromagnetic devices, a change in dimensions must be accompanied by the proper changes in the electrical and magnetic properties of the materials used and in the operating frequency.

The relations between physical dimensions, operating frequency, and the properties of the materials may be derived by suitable manipulation of Maxwell's equations. Stratton¹ shows how this principle of electrodynamic similitude leads to the following relations:

$$\mu\epsilon l^2\nu^2 = A, \quad (201)$$

$$\mu\sigma l^2\nu = B. \quad (202)$$

Here A and B are constants to be discussed presently and l is any length which establishes the dimensional scale factor of the device being considered; it might be, for example, the radius of a spherical cavity or the width of a rectangular waveguide. In scaling, *all* dimensions of the device must be changed by the same factor as is l . When the dimensions are scaled in this way, the operating frequency ν and the characteristics

¹ J. C. Stratton, *Electromagnetic Theory*, McGraw-Hill, New York, 1941, p. 488.

μ , ϵ , and σ of *each* of the materials throughout the entire apparatus must be altered in such a way that the constants A and B retain their old values. To be specific, each of the constants A and B will have a series of values A_i and B_i uniquely determined by the properties μ_i , ϵ_i , and σ_i of the material constituting that particular part of the original apparatus. Equations (201) and (202) then become

$$\mu_i \epsilon_i l^2 \nu^2 = A_i, \quad i = 1, 2 \dots \quad (203)$$

$$\mu_i \sigma_i l^2 \nu = B_i, \quad i = 1, 2 \dots \quad (204)$$

As an example of the application of this principle, let us double the characteristic length l of a particular device. The constants A_i of Eq. (203) remain unchanged if ν should be halved, and if μ_i and ϵ_i should be left unchanged. In order to satisfy Eq. (204), however, we must double σ_i . The doubling of all conductivities throughout the apparatus may in some cases be extremely important to the proper functioning of the device. This is particularly true of those circuits, such as cavity resonators, in which the power absorbed in conducting surfaces or dielectric medium plays an important role in determining performance.

On the other hand, there are a large number of circuits in which the power lost to the conductors and dielectrics of the device is a negligibly small fraction of the input power. For such devices (and nearly all of those described in this volume fall into this class), the conductivity is relatively unimportant in determining the electric and magnetic field patterns. The impedance which is determined by these fields therefore shows little dependence on conductivity. Hence, the plot of impedance against scaled frequency is essentially the same for the scaled-down device as for the original one, even though the conductivity is not scaled. In many practical problems, therefore, it is not necessary to satisfy Eq. (204).

Although the fraction of the input power lost in passing through the apparatus may be very small in both the original and the scaled-down circuits, the two figures may differ from each other by a considerable factor if the conductivities are not scaled. It can be shown¹ that for a circuit whose dimensions are scaled down by a factor p from a larger one, the percentage of the incident power lost in passing through the smaller apparatus at a frequency p times higher bears the following relationship to that lost in the larger: loss in dielectric, *smaller* by the factor p ; loss in conductors, *larger* by the factor \sqrt{p} . It must be remembered that we are considering the case where the over-all length, as well as the other dimensions, is scaled down, and the characteristics ϵ , μ , and σ are kept constant.

It should be noted that constancy of the loss tangent (essentially equal

¹The special case of attenuation in rectangular waveguide may be verified by converting Eqs. (150) and (151) into loss per wavelength.

to the power factor) of a dielectric with change of frequency corresponds to the scaling of σ in the manner required. This fact is easily seen by converting Eq. (92)

$$\epsilon_1'' = \frac{\sigma_1}{\omega} \quad (2.92)$$

into the form

$$\sigma_1 = \omega \epsilon_1'' = \omega \epsilon_1' \left(\frac{\epsilon_1''}{\epsilon_1'} \right). \quad (205)$$

It is evident that if the dielectric constant ϵ_1' and the loss tangent (ϵ_1''/ϵ_1') remain constant, then σ will be proportional to ν as required by Eqs. (203) and (204) when scaling without change of μ_i or ϵ_i .

Thus far we have considered only the adjustment of l , ν , and σ_i in applying Eqs. (203) and (204) to scaling problems, keeping μ_i and ϵ_i constant. Although this application is the most useful for these equations, there are several others. One which is occasionally useful is that in which the size of a circuit is reduced while the same operating frequency is retained. This reduction and maintenance of frequency may be accomplished most easily by the introduction of a new dielectric with a higher value of ϵ . If it is desired to decrease l by a factor p , then ϵ must be increased by the factor p^2 in order to satisfy Eq. (203), μ and ν remaining unchanged. In order to satisfy Eq. (204), σ_i must be increased by the same factor p^2 . As remarked in connection with the preceding example, it is, in many practical problems, not necessary to satisfy Eq. (204).

A third possibility is that of keeping l and μ_i fixed, and varying ϵ_i and ν to satisfy Eq. (203). Other combinations in which μ_i is varied are possible, in principle, but rather impractical. There are also numerous possibilities in allowing three or even all four of the quantities on the left of Eq. (203) to vary.

To be exact, *all* dimensions must be scaled, but it is obvious from a practical standpoint that some dimensions are not at all important. Thus it is only the internal dimensions of a metal waveguide that need be scaled. Similarly, only the internal diameter of the outer conductor and the outer diameter of the inner conductor of a coaxial line have any significance. In general, only those dimensions involving the dielectric material in which electric and magnetic fields occur and the metal surfaces adjacent to this region are significant.

Unfortunately the practice of scaling dimensions is considerably hampered by the fact that the pertinent dimensions of standard coaxial lines and rectangular tubes seldom have the proper relationships. This is, in the case of rectangular waveguides, chiefly due to the fact that the tubing used is standard stock tubing, sized according to its external dimensions. Very rarely do the inside dimensions of one tube scale at all

closely to that of a different size. Similarly it is difficult to obtain, from stock tubing, a series of lines of different sizes with approximately the same diameter ratio. Nevertheless, the principles of scaling by similitude argument give one a fair start on a new design if applied as carefully as inconsistencies in the scale factors of standard tubings permit.

2-15. Impedance-matching Transformers.—There are times when it becomes desirable to incorporate into a design a fixed transformer section. This section is usually introduced for the purpose of matching the circuit in question to the characteristic impedance of the transmission line or waveguide. In some special cases, however, it is necessary to cause a specified impedance to occur at a given point. An example of this application is found in the case of the transformer which is sometimes used to cause the optimum load impedance to appear at the terminals of a transmitter tube such as a magnetron. In regard to the use of a transformer to compensate for the mismatch of a circuit being designed, it is usually preferable to obtain a satisfactory match by the methods outlined in Sec. 2-14; but if these methods fail to give the degree of match desired, several types of simple transformers are available.

Quarter-wavelength Transformers.—The simplest types of coaxial-line transformers fall into this classification. Quarter-wavelength transformers may be used in waveguides, but it is more common to use shunt susceptance elements in waveguide work. The quarter-wavelength transformers used in coaxial lines usually take the form of sections of line in which the inner conductor is enlarged by slipping onto it a metallic sleeve of the appropriate thickness. This and other forms of transformers for coaxial lines are discussed in Sec. 4-5, while some forms of waveguide transformers are taken up in Sec. 4-16.

One frequently hears it said that a quarter-wavelength line section "inverts the impedance." This statement may be understood by noting that it is the *normalized* impedance, expressed in terms of the characteristic impedance of the quarter-wavelength section, which is inverted. Thus if a load impedance Z_r terminates a quarter-wavelength section of characteristic impedance Z'_0 , the *normalized* output impedance Z_r/Z'_0 is transformed at the input end to the *normalized* input impedance

$$\frac{Z_i}{Z'_0} = \left(\frac{Z_r}{Z'_0} \right)^{-1} = \frac{Z'_0}{Z_r} \quad (206)$$

Writing the equation in this form brings out the inversion property of the quarter-wavelength line more clearly than does the frequently used form (Item 8 of Table 2-1)

$$Z_i = \frac{Z'^2_0}{Z_r} \quad (207)$$

In any case, the characteristic impedance of the quarter-wavelength section which can transform the output impedance Z_r to the input impedance Z_i is given by

$$Z'_0 = \sqrt{Z_r Z_i}. \quad (208)$$

A simple example of the inversion property of a quarter-wavelength line section is clearly evident from an inspection of the impedance chart of Fig. 2-35. Consider the normalized impedance point $R = 2$, $X = 0$. This point lies on the real axis at the point where the ($r = 2$)-circle crosses it. If this ($r = 2$)-circle is followed in the clockwise direction (that is, if the impedance transformation is traced at points along the line toward the generator) for a quarter wavelength, we arrive at the normalized impedance $R = \frac{1}{2}$, the reciprocal of the normalized load impedance $R = 2$. Conversely, if we start with the normalized load impedance $R = \frac{1}{2}$ and follow the upper arc of the ($r = 2$)-circle for a quarter wavelength, we obtain the input impedance $R = 2$, the reciprocal of the load impedance $R = \frac{1}{2}$. It is easily verified for any of the constant- r circles that the two points of intersection with the real axis bear this reciprocal relationship.

A quarter-wavelength transformer may be used to obtain an input impedance equal to the characteristic impedance Z_0 of the transmission line if, for any *real* load impedance Z_r , the characteristic impedance of the transformer section is chosen to be that required by Eq. (208); namely,

$$Z'_0 = \sqrt{Z_r Z_0}. \quad (209)$$

In the general case the load impedance will be complex rather than real. Fortunately, however, points of real impedance occur at every voltage-minimum or voltage-maximum point along the line on the input side of the circuit being matched. If one of these were chosen as a reference point, the effective load impedance at that point would be real, and the above method of transforming a real load impedance to Z_0 would be valid.

If a point of minimum voltage is chosen as the reference point, the load impedance will be

$$Z_{\min} = \frac{Z_0}{r_1}, \quad (210)$$

where r_1 is the value of the VSWR introduced by the circuit to be matched. The characteristic impedance of the transformer section is then

$$Z'_0 = \sqrt{Z_{\min} Z_0} = \frac{Z_0}{\sqrt{r_1}}, \quad (211)$$

and the impedance transformation is as shown in Fig. 2-46a. The circle *cd**f* represents the circle for which $\text{VSWR} = r$, for an impedance chart

based on the impedance Z_0 . The actual load impedance lies somewhere on this circle (say at point d or at point f) but we need not be concerned about its location in the present instance. Locating the point e of minimum voltage is important; this may be accomplished by extrapolating an integral number of half wavelengths toward the load from one of the voltage minima which occur in the slotted section of line used to measure r_1 . Usually the point e should be chosen as the voltage minimum that is as close as possible¹ to the circuit being matched, in order to obtain the least frequency-sensitive response. This choice is made because of the fact that the rate of change of input impedance with wavelength is, for a given load impedance, greater for long lines than for short ones. If the

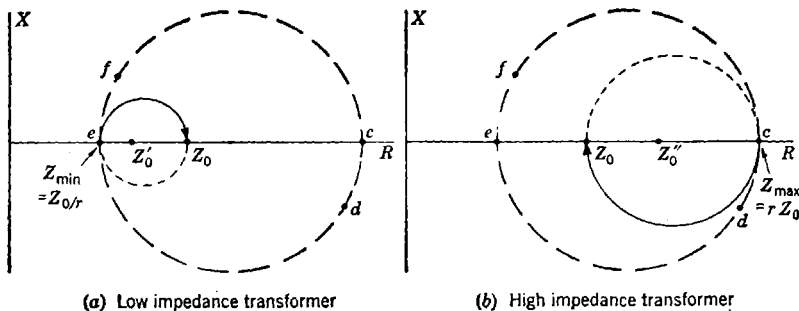


FIG. 2-46.—Impedance diagrams for quarter-wave transformer.

point e is made the terminal end of the quarter-wavelength transformer whose characteristic impedance is given by Eq. (211), the impedance transformation along the transformer section will follow the arc eZ_0 , resulting in an input impedance equal to the characteristic impedance Z_0 of the line.

In a similar way, one may choose for the reference point the point c where the voltage is a maximum and the impedance is

$$Z_{\max} = r_1 Z_0. \quad (212)$$

The required characteristic impedance of the transformer section is

$$Z''_0 = \sqrt{Z_{\max} Z_0} = \sqrt{r} Z_0, \quad (213)$$

and the impedance transformations are as shown in Fig. 2-46b.

The problem of creating a prescribed impedance at a given point by the introduction of a transformer section into a matched transmission line is essentially the inverse of the above problem. If the desired impedance lies on the curve where $VSWR = r_1$, either of the two transformers

¹ For discussion of an exception to this general rule see, below, the subsection title "Use of Admittance Charts."

described above is suitable. For example, if it is desired to produce the impedance f at a given point, the input end of the transformer of impedance Z'_0 can be placed the proper distance (represented by the arc ef) on the load side of the given point. The transformation is then, working from the matched line impedance Z_0 back to the desired impedance at f , from Z_0 via the dotted arc to e , thence along the dashed arc ef .

Shunt Susceptance Elements.—A type of impedance-matching element which is particularly useful in waveguides is that which behaves essentially like a pure susceptance shunting the line. The mechanical details and design data for waveguide structures used to accomplish this shunting action are discussed in Secs. 4-13, 4-14, and 4-15. The most common structure is the so-called "inductive diaphragm," which adds a negative susceptance with a magnitude dependent on the dimensions.

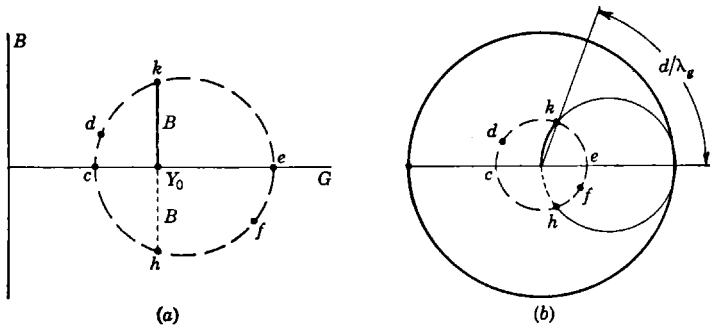


FIG. 2-47.—Admittance charts for waveguide matching, (a) using rectangular chart; (b) using circular chart.

The way in which such an element is used to match a given circuit to the characteristic impedance (or admittance) of the waveguide is indicated in Fig. 2-47. These diagrams represent the impedances of Fig. 2-46 transformed onto an admittance chart. Again, we are not concerned with the actual load admittance but are interested merely in finding the point along the standing-wave pattern where the admittance has the desired value. In this case we seek the point where the admittance has the form $Y = 1 + jB$, represented by the point k in the diagrams. At this point an inductive diaphragm whose susceptance is $-B$ may be added and the matched condition achieved.

For this type of matching the point e , at the voltage minimum, has no particular significance; however, it furnishes a convenient reference point with respect to which the matching diaphragm may be located. The magnitude B of the susceptance and the distance d between voltage minimum and proper diaphragm position may be read from the admittance chart after the experimental data on phase and magnitude of the

VSWR have been plotted. As a matter of fact both B and d are completely determined by the magnitude of the VSWR and may be calculated by formulas, Eqs. (4-55) and (4-56), or determined from graphs, Figs. 2-12 and 4-61. A discussion of the advantages to be obtained under certain conditions by the use of admittance charts is presented in the next subsection.

The preceding discussion was based on the use of an inductive (negative) susceptance to effect matching. Such an element is to be placed at the point k , Fig. 2-47, which is a distance d toward the *load* (counterclockwise) from the voltage minimum at e . There is a corresponding point h at the same distance d toward the *generator* from the voltage minimum at which a capacitive (positive) susceptance may be placed to effect matching.

Use of Admittance Charts.—It has been shown above that the characteristic impedance and placement of a quarter-wavelength transformer may be determined very simply without the aid of an admittance (or impedance) chart. Similarly, reference was made to simple graphs and formulas by which the magnitude and placement of susceptive elements may be determined. In case the matching is to be done on the basis of a single measurement at a given frequency these methods present the simplest and most accurate solution. In most design work, however, it is desired to obtain the best possible match over a given band of frequencies. It has been found that an admittance chart is of great assistance in achieving this goal.

The usual procedure consists of taking data on the magnitude and phase of the VSWR introduced by the given circuit at a number of frequencies within the operating band of the device to be matched. Some convenient reference point within the device or its input line is then chosen, and the admittance at that point is plotted for each frequency used in the measurements. Let us first assume that we are dealing with a waveguide circuit and that we have been particularly fortunate in the choice of a reference point so that the admittances cluster about the point k . We can then try adding an inductive susceptance of appropriate magnitude and predict the admittance plot to be expected from the device if matched in this manner. It may very well turn out that, in order to obtain the optimum over-all performance within the operating band, a compromise susceptance will be used which is not intended to produce a perfect match at any wavelength within the band. An example of this type of matching procedure is to be found in Sec. 6-6, the corresponding admittance diagram being shown in Fig. 6-17.

There are numerous complications and variations which need to be considered in actually applying the procedure indicated above. In the example given, the variation of the magnitude of the susceptance B with wavelength must be taken into consideration, and this variation differs

from one type of matching structure to another. Then, too, one is seldom fortunate enough to choose the optimum position of the matching device as a reference point. In general one must choose, on the basis of the admittance plot at the initially chosen reference point, a new reference point. The admittance must then be replotted at this new point; it is unfortunately true that a simple rotation of the chart will not suffice because the phase length between points is different for different wavelengths.

It sometimes happens that this difference in phase length can be used to advantage in increasing the bandwidth of a circuit. An illustration of this effect is afforded by the example from Sec. 6-6 mentioned above. The method of design discussed in Sec. 6-6 is, in fact, one of the most useful methods of achieving broadband circuits.

Although the above discussion has been based on waveguide circuits, similar considerations apply to coaxial circuits. The choice of the initial reference point is again rather arbitrary, but in the coaxial circuits the admittance points should cluster about either point c or e , depending on the use of a transformer section of either low or high characteristic admittance. Corresponding to the variation of susceptance with frequency, there will be a variation in transformer action with frequency, because the transformer is a quarter wavelength long at only one wavelength. All these considerations may be worked out very nicely by means of admittance (or impedance) diagrams.

The broadbanding technique described in Sec. 6-6 for a waveguide circuit may be applied in suitably modified form to coaxial circuits. It was by the use of such a technique that the broadband coaxial-stub angle of Fig. 4-31 was designed.

2-16. Other Design Factors. *Manufacturability.*—Although it is no doubt true that almost anything one might design could be manufactured if sufficiently elegant methods of fabrication are sought, a little thought as to problems of manufacture may often avoid needlessly involving slow and expensive fabricational techniques without sacrificing performance. At times there may arise a serious conflict between considerations of simplicity of fabrication and some other characteristics to be mentioned presently. In particular, the streamlining which leads to better breakdown characteristics is often difficult to achieve if conventional machining methods are to be used. In such cases, circumstances may indicate a choice, or some compromise may be reached.

Power-handling Capabilities.—As has just been indicated, streamlining by eliminating sharp corners is frequently desirable. If sharp corners occur in a region of high electric fields, they seriously reduce the breakdown power. It is sometimes sufficient merely to remove the machining burrs by using emery cloth or to go one step further and round the edge

by introducing a radius of curvature of a few thousandths of an inch. However, if the ultimate in breakdown resistance is needed, special streamlined contours or large radii of curvature, calling for special design, become necessary. Examples of this type of design are the high-power E_0 -transition in Fig. 6-77 and the "doorknob"-type transition from coaxial line to waveguide in Fig. 6-37. In the doorknob design, considerable difficulty with manufacturability has been experienced, illustrating the point about the conflict between manufacturability and other factors.

The use of dielectrics is to be avoided wherever possible if high-power operation is desired, both because surface flashover is likely to occur along the dielectric-to-air interface and because most dielectrics are permanently damaged if such breakdown occurs.

Highly frequency-sensitive devices are usually unsuitable for high-power transmission. Usually they include either a section of line in which high standing waves exist or else a small gap across which a high voltage builds up. In either case abnormally high electric fields occur, leading to low power-handling capacity.

It is possible to have a device which includes objectionably small gaps even though it is not very frequency-sensitive. An example of this is the probe-type transition from coaxial line to waveguide, Fig. 6-9, in which the small gap between the end of the probe and the opposite wall of the waveguide leads to low breakdown figures. This limitation may become less serious if the gap is increased by bulging out the waveguide wall in that region. This change alters the impedance match, so one must compensate for it by readjusting the junction parameters.

Bandwidth.—Of all the factors which enter into microwave-circuit design, the problem of maintaining a low VSWR over broad frequency bands is without doubt the most difficult. It is a relatively simple matter to conceive the basic design for a circuit which will perform the required function; for example, a method of coupling from a given coaxial line to a given waveguide. With reasonable provisions for adjustable design parameters, and with due regard for high-power and manufacturability factors, a design may be readily evolved which is reasonably well matched at a given wavelength. If further improvement in the impedance match is desired, a simple impedance transformer may be inserted to give essentially perfect match at this wavelength. If the performance of this device at a series of frequencies is then investigated, it will give an estimate of what may be called the "inherent" frequency sensitivity of the design. This inherent sensitivity varies widely from one circuit to another but will usually be low enough to make operation over a band of about one per cent width satisfactory with a VSWR below 1.10. Some relatively simple circuits give satisfactory performance over a band of ten per cent width, but many others fall far short of this; and it is rare indeed that an appreciably broader inherent bandwidth is found.

As an example of one important factor which influences inherent bandwidth let us consider the simple circuit of Fig. 2-48. A resistance card, whose surface impedance is equal to the wave impedance of the waveguide at midband, is placed a quarter of a midband guide wavelength from the end plate which terminates the waveguide. This impedance has the value, for all *TE*-type waves, of $377 \lambda_{g0}/\lambda_0$ ohms per square, where λ_0 is the midband wavelength and λ_{g0} is the corresponding guide wavelength. For coaxial lines, it is simply 377 ohms per square. The wavelength sensitivity of such a load is given by Fig. 2-49 for various choices of midband wavelength relative to cutoff wavelength. The wavelength sensitivity of the equivalent coaxial line load is given for comparison and is the limiting curve which would be obtained for $(\lambda_0/\lambda_c) = 0$. It is important to note that the closer the midband wavelength is to cutoff, the more sensitive to wavelength the load becomes.

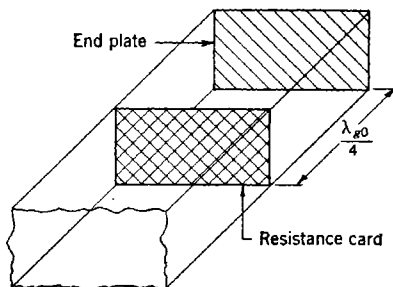


FIG. 2-48.—Resistance card load in waveguide matched at $\lambda = \lambda_0$. Surface resistance of card is equal to wave impedance of guide at λ_0 .

This is, of course, because of the rapid change of guide wavelength near cutoff.

This simple circuit is rather typical of a large number of those which include a quarter-wavelength stub in shunt with the line. The coaxial-load curve might equally well be considered to represent that of an ordinary quarter-wavelength T-stub support. The waveguide curves bear a close relation to a transition from coaxial line to waveguide of the commoner types (see Sec. 6-9).

In general, circuits tend to behave in a manner similar to this. Bandwidths are usually better for circuits operating far from

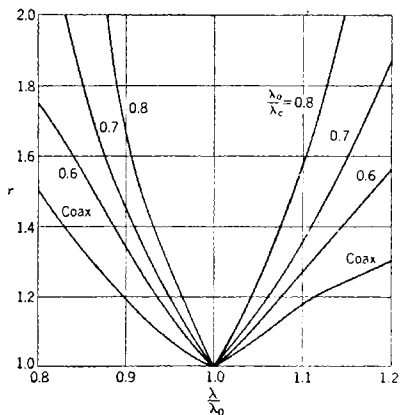


FIG. 2-49.—Wavelength sensitivity for resistance card loads matched at $\lambda = \lambda_0$ in a waveguide whose cutoff wavelength is λ_c . The equivalent coaxial load is given for comparison.

cutoff. A note of warning is in order, however, since difficulties arise as the wavelength approaches the cutoff value for the next higher mode. The higher-mode fields set up by waveguide discontinuities are not attenuated rapidly enough, and undesirable interactions between discon-

tinuities occur. The wavelength at which these difficulties set in depends on such factors as the nature of the discontinuities, but for any wavelength below about $0.6\lambda_c$ caution is advisable.

If the inherent bandwidth of a circuit falls below that desired, either it must be discarded and replaced by a basic design of greater inherent bandwidth, or it must be given greater breadth of band by resorting to some form of broadbanding technique. These techniques usually consist of the introduction of some other element whose frequency sensitivity is roughly equal to that of the original unit and which is placed in such a position that the reflections from the two circuits tend to cancel over a considerable frequency band.

The details of the circuits involved may take various forms. Although there is some overlapping of categories, a classification according to the form of the broadbanding element will be attempted, and an example or two of each group given.

To broadband a simple device such as a bead support or simple stub support, an identical unit may be added at a point in the line which is effectively a quarter of a wavelength away. This is the most obvious way of obtaining cancellation between units of equal frequency sensitivity and is discussed in Secs. 4-3 and 4-4.

Another method which sometimes presents itself is that of adjusting the distance between two circuit components both of which are already present and which have approximately equal frequency sensitivities. An example of this is to be found in the judicious spacing of a simple coaxial-line stub support with respect to the probe-type transition from coaxial line to waveguide described in Sec. 6-7.

A third method consists of introducing an additional element for the express purpose of broadbanding. This element may take the form of a section of line whose length is half a wavelength and whose characteristic impedance differs from that of the rest of the line. This half-wavelength transformer introduces no mismatch at midband and its frequency sensitivity may be varied by altering its characteristic impedance. For example, the added element may be a transformer consisting of a dielectric-filled section of coaxial line. The frequency sensitivity of such a half-wave dielectric "bead" is given by Fig. 4-15. The added element might consist of other resonant combinations, such as a resonant slit in waveguide or a pair of inductive irises spaced to cancel reflections at midband.

Another method, closely related to the last, is to place the added element more or less symmetrically on the output and input sides of the original circuit component. One example of this is afforded by the placement of a low-impedance half-wavelength sleeve transformer symmetrically with respect to a simple coaxial-line stub support in order to obtain the broadband stub described in Sec. 4-4. The technique of using two

elements, one in the output line and one in the input, is illustrated by the discussion of Sec. 6-14 in connection with Fig. 6-79. The procedure outlined there is to a large extent one of trial and error in regard to the size and location of the element in the output line. It is quite possible that a more straightforward method could be evolved if the broadbanding procedure were based on measurements of the complete equivalent circuit characteristics of the component at a number of frequencies in the desired band.

Instead of adding an element in the output line, as in the preceding method, the design parameters may be varied in such a way that the variation of impedance with frequency takes on a desirable form. It then becomes possible to add an impedance transformer in the input line, just as in the preceding case, which restores match at midband and gives, by virtue of the sensitivity of the effective length of the intervening line section to frequency, a broad bandwidth. Examples of this technique are to be found, in Sec. 6-6, applied to the crossbar transition between coaxial line and waveguide.

Although their applicability is restricted to certain simple problems, tapers form the basis of the most familiar of all broadbanding techniques. Use of tapers is made in the design of transitions between different sizes of coaxial lines, Sec. 6-1, and different sizes of waveguides, Sec. 6-3.

The final class of broadbanding techniques to be discussed is probably one of the most familiar; namely, the use of a properly chosen series of quarter-wavelength transformers. Slater¹ discusses this method of achieving broadband performance; an example is to be found in the coaxial-line phase shifter of Sec. 9-5.

Mode Purity and Resonances.—In some devices, additional considerations enter the picture to complicate the design problem and limit the freedom of variation of design parameters. For instance, in designing a transition from rectangular waveguide operating in the lowest or TE_{10} -mode to round waveguide operating in the second or TM_{01} -mode, the lowest or TE_{11} -mode may also be excited in the round guide. Particular care must be taken in providing design parameters which may be adjusted for minimum excitation of the unwanted lower mode. At the same time attention must be paid to the impedance match, for there may be a conflict between the two considerations when adjusting the design parameters. This conflict may be dealt with in the manner illustrated by the discussion of Sec. 6-4.

When the round waveguides of two such transitions are joined to form a rotary joint, an additional complication arises. Even though the excitation of the unwanted mode may be exceedingly small, certain over-all lengths of round waveguide lead to trouble because of resonance in that

¹ J. C. Slater, *Microwave Transmission*, McGraw-Hill, New York, 1942, pp. 57-62.

mode. The resonant wavelength depends in a rather complicated way on the angle as the rotary joint turns. A thorough discussion of this resonance problem is given in Secs. 7-10 to 7-16.

Even though a round waveguide may be too small for any propagation except in the lowest mode, there still remains the possibility of the existence of either of two perpendicular polarizations. It is this ambiguity about polarization which makes round waveguide unsuitable for most transmission-line applications; however, use is made of this property in the rotary joint using circular polarization, Sec. 7-17. In this application, care must be taken to excite a circular polarization, rather than elliptical; such care presents a design problem closely analogous to that of mode purity in the design of transitions to TM_{01} -mode. There arises, similarly, the problem of avoiding resonances in the round waveguide; this topic is discussed in Sec. 7-18. Similar problems, in connection with a rotary joint using a device which rotates the plane of polarization, are discussed in Sec. 7-19.

2-17. Series Branches and Choke or Capacity Coupling.—Frequently the coupling of two sections of transmission lines is desired under circum-

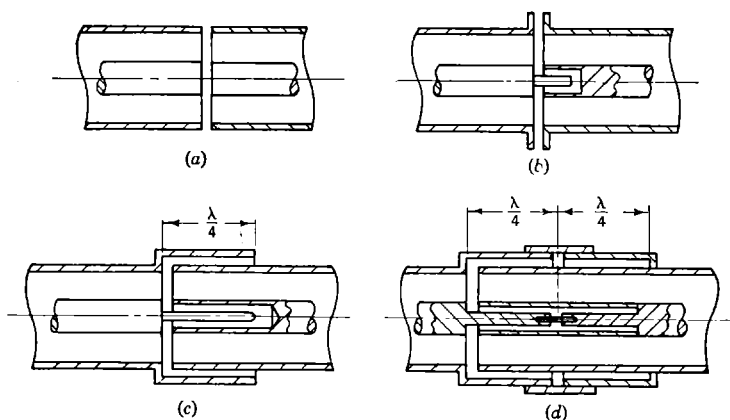


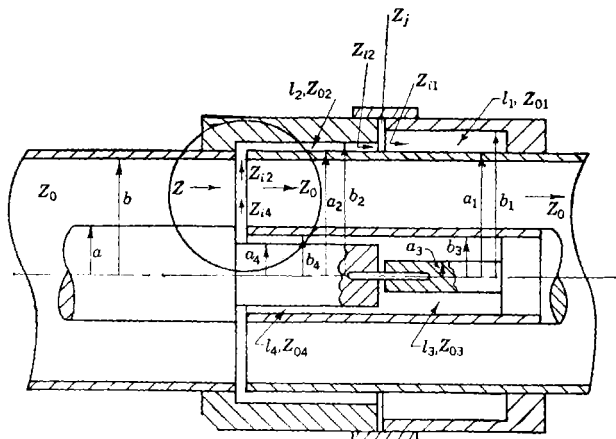
FIG. 2-50.—Evolution of capacity or choke coupling for coaxial line.

stances that make the attainment of good metallic contact rather difficult. This requirement is encountered in the design of many components for both coaxial lines and waveguides. The following examples, described in later chapters, are typical: waveguide couplings, Chap. 4; rotary joints and other types of motional joints, both in coaxial lines and in waveguides, Chap. 7; switches, short-circuiting plungers, and phase shifters, Chap. 8.

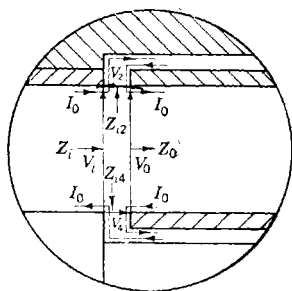
Since this problem is of such common occurrence, it seems advisable to describe in some detail the most usual method of solving it. In doing so, many of the transmission-line and impedance-transformation equations

developed previously will be used; thus the discussion will give an illustration of the use of these equations, as well as results which are themselves useful in many practical problems.

The problem proposed is usually solved by what is frequently, though somewhat inaccurately, termed "capacity coupling" or "choke coupling."



(a)



(b)

Fig. 2-51.—Series-branching lines forming choke or capacitive coupling. An enlargement of the encircled portion of (a) is shown in (b).

One simple form of this circuit is illustrated by Fig. 2-50, where it is obvious that the term "series-branching lines" is appropriate. Its evolution from true "capacity" couplings and improvement by the addition of another section of line acting as a "choke" is indicated by the series of sketches of Fig. 2-50.

The performance of such a circuit may be analyzed by means of the simple line theory which we have developed in the preceding sections.

Referring to Fig. 2-51, it is evident that the branch lines communicating with the gaps in both inner and outer conductors will be excited by radio-frequency energy, since the main-line current is interrupted by them. Assuming the gaps in inner and outer conductors to be small compared with a wavelength, we may write (see Fig. 2-51)

$$V_i = V_0 + V_2 + V_4. \quad (214)$$

Dividing through by I_0 , which is common to all branches, we obtain the series-impedance relation

$$Z_i = Z_0 + Z_{i2} + Z_{i4}. \quad (215)$$

The main line is assumed to be terminated in its characteristic impedance Z_0 . It is evident that if Z_{i2} and Z_{i4} , the input impedances of the branch lines, can be made very small compared to Z_0 , the gaps will not present an appreciable mismatch to waves transmitted along the main line. This will be the case if the branch lines are each made a half wavelength long, since the input impedance for a half-wavelength line terminated in a short circuit is zero, neglecting losses. Furthermore, in such a line section, the current is high at the short circuit, zero at a point a quarter wavelength away, and high again (equal to I_0) at the half-wavelength point. If the break in the branch lines is made at the quarter-wavelength point, it will not be necessary to provide good contact since no current is flowing at that point.

It is obvious that these conditions will prevail, for a given circuit, only at one particular wavelength; the question then arises as to its performance at other wavelengths. This performance, of course, depends on such geometrical factors as the radii, a_1, b_1, a_2, b_2 of the branch lines. It is also natural to be somewhat apprehensive as to how the breakdown-power limitation of the branch lines compares with that of the main line. These questions will now be investigated.

Impedance Relations.—The relations for the outer-branch line of Fig. 2-51 will be derived first. Beginning at the short-circuited (right-hand) end, and working back to the gap in the main line, we have

$$Z_{i1} = jZ_{01} \tan \theta_1, \quad (216)$$

where $\theta_1 = 2\pi l_1/\lambda$ and line losses are neglected. The length l is chosen equal to a quarter of the midband wavelength λ_0 , so that

$$\theta_1 = \frac{\pi}{2} \frac{\lambda_0}{\lambda}. \quad (217)$$

At or near midband, $\tan \theta_1$ will be very large—infinite at midband, and about six for a wavelength 10 per cent either side of midband. If the junction impedance Z_j (contact resistance, radiation resistance if an open junction, and other discontinuity effects) is kept less than, or comparable

to, the characteristic impedance Z_{01} , it may be neglected compared with Z_{i1} . This suggests the desirability of making Z_{01} as high as possible, which is desirable for other reasons as well. Neglecting Z_j , then, the impedance terminating the next section of line is

$$Z_{i2} = Z_{i1} = jZ_{01} \tan \theta_1, \quad (218)$$

which transforms [by Eq. (40)] to

$$\begin{aligned} Z_{i2} &= Z_{02} \frac{Z_{i2} + jZ_{02} \tan \theta_2}{Z_{02} + jZ_{i2} \tan \theta_2} \\ &= jZ_{02} \frac{Z_{01} \tan \theta_1 + Z_{02} \tan \theta_2}{Z_{02} - Z_{01} \tan \theta_1 \tan \theta_2}. \end{aligned} \quad (219)$$

Normalizing in terms of the main-line impedance Z_0 and rearranging, we obtain

$$\frac{Z_{i2}}{Z_0} = -j \left(\frac{Z_{02}}{Z_0} \right) \cot \theta_2 \frac{1 + \frac{Z_{02} \cot \theta_1}{Z_{01} \cot \theta_2}}{1 - \frac{Z_{02}^2 \cot \theta_1 \cot \theta_2}{Z_{01}^2}}. \quad (220)$$

If we make $l_1 = l_2 = \lambda_0/4$, we may write, as in Eq. (217),

$$\theta_1 = \theta_2 = \theta = \frac{\pi \lambda_0}{2 \lambda}. \quad (221)$$

Ordinarily, $Z_{02}/Z_{01} \leq \frac{1}{2}$ and near midband $\cot \theta \ll 1$; therefore we may neglect $\frac{Z_{02}}{Z_{01}} \cot \theta_1 \cot \theta_2$, compared to unity, in the denominator. In addition, near midband, $\cot \theta$ is well approximated by

$$\cot \theta = \tan \left(\frac{\pi}{2} - \theta \right) \approx \left(\frac{\pi \Delta \lambda}{2 \lambda} \right), \quad (222)$$

where $\Delta \lambda$ is defined by $\Delta \lambda = \lambda - \lambda_0$. Equation (220) may be approximated by

$$\frac{Z_{i2}}{Z_0} \approx j \left(\frac{Z_{02}}{Z_0} \right) \left(\frac{\pi \Delta \lambda}{2 \lambda} \right) \left(1 + \frac{Z_{02}}{Z_{01}} \right). \quad (223)$$

These approximations lead to a result which is slightly larger than that of Eq. (220), but the error is less than 5 per cent for $0.80 < \lambda/\lambda_0 < 1.33$ provided $Z_{02}/Z_{01} \leq \frac{1}{2}$. It rises to 15 per cent over the same wavelength range if $Z_{02}/Z_{01} = 1$. Since the losses have been neglected, the impedance Z_{i2} is naturally purely reactive. The normalized reactance, referred to Z_0 of the main line, is

$$X'_{i2} = \frac{X_{i2}}{Z_0} \approx - \left(\frac{Z_{02}}{Z_0} \right) \left(\frac{\pi \Delta \lambda}{2 \lambda} \right) \left(1 + \frac{Z_{02}}{Z_{01}} \right). \quad (224)$$

In the case of the coaxial-line example of Fig. 2-51, a similar analysis of the line within the center conductor leads to

$$X'_{i4} \approx - \left(\frac{Z_{04}}{Z_0} \right) \left(\frac{\pi \Delta\lambda}{2 \lambda} \right) \left(1 + \frac{Z_{04}}{Z_{03}} \right). \quad (225)$$

The input impedance is then given by

$$Z' = 1 + j(X'_{i2} + X'_{i4}). \quad (226)$$

Since the branch lines present reactances of the same sign, their contributions to the over-all mismatch of the circuit are, roughly speaking, additive. They may be made approximately subtractive by spacing the gaps in outer and inner conductors a quarter of a midband wavelength apart. Such an arrangement, combined with a reversal of the orientation of the center-conductor branch which may be desirable mechanically, is shown

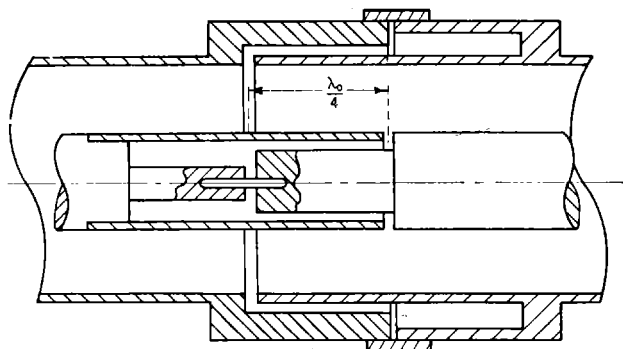


FIG. 2-52.—Alternative arrangement of Fig. 2-51 providing broader bandwidth.

in Fig. 2-52. The outer-branch line and inner-branch lines are now each in series with the main line at different points. The VSWR which each separately would introduce into a matched line may then be calculated from Eq. (7c) of Table 2-2:

$$\left. \begin{aligned} \frac{r_2 - 1}{\sqrt{r_2}} &= |X_{i2}| \\ \frac{r_4 - 1}{\sqrt{r_4}} &= |X_{i4}| \end{aligned} \right\} \quad (227)$$

For small values of r , the mismatch, which we shall define as $(r - 1)$, is approximately equal to $|X|$. Thus, the mismatch introduced by the outer-conductor branch line is given approximately, using Eqs. (224) and (227), by

$$r_2 - 1 \approx \left(\frac{Z_{02}}{Z_0} \right) \left(\frac{\pi |\Delta\lambda|}{2 \lambda} \right) \left(1 + \frac{Z_{02}}{Z_{01}} \right). \quad (228)$$

Neglecting \sqrt{r} in Eq. (227) leads to an estimate of the mismatch which is too low, but the error is less than 10 per cent for $r < 1.2$. This error is opposite in sign to the errors made in the approximations leading to Eq. (224), so that Eq. (228) is actually a rather good approximation (that is, in error by less than 10 per cent) for $r_2 \leq 1.2$, $|\Delta\lambda/\lambda| \leq .25$ and

$$\frac{Z_{02}}{Z_{01}} \leq 1.$$

It will be noted that the mismatch is proportional to: (a) Z_{02}/Z_0 , (b) $(|\Delta\lambda|/\lambda)$, and (c) $(1 + Z_{02}/Z_{01})$. Therefore, to maintain the lowest possible mismatch over a band of wavelengths about λ_0 , it is desirable, in view of (a), to make Z_{02} as small as possible compared with Z_0 . In view of (c) it is desirable to make Z_{01} as large as possible compared with Z_{02} ; the desirability of making Z_{01} large, for another reason, was pointed out in the discussion leading to Eq. (218).

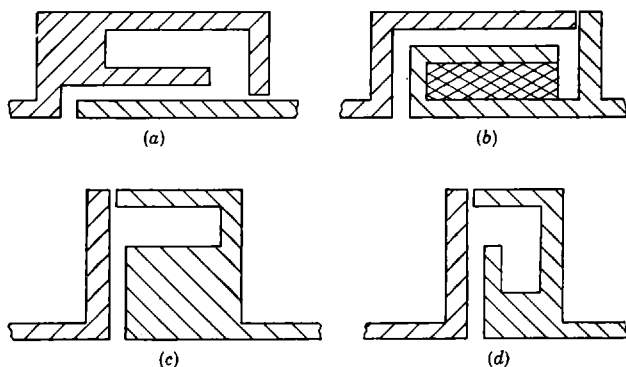


FIG. 2-53.—Variations in outer conductor of branch lines. In each case, the actual circuit is a figure of revolution generated by rotation about a horizontal axis to be imagined to exist below the figure.

A number of alternative physical arrangements of branch lines for the outer conductor of coaxial lines is shown in Fig. 2-53. The center-conductor branch line is pretty closely restricted, because of physical considerations, to the two forms *c* and *d* of Fig. 2-50. The arrangement of Fig. 2-53*a* is the one most frequently used in coaxial rotary joints since it is fairly economical of space, both radially and axially, and involves no dielectric.

For those arrangements which include radial sections of transmission line, the simple equations given are not accurate. Radial lines require a special treatment which will not be given here. Curves giving the radial dimensions of effective quarter-wavelength lines are given in Figs. 4-46 and 4-47 and may be used in design work. In estimating wavelength

sensitivity the results given here for coaxial branch lines should give a fairly good approximation. The characteristic impedance of a radial line is fairly well approximated by considering the radial line to be roughly equivalent to a coaxial line whose cylindrical conductors are separated by the same distance as are the plates of the radial line, and whose mean radius is equal to the mean radius of the section of radial line. Thus close spacing between conductors leads to a low characteristic impedance, wide spacing to a high characteristic impedance.

As an example of the use of Eq. (228), the frequency sensitivity of the preferred type of coaxial rotary joint for standard $\frac{1}{8}$ -in. coaxial line (see Fig. 7-4) may be calculated. The outer branch line has the form of Fig. 2-53a, the inner that of Fig. 2-51a. The constants are given in Table 2-3.

TABLE 2-3.—CHARACTERISTICS OF $\frac{1}{8}$ -IN. COAXIAL-LINE ROTARY JOINT, FIG. 7-4
All impedances in ohms

Line	Z_0	Z_{01}, Z_{03}	Z_{02}, Z_{04}	$\frac{Z_{02}, Z_{04}}{Z_0}, \frac{Z_{04}}{Z_0}$	$\frac{Z_{02}, Z_{04}}{Z_{01}}, \frac{Z_{04}}{Z_{03}}$
Outer	46.6	13.4	4.2	0.090	0.31
Inner	46.6	28	13.4	0.29	0.48

The values of mismatch which would be caused by each branch separately are

$$r_2 - 1 \approx (0.090) \left(\frac{\pi}{2} \frac{|\Delta\lambda|}{\lambda} \right) (1.31) \approx 0.19 \frac{|\Delta\lambda|}{\lambda}, \quad (229)$$

$$r_4 - 1 \approx (0.29) \left(\frac{\pi}{2} \frac{|\Delta\lambda|}{\lambda} \right) (1.48) \approx 0.97 \frac{|\Delta\lambda|}{\lambda}. \quad (230)$$

In the actual design the gaps were, for economy of space, at the same point in the line (see Fig. 2-51). Hence the actual mismatch was approximately the sum of these, namely,

$$r_s - 1 \approx (0.97 + 0.19) \frac{|\Delta\lambda|}{\lambda} \approx 1.16 \frac{|\Delta\lambda|}{\lambda}. \quad (231)$$

If they were separated by a quarter wavelength, (see Fig. 2-52), the mismatch would be approximately their difference,

$$r_d - 1 \approx (0.97 - 0.19) \frac{|\Delta\lambda|}{\lambda} \approx 0.78 \frac{|\Delta\lambda|}{\lambda}. \quad (232)$$

These results are plotted graphically, over a range of wavelengths, in Fig. 2-54.

Breakdown.—One would expect to find that the small clearances and small diameters occurring in these branch lines lead to a serious decrease

in the power-handling capacity of the coaxial line. On examination it is discovered that the small diameters of the inner conductor branch d_0 lead to such a reduction, but it is found that the smallness of the clearances *does not* lead to high electric fields, since the total voltage across the gap goes down quickly enough, as the gap is decreased, to avoid trouble.

Referring to the center-conductor branch of Fig. 2-51, we may demonstrate this point. The highest voltage in this branch occurs across the line where the center conductor changes diameter. The branch is excited by the current of amplitude I_0 where it joins the main line, at the left end of Line 4. Let us first consider the situation at midband, where Line 4 is exactly a quarter wavelength long. The voltage at the right end of Line 4 has the amplitude

$$V_4 = I_0 Z_{04} = I_0 60 \ln \frac{b_4}{a_4}. \quad (233)$$

The amplitude of the maximum electric field E_4 , at the center conductor, is related to the voltage amplitude by

$$V_4 = \int_{a_4}^{b_4} \frac{E_4 a_4}{r} dr = E_4 a_4 \ln \frac{b_4}{a_4}. \quad (234)$$

Equating Eqs. (233) and (234), we obtain

$$E_4 = \frac{60 I_0}{a_4}. \quad (235)$$

In the main line, the maximum field, at the center conductor of radius a , is found by the same method to be

$$E_a = \frac{60 I_0}{a}. \quad (236)$$

Therefore, the maximum field in Line 4 is larger than that of the main line by the factor

$$\frac{E_4}{E_a} = \frac{a}{a_4}. \quad (237)$$

That is, the field in the branch line is larger than that of the main line by exactly the same factor as that relating the inner conductors of the respec-

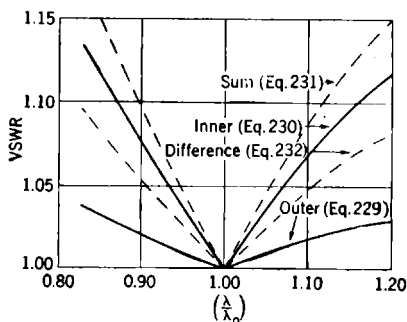


FIG. 2-54.—Performance of coaxial-line rotary joint of Table 2-3.

tive coaxial line. To avoid breakdown in Line 4, the fields in the main line must be lowered from their break down value by this factor. Since the power being transmitted varies as the square of the fields, the power reduction factor caused by the smaller diameter in the branch line is

$$\frac{\text{Power with branch}}{\text{Power without}} = \left(\frac{a_4}{a}\right)^2. \quad (238)$$

Of course, the same voltage V_4 appears also across the left end of Line 3, but it is very unlikely that the electric field at the conductor of radius a_3 would exceed that at a_4 . For a given outer-conductor diameter ($b_3 = b_4$) a line whose diameter ratio is 2.72 ($Z_0 = 60$ ohms) gives minimum electric field for a given applied voltage. In practice both lines have diameter ratios considerably smaller than this, and that of Line 3 is nearer to the optimum value.

Equations (237) and (238) are exact mathematically, but we have neglected the effect of the discontinuity in conductor diameter in passing from Line 3 to Line 4. In order to avoid increased fields in this region, the ends of the center conductors should be rounded with radii of curvature no less than their respective cylindrical radii.

Applying the same equations to the outer branch Lines 1 and 2, one finds that the minimum field occurs at the right end of Line 2 and is given by

$$\frac{E_2}{E_0} = \frac{a}{a_2}. \quad (239)$$

Since this gives E_2 less than E_0 , no difficulty from breakdown in the outer branch is to be expected. It is, of course, advisable to avoid sharp edges where Lines 1 and 2 join.

The preceding discussion is accurate only for midband conditions. However, changing the wavelength by a considerable amount does not alter the conclusions appreciably, since the feeding current and maximum voltage are at the crests of distributions varying sinusoidally along the line.

The $\frac{7}{8}$ -in. coaxial-line rotary joint of Table 2-3 has $a = 0.187$ in. and $a_4 = 0.125$ in.; therefore the power-reduction factor is, for this capacity coupling, 0.44.

Contact and Radiation Losses.—In Eq. (218) the junction impedance Z_j was neglected entirely compared with the input impedance of Line 1. If we assume that the junction presents a small resistive impedance R , because of contact or radiation effects, we have, instead of Eq. (218),

$$Z_{i2} = R + jZ_{01} \tan \theta_1. \quad (240)$$

When the succeeding steps are carried through and small quantities neglected, as before, in the final result, it is found that the reactance is that

given by Eq. (224), but that there now appears a resistive component of input impedance given by

$$R_{i2} = R \left(\frac{Z_{02}}{Z_{01}} \right)^2 \left(\frac{\pi \Delta\lambda}{2\lambda} \right)^2. \quad (241)$$

It has been assumed, in making the simplifying approximations in the final result, that R^2 may be neglected as compared with $Z_{01}^2 \tan^2 \theta_1$. Thus the result is valid only if this is the case.

The main-line current I_0 flows in this input resistance; hence the power dissipated with a resistance R present in the branch line is

$$P_z = \frac{1}{2} I_0^2 R_{i2} = \frac{1}{2} I_0^2 R \left(\frac{Z_{02}}{Z_{01}} \right)^2 \left(\frac{\pi \Delta\lambda}{2\lambda} \right)^2. \quad (242)$$

Had the resistance R appeared directly in series with the outer conductor, rather than in a branch line, the power dissipated in it would be

$$P = \frac{1}{2} I_0^2 R. \quad (243)$$

Therefore, the power dissipated in the resistance R is decreased, by the branch-line arrangement, by the factor

$$\frac{P_z}{P} = \left(\frac{Z_{02}}{Z_{01}} \right)^2 \left(\frac{\pi \Delta\lambda}{2\lambda} \right)^2. \quad (244)$$

For practical capacity-coupling (or choke-coupling) circuits this factor represents a tremendous benefit. Taking the coaxial circuit whose characteristics are given in Table 2-3 and a value of $\Delta\lambda/\lambda$ of 0.25, the loss-reduction factor is 0.015 for the outer conductor and 0.036 for the inner.

Incidentally, it should be pointed out that the ratio Z_{02}/Z_{01} comes in squared in the loss-reduction calculation, again indicating in no uncertain terms the advantage of making Z_{01} large compared to Z_{02} .

Extension to Waveguides.—The principles and equations developed for coaxial lines may be carried over, with suitable modifications, to waveguide capacity or choke couplings. The problem of providing such couplings for round waveguide operating in the TM_{01} -mode is an exceedingly simple one. Since this mode is a symmetrical one, the current flow in the waveguide wall is of uniform density, just as in a coaxial line; the branch line is excited in exactly the same manner as if it were connected to the outer conductor of a coaxial line. Any of the forms of outer-conductor branch line used for coaxial line may be used for the TM_{01} -mode in round waveguide. This mode is widely used in waveguide rotary joints, and such couplings are quite common. All the equations previously developed carry over exactly, provided the main-line characteristic

impedance Z_0 is correctly chosen to suit the waveguide mode. This impedance is that associated with radial voltage and total current; namely,

$$Z_0 = 48 \sqrt{1 - \left(\frac{\lambda}{\lambda_c}\right)^2}. \quad (245)$$

That this is the proper impedance to use may be seen by referring to Fig. 2-55 and noting the fact that

$$V_i = V_0 + V_{i2}, \quad (246)$$

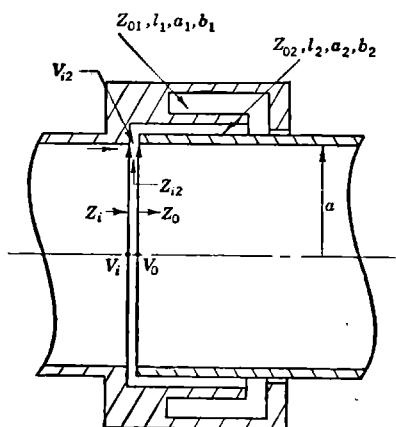


FIG. 2-55.—Branch-line coupling for round waveguide carrying TM_{01} -mode.

where V_0 and V_i are the integrated values of the radial field E_r taken from the center, where $E_r = 0$, to the inner surface of the waveguide, and V_{i2} is the voltage across the coaxial branch line excited by the current I_0 . Dividing Eq. (246) by the common current I_0 , one obtains the impedance relation

$$Z_i = Z_0 + Z_{i2}, \quad (247)$$

where it is clear that the characteristic impedance used in the waveguide is that defined by

$$Z_0 = \frac{V_0}{I_0}. \quad (248)$$

As an example of the application of these and previously derived formulas, Fig. 2-56 gives the performance curve calculated for the typical 3-cm band TM_{01} -coupling whose characteristics are listed in Table 2-4.

TABLE 2-4.—CHARACTERISTICS OF A TM_{01} -CAPACITY COUPLING* DESIGNED FOR $\lambda_0 = 3.33$ CM

a	λ_c	Z_{01}	Z_{02}
0.576-in.	3.83 cm	8.1 ohms	3.1 ohms

* See Fig. 2-56.

A comparison of Fig. 2-56 with Fig. 2-54 shows that the waveguide coupling is somewhat more frequency-sensitive than the outer-conductor branch coupling, but not as frequency-sensitive as the inner. The waveguide coupling is restricted by the cutoff wavelength of the TM_{01} -mode on the long-wave side of midband, and trouble occurs because of the

possibility of propagation of the next higher mode on the shorter-wavelength side of midband. The region of wavelengths shown in Fig. 2-56 is about all that is practical in view of these limitations.

Round waveguides operating in the lowest or TE_{11} -mode may be coupled in the same manner, but the branch lines are then asymmetrically

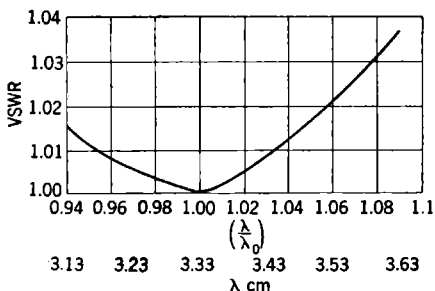


Fig. 2-56.—Performance of TM_{01} -coupling (see Fig. 2-55 and Table 2-4).

excited by the waveguide currents. Branch lines with coaxial geometry will be excited in the second coaxial mode, so the phase constant associated with them is no longer simply that of transverse electromagnetic wave but rather that of a mode with cutoff characteristics (see Fig. 2-22).

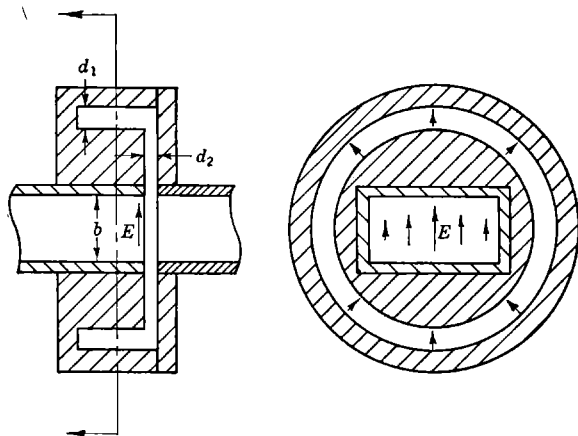


Fig. 2-57.—Capacitive or choke coupling for rectangular waveguide.

Similarly, radial sections will be excited in the second radial mode, for which design curves are given in Fig. 4-46.

Although these complications make more difficult the quantitative analysis of the behavior of the capacity-coupling circuit, the principles to be observed for low mismatch over a broad band of wavelengths are still

the same. That is, the Line Section 2, next to the main line, should have a low characteristic impedance or closely spaced conducting surfaces, but Section 1 should have a higher characteristic impedance or more widely separated conducting surfaces.

Rectangular waveguides transmitting the lowest or TE_{10} -mode have a field structure and current distribution rather like that of the lowest mode in round waveguide, just discussed. The various forms of capacity coupling shown for coaxial lines should, with suitable modifications, be applicable to rectangular waveguides in somewhat the same way in which they were applied to round waveguide. The form most frequently used is that of Fig. 2-57, the design of which is discussed in considerable detail in Sec. 4-9. Alternative types of capacity-coupling circuits devised

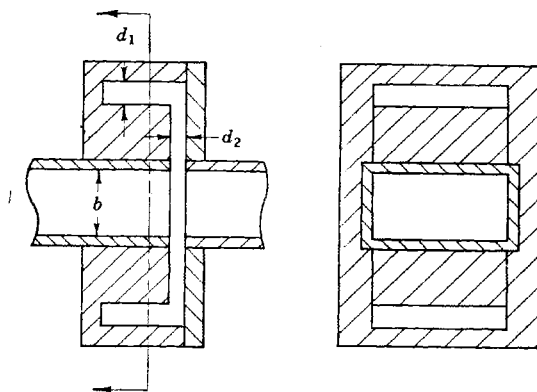


FIG. 2-58.—Simple branch circuit approximately equivalent to Fig. 2-57.

especially for use with rectangular waveguides are discussed there, also. The simple branch circuit of Fig. 2-58 is approximately equivalent to the common coupling of Fig. 2-57. The two grooves of height d_1 of the former have been widened, bent into semicircular form, and joined to form the circular groove of the latter. The simple coupling would not be expected to be an effective capacity-coupling circuit, however, since the currents flowing in the side walls of the waveguide branch line of height d_2 are large and must flow through contacting surfaces. Neglecting this fact, the mismatch introduced by such a circuit may be calculated by modifying slightly the coaxial-line equations. It is merely necessary to change λ to λ_g and $\Delta\lambda$ to $\Delta\lambda_g$ in Eq. (228) to obtain the mismatch due to one of the two series branches. Since there are two equal branches, the total mismatch is twice this value. The characteristic impedances are, since all branch lines have the same width as the main waveguide, simply proportional to the respective waveguide heights b , d_1 , and d_2 , [see Eq. (158)]. Equation (228) then becomes, for the complete coupling,

$$r - 1 \approx 2 \left(\frac{d_2}{b} \right) \left(\frac{\pi \Delta \lambda_g}{2 \lambda_g} \right) \left(1 + \frac{d_2}{d_1} \right). \quad (249)$$

Although there is a considerable difference between this coupling and the common coupling of Fig. 2-57, enough similarity exists for this result to give a fair prediction of the performance of the capacitive coupling. A comparison is made in Fig. 2-59 between values of VSWR measured for two different choke couplings and the performance predicted by Eq. (249). It will be noted that, although the agreement is not bad, the mismatch of the actual circuit is consistently lower than that predicted by the formula, especially at longer wavelengths. It may be reasoned that this is due to the fact that the branch lines are effectively wider than the main line; hence, they have lower characteristic impedance and slower variation of λ_g than assumed in the formula. This would be especially noticeable at longer wavelengths, since the main line would approach cutoff long before the branch lines.

Since Eq. (249) gives fair agreement with measurements made on common couplings, one is encouraged to expect other equations, based on the simple coupling of Fig. 2-58, to do likewise. One would not expect to have breakdown trouble. The voltage amplitude in the main line of Fig. 2-58 is

$$V_0 = I_0 Z_0, \quad (250)$$

where I_0 is the longitudinal current in the main line and Z_0 is the appropriately defined characteristic impedance [$Z_{v,1} \propto$ waveguide height b , Eq. (158)]. The maximum voltage in Line 2 is, at midband,

$$V_2 = I_0 Z_{02}, \quad (251)$$

where Z_{02} is similarly defined and is proportional to d_2 . Dividing Eq. (251) by Eq. (250), one obtains

$$\frac{V_2}{V_0} = \frac{Z_{02}}{Z_0} = \frac{d_2}{b}. \quad (252)$$

Rearranging, one obtains

$$\frac{V_2}{d_2} = \frac{V_0}{b}, \quad (253)$$

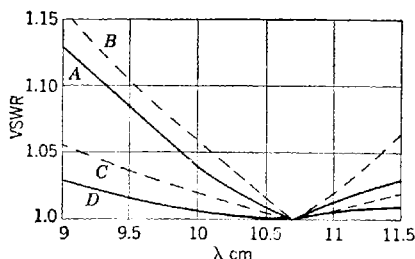


FIG. 2-59.—Performance of waveguide choke couplings of Fig. 2-57. For the two upper curves, $d_1 = 0.150''$ and $d_2 = 0.104''$. For the lower curves, $d_1 = 0.250''$, $d_2 = 0.050''$. Solid lines are experimental, dashed lines calculated by Eq. (249).

where the terms represent the maximum electric field amplitudes in the branch line and in the main line of the simple circuit. Since in the actual coupling the fields tend to fan out to fill the circular groove, it would be expected that breakdown is even less likely in the choke coupling than in the main line.

Similarly, Eq. (244) may be modified to give the loss-reduction factor for the simple circuit; namely,

$$\frac{P_2}{P} = \left(\frac{d_2}{d_1}\right)^2 \left(\frac{\pi}{2} \frac{\Delta\lambda_g}{\lambda_g}\right)^2. \quad (254)$$

For the worst wavelength, 9 cm, on the curves of Fig. 2-59, this factor is 0.18 for the older design, upper curves, and 0.015 for the improved version lower curves. Although the application of Eq. (254) to the actually used couplings is certainly not expected to give an accurate figure, it should serve as a rough estimate.

CHAPTER 3

MATERIALS AND CONSTRUCTION TECHNIQUES

BY RICHARD M. WALKER

The materials usually used in the design of microwave transmission circuits are good metallic conductors and low-loss dielectrics with dielectric constants between 2 and 4. Metallic conductors and miscellaneous parts are usually made of brass or copper, sometimes plated with a highly conductive metal if low attenuation is desired, and often protected against corrosion and fungus growth by lacquers or other finishes. Dielectric materials are used frequently for supporting center conductors in cables and coaxial lines, and for pressurizing waveguides and coaxial lines.

In this chapter, materials are considered from the standpoint of durability, strength, and electrical characteristics at microwave frequencies. Tables of materials and their characteristics presented here include only those materials that have been used successfully in microwave transmission systems and those that show promise for future applications. Construction techniques are discussed from the standpoint of tolerances, economy, and application to the construction of microwave transmission lines and components in the laboratory and in the factory.

METALLIC MATERIALS

3-1. Tubing for Coaxial Lines and Waveguides.—Brass is the most widely used metal for coaxial lines and waveguides because it is easily machined and soldered and has relatively low electrical loss. Rectangular and circular seamless brass tubing is available in many standard sizes that are quite adequate for general use in microwave transmission lines. Stainless-steel tubing is used in applications where attenuation is not a serious consideration. For good conductivity the tubing is plated with copper or silver, or made with a copper or silver lining.

For optimum performance at microwave frequencies, special care must be taken in the selection and fabrication of tubing. The conditions for optimum performance of a microwave transmission line are smooth wall surfaces, high conductivity in the metallic walls, and protection against corrosive atmospheres and fungus growth. Rough wall surfaces are objectionable for several reasons. Sharp burrs or edges on the wall surface considerably decrease the maximum peak power that a line can

handle without voltage breakdown. A rough wall surface also increases the effective resistance of the transmission line, and the attenuation per unit length of line is therefore increased. This increase in resistance can be explained in terms of the skin effect in a conductor at high frequencies. The effective skin depth δ is defined as the depth at which the current density is $1/e$ times the current density at the surface; it is given in meters by the formula¹

$$\delta = \sqrt{\frac{1}{\pi\sigma\mu c}} \sqrt{\lambda_0}, \quad (1)$$

where λ_0 is the free-space wavelength in meters, σ is the conductivity in mhos per meter, μ the permeability of the metal in henrys per meter, and c the velocity of light in meters per second. [See Eq. (2-78).] From Eq. (1) it is seen that, for a given wavelength, δ is inversely proportional to the square root of the conductivity of the metal. For copper, the value of δ at 10-cm free-space wavelength is 1.2×10^{-4} cm or 4.7×10^{-5} in.

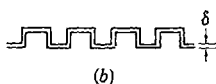
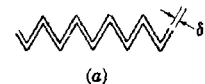


FIG. 3-1.—Corrugated wall surfaces.

The attenuation per unit length of line is increased if the wall surfaces are scratched or corrugated as shown in Fig. 3-1. The increase in attenuation is believed to be caused by two effects: (1) the effective length of the conductor, which is a section of the wall surface of thickness δ , is increased; (2) the concentration of currents at the edges of each corrugation increases the effective resistance of the skin. The contribution of the increased effective length can be calculated for known configurations in the corrugated surface.

The effective length for the triangular grooves of Fig. 3-1a is twice the actual length of the line, if the triangle is equilateral, for any depth of groove. Similarly, for square grooves or corrugations, as shown in Fig. 3-1b, the effective length of the line is also twice the actual length of line.

An example of one form of the square type of corrugation is the flexible waveguide known as "Titeflex" (see Secs. 5-14 and 5-15). Measurements made at Radiation Laboratory on six samples of Titeflex flexible waveguide showed that the attenuation is 3.2 to 3.6 times the calculated value for smooth wall surfaces. The samples of 1.5- by 3-in. Titeflex were 2 ft long and the corrugations were 0.060 in. square. Four samples were silver-plated 70-30 brass and the other two were unplated 70-30 brass. Measurements at 10.4 cm showed an average loss of 0.069 db/m in the silver-plated samples and of 0.127 db/m in the unplated samples. Comparison of these values with the calculated loss of 0.019 db/m for silver waveguides and of 0.040 db/m for 70-30 brass waveguides with smooth

¹ J. C. Slater, *Microwave Transmission*, McGraw-Hill, New York, 1942, p. 114.

walls, shows that the actual loss is respectively 3.6 and 3.2 times the calculated losses. The results indicate that there are losses other than those caused by the increased length of line. These losses may result from the concentration of currents at the edges of the corrugations.

There is evidence that the added loss caused by surface imperfections such as oxide films and die marks is also a function of the wavelength. This result is to be expected since such surface imperfections become comparable in dimensions to the skin thickness as the wavelength decreases. Loss measurements on commercially drawn tubing at 3 cm agree with theoretical calculations within an estimated experimental error of ± 5 per cent. Similar measurements at 1.25 cm gave results that were 10 to 20 per cent higher than the theoretical loss values,¹ and at 0.54 cm the loss was about 50 per cent higher than the theoretical values.² The above measurements were made in waveguide of dimensions 0.400- by 0.900-in. ID, 0.170- by 0.420-in. ID, and 0.086- by 0.180-in. ID, respectively. It seems probable that the increased attenuation is caused by surface irregularities of some nature. These irregularities must be numerous and submicroscopic in size. Further investigation of these effects is particularly desirable. It is extremely likely, however, that the over-all attenuation of a transmission system may be seriously increased by rough wall surfaces in applications where long lengths of line are used, especially at the lower wavelengths.

In the manufacturing process, round seamless tubing is drawn from a flat sheet into a series of cylindrical cups by means of a conventional hydraulic press that presses the metal into successive dies. Each die reduces the diameter of the tubing and increases its length until the length of the deep-drawn tubing reaches the limit of the press. The operation is then continued on a draw table, on which the tubing is drawn horizontally through a die and over a sizing plug until the proper diameter is reached. Annealing is usually required after each drawing operation because the metal becomes work-hardened. Dies for drawing rectangular tubing are made by accurately ground and fitted rollers. Rectangular tubing is drawn from circular tubing. Silver-lined tubing is made in the same manner. The flat sheet, however, is made by silver-soldering a plate of silver to a block of the base metal desired. This block is then rolled into a flat sheet. The ratio of the thickness of silver to that of the base metal remains constant throughout the process.

3-2. Dimensional Tolerances.—The dimensional tolerances of the tubing depend on the accuracy of the die and plug, and the finish depends on the finish of the die and plug. Best finishes are produced by use of a

¹ E. Maxwell, "Conductivity Loss Measurements at K-band," RL Report No. 854, Jan. 15, 1946.

² E. R. Beringer, unpublished data.

die-and-plug combination of very hard steel that has been highly polished and plated with chromium. Tolerances in drawn tubing are limited by the wear permitted on the die and plug before they are replaced. The die is usually made to the minimum diameter within the specified tolerance and allowed to wear until it reaches the maximum allowable diameter. Commercial tolerances to be expected on the inside or outside of round and rectangular standard tubing are given in Table 3-1. The table also shows the maximum standing-wave voltage ratio, at the given wavelength, that will result from joining two pieces of tubing with the maximum tolerance in opposite directions. The VSWR introduced by a junction between two waveguides of different inside dimensions is approximately equal to the ratio of the impedances of the two lines and is given by Eq. (2-160), which may be written

$$r = \frac{\lambda_g a' b}{\lambda_g' a b'} \quad (2)$$

TABLE 3-1.—COMMERCIAL TOLERANCES IN ROUND AND RECTANGULAR TUBING
Coaxial lines

Outer conductor diameter OD, in.	Wall thickness, in.	Inner conductor diameter OD, in.	Tolerance outer cond. ID, in.	Tolerance inner cond. OD, in.	Maximum VSWR at joint,* in.
$\frac{5}{16}$	0.025	0.125	± 0.002	± 0.002	1.065
$\frac{1}{2}$	0.032	0.1875	± 0.002	± 0.002	1.036
$\frac{5}{8}$	0.035	0.250	± 0.0025	± 0.002	1.035
$\frac{7}{8}$	0.032	0.375	± 0.0025	± 0.002	1.025
$1\frac{1}{4}$	0.049	0.500	± 0.003	± 0.002	1.020
$1\frac{5}{8}$	0.049	0.625	± 0.003	± 0.0025	1.012

Rectangular tubing

Tube size, in.	Wall thickness, in.	OD or ID tolerance, in.	Wall tolerance, in.	Maximum radius on inside corners, in.	Maximum VSWR at joint*	λ_0 , cm
3.0 × 1.5 OD	0.080	± 0.005	± 0.005	0.016	1.012	10.4
2.75 × 0.375 ID	0.049	± 0.005	± 0.005	0.016	1.032	10.4
1.25 × 0.625 OD	0.064	± 0.004	± 0.004	0.030	1.016	3.3
1.0 × 0.5 OD	0.050	± 0.002	± 0.0035	0.030	1.018	3.3
0.5 × 0.25 OD	0.040	± 0.002	± 0.003	0.010	1.040	1.25

* The VSWR given in this column was calculated for the given wavelength assuming two tubes were joined giving the greatest possible mismatch within the above tolerances. Shunt capacity is negligible in all cases.

where a and b are respectively the wide and narrow inside cross-sectional dimensions of one waveguide, and a' and b' the corresponding dimensions

of the other waveguide; λ_0 and λ'_0 are the guide wavelengths. The reactance at a step of this order of magnitude is negligible in comparison with the resistive mismatch. From the formula, we see that the mismatch is at a maximum when a'/a and b/b' are maximum—that is, when one waveguide is larger than the other in the a dimension but smaller in the b dimension. Steps in coaxial lines may cause mismatches that are more reactive than resistive, or vice versa, depending on whether the steps on the outer and center conductors are in the same direction or opposite directions, respectively. The values given are for steps in the opposite direction on the two conductors, in which case the mismatch is due mainly to the change in characteristic impedance. For complete analysis of the problem of discontinuities in coaxial lines, reference should be made to Sec. 4-6. From Table 3-1 it is seen that the mismatch introduced by junction steps in tubing is not excessive. Care must be taken to remove burrs from junctions to prevent voltage breakdown.

Brass waveguides and tubing of special sizes for coaxial lines are sometimes needed in the laboratory and in product on. The manufacture of such tubing requires a new set of dies and sizing plugs for large-scale production. When only a few pieces of tubing are needed, the cost of retooling is often too expensive and requires too much time. In such cases the drawing process may be speeded up by using coin silver, which can be drawn more easily. The dies and plugs for drawing coin silver need not be hardened or chromium-plated.

Tubing for coaxial lines of special sizes may be made in short lengths in the laboratory shop by turning on a lathe or by reaming out undersize tubing. Waveguides of special sizes may be made by casting two halves and milling the inside to the correct dimensions, or by cutting down oversize waveguide. In either case, the break should come in the center of the broad side of the waveguide to minimize current flow across the junction. The two halves may be adequately held together by clamps, or soldered. Care must be taken in soldering to avoid warping of the metal.

3-3. Miscellaneous Metallic Parts.—Special applications require the use of metals other than brass because of their thermal expansion coefficients, elasticity, sliding friction, and other properties. An iron-nickel-cobalt alloy containing 54, 28, and 18 per cent of the metals respectively is widely used in making seals to glass for pressurizing lines because its expansion coefficient is the same as that of Corning Glass Nos. 704, 705, 7052, and 706 (see Sec. 4-19). This alloy is designated by the trade names Kovar and Fernico. Phosphor bronze, beryllium copper, and chromium copper are used in making sliding contacts, such as bullets in coaxial lines (see Sec. 4-2), and movable plungers for coaxial lines (see Sec. 8-3). These alloys are desirable for sliding-contact applications because they have good elasticity and good electrical conductivity. Anaconda Beryl-

TABLE 3-2.—CONDUCTIVITY AND ATTENUATION OF METALS AND ALLOYS
 Values given for 20°C

Metal	Conductivity, mhos/meter	Relative attenuation	Waveguide attenuation, db/meter*
Copper, pure.....	5.8005×10^7	1.00	0.117
Aluminums			
Pure.....	3.475	1.29	0.151
Si 0.29 %, Fe 0.14 %.....	3.475	1.29	0.151
Die-casting alloys.....	1.05-2.64	2.35-1.48	0.275-0.174
Brasses, annealed			
Cu 90 %.....	2.52	1.52	0.178
Cu 80 %.....	1.882	1.75	0.206
Cu 70 %.....	1.51	1.95	0.229
Cu 60 %.....	1.65	1.88	0.220
Brass, hard-drawn			
Cu 70 %.....	1.22	2.18	0.255
Bronze, phosphor.....	0.817-2.52	2.66-1.52	0.312-0.178
Coppers			
Be 2.15 %, Pb 0.35 %.....	0.983	2.43	0.285
Same, heat-treated.....	1.05-1.45	2.34-2.00	0.275-0.234
Cr 0.85 %, Si 0.10 %.....	2.32	1.58	0.185
Same, heat-treated.....	4.64	1.12	0.131
Chromium.....	2.23	1.61	0.189
Constantan.....	0.204	5.33	0.624
Gas carbon.....	0.002	54.00	6.320
Graphite.....	0.0125	21.60	2.530
Gold.....	4.10	1.19	0.139
Lead.....	0.454	3.58	0.418
Magnesium			
Pure.....	2.175	1.64	0.192
Dow M.....	1.525-2.00	1.95-1.70	0.229-0.200
Other alloys.....	0.558-1.00	3.20-2.40	0.380-0.280
Mercury.....	0.1044	7.45	0.874
Nichrome.....	0.0999	7.63	0.894
Palladium.....	0.907	2.53	0.296
Platinum.....	0.999	2.41	0.283
Rhodium.....	1.960	1.72	0.202
Silver, pure.....	6.275	0.96	0.113
Silver, coin (10 % Cu).....	4.960	1.08	0.127
Steel, cold-rolled.....		10.20	1.193†
Steel, cold-rolled.....		16.00	1.9‡
Steel, stainless.....		7.00	0.8‡
Steel, stainless.....		10.35	1.212§
Tin.....	0.654	2.95	0.346
Tungsten, drawn.....	1.780	1.80	0.221
Zinc.....	1.725	1.84	0.215

* For 0.400" × 0.900" ID rectangular tubing at 3.20-cm wavelength.

† W. A. Edson BTL Memo 3510-W.A.E.—3/12/45.

‡ Very rough estimate based on an old experiment at 10-cm wavelength.

§ Measured at 3.20 cm wavelength at Radiation Laboratory.

lium Copper 175 has the best elasticity of the three but its conductivity is slightly lower than that of 70-30 brass.¹ Anaconda Phosphor Bronze 356 and Chromium Copper 999 are somewhat higher in electrical conductivity than 70-30 brass.

Table 3-2 gives values of the conductivity of various metals used in the design of microwave transmission lines and components and the relative attenuation in each metal. The conductivity values for pure metals were assembled from data in the *Handbook of Chemistry and Physics*,² and the values for alloys were taken from data in *Sweet's File for Product Designers*.

The attenuation of rectangular waveguide 0.400- by 0.900-in. ID at a free-space waveguide of 3.2 cm is also given in Table 3-2 for the various metals. The attenuation was calculated from equations developed in Chapter 2 for most of the metals. The attenuation values for magnetic metals were determined experimentally by direct loss measurements.

3-4. Construction Techniques.—Special construction techniques have been necessary in the manufacture of microwave transmission-circuit components that have peculiar geometrical shapes. These special techniques include electroforming and several forms of precision casting.

Electroforming is a process for producing hollow metal parts of irregular shape by electroplating a low-melting-point metallic alloy on wax molds made to reproduce the interior of the part desired. The process serves in some cases as an interim between model-shop specimens and production parts, but it has also been used successfully on a large scale in the production of parts. The mold is usually made of Wood's metal, Cerrobend, or electrotyping wax. The electroforming metal is usually copper or nickel, which is deposited to the thickness required for the desired mechanical strength. The mold is then melted out leaving the part with very accurate internal dimensions. Matching windows or other inserts may be molded into the alloy at the correct positions so that they will become attached to the plated part in the plating process. These inserts are very easily located with accuracy and are well bonded to the copper or nickel during the plating process. Electroformed parts of nickel which are very light yet mechanically strong can be produced. For good electrical conductivity the nickel is usually plated with silver after the mold is melted out. Electroforming may be done in any laboratory that has equipment for electroplating. Although the process is not limited to the use of copper and nickel, it is not practical for some metallic platings because of the difficulties in applying thick deposits. The thicker the plate becomes during plating the more porous is the surface last

¹ *Sweet's File for Product Designers*, F. W. Dodge Corporation, New York, 1943.

² *Handbook of Chemistry and Physics*, 26th ed., Chemical Rubber Publishing Co., Cleveland, 1942.

deposited because the metal deposits faster on the high spots. A combination of platings may also be used in electroforming.

The production of some transmission-line components of peculiar geometrical shapes difficult to fabricate or otherwise produce has been achieved by use of precision-casting methods. In comparison with conventional sand casting these methods have advantages of cleaner, sharper definition and much closer dimensional tolerances. Precision-casting methods can be grouped into three general classes: die castings, centrifugal castings, and "lost wax" castings.

Die-casting techniques are of course well known and widely used. The molten metal is forced under pressure into steel molds of extreme accuracy and high finish. This method produces the finest castings and is the most economical for large-scale production. It is, however, limited to metals and alloys with relatively low melting points because the temperature of the molten metal must be considerably lower than that of the die metal. Copper, aluminum, and zinc alloys may be easily die-cast in steel molds. The accuracy is determined by the tolerance of the mold and the difference in contraction of the two metals during cooling. Tolerances of ± 0.002 in. may be held consistently in small parts. Tools must be replaced when worn beyond tolerances. The tool cost limits the practical use of die-casting to the production of large quantities.

Centrifugal casting is a process intermediate between sand-casting and die-casting. This method is used when dimensional and finish requirements are not too exacting. Accurate molds are made of plaster of paris, baked sand, or special clay, and mounted off center on a revolving table. The molten metal is poured into a cup or hole in the center of the table and forced through channels into the molds by centrifugal action. The resulting castings are much superior to sand castings because air pockets are prevented by the centrifugal action. This is an ideal method where some machining of the casting is possible to insure the accuracy of critical dimensions.

The "lost wax" method of casting is an ancient technique modernized by the dental profession. Briefly, it consists of making a wax impression of the part to be molded, burying the impression in special clay, and baking the clay. During the baking, the wax is lost by evaporation through the pores of the clay. Thus there is produced a ceramic mold that will withstand extremely high temperatures. Such a mold is porous enough to permit the escape of air and gas, so that a casting made from it will be free of blow holes and bubbles. The molten metal is drawn into the mold by vacuum action on the porous ceramic mold. This process is highly technical and the many trade secrets involved are closely guarded by the various manufacturers. The results are excellent but sometimes expen-

sive. This method is capable of producing castings that could be made by no other means.

Powder metallurgy—a process of molding powdered alloys of copper, aluminum, and zinc—affords an alternate for casting. This process provides unusual production economy, particularly in the case of complex parts, the production of which normally requires a series of forming, working, or machining operations. The powdered metal is screened and compressed, or briquetted, in a mold under pressures of 50,000 to 100,000 lb/in² to form a sustaining compact mass that will withstand the necessary handling during transfer to the sintering furnace. Thin wall sections should be avoided because they cause die failures at pressures of this magnitude. In the sintering furnace the metal is heated nearly to the melting point, a process that fuses the powder into a hard metal comparable in strength to a casting. Die costs and costs of setting up production are so high that the process is not economical except for large quantities of identical parts. The finished parts are often porous and cannot be used where pressurization is required. Dimensional tolerances to be expected on the briquette as sintered are ± 0.004 in. on the diameter and ± 0.008 in. on the length. Re-pressing or coining will improve the tolerance on the diameter but will not improve the tolerance in the direction of pressing. Powder metallurgy has also been used for making oilless bearings by mixing graphite with the powdered metal.

Many microwave transmission components must be made in two or more parts which are then joined by soldering. It is advisable to locate such joints so that minimum current flows across the joint, in which case radiation and reflection in poorly soldered joints are minimized.

Two methods of soldering are used in making joints in microwave components: silver soldering and soft soldering. Silver soldering—sometimes referred to as hard soldering—may be defined as the joining of metals by means of a nonferrous filler alloy containing silver, which melts at a temperature near but below the melting point of either metal to be joined. Joints properly made have strength comparable to that of the parent metal. Any of the commercial silver solders such as Sil-fos or Easy-flo give strong durable joints on copper, brass, or bronze. Gas brazing with a torch, using oxygen and acetylene or other suitable fuel gas, is the most common heating method and gives excellent results, especially in the hands of a skilled operator. Control of the heating, to bring the joint surfaces of both parts simultaneously to the proper temperature, is effected by application of the flame away from the joint. Thus the flame is not allowed to impinge directly on the solder, and the solder is melted by the heat of the parts. Initial cleanliness is of paramount importance. This may be ensured by the use of a suitable flux

which aids in protecting metal from oxidation by dissolving oxides that may form and by promoting free flow of the molten solder into the joint. After soldering, it is desirable to clean the parts thoroughly since the flux may cause corrosion. Common fluxes are water-soluble and are easily removed by hot water or steam. Clearances between parts to be soldered are important and vary according to the materials. For joining brass, a clearance of 0.002 to 0.003 in. gives good results. Silver solder usually has a composition of copper, zinc, and 40 to 50 per cent silver. The melting-point range is 1150° to 1600°F.

Soft solder contains tin and lead in ratios that vary according to the manufacturer. A common composition for electrical work is 45 per cent tin and 55 per cent lead. The more lead above 38 per cent, the higher the melting point. Soft solders melt at 350° to 600°F depending on the composition. Joining of this type is not suitable for assemblies requiring strength or for a situation in which vibration is likely to occur. Soft solder is often used to solder beryllium-copper fingers where high temperatures would ruin the temper. Other applications are the joining of small, light parts that do not require strength and are not subject to vibration.

Resistance and spot welding are very seldom used in the fabrication of microwave transmission lines and components. A method of soldering copper and copper-plated steel in a hydrogen atmosphere using various high-melting-point solders has been much used recently for the construction of microwave tubes. It might well be applied to the construction of other components as it is easy to use and gives excellent results. The process cannot be used for brass. Further details are given in Chap. 14 of Vol. 31 of this series.

FINISHES AND ELECTROPLATING

Metallic transmission lines and components are often subjected to corrosive atmospheres, to humidity, and to fungus growth. In tropical regions these agents may increase the attenuation in lines and components to such an extent that frequent replacement of parts is necessary if adequate protection has not been provided. The increase in loss is caused by the pitting of wall surfaces, the formation of lossy metallic compounds, and the flaking of platings. Metallic surfaces may be protected by one or both of two processes: (1) nonmetallic finishes, and (2) electroplating. These processes will be discussed in Secs. 3-5 and 3-6, respectively. Section 3-7 is a discussion of testing procedures used for determining the corrosion resistance of conductors by the effect of corrosion on the electrical loss in the wall surfaces.

3-5. Nonmetallic Finishes.—Corrosion may be prevented with some success by two nonmetallic finishing processes: a chemical surface treat-

ment, and a special varnish treatment. Both processes have been used successfully in field applications for protecting microwave transmission lines and components. The Ebonol process, an example of chemical surface treatment, consists of dipping the cleaned metallic part into a solution of Ebonol salts until a black oxide coating is formed. Ebonol "C," "S," "Z," and "A" salts are used, respectively, for blackening copper and its alloys, iron and steel, zinc and its alloys, and aluminum and its alloys. The Ebonol salts are produced and distributed by the Enthone Company of New Haven, Conn. The Ebonol "C" coating has proved satisfactory for corrosion protection of brass. However, the loss in brass transmission lines is increased slightly if the coating is too thick. The thickness of the coating can be controlled by the length of time the metal is submerged and can be judged by the color of the surface. Blackening is accomplished in from 3 to 5 min for pure copper and in from 10 to 25 min for copper alloys ranging from 70 to 80 per cent copper. When copper or brass lines or parts that have been soldered together are treated, the solder is not affected by the solution. Therefore, it is advisable to copper-plate the assembly after all soldering has been done and before using the blackening process. The Ebonol "A" process has also been used successfully for blackening and protecting aluminum. Bulletins are available from the Enthone Company which give details on cleaning surfaces and preparing the solutions.

The most satisfactory varnish coating investigated to date is a phenol formaldehyde varnish, developed by E. I. du Pont de Nemours and Company. This varnish is prepared by mixing two parts by volume of their VGT-1112 varnish with one part by volume of T-8802 thinner. It is applied to a chemically or electrically cleaned surface by spraying or dipping. The coated surface is then baked for 20 min at 340°F. A smooth hard finish is produced which is very adherent and which provides very good corrosion protection. The varnish when baked too long becomes brittle and changes to an opaque dark color instead of a transparent yellow. When it is baked too long or at too high temperatures the adhesion is poor, and cracks appear which impair the corrosion protection.

The varnish-coating process can be applied to any metallic surface or combination of metallic surfaces in one component. The Ebonol process requires a different solution for each metal. Where silver-plating is done to obtain optimum conductivity, the varnish coating may be applied over the plating. Both finishes give protection from the corrosive action of fungus growth. The protection against fungus growth is due not to a chemical which kills fungi but to the fact that fungi cannot live on the contents of either finish.

3-6. Electroplating.—Plating of waveguide, coaxial line, and other microwave line components has been, until recently, the accepted proce-

ture for corrosion protection. It has been known, however, for many years that under outdoor weathering conditions most electroplated deposits show a very high percentage of failures. Porosity of the electroplated deposits has been one of the chief contributing factors. Plated deposits such as zinc, cadmium, nickel, chromium, and more recently antimony, have been successful in some outdoor applications. To achieve satisfactory results with respect to corrosion, very stringent specifications must be set up for the plating process. Deposits of electroplated nickel 0.001 to 0.003 in. thick have high corrosion resistance when carefully prepared. Chromium is tarnish-resistant under ordinary conditions but will fail rapidly in the presence of chlorides. Because chromium plating is also highly porous, it is necessary to protect the base metal with 0.001 to 0.002 in. of nickel. Gold is highly corrosion-resistant but the cost of deposits of suitable thickness prohibits its extensive use. In general, it is not easy to electroplate thick deposits of the platinum metals. Their cost is also a factor in limiting their use.

Silver and copper are the most desirable plating materials from the microwave standpoint because of their high electrical conductivity. Since, however, these metals corrode or tarnish under outdoor weather conditions, they may profitably be protected with thin coats of low-loss varnish or the Ebonol finish. A thin "flash" plating of a noncorroding metal like palladium, described later in this section, offers good protection.

Porous electroplated deposits are objectionable not only because the rough surfaces increase the attenuation but also because the porosity greatly decreases the protection against corrosion. The pores allow solutions to produce, at the junction of the dissimilar metals, electrolytic action that may result in highly accelerated corrosion. In general, contacts between metals at the extremes of the electrochemical series are undesirable because of the large potential differences set up between them.

Because of its high electrical conductivity, silver plating has often been used on microwave transmission components. Copper has about the same electrical conductivity as silver but it corrodes very rapidly. Considerable success has been achieved in obtaining nonporous silver-plated deposits. These results have been achieved, however, under ideal laboratory conditions. The degree of control necessary to produce nonporous silver deposits is too exacting for general commercial practice. It should be kept in mind that in ordinary decorative silver plating 15 or more individual steps are necessary to produce a smooth, adherent surface. To minimize porosity and maximize electrical conductivity a number of additional and very exacting controls must be imposed upon the usual plating process. Not only is it necessary to exercise a very precise and elaborate control over the actual plating process, but it is also essential to select and prepare carefully the metallic surfaces that are to be

plated. Heterogeneity in chemical composition and roughness of the base-metal surface are the major factors that produce low-quality electroplated deposits. The subject of nonporous plating is treated with some thoroughness in the literature on electroplating; therefore only the aspects of the problem of porosity that influence the electrical conductivity of the wall surface at microwave frequencies will be mentioned here. At such frequencies, a plated film of the usual thickness (0.0005 to 0.001 in.) carries practically all of the electric current. Therefore, the effective electrical conductivity of a conductor plated with a metal of high conductivity is a maximum when the surface is perfectly smooth and nonporous (see Sec. 3-1). Buffing of a silver deposit by an experienced

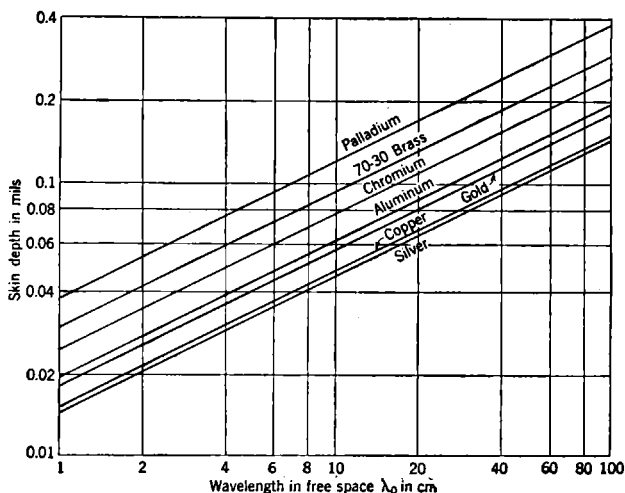


FIG. 3-2.—Skin depth in metallic conductors at microwave frequencies.

operator greatly reduces the porosity and smooths the surface, but, on the other hand, buffing compound may be incorporated into the silver deposit with a resulting reduction of electrical conductivity. Ball burnishing, when properly controlled, produces a smooth silver surface of low porosity, and it has little tendency to contaminate the plate. Both burnishing and buffing tend to produce a dense deposit, but, at the same time, they produce some strain as the result of cold-working of the surface. Excessive cold-working of a silver deposit tends to reduce the electrical conductivity. The strain induced by cold-working may be released by heat-treating the plate at approximately 200°C to induce recrystallization of the silver. Heat-treating may also be utilized to release crystallization strain in freshly electroplated deposits, and thus to increase the electrical conductivity.

Theoretically, a highly conductive plating on a low-conductivity base metal increases the effective conductivity of the metallic wall in accordance with the curves shown in Fig. 3-3. The attenuation approximates that of a metallic wall made of the highly conductive metal if the plating thickness is equal to, or greater than, a skin depth. Figure 3-2 is a curve showing the skin depths for seven common metals, plotted against the free-space wavelength. The attenuation in the walls of a waveguide or

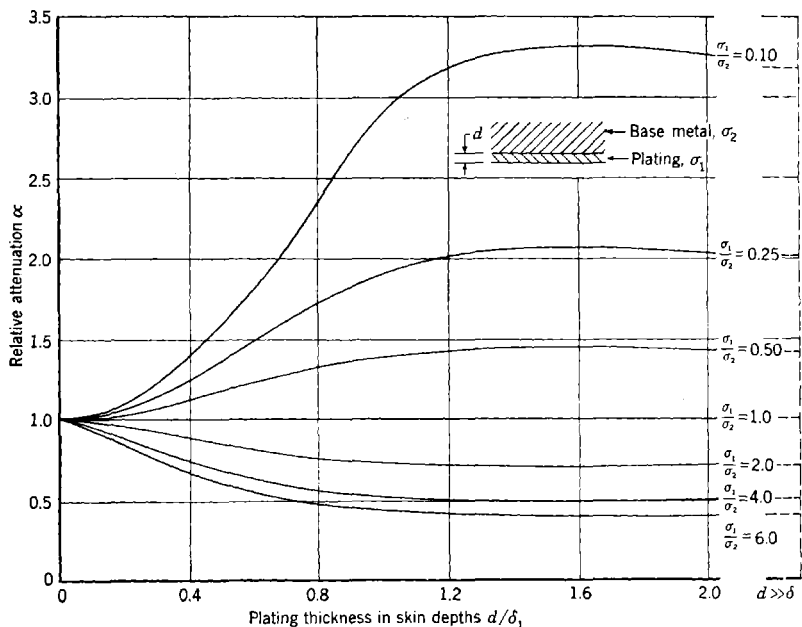


Fig. 3-3.—Attenuation in plated conductors. The relative attenuation α is the ratio of the attenuation of the combination to the attenuation of the base metal.

coaxial line is proportional to the real part of the impedance looking into the wall. This impedance, for a good conductor plated with another conductor, may be determined from the characteristic impedances Z_2 and Z_1 of the metals, the reflection coefficient between layers, and the propagation function γ_1 in the metallic plating. These quantities are given [see Eq. (2-132)] by

$$\left. \begin{aligned} Z_2 &= \sqrt{\frac{j\omega\mu_2}{\sigma_2}} = (1+j) \sqrt{\frac{\pi f\mu_2}{\sigma_2}}, & (a) \\ Z_1 &= \sqrt{\frac{j\omega\mu_1}{\sigma_1}} = (1+j) \sqrt{\frac{\pi f\mu_1}{\sigma_1}}, & (b) \end{aligned} \right\} \quad (3)$$

$$\Gamma = \frac{Z_2 - Z_1}{Z_2 + Z_1} = \frac{\sqrt{\sigma_1} - \sqrt{\sigma_2}}{\sqrt{\sigma_1} + \sqrt{\sigma_2}} \quad (4)$$

$$\gamma_1 = j\omega \sqrt{\frac{\mu_1 \sigma_1}{j\omega}} = (1 + j) \sqrt{\pi f \mu_1 \sigma_1} = \frac{1 + j}{\delta_1} \quad (5)$$

where δ_1 is the skin depth in the plating; γ_1 , σ_1 , and γ_2 , σ_2 are the propagation functions and electrical conductivities of the plating and the base metal, respectively. The wavelength in the plating is

$$\lambda_1 = \frac{2\pi}{\text{Im}(\gamma_1)} = 2\pi \sqrt{\frac{2}{\omega \mu_1 \sigma_1}} \quad (6)$$

hence the phase shift in the plating metal is d/λ_1 , where d is the plating thickness.

The impedance looking into the surface of a plated metallic conductor may be calculated from the usual impedance transformation equation¹

$$Z = \frac{\gamma_1}{\sigma_1} \frac{\sinh \gamma_1 d + \frac{\gamma_2 \sigma_1}{\gamma_1 \sigma_2} \cosh \gamma_1 d}{\cosh \gamma_1 d + \frac{\gamma_2 \sigma_1}{\gamma_1 \sigma_2} \sinh \gamma_1 d} \quad (7)$$

Figure 3-3 shows curves of relative attenuation in a plated conductor, in terms of the attenuation in a solid conductor of the base metal, plotted against the plate thickness in skin depths. The curves were calculated from Eq. (7) and checked by the impedance-chart method. Figure 3-2 was calculated from Eq. (1). Both figures are based on the assumption that the surfaces are smooth and nonmagnetic. The theoretical curves of Fig. 3-3 have not been checked experimentally because of the difficulty in measuring plating thickness and because of the porosity of plated films. However, experiments at Pratt Institute in Brooklyn and at Radiation Laboratory, in which silver was plated on brass, indicated that a thickness much greater than the skin depth is required to obtain a silver-plated waveguide with a loss comparable to that of a pure silver waveguide.² Since all platings are somewhat porous, it is advisable to use a plating thickness several times greater than a skin depth if the plating has to form the conducting film.

The most effective highly conductive plating combination used so far in the manufacture of microwave lines and components is a combination of palladium and silver developed by the Sperry Gyroscope Company.

¹ Ramo and Whinnery, *Fields and Waves in Modern Radio*, Wiley, New York, 1944, p. 217.

² R. M. Walker, "X-Band Waveguide Corrosion Proofing," RL Report No. S-29, Oct. 6, 1944; T. G. Dixon, "Protection of R.F. Transmission Lines," Pratt Institute Report P.I.-X-1, July 31, 1945.

A flash plating of palladium is applied to the brass or copper base metal, which leaves a film for protection against corrosion of the base metal. The palladium flash is followed by a silver plating which appears to be less porous than a silver plating deposited directly on brass or copper since it gives a lower attenuation. This silver plating is made thick enough to form a good conductive skin (at least 0.0006 in. at 3.0 cm) and is followed by another flash coating of palladium for its protection. Since the conductivity of palladium is about one quarter that of silver this final flash coating must be much thinner than a skin depth if increased loss is to be avoided. From Fig. 3-3 we note that a flash thickness of one-fifth skin depth of palladium on silver increases the attenuation by only about 7 per cent, whereas the attenuation is doubled by a full skin depth.

3-7. Corrosion Tests and Measurements.—Corrosion tests are usually made in a test chamber into which is sprayed a fine mist containing the corrosive elements and compounds. The solution to be sprayed may be made up in the approximate proportions to simulate actual outdoor weather conditions in a particular locality, or it may be concentrated with particular compounds to speed up the corrosive action. The action in either case is much faster than under outdoor weather conditions because all parts are exposed continuously to the spray. The outdoor weather-corrosion rate is variable depending upon location and exposure.

TABLE 3-3.—COMPOSITION OF SALT SPRAY, AN-QQ-S-91

Metal chloride	g per l of H ₂ O	Percentage
NaCl.....	28	2.8
KCl.....	0.8	0.08
CaCl ₂	4.0	0.4
MgCl ₂	4.0	0.4
Others.....	...	0.8

Ordinary rain water contains oxygen, nitrogen, carbon dioxide, oxides of sulfur, oxides of nitrogen, ozone, hydrogen, sulfides, and ammonia. In industrial areas the concentration of carbonic and sulfurous acids may run very high. Over the sea and in adjacent regions the concentration of salt may be very high. As a result of the wide range of weather conditions encountered in outdoor use of microwave transmission lines and components, corrosion testing can provide only a comparison of the corrosion rates of various metals under similar conditions.

The degree of corrosion of various metals may be determined by measuring the loss of samples of waveguides or coaxial lines before and after corrosion. The salt-spray test for corrosion of electroplated deposits is the generally accepted method. Although salt-spray testing has been used for many years, the method is subject to considerable criticism

because of lack of reproducibility of the tests. Therefore considerable caution must be exercised in comparing the results of tests made in different chambers or at different times in the same salt-spray test chamber. The rate of corrosion in any given chamber will vary widely depending upon the location and position of the test piece in the chamber. If the temperature of the chamber and the concentration of the salt solution are not controlled, even wider variations in results may occur. For best

TABLE 3-4.—CORROSION TEST DATA ON PLATED AND SURFACE-COATED WAVEGUIDE

Waveguide base metal and plating or surface coating, mils*		Loss after plating or coating, db/m	Loss after 200-hr salt spray, db/m	Where measured
70-30 brass	Cu flash, 0.1 Ni, 0.15 Ag . . .	0.16	0.21	Radiation Laboratory
	Cu flash, 0.1 Ni, 0.3 Ag . . .	0.14	0.33	Pratt Institute
	0.1 Ni, 0.3 Ag, Pd flash . . .	0.32	0.36	Radiation Laboratory
	0.1 Ni, 0.3 Ag	0.17	0.29	Pratt Institute
	0.1 Ni, 0.3 Au	0.19	0.26	Pratt Institute
	0.5 Ag, 0.2 Au	0.25	0.31	Pratt Institute
	0.3 Ag, Pd flash	0.15	0.23	Radiation Laboratory
	Pd flash, 0.6 Ag, Pd flash . .	0.14	0.28	Pratt Institute
	Pd flash, 0.3 Ag, Pd flash . .	0.13	0.16	Radiation Laboratory
	0.3 Ag	0.19	0.22	Pratt Institute
	Heavy Ag plate	0.12	0.18	Pratt Institute
	0.16 Au	0.29	0.40	Pratt Institute
	0.3 Cd	0.21	0.30	Radiation Laboratory
	Cu flash, 0.3 Ag, 0.1 Cd . . .	0.20	0.25	Radiation Laboratory
	Ebonol coating	0.26	0.26	Radiation Laboratory
	Ebonol coating	0.29	0.30	Pratt Institute
Phenol formaldehyde 1.0 . . .	0.26	0.26	Radiation Laboratory	
Phenol formaldehyde 1.0 . . .	0.28	0.30	Pratt Institute	
Aluminum 2S	Anodized	0.15	0.41	Radiation Laboratory
	Silver plated	0.23	7.40	Radiation Laboratory

*Coatings or plating listed in the order of their deposit.

results all specimens should be run at the same time and transposed at regular intervals.

Various combinations of metallic platings and nonmetallic coatings were included in a series of tests to find a method of protecting waveguide from corrosion and to determine the relative resistance of the surfaces to corrosion and fungus growth. These tests were made at Radiation Laboratory and at Pratt Institute in Brooklyn. The samples were pieces of tubing, $\frac{1}{2}$ by 1 in. OD, with 0.050-in. wall, 1 m long. The rela-

tive resistance to corrosion was determined by measuring the attenuation of each sample at a frequency of 9000 Mc/sec ($\lambda_0 = 3.33$ cm) before and after exposure to a 200-hr salt spray. The salt-spray test chambers were operated according to Army-Navy Aeronautical Specification AN-QQ-S-91, which requires the composition of spray given in Table 3-3. Results of these tests are tabulated in Table 3-4. Most of the samples tested were plated by commercial establishments according to their own control. These methods are trade secrets in most cases; therefore the results only indicate what may be expected in commercially plated waveguides.

DIELECTRIC MATERIALS

3-8. Uses and General Requirements.- Many design requirements for microwave transmission lines and components make dielectric materials desirable for the following uses:

1. Mechanical support of center conductors for coaxial lines.
2. Pressure sealing of coaxial and waveguide lines, resonant cavities, and other components.
3. Impedance-matching, slugs in slug tuners, etc.
4. Power absorption in line terminations.
5. Sealing pores in other materials.

Design procedures for coaxial bead supports, pressure windows, and slug tuners are discussed in Secs. 4-3, 4-18, and 8-5, respectively. Line terminations are discussed in Vol. 23 of this series.

The requirements for electrical and mechanical characteristics of dielectric materials for the uses just listed are varied. Bead supports, pressurizing units, and impedance-matching units require dielectric materials with low dielectric constants and low-power factors as well as good mechanical strength and heat resistance. Thermal expansion coefficients are very important in the design of pressure windows. Special mixtures of glass and polystyrene that have expansion coefficients approximately equal to the expansion coefficient of brass were developed at M.I.T. The material called "polyglas"¹ can be molded into intricate shapes and cemented into waveguide and coaxial lines to form a pressure seal over wide temperature ranges. Special types of glass are sealed to Kovar or Fernico for resonant-aperture pressurizing windows as mentioned in Sec. 3-3, (see also Sec. 4-19).

Moisture absorption, oxidation, and fungi are the chief enemies that destroy the good electrical properties of dielectric materials. Absorbed moisture even in very small quantities appreciably increases dielectric loss at microwave frequencies. To combat this effect in tropical regions,

¹ A. Von Hippel, S. M. Kingsburg, and L. G. Wesson, "Low Expansion Plastics," NDRC Report 14-539, M.I.T., Nov. 1945. A. Von Hippel, "Tables of Dielectric Materials," NDRC Report 14-425, M.I.T., June 1945.

small amounts of paraffin or certain silicones have been incorporated into some materials during manufacture. It was found that 0.2 per cent of paraffin is effective in minimizing moisture absorption in polystyrene, but larger amounts of paraffin produce scarcely any further improvement. Paraffin alone is only mildly effective in reducing the moisture absorption of polystyrene-glass mixtures, presumably because water is strongly adsorbed on the glass surface. In this case, the addition of 0.1 per cent of a silicone (Dow Corning Ignition Sealing Compound No. 4), which is preferentially adsorbed on glass, has proved an effective remedy. The best results are obtained when both paraffin and the silicone are added. Oxidation also increases the loss of dielectric materials at microwave frequencies. Oxidation occurs most readily during the molding or casting operation and can be minimized by careful control of the molding temperature.

Materials with a high-power factor and low dielectric constant are used for line terminations. Graphite or a specially prepared form of iron is often used for the lossy material. Graphite is mixed with Portland Cement or X-pandotite Cement made by the Dixon Crucible Company of Jersey City, N.J.; and specially prepared iron is suspended in very fine particles in a ceramic or bakelite filler to form a material, polyiron, much used as a core material in r-f transformers. One source of this material is Henry L. Crowley and Company, Inc., of West Orange, N.J. The resulting mixture in either case is a poorly conducting medium, which can be cast into a section of transmission line to absorb the electromagnetic power. Since both materials are quite porous, they absorb enough moisture to change their characteristics considerably. Therefore, it is necessary to seal the pores with silicone liquids or similar materials to keep out moisture.

3-9. Characteristics of Dielectric Materials.—Many low-loss plastics were developed during World War II, but relatively few have been used extensively in microwave transmission-circuit design because of failure to meet the requirements outlined previously in this chapter. Electrical and mechanical characteristics of the most widely used dielectric materials are given in Table 3-5. The specific dielectric constant k_e and loss factor $\tan \delta$ are given for each material at three wavelengths in the microwave region.

The complex dielectric constant of a medium is expressed as

$$\epsilon = \epsilon' - j\epsilon''$$

in Eq. (2-90). In the table, $k_e = \epsilon'/\epsilon_0$ and $\tan \delta = \epsilon''/\epsilon'$ where ϵ_0 is the permittivity of free space. The value of ϵ''/ϵ' is often called the loss tangent or power factor and the loss in the dielectric material can be calculated from it (Sec. 2-5).

TABLE 3-5.—ELECTRICAL AND MECH
 All values given for room temperature,

Material trade name	Manufacturer	k_e at 30 cm	$\tan \delta$ at 30 cm	k_e at 10 cm	$\tan \delta$ at 10 cm	k_e at 3 cm	$\tan \delta$ at 3 cm
Glasses							
No. 705	Corning Glass Works	4.70	4.80×10^{-3}	4.72	5.20×10^{-3}	4.71	6.10×10^{-3}
No. 7052		5.05	5.00	5.04	5.80	4.93	8.10
No. 707		3.97	1.20	4.00	1.90	3.99	2.10
No. 790		3.87	0.60	3.84	0.68	3.82	0.94
No. 774		4.92	8.80	4.89	8.90	4.82†	8.90†
Polyglas							
P†	Mass. Inst. of Tech.	3.36	0.77	3.35	0.78	3.32	0.84
S†	Mass. Inst. of Tech.	3.55	3.40	3.55	4.00	3.53	4.60
D†	Monsanto Chem. Co.	3.22	0.76	3.22	1.20	3.22	1.30
M†	Hood Rubber Co.	4.80	13.00	4.86	33.90	5.22	66.00
Polystyrene							
XMS 10023	Bakelite Corp.	2.55	0.45	2.55	0.50	2.55†	0.70†
Styron C-176	Dow Chemical Co.	2.56	0.30	2.55	0.26	2.54	0.30
Laolin	Catalin Corp.	2.50	0.10	2.49	0.22	2.49†	0.30†
Lustron D-276	Monsanto Chem. Co.	2.52	0.40	2.51	0.41	2.50†	0.60†
D-334	Monsanto Chem. Co.	2.55	0.27	2.54	0.24	2.54†	0.40†
Poly 2-5 Dichloro- styrene							
D-1385	Monsanto Chem. Co.	2.59	0.23	2.62	0.23	2.60	0.23
Styramic HT F-1891	Monsanto Chem. Co.	2.56	0.34	2.55	0.38	2.55	0.40
Polyethylene							
M 702-R	Acadia Syn. Prod.	2.26	0.40	2.26	0.40	2.26†	0.50†
KLW A-3305	Bakelite Corp.	2.23	0.19	2.21	0.19	2.15†	0.20†
	E. I. du Pont de Nemours and Co., Inc.	2.25	0.22	2.25	0.22	2.25†	0.22†
Silicone Liquids							
No. 200	Dow Corning Corp.	2.80	4.00	2.79	10.00
No. 500	Dow Corning Corp.	2.20	0.80	2.20	1.45
Ignition Sealing Compound No. 4	Dow Corning Corp.	2.78	6.60	2.77	10.00
Ceramics							
Titanium Dioxide	E. I. du Pont de Nemours and Co., Inc.	99†	1.00†
Steatite Ceramic F-66	BTL	6.25	0.54	6.25	0.55
Crolite No. 29	H. J. Crowley Co.	5.85	1.90	6.25	2.40	6.25	3.15
Miscellaneous							
Poly F-1114	E. I. du Pont de Nemours and Co., Inc.	2.10	0.20	2.10	0.20	2.10†	0.20†
No. 1421 Resin	General Electric Co.	2.56	0.45	2.53	0.50	2.52	0.56
Q-200.5	Dow Chemical Co.	2.55	0.45	2.52	0.44	2.50†	0.50†
Styraloy 22	Dow Chemical Co.	2.38	3.85	2.38	3.30	2.38	2.40
Ruby Mica	General Electric Co.	5.40	0.25	5.40	0.30	5.40†	0.30†
Mycalex 1364	General Electric Co.	6.92	3.00	6.91	3.60	6.90†	4.45†

* Data from "Tables of Dielectric Materials," Vols. I and II, NDRC Reports 14-237, Feb. 1944;
 † Treated to prevent moisture absorption.

ANICAL PROPERTIES OF DIELECTRICS*
 25°C; wavelengths refer to free space

Heat distortion temperature T_{dis} , °C	Thermal conductivity σ_t , Cal/cm ² Sec per °C/cm	Thermal expansion coefficient α_t , parts/°C	Molding methods	Machinability	Moisture absorption, percentage weight at 90% humidity	Remarks and uses
703	20-30 × 10 ⁻⁴	0.46 × 10 ⁻³		No	Seals to Kovar Mo.W.
710	27	0.47		No	Seals to Kovar Mo.W.
746	27	0.31		No	Seals to tungsten
1450	20-30	0.08		No	Seals to tungsten
819	20-20	0.33		No	Seals to tungsten
86.7	1.66	Compression	Poor	0.07	Pressure windows
.....	2.10	Comp.	Poor	nil
112.6	1.74	Comp. and inj.	Poor	0.06	Pressure windows
150.0	1.30	Comp.	Poor	3.67
77-83	1.8-2.0	6.5-7.6	Comp., inj., extr.	Good	0.00	Beads for coaxial lines
82	1.8-2.0	Comp., inj.	Good	nil	
74-88	1.8-2.0	0.6-0.8	Comp., inj., extr.	Good	0.40	
76	1.90	6.0-8.0	Cast and comp.	Good	0.06	
76	1.90	6.0-8.0	Cast, comp., inj.	Good	0.06	
113	Cast, comp., inj.	Good	0.03	Beads for coaxial lines
110	5.93	Extr., comp., inj.	Good	0.03	
95-105	15.00	25	Comp. and extr.	Good	0.03	Flexible cables
95-105	10.30	19	Comp., inj., extr.	Good	0.03	Flexible cables
95-105	10.30	19	Comp., inj., extr.	Good	0.025	Flexible cables
.....	96.8	Fluid 200 cs	0.1	Sealing and lubrication
.....	160	Fluid 0.65 cs	nil	Sealing and lubrication
.....	63	Light grease	nil	Sealing and lubrication
1350	Die-press and firing	No	Delay lines
1225	Comp. mold	No	0.1	Insulator
1000	0.77	Die-press	Poor	Insulator
66	4.82	9	Machining	Good	0.00	Chem. resistant
.....	Good	0.1	Subst. for polystyrene
100	Good	Low	Subst. for polystyrene
62-65	4.00	5.9	Comp., extr., inj.	Poor	0.04	Flexible seals
.....	18.00	Mica windows
.....	13.70	0.80	Comp.	Fair	0.003	Substitute for mica

14-425, June 1945.

‡ Estimated values.

The dielectric constant of a dielectric material and the loss in it are produced by contributions of three molecular mechanisms,¹ namely: (1) electronic and atomic polarization, (2) orientation of permanent dipoles, (3) ionic or electronic conduction.

1. Polarization is the response of the charge carriers in a dielectric medium to an applied electric field. These carriers may be locally bound, as electron clouds are bound by the change of a nucleus, or as ions are bound in crystal structures. An exterior field in this case displaces the positive charge carriers slightly with respect to the negative ones, thus producing dipole moments by "electronic" or "atomic" polarization. This "induced" polarization has its resonance frequencies in the optical range. At high electrical frequencies and up to optical frequencies approaching the resonant value, the displacement of charge follows closely the applied field so that the resulting current is out of phase with the field. This behavior produces no loss but leads to a frequency-independent contribution k'_{e1} to the dielectric constant and to a corresponding contribution $n_1 = \sqrt{k'_{e1}}$ to the index of refraction. This contribution to k_s depends on temperature only because the number of molecules per cubic centimeter varies with temperature. This change in k'_{e1} due to temperature is approximately given by

$$\frac{\Delta k'_{e1}}{k'_{e1}} = (k'_{e1} - 1)(k'_{e1} + 2)\alpha t, \quad (8)$$

where α is the thermal expansion coefficient given in Table 3-5. For most dielectrics the temperature effect is small (about .05 per cent per °C).

2. In addition to the induced dipoles, there exist in many molecules permanent dipoles produced by the difference in electron affinity of their atoms. Such dipoles tend to produce polarization by orientation of the molecules in the applied field. Gas molecules are free to rotate with little restraint; therefore they follow the field more or less instantaneously. Resonance frequencies are found in the infrared, but for heavy molecules they extend into the microwave range. In liquids and solids, however, the freedom of rotation is normally impeded by the interaction of the neighboring molecules. The resonance phenomenon degenerates into an aperiodic orientation under high friction, which is very temperature-sensitive. The orientation of permanent dipoles appears pronounced in the fre-

¹ A. Von Hippel, "Tables of Dielectric Materials," Vols. I and II, NDRC Reports 14-237 and 425, M.I.T., Feb. 1944, and June 1945. A. Von Hippel and R. G. Breckenridge, "The Interaction Between Electromagnetic Fields and Dielectric Materials," NDRC Report 14-122, M.I.T., Jan. 1943.

quency characteristics of many materials. Its principal feature is that, with increasing frequency, the dipoles begin to lag more and more behind the field; that is, their contribution to the dielectric constant decreases, and the loss tangent or power factor increases to a maximum and decreases again as the dipole effect dies out. If only one dipole type is present, orientating itself in a viscous medium without mutual interaction, the electrical behavior of the dielectric can be represented by a simple RC -circuit. After removal of the field, the polarization would die down exponentially with a "relaxation time" τ . The dielectric constant should decrease to about 0.2 of its maximum value in one decade of frequency increase. With increasing temperatures the viscosity decreases, the relaxation time shortens, and the whole dispersion region moves to higher frequencies. Most dielectrics, especially plastics, contain dipoles of many types; and each dipole, because of the varying location of neighboring molecules, finds itself in slightly different surroundings. Therefore, a wide distribution of relaxation times exists, and the k_e and $\tan \delta$ curves are flattened out. This condition is present in most of the dielectrics given in Table 3-5. Plasticizers inevitably lower the relaxation times in polymers and thereby shift the loss maximum to higher frequencies.

3. The last contribution to k_e and $\tan \delta$ is the ionic or electronic conduction, which has a small effect in the materials listed in Table 3-5. This effect, caused by the migration of electrons or ions through the material, produces a frequency-independent conductivity and a contribution to the loss tangent inversely proportional to the frequency. If the electrons or ions, after migrating over some distance, are stopped—as, for instance, at the boundary of a carbon particle embedded in rubber—a field distortion results. To the observer this gives the impression of a high dielectric constant. Dielectric constant and loss in this case are frequency-dependent and influenced fundamentally by the nature and distribution of the conducting particles. It is, therefore, important to keep dielectric materials free from such particles and also to prevent carbonizing of their surfaces by too much heat during the molding process. Fillers are often polar (wood flour) or poorly conducting (carbon black) and thus may increase $\tan \delta$.

3-10. Construction of Dielectric Parts.—Dielectric material for the construction of parts is usually furnished by the manufacturer in a powder form. This powdered material is then polymerized and formed into various shapes by heating the material in a mold until polymerization of the liquid material in the mold is complete. The temperature, curing

time, and pressure requirements should be obtained from the producer of the raw material as they are critical for some materials. Construction techniques for dielectric parts are divided into five general classes: (1) compression molding, (2) transfer molding, (3) injection molding, (4) extrusion molding, (5) casting.

Compression molding is the simplest of the forms of plastic molding which use heat and pressure. The powdered material is poured into a cavity into which a closely fitted piston descends, compressing the powder while it is hot into the cavity. The piston is then withdrawn, leaving the finished part, which is pushed out by an ejection pin, and the cycle is repeated. The temperature and pressure used must be correct for the material and must be properly controlled. Only one piece in each cavity is made in one cycle.

Transfer molding is a double-step compression method. The correct amount of powder is heated and pressed into a block of semisolid form, then transferred while hot to an adjoining cavity where it is further pressed and cured into the finished part. This method is used when the finished part has an irregular cross-sectional area or when it requires inserts that must be accurately positioned.

Injection molding is a continuous process accomplished with an automatic machine in which the molding powder is heated to a semifluid state and injected into the mold where the finished part is formed and removed automatically. Such a machine is expensive and requires skilled operators, but it does fast and accurate work.

Extrusion molding is used only for tubes, rods, and bars of continuous cross section. The powdered material is heated to a plastic state and slowly forced through a die of the required shape and size. The material hardens as it comes out of the die. Many plastic materials cannot be extruded.

Casting is the simple process of placing the material to be formed into a mold or container of the desired shape and curing the material, with or without heat, until it hardens. No pressure is used in this process.

Ceramic materials, such as porcelain, titanium dioxide, steatite, and Crolite are sometimes used in the construction of microwave transmission components. Titanium dioxide is used in delay lines because of its high dielectric constant and low loss. The other materials are used for crystal casings and, in mixtures with graphite and other lossy materials, for line terminations. Ceramic parts are made by the die-press method. The dry powder is mixed with water or any organic binder that dries out during heating. The mixture is put in a die of the desired shape and compressed, at room temperature, into a compact mass strong enough to be transferred to a furnace for baking. The baking temperatures range from 1000° to 1600°C depending on the density required. Ceramic parts are

usually porous and require glazing to produce a surface. Glazing is a process of sealing the surface pores in the ceramic by applying suspensions of essentially low-melting glass and firing at suitable temperatures to melt the glaze and form an impervious coating.

The surface condition of finished dielectric parts is determined mainly by the surface of the mold in which it was formed. The metal used for the mold is very important when materials such as polyglas requiring high temperatures and pressures are to be molded. The polyglas materials are particularly difficult to mold because of the abrasive quality of the molding powder. In this case, the mold is made of very hard steel, polished and plated with chromium to prevent the molding powder from scratching the mold during the pressing operation of the compression- and transfer-molding processes. It is also advantageous to lubricate the mold with one of the silicone liquids or paraffin when molding materials such as polyglas. The lubricant not only lubricates the mold, allowing the material to be completely pressed into corners, but it also tends to fill in the surface pores of the part being formed, thereby making it moisture-proof. Pores in ceramics may also be sealed with silicone liquids or paraffin.

In designing dielectric parts of intricate shapes it is important in most cases to allow rounded corners and slight tapers in dimensions so that the finished parts may be removed from the molds without breakage. It is also advisable to limit the thickness of a molded part to a small value because most dielectric materials have very low heat conductivity and are therefore heated very slowly on the inside of a thick piece.

PRESSURIZATION PROBLEMS

Pressurization of microwave transmission systems consists ideally of sealing the entire system, or separate units of the system, against air leakage to ensure constant pressure inside and to keep out moisture and water vapor. A decrease in the air pressure inside a transmission line or component decreases the maximum power that the unit will handle without voltage breakdown. Therefore, pressurization is essential, even under ideal weather conditions, for high-power systems at high altitudes. Damp weather and high-humidity conditions cause an increase in the loss of the system and a corrosion of metallic parts, which also increases the loss in the metallic walls. Moisture and high humidity encountered in tropical climates also promote the growth of fungi.

In actual practice ideal pressurization is not easy to attain. Small leaks are usually present, and it is difficult to design large lightweight parts that will stand the pressure differential encountered by high-flying aircraft. Therefore alternative methods have been used to control the pressure inside the system and keep out moisture. Two such methods have been developed:

1. Sealing the antenna feed and couplings as well as possible and leaving the small leaks to breathe very slowly. This method is used without a pump or relief valve on some shipborne and ground installations. For airborne equipment in which this method is used, a relief valve must be provided which operates at the maximum allowable pressure in the system. In this case it is advisable that the modulator, the receiver, and the line constitute one pressurized container. For a given leakage rate, a decrease in the rate of change of pressure in the system will, of course, accompany this volume increase. This method permits a large amount of breathing under conditions of extreme pressure and the temperature changes encountered in airborne application, but it gives adequate protection in ground and shipborne applications. However, protection of individual units must be provided for shipment and storage.
2. Sealing the antenna feed and couplings as well as possible and using an automatic pump to keep the inside pressure constant in spite of small leaks. The air taken in by the pump is dried by a chamber filled with silica gel and crystals of cobaltous chloride, which are a dull blue when dry but turn pink when saturated with moisture. This change in color is an indication that the chamber must be replaced or refilled. Replacement chambers are usually furnished as spare parts. The moisture may be removed from the saturated chamber by heating after the chamber is removed from the system. This method is very effective in both ground and airborne applications, but it is objectionable in airborne applications because the pump and associated equipment add weight to the system.

Pressurization of each unit or group of units by one of these two methods is necessary to protect the disassembled system during shipment and storage as well as during operation.

The most effective method for a specific application naturally depends on the amount of breathing permitted in the application and the minimum leakage attainable in the individual components of the system. The remainder of this chapter deals with the methods used in pressurizing the individual components and suggestions for improvements using new materials that show promise. Components requiring special sealing methods are (1) lines and couplings, and (2) rotating shafts and joints.

3-11. Sealing of Transmission Lines and Couplings.—Transmission-line output terminals of units are often sealed for protection during shipment. For this purpose, seals known as "pressurizing windows" have been used. Waveguide pressurizing windows of two types are discussed from the standpoint of electrical design in Sec. 4-22. The slug

type is made of polyglas which has a coefficient of expansion approximately equal to that of brass. The dielectric is molded into a solid piece of the correct dimensions and cemented into the waveguide to form a pressure seal. A very thin cement is required which will flow into a small clearance space of about 2 or 3 mils between the slug and the waveguide wall. Vinylseal cements¹ NA 28-14 and T 24-9 thinned with acetone or toluene respectively have given the best results so far obtained. Two or three applications of the cement are usually required for a good pressure seal because the evaporation of the solvent tends to leave air pockets. When properly cemented the unit makes an airtight seal over a wide temperature range. One application of cement is sufficient for holding the slug in place and keeping out moisture and dirt during shipment. Coaxial lines may be pressurized by dielectric beads similar in design to the waveguide windows of the slug type. This design is illustrated in Fig. 4-8.

The resonant-aperture pressurizing window was developed and manufactured by Westinghouse. This window, as shown in Fig. 4-76, is made by sealing glass into a Kovar disk to form an airtight seal. The Kovar disk is then soft-soldered to a choke coupling to complete the operation. This seal will stand extreme pressures and temperatures.

Synthetic rubber rings are used in waveguide and coaxial couplings to pressure-seal the junctions. They are very simple in construction, as shown in Fig. 4-44. The rectangular groove that holds the doughnut-shaped rubber ring is designed so that the rubber ring practically fills the groove when the two metallic parts are clamped together. The rubber ring must retain its elasticity over the temperature ranges encountered in the use of the system being designed.

3-12. Rotary-joint Pressure Seals.—Rotary-joint pressure seals have been the chief cause of leaks in pressurized systems. No completely satisfactory solution of the problem has been found because materials having the proper characteristics have not been developed. Several designs have been used, however, with a fair degree of success.

To meet the restrictions usually encountered in the operation of a rotary joint, the rotary seal must: (1) operate at speeds up to 3000 rpm; (2) operate over a temperature range from 70° to -50°C; (3) impose low frictional torque; (4) require small space; (5) be easily reproducible; (6) operate continuously.

The following types of rotary seal have been recommended: (1) the synthetic-rubber-lip type, (2) the Sealol type, (3) the bellows type.

The synthetic-rubber-lip seal, developed at Radiation Laboratory and manufactured by Graton and Knight² has proved to be the most economi-

¹ Manufactured by Carbide and Carbon Chemicals Corp., New York, N.Y.

² Graton and Knight Co., 356 Franklin Street, Worcester, Mass.

cal and dependable of the three types. Figure 3-4a shows the construction of the rubber-lip seal. The rubber is held firmly in the outer housing in such a way that pressure on the high-pressure side tends to tighten the seal on both the rotating shaft and the outer housing.

This type has the advantages of extremely low cost and very small space requirement. The rubber rings are readily interchangeable; thus the unit is easily serviced. Test samples have run continuously for

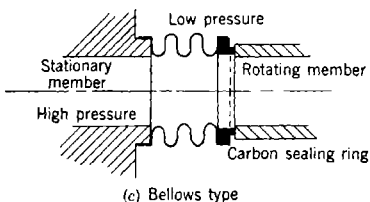
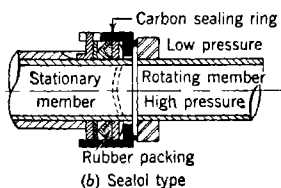
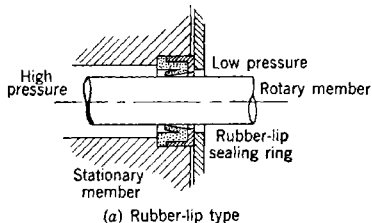


FIG. 3-4.—Rotary-joint pressure seals.

months without excessive air loss; a loss of 1 in.³ in 2 hr at an internal pressure of 15 lb/in.² is not considered excessive. The torque required is 1 to 2 lb-in. for a 1-in. shaft seal holding 15-lb pressure. The lip must be thick enough to ensure accurate trimming, and the angle of slope should be as small as practicable for low torque. The metal housing ring should have appreciable grooves and should be nickel-plated to achieve a satisfactory bond to the rubber. The housing ring should provide support at the rear of the seal for maintenance of low torque.

The rubber used in the rubber-lip seal is very important. Graton and Knight Formula 93, a Hycar base preparation, is recommended. Results of tests on many types of rubber indicate a stress-deformation hysteresis period inversely proportional to the temperature. Even though the rubber samples themselves are flexible down to -70°C , the stationary sealing limit is about -50°C and, with the shaft rotating, the limit is -20°C . Therefore, for very low temperatures, electric heaters are required for seals made of this compound.

The Sealol type of rotary seal illustrated in Fig. 3-4b utilizes a carbon cylinder sealed by a rubber packing to a stationary member running against a lapped steel shoulder on the rotating member to form the seal. The success of the design depends upon the finish of the carbon and steel mating surfaces—a fact that makes manufacturing tolerances critical. The carbon must be nonporous and the contact surface smooth and round.

Morganite MM₁ and MM₂ made by the Morgan Brush Company of Long Island City, N.Y., or Graphitor No. 35 and No. 39, made by the U. S. Graphite Company of Saginaw, Mich., are recommended for Sealol rotary seals when used with hardened tool steel. Speed is no problem except for temperature rise with dry operation. At 3500 rpm this rise over ambient temperature is about 70°C for a 1-in. shaft. The torque requirement for a 1-in. shaft seal at a gauge pressure of 15 lb is 2 to 5 lb-in. After a 10- to 20-hr run-in period at 2000 rpm required to lap the surfaces, the leakage can be brought down to 1 in.³ in 20 hr at 15 lb/in.²

Bellows seals as shown in Fig. 3-4c are less reliable because they have mechanical flexibility, require more room, and require the same precise manufacturing as the Sealol type. The fact that the seal utilizes a carbon or bronze foreplate, bearing against a lapped steel shoulder, makes its operation independent of temperature.

The success of either type depends on the characteristics of the sealing material. No material that has been tried has given a completely satisfactory seal; however, new developments in the field of plastics may offer solutions to the sealing problem.

New silicone rubber developed by Dow Corning Corporation and General Electric appears to offer a possible solution to the low-temperature problems of the rubber-lip seal. Silicone rubber retains its elasticity at very low temperatures.

Another new material, developed by E. I. du Pont de Nemours and Company, appears to have promising possibilities for use in all types of seals. The new material, known as "Teflon" and designated by du Pont as "Poly F-1114," is a soapy-feeling plastic that causes very little friction when rotated in contact with a machined metallic surface. It is not so pliable as rubber but has much better low-temperature characteristics. Teflon is also very resistant to chemical action and absorbs no moisture.

CHAPTER 4

RIGID TRANSMISSION LINES

BY G. L. RAGAN AND RICHARD M. WALKER

COAXIAL LINES

BY G. L. RAGAN

4-1. Factors Governing Choice of Dimensions.—The primary considerations in choice of rigid-line dimensions are high power-carrying capability and low attenuation. Mention of such other characteristics as maximum voltage between conductors, maximum impedance of resonant line, and minimum impedance of resonant line is frequently made. These considerations, which are of importance in some types of work, are rarely, if ever, considered important at microwave frequencies and still less often are considered important in microwave transmission lines. The consideration of maximum voltage may be useful in case the frequency is so low or the line so short that it contains considerably less than one-half wavelength. In this case the voltage on the line is essentially constant along its length regardless of impedance-matching and is of prime importance in the transfer of power. In microwave lines, however, this is almost never the situation. Such lines are usually much longer than one half wavelength so that the load impedance must match the line impedance if standing waves are to be avoided. It is in this matched condition that a given line carries maximum power to a load; high power-carrying capability therefore is calculated on this basis. The resonant impedance behavior of a coaxial line enters into certain resonator problems at microwave frequencies but not into the choice of dimensions for a transmission line.

In seeking the dimensions of a transmission line to obtain optimum performance with respect to some selected characteristic, the problem must be limited further in one of the following ways. One may seek those dimensions consistent with the restriction that only the fundamental *TEM*-mode be propagated at a given wavelength in the resulting line; this restriction sets an upper limit, in a certain manner, on the size of the line for a given wavelength. Or one may be limited for mechanical reasons to an even smaller line size. Usually, in this case, the limitation will be the diameter of the outer conductor.

The two primary factors, high power-carrying capability and low attenuation, will be considered now under these two types of limitation.

Maximum Power-carrying Capacity for a Given Wavelength.—The power being transmitted by a coaxial line in the absence of standing waves is given by Eq. (2-77),

$$P = \frac{E_a^2 \sqrt{k_e} a^2}{120} \ln \eta, \quad (1)$$

where $\eta = b/a$ is the diameter ratio of the conductors. The critical dimensions for cutoff of the second or TE_{10} -mode are well approximated by the relation indicated in Fig. 2-22.

$$\lambda_c \approx \sqrt{k_e} \pi (a + b); \quad (2)$$

therefore,

$$a \approx \frac{\lambda_c}{\pi \sqrt{k_e} (1 + \eta)}. \quad (3)$$

Substituting this value for a in the above equation, one obtains

$$P = \frac{E_a^2 \lambda_c^2}{120 \pi^2 \sqrt{k_e} (1 + \eta)^2} \ln \eta. \quad (4)$$

Normally one would operate at a wavelength slightly longer than cutoff. This effectively reduces a in Eq. (3) by the desired wavelength factor and

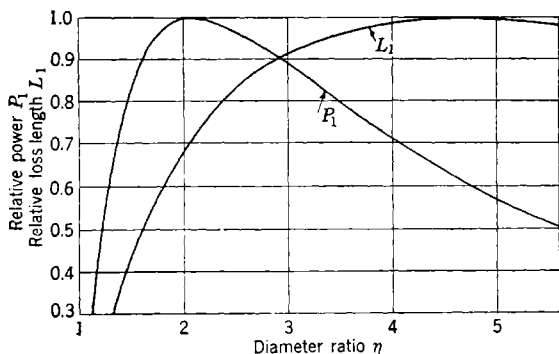


FIG. 4-1.—Relative power-handling capacity and loss length vs. diameter ratio for coaxial line, at a given wavelength.

reduces P in Eq. (4) by the square of this factor. The form of the equations is unchanged. Relative values of P are plotted as a function of η in Fig. 4-1. The maximum value of the last term, $\ln [\eta / (1 + \eta)^2]$, is found to be 0.0774. This occurs when η has the value 2.09 and means $Z_0 = 44.4$ ohms for air-filled line. When numerical values are inserted, the maximum power is given by

$$P_{\max} = 6.53 \times 10^{-5} \frac{E_a^2}{\sqrt{k_e}} \lambda_c^2, \quad (5)$$

and the corresponding conductor radii are

$$a = 0.097 \frac{\lambda_c}{\sqrt{k_e}}, \quad (6a)$$

$$b = 0.215 \frac{\lambda_c}{\sqrt{k_e}}, \quad (6b)$$

where $k_e = 1$ for air, and a reasonable value for E_a is 3×10^6 volts/m at breakdown. Hence, Eq. (5) becomes

$$P_{\max} = 5.88 \times 10^8 \lambda_c^2. \quad (7)$$

For example, $\lambda = 0.1$ m gives

$$\begin{aligned} P_{\max} &= 5.88 \text{ Mw,} \\ 2a &= 1.94 \text{ cm (0.764 in.)} = \text{center conductor OD,} \\ 2b &= 4.30 \text{ cm (1.692 in.)} = \text{outer conductor ID.} \end{aligned}$$

Minimum Conductor Loss for a Given Wavelength.—The attenuation in coaxial conductors may be written [slightly modifying Eq. (2-82)]

$$\alpha = 0.04566 \sqrt{\frac{k_e}{\sigma \lambda}} \frac{1 + \eta}{b \ln \eta} \text{ nepers/m.} \quad (8)$$

Applying the same limit as above to the size of conductors at a given wavelength, we find that

$$b = \eta a = \frac{\lambda_c}{\pi \sqrt{k_e}} \frac{\eta}{1 + \eta}. \quad (9)$$

If this value of b is substituted in the previous equation, the result is

$$\alpha = 0.1435 \frac{k_e}{\sqrt{\sigma} \lambda_c^{3/2}} \frac{(1 + \eta)^2}{\eta \ln \eta} \text{ nepers/m.} \quad (10)$$

Relative values of loss length, the reciprocal of α , are plotted against η in Fig. 4-1. The minimum value of the last term, $(1 + \eta)^2 / \eta \ln \eta$, is 4.45 and occurs when $\eta = 4.68$. The impedance is 92.6 ohms for air-filled line, and the minimum attenuation for a given wavelength is

$$\alpha_{\min} = 0.6368 \frac{k_e}{\sqrt{\sigma} \lambda_c^{3/2}} \text{ nepers/m.} \quad (11)$$

The line dimensions are

$$a = 0.056 \frac{\lambda_c}{\sqrt{k_e}}, \quad (12a)$$

$$b = 0.262 \frac{\lambda_c}{\sqrt{k_e}}. \quad (12b)$$

For an air-filled copper line ($\sigma = 5.80 \times 10^7$ mhos/m) the result is

$$\alpha_{\min} \begin{cases} = 8.38 \times 10^{-5} \lambda_c^{-3/2} & \text{nepers/m} \\ = 7.27 \times 10^{-4} \lambda_c^{-3/2} & \text{db/m.} \end{cases} \quad (13)$$

If $\lambda_c = 0.1$ m, then

$$\begin{aligned} \alpha_{\min} &= .0232 \quad \text{db/m,} \\ 2a &= 1.12 \text{ cm (0.441 in.)} = \text{OD of inner conductor,} \\ 2b &= 5.24 \text{ cm (2.065 in.)} = \text{ID of outer conductor.} \end{aligned}$$

Maximum Power-carrying Capacity for a Given Outer-conductor Size.— Equation (1) may be written in terms of b

$$P = \frac{E_a^2 \sqrt{k_e} b^2 \ln \eta}{120 \eta^2} \tag{14}$$

Relative values of P are plotted against η in Fig. 4-2. Since b is given, the problem is to find the value of η which makes the last term $\ln \eta/\eta^2$ a

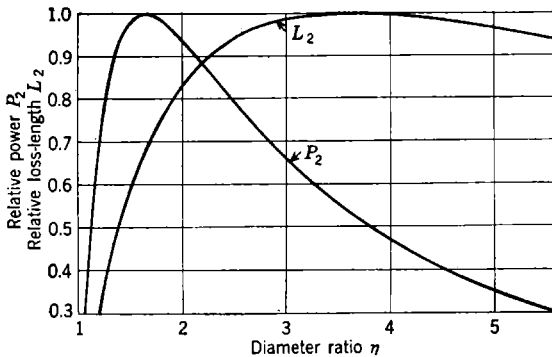


FIG. 4-2.—Relative power-handling capacity and loss length vs. diameter ratio for coaxial line for a given outer-conductor radius.

maximum. This maximum occurs for $\eta = 1.65$, giving an impedance of 30 ohms if the line is air-filled. For this case, assuming breakdown to occur when $E_a = 3 \times 10^6$ volts/m, the maximum power is

$$P_{\max} = 1.377 \times 10^{10} b^2. \tag{15}$$

Minimum Conductor Loss for a Given Outer-conductor Diameter.— In this case b is constant and η the variable; consequently, Eq (8) has the proper form. In Fig. 4-2 relative values of loss length, $1/\alpha$, are plotted against η . The term $(1 + \eta)/\ln \eta$ is a minimum when $\eta = 3.6$, which makes the characteristic impedance 77 ohms for air-filled line. For air-filled copper line

$$\alpha_{\min} = 0.0215 \lambda^{-1/2} b^{-1} \quad \text{nepers/m.} \tag{16}$$

Some Mechanical Considerations.—Aside from these r-f factors, there are some factors of mechanical nature. For instance, the line should be as rigid as possible in order to withstand shock and vibration with a minimum disturbance of characteristic impedance and power-carrying

capacity. Assuming the inner conductor to be a tube and of the same metal as the outer conductor, it seems that a relatively large center tube is desirable. This makes the two tubes approximately equal in size and their behavior under shock and vibration is comparable. Both the center and outer tubes should be large and supported at frequent intervals in order to keep the resonant frequency of each section of tubing above any vibration frequencies likely to be encountered in use. A large center tube and frequent supports are also an aid in preventing relative motion

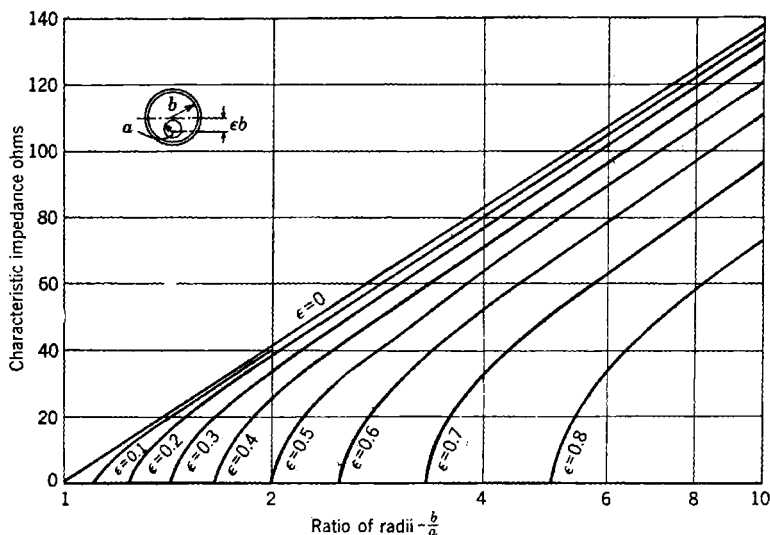


FIG. 4-3.—Characteristic impedance of an eccentric line.

between inner and outer tubes when the line is subjected to shock. The diameter ratio should not be made too small, however, since the effect of eccentricity is much more pronounced for low-impedance lines. Fig. 4-3 illustrates this eccentricity effect.

In manufacturing small lines, particularly for the short-wavelength end of the microwave region, it is desirable to use a relatively large center conductor. The upper limit upon the size of center conductor comes from the previously mentioned effect of eccentricity. Within the limitation imposed by this effect, a large center conductor makes it easier to fabricate such structures as stub supports, slotted center-conductor contacts (bullets), and center-conductor capacity couplings like those used for rotary joints.

The summation of these mechanical considerations leads to a compromise between the very low diameter ratio indicated by most of these considerations and the practical limitation imposed by the increased

sensitivity of low-impedance lines to eccentricity effects. Probably a diameter ratio of 1.5 to 2 is an acceptable figure. This ratio gives a characteristic impedance for air-filled line of 25 to 42 ohms—values that are about the same as those for maximum power-carrying capacity, 30 ohms and 44.4 ohms for the two cases already discussed.

The 50-ohm Line as a Compromise Standard.—When choosing a coaxial line to serve a given purpose one might choose the line impedance to suit the requirements peculiar to the individual application. Depending on which of the five characteristics already mentioned is considered most important, this procedure would lead to the use of a number of different impedances over a threefold range, 30 to 93 ohms. Under such a system each transmission-line circuit element is a special design problem requiring its own special test equipment, such as slotted lines for impedance measurement. Obvious economy both in test equipment and in design work can be achieved if a single impedance can be chosen as a compromise standard. It has been found convenient to adopt 50 ohms as an impedance level offering a satisfactory compromise. For air-filled coaxial line this requires a diameter ratio of 2.3, and for polyethylene ($k_e = 2.25$) a ratio of 3.5. By reference to Figs. 4-1 and 4-2 the performance of the 50-ohm line may be compared with that of the line whose diameter ratio has the optimum value for each of the four characteristics presented there. The results of such an examination are given in Table 4-1.

TABLE 4-1.—COMPARISON OF 50-OHM PERFORMANCE WITH THAT OF OPTIMUM LINES

Characteristic	Optimum value of η	Relative values for 50-ohm line	
		$k_e = 1, \eta = 2.3$	$k_e = 2.25, \eta = 3.5$
For a given wavelength:			
Power handled.....	2.09	0.99	0.80
Loss length.....	4.68	0.78	0.96
For a given outer conductor:			
Power handled.....	1.65	0.86	0.56
Loss length.....	3.60	0.91	1.00

Quite apart from line-impedance considerations, a number of different line sizes are required in order to meet mechanical requirements and to accommodate various wavelengths. A list of some air-filled lines which have been used, together with some of their characteristics, is given in Table 4-2.

The theoretical maximum power tabulated is for a peak voltage gradient of 30,000 volts/cm and for coaxial cylinders in the absence of supports. The recommended maximum powers are based on experi-

TABLE 4-2.—SOME COAXIAL-LINE CHARACTERISTICS

Line size OD, in.	Wall, in.	Inner- conductor diam., in.	Impedance, ohms	Support	Theoretical maximum power, kw	Recommended maximum power, kw	Attenuation, db/m	Lowest safe wavelength, cm
$\frac{1}{16}$	0.025	0.125	44.4	bead	140	5	0.21	1.70
$\frac{1}{8}$	0.032	0.1875	50.6	stub	358	50	0.20	2.70
$\frac{3}{16}$	0.035	0.250	47.8	bead	598	20	0.095	3.50
$\frac{1}{4}$	0.032	0.375	46.4	stub	1310	200	0.066	5.28
$\frac{5}{16}$	0.049	0.500	50.0	stub	2530	400	0.045	7.18
$\frac{3}{8}$	0.049	0.625	53.4	stub	4200	600	0.033	9.30

ence with $\frac{7}{8}$ -in. stub-supported lines and $\frac{5}{8}$ -in. bead-supported lines in system use. These have shown signs of failure in carefully made laboratory systems at powers of about 500 and 50 kw, respectively. A safety factor of 2.5 in power (1.6 in voltage) is allowed in each case. These figures give a factor of 0.15 between theoretical maximum and design maximum for the stub-supported series and 0.033 for the bead-supported series. The low rating for the bead-supported lines is explainable on the basis of flashover along the insulator and high fields in air spaces between bead and center conductor. The attenuation figures given are for copper lines. For the $\frac{1}{8}$ -in. line, the wavelength is 3.3 cm; in all others it is 10 cm. Silver-plated lines are some 60 per cent higher in attenuation. Lines made of brass tubing have about twice the attenuation of copper lines. In Table 4-2, the lowest safe wavelengths listed are taken as 12 per cent above the cutoff wavelength for the second coaxial mode, a criterion based on experience with the $1\frac{1}{8}$ -in. line. It was found that this line was usable down to a wavelength of about 9.3 cm, which is 12 per cent longer than that calculated as cutoff for the second coaxial mode. These lines have been approved by the Army-Navy Cable Coordinating Committee as standards for microwave use. It is common practice to refer to a line by the outer diameter of the outer conductor. Thus, the largest line listed is commonly referred to as the $1\frac{5}{8}$ -in. line.

4-2. Couplings for Coaxial Lines.—

The principal points to consider in such couplings are these. First, both outer and inner tubes should be joined with a minimum of discontinuity in order to minimize reflection of r-f power

and to prevent any local concentration of fields, by sharp corners, which would lower the breakdown power level. Second, the contact resistance of both outer and inner junctions should be kept low in order to minimize losses and to prevent burning and consequent deterioration of the contacts by the high currents involved. Third, it is frequently desirable to provide a pressure-tight junction in the outer tube to prevent the entrance of moisture or of corrosive atmosphere or to maintain an actual pressure differential. Finally, such features as

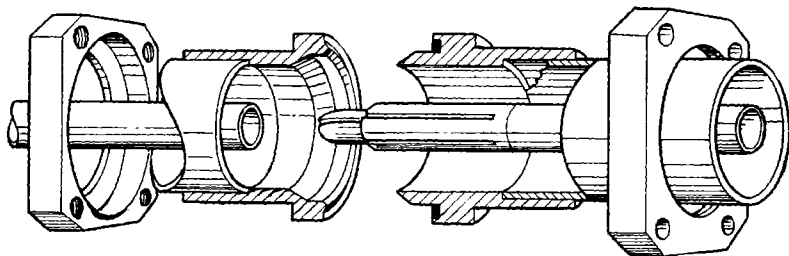


FIG. 4-4.—Coupling for coaxial line; polarized connector.

convenience in use and positive clamping action should be considered. The following types of connector have been found to satisfy these requirements.

Polarized Connectors.—The coaxial connector most used in microwave lines is shown in Fig. 4-4. It is a polarized connector; that is, the two mating units are not identical. The junction of the outer conductors is made by forcing into a female taper a piece bearing a male taper of slightly sharper angle. This insures contact's being made at the tip of the male piece and hence at the desired point, the inner wall of the outer conductor. The connector is drawn up by means of four screws passing through clearance holes in a square flange surrounding the male outer connector. The female outer connector is surrounded by a similar flange with tapped holes to receive these four screws. A neoprene gasket is compressed between the two outer-connector pieces to provide pressurization. Its dimensions must be right within small tolerances; it must be thick enough to obtain sufficient compression to insure pressurization, and yet not so thick that it will prevent a good contact between the male and female tapers.

The center-conductor junction is formed by plugging the slotted "bullet" of the male connector into the end of the center-conductor tube of the female connector. The nose of the bullet is very slightly tapered at the point of contact, so that contact is made to the inside of the female center tube at its end only. This prevents any reentrant cavity's being formed between the inside of the female tube and the outside of the

bullet nose. The circular gap between the end of the female tube and the shoulder on the bullet is kept as small as mechanically feasible in order to minimize the impedance and field discontinuities set up thereby. In the case of the $\frac{7}{8}$ -in. OD coaxial line, the gap is held to a maximum of 0.032 in. The standing wave introduced by this discontinuity is certainly less than 1.03 at a wavelength of 10 cm. It is very important that the bullet shoulder should not be forced against the end of the female tube before the outer-conductor coupling is completely sealed. If this should occur, the center conductor would tend to buckle under the longitudinal compression so introduced. For this reason the extension of the female center tube and the male bullet shoulder are each specified according to their respective outer-conductor parts in such a way that there is a gap (nominally, 0.016 in. with a tolerance of ± 0.016 in. in the case of the $\frac{7}{8}$ -in. line) between them when the coupling is drawn together completely. It is very important that the slotted bullet be springy enough to make good tight contact with the inner wall of the female tube. Normally a springy metal (see Sec. 3-1) such as heat-treated beryllium copper is used for the bullet. A heat-treated chrome-copper alloy has been found to have satisfactory mechanical properties and, in addition, to afford better thermal conductivity. The quality of conductivity is sometimes desirable as, for instance, in plugging into a transmitter tube. The heat generated in the contacts and in the glass seal is then conducted away more rapidly, reducing the temperature at the glass seal. In soldering this bullet into the male center tube, a low-melting solder must be used and care must be exercised to prevent injuring the temper of the bullet by overheating. In fabrication the bullet is sprung out so that it is under radial compression when plugged into the female tube.

Several convenient features of this connector may be indicated. There are no loose pieces in the assembly; all the elements of the connector are self-contained except the four standard screws, and these can be made captive screws if desired. This feature prevents loss of parts and also makes it impossible to omit any vital part in making a connection, an omission which has occurred in the case of the double-ended bullet of the unpolarized connector discussed later. Another desirable feature is that a line to which a connector is to be attached is prepared simply by making certain that the outer and inner tubes end flush with each other, because the total length of the two outer-conductor parts when coupled is exactly the same as the length of bullet plus gap allowance. A third feature is that a certain amount of angular misalignment of the axes of the connected lines is permitted by the tapers of the outer- and inner-conductor contacts. This misalignment cannot be allowed to become large, however, since the tapers are slight

and since the pressurizing gasket will not be properly compressed if the misalignment is large.

In the use of any polarized connector, it is advisable to establish a convention to be followed in assembling connectors to line sections or line components. It is customary to follow the same convention as in connecting garden hose; namely, at a connection the power (water) flows from transmitter (water main) through a male coupling into a female coupling. Thus, the male coupling always points toward the antenna (or hose nozzle). In case the line is also used for reception, or for reception alone, the male coupling still points toward the antenna.

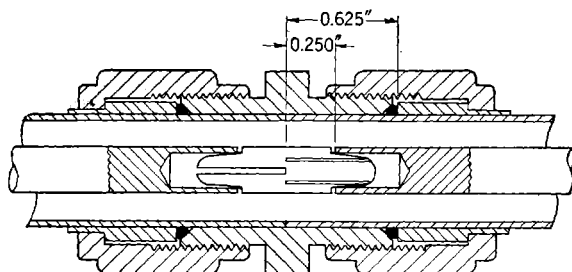


FIG. 4-5.—Five-eighths-inch line coupling; unpolarized connector.

This convention is recommended for all transmission lines, whether of coaxial or waveguide type.

Unpolarized Connectors.—Another type of connector which has had considerable use is that shown in Fig. 4-5. Since the two line ends joined are identical, this connector is said to be “unpolarized.” The unpolarized connector has certain obvious advantages in permitting the assembly of lines and components in any order or in the turning of any piece end-for-end; but it has the disadvantage of requiring two loose pieces—the center-contact “bullet” and the outer union. In addition to the possible loss of these loose parts, there is also the possibility of omitting a bullet or of its falling out of place during assembly. This is especially serious in a line containing dielectrics—for example bead supports or vacuum seals, since the high standing waves resulting may cause permanent damage to the dielectric before the power can be shut off. Even if this problem does not exist, as in purely receiving or low-power transmitter lines, it is a nuisance to have to take many couplings apart until the faulty connector assembly is found.

The inner-conductor bullet is exactly like the bullet of the unpolarized connector on each end. A double-ended bullet is usually shorter than the single-ended type, although to obtain the same mechanical properties, such as springiness, it should be about twice as long as the latter. Since

it is not soldered in place, the problem of detempering by the heat of soldering is avoided.

The outer contact is made between the outer tubes directly, the union sleeve providing the necessary alignment. In order to get good contact all around, the tube ends must be finished flat and in a plane perpendicular to the tube axis. The special trimming tool shown in Fig. 4-6 drawn to a larger scale does this, and at the same time it trims to the proper length the sleeve against which the pressurizing gasket is compressed by the union.

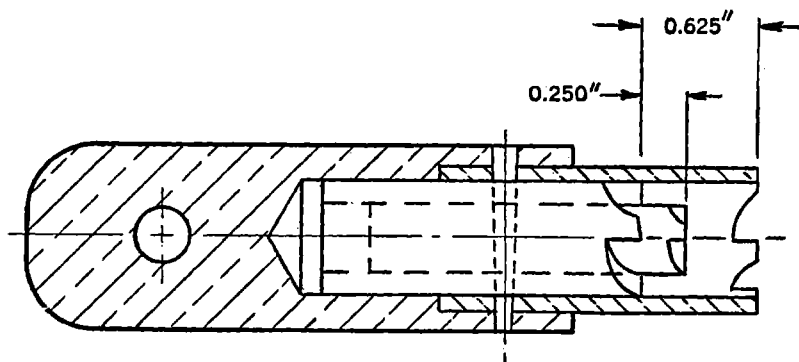


FIG. 4-6.—Trimming tool for unpolarized connector.

This connector has been largely superseded by the polarized connector discussed before and is not recommended because of the difficulties just mentioned.

Other Connectors.—Several other connectors which have been used to some extent are shown in Fig. 4-7. They are essentially like one or the other of the two connectors already discussed, or combine features of the two. The connector shown in Fig. 4-7a requires special care in soldering and in finishing the tube ends and is intended for laboratory test work only. The connectors shown in Figs. 4-7b and c are designed primarily for aluminum lines and do not require any soldering.

Although the soldering and brazing techniques for aluminum are now being worked out, they are still difficult. Corrosion of aluminum in general, in soldered or brazed joints, and in contacts with other metals gives considerable trouble. Another difficulty encountered with aluminum connectors is that the resistance of aluminum contacts is fairly high. Since it is presumably caused by a surface film of insulating aluminum oxide, the high resistance might be expected to be less troublesome in the microwave region where the frequency is so high that the capacitive reactance across the insulating layer becomes small compared to the contact resistance. To improve the contacts, a silver layer has

sometimes been applied, either by electroplating or by spraying molten silver onto the contact surface. The conductors may be made of aluminum tube clad on the inside with a thin silver lining in the process of tubing manufacture. The outer tube can then be flared out so that the silver surfaces form the contact. The silver lining inside the center tube would not serve to decrease the attenuation of the line as it does in the case of the outer conductor and thus would be wasted except at the contact.

4.3. Bead Supports.—One of the major problems in connection with coaxial lines is that of supporting the center conductor. The obvious method of accomplishing this is to use dielectric insulating washers, commonly referred to as “beads.” While these beads alter the characteristic impedance and propagation constant of the line throughout the bead thickness, the impedance discontinuity so produced is rather unimportant at very low frequencies. In this case there are usually many beads per wavelength, and one simply modifies the characteristic impedance and propagation constant of the air-filled line to take into account the presence of a partial dielectric filling.¹ In microwave lines, on the other hand, the beads are an appreciable fraction of a wavelength thick, so that the impedance discontinuity is sizable. Furthermore, there are few, rather than many, beads per wavelength. For these reasons, simply modifying the line characteristics is not sufficient. A

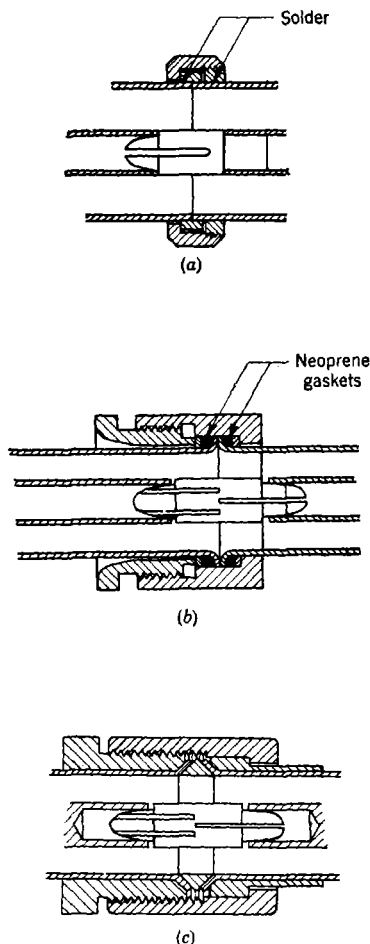


FIG. 4.7.—Miscellaneous connectors. (a) Unpressurized laboratory connector (Raytheon Company). (b) Solderless connector for aluminum line, pressurized by neoprene gaskets (General Electric Company). (c) Solderless connector for aluminum line with metallic compression-type pressurization (Radiation Laboratory).

¹ H. T. Kohlhaas, *Reference Data for Radio Engineers*, Federal Telephone and Radio Corp., 1943, p. 116.

number of schemes have been devised to circumvent these impedance difficulties, as shown in Fig. 4-8. They will be discussed in detail later in this section.

At low frequencies, dielectric losses in lines are usually negligible compared to conductor losses, but at microwave frequencies dielectric losses become comparable to, and in some cases greater than, conductor losses. The dielectric attenuation constant in a line completely filled with dielectric is, by Eq. (2-99),

$$\alpha_{di} = \frac{27.30 \sqrt{k_e}}{\lambda} \tan \delta \quad \text{db/m.} \quad (17)$$

This figure is independent of diameter ratio but assumes the dielectric-filled line to be matched. This equation applies directly to the undercut bead, Fig. 4-8c, since the bead is matched—that is, it is terminated in its characteristic impedance. In other arrangements the beads are not matched, and as a result the dielectric attenuation constant is larger.

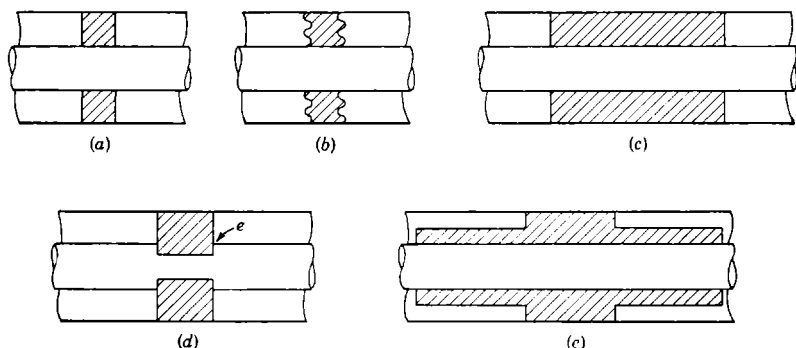


FIG. 4-8.—Several forms of bead support. (a) Thin bead. (b) Bead grooved to increase surface leakage path. (c) Half-wave bead. (d) Undercut (constant impedance) bead. (e) Stepped three-quarter-wave bead.

An effect that may be of comparable magnitude is the increase in the beaded section of the conductor loss caused by the introduction of dielectric. Fortunately, this increase does not occur for very thin beads, since the current flowing in the conductors is the same as that in the main line.

A problem common to both low and high frequencies is that of voltage breakdown. This problem acquires increased importance, however, in lines carrying pulses of high peak power, a requirement that is frequently imposed in microwave applications. In this connection three effects are of importance. The first is flashover radially along the air-dielectric interface, which occurs at a lower field than that required to break down either material alone; the extent to which this limits the

power is difficult to estimate, and it depends on the character of the surface and on humidity effects. The bead faces are sometimes corrugated by concentric grooves similar to those shown in Fig. 4-8*b* to increase the leakage path for surface currents. The second consideration is the limitation imposed by breakdown within the insulator itself at microwave frequencies and is an element that is hard to evaluate. The dielectric strength, however, of practically all dielectrics is known to exceed that of air by a large factor at ordinary frequencies. This is known to be also true of the dielectrics used in flexible coaxial cables at microwave frequencies. Hence one does not anticipate any limitation on power by reason of breakdown in the body of the dielectric. The third effect is the increased field in the air film which is likely to exist between bead and conductor. If a cross section such as that of Fig. 4-9 is considered, it is recalled that the electric displacement must be constant across the boundary c

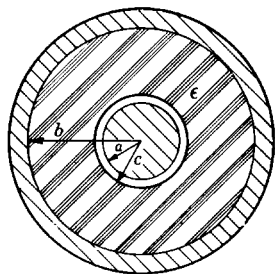


FIG. 4-9.—Loose-fitting coaxial bead.

$$E_c(\text{air}) = k_e E_c(\text{dielectric}). \quad (18)$$

For very thin air films this may be written

$$E_f = k_e E_a, \quad (19)$$

where E_f is the electric field strength in the air film and E_a that in the dielectric at $r = c \approx a$. The air film may be thin enough to give a negligible contribution to line voltage, characteristic impedance, power transmission, and so forth, but still so thick that it contains enough gas to give breakdown trouble. Any thickness that is large (compared with mean distance through which an accelerated electron moves between collisions with the molecules of the gas) would be sufficient to cause such breakdown trouble. Since this mean distance is of the order of 10^{-5} cm at atmospheric pressure, it is clear that films of air of several orders of magnitude greater than this figure might easily occur. The critical field strength at breakdown may be assumed to be the same in the air film as in the main line, but there is evidence¹ to indicate that larger r-f fields may be tolerated in small gaps, just as in d-c breakdown. Therefore, any estimate of power-handling capability based on this assumption may be regarded as fairly conservative.

In the case of thin beads, the total voltage across the line is the same in the bead as in the unbeaded line; therefore, the field in the dielectric

¹ D. Q. Posin, I. Mansur, H. F. Clarke, "Experiments in Microwave Breakdown," RL Report No. 731, Nov. 28, 1945.

would be identical with that in the unbeaded line at any given radius. If a very thin air film were present, the field in it would be given by Eq. (19); hence, the power transmitted by the line must be reduced by the factor k_e^2 to prevent breakdown in the air film. If the bead is of polystyrene, $k_e = 2.56$, the power-reduction factor is 6.6 (multiplying factor 0.15). The same factor applies to the half-wavelength line, since the maximum voltage occurs at the ends where it is equal to that in the unbeaded line.

For the undercut bead, the total voltage is again the same as that of the unbeaded line, but the center-conductor diameter has been decreased. Since the undercut section is matched, Eq. (14) is applicable, where E_a is the field in the dielectric at $r = c \approx a$. In view of Eq. (19) E_a may be replaced by E_f/k_e . The power transmitted by a matched dielectric-filled line in which an air film is present is then given by

$$P_f = \frac{E_f^2 b^2}{120 k_e^{3/2}} \frac{\ln \eta}{\eta^2} \quad (20)$$

Comparison with the power P_0 carried by an air-filled line of the same characteristic impedance and same outer-conductor radius gives the power-carrying factor

$$\frac{P_f}{P_0} = k_e^{-1} \left(\frac{\eta}{\eta'} \right)^2 = k_e^{-1} \eta^{-2} (\sqrt{k_e} - 1), \quad (21)$$

where η is the diameter ratio in the air-filled line and η' that in the undercut beaded line ($\ln \eta = \ln \eta' / \sqrt{k_e}$).

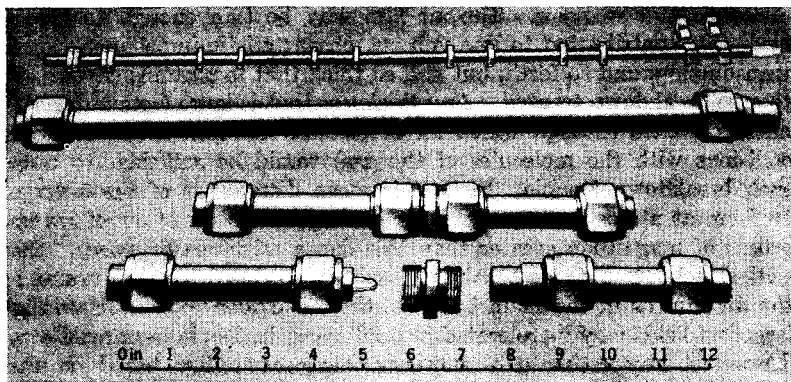


FIG. 4-10.—Bead lines.

Thin Beads.—While bead-supported lines have largely been supplanted by stub-supported ones, some of the early transmission lines were beaded. The standard $\frac{5}{8}$ -in. OD line was used, both outer and

inner conductors being of copper tubes. Sections of such a line are shown in Fig. 4-10. The beads were of polystyrene, and the dimensions were made in such a way that the beads fitted tightly onto the center tube but loosely into the outer. This permitted affixing the beads at the proper intervals onto the center tube and then pulling the assembly into place within the outer tube. Since the tubes were of soft copper and the beads gave support at frequent intervals, gentle bends in the completed line were permissible. With sufficient care, a bending tool could be used to obtain bends on a radius as small as four inches. The molded polystyrene beads were 0.100 in. thick, 0.254 in. in inner diameter to fit closely around the 0.250-in. inner tube, and 0.500 in. in outer diameter to permit a loose fit within the 0.555-in. ID outer tube.

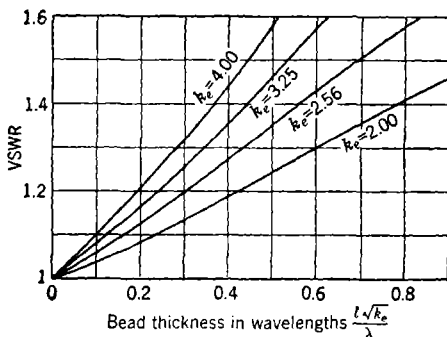


FIG. 4-11.—Mismatch introduced by thin beads.

The mismatch introduced by a bead that fits tightly against both outer and inner conductors is easily calculated (see Fig. 4-11). Figure 4-11 gives an enlargement of that portion pertaining to thin beads. From this graph it is found that a 0.100-in. (.04 wavelengths at $\lambda = 10$ cm) polystyrene bead is expected to give a VSWR of 1.27. Since the bead fits loosely in the outer tube, the VSWR should be reduced, and $r = 1.23$ is the experimentally determined¹ value. The figure is further reduced by the crimping technique used to hold the bead in place on the center tube, because the crimping, which consists of deforming the center tube on both sides of the bead by squeezing it between parallel knife edges, increases the characteristic impedance in the crimped portion of the line. These short sections of high-impedance line partly compensate for the section of low-impedance line formed by the bead. The crimping used in the $\frac{5}{8}$ -in. line was found by Reed² to reduce the VSWR from 1.23 to 1.15 at $\lambda = 10$ cm. Since the crimping has a rather large effect on the VSWR introduced, it must be carefully controlled.

¹ J. Reed, "Broad-band Bead Spacing," M.I.T. Bachelor's Thesis, January 1943.

² *Ibid.*

A number of bead-spacing schemes have been proposed.¹ Theoretical analyses of the performance of some of these schemes have been made by Condon² and by Hansen.³ The more promising schemes are based on the cancellation of the reflections of two beads when spaced approximately a quarter wavelength apart, as in Fig. 4-12a. Figure 4-13 gives the performance of a pair of $\frac{1}{8}$ -in. polystyrene beads spaced for cancellation $\lambda = 10$ cm in Curve II, and for comparison, that of a single bead in Curve I. Using the nomenclature of Fig. 4-12a, it can be shown that the condition for reflectionless spacing of a pair of beads is

$$\tan \alpha \tan \beta = \frac{2 \sqrt{k_e}}{1 + k_e} \quad (22)$$

Since the right-hand member of this equation is approximately unity, one may write an approximation which is extremely good for thin beads,

$$\alpha + \beta \approx \frac{1}{4}\lambda, \quad (23)$$

where all electrical angles are expressed in terms of wavelengths. For example, the angles of Fig. 4-13 are $\beta = 0.05$, $\alpha = 0.195$, and

$$\alpha + \beta = 0.245.$$

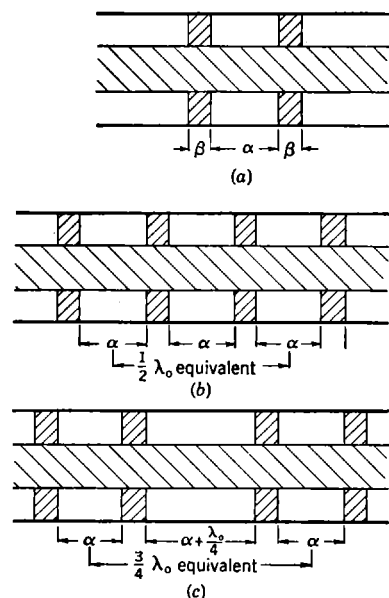


FIG. 4-12.—Basic bead spacings. (a) Quarter-wave-spaced pair. (b) Uniform quarter-wave spacing. (c) Lawson spacing for four.

Building up a bead-spacing scheme based on pairs spaced a quarter wavelength apart, one may use uniform spacing between beads as in Fig. 4-12b keeping the total number of beads even. The spacing between pairs is equivalent to a half wavelength; consequently, the reflections from the two pairs are approximately in phase and lead to the high wavelength sensitivity of Curve III of Fig. 4-13. If the two pairs are spaced

¹ J. L. Lawson, "Design and Test of Concentric Transmission Lines," RL Report No. 141, July 14, 1941; W. W. Salisbury, unreported early work using half-wave air line between beads; John Reed, *op. cit.*

² E. U. Condon, "Low-loss Coaxial Cables for Micro-Waves," Research Report R-94293-E, Westinghouse Research Laboratories, Apr. 17, 1941.

³ W. W. Hansen, "Notes on Microwaves," Chap. VII of the notes prepared by S. Seeley and E. C. Pollard based upon Hansen's lectures to the personnel of Radiation Laboratory in 1941-1942.

the equivalent of three-quarters wavelength apart, as in the Lawson system of Fig. 4-12c, the response curve is flattened as indicated by Curve IV of Fig. 4-13. This gives a great improvement near midband, but it should be noted that at about 8.3 and 12.5 cm the curves cross, the Lawson spacing going to much higher values than that of the uni-

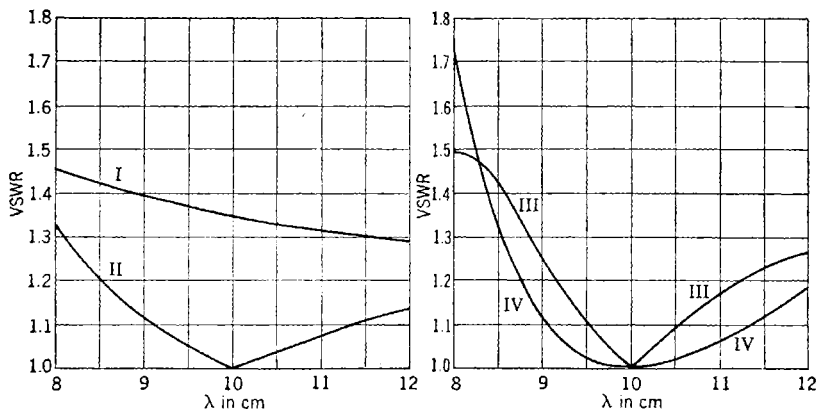


FIG. 4-13.—VSWR for $\frac{1}{8}$ -in. polystyrene bead as a function of wavelength. Curve I, single bead; Curve II, quarter-wave-spaced pair as in Fig. 4-12a; Curve III, uniform quarter-wave spacing, four beads as in Fig. 4-12b; Curve IV, Lawson spacing for four beads as in Fig. 4-12c.

form spacing. Hansen¹ has analyzed, by an approximate method, the behavior of these curves as more and more beads are added. His results may be summarized in the following manner.

1. The curve for the uniformly spaced line becomes steeper and steeper, whereas that for the Lawson line becomes flatter and flatter, in the neighborhood of midband.
2. The maxima on either side of midband wavelength move in closer and closer and secondary, tertiary, etc. maxima enter the range of wavelengths being considered.
3. It can be shown that the amplitudes of the maxima in the case of the uniform line are limited to approximately that of Curve I for a single bead in the wavelength region considered in Fig. 4-13. On the other hand, the maxima of the Lawson line are not thus limited, and as a result extremely high standing waves will occur at a wavelength fairly close to midband if many beads are used.
4. Hansen concludes that for short lines having few beads the Lawson line is best, but for long lines the quarter-wave uniform spacing is to be preferred. If a total bandwidth of $\Delta\lambda$ at a midband wave-

¹ Hansen, *op. cit.*

length λ_0 is desired, then the Lawson spacing is not bad, providing the number of beads is less than

$$n = 2 \frac{\lambda_0}{\Delta\lambda}$$

Fluctuations in bead thickness, variations in crimping, and errors in positioning of beads may introduce enough randomness to alter the predicted behavior markedly. Line losses also tend to reduce the cumulative effect of reflections. Reed has suggested that beads be assembled in groups of eight, the spacing between groups to be random.

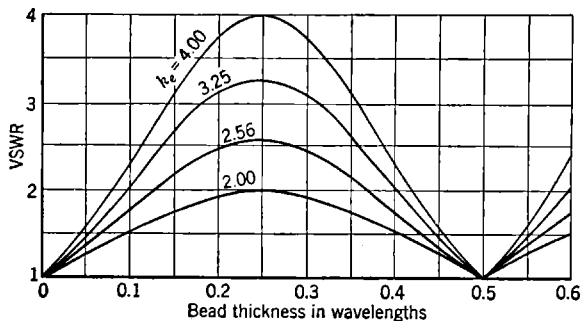


FIG. 4-14.—Mismatch caused by a bead as a function of thickness.

His system for the eight beads is as follows: the spacing between beads in each pair to be right for one wavelength, that between pairs in a set of four to be right for another, and that between the two sets of four to be right for a third wavelength. By choosing the three wavelengths properly a low VSWR may be obtained over a considerable band.

Half-wavelength Bead.—Since the input impedance of a half-wavelength section of transmission line is equal to its output impedance regardless of its characteristic impedance, a bead whose thickness is half a wavelength (in dielectric) introduces no mismatch. If the bead length is chosen properly for midband the VSWR introduced will be a function of the deviation from half wavelength, as indicated by Fig. 4-14. The performance of beads which are made a half wavelength long at 10 cm is shown in Fig. 4-15. Comparison of the curve for the half-wave polystyrene bead with those of Fig. 4-13 for thin beads reveals the relatively high wavelength sensitivity of the half-wave bead.

Because of its high frequency sensitivity, its high dielectric loss (because of the large amount of dielectric present), and because of various mechanical reasons, half-wavelength beads are not used for transmission-line supports. They have found limited use as frequency-sensitive

elements purposely introduced to cancel the frequency sensitivity of some other circuit.

Undercut Bead.—If the size of the inner conductor is reduced by the proper amount, the characteristic impedance in the bead-filled line can be made equal to that in the air-filled line (see Fig. 4.8*d*). In

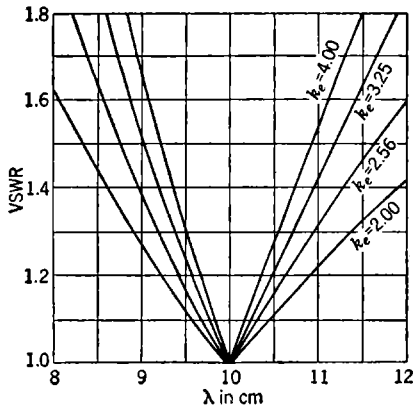


FIG. 4.15.—Performance of half-wave beads of various dielectrics.

order to achieve this equality the inner conductor must be reduced from a radius of a to a radius a' , so that

$$Z_0 = 60 \ln \frac{b}{a} = \frac{60}{\sqrt{k_e}} \ln \frac{b}{a'} \quad (24)$$

While at first this seems an ideal solution to the problem, there are practical difficulties. The problem of assembling the bead onto the undercut section may be solved by making the beads in two halves, split along a diameter; or it may be preferable to make the center conductor in many sections, one for each bead, and to assemble the sections by screwing or press-fitting each section to the next with the bead in place.

High-power breakdown may occur more readily in an undercut bead than in other types, because the sharp edge e shown in Fig. 4.8*d* naturally leads to a high electric-field concentration. Since this edge occurs at the bead surface, flashover along the dielectric surface is likely to occur. This tendency may be greatly reduced by rounding the edge; at the same time this rounding probably tends to decrease the net shunt-capacity effect (see below) at the junction. If such rounding is used, it is felt that breakdown is less likely to occur here than at the other vulnerable spot, namely, in the air film between the bead and the center conductor whose diameter has been reduced.

As discussed in Sec. 4.5, whenever a change of diameter occurs in

either of the coaxial conductors, or in both, the effect of the fringing fields so produced is equivalent to adding a certain capacity in shunt with the line at that point. If an undercut bead support is designed without compensating for this, a certain amount of mismatch will result. In the case of the 0.25-in. polystyrene bead in the $\frac{5}{8}$ -in. line of Table 4-1, calculation shows the shunt capacity introduced by the step at each end separately to be 6.8×10^{-14} f. At $\lambda = 10$ cm this leads to a capacitive susceptance of $0.062Y_0$, but the proximity effect, caused by the two discontinuities being relatively close together, reduces this to $0.055Y_0$. The over-all mismatch for the bead then amounts to a VSWR of 1.09.

In discussing power-handling capacity, it was remarked that rounding the corner where the center conductor changes diameter would be

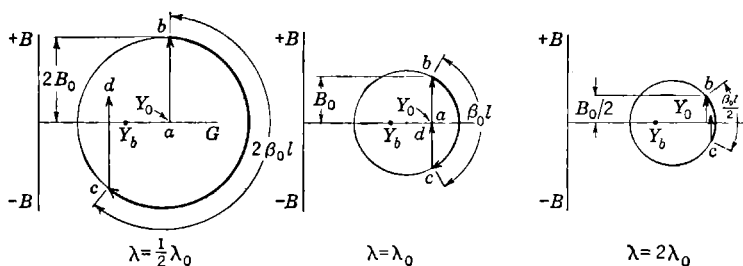


FIG. 4-16.—Admittance diagrams for compensated undercut bead.

expected to decrease the net shunt-capacity effect. This surmise is based on the fact that a decrease in the diameter of the center conductor gives rise to a short section of high-impedance line, which has an inductive effect. The degree of rounding required to give perfect compensation could be easily determined experimentally.

A simple and effective way of compensating for the shunt-capacity effect, in the case of beads that are thin compared with a wavelength, is to reduce the characteristic admittance Y_B in the beaded section. The rectangular-coordinate admittance diagrams of Fig. 4-16 show how this reduction accomplishes the desired result. The vertical lines ab and cd represent the shunt susceptance at the two bead surfaces, and the arc bc represents the electrical length of the bead. The input admittance is represented by d , and the error in closure da is a measure of the mismatch introduced. For a given bead thickness, Y_B is chosen to give perfect compensation near the shortest wavelength to be used. Since both the susceptance and the bead thickness in wavelengths are inversely proportional to wavelength, a reasonably low VSWR results for any $\lambda > \lambda_{\min}$. The thinner the bead is, the better the broadband performance. Unfortunately, decreasing the characteristic admittance in the bead means still larger steps in the conductor size and hence larger

shunting effects. Practically, however, this is not a serious effect. Figure 4-17 gives the dimensions for such a compensated bead designed for 10 cm and its calculated wavelength performance.

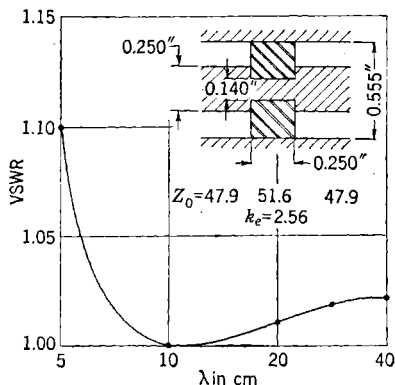


FIG. 4-17.—Undercut bead with high-impedance compensation.

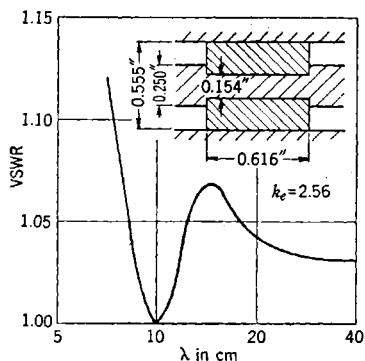


FIG. 4-18.—Undercut bead with quarter-wave compensation.

Another method of compensation is to make the bead a quarter wavelength long, leaving its characteristic admittance the same as that of the main line. This spacing of the two shunt-capacity effects gives cancellation at the design wavelength but does not perform especially well over a broad band. Figure 4-18 gives the dimensions and performance for such a bead.

Having designed beads in this way to have as low a mismatch as possible, it is further advisable to space them at odd quarter-wavelength intervals. This avoids cumulative addition of the reflections which, though individually small, may attain very large values if a number combine in phase. The discussions given previously relative to quarter-wave and alternative spacing schemes apply here although, of course, in the present case the mismatch per bead is much smaller.

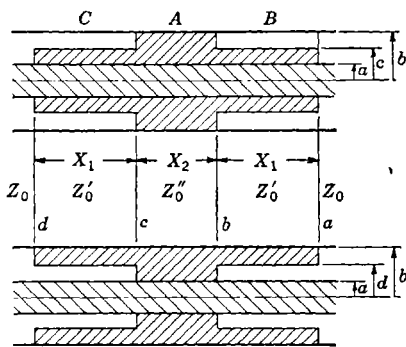


FIG. 4-19.—Three-quarter-wave beads with steps.

Three-section Bead.—It is sometimes convenient to have a bead that is a complete well-matched unit. The half-wave bead is of this type, but it is not desirable because of its high frequency sensitivity. A broad-

band bead may be made in the forms indicated by Fig. 4-19. The characteristic impedance Z''_0 of section *A* is easily calculated by use of Eq. 74. The characteristic impedance Z'_0 of sections *B* and *C* is to be

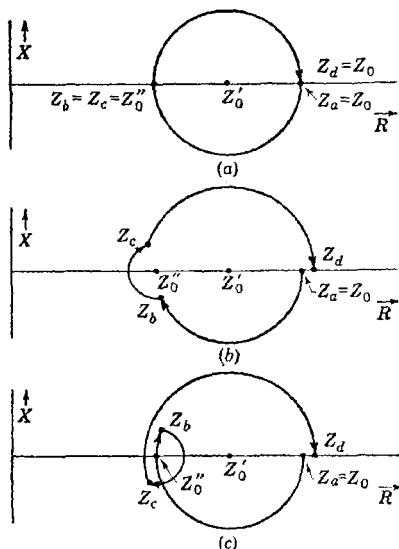


FIG. 4-20.—Impedance transformations in three-section bead ($Z'_0 = \sqrt{Z_0 Z''_0}$). (a) Midband, $\lambda = \lambda_0$; X_1, X_2, X_3 all equal to $\lambda/4$. (b) $\lambda > \lambda_0$; X_1, X_2, X_3 less than $\lambda/4$. (c) $\lambda < \lambda_0$; X_1, X_2, X_3 greater than $\lambda/4$.

terminated in the impedance $Z_a = Z_0$, and from this point on Fig. 4-20 an arc is described clockwise about the impedance Z'_0 to obtain the impedance Z_b . From *b* to *c*, the arc is about Z''_0 and from *c* to *d* it is again about Z'_0 .

made the geometric mean between Z_0 and Z''_0 , and the length X_1 is to be made an effective quarter wavelength, in order to provide matching transformers between Z_0 and Z''_0 . Since the completely filled section *A* is thereby operating in the matched condition, its length X_2 might seem to be unimportant. However, if X_2 is chosen to be a quarter wavelength, a very desirable broadband response is obtained.

The impedance transformations involved are shown in the rectangular impedance plots of Fig. 4-20. The source is considered to be at the left in Fig. 4-19 and the line to the right is assumed to be matched.

It is desired to follow the impedance transformations along the bead from point *a* to *b*, *c*, and *d* of Fig. 4-19. The output end *a* is

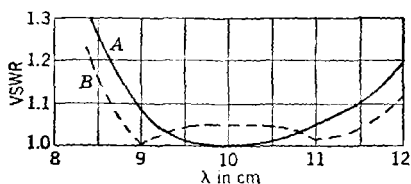


FIG. 4-21.—Performance of three-section bead made of polystyrene. (a) $Z'_0 = \sqrt{Z_0 Z''_0}$. (b) $Z'_0 = 0.988 \sqrt{Z_0 Z''_0}$.

(Strictly speaking, the arcs on the diagram are not centered exactly at the impedances Z'_0 and Z''_0 , but for the purpose of qualitative argument one need not worry about this discrepancy.) At midband, Fig. 4-20*a*, the center section *bc* is matched at the impedance level Z''_0 . Above

midband wavelength (Fig. 4-20*b*) and below (Fig. 4-20*c*) the section *bc* tends to compensate for the departure of the lengths of the end sections from the quarter-wave value. The calculated performance of such a bead, made of polystyrene and designed for a midband wavelength of 10 cm, is given by Curve *a* of Fig. 4-21. Comparison reveals that this type of bead is considerably better than the half-wavelength bead of Fig. 4-15 and that it is slightly better than the Lawson spaced set of four beads, Curve IV of Fig. 4-13.

A slightly broader band may be obtained, at the expense of introducing a mismatch at midband, by reducing the impedance Z'_0 . The effect of this reduction may be seen on the impedance diagrams of Fig. 4-22. There will be a pair of wavelengths, one above and one below midband, for which the modified bead will be perfectly matched, as indicated in the diagrams *b* and *c* of Fig. 4-22. It may be shown that if the impedance Z'_0 is reduced so that it is given by

$$Z'_0 = \frac{1}{F} \sqrt{Z_0 Z''_0},$$

then the VSWR at midband is

$$r = F^4.$$

If the midband VSWR is to be kept below 1.05, F may be chosen equal to 1.012. The resulting performance for a polystyrene bead is given by Curve *b* of Fig. 4-21. The band within which r is below 1.05 has been increased by this means from a full width of 2 per cent to one of 2.8 per cent. The shape of the curve is that characteristic of a double-tuned circuit.

The design equations for the original bead, matched at a midband wavelength λ_0 , are as follows:

$$X_2 = \frac{\lambda_0}{4} k_e^{-1/2}, \tag{25a}$$

$$X_1 = \frac{\lambda_0}{4} k_e^{-1/4}, \tag{25b}$$

$$c = b \left(\frac{k_e - \sqrt{k_e}}{k_e - 1} \right) a \left(\frac{\sqrt{k_e} - 1}{k_e - 1} \right) \tag{25c}$$

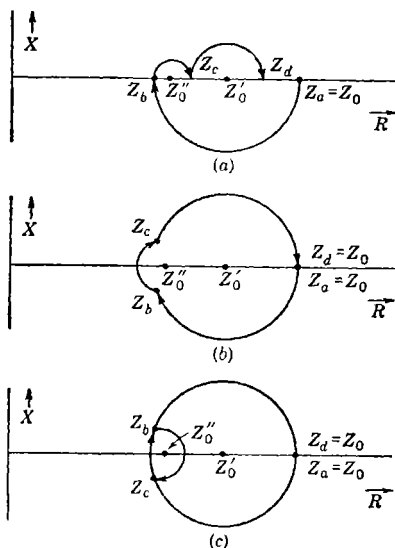


FIG. 4-22.—Impedance transformations for broadband bead ($Z'_0 < \sqrt{Z_0 Z''_0}$). (a) Midband, $\lambda = \lambda_0$; X_1, X_2, X_3 all equal to $\lambda/4$. (b) $\lambda > \lambda_0$; X_1, X_2, X_3 less than $\lambda/4$. (c) $\lambda < \lambda_0$; X_1, X_2, X_3 greater than $\lambda/4$.

Relation (25a) merely expresses the fact that X_2 is a quarter of the wavelength $\lambda_0/\sqrt{k_e}$ in a completely filled line section. Relation (25b) comes from a consideration of the fact that both the effective wavelength and characteristic impedance in a transmission line vary as $1/\sqrt{C}$ if L is kept constant (see Table 2-1, Items 2 and 4). Since the characteristic impedance Z'_0 is the geometric mean of Z_0 and Z''_0 , the corresponding effective wavelengths, λ'_0 , λ_0 , and λ''_0 , must bear the same relationship,

$$\lambda'_0 = \sqrt{\lambda_0 \lambda''_0}.$$

The characteristic impedance of a partially filled section of line (Fig. 4-19) is

$$Z'_0 = 60 \ln \frac{b}{a} \sqrt{\frac{k_e \ln \frac{b}{c} + \ln \frac{c}{a}}{k_e \ln \frac{b}{a}}}. \quad (26)$$

This equation is derived by calculating L , the inductance per unit length, and C , the capacitance per unit length, and using the relation $Z = \sqrt{L/C}$. When this is solved simultaneously with

$$Z'_0 = \sqrt{Z_0 Z''_0} = 60 k_e^{-1/4} \ln \frac{b}{a}, \quad (27)$$

the result is Eq. (25c), which may be written in the alternative form

$$\log_{10} c = \frac{\sqrt{k_e} - 1}{k_e - 1} (\sqrt{k_e} \log_{10} b + \log_{10} a). \quad (28)$$

For the second type of bead shown in Fig. 4-19 the lengths X_1 and X_2 are the same as before and are given by Eqs. (25a) and (25b). The dimension d may be shown to be given by

$$\log_{10} d = \frac{\sqrt{k_e} - 1}{k_e - 1} (\log_{10} b + \sqrt{k_e} \log_{10} a). \quad (29)$$

This type of bead recommends itself particularly at the shorter wavelengths, where it is very difficult to make a bead thin enough to obtain a low VSWR. For the longer wavelengths this bead may be too long to be practical in many cases. The long bead-to-conductor contact surface (along the inner conductor of the first type of Fig. 4-19 and along the outer on the second) may be especially objectionable. The contacting surfaces may be limited to the central quarter-wavelength section by making the partial filling of dielectric occupy a position intermediate between conductors without contacting either.

One would expect all forms of this bead to be relatively good for handling high power. The center section is matched, and the fields

in the air gaps in the end section, while larger than those in the main line, are not so high as those in the air gaps of the beads discussed previously.

There is some fringing of the electric fields at all points of impedance change, since the fields in the main line and in the completely filled section are purely radial and fall off radially as $1/r$, while those in the partly filled section suffer a discontinuity at air-to-dielectric boundaries. As a matter of fact, some component of electric field in the Z -direction (parallel to the axis of the line) must exist in the partly filled sections. These fringing fields would be expected to contribute a shunt-capacity effect paralleling the line at the points a , b , c , and d . Since these points are spaced by a quarter wavelength, some degree of cancellation results.

An experimental model of the first type of bead of Fig. 4-19 was made for the $\frac{1}{2}$ -in. coaxial line for operation at 3.33-cm midband. The dielectric used was Teflon ($k_e = 2.1$), and the dimensions were

$$\begin{aligned} X_1 &= 0.272 && \text{in.}, \\ X_2 &= 0.226 && \text{in.}, \\ 2a &= 0.1875 && \text{in.}, \\ 2b &= 0.437 && \text{in.}, \\ 2c &= 0.310 && \text{in.} \end{aligned}$$

The voltage standing-wave ratio was measured from $\lambda = 3.02$ to $\lambda = 3.65$ cm, and it was found to agree, within experimental error, with the predicted behavior. The experimental error caused by load, connectors, and slotted section was unfortunately of the order of $r = 1.06$, but it could safely be said that the VSWR was lower than approximately 1.12 over this band.

The possibility of the existence of a resonance, caused by the second coaxial mode, was not entirely eliminated. The dimensions of the coaxial line are such that this mode may propagate in the completely filled section and in all probability it can do so in the partly filled sections. There should be little tendency to excite this mode, however, because it is an asymmetrical mode while the bead is supposed to be made as nearly symmetrical as possible. One should bear in mind the possibility of encountering resonance trouble, especially if the beads themselves are not symmetrically made or if they are placed near some circuit which tends to excite the second coaxial mode. For example, such beads should not be placed near a transition unit from coaxial line to waveguide, nor near a coaxial-line stub support.

This same warning is applicable, to some extent, to most coaxial-line beads. It is particularly pertinent when the line size is so large compared with the operating wavelength that propagation of the second mode becomes possible in the bead. In such large lines the second mode

is not attenuated very rapidly in the air-filled part of the line; consequently, special care must be taken to keep beads at a safe distance from asymmetrical circuits. As an example of this difficulty, erratic behavior was noticed in an attempt to design a transition from coaxial line to waveguide for a wavelength of 3.3 cm, and the trouble was traced to the bead of the type N connector which supported the coaxial line about a quarter inch from the waveguide wall. When this bead was moved to a distance of about three-quarters of an inch, normal behavior was obtained.

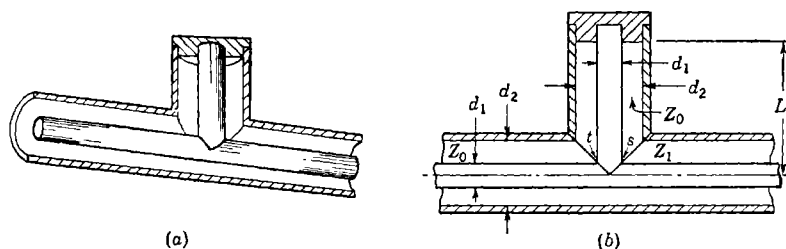


FIG. 4-23.—Simple T-stub support for coaxial line.

4.4. Stub Supports and Angles.—The impedance mismatch introduced by dielectric bead supports in coaxial lines causes increasing difficulty as the wavelength becomes shorter. It is fortunate that an alternative method of supporting the central conductor becomes practical at these shorter wavelengths. This method employs a branch line of the type illustrated in Fig. 4-23, which is commonly referred to as a “stub support.”

Simple T-stub Supports.—The principle of operation of such a stub support is briefly as follows: at the junction point, the voltage between inner and outer conductors of the branch line is the same as that across the main line at that point, and the current flowing into the junction from the input line (for example, that in the center conductor from the left-hand branch) is divided between the branch line and the output line. On the basis of these observations it can be said that the stub line is a shunt circuit in parallel with the main line.

The stub line is terminated in a metallic short circuit, so that it presents a purely susceptive admittance at the junction.

$$Y_s = -jY_0 \cot \frac{2\pi l}{\lambda} = jB_s. \quad (30)$$

The characteristic admittance of the stub line is assumed to be equal to that of the main line Y_0 since it will be in the usual type of stub in which the same size conductors are used in both the stub and the main line. At any given wavelength λ the length l may be chosen equal to $\lambda/4$,

in which case Eq. (30) becomes

$$Y_s = -jY_0 \cot \frac{\pi}{2} = 0. \quad (31)$$

Under these conditions the stub line presents zero susceptance at the junction, so that it does not introduce any mismatch into the main line.

If the stub line is made of length $l = \lambda_0/4$, the susceptance introduced by the stub at any wavelength λ is, by Eq. (30),

$$B_s = -Y_0 \cot \left(\frac{\pi \lambda_0}{2 \lambda} \right). \quad (32)$$

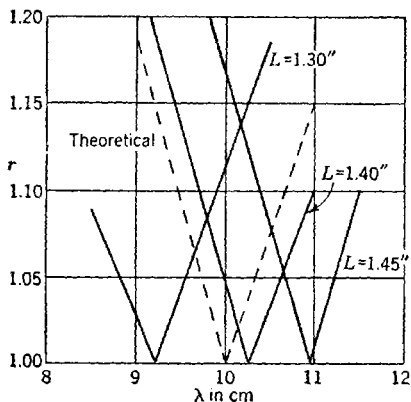


FIG. 4-24.—Performance curves for simple T-stub.

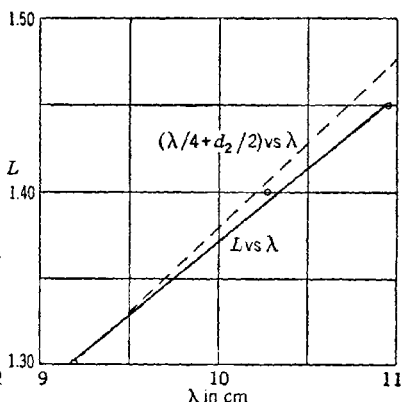


FIG. 4-25.—Stub length vs. wavelength for match for stubs of Fig. 4-24.

The voltage standing-wave ratio introduced into the input line by this susceptance shunting the main line is given by Item 8 of Table 2-2 and by the curve of Fig. 2-12. The theoretical-performance curve for a simple T-stub of this type is given by Curve *a* of Fig. 4-24. Measurements reported by Pound¹ on three experimental models are plotted as Curves *b*, *c*, and *d*. The frequency sensitivity of the actual stubs is seen to be in good agreement with that predicted by simple theory.

In Fig. 4-25, the stub length giving perfect match at a wavelength λ is plotted against λ for the three stubs of Fig. 4-24. Comparison with calculated quarter-wave values shows marked deviation between experiment and simple theory. An extremely useful correlation which is approximately valid for many line sizes and wavelengths is presented in Curve II which indicates that the stub length should be approximately a quarter wavelength, measured from the inner surface of the

¹ R. V. Pound, "Stub Supports in $\frac{7}{8}$ -in. Coaxial Line," RL Report No. 232, May 19, 1942.

outer conductor. The simple theory does not predict the correct stub length because the fields and currents in the region of the junction are badly distorted, and the region within which such distortions exist is an appreciable fraction of a wavelength. The approximate correlation between the quarter-wave value and the stub length measured from the inside surface of the outer conductor of the main line could hardly be other than fortuitous, but it is nevertheless a bit of information worth remembering.

In view of the discussion of the preceding paragraph it might be felt that it is rather remarkable that *any* stub length may be found that

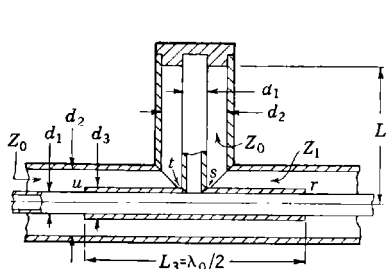


FIG. 4-26.—Broadband T-stub support.

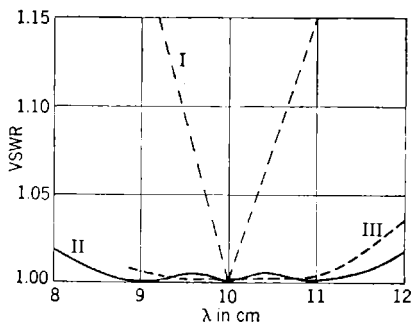


FIG. 4-27.—Performance of broadband stub in $\frac{1}{8}$ -in. coaxial line. I = theoretical simple stub; II = theoretical broadband; III = experimental.

yields perfect match past a T-stub. As a matter of fact, perfect match is not achieved by any choice of stub length in the right-angle stub support to be discussed presently (see Fig. 4-26). The obvious difference between these two types of stub supports is that the straight-through T has perfect output-input symmetry with respect to the plane passing through the stub perpendicular to the axis of the main line, while there is no such plane of symmetry in the right-angle stub.

It can be shown in a perfectly general way that any circuit that possesses this property of symmetry can be adjusted to give a perfect match, while those not possessing such symmetry cannot, in general, yield perfect match. The methods by which this general proof is given are discussed in another volume of this series (see Vol. 8, Chap. 9).

Throughout the foregoing discussion the stub is assumed to be of perfectly conducting metal and hence loss-free. An accurate calculation of the loss to be expected from a stub support is extremely difficult mathematically, but an estimate may be easily made based on simple theory which should be approximately correct. It is likely that the actual loss is somewhat higher than this estimate because of additional

currents in the junction region that are associated with the fringing fields existing there. According to the simple theory the maximum voltage amplitude in the stub branch occurs at the junction and is just equal to that in the main line, while the maximum current amplitude occurs at the short-circuiting plug and is just equal to the current amplitude in the main line. The amplitude of the current decreases cosinusoidally from the short-circuiting plug to zero at the junction. Since the conductor losses at any point in a line are proportional to the square of the current amplitude at that point, the losses in a quarter-wave stub may be shown to be just half that in a quarter wavelength of the main line.

The power-handling capacity of a stub-supported line is, of course, less than that of the section between supports, but the magnitude of this effect for a simple stub is not well known, either theoretically or experimentally. An indication of the magnitude is obtained from experiments on the standard $\frac{7}{8}$ -in. coaxial line, which would be expected to break down at about 1200 kw pulse power, assuming the critical or breakdown field to be 30,000 volts/cm. A short smooth section of such a line, held between sections tapering from a larger size line, gave breakdown at about 800 kw, while a section of line supported by the broadband stub (to be discussed later in this section) broke down at about 600 kw.

Broadband T-stubs.—The wavelength sensitivity of the simple stub support was higher than desirable. The first attempts to circumvent this difficulty followed the earlier procedure used in bead supports, namely, spacing two such stubs at one-quarter or three-quarters wavelength apart. By choosing individual stub lengths correct for one wavelength and spacing them for cancellation at another, an acceptable double-tuned circuit response was achieved.¹

An ingenious method of compensating for the frequency sensitivity of a single stub was proposed by Pound.² The view of Fig. 4-26 shows the structure, and the admittance charts of Fig. 4-28 illustrate the principle. The points on the admittance diagrams labeled *r*, *s*, *t*, and *u* correspond to the same points on Fig. 4-26. Assuming a generator to be located at the left of the stub and the output line at the right to be matched, the admittance may be traced through the stub assembly from right to left. At midband, Fig. 4-28*a*, the stub length has been chosen so that it will introduce no shunting effect at the point *st*; and the low-impedance section *ru* is exactly half a wavelength long so that its input admittance is equal to its output admittance Y_0 . Thus the stub is perfectly matched at λ_0 . At a particular wavelength $\lambda_2 > \lambda_0$,

¹ W. P. Mason, "A Band Pass Metallic Support for Coaxial Transmission Lines," BTL Report MM-42-160-1, Jan. 3, 1942.

² Pound, *op. cit.*

the line section rs is less than $\lambda_2/4$ in length; consequently, the admittance at s is capacitive as shown in Fig. 4-28*b*. But the stub length is also less than $\lambda_2/4$; therefore, it adds a shunt inductance effect to bring the admittance to the point t , symmetrically below s . The other half tu of the broadbanding transformer then transforms this admittance back

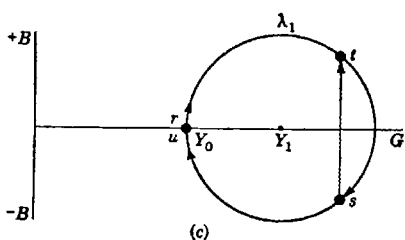
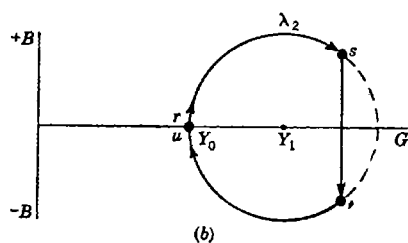
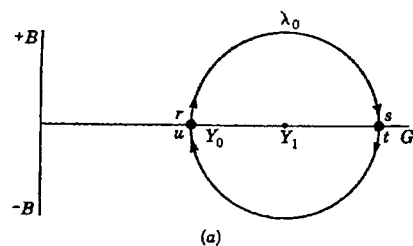


FIG. 4-28.—Admittance diagrams for broadband T-stubs. (a) Stub is equal to $\lambda_0/4$ and adds nothing. (b) Stub is less than $\lambda_2/4$ and adds inductance. (c) Stub is greater than $\lambda_1/4$ and adds capacity.

manipulation of Eq. (33) gives

$$\lambda_0 = \frac{2\lambda_1\lambda_2}{\lambda_1 + \lambda_2}, \quad (35a)$$

$$\nu_0 = \frac{1}{2}(\nu_1 + \nu_2), \quad (35b)$$

$$p^2 = \tan^2\left(\frac{\pi\lambda_1}{\lambda_1 + \lambda_2}\right), \quad (36a)$$

$$p^2 = \tan^2\left(\frac{\pi\nu_2}{\nu_1 + \nu_2}\right). \quad (36b)$$

to the value of the output admittance Y_0 , and results in perfect match at λ_2 . At some particular wavelength $\lambda_1 < \lambda_0$ the conditions are as depicted in Fig. 4-28*c*. The admittance at s is now inductive, while the stub adds capacitance to give the symmetrical admittance point t which is then transformed by the section tu back to Y_0 .

It can be shown by simple transmission-line theory that the design relations required to achieve perfect match at wavelengths λ_0 , λ_1 , and λ_2 , are

$$\tan^2\left(\frac{\pi}{2}\frac{\lambda_0}{\lambda_1}\right) = \tan^2\left(\frac{\pi}{2}\frac{\lambda_0}{\lambda_2}\right) = p^2, \quad (33)$$

$$\left(\frac{Z_1}{Z_0}\right)^3 + 2\left(\frac{Z_1}{Z_0}\right)^2 + \frac{1}{p^3}\left(\frac{Z_1}{Z_0}\right) - 2 = 0. \quad (34)$$

Any two of the wavelengths λ_0 , λ_1 , and λ_2 may be chosen at will; the third and the value of p^2 will then be determined by Eq. (33) and the impedance Z_1 will be determined by Eq. (34). A little

On a frequency scale, midband is simply the arithmetic mean of the other two values, while on a wavelength scale the relation is more complicated.¹

The theoretically predicted and experimentally observed performances of a stub of this type are given in Fig. 4-27. That of a narrow-band stub is given for comparison. In Table 4-4 are given the dimensions that have been experimentally determined for a number of stub supports of this type. For a given line size and wavelength band all dimensions except the stub length L are calculated from the design equations. The stub length is made the design variable and is adjusted until the desired performance curve is obtained.

TABLE 4-4.—DIMENSIONS FOR BROADBAND T-STUBS (FIG. 4-26)
All dimensions in inches, wavelengths in centimeters

Line size	Z_0	Conductors		Transformer		Stub length L	λ_0
		d_1	d_2	d_3	L_3		
$\frac{1}{8}$	51	0.187	0.437	0.218	0.630	0.516	3.2
$\frac{5}{8}$	48	0.250	0.555	0.283	1.600	1.113	8.1
$\frac{7}{8}$	46	0.375	0.811	0.425	1.600	1.238	8.1
$\frac{7}{8}$	46	0.375	0.811	0.425	1.950	1.450	9.9
$\frac{7}{8}$ *	44	0.375	0.785	0.425	1.950	1.450	9.9
1†	75	0.250	0.875	0.327	1.970	1.311	10.0
1 $\frac{1}{4}$	50	0.500	1.152	0.573	1.600	1.425	8.1
1 $\frac{5}{8}$	53	0.625	1.527	0.725	1.950	1.750	9.9

* Not a standard line. An early line used in Pound's original design.

† Not a standard line of the 50-ohm series. Data taken from *Microwave Transmission Design Data*, Sperry Gyroscope Co., May 1944, p. 57.

It is interesting to note the similarity between the response curve of Fig. 4-28 and that of a triple-tuned circuit. These stubs have been designed to give perfect match at three wavelengths differing by some 10 per cent. As the wavelengths λ_1 and λ_2 are chosen closer and closer to λ_0 , p of Eq. (33) becomes larger and larger. In the limit, when $\lambda_1 = \lambda_0 = \lambda_2$, the coefficient $1/p^2$ of the linear term of Eq. (34) becomes zero. Equation (34) then becomes

¹ This observation is in keeping with the more general principle that the behavior of most circuits tends to be more symmetrical when plotted on a linear frequency scale than when plotted on a linear wavelength scale. Specific examples of this principle, in which perfect symmetry in the plot of VSWR vs. frequency is given by the theory, are (a) the half-wave bead and three-quarter-wave beads of Sec. 4-3, (b) the simple T-stub of this section, and (c) the complete broadband stub assembly being discussed here. Usually, any simple device, matched at a frequency ν_0 and involving only elements whose electrical angles are some multiple n , either even or odd, of $\pi/2$ at midband, will possess this symmetry. These observations constitute a rather strong argument in favor of plotting performance curves in terms of frequency.

$$\left(\frac{Z_1}{Z_0}\right)^3 + 2\left(\frac{Z_1}{Z_0}\right)^2 - 2 = 0, \quad (37)$$

which has the solution

$$\frac{Z_1}{Z_0} = 0.8393. \quad (38)$$

This solution corresponds to the critically coupled triple-tuned circuit which is perfectly matched at midband, and at midband only, and which has a very flat response curve in the neighborhood of midband. As Z_1 decreases from the value Z_0 toward the value $0.8393Z_0$, the performance curve starts from that of a simple stub and becomes progressively flatter until it reaches critical coupling. Any further decrease in Z_1 causes the overcoupling response curve to appear, and the spread in the wavelengths λ_1 , λ_0 , λ_2 becomes progressively larger as Z_1 decreases. If Z_1 is decreased too much, rather high mismatch will begin to appear in the intervals between these three wavelengths. For the stubs of Table 4-4 the VSWR remains well below 1.01 (by calculation) in these intermediate intervals. Incidentally, the wavelengths λ_1 and λ_2 spread rapidly as Z_1 decreases. For $\lambda_1 = 0.9\lambda_0$, one obtains $Z_1 = 0.835Z_0$, which is only one-half of 1 per cent lower than the critically coupled value, 0.8392. A variation of another half per cent to $Z_1 = 0.831Z_0$ makes $\lambda_1 = 0.87\lambda_0$.

There is a small phase distortion in the broadband T-stub which should be taken into consideration when the application demands high precision in this regard. Pound¹ evaluated this distortion, both theoretically and experimentally, for the $\frac{7}{8}$ -in. line version. The correction ΔL to be applied to the mechanical length of line containing such a stub in order to obtain its equivalent electrical length was found to have the values given in Table 4-5.

TABLE 4-5.—PHASE DISTORTION IN BROADBAND STUB SUPPORT OF FIG. 4-28

Electrical length = mechanical length + ΔL .

All units are in centimeters

λ	8.4	9.0	10.0	11.0	11.4
ΔL	-0.15	-0.08	0	+0.10	+0.15

Right-angle Stubs.—Stub-supported coaxial lines are usually made of rigid tubing supported at fairly large intervals, so that the line is not easily bent. The necessary changes in direction required of the line are accomplished by means of stub angles which are modifications of the T-stub previously discussed. It is nearly always possible to lay out the transmission-line arrangement in such a way that simple 90° changes

¹ R. V. Pound, "Phase Distortion in Broad Band Stub Supports," RL Report No. 53-6, Aug 17, 1942.

of the axial direction of the line accomplish the desired interconnections between circuits in a straightforward manner.

The physical arrangement and performance of simple stub angles having various stub lengths are given by Fig. 4-29. These performance curves, unlike those of the T-stubs discussed earlier, do not present a perfect match to the input line at any wavelength. Each curve goes through a minimum VSWR at a different wavelength, and the stub

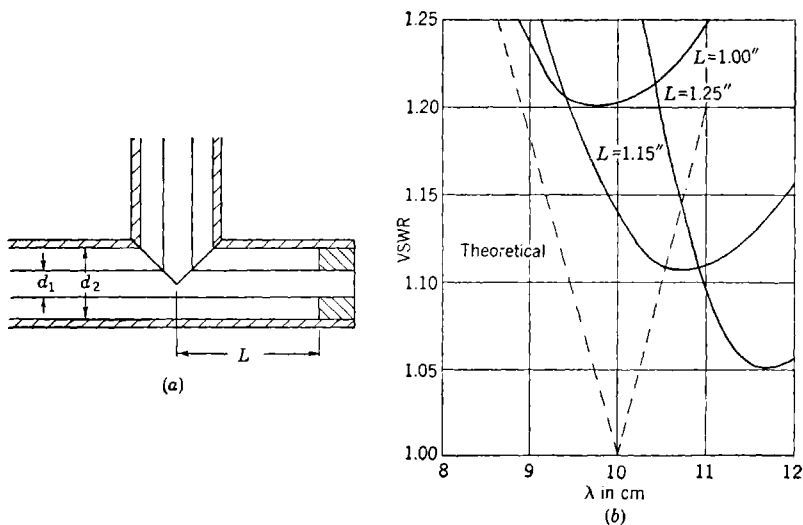


FIG. 4-29.—Simple stub angle. (a) Dimensions. (b) Performance curves for a line with $d_1 = 0.375''$ and $d_2 = 0.785''$.

length is plotted against the associated optimum wavelength as Curve I of Fig. 4-30b. The stub length L is rather close to the quarter-wave value, Curve II. As the wavelength of best match becomes longer the minimum VSWR goes down, as clearly illustrated by Fig. 4-30a. This type of behavior is expected because, as the wavelengths become large compared with the line dimensions, junction effects should become of decreasing importance. Unfortunately this type of stub angle lacks the T-stub property of symmetry that is responsible for attaining perfect match.

In order to obtain a matched stub angle it is necessary to introduce an impedance transformer. One such design and its performance curve is given in Fig. 4-31. This design is based on Pound's work,¹ which gives impedance diagrams showing how the broadbanding, evident by comparison with the dashed curve representing a theoretical stub, is achieved.

Soon after this design was completed, the wall thickness of the outer

‡ *Ibid.*

conductor of the $\frac{7}{8}$ -in. line was changed from 0.045 to 0.032 in., and it was assumed that this slight change would not affect the performance enough to require a redesign. Later it was found that the stubs being

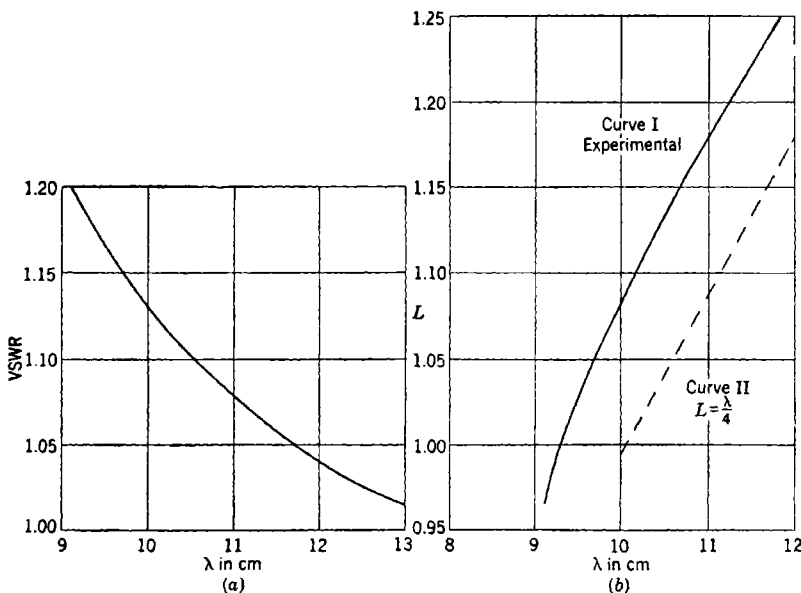


FIG. 4-30.—Minimum VSWR (a) and optimum stub lengths in inches (b) for stub angles of Fig. 4-29.

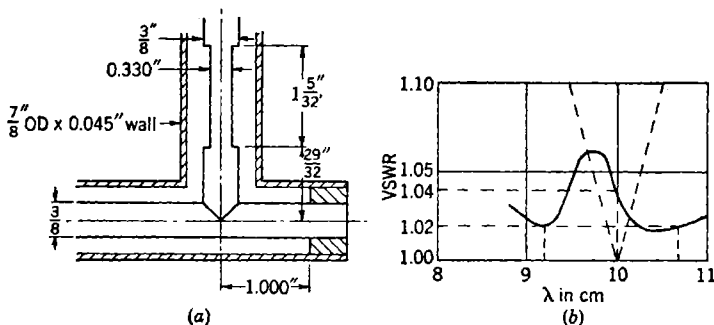


FIG. 4-31.—Stub angle matched by undercut transformer. (a) Dimensions. (b) Performance curve.

made according to this design but using the thinner tubing gave a VSWR of about 1.10 at wavelength of 10.7 cm. It does not seem likely that the small change in wall thickness could have caused such a large mismatch to appear, but no other source for the error has appeared.

In some applications, the length of the side branch (over two inches to the end of the transformer section) is objectionable. For this reason, as well as that of the unexplained mismatch previously mentioned, alternative stub angles are preferred. One alternative is that of using the simple sleeve transformer of Fig. 4-32a. The sleeve transformer is

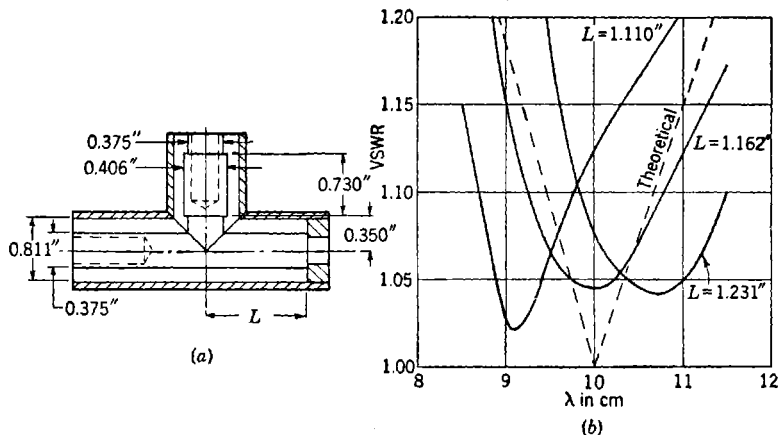


FIG. 4-32.—Stub angle matched by sleeve transformer. (a) Design. (b) Performance.

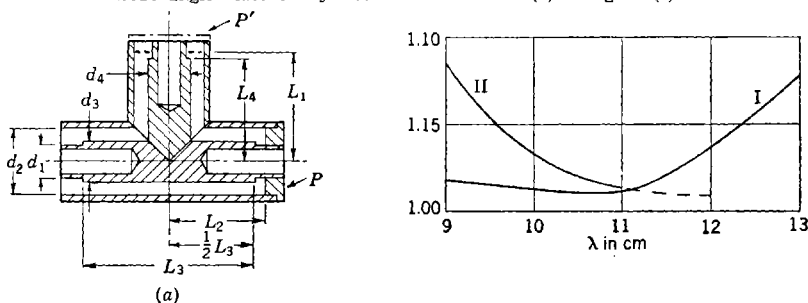


FIG. 4-33.—Universal stub. (a) Dimensions. (b) Performance curves for $\frac{3}{8}$ -in. stub for $\lambda_0 = 10$ cm. Curve I, straight T-stub; Curve II, stub angle.

fairly short, leading to an extremely compact stub. Since the response curves (see Fig. 4-32b) are about like those of a theoretical stub, this design is not to be recommended for bands of width greater than about 6 to 8 per cent. This design was evolved especially for operation at a wavelength of 9.1 cm, where none of the other stub angles was well matched. It was later discovered that a simple change of stub length gave fair results at other wavelengths.

Universal Stubs.—A stub which may serve either as a straight-through T-stub or as a stub angle, depending on the way in which the parts are assembled, is shown in Fig. 4-33a. When the short-circuiting plug is

assembled as shown in solid lines at position P , a stub angle results. Ordinary coaxial-line connectors are then attached to the left and top branches for connection to other sections of line. If the plug is assembled at position P' (shown in phantom) and a standard connector is attached to the right-hand branch line, a straight-through T-stub results. The dimensions for three such stubs are given in Table 4-6. The performance curves for the universal stub in the $\frac{7}{8}$ -in. line size are given in Fig. 4-33*b* and the dimensions are those given in Table 4-6. It was found necessary to increase the original value of L_1 by 0.070 in. in order to obtain the result of Curve I. It may be that some modification of L_2 would improve the stub-angle performance of Curve II.

TABLE 4-6.—DIMENSIONS FOR UNIVERSAL STUBS OF FIG. 4-33
All dimensions in inches, wavelengths in centimeters

Line size	Z_0	d_1	d_2	d_3	d_4	L_1	L_2	L_3	L_4	λ_0
$\frac{3}{8}$ *	48	0.250	0.555	0.283	0.294	1.181	1.050	1.950	1.100	9.9
$\frac{1}{2}$ †	46	0.375	0.811	0.425	0.445	1.323	1.094	1.950	1.141	9.9
1 †	75	0.250	0.875	0.327	0.342	1.410	1.100	1.970	1.310	10.0

* Designed by Polytechnic Institute of Brooklyn; Report R-25-43, PIB-9, Contract OEMsr-335, July 1, 1943.

† Not a standard line of the 50-ohm series. Data taken from *Microwave Transmission Design Data*, Sperry Gyroscope Co., May 1944, p. 58.

Miscellaneous Stubs.—A number of other types of stub have been proposed to fulfill special requirements. A few of these are illustrated in Fig. 4-34. Figure 4-34*a* is a modification of the broadband T-stub which has the advantages of greater rigidity and of mechanical balance. It is especially well suited to applications in which it is required to support a section of coaxial line which is rotating at high speed about its axis.

The stub of Fig. 4-34*b* is a special type of stub angle in which symmetry between input and output halves has been introduced. It was pointed out in the discussion of ordinary T-stubs and stub angles that it is usually possible to obtain an impedance match with simple symmetrical circuits (for example, simple stub angle). It was indicated in Fig. 4-22 that this effect becomes more pronounced as the wavelength becomes shorter, and extremely poor conditions can be expected to arise as the wavelength approaches that corresponding to the cutoff of the second coaxial mode. The stub of Fig. 4-34*b* was designed for the largest line usable in the 10-cm band, and it was very satisfactory, whereas attempts to make a stub angle of the usual type had proved most unsatisfactory. The enlargements of the center conductor are not needed for matching but serve rather as broadbanding transformers.

Diagram 4-34c illustrates the use of a smaller coaxial line within the center conductor of the standard $\frac{7}{8}$ -in. line, the $\frac{3}{8}$ -in. tube being common to both lines. In the diagram the outer line is supported by a broadband T-stub, while the smaller line is a simple narrowband stub matched for a wavelength of 9.1 cm.

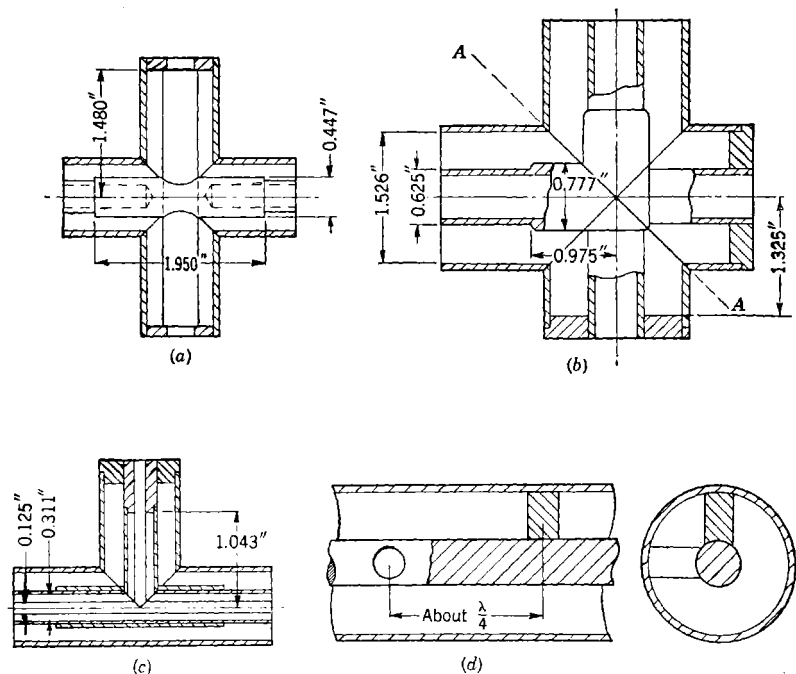


FIG. 4-34.—Miscellaneous stubs. (a) Cross stub support in standard $\frac{1}{2}$ -in. line ($\lambda_0 = 10$ cm). (b) Cross stub angle in standard $1\frac{1}{2}$ -in. line ($\lambda_0 = 9.9$ cm). (c) Stub within a stub in standard $\frac{7}{8}$ -in. line (inner stub for $\lambda = 9.1$ cm). (d) Internal stubs in a large line (dimensions comparable to λ).

A simple stub of the type shown in Fig. 4-34d might be expected to present an almost complete short-circuiting effect to the line. For wavelengths that are long compared with the line dimensions this is indeed the case, but for lines that are almost large enough to propagate the second coaxial mode the mismatch due to such a stub is surprisingly small. It was found that a single $\frac{3}{8}$ -in. rod used in this manner to support the $\frac{5}{8}$ -in. center conductor of the $1\frac{1}{2}$ -in. line gave a VSWR of about 1.2 at 9.1 cm, increasing linearly with wavelength to a value of 2 at about 10.7 cm. A spaced pair showed some promise ($r < 1.10$ from $\lambda = 9.0$ to 9.5 cm), but the problem was not pursued further as

there seemed little prospect of a good broadband performance in the 10- to 11-cm wavelength region for which a stub was desired.

It may be that the approach of the wavelength toward propagation of the second coaxial mode is the essential factor in giving a low VSWR, but it is also possible that the fact that the stub length approaches the quarter-wave value at about the same time is the more important. If the latter explanation is the true one, a better performance would be expected from higher-impedance lines, since the radial distance between outer and inner conductors is greater for a high-impedance line than for a

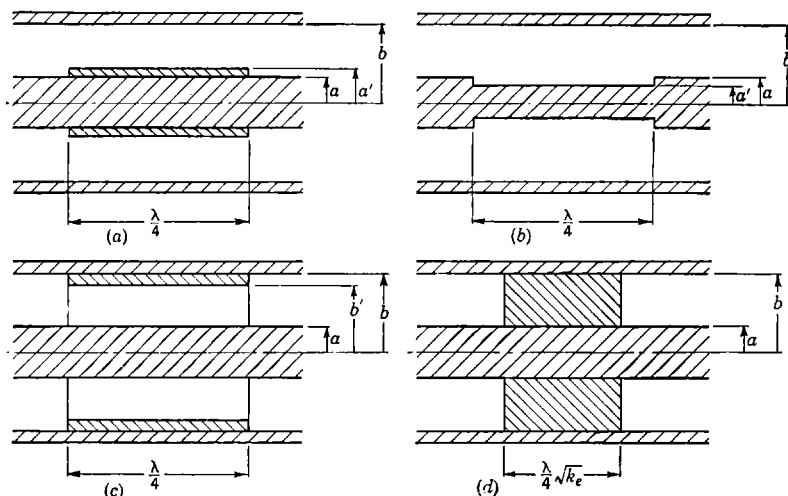


FIG. 4-35.—Simple types of quarter-wave coaxial transformers.

low-impedance line having the same cutoff wavelength for the second mode.

In addition, various "trick" shapes may be tried for support. Making the supporting rod of smaller diameter may be beneficial. It has been reported that the Raytheon Laboratories have had success with shapes that introduce a "capacity-loading" effect, while the Sperry Laboratories have found a thin wafer-like structure with a spiral effect to be extremely handy as a completely internal metallic support.

The chief limitation of the stub shown in Fig. 4-34*d* and the other types of internal stub mentioned seems to be in their power-handling capacity. Experimental results are not known to the author, but it does not seem likely that any of these supports would be applicable where high peak powers are transmitted.

4-5. Coaxial Impedance Transformers.—Four simple types of coaxial-line transformers are illustrated in Fig. 4-35. For a general discussion

of the principles underlying the use of transformers in impedance-matching the reader is referred to Sec. 2-15 and to Slater.¹ There are of course other ways of changing the characteristic impedance of a coaxial line, including combinations of those shown, and any such arrangement may be used as a transformer. Those shown include the more important ones, however.

The most commonly used type is that of Fig. 4-35a. It is shown as a sleeve to be slipped over the center conductor, in which form it is very convenient to use as a trial transformer. A narrow longitudinal slot may be sawed the full length of the sleeve in order to permit sliding it along the line. After the proper size and position of the trial transformer sleeve have been found, it is advisable to make a confirming measurement with the sleeve soldered in place because of the possibility of faulty contacts between sleeve and center conductor. In manufacturing practice the transformer may be a soldered sleeve or it may be formed by machining the center conductor and transformer from a solid rod of larger diameter. Machining is usually more practical for short sections and the sleeve technique is preferred for longer lengths.

The characteristic impedance of the transformers shown may be calculated from the usual formula

$$Z_0 = \frac{138.2}{\sqrt{k_e}} \log_{10} \frac{b}{a}, \quad (39)$$

or read from Fig. 4-36. The radii b and a and the relative dielectric constant k_e are, of course, those in the transformer section. It is evident that the characteristic impedance may be decreased compared with that of the main line (1) by increasing a (Fig. 4-35a), (2) by decreasing b (Fig. 4-35c), or (3) by increasing k_e (Fig. 4-35d). The impedance may be increased (1) by decreasing a (Fig. 4-35b), (2) by increasing b (not shown, because it is little used), or (c) by decreasing k_e (a possibility only if the main line is dielectric-filled). Various combinations of these six alternatives are possible, and the resulting characteristic impedance may be calculated by Eq. (39) or read from Fig. 4-36.

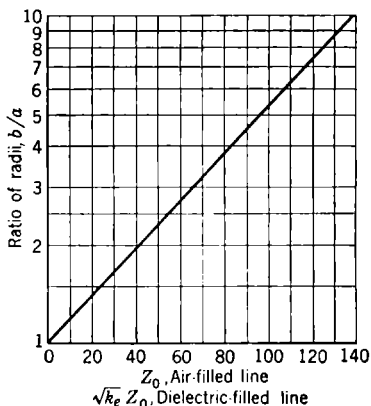


FIG. 4-36.—Characteristic impedance of coaxial line.

¹ J. C. Slater, *Microwave Transmission*, McGraw-Hill, New York, 1942, pp. 55-63.

Of the transformers shown in Fig. 4-35, only that of Fig. 4-35*d* is free from distortions in the electric and magnetic fields at the junction between main line and transformer. It was mentioned in Sec. 2-12 that a change in diameter of either or both conductors of a coaxial line sets up fringing fields which introduce a shunt-capacity effect, as indicated by the equivalent circuit of Fig. 2-41. More will be said about this effect in the following section. It is well to point out at this time that this shunting effect must be taken into consideration if extreme precision is required in the use of matching transformers. Fortunately, the two shunt capacitances are spaced a quarter wavelength apart and as a result tend to cancel each other to a certain extent.

As an illustration of the magnitude of the error introduced by neglecting the discontinuity capacitances, a typical numerical example should be considered. At a wavelength of 10 cm in the standard $\frac{7}{8}$ -in. OD coaxial line, a sleeve transformer is to be used (Fig. 4-35*a*) to match out a VSWR of 2.56. On the basis of simple theory, this requires a transformer of characteristic impedance $Z_0/1.6$ and of length 2.50 cm placed with its output end at a voltage-minimum point. The susceptance that may be calculated¹ at each end of the transformer amounts to $0.04Y_0$, and experimental values are in good agreement. If the transformer is placed with its output end exactly at the voltage minimum, the resulting VSWR will be about 1.025 rather than 1.000 as expected from simple theory. The input admittance is slightly capacitive and is almost identical with that which would be predicted by simple theory for a transformer placed 0.004λ (0.016 in.) too close to the generator. As one might infer from the last observation, almost perfect match may be achieved by displacing the transformer an equal distance toward the load.

4-6. Coaxial-line Discontinuities.—Several references (Secs. 2-12, 2-15, 4-3, 4-5) have already been made to the existence of an equivalent shunt capacity at the point where either conductor (or both) of a coaxial line undergoes an abrupt change of diameter. The purpose of this section is to present a very brief qualitative explanation of this effect and to give a few useful curves and illustrative examples. Thorough theoretical treatments² and numerical results³ exist in the literature, and the reader is referred to them if additional material is desired.

¹J. R. Whinnery and H. W. Jamieson, "Coaxial-line Discontinuities," *Proc. I.R.E.*, **32**, 695-709 (November 1944); also Sec. 4-6 of this volume.

²Vol. 10, Radiation Laboratory Series; J. R. Whinnery and H. W. Jamieson, "Equivalent Circuits for Discontinuities in Transmission Lines," *Proc. I.R.E.*, **32**, 98-115 (February 1944).

³J. R. Whinnery, H. W. Jamieson, and Theo Eloise Robbins, "Coaxial-Line Discontinuities," *Proc. I.R.E.*, **32**, 695-709 (November 1944).

The field structure in the neighborhood of a step discontinuity is of the form shown in Fig. 4-37a. All field lines end normal to the metallic boundary since no tangential component of E may exist there. The principal- or lowest-mode field is purely radial; consequently it is obvious that there are some longitudinal components of field present which do not belong to this mode. The longitudinal components may be thought of as belonging to higher mode E -waves (those modes with longitudinal component of E but not of H , also called " TM -waves"). If the dimensions of either (or both) of the lines are large enough to propagate any of these higher mode E -waves, a part of the power incident on the discontinuity will be transformed into such E -mode waves traveling away from the discontinuity in the large line (or lines). Usually this is undesirable, and in order to avoid transfer of power into higher-mode waves of both E and H types the dimensions of lines actually used are limited so that only the lowest mode may be propagated.

It is shown in the theoretical references that the effect of the discontinuity is exactly represented by an equivalent circuit of the type given in Fig. 4-37c provided the lines are both capable of propagating only the lowest mode. This equivalent circuit is valid

only for impedance measurements made at a distance from the discontinuity which is large enough to ensure that the higher order fields have been attenuated to negligible values. It assumes also that no other discontinuity occurs close enough to couple to these higher order fields. This consideration is sometimes termed the "proximity effect," and methods of treating it are given in the references. Usually, the proximity effect lowers the capacity of each discontinuity by an amount depending on the physical arrangements of the discontinuities and on their separation. If two discontinuities are separated by a distance greater than the separation between inner and outer conductors of the line between them, little interaction results, and the reduction in individual capacitances is negligible. For certain arrangements, namely those for which the fields

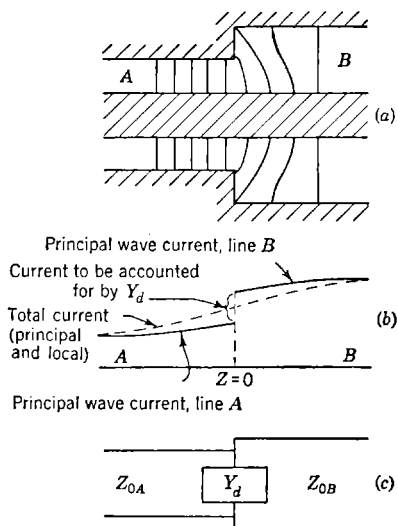


FIG. 4-37.—Step discontinuity in coaxial line. (a) Electric fields at the discontinuity. (b) Plot of the variation of the currents across the discontinuity. (c) Equivalent circuit of the discontinuity.

between the discontinuities are relatively undistorted (as in line A of Fig. 4-37a), much closer separations may be tolerated.

Four common types of step discontinuity are given in Fig. 4-38. By using the formulas given in the legend, in conjunction with the curve

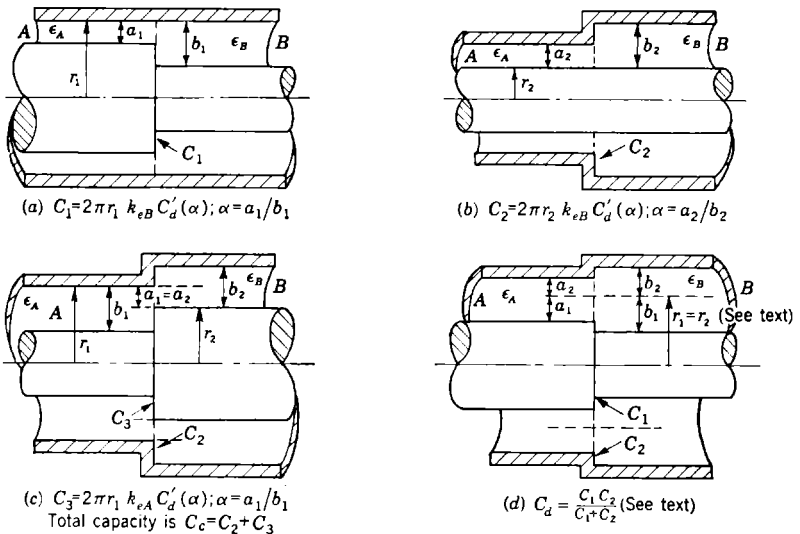


FIG. 4-38.—Examples of coaxial-line step discontinuities (C'_d from Fig. 4-39).

of Fig. 4-39, a good estimate of the junction capacity may be made. The equivalent circuits are all of the type given in Fig. 4-37c, where

$$Y_d = jC\omega, \quad (40)$$

and Z_{0A} and Z_{0B} are the ordinary characteristic impedances of the coaxial lines A and B.

Figure 4-39 is taken from Whinnery and Jamieson (*loc. cit.*) and applies exactly only for step discontinuities in parallel-plane transmission lines. It gives accurately the capacity per unit width caused by a step in such a line; when this value is multiplied by the appropriate circumference ($2\pi r_1$ or $2\pi r_2$ as indicated in the legend of Fig. 4-38), a good approximation to the discontinuity capacity in a coaxial line of the same step ratio α is obtained. It may be noted that the appropriate radius is that common to lines A and B. The error involved in the approximation depends, for a given step ratio, on the diameter ratio of the coaxial conductors. If the largest diameter ratio of either line is below five, the approximation is good to within better than 20 per cent for all values of α plotted. Greater accuracy may be obtained by study of the references cited above.

The appearance of the dielectric constant k_e in the formulas of Fig. 4-38 requires further explanation. Referring to Fig. 4-37a it will be noticed that the field in line *A* is relatively undistorted; therefore the value of the dielectric constant in line *A* should have little effect on the higher mode fields. It is the dielectric constant in line *B*, where the principal distortions of field occur, that has the major influence on the higher-mode fields and hence on the discontinuity capacity. The values of C'_d from Fig. 4-39 are based on air dielectric and thus must be multiplied by the appropriate dielectric constant to obtain the actual capacity. In all cases except C_3 of Fig. 4-38, the major field distortions occur in line *B*.

In the case of the double step of Fig. 4-38c, the total junction capacity is well approximated by considering it to be composed of the two capacitances C_2 and C_3 added in parallel. To justify this statement, the outer conductor can be visualized as displaced slightly to the right creating an intermediate section of line of outer radius r_1 and inner radius r_2 . In this intermediate section the fields are relatively free of distortion; hence, there is little interaction between the two discontinuities and their capacities may be calculated separately. In view of the remarks of the preceding paragraph, the dielectric constant k_{eA} is appropriate to the capacity C_3 , while k_{eB} is used in calculating C_2 . As the outer conductor is brought back to the position indicated in the figure these two capacities remain essentially separate, but their shunting actions become located at the same point in the line.

The situation existing in Fig. 4-38d is more complicated, since the fringing fields caused by the two steps are intimately associated. An approximate method of treating the problem, due to Whinnery, gives results which agree fairly well with experiment. An intermediate cylindrical sheet of radius $r_1 = r_2$ (properly chosen) could be inserted as indicated in the figure and the junction capacitances C_1 and C_2 of the

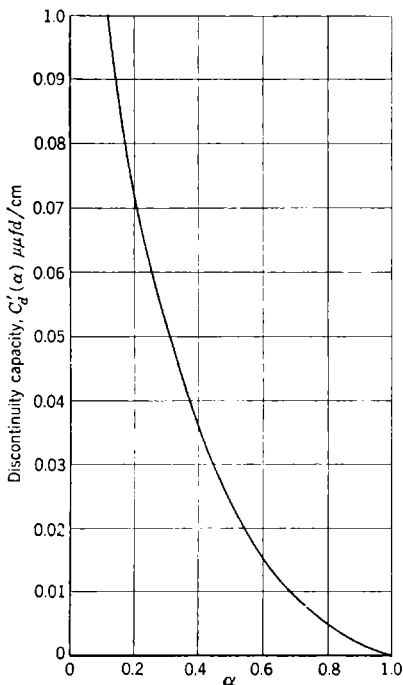


FIG. 4-39.—Approximate discontinuity capacitance for coaxial steps.

internal and external lines that are formed by the methods outlined in connection with Figs. 4·38*a* and *b* could be calculated. These junction capacitances are treated first by placing them in series with each other and then by connecting the combination across the line.

The value of $r_1 = r_2$ is chosen as that value which makes the total capacitance C_d a maximum. Being at a maximum, the value of C_d is not very sensitive to slight variations of $r_1 = r_2$ from the correct value.

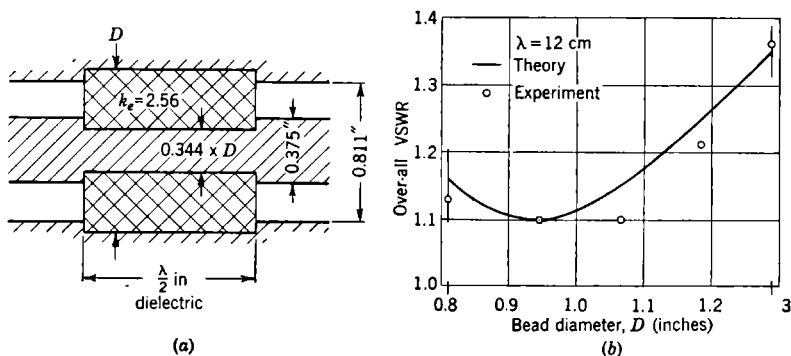


FIG. 4-40.—Some experimental results on coaxial steps. (a) Dimensions. (b) Comparison between theory and experiment.

A series of measurements¹ which provides a check on the validity of this procedure is summarized graphically in Fig. 4-40. Unfortunately the experimentally measured values of VSWR are to be trusted to an accuracy of only about ± 0.03 ; consequently it is difficult to ascertain if the discrepancy between theory and experiment is real. At any rate, the prediction of theory is certainly close enough to be very useful in many applications.

WAVEGUIDES

BY RICHARD M. WALKER

4·7. Factors Governing Choice of Dimensions.—The choice of dimensions for a waveguide to be operated at a given wavelength involves the following considerations: (1) mode of operation; (2) cutoff wavelength for the operating mode and the next higher mode; (3) attenuation in the wall surfaces; and (4) voltage breakdown. Waveguide dimensions are usually selected so that only the lowest or fundamental mode can be propagated at the desired wavelength. With such a choice of dimensions, propagation of a higher mode excited by components in the system is rapidly attenuated and the impedance of the system is not changed appreciably. Therefore, the design of components that may excite a

¹ B. P. Washburne, "Coaxial-Line Step Discontinuity Admittances," RL Group Report No. 53, July 25, 1945.

higher mode, such as couplings, rotating joints, switches, transitions, and so forth, is simplified. This choice of dimensions also makes it possible to use matching elements such as capacitive and inductive irises and the resonant ring which excite higher modes in the waveguide. Two components or elements in the transmission line which excite a higher mode may form a resonant cavity, the Q of which is determined by the distance between them. Since the attenuation is high for the higher modes, the cavity Q can be made very low by moving the components far enough apart (see Sec. 2.3 for attenuation formulas). An exception to this consideration is made in some cases such as the circular-pipe section of a waveguide rotary joint discussed in Sec. 7.3 where the TM_{01} -mode is essential for the rotary-joint operation. The TE_{11} -mode that may also be propagated in the circular waveguide is suppressed by resonant rings and by special design to prevent its excitation.

Usually, waveguide transmission systems are similar to high-pass filters in that, for a given choice of inside dimensions, all wavelengths below the cutoff wavelength λ_c may be propagated. However, where propagation is limited to one mode, the pass band has a lower wavelength limit, determined by the cutoff wavelength for the second waveguide mode. The cutoff wavelengths for any mode may be calculated from the inside dimensions of the waveguide. Formulas for calculating the cutoff wavelengths of rectangular and circular waveguides in the fundamental and higher modes are given in Sec. 2.10.

So far the pass band has been discussed for a waveguide with given internal dimensions. This pass band is fairly wide compared with the operating wavelength band of a radar system. Since the waveguide-attenuation and voltage-breakdown characteristics change considerably over the pass band, a portion of the pass band that gives the best over-all operating characteristic may be selected. Figure 4.41 shows the variation of attenuation over the pass band for rectangular waveguide operating in the TE_{10} -mode. The curve was calculated from the equation¹

$$\alpha_c = \frac{0.01107}{a^{3/2}} \left[\frac{\frac{1}{2} \frac{a}{b} \left(\frac{\lambda_c}{\lambda_0} \right)^{3/2} + \left(\frac{\lambda_c}{\lambda_0} \right)^{-1/2}}{\sqrt{\left(\frac{\lambda_c}{\lambda_0} \right)^2 - 1}} \right] \text{ db/ft,} \quad (41)$$

where α_c is the conductor loss, a and b the wide and narrow inside dimensions, respectively, in inches, and λ_0 and λ_c the free-space and cutoff wavelengths, respectively. In Fig. 4.41 $\alpha_c a^{3/2}$ is plotted against λ_0/λ_c for three ratios of a/b —2.12, 2.25, and 2.47. For convenience, the dimension a for Fig. 4.41 is in inches.

¹ *Microwave Transmission Design Data*, Sperry Gyroscope Co., May 1944, p. 77

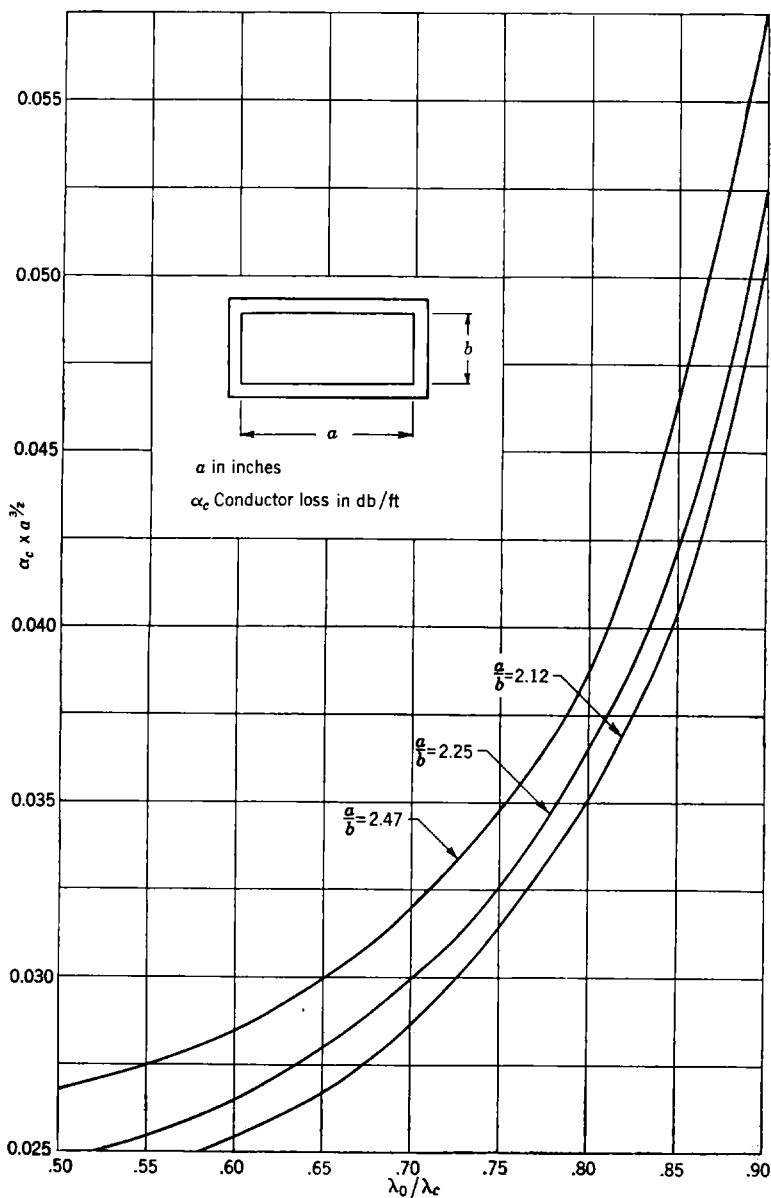


FIG. 4.41.—Variations of attenuation with λ_0/λ_c in rectangular copper waveguide; a is in inches; α_c is conductor loss in decibels per foot.

The maximum power that can be carried by a rectangular waveguide operating in the TE_{10} -mode with $a > b$ is given by the equation¹

$$\frac{P}{E_{\max}^2} = 6.63 \times 10^{-4} ab \left(\frac{\lambda}{\lambda_g} \right). \quad (42)$$

If a and b are in meters, and the electric field strength E is in volts per meter, the power is in watts. Since

$$\frac{\lambda}{\lambda_g} = \sqrt{1 - \left(\frac{\lambda_0}{\lambda_c} \right)^2},$$

$$\frac{P}{E_{\max}^2} = 6.63 \times 10^{-4} (ab) \sqrt{1 - \left(\frac{\lambda_0}{\lambda_c} \right)^2}. \quad (43)$$

Figure 4-42 shows the variation of P/abE_{\max}^2 with changes in λ/λ_c over the pass band.

TABLE 4.7.—SOME WAVEGUIDE CONSTANTS

Guide size OD, in.	Wall, in.	Wave- length, cm	$\frac{P}{E_{\max}^2}$	Power,* Mw	Loss, † db/m (copper)	Wave- length ‡ band, cm
A. Rectangular (TE_{10} -Mode)						
3 × 1.5	0.080	10.0	11.7×10^{-3}	10.5	0.0199	7.3–13.0
2.75 × 0.375 (ID)	0.049	10.0	3.08	2.77	0.0575	7.0–12.6
2 × 1	0.064	6.5	5.39	4.86	0.0310	4.8–8.5
1.5 × 0.75	0.064	5.0	2.54	2.29	0.0633	3.6–6.3
1.25 × 0.625	0.064	3.2	1.97	1.77	0.0725	2.9–5.1
1.0 × 0.5	0.050	3.2	1.10	0.99	0.117	2.3–4.1
0.5 × 0.25	0.040	1.25	0.248	0.223	0.346	1.07–1.9
B. Round (TE_{11} -Mode)						
3 ID	10.0	18.4×10^{-3}	16.6	0.0140	10.0–11.7
1 OD	0.032	3.2	17.3	1.57	0.0847	3.18–3.64

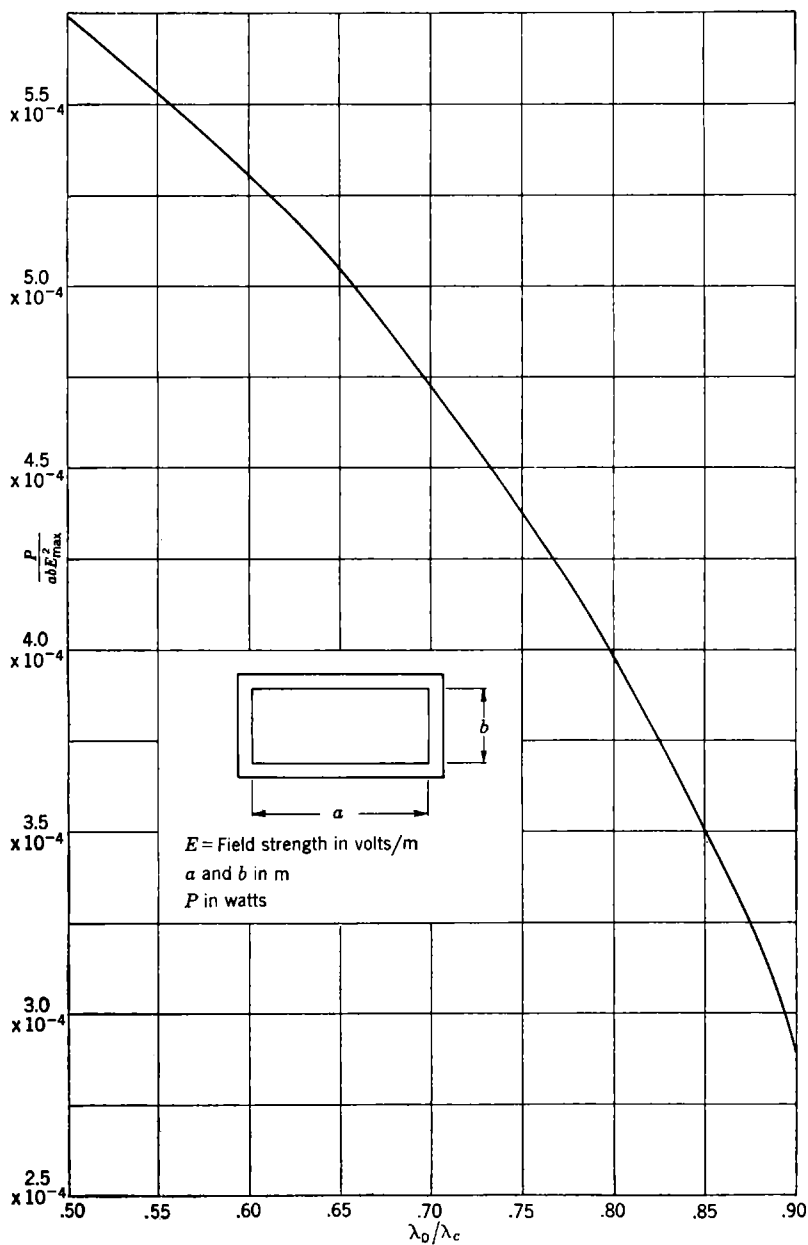
* Calculated values assuming 30,000 volts/cm.

† Calculated values for copper.

‡ Based on maximum wavelength 10% below cutoff for lowest mode and minimum wavelength 1% above that allowing propagation of another waveguide mode. At 10% below cutoff, the attenuation is roughly twice, and breakdown power roughly half, that for the short-wave limit. Both become very rapidly worse as cutoff is approached.

As the cutoff wavelength is approached, the attenuation of a waveguide increases rapidly and the breakdown power decreases rapidly. Therefore, the entire pass band as described above is not used. The use of a range from about 1 per cent above the cutoff wavelength for the second mode to 10 per cent below cutoff for the lowest mode is considered good practice. For narrow-band systems, it is advisable to operate

¹ *Ibid.*, p. 73.

FIG. 4-42.—Variations in breakdown with λ_0/λ_c in rectangular waveguide.

near the center of this wavelength range. At 10 per cent below cutoff for the dominant or TE_{10} -mode, the attenuation is roughly twice, and the breakdown power roughly half, that for the short wavelength limit.

The more important characteristics of several commonly used waveguides are presented in Table 4-7.

WAVEGUIDE COUPLINGS

Two general classes of couplings are used for connecting waveguide sections: (1) the contact coupling, and (2) the choke-flange coupling. The losses and reflections from a contact joint between two sections of tubing are negligible if care is taken to have the sections line up and make good contact across the entire surface. It is considered good design practice to use the more complicated "choke-flange" coupling in service applications instead of the contact coupling because clean, flat, parallel surfaces are hard to achieve and maintain.

4-8. Contact Couplings.—The contact coupling is usually made of flat flanges which are soldered to the ends of the tubing and bolted together as shown in Fig. 4-43. A joint of this type is often used in experimental impedance-measuring equipment where extreme accuracy is desired. This assembly is usually made by inserting into the line at the junction a plunger carefully machined to make a slip fit in the tubing. After the bolts are tightened, the plunger is pulled out of either end. Each time the coupling is assembled the mating surfaces are usually cleaned to remove corrosion and thereby ensure good contact. By moving one flange back a few mils from the end of the tubing as shown in Fig. 4-43,

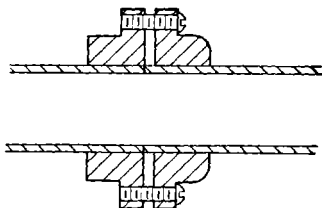


FIG. 4-43.—Contact coupling.

a greater pressure may be applied to make good contact over the entire surface. This procedure reduces the mechanical strength of the joint; therefore, the line should have additional support. Reflections from such a coupling can be kept consistently below 1.01 in VSWR by use of this procedure. Tests have shown that a coupling of this type, when carefully made, is better than the average soldered guide-to-guide joint. The contact coupling is not frequency-sensitive.

4-9. Circular-groove Choke-flange Couplings.—Choke-flange couplings consist essentially of a series-branching transmission line whose length is one-half wavelength, thus presenting zero series impedance to the main line. The important feature of such a coupling is that it is broken at a low-current point B (Fig. 4-44) in the branch line; thus contact troubles are minimized. It is common practice to make the outer quarter-wavelength section in the form of a circular groove. The depth

d of this groove is chosen a quarter wavelength in order that the minimum-current point will occur at the contact between the choke and flange.

For the rectangular-waveguide coupling, the outer groove may be considered as a low-impedance coaxial line excited principally in the second TE_{10} -mode as in Fig. 4-44a. Figure 4-44 illustrates standard choke-coupling designs for rectangular waveguide operating in the fundamental

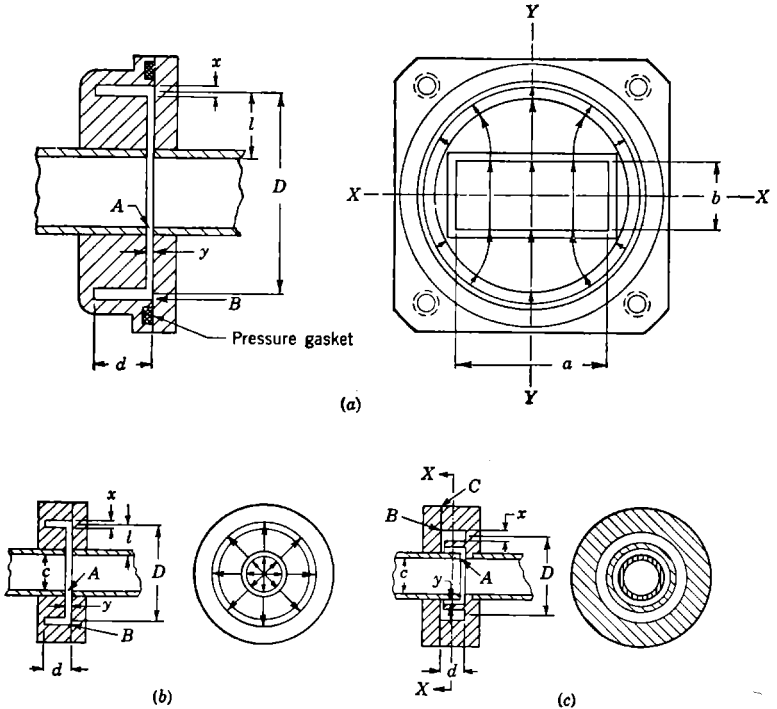


FIG. 4-44.—Continuous circular-groove choke coupling. (a) Rectangular-waveguide coupling, TE_{10} -mode. (b) and (c) Circular-waveguide couplings, TM_{01} -mode.

TE_{10} -mode and for circular waveguide operating in the TM_{01} -mode. From the symmetry of fields and currents about the vertical line YY and the equal but opposite (mirrored) symmetry about the horizontal line XX , it is obvious that the excitation of the choke section must be such that it will excite only coaxial modes of similar symmetry. Hence, the TE_{20} -mode would not be excited under normal conditions. If the choke and flange are not lined up perfectly, the TE_{20} -mode will be excited to some extent. It is quite likely that a good deal of excitation of the TE_{30} -mode is normally present. The currents flowing in the waveguide do not tend to excite the side portions of the circular groove (that is, the portions of

the groove adjacent to the narrow sides of the waveguide). This fact seems to indicate that the fields in the circular groove cannot be adequately described by the TE_{10} -mode alone but that a fairly large TE_{30} -term plus smaller amounts of higher TE -modes are required.

Since the currents in the side walls of the waveguide have no longitudinal component, it is not necessary to provide any choke action along the narrow sides of the waveguide. Therefore, the circular groove may be filled up with metal or not cut at all in this region as indicated in Fig.

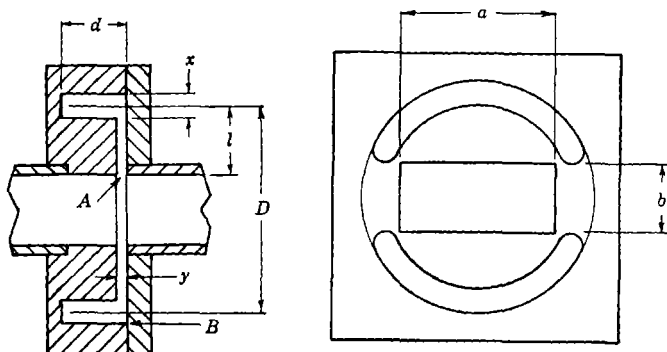


FIG. 4-45.—Discontinuous circular-groove choke coupling.

4-45. This procedure is desirable when misalignment between the choke and flange is contemplated as in motional joints (see Sec. 5-20). By this procedure the choke is broken up into two separate portions, one excited by the currents in the top wall and the other by the currents in the lower wall of the waveguide. The two portions may now be considered as separate waveguides. Moreover, the currents in the broad walls of the waveguide, being sinusoidal in their transverse variation, tend to excite the TE_{10} -mode in a fairly pure manner.

A coupling of this type is difficult to manufacture; therefore, the circular-groove type has been used for rigid-waveguide couplings. The cutoff wavelengths for the TE -modes are given with very good accuracy, for these low-impedance coaxial lines, by the approximate equation

$$\lambda_c = \frac{\text{average circumference}}{n}, \quad (44)$$

where n is the order of the mode (TE_{n0}). By use of the usual equation relating guide wavelength to free-space and cutoff wavelengths, the depth of groove d in Fig. 4-44a can be calculated; a quarter guide-wavelength depth is required. Since the TE_{10} -mode is the one chiefly excited, the groove is made a quarter wavelength deep for this mode. The average circumference of the groove is such that the TE_{30} -mode will

not propagate at the longer wavelengths for which the choke is designed. At the shorter wavelengths, the depth is a very small fraction of a quarter wavelength for the TE_{30} -mode.

In the choke coupling for circular waveguide operating in the TM_{01} -mode, Fig. 4-44b, the coaxial groove is excited uniformly over the circumference in the fundamental coaxial mode (assuming perfect alignment). Therefore, the wavelength in this section is equal to the free-space wavelength. The groove depth must be adjusted to balance

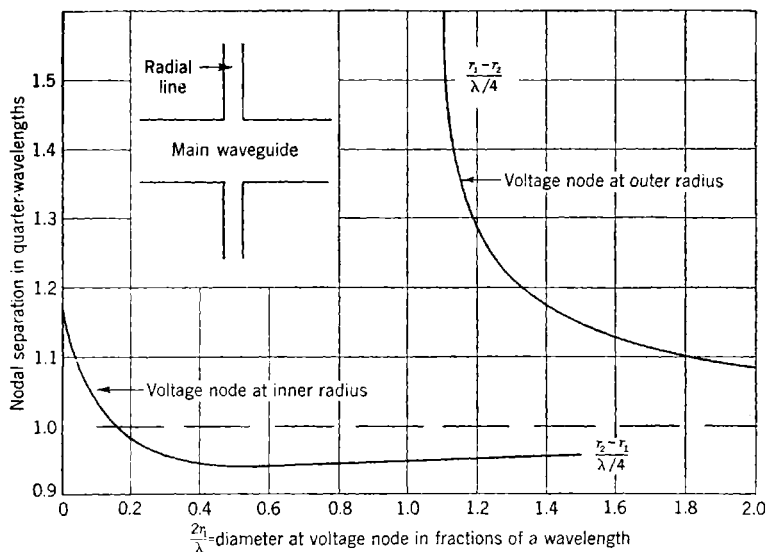


FIG. 4-46.—Voltage and current nodes in a radial-transmission line; r_1 corresponds to a voltage node; r_2 corresponds to a current node; for $n = 1$, cylindrical wave.

junction effects, which makes it deeper than $\lambda/4$. An experimental method for determining the proper groove depth is described later in this section.

To determine the average circumference in a circular-choke groove that is cut in such a way that the point B on diameter D is at a current minimum position and also a quarter wavelength from point A , the section of line between A and B must be considered. This section of line between the main line and the coaxial groove is a radial-transmission line. The proper groove diameter D , Fig. 4-44a, is usually determined by empirical methods. A method for determining this diameter, proposed by Pierce of Bell Telephone Laboratories,¹ is to vary the radius r_1 of a purely radial

¹ J. R. Pierce, "Design Procedure for Disk Choke Couplings," BTL Report MM-44-120-22, Apr. 26, 1944.

transmission line until no discontinuity is presented in the main-waveguide line. The width of this radial line should be the same as that used in the final choke design (y of Fig. 4.45). From this radius r_1 , the radius r_2 of a circle at the antinode or high-impedance point may be found for the rectangular-waveguide case from the curves of Fig. 4.46, which is reproduced from Pierce's report. It should be mentioned here that in some instances the proper groove diameter will intersect the waveguide. If this is so it is impossible to make a simple circular choke which will give both a perfect match and very low leakage. Either match or low leakage

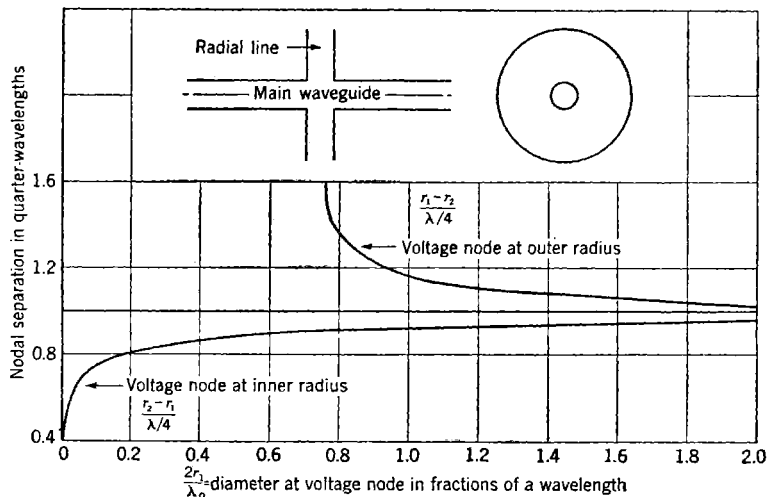


FIG. 4.47.—Voltage and current nodes in a radial-transmission line; r_1 = voltage node; r_2 = current node; $n = 0$, cylindrical wave.

must be sacrificed. This situation has been encountered in 0.170- by 0.420-in. ID and $1\frac{1}{8}$ - by $\frac{3}{8}$ -in. ID waveguides operating at free-space wavelengths of 1.25 cm and 3.3 cm, respectively. The only way to preserve both is to go to some other groove shape or to a discontinuous circular groove as illustrated in Fig. 4.45. Grooves of other shapes for choke couplings are discussed later in Sec. 4.9. For the circular-waveguide choke coupling, Fig. 4.47 gives the same relations.

Having calculated the groove depth for the correct diameter D as outlined, it may be desirable to check experimentally to see that this depth gives the expected current minimum at the choke-flange contact. In the same report, Pierce has proposed one such check. Figure 4.48 illustrates the Pierce method for determining the correct groove depth. The method consists essentially in opening the choke-flange contact and inserting at this point a variable-length transmission line short-circuited

at its outer diameter. This transmission line may be coaxial or radial as shown in Fig. 4-48. With this arrangement, the main line is short-circuited a half wavelength beyond the choke opening to give maximum excitation of the choke, and the position of the minimum voltage L_1 is found for various lengths of the added line L_2 . Figure 4-48 shows the

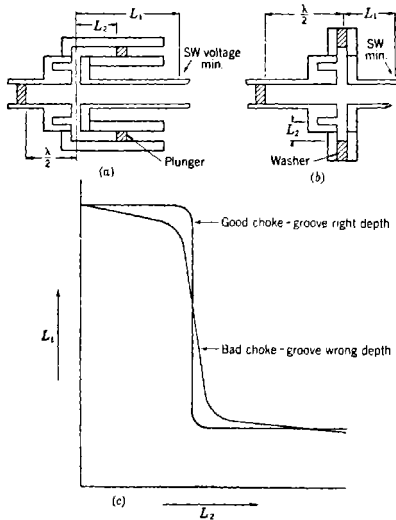


FIG. 4-48. —Pierce method for design of choke grooves. (a) Coaxial-plunger method. (b) Washer method. (c) Curves showing good and bad chokes.

form of the L_1 -vs.- L_2 curves for good and bad choke designs. The curves show essentially the sharpness of the resonance created when the variable-line length L_2 is approximately $\lambda/4$, since the choke depth is also a quarter wavelength. Since a gap is created in place of the choke-flange contact, the conditions at this junction are not quite the same as those in actual practice; however, if the gap is kept small, this objection is probably not very serious.

Where choke-flange couplings are to be separated to eliminate shock mounting, it is advisable to limit the external diameter of the coupling so that the outer edge is a quarter wavelength from B . In this case the open circuit at the edge is transformed to a low impedance across the gap at B . This low impedance is in series with a much higher impedance so that leakage is minimized.

So far no mention has been made of the factors affecting the performance of such a coupling over a broad band of wavelengths. Obviously the choke groove cannot be the right depth to give zero current at the contact over a broad band. Hence, a certain amount of leakage and contact losses will occur on each side of the design wavelength. Similarly, the effective over-all choke length cannot be half a wavelength over a broad band; consequently some mismatch will occur at each side of the design wavelength. Such effects may be minimized by making the characteristic impedance Z_x of the outer groove much larger than that of the radial section Z_y , as shown in Fig. 4-44. The impedance at point B in Fig. 4-44 is

$$Z_B = jZ_x \tan \beta_1, \quad (45)$$

where $\beta_1 = 2\pi d/\lambda_z$, and λ_z is the guide wavelength in the outer groove.

Then at point A the impedance Z_A can be calculated from the usual line-theory formula using Z_B as the load for the radial line. The impedance at point A is then

$$Z_A = Z_y \frac{Z_B + jZ_y \tan \beta_2}{Z_y + jZ_B \tan \beta_2}, \quad (46)$$

where β_2 is the effective angular length of the radial-line section. The relation between effective and actual length of the radial line is not important. In this discussion it is assumed that l' and λ_y' are the effective values of length and guide wavelength for the radial section; then,

$$\beta_2 = \frac{2\pi l'}{\lambda_y'}. \quad (47)$$

Inserting the value of Z_B given by Eq. (45) into Eq. (46) and simplifying, we have

$$Z_A = jZ_y \frac{(Z_x \tan \beta_1) + (Z_y \tan \beta_2)}{Z_y - Z_x \tan \beta_1 \tan \beta_2}. \quad (48)$$

In practice, both β_1 and β_2 are very nearly $\pi/2$; hence if β_1 is equal to $\pi/2 + \delta_1$ and β_2 is equal to $\pi/2 + \delta_2$, $\tan \beta_1$ and $\tan \beta_2$ are approximately $-1/\delta_1$ and $-1/\delta_2$, respectively. Using these assumptions

$$Z_A \approx -jZ_y \frac{\delta_2 + \frac{Z_y}{Z_x} \delta_1}{\frac{Z_y}{Z_x} \delta_1 \delta_2 - 1}, \quad (49)$$

and in practice $(Z_y/Z_x)\delta_1\delta_2 \ll 1$; therefore

$$Z_A \approx -jZ_y \left(\delta_2 + \frac{Z_y}{Z_x} \delta_1 \right). \quad (50)$$

This reactance appears in series with the line impedance of the main waveguide.

The voltage standing-wave ratio introduced in the main line is very nearly $1 - Z_A/Z_0$. The important points to be noted from the above discussion are these:

1. The mismatch is directly proportional to Z_y/Z_0 ; hence for lowest mismatch Z_y should be as low as practical (that is, y as small as practical).
2. If $Z_x \gg Z_y$, the contribution to the mismatch by δ_1 is negligible compared to that by an equal δ_2 , hence Z_x should be made large compared to Z_y (that is, $x \gg y$). This makes the mismatch more sensitive to choke-groove diameter D than to the depth d . In general, x is made from two to five times as large as y .

4-10. Other Choke Couplings.—Two general types of grooves other than circular ones discussed in Sec. 4-8 have been used in the design of choke-flange couplings for rectangular waveguide. One is known as the British-type choke, Fig. 4-49*a*, and the other type, the Chu choke, is represented by the two chokes shown in Figs. 4-49*b* and *c*. Both types are similar in operation to the discontinuous circular-groove choke couplings in that no choke action is used along the narrow-waveguide walls. Although both types are quite good electrically, they are very difficult to manufacture; therefore they have only been used in special applications.

The British-type choke can be designed quite successfully and easily by direct calculations since the guide wavelength is the same as that in the main-line waveguide. The path lengths l and d in Fig. 4-49*a* are

$$l = \frac{\lambda g}{4} - \delta_l \quad (51)$$

$$d = \frac{\lambda g}{4} - \delta_d \quad (52)$$

where δ_l and δ_d are small corrections which may be obtained from the equivalent circuit analysis of E -plane T -junctions (see Vol. 10 of this series).

The two types of Chu-choke couplings are illustrated in Fig. 4-49. Their operation may be analyzed by considering the current flow in the half-wavelength cavity resonator shown in Fig. 4-50. The cavity-choke coupling of Fig. 4-50 is not a good design because the choke-flange contact is at a maximum position over the entire perimeter. However, its operation is the basis for the design of Chu-choke couplings. The cavity is excited in the TE_{10} -mode and, since its width is a , its guide wavelength is the same as that in the main waveguide. The solid lines of Fig. 4-50*b* show the direction of current flow in the cavity walls. The dotted lines show the direction of the magnetic field. When $c = a$, the cavity has several features which are utilized in the design of Chu-choke couplings. (1) The diagonal lines df and eg and the axes YY and XX are parallel to the current flow. (2) The diagonals fall at positions of minimum current density. (3) The current flow lines and field lines are symmetrical about the diagonals and also about the XX - and YY -axes.

From the first two features, it is seen that the diagonal lines are ideal positions for a choke-flange contact. Choke-flange contact may be made along the diagonals in two ways: (a) by removing section A and folding the sections B and B' to join lines go and do to form the variable-groove-depth type of coupling shown in Fig. 4-49*b*, and (b) by removing sections B and B' and folding section A about the XX -axis to join lines go and do to fo and co , respectively, thus forming the fold-back

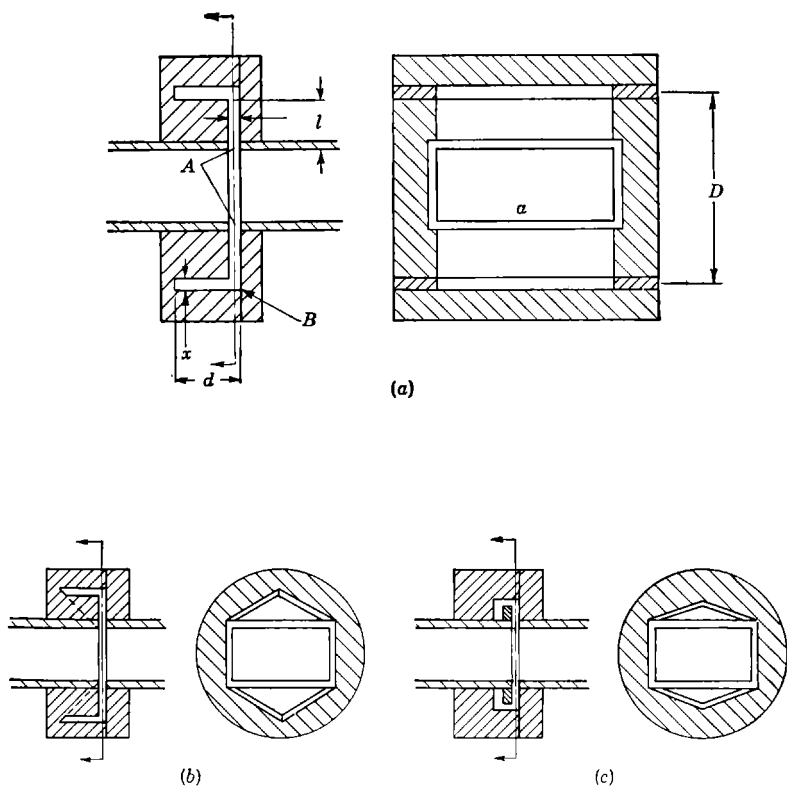


FIG. 4-49.—Other choke couplings. (a) British-choke coupling. (b) and (c) Chutype choke coupling; (b) is a variable-groove-depth type and (c) is a fold-back type.

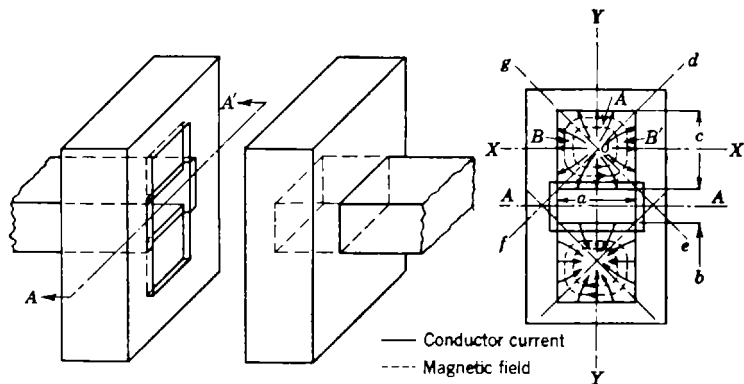


FIG. 4-50.—Half-wavelength cavity choke coupling. Solid line shows conductor current; dashed line shows magnetic field.

type of coupling (Fig. 4-49c). In either case symmetry and continuous magnetic fields still exist.

So far only conditions for low leakage at the contact between choke and flange have been discussed. For minimum mismatch in the main-line waveguide, c must be a half-guide wavelength and, since c must equal a for the low-leakage conditions outlined above, a must be a half-guide wavelength. Therefore, the choke may be used only when $\lambda_a = \lambda_c$ or, in terms of free-space wavelength, when $\lambda_0 = \lambda_a/\sqrt{2} = \lambda_c/\sqrt{2}$. For $\frac{1}{2}$ - by 1-in. (0.050-in. wall) waveguide, the Chu chokes operate best at a free-space wavelength of 3.23 cm. The operation of this type of coupling over a wide range of wavelengths should be at least as good as the other types if the impedance in the outer groove is made large in comparison with the impedance in the section between the choke and flange units as discussed in Sec. 4-8. Both designs have been checked experimentally and have been found to give satisfactory results; however, manufacturing problems prevent further development.

TABLE 4-8.—CHOKE-COUPLING DESIGN DETAILS

Army-Navy type choke flange	Guide dimen- sions, in.		Choke dimensions, in.				Fig. no.	Design wave- length, cm	Band- width for $r = 1.05$, %
			D	x	y	d			
	a	b	Rectangular-waveguide choke. TE_{10} -mode						
UG-54/U-53/U	2.84	1.34	4.015	0.250	0.050	1.120	4.44a	10.7	± 15
U-200/U-214/U	2.84	1.34	3.75	0.250	0.030	0.865	4.44a	9.0	± 15
UG-40/U-39/U	0.90	0.40	1.183	0.063	0.031	0.347	4.44a	3.20	± 6
UG-52/U-51/U	1.125	0.50	1.332	0.063	0.031	0.347	4.44a	3.20
None	0.900	0.40	1.155	0.125	0.010*	0.355*	4.44a	3.30	$> \pm 6$
UG-117/U-116/U	0.420	0.170	0.501	0.029	0.008	0.137	4.44a	1.25	$> \pm 2$
None	0.420	0.170	0.589	0.063	0.008	0.156	4.44a	1.25	$> \pm 4$
	c		Circular-waveguide chokes. TM_{01} -mode						
None	0.4675		0.713	0.050	0.015	0.153	4.44b (1)	1.25	$> \pm 4$
None	1.187		1.479	0.093	0.030	0.312	4.44b (2)	3.30	$> \pm 6$

* Designed for 0.115-in. separation between choke and flange (see Sec. 5.21).

4-11. Summary of Choke-coupling Designs.—Choke-flange couplings have been standardized by the Army and Navy for several sizes of waveguides. The continuous circular-groove type shown in Fig. 4-45 has been favored because it is much easier to make on a large scale. Dimensions for choke-coupling designs are tabulated in Table 4-8 with the numbers of the figures in this chapter to which they refer so that any

of the choke couplings listed can be reproduced. The bandwidth in per cent on each side of the design wavelength when the voltage standing-wave ratio is below 1.05 is given in the table.

CORNERS, CIRCULAR BENDS, AND TWISTS

Waveguide corners and circular bends are similar to elbows in water and gas pipe in that they change the direction of energy flow. Twists are used to change the polarization. These units are very important in the design of compact assembly units. Corners and circular bends for rectangular waveguide operating in the TE_{10} -mode are made in the E - and H -planes. An E -plane bend or corner is defined as one whose axis lies in a plane parallel to the electric field lines. The H -plane bend or corner is defined as one whose axis lies in a plane parallel to the magnetic field lines. So far, in practice, circular waveguide has been used only in short lengths such as rotary-joint sections; consequently, there has been no need for circular-waveguide corners or bends.

Waveguide corners, circular bends, and twists must be carefully designed to avoid impedance mismatch and to prevent voltage breakdown. These design features are discussed in the following sections.

4-12. Waveguide Corners.—Corners for rectangular waveguide are made in two types as shown in Fig. 4-51. The characteristics of the

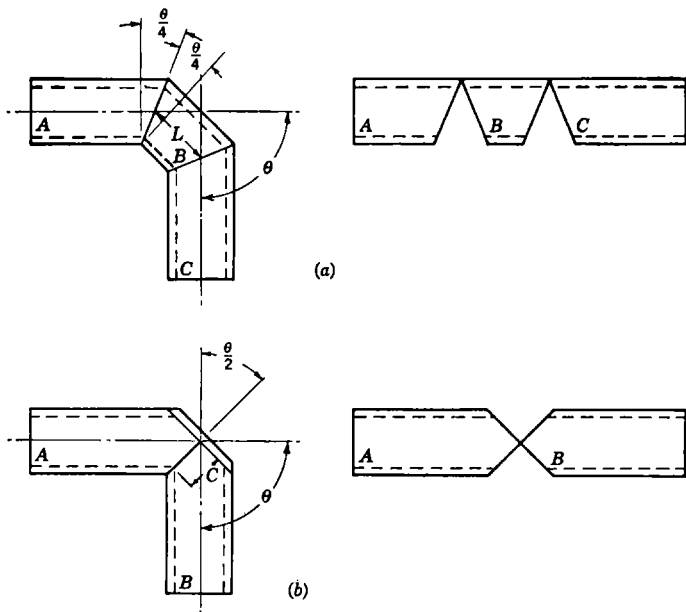


FIG. 4-51.—Waveguide corners. (a) Double-mitered type. (b) Single-miter, cutoff type.

double-mitered type may be determined from the mismatch set up by a single-mitered corner. The equivalent circuit for an E -plane single-mitered corner and its parameters for 1- by $\frac{1}{2}$ -in. waveguide at 3.0, 3.2, and 3.4 cm are shown¹ in Figs. 4-52 and 4-53. The dotted lines are the reference planes corresponding to the equivalent circuit and its parameters. The same characteristics for an H -plane single-mitered junction are shown in Figs. 4-54 and 4-55. These parameters are plotted as a function of wavelength and angle of bend. From these curves the mismatch produced by a simple junction may be determined.

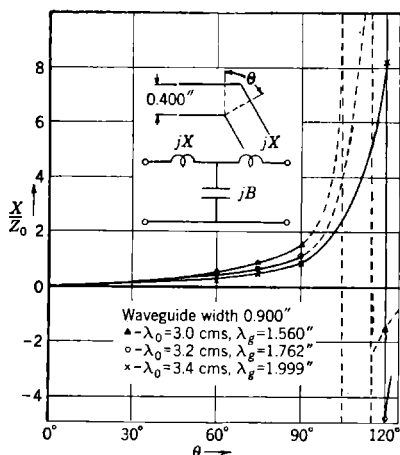


Fig. 4-52.—Series reactance of simple waveguide corners, E -plane.

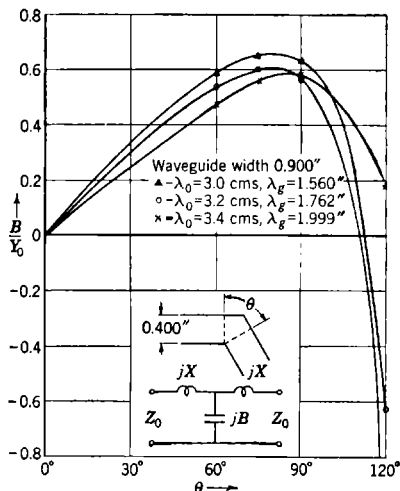


Fig. 4-53.—Shunt susceptance of simple waveguide corner, E -plane.

In the double-mitered corner, two of the single-mitered corners are spaced in such a way that their reflections cancel each other at the desired wavelength. The proper spacing (L in Fig. 4-51) may not be calculated from the equivalent circuit parameters of a single corner since higher mode propagation cannot be neglected. It is necessary to determine L experimentally.

The mean length L for cancellation of reflections in a double-mitered E -plane corner is very nearly a quarter-guide wavelength as shown by experimental measurements. Measurements also show that L must be larger than a quarter-guide wavelength for H -plane double-mitered corners. An experimental design curve for 90° double-mitered H -plane corners in waveguide $1\frac{1}{2}$ by 3 in. OD, 0.080-in. wall, is shown in Fig.

¹ The curves of Figs. 4-52, 4-53, 4-54, and 4-55 were plotted from measurements made at California Institute of Technology, Contract OEMsr-1311, W. H. Pickering, Official Investigator.

4-56. The mean length L in terms of guide wavelengths is plotted against λ_0/λ_c , where λ_0 is the free-space wavelength at which the corner is to be designed and λ_c the cutoff wavelength of the waveguide. This curve has been checked experimentally at a few points (λ_0/λ_c 0.65 to 0.75) for other waveguide sizes and found to be accurate within experimental errors in measurements. The deviation of L from a quarter-guide wavelength for cancellation of reflections between the two junctions is theoretically zero for $\theta = 0$, and it is small if θ is small (see Figs. 4-54 and 4-55).

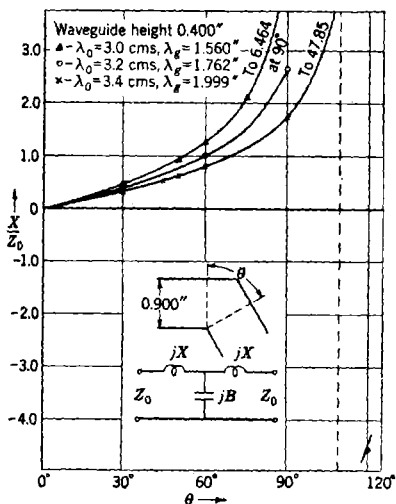


FIG. 4-54.—Series reactance of simple waveguide corner, H -plane.

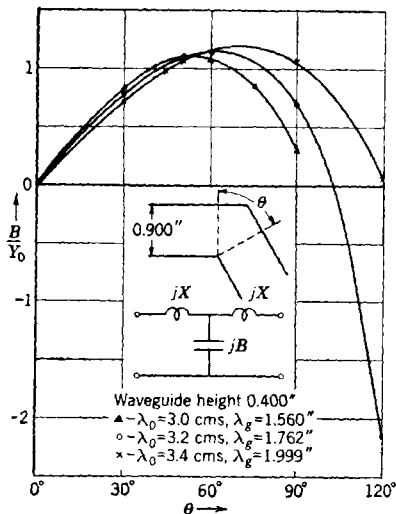


FIG. 4-55.—Shunt susceptance of simple waveguide corners, H -plane.

The mismatch of double-mitered corners over a given band of wavelengths depends on the magnitude of the reflection set up at each junction and the spacing between junctions. Maximum bandwidth for a given mismatch is obtained when the spacing between junctions is a quarter-guide wavelength plus the correction already discussed. However, it may be desirable in some instances to make L equal to $\frac{3}{4}$ or $\frac{5}{4}\lambda_c$. Since the reflection from each junction in a 90° double-mitered corner varies with wavelength, the bandwidth also varies with wavelength. This variation is shown for the $1\frac{1}{2}$ waveguide by 3 in. OD, 0.080-in. wall, in Fig. 4-57 which was determined experimentally. The bandwidth was taken as the wavelength band in per cent over which the voltage standing-wave ratio was below 1.06. This curve can also be applied to other waveguide sizes. This type of mitered corner will

stand as much power before arcing as the waveguide itself if the joints are properly soldered.

The cutoff type of mitered corner has not been used widely since the double-mitered corner was conceived, because it is more difficult to fabri-

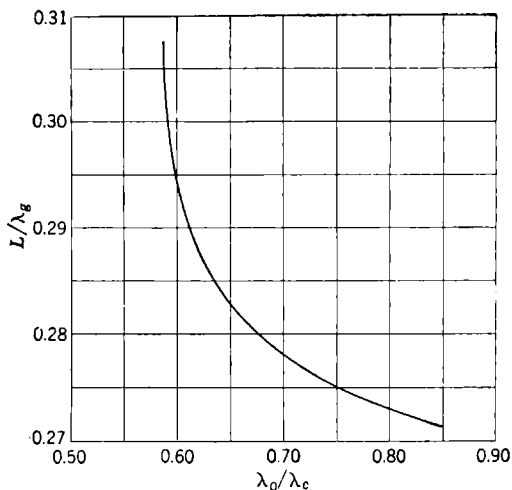


FIG. 4-56.—Design curve for double-mitered *H*-plane corners.

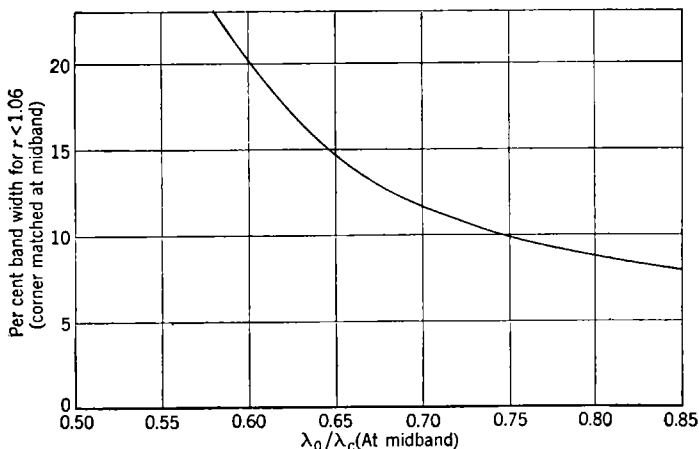


FIG. 4-57.—Bandwidth curve for double-mitered *H*-plane corners.

cate; the dimension C in Fig. 4-51 is critical; and it arcs over at much lower power levels than the waveguide. Arc-over problems are particularly bad in the *E*-plane cutoff corners because the effective guide height b is decreased. No theoretical analysis has been worked out for the cutoff

type of mitered corners. Empirical curves for the design of such corners are shown in Figs. 4-58 and 4-59. In these curves the percentage amplitude reflection is plotted as a function of c/d_0 for five angles. Data for these curves were taken from British measurements using waveguide 7 cm by 3.25 cm ID at 10.84 cm. The reflection coefficient is defined as the ratio of the amplitude of the reflected wave to that of the incident wave. The reflection coefficient has been arbitrarily plotted in such a way that it goes through zero and changes its sign, thereby avoiding cusps that would occur if only positive values were employed. From both figures, it is evident that, at any bend angle, a design is possible which essentially allows perfect transmission around the corner. Evidently the *E*-bend is more satisfactory in the sense that the curves are flatter and hence the dimension c is not so critical.

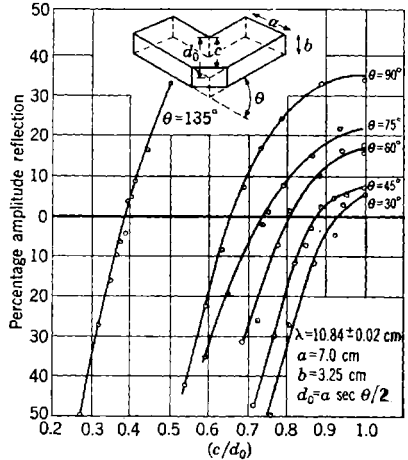


FIG. 4-58.—Reflection from *H*-plane cutoff corners.

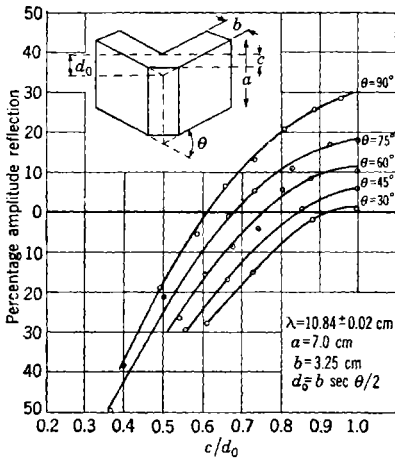


FIG. 4-59.—Reflection from *E*-plane cutoff corners.

4-13. Waveguide Bends and Twists.

—A circular bend in waveguide may be considered as a section of line with a characteristic impedance differing from that in the straight waveguide by an amount depending on the angle of the bend, its radius, and the mechanical tolerances of its cross section. If the bend is uniform, it acts as a transformer, setting up reflections at each end, both of which are equal in magnitude. The transformation is from a higher to a lower impedance at one end and from the lower back to the higher at the other, or vice versa. Therefore, the bend should be any number of half wavelengths long, measured along its axis for cancellation of reflections. These reflections increase as

the radius of curvature of the bend is decreased. The guide wavelength in the bend is almost equal to that in straight waveguide for smooth undistorted bends. Two alternatives are presented in designing circular bends for wide wavelength ranges: (1) the radius of curvature may be made very large so that the reflections from each end are negligible; or (2) the radius may be made very short ($\lambda_g/2$) so that the deviation of the bend length from $\lambda_g/2$ is small over a wide range of wavelengths. Both methods have been used successfully in practice; however, the short radius is preferred because of space and weight limitations.

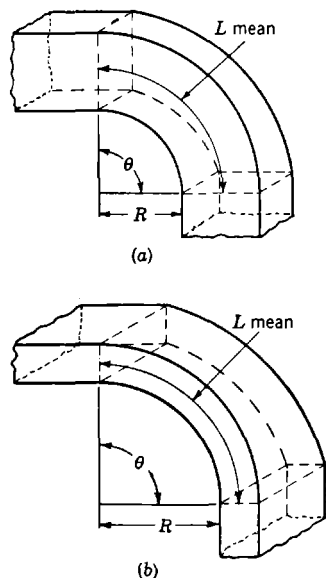


FIG. 4-60.—Waveguide bends.
(a) *H*-plane bend. (b) *E*-plane bend.

Figure 4-60 illustrates the *E*- and *H*-plane circular bends in rectangular waveguide. These bends may be made by filling a straight section of waveguide with cerrobend or Wood's metal and bending the section by a machine or press, by the electroforming process discussed in Sec. 3-2, or by machining. After bending in the first method, the filler is melted out. The bending method is the most economical and is adequate for bends of large radius. For bends of small radius, the bending process produces excessive distortion in the waveguide walls which causes impedance mismatch. The electroforming process is recommended for bends of short radius. The machining process is applicable to any size. The bend is turned on a lathe in the form of two U-shaped circular troughs in such a way that the seam

is in the center of the wide side wall. The two halves are then soldered together and the unit is cut into bends of any desired angle.

Twists in rectangular waveguide are very similar to circular bends since they are best matched when their length is any number of half-guide wavelengths. The guide wavelength in the twisted section is nearly equal to that in the straight waveguide if the cross-sectional dimensions of the twist at any point are the same. Twists are made by filling a waveguide section with cerrobend or Wood's metal and twisting the section in a vice or machine to the desired angle.

The results of tests on several waveguide circular bends and twists are given in Table 4-9. The dimensions for circular bends are illustrated in Fig. 4-60.

TABLE 4-9.—PERFORMANCE OF WAVEGUIDE CIRCULAR BENDS AND TWISTS

Type	Waveguide size ID, in.	Inside radius R , in.	θ	Design wave-length, cm	Bandwidth for r below 1.05, per cent
<i>E</i> -plane bend	1.34 × 2.84	6	45°	10	> ±20
	1.34 × 2.84	6	90°	10	> ±20
	1.125 × 0.50	2	90°	3.3	±9
	0.90 × 0.40	0.50	180°	3.3	> ±9
	0.90 × 0.40	0.25	90°	3.3	> ±9
	0.90 × 0.40	3.00	90°	3.3	> ±9
	0.420 × 0.170	0.50	90°	1.25	> ±4
<i>H</i> -plane bend	1.34 × 2.84	6	45°	10	±10
	1.34 × 2.84	6	90°	10	> ±20
	1.125 × 0.50	2	90°	3.3	> ±9
	0.90 × 0.40	0.192	90°	3.35	±4
	0.90 × 0.40	1.1875	90°	3.30	±9
	0.420 ± 0.170	0.50	90°	1.25	> ±4
Type	Waveguide size ID, in.	Length, in.	Design wavelength, cm	Bandwidth for r below 1.05, per cent	
Twists	0.900 × 0.400	2	3.4	±6	
	0.900 × 0.400	3	3.4	±3.7	
	1.125 × 0.500	4	3.3	> ±9	
	0.420 × 0.170	1½	1.25	> ±4	
	0.420 × 0.170	2½	1.25	> ±4	

IMPEDANCE-MATCHING

Impedance-matching devices in waveguide are sometimes necessary to correct for the mismatch of a component or assembly of components in the line. The matching consists of introducing into the line a reflecting element that sets up a reflection equal in magnitude but 180° out of phase with the existing reflection. If the reflecting element is a perfect conductor, its action is equivalent to some combination of series and shunting reactors in an ordinary transmission line which absorb no power. Many reflecting elements whose dimensions along the guide axis are small compared with a wavelength are equivalent to simple shunting reactances in the line. The equivalent reactance for elements discussed in the following sections have been determined theoretically and verified experimentally. This equivalent reactance is given as the normalized susceptance B . The normalized input admittance Y to such reflecting elements when introduced into a matched waveguide is

$$Y = 1 + jB. \quad (53)$$

The voltage standing-wave ratio set up in a matched line by an element of normalized susceptance B is¹

$$r = \frac{\sqrt{4 + B^2 + B}}{\sqrt{4 + B^2 - B}} \quad (54)$$

The susceptance B required to correct a given voltage standing-wave ratio r may be written as

$$B = \frac{r - 1}{\sqrt{r}} \quad (55)$$

The location of the reflecting element for correction of the mismatch r is determined by

$$d = \frac{90^\circ - \tan^{-1} \left| \frac{B}{2} \right|}{720^\circ} \lambda_g, \quad (56)$$

where d is the distance between the reflecting element and a voltage minimum. If the reflecting element is inductive (B is negative), it should be placed at a distance d on the load side of a minimum; and if

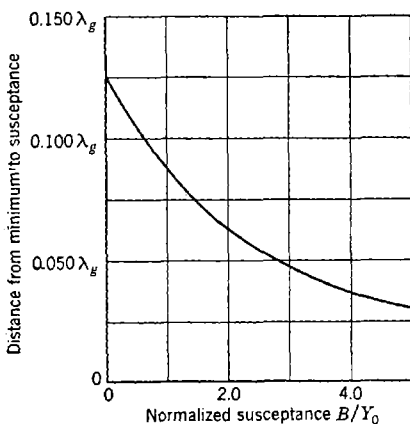


FIG. 4-61.—Distance between voltage minimum and position of matching susceptance.

capacitive, it should be at a distance d on the generator side of a minimum. For best operation over a broad band, the minimum position mentioned above should be the first one on the generator side of the component or discontinuity causing the reflection.

Curves of r vs. B and d/λ_g vs. B are given in Figs. 2-12 and 4-61. The effect of higher modes (fringing fields) is neglected in the calculation of the curves. This higher mode effect has been troublesome only in

¹ *Microwave Transmission Design Data*, Sperry Gyroscope Co., May 1944, p. 97.

cases where large susceptances were used in waveguides operated at a wavelength just above their cutoff wavelength.

The simple shunting reactance elements which have been used extensively in microwave-transmission systems and which will be discussed here are (1) inductive diaphragms, (2) capacitive diaphragms, (3) capacitive buttons and dents, and (4) quarter-wavelength transformers.

4-14. Inductive Matching Diaphragms.—A diaphragm in waveguide is an aperture in a thin metal diaphragm that extends transversely across the guide. In the inductive diaphragm, the aperture extends completely across the guide, the edges being parallel to the electric-field vector for the lowest mode. Inductive diaphragms are made in two types, symmetrical and asymmetrical, which are illustrated in Fig. 4-62a.

In the symmetrical type the aperture of width d is centered between the guide walls. The shunt susceptance for this type has the theoretical value¹

$$B = -\frac{\lambda_g}{a} \cot^2 \left(\frac{\pi d}{2a} \right), \quad (57)$$

where λ_g is the guide wavelength of the lowest mode and a is the longer of the cross-section inside dimensions of the guide. Figure 4-63 shows the theoretical variation of B with d/a computed by a more accurate expression than Eq. (57).

In the asymmetrical type, the center line of the aperture is displaced from the half-way position between the guide walls. If X_0 is the center-line position measured from the nearest side wall of the guide ($X_0 = a/2$ for the centered diaphragm), the theoretical susceptance is

$$B = -\frac{\lambda_g}{a} \cot^2 \frac{\pi d}{2a} \left(1 + \sec^2 \frac{\pi d}{2a} \cot^2 \frac{\pi X_0}{a} \right). \quad (58)$$

The approximation in deriving this formula is the same as for the symmetrical type but is not so good here because of the asymmetry. The special case for which one edge of the diaphragm coincides with the guide

¹ N. H. Frank, Report T-9, Sec. III, p. 14. This formula was derived by assuming that the cutoff wavelengths for all the higher modes that are excited are so large compared with the free-space wavelength that these may be neglected relative to the cutoff wavelength.

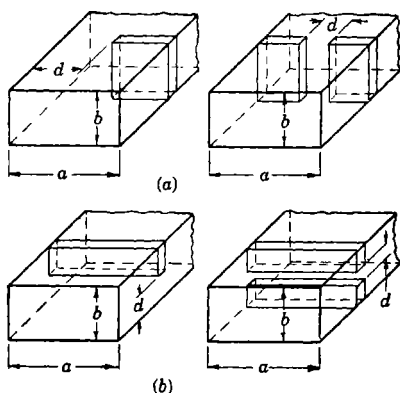


FIG. 4-62.—Inductive and capacitive diaphragms in rectangular waveguide. (a) Inductive diaphragms. (b) Capacitive diaphragms.

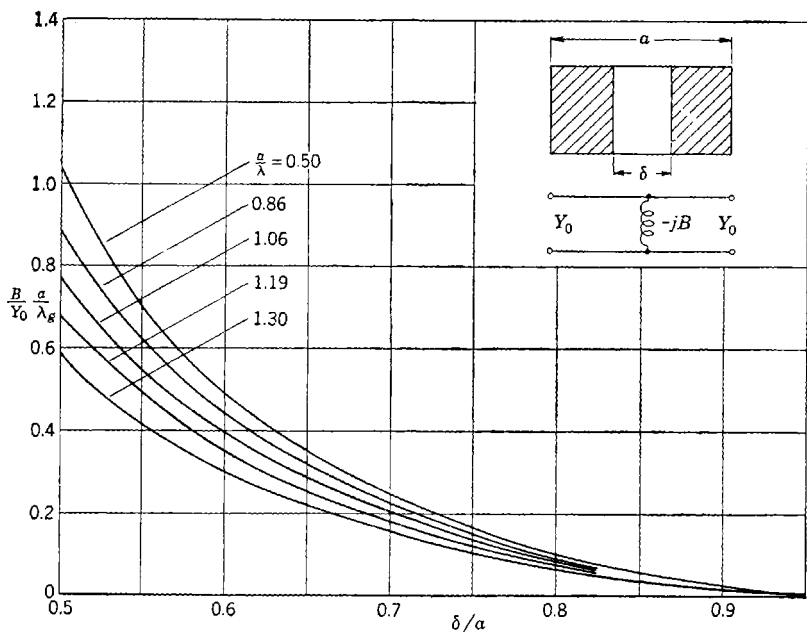


FIG. 4-63.—Normalized susceptance of symmetrical inductive diaphragm.

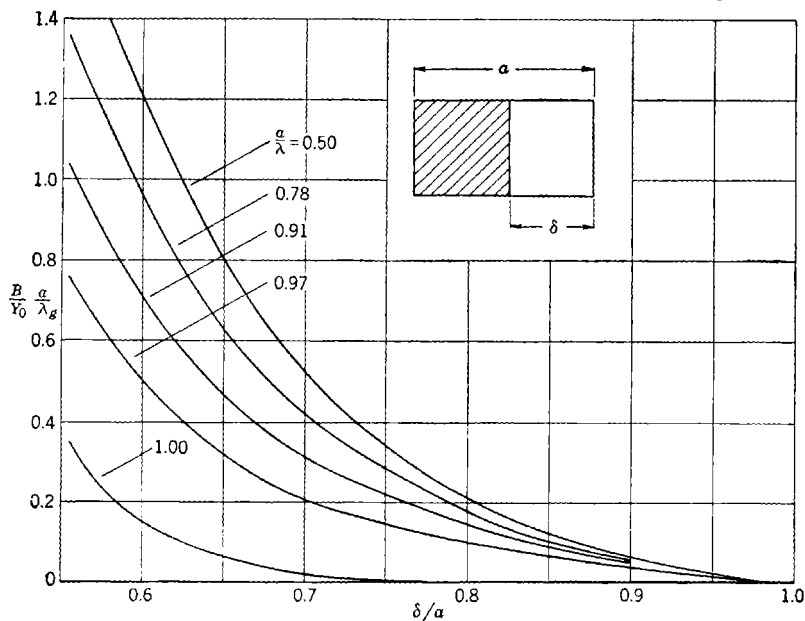


FIG. 4-64.—Normalized susceptance of asymmetrical inductive diaphragm.

wall is contained in this equation, if one sets $X_0 = d/2$. For this special case, the shunt susceptance is given by

$$B = -\frac{\lambda_g}{a} \cot^2 \frac{\pi d}{2a} \left(1 + \csc^2 \frac{\pi d}{2a} \right). \quad (59)$$

Figure 4-64 is a plot of the variation of $B(a/\lambda_g)$ with d/a for this special case for an accurate theoretical formula.

A circular aperture centered in a waveguide of circular cross section as shown in Fig. 4-65 is inductive. Measurements have been made at

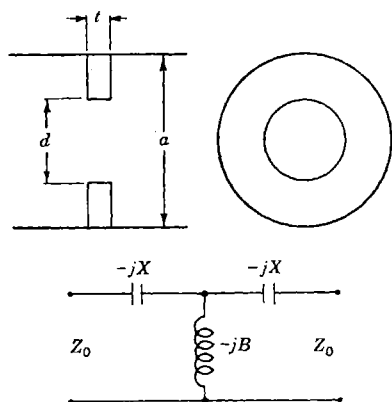


FIG. 4-65.—Inductive window for circular waveguide.

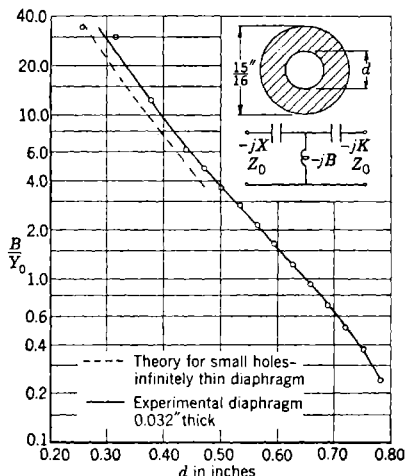


FIG. 4-66.—Normalized susceptance of inductive diaphragm in circular waveguide, $\lambda = 3.20$ cm.

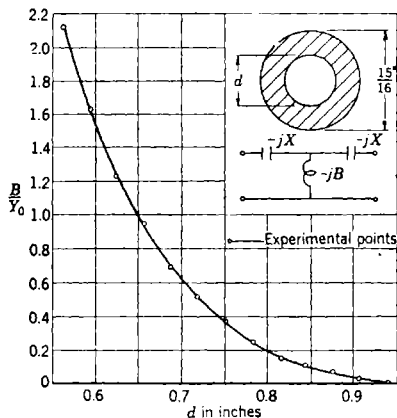


FIG. 4-67.—Normalized susceptance of inductive diaphragm in circular waveguide; $\lambda = 3.20$ cm.

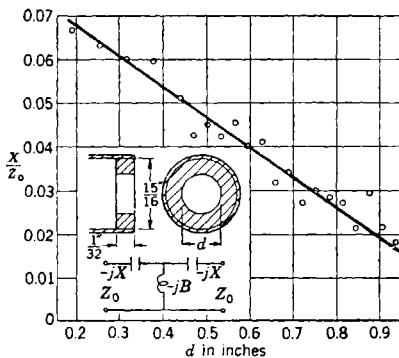


FIG. 4-68.—Series reactance of inductive diaphragm in circular waveguide; $\lambda = 3.20$ cm.

$\lambda_0 = 3.20$ cm ($\lambda_g = 2.026$ in.) for a waveguide $\frac{1\frac{1}{2}}$ -in. ID (TE_{11} -mode). The equivalent circuit parameter B , plotted against d , is given in Figs. 4-66 and 4-67 for a $\frac{1}{32}$ -in. diaphragm. Figure 4-66 also gives a theoretical curve, the theory assuming small holes in an infinitely thin barrier.

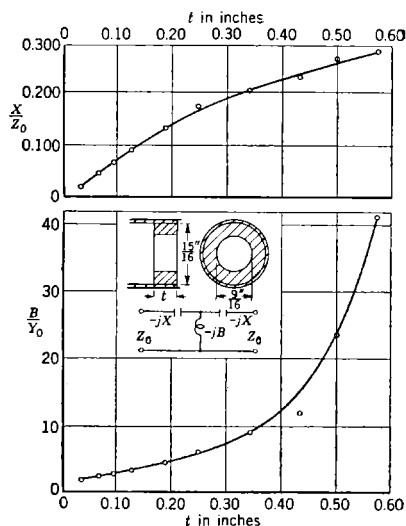


FIG. 4-69.—Variation of equivalent circuit parameters with thickness of diaphragm; $\lambda = 3.20$ cm.

the guide, and d is the width of the aperture. For an asymmetrical diaphragm (see Fig. 4-62*b*),

$$B = \frac{8b}{\lambda_g} \ln \csc \frac{\pi d}{2b}. \quad (61)$$

Figure 4-70 shows the theoretical and observed variations of B with d/b for waveguide 3.44 cm by 7.21 cm ID at a wavelength of 9.8 cm. The theoretical value is derived to the same degree of approximation as in the inductive case. The experimental observations were made at the Research Laboratory of the General Electric Company.

The thickness of the diaphragm has a large effect on the susceptance of capacitive diaphragms. For small but finite diaphragm thickness, the following theoretical formulas have been derived.

$$\left. \begin{aligned} B &= B_0 + \frac{2\pi t}{\lambda_g} \left(\frac{b}{d} - \frac{d}{b} \right) \\ G &= \frac{2\pi t}{\lambda_g} B_0 \frac{d}{b} \end{aligned} \right\}, \quad (62)$$

Figure 4-68 gives a plot of X/Z_0 vs. d for the same case; and Fig. 4-69 is a plot of B/Y_0 and X/Z_0 vs. t for $d = \frac{9}{16}$ in.

4-15. Capacitive Matching Diaphragms.—The aperture in a capacitive diaphragm extends across the guide, as shown in Fig. 4-62*b*, the edges being parallel to the longer cross-section dimension a of the guide. The theoretical shunt susceptance of such a diaphragm centered between the guide walls is, for infinitely thin diaphragms,

$$B = \frac{4b}{\lambda_g} \ln \csc \frac{\pi d}{2b}, \quad (60)$$

where λ_g is the guide wavelength of the lowest mode, b is the shorter cross-section inside dimension of

where B and G are the shunt susceptance and shunt conductance of the diaphragm of thickness t , B_0 being the value given by Eq. (61). These values refer to the entrance planes of the diaphragm.

The use of the capacitive diaphragm is limited to relatively low-power systems because of the danger of voltage breakdown.

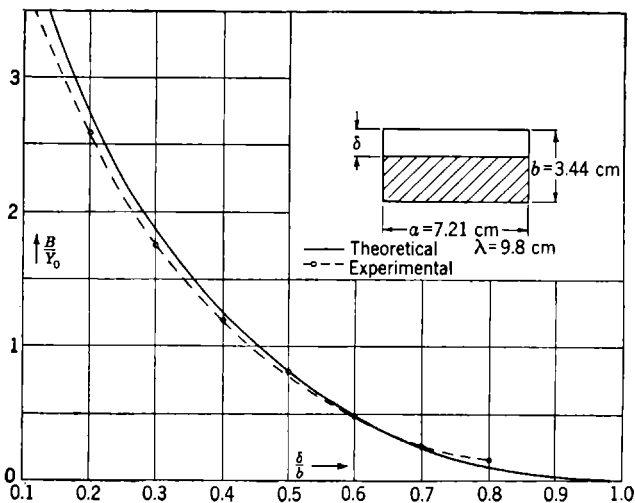


FIG. 4-70.—Normalized susceptance of asymmetrical capacitive diaphragm.

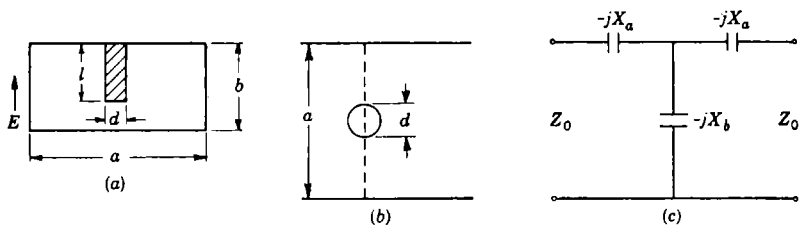


FIG. 4-71.—Capacitive post or button; (a) section view, (b) top view, (c) equivalent circuit at the reference plane (shown dotted in b).

4-16. Capacitive Buttons and Dents.—Capacitive buttons are sometimes used for matching of components and transmission systems. The capacitive button consists of a metallic cylindrical rod of finite length inserted into the center of the wide side of the waveguide so that its axis is parallel to the electric field. Such a device is shown (for rectangular waveguide, TE_{10} -mode) in Fig. 4-71. The cylindrical post of length l and diameter d is joined to the wide side of the waveguide. An equivalent circuit referred to the reference plane in Fig. 4-71 is a T -network whose series and shunt arms are capacitive elements for small lengths of

obstacle (and $d/\lambda \ll 1$). For lengths approximately one-quarter of free-space wavelength, the shunt element becomes series resonant. When used as a matching element such buttons are slightly rounded on the end to reduce field concentration on the edges and thus to increase the breakdown power level in the guide in which the matching button is installed. Even with rounded edges, buttons decrease the breakdown power level of the waveguide.

A plot of experimental data for the relative reactances of the series and shunt arms as a function of the obstacle length for the case $d = 0.25$ in., $a = 0.90$ in., $b = 0.40$ in., and $\lambda = 3.2$ cm, is given in Fig. 4-72.

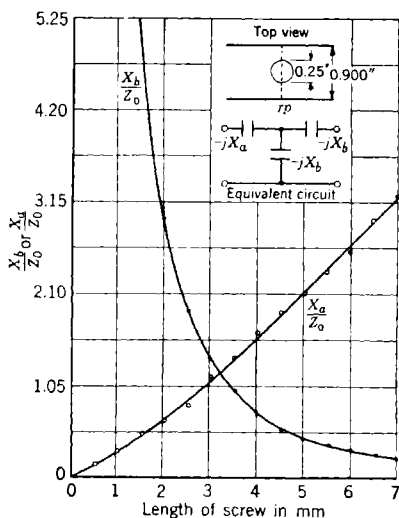


Fig. 4-72. Reactances of a capacitive tuning screw; $\lambda = 3.20$ cm.

The data were taken on a tuning screw with slightly rounded edges. The choke on the tuning screw introduced a small reactance (≈ 0.05) even for zero length; this reactance has been subtracted from the X_a/Z_0 plot.

Dents may be used in matching components after assembly to correct for manufacturing tolerances. Dents are very similar to the capacitive button since a dent in the center of the wide side of a waveguide is capacitive, and it reduces the breakdown power level of the waveguide. Dents can easily be made at any desired position along the line for final matching of a component or system. To find the correct position,

a clamp may be placed on the waveguide at different points to squeeze the waveguide just enough to see if a dent at that point would decrease the reflection. After removing the clamp, the waveguide springs back almost to its original position if the dent is not deep. When the correct position is reached, the dent is made deep enough so that when the clamp is removed the depth of the penetration is correct for matching. This procedure is quite satisfactory when a directional coupler is used to indicate the reflected power. When a slotted section of waveguide is used to measure the reflected power, it is more convenient to calculate the proper location for the dent. The proper distance from a voltage minimum position is shown in Fig. 4-61 where the distance d is plotted against the voltage standing-wave ratio. For a capacitive element such as the dent, the proper distance between the voltage minimum and the element measured toward the load is $\lambda/2 - d$.

The reflection from a dent measured in r^2 increases linearly with the depth of the dent. Experimental results on waveguide 0.500 by 1.125 in. ID show an increase in r^2 of 0.08 per $\frac{1}{32}$ -in. depth.

4-17. Quarter-wavelength Transformer.—A transformer in a waveguide is made by an abrupt change of either or both cross-sectional inside dimensions of the guide. The quarter-wavelength transformer is equivalent to a matching diaphragm with a thickness of one-quarter guide wavelength. If the original dimensions are called a and b and the reduced dimensions a' and b' , the ratio of the impedance of the smaller to the larger may be calculated from Eq. (2-160) for changes in either or both dimensions. The ratio is

$$\frac{Z'_0}{Z_0} = \frac{b' a \lambda'_g}{b a' \lambda_g} \quad (63)$$

In addition to this change in characteristic impedance, a shunt susceptance is introduced at each junction. Higher modes are also set up at such junctions especially when the change is asymmetrical (guide axis shifted in transformer section). These higher modes are damped out

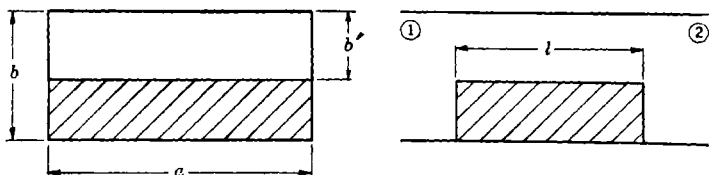


FIG. 4-73.—Asymmetrical quarter-wavelength transformer.

rapidly by a transformer of smaller dimensions than the waveguide and therefore cause little trouble in quarter-wavelength transformers. Since the quarter-wavelength transformer is essentially a matching diaphragm which is one-quarter wavelength in thickness, the junction susceptance may be estimated from the preceding formulas and curves for matching diaphragms. Since asymmetrical transformers involving a change in only one guide dimension are more practical from the manufacturing standpoint, they are frequently used. The asymmetrical capacitive transformer shown in Fig. 4-73 is usually used because in this type the cutoff characteristics of the guide for the TE_{10} -mode are not changed and the construction is very simple. For small changes in the characteristic impedance, the junction effects are small. The input admittance seen at the generator side when the load end is matched is given by

$$\frac{Y}{Y_0} \approx \left(\frac{b}{b'} \right)^2 \quad (64)$$

The transformer may be designed to cancel a given mismatch by the

above formula. To avoid difficulty in locating the transformer at the correct position, it may be made to slide in the guide after being tinned with solder on the bottom and sides. A small hole in the center of the broad face of the guide will enable the operator to move the transformer until a match is obtained; then the transformer is soldered in place by heating the outside of the guide.

PRESSURIZING WINDOWS

Pressurizing windows are structures sealed in the line for protection of an entire transmission system or of individual components from

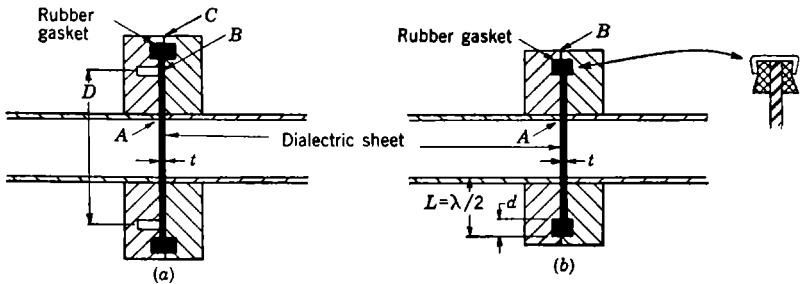


FIG. 4-74.—Thin-sheet, nonresonant windows.

moisture, fungus growth, and corrosion during shipment, storage periods, and operation. Pressurizing windows also increase the voltage breakdown limit of a microwave transmission system, if the system is sealed under pressure as discussed in Chap. 3.

Four types of pressurizing windows are known for sealing waveguide systems: (1) thin sheets, nonresonant; (2) thin sheets in resonant mount; (3) half-wavelength dielectric plugs; and (4) T-shaped dielectric plugs three-quarters wavelength long. All types make use of low-loss dielectric materials for transmission of power without attenuation. The material must be low loss to prevent r-f heating and consequent destruction of the dielectric material as well as undesirable results in matching. The electrical and mechanical characteristics of these materials and techniques for handling them are discussed in Chap. 3. Therefore, the following sections are discussions of each type principally from the standpoint of electrical design.

4-18. Thin Sheets, Nonresonant.—Pressurizing windows of this type make use of a transverse sheet of nonporous dielectric material sealed into the waveguide. The seal is made by supporting the sheet between a choke and flange with glue on each side or by clamping with a gasket on each side as shown in Fig. 4-74. In Fig. 4-74a the impedance added in series with the line at A by the dielectric-filled radial line and the

circular-choke groove is made small by the same methods used for the design of choke couplings (see Sec. 4-9). Radiation at B may be eliminated by the metal contact and by using a lossy rubber for the gaskets. The choke-groove diameter D for minimum current at B will be smaller in this case than in the ordinary choke coupling because the dielectric sheet increases the effective length of the gap. Sheets of mica or Teflon 0.010 in. thick have been used between standard choke-flange couplings in waveguide 1 by $\frac{1}{2}$ in. with 0.050-in. wall at 3.2 cm without excessive reflection. Some method of preventing radiation should be used in such a case, however, if a receiver is located near the coupling. Figure 4-74b shows another method using a half-wavelength radial line filled for a quarter wavelength with the rubber gaskets to seal the dielectric sheet on either side ($d \approx \lambda/4$). The high dielectric constant of the rubber makes the guide wavelength in this section very short. Leakage at B may be prevented by a thin ring of soft copper clamped around the two gaskets as shown in the insert. The copper ring makes a good short circuit at B and provides a method for making a unit for easy replacement. The considerations for making the impedance at A small over a broad band of wavelengths are the same as those discussed in Sec. 4-9 for choke couplings; namely, the characteristic impedance in the outer $\lambda/4$ section should be high compared to that in the inner section ($x \gg y$), and y should be as small as practical from the standpoint of strength of the dielectric sheet. The edges of the waveguide at A should be rounded slightly to prevent cutting of the dielectric sheet when pressure is applied on one side.

The reflection from the sheet across the waveguide can be calculated assuming a section of dielectric material of thickness t fitted into a section of waveguide in a plane perpendicular to the guide axis. If the guide is viewed from the generator side with a matched load beyond the window, a normalized impedance Z_s is seen at the face of the dielectric sheet which is

$$Z_s = Z_0'' \frac{1 + jZ_0'' \tan \theta}{Z_0'' + j \tan \theta}, \quad (65)$$

where Z_0'' is the normalized impedance of the dielectric-filled guide [Eq. (2-168)], and θ is $2\pi t$ divided by the guide wavelength in the dielectric-filled guide λ_g'' given by Eq. (2-147). By dividing out the right-hand side of Eq. (65) to form a power series, the following equation is obtained.

$$Z_s = 1 + j \tan \theta \left(Z_0'' - \frac{1}{Z_0''} \right) + \tan^2 \theta \left[1 - \frac{1}{(Z_0'')^2} \right] - j \tan^3 \theta \left[\frac{1}{Z_0''} - \frac{1}{(Z_0'')^3} \right] + \dots \quad (66)$$

Since θ is small for thin sheets, the squared term is negligible and $\tan \theta = \theta = 2\pi t/\lambda_g''$; consequently,

$$Z_s = 1 + j \frac{2\pi t}{\lambda_g''} \left(Z_0'' - \frac{1}{Z_0''} \right). \quad (67)$$

The guide wavelength in the dielectric-filled section is equal to the product of λ_g (air-filled) and Z_0'' . Equation (67) therefore reduces to

$$Z_s = 1 + j \frac{2\pi t}{\lambda_g} \left[1 - \frac{\lambda_g^2}{(\lambda_g'')^2} \right]. \quad (68)$$

From Eq. (2-147) this may be expressed in terms of the dielectric constant k_e of the sheet,

$$Z_s = 1 - j \frac{2\pi t \lambda_c^2}{\lambda_g (\lambda_c^2 - \lambda_0^2)} (k_e - 1). \quad (69)$$

Equation (69) shows that the thin sheet of dielectric material acts like a series capacitive reactance in the waveguide. At a given wavelength,

this reactance is directly proportional to the thickness and to the dielectric constant minus one. Figure 4-75 shows the value of this normalized reactance per mil thickness plotted against the dielectric constant k_e for three common waveguide sizes. This reactance is nearly equal to $r - 1$ for thin sheets.

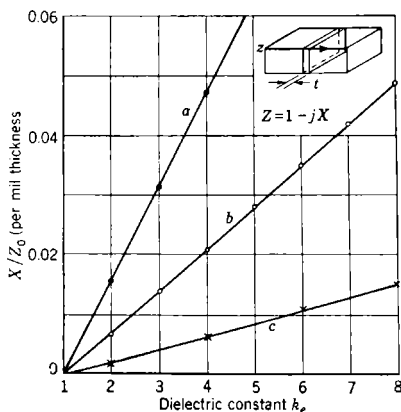


FIG. 4-75.—Reflections from thin-sheet, nonresonant windows. (a) Waveguide $\frac{1}{2}$ by $\frac{1}{4}$ in. by 0.040-in. wall at $\lambda_0 = 1.25$ cm. (b) Waveguide 1 by $\frac{1}{2}$ in. by 0.050-in. wall at $\lambda_0 = 3.3$ cm. (c) Waveguide 3 by $1\frac{1}{2}$ in. by 0.080-in. wall at $\lambda_0 = 10$ cm.

band of a given waveguide operating in a single mode (see Sec. 4-7). A pressurizing window of this type may be matched with an inductive matching diaphragm at the front face of the dielectric sheet. A symmetrical matching diaphragm is preferable because asymmetry would cause higher mode excitation in the choke.

4-19. Thin Sheets in Resonant Mount.—A pressurizing window of this type consists of a resonant aperture in a thin metallic sheet filled with

glass. Two such designs have been developed as shown in Figs. 4-76*a* and *b*. These developments were carried out at the General Electric Company and the Westinghouse Electric and Manufacturing Company, respectively. Both units consist of a Kovar (or Fernico) disk or plate

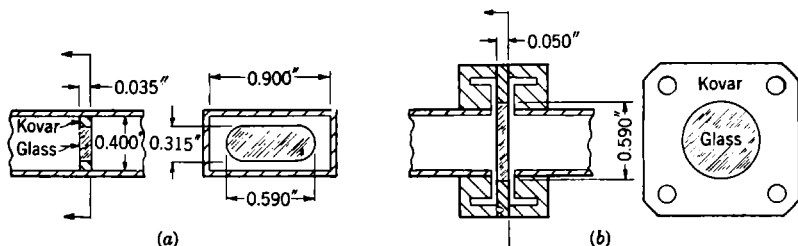


FIG. 4-76.—Resonant window in rectangular waveguide. (a) Rectangular aperture window. (b) Circular aperture window.

with a resonant opening into which glass with the same thermal properties as the metal is sealed.

The first design may be soft-soldered into the waveguide directly as shown in Fig. 4-76*a*. A structure of this kind is known as a “transmitting screen” or “resonant aperture.” It has been found experimentally that the appropriate dimensions for a rectangular resonant opening is given approximately by the relation

$$\frac{a}{b} \sqrt{1 - \left(\frac{\lambda_0}{2a}\right)^2} = \frac{a'}{b'} \sqrt{1 - \left(\frac{\lambda_0}{2a'}\right)^2} \quad (70)$$

This empirical rule is extremely useful in obtaining approximate dimensions of the opening for resonance; and information contained in it can be represented by the following geometrical construction. In a cross section of the waveguide as shown in Fig. 4-77, a line *AB*, of length $\lambda_0/2$ (λ_0 is the free-space wavelength), may be drawn with its center at the waveguide axis. Two hyperbolas may then be constructed with their vertices at *A* and *B*, respectively, which pass through the corners of the guide cross section, as shown. Then the corners of a resonant opening lie on these two hyperbolas, as, for example, those of the opening of dimensions a' and b' . A resonant diaphragm with such an opening will be matched if the diaphragm is very thin. This condition is changed somewhat in the pressurizing window because of the dielectric filling and because the thickness must be appreciable for mechanical support.

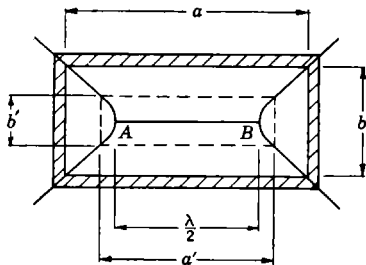


FIG. 4-77.—Resonant rectangular aperture.

The effective thickness of the resonant diaphragm is increased and the characteristic impedance in the aperture is reduced by the dielectric material. Both the thickness of the diaphragm and the presence of the dielectric material have the effect of adding capacitance at the input side of the opening. To correct for this added capacitance, the dimension a' may be made smaller. The amount of the decrease in a' for complete correction is directly proportional to the thickness, as seen in the

analysis of Sec. 4-18. In practice, this decrease may be made larger than necessary and the thickness of the finished diaphragm reduced on a grinding wheel until resonance occurs at the desired wavelength. This procedure corrects for tolerances and variations in the characteristics of the dielectric material used. The dimensions of a reso-

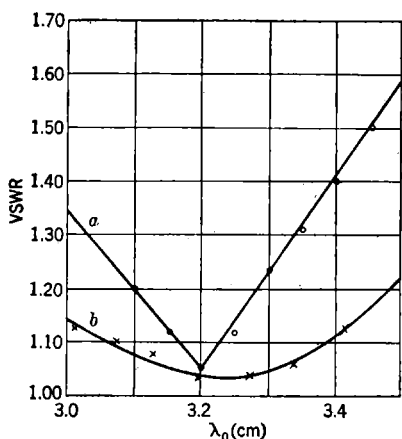


FIG. 4-78.—Mismatch of resonant windows. Curves a and b are for corresponding designs of Fig. 4-76.

nant window for 1- by $\frac{1}{2}$ -in. (0.050-in. wall) waveguide are shown in Fig. 4-76a. Curve a of Fig. 4-78 shows the mismatch¹ caused by such a design over a 12 per cent wavelength band.

The second design is much the same as the first except that the aperture is circular. The correct diameter for resonance in such a design is larger than the narrow inside dimension of the waveguide a . For this reason the resonant diaphragm is supported in the line between two choke couplings as shown in Fig. 4-76b. Dimensions are given for a resonant window of this type for use between two standard choke couplings (see Table 4-7) designed for 1- by $\frac{1}{2}$ -in. (0.050-in. wall) waveguide as shown in the figure. The mismatch caused by such a design over a 12 per cent wavelength band is also shown in Fig. 4-78, Curve b .

4-20. Half-wavelength Dielectric Plugs.—A simple pressurizing window for narrow-band operation may be made by inserting a half-wavelength dielectric plug into waveguide as shown in Fig. 4-79. The guide wavelength in the dielectric-filled section is given by the formula

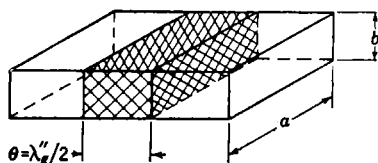


FIG. 4-79.—Half-wavelength dielectric plug in a section of waveguide.

¹ R. M. Walker, RL Report No. 587, June 29, 1944.

$$\lambda_g'' = \frac{\lambda_0}{\sqrt{k_e - \left(\frac{\lambda_0}{2a}\right)^2}}, \quad (71)$$

where k_e is the dielectric constant of the medium. The normalized impedance looking into the face of the plug from the generator side with a matched line on the other side is given by Eq. (65). From this equation

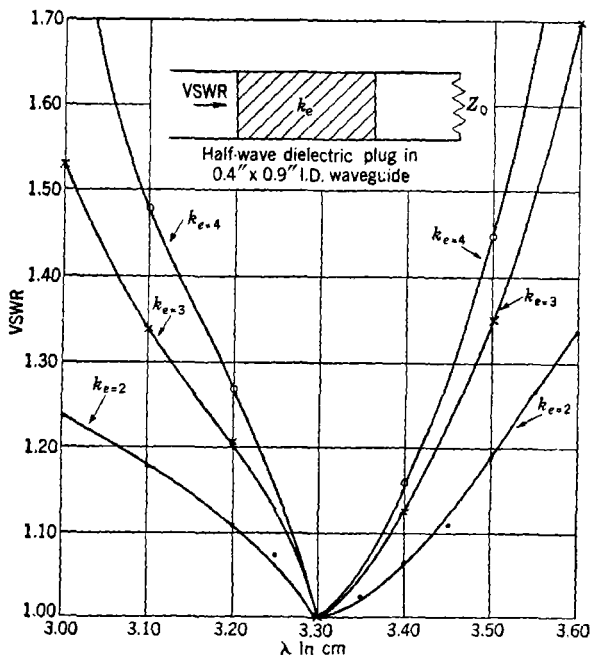


FIG. 4-80.—Mismatch vs. wavelength for half-wavelength dielectric plug.

it can be seen that, when θ is 180° or $\lambda_g''/2$, the normalized input impedance is unity and the line is matched. The frequency sensitivity of the half-wavelength dielectric plug depends upon the dielectric constant of the material used. The mismatch in voltage standing-wave ratio introduced into a 1- by $\frac{1}{2}$ -in. (0.050-in. wall) waveguide by a dielectric plug which is a half wavelength long at $\lambda_0 = 3.3$ cm is plotted against λ_0 for three values of the dielectric constant k_e in Fig. 4-80.

4-21. T-shaped Plugs Three-quarters Wavelength Long.—A pressurizing window of this type is a modification of the type discussed in Sec. 4-20, which is much less frequency-sensitive. Referring to Fig. 4-81, the center section *A* completely fills the waveguide and provides the pressure seal. In sections *B* and *C*, the waveguide is only partly

filled with dielectric and the characteristic impedance is the geometric mean between that in section *A* and that in the air-filled guide. Sections *B* and *C* thus serve as quarter-wavelength matching sections from air-filled guide to dielectric-filled and back to air-filled. As will be seen later, this leads to a broadband impedance match. Other shapes were tried but they failed to give the desired bandpass characteristics—probably because of higher mode excitation in the dielectric-filled section.

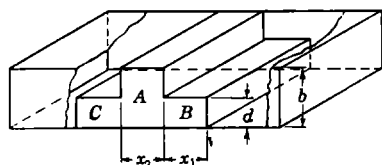


FIG. 4-81.—T-shaped plug three-quarters wavelength long.

From the transmission-line equation, Eq. (65), the impedance seen looking into a line of characteristic impedance Z_c that is one-quarter wave-length long and is terminated in an impedance Z_R is Z_c^2/Z_R . Applying this formula to

each of the three sections of the window in Fig. 4-81 from right to left, assuming a matched line to the right of the window, it is found that the impedance at the left face of section *C* is

$$Z = \frac{(Z'_0)^4}{Z_0(Z''_0)^2}, \quad (72)$$

where Z_0 , Z''_0 , and Z'_0 are the characteristic impedances of the air-filled guide, section *A*, and sections *B* and *C*, respectively. From Eq. (72) it is seen that no mismatch occurs when Z'_0 is equal to the square root of $Z_0 Z''_0$. From Eq. (2-168) it appears that this condition is also satisfied when λ'_0 is equal to the square root of $\lambda''_0 \lambda_0$. The equation for determining the quantities λ''_0 and λ_0 is Eq. (2-147). Referring to Fig. 4-81, x_1 and x_2 are made one-quarter λ'_0 and λ''_0 , respectively.

Now except for dimension d/b , all the dimensions of the three-quarter-wavelength T-shaped pressurizing window have been determined (see Fig. 4-81). Theoretical considerations of the boundary conditions at the air-dielectric surface lead to the following equation relating the guide wavelength in the partly filled line to that in air-filled line (see Vol. 8, Chap. 11):

$$\tan A(b - d) = \frac{A'}{k_e A} \tan 2\pi A' d \quad (73)$$

where

$$A = 2\pi \sqrt{\frac{1}{\lambda_0^2} - \frac{1}{\lambda'_0{}^2} + \frac{1}{4a^2}},$$

$$A' = 2\pi \sqrt{\frac{k_e}{\lambda_0^2} - \frac{1}{\lambda'_0{}^2} + \frac{1}{4a^2}}.$$

Figure 4-82 shows a curve of d/b for $a = 0.900$ in., $b = 0.400$ in., and $\lambda_0 = 3.3$ cm when λ'_0 is the square root of the product of λ_0 in air and λ_0 in completely filled guide. The curve gives the theoretical percentage

filling for the outer sections of the three-quarter-wavelength T-shaped windows in the given waveguide at 3.30-cm free-space wavelength. An experimental curve is also drawn in dotted lines for the same conditions. The experimental curve is consistently above the theoretical curve, the deviation becoming greater as k_e increases. This deviation is partially caused by the junction effects that would be shunt capacitive reactances across the line. The junction effects could have been corrected by lengthening the outer sections, the center section, or both. Increasing the dimension d effectively increases the length of the outer sections by decreasing the guide wavelength in the partly filled guide and in addition makes a double-tuned circuit which increases the bandwidth of the window. Experiments show that the maximum bandwidth is obtained by a combination of the above effects, increasing d and thereby correcting for junction capacitance in the outer sections and forming a double-tuned circuit and also increasing the length of the center section.

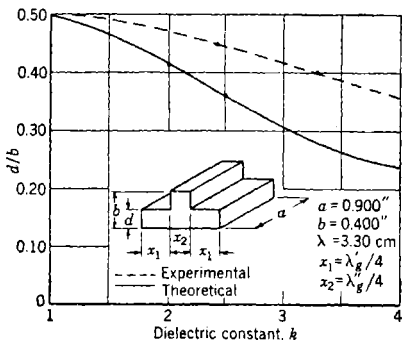


FIG. 4-82.—Design curve for T-shaped plug in rectangular waveguide.

The reason that a construction of this type leads to a broadband window is indicated by the impedance charts of Fig. 4-83. In the figure the three-quarter-wavelength T-shaped plug is compared to the half-wavelength plug. At midband where the dimensions are correct both types are matched as shown in Fig. 4-83a. At a longer wavelength (Fig. 4-83b) the half-wavelength plug transforms the impedance $Z'_a = Z_0$ along the dashed circle about the center Z''_0 to the impedance Z'_d . At this longer wavelength, the length x_3 is shorter than a half wavelength by 2β . Hence, Z'_d is rather poorly matched to Z_0 . The three-quarter-wavelength T-shaped window is better matched, and the following transformations occur. The section B transforms Z_0 (along the circle of radius r_3) about its characteristic impedance Z'_0 . This fails to match into the impedance Z''_0 of the next section, as indicated, since the length ab is now shorter than a quarter-guide wavelength. This impedance Z_b is then transformed by the center section bc to a point Z_c which is almost symmetrically above Z_b ; consequently, the section cd transforms it along the arc Z_c to Z_d almost symmetrically above the arc Z_a to Z_d . This leads to an impedance Z_d which is quite well matched to Z_0 . A similar line of reasoning shows that below midband Z_d is also well matched.

The bandwidth for this type may be further increased by making

Z'_0 slightly less than the square root of $Z_0 Z'_0$. The window then acts like a double-tuned circuit which is matched to the characteristic impedance of the guide at two wavelengths, one on each side of the original design wavelength; and a slight mismatch occurs at the design wavelength. This mismatch is about 1.03 in voltage standing-wave ratio for a change of 2 per cent in Z'_0 .

4-22. Summary of Pressurizing-window Designs.—The various types of pressurizing windows already discussed have been used in microwave transmission circuits extensively except for the half-wavelength dielectric plug which is too frequency-sensitive for systems covering a wide wavelength range.

Each type has its limitations, however, with regard to ruggedness, sealing difficulties, breakdown characteristics, attenuation, and mismatch as a function of wavelength. The resonant sheet window made of glass sealed in a Kovar disk is considered the most rugged design and makes a permanent seal. For this reason it is used in applications where replacements cannot be made in the field such as cavity magnetron and TR switch output seals. The other types have better breakdown characteristics and introduce lower mismatch over a wide band of wavelengths. A summary of these characteristics

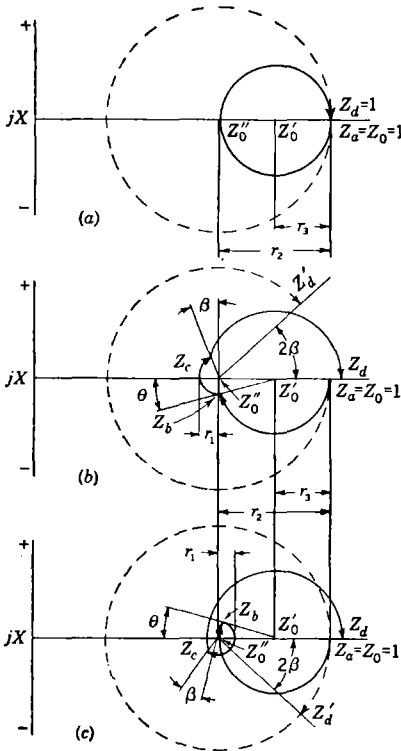


FIG. 4-83.—Waveguide impedance curves for dielectric plugs. (a) At midband; $x_1 = \lambda'_0/4$; $x_2 = \lambda''_0/4$; $x_3 = \lambda'''_0/2$. (b) Above midband; $x_1 < \lambda'_0/4$; $x_2 < \lambda''_0/4$; $x_3 < \lambda'''_0/2$. (c) Below midband; $x_1 > \lambda'_0/4$; $x_2 > \lambda''_0/4$; $x_3 > \lambda'''_0/2$. The dashed circle, z'_d , and x_3 refer to a half-wave bead (see Fig. 4-79). Full circles, z_d , x_1 and x_2 refer to T-shaped plug (see Fig. 4-81).

for the window types discussed is given in Table 4-10. Dimensions are given for each type as well as the free-space wavelength for which they were designed. The mismatch characteristics are given as the wavelength band obtained in the particular design for a voltage standing-wave ratio less than 1.10. This wavelength band is given as percentage of the design wavelength, the design wavelength being midband. The breakdown power level is given in kilowatts at an altitude of 50,000 ft (≈ 12 cm Hg).

TABLE 4-10.—PRESSURIZING WINDOWS IN RECTANGULAR WAVEGUIDE

Type	Fig. No.	Dielectric*	Window dimensions, in.			Waveguide dimensions, † in.		Loss, db	Wave-length band for $r < 1.10$, cm	Breakdown power at 50,000 ft, kw
			x_1	x_2	d	a	b			
Three-quarter-wavelength plug	4.81	Polystyrene	0.315	0.225	0.180	0.900	0.400	0.005	$3.3 \pm 6\%$	60
	4.81	Polyglas p‡	0.300	0.220	0.160	0.900	0.400	<0.040	3.3 ± 6	65
	4.81	Polyglas p‡	0.285	0.225	0.310	1.122	0.500	3.3 ± 5	..
	4.81	Polyglas p‡	0.104	0.072	0.068	0.420	0.170	1.25 ± 3	..
Sheet in resonant mount	4.81	Polyglas p‡	0.940	0.608	0.503	2.84	0.134	10.00 ± 15	..
	4.76a	Glass §	0.315	0.590	0.035	0.900	0.400	0.200	3.2 ± 1.5	36
Nonresonant sheet	4.76b	Glass	0.590	0.050	0.900	0.400	0.060	3.2 ± 5	50
	4.74	Mica	0.002	0.900	0.400	0.010	3.3 ± 6	65
	4.74	Teflon	0.010	0.900	0.400	0.015	3.3 ± 6	65

* See Table 3.5 for characteristics.

† Column a is the wide and b the narrow cross-sectional inside dimension.

‡ Treated to prevent moisture absorption.

§ Test on a single sample, may not be representative.

|| Mounted between two choke-flange couplings.

VOLTAGE BREAKDOWN AT MICROWAVE FREQUENCIES

BY G. L. RAGAN

With the introduction of the technique of using short pulses of r-f energy at a high-power level, the problem of voltage breakdown in the transmission lines and waveguides becomes a serious one. In order to gain a better understanding of the factors that influence the power level at which microwave breakdown occurs, a series of experiments was performed.¹ An attempt was made to obtain quantitative data regarding those factors which were found to be relatively important.

4-23. Apparatus and Methods.—In these experiments the r-f power sources used were microwave magnetrons energized by high-voltage d-c pulses of short duration supplied by a pulse-generating power supply usually referred to as a "modulator." The maximum power available at the three wavelengths used is given in Table 4-11, the lower values being the powers regularly available in most of the experiments, the higher values being available for only a small fraction of them. An attempt was made to obtain a combination of magnetron and modulator that would

¹ D. Q. Posin, Ina Mansur, H. Clarke, "Experiments in Microwave Breakdown," RL Report No. 731, Nov. 28, 1945. Unless otherwise stated, all figures and conclusions given in the text are based on these experiments.

H. F. Clarke, G. L. Ragan, R. M. Walker, I. Mansur, "Summary of High Power Breakdown Tests on Microwave Components," RL Report No. 1071, Jan. 10, 1946. This article contains a thorough treatment of methods and techniques, including magnetron type numbers, modulator model numbers, water-circulating system, and so forth.

furnish the highest powers provided by contemporary design in these fields. Wherever possible a modulator was used that was capable of furnishing a number of different pulse lengths and repetition rates.

TABLE 4-11

Nominal wavelength, cm	Maximum power available, kw	
	Usually	Sometimes
10.5	1000	1500
3.2	125	250
1.25	50	125

It was decided to use rectangular waveguides exclusively in these experiments, since they provide an electric field that is uniform in the direction of the field. In order to provide increased fields, waveguide

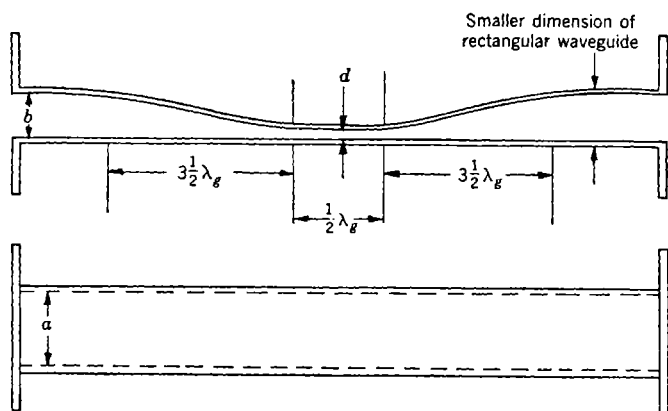


FIG. 4-84.—Experimental waveguide section.

sections of the type shown in Fig. 4-84 were used. The long tapered sections provide impedance-matching between the normal-size waveguide and the constricted portion. Dimensions of the various test sections used are given in Table 4-12. The relation between electric field and power transmitted in a matched waveguide of width a and height d (sometimes referred to as “gap” in the following discussion) is

$$\frac{P}{E_{\max}^2} = 6.63 \times 10^{-4} ad \left(\frac{\lambda}{\lambda_u} \right). \quad (74)$$

In order to determine the electric field strength, it is necessary to

measure the power being transmitted. This is done by the use of a directional coupler that transmits a known fraction of the power in the incident wave to a power-measuring thermistor bridge (see Vol. 11, Chap. 3). An alternative method is that of absorbing the r-f power in a

TABLE 4-12

Nominal wave length, cm	Guide width a , in.	Guide height d , in.	Reference symbol on curves
10.5	2.840	0.110	S 110
		0.040	S 40
3.2	0.900	0.006	X 6
		0.017	X 17
		0.038	X 38
1.25	0.420	0.006	K 6
		0.016	K 16
		0.036	K 36
		0.059	K 59

“water load.” In this device the r-f power is absorbed in a flowing stream of water, and the average power is computed from the heating of the water by ordinary calorimetric methods. With careful use, the

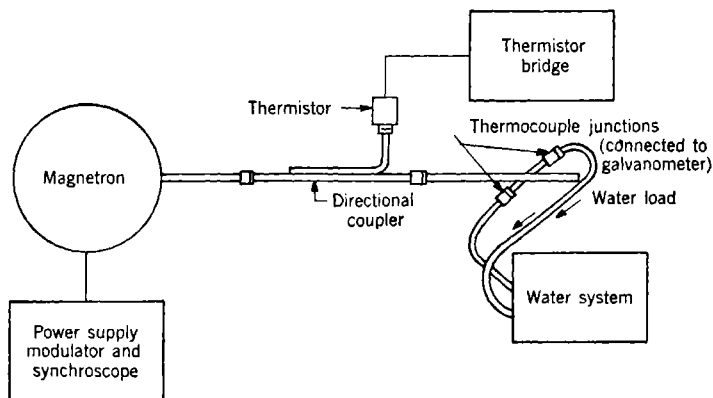


FIG. 4-85.—Arrangement of apparatus for calibration.

water load is felt to be the most accurate power-measuring instrument available, but it is too slow in response to be very useful in general breakdown measurements. In practice, the combination of directional coupler and thermistor bridge was calibrated by comparison with a water load, with the apparatus arranged as indicated in Fig. 4-85. The

thermistor combination was then used in the actual measurements, the arrangement being that indicated in Fig. 4-86.

The pulse length and repetition rate were measured by the use of a synchroscope (Vol. 5, Sec. 16-5). This instrument is basically a cathode-ray tube provided with a circuit for generating pulses that are used to trigger the modulator which applies power to the magnetron and simultaneously to start the horizontal sweep of the cathode-ray tube. The

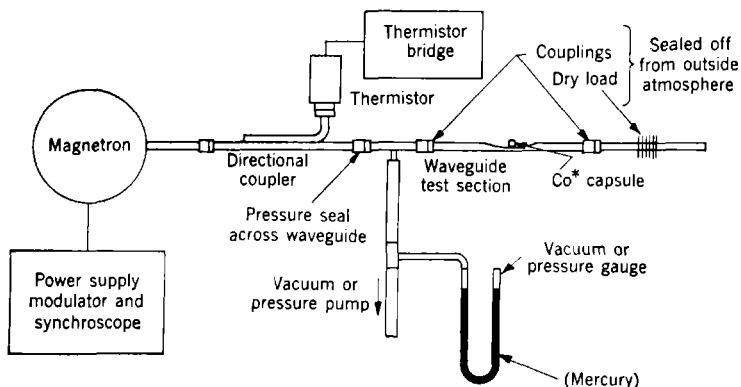


FIG. 4-86.—Arrangement of apparatus used in experiments.

magnetron current or voltage is indicated by the vertical deflection on the cathode ray screen. From the data on pulse length, repetition rate, and average power it is a simple matter to obtain the pulse power, that is, the average power during the time interval in which the magnetron is oscillating.

An analysis of sources and estimate of the magnitudes of the errors encountered in the present experiments may be useful, both in evaluating the data given and in suggesting improvements in future experiments. The largest single source of error is felt to be that caused by the existence of standing waves in the test section. In practically all cases the VSWR was below 1.10, averaging about 1.05. Since the constricted portion of the waveguide test sections was half a guide wavelength long, a maximum of the standing-wave voltage pattern always occurred within the constricted section. As indicated in Table 2-2, the breakdown field in the presence of a standing wave occurs at a power that is lower by the factor r (the value of the VSWR) than the power that would be required to achieve breakdown if the line were perfectly matched. On this basis it is estimated that the data on power, quoted without correction, in the following pages are subject to a systematic error which gives powers, on the average, about 5 per cent low.

Other sources of error are usually random rather than systematic. The errors in pulse length τ and gap height d are estimated at about ± 5 per cent, on the average. Both τ and d are considerably less accurate than this for small values and more accurate for large values since their errors tend to be constant in absolute magnitude rather than on a relative basis.

A number of other sources of error, each averaging about ± 0.5 per cent in magnitude, are as follows: (1) thermal leakage in water-load measurements; (2) thermocouple and galvanometer errors in using a water load; (3) errors in thermistor bridge; (4) errors in measuring repetition rate; (5) attenuation in waveguide between measuring section and test section. There is, in addition, a rather large error in any given measurement, caused perhaps by statistical fluctuations in the ionization existing in the gap just before and during the pulse. A method of reducing this uncertainty by the use of ionizing radiations is discussed in the following section.

It is believed that each individual measurement of power made in these experiments is subject to about 5 per cent systematic error (the measured values being too low) and about ± 10 per cent random error from all causes. Since each point is the average of a number of observations, it is felt that the powers indicated are accurate to about -5 per cent (systematic error) and ± 5 per cent (random error); thus half the observations of power fall within the range of errors between 0 and -10 per cent of the true values. Since the field strength E is proportional to the square root of the power, the probable error in E is only about half as large, namely, -2.5 per cent ± 2.5 per cent (ranging from 0 to -5 per cent).

4-24. Preliminary Considerations.—One of the problems confronted at the outset of the experiments was that of obtaining consistent and repeatable data. It was noticed in earlier work that rather large discrepancies exist between measurements made at different times, and smaller but still bothersome discrepancies occur even between successive measurements.

It was felt that these discrepancies were caused in part by a failure to control certain parameters, and it was planned to investigate these sources. The discrepancies between successive measurements were thought to be due, however, to causes of a statistical nature, and it was felt that some improvement might result from irradiating the test gap to provide a source of ions. This is a technique familiar in low-frequency breakdown studies where the presence of additional ions, while providing much more consistent performance, is found to have little effect on the average breakdown figures.

To provide the ionization desired within the waveguide gap, a strong

source of gamma-radiation in the form of radioactive cobalt chloride was obtained from the Cyclotron Laboratory of the Massachusetts Institute of Technology. A very intense source was required (3 millicuries radium equivalent) and it was placed in the form of a small capsule directly in contact with the broad surface of the waveguide. Although this amount was barely sufficient to cause a noticeable improvement in

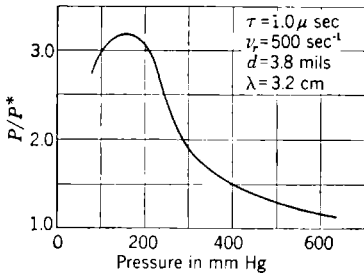


FIG. 4-87.-Effect of radioactive cobalt on breakdown power. P^* is the breakdown power when Co^* is used, P is the breakdown power without radioactive irradiation, τ is pulse width, ν_r is repetition frequency, d is gap (see Fig. 4-84), λ is wavelength.

the repeatability, it had a large effect on breakdown measurements. This is in marked contrast to the experience at lower frequencies where it is found that statistical reliability may be achieved without increasing the ionization to such an extent that the measurements are affected.

The degree of lowering of breakdown power for a typical waveguide section is shown, as a function of pressure, in Fig. 4-87. Curves of similar form were obtained for other sections. In general, the irradiation has its greatest effect at pressures of about one-sixth to one-third of an

atmosphere, and the effect appears to be somewhat larger in magnitude for waveguide sections of smaller gap dimension d .

It is interesting to obtain a crude estimate of the ionization caused by the radioactive Co^{60} . The gamma rays emitted have an energy of 1.3 Mev and decay with a half life of 5.3 yr. Since one millicurie gives, by definition, 3.7×10^7 disintegrations per second, the 3.2-millicurie source used emits roughly 10^8 quanta per second or 100 per microsecond. From the geometry of the experiment it is estimated that roughly one-tenth of the quanta, that is, 10^7 per second, are emitted in such a direction that they might cause ionization in a part of the gap where the fields are large. The absorption of the gamma rays in the gas furnishes negligible ionization compared with that furnished by secondary electrons knocked out of the brass walls of the waveguide. The range of an electron whose energy is 1.3 Mev, which is the maximum energy available, is about 0.06 cm (0.024 in.). Only those gamma rays absorbed in the waveguide wall within this distance of the inner surface may be effective in causing ionization in the gap. Since it requires 1.5 cm of copper to absorb half the gamma radiation, only about 3 per cent will be absorbed in a 0.06-cm layer. These observations lead to a final estimate, crude but probably right as to order of magnitude, of 3×10^5 ionizing events per second. On the average, it would be expected that one such event would occur every three microseconds.

It may be assumed that ions formed within the first 10 per cent of the pulse time are almost completely effective.¹ For 1- μ sec pulses, the probability of occurrence of an ionizing event within the first 10 per cent is seen to be about 1 in 30. For the shortest pulse width used in the experiments, 0.2 μ sec, it would be 1 in 150.

Each secondary electron passing through the air in the gap causes the formation of a number of ion pairs along its path. While the number of pairs per unit length is dependent on the energy of the secondary electron, it may be taken as about 100, on the average, at atmospheric pressure. Multiplying this figure by the 3×10^5 events per second, an estimate of 3×10^7 ion pairs per second per centimeter of path is obtained. From the geometry of the apparatus it is estimated that the effective secondary electrons are emitted from a wall surface of roughly 3 cm² so that the number of ion pairs formed per cubic centimeter of gas volume is estimated to be 10^7 per second.

A comparison of the frequency of ionizing events with the number normally present as a result of cosmic rays and natural radioactivity is enlightening. The latter figure is usually taken as about two per minute per square centimeter of wall area or six per minute for the 3-cm² area being considered. From the comparison of this small number with the 3×10^5 events per second estimated above, a vast improvement in statistical reliability when using the radioactive cobalt is expected.

The improvement, while noticeable, is not so great as it is desirable to obtain. A series of 28 trials with the Co* in place was alternated with an equal number without artificial ionization. This number of trials is not sufficient to justify a thorough analysis of the statistics involved, but the following behavior seemed to be indicated: (1) There were considerably fewer large departures from the mean value when Co* was used. (2) Half the values fell within a ± 5 per cent range when Co* was used, whereas the corresponding range was ± 6 per cent without it. (3) The breakdown power was about half as high when Co* was used as when it was not.

Perhaps the best indication of the improvement in repeatability which was provided by the Co* is to be found in the data obtained in a series of breakdown measurements in which the pressure is varied. It was found that if a single observation is made at each pressure, the resulting curve of breakdown power vs. pressure was much smoother when Co* was used. In order to obtain satisfactory curves without Co*, the average of a number of observations was required. One such pair of curves is given in Fig. 4-88, from which Fig. 4-87 is derived.

¹ This assumption is rather well justified by data presented in the next section that show that a 10 per cent change in pulse duration (which is for practical purposes equivalent to an equal change in the time of introduction of a burst of ions) leads to a change in breakdown power of only about 3 per cent.

In addition to the problem of achieving the repeatability, a cursory investigation of two other factors that might be expected to influence breakdown was made. The first of these factors was the effect of humidity, and the second was that of sharp points on the metal walls.

Tests were made using approximately saturated air (relative humidity conservatively estimated to be greater than 80 per cent) provided by circulating air that had been bubbled through water at room temperature. These results were compared with those obtained using dry air (conservatively estimated to have a relative humidity of less than 10 per cent)

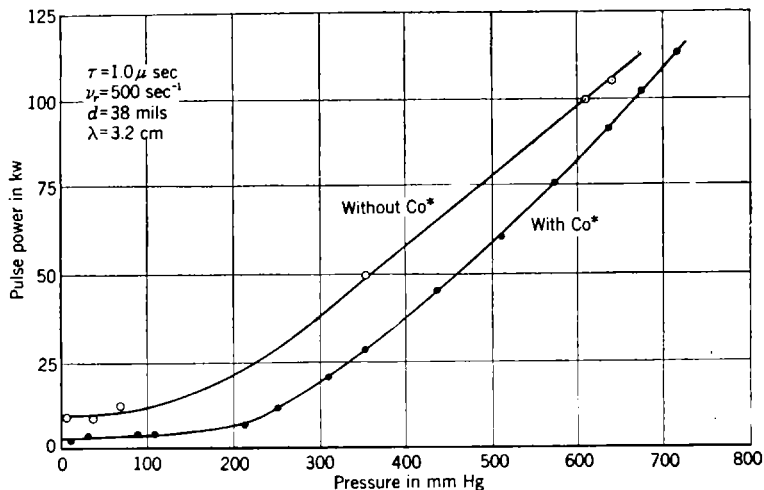


Fig. 4-88.—Variation of breakdown power with pressure, with and without Co*.

provided by circulating air which had been drawn through a trap cooled by dry ice. In a series of measurements using alternately dry and wet air, the average of breakdown values of seven trials with dry air was 5 per cent higher than that of the six interspersed trials using wet air. These experiments were not intended to afford a precise measurement of the effect of humidity but rather to serve as a guide in judging whether or not special precautions as to the control of humidity in conducting subsequent experiments were necessary. It was felt that since only a 5 per cent change was indicated under these extreme conditions of humidity, it would not be necessary to take special precautions.

In order to study the effect of sharp points, a quantity of fine brass chips whose average size was from 2 to 5 mils was introduced into a waveguide section of 40-mil gap and tested at a wavelength of 1.25 cm. Breakdown with a large quantity of these "shop dust" particles present was about one-third of that observed before their introduction. The

same low figure was observed even after the particles were poured out of the waveguide section. The few remaining particles adhering to the walls were sufficient to maintain the low breakdown power. When these were removed by blowing out the waveguide section with a strong stream of compressed air, the original high breakdown power was again observed. Although these experiments are quite crude, they serve to indicate the importance of carefully removing all foreign particles from transmission-line components and serve to emphasize the desirability of removing burrs and rounding sharp corners. In all subsequent experiments, care was taken to observe these precautions in the waveguide test sections.

4-25. Effect of Duration and Repetition Rate of Pulses.—An investigation of breakdown phenomena at microwave frequencies is complicated by the necessity of using short pulses of r-f power. The use of short pulses in such investigations is required both by the fact that pulses are commonly used in microwave applications and also by the fact that it is in this way that the extremely high electric fields desired may best be produced.

It is to be expected that the fields required to produce breakdown within the short time interval represented by the pulse would exceed those corresponding to continuous wave conditions. It has been observed that the delay between the time of application of a d-c voltage and the resulting breakdown is a rather strong function of the "over voltage." That is, a rather long time will be required for the formation of a spark if the voltage is just sufficient to cause breakdown, whereas the time becomes increasingly shorter as the voltage is increased above this critical value. This is to be expected since the rate of multiplication of ions is increased when the voltage is made greater.

A careful study of the dependence of breakdown power on the pulse width was made, and the resulting data are plotted in Fig. 4-89. From the average of the slopes of the three lines of Fig. 4-89, the empirical relation $P \propto \tau^{-0.23}$ is obtained. Other data have been taken which indicate a considerably stronger dependence on pulse length, and there are indications that under some conditions the data are better represented by $P \propto \tau^{-0.5}$. It is suggested that $P \propto \tau^{-1/2}$ represents a rather good approximation under average conditions.

The method of measuring the pulse power in taking the data of Fig.

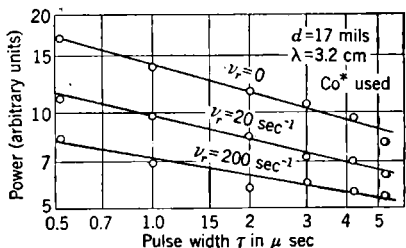


FIG. 4-89.—Dependence of breakdown power on pulse width, at three different repetition rates. Average result: $P \propto \tau^{-0.23}$.

4.89 deserves mention, since it is entirely different from that usually employed. The magnetron current was passed through a noninductive 1-ohm resistor, and the voltage drop across the resistor was applied to the vertically deflecting plates of the synchroscope. If the performance chart of the 4J53 magnetron used is consulted, it will be found that the

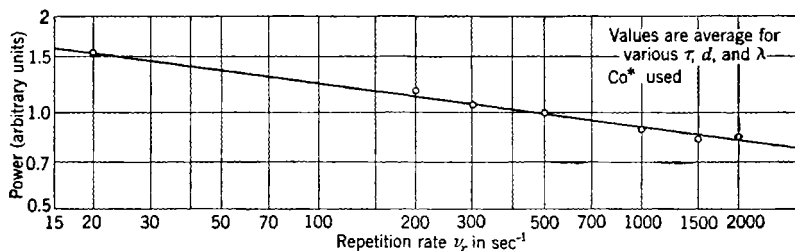


FIG. 4-90.—Dependence of breakdown power on repetition rate. Average result: $P \propto \nu_r^{-0.13}$.

efficiency of the tube does not vary appreciably over the range of currents used. The voltage applied to the input terminals of the magnetron is almost constant over the same range of currents; consequently, the magnitude of the current is closely proportional to the power supplied to the tube and, by virtue of the constancy of efficiency, to the r-f power delivered by the tube. The power scale of Fig. 4.89 represents the height of the deflection on the synchroscope, which is proportional to the current through the magnetron.

This method of measurement of pulse power was especially needed for the single pulse breakdown work, denoted by $\nu_r = 0$. The method also is advantageous for general use since the measurement of pulse power is not dependent on the accuracy of measuring pulse length and repetition rate.

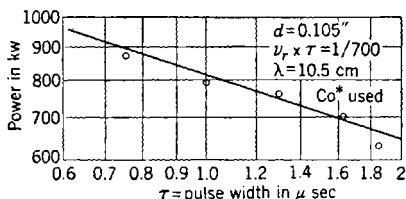


FIG. 4-91.—Dependence of breakdown power on pulse length at constant duty factor. Average result: $P \propto f(\mu\tau)\tau^{-0.34}$.

that any appreciable dependence on repetition rate should be observed. The shortest interval between pulses, about 500 μ sec for $\nu_r = 2000$ per second, is so long that the ionization held over from one pulse to the next would be expected not to be very important. Nevertheless, a very definite dependence is observed as indicated by Fig. 4-90. The data plotted represent averages for a number of different conditions in which τ , d , and λ are varied. The effect may be represented empirically as $P \propto \nu_r^{-0.13}$ or simply $P \propto \nu_r^{-1/6}$.

Since the dependence of breakdown power on pulse length is stronger than its dependence on repetition rate, it is to be expected that breakdown power will increase with decreasing pulse length if the product $\tau \times \nu_r$, sometimes called the "duty factor," is kept constant. Figure 4-91 illustrates this. Combining the empirical relations suggested above, one would expect to obtain

$$P \propto \tau^{-1/2} \nu_r^{-1/2} \\ \propto (\nu_r \tau)^{-1/2} \tau^{-1/2}.$$

The slope of Fig. 4-91 corresponds to a somewhat stronger dependence on pulse length but is in qualitative agreement with expectations.

4-26. Effect of Pressure, Gap, and Wavelength.—In d-c measurements on breakdown the two variables ordinarily considered are pressure and gap. A third, which is inevitable in a-c work, is that of frequency

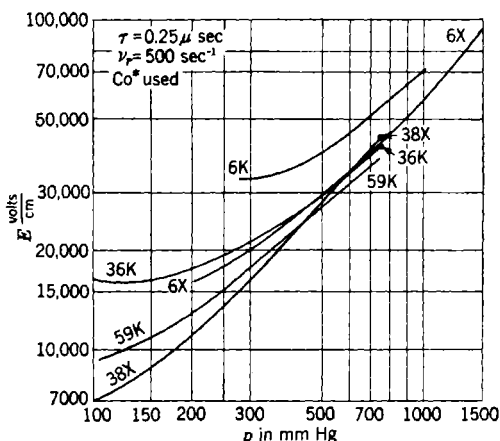
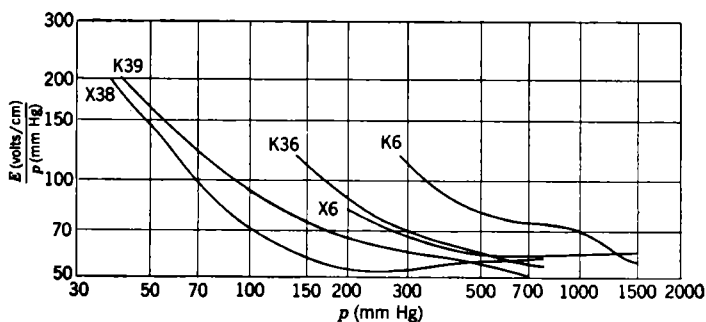
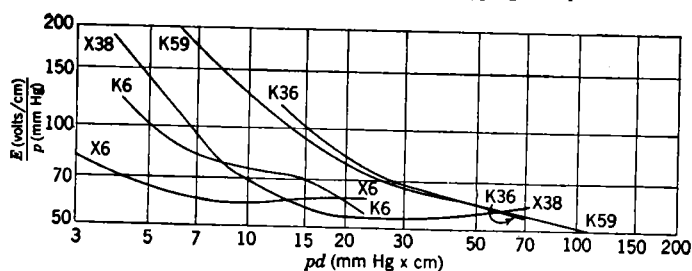
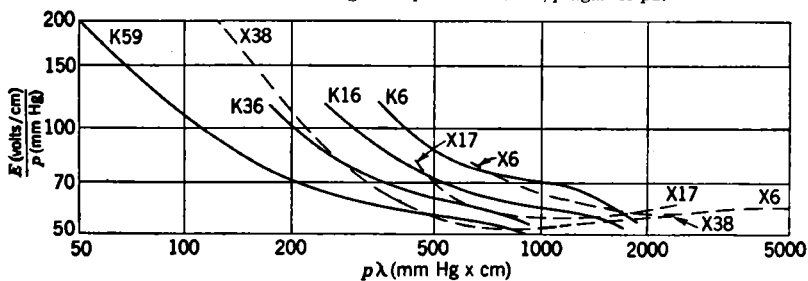
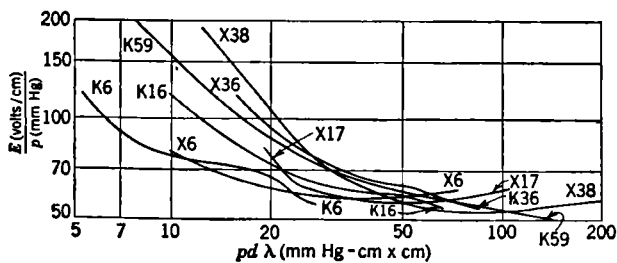


FIG. 4-92.—Relation between breakdown field strength and pressure for the gap heights, and wavelengths indicated on curves. The meaning of the symbols on the curves is given in Table 4-12.

or wavelength, and the additional parameters, pulse length and repetition rate, enter whenever pulsed operation is considered. Now that the effect of these latter parameters has been described, the study of the dependence of breakdown fields on pressure, gap, and wavelength, keeping fixed the parameters associated with the pulse, is to be considered.

The data to be presented in connection with this study were taken at wavelengths of 1.25 and 3.20 cm. The gaps used at the shorter wavelength were 6, 16, 36, and 59 mils and, at the longer wavelength, 6, 17, and 38 mils. In all cases the pulse length was 0.25 μ sec, the repetition rate 500 per second; and the radioactive-cobalt capsule was used. The data are presented in a number of different ways in Figs. 4-92 through 4-96.

Fig. 4-93.—Data of Fig. 4-92 plotted with E/p against p .Fig. 4-94.—Data of Fig. 4-92 plotted with E/p against pd .Fig. 4-95.—Data of Fig. 4-92 plotted with E/p against $p\lambda$.Fig. 4-96.—Data of Fig. 4-92 plotted with E/p against $pd\lambda$.

In all cases it was found that for pressures of about one-half to one atmosphere, the electric field at breakdown was essentially the same for all gaps and for both wavelengths, as illustrated by Fig. 4-92. In addition, the electric field became more or less proportional to the pressure at these high pressures. This fact is demonstrated graphically in Fig. 4-93 where the ratio E/p is plotted as the ordinate and the constancy of this ratio at high pressures indicates linearity of the relationship.

In d-c work it is found that the product pd of the two variables, pressure and gap width, is a significant quantity. A relation known as Paschen's law is verified both experimentally and theoretically in the case of d-c breakdown. One formulation of the law states that the breakdown voltage Ed is a function of the product pd , and when the breakdown voltage is plotted against pd a unique curve results. The law may be stated in several other forms but is not to be misinterpreted as asserting that breakdown voltage is *proportional* to pd . An alternative formulation of the law, easily derived from that just given, is that E/p is a function of pd . It has been shown,¹ providing certain assumptions are made regarding the processes involved in the discharge and certain restrictions imposed on the values of ω , p , and d , that E/p should be a function of pd in high-frequency discharges. In order to see whether or not Paschen's law has significance for these microwave breakdown data, the quantity E/p is replotted against pd in Fig. 4-94. For the higher values of pd , it appears that all the curves approach constancy of E/p and the value approached seems to be about the same as the d-c figure of 40. The agreement with the d-c value is probably fortuitous since there are several complicating factors in the microwave data. Chief among these factors are the tendency of the Co^* to cause a reduction in breakdown field and the counterbalancing tendency of short pulses tending to raise the breakdown fields. It can hardly be said that the Paschen plot Fig. 4-94 represents an appreciable improvement on the simple pressure plot of Fig. 4-93, except at the higher values of pd .

A general principle of similarity for a-c discharges has been pointed out by Margenau.² The principle is strictly valid only for steady-state discharges in which the a-c field is continuously applied and in which the effect of metal walls is negligible, as it is in the so-called "electrodeless" discharge. Within these limitations the principle states that no changes in the properties of the discharge should occur so long as the ratios E/p and ω/p are both constant, provided that the changed conditions do not activate additional sources of ionization or destroy active ones. While

¹ T. Holstein, "Initiation of High Frequency Gas Discharges," *Phys. Rev.*, **69**, 50-51 (Jan. 1 and 15, 1946).

² Henry Margenau, "Theory of Alternating Current Discharges in Gases," RL Report No. 967, Jan. 10, 1946.

the present experiments do not fulfill the requirements on which this principle is based, it was felt that its application might lead to some improvement in presentation. Accordingly, the data on E/p were plotted against $p\lambda$, a quantity proportional to the reciprocal of ω/p , with the result shown in Fig. 4-95. It may be seen that the data at the two wavelengths for a given gap dimension are brought into fairly good agreement by a plot of this type. This correlation is encouraging, and it would be desirable to check it by performing further experiments. Two additional curves, K16 and X17, which were omitted in the previous graphs to avoid confusing them, are included in order to give added evidence of the correlation indicated.

In an attempt to obtain a better correlation between the various gap widths of Fig. 4-95, the gap width d was introduced as a multiplying factor in the abscissa, with the result shown in Fig. 4-96. With the exception of the 6-mil curves, a considerable improvement in the presentation results. If instead of the multiplier d its square root is introduced, the 6-mil curves are in better agreement with the others, while the 59-mil curve is then detached from the others. While the plot of Fig. 4-96 is not so good as one might hope to obtain, it seems to represent one of the most significant ways of presenting the data. The justification for such a plot is largely empirical, although it may be argued that if λ is kept constant it makes E/p a function of pd , as suggested by Holstein, and if d is kept constant it makes E/p a function of $p\lambda$, as suggested by Margenau.

4-27. Summary and Discussion of Breakdown Results.—The data discussed in the preceding sections lead to some very definite conclusions but certain inconsistencies in the data presented indicate the desirability of obtaining additional data. Certain changes in experimental technique and the desirability of investigating effects not definitely established are also suggested by a survey of the data. Both a résumé of these results and recommendations in regard to future experiments are presented in this section.

1. The repeatability of the data was definitely improved by the use of radioactive cobalt, but the breakdown power was decreased by a rather large factor, and this factor appeared to be dependent on such parameters as pressure and gap. It is suggested that the use of an ionizing agent such as ultraviolet illumination that would produce a more continuous supply of low-energy electrons would be preferable. The fact that the Co^* ionizes in large bursts at irregular intervals may be undesirable when the electrical field is applied in pulses.
2. The data indicate that humidity is rather unimportant. The fact that no more than 5 per cent difference occurred between

breakdown powers with "wet" and "dry" air was definitely indicated.

3. The effect of sharp corners was found to be very large. This emphasizes the desirability of removing machining burrs and of rounding sharp corners.
4. It was definitely shown that breakdown power increases as the pulse length is reduced. While certain quantitative variations were observed from one set of data to another, an average of all the data indicates the empirical relation $P \propto \tau^{-1.5}$. An investigation of the factors that cause the discrepancy between different sets of data might be profitable.
5. The breakdown power was found to decrease, as the repetition rate was raised. The empirical relation indicated was $P \propto \nu_r^{-1.8}$.
6. When the product $\nu_r \tau$, frequently referred to as the "duty factor," is kept constant, the effect of pulse length predominates. Combining the two empirical relations discussed under Paragraphs (4) and (5) gives

$$P \propto (\nu_r \tau)^{-1.8} \tau^{-1.5}$$

More data are needed to verify this relation.

7. At higher pressures, namely, above about one-half atmosphere, all data tend to show that the electric field E is proportional to the pressure p ; that is, E/p is approximately constant.
8. For a given value of pulse length τ and repetition rate ν_r , there appears to be good evidence to support the relation

$$\frac{E}{p} = f\left(\frac{\omega}{p}\right)$$

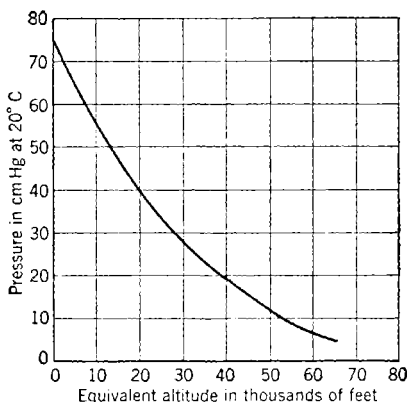


FIG. 4-97.—Altitude at which air density equals that at the indicated pressure and temperature.

9. There is less definite indication that the relation $E/p = f(pd)$ is valid; however, a combination in which E/p is plotted against λpd represents the data fairly well.
10. A summary of the above empirical relations will tend to indicate that for values of λpd (cm \times mm Hg \times cm) exceeding about 50, the following empirical relation is fairly good:

$$\frac{E}{p} = 42\tau^{-1/6}\nu_r^{-1/6},$$

where τ is in microseconds, ν_r is in thousands of pulses per second, E is in volts per centimeter, and p is in millimeters of mercury.

11. The dependence of breakdown field strength or power on altitude may be determined by using these results in conjunction with Fig. 4-97.

CHAPTER 5

FLEXIBLE COUPLING UNITS AND LINES

BY F. E. EHLERS AND F. T. WORRELL

Although the transmission of power at microwave frequencies is most effectively accomplished by means of rigid coaxial lines or waveguides, certain applications demand the use of flexible units. Such units are necessary when allowance must be made for the relative motion of two components, either because of vibration, or because such motion is an essential part of the function of the device. Flexible coupling units fall naturally into two classes: those employing coaxial lines, and those in which waveguide techniques are used.

FLEXIBLE COAXIAL CABLES

BY F. E. EHLERS

Two types of coaxial cables have been used for r-f transmission: beaded cables and solid dielectric cables. A beaded cable is made by slipping "fish spine" beads over a copper wire used as a center conductor, and braiding a wire shield over the beads as an outer conductor. The construction is shown in Fig. 5-1. This type of cable has been largely replaced by the solid dielectric cable which is made by extruding a dielectric (usually polyethylene) over a conductor, either solid or stranded, and by braiding a shield over the dielectric. On some cables two braids are used in order to obtain better shielding. Over the outer braid, a jacket, usually of some vinylite plastic, is either extruded or tubed. For naval installations, in addition to the plastic jacket sometimes a steel braided armor is woven over the cable. Solid dielectric cables are much more rugged than the beaded cables since polystyrene beads, being brittle, are easily broken, and thereby introduce losses by reflection and possible short-circuiting of the cable.

For the purpose of facilitating the production of r-f cables, rigid lines, and connectors for radio and radar equipments for the Army and Navy, a joint Army-Navy R-f Cable Coordinating Committee has been set up with headquarters in Washington, D. C. This committee, with the aid of the services, laboratories, and manufacturers, has determined standards for rigid lines, coaxial cables, connectors, and adapters. A numbering system to facilitate the description and ordering of transmission lines and fittings has also been established. For r-f transmission lines, the

number system RG-/U was designated. This includes flexible cables, rigid coaxial lines, and waveguides. The UG-/U numbering system was assigned to connectors and adapters used with these transmission lines. These systems may be remembered more easily by means of the following interpretation: "RG" means "radio guide," and "UG" means "union guide." The final "U" means "universal." As this committee is a

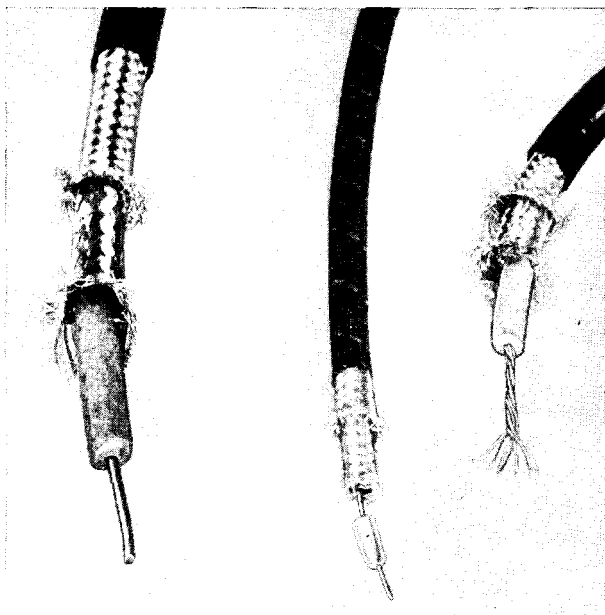


FIG. 5-1.—Construction of beaded and solid-core cables, showing braid, core, center conductor, and jacket.

wartime agency, it will soon cease to function; but a new committee will be formed to carry on a similar work for the postwar period.

The Army-Navy R-f Cable Coordinating Committee has from time to time published specifications of all cables, lines, and fittings recommended for Army and Navy equipment. These particulars were not meant to be restrictive in any way, and when improvements were made they were described in detail. The latest specifications on coaxial cables are those of JAN-C-17 which were published July 31, 1945. A complete index of r-f transmission lines and fittings was published by the same committee on June 15, 1945. Some of the material in this chapter is taken from these two publications. Although the present discussion is not intended to be exhaustive, it covers rather completely the cables, connectors, and adapters that are suitable for microwave frequencies. The discussion is

limited to flexible cables having a nominal characteristic impedance of 52 ohms since such cables match approximately the rigid lines used at microwave frequencies. With the tolerances that cable manufacturers can now hold, the characteristic impedance of these cables is within ± 2 ohms of this nominal value.

5.1. Attenuation in Flexible Cables.—The attenuation in a flexible coaxial cable is made up of two kinds of losses: series losses in the center and outer conductors, and shunt losses in the dielectric. The series losses are proportional to the square root of the frequency and may be calculated from the following formula¹ for the series attenuation A_s in decibels per meter:

$$A_s = \frac{27.37}{Z_0} \frac{1}{\sqrt{\lambda}} \left(\frac{\sqrt{\rho_c} K_c}{a} + \frac{\sqrt{\rho_0} K_0}{b} \right). \quad (1)$$

Here, Z_0 equals the characteristic impedance of the cable; ρ_c and ρ_0 are the resistivities of the center and outer conductors, respectively; and K_c and K_0 are the factors of attenuation of the stranded and braided conductors as compared with that of perfect cylinders of the same material.

Shunt losses are caused by the conductivity of the insulating material. The dielectric constant of an imperfect dielectric may be expressed as a complex quantity, the imaginary component designating the conducting or dissipating property of the material. For example, a lossless coaxial line may be said to have a shunt capacitive susceptance per unit length, which will be called $j\omega ck_c$, where ω is the angular frequency, c is the capacity per unit length with air as the dielectric, and k_c is the relative dielectric constant of the insulator. If we substitute an imperfect dielectric so that $k_c = k'_c - jk''_c$, we have the following shunt admittances:

$$j\omega c(k'_c - jk''_c) = j\omega ck'_c + \omega ck''_c = g + j\omega c.$$

From the above equation it can be seen that $\omega ck''_c$ is the shunt conductance of a coaxial line and is directly proportional to frequency. The power factor for a low-loss dielectric is well approximated by the formula

$$P \approx \frac{k''_c}{k'_c}.$$

For polyethylene, which is used in all cables at microwave frequencies, the power factor is about 0.0004. The shunt losses A_p of a coaxial line may be calculated from the equation

$$A_p = 0.091 \times 10^{-5} \sqrt{k'_c} P \nu \quad \text{db/m.} \quad (2)$$

An examination of Eqs. (1) and (2) reveals that shunt losses are inde-

¹ J. C. Slater, *Microwave Transmission*, McGraw-Hill, New York, 1942, p. 162; Vol. 8, Sec. 2-19, Radiation Laboratory Series.

pendent of the size of the cable but that the series losses in each conductor are inversely proportional to its radius.

To illustrate the effect on the attenuation of braid, as compared with the attenuation of a solid cylindrical conductor of the same metal, let us take the RG-14/U cable which has the following characteristics:

$$\begin{array}{ll}
 a = 0.101 \text{ in.} = 0.00258 \text{ m} & \text{total attenuation} = 0.14 \text{ db/ft} \\
 b = 0.370 \text{ in.} = 0.00940 \text{ m} & k'_e = 2.25 \\
 \rho = 1.724 \times 10^{-8} \text{ ohm-meters} & Z_0 = 52 \text{ ohms} \\
 & \text{for copper} \quad P = 0.0004 \\
 \lambda = 10 \text{ cm} = 0.1 \text{ m} &
 \end{array}$$

From Eq. (2), the attenuation caused by the polyethylene dielectric is 0.05 db/ft. Substituting proper values in the first term of Eq. (1), after letting $K_e = 1$ since the conductor is not stranded, gives 0.052 db/ft for the loss in the center conductor and hence leaves another 0.038 db/ft for the attenuation of the braid. Assuming a perfect cylinder of copper, from Eq. (1), we calculate the loss in the outer conductor and obtain a value of 0.014 db/ft. Thus the "braid factor" is

$$\begin{aligned}
 0.014K_b &= 0.038, \\
 K_b &= 2.7.
 \end{aligned}$$

Nominal values for well-woven braids vary from 2.5 to 3.

A brief explanation of braid construction will serve to point out some of the aspects of the design of flexible cables for a minimum braid factor. The first step in the design of a braid is the choice of the wire that will produce a braid rugged enough to minimize the contact resistance between individual wires. A number of thin wires are combined to form a carrier that we might compare to a single flat reed in a woven basket; a number of these carriers are woven in and out to form the braid. Around 99 per cent coverage is required for a braided conductor in order to avoid excessive loss by radiation and to ensure proper shielding. This coverage is determined by the number of ends per carrier, the number of carriers, and the number of "picks" per inch which make up the braid. The number of picks per inch is the number of times that a single carrier crosses over or under another carrier in an inch of cable. Another term applied to this characteristic of the braid is the word "lay"; this is the length of cable required for the carrier to make one complete revolution around it. Since the currents in a coaxial conductor are always in the direction of propagation, a braid having a long lay will have less attenuation than one having a short lay since less energy is dissipated in contact resistance. Mechanical considerations, however, limit the lay of the braid, and greater stability with flexing can be attained with a shorter lay. The tightness with which the braid is woven is also impor-

tant in eliminating instability under flexing and in decreasing the contact resistance between braid wires. It is also important that the individual braid wires should not be embedded in the dielectric and that jacketing material should not penetrate between them.

5-2. Jacketing Materials.—The two jacketing materials most widely used on flexible cables are regular vinyl and noncontaminating vinyl. The development of the noncontaminating type was undertaken because the plasticizer from the old type of vinyl jacket leached out, was absorbed in the polyethylene, and increased the power factor. The use of cables with the new type of jacket is especially important where the cables

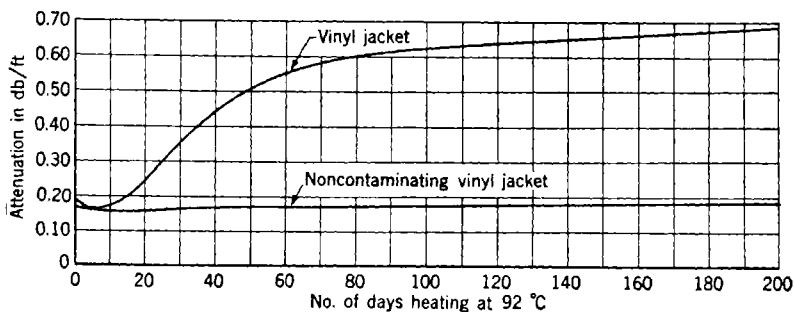


FIG. 5-2.—Contamination of polyethylene by vinyl jacket. The attenuations were measured at room temperature, $\lambda = 10$ cm. The first 9 days of heating were at 68°C.

will be subjected to high temperatures. Figure 5-2 gives a comparison of attenuation, as a function of the number of days at a temperature of 92°C,¹ of two samples of RG-9/U cable, one having the old vinyl jacket and the other, the new noncontaminating vinyl jacket. After 200 days, the total attenuation of the cable with the regular vinyl jacket had increased by a factor of almost 4 whereas the attenuation of the cable with the noncontaminating vinyl jacket had increased only 0.01 db/ft or about 6 per cent.

An examination of the copper braids of both cables indicated considerable tarnishing and corrosion and the formation of a coating of green waxy material. Although the plasticizer from the new jacket attacked the copper more vigorously than did the old material, its effect on the dielectric power factor was considerably smaller.

Both types of jacketing materials are flexible within the temperature range from -25° to $+90^{\circ}$ C but are, of course, stiffer at the lower temperatures. For temperatures below -25° C, however, the jacket is very brittle and is likely to crack if the cable is bent. The regular vinyl jacket is slightly more flexible than the noncontaminating vinyl jacket at

¹ G. J. Schaible, "S-band Attenuation and Capacity Stability of RG-9/U Cable," BTL Report No. GJS-3710, June 1945.

temperatures lower than -25°C ; it reaches a brittle state at about -35°C

These jackets are thermoplastic; that is, they may be deformed or softened by excessive heat or pressure. In general, they can be cut easily but do not tear readily; they also have good abrasion resistance. These materials have practically no permeability to gasoline or water.

5-3. Cables for Low-power Levels.—For low-power levels, the three cables most frequently used at microwave frequencies are the types RG-9/U, RG-21/U, and the RG-5/U. The RG-9/U cable is a double-braided cable containing a polyethylene dielectric core with a stranded

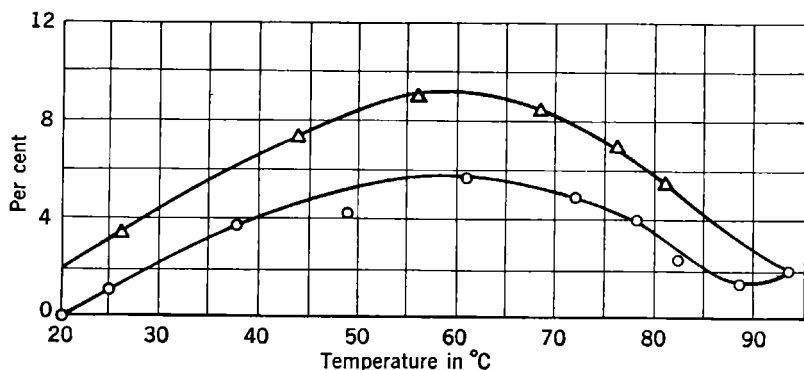


FIG. 5-3.—Variation of attenuation with temperature for an RG-9/U cable. The ordinates are the change in attenuation from the value at 20°C . $\lambda = 10$ cm. Circles, temperature increasing; triangles, temperature decreasing.

center conductor that is made of seven strands of 21 AWG silver-clad wire. The inner braid is made of silver-clad copper in order to obtain lower contact resistance between the wires at high frequencies than would be attained with the use of pure copper. The diameter over the dielectric is 0.285 in.; and the total diameter over the jacket, which is the non-contaminating type, is about 0.440 in.

The attenuation of this cable at a wavelength of 10 cm is about 0.16 db/ft, and there is little or no variation of attenuation with flexing or with changes in temperature. Some recent measurements have been made at Bell Telephone Laboratories on the effect of heat on the attenuation of RG-9/U cable at 10 cm, between 20° and 94°C . A maximum increase of 6 per cent in the attenuation occurred at 60°C during the period of increasing temperature (see Fig. 5-3). However, during the cooling period a maximum increase of 9 per cent occurred at the same temperature. This represents a maximum deviation of about 0.014 db/ft from the 20°C value and agrees very closely with results on a similar type of cable obtained some time ago at the Radiation Laboratory.

The stability of transmission for wavelengths smaller than 3.53 cm, however, is much worse. Variations of about 0.4 db in the r-f transmission through the cable were encountered by flexing a 20-ft length; the measured attenuation of long lengths of cable varied as much as 0.02 db/ft depending on how tightly they were coiled. In the temperature range of -40° to $+70^{\circ}\text{C}$, at a wavelength of 3.30 cm, the attenuation varied erratically between 0.30 and 0.40 db/ft (see Fig. 5-4).

Each successive heating cycle caused a permanent increase of about 0.01 db/ft in the attenuation until, after about nine cycles of heating to a temperature of 60°C or more and cooling to room temperature, the

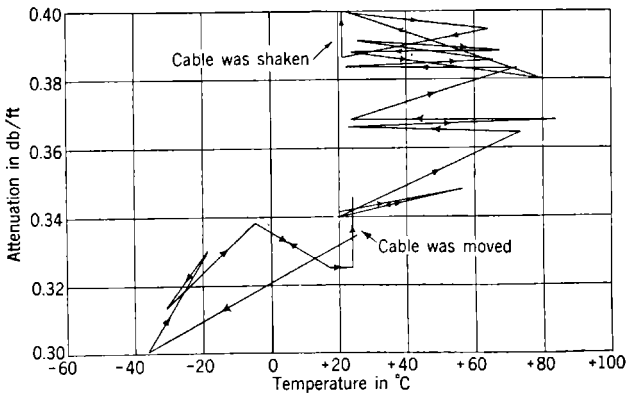


FIG. 5-4.—Attenuation of RG-9/U cable vs. temperature. $\lambda = 3.3$ cm.

attenuation stabilized near 0.40 db/ft. This random variation of attenuation with temperature cycling is undoubtedly caused by the expanding polyethylene disturbing the contacts between the braid wires. To lessen this variation, or possibly to eliminate it entirely, a new cable, which is designated as RG-9A/U, has been designed with the silver inner braid having a shorter lay to give better stability. This special high-frequency cable will have slightly larger attenuation because of the shorter lay.

Measurements of the frequency sensitivity of the attenuation of RG-9/U cable have been made in the wavelength range from 3.15 to 3.55 cm. Because of the effect of flexing upon the attenuation, the cable was fastened to a board while the attenuation was measured, to ensure reproducible results. Over this wavelength range, the attenuation varied from 0.303 db/ft at 3.55 cm to 0.341 db/ft at 3.162 cm, a variation of about 12 per cent. The results are shown in Fig. 5-5.

The RG-21/U cable is an attenuating cable that is used when one piece of equipment must be isolated from another to eliminate interaction

between them; it is used, too, when a given amount of attenuation is needed to decrease the sensitivity of some piece of test equipment. This cable, like the RG-9/U cable, has a double braid: an inner one of silver-clad copper and an outer one of copper with a noncontaminating vinyl jacket. In order to achieve the desired attenuation, a high-resistance No. 16 AWG Nichrome center wire is used. As most of the

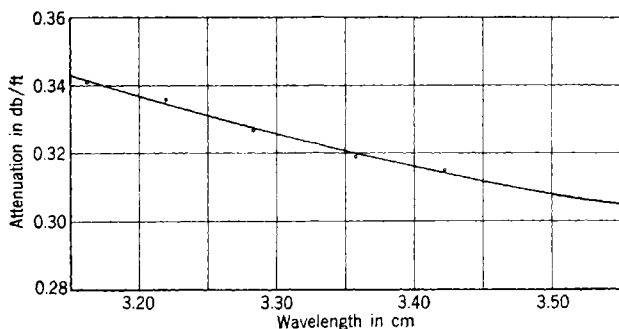


FIG. 5-5.—Attenuation of RG-9/U cable vs. wavelength.

dissipation is in the center conductor, the attenuation in decibels is nearly proportional to the square root of the frequency. This cable was designed to replace the RG-38/U cable which uses "lossy" rubber dielectric with a power factor of about 0.006 as the dissipating element. In the RG-38/U cable, the attenuation is nearly proportional to fre-

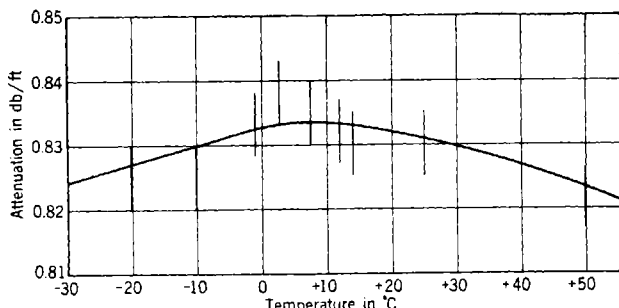


FIG. 5-6.—Attenuation of RG-21/U cable vs. temperature at 10-cm wavelength.

quency, and in addition the power factor of the rubber has a high temperature coefficient, about 0.008 db/ft per °C. The RG-21/U cable was developed to have a low temperature coefficient of attenuation. From -40° to $+60^{\circ}\text{C}$ the attenuation at a wavelength of 10 cm has a maximum value of 0.84 db/ft at $+10^{\circ}\text{C}$; and it decreases to 0.82 db/ft at each end of the temperature range, a total change of only 2.5 per cent (see Fig.

5-6). In the wavelength range from 8.6 to 12.6 cm, the attenuation varies from 0.74 to 0.90 db/ft as shown in Fig. 5-7.

Like the RG-9/U cable, the RG-21/U cable has a very good stability of transmission with flexing and temperature cycling, in the region from

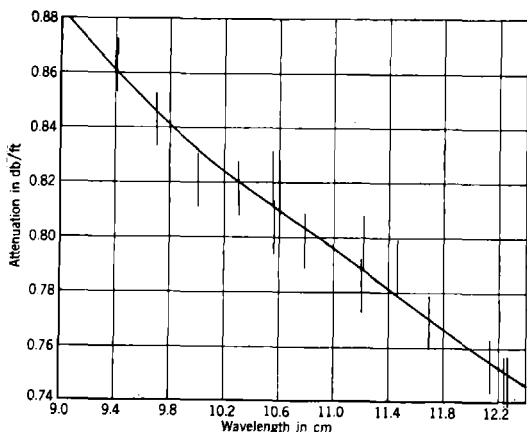


Fig. 5-7.—Attenuation of RG-21/U cable vs. wavelength (10-cm band).

8 to 12 cm. However, at wavelengths of 3.53 cm and below, bending and flexing cause considerable variation. When a cable carrying r-f power at these high frequencies is bent or flexed, the attenuation increases, and several minutes are required for the transmission to return to the original level. Since most of the loss is in the center conductor, the effect of temperature on attenuation is less than in the RG-9/U cable and is in the opposite direction; that is, the attenuation decreases with increasing temperatures, as does the resistivity of Nichrome. Over the range from -46° to $+61^{\circ}\text{C}$, the attenuation varies from 1.68 to 1.56 db/ft. The variation is illustrated in Fig. 5-9. Over the wavelength range from 3.13 to 3.53 cm, the attenuation varies from 1.70 to 1.52 db/ft, as shown in Fig. 5-8.

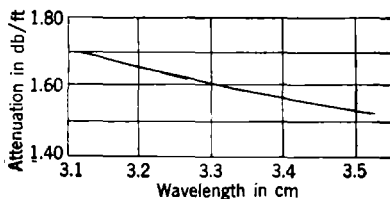


Fig. 5-8.—Attenuation of RG-21/U cable vs. wavelength (3-cm band).

The RG-5/U cable is the same size as the RG-21/U cable. Instead of the Nichrome wire, No. 16 copper wire is used as the center conductor. The shield consists of two copper braids, and the jacket is a regular vinyl jacket instead of the noncontaminating type. This cable has not had as widespread usage for microwaves as the RG-9/U cable since there is

little gain in flexibility and the electrical properties are not so good. The attenuation of RG-5/U cable at 10 cm is about 0.22 db/ft. It has been used principally for a flexible coupling from Sperry Klystrons since

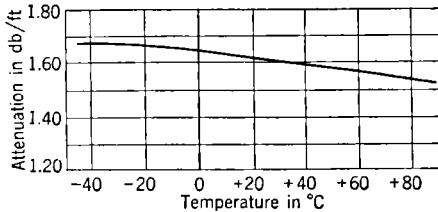


FIG. 5-9.—Attenuation of RG-21/U cable vs. temperature (3-cm band).

the SKL fittings used on these Klystrons will fit the RG-5/U cable but not the RG-9/U. These SKL fittings are shown in Figs. 5-37 and 5-38 at the end of Sec. 5-11.

5-4. High-power Cables.—For high-power transmission, there are two cables that have been most widely used. These are the RG-14/U

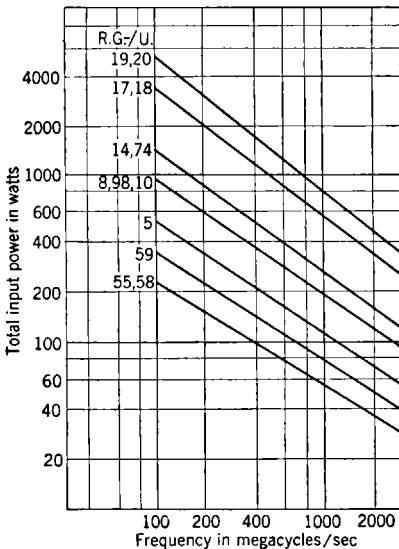


FIG. 5-10.—Average power transmitted by cables of various sizes. RG-U numbers on curves refer to Table 5-5.

tubing of 0.188 in. diameter. A single copper shield is braided over the core, and a noncontaminating jacket of 0.760 in. diameter is tubed or extruded over the braid. The attenuation is 0.096 db/ft at a wavelength of 5.00 cm where the cable begins to transmit the *TE*-mode.

cable, its armored equivalent RG-74/U, and the RG-17/U cable with its armored equivalent RG-18/U. The RG-14/U cable has a polyethylene dielectric core of 0.375 in. diameter, with a No. 10 AWG copper wire for the center conductor. There are two copper braids over the core covered by a noncontaminating vinyl jacket. The resulting over-all diameter is about 0.550 in. The attenuation of this cable at 10 cm is 0.14 db/ft. Since the diameter is slightly larger than that of the RG-9/U cable, the series conductor losses and therefore the total attenuation are somewhat less.

The RG-17/U cable has a polyethylene core which has a 0.680 in. diameter and contains a center conductor of copper rod or

The power breakdown for the dielectric-filled cables is of two kinds: thermal breakdown, and voltage breakdown. Thermal breakdown occurs when the dielectric softens because of the heating under high average power and allows the center conductor to move with respect to the outer conductor. Voltage breakdown occurs when the r-f voltage exceeds the dielectric strength of the insulation. Figure 5-10 shows a graph giving the average power rating of the cables of various sizes, including the RG-14/U and RG-17/U cables. These curves are calculated on the basis of a center-conductor temperature of 175°F and an ambient temperature of 104°F. As the frequency of the r-f current is increased, the power rating of the cable is decreased. This is because the amount of heat to be dissipated per unit length increases with the attenuation.

The RG-14/U cable has been tested under pulsed r-f power, at a wavelength of 10 cm, with a 1- μ sec pulse and a repetition rate of 1000 pps. True voltage breakdown was not attained in this way, but just above a pulse power of 300 kw failures usually occurred in the r-f connectors. This cable certainly should not be run at peak powers greater than 300 kw at microwave frequencies, although the maximum operating voltage as recommended by the Army-Navy R-f Cable Coordinating Committee is 5500 volts rms, which corresponds approximately to 500 kw pulse. This pulse power rating, of course, is limited by the amount of average power which the cable will transmit safely.

The RG-17/U cable was run for an hour at 1.2 Mw pulse power with a duty ratio of 1/1000 without any noticeable change. The voltage rating on this cable is 11,000 volts rms.

5.5. Resonances in Coaxial Cables.—Some flexible coaxial cables have been found to exhibit bad resonances at certain frequencies. These resonances are caused by certain periodic variations in the characteristic impedance of the cable which result from the periodic fluctuations of the diameter of the dielectric, the centering of the center conductor, or the ellipticity of the core. These resonances are characterized by a rapid change, with wavelength, in the standing-wave ratio looking into the cable and by an increase in the attenuation. They have been observed, at the Radiation Laboratory, in the RG-8/U and RG-9/U cables in the region of wavelengths from 8 to 10 cm. The standing-wave ratio changed from 1.1 to about 2 in voltage and dropped back to 1.1 in about 0.3 per cent change in wavelength, or in about 10 Mc/sec. At the resonance frequency, the transmission decreased by about 20 to 50 per cent of the transmission off resonance. In six samples, resonances were found at 8.4, 9.2, 9.4 cm (see Fig. 5-11). It is apparent that these resonances are caused by periodic variations because, if a cable that resonates is cut in half, each half will resonate at the same frequency as the original length.

The Naval Research Laboratory has reported finding resonances in

the RG-17/U, the RG-18/U, and the RG-9/U cables in the wavelength range from 46 to 22 cm. Nearly all the samples tested exhibited resonances with maximum voltage standing-wave ratios varying from 1.4 to 8. Measurements on the diameters revealed a definite periodicity (see Fig. 5-12). Cables in which abrupt changes occurred in the diameter showed much higher standing-wave ratios at resonance. One cable sample in which the resonance was small did not have very abrupt changes in the diameter but had a more gradual periodic variation. From the standpoint of transmission-line theory, gradual changes, even if periodic

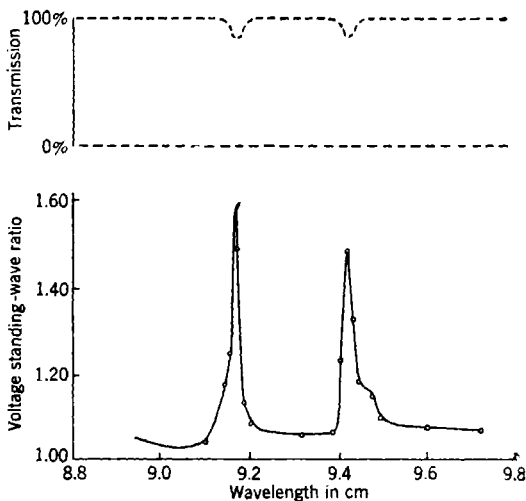


FIG. 5-11.—Resonances in RG-9/U cable.

would cause little reflection. However, abrupt discontinuities that are repeated periodically will add up to a very large mismatch at the input end of a long cable at those frequencies for which these abrupt discontinuities are spaced by an integral number of half cycles.

The RG-8, 9, 17, 18/U cables are the only cables that have been tested for resonances, but it is presumed that, since the extrusion is done in a similar way for other types of cables, they too may exhibit resonance effects. In very short lengths of cable, the effect of resonance is less noticeable; but in long lengths, the standing-wave ratio may become very high. As refinements are made in the techniques of manufacture these resonances may be eliminated or considerably lessened.

5-6. Flexibility and Durability of Coaxial Cables.—Tests of the flexibility and durability of coaxial cables are inadequate, but some results on the RG-14/U cable will give an indication of what may be expected of a cable under flexing. Table 5-1 gives the results and a

description of tests on three samples of RG-14/U cable flexed at the rate of 90 cycles per minute.

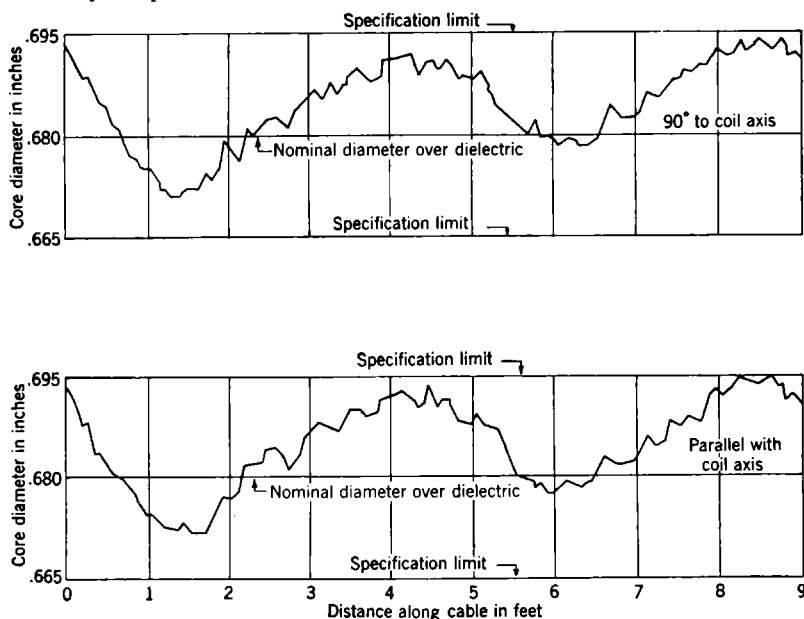


FIG. 5-12.—Periodicity in core diameter of RG-17/U cable.

TABLE 5-1.—EFFECTS OF REPEATED FLEXING OF COAXIAL CABLES

Sample No.	Description of tests	Time flexed	Number of flexings	Condition after flexing
1	From straight to a 3½-in. radius	2 hr	1080	Ragged copper braid, broken center conductor, dielectric and jacket unharmed.
2	From straight to a 5-in. radius	12 hr, 18 min	71,820	Inner braid slightly disturbed, center conductor broken, dielectric and jacket unharmed.
3	From straight to 6-in. radius	25 hr, 37 min	138,330	Center conductor broken in three places. Braid, dielectric, and jacket unharmed.

These cables are early samples of RG-14/U and contain a center conductor of copper-weld wire, which is copper drawn over a steel center core. With this construction, the wire is brittle and inclined to break from metal fatigue under flexing. The present RG-14/U cable uses solid copper wire, and therefore, under the same conditions, will probably

last longer than the samples described above. The RG-9/U cable is much more flexible than the RG-14/U. A 4-oz force is required to bend a straight 1-ft length of RG-9/U cable to a radius of curvature of about 8 in., whereas a 10-oz force is required to bend a straight 1-ft length of RG-14/U cable to a radius of curvature of about 16 in. In permanent installations, the Navy recommends that bends having radii of curvature not less than ten times the diameter of the cable be used. This certainly ought to be the lowest limit in the radius of curvature of a cable under repeated flexing.

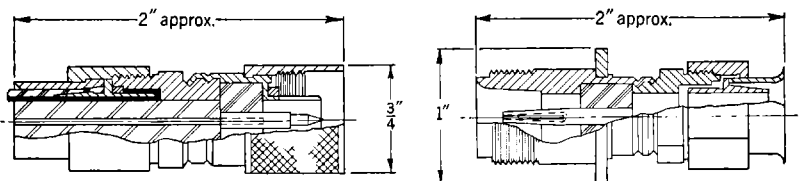


FIG. 5-13a.—Type N connectors, UG-21/U, UG-22/U.

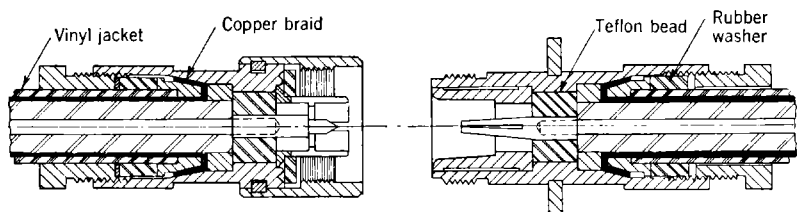


FIG. 5-13b.—Type N connectors, UG-21b/U, UG-22b/U.

5-7. Connectors for Cables for Low Power.—The connector that is used most prevalently on low-power cables is the type N. Cross-sectional drawings for two types of N connectors are shown in Figs. 5-13. The first type uses a polystyrene bead 0.254 in. long. The second is a modification of the polystyrene connectors and uses Teflon, a material with a low dielectric constant, for the insulating bead. In this new design, an improvement was made in the technique of coupling the braid and jacket to the body of the connector. The original type N connector, shown in the drawing on the left side of Fig. 5-13, was somewhat unsatisfactory because the cable core worked away from the bead of the connector, and the braid was stretched from bending and flexing with use. In the new design, shown in the drawing on the right-hand side of Fig. 5-13, a rubber washer is compressed by a nut and grips the jacket, braid, and cable core to the main body of the connector. In this construction, there is less likelihood of the braid stretching to allow the dielectric and center conductor to pull away from the connector bead. An additional advantage in the new design is the step in the outer

conductor of the plug; this step reduces the mismatch caused by a gap between the plug pin and jack center contact. This allows an adjustment in the tolerances so that there is always a gap that will prevent the spreading of the jack fingers by the shoulder against the plug pin. An interim design embodying these mechanical properties, but using polydichlorostyrene dielectric instead of Teflon, has been made. These three types are designated in the following way: the original connector has an ordinary UG-/U number; the mechanically improved design with the

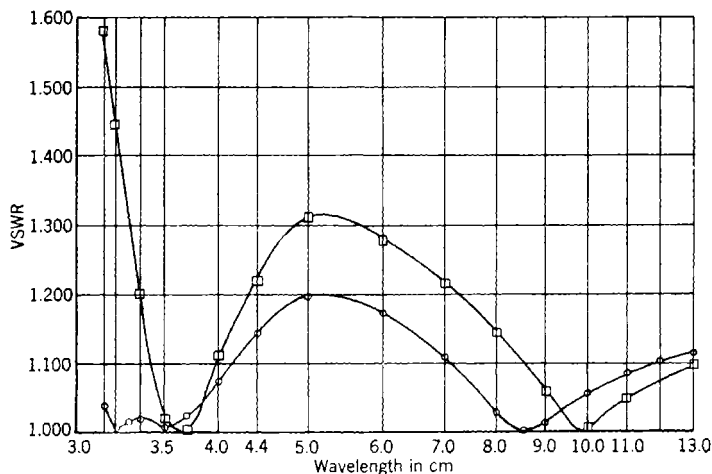


FIG. 5-14.—Theoretical performance of type N connectors. The circles represent the improved type with a Teflon bead, the squares the original type with a polystyrene bead.

polydichlorostyrene dielectric bead is designated by a UG-A/U number; the Teflon-dielectric connectors are designated by a UG-B/U number. A complete listing of the connectors designed for each cable is found in the table at the end of the section on flexible cables.

Figure 5-14¹ shows a graph of the performance of the type N connectors with the 0.254-in. polystyrene or polydichlorostyrene beads and the modified connectors using Teflon dielectric beads. The dielectric constant for Teflon is low (2.1) compared with that for polystyrene (2.56). This low dielectric constant reduces considerably the maximum mismatch that can occur in a pair of connectors because of the shunt capacities at the steps that result from the introduction of the beads. For the Teflon connectors at a wavelength of 5 cm, the maximum standing-wave ratio is 1.2 in voltage whereas the ratio for the polystyrene

¹ The development of Teflon-dielectric connectors was carried out at the Polytechnic Institute of Brooklyn, under contract from OSRD. The calculations embodied in this figure were taken from a progress report of work on this contract.

connectors is 1.3 at the same wavelength. Most of the improvement in match was made in the wavelength range from 3.0 to 3.5 cm. The length of the Teflon was made nearly a quarter wavelength at 3.3 cm in order to cancel out the shunt capacity of the step in the outer and inner conductors which was caused by the introduction of the bead. In this way each bead is compensated to be well matched from 3.0 to 3.5 cm. The two beads are spaced so that the reflections from them cancel each other at a wavelength of 9.3 cm. This spacing was made in order to have a single connector design that would be good from 8 to 12

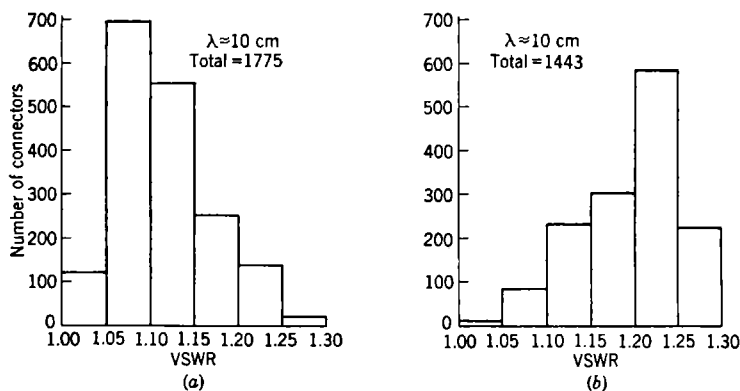


FIG. 5-15.—Histogram of voltage standing-wave ratios observed on commercial type N connectors; (a) is for RG-9/U cable, (b) is for RG-21/U and RG-5/U cables.

cm as well as from 3.0 to 3.5 cm in wavelength and that ultimately would replace the original polystyrene type of connector.

The curve in Fig. 5-14 indicates only relatively what may be found in actual cables and connectors. The plug-and-jack center contacts introduce reflections that are erratic and unpredictable. In the 3-cm band, the center contacts alone have been found to produce standing-wave ratios as high as 1.1 in voltage. For best match, the extreme ends of the fingers of the jack center conductor should make contact with the plug. Since the characteristic impedance of the cable varies ± 4 per cent and may not be uniform along the whole length, the magnitude and phase of input impedance of the cable may vary over a considerable range. Data on voltage standing-wave ratio have been obtained from 1775 UG-21/U and UG-22/U connectors attached to RG-9/U cables by technicians during the last two and a half years at the Radiation Laboratory. Seventy-seven per cent of these connectors had a voltage standing-wave ratio of 1.15 or less around 10-cm wavelength, and 46 per cent had a VSWR of 1.10 or less (see Fig. 5-15). The results on the RG-5/U and RG-21/U cables were not so good. Only 23 per cent of the connectors

had a VSWR of 1.15 or less, and 61 per cent of the connectors had a VSWR between 1.16 and 1.25. Since these cables are smaller than the RG-9/U, the shunt reactance at the junction between the cable and the connector is greater and undoubtedly causes the higher standing-wave ratio.

In the range of wavelengths from 3.1 to 3.5 cm, the UG-21/U and UG-22/U connectors on the RG-9/U cable are badly mismatched. Four pairs of connectors were tested with the following average results:

Wavelength.....	3.1 cm	3.3 cm	3.5 cm
VSWR.....	1.58	1.32	1.25

This cable connector has been used at these frequencies but only in conjunction with a transition from coaxial line to waveguide, or in some r-f component for which the connector mismatch has been compensated in the design. Results for the Teflon-dielectric connector in the 3-cm wavelength range are somewhat comparable to those for the polystyrene connectors for RG-9/U cable at 10 cm. The following are data taken at the Polytechnic Institute of Brooklyn.

TABLE 5-2.—TEFLON CONNECTORS

Number of pairs tested	Average VSWR		
	3.1 cm	3.3 cm	3.5 cm
14	1.12	1.18	1.10
12	1.13	1.13	1.11
5	1.11	1.06	1.08
6	1.07	1.15	1.11
Average.....	1.11	1.10	1.10
	9 cm	10 cm	11 cm
14	1.09	1.10	1.13
12	1.13	1.12	1.14
5	1.07	1.06	1.06
Average.....	1.10	1.10	1.12

Type N Adapters.—Since type N connectors are very widely used, a series of adapters has been designed. These include not only couplers to the various rigid lines but also such adapters as shunt T's and pressurizing fittings. In Table 5-3, these adapters are listed, information concerning the match at wavelengths of 3.2 and 10 cm being given where it is known. Figures 5-16 give cross-sectional sketches of some of these adapters.

5-8. HN Connectors.—The type HN connectors (UG-59, 60, 61/U) have been designed for applications using the RG-8/U cable, which require higher voltages than the type N connectors will safely transmit. These connectors, which are shown in Figs. 5-17, are designed so that the path length in air between the dielectric surfaces is as long as possible. This air path is increased by trimming the polyethylene core of the cable

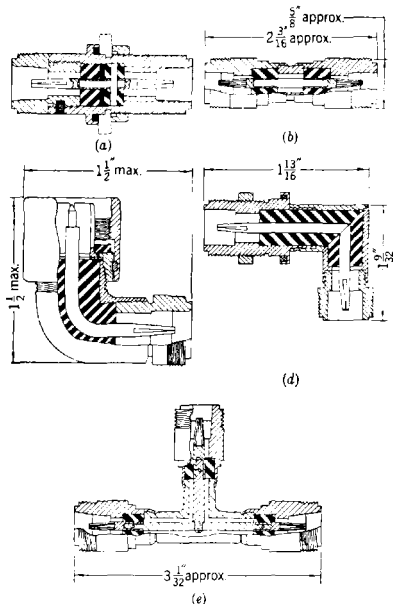


FIG. 5-16.—Type N adapters; (a) UG-30/U; (b) UG-29/U; (c) UG-27A/U, (d) UG-202/U; (e) UG-107/U.

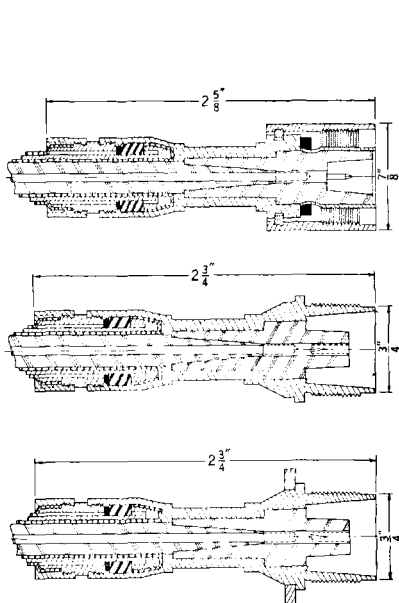


FIG. 5-17.—HN connectors; (a) UG-59A/U, (b) UG-60A/U, (c) UG-61A/U.

in the shape of a cone which fits into the polystyrene bead. The tool required for this is like a simple hand pencil sharpener and is designated by the Army and Navy number MX-103/U. Also, the bead of the jack is cut so that it will fit into the polystyrene bead of the plug. The Army-Navy R-f Cable Coordinating Committee rates this connector for 4000 volts peak at an altitude of 50,000 ft.

5-9. High-power Connectors to Rigid Lines.—The Army-Navy R-f Cable Coordinating Committee has designed a field-assembly connector for joining the RG-14/U cable to $\frac{7}{8}$ -in. stub-supported line. In this cable connector, designated UG-207/U, the center contact is forced under the dielectric for about $\frac{1}{2}$ in. and is soldered to the center wire at the end of the dielectric. Then the cable core is pushed into the polydichlorostyrene bead, the outer diameter of which is such that the characteristic imped-

ance is 52 ohms (see Fig. 5-18). This feature gives a long path length, so that the possibility of breakdown through the air between the cable dielectric and the bead is considerably lessened. A butyl-rubber washer

TABLE 5-3.—TYPE N ADAPTERS

Army-Navy number	Description	Figure number	Voltage standing-wave ratio	
			10 cm	3.2 cm
UG-30/U	Adapter from N plug to N plug for pressurizing a unit.	5-16	1.10-1.15	1.20-1.30
UG-29/U	Adapter from N plug to N plug, not pressurized.	5-16	1.15-1.20*
UG-27/U	Right angle, fits between N plug and jack.	1.15-1.25*
UG-27A/U	Right angle, fits between N plug and jack, better matched than UG-27/U.	5-16	1.10-1.15*
UG-202/U	Right angle from N plug to N plug.	5-16*
UG-28/U	Branched T, coupling to N plugs on all arms.	5-16	1.5
UG-107/U	Branched T, one branch couples to plug; other two to jacks.	5-16†	1.5

* Appears as very high reactance since braided section propagates coaxial *TE*-mode.

† Same except plug on vertical arm.

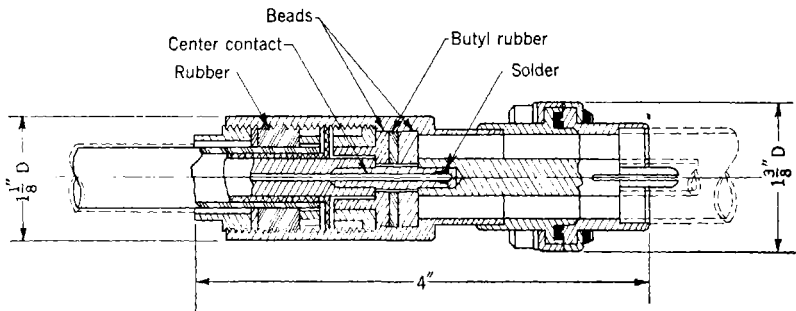


FIG. 5-18.—UG-207/U connector.

is compressed between the two polydichlorostyrene beads in order to seal hermetically the line to which the connector is coupled. To reduce the possibility of corona in the air gaps, Dow Corning Ignition Sealing Compound is applied liberally to the cable core and center contact before inserting them into the bead at assembly.

One bad feature of this connector is that the center contact is not

soldered to the center wire of the cable at the end that is forced under the dielectric. Should the diameter of the hole in the center contact which fits over the cable center wire be large, and should some dielectric be forced into it between the center conductor and the center contact, at this point a reentrant section of line would be formed in series with the main coaxial line. At microwave frequencies, this section could be an appreciable part of a wavelength and might therefore introduce considerable reflection. In assembling a connector of this type care must be exercised to ensure a good contact at this tip.

Electrical tests have been made on the UG-207/U connector in which 290 ft of RG-14/U cable were used as a termination. The following results were obtained.

TABLE 5-4.—REFLECTION FROM THE UG-207/U CONNECTOR

Wavelength, centimeters	Voltage standing-wave ratio
9.25	1.25
9.43	1.11
9.60	1.23
9.79	1.31
9.99	1.15
10.16	1.08
10.33	1.09
10.48	1.14

The Radiation Laboratory design of the connector between RG-14/U cable and $\frac{7}{8}$ -in. line, Figs. 5-19, 5-20, utilizes a taper from the size of the cable to the outer diameter of the $\frac{7}{8}$ -in. line. There is a step in the inner

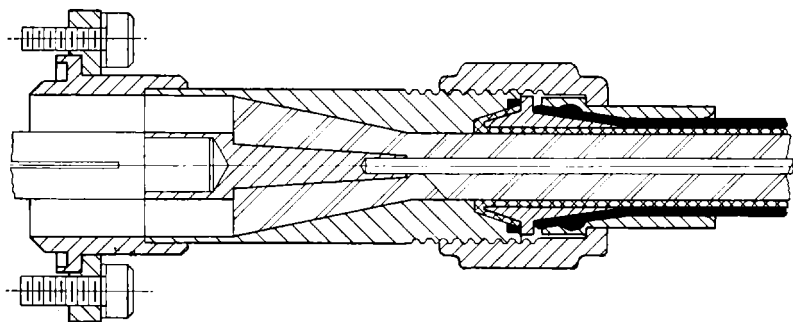


FIG. 5-19.—Connector for $\frac{7}{8}$ -in. line to RG-14/U cable.

conductor to compensate for the change in dielectric from polyethylene to air and to maintain constant impedance. The dielectric for the taper must be extruded into the connectors, and, if a good bond is made to the cable dielectric, the connector will stand nearly as much power as the cable. The most frequent incidence of breakdown is across the

dielectric face of the junction, between the dielectric and the air line. The path across this dielectric face may be made longer by a series of circular grooves in the dielectric surface. Two such connectors with extruded polyethylene dielectric were tested at a wavelength of 10.4 cm with a pulse length of $1.04 \mu\text{sec}$ and a repetition rate of 500 pps. Break-down across the dielectric face occurred at 575 kw pulse power for one connector and 662 kw pulse power for the other. With a safety factor of 2, a connector of this type may be rated at 300 kw pulse power, subject of course to the average-power limitation.

The voltage standing-wave ratio that can be expected to be set up by a single connector is between 1.1 and 1.2 for wavelengths greater than

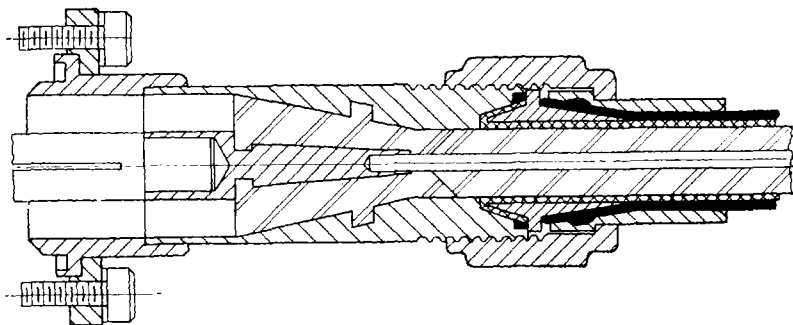


FIG. 5-20.—Modified connector for $\frac{1}{2}$ -in. line to RG-14/U cable.

9 cm. Considerable variation is found among connectors. This is undoubtedly caused by differences in the characteristic impedance of the cable and in the manner in which the dielectric is extruded.

In the design of connectors for the microwave region, the maintenance of constant impedance throughout is not the only requirement for obtaining a well-matched connector. At these frequencies, abrupt changes in the diameter of the line, which are caused by introducing a bead with a fairly large dielectric constant, result in a large capacitive susceptance. Such a mismatch may be canceled by another susceptance of the same value spaced about a quarter wavelength from the first, as explained in the preceding chapters in this book. Another method for eliminating this capacitive susceptance is to use a short section of high-impedance line at the step, as shown in the sketch in Fig. 5-21. The explanation of this technique follows. If we assume that Z_1 is terminated in its characteristic impedance, the capacitive susceptance introduces a mismatch shown on the admittance chart by A . If we normalize the admittance to the characteristic admittance of the high-impedance line Z_2 , we move our admittance to point P . Next, we transform the admittance P through a length l of the high-impedance line to point C . Then by

normalizing the admittance C to the characteristic admittance of the line Z_3 we arrive at D , and by adding the capacitive susceptance at this step, we obtain a perfect match. A modification of the Radiation Laboratory design of the connector between RG-14/U cable and $\frac{7}{8}$ -in. line has been made, using this principle for matching the capacity step

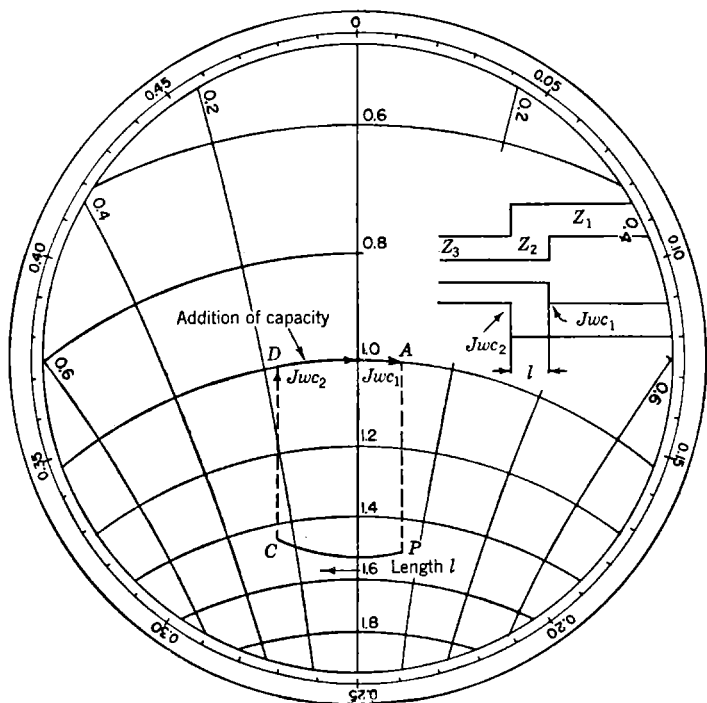


FIG. 5-21.—Admittance diagram of step compensation.

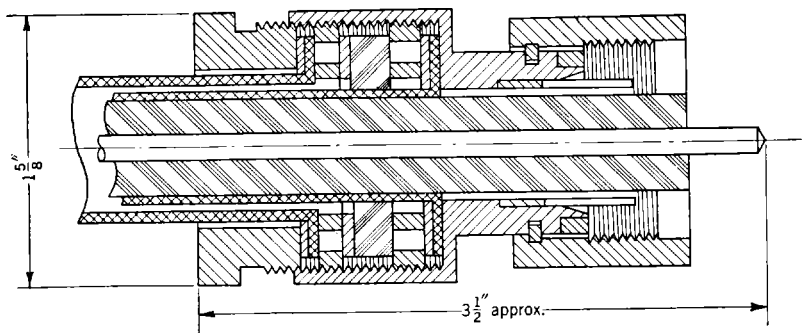


FIG. 5-22.—UG-154/U plug.

(see Fig. 5-20). The undercuts were introduced to hold the dielectric core and center conductor firmly in place.

The Army-Navy R-f Cable Coordinating Committee has designed for the RG-17/U cable a connector, the UG-154/U, which is suitable for field assembly and is shown in Fig. 5-22. This connector utilizes the

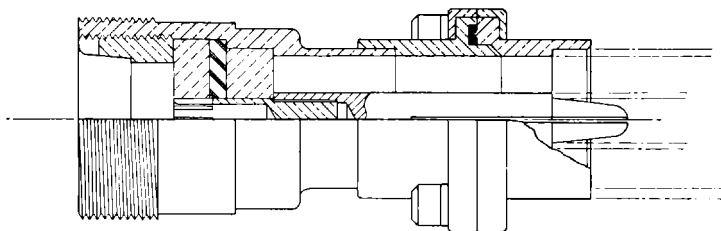


FIG. 5-23.—UG-237/U adapter.

center wire of the cable as the center contact. This center wire fits into the center tube of the mating connector and contact is secured by slotting and compressing this tube. For low-voltage use (less than 200 kw pulse power), the cable dielectric is cut off flush as in Fig. 5-22. Dow Corning Ignition Sealing Compound is used to fill up the air gaps. Couplings to various rigid lines are made by means of adapters; for the

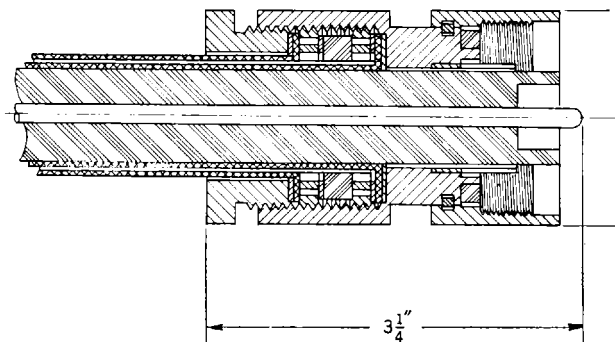


FIG. 5-24.—UG-156/U plug.

$\frac{7}{8}$ -in. stub line, the adapter is the UG-237/U shown in Fig. 5-23. The bead section in this adapter is a quarter wavelength long at about 10 cm; its characteristic impedance is 49.2 ohms. Thus the connector acts as a matching transformer from the 52-ohm cable to the 46-ohm $\frac{7}{8}$ -in. line for a wavelength of 10 cm, and the quarter-wavelength spacing helps to cancel the shunt capacity caused by the step in the diameter of the line.

For high-voltage use, the RG-17/U cable dielectric is trimmed as

shown in Fig. 5-24. This trimming enables the cable dielectric to fit into the bead of the connector, and thus to increase the path length for the voltage breakdown from the center conductor to the outer conductor. Dow Corning Ignition Sealing Compound is used to fill the air gap around

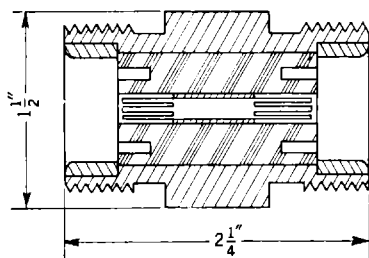


Fig. 5-25.—UG-155/U adapter.

the center conductor and between the dielectric surfaces and to decrease corona and the possibility of breakdown. This connector, if used with the UG-155/U connector, Fig. 5-25, to couple two sections of cable together, will withstand nearly as much voltage as the cable.

To increase the length of the air path across the surface of the dielectric, the connector may be tapered as shown in Fig. 5-26. The characteristic impedance of any cross section in this taper can be calculated from the equation

$$Z_0 = 138 \sqrt{\left[\frac{\log_{10} \left(\frac{d_1}{d_2} \right)}{k_e^{(2)}} + \frac{\log_{10} \left(\frac{d_2}{d_1} \right)}{k_e^{(1)}} \right] \log_{10} \left(\frac{d_3}{d_1} \right)}. \quad (3)$$

This equation assumes that the capacity per unit length of a coaxial line made up of two dielectrics whose common boundary is the surface of a cylinder of diameter d_2 (Fig. 5-27) consists of two capacities in series,

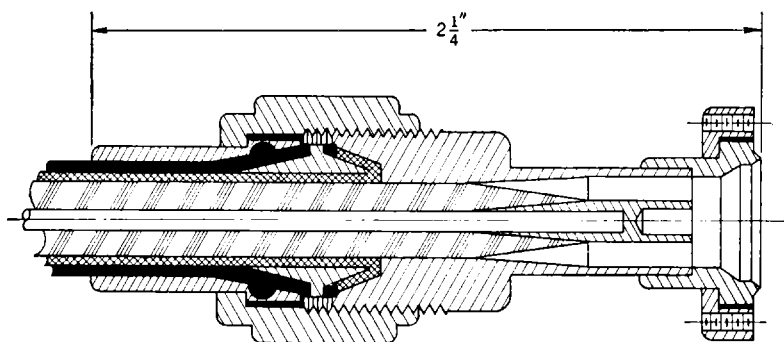


Fig. 5-26.—AN-type adapter from RG-14/U cable to $\frac{3}{8}$ -in. rigid line.

calculated from the two coaxial lines which would be formed if a thin metal tube were at this boundary. The inductance per unit length of the coaxial line is assumed to be unchanged since the magnetic permeability of most low-loss dielectrics is nearly the same as that of air. If the tapers of the conductors are straight lines, then Eq. (3) may be

used to calculate the shape of the dielectric in this section to ensure a taper with a gradually changing characteristic impedance. For a taper longer than a half wavelength, however, straight tapers of both conductors and dielectric will give a fairly good match since the change in the characteristic impedance will be gradual.

5-10. Polyglas Connectors.—In certain applications where a connector must maintain the pressure in the air-filled line to which it is coupled, it is possible to obtain a seal by means of an extruded polyglas bead in the connector. Polyglas has the property of adhering to the metal of the center and outer conductors and thus of securing a seal. It has, further, a coefficient of expansion equal to that of brass; this enables the connector to seal the line hermetically over a range of temperatures greater than would be obtained with the use of a butyl-rubber washer squeezed between two polydichlorostyrene beads. The dielectric constant of polyglas D, the material which is most satisfactory at present,

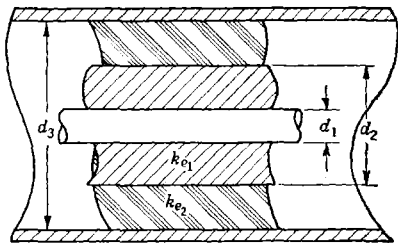


FIG. 5-27.—Coaxial line with two dielectric layers.

is rather high: 3.22, as compared with 2.25 and 2.56 for polyethylene and polydichlorostyrene, respectively. This high dielectric constant makes it necessary to introduce a large step in the conductors, and therefore

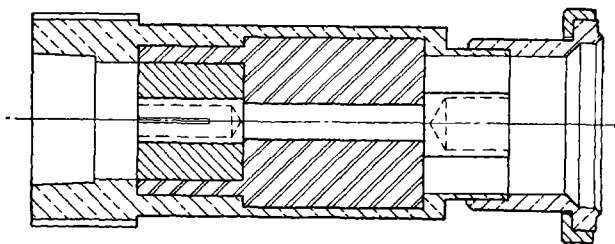


FIG. 5-28.—Adapter from UG-154/U connector to $\frac{1}{8}$ -in. line.

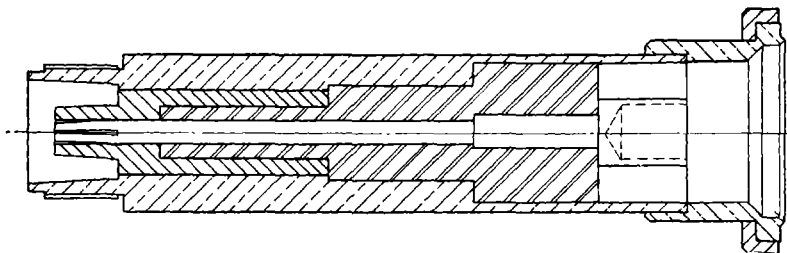


FIG. 5-29.—Adapter from HN connector to $\frac{1}{8}$ -in. line.

is rather high: 3.22, as compared with 2.25 and 2.56 for polyethylene and polydichlorostyrene, respectively. This high dielectric constant makes it necessary to introduce a large step in the conductors, and therefore

causes high capacitive mismatches at the steps. The mismatch may be lessened if the conductors are stepped in opposite directions from those of the conductors of the connecting line; that is, if the center-conductor diameter is decreased while the outer conductor is increased in diameter.

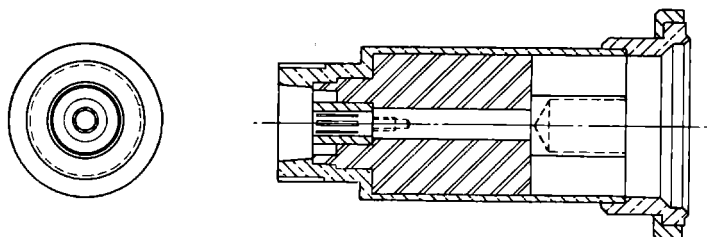


FIG. 5-30.—Adapter from UG-154/U connector to 1½-in. line.

By using the formulas from Sec. 4-6, which give the capacity of a step in terms of the dimensions of the line, the length of the bead may be selected so that a matched connector can be obtained. Figures 5-28

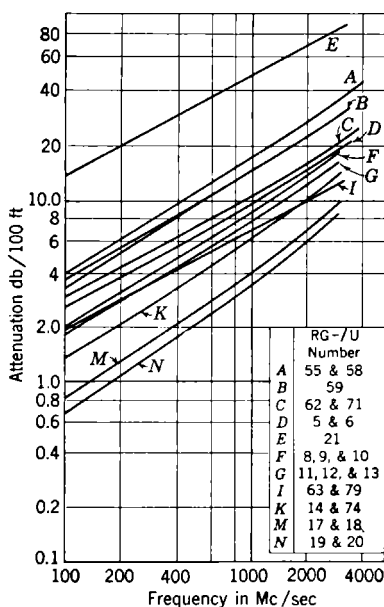


FIG. 5-31.—Attenuation of standard cables vs. frequency.

through 5-30 show several such connectors designed to fit various lines and fittings. These connectors are matched at a wavelength of 30 cm.

The adapter shown in Fig. 5-28 shows the insertion of a polyethylene bead into the polyglas. In this way a more elastic dielectric is used over the fingers of the slotted center conductors of the adapter so that these fingers will be able to expand when the plug center contact is forced into them. The characteristic impedance of this two-dielectric section may be calculated on the basis of Eq. (3). The termination of the Radiation Laboratory prevented the completion of tests on this sort of adapter. It is not known how satisfactory it might be to manufacture. Other polyglas materials that have similar properties, but with a lower dielectric constant, are being developed.

5-11. Summary.—In the preceding sections of this chapter a somewhat detailed but not exhaustive description of a few of the most widely

TABLE 5-5.—ARMY-NAVY STANDARD LIST OF R-F CABLES
15 October 1944

Class of cables	Army-Navy type number	Inner conductor	Nominal diameter of dielectric, in.	Shielding braid	Protective covering	Nominal over-all diam., in.	Weight, lb/ft	Nominal impedance, ohms	Nominal capacitance, $\mu\text{f}/\text{ft}$	Max. operating voltage, volts rms	Remarks
Single braid	RG-58/U	20 AWG Copper	0.116	Tinned copper	Vinyl	0.195	0.025	53.5	28.5	1900	General-purpose, small-size flexible cable
	RG-8/U	7/21AWG Copper	0.285	Copper	Vinyl	0.405	0.106	52.0	29.5	400	General-purpose, medium-size, flexible cable
	RG-10/U	7/21 AWG Copper	0.285	Copper	Vinyl (noncontaminating) and armor	(Max.) 0.475	0.146	52.0	29.5	4000	Same as RG-8/U armored for Naval equipment
	RG-17/U	0.188 Copper	0.680	Copper	Vinyl (noncontaminating)	0.870	0.460	52.0	27.5	11,000	Large, high-power, low-attenuation, transmission cable
	RG-18/U	0.188 Copper	0.680	Copper	Vinyl (noncontaminating) and armor	(Max.) 0.945	0.585	52.0	29.5	11,000	Same as RG-17/U armored for Naval equipment
	RG-19/U	0.250 Copper	0.910	Copper	Vinyl (noncontaminating)	1.120	0.740	52.0	29.5	14,000	Very large, high-power, low-attenuation, transmission cable
	RG-20/U	0.250 Copper	0.910	Copper	Vinyl (noncontaminating) and armor	(Max.) 1.195	0.925	52.0	29.5	14,000	Same as RG-19/U armored for Naval equipment
Double braid	RG-55/U	20 AWG Copper	0.116	Tinned copper	Polyethylene	(Max.) 0.206	0.034	53.5	28.5	1900	Small-size, flexible cable
	RG-5/U	16 AWG Copper	0.185	Copper	Vinyl	0.332	0.087	53.5	28.5	2000	Small microwave cable
	RG-9/U*	7/21AWG Silvered Copper	0.280	Inner, silver-coated copper; outer, copper	Vinyl (noncontaminating)	0.420	0.150	51.0	30.0	4000	Medium-size, low-level circuit cable
	RG-14/U	10 AWG Copper	0.370	Copper	Vinyl (noncontaminating)	0.545	0.216	52.0	29.5	5500	General-purpose, semiflexible, power-transmission cable
	RG-74/U	10 AWG Copper	0.370	Copper	Vinyl (noncontaminating) and armor	0.615	0.310	52.0	29.5	5500	Same as RG-14/U armored for Naval equipment

* RG-9A/U is identical with RG-9/U except that the inner braid is woven with a shorter lay. This should result in a greater stability under flexing.

TABLE 5-6.—R-F CABLE CONNECTORS

Cable No.	$\frac{3}{8}$ -in. stub-line coupling	Type N (polystyrene equivalent)	Type N modified (Teflon dielectric)	Other couplings
RG-58/U } RG-58A/U }		*UG-188/U plug Fig. 5-32		BNC connectors UG-88/U plug Fig. 5-35 UG-89/U jack Fig. 5-36 UG-90/U panel jack (VSWR < 1.16 for wave-lengths < 7.5 cm)
RG-5/U } RG-21/U }		UG-18/U plug UG-18A/U plug UG-19/U panel jack UG-19A/U panel jack UG-20/U jack UG-20A/U jack Fig. 5-13	UG-18B/U plug UG-19B/U panel jack Fig. 5-13 UG-20B/U jack	*SKL fittings— Fig. 5-37 UG-275/U straight UG-276/U right angle (not constant impedance) Fig. 5-38
RG-8, 9/U } RG-9A/U } RG-10/U }	Similar to Fig. 5-19	UG-21/U plug UG-21A/U plug UG-22/U panel jack UG-22A/U panel jack UG-23/U jack UG-23A/U jack Fig. 5-13	UG-21B/U plug UG-22B/U panel jack UG-23B/U jack Fig. 5-13	HN connectors Fig. 5-17 UG-59/U plug Fig. 5-17 UG-60/U jack Fig. 5-17 UG-61/U jack Fig. 5-17
RG-14/U } RG-72/U } RG-74/U }	UG-207/U field assembly Fig. 5-18 Fig. 5-19	UG-204/U plug Fig. 5-33		LN connectors Figs. 5-39, 5-40 UG-100/U plug UG-101/U panel jack UG-279/U jack
RG-17/U } RG-18/U }	†UG-237/U Fig. 5-23 Rad. Lab. Design Fig. 5-26	UG-167/U plug Fig. 5-34		UG-192/U couples to $1\frac{5}{8}$ -in. line. Fig. 5-41

* Not weatherproof.

† Couples to UG-154/U.

used cables, connectors, and adapters has been given. The various types of connectors which have been discussed in detail were chosen not only on the basis of their general use but also to suggest to the reader various ways in which other connectors for new cables and lines for microwave frequencies may be designed. In order to give a more comprehensive list

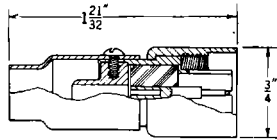


FIG. 5-32.—UG-188/U plug.

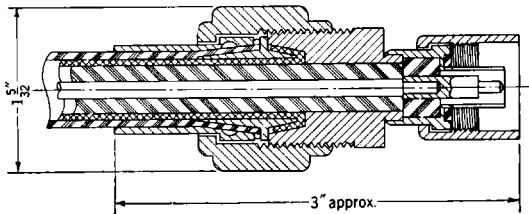


FIG. 5-33.—UG-204/U plug.

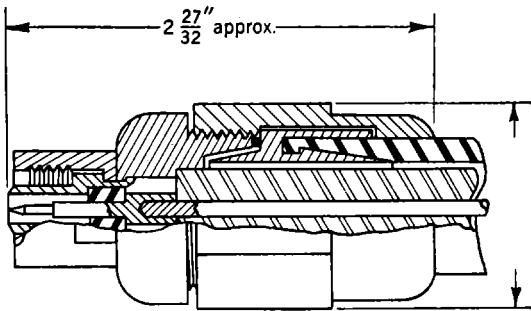


FIG. 5-34.—UG-167/U plug.

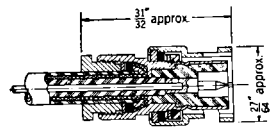


FIG. 5-35.—UG-88/U plug.

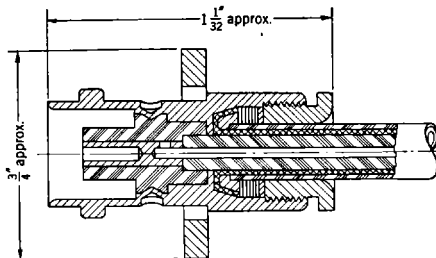


FIG. 5-36.—UG-89/U jack.

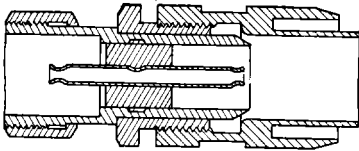


FIG. 5-37.—UG-275/U Klystron connector.

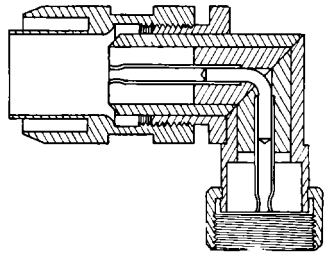


FIG. 5-38.—UG-276/U Klystron right-angle connector.

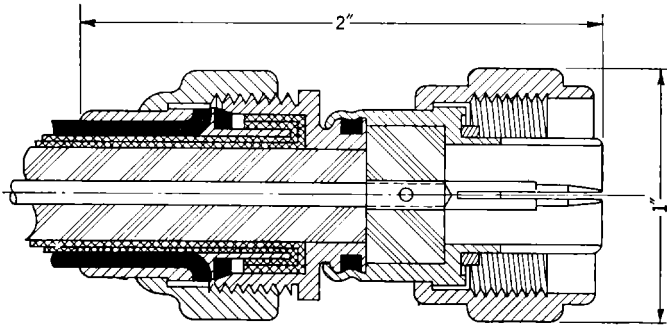


FIG. 5-39.—UG-100/U plug.

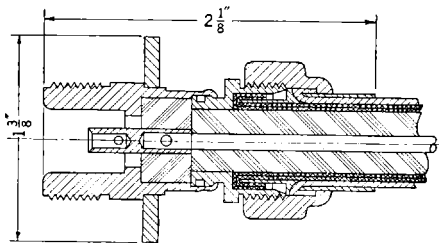


FIG. 5-40.—UG-101/U jack.

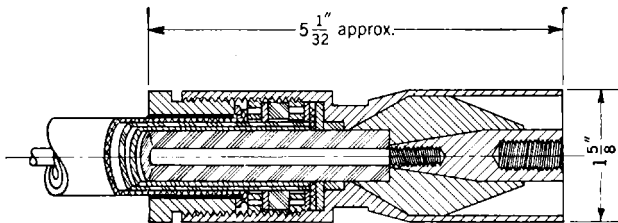


FIG. 5-41.—UG-192/U adapter.

of the cables and connectors, Table 5-5 has been prepared. The physical and electrical properties of all the 52-ohm cables on the standard list of cables published by the ANRFCOC are given in this table. Figure 5-31 shows the variation of attenuation with frequency for these cables. The corresponding connectors and adapters which are designed to be used with them are shown in Table 5-6 and various figures illustrate these connectors. Included also is a list, Table 5-7, of various adapters used to couple one connector to another. These adapters are not necessarily matched at microwave frequencies and therefore are recommended only where a good match is not needed.

TABLE 5-7.—PARTIAL LIST OF ADAPTERS FOR COAXIAL CONNECTORS

Number	Description
UG-97/U	Right angle: fits between LN plug and jack.
UG-108/U	Fits between LN and N plugs.
UG-109/U	Adapts from LN plug to LN plug.
UG-110/N	Adapts from type N jack to SKL male fitting.
UG-131/U	Adapts from type N plug to female SKL fitting.
UG-201/U	Adapts from type N jack to BNC plug.
UG-212/U	Right angle: fits between HN plug and jack.
UG-213/U	Adapts from type N plug to LN jack.
UG-217/U	Adapts from LN plug to UG-154/U connector
UG-252/U	Adapts from UG-215/U connector to LN plug.
UG-274/U	T containing one male BNC connector and two female BNC ends.
UG-306/U	Right-angle adapter; fits between BNC plug and jack.

WAVEGUIDE UNITS

BY F. T. WORRELL

Flexible waveguide units can be divided into two main classes: nonresonant and resonant. The first includes varieties which are essentially continuous waveguides made of some special flexible conductor; the second includes varieties which consist of a flexible choke-to-flange junction, or a number of flexible choke junctions in cascade.

Before discussing these flexible waveguides in detail, the various applications in which a flexible waveguide may be used should be considered. These are listed below.

1. *General Service Unit.* This unit is used for connecting two pieces of equipment, or for connecting test equipment to a system, and for any sort of "patch cord" service. This application generally requires long sections of flexible waveguide.
2. *Alignment Section.* This is a section, generally short, which is used to connect two rigidly mounted units that are expected to be misaligned, relative to the nominal alignment, by an amount sufficient to prohibit the use of a piece of rigid waveguide.

3. *Vibration Section.* This section can be used to connect two pieces of equipment that vibrate with respect to each other.
4. *Flexure Section.* One of these sections can be flexed continually through fairly large amplitudes at a relatively slow rate, that is, slow compared with variation rates.
5. *Flexible Waveguide for Emergency Repair.* This flexible waveguide may be used to replace damaged sections of rigid waveguide for temporary service until more permanent repairs can be made. An emergency-repair waveguide must be of such a design that it can be cut to arbitrary lengths.

In general, no given kind of waveguide will fall into only one of the classes listed above, but will have properties putting it in several of the classes. The combination of properties needed for a given application will determine the type of waveguide to be selected.

NONRESONANT FLEXIBLE WAVEGUIDE

The flexible waveguides that come under this heading are wound metal hose, Titeflex, seamless corrugated waveguide, plastic and plastic-filled waveguides, and wire-screen waveguides.

5-12. Wound Metal Hose.—At Radiation Laboratory the first piece of flexible waveguide was made by forcing a piece of breeze cable, which

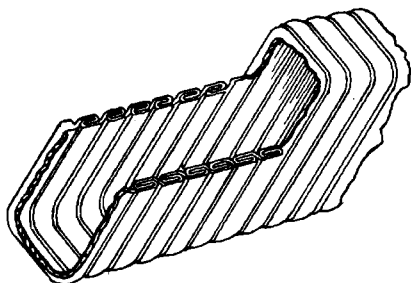


FIG. 5-42.—Wound-metal-hose waveguide.

is similar to ordinary BX armor, into approximately the cross section of the rigid waveguide with which it was to be used. It was, of course; lossy (about 1.5 db/m) but showed enough promise to warrant development of a more elegant version. This version is the wound-metal-hose flexible waveguide.

The construction of wound-metal-hose¹ waveguide is illustrated in Fig. 5-42. The waveguide is formed by winding a narrow strip of silver-clad brass in a spiral on a rectangular form and crimping the edges of the strip

¹ Manufactured by American Metal Hose Branch, American Brass Co., Waterbury, Conn.

as it is wound so that the adjacent turns are linked together. Since the crimping is quite tight, there is good electrical contact between the turns. When the waveguide is flexed, the successive convolutions in the winding slide over one another without breaking the contact. It is evident that such waveguides can be supplied in rather long pieces; these pieces can be cut to the desired length, and connectors can be soldered to them. The sizes in which wound-metal-hose waveguides are made are listed in Table 5-8.

TABLE 5-8.—SIZES OF WOUND-METAL-HOSE WAVEGUIDE

Wave-length region, cm	Type No.	Inside dimensions,* in.	Mating rigid waveguide OD, in.	Mating rigid waveguide,† type No.	Rubber-covered assembly, type No.
1	CG-162/U	0.170 × 0.420	$\frac{1}{4} \times \frac{1}{2}$	RG-53/U, RG-66/U	CG-163/U
3	CG-179/U	0.400 × 0.925	$\frac{1}{2} \times 1$	RG-52/U, RG-67/U	CG-164/U
3	CG-165/U	0.497 × 1.122	$\frac{5}{8} \times 1\frac{1}{4}$	RG-51/U, RG-68/U	CG-165/U
5		$\frac{5}{8} \times 1\frac{3}{8}$ $\frac{3}{4} \times 1\frac{5}{8}$	$\frac{3}{4} \times 1\frac{1}{2}$?	RG-50/U‡
6.5	CG-167/U	$\frac{7}{8} \times 1\frac{7}{8}$	1 × 2	RG-49/U	CG-168/U
6.5		$\frac{7}{8} \times 1\frac{3}{4}$?	‡
10	CG-169/U	1.338 × 2.838	1½ × 3	RG-48/U, RG-75/U	CG-170/U
10		$\frac{3}{8} \times 2\frac{3}{4}$.473 × 2.848 ($\frac{3}{8} \times 2\frac{3}{4}$ ID .049 wall)		
30		3¼ × 6½	3.41 × 6.66 (3¼ × 6½ ID 0.080 wall)	RG-69/U	

* All sizes have a radius on the corners of the order of $\frac{1}{8}$ in. Exact values are not quoted here.

† When two numbers are listed, the first is the more commonly used (brass) waveguide, the second the less common (aluminum) waveguide. Exception: RG-66/U is silver.

‡ Rubber-covered assemblies have been made in these sizes, but no type numbers have been assigned.

This type of waveguide is suitable for essentially the same frequency range as is the corresponding rigid waveguide. Since the irregularities in the inner wall of the waveguide are small and frequently spaced, and since the contact loss in the windings is small, the mismatch introduced by the flexible waveguide is mainly that caused by the discontinuity at the connection between the rigid and the flexible waveguides. Such a discontinuity does exist, since the corners of the flexible sections must be rounded. The effect of this discontinuity can be minimized by making the nominal inside dimensions of the flexible waveguide different from those of the rigid waveguide. To date only

the dimensions of the CG-179/U waveguide have been changed in this way. Flexible waveguides for the longer wavelengths are not badly enough mismatched by this discontinuity to warrant making a change in the cross section. The smaller CG-162/U waveguide needs a considerable change in cross section.

A certain amount of mismatch may be introduced at the point where the metal hose is soldered to the connector. This mismatch is random in character and can be detected by standing-wave measurements. It should be noted here that the effect of any changes in design of this waveguide can be found only by testing many samples and making a statistical analysis since the scattering in impedance among the various samples is appreciable.

Metal hose that has no covering material is fairly flexible. Samples of various sizes have been tested, at the American Brass Company, for minimum bending radius by bending them over uniform drums of different radii. Recommended minimum radii for bending in the *E*- and *H*-planes are listed in Table 5-9. If the waveguide is bent to a smaller radius, the loss will increase. The waveguide is wound to such a tightness that when the recommended minimum radius has been reached, the difficulty of further bending of the waveguide makes this fact apparent.

TABLE 5-9.—MINIMUM BENDING RADII OF METAL-HOSE WAVEGUIDES

Inside dimensions, in.	Minimum bending radius, <i>E</i> -plane	<i>H</i> -plane, in.
0.170 × 0.420	20	..
0.400 × 0.925	9	18
0.500 × 1.125	9	18
$\frac{5}{8} \times 1\frac{3}{8}$	10	20
$\frac{7}{8} \times 1\frac{7}{8}$	20	30
$\frac{7}{8} \times 1\frac{3}{4}$	20	30
1.338 × 2.838	24	36

The large bending radius specified for the 0.170- by 0.420-in. size should be noted. It has been found that any bending sharper than that specified causes considerable distortion of the cross section of the waveguide and a large increase in the loss.

Standing-wave-ratio specifications for the different sizes vary but, in general, one can expect that the voltage standing-wave ratio will be between 1.00 and 1.05 per end for any size the design of which has passed beyond the experimental stage. This means that a given length of waveguide may have an over-all voltage standing-wave ratio between 1.00 and 1.10, depending on the reflection from each end and on the electrical length of the line. In a long line the loss may be large enough

to affect the over-all standing-wave ratio. Further properties will be discussed in the section on the rubber-covered version, which in general has the same electrical characteristics.

The uncovered wound-metal-hose waveguide has several disadvantages. It deteriorates fairly rapidly with use since the flexing, by tending to open the convolutions, makes the contacts poorer and the waveguide more lossy and allows sparking between the convolutions. If exposed to salt spray, or even to ordinary atmospheric corrosion, this waveguide deteriorates because it is unprotected on the outside. Since it is not jacketed, it cannot be used in a pressurized system. However, it is useful in laboratory systems where there is no appreciable trouble with atmospheric corrosion, and in hastily assembled equipment where the extra losses are not important. Its chief importance in complete systems is for emergency patching of a damaged piece of rigid waveguide. In such a case the damaged section can be removed, and a piece of the flexible waveguide, cut to the proper length, can be soldered in place as a temporary expedient.

5-13. Wound Metal Hose, Rubber-covered.—This construction is a refinement of that described in the previous section. The flexible section has connectors soldered to each end and a rubber jacket molded around the entire unit. The sizes of waveguide for which a rubber-covered version has been made are listed in Table 5-8. A typical CG-164/U assembly is shown in Fig. 5-43. Because of the construction, units of this kind are supplied only in standard lengths. At present, it is made in lengths up to 48 in., in 6-in. steps, and also in 60- and 72-in. lengths. Although any type of connector may be used on this waveguide, the standard assembly is fitted on each end with a flange, mating with the standard rigid-line choke coupling. The exception is the CG-163/U waveguide, which has a choke at one end and a flange at the other, mating with the UG-116/U and the UG-117/U connectors, respectively. The rubber jacket makes the waveguide inherently less flexible, but since it prevents the convolutions from opening, the functional life of the waveguide is much longer. The jacket seals the waveguide so that it may be used in a pressurized system and affords protection against corrosion.

Power-breakdown troubles may be of two kinds: arcing across the waveguide in the direction of the E -vector, and arcing in the convolutions. No breakdown across the waveguide was observed, when the following powers were applied to the various sizes of waveguide: CG-170/U waveguide at a wavelength of 10.3 cm, 800 kw; CG-164/U at 3.2 cm, 200 kw; CG-163/U at 1.25 cm, 150 kw. The determination of the power level at which arcing occurs in the convolutions is difficult, for considerable arcing may occur without being visible to an observer looking down the inside of the waveguide. It is possible to detect such

arcng by measuring the loss in a piece of waveguide under high-power conditions and comparing this loss with that which is measured at low powers. This has been done on an 8-ft section of CG-164/U at 3.2 cm for powers ranging from 50 to 200 kw. The power loss was, within experimental error, constant over this range, a fact which leads to the belief that no appreciable sparking occurs up to 200 kw.

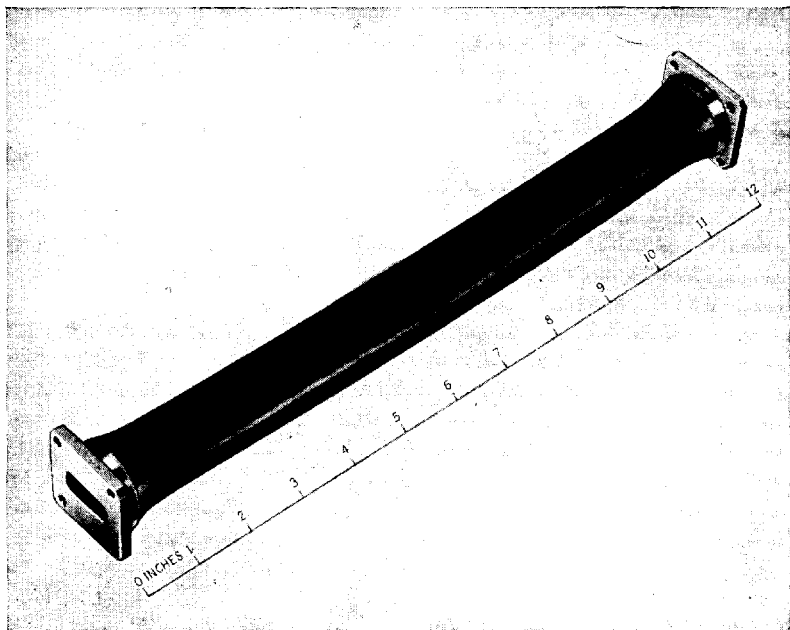


FIG. 5-43.—Rubber-covered wound-metal-hose assembly.

Waveguide of this type is moderately flexible. Permissible distortions of various sizes are listed in Table 5-10. These figures are obviously

TABLE 5-10.—FLEXIBILITY OF VARIOUS RUBBER-COVERED METAL-HOSE WAVEGUIDES

Type No.	Allowable <i>E</i> -bend radius, in.	Length required for 90° twist, in.
CG-170/U	45	
CG-166/U	8	24
CG-164/U	8	18
CG-163/U	6	9

only approximate. The variation in flexibility with dimensions of the waveguide does not appear, from the table, to be as smooth as one would expect. The units are "preflexed" in the factory before being tested. It should be noted that these figures are, in general, smaller than those

for the uncovered waveguides (Table 5-9). At first glance this seems inconsistent since the rubber jacket tends to stiffen the waveguide. However, it has been found that, even though the covered waveguides are inherently stiffer than the uncovered ones, the former can be flexed until they are more pliable than the latter without deterioration of electrical properties. This apparently is because the rubber jacket holds the convolutions in place and keeps the contacts good. In the case of the smallest size, the rubber also holds the cross section uniform.

No figures have been given for *H*-plane bending because the flexibility of the waveguide in the *H*-plane is so small that it is almost impossible to distort the guide without breaking it. An *E*-plane bend and a 90° twist should be used instead of an *H*-plane bend.

Vibration-table tests indicate that rubber-covered metal hose is satisfactory for vibration service. Data have been accumulated at the American Brass Company on the life expectancy of units of types CG-166/U and CG-164/U. A number of assemblies, each 12 in. long, of both types, were mounted in a machine that displaced one end of the assembly by $\frac{1}{8}$ in. on either side of the neutral position, in the *E*-plane, at a rate of 1400 cycles per minute. Under these conditions almost all the samples lasted at least one million cycles, and about 25 per cent of them lasted more than ten million cycles; two were still good after 60 million cycles. Some caution must be used in interpreting these data since it is suspected that the vibration table may not have given the simple type of motion described above but may have put additional stresses on the waveguide which would tend to shorten its life. However, the tests did show improvement in both strength and flexibility over an earlier model tested in the same way.

Flexure tests have been run at the American Brass Company on the CG-166/U unit. Six 12-in. samples have been flexed in the *E*-plane, 10° on either side of the neutral position in a continuous arc at a rate of 20 cycles per minute. All but one, which broke early in the test, were flexed 3.5 to 4.0 million cycles before breaking. In both the vibration and flexing tests, loss and standing-wave measurements were made at frequent intervals. In general, during the test the samples showed no marked change in either loss or standing-wave ratio until they were actually broken.

The effect of temperature on the rubber jacket is not definitely known; however, jackets occasionally crack when flexed at extremely low temperatures. This type of waveguide has proved satisfactory in general and is particularly suitable for vibration and flexure service.

5-14. Titeflex.—The construction of Titeflex¹ is shown in Fig. 5-44. Like the metal-hose waveguide, it is made by winding a narrow metal strip spirally on a rectangular form. In this case, however, the strip is

¹ It will be seen that this type is also a wound metal hose. To distinguish it from

considerably thinner, and the adjacent turns are crimped only a small amount over each other. The crimped edges are soft-soldered after

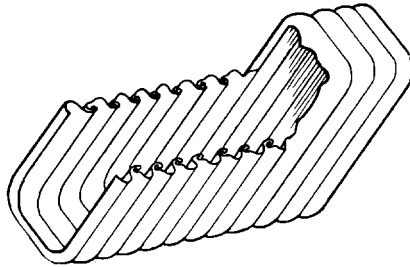


FIG. 5-44.—Titeflex waveguide.

the winding is finished. Thus, when the waveguide is flexed, there is no sliding of adjacent convolutions over each other, but rather a flexing of each convolution. The sizes in which Titeflex is made are listed in Table 5-11.

TABLE 5-11.—SIZES OF TITEFLEX

Wave-length region, cm	Type No.	Inside dimensions,* in.	Mating rigid waveguide OD, in.	Mating rigid waveguide,† type No.	Rubber-covered assembly, type No.
1	CG-162/U	0.170 × 0.420	$\frac{1}{4} \times \frac{1}{2}$	RG-53/U, RG-66/U	CG-162A/U
3	CG-179/U	0.400 × 0.900	$\frac{1}{2} \times 1$	RG-52/U, RG-67/U	CG-179A/U
3	CG-165/U	0.497 × 1.122	$\frac{5}{8} \times 1\frac{1}{4}$	RG-51/U, RG-68/U	CG-165A/U
5	$\frac{5}{8} \times 1\frac{3}{8}$	$\frac{3}{4} \times 1\frac{1}{2}$	RG-50/U	
6.5	CG-167/U	$\frac{7}{8} \times 1\frac{7}{8}$	1 × 2	RG-49/U	
10	CG-169/U	1.338 × 2.838	1½ × 3	RG-48/U, RG-75/U	CG-169A/U
10	$\frac{3}{8} \times 2\frac{3}{4}$.473 × 2.848 ($\frac{3}{8} \times 2\frac{3}{4}$ ID, .049-in. wall)		

* All sizes have a radius on the corners of the order of $\frac{1}{8}$ in. Exact values are not quoted here.

† When two numbers are listed, the first is the more commonly used (brass) waveguide, the second the less common (aluminum) waveguide. Exception: RG-66/U is silver.

Compared with the metal hose, Titeflex is considerably more flexible in some respects, less in others. Being made of a thinner strip, it can be bent to a small radius. It breaks, however, if flexed repeatedly after

other types, this is referred to by its convenient trade name. Titeflex is manufactured by Titeflex, Inc., 500 Frelinghuysen Avenue, Newark, N. J.

bending to the limiting radius, because large localized deformations then occur. Its great flexibility for a single bending makes Titeflex useful for alignment sections. It can be said, in general, that Titeflex is more flexible but more fragile than its metal-hose counterpart. It differs further from the metal hose in that its construction allows the waveguide to stretch or compress slightly; however, it cannot twist. Furthermore, it is airtight and can therefore be used in a pressurized system without need for a rubber jacket. Only one difficulty arises here; namely, that the waveguide will tend to stretch slightly when in a pressurized system. This stretching is noticeable only in the larger sizes, and can be made negligible in many cases by having the rigid r-f components associated with the flexible waveguide mounted strongly enough to take the stress. Like the metal hose, Titeflex is available in long sections and can be used for repairing damaged rigid waveguide. It is more likely to be damaged in use than the metal hose is, but it is less subject to deterioration from atmospheric corrosion.

No systematic program of testing has been undertaken, but a number of miscellaneous tests have been made to determine the flexibility of this type of waveguide. Some 24-in. samples of uncovered Titeflex in the 1.340- by 2.840-in. size have been tested to find the effect of distortions on the standing-wave ratio. The test samples were distorted, without any mechanical troubles or appreciable changes in the standing-wave ratio, by these amounts: 90° *H*-bend, 120° *E*-bend, 5-in. *H*-plane shear, 9-in. *E*-plane shear, 1-in. stretch, and $\frac{1}{2}$ -in. compression. The waveguides tended to take a set at the extreme values of distortion listed; therefore, such distortions could not be recommended for flexing service.

5.15. Titeflex, Rubber-covered.—Titeflex of this type is made in standard lengths with connectors soldered to the ends. A rubber jacket is molded around the outside of each unit. The jacket has the effect of stiffening the waveguide somewhat and making it considerably more sturdy. The standard lengths available and the specifications on their electrical properties are the same as those for the rubber-covered metal hose.

The only life-test data available are those made on a few samples of CG-164A/U waveguide, 12 in. long. These samples were run through a flexing test in which they were flexed 15° each side of the neutral position. The test was discontinued after a half-million cycles, at which time all the samples were still good.

The power-handling capacity of Titeflex has not been measured systematically. It is believed that this guide can handle at least those powers at which the metal hose has been tested (see Sec. 5-13). Its breakdown power may be lower than that of the metal hose because the ridges in the wall of the waveguide are higher and narrower.

5-16. Seamless Corrugated Waveguide.—The construction of seamless corrugated waveguide¹ is shown in Fig. 5-45. Like the common circular bellows or Sylphon bellows, this waveguide is made from thin-walled rectangular tubing that has corrugations formed in its walls.

The design problems here are not so straightforward as in the previously mentioned types. In the original design the inside dimensions of the flexible section were made equal to those of the rigid waveguide,

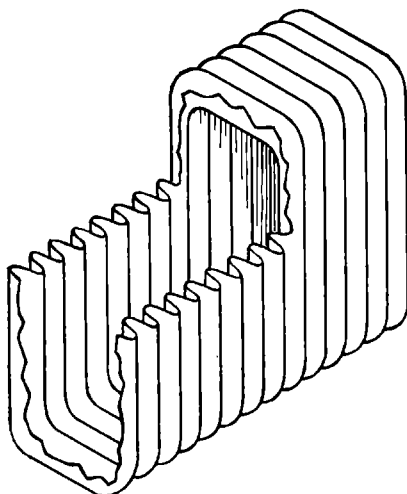


FIG. 5-45.—Seamless corrugated waveguide.

the impedance of which it was supposed to match. The depth of the corrugations was made small compared with the wavelength in the hope that the discontinuities introduced would be small, and yet large enough to provide a reasonable flexibility. Also, the corners of the waveguide had to be rounded to ensure flexibility. The units made according to this design do not match the rigid waveguide in impedance. Theoretical analyses² have been made of waveguide with corrugations in one or both of the broad faces. The analyses show that these waveguides transmit electromagnetic radiation in modes that do not have the same geometry as those in the smooth-walled rectangular waveguide. No analysis has been made of waveguides with corrugations in all four walls, but it seems logical to assume that the same theory of transmission is true in these

¹ Manufactured by American Metal Hose Branch, American Brass Co., Waterbury, Conn.

² C. C. Cutler, "Electromagnetic Waves Guided by Corrugated Conducting Surfaces," BTL Report No. MM-44-160-218, Oct. 25, 1944; H. Goldstein, "The Theory of Corrugated Transmission Lines and Waveguides," RL Report No. 494, Apr. 6, 1944.

waveguides. Therefore, one would expect that a smooth-walled rectangular waveguide and a corrugated waveguide of the same inner dimensions would not have the same impedance. As a matter of fact, experimental data indicate that the corrugated waveguide has the same impedance as a smooth rectangular waveguide the inside dimensions of which are approximately the mean of the inner dimensions of the corrugated waveguide and the dimensions at the bottom of the corrugations.

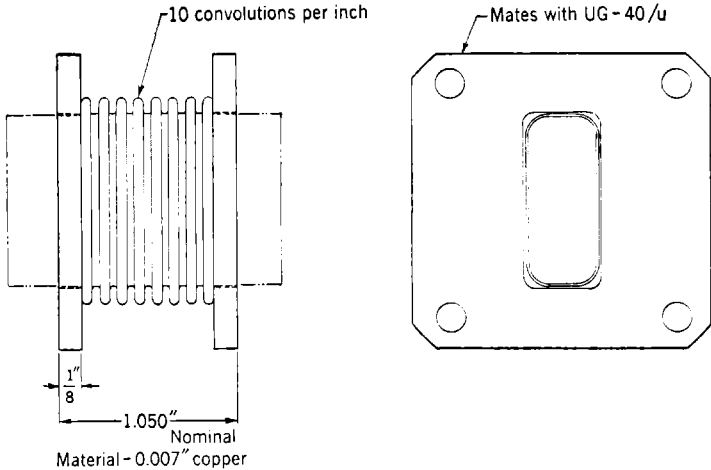


FIG. 5-46.—Seamless-corrugated-waveguide assembly for connecting two pieces of RG-52/U waveguide.

At the time of writing, waveguide of this type is available in two sizes: 0.400 by 0.940 in. ID, $\frac{1}{8}$ -in.-radius corners, corrugations 0.100 in. deep, to be used with RG-52/U waveguide (0.400 by 0.900 in. ID); and 0.500 by 1.125 in. ID, $\frac{1}{8}$ -in.-radius corners, corrugations 0.100 in. deep, to be used with RG-51/U waveguide. It can be seen from the previous remarks that these waveguides will not match the rigid waveguides with which they are used. As a matter of fact, the voltage standing-wave ratio, observed when one looks from a piece of UG-52/U waveguide into the smaller of the above-mentioned sizes of corrugated waveguide terminated at the far end, is about 1.10 to 1.15. The conclusion stated in the previous paragraph would indicate that the proper inside dimensions of the two guides, each having corrugations 0.100 in. deep, would be 0.300 by 0.800 in. and 0.400 by 1.025 in., respectively. In early developmental work, there was no time to perfect the design of this waveguide; consequently, until the proper dimensions could be found, a makeshift had to be constructed for the small size since usable units were urgently required. The small size was needed for two appli-

connections; namely, as an alignment section between two sections of RG-52/U waveguide and as an alignment section between a piece of RG-51/U waveguide and a piece of RG-52/U waveguide. In each case an optimum

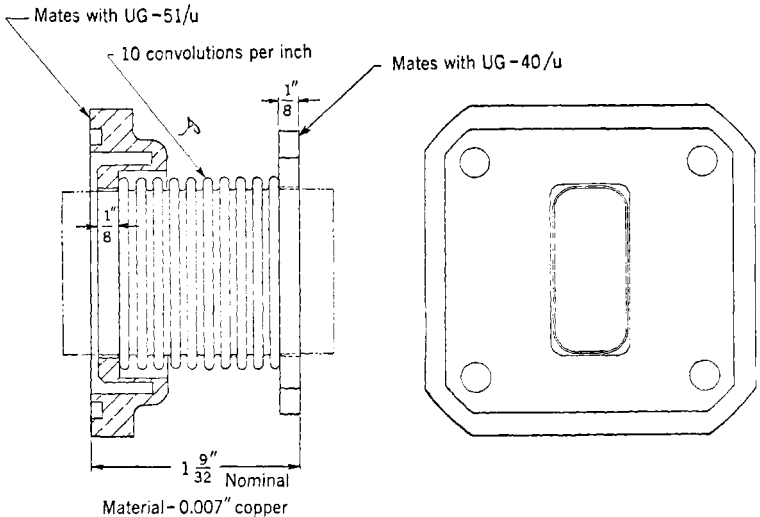


FIG. 5-47.—Seamless-corrugated-waveguide assembly for connecting RG-51/U to RG-52/U waveguide.

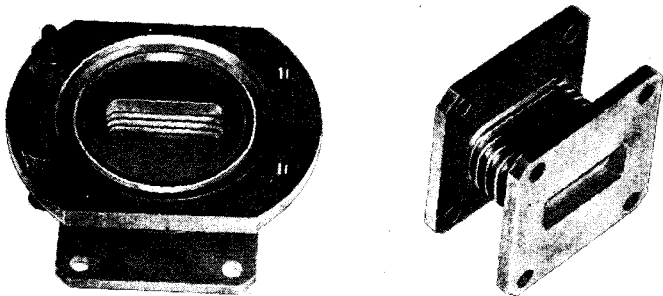


FIG. 5-48.—Finished assemblies of seamless-corrugated-waveguide connectors.

length was determined experimentally, so that the flexible unit was well matched over the wavelength band from 3.1 to 3.5 cm. Drawings of these two units are shown in Figs. 5-46 and 5-47. Finished assemblies are shown in Fig. 5-48.

This type of waveguide is about the most flexible that is available; it lacks only the ability to twist. Its flexibility is approximately the

same as that of uncovered Titeflex, but it rates higher in compression and extension. The small size can be bent on a $\frac{3}{4}$ -in. radius in the E -plane, or on a $1\frac{1}{2}$ -in. radius in the H -plane, or stretched or compressed 10 per cent, without appreciably changing the standing-wave ratio. A unit with ten corrugations can be sheared $\frac{1}{8}$ in. in the H -plane and $\frac{1}{4}$ in. in the E -plane without changing the standing-wave ratio.

One assembly in this same size with nine corrugations has been tested at a wavelength of 3.2 cm at a power of 250 kw, pulse length of 0.8 μ sec, 1300 pps. No breakdown occurred for the following distortions: 30° H -bend, 45° E -bend, $\frac{1}{4}$ -in. stretch, and $\frac{1}{4}$ -in. compression. Apparently the distortion is limited by the standing-wave ratio and by the mechanical limitations of the waveguide.

Corrugated waveguide is airtight, but it cannot be pressurized, except within certain limitations. A 3-cm small waveguide assembly was tested at 20 lb/in², and was found to stretch 15 per cent. It did not bulge radially at pressures up to 30 lb/in². Therefore, a guide of this size can be used in a pressurized system at a pressure of 20 lb/in² if the rigid waveguide sections to which the flexible section is connected can stand a stress of about 10 to 12 lb.

At present, the corrugated waveguide is made of soft annealed copper to give it maximum flexibility as an alignment section. Therefore, it is not suitable for repeated flexing or for vibration service. By the use of different materials, units satisfactory for such service may be developed eventually, but since rubber-covered Titeflex is already available for these uses, there is no urgent need for such development.

5-17. Plastic and Plastic-filled Waveguides.—It is well known that light can be conducted down a dielectric rod without appreciable loss of light through the walls, even if there is no metallic reflecting surface on the walls. In the optical case, if one uses a rod of appreciable cross section the light will be carried in numerous modes, perhaps thousands. In microwave work, carrying the power in only one mode is of interest; consequently, the problem is somewhat different. Some theoretical work has been done on this problem.¹ Two cases were considered: that of a rod of uniform dielectric constant; and that of a rod whose dielectric constant varied from a large value at the center to 1.0 at the surface. For simplicity, the calculations were made for the TE_{01} -mode. In each case it was found that the electric field at the surface was about 40 per cent of the maximum field in the interior of the rod, and that 55 to 60 per cent of the radiation was transmitted along the outside of the rod. This means that any external supports would cause large reflections of power. Ways of making slight improvements have been

¹ R. M. Whitmer, "Waveguides Without Metal Walls," RL Report No. 726, May 10, 1945.

suggested, but on the whole, it is believed that this system of transmitting power is impractical.

Although a simple plastic-rod waveguide will not work, a metal waveguide filled with plastic should be satisfactory. A plastic-filled waveguide would have the following advantages over a hollow waveguide.

1. The width of the waveguide would be $1/\sqrt{2k_e}$ times the width of air-filled waveguide for the same cutoff frequency.
2. The height of the guide, which is kept close to $\lambda/2$ in air-filled waveguides in order to get maximum power-handling capacity, could be proportionately much less since the breakdown strength of a solid dielectric is much higher than that of air.
3. The walls of the waveguide could be thin because the dielectric provides support and holds the shape.
4. The waveguide would be flexible since the thin metal wall could be distorted.

The dielectric-filled waveguide would have these disadvantages.

1. Voids in the dielectric would cause large reflections.
2. Transitions to the air-filled rigid waveguide would be required.
3. The attenuation would be higher, even if the dielectric were lossless.

To explain the higher attenuation an example may be considered. At a wavelength of 10.0 cm, a standard 1.5- by 3-in. copper waveguide will have a loss of 0.0199 db/m. If this waveguide is filled with polyethylene, $k'_e = 2.25$, and if the width is then reduced by $\sqrt{k'_e}$ to keep λ_e the same as before, and the height is reduced by the same factor, the copper loss will be increased by the factor k_e to a value of 0.0448 db/m. In addition, polyethylene, for which $\sqrt{k''_e} = 0.0009$, will cause a loss of 0.184 db/m. The total loss is, therefore, 0.229 db/m.

Attempts have been made to develop flexible dielectric-filled waveguides for the 1-cm region.¹ In one variety a thin lead sleeve was used over a polyethylene core. This waveguide had a loss of 4 or 5 db/m, which could have been reduced by silver-plating the inside of the lead sleeve. In another version that was tried, du Pont conducting silver paint² was applied to the outside of a polyethylene rod. The lowest loss obtained in this case was about 7 db/m. Moreover, after drying, the paint flaked off when the rod was flexed. These results, it must be admitted, are not encouraging, but it seems reasonable to assume that

¹ H. E. Kallman, "Rudiments of Flexible Waveguides," RL Group Report No. 41-9/26/45.

² Made by E. I. du Pont de Nemours, Arlington, N. J.

a successful version could be developed. It has been suggested that a more flexible binder be used, and that a flexible sheath be put over the paint to prevent the cracking. If such a waveguide were perfected, it would still have a loss about three times that of the rigid waveguide and would thus be used only in special applications. One advantage is that it would not radiate small amounts of power as do metal hose and vertebrae. For use with signal generators, the high loss would not be objectionable.

5-18. Wire-screen Flexible Waveguides.—The British have developed waveguides having copper screen walls. Two different varieties have

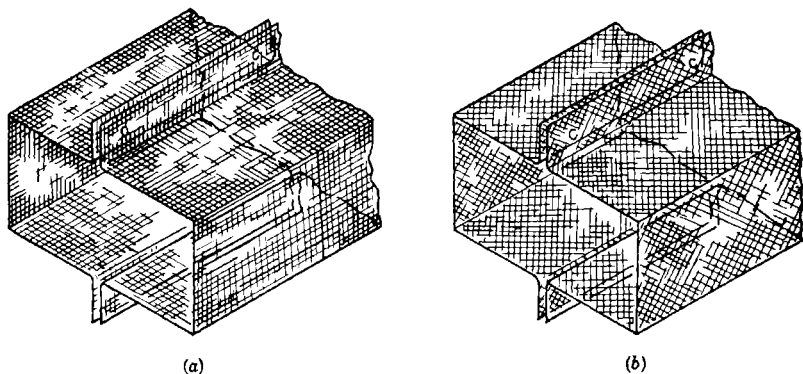


FIG. 5-49.—British flexible waveguide; (a) wires parallel to waveguide axis, (b) wires on the bias.

been used, as shown in Fig. 5-49. One has the wires in the screen running parallel and perpendicular to the axis of the waveguide; the other has the wires on the bias. Both varieties have rubber jackets molded over the screen. The first kind can be twisted but is stiff in bending; the second cannot be twisted but is fairly flexible in bending. Each has a loss of roughly 0.4 db/m and voltage standing-wave ratio of 1.03.

Some life tests were made of this type of waveguide. A flexure test was accomplished by mounting one end of a sample eccentrically on a rotating table while holding the other end in a fixed position. The table rotated at 110 rpm. Two samples were tested: a 15-in. sample was sheared 3 in., and a 6-in. sample was sheared $\frac{1}{4}$ in. After about 500,000 flexures, the loss had increased about 50 per cent, presumably as a result of loosening of the braid. One sample was vibrated at an amplitude of 0.013 in. at 2000 rpm for 12 hr with no change in loss. Samples have also been held at a temperature of 60°C for 76 hr with no change, particularly with regard to adhesion of the rubber to the metal braid.

This is important, since, without the rubber jacket, the braid would collapse when the waveguide was bent.

RESONANT FLEXIBLE WAVEGUIDE AND COUPLING UNITS

5-19. Flexible Bellows.—A flexible-bellows section consists of a radial choke made of flexible material. For round waveguide carrying the TE_{11} -mode, the design is quite straightforward. The choke consists of a section of radial transmission line one-half wavelength long, with a short circuit at the end, as shown in Fig. 5-50. The theory of operation of radial chokes has been treated in Sec. 4-9 and will not be discussed here. For greater flexibility than is provided by one of these sections, a

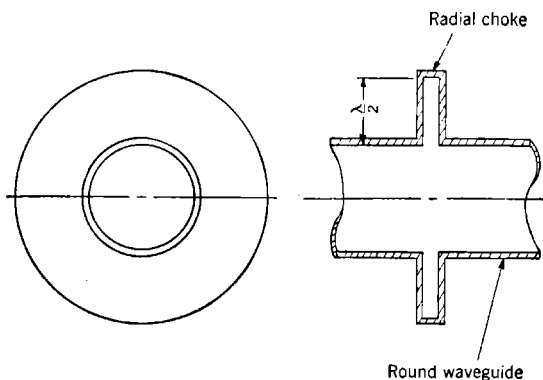


FIG. 5-50.—Flexible bellows for TE_{11} -waveguide.

series of sections can be stacked, one on the other, forming, in essence, a flexible waveguide. Not much use has been made of this type because the round waveguide is used infrequently. Bellows can, however, also be used in rectangular waveguide. The design of a single section is practically the same as that of the round waveguide. When a number of these are stacked together, however, they must be separated by partitions having rectangular holes the same size as the waveguide.

Two different kinds of bellows have been made. In one,¹ a complete section is spun in one piece, in much the same way as in the manufacture of circular Sylphon bellows. This spun type is shown in Fig. 5-51. In Fig. 5-52 is shown an individual bellows. The method of assembly is shown in Fig. 5-53. It should be noted that the dimension A is bigger than the dimension B . Consequently the impedance of the inner section of the radial choke, which corresponds roughly to the first quarter-wave section, is larger than the impedance of the outer section, which corresponds to the second quarter-wave section. This situation is

¹ Manufactured by Fulton Sylphon Co., Knoxville, Tenn.

opposite to the low-impedance-high-impedance design that is characteristic of a broadband choke. Therefore, this bellows is satisfactory only over a narrow band. It also has other disadvantages: it is subject to high-power breakdown across the rectangular hole; and its life under

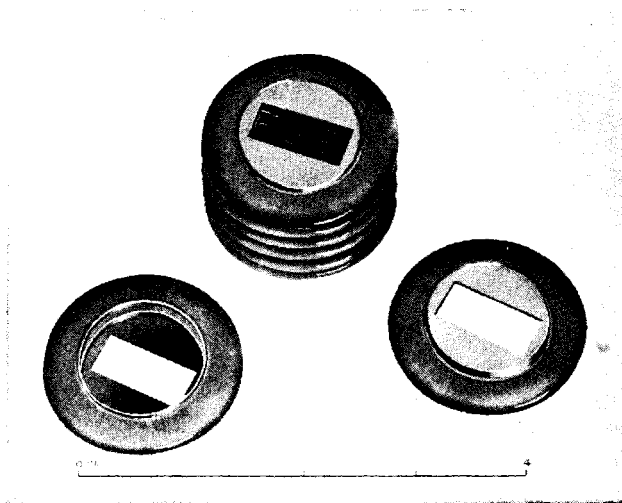


FIG. 5-51.—Spun bellows

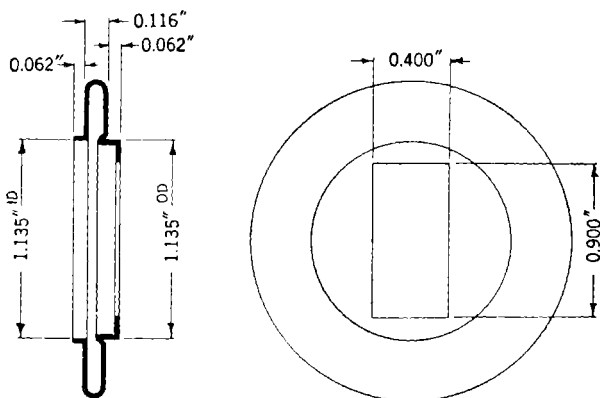


FIG. 5-52.—Details of a 3-cm spun bellows.

constant flexure or vibration is short. However, it has good flexibility and is airtight, although it cannot be pressurized unless the connecting rigid waveguide can stand the stresses introduced by having air inside the bellows at a pressure above atmospheric.

Detailed data are not available on this kind of bellows. Power-

handling tests have been made from time to time, and the results are variable. The breakdown seems to depend upon the thickness of the edge of the rectangular hole and upon the tolerance in the diameter of the radial choke. Some standing-wave measurements taken on an

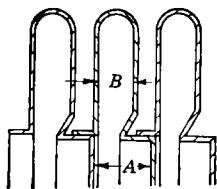


FIG. 5-53.—Cross section of a spun-bellows assembly.

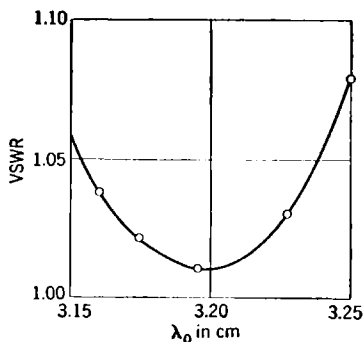


FIG. 5-54.—Performance of a 3-cm spun-bellows assembly with three sections.

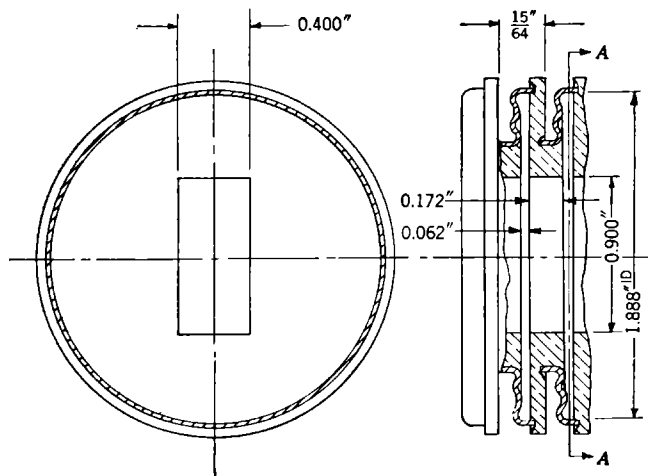


FIG. 5-55.—Typical design of a Cook bellows for rectangular waveguide.

early model are plotted in Fig. 5-54. These are only generally indicative of the performance of bellows of this variety.

The bellows of the second variety¹ consists of two pieces of thin, flexible stock and a partition with a rectangular hole, all of which are assembled as shown in Fig. 5-55. Although the Cook bellows is generally less flexible than the spun bellows, it has several advantages, most of which result from the proper design of the partition. If the partition is

¹ Manufactured by Cook Electric Co., Chicago, Ill.

fairly thick, the breakdown power is higher because of the thicker edge on the rectangular hole. Also, the design of the choke more nearly fulfills the ideal low-impedance-high-impedance condition since the effect of a thick partition is to narrow the first quarter-wavelength section of the choke. Another advantage of this bellows is that they are more rugged than those of the previously mentioned variety.

The Cook bellows are good over a broader band than are the spun bellows, as can be seen from the curve in Fig. 5-56 which shows the voltage standing-wave ratio as a function of wavelength for a recent model of bellows for rectangular waveguide. Tests with a frequency-modulated oscillator indicate that there are serious resonances in one part of the pass band. Bellows of this recent model have not been tested at high power, but tests on earlier models indicated that they could handle a higher pulse power than the spun bellows.

In general, it can be said that bellows are not particularly satisfactory. They are not so flexible as some other types of waveguide, and their pass band is relatively small, not exceeding 6 per cent.

5-20. Open Choke-flange Junctions.—It is sometimes convenient when assembling a system to allow for possible small misalignments in the r-f line components by leaving one of the choke-to-flange junctions open a bit. Although this expediency has been used for some time, it is only recently that detailed measurements have been made to determine exactly what happens in such an open joint. The work was done on chokes of two designs, one for use at a wavelength of 10.7 cm, and the second for a wavelength of about 9 cm. In each case it was found that when the choke and flange were slightly displaced sidewise, relative to each other, and at the same time separated by a small amount, bad resonances occurred. Typical performance is shown in Fig. 5-57 where transmission loss is plotted as a function of the separation Δz of choke and flange for a displacement Δy of 0.125 in. in the direction of the small dimension of the cross section, and a displacement Δx of 0.100 in. in the perpendicular direction. These measurements were made on the first-mentioned choke at a wavelength of 10.4 cm. Similar data were taken for several other values of Δy and Δx , and standing-wave measurements were made under all these conditions. The curves obtained were all similar to the one shown, differing in the magnitude of the peak, and in the position of the peak relative to Δz .

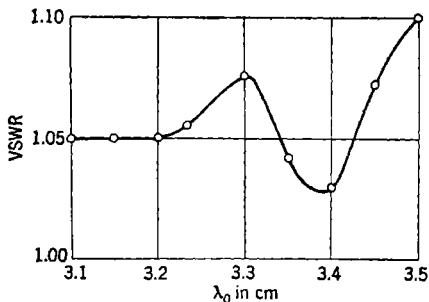


FIG. 5-56.—Performance of Cook bellows for rectangular waveguide.

Some information as to what is happening when these resonances occur can be found by comparing VSWR and transmission curves for a given pair of values of Δx and Δy . One particular pair of curves indicates that where the resonance occurs the voltage standing-wave ratio is about 2.0, and the transmission is about 50 per cent. The power reflection corresponding to a standing-wave ratio of 2.0 is $\frac{1}{3}$, or 11 per cent. Therefore, the other 39 per cent must be either radiation loss or resistive loss in the walls of the resonant cavity which exists between the choke and flange, or, more likely, a combination of the two.

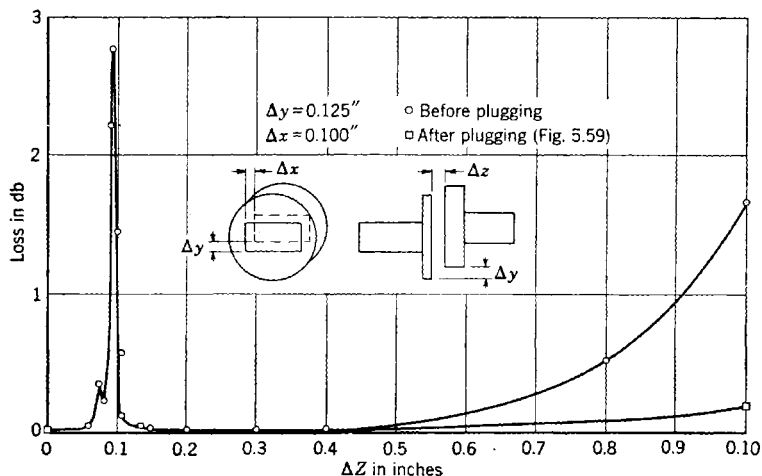


Fig. 5-57.—Transmission loss of 10.7-cm choke-flange junction as a function of separation.

Further information on this effect was found in the process of checking the design of a special open choke junction by the use of Pierce's method.¹ There were a number of positions of the variable short-circuiting plunger where the customary phase shift was observed. These positions were separated in such a way that there seemed to be two sets of positions, one corresponding to radiation in the TE_{10} -mode, the other to radiation in the TE_{30} -mode. When the depth of the choke groove was correct, the TE_{10} -radiation was not noticeable, but the other was still present. The existence of this radiation in the TE_{30} -mode is, of course, to be expected.

If the ordinary choke for rectangular waveguide is now examined, it is found that the choke ditch is actually a section of coaxial line. Because of the symmetry of the electromagnetic field in the rectangular waveguide, the radiation excited in the section of radial transmission line

¹ Specifically, the method using a coaxial-line short-circuiting plunger, as described in Sec. 4-9.

between the waveguide and the choke ditch is predominantly in the TE_{10} -mode; therefore the excitation of the choke ditch is also in this mode, as shown in Fig. 5-58. The depth of the ditch is therefore made a quarter-guide wavelength for the TE_{10} -mode at the design wavelength. If there were no other modes present, no trouble would occur. However, the TE_{30} -mode is also excited in the waveguide. The circumference of the choke ditch is large enough to allow the ditch to propagate radiation in this higher mode. Since the ditch, however, is not far from cutoff for this higher mode, the guide wavelength in this mode is long; therefore, the depth of the ditch is considerably less than $\frac{1}{4}\lambda_g$ for this mode. Consequently, the ditch, instead of presenting an infinite impedance at the top, presents a fairly small impedance, which may be of the order of jZ_0 or less. In series with this impedance, there is the impedance, reflected back to the choke ditch, of the outer edge of the choke-flange joint. The distance from the ditch to the edge of the choke joint is generally something between $\frac{1}{8}\lambda_g$ and $\frac{1}{4}\lambda_g$. Since the impedance at the outer edge of the joint looking out into free space is high, the impedance seen at the edge of the choke ditch will be low, with the imaginary part capacitive.

This capacitance in series with the inductance of the choke ditch forms a series-resonant circuit. It would, therefore, be quite possible to have the resonant condition that has been found. To remedy this trouble, the sections of the choke ditch adjacent to the narrow edge of the waveguide were plugged, as illustrated in Fig. 5-59, which made the remaining arcs of the ditch short enough to prevent propagation of the TE_{30} -mode. This method has been used successfully in every device where trouble had previously been experienced. The performance of a 10.7-cm joint with plugged ditches is shown in Fig. 5-57. The plugged chokes showed no resonances for displacements up to $\frac{1}{2}$ in. in x and y directions. Similar tests have been made of 3-cm chokes. The standard choke coupling showed resonances which were not completely removed by plugging. It is believed that these were caused by reflections from the outer edge of the coupling, which is square, since a round choke having the same internal dimensions showed no resonances after plugging, for displacements of at least $\Delta x = 0.100$ in. and $\Delta y = 0.063$ in.

Since the choke ditch of one of these plugged choke joints is beyond cutoff for the TE_{30} -mode, it presents a very low reactance to radiation

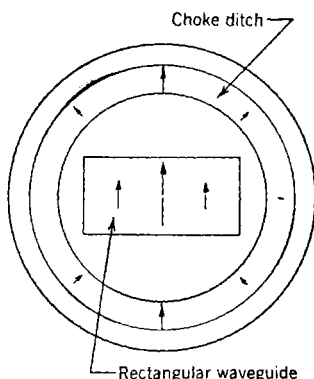


FIG. 5-58.—Excitation of typical choke. The vectors represent electric fields.

waves with great accuracy, and the single-screw tuner has proved adequate for most low-power work.

8-12. Waveguide Double-slug Tuners.—Since a dielectric slug is limited in the amount of reflection that it can introduce, such elements

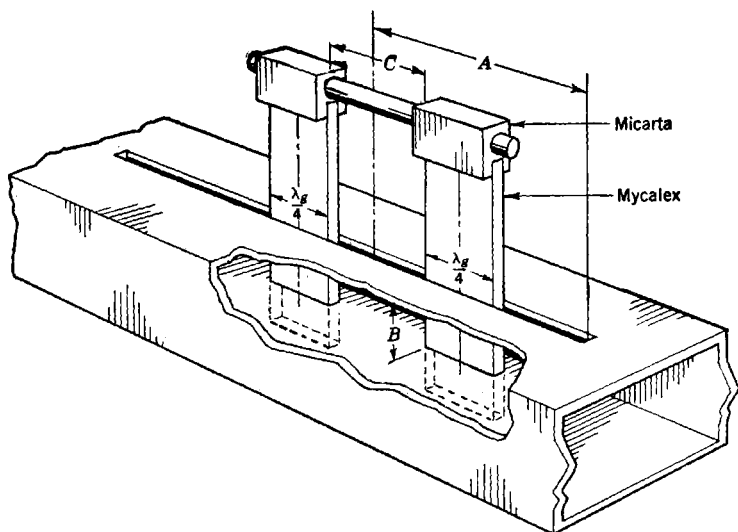


FIG. 8-30.—Mycalex double-slug tuner for waveguide.

may be used in pairs, as shown in Fig. 8-30, to increase the tuning range. The maximum reflection from two slugs $\lambda_g/4$ in length occurs when the

separation C is $\lambda_g/4$ where λ_g is the guide wavelength. The normalized impedances at different points in the tuner section are given in Fig. 8-31. These impedances are obtained by application of the usual transmission-line equation as discussed in Sec. 8-11. If z_1 is the normalized characteristic impedance in the region of the dielectric, then the combination, when followed by a matched line, has an input impedance z_1^4 as

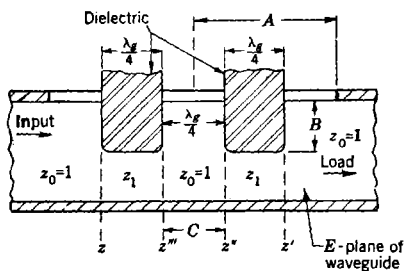


FIG. 8-31.—Normalized impedances in waveguide double-slug tuner. $z' = 1$, $z'' = z_1^2$, $z''' = 1/z_1^2$, $z = z_1^4$.

compared with z_1^2 for a single element.

Tuning is accomplished in either of two ways: (1) by varying the depth of insertion B and the position along the line A of the two slugs together without changing their separation C , or (2) by varying the sepa-

The chief problem in designing the 3-cm vertebrae is to design a choke that can be moved about freely in the immediate vicinity of the flange without producing high standing waves or large losses. The dimensions of the choke ditch are therefore slightly different from those of the ditch in the rigid-line couplings. In the first place, the choke is designed for a separation from the flange of $\frac{1}{16}$ in.; therefore, the ditch is shallower than for a contact joint. Second, since the separation of choke and flange is greater here than in the contact joint, the choke ditch must be made wider in an attempt to preserve the desirable low-impedance-high-impedance condition. If this is done, variations of impedance of the choke-flange junction with wavelength and with distortions, that is, relative motion of the choke and flange, will be minimized. Finally, the sections of the choke ditch adjacent to the narrow edges of the rectangular waveguide are plugged, as described in Sec. 5-20. An example of the improvement of performance resulting from the plugging is shown in Fig. 5-60, in which is shown the loss in a 3-cm vertebral assembly at a wavelength of 3.2 cm, before and after plugging, as a function of the amount of bending in the H -plane. It should be noted here that the resonance trouble is more likely to appear at the shorter wavelengths. In fact, the unplugged vertebrae gave no trouble in the region from 3.3 to 3.5 cm.

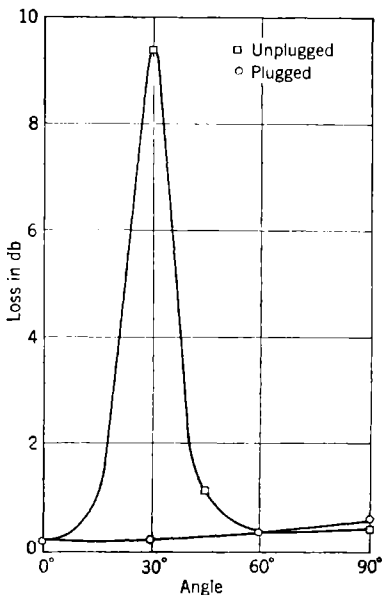


FIG. 5-60.— Comparison of H -bend performance of plugged and unplugged vertebrae at 3.2 cm.

The general construction of a 3-cm vertebral assembly is shown in Fig. 5-61. In Fig. 5-62 are shown details of construction of the disk inserts. The choke-to-flange junctions consist of a series of disks separated $\frac{1}{16}$ in. In each disk is a rectangular hole 0.400 in. by 0.900 in., forming the waveguide. In one face of the disk is the choke ditch. The opposite face of the disk is plane and forms the flange for the next choke-flange joint. The thickness of each disk is such that the distance between successive choke-flange joints is a quarter of the guide wavelength in the undistorted position of the vertebral assembly. Vertebral assemblies are designed to have even numbers of joints so that small

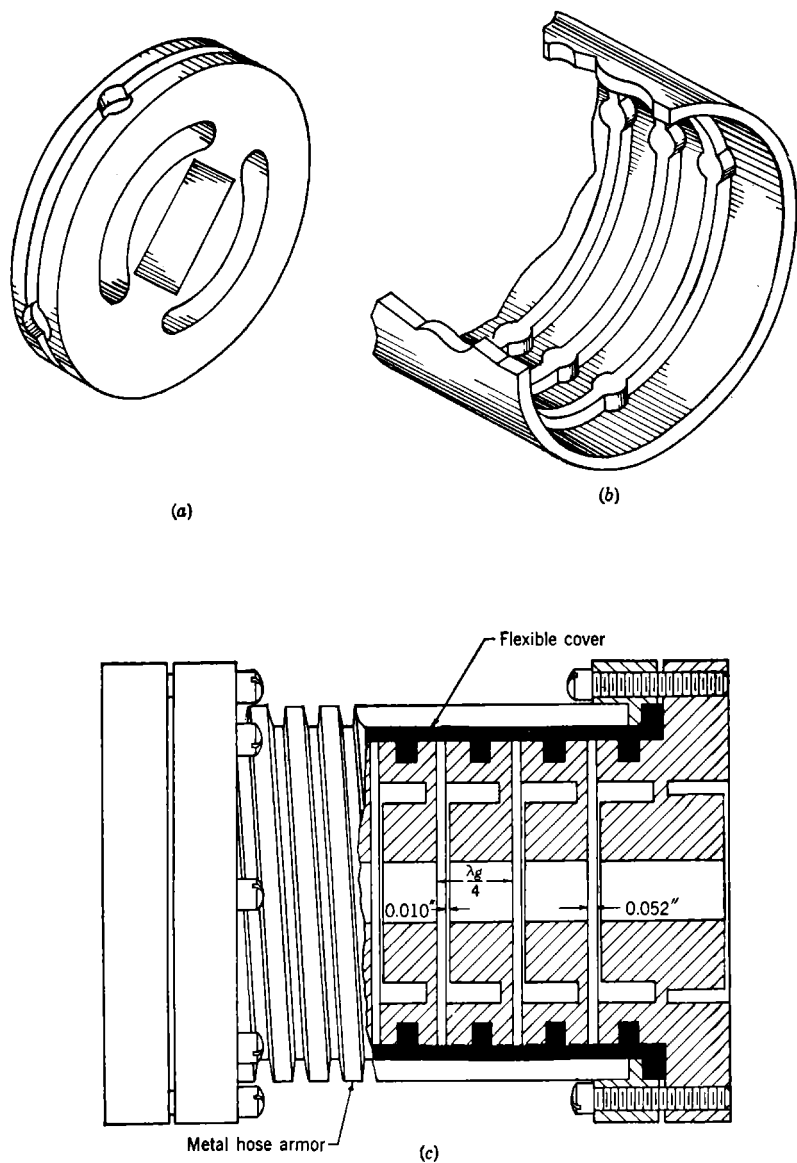


FIG. 5-61.—3-cm vertebrae assembly; (a) is a single choke disk, (b) is the flexible cover, (c) parts assembled.

mismatches in the individual junctions are canceled out. The disks are assembled in a neoprene jacket that serves to hold them in the proper relationship, one to another. This is accomplished by having ribs in the rubber jacket which fit into grooves in the disks.

The vertebral assemblies have end pieces with choke couplings that mate with standard rigid-line flange couplings. Around the outside of the rubber jacket is a flexible metal hose that helps pressurize the assembly by preventing radial expansion of the jacket. Longitudinal expansion must be restrained by the waveguide sections to which the unit is attached. The metal hose restricts the flexibility of the waveguide to a certain extent, but the units can be used without the sheath if extra flexibility is needed and pressurization is not. The 3-cm vertebrae are supplied, at present, in 5- and 9-choke units.

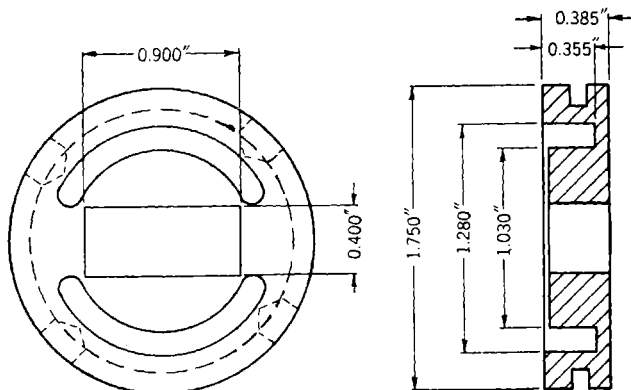


FIG. 5-62.- Disk insert for 3-cm vertebrae.

The loss and standing-wave ratio caused by various distortions of a 9-choke unit at various wavelengths are shown graphically in Fig. 5-63. These data may be summarized as follows: in the range from $\lambda = 3.10$ cm to $\lambda = 3.50$ cm, the waveguide assembly can be (1) twisted 45° , (2) stretched at least 1 in., (3) compressed $\frac{1}{4}$ in., (4) bent in the E -plane 60° , (5) bent in the H -plane 60° , (6) sheared in either plane 1 in.; all this can be done without introduction of a loss greater than 0.5 db or a VSWR greater than 1.10.

The power-handling capacity of the 3-cm vertebrae is adequate for powers in use at the present time. At 250 kw pulse power, 0.8- μ sec pulses, 1300 pps, the same 9-choke unit mentioned above could be distorted at least the following amounts without breakdown: $\frac{1}{4}$ -in. compression, $\frac{1}{2}$ -in. stretch, 1-in. H -plane shear, 45° E - and H -bend, 45° twist. The maximum E -plane shear is $\frac{1}{4}$ in. At 100 kw pulse power this last figure increases to at least 1 in.

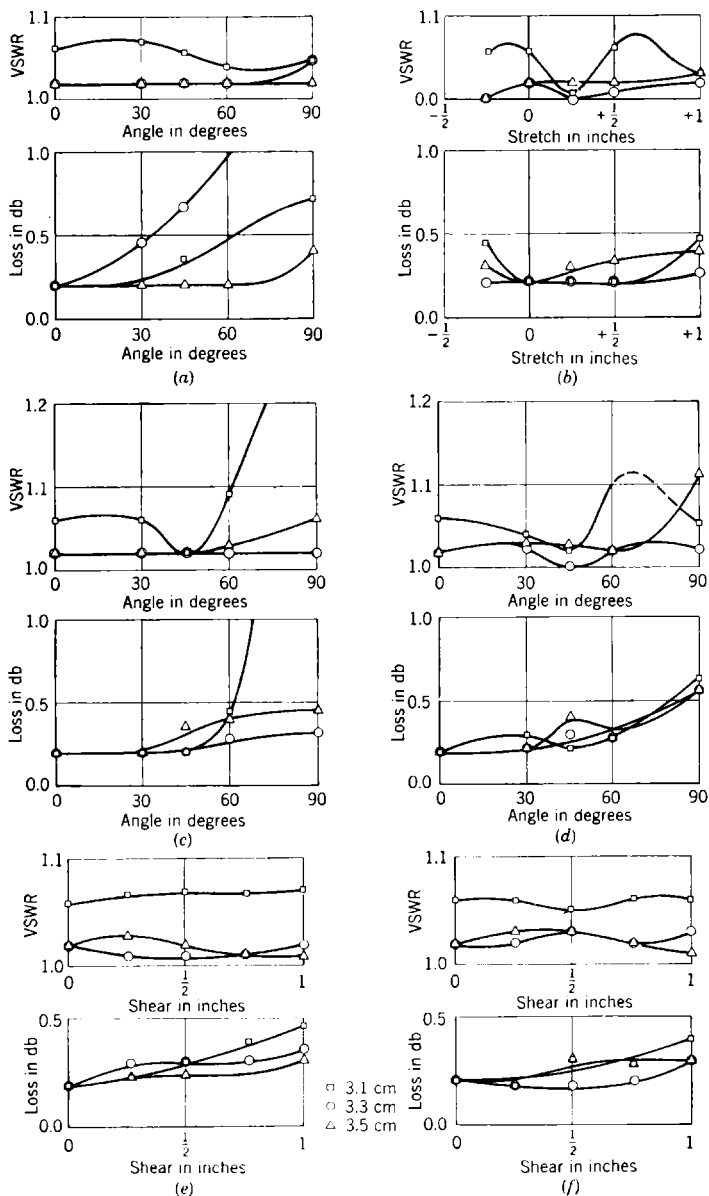


FIG. 5-63.—Loss and SWR for deformations of 3-cm vertebral assembly: (a) twist; (b) stretch; (c) *E*-bend; (d) *H*-bend; (e) *H*-plane shear; (f) *E*-plane shear.

Vertebrae suffer from one disadvantage that is sometimes serious: they have an appreciable amount of r-f leakage. It should be noted that this leakage is small compared with the power transmitted by the vertebrae and is noticeable only when the vertebrae are in an enclosed space or near a sensitive detector or receiver.

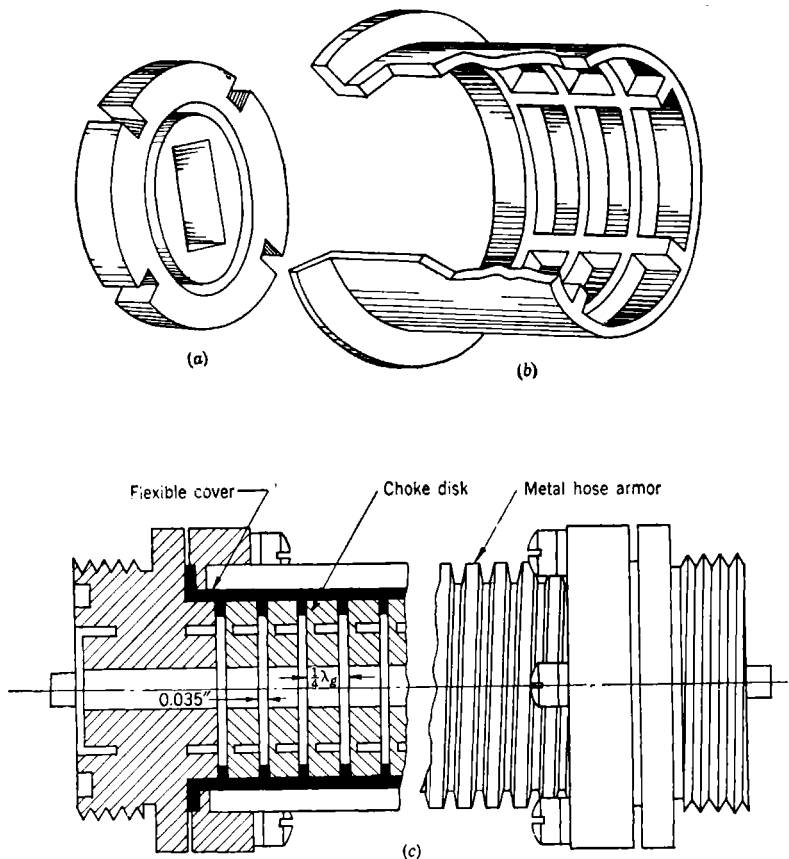


FIG. 5-64.—1-cm vertebral assembly; (a) choke disk, (b) flexible cover, (c) assembly.

The problems involved in the design of the 1-cm vertebrae differ from those of the 3-cm version. In the first place, since only a 4 per cent wavelength band needs to be covered, it is not necessary to plug the choke groove to avoid resonances. In the second place, the ideal diameter of the choke ditch for a choke coupling on the standard 1-cm waveguide would be such that the ditch would cut across the corners of the waveguide. When the ditch is made large enough in diameter to

avoid this trouble, the choke coupling is not well matched. In rigid-line couplings, this mismatch is minimized by making the separation between the choke and the flange small, thus achieving an alternating low-impedance-high-impedance condition. With vertebrae, however,

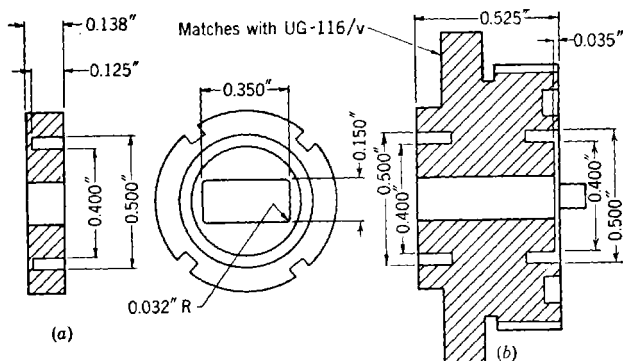


FIG. 5-65.—Details of 1-cm vertebrae; (a) is choke disk, (b) end piece.

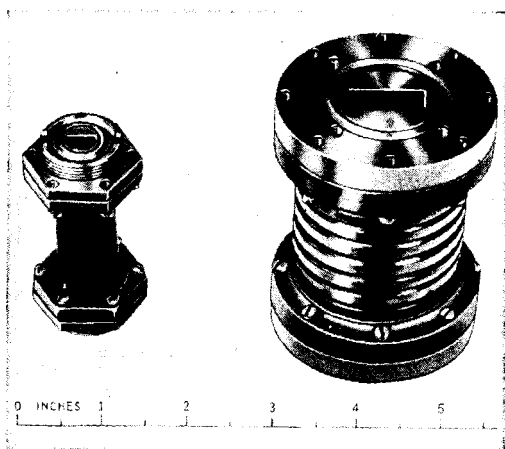


FIG. 5-66.—Typical 3- and 1-cm vertebral assemblies.

this cannot be done; therefore, the design of the choke ditch must be better. The design was improved to a great extent by reduction of the size of the rectangular waveguide within the vertebrae to the point where a choke ditch of nearly the correct diameter could be used. The use of undersized waveguide gave rise to a further problem of matching the vertebrae to standard waveguide. The matching was accomplished by the use of a choke groove of a special size in the connectors on the ends of the assembly; this, of course, required that the end connectors

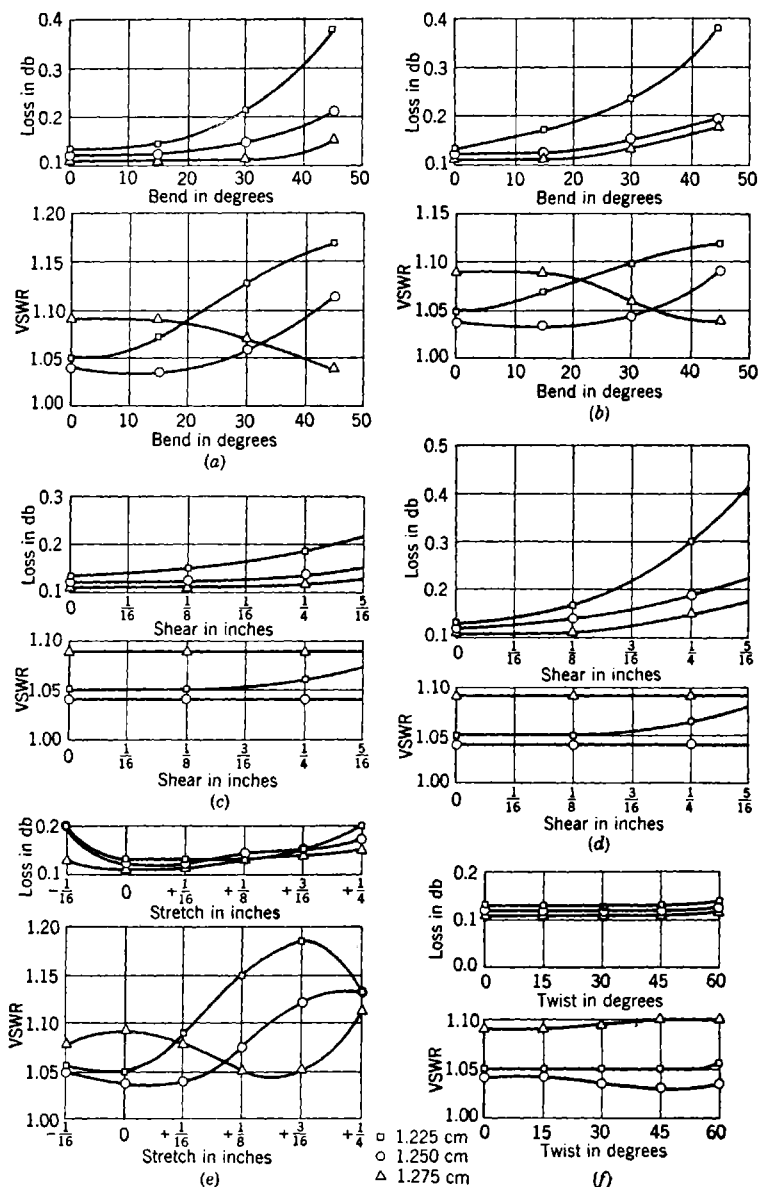


FIG. 5-67.—Loss and SWR for deformations of 1-cm vertebral assembly: (a) *E*-plane bend; (b) *H*-plane bend; (c) *E*-plane shear; (d) *H*-plane shear; (e) stretch; (f) twist.

on the vertebral assembly be chokes and not flanges. A typical vertebral assembly for 1 cm is shown in Fig. 5-64. In Fig. 5-65 are shown details of the disk inserts and the end piece of the vertebral assembly. In Fig. 5-66 are shown typical 3- and 1-cm vertebral assemblies.

Assemblies of 1-cm vertebrae sheathed with flexible metal hose are available. In the 1-cm size the extension force is much smaller than in the larger 3-cm size when used in a pressurized system; therefore, the rubber jacket keeps the extension of the unit down to fairly small values. This size can be considered for pressurizing, if it has the metal jacket to prevent radial expansion. At present 1-cm vertebrae are assembled in units containing 11, 21, and 41 chokes with standard end connectors.

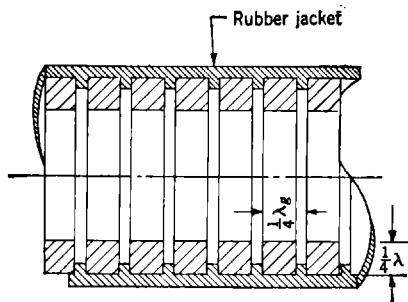


FIG. 5-68.—A possible assembly of TE_{01} -vertebrae.

Also, a small 5-choke unit for a particular alignment application has been made, as well as a 41-choke unit with a special adapter on one end to mate with a standard rigid-line choke.

The voltage standing-wave ratio and loss of an 11-choke unit, under various conditions of distortion, are shown in Figs. 5-67.¹ Experiments on the power-handling capacity of these vertebrae indicate that operation is possible at levels around 100 kw for any distortion that is possible from the standpoint of loss and standing-wave ratio.

This discussion has been concerned only with vertebrae designed for use with rectangular waveguide carrying power in the TE_{10} -mode. Vertebrae can be made also for round waveguide carrying power in the TE_{11} -mode. Vertebrae can also be constructed for use in waveguide in the TE_{01} -mode. In waveguide carrying this mode, the currents in the wall are circular in a plane perpendicular to the axis of the waveguide; therefore, if the waveguide is cut in this plane, no power will leak out of the waveguide, and no choke will be needed. One might expect that a vertebral assembly could be made that uses a series of rings supported in some sort of flexible jacket as shown in Fig. 5-68. This arrangement

¹ E. L. Younker, "An Improved K Band Vertebrae Waveguide," RL Report No. 776, Aug. 25, 1945.

has two faults: first, it requires transitions to rectangular waveguide at the ends if it is to be used in the conventional type of system; and second, as soon as the assembly is bent in any way the asymmetry introduced will allow lower waveguide modes to be generated. As soon as the lower modes, namely, the TE_{11} - and TM_{01} -modes, are present, the circular slots in the waveguide wall will cause large reflections of power and will allow large amounts of power to radiate.

5-22. Summary.—The previous discussion can best be summarized by a brief listing of the various types of flexible waveguide according to the applications to which they are suited.

General Service Unit.—The rubber-covered wound metal hose and rubber-covered Titeflex are to be preferred. In case of emergency, if these are not available, the uncovered varieties of wound metal hose and Titeflex may be used. Their use is not recommended because they are not so strong mechanically, and they deteriorate more rapidly in service, especially when exposed to salt spray or corrosive vapors.

Alignment Section.—For the 1-cm band, the vertebrae are to be preferred at present, partly because of availability. Seamless corrugated waveguide and Titeflex, when they are developed, may be more satisfactory from certain standpoints. For the 3-cm band, the seamless corrugated waveguide is preferable. Uncovered Titeflex is slightly less flexible. Vertebral sections, which are bulkier, may be considered when the bulk does not matter since they have more degrees of freedom than the others. For the 10-cm band, uncovered Titeflex is to be preferred because of its flexibility and general availability. Vertebrae at these wavelengths do not seem to be practical. Seamless corrugated waveguide is under development, and it is not known whether it will be practical in this size. In addition to these, an open choke-flange junction is suitable, if the choke ditch is plugged.

Vibration Section.—At 1 cm, for lengths greater than 8 in., the rubber-covered wound metal hose is preferable. For shorter lengths, the vertebrae are best. At 3 cm, the rubber-covered Titeflex or wound metal hose in the long lengths are good. For short lengths, the vertebrae are satisfactory. Other considerations, such as r-f leakage, will determine which is to be used. On the 10-cm band, about the only type available at present is the rubber-covered wound metal hose. Rubber-covered Titeflex, when it is available, may be preferable because of greater flexibility. An open choke-flange junction with the choke plugged is suitable for small amplitudes of vibration.

Flexure Section.—Any of the types except corrugated waveguide can be recommended at present, the choice depending, among other things, on the sharpness of bending required. The corrugated waveguide may some day be developed to the state where it, too, can be used. The

uncovered varieties of the wound metal hose and Titeflex are, of course excluded.

Pressurized Unit.—On all bands, the rubber-covered wound metal, hose, rubber-covered Titeflex and the uncovered Titeflex can be used. In addition, for the 3-cm band and, it is expected, for the 1-cm band, the corrugated waveguide will be suitable, if certain limitations that have already been mentioned are taken into account. With the same restrictions, vertebrae will be suitable at 1 cm, and perhaps at 3 cm.

Emergency Repair Type.—For emergency repairs of damaged waveguide, where, for instance, a piece of flexible waveguide is to be soldered in the place of a damaged section of rigid waveguide which has been removed, uncovered metal hose or Titeflex can be recommended. Neither is to be considered permanent since each deteriorates rapidly.

CHAPTER 6

TRANSITION UNITS

TRANSITIONS FROM ONE COAXIAL LINE TO ANOTHER

BY G. L. RAGAN

It is frequently desirable to pass from one coaxial line to another without setting up reflections resulting in standing waves. Some of the variations most commonly encountered are these: (1) change of line size with little or no change of diameter ratio or characteristic impedance; (2) change of dielectric (for example, air-filled line to flexible cable), usually with a change of diameter ratio to preserve approximately constant impedance; (3) change of dimension of one conductor only with consequent change of characteristic impedance; (4) combinations of these variations. A discussion of some of the variations associated with the use of coaxial cables was given in Sec. 5-6. A general treatment of the problem will be given in the following sections.

6.1. Tapers in Coaxial Lines.—One of the simplest ways of joining two dissimilar coaxial lines is by means of an intermediate taper section which introduces the change in line characteristics gradually. A simple example of such a taper is given in Fig. 6-1. If the change occurs gradually enough only negligible reflected waves should be generated. To a first approximation this expectation is realized, and indeed the reflected wave approaches zero as the taper length approaches infinity. Frank¹ has shown that the reflection coefficient for a taper of length d within which the line constants are slowly varying is approximately

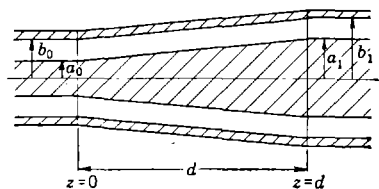


FIG. 6-1.—Coaxial line taper.

$$\Gamma = \frac{1}{4\gamma_0} \left[\frac{d(\ln Z)}{dz} \right]_0 - \frac{1}{4\gamma_d} \left[\frac{d(\ln Z)}{dz} \right]_d e^{-2\int_0^d \gamma dz}, \quad (1)$$

where γ is the propagation constant, Z is the characteristic impedance, and the subscripts 0 and d denote values at the points $z = 0$ and $z = d$.

¹ N. H. Frank, "Reflections from Sections of Tapered Transmission Lines and Wave Guides," RL Report No. 189, Jan. 6, 1943.

Usually the value of the logarithmic derivatives will be discontinuous at the ends of the taper; the values to be used are those just inside the tapered portion.

In applying Eq. (1) it is necessary to obtain expressions for γ and Z in terms of z and then perform the indicated operations. This was done by Frank for the parallel-plate transmission line indicated in Fig. 6-2. An ideal dielectric for which $k_e = 2.56$ fills the output line, and a linear physical taper of the dielectric is used. The over-all VSWR is given as a function of the length by the graph of Fig. 6-2. It is apparent that certain optimum lengths exist. These lengths— $0.8\lambda_0$, $1.2\lambda_0$, and

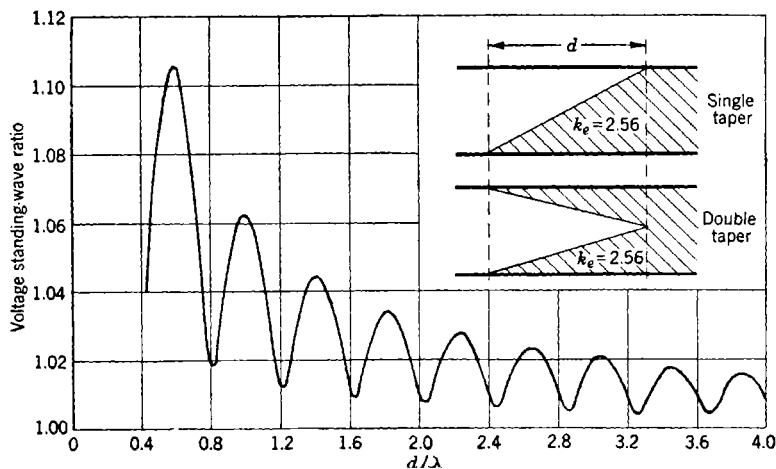


FIG. 6-2.— Voltage standing-wave ratio produced by reflections from a tapered dielectric plug in a parallel-plate transmission line.

so on—are electrically equivalent to integral numbers of half wavelengths, the average wavelength in the taper being reduced, because of the dielectric, to about 80 per cent of that in free space. Lengths equivalent to odd numbers of quarter wavelengths lead to maximum values of VSWR. As the taper becomes longer and longer, the magnitude of the oscillations of the curve decreases and both maxima and minima approach perfect match.

Since the problem just discussed deals with a transmission-line or *TEM*-mode, it applies in the limiting case of a coaxial line whose diameter ratio approaches unity. It would be expected to represent fairly accurately the situation for low-impedance coaxial lines, becoming less accurate as the diameter ratio departs appreciably from unity. The problem of dielectric tapers in coaxial line of higher diameter ratios may be worked out in a straightforward, though somewhat laborious, manner by the application of Eq. (1).

A problem which is much more frequently encountered is that of a taper between coaxial lines both of which are air-filled. In this problem $\lambda_0 = \lambda_d = \epsilon (2\pi/\lambda)$, so that Eq. (1) becomes

$$\Gamma = -j \frac{\lambda}{8\pi} \left\{ \left[\frac{d(\ln Z)}{dz} \right]_0 - \left[\frac{d(\ln Z)}{dz} \right]_d e^{-j\frac{4\pi d}{\lambda}} \right\}. \quad (2)$$

It has been pointed out¹ that if the taper is made in such a way that the function $\ln Z$ varies linearly over the length of the taper, Eq. (2) gives

$$\Gamma = -j \frac{\lambda}{8\pi d} \ln \frac{Z_1}{Z_0} (1 - e^{-j\frac{4\pi d}{\lambda}}). \quad (3)$$

It follows that Γ has the magnitude

$$|\Gamma| = \frac{1}{2} \ln \frac{Z_1}{Z_0} \frac{|\sin \theta|}{\theta}, \quad (4)$$

where $\theta = 2\pi d/\lambda$ is the electrical length of the taper. Equation (4) and the relation

$$r = \frac{1 + |\Gamma|}{1 - |\Gamma|} \quad (5)$$

may be used to determine the VSWR introduced by a given taper. The curve of Fig. 6-3 gives the values of r^2 , the square of the usual VSWR, as a

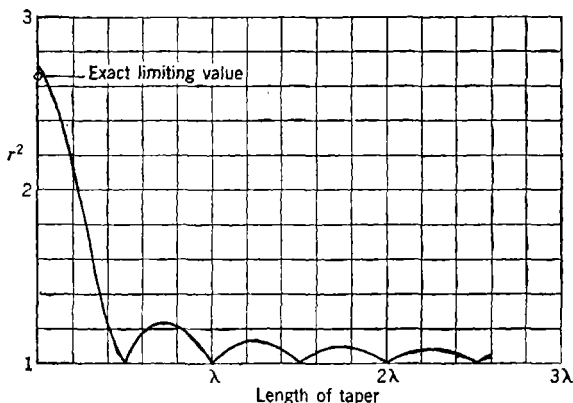


Fig. 6-3.—Standing-wave ratio introduced by tapered section of coaxial line, 75 to 46 ohms. Ordinate is the square of the VSWR.

function of taper length for a logarithmic taper between 46- and 75-ohm lines. The existence of the best taper lengths (integral numbers of half wavelengths) and worst lengths (odd numbers of quarter wavelengths) is evident. The decreasing amplitude of the oscillations of the function

¹ *Microwave Transmission Design Data*, Sperry Gyroscope Co., May 1944, p. 35.

$\sin \theta/\theta$ is also brought out. The "exact limiting value" indicated is not strictly accurate, since there will be a shunt capacity effect at the step in the conductors. This effect is quite important for the usual microwave lines (see Sec. 4-6).

For small values of $|\Gamma|$, Eq. (5) becomes

$$r \approx 1 + 2|\Gamma|. \quad (6)$$

As a matter of fact, Frank points out that the accuracy of Eq. (6) is about the same as that of Eq. (1), both being based on the assumption that only small reflections are present. Substitution of $|\Gamma|$ from Eq. (4) into Eq. (6) gives

$$r \approx 1 + \ln \frac{Z_1}{Z_0} \frac{|\sin \theta|}{\theta}. \quad (7)$$

It should be recalled that Eqs. (3), (4), and (7) and Fig. 6-3 apply only to tapers for which the function $\ln Z$ varies linearly. This may be quite different from the usual taper in which one or both conductors are given a physically linear taper. For tapers involving little change of diameter ratio, the difference between linear logarithmic and linear physical taper is not great, therefore the preceding discussion represents either situation fairly well.

It can be shown that for a linear physical taper, whose dimensions are indicated in Fig. 6-1, the logarithmic derivatives appearing in Eq. (2) are

$$\left[\frac{d(\ln Z)}{dz} \right]_0 = \frac{60}{Z_0 d} \left(\frac{b_1}{b_0} - \frac{a_1}{a_0} \right), \quad (8)$$

$$\left[\frac{d(\ln Z)}{dz} \right]_d = \left[\frac{d(\ln Z)}{dz} \right]_0 \frac{a_0 b_0 Z_0}{a_1 b_1 Z_1}. \quad (9)$$

Both derivatives are identically zero if

$$\frac{b_1}{a_1} = \frac{b_0}{a_0}. \quad (10)$$

This relation implies, of course, a taper of the constant-impedance type. It is evident from Eq. (2) that for such tapers, Γ is identically zero regardless of taper length. For tapers whose length is an integral number of half wavelengths, the exponential factor in Eq. (2) becomes unity, so that Γ is proportional to the difference between the logarithmic derivatives, Eqs. (8) and (9). An inspection of Eq. (9) indicates that equality of the two derivatives results if

$$a_0 b_0 Z_0 = a_1 b_1 Z_1. \quad (11)$$

This relation furnishes a criterion for making reflectionless half-wavelength tapers by giving the proper linear physical tapers to the con-

ductors. To be sure, all the quantities appearing in Eq. (11), involving the dimensions and impedance of the two lines to be joined, are usually specified in a given problem and rarely would they be consistent with Eq. (11). The difficulty is to design reflectionless linear tapers to solve practical problems. It has been suggested¹ that the general problem be solved by using a double taper. The procedure would be: (1) to design an integral half-wavelength taper whose actual dimensions are uniquely fixed by Eq. (11), from one of the given lines to an intermediate line of the same impedance as the second; and (2) to pass directly, by means of a constant-impedance taper whose length is not important, from this intermediate line to the second of the given lines.

It will usually be found more convenient to solve Eq. (11) explicitly for a dimension of the intermediate line, assuming a_0 , b_0 , Z_0 , and Z_1 to be given. The radius b_1 of the outer conductor is

$$b_1 = b_0 \sqrt{\frac{\eta_1 \ln \eta_0}{\eta_0 \ln \eta_1}} \quad (12)$$

where $\eta_0 = b_0/a_0$ and $\eta_1 = b_1/a_1$. It is convenient to choose as a reference line, a line of unit outer-conductor radius b_0 and of diameter ratio $\eta_0 = e = 2.72$. For any other diameter ratio η_1 the outer-conductor radius b_1 is easily determined from Eq. (12) and the corresponding radius $a_1 = b_1/\eta_1$ computed. The result for values of η_1 between 1.5 and 6 is given graphically in Fig. 6-4. It is easily shown that, for any two values of η which may be chosen, the corresponding values of b and a read from these curves satisfy Eqs. (11) and (12). Hence these curves may be considered as giving, on a relative scale, values of b and a to be used in the design of reflectionless half-wavelength tapers between lines of specified diameter ratio (or impedance).

An important fact is at once apparent in Fig. 6-4; namely, that for a taper between lines whose diameter ratios are in the neighborhood of $\eta = e = 2.72$, little change of outer-conductor size is indicated. Fortunately, the lines in common use at microwave frequencies have diameter ratios of about this value; consequently, tapers in which the outer-conductor diameter remains unchanged should be good. Less than 3 per cent change in outer-conductor size is required for any two lines with diameter ratios lying between 2 and 4 (impedances between 42 and 83 ohms).

¹ A. W. Gent and P. J. Wallin, "Impedance Matching by Tapered Transmission Lines," Valve Laboratory Report No. G 78, July 1944. These authors, using a different mathematical method, obtained Eq. (10) and the following modified relation in place of Eq. (11): $a_0 b_0 = a_1 b_1$. A critical comparison of their derivation with that of Frank which led to Eq. (1) seems desirable. Both methods involve certain approximations, and it is not known which analysis leads to the more accurate result.

The frequency sensitivity of coaxial tapers is a matter of considerable importance in some applications. It is convenient to introduce this subject by a consideration of the logarithmic taper to which Eq. (7) applies. If d is chosen equal to an integer n times half the midband

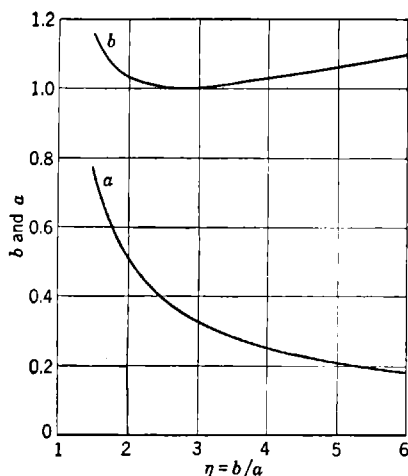


FIG. 6-4.—Design curves for reflectionless half-wave tapers. The vertical scale gives values of b and a on an arbitrary scale.

wavelength λ_0 , it follows from Eq. (7) that the mismatch, defined as $r - 1$, is

$$(r - 1) \approx \ln \frac{Z_1}{Z_0} \left| \frac{\sin \left(\frac{n\pi\lambda_0}{\lambda} \right)}{\left(\frac{n\pi\lambda_0}{\lambda} \right)} \right|. \quad (13)$$

For small departures of the electrical length $n\pi\lambda_0/\lambda$ from the value $n\pi$ which it has at midband, Eq. (13) is well approximated by

$$(r - 1) \approx \ln \frac{Z_1}{Z_0} \left(\frac{\Delta\lambda}{\lambda_0} \right). \quad (14)$$

This approximation to the mismatch is good to about 10 per cent for departures up to about $\pi/4$ in electrical length. In other words, it is this good for values of $\Delta\lambda/\lambda$ less than $1/(4n)$. For half-wavelength tapers ($n = 1$) this amounts to a band of about ± 25 per cent, for one-wavelength tapers ± 12 per cent, and so forth. This result implies, of course, that the full-wavelength taper presents little advantage over a half-wavelength taper for bands narrower than ± 12 per cent. For bands appreciably broader than this, however, the longer taper offers a material reduction in mismatch.

The reflection coefficient for a linear physical taper designed according to Eq. (11) varies in exactly the same way with wavelength as that for a logarithmic taper, since both are determined by Eq. (2) and in both instances the logarithmic derivatives at $z = 0$ and $z = d$ are equal—although the actual value of the derivative for the linear physical taper may be different from that for the logarithmic taper. As a matter of fact, the values will probably be found almost identical in the two types of tapers for most practical problems; this is true at least for the 46- to 75-ohm taper. It does not seem profitable, therefore, to discuss the frequency sensitivity of the linear physical taper. It is possible, however, to state that the discussion of the frequency sensitivity of the logarithmic taper applies here accurately.

6.2. Transformer Sections between Coaxial Lines.—Some general aspects of transformers in coaxial lines have been discussed in Sec. 4.5.

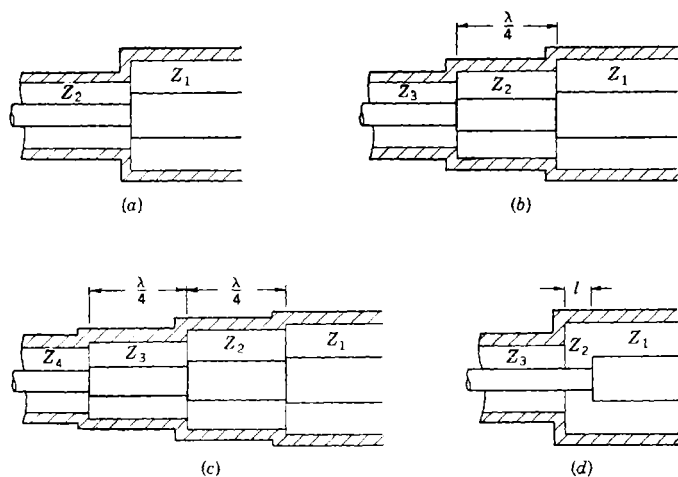


FIG. 6.5.—Coaxial-line transformers.

In the present section specific application of these principles to the problem of joining two coaxial lines will be treated. In addition, the merits of this method of joining coaxial lines as compared with that of using tapers will be considered.

In discussing the use of coaxial-line transformers it is customary to neglect the effect of the discontinuity capacitance arising from the fringing fields in the neighborhood of an abrupt change in the diameter of one or both conductors. It has been pointed out in Secs. 4.5 and 4.6 that this junction effect may be rather large; therefore, it should be taken into consideration if large changes in conductor size occur.

If two lines are joined directly as illustrated by Fig. 6.5a there will

be introduced a VSWR equal to the ratio of the two characteristic impedances, if the junction susceptance B_{12} between Lines 1 and 2 is negligible. If $Z_1 = Z_2$ the only mismatch arising will be that due to B_{12} , but if the steps in conductor diameter are large this mismatch may not be negligible. Furthermore, the restricted space between inner and outer conductors is undesirable and in extreme cases would lead to a complete short circuit. In order to (1) provide impedance-matching, (2) reduce the effect of discontinuity capacitances, and (3) reduce the restriction of the inner-conductor gap, an impedance transformer section or sections such as those shown in Figs. 6-5*b* and *c* may be inserted.

It has been shown in Sec. 2-14 that the condition for matching by means of a transformer of the type illustrated by Fig. 6-5*b* is

$$Z_2 = \sqrt{Z_1 Z_3}. \quad (15)$$

It is easily shown, by means of the transmission-line equation, Eq. (2-41), that if junction susceptances B_{12} and B_{23} exist at the junction of the lines indicated by the double subscripts, exact cancellation of the two susceptances will occur at the design frequency, provided that

$$\frac{B_{12}}{Y_1} = \frac{B_{23}}{Y_3} \quad (16)$$

Ordinarily the values of B_{12} and B_{23} will be found to be so small that they may be safely neglected, but it is advisable to make the steps in conductor size at the ends of the transformer section of comparable magnitude in order to take advantage of a certain amount of cancellation.

The frequency sensitivity of a single quarter-wavelength transformer may be determined rather easily by applying the transmission-line equation. Neglecting B_{12} and B_{23} , the mismatch, defined as $r - 1$, introduced at a wavelength, is approximately

$$r - 1 \approx \frac{\pi}{2} \frac{Z_1 - Z_3}{\sqrt{Z_1 Z_3}} \left(\frac{\Delta\lambda}{\lambda} \right), \quad (17)$$

where $\Delta\lambda$ is the difference between λ and the wavelength for which the transformer is designed. For values of $r - 1$ below about 0.2 and values of $\Delta\lambda/\lambda$ below about 0.2, Eq. (17) gives $r - 1$ to about 10 per cent accuracy.

It is of interest to compare the frequency sensitivity indicated by Eq. (17) with that given by Eq. (14) for a taper. For small changes in impedance between input and output line, Eq. (17) may be written

$$(r - 1) \approx \frac{\pi}{2} \frac{\Delta Z}{Z} \frac{\Delta\lambda}{\lambda}, \quad (18)$$

while, with the same restriction, Eq. (14) for a taper becomes

$$(r - 1) \approx \frac{\Delta Z}{Z} \frac{\Delta \lambda}{\lambda_0}. \quad (19)$$

It is readily seen that the mismatch introduced by the transformer is larger by the factor $\pi/2$.

A greatly decreased frequency sensitivity may be achieved by using a two-section transformer of the type represented by Fig. 6-5c. This design also presents another desirable feature, which is especially important if large changes of line size or impedance are required; namely, the diameter changes are divided among three steps rather than two. Slater¹ gives a good explanation of the decreased frequency sensitivity afforded by multiple-section transformers. He points out that in order to obtain this low frequency sensitivity the impedances should be chosen to satisfy the relation

$$\left(\frac{Z_1}{Z_2}\right)^2 = \left(\frac{Z_2}{Z_3}\right) = \left(\frac{Z_3}{Z_4}\right)^2. \quad (20)$$

If the junction susceptances are sizable, it seems advisable to arrange the conductor steps in such a way that the susceptances will satisfy the relation

$$\frac{B_{12}}{Y_1} = \frac{B_{23}}{2\sqrt{Y_1 Y_4}} = \frac{B_{34}}{Y_4}. \quad (21)$$

This arrangement gives cancellation at the design wavelength, and a line of reasoning similar to that of Slater concerning frequency sensitivity leads one to favor such a relation.

It may be shown by a tedious calculation using the transmission-line equation that the mismatch in the input line is given, for the two-section transformer, by

$$(r - 1) \approx \frac{\pi^2}{4} \frac{Z_1 - Z_4}{\sqrt{Z_1 Z_4}} \left(\frac{\Delta \lambda}{\lambda}\right)^2. \quad (22)$$

The accuracy of the approximation is about the same as that of Eq. (17) under the same restrictions.

A comparison of the frequency sensitivity of a taper, single-section transformer, and two-section transformer is given by Fig. 6-6. The quadratic behavior of Eq. (22) makes the two-section transformer superior over the wavelength range presented. It is, of course, expected that the taper would give the best results for very broad wavelength ranges.

In the event that the two lines joined have the same impedance but different diameters, a short transformer section of the type indicated in Fig. 6-5d is sometimes useful. The conductors are displaced axially

¹ J. C. Slater, *Microwave Transmission*, McGraw-Hill, New York, 1942, p. 57.

by a distance l which is chosen in order that the susceptances B_{12} and B_{23} may be compensated for by the transforming action of the short section of line of high impedance Z_2 . It is well known that the insertion of a section of high-impedance line, the length of which is short compared to a wavelength, gives an inductive effect. The two capacitive junction susceptances and inductive-line section are spaced so closely together in terms of wavelengths that they cancel in a manner approximating lumped-circuit behavior. The length l may be easily determined experimentally; it would be rather difficult to calculate accurately because of the large interaction between the junctions. It is sometimes found

desirable to fill the line Z_2 with a dielectric supporting material that decreases the impedance Z_2 , thus rendering it less inductive for a given length.

There are of course endless variations of the transformers that have been presented here. In particular, there are special cases in which either inner or outer conductors are the same size in the

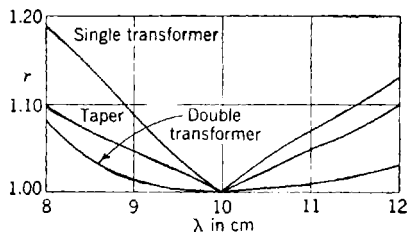


FIG. 6-6—Wavelength sensitivity of 75- to 46-ohm transitions.

two lines to be joined. The use of dielectrics in one or more of the lines or transformer may be required or may be found desirable.

In neither this section nor in the preceding section on tapers were experimental results or actual designs presented. It did not seem profitable to do so, since the principles of design, the dimensions required, and the equations giving performance characteristics are quite reliable and complete.

TRANSITIONS FROM COAXIAL LINE TO WAVEGUIDE

BY F. L. NIEMANN

6-3. The Transition Problem.—In microwave transmission lines it is frequently desirable and often necessary to change from waveguide to coaxial line. Many components, such as duplexers, bridge circuits, and antenna feed horns, are more easily constructed in waveguide. However, many microwave oscillators have coaxial output terminals; also, it is frequently more convenient (at longer wavelengths, for example) to produce a symmetrical field for application to rotary joints by the use of the coaxial mode. Except in special applications, not to be treated here, the problem is to provide for a transition between the principal coaxial TEM -mode and the dominant TE_{10} -mode in the rectangular guide. The field configurations for these modes are shown in Figs. 6-7a and b. The basic methods for exciting this waveguide mode with a

coaxial line can be used in different arrangements to excite one of the modes of higher order, if desired.

The fundamental way of establishing a desired mode in a waveguide is the excitation of either the electric or the magnetic field identified with

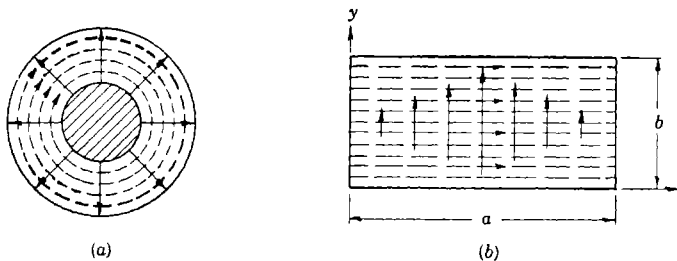


FIG. 6-7.—Field configurations for lowest coaxial-line and waveguide modes; (a) the principal or $TEM = coaxial$ mode; (b) the dominant or TE_{10} -waveguide mode. The E -lines are solid; the H -lines are dashed. The direction of propagation is into the page.

that mode. This is done either by means of an “antenna” element parallel to the electric field, or by means of a loop, the plane of which is normal to the magnetic field. An example of each of these methods for the TE_{10} -mode in waveguide is shown in Fig. 6-8. Although each type has had some application, transitions based on the waveguide antenna for electric coupling are much more widely used at present.

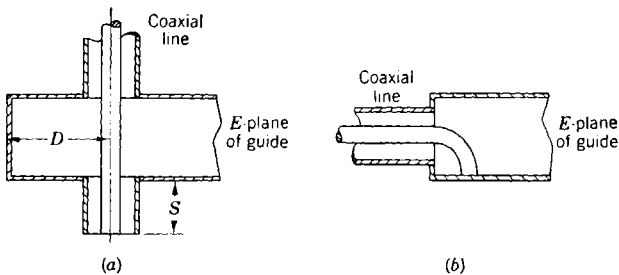


FIG. 6-8.—Basic methods of coupling from coaxial line to waveguide for the lowest modes; (a) crossed transition for excitation of the electric field; (b) loop transition for coupling to the magnetic field.

The crossed transition from coaxial line to waveguide is treated theoretically by Slater,¹ who has shown that a transition of this type can be matched by variation of the end-plate and coaxial-plunger positions, dimensions D and S of Fig. 6-8. In particular, the coaxial stub constitutes a variable reactance in series with the waveguide antenna (that

¹ J. C. Slater, *Microwave Transmission*, McGraw-Hill, New York, 1942, Chap. VII.

portion of the coaxial center conductor which extends across the guide); and, by means of variations in the length of the short-circuited section of guide, it is possible to adjust the radiation resistance of this antenna. It is possible, therefore, to make the reactance of the antenna zero and its resistance equal to the characteristic impedance of the coaxial line whenever this is less than twice the characteristic impedance of the waveguide. This limit holds for transitions in which the coaxial line is centered on the wide side of the guide.

Other theoretical treatments¹ give methods for calculating the dimensions which will match the transition. These are, however, much more easily obtained experimentally as will be shown later.

A modified version of this transition, in which the center conductor of the coaxial line extends only part way into the guide (the probe transition), has also been treated theoretically, and to some extent experimentally, by Slater.² Since this has proved one of the more successful types of transition, it will be treated in detail later. Both the crossed coaxial-line-to-waveguide transition and the probe transition have been used for the excitation of the TE_{11} -mode in round waveguide.³

Heretofore, the magnetic coupling has been given little theoretical study and the types of electric coupling used in modern practice are different from the crossed coaxial-line-to-waveguide transition which has been treated theoretically. Therefore, the purpose here is to describe the transitions most used today and to present, in terms of transmission-line concepts, the experimental techniques used in designing them and in matching them over comparatively broad wavelength bands.

In practice it has usually been necessary to provide a transition from one of the standard coaxial lines, having an impedance of about 50 ohms, to one of the standard rectangular waveguides used at 3 or 10 cm. Thus, the impedance of the line or guide itself is seldom used as a factor in impedance-matching. In all standard transitions the characteristic impedance of the coaxial line is well within the limit required for matching; that is, it is considerably less than twice that of the rectangular guide.

The transitions to be described are as follows:

1. Transitions from waveguide $1\frac{1}{2}$ by 3 in. OD at a wavelength of 10 cm to coaxial lines of sizes

¹ S. Kuhn, "The Coupling between a Rectangular Waveguide Carrying an H_{01} -Wave and a Concentric Line," Admiralty Research Establishment Report M439, Haslemere, Surrey, England, September 1942.

² J. C. Slater, "Properties of the Coaxial-Waveguide Junction in the 725-A and 2J51 Output," BTL Memorandum 44-180-4, November 1944.

³ "The Coaxial to Wave Guide Transformer," British Royal Society Report G8/102/W. D. Allen, January 1942.

- a. $\frac{1}{2}$ in. OD
 - b. $\frac{7}{8}$ in. OD
 - c. $1\frac{1}{4}$ in. OD
 - d. $1\frac{5}{8}$ in. OD.
2. Transitions from waveguide $\frac{1}{2}$ by 1 in. OD and waveguide $\frac{5}{8}$ by $1\frac{1}{4}$ in. OD at a wavelength of 3 cm to coaxial lines of sizes
- a. $\frac{1}{2}$ in. OD
 - b. $1\frac{5}{8}$ in. OD.

A discussion of these transmission-line dimensions and the factors governing their choice is to be found in Chap. 4.

6.4. Matching Techniques.—Since the techniques for matching transitions from coaxial line to waveguide are applicable to all types, they will be discussed separately, with examples for which detailed development data are available. The theory of impedance-matching at microwave frequencies is discussed in Chap. 2. The necessary experiments consist of measuring the magnitude and phase of the standing waves set up by reflections from the transition as an element in a transmission line terminated in a matched load. Measurements may be made either in the coaxial line or in the waveguide. However, measurements in the waveguide are preferable because the final matching may then be done by means of an iris which affects the power-handling capacity of the unit less than does a coaxial transformer. From measurements in the guide, the sizes and positions of these irises may be calculated very accurately. Measurements in the coaxial line necessitate the experimental determination of the iris dimensions or the use of a coaxial transformer which further limits the breakdown power of the coaxial line.

By the use of the Smith impedance (or admittance) chart, the data from these standing-wave measurements may be plotted in terms of the associated reflection coefficients and their phase angles. This chart also presents the real and imaginary components of the normalized impedance of the discontinuity represented by the transition. Contours of constant resistance (or conductance), and contours of constant reactance (or susceptance) appear as arcs of circles on such a chart. So it is possible, by the measurement of the voltage standing-wave ratio and the position of a voltage minimum and by the performance of the proper transformations on the Smith chart, to obtain the impedance at any desired reference plane between the point of measurement and the transition. Usually impedances are referred to the plane of the coaxial line (for example, in right-angle transitions) for measurements in the waveguide and to the end of the coaxial line at the inside surface of the waveguide wall for measurements in the coaxial line. Plots of the impedances or, more often, the admittances as functions of the transition dimensions

and as functions of wavelength, show how the dimensions must be varied to produce a match and how the impedance will vary with the wavelength.

6-5. Narrowband Matching.—The matching of these transitions, when the sizes of the coaxial line and the waveguide are fixed, is accomplished in one of two ways. The dimensions within the transition may be varied, such as the position of the waveguide short circuit (end plate), the coaxial stub length, or the loop size or probe depth, depending upon the type of transition to be used. Thus, it is usually possible to obtain sufficient variation of both conductance and susceptance to match the transition at nearly any wavelength for which both the coaxial line and

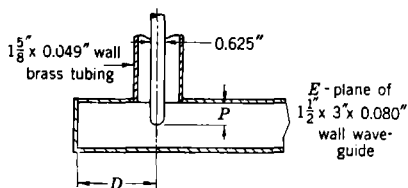


Fig. 6-9.—Probe transition for $1\frac{5}{8}$ -in. coaxial line to waveguide.

the waveguide support their lowest modes. This is called "narrowband" matching in contradistinction to the second method; in the latter, the transition is adjusted to have a certain type of variation of admittance with wavelength (generally not matched), which may then be matched over a considerably wider band by means of a

transformer or, more often, a waveguide iris. This is called "broadband" matching and will be discussed in detail later.

In microwave systems, the application for which a component is intended determines the wavelength band over which the component must operate and the quality of impedance match which is required over this band. In receiving systems, the primary consideration is that of power loss. In transmitting systems the requirements are more stringent because reflections from an impedance mismatch which produce negligible power loss may seriously affect the operation of the oscillator or some other r-f component. Since the components described here are used either for transmitting alone or for transmitting and receiving, only small reflections can be tolerated. The usable bandwidth of a component is therefore defined as the wavelength range over which the voltage standing-wave ratio caused by reflections from that component is 1.10 or less. The limit of 1.10 is imposed for design purposes; it is usually necessary to allow voltage standing-wave ratios as high as 1.15 on production models.

The development of the probe transition from $1\frac{5}{8}$ -in. coaxial line to waveguide,¹ shown diagrammatically in Fig. 6-9, provides an example of the narrowband matching technique. Figure 6-10 is an enlarged section of a Smith chart on which is plotted the admittance of this

¹ M. Clark, Jr., "Coupling between $1\frac{5}{8}$ -in. Coaxial Transmission Line and $1\frac{1}{2}$ -in. \times 3-in. Waveguide," BS Thesis, M.I.T., January 1943.

transition, at a wavelength of 10.92 cm, for different end-plate positions and probe depths. Measurements were made in the waveguide and admittances are referred to the center of the coaxial line. At this point, variations in the end-plate distance appear as almost purely susceptive changes in the admittance. Variations in probe depth change both the conductance and susceptance at roughly the same rate.

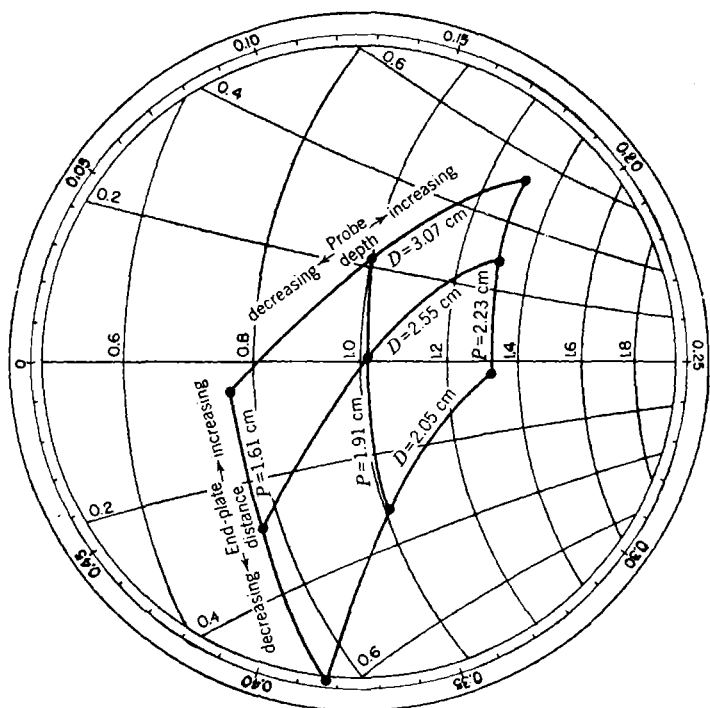


FIG. 6-10.—Admittance as a function of dimensions for probe transition from $1\frac{5}{8}$ -in. coaxial line to waveguide, measured in guide, plotted at the center of the coaxial line. D = end-plate distance, P = probe depth, $\lambda = 10.92$ cm.

These measurements show that the dimensions for best match, at a wavelength of 10.92 cm, are 2.55 cm for the end-plate distance measured to the center of the coaxial line, and 1.91 cm for the probe depth measured from the inside of the guide to the end of the probe. It is also possible to estimate from these data the tolerances necessary to keep the mismatch below a certain limit; for example, the unit will have a voltage standing-wave ratio of less than 1.05 for a variation in the end-plate distance of ± 0.093 cm (0.037 in.). However, since several dimensions may vary in any unit, design tolerances should be considerably smaller than this.

Figure 6-11 is a Smith-chart plot which shows the variation of the admittance with the wavelength for this transition when it has the dimensions for best match at the 10.92-cm wavelength. The resulting voltage standing-wave ratios at the different wavelengths are plotted in Fig. 6-12. By measurements over a range of wavelengths, the dimensions for the best match at any particular wavelength in the 10- to 11-cm region can be determined. Figure 6-13 gives the end-plate distance for best match as a function of the wavelength for which the match occurs.

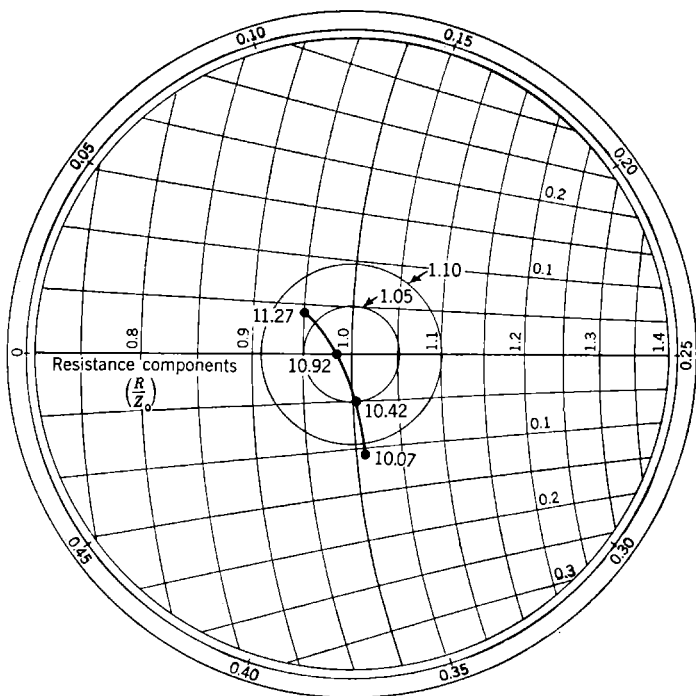


FIG. 6-11.—Admittance as a function of wavelength for the probe transition from $1\frac{5}{8}$ -in. coaxial line to waveguide matched at 10.92 cm; measured in guide, plotted at center of coaxial line.

Practically no variation of probe depth is required to obtain best match in this wavelength range. The value of 1.87 cm given for this dimension is the average of values having variations less than ± 0.05 cm which are hardly significant.

In this method, which utilizes variations of two dimensions to produce an impedance match at a single wavelength, the resulting bandwidth is determined by the characteristics of the transition at that wavelength. For the case in which the end plate is less than a half guide wavelength

from the probe, there is but one combination of end-plate distance and probe insertion which will match the transition at a given wavelength. The impedance of the short-circuited section of waveguide is, of course, the same, if the length of the section is increased by some integral multiple of half guide wavelengths. However, such an increase in the end-plate distance serves only to increase the frequency sensitivity of the transition. Additional parameters must be used, therefore, to increase the bandwidth.

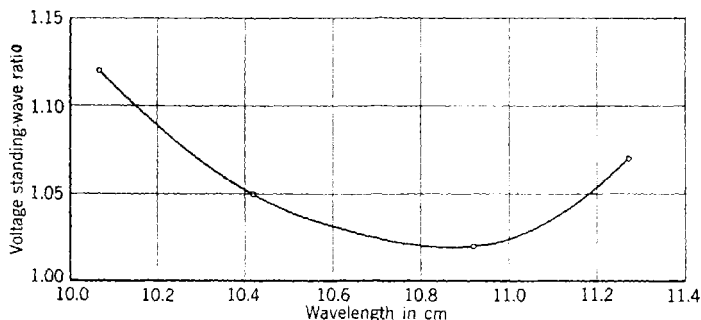


FIG. 6-12.—Voltage standing-wave ratio vs. wavelength for probe transition from $1\frac{1}{8}$ -in. coaxial line to waveguide.

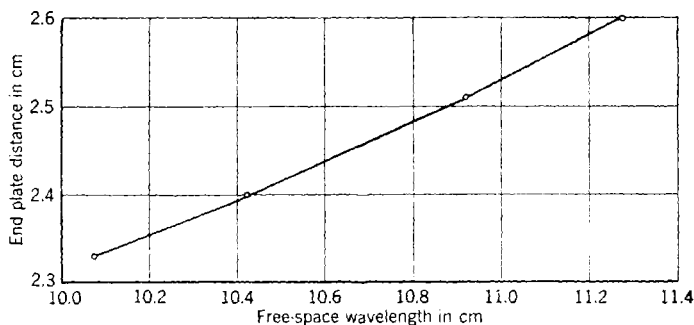


FIG. 6-13.—End-plate distance for best match as a function of wavelength for the probe transition from $1\frac{1}{8}$ -in. coaxial line to waveguide; probe depth 1.87 cm.

An investigation has been made of the effect upon frequency sensitivity of terminating the probe in a sphere. Spheres of different diameters were attached to the end of the probe and the frequency sensitivity of the transition as a function of sphere diameter was measured. The transition becomes more frequency-sensitive as the diameter is increased, although the effect is small for spheres of diameters up to about 1.2 times that of the coaxial center conductor. From this result, together with results obtained with other transitions to be discussed, it appears that the larger the object in the region of the transition, the greater is the

frequency sensitivity when the transition is matched by varying only two parameters. For this reason, at a given midband wavelength, the probe transition inherently covers a broader band than do other types of transitions having the same impedance discontinuity between the coaxial line and the guide. However, this type of transition has certain disadvantages; it has been replaced in many applications by other types which, although having inherently a smaller bandwidth when matched by the two-parameter method, can be matched over wide bands by the method to be described next.

6-6. Broadband Matching with Waveguide Irises.—There are several ways in which the impedance characteristics of a transition may be altered by the variation of more than two parameters: for example, by placing the coaxial line off-center, by using dielectrics, by changing the shape of the short-circuited waveguide section, and by matching with coaxial stubs. Nearly all of these methods have been developed experimentally for special applications. The broadband matching described here is a systematic method which has been applied successfully to several types of transitions and is, therefore, of more general interest.

This method utilizes several important impedance properties of these transitions and of waveguide obstacles in general. In discussing these properties, it should be recalled that the use of a Smith chart involves a polar plot of the magnitude and phase of the reflection coefficient associated with a given admittance or impedance. These two quantities are uniquely specified by that admittance or impedance. On the Smith chart they are plotted in terms of the voltage standing-wave ratio and the distance in wavelengths from a voltage minimum (admittance maximum or impedance minimum) to the desired reference plane. The chart also gives the values of conductance and susceptance components of any admittance. Admittance plots are used exclusively in this discussion because the broadband matching techniques presented involve the application of shunt susceptances.

The procedure in this method is applicable to a transition which has been, or can be, matched by the two-parameter variation method described in the last section. The admittance as a function of wavelength over the desired band is determined for different values of these two parameters. This permits the adjustment of the transition admittance to have certain desired characteristics. The transition is then mismatched to a voltage standing-wave ratio between 1.5 and 2.0 and to an admittance function having the proper distribution in phase, to be described later. By performing transformations on the Smith chart of this admittance-vs.-wavelength function, it will be possible to find a point some distance along the line from the transition toward the generator at which the admittance is nearly constant over the desired wavelength

range. If this point occurs near the circle of unity conductance on the chart, as can be arranged by a proper initial mismatch of the transition, a waveguide iris or other susceptance can be used at this point to match the transition over the entire band. Further, it is sometimes possible, with the proper initial spread of voltage standing-wave ratios with wavelength, to secure a reduction in this spread by making use of the variation with wavelength of the susceptance of the matching element.

To illustrate the application of this technique, the development of the crossbar transition from $\frac{7}{8}$ -in. coaxial line to waveguide shown diagrammatically in Fig. 6-14, will be presented in some detail. This is essentially a modification of the probe transition, but it can be built more accurately and will carry more power than one of the probe type. Since

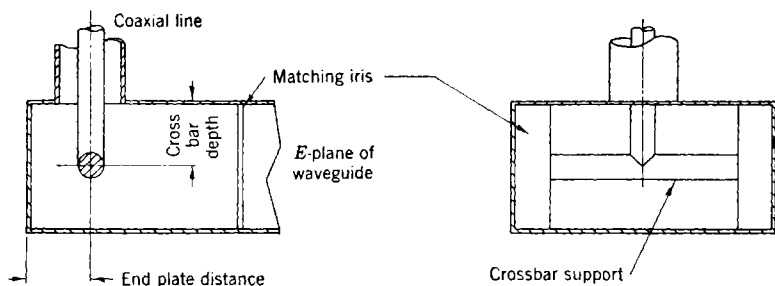


FIG. 6-14.—Crossbar transition from coaxial line to waveguide. End-plate distance and crossbar depth are indicated.

it has been matched by both the narrowband and the broadband methods, it provides a comparison of the results obtained by these two techniques.

In Fig. 6-15 is plotted the admittance as a function of wavelength, for this transition, for different combinations of end-plate and crossbar positions. These dimensions are first adjusted roughly to give a voltage standing-wave ratio of less than 2.0 over the band desired (10.3 to 11.1 cm) and Curve 1 is plotted. Increasing the end-plate distance by 0.080 in. produces the admittance function, Curve 2. Next, increasing the crossbar insertion 0.030 in. gives Curve 3. By a slight further adjustment of both of these parameters the properly centered narrowband match plotted in Fig. 6-16 results. This design has a VSWR of less than 1.05 for a 2 per cent band centered at 10.7 cm. In matching over a broad band, of course, this intermediate step, used as an illustration of the narrowband method, is not necessary. It is presented for the purpose of comparing the methods. The transition can be adjusted directly to have the admittance function represented by Curve 5, Fig. 6-15.

In mismatching the transition so that the admittance-vs.-wavelength function moves from Curve 3 to Curve 5, Fig. 6-15, an important property

of these transitions is seen. A comparison of these curves shows that, although there is considerable change of admittance with changes in the dimensions of the transition, the general distribution and relative orientation of points on the curves is little changed by these variations in dimensions. This is true, at least, when the admittance function lies in the region near match as obtained by the two-parameter variation method. In other words, to a first approximation, for comparatively

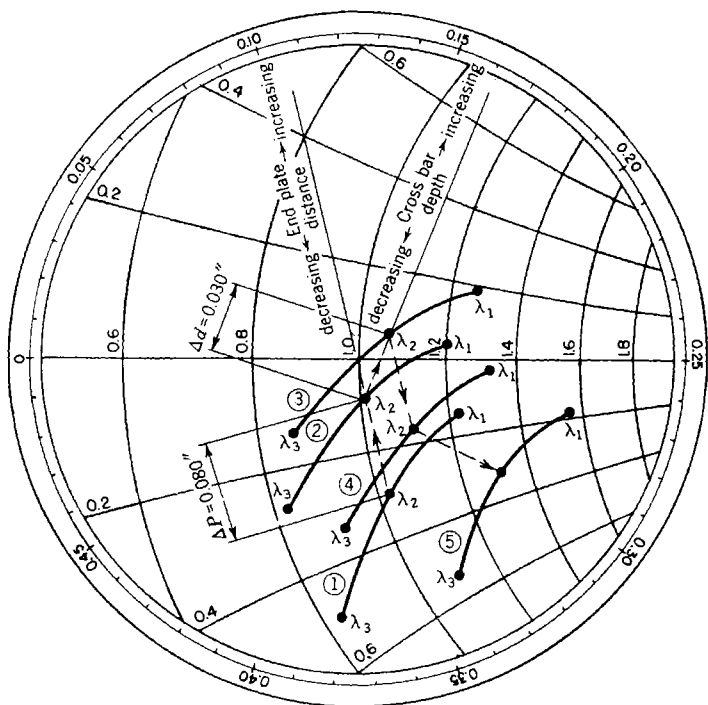


FIG. 6-15.—Admittance of crossbar transition from $\frac{7}{8}$ -in. coaxial line to waveguide as a function of wavelength and dimensions; admittance measured in guide and referred to center of coaxial line; $\lambda_1 = 10.3$ cm, $\lambda_2 = 10.7$ cm, $\lambda_3 = 11.1$ cm.

small changes in dimensions, the dispersion of admittance with wavelength is relatively independent of the dimensions. This means, however, that the dispersion with wavelength of the standing-wave ratio and reflection phase angle as plotted on the Smith chart can be greatly reduced, simply by mismatching the transition as shown. This may be seen by comparing the spread of these two quantities with the wavelength in Curves 3 and 5.

When the characteristic is that given by Curve 5, the transition is no longer matched, but the variation with wavelength of both the magni-

tude and phase of the reflection is considerably reduced. The curve for the admittance as a function of wavelength does not change appreciably in either size or shape in going from the matched to the mismatched condition. Thus, it is possible to obtain a reduction in the variation with wavelength of either the voltage standing-wave ratio or the reflection phase angle or both, depending upon the orientation of the admittance function and the direction on the Smith chart in which the mismatch

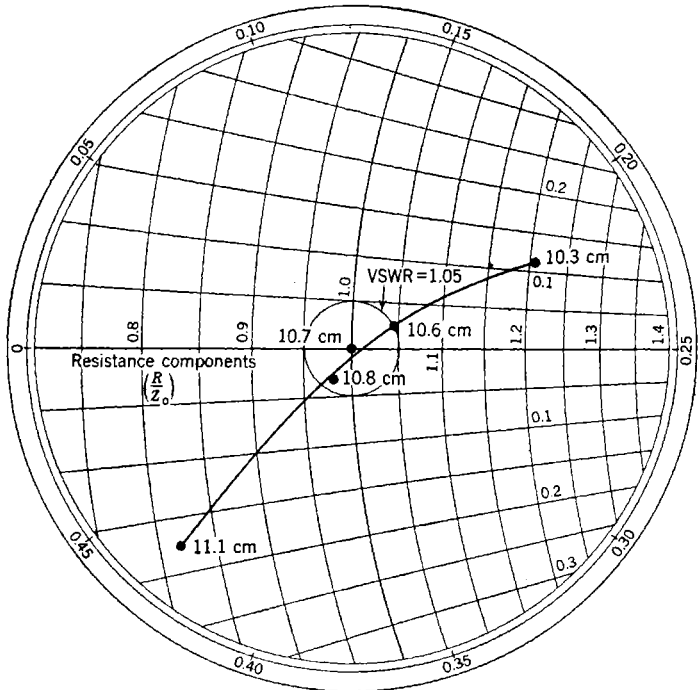


FIG. 6-16.—Admittance of narrowband $\frac{1}{4}$ -in. coaxial-line crossbar transition measured in guide and referred to center of coaxial line.

occurs. However, it will appear in the following discussion that there are only certain ways in which the transition may be mismatched to permit broadband matching by the addition of a properly placed shunt susceptance.

The second property utilized in this method is quite familiar and is characteristic of all transmission lines with reflecting discontinuities. It is essentially true that in transforming impedances along the line by rotation about the center of a Smith chart, a given physical length of line represents more rotation on the chart at short wavelengths than it does at longer ones. If the transition is mismatched in the proper manner

for broadband matching, it will have an admittance-vs.-wavelength characteristic similar to that represented by Curves 5 in Figs. 6-15 and 6-17. Since these admittances are referred to the plane of the junction from measurements in the waveguide, they may be transformed along the guide toward the generator in the usual way (by rotation of the points clockwise about the center of the chart), the differences in guide wavelength being taken into account. If the admittance at midband (10.7

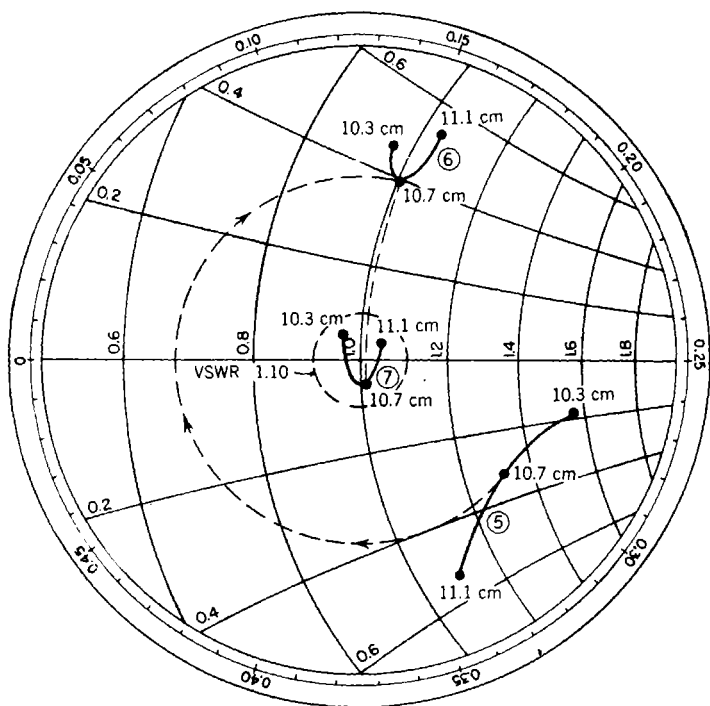


FIG. 6-17.—Broadband matching of $\frac{1}{8}$ -in. coaxial-line crossbar transition. Curve 5: admittance at center of coaxial line measured in guide. Curve 6: calculated admittance in guide at position for iris $0.339 \lambda_g$ at 10.7 cm toward generator from coaxial line. Curve 7: calculated admittance at same point with inductive window of $B = 0.45$ at 10.7 cm.

cm) is transformed as shown on Curve 6, Fig. 6-17, until it falls near the curve of unity conductance on the positive (capacitive) susceptance side of the chart, a shunt inductive susceptance such as a waveguide iris may be added at this point to match the transition for this wavelength. However, the physical distance corresponding to this electrical transformation represents a larger fraction of a guide wavelength (more rotation) at 10.3 cm, and a smaller fraction (less rotation) at 11.1 cm, than at midband. Consequently, the variation with wavelength of the admittance function is considerably less at this point than it is at the

junction, as is seen by comparing Curves 5 and 6, Fig. 6-17. With an inductive iris at this point, therefore, it is possible to match the transition to a small VSWR over the entire wavelength range shown. This effect can be utilized, of course, only if the admittance function at the junction of the mismatched transition has the proper variation of reflection phase angle with wavelength. Specifically, the admittances for the shorter wavelengths must have larger phase angles than those for the longer wavelengths.

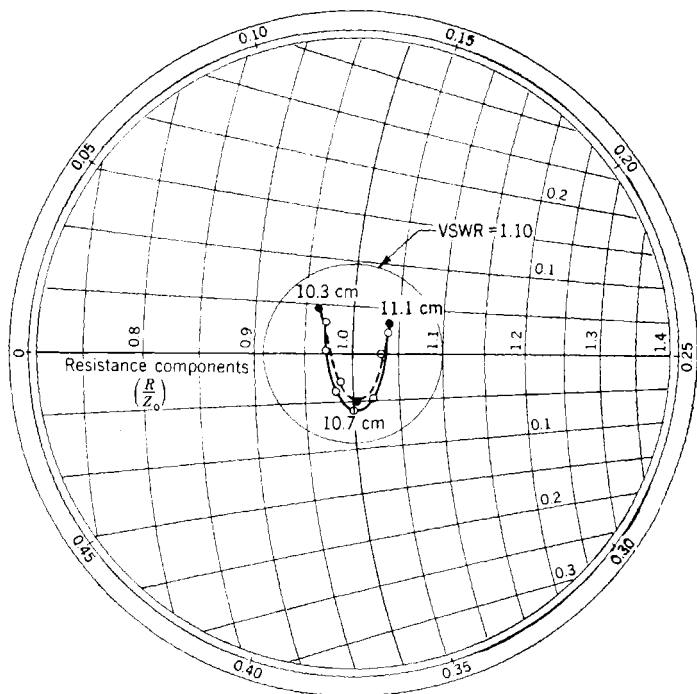


FIG. 6-18.—Admittance at matching iris of broadband crossbar transition. The full curve and open circles are experimental; the dashed curve and filled circles are predicted by Fig. 6-17.

As mentioned previously, the variation with wavelength of the susceptance of the waveguide iris can be used in this method of matching in such a manner as to reduce the spread in the VSWR of the transition with wavelength. In the example given, an inductive iris is used. The susceptance added by such an iris is proportional to the wavelength. The longer the wavelength then, the greater is the susceptance added by an iris of given physical dimensions. If the transition, as mismatched for matching over a broad band, has a VSWR which increases with wavelength, more susceptance is required to match it at longer wavelengths.

Therefore the spread in standing-wave ratio with wavelength can be reduced further by adjusting the transition so that it will have such a characteristic, and by using an iris in this manner. This effect is better understood by comparing Curves 6 and 7, Fig. 6-17, which show that the admittance function at the iris is not only centered on the chart but is also somewhat reduced in its spread.

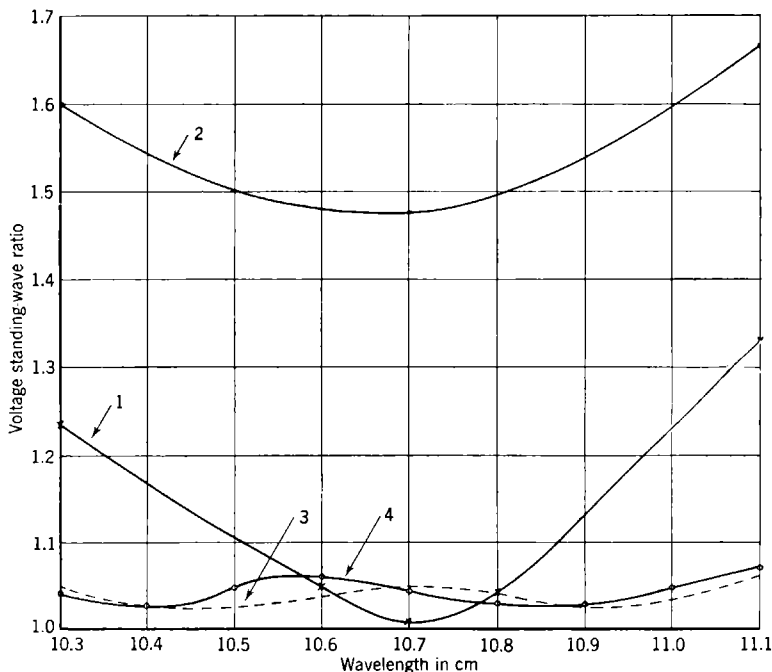


FIG. 6-19.—Voltage standing-wave ratio for crossbar transition from $\frac{1}{8}$ -in. coaxial line to waveguide under different conditions of match. (1) Matched with end-plate and crossbar dimensions only. (2) Mismatched for broadband matching with iris. (3) Predicted results with matching iris. (4) Experimental results with matching iris.

Curves 6 and 7 in Fig. 6-17 are calculated from the initial admittance function of the mismatched transition, Curve 5, which was measured experimentally. Figure 6-18 shows the accuracy with which these calculated results may be duplicated experimentally. A comparison of Figs. 6-16 and 6-18 shows the difference in the results obtained by the narrowband and broadband methods of matching this transition over the same wavelength range. The voltage standing-wave ratios as functions of wavelength for this transition under different conditions of match are plotted in Fig. 6-19. This makes the same comparison in terms of VSWR-vs.-wavelength functions for the two methods. Also shown are

the amount of mismatch necessary and the type of VSWR function with which an inductive iris can be used to obtain this bandwidth.

It sometimes happens, when this matching technique is used, that the proper reduction in the spread of the reflection phase angle with wavelength must be obtained by transformation of the junction admittance to the circle of unity conductance on the negative (inductive) susceptance side of the Smith chart. Matching is then accomplished by the use of a capacitive iris. For this, the VSWR-vs.-wavelength characteristic of the transition in the mismatched condition should be the opposite of that shown in Fig. 6-15; that is, the smaller ratios should occur at the longer wavelengths since the susceptance of a capacitive iris is inversely proportional to the guide wavelength. In practice, however, the use of the capacitive iris is avoided whenever possible, since this decreases the dimension of the guide parallel to the electric field and, therefore, decreases the voltage at which breakdown occurs.

There are several general considerations in the use of this broadband matching method. It will be noted that a reduction in the spread with wavelength of the reflection phase angle is accomplished in two ways. First, considering what an admittance-vs.-wavelength plot represents on a Smith chart, a simple mismatch of the transition constitutes such a reduction. Second, because of the different rates at which the various wavelength-vs.-admittance points rotate on the Smith chart, the junction admittance may be transformed along the line to some point nearer the generator where this spread is less. In obtaining maximum bandwidth these two operations are interdependent. The form of junction admittance as a function of frequency when the device is matched at a given frequency is determined by the type of junction. If a desired reduction in the spread of the reflection phase angle is specified, then neither the extent of the mismatch nor the transformation distance (rotation) necessary is uniquely determined; that is, the same reduction may be accomplished by a large mismatch and a small rotation or vice versa. In this connection a "large mismatch" implies a VSWR of from 1.5 to 2.0. A "large rotation" is, arbitrarily, one greater than a half wavelength or 360° on the Smith chart. For example, compare Curves 4 and 5 of Fig. 6-15. By the proper transformation along the line, the spread in phase of the points on either of these curves can be reduced to about the same amount. The transformation necessary to produce the effect, however, differs in the two cases. On Curve 4, to group the points on the circle of unity conductance in the capacitive side of the chart, so that an inductive iris may be used, a rotation of nearly 0.9 guide wavelengths is required. In the case of Curve 5, a rotation of less than 0.4 guide wavelengths produces the same result. Further, the average standing-wave ratio is less for Curve 4, but its variation of VSWR with wavelength is consider-

ably greater than that for Curve 5. Both these conditions are undesirable. The first implies that only a small susceptance is required to center the rotated Curve 4 about the point of match on the chart. The second means that a larger *total* variation with wavelength of the matching susceptance is required to cancel this spread of VSWR with wavelength in Curve 4 which appears as a spread in susceptance at the point where the iris is added. However, the total variation, with wavelength, of the iris susceptance is proportional to the size of the iris. Hence the small iris does not appreciably reduce the spread of VSWR with wavelength in Curve 4 which was larger than that of Curve 5 in the beginning.

These alternative procedures may be compared in general for a given transition admittance function. If the initial mismatch is small, the rotation required will be large. This means that the iris will be some distance from the transition which makes the unit larger. The iris will be small and less critical as to position; but, because only a small amount of susceptance is required for matching, it will not take advantage effectively of the variation in susceptance with wavelength of the iris which, as has been shown, can be used to reduce the spread in the VSWR with wavelength. If the initial mismatch is large, the rotation required will be small. A large matching iris will be necessary, and its position will be more critical. Further, if the initial mismatch is increased too much, the form of the admittance-vs.-wavelength function may no longer be independent of the dimensions; and the maximum bandwidth obtainable in this method may be decreased rather than increased. In addition, there will be larger standing waves in the region between the transition and its matching iris. This condition may decrease the power-handling capacity, though tests show that the effect is very small for standing waves of the order occurring in the transition described in this section. All these properties must be considered, when the transition is initially mismatched, for matching over the maximum wavelength range by this method. In practice it has been found that the use of a comparatively large initial mismatch gives the best results.

Because of the importance of the use of susceptive elements in this method of broadband matching, a note on their use for impedance matching is in order. The required susceptance may be introduced in the proper phase by the use of either a waveguide iris (or diaphragm) or a coaxial transformer. The general technique of this use of susceptance elements is described in Sec. 2-7. There are several reasons, however, for the fact that the waveguide iris has been used almost exclusively in the matching of transitions from coaxial line to waveguide. First, in the experimental development of these transitions, it is much more convenient to insert such an iris after the transition is built when the size and position of the matching susceptance must be determined from

measurements on the transition. Second, the power-handling capacity of the transition must be considered. In an ideal transition, this will be limited only by the breakdown power of the coaxial line. In certain improved versions of the transitions already described this is, in fact, the case. High-power tests have shown that there is considerable asymmetry of the electric field for a short distance into the coaxial line from these transitions. Almost any discontinuity in the coaxial-line center conductor in this region is likely to decrease the power required to cause the unit to arc at high powers. Third, there is no particular advantage of the coaxial transformer over the waveguide iris for the measuring techniques required in this impedance matching. In the design of components as critical as these transitions, it is generally necessary to make standing-wave measurements on both sides of the transition to be certain that the line is terminated with a perfectly matched load, as well as to obtain measurements of the transition characteristics. For these reasons the impedance matching is almost never done from the coaxial side of the transition.

Both symmetrical and asymmetrical irises have been used successfully in this matching. The asymmetrical iris is, of course, much simpler to use than the symmetrical iris, and its size and position can be calculated just as accurately. However, because of the amount of the next higher waveguide mode—the TE_{20} -mode—which it excites, it should be avoided whenever the iris is placed too close to the transition or any other waveguide discontinuity such as a choke-flange coupling. The "safe" distance depends upon both the susceptance of the iris and the wavelength. The field strength of the second waveguide mode excited by such an iris increases with the size of the iris; and the rate of its attenuation decreases with the wavelength. For example, the amount of the TE_{20} -mode set up by an asymmetrical iris having a susceptance of 0.70 (equivalent to a VSWR of 2.0) is attenuated to 1 per cent (40 db) of that for the TE_{10} -mode incident upon the iris in 0.60 free-space wavelengths at 10.0 cm. At 9.0 cm the corresponding distance for the same conditions is 0.82 wavelengths, and at 8.0 cm it is 1.29 wavelengths. These figures are given for the standard rectangular tubing $1\frac{1}{4}$ by 3 in. by 0.080-in. wall used as a waveguide at 10 cm. This has a cutoff wavelength of 7.22 cm for the TE_{20} -mode. At the 3-cm wavelengths now used for radar, and with the standard rectangular tubing $\frac{1}{2}$ by 1 in. by 0.050-in. wall having a cutoff wavelength for the second mode of 2.29 cm, the effect is not so critical since those wavelengths are proportionately farther from cutoff. An asymmetrical iris used to match a voltage standing-wave ratio of 1.5 to 2.0 should not be placed closer than a quarter guide wavelength to a discontinuity, when the free-space wavelength is greater than the cutoff wavelength of the TE_{20} -waveguide mode by 15 per cent or less. The

theory of (and data for) the use of the asymmetrical waveguide iris is developed elsewhere.¹

6-7. Broadband Matching with Coaxial Stubs.—It is possible by means of a properly placed narrowband coaxial stub support to improve considerably the match of a transition, from coaxial line to waveguide over a given band. By narrowband stub support is meant one not having a broadband coaxial matching transformer such as that described in Sec. 4-4. The reason for the use of the narrowband stub will appear in this discussion. Although used in only one specific application, this

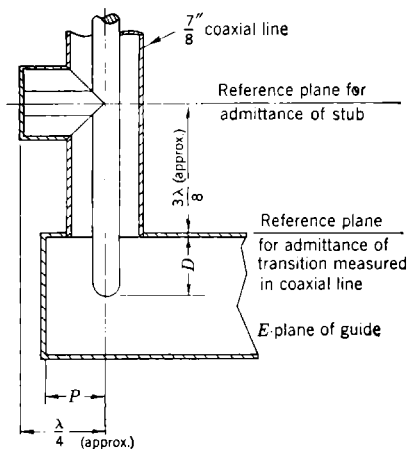


FIG. 6-20.—Probe transition for $\frac{7}{8}$ -in. coaxial line to waveguide with coaxial matching stub.

method should be applicable to all transitions having the proper junction admittance function. However it is neither so simple and convenient mechanically, nor so effective electrically, as the method described in the last section.

This method is particularly applicable to high-power transitions, which, operated at powers too high for beads, require a stub support on the center conductor whether or not this stub is used in the matching of the transition. It consists of reducing the variation of susceptance with wavelength of the probe transition by means of a quarter-wavelength, coaxial, short-circuited section (stub support) properly placed in shunt with coaxial line. The susceptance function of such an element is

¹ A. E. Heins, "The Susceptance of Asymmetrically Located Windows in Rectangular Wave Guides," RL Report No. 183, October 1942; N. H. Frank, *Wave Guide Handbook*, Sec. III, RL Report T-9, November 1942; W. Sichak, "One Sided Inductive Irises and Quarter-wave Capacitive Transformers in Waveguide," RL Report No. 426, November 1943.

nearly the same form as that of the probe transition alone; but it has the opposite sign with respect to wavelength.

The method was used in the broadband matching of a transition between $\frac{7}{8}$ -in. coaxial line (with $\frac{3}{8}$ -in. center conductor) and the standard $\frac{1}{2}$ - by 3-in. rectangular waveguide in the region of 9 cm. The construction of this unit is shown in Fig. 6·20. The design was developed in the following manner. The probe transition, without the coaxial stub support,

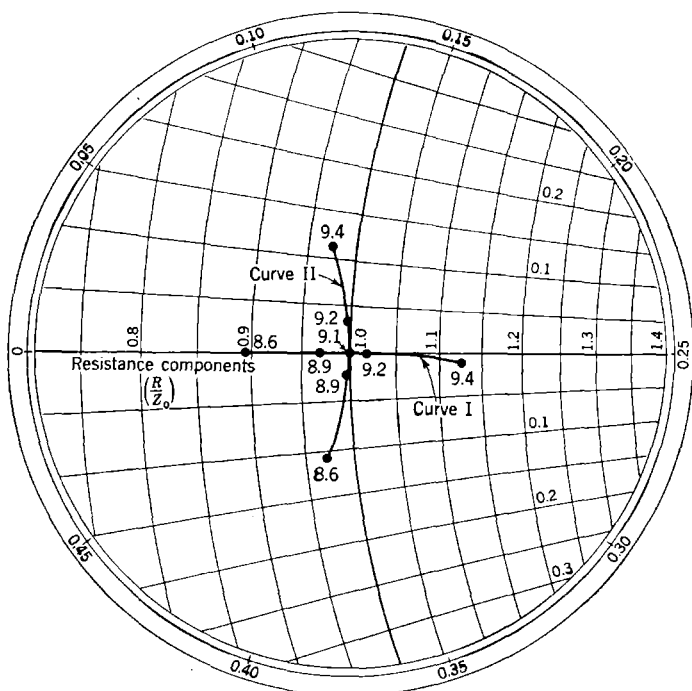


Fig. 6·21.—Admittance as a function of wavelength for $\frac{7}{8}$ -in. coaxial-line transition, measured in coaxial line. Curve I: admittance at junction (see Fig. 6·20). Curve II: admittance approximately $\frac{3}{8}$ λ away from junction in coaxial line.

was matched at 9.1 cm by variation of the probe and end-plate positions, dimensions P and D in Fig. 6·20. (The probe was supported from the input end of the coaxial slotted section used for measuring standing waves.) The admittance of this transition, measured from the coaxial side and plotted at the reference plane indicated in Fig. 6·20, has the characteristics shown as Curve I on the Smith chart, Fig. 6·21. Approximately three-eighths of a wavelength back in the coaxial line (rotation toward the generator on the chart) this transforms into the admittance function shown as Curve II. This is almost a purely susceptive variation

with wavelength, having negative (inductive) susceptances for wavelengths shorter than 9.1 cm and positive (capacitive) susceptances for those longer. A quarter-wavelength short-circuited section of line added in shunt at this point will have a similar variation in susceptance but one of opposite sign with respect to wavelength. This is seen from the

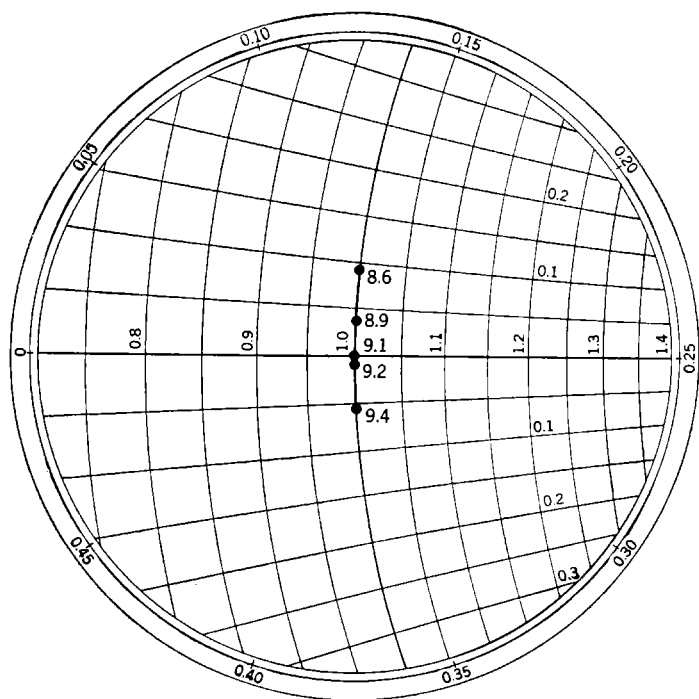


FIG. 6-22.—Calculated admittance as a function of wavelength at center of $\frac{7}{8}$ -in. coaxial stub. Admittance is that of stub alone.

formula for the admittance of short-circuited section of lossless transmission line,

$$\frac{Y}{Y_0} = -j \cot \frac{2\pi l}{\lambda}.$$

The calculated admittance as a function of wavelength for such a stub is plotted in Fig. 6-22 for the same wavelength range over which the transition was measured. A broadband stub support does not have this characteristic, and therefore it cannot be used for matching in this way. When the stub and probe susceptance functions are combined in the proper phase, the variation of match of the combination is considerably reduced over that of either unit alone, as shown in Fig. 6-23. The

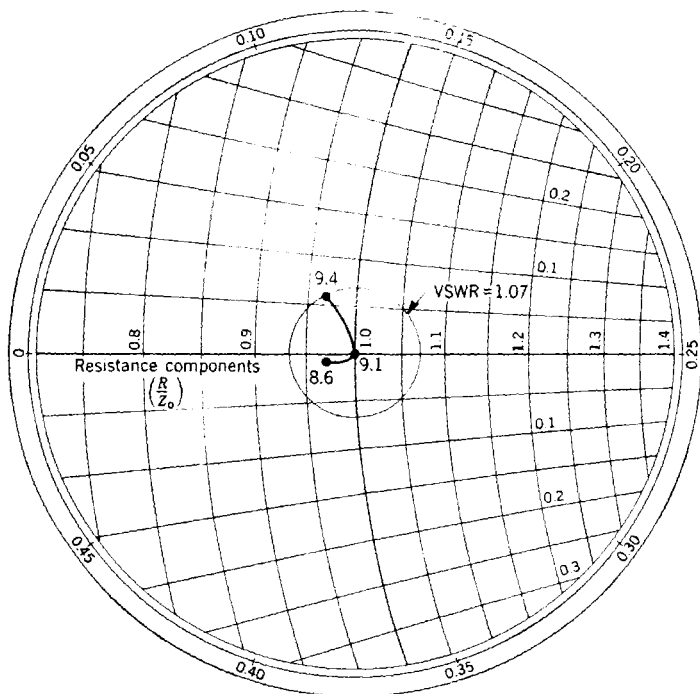


FIG. 6-23.—Admittance as a function of wavelength for $\frac{7}{8}$ -in. coaxial stub-supported probe transition measured in coaxial line and referred to center of stub. Admittance is for combination of transition and stub.

maximum voltage standing-wave ratio over the range measured has been reduced from 1.13 to 1.07. This effect in terms of VSWR as a function of wavelength is shown in Fig. 6-24. Further improvement could probably be effected by using a stub of characteristic impedance different from that of the line and by redetermining the stub position and the transition dimensions for proper centering of the match in the range measured. However, since this result was adequate for the requirement at the time, no further improvement was attempted. Further, it is possible to match this transition over wider

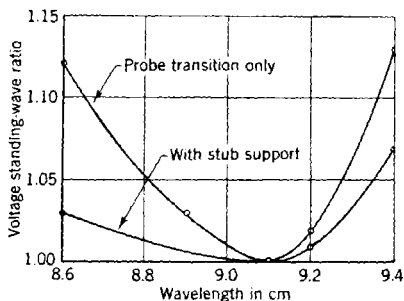


FIG. 6-24.—Voltage standing-wave ratio as a function of wavelength for probe transition from $\frac{7}{8}$ -in. coaxial line, stub-supported, to waveguide.

wavelength bands, or to adapt it to other bands by the use of the waveguide matching iris in the manner described in the last section. A summary of these results will be given later.

6-8. Tuning Adjustments.—The earliest transitions from coaxial line to waveguide, which were usually of the crossed coaxial-line-to-waveguide type shown in Fig. 6-8, were quite frequency-sensitive and were, therefore, built with adjustable plungers in the waveguide and coaxial short-circuited sections so that the transition could be tuned to the desired frequency. These were soon replaced by fixed-tuned transitions of somewhat different types, which are better matched over a broad band. It has been found that when bandwidths of about 10 to 20 per cent are desired, the dimensions of such transitions are critical; and it is difficult to duplicate the impedance characteristics of the original design. This realization led to the development of a method for adjusting the match of subsequent experimental and production units to obtain maximum bandwidth and optimum match.

Since the amount of tuning required is generally small, and because they are easily constructed and have a smaller effect than other tuners on the power-handling capacity of the units, waveguide tuning screws are used as the final matching adjustment on some of these transitions. The general use of screws as tuning elements is discussed in Sec. 8-14. Application to transitions from coaxial line to waveguide will be presented here.

In building a number of 10-cm broadband transitions to the same design, it has been found that the matching iris dimensions required to give the maximum bandwidth or the optimum match over a given broad band vary as much as ± 0.040 in. in both position and aperture, indicating that the transition characteristics are not identical with those of the original design. However, in most instances it is possible, by the calculation of new iris dimensions from measurements on the transition without the matching iris, to obtain bandwidths and degrees of match quite comparable with those of the original design model. By a slight adjustment, then, of the amount and phase of the matching susceptance, it would be possible to match, over a broad band, transitions which do not duplicate exactly the characteristics of the original design. This matching can be done much more easily with tuning screws than by the calculation of new matching iris dimensions from standing-wave measurements on the transition. Further, when so tuned, the screw tuners can be locked or soldered and no further adjustment is necessary. This technique has proved very useful in the laboratory; it also expedites the production of satisfactory units using these transitions, such as magnetron couplings, antennas, and rotary joints. This technique should

not be used, however, as a substitute for the development of accurate production assembly methods.

One arrangement which has been used effectively is that shown in Fig. 6-25. With screws of fairly large diameter (about 1 in. at 10 cm), it is possible to obtain quite large capacitive susceptances and inductive susceptances of the order of 0.15 (normalized) or slightly larger. In the arrangement shown, these screws are in the center of the wide side of the guide, one centered on the matching iris, and the other one-eighth guide wavelength away toward the transition. Each screw can be moved from about 0.2 in. projection into the guide to about 1 in. back into its housing. This gives a continuous variation in susceptance

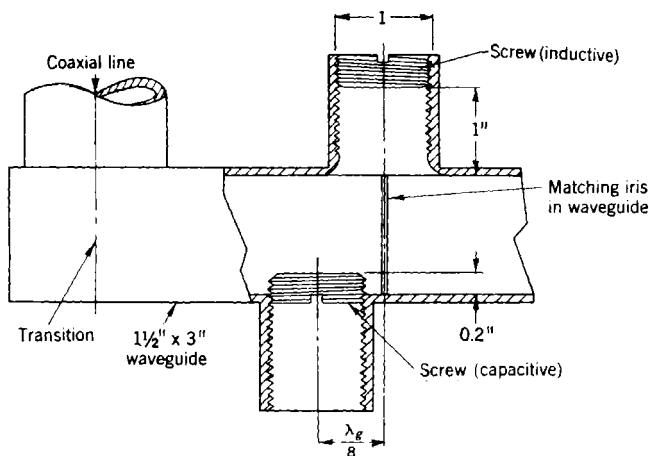


FIG. 6-25.—Tuning screws for adjusting match of 10-cm transition.

from about $+0.3$ capacitive to about -0.15 inductive. In the figure, one screw is shown in the position which gives maximum inductive susceptance and the other in the position for a capacitive susceptance. Capacitive susceptances which are considerably larger than the value given are obtainable with such a screw. However, the value given for the inductive susceptance is about the maximum that may be obtained from a screw of this diameter at 10 cm. This limits the magnitude of admittance variation which may be produced in any phase by two screws used in this manner.

The screw centered on the iris produces at this point a variation of susceptance which is effectively an adjustment of the iris aperture. The other screw gives a variation of susceptance one-eighth guide wavelength

away. This appears at the iris as a change in conductance which effectively adjusts the iris position.

Since the mismatch which is to be canceled may occur in any phase, the limiting factor of this device is the maximum inductive susceptance obtainable with a given size screw. With the 10-cm screw tuner described above, a reflection of any phase may be reduced by a factor of about 1.15 in terms of the voltage standing-wave ratio. Similar results are obtained at 3 cm when the dimensions are scaled according to the guide wavelengths. Screws of larger diameter have been used to obtain a greater inductive susceptance, but these do not give purely susceptive tuning when used to introduce capacitance; sometimes, they actually produce a shunt resonance. Screws of the size discussed above are about the optimum for applications in which the same diameter screw is used for capacitive and inductive tuning. Other types of screws for general application are discussed in Chap. 8.

This type of tuning adjustment can, of course, be applied equally well to other devices, particularly to transitions matched by the narrow-band method. In each type this amount of corrective tuning on production units has proved sufficient to bring the voltage standing-wave ratios well within the desired limits which are usually 1.10 and 1.15.

This method of adjusting the final match of these transitions is particularly simple and convenient for narrowband matching. The reflection from the transition is measured at the proper frequency and the screws are adjusted to give a minimum standing-wave ratio and then soldered in position. This is a feasible production technique. Broadband matching however, which is more often necessary, is more difficult to accomplish by this method. In this case, it is necessary to make a plot of admittance vs. wavelength, or to obtain the equivalent information by means of a microwave impedance bridge, an instrument which measures the voltage standing-wave ratio simultaneously at several different frequencies in the desired band. The reason for this procedure may be seen by reference to Fig. 6-17 or to Fig. 6-18. The transition can be adjusted, by means of the screw tuner, to have a standing-wave ratio of unity at midband (10.7 cm). This would occur, however, through the addition of capacitive susceptance which would shift the entire curve upward and cause the mismatch at the ends of the band to increase. Therefore the screw tuner must be used to center the admittance curve for a broadband transition about the point of match on the chart, rather than to match it at a specific wavelength.

6-9. Examples of Transition Construction.—Many mechanical arrangements have been employed in the construction of coaxial-line-to-waveguide transitions with differences depending upon the application and the conditions under which the unit is to be operated. A number

of these are diagrammed in Fig. 6-26 for easy reference and in order to facilitate comparisons between different designs. By adjustment of the proper dimensions, it is possible to obtain an impedance match for nearly any geometrical shape of transition region, at nearly any wavelength in the range for which the waveguide and coaxial line support only their lowest modes. However, the impedance characteristics of different types of transitions differ considerably for wavelengths, in the region of that for which the transition is best matched. Since the transition dimensions are usually critical, and since there are few instances in which a desired type of electrical characteristic cannot be obtained with one of the geometrically simple constructions shown, the practice has been to use the simplest possible arrangement by which a given impedance characteristic can be obtained. Most of the transitions shown in Fig. 6-26 are based on the waveguide antenna or electric-coupling method described in Sec. 6-3. However, the distinction between this and the magnetic or loop-coupling method is hardly significant in some of the more complicated constructions.

6-10. Crossed Transitions from Coaxial Line to Waveguide.—The earliest method of providing a transition from the principal coaxial mode to the lowest rectangular (or round) waveguide mode is the crossed line and guide transition shown in Fig. 6-26*a*. As discussed in Sec. 6-3, matching is accomplished by adjusting the lengths of the waveguide and coaxial-line short-circuited sections, dimensions D and S in the figure. In the region of match, this transition has always proved very frequency-sensitive and, therefore, has been used either as a tunable device or as a narrowband fixed-tuned transition. Figure 6-27 shows the detailed construction and electrical characteristics for this type of transition between $\frac{5}{16}$ -in. coaxial line and rectangular waveguide $\frac{1}{2}$ by 1 in. by 0.050-in. wall in the 3-cm region. Measurements for its development are made in the waveguide; and a long length of RG-9/ U cable (see Sec. 5-1) is coupled to the coaxial line with a type N connector, UG-58/ U (see Sec. 4-2), used as the coaxial load. The mismatch of the cable section was about 1.14 in voltage at 3.2 cm. This design met requirements for a rugged, easily constructed transition matched reasonably well for a narrow band. It has been used in microwave test equipment as a low-power, type N connector to 3-cm waveguide adapter.

Another type of crossed coaxial-line-and-waveguide transition, tuned in another way, is that shown in Fig. 6-26*b*. In this unit the outer conductor of the coaxial line extends into the waveguide from both sides, forming a tunable coupling gap. It is used as a tuning device to match power into a coaxial crystal mount in a 3-cm standing-wave detector. Tuning is accomplished by varying the coaxial stub length S and the gap in the coaxial line G . It is a narrowband tunable device; its charac-

teristics are, of course, also determined by the position of the waveguide short circuit which is fixed in this unit. By making all three dimensions variable, it should be possible to adjust the bandwidth to some extent, as well as to match the transition at a given wavelength. This, however, is an unnecessary complication in a tunable device.

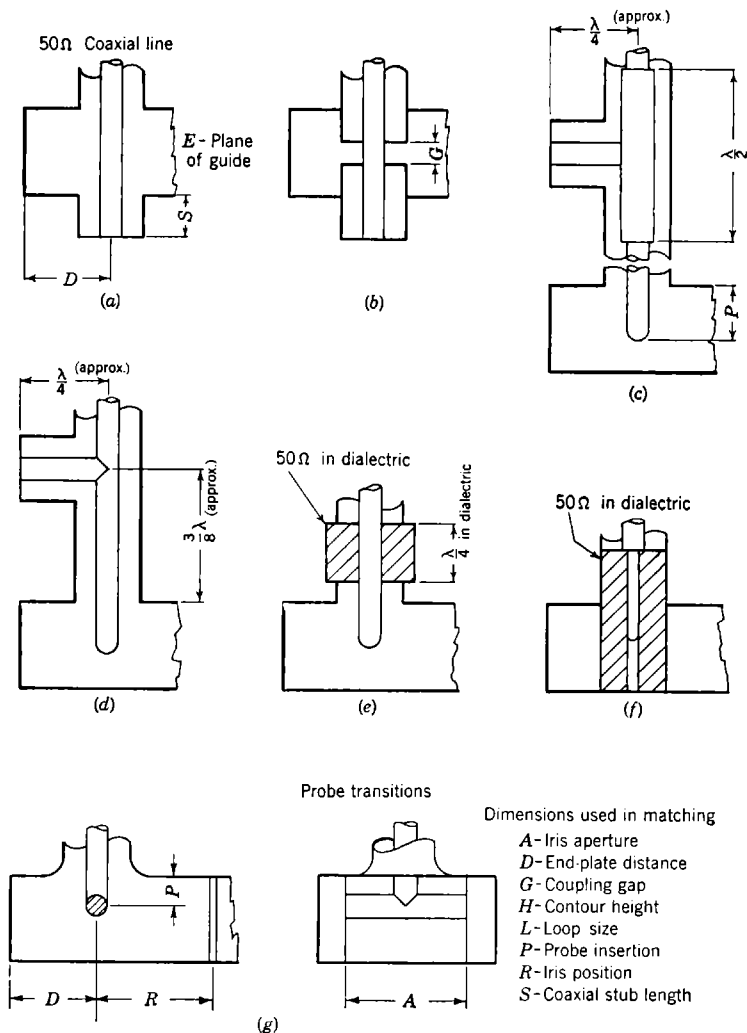
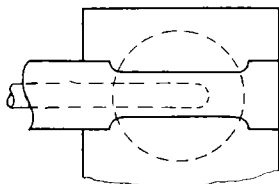
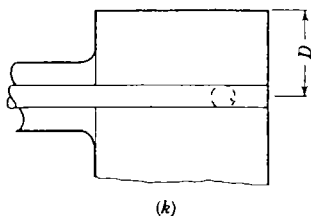
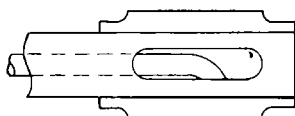
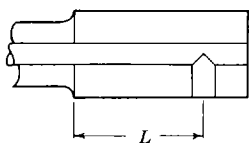
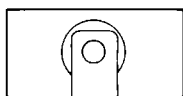
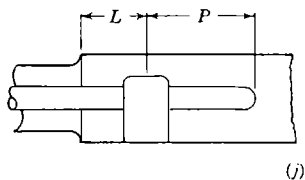
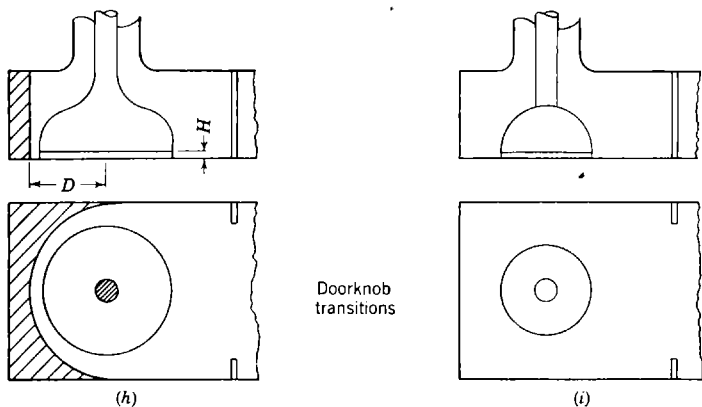


FIG. 6-26. —Transitions from coaxial line to waveguide. (a) Crossed transitions from coaxial line to waveguide; (b) crossed transition with adjustable gap *G*; (c) probe transition with broadband stub support; (d) broadband probe transition with matching stub support

6-11. Probe Transitions.—In terms of the impedance match and the bandwidth obtainable without special matching techniques, the probe transition is the most desirable type and has had considerable application in microwave systems and test equipment. Some of the possible differ-



(e) bead-supported probe; (f) dielectric-supported probe; (g) crossbar transitions; (h) wine glass or Grecian urn; (i) hemisphere; (j) *E*-plane loop coupling; (k) *H*-plane loop coupling; (l) resonant-slot coupling.

ent constructions of this transition are shown in Figs. 6-26c to f. The chief problem involved in the design of such a transition is the support of the coaxial center conductor which should not limit the power-handling capacity of the unit to less than that of the transition itself.

Figure 6-26c shows a method of supporting the center conductor of the coaxial line by means of a quarter-wavelength coaxial stub having a half-wavelength coaxial transformer for broadband matching of the stub only. Such a stub is very well matched (VSWR less than 1.05) over as

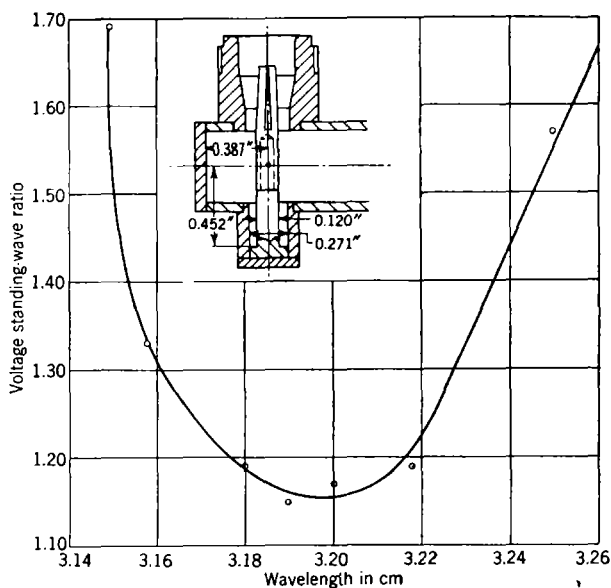


FIG. 6-27.—Voltage standing-wave ratio characteristics of adapter from type N connector to waveguide.

much as a 30 per cent band and is the basis of the broadband stub-supported coaxial line discussed in Chap. 4. The characteristics of the transition are very little affected by the presence of the stub, and the coaxial line is broken in the figure to indicate that the position of the stub along the line is unimportant. However, in order to support the probe accurately, the stub should be placed as close to the waveguide as possible. On the other hand, it probably should not be designed to come less than a half wavelength from the transition in order that the higher modes set up in the region of such discontinuities are damped sufficiently to prevent interference with the functions of either the stub or the transition. The development of this transition and its electrical characteristics have been discussed in detail in Secs. 6-5 and 6-7. Typical plots of voltage

standing-wave ratio vs. wavelength for probe transitions from $1\frac{1}{8}$ -in. and $\frac{7}{8}$ -in. coaxial lines are to be found in Figs. 6-12 and 6-24, respectively; such a plot is shown in Fig. 6-24 by the curve labeled "probe transition only." This type of transition has been used successfully in units requiring transitions from coaxial line to waveguide at both 10- and 3-cm wavelengths.

The effect obtained in using a narrow-band coaxial stub support to reduce the frequency sensitivity of a probe transition has been discussed

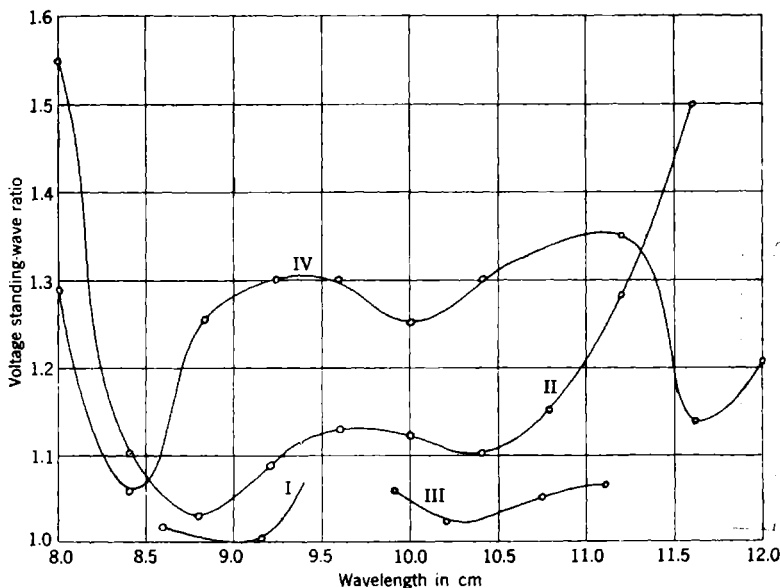


FIG. 6-28.—Probe transition from $\frac{7}{8}$ -in. coaxial line to waveguide with simple stub support. Curve I: original design. Curve II: average for two production units of original design. Curve III: transition matched with iris for 9.9 to 11.1 cm (average of three individually matched units). Curve IV: transition matched with iris for 8 to 12 cm (average of two individually matched units).

in Sec. 6-7. The basic construction of this transition is shown in Figs. 6-20 and 6-26d. The application of this technique to the probe transition from $\frac{7}{8}$ -in. coaxial line to waveguide, described previously, has resulted in a particularly useful transition in the 10-cm region. Its properties are given in the VSWR-vs.-wavelength plot in Fig. 6-24 and by Curve I, Fig. 6-28. By the use of matching irises in the manner described in Sec. 6-6, it has been possible to adjust the frequency of best match and, to some extent, the bandwidth of this transition over a considerable range. This has been done without variation of the transition-matching dimensions (end-plate distance, probe insertion, and stub position) from

those of the original design. Results of these further modifications are given in Fig. 6-28. Curve II is voltage standing-wave ratio as a function of wavelength, averaged from two production units made to the original design, but measured over a considerably wider wavelength range than that for which the transition was intended. To meet requirements for transitions handling appreciable power and being sufficiently well matched, in the 9.9- to 11.1-cm band, to be used for measuring equipment, three production models were individually matched with waveguide irises. Each transition was measured over this band, and separate matching irises were calculated for each one. The results for these three transitions are averaged in Curve III. A similar type of experimental

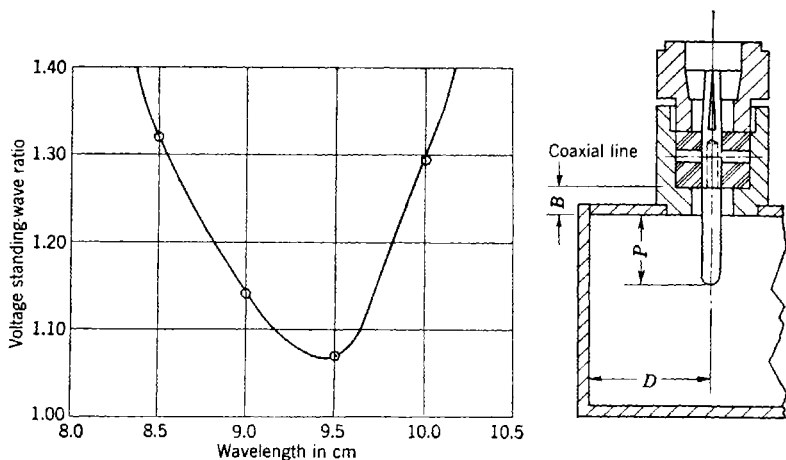


FIG. 6-29.—Bead-supported probe transition in $\frac{5}{16}$ -in. coaxial line.

development is shown in Curve IV. In this instance an attempt was made to secure the best possible match over the entire 8- to 12-cm wavelength range by the use of matching irises. This was done with two production units built to the original design for the stub-matched probe transition.

Although the coaxial-stub method of supporting the center conductor does not limit the power-handling capacity of the probe transition (which is generally less than that of the coaxial line itself), it has another disadvantage. The electrical characteristics of these transitions are sensitive to the centering and insertion of the probe. These dimensions are particularly difficult to hold accurately in assembly since the supporting stub is some distance from the transition region. Because of this fact and because the probe transition has a lower breakdown power than the coaxial line, this transition has been replaced by other types in applications where high power is used and a very good match is required.

In instances where power limitations and sizable reflections are not serious considerations, such as in certain test equipment, the probe may very conveniently be supported by a dielectric (usually polystyrene) as shown in Figs. 6-26*e* and *f*. The bead shown in Fig. 6-26*e* is frequently part of a type N coaxial connector in $\frac{5}{16}$ -in. line. The outer-conductor diameter is increased at the bead in order to maintain a 50-ohm characteristic impedance in the dielectric-filled region. The length of the

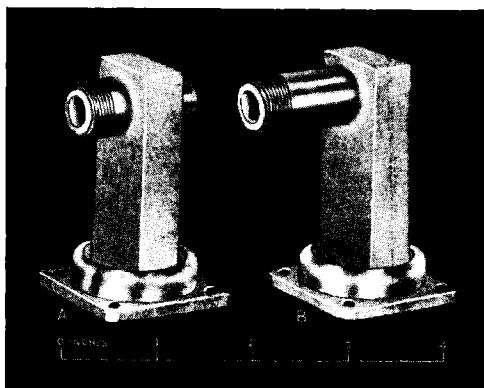


FIG. 6-30.—Adapter from type N connector to 3-cm waveguide (dielectric-supported probe transition).

bead is a quarter wavelength in the dielectric so that the capacitive mismatch occurring at one end cancels that at the other. This transition has been used extensively in test equipment and other low-power microwave applications at both 10- and 3-cm wavelengths. Figure 6-29 shows the detailed construction of a typical adapter from type N coaxial connector to waveguide with a representative plot of the VSWR as a function of wavelength for the design matched at about 9.5 cm. Table 6-1 gives the dimensions for matching at other wavelengths. Relative to other types of transitions these adapters are limited by the inconsistencies and frequency sensitivity of the type N connectors, but they have been

TABLE 6-1.—DIMENSIONS FOR ADAPTER FROM TYPE N COAXIAL CONNECTOR TO WAVEGUIDE* FOR BEST MATCH AT VARIOUS WAVELENGTHS

λ	Coaxial line, in.		Waveguide, in.	B , in.	D , in.	P , in.	Band VSWR < 1.10, %
3.3	0.296	0.125	$\frac{1}{2} \times 1 \times 0.050$	0.500	0.310	0.250	± 1
9.5	0.296	0.125	$1\frac{1}{2} \times 3 \times 0.080$	0.143	0.707	0.765	± 3
11.0	0.296	0.125	$1\frac{1}{2} \times 3 \times 0.080$	0.143	0.725	0.862	± 3

* See Fig. 6-29.

widely used in low-power microwave systems. A bead-supported 3-cm adapter of this type and one having a crossed coaxial-line-and-waveguide transition are pictured in Fig. 6-30.

A somewhat more rugged and accurate method of supporting the probe by means of dielectric is that shown in Fig. 6-26f. The detailed construction and electrical characteristics of this type of transition used as a type N coaxial-connector-to-waveguide adapter are shown in Fig.

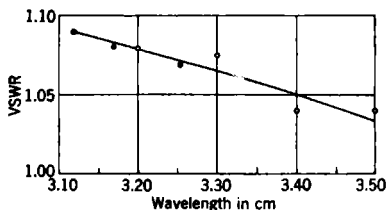
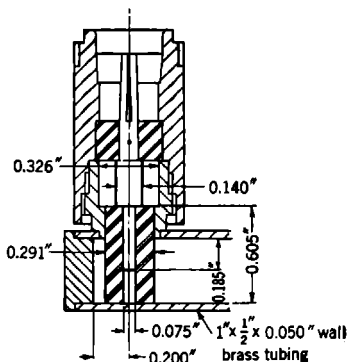


FIG. 6-31.—Type N coaxial connector to 3-cm waveguide probe transition.

6-31; those dimensions which are more important in matching are indicated. In this design the size of the coaxial line varies for structural reasons, but a 50-ohm characteristic impedance is maintained in both the air- and dielectric-filled regions. Matching was accomplished by varying the end-plate distance, the probe insertion, and the length of the dielectric support. This adapter has proved to be a superior type at 3-cm wavelengths; the same construction has not yet been used for 10-cm applications. It is consistently better matched for a broader band in production than the types discussed above, probably because of the more accurate method of positioning the probe.

6-12. Crossbar Transitions.—

In order to simplify the construction of coaxial-line-to-waveguide transitions and to permit a more accurate support of the center conductor, the "crossbar" transition,¹ shown in Fig. 6-26g, was developed for use in a 3-cm coaxial rotary joint of 70-ohm characteristic impedance with transitions to waveguide on either end. Dimensions and voltage standing-wave ratio characteristics for this transition are given in Fig. 6-32. In this development it was possible to achieve an adequate impedance match and bandwidth without resorting to additional matching elements such as waveguide irises or coaxial transformers. This same type of transition, for wavelengths near 10 cm using standard waveguide and $\frac{7}{8}$ -in. coaxial line having a characteristic impedance of 50 ohms, has proved considerably more frequency-sensitive.

¹ C. F. Edwards, "Preliminary Report on a Waveguide Rotary Joint," BTL Memorandum 43-160-120, July 1943.

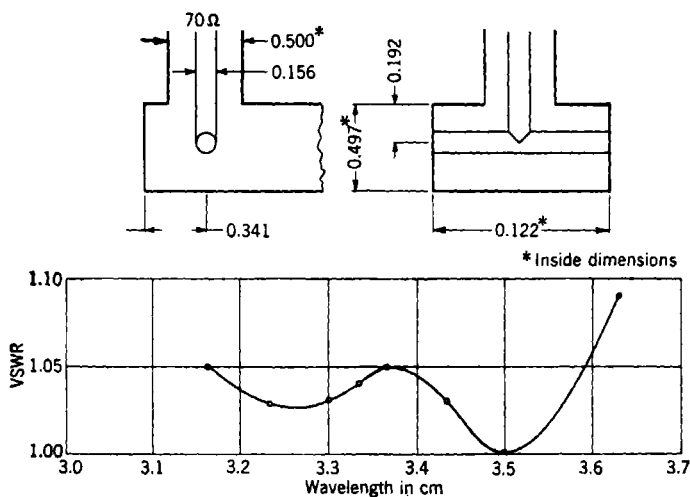


FIG. 6-32.—Crossbar transition from 3-cm coaxial line to waveguide (data from Ref. 6).

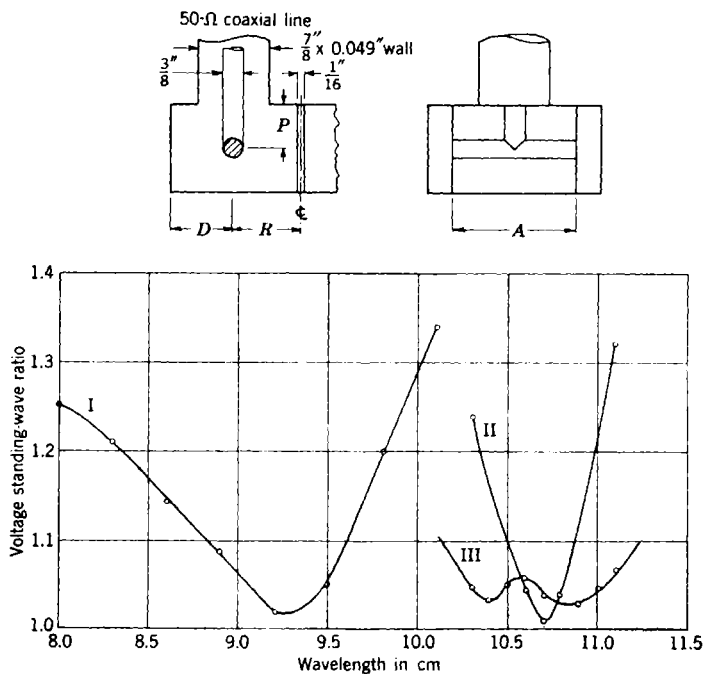


FIG. 6-33.—Crossbar transitions from $\frac{7}{8}$ -in. coaxial line to waveguide in the 10-cm region.

TABLE 6-2.—DIMENSIONS FOR CURVES SHOWN IN FIG. 6-33

Curve	D , in.	P , in.	R , in.	A , in.	Band, cm (VSWR < 1.10)
I	0.696	0.509	9.25 ± 4%
II	1.670	0.653	10.7 ± 2%
III	0.530	0.705	2.200	2.120	10.2 to 11.2

One method of matching this transition over a broad band by means of a waveguide iris has been described in Sec. 6-6. A summary of the

different design dimensions for crossbar transitions in the 8- to 11-cm wavelength region may be found in Fig. 6-33 and in Table 6-2. The broadband model is pictured in Fig. 6-34.

The differences in the properties of the transitions shown in Figs. 6-32 and 6-33 is easily understood in terms of the relative guide wavelengths. First, the formula for the guide wavelength is

$$\lambda_g = \frac{\lambda_0}{\sqrt{1 - \left(\frac{\lambda_0}{\lambda_c}\right)^2}}$$

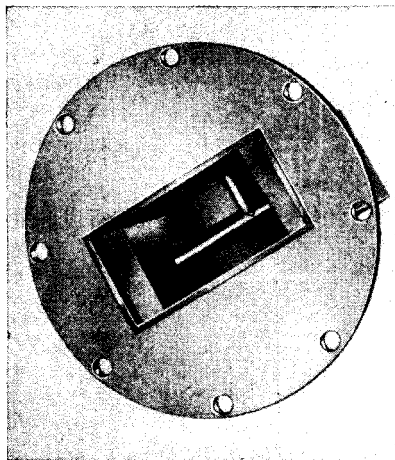


FIG. 6-34.—Broadband crossbar transition from $\frac{1}{8}$ -in. coaxial line to waveguide.

where λ_0 is the free-space wavelength, and λ_c is the cutoff wavelength (equal to twice the inside wide dimension of the guide). Now, as λ_0 approaches λ_c , the rate of change of λ_g with λ_0 will increase; that is, the nearer the waveguide component is operated to the cutoff wavelength, the more frequency-sensitive it becomes. The ratio of free-space to cutoff wavelength for the three different transitions is as follows:

λ_0 (midband), cm	λ_0/λ_c
3.3	0.579
9.2	0.637
10.7	0.741

If all dimensions of the different transitions were scaled according to the wavelength, the electrical properties, of course, would remain unchanged. This method has been used to great advantage in special applications where a component of the desired characteristics has been developed for another wavelength. However, the waveguide and coaxial-line sizes for the different wavelength bands are predetermined

and usually are not in the correct ratio for "scaling," in terms of guide wavelengths. In comparing these crossbar transitions, the effect is complicated even further by the difference in the characteristic impedance of the coaxial line which is 70 ohms for the 3.3-cm transition and 50 ohms for the other two.

6-13. "Doorknob" Transitions.—The only limit on the power which may be safely transmitted by a coaxial-line-to-waveguide transition under given conditions should be that imposed by the breakdown voltage of the coaxial line alone. Although the crossbar transition can carry more than twice the power of which the stub-supported probe transitions are capable, this desired maximum power limit was not obtained with either design. In order to achieve this, a transition¹ was developed in which the center conductor of the coaxial line terminates on the opposite side of the guide (for an *E*-plane, right-angle transition) in a knob of the proper size to permit impedance-matching and of a "streamlined" shape to increase the power required for breakdown. This general type of transition, two versions of which are shown in Figs. 6-26*h* and *i*, is widely known as the "doorknob" transition and occasionally by more colorful names which identify different shapes of doorknobs.

The doorknob may be thought of as an "inverted" stub in a crossed coaxial-line-and-waveguide transition. The purpose of this stub is to match the susceptance (as measured in the coaxial line) of the "antenna" (that portion of the coaxial center-conductor extending across the guide) which excites the waveguide, as discussed in Sec. 6-3. The proper shunt susceptance for this matching can be added by "building up" the inside of the guide in this region as well as by using a short-circuited section of coaxial line having the proper input susceptance. Further, as might be expected, this arrangement proves slightly less frequency-sensitive than one in which the susceptance matching the waveguide antenna depends upon the electrical characteristics of an appreciable length of coaxial line.

This type of construction has very successfully improved the power-carrying capability of the coaxial-line-to-waveguide transition to the point where it is limited only by the breakdown power of the coaxial line. An extensive series of high-power tests on different types of doorknob transitions has been made under a number of different conditions of pressure, standing waves, and ionizing radiation. These have shown that a well-made transition of this type, operating in a reasonably well-matched transmission line, will break down only at powers necessary to cause arcing in the coaxial line. These transitions have had wide

¹ N. A. Schuster and G. L. Hollingsworth, "Development of an Improved Conversion Unit for Coaxial Line to Waveguide Feed," General Electric Co. Engineering Memorandum EMT-521, January 1943.

application in 10-cm waveguide systems using magnetrons with coaxial-output or coaxial-mode rotary joints. This construction also has been used in 3-cm rotary joints and in certain test equipment. It has been used in 1-cm applications, chiefly as a means of matching power into a crystal. Some of these applications are largely experimental, and such transitions generally have adjustable dimensions to permit tuning.

When matched only by adjustment of the transition dimensions (end-plate distance, and doorknob size and shape), these transitions are comparatively narrow band; that is, they have a VSWR of less than 1.10 for a bandwidth of only a few per cent. By mismatching the transition and matching over a broad band with a waveguide iris, in the manner

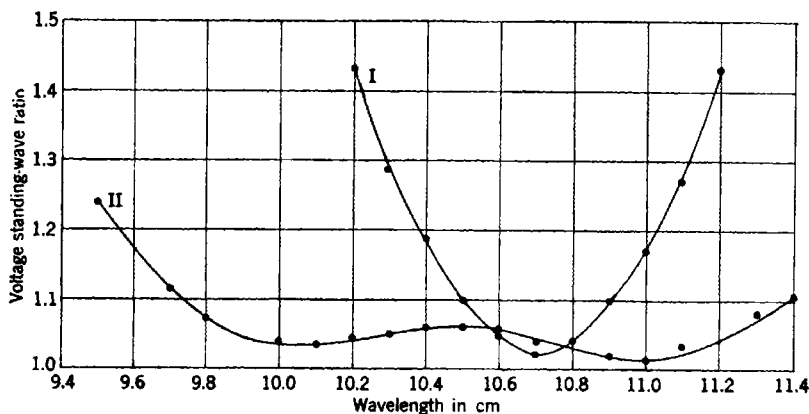


FIG. 6-35.—Doorknob transition from $1\frac{1}{8}$ -in. coaxial line to waveguide. Curve I: narrowband model (data from Ref. 7). Curve II: average of four design models for broadband transition.

described in Sec. 6-6, bandwidths of the order of 10 to 20 per cent are obtainable. This has been done for a number of different 10-cm transitions; it has not been done, to any extent, for the 3-cm transitions since coaxial line is seldom used in high-power applications at this wavelength. Requirements for the match are not so stringent for low-power transitions.

Although the doorknob transition is quite satisfactory in terms of its power-handling capacity and bandwidth (if properly "broadbanded" with an iris), it is extremely critical as to dimensions. Since the specifications for its construction are detailed, they cannot be included here. However, some representative electrical characteristics for different designs will be presented with references from which more detailed design information may be obtained.

Figure 6-35 shows the voltage standing-wave ratio as a function of wavelength for two designs of doorknob transitions from $1\frac{1}{8}$ -in. coaxial

line to standard 10-cm waveguide. Both have the same general construction shown in Fig. 6-26*h*. The characteristic of the narrowband model is plotted as Curve I. This design differs from that for the broadband model in that it has no matching iris and has a flat end plate some distance farther from the doorknob than is the semicircular end plate in the broadband model. These curves show the frequency sensitivity of the basic design of doorknob transition in this wavelength range as well as the improvement which may be obtained by broadband matching with an inductive waveguide iris. Curve II for the broadband model is the average of the data taken from measurements on four units for which individual matching irises had been calculated.

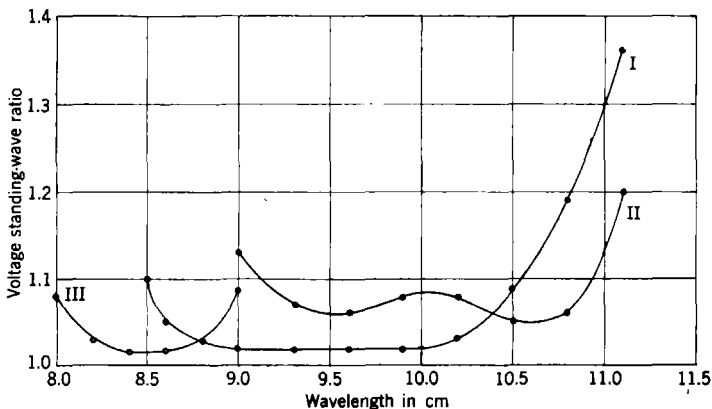


FIG. 6-36.—Doorknob transitions from $\frac{7}{8}$ -in. and $1\frac{1}{4}$ -in. coaxial line to waveguide. Curve I: average for four preproduction models individually matched for maximum bandwidth, $\frac{7}{8}$ -in. coaxial line. Curve II: average for 10 preproduction models of same design as for Curve I, but with different iris for longer wavelengths, $\frac{7}{8}$ -in. coaxial line. Curve III: design model $1\frac{1}{4}$ -in. coaxial transition hemispherical doorknob.

Some results for doorknob transitions with different sizes of coaxial line at different wavelengths in the 10-cm region are shown in Fig. 6-36. Curve I represents the characteristics of the broadband $\frac{7}{8}$ -in. coaxial-line-to-waveguide doorknob transition which has the same general design in the transition region as that discussed above and shown in Fig. 6-26*h*. This result was obtained in the usual way, by varying the transition dimensions to give the proper mismatch and by matching with a waveguide iris calculated to give the maximum bandwidth. Curve II is the characteristic curve of the same transition design with a slightly different position of matching iris to improve the match in the region of 11 cm. It should be noted that this can be done only at the expense of a standing-wave ratio with a slightly higher average over the band and a somewhat decreased bandwidth. Curve III is the VSWR as a function of wavelength for a hemispherical doorknob transition from $1\frac{1}{4}$ -in.

coaxial line to waveguide for use in the 8- to 9-cm band. This has the construction shown in Fig. 6-26*i*.

Similar transitions have been built for 3-cm wavelengths, though they have had far less application than those for 10 cm. So far, little work has been done in attempting to increase the bandwidth of these transitions by means of a waveguide iris. Figure 6-37 shows the voltage standing-wave ratio as a function of wavelength for two experimental models of doorknob transitions matched in the region of 3.2 cm. Both of these were matched by adjustment of the end-plate position and shape and the doorknob size and shape. One form was used¹ at the Tele-

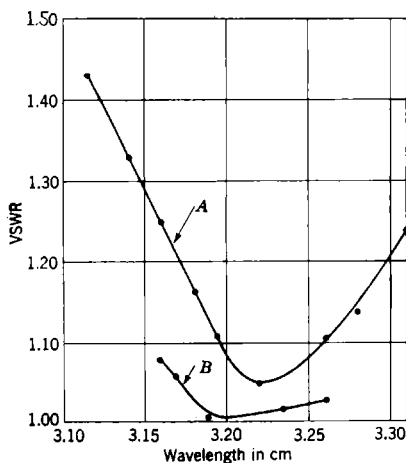


FIG. 6-37.—Doorknob transition from 3-cm coaxial line to waveguide. Curve A: British (TRE) hemispherical doorknob transition similar to Fig. 6-26*i* except that a semicircular end plate and no matching iris are used. Curve B: General Electric transition similar to Fig. 6-26*h* without matching iris.

communications Research Establishment in matching power from 3-cm waveguide into a thermistor for low-level power measurements. It has a hemispherically shaped doorknob similar to that shown in Fig. 6-26*i*, and a semicircular end plate very close to the doorknob, similar to the arrangement shown in Fig. 6-26*h*. An improved design has been developed, but the details are not yet available. The transition as developed at the General Electric Company² has the same general construction as that shown in Fig. 6-26*h* but with no matching iris. This was an experimental development intended for use in a 3-cm coaxial-mode rotary joint.

¹ P. R. Tunnicliffe, "An RF Wattmeter for Low-Level Power Measurements at 3 cm," TRE Report T 1663, May 1944.

² K. M. Uglow, General Electric Co., Transmitter Engineering Division, Letter of Feb. 19, 1944, to G. L. Ragan, Radiation Laboratory, M.I.T.

In terms of its power-handling capabilities, bandwidth, and degree of match attainable, the doorknob transition has proved the most satisfactory type for high-power work. Furthermore, it has the advantage in applications to rotary joints that, since the center conductor terminates on the bottom of the guide, a second low-power coaxial rotary joint may be built within the center conductor. This is a great advantage in certain types of installations. However, the doorknob transition is very difficult to build because its dimensions are quite critical. This is to be expected for the broadband models in which the transition is actually adjusted to have a considerable mismatch of the proper distribution with wavelength in magnitude and phase so that it may be matched over a broad band by means of a waveguide iris. There has been considerable difficulty in securing consistent production units. The machining tolerances required by most designs are not unduly small and can be met, with care. It appears, however, to be much more difficult to maintain the assembly dimensions because of the distortion and movement of the parts at the temperatures required for silver soldering.

Calculations of new matching irises from measurements on individual transitions can compensate for these deviations. This, however, is laborious; the same result can be accomplished by the use of tuning screws to adjust the iris impedance slightly in the manner described in Sec. 6-8. But, since the calculation of matching irises for individual units is not practical and tuning adjustments are undesirable as production techniques, several different methods of manufacturing these transitions have been tried. The doorknob contour itself can be machined with a sufficient accuracy; and it is not likely to distort in assembly if properly designed. The chief problem arises in maintaining accurate dimensions in the waveguide section. Ordinary rectangular tubing is not sufficiently accurate; and it is subject to considerable distortion. Attempts to cast waveguide sections have not, so far, proved satisfactory. Electroformed sections are slightly more accurate, but they lack mechanical strength at the junction between the coaxial outer conductor and the waveguide wall. Machined sections are, usually, unnecessarily heavy and too expensive for practicability. The best results have been obtained by using a well-annealed precision waveguide that is very carefully handled during the assembly process. Furnace-assembly soldering of the parts, accurately held in position with soldering jigs, is required to minimize variations in production units. Since considerable work has been done on the problem of manufacturing well-matched doorknob transitions, all the results cannot be given here. Further information and design details may be obtained from previous references and elsewhere.¹

¹ F. L. Niemann, "10-Cm Coaxial Line-to-Rectangular Waveguide Transitions," RL Report No. 802, December 1945.

6-14. Magnetic and Resonant-slot Couplings.—The transitions described thus far have been of the electric-coupling type in which various means of supporting a waveguide-exciting antenna are employed. As discussed in Sec. 6-3, there is also the magnetic-coupling transition which is formed by terminating the coaxial line in a loop, the plane of which is orthogonal in the waveguide to the magnetic field associated with the TE_{10} -mode. Several different versions of this transition have been developed, and a few have had limited application. They are, in general, difficult to match, quite frequency-sensitive, and critical as

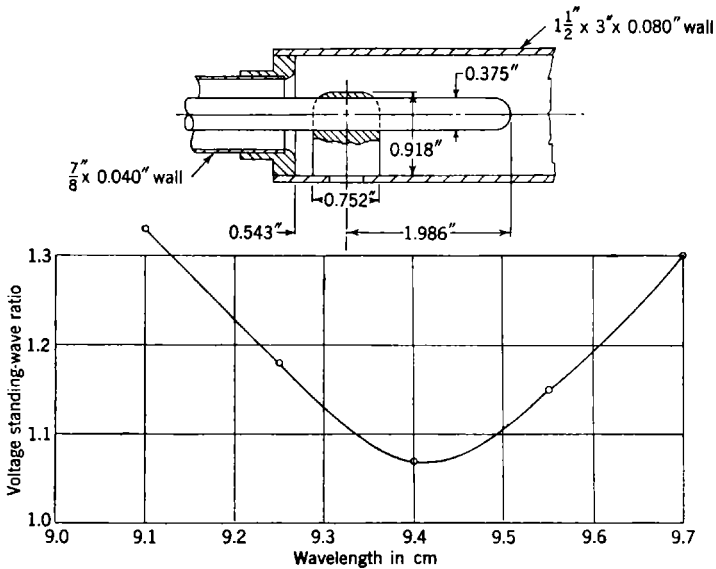


Fig. 6-38.—Straight-through transition from $\frac{7}{8}$ -in. coaxial line to waveguide.

to dimensions, so that they have a number of disadvantages when compared with the electric-coupling type of transition. In one instance in which a straight-through E -plane transition at 9.4 cm was required, the construction shown in Fig. 6-26j was used with limited success. The dimensions and electrical characteristics of this transition are given in Fig. 6-38. It was matched by variation of the loop size L and the probe depth P (Fig. 6-26j). A particularly long probe was necessary to obtain the proper susceptance. The supporting post was arbitrarily chosen fairly large in order to minimize high-power breakdown to the opposite side of the guide.

Figures 6-26k and l show two right-angle H -plane transitions for the 10-cm region used by the Raytheon Manufacturing Company. The

first is a straightforward loop coupling which could be matched by variation of the loop size and end-plate distance, but which proved too frequency-sensitive to be of much use. The second is based on the idea that the distribution of electric field in a resonant slot in the coaxial line is similar to that required to excite the TE_{10} -mode in rectangular waveguide. The slot region is excited by magnetic coupling from the loop formed by grounding the center conductor to the outer conductor in the region of the slot. This transition proves somewhat broader band than the other with a VSWR of less than 1.10 for a ± 3 per cent band when the unit is well made. Matching of this transition is accomplished by variation of the slot width and length, the end-plate distance, the loop size, and the guide height which provides the proper susceptance. As in the case of any transition of complicated geometry most of these dimensions prove rather critical, and the desired characteristics are difficult to reproduce. This transition was used in one model of a production radar system but was replaced in later models by a probe-type transition.

6-15. Applications and Special Transitions.—In addition to providing transitions between the different standard coaxial lines and waveguides, some of the units described have been combined with other devices for specific applications. The most frequently used examples are the magnetron-to-waveguide input couplings, and the coaxial rotary joints between waveguide sections. The applications to rotary joints will be discussed in Chap. 7. Two different kinds of magnetron couplings will be described here.

One type of waveguide coupling for a high-power 10-cm magnetron having coaxial output section is shown in Fig. 6-39. In this design the magnetron may be removed from the coupling unit. The outer conductors are coupled by means of the conventional half-wavelength coaxial choke (see Chaps. 2 and 7). The center conductors are connected by a double-ended "bullet" designed to maintain spring contact at each end. It is made of beryllium copper and is heat-treated after machining for maintenance of its properties while operating at a fairly high temperature. A pressurizing gasket seals the outer case of the magnetron output section to the coupling unit so that the r-f line may be operated under pressure to reduce the possibility of breakdown. The unit shown is a doorknob transition for $1\frac{5}{8}$ -in. coaxial line with a $\frac{3}{8}$ -in.-diameter center conductor. Its characteristics are those given by Curve II, Fig. 6-35. It is used with the 4J31-35, 43-47, and 74-77 types of magnetrons. A second magnetron-to-waveguide coupling is that shown in Fig. 6-40. To ensure the proper positioning of the probe, the coupling is designed to be a permanent part of the tube. When this construction is used, the probe may be contained within the tube seal, an arrangement which greatly increases the power-handling capacity of the unit. The

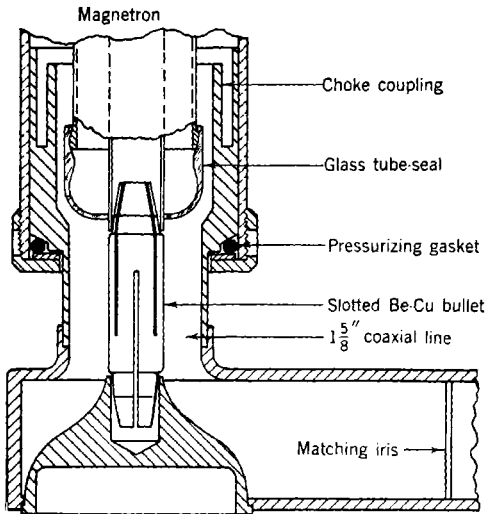


FIG. 6-39.—Waveguide input coupling for high-power 10-cm magnetron.

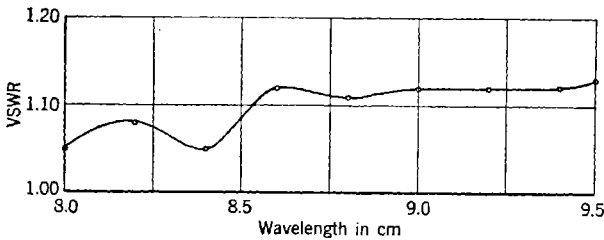
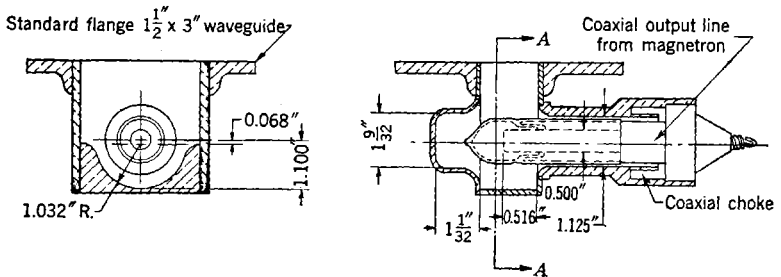


FIG. 6-40.—Coupling from coaxial line to waveguide for high-power tunable magnetron (sealed-in-glass probe transition).

enlarged waveguide section in the region of the probe also aids in this respect. Matching is accomplished in the usual way, by variation of the end-plate distance and the probe depth. The results, shown in the curve of voltage standing-wave ratio as a function of wavelength, were obtained without the use of a matching iris. This is the type of construction used on the 4J70-73 tunable magnetron. It has given no evidence of breakdown at the maximum powers (about one megawatt) presently available.

A special application, in which a combination of transitions is used to advantage, is shown in Fig. 6-41. This arrangement reduces the complexity in construction of r-f components in a radar system that uses separate antennas for transmitting and receiving.¹ Two adjacent collinear coaxial antennas were designed to be operated in a vertical position and to have symmetrical field patterns in a horizontal plane. The two concentric coaxial-line-to-waveguide transitions, one a crossbar-supported probe and the other essentially

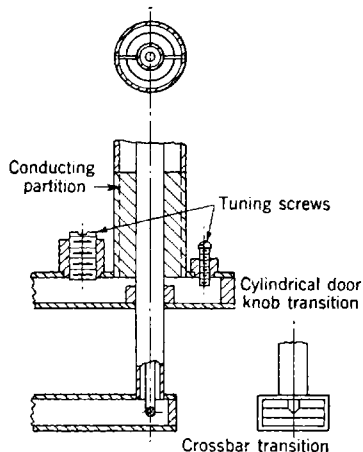


FIG. 6-41.—Concentric transitions for double antenna.

one a crossbar-supported probe and the other essentially

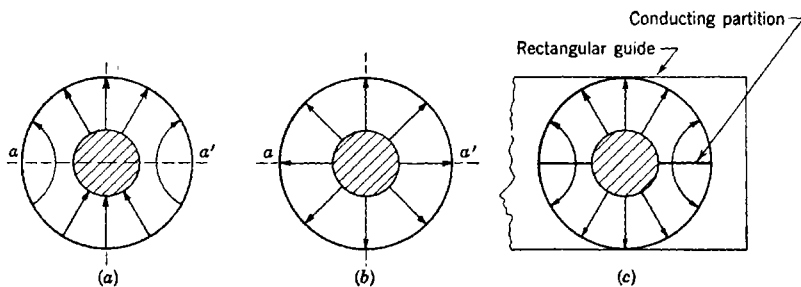


FIG. 6-42.—Field configurations in large coaxial line of double-coaxial coupler; (a) shows the electric field configuration in the TE_{10} -mode; (b) that in the TEM -mode; (c) shows the orientation of the conducting partition for symmetrical excitation of the coaxial line.

a cylindrical doorknob transition, allow coupling to both antennas in such a manner that neither field pattern is distorted by the presence of the transmission line to the other antenna. This device was used in a system

¹ R. M. Fano, "Double Coaxial Coupler for BUPX Antenna," RL Report No. 736, May 28, 1945.

operating in the 3-cm region. At these wavelengths, in order for the inner coaxial line not to become too small, the larger coaxial line is of a size such that it allows the transmission of the undesirable TE_{11} -coaxial mode illustrated in Fig. 6-42a. This mode cannot be used because of the requirement of azimuthal symmetry on the field of the antenna. The desired symmetrical TEM -coaxial mode is shown in Fig. 6-42b. The elimination of the TE_{11} -mode from the large coaxial line was accomplished in the following manner. It is evident from the field configuration of this mode, shown in Fig. 6-42a, that the plane $a-a'$ constitutes an equipotential surface to which the components of the field are orthogonal, so that it may be replaced by a thin conducting partition without disturbing the field configuration.

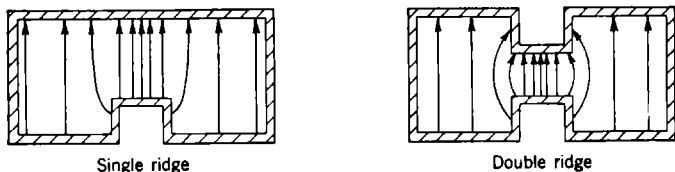


FIG. 6-43.—Electric field configurations for TE_{10} -mode in single- and double-ridged waveguide.

If this is done, the only orientation for which the TE_{11} -mode may be propagated in such a transmission line is that for which the field is as shown in (a) or (c). If this partition is oriented in the transition as shown in Fig. 6-42c, then the coaxial line following the partition will be symmetrically excited. Any other fields are rapidly attenuated. This is particularly important since there is known to be considerable distortion of field in right-angle transitions of this sort. The length of this strip is that which is necessary for the desired amount of attenuation of the unwanted modes.

These transitions were matched by the usual techniques already discussed. The transition to the larger coaxial line proved to be somewhat critical as to dimensions and for that reason tuning screws were provided to permit factory adjustment of the transition after assembly. Both transitions when properly made and tuned have a voltage standing-wave ratio of less than 1.1 for a bandwidth of about 9 to 10 per cent.

In developing a very wideband transition from coaxial line to waveguide considerable work has been done by the Radio Research Laboratory at Harvard University on the properties of "ridge" waveguide¹ and its application to the transition problem.² This type of waveguide is

¹ S. B. Cohn, "Properties of Ridge Waveguide," RRL Report No. 411-211, August 1945.

² S. B. Cohn, "Design of Simple Broad-band Waveguide-to-Coaxial Line Junctions," RRL Report No. 411-186, July 1945.

also discussed in Sec. 2-9. The electrical field configurations for single- and double-("H-shaped") ridge waveguide are shown in Fig. 6-43. The approximate distribution in intensity is suggested by the density of the lines of force.

This type of waveguide has several properties which make it applicable to broadband components in general, and to coaxial-line-to-waveguide transitions in particular. For given over-all dimensions it has a longer cutoff wavelength (lower cutoff frequency) than the same size of rectangular guide. Its characteristic impedance can be made considerably lower than that of ordinary guide; and in particular, it can be made equal

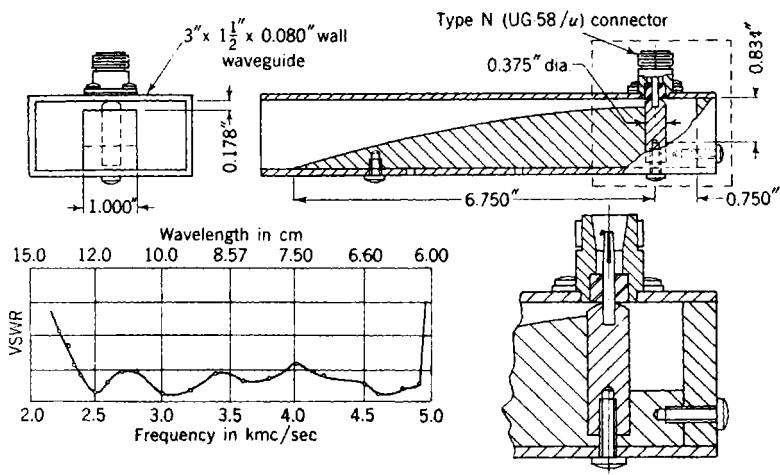


FIG. 6-44.—Adapter for type N connector (UG-58/U) to waveguide with single-tapered ridged waveguide.

to that of the standard coaxial lines. Further, the range between the cutoff wavelengths of the various modes is considerably increased, making it useful for very broadband requirements. However, it has certain disadvantages. In addition to being somewhat more complicated to construct accurately, its attenuation is several times that of ordinary waveguide, and its breakdown is obviously less than that of the standard guide. This limits its use to those receiving or low-power transmitting systems which employ a fairly short length of this guide.

In using ridged waveguide in a transition from coaxial line to standard waveguide, the coaxial line is terminated in a ridged waveguide section with an input characteristic impedance equal to that of the coaxial line. The "ridge" then is tapered gradually into the standard guide. Since the ridged waveguide is symmetrical, the asymmetrical TE_{20} -mode is not excited in the rectangular guide; and, since in the ridged guide the

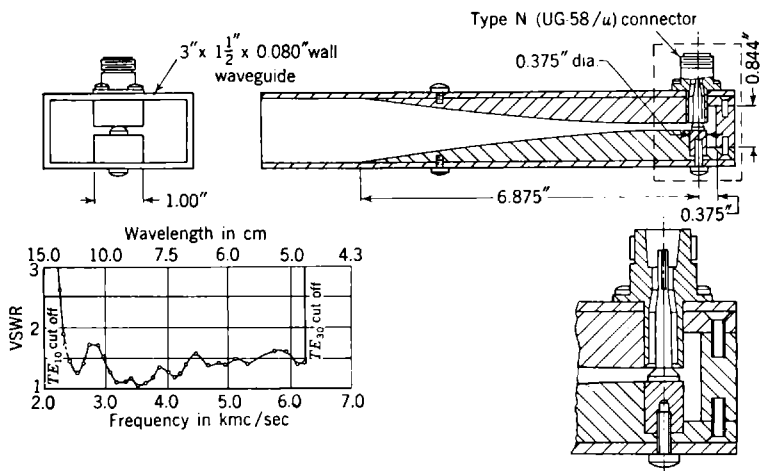


FIG. 6-45.—Adapter for type N (UG-58/U) connector to waveguide with double-tapered ridged waveguide.

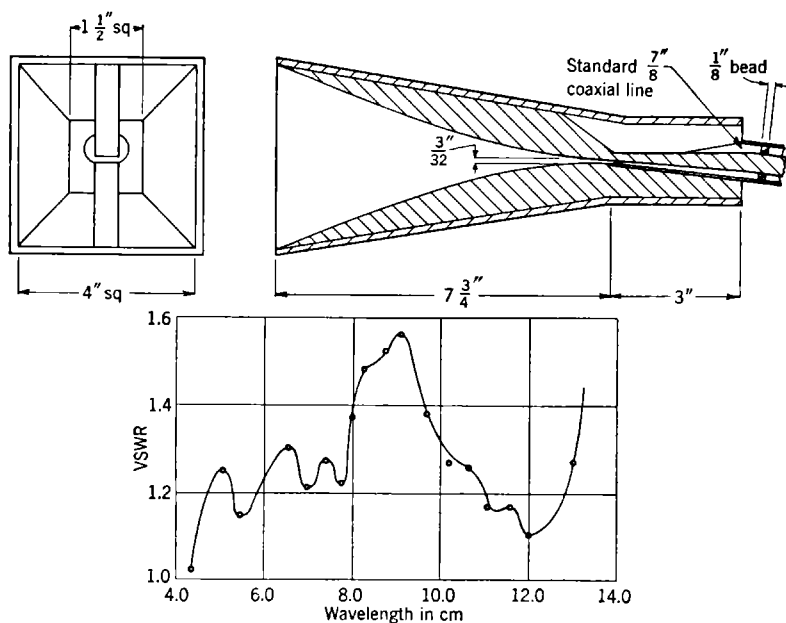


FIG. 6-46.—Dimensions and performance curve of transition from 7/8-in. coaxial line to ridged waveguide horn. (See Fig. 6-47.)

TE_{30} -mode has a much shorter cutoff wavelength than in the standard guide, most of the field of this mode excited by the transition is damped out before it reaches the rectangular guide. It is sometimes possible to use such a transition over almost the entire region between the cutoff wavelengths of the TE_{10} - and the TE_{30} -modes in the standard guide.

Figures 6-44 and 6-45 show, respectively, the use of single and double-tapered ridged waveguide sections in the construction of a broadband coaxial-line-to-waveguide transition. These units, designed by the

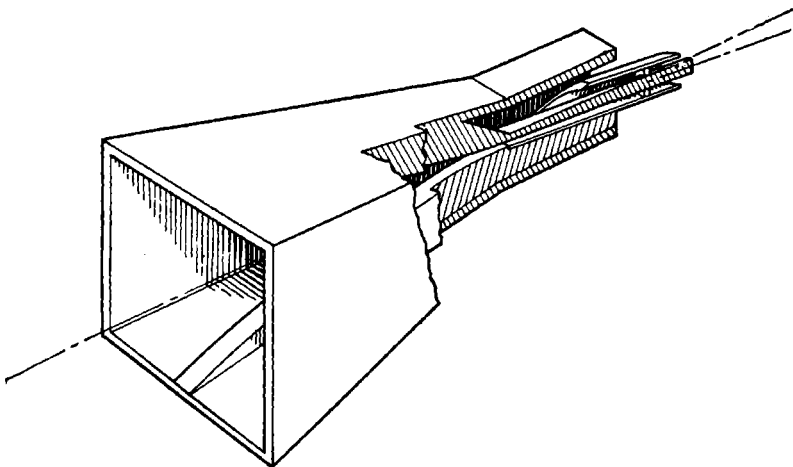


FIG. 6-47.—Transition from $\frac{7}{8}$ -in. coaxial line to ridged waveguide horn (see Fig. 6-46).

Radio Research Laboratory, are for the standard type N (UG-58/U) connector in bead-supported $\frac{5}{16}$ -in. coaxial line. An example of a similar application to a broadband antenna "feed" horn, with a transition from standard $\frac{7}{8}$ -in. coaxial line to a special size of guide developed at the Radiation Laboratory, is shown in Figs. 6-46 and 6-47. The flared horn provides an approximate match to free space. The results, plotted in terms of voltage standing-wave ratio as a function of wavelength, were measured in the coaxial line.

LOWEST MODE IN THE WAVEGUIDE TRANSITIONS

By F. E. EHLERS

6-16. The Transition between Rectangular Waveguides of Different Sizes.—It is often desirable to transform from rectangular waveguide of one size, carrying the TE_{10} -mode, to that of another size in which the same mode is propagated. This may be done by means of a quarter-wavelength matching transformer, or by a taper from one set of dimensions to the other.

Although the concept of characteristic impedance in waveguide is not so well defined as it is in coaxial line, it is convenient to use regular transmission-line theory in determining the dimensions of a quarter-wavelength transformer. Consequently, the following formula for the equivalent impedance of rectangular waveguide in the TE_{10} -mode may be taken from Slater.¹

$$Z_{\text{equ}} = \sqrt{\frac{\mu}{\epsilon}} \frac{1}{\sqrt{1 - \left(\frac{\lambda_0}{2a}\right)^2}} \frac{b}{a} = \sqrt{\frac{\mu}{\epsilon}} \frac{\lambda_0}{\lambda_0} \frac{b}{a} \quad (23)$$

If this formula is assumed, the equivalent circuit of the discontinuity between the different waveguides is that shown in Fig. 6-48 provided that the change from Z_1 to Z_2 is not too great and that neither waveguide will transmit higher modes.

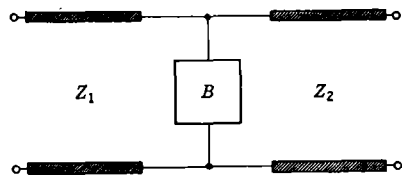


FIG. 6-48.—Equivalent circuit of discontinuity between different waveguides.

be rewritten in the following form:

$$b^2 = \frac{\epsilon}{\mu} Z_{\text{equ}}^2 \left[a^2 - \left(\frac{\lambda_0}{2} \right)^2 \right].$$

This is the equation of an hyperbola, connecting a and b if Z_{equ} is kept constant. For a given choice of a greater than a half wavelength, a value of b for the waveguide is determined which will match the impedance of another waveguide of the same equivalent impedance.

If the two waveguides differ only in the narrow dimension, the calculation of a quarter-wavelength transformer becomes very simple since the characteristic impedance is proportional to the narrow dimension only. Thus, the narrow dimension of the transformer section is

$$b_t = \sqrt{b_1 b_2},$$

where b_1 , b_2 , and b_t are shown in Fig. 6-49.

At each junction between the waveguide and the transformer, there will be a shunt capacitive susceptance. If the discontinuities are not too large, however, the shunt susceptances, having about the same

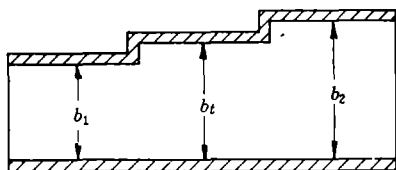


FIG. 6-49.—Narrow dimensions of a transformer section.

¹ J. C. Slater, *Microwave Transmission*, McGraw-Hill, New York, 1942.

magnitude, will nearly cancel each other because of the quarter-wavelength spacing. If the two waveguides differ in the wide dimensions only, the problem is a little more difficult since the guide wavelength must be taken into account. For this sort of change, the shunt susceptance at the steps will be inductive instead of capacitive. If two waveguides differ in both dimensions b and a , the transformer section may be chosen to make the shunt susceptance of the ends approach equality or vanish altogether. Such a quarter-wavelength transformer has been designed for the junction between $1\frac{1}{4}$ - by $\frac{5}{8}$ -in. rectangular waveguide with 0.064-in. wall, and 1- by $\frac{1}{2}$ -in. waveguide with 0.050-in. wall. The dimensions of this transformer are shown in Fig. 6-50. The voltage standing-wave ratio introduced by the transformer is less than 1.03 over the wavelength band from 3.13 to 3.53 cm.

A simple way to transform from a waveguide of one size to one of another size is to taper the dimensions linearly. In Frank's report,¹ the ratio of incident to reflected waves from a tapered section of transmission line, if the second waveguide is terminated in its characteristic impedance, is shown to be (see Eq. 1)

$$\frac{B}{A} = \frac{1}{4\gamma_0} \left[\frac{d \ln Z}{dx} \right]_0 - \frac{1}{4\gamma_1} \left[\frac{d \ln Z}{dx} \right]_1 \exp \left(-2 \int_0^d \gamma dx \right). \quad (24)$$

If the two terms of Eq. (24) representing the magnitude of the discontinuities at both ends of the taper are equal, and if the length of the taper is equal to an integral number of half wavelengths, the reflection from the taper will be zero, according to the formula above. If these two terms are different, the mismatch of the taper will be at a minimum for length of the taper equal to an integral number of half wavelengths. For a taper in which the dimensions change linearly, a_0 may be defined as the wide dimension of the smaller waveguide and d as the length of the taper. Then the corresponding dimension of any cross section in the taper is

$$a = a_0 + \frac{\delta x}{d},$$

¹ N. H. Frank, "Reflections from Sections of Tapered Transmission Lines and Waveguides," RL Report No. 189, Jan. 6, 1943.

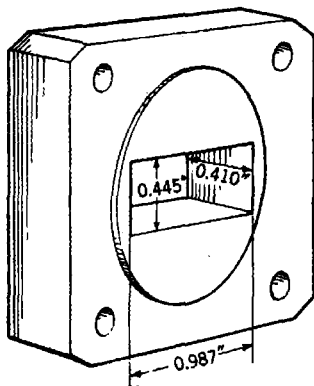


FIG. 6-50.—Quarter-wavelength transformer from 1- by $\frac{1}{2}$ -in. rectangular waveguide (0.050-in. wall) to $1\frac{1}{4}$ - by $\frac{5}{8}$ -in. rectangular waveguide (0.064-in. wall). Army-Navy designation UG-80/U.

where δ is the difference between the wide dimensions of the two waveguides. For calculating the length of an integral number of half wavelengths, the following formula may be used:

$$n\pi = \int_0^d \frac{2\pi}{\lambda_g} dx = 2\pi \int_0^d \frac{\sqrt{1 - (\lambda/2a)^2}}{\lambda} dx,$$

$$n\pi = \frac{2\pi d}{\delta\lambda} \int_{a_0}^{a_1} \frac{\sqrt{(2a)^2 - \lambda^2}}{2a} da.$$

Integrating and simplifying,

$$d = \frac{n\lambda\delta}{\sqrt{(2a_1)^2 - \lambda^2} - \sqrt{(2a_0)^2 - \lambda^2} - \lambda \left(\cos^{-1} \frac{\lambda}{2a_1} - \cos^{-1} \frac{\lambda}{2a_0} \right)}$$

This formula may be rewritten for convenience in the parameters of waveguide wavelengths and the wide dimensions for the two terminating waveguides.

$$d = \frac{n(a_1 - a_0)}{\left(\frac{2a_1}{\lambda_{g_1}} - \frac{2a_0}{\lambda_{g_0}} \right) - \cos^{-1} \left\{ \frac{\lambda^2}{4a_0a_1} \left[1 + \left(\frac{2a_0}{\lambda_{g_0}} \right) \left(\frac{2a_1}{\lambda_{g_1}} \right) \right] \right\}}$$

Two such tapers, 0.817 in. and 1.635 in. long, were constructed and tested. The first was calculated from the above formula to be a half wavelength long and the other, a full wavelength, at 3.22 cm. The voltage standing-wave ratios of both transitions were 1.05 or less over a wavelength range from 3.14 to 3.52 cm.

6-17. Transition from Rectangular to Cylindrical Waveguide.—As the primary modes in both the round and rectangular waveguides are similar, being *TE*-modes, the cylindrical waveguide may be excited directly from the end, utilizing a gradual taper or a quarter-wavelength transformer. If the rectangular waveguide is terminated abruptly in the cylindrical waveguide, the voltage standing-wave ratio is about 2. The admittance of such a transition from $\frac{1}{4}$ - by $\frac{1}{2}$ -in. waveguide with 0.040-in. wall to 0.350-in. ID tubing at a wavelength of 1.25 cm is $Y = 0.45 - j0.15$ referred to the junction point between the two waveguides. Thus, to match such a transition with a quarter-wavelength transformer the equivalent characteristic admittance of the transformer section relative to the rectangular waveguide must be 0.67; and the susceptance of the two junctions of the transformer must be equal. Since the transition is from rectangular to round waveguide, this condition will be more easily obtained by a waveguide that has a cross section intermediate between round and rectangular. As the guide wavelength and the characteristic admittance cannot be calculated in a waveguide with round corners, both the length and the size of the transformer must be determined experimentally. The admittance that would be obtained with a transformer

whose characteristic admittance is correct for matching the two waveguides may be calculated on the basis of transmission-line theory as a function of its length. The resulting curve passes through the center of the Smith chart in Fig. 6-51. There are two other curves in Fig. 6-51 which show the variation of admittance with length for transformers with too large and too small a characteristic admittance. These curves have

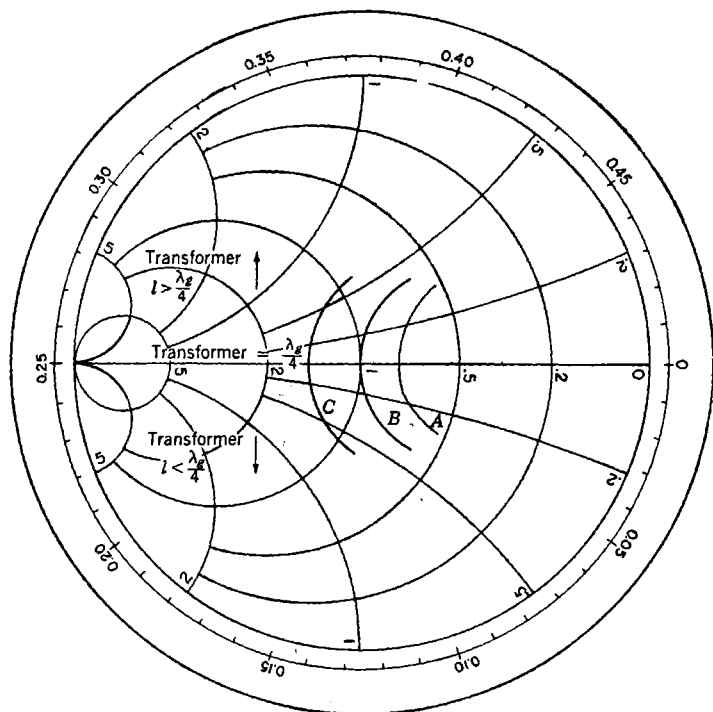


FIG. 6-51.—Curves for correct and incorrect transformer characteristic admittance; (A) transformer characteristic admittance too small; (B) correct transformer characteristic admittance too large. The admittance chart has been rotated 180° from the usual position (see Sec. 2-12). Some users prefer this position since it gives positional correspondence with impedance chart.

been calculated with the assumption that no shunt susceptance exists at the junctions of the transformers. With such susceptances present there would be some rotation and shifting of these curves. However, when these curves are taken as indicative of the general trend of admittances that would be encountered, the dimensions of the transformer may be determined empirically by a series of approximations. It should be remembered, however, that the characteristic admittance is proportional to a/λ_g , which increases with the wide dimension of the guide and is

inversely proportional to the narrow dimension [see Eq. (23)]. Such a transformer from $\frac{1}{2}$ - by $\frac{1}{4}$ -in. waveguide with 0.040-in. walls to round waveguide 0.350 in. ID was designed for 1.25-cm wavelength and is shown in Fig. 6-52.

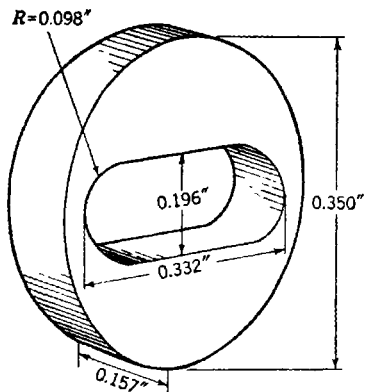


FIG. 6-52.—Transformer from $\frac{1}{2}$ - by $\frac{1}{4}$ -in. waveguide with 0.040-in. wall to round waveguide 0.350 in. ID.

Another way to construct a quarter-wavelength transformer is to fill in a section of the round waveguide as shown in Fig. 6-53. This has been tried in transforming from $\frac{1}{2}$ - by $\frac{1}{4}$ -in. waveguide with 0.040-in. wall to round waveguide 0.350 in. ID, with less success than the design of Fig. 6-52. This design is also not so easy to make as the transformer described in the preceding paragraph.

A taper from rectangular to round waveguide may be constructed as shown by the sketch in Fig. 6-54. In this construction, the cross section changes gradually from a rectangular shape to a circular one. If this transition section is made longer than a wavelength, the match will, in general, be quite satisfactory. One is assured of a good match if this transition is made very long, for the change will be gradual enough to cause little mismatch. Figure 6-54 gives the

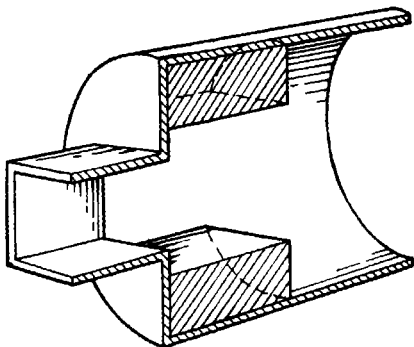


FIG. 6-53.—Quarter-wavelength transformer.

dimension of such a taper from 1- by $\frac{1}{2}$ -in. rectangular waveguide with 0.050-in. wall to 1-in. round waveguide with 0.032-in. wall. This taper is between one, and one and a half wavelengths long and the voltage standing-wave ratio is 1.10 or less from 3.14 to 3.47 cm.

It is also possible to transform from rectangular waveguide to round

waveguide with the two waveguides at right angles. There are two types of coupling, series and shunt. In the series coupling, the wide dimension of the waveguide is transverse to the axis of the round guide. This is not so easy to match as the shunt coupling since there is a greater distortion of the magnetic and electric fields at the junction between the

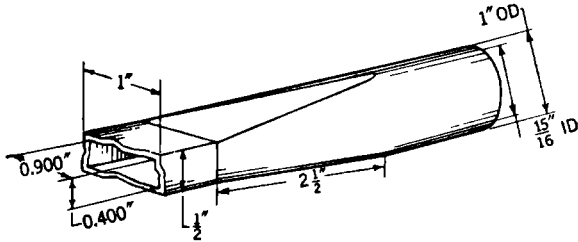


FIG. 6-54.—Taper from rectangular to round waveguide.

rectangular and round waveguides. However, if a wedge is placed extending from one wide side of the rectangular waveguide to the opposite wall of the round waveguide as in Fig. 6-55, a match may be obtained. This wedge helps to bend the wave around the corner. Data of voltage standing-wave ratio vs. wavelength for wedges of three sizes are shown in the graph Fig. 6-56 for 1-by 1/2-in. waveguide with 0.050-in. wall and round waveguide 1 1/8 in. ID. Better results may possibly be obtained if some matching device, such as inductive window, is used in conjunction with the wedge.

A transition, using shunt coupling from 1/2-by 1/4-in. waveguide with 0.040-in. wall to round waveguide 0.350 in. ID, may be matched at 1.25-cm wavelength by adjusting a short-circuiting plunger in one arm of the round waveguide. This combination of waveguide dimensions is such that at this wavelength no matching irises or transformers are needed. For waveguides of different relative sizes, some additional means of matching must be employed.

In designing such a transition, one must avoid using a waveguide too near cutoff for the TM_{01} -mode. Since the rectangular waveguide opening

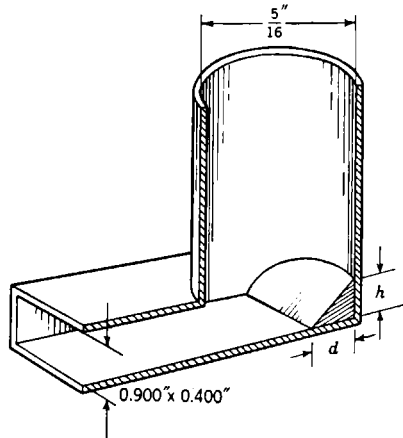


FIG. 6-55.—Right-angle transition from rectangular to round waveguide. The waveguide width is 0.900 in. ID.

increases the cutoff wavelength of this mode in this short section of round waveguide, resonances may occur which would introduce serious reflection. In case the diameter of the round waveguide cannot be reduced in a particular application, these resonances may be eliminated by

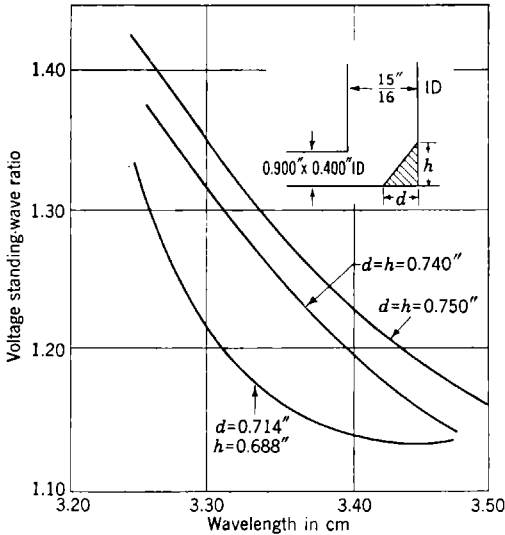


Fig. 6-56.—Voltage standing-wave ratio for different size wedges from rectangular to round waveguide.

placing across the opening narrow bars which are parallel to the wide dimension of the rectangular waveguide. These bars, being perpendicular to the electric field in the rectangular waveguide, have little effect upon the match but, by closing the opening, they reduce the cutoff wavelength of the TM_{01} -mode to a safe value.

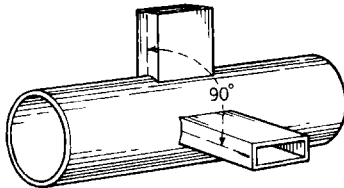


Fig. 6-57.—Transition from rectangular to round waveguide with two rectangular waveguides.

With a single rectangular-waveguide input wave, one polarization will be excited, of which the maximum radial electric-field component will be transverse to the wide dimension of the rectangular waveguide. It is possible to couple another waveguide the same distance from the short-circuiting plug

about 90° in azimuth from the location of the first rectangular waveguide (see Fig. 6-57). In this way, another polarization may be fed into, or coupled out of, the round waveguide. However, the waveguides are not strictly independent for there will be some coupling from one to the other.

This coupling to the second arm of r-f power from the first will reflect from the second opening some TE_{11} -power, with the polarization 90° to the wave set up by the first arm. The phase of this reflected wave may be different from that of the input wave so that, in adding with the input wave, it will cause some of the energy to be circularly polarized.

Another means of coupling the other polarization is by feeding the round waveguide end-on with a quarter-wavelength transformer, as in Fig. 6-53. The quarter-wavelength transformer will act as a short-circuiting plug in the round waveguide, for the wave from shunt arm providing the narrow dimension of the transformer is beyond cutoff for the incident frequency. Figure 6-58 gives the details of this transition. The distance from the edge of the quarter-wavelength transformer to the inside dimension of the rectangular waveguide, as shown, is somewhat less than the distance for a short-circuiting plug. The effective short circuit is slightly beyond the face because the transformer waveguide is beyond cutoff for this polarization.

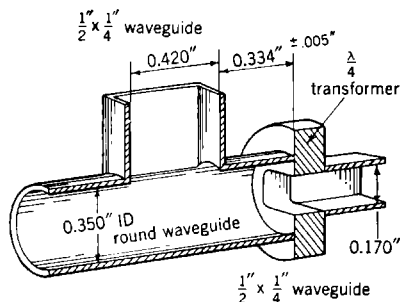


FIG. 6-58.—Transition from rectangular waveguide to two polarizations in round waveguide.

6-18. Circular Polarization of the TE_{11} -mode.

—The radial component of the electric field of a single polarization of the TE_{11} -mode at a fixed radial distance $r < a$ is of the general form

$$E_r = E \sin \phi' e^{j(\omega t - \beta x)}.$$

Now this single wave may be broken up into the sum of two waves whose maximum amplitude is 90° apart in azimuth; thus,

$$E_r = E_1 \sin \phi e^{j(\omega t - \beta x)} + E_2 \cos \phi e^{j(\omega t - \beta x)}, \quad (25)$$

where ϕ has undergone some angle of rotation from ϕ' , depending upon the relative magnitude of E_1 and E_2 .

If the second wave had undergone a shift in phase of θ' radians, it would be designated for conveniences which will become clear later in the discussion as $\theta' = \theta + (\pi/2)$, where θ is now the phase shift greater (or less) than a quarter wavelength. Equation (25) now becomes

$$E_r = E_1 \sin \phi e^{j(\omega t - \beta x)} + E_2 \cos \phi e^{j(\omega t + \frac{\pi}{2} + \theta - \beta x)}$$

$$E_r = E_1 \sin \phi e^{j(\omega t - \beta x)} + E_2 \cos \phi (-\sin \theta + i \cos \theta) e^{j(\omega t - \beta x)}. \quad (26)$$

If, to the right-hand member of this equation, we add

$$E_2 \sin \phi \cos \theta e^{j(\omega t - \beta x)} - E_2 \sin \phi \cos \theta e^{j(\omega t - \beta x)} \equiv 0$$

and regroup the terms, the equation for the electric field becomes

$$E_r = [E_1 \sin \phi - E_2 \sin (\phi + \theta)]e^{j(\omega t - \beta x)} + E_2 \cos \theta e^{j\left(\omega t - \phi + \frac{\pi}{2} - \beta x\right)}. \quad (27)$$

The first term represents a plane-polarized wave. The second term, however, has an amplitude which is independent of angle and therefore is symmetric. This symmetry is, however, false since, at any instant t' , the electric field has the same pattern as a single plane-polarized wave. To determine the angular position of the maximum electric field, the exponent must be set equal to zero.

$$\omega t - \phi + \frac{\pi}{2} - \beta x = 0$$

$$\phi = \omega t + \frac{\pi}{2} - \beta x.$$

At any cross section in the waveguide, therefore, the maximum amplitude rotates with an angular velocity of ωt . Hence, the resultant of any two plane-polarized waves which differ in phase consists of the sum of a single plane-polarized wave and a circularly polarized wave. The E_ϕ component of the TE_{11} -mode, which for constant $r < a$ has the form $E = E \cos \phi e^{j(\omega t - \beta x)}$, can thus be represented in a manner similar to Eq. (27). The derivation of the E_ϕ component then, will be omitted from this discussion.

If the amplitudes E_1 and E_2 of the two waves were equal, then

$$\begin{aligned} E_r &= E_1 [\sin \phi - \sin (\phi + \theta)]e^{j\omega t - \beta x} + E_1 \cos \theta e^{j\left(\omega t - \phi + \frac{\pi}{2} - \beta x\right)} \\ E_r &= -2E_1 \sin \frac{\theta}{2} \cos \left(\phi + \frac{\theta}{2}\right) e^{j(\omega t - \beta x)} + E_1 \cos \theta e^{j\left(\omega t - \beta x - \phi + \frac{\pi}{2}\right)}. \end{aligned} \quad (28)$$

The angle θ is the difference in phase shift from $\pi/2$ radians, or a quarter wavelength; thus, if $\theta = 0$, all the energy from two waves of equal amplitude whose polarizations differ by 90° is transmitted into the circularly polarized mode, when a phase shift of $\pi/2$ radians or a quarter wavelength is introduced into one of the two waves. If the phase shift is greater or less than $\pi/2$, the ratio between the amplitudes of the plane-polarized wave and the circularly polarized wave from Eq. (28) is

$$\frac{E_p}{E_c} = \left| \frac{2 \sin \frac{\theta}{2}}{\cos \theta} \right|; \quad (29)$$

and the ratio of the powers in the two waves is

$$\frac{P_p}{P_c} = \frac{4 \sin^2 \frac{\theta}{2}}{\cos^2 \theta}. \quad (30)$$

If a probe is inserted into a waveguide which is matched to all polarizations and which carries two such waves, and the probe is rotated around the tube, the symmetry of the resulting wave can be determined. From Eq. (26), the magnitude of the square of the electric field as a function of ϕ and θ , after setting E_2 equal to E_1 , may be calculated.

$$E_p^2 = E_1^2 (1 + \sin 2\phi \sin \theta), \quad (31)$$

which has maxima at $\phi = \pi/4, 5\pi/4$ and minima at $\phi = 3\pi/4, 7\pi/4$ for $\pi > \theta > 0$. The maximum to minimum voltage ratio is

$$r = \sqrt{\frac{1 + \sin \theta}{1 - \sin \theta}} = \cot \left(\frac{\theta}{2} + \frac{\pi}{4} \right). \quad (32)$$

Combining Eqs. (29) and (32), and (30) and (32), we get

$$\frac{E_p}{E_c} = \frac{2 \sin \left(\cot^{-1} r - \frac{\pi}{4} \right)}{\cos \left(2 \cot^{-1} r - \frac{\pi}{2} \right)} = \frac{2 \sin \left(\cot^{-1} r - \frac{\pi}{4} \right)}{\sin \left(2 \cot^{-1} r \right)},$$

and

$$\frac{P_p}{P_c} = \frac{1 - \sin 2(\cot^{-1} r)}{\sin^2 2 \cot^{-1} r}.$$

With the above relations there is sufficient information to design a quarter-wave plate in the TE_{11} -mode in order to obtain a circular polarization. Various schemes for obtaining it have been tried. Usually, these schemes consist of inserting a metal fin or a dielectric slab at a 45° angle to the incident wave. At this fin the incident wave can be resolved into two waves of equal amplitude at 45° . If the fin is very narrow, its effect on the polarization, of which the radial vector is maximum 90° in azimuth away from the fin, is very small; this is true since the electric field E_r is perpendicular to its surface and the radial component E_r is equal to zero. For fins that are rather thick, however, there is some phase shift in one polarization, and considerable phase shift in the polarization that has a maximum electric field at the fin. For a 0.062-in. fin in round waveguide of 0.350 in. ID at 1.25 cm, the guide wavelength, as a function of the amount of insertion of the fin into the waveguide, is plotted in Fig. 6-59 for the two polarizations. Another way of obtaining a quarter-wave plate is by filling in part of the waveguide with a metal plate as shown in the cross-section sketch in Fig. 6-60. In this figure also is a plot of guide wavelength as a function of the thickness of this metal plate.

The quarter-wave plate must be matched to both polarizations and particularly to the polarization in which it causes the greater phase shift. This matching is accomplished by using a quarter-wavelength step in the plate which must be determined experimentally after the dimensions

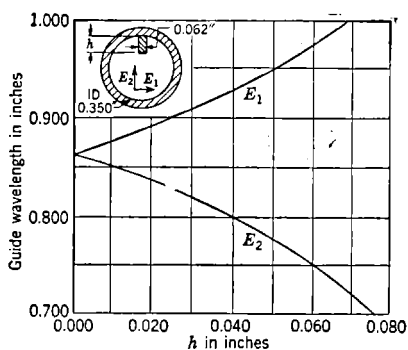


FIG. 6-59.—Guide wavelength in two polarizations of TE_{11} -mode for metal fin in round waveguide.

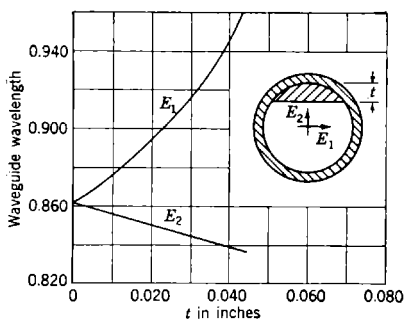
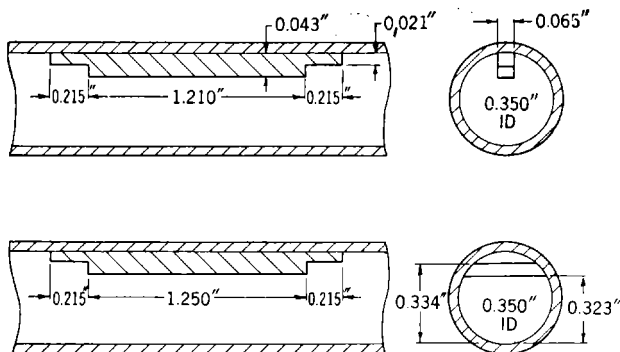


FIG. 6-60.—Waveguide wavelength for two polarizations of TE_{11} -mode.



FIGS. 6-61 and 6-62.—Quarter-wave plates; 1.25-cm wavelength.

of the matching transformers are determined. The length of the quarter-wave plate may be calculated as follows:

$$2l' \left(\frac{1}{\lambda_{t_1}} - \frac{1}{\lambda_{t_2}} \right) + l \left(\frac{1}{\lambda_1} - \frac{1}{\lambda_2} \right) = \frac{1}{4},$$

where l' is the length of the quarter-wave transformer, λ_{t_1} and λ_{t_2} are the guide wavelengths of the quarter-wavelength transformer for the two polarizations, and l is the remaining length of the quarter-wave plate with λ_1 and λ_2 the corresponding guide wavelengths of the two polarizations as shown in Figs. 6-59 and 6-60. Dimensions for two quarter-wave plates are shown in Figs. 6-61 and 6-62 for 1.25-cm wavelength in round waveguide 0.350 in. ID.

A quarter-wave plate may be obtained by means of a number of lumped susceptances spaced in the round waveguide. These lumped susceptances may be in the form of rods, as in Fig. 6-63, which protrude

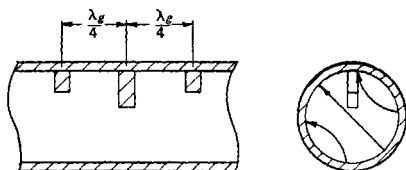


FIG. 6-63.—Quarter-wave plate with lumped susceptance.

into the waveguide. These rods act like shunt capacities; and if the values of their susceptances are known, the spacing between them may be determined by means of the Smith chart so that a perfect match is obtained. If the shunt capacity of these elements is not too large, a match over a broad band may be obtained by spacing several of these elements about a quarter wavelength if the relative magnitudes of these susceptances follow the values of the binomial coefficients. For example, if two susceptances are used, their magnitudes are equal; if three susceptances are used, then their magnitudes should have the relative values of ωc , $2\omega c$, and ωc , respectively. Several typical values are as follows:

Number of elements	Value of capacities				
2		ωc		ωc	
3		ωc	$2\omega c$	ωc	
4	ωc	$3\omega c$	$3\omega c$	ωc	
5	ωc	$4\omega c$	$6\omega c$	$4\omega c$	ωc

Equal spacing of equal elements may also be used but the broadband match may not be so good. By trying various matched combinations of these elements, the values of the susceptance and the number of elements may be determined experimentally so that circular polarization

is attained. This technique is rather cumbersome to design. Sufficient work has not been done to determine whether there is any gain in bandwidth over the continuous type of quarter-wave plates.

It is also possible to couple from rectangular waveguide directly to

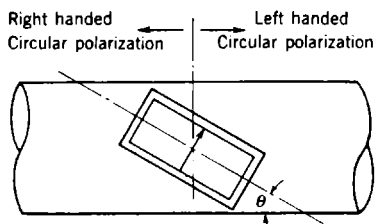


FIG. 6-64.—Double circular polarizer with right- and left-handed circular polarizations.

round waveguide in circular polarization without means of a quarter-wave plate. The shunt rectangular-waveguide arm as shown in Fig. 6-64 couples to the TE_{11} -mode by cutting transverse currents in the round waveguide. The instantaneous currents in circular polarization wind spirally around the waveguide making a complete revolution in a waveguide wavelength. Thus, if these currents are excited by orienting the rectangular waveguide at the proper angle with the axis of the round waveguide, circular polarization can be set up. This angle can be approximated by the formula

$$\theta = \tan^{-1} \frac{2\pi a}{\lambda_0}$$

where a is the radius of the round waveguide and λ_0 the waveguide wavelength. If both ends of the round waveguide are matched, then a right-handed circular polarization will be excited in one direction and a left-handed circular polarization in the other. Data at 1.25-cm wavelength for such a transition as a function of the orientation angle of the rectangular waveguide with respect to the round-waveguide axis are shown in Fig. 6-65.

If a movable short-circuiting plunger is introduced into one of these arms, some interesting results may be obtained. A left-handed polarization will be reflected back as a right-handed polarization, looking in the direction of propagation, and will add to the original right-handed circularly polarized wave. As the phase of this reflected wave is adjusted by the short-circuiting plunger, the resulting wave propagated in the matched arm may vary

round waveguide in circular polarization without means of a quarter-wave plate. The shunt rectangular-waveguide arm as shown in Fig. 6-64 couples to the TE_{11} -mode by cutting transverse currents in the round waveguide. The instantaneous currents in circular polarization wind spirally around the waveguide making a complete revolution in a waveguide wavelength. Thus, if these currents

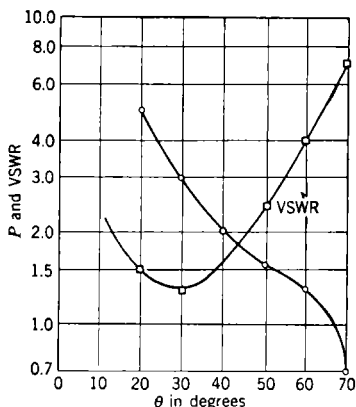


FIG. 6-65.—Performance of double circular polarizers of Fig. 6-64 at 1.25-cm wavelength with VSWR measured in rectangular waveguide and P equal to the ratio of the major axis voltage to the minor axis voltage of the polarized wave.

gradually from circularly polarized wave to plane-polarized wave. If the reflected wave is 180° out of phase with the other wave in the matched arm, then there is no propagation, and all the energy is reflected from the junction.

Circular polarization may also be excited by means of a transition which has been aptly designated as a "turnstile" transition. This consists of two cross arms of rectangular waveguide with a round waveguide coupled out of the section that is common to the two arms. The narrow dimensions of the rectangular waveguide are lined up with the round-waveguide axis. If the transition is matched so that the symmetry is preserved, then some interesting results are obtained. This matching is done by adjusting the dimensions of a post which is set in the bottom of the rectangular waveguide along the axis of the round waveguide as in Fig. 6-66. The data for Fig. 6-66 are taken from Table 6-3. The

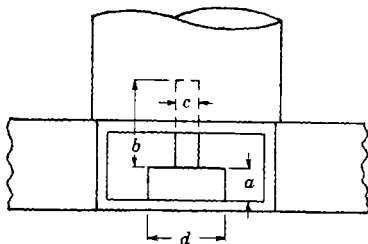


Fig. 6-66.—Matching of turnstile junction of Fig. 6-67; data taken from Table 6-3.

TABLE 6-3.—DIMENSIONS* TO ACCOMPANY TURNSTILE JUNCTION OF FIG. 6-66

Center wavelength, cm	a, in.	b, in.	c, in.	d, in.	Round waveguide, ID, in.	Rectangular waveguide, in.
3.33	0.181	0.509	0.125	0.4375	0.9375	$1 \times \frac{1}{2}$ (.050 wall)
3.57	0.160	0.502	0.125	0.5315	1.000	$1 \times \frac{1}{2}$ (.050 wall)
1.25	0.070	0.175	0.065	0.188	0.350	$\frac{1}{2} \times \frac{1}{4}$ (.040 wall)

* All letter symbols pertain to Fig. 6-66.

height and diameter of the lower part of the post have a greater effect on the match looking into one rectangular waveguide with matched loads in the other four arms, while the narrow post has greater effect on the match looking into the round waveguide. Thus a transition is obtained with the following characteristics:

1. The wave is matched looking into the round waveguide with matched loads in the four rectangular arms.
2. Each rectangular arm is matched with matched loads in the other arms.

With these conditions, if power is fed into Arm A Fig. 6-67, one half of the power is transmitted in the round waveguide, and the other half is divided between Arms B and D with no power propagated in Arm C.

Since B and D are in shunt with Arm A , the phase at the planes represented by narrow sides of waveguides A and C will be equal for the two waves. If arms B and D are short-circuited and are equal in length, the two reflected waves arrive back at the junction in phase, and the reflected power is equally divided between Arms A and C . No reflected power enters the round waveguide since the two reflected waves will set up polarizations in the round guide which are 180° out of phase and, therefore, will be canceled out.

If one arm is a quarter wavelength longer than the other, then the reflected waves from the two arms are out of phase and will set up a polarization in the round guide which is aligned with the axis of the short-circuited arms. Thus, there are two waves of equal amplitude, whose polarizations differ by 90° , propagated in the round waveguide. As the length of the arms is adjusted, keeping a quarter-wavelength difference in lengths between the two, the phase of the polarization set up by the reflected waves will be varied. If the phase

difference between the polarizations is equal to zero, then a plane-polarized wave oriented at 45° to the cross arms is propagated. If this phase difference is equal to π , then there is propagated a plane-polarized wave, oriented at 90° in azimuth from the wave resulting from a phase difference

TABLE 6-4.—DIMENSIONS AND VSWR FOR THE TURNSTILE JUNCTIONS OF FIG. 6-66

VSWR with matched loads in the three rectangular arms and in the round waveguide	Circular polarizer			Plane polarizer		
	$d_1,^*$ in.	$d_2,^*$ in.	VSWR	$d_1,^*$ in.	$d_2,^*$ in.	VSWR
1.03 for $\lambda = 3.33$ cm	1.367	0.864	1.616	1.146
1.01 from $\lambda = 3.407$ to 3.746 cm	1.356	0.763	1.12 at 3.525 cm 1.05 at 3.605 cm 1.02 at 3.654 cm
1.05 for $\lambda = 1.25$ cm	0.457	0.308	1.08 at 1.215 cm 1.10 at 1.224 cm 1.05 at 1.255 cm 1.10 at 1.250 cm 1.11 at 1.265 cm 1.16 at 1.280 cm

* d_1 and d_2 are lengths of arms B and D .

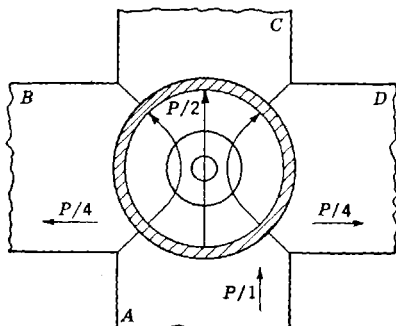


FIG. 6-67.—Cross section of turnstile transition.

of zero. If this phase difference is $\pi/2$, $3\pi/2$, the resulting wave is circularly polarized in the round waveguide; while in between these values of phase difference the resulting wave is elliptically polarized.

Table 6-3 gives the dimensions of three turnstile transitions centered at wavelengths of 3.33, 3.57, and 1.25 cm. Complete data have not been collected on these transitions since each transition was designed for a specific application, and only sufficient data were taken for this application. Table 6-4 gives the length of short-circuited arms for circular

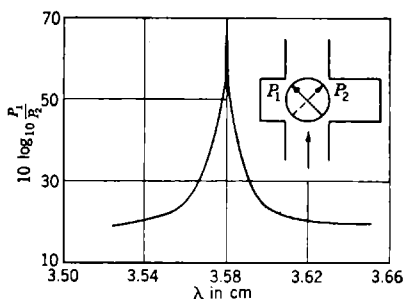


FIG. 6-68.—Characteristics of turnstile used as linear polarizer. Dimensions are given in the second line of Table 6-4.

polarization and for plane polarization, with the voltage standing-wave ratios obtained for these applications.

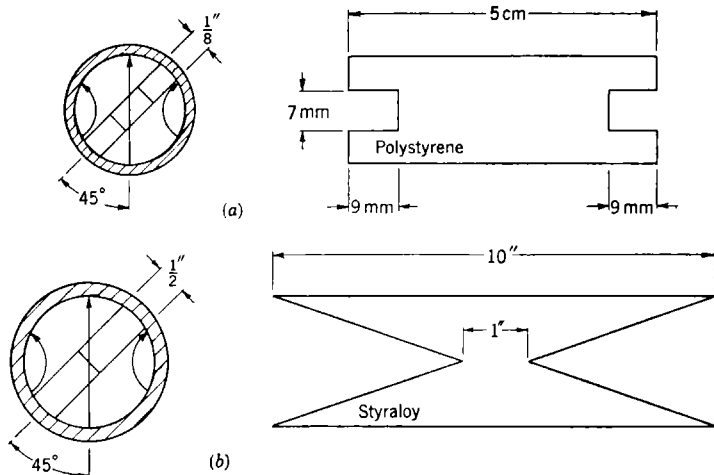


FIG. 6-69.—Dielectric quarter-wave plates. (a) Waveguide $1\frac{5}{8}$ in. ID at 3.2-cm wavelength with polystyrene; (b) waveguide 3 in. ID with styraloy.

While the voltage standing-wave ratio is very good over a broad band, the useful wavelength region may be limited further by the frequency

sensitivity of the lengths of the short-circuited arms. Figure 6-68 shows a plot of the ratio between the power found in the two polarizations in the second transition of Table 6-4, over a part of the frequency band,

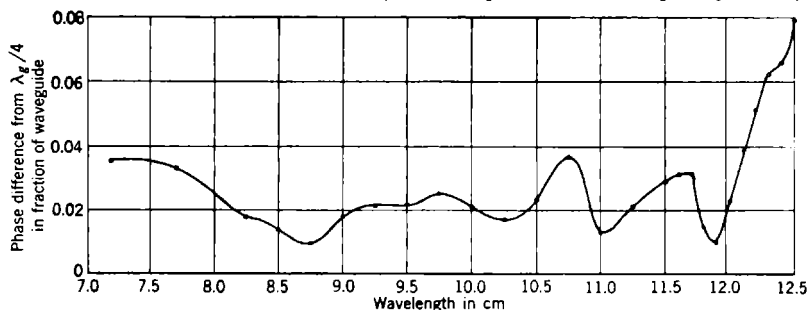


FIG. 6-70.—Circular-polarization tests on styraloy quarter-wave plate of Fig. 6-69b.

when the transition is used as a linear polarizer. The amount of P_2 in the figure is very small at 3.58-cm wavelength but increases very rapidly toward each end of the band. This P_2 wave will be out of phase with the P_1 wave, thus setting up some circular polarization. For some applications the ratio must be greater than 30 db.

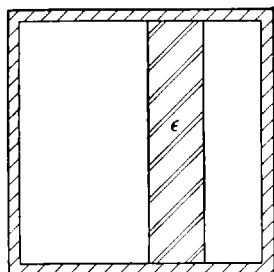


FIG. 6-71.—Circular polarizer in rectangular waveguide. Cross-section view.

Another way to construct a quarter-wave plate is to place a narrow slab of dielectric material, as shown in the drawings in Fig. 6-69, at an angle of 45° to the incident polarization. The dielectric has a greater effect on the guide wavelength of that component, the polarization of which is parallel to its width, than in the component at 90° .

The notches and the tapers match the plate to the incident wave. Apparently better results are obtained with a fairly thick slab of dielectric than with a very thin sheet. Experimental results of the tapered quarter-wave plate of Fig. 6-69 are shown on the graph of Fig. 6-70. The small maxima and minima are probably due to multiple reflections from the two tapers in the two component polarizations.

6-19. Circular Polarization in Square Waveguide.—It is possible to propagate a circularly polarized wave in square waveguide, as well as in round, by dividing the power in half so that two TE_{10} -modes are propagated at right angles, and by introducing a phase shift of $\pi/2$ in one of these modes. This phase shift may be obtained by using a section of rectangular waveguide with a slab of dielectric as in Fig. 6-71. Since the boundary conditions are not complicated, the cutoff wavelengths

for the primary modes in the two polarizations may be calculated accurately. This technique of exciting circular polarization gives us several parameters which must be adjusted in order to obtain a broad band. By selecting the dimensions a and b , and the thickness and dielectric constant of the slab, a waveguide section may be obtained in which the phase difference between the two polarizations, as a function of free-space wavelength, is at a minimum in the center of the selected band. In this way, theoretical bandwidths of 3 to 1 and 5 to 1 can be obtained using the maximum ratio of 3 db, between the major axis and the minor axis of the wave, as a criterion.

TRANSITIONS INVOLVING A CHANGE IN WAVEGUIDE MODE

BY F. E. EHLERS

For certain specialized applications, it is often necessary to transform the dominant mode of one type of waveguide to a higher mode of another. The higher waveguide mode most often used is the TM_{01} -mode in round waveguide. The advantage of this mode is that it has radial symmetry and, therefore, is desirable for use in rotary joints, in antennas in which a uniform azimuth is desired, and in other applications requiring symmetry.

6-20. Transitions to the TM_{01} -mode.—Transitions to the TM_{01} -mode are more difficult to design than are transitions between two different waveguides in which only the lowest mode is propagated, because the TM_{01} -mode has to be excited without setting up an appreciable amount of TE_{11} -mode. The cutoff wavelength for the TM_{01} -mode is

$$\lambda_c = \frac{2\pi a}{2.405},$$

while the cutoff wavelength for the TE_{11} -mode is

$$\lambda_c = \frac{2\pi a}{1.841}.$$

Therefore, if the diameter of the waveguide is selected to propagate the TM_{01} -mode, it will also propagate the TE_{11} -mode. From the standpoint of electromagnetic theory, the round waveguide must be excited with a field as nearly symmetrical as possible.

Since nearly all microwave transmission line is rectangular waveguide, the most logical type of transition to the TM_{01} -mode is from the TE_{10} -mode in rectangular guide. From Fig. 6-72 it is seen that the TM_{01} -mode is very similar to the coaxial TEM -mode. The first type of TM_{01} -transition from rectangular waveguide contained first a right-angle transition from rectangular waveguide to a coaxial line which was beyond cutoff for all waveguide modes. Then an antenna, formed by the extension of

the center conductor of the coaxial line into the round waveguide, excited the TM_{01} -mode. In this construction, there is perfect symmetry so that no TE_{11} -mode (see Fig. 6-73) is set up in the round waveguide unless the coaxial section is so short that higher modes, set up in the coaxial line by the junction at the rectangular waveguide, are not attenuated sufficiently. This transition was satisfactory only over a very narrow band of wavelengths. It was matched to the transmitter frequency by

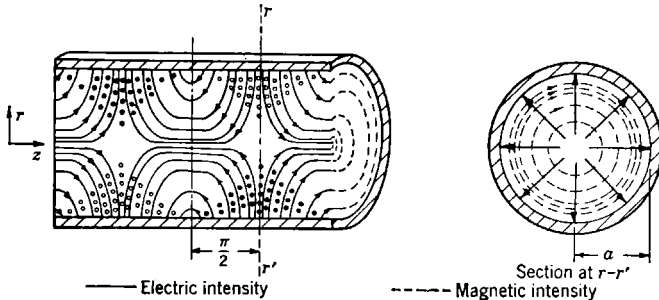


FIG. 6-72.—Instantaneous fields in TM_{01} -mode showing electric and magnetic intensities.

adjusting the plunger in the rectangular waveguide, the plunger in the coaxial stub, and then three capacitive screws. The disadvantage of such a transition, beyond the mechanical complications, is that the power capacity of the transition is limited by the narrow coaxial section. The device would be much easier to make if power could be coupled directly from the rectangular waveguide to the round waveguide without this narrow constriction. Therefore, from a study of the fields of the TE_{10} -mode in rectangular waveguide and of the TM_{01} -mode in round wave-

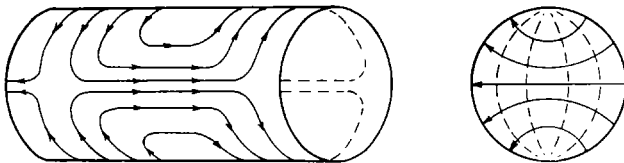


FIG. 6-73.—Instantaneous currents on conductor surface in TE_{11} -mode. The corresponding E and H fields are shown on the right.

guide, the most logical method of exciting the TM_{01} -mode directly from the rectangular waveguide should be determined. From Fig. 2-19 it can be seen that, in a plane across the narrow dimension of the rectangular waveguide and parallel to the wide side, the magnetic field forms closed loops somewhat circular in shape, and the electric field is always perpendicular to the plane. Now if the magnetic field lines of the TM_{01} -mode in a circular cross section of the round waveguide are examined, it is found that they form closed circles. Moreover, at the instant shown

by the line *A* in Fig. 6-72 when the radial component of the electric field is equal to zero, the electric field is axial. This analysis of the fields suggests that the *TM*₀₁-mode can best be excited by coupling from the wide dimension of the rectangular waveguide. The diameter of the round waveguide must be large enough to propagate the *TM*₀₁-mode but not large enough to propagate the next higher mode, the *TE*₂₁-mode, whose cutoff wavelength is $2\pi a/3.048$. To complete the transition, a short-circuiting plug which fits the rectangular waveguide is adjusted to excite the maximum electric vector in the center of the round waveguide; a matching device may be placed either in the round waveguide or in the rectangular waveguide, or both, to reduce the reflections. Such a simple type of transition is possible for certain sizes of rectangular and round waveguides, but in designing such a transition, some technique for determining the purity of the *TM*₀₁-mode must be used.

Only one polarity of the *TE*₁₁-mode is excited by this type of transition—the one in which the maximum electric vector lies along the diameter of the cylindrical waveguide that is parallel to the axis of the rectangular waveguide. This can be readily seen by a study of the geometry of the transition. The *TE*₁₀-mode in rectangular waveguide has an electric vector which is perpendicular to the axis of the rectangular guide and parallel to the narrow dimension. Its magnitude is maximum in the center and decreases sinusoidally to zero at the edges of the waveguide. Thus, there is symmetry about the center of the rectangular waveguide which precludes the excitation of the mode in the round pipe which is not symmetric about this center line. This property of the transition, to excite only one polarization of the *TE*₁₁-mode, makes it possible to use the technique outlined in the following paragraphs.

6-21. Determining Percentage of *TE*₁₁-mode in Cylindrical Waveguide.—When r-f power is propagated simultaneously in the *TE*₁₁- and *TM*₀₁-modes in a cylindrical waveguide, it is possible to determine the relative amount of power in the two modes by measurements of the electric field in the waveguide. Since a probe inserted into a waveguide will be excited by the electric field which is directed along its length, only the radial component of the electric vector in cylindrical waveguide need be considered. For the *TM*₀₁-mode, the radial component of the electric field at the periphery of the pipe will vary according to the formula

$$E_r = E_E e^{j\left(\omega t - \frac{2\pi x}{\lambda_{01}}\right)}, \quad (33)$$

where E_E = voltage amplitude of *TM*₀₁-wave, x = distance along the axis, and λ_{01} = the waveguide wavelength in the *TM*₀₁-mode. For the *TE*₁₁-mode,

$$E_r = E_H \sin \phi e^{j\left(\omega t - \frac{2\pi x}{\lambda_{11}}\right)}, \quad (34)$$

where E_H = the amplitude of the TE_{11} -wave, and ϕ = angle of azimuth. If the two modes are propagated simultaneously and the waveguide is matched to each mode, then the radial component of the electric field becomes

$$E_r = E_E e^{j\left(\omega t - \frac{2\pi x}{\lambda_{01}}\right)} + E_H \sin \phi e^{j\left(\omega t - \frac{2\pi x}{\lambda_{11}} + \alpha\right)}, \quad (35)$$

where α is the phase difference between the two modes at $x = 0$ and $t = 0$.

If the two terms are divided by $e^{j\left(\omega t - \frac{2\pi x}{\lambda_{01}}\right)}$ and only the amplitude of the electric field is considered,

$$E_r = E_E + E_H \sin \phi e^{j\left(\frac{2\pi x}{\lambda'} + \alpha\right)},$$

where $\frac{1}{\lambda'} = \frac{1}{\lambda_{11}} - \frac{1}{\lambda_{01}}$. From this relation, it is seen that, at the point

along the pipe where $e^{j\left(\frac{2\pi x}{\lambda'} + \alpha\right)} = \pm 1$, the values of maximum and minimum are obtained by rotating around the pipe;

$$\text{and } \left. \begin{aligned} E_{\max} &= E_E + E_H \\ E_{\min} &= E_E - E_H \end{aligned} \right\} \quad (36)$$

If the ratio of maximum to minimum fields measured around the waveguide is defined as

$$r = \frac{E_{\max}}{E_{\min}}, \quad (37)$$

Eqs. (36) may be combined to give

$$\frac{E_H}{E_E} = \frac{r - 1}{r + 1}. \quad (38)$$

This maximum ratio will occur every $\lambda'/2$ along the axis of the waveguide, or $5\frac{1}{2}$ to $7\frac{1}{2}$ cm, for tubing 1.152 in. ID over the band from 3.13 to 3.53 cm. These same values of maximum and minimum are obtained if $\sin \phi = \pm 1$, and the probe is moved along the axis of the waveguide; however, the technique of rotating the waveguide and inserting the probe into holes along the waveguide is preferable in order to avoid radiation in the TE_{11} -mode and possible resonances caused by the slot. For round waveguide with inner diameters of 1.152 in. and 1.188 in. about 15 holes spaced $\frac{1}{2}$ in. apart are sufficient to obtain accurate results in the wavelength range of 3.13 to 3.53 cm. For a matched load in the waveguide, one may use a cone of finely grained wood 14 in. long with a 14-in. shank machined to a slide fit in the tubing. The reflections introduced by the cone may be detected by changing the position of the cone in the guide, and by observing the resulting variation in the power

extracted by a fixed probe. For a waveguide .467 in. in diameter, 14 holes spaced $\frac{3}{16}$ in. apart were used satisfactorily over the range from 1.21 to 1.27 cm with a 6-in. wooden cone as a load.

To make use of the variation in power around the pipe in calculating the relative amount of power transmitted in the TE₁₁-mode, the ratio of the r-f power transmitted to the square of the voltage amplitude at the periphery of the waveguide for each of the modes should be known.¹ These formulas may be checked by calculating the total power from the component of Poynting's vector in the direction of propagation from the equations²

$$P_z = \frac{1}{2} \int \int p_z ds$$

$$P_z = \frac{1}{2} \int_{\phi=0}^{\phi=2\pi} \int_{r=0}^{r=a} R(E_r' H_\phi' - E_\phi' H_r') r dr d\phi. \quad (39)$$

The field equations for the TE₁₁-mode were taken from the equations

$$\left. \begin{aligned} E_z &= 0 \\ E_r &= j \left[A' \omega \mu_1 \left(\frac{a}{r'_{nm}} \right) 2 \frac{n}{r} \sin n\phi J_n \left(r' \frac{r'_{nm}}{a} \right) \right] e^{j(\omega t - \beta_{nm} x)} \\ E_\phi &= j \left\{ A' \omega \mu_1 \left(\frac{a}{r'_{nm}} \right)^2 \cos n\phi \left[\frac{n}{r} J_n \left(r' \frac{r'_{nm}}{a} \right) \right. \right. \\ &\quad \left. \left. - \left(\frac{r'_{nm}}{a} \right) J_{n+1} \left(r' \frac{r'_{nm}}{a} \right) \right] \right\} e^{j(\omega t - \beta_{nm} x)} \\ H_z &= \left[A' \cos n\phi J_n \left(r' \frac{r'_{nm}}{a} \right) \right] e^{j(\omega t - \beta_{nm} x)} \\ H_r &= -j \left\{ A' \beta_{nm} \left(\frac{a}{r'_{nm}} \right)^2 \cos n\phi \left[\frac{n}{r} J_n \left(r' \frac{r'_{nm}}{a} \right) \right. \right. \\ &\quad \left. \left. - \left(\frac{r'_{nm}}{a} \right) J_{n+1} \left(r' \frac{r'_{nm}}{a} \right) \right] \right\} e^{j(\omega t - \beta_{nm} x)} \\ H_\phi &= j \left[A' \beta_{nm} \left(\frac{a}{r'_{nm}} \right)^2 \frac{n}{r} \sin n\phi J_n \left(r' \frac{r'_{nm}}{a} \right) \right] e^{j(\omega t - \beta_{nm} x)} \end{aligned} \right\} H_{nm} \text{ waves in the dielectric} \quad (40)$$

and those for the TM₀₁-mode were taken from the equations

$$\left. \begin{aligned} E_z &= A J_0 \left(r' \frac{r_{01}}{a} \right) e^{j(\omega t - \beta_{01} x)} \\ E_r &= j A \frac{\beta_{01}}{r_{01}} a J_1 \left(r' \frac{r_{01}}{a} \right) e^{j(\omega t - \beta_{01} x)} \\ H_\phi &= j A \frac{\omega \epsilon_1}{r_{01}} a J_1 \left(r' \frac{r_{01}}{a} \right) e^{j(\omega t - \beta_{01} x)} \end{aligned} \right\} E_0 \text{ waves in the dielectric} \quad (41)$$

¹ F. E. Ehlers, "E₀ Rotary Joints for the 3-Centimeter Band," RI. Report No. 853, Dec. 4, 1945.

² Sarbacher and Edson, *Hyper and Ultrahigh Frequency Engineering*, Wiley, New York, 1943, p. 263, Eq. (7.114); p. 258, Eq. (7.104); p. 250, Eq. (7.82), respectively.

Dividing the axial component of Poynting's vector by the square of the amplitude of the radial component of the electric vector at the surface of the waveguide, we obtain for the TE_{11} -mode,

$$\frac{P_H}{E_H^2} = \frac{a^2}{200} \frac{\lambda}{\lambda_{11}}, \quad (42)$$

where λ_{11} is the guide wavelength in this mode and a is the radius of the waveguide. For the TM_{01} -mode

$$\frac{P_E}{E_E^2} = \frac{a^2}{240} \frac{\lambda_{01}}{\lambda}. \quad (43)$$

After combining Eqs. (42) and (43),

$$\frac{P_H}{P_E} = 1.20 \frac{\lambda^2}{\lambda_{11} \lambda_{01}} \frac{E_H^2}{E_E^2} \quad (44)$$

$$\frac{P_H}{P_E} = 1.20 \frac{\lambda^2}{\lambda_{11} \lambda_{01}} \frac{(r-1)^2}{(r+1)^2}, \quad (45)$$

where r is the ratio of maximum to minimum voltage at that point along the axis of the waveguide where the rotational asymmetry is greatest. The coefficient of $(r-1)^2/(r+1)^2$ is plotted against λ/a in Fig. 6-74.

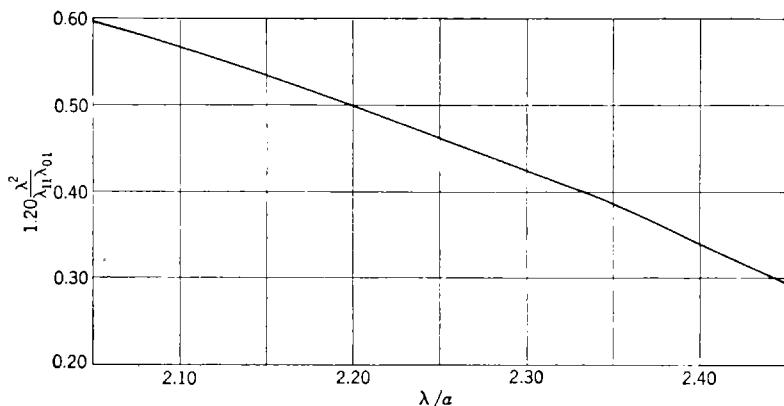


FIG. 6-74.—Factor in Eq. (45) plotted against λ/a .

For some applications, the requirements for the purity of the TM_{01} -mode in the round waveguide may not be very severe. In applications for rotary joints, however, there must be less than 0.5 per cent of the power in the TE_{11} -mode. In the design of the transitions developed at the Radiation Laboratory, attempts were made to secure this degree of mode purity, and various techniques were tried to reflect from the round waveguide, or otherwise suppress, the energy in the TE_{11} -mode. How-

ever, before discussing these techniques, two transitions from rectangular waveguide to round waveguide in the TM_{01} -mode will be described in which no devices are needed to obtain the desired mode purity.

A simple transition in which the round waveguide is attached to the wide side of the rectangular waveguide, at right angles to it, has been described earlier in this chapter. Such a transition has been designed, for use at a wavelength of 1.25 cm, in which rectangular guide $\frac{1}{2}$ by $\frac{1}{4}$ in. with 0.040-in. wall and round waveguide with an inside diameter of 0.4675 in. are used. A rectangular plug is inserted into the rectangular waveguide as shown in Fig. 6-75. In this particular transition, the dimensions of the rectangular guide are such that it is possible to select round guide of a diameter which achieves, simultaneously, a nearly perfect match and a mode purity satisfactory for use in rotary joints. This optimum diameter for the round guide was determined experimentally. For each of several diameters tried, the short-circuiting plug was adjusted so that the minimum voltage standing-wave ratio was obtained at 1.25 cm, the center wavelength of the band. Figure 6-76 shows a plot of this minimum voltage standing-wave ratio as a function of the diameter of the round waveguide. The match of the finished transition as a function of wavelength is shown in Fig. 6-77. The bandwidth of

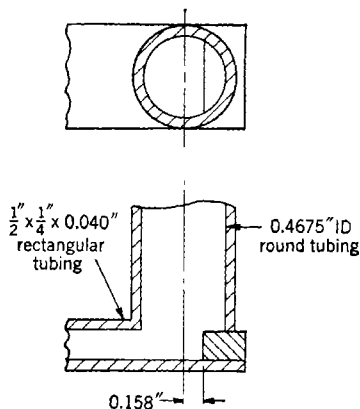


Fig. 6-75.— TM_{01} -mode transition for 1.25-cm wavelength.

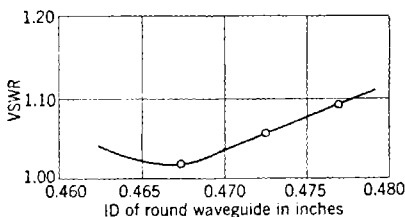


Fig. 6-76.—Voltage standing-wave ratio of transition from $\frac{1}{2}$ -by $\frac{1}{4}$ -in. rectangular waveguide to E_{01} -mode.

the transition for a maximum voltage standing-wave ratio of 1.05 is about 4 per cent.

Because of the urgency with which this type of transition was developed, no systematic data were taken by which the ratios between the dimensions of the waveguides and the wavelength could be determined

for any wavelength band. It is possible, however, to scale the dimensions of this particular transition according to the ratio of the desired wavelength to 1.25 cm and thus to obtain comparable results.

In the design of a transition from $1\frac{1}{4}$ - by $\frac{3}{8}$ -in. waveguide with 0.064-in. wall to a round waveguide of 1.188-in. inner diameter, it was found that better mode purity could be obtained by use of a round short-circuiting plug having the same diameter as the wide dimensions of the rectangular waveguide. Because first consideration was given to the purity of the mode excited in the round waveguide, the location of the plunger was determined as that which gave minimum asymmetry at 3.20 cm. The purity of the TM_{01} -mode in the resulting transition is shown in Fig. 6-78.

Since the transition was so simple in construction, it was decided to round the corners, as shown in Fig. 6-79, so that the transition would be able to transmit very high power. The position of the plug with the rounded corners was redetermined, and a tapered section from rectangular waveguide 1 by $\frac{1}{2}$ in. with 0.050-in. wall was added. An inductive window was placed in this taper to match the transition at 3.20 cm, since the voltage standing-wave ratio without the window was 1.4. With this window, the transition had a voltage standing-

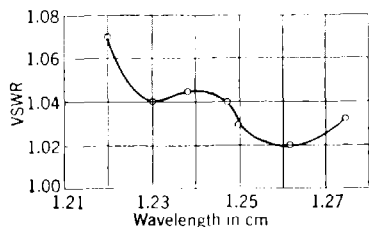


FIG. 6-77.—Voltage standing-wave ratio of right-angle transition to TM_{01} -mode, $\frac{1}{2}$ -in. by $\frac{1}{4}$ -in. rectangular waveguide.

ratio of 1.10 or less from $\lambda = 3.162$ cm to $\lambda = 3.250$ cm (see Fig. 6-80).

The only means of manufacturing this transition is by the process of electroforming over a cerrobased form. The cerrobased is then melted out and the transition cleaned.

Since this technique has not been satisfactory for large-scale manu-

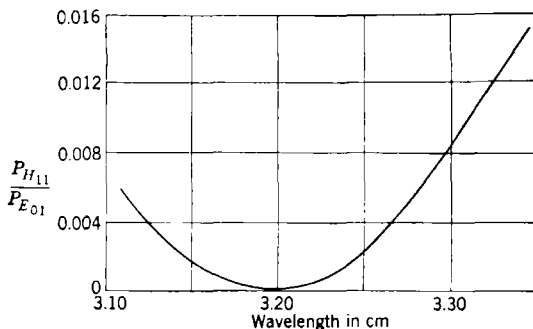


FIG. 6-78.—Purity of TM_{01} -mode for electroformed or die-cast high-power rotary joint.

Since this technique has not been satisfactory for large-scale manu-

facture, the transition was redesigned for the process of die-casting. In the die-casting technique, a core must be drawn out of the rectangular waveguide and also out of the round-waveguide end of the casting; therefore the taper was eliminated. Also, a different technique for matching the transition was used: a matching iris was placed in the round waveguide as well as an inductive window in the rectangular waveguide in order to obtain a broader band. To demonstrate the advantage of two matching devices, the admittance plots of the transition will be examined first without any inductive matching devices. Figure 6-81 gives a plot on the Smith chart of the transition with the admittance referred to an arbitrary position in the rectangular waveguide chosen so that, if an inductive window of the correct aperture were placed there, the best broadband match would be obtained. With such a window, the bandwidth between maximum standing-wave ratios of 1.10 is 3.16 to 3.25 cm or about 4 per cent. Now let us insert an iris into the round waveguide and adjust the aperture and position so that the smallest spread of admittances is obtained. The dotted lines in Fig. 6-81 show the path through which the iris moves the admittance at each particular wavelength. Since the iris adds capacitive susceptance, the admittance of the transition without the iris and the admittance point with the iris may be rotated together to the place on the chart at which these two points lie along some line of constant conductance. In this way the dotted lines in Fig. 6-81 can be traced. Since the susceptance of a capacitive iris is inversely proportional to the guide wavelength in the round waveguide, corrections can be made in the first data in order to determine the size of aperture of the new iris and its position in obtaining the desired admittance pattern. In this way was obtained the admittance plot in Fig. 6-81, which, with an inductive window in the rectangular waveguide matched the transition to a maximum standing-wave ratio of 1.04 in voltage from 3.13-cm to 3.26-cm wavelength.

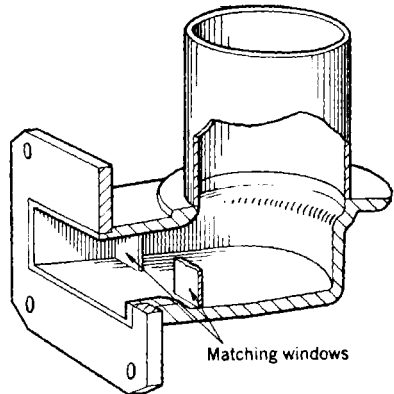


FIG. 6-79.—High-power E_0 -transition with matching windows.

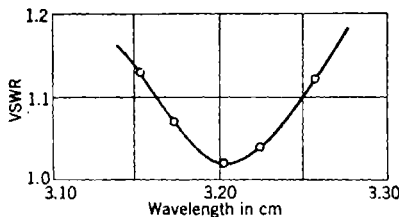


FIG. 6-80.—Performance curve for transition of Fig. 6-79.

This technique of matching may be used on other types of transition, such as rectangular to round in the TE_{11} -mode. Separating the matching devices between the output and the input lines makes it much easier to attain a broadband device.

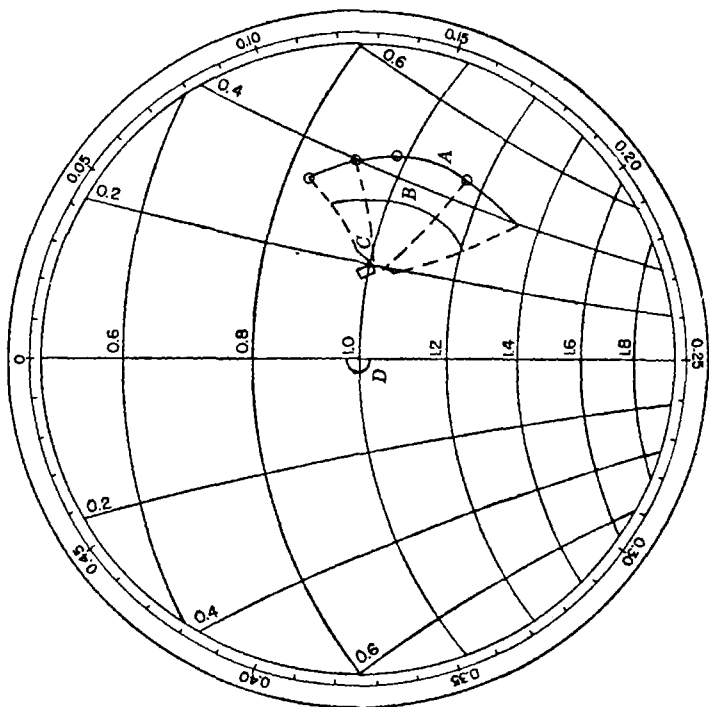


FIG. 6-81.—High-power die-cast TM_{01} -transition. A = admittance without iris; B = admittance with too small an iris; C = best admittance for broad band; D = completed transition with inductive window in rectangular waveguide.

6-22. TE_{11} -mode Filters.—In the two transitions discussed in the foregoing paragraphs, the dimensions of the respective waveguides were such that, at the chosen wavelength bands, the mode purity was satisfactory. In some transitions these dimensions, together with wavelength, may not be so fortunate. Consequently, some means of suppressing the TE_{11} -mode must be employed. This was first done by means of an extension of the round waveguide below the rectangular waveguide, terminated by a short circuit. This is shown in Fig. 6-82. If this extension stub is a quarter wavelength in the TE_{11} -mode measured from the short circuit to the center of the rectangular waveguide, a nearly pure TM_{01} -mode is propagated in the round waveguide. Unfortunately, this stub is also nearly a quarter wavelength in the TM_{01} -mode,

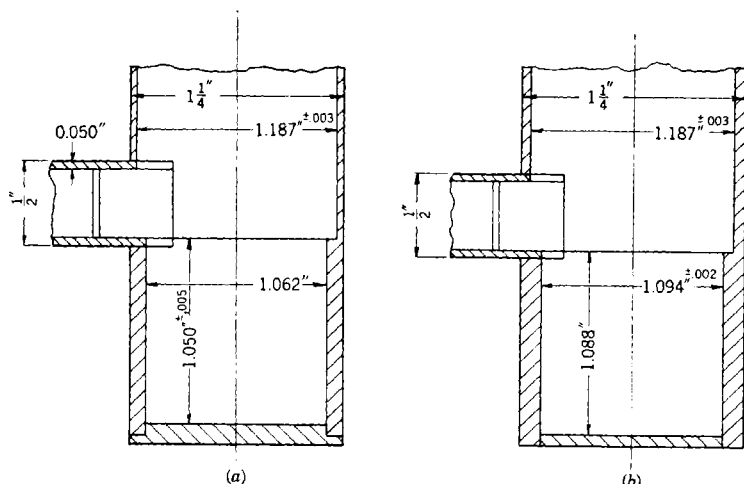


FIG. 6-82.—Details of Preston TM_{01} -transition; (a) stub transition for 3.17 to 3.23 cm; (b) stub transition for 3.27 to 3.33 cm.

and thus causes a large mismatch which must be cancelled. A better result is obtained if this stub is made three-quarters guide wavelength in the TE_{11} -mode. Then the diameter of the stub can be chosen experimentally so that when the length of the short-circuited stub becomes three-quarters waveguide wavelength in the TE_{11} -mode, it is a half-waveguide wavelength in the TM_{01} -mode. In this way, the voltage standing-wave ratio of the transition can be made small enough (about 1.5) to be matched easily by an inductive window. Such a transition was designed from 1- by $\frac{1}{2}$ -in. waveguide with 0.050-in. wall to round waveguide 1.188 in. ID at a wavelength of 3.20 cm. The dimensions of this transition are shown in Fig. 6-82. The voltage standing-wave ratio is below 1.1 for a 2 per cent band centered at 3.20 cm, and the ratio of TE -mode to TM -mode is about 0.5 per cent over this band.

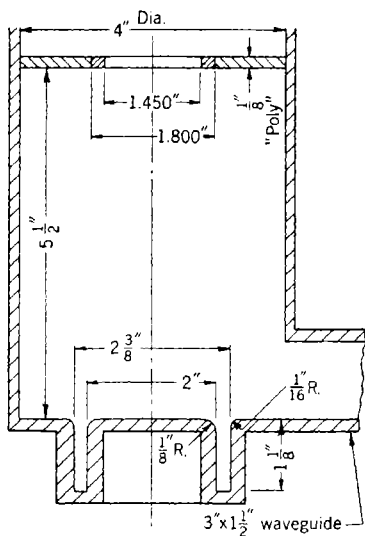


FIG. 6-83.— TM_{01} -transition for 10.7 cm with coaxial stub TE_{11} -mode suppressor.

Another way of suppressing the TE_{11} -mode is by means of a coaxial

stub on the axis of the round waveguide placed below the rectangular waveguide as in Fig. 6-83. This has one advantage over the round waveguide stub: it has little effect on the TM_{01} -mode, since the maximum

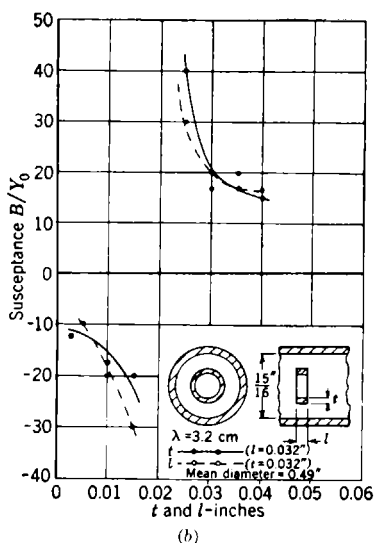
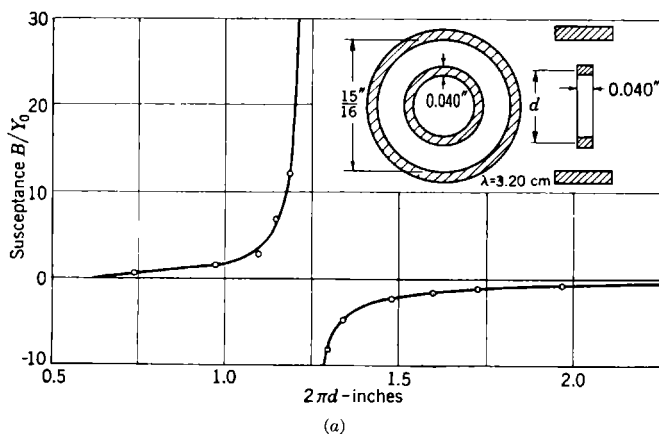


FIG. 6-84.—Susceptance of a ring mounted in a waveguide: (a) as a function of mean circumference; (b) as a function of cross-section dimensions.

electric field for this mode occurs at the center conductor of the coaxial stub and is not coupled into it. Therefore, the stub can be made a quarter wavelength long in the TE_{11} -coaxial waveguide mode, and it

will present a very high impedance to the round waveguide TE_{11} -mode. This device is not so effective a suppressor as the compound TE - TM -stub discussed in the earlier part of this section, and the introduction of the poly-supported resonant ring is necessary to obtain sufficient purity of the TM_{01} -mode. This particular transition has a standing-wave ratio of 1.10 or less over the band from 10.61 to 10.81 cm.

Possibly the most effective filter for the TE_{11} -mode is the resonant ring. If a circular metal ring of the correct diameter is placed in a round waveguide propagating a plane wave such as the TE_{11} -mode, nearly all the energy will be either absorbed or reflected away from this ring. The TM_{01} -mode, however, will be little affected, since the electric field is nearly always perpendicular to the edges of the ring. Thus, if this ring is inserted in the round waveguide in which the amount of TE_{11} -mode is larger than desired, a large proportion of this energy will be filtered out of the round waveguide. The resonant ring is a satisfactory mode filter if about 90 to 95 per cent of the energy is in the TM_{01} -mode.

If this ring is aligned axially and centered in the round waveguide, it acts like a resonant circuit parallel to the impedance of the line. As the periphery of the ring is increased from a very small diameter, it first has increasing capacitive susceptance. Then, as the periphery is increased beyond the resonant point, the ring becomes inductive. Figure 6-84 shows the effect of the diameter of the ring whose metal cross section is 0.040 in. square. These data were taken in waveguide $\frac{1}{8}$ in. ID at a wavelength of 3.20 cm. A complete study of the effect of resonant rings in round waveguide was made at the Telecommunications Research Establishment in Great Britain. At 9.1-cm wavelength, British physicists found that the resonant outer periphery was slightly greater than a free-space wavelength and increased as the thickness of the ring material was increased. To a first approximation, the resonant inner periphery is independent of ring thickness. Figure 6-85 shows a chart of the amplitude of the transmission coefficient vs. the periphery of the resonant ring for different diameters of the wire, taken in waveguide $2\frac{1}{2}$ in. ID. The effect of the waveguide diameter is of a second order, for a ring with a periphery of 1.15λ will resonate in waveguide $2\frac{1}{2}$ in. ID

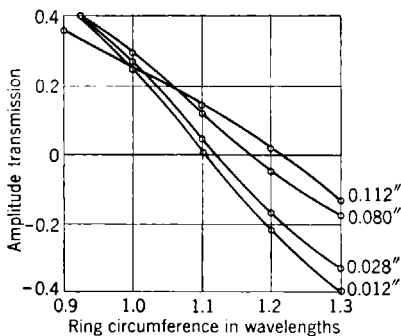


FIG. 6-85.—Amplitude transmission coefficient vs. ring circumference in wavelengths. The wavelength was 9.1 cm, the waveguide had an ID of $2\frac{1}{2}$ in. The diameters of wire used for the rings are indicated on the curves.

at 9.1 cm, while it requires a ring with a periphery of 1.18λ for waveguide $3\frac{3}{8}$ in. diameter.

Another significant effect of increasing the thickness of the ring material is that the frequency sensitivity is decreased. This can be seen from Fig. 6-85 by the fact that the slope of the curves giving the amplitude of the transmission coefficient decreases for increasing ring thickness. Telecommunications Research Establishment found that at 9.1 cm the frequency sensitivity is $2\frac{1}{2}$ times less for a wire of 0.116 in. diameter than it is for a wire of 0.012 in. diameter.

One of the first applications of the resonant ring was to increase the bandwidth of the transition which used a round waveguide stub to filter

the TE_{11} -mode. A resonant ring was placed in the stub as in Fig. 6-86, so that the length of the stub appeared to be a quarter wavelength in the TE_{11} -mode. The total length of this stub from the center of the rectangular waveguide to the short-circuiting plug was made a half guide wavelength in the TM_{01} -mode. Since the distance to the ring was shortened from three-quarters of a wavelength to a quarter wavelength

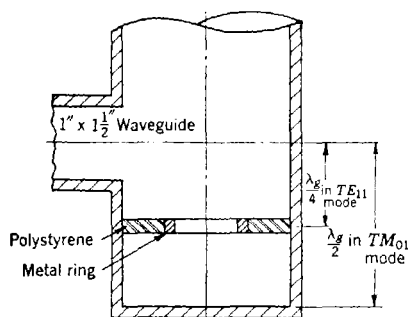


FIG. 6-86.—Stub filter with resonant ring.

and the resonant ring is a broadband device, some improvement in bandwidth was obtained over the compound TE - TM -stub. This type of transition was not used because of the mechanical difficulty of supporting the resonant ring by a polystyrene or mica disk, and because the compound TE - TM -stub had sufficient bandwidth to satisfy the requirements at that time.

In subsequent designs of TM_{01} -transitions, a better means of supporting this resonant ring was devised. If the electric field of the TE_{11} -mode in Fig. 6-73 is examined, it will be found that a metal sheet can be placed along a diameter across the waveguide so that it is perpendicular to the electric field and, therefore, will cause no disturbance of this field. Similarly, if metal struts which lie along this diameter to support the resonant ring are used, the effectiveness of the resonant ring for this polarization is unimpaired. However, if the struts are aligned in the direction of the electric vector, the ring is only 50 per cent effective. From the discussion in the beginning of this chapter it is seen that only one polarization of the TE_{11} -mode can be excited in the right-angle transition; that is, the one in which the polarization is along the axis of the rectangular waveguide. Therefore, if the struts are oriented

perpendicular to the axis of the rectangular waveguide, the resonant ring will filter out the TE₁₁-mode.

With the use of the strut-supported ring, a TM₀₁-mode transition was designed to cover the band from 3.13- to 3.53-cm wavelengths. In order to obtain a transition from 1- by $\frac{1}{2}$ -in. waveguide with 0.50-in. wall which would be easy to manufacture and which would have no stub extending below the rectangular waveguide, the construction shown in the drawing in Fig. 6-87 was tried. The 0.980 in. diameter of the hole concentric with the round waveguide was experimentally found

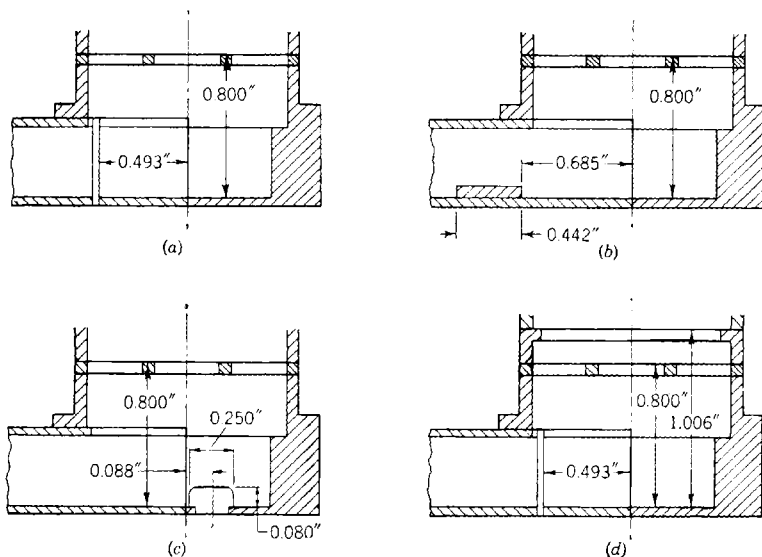


Fig. 6-87.—Filter-ring transitions. The basic construction is similar to that of the upper view of Fig. 6-93.

to give the smallest amount of TE₁₁-mode and the best possible match at 3.20-cm wavelength with round waveguide 1.188 in. ID. The diameter of 0.980 in. matched the transition to about 1.1 and from 5 to 7 per cent of the energy was propagated in the TE₁₁-mode. With the addition of a strut-supported resonant ring, the amount of TE₁₁-mode was reduced to 1 per cent or less from 3.1 to 3.5 cm. With the ring located about $\frac{1}{16}$ in. from the bottom, the transition was matched by a symmetric inductive window to 1.1 or less over this band. However, as the amount of TE₁₁-mode exceeded the allowable half per cent for the high-wavelength end of this band, the size of the waveguide was changed to see if better mode purity could be obtained. With the waveguide of 1.152 in. ID ($\frac{1}{4}$ -in. tubing with 0.049-in. wall), it was found that the transition could be matched over the band from 3.13 to 3.53 cm with a

voltage standing-wave ratio of 1.1 or less, with an inductive window; the amount of power to the TE_{11} -mode was less than one-half per cent over this band (see Figs. 6-87, 6-88, and 6-89). The position of the resonant ring was chosen principally to obtain an r-f admittance which could be matched over a broad band by an inductive window in the rectangular waveguide. Its effect on the purity of the TM_{01} -mode is practically independent of the distance from the bottom of the rectangular waveguide. However, for positions nearer the bottom than $\frac{3}{4}$ in., its effective-

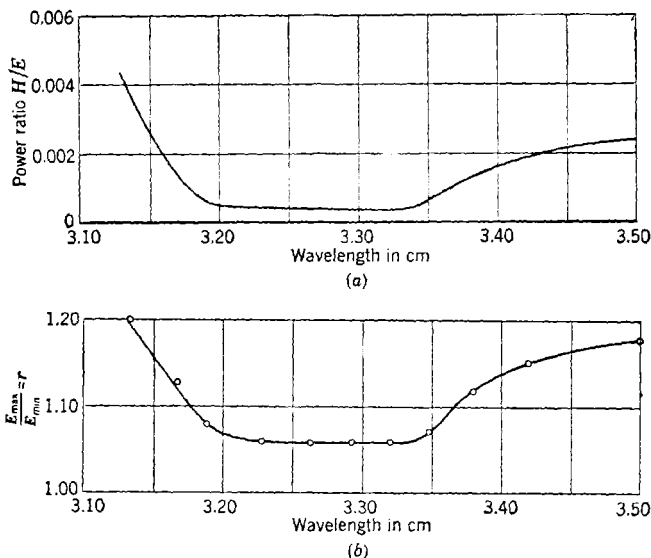


FIG. 6-88.—Purity of E_{01} -mode for filter-ring transition (Fig. 6-87a). The ordinate of (a) is P_H/P_E as given by Eq. (45), and is derived from the data plotted in (b).

ness diminishes. Section 7-3 contains a discussion of the application of these transitions in rotary joints and an explanation of the effect of the strut-supported ring on the TE_{11} -mode resonances.

Although a standing-wave ratio in voltage of 1.1 or less is satisfactory for most uses, a better match can be obtained by using a capacitive iris in the round guide as well as an inductive window in the rectangular waveguide (Fig. 6-87d); this is the same method used in the transition from $1\frac{1}{4}$ - by $\frac{5}{8}$ -in. waveguide which was discussed in a previous part of this chapter. The graph in Fig. 6-90 shows the standing-wave voltage ratio as a function of wavelength for the initial model.

Because of the wide use of these transitions, and because of the different processes by which they were constructed, two more ways of matching were employed: a quarter-wavelength transformer, and a capacitive

button. The quarter-wave transformer, which is shown in Fig. 6-87*b*, was used to obtain a match at 3.20 cm. Because it has a simple geometry, the transformer is especially adapted to the process of electroforming. The voltage standing-wave ratio of the transition with this transformer is 1.04 or less, from 3.15 to 3.25 cm (Fig. 6-91).

Button matching is especially suitable to the process of die-casting. In this process, a die must be drawn from a rectangular waveguide and another from the round-waveguide section of the transition casting. By putting a capacity button 0.080 in. high and $\frac{1}{4}$ in. in diameter at the

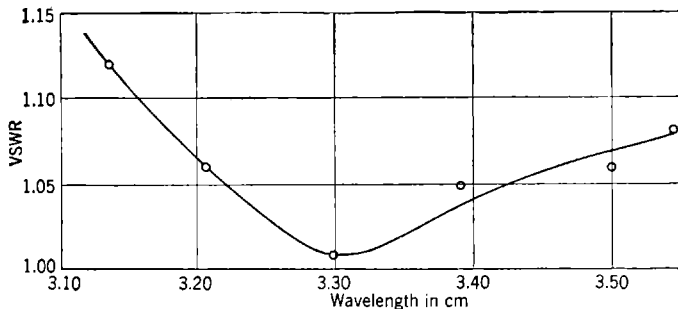


FIG. 6-89.—VSWR vs. λ for the transition of Fig. 6-87*a*.

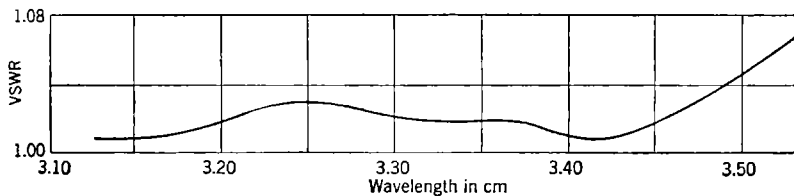


FIG. 6-90.—VSWR vs. λ for the transition of Fig. 6-87*d*.

bottom of the transition along the axis of the rectangular waveguide, but off the axis of the round guide toward the back of the transition, the transition can be matched without the additional machining necessary to put in a quarter-wave transformer or an inductive window. Each transition will be matched to 1.03 VSWR or less from 3.13 to 3.29 cm with a maximum of 1.06 at 3.33 cm as in Fig. 6-92.

The following procedure was used to determine the position of the button. The position of the minimum in the standing-wave ratio of the transition without the button was used as a reference point. A small button, not quite large enough to remove the mismatch caused by the transition, was placed in the transition where it reduced the voltage standing-wave ratio. The admittance was plotted with respect to the position of the voltage minimum without the button. Having

assumed that the button would add shunt capacitance, the two admittances were rotated on the Smith chart until they lay along some constant conductance circle. Successive adjustments of the position were made until the button moved the admittance along the conductance circle of 1. Then, that height of the button which would bring it into the center of the chart was determined experimentally. Locating the proper position only by rotating the admittance of the transition toward the load is subject to considerable error since the guide wavelength in the transition section is not known.

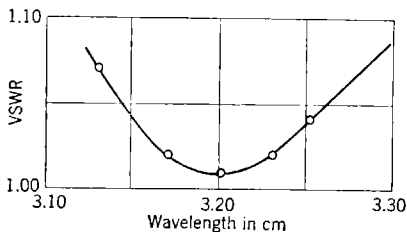


FIG. 6-91.—VSWR vs. λ for the transition of Fig. 6-87b.

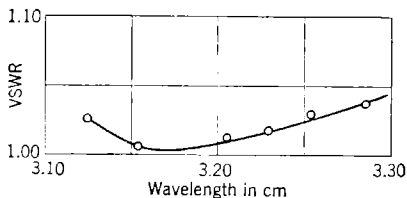


FIG. 6-92.—VSWR vs. λ for the transition of Fig. 6-87c.

The optimum bandwidth is attained when the button is 0.088 in. from the center line of the round guide. To improve the match for the higher wavelengths, the button must be nearer the load; if the button is moved farther back, its effect diminishes, and it becomes critical with respect to position. Consequently, there is no satisfactory position to match for the wavelengths above 3.3 cm.

The most critical part in this type of transition is the resonant *H*-ring. Tilting an *H*-ring with the supporting struts as axes tends to affect its resonant frequency. One transition was tested in which the ring was tilted 0.018 in. (the difference between the height of one end and the height of the other end of the ring). Then the ring was adjusted to an 0.010-in. tilt. The following table gives a comparison of the results.

TABLE 6-5.—RESULTS OF TILT OF *H*-RING

λ	VSWR	VSWR
	0.018 in.	0.010 in.
3.16	1.16	1.09
3.20	1.07	1.05
3.23	1.06	1.00
3.30	1.13	1.09

Assuming that a change of 0.008 in. in tilt from the level position has the same effect as a change from 0.010 in. to 0.018 in., we find that a

tolerance of ± 0.002 in. is allowed for a change of 0.01 in voltage standing-wave ratio. Variation in the height of the H -ring is less critical; ± 0.005 in. will cause a change in voltage standing-wave ratio of 0.01.

Another means of eliminating this objectionable TE_{11} -mode is to use a metal fin as shown in Fig. 6-93. It has been shown that only one polarization of the TE_{11} -mode can be excited in the round waveguide

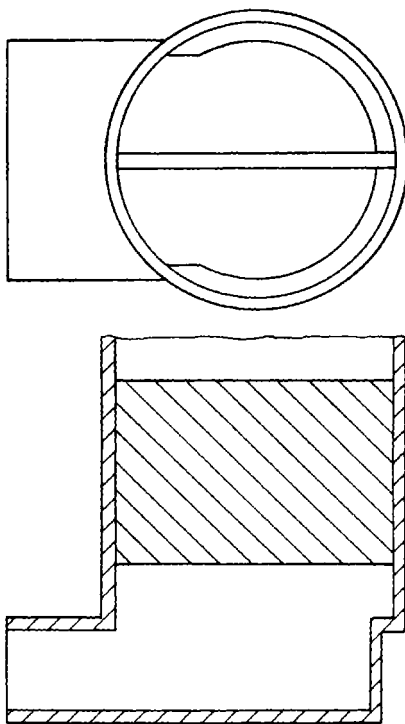


FIG. 6-93.—Fin TE_{11} -mode filter.

by a right-angle transition from rectangular to round waveguide; therefore, if there is inserted across the diameter of the waveguide a metal fin aligned along the axis of the rectangular waveguide, this polarization is short-circuited. One requirement of the fin is that it must be very well centered. The type of mode propagated in this half round-waveguide section is essentially the TE_{11} -mode, with one half 180° out of phase with the other half, so that a symmetric mode is set up at the transmitting end of the fin. If, however, the fin is not centered, then the waveguide wavelength in one half is different from that in the other half, and a shift in phase between these two halves results in some

TE_{11} -mode being excited by the fin (see Fig. 6-94a). This fin also must be long enough so that the higher mode in Fig. 6-94b is sufficiently attenuated.

The mismatch of the fin to the TM_{01} -mode, with the edge rounded, is very highly inductive, so that the fin is nearly matched if it is about a half guide wavelength long. Figure 6-95 shows a plot of various fin sizes and the resulting match to the TM_{01} -mode as a function of wavelength. The straight fin will stand no more power than the resonant ring. Corona forms along the edge of the fin; and, although rounding the edges has a salutary effect on the breakdown, it does not eliminate this corona entirely.

Another means of reflecting the TE_{11} -mode is to couple out this mode into shunt arms of rectangular waveguide in the same manner as the right-angle transitions described in Sec. 6-17. However, instead of using the full rectangular opening into the round waveguide, a narrow resonant slot may be used to couple into the waveguide. Four such waveguides may be spaced 90° around the TM_{01} -waveguide so that all polarizations are coupled into the rectangular waveguides. If the short-circuiting plungers in each arm are adjusted so that an effective short circuit is placed at the center of the waveguide, all the energy is reflected back and the device is a resonant mode filter.

This type of filter is a selective device, for it will have little effect on the TM_{01} -mode transmitted in the round waveguide. The currents in the TM_{01} -mode are always in the direction of propagation; they are, therefore, parallel to the slots which will not, consequently, cut across any currents in this mode.

Some experiments have been done on this type of mode filter but no appreciable band was attained. Figure 6-96 shows the plot of the transmission of TE_{11} -mode past a single arm of $1\frac{1}{4}$ - by $\frac{5}{8}$ -in. waveguide on round waveguide 1.152 in. ID. It was thought that by spacing the opposite arms a quarter wavelength away as in Fig. 6-97 the bandwidth could be increased; but there was some interaction between the two sets of arms. At certain wavelengths, more energy was propagated in the TE_{11} -mode with this type of filter than without it. One fundamental fault of this design was that the symmetry of the round-waveguide section was not preserved.

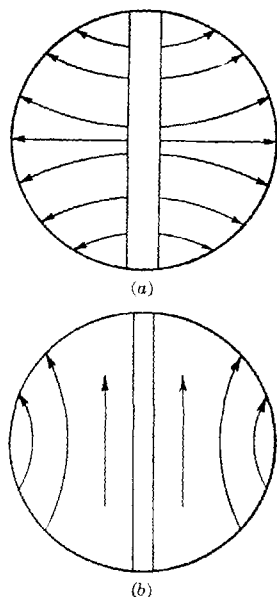
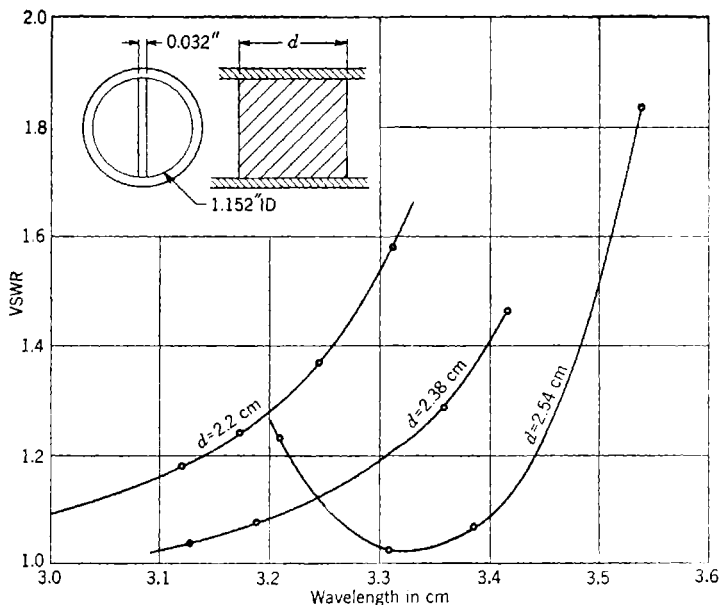
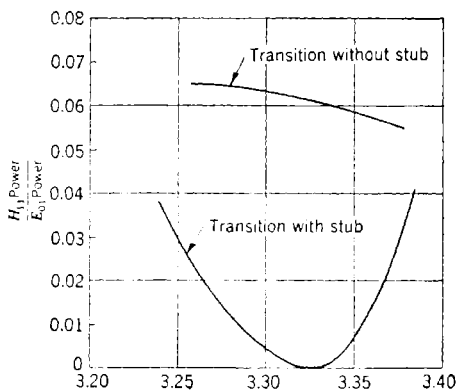


FIG. 6-94.—Propagated (a) and attenuated (b) modes in fin section.

FIG. 6-95.—Match of fin to TM_{01} -mode in round waveguide.FIG. 6-96. Plot of transmission of TE_{11} -mode past single arm of mode filter of the shunt-stub type (see Fig. 6-97).

The purpose of using resonant slots to couple into the waveguide was to ensure the TE_{11} -mode filter's introducing as little disturbance as possible to the incident TM_{01} -mode. Since, however, there is very little coupling of the TM -mode into a shunt waveguide arm with a full opening, it is possible that a more satisfactory filter may be made, using four short-circuited arms 90° apart around the waveguide as in Fig.

6-98a. Since this is symmetric it will not excite any TE_{11} -mode. Some

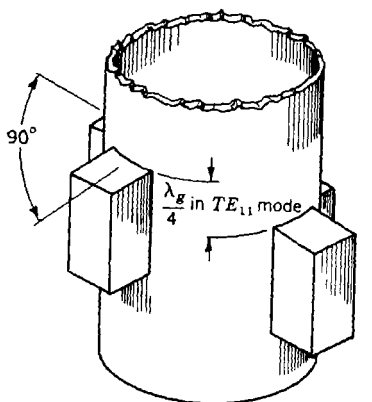


FIG. 6-97.—Mode filter with two sets of stubs spaced $\lambda_g/4$ apart in round waveguide. Stubs to reflect TE_{11} -mode.

of the TM_{01} energy will be reflected back as well as the TE_{11} -mode, to be sure, but if this reflection is not too large, it may be matched out by inductive diaphragms or it may be spaced to cancel the reflection from the transition. One is limited somewhat in spacing the filter in the round waveguide since that section between the filter and the transition itself may become resonant in the TE_{11} -mode at certain frequencies. One might also extend this further and use a long section of waveguide, the cross section of which is shown in Fig. 6-98, which might be designed so that it will not propagate the TE_{11} -mode.

Another device which may be used to excite the TM_{01} -mode is shown in Fig. 6-99. This should transform nearly all the energy into the TM_{01} -mode without the necessity of any mode filters. The wave propagated in the two arms of the rectangular waveguide T from the input shunt arm have the same phase relation. Since the two path lengths from the T, around the rectangular bands to the center of the round waveguide, are equal, this waveguide will be excited by a symmetric field which theoretically should prevent any of the TE_{11} -mode from being propagated.

6-23. Straight-on TM_{01} -mode Transitions.—In Sec. 6-20, the easiest way of exciting the TM_{01} -mode was discussed, and it was decided that this could best be done by coupling the round waveguide at right angles to the wide side of the rectangular waveguide. It is often desirable, however, to have the two waveguides on the same axis. Some means must be used to excite the waveguide with a symmetrical field. This may be done by a tapered fin. This fin, when aligned with the maxi-

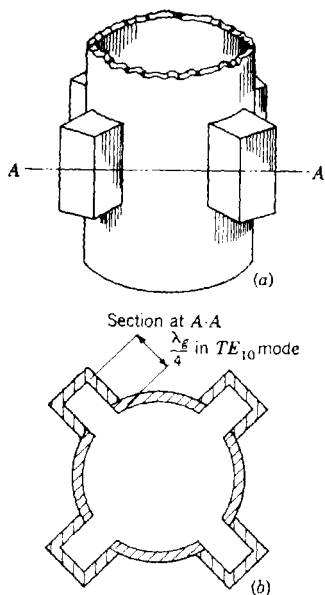


FIG. 6-98.—Four stubs to reflect TE_{11} -mode.

imum electric vector in the TE_{11} -mode in the round waveguide, will divide the waveguide mode into two half-round TE_{11} -modes of equal power. In Fig. 6-100 there are sketches of the electric field in various cross sections of this tapered section showing how the field is gradually divided into two sections with one side 180° out of phase with the field in the other half. If the round waveguide is tapered to a larger size to transmit the TM_{01} -mode, then a terminating antenna may be used to match the waveguide to the TM_{01} -mode. This device, if the fin is centered carefully, will excite very little energy in the TM_{11} -mode since the symmetry is not dependent in any way on frequency.

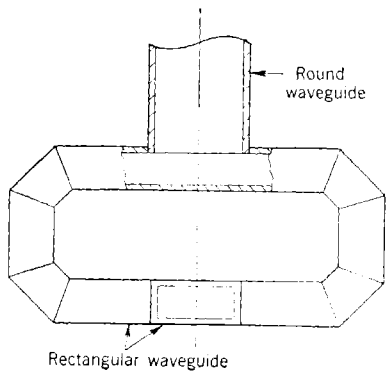


FIG. 6-99.— TM_{01} -transition with exciting round waveguide in a symmetrical manner. The input waveguide, at the bottom, branches by means of an H -plane T.

The length of the taper for this transition was determined to obtain the best match for 3.2 cm, which for round waveguide $\frac{1}{8}$ in. ID is 1.125

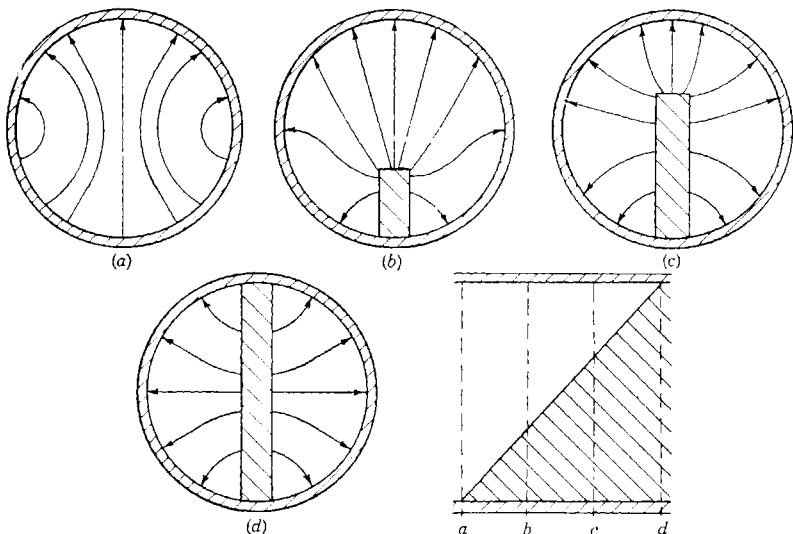


FIG. 6-100.—Field configurations in round waveguide with tapered fin.

in. A metal rod of $\frac{1}{8}$ in. diameter was soldered over this taper to provide rounded edges in order to cut down the possibility of corona and voltage

breakdown. On the basis of the theory of tapered transmission lines, it would be expected that if this taper were made very long it would be very well matched over a broad band. Lengthening this type of taper, however, makes the mismatch worse. A study of the cutoff wavelength

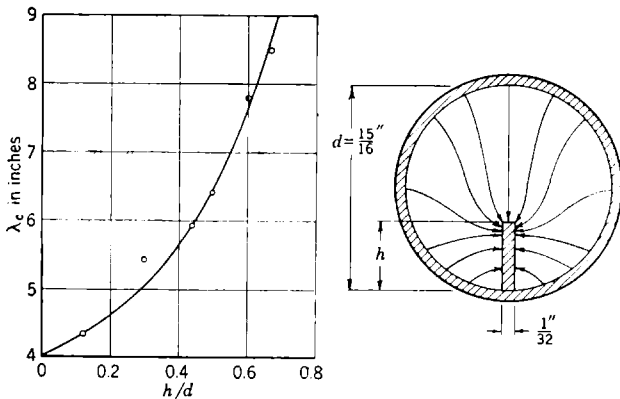


FIG. 6-101.—Cutoff wavelength for round waveguide with fin, TE_{11} -mode.

as a function of the dimension of the fin in Fig. 6-101 indicates that the cutoff wavelength may become infinite as the height of the fin approaches the diameter of the waveguide. This, of course, would introduce a large discontinuity in the impedance at this point. The design of this transition has not been finished. If a capacitive iris in the round waveguide, together with an inductive iris in the rectangular waveguide, is used to match this transition, a good match may be obtained over a fairly broad band.

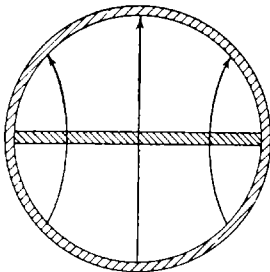


FIG. 6-102.—Fields in waveguides divided by a diametral plane.

Another technique of obtaining a straight-on TM_{01} -transition is shown in Fig. 6-102. In this transition a fin is placed across a diameter in the round waveguide so that it is perpendicular to the electric field. In this way, the incident power is divided in half with very little mismatch. Now, if a phase shift of 180° is introduced into one half of this waveguide section, then a symmetrical field

may be formed exactly like the right-hand sketch in Fig. 6-100. This phase shift may be accomplished by a section of dielectric or a metal half-round rod as in Fig. 6-103. The half-round rod has some advantages since this section of waveguide will propagate only the TE_{11} -coaxial mode; and then its cutoff wavelength can be calculated. As in the previous design, the

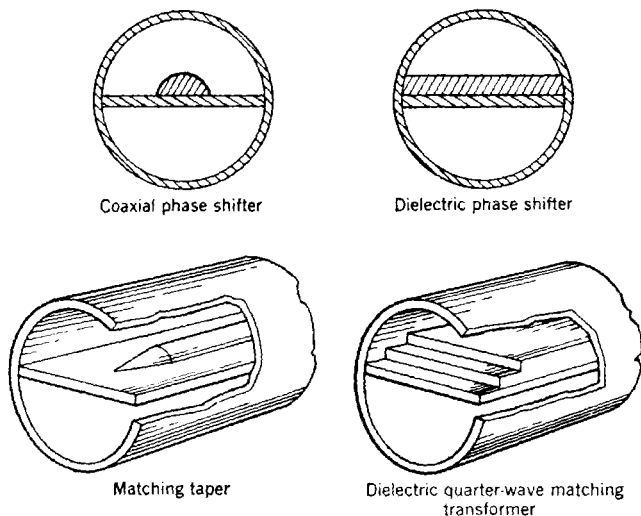


FIG. 6-103.—Two possible means of obtaining a phase shift and appropriate matching sections.

round waveguide should be tapered to one of larger size which propagates the TM_{01} -mode; the same terminating antenna may be used. The addition in the round waveguide of some filter, such as a resonant ring, will increase the bandwidth.

A shorter straight-on transition is possible if a stub is used to introduce the phase shift. In this transition, the dividing fin is placed in the rectangular waveguide and a series stub is placed on one side as shown in Fig. 6-104. This fin is also extended into the round waveguide, and no gradual taper from the rectangular section to the round is needed. The same antenna is used to terminate this fin. With the introduction of a resonant ring, such a device appears to be capable of being matched over a broad band.

6-24. High-power Capacity.—In the course of designing these transitions, some tests were made on their power capacity. For most of these tests, the round waveguide was matched to space by means of a flared horn. This made it possible to observe where breakdown actually

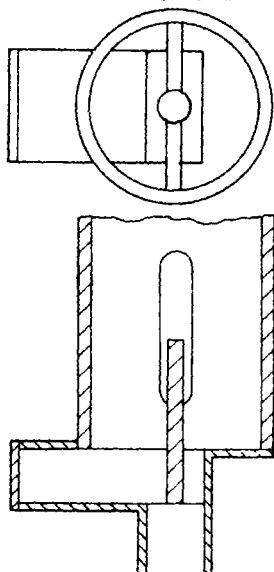


FIG. 6-104.—Straight-on TM_{01} -transition with stub phase shifter.

occurred in the transition. Since only 100 to 200 kw peak power was available for test, the transition with its matched horn was placed inside a bell jar of a vacuum system. Then the air was drawn out until arcing occurred. The following chart of power breakdown for atmospheric pressure was calculated, assuming that the peak-power breakdown varies directly as the $\frac{4}{3}$ power of the pressure and is inversely proportional to the square root of the pulse width up to 2 μ sec. If the repetition rate is increased by a factor of 4, the peak power necessary for breakdown is decreased by 30 per cent.

There are many factors that determine the power capacity of a transition, such as the width of air gaps in the transition and the presence of sharp corners and of dust or fine metal filings. Cleanliness seems to be an especially important factor in ensuring the best power capacity of a particular design. When each transition was tested at first, frequent "splitting" or "sputtering" occurred from the sharp corners, but as the transition was continued under high power, this spitting gradually ceased. Greater consistency is obtained if the sharp corners are eliminated by rubbing with steel wool and the transition is blown clean by an air blast.

6-25. Summary.—In the previous paragraphs we have discussed in detail the transitions that were developed, or were attempted, at the Radiation Laboratory. In designing these transitions, with the possible exception of the round waveguide in the transition for 1.25 cm, the inquiry was consistently limited to standard tubings. This was especially true in the case of the rectangular waveguide which was standardized by the Army and Navy. Therefore, if a simple transition, containing no filters for the TE -mode, excited nearly pure mode, this was a happy coincidence; and if the combination of waveguides and wavelength were not right, various TE -mode filters had to be tried to obtain the satisfactory TM_{01} -mode purity. It is possible that the purity of the mode in the round waveguide in such a simple transition results from the optimum adjustment of four dimensions: the height and the width of the rectangular waveguide, the diameter of the round waveguide, and the position of the short-circuiting plunger. There were not many parameters with which to work, but it is possible that broader bands could have been obtained if a greater investigation of these parameters had been made. For instance, one might investigate the effect that the height of the rectangular waveguide would have upon the mode purity in a waveguide of a given diameter when the plunger is adjusted for minimum excitation of the TE_{11} -mode. Also, the effect of the wide dimension of the rectangular waveguide might be investigated. If these investigations were made over the entire frequency range where the TM_{01} -mode will operate without higher modes, they would give adequate data to

enable an engineer to design a simple transition which could be manufactured for any desirable band from standard tubings. Of course one could scale the transitions described in this text by the ratio of the wavelengths for the known transition to the wavelength of the new band and obtain a set of dimensions which would be as good for the new band; but in a great majority of the cases, these dimensions would be very odd indeed, and would not correspond to any standard tubings available. Consequently, a fundamental series of investigations, such as those proposed here, would be desirable if further designs of the TM_{01} -transitions were contemplated.

TABLE 6-6.—BREAKDOWN OF TM_{01} -TRANSITIONS

Transition	Fig. No.	Wave-length, cm	Break-down, kilo-watts, at 1 μ sec. 1000 cps	Rating, kw, for factor of safety of 2	Weakest point
Compound $TE-TM$ stub.	6-82	3.2	250	125	Across rectangular waveguide edges at opening into round waveguide
Strut-supported resonant-ring filter.	6-87	3.2	900*	450	Junction of rectangular and round to bottom of rectangular corner of ring
Fin filter (breakdown at fin)	6-93	3.2	550	276	Along edges of fin
High-power transition, rounded corners.	6-79	3.2	1250	No arcing at 200 kw peak power to 10 cm pressure
Straight-on tapered fin	6-100	3.2	440	220	From top of taper to top of round waveguide near point where fin is nearly across waveguide
Transition with rectangular plug in bottom.	6-75	1.25	70	35	Junction of rectangular and round to bottom of rectangular

* Sharp edges taken off with steel wool, and transition thoroughly cleaned by air blast.

CHAPTER 7

MOTIONAL JOINTS

BY F. L. NIEMANN, F. E. EHLERS, AND F. T. WORRELL

In microwave system installations it is usually necessary to provide for relative motion between components at one or more points in the r-f transmission line. The shock-mounting of the different components and the searching or scanning motions performed by radar antennas, for example, require motional joints in the coaxial line or waveguide which have a variety of degrees of freedom. It is the purpose of this chapter to discuss the electrical design of the various devices that fulfill these requirements. The mechanical aspects are treated in other books of this series, e.g., "Radar Scanner Engineering," and will be mentioned here only in so far as they affect, or are affected by, the electrical characteristics.

There are two general electrical considerations that apply to all motional joints. First, they must provide a good impedance match (a voltage standing-wave ratio of about 1.2 or less) for all required displacements. This involves the problem of mode purity, in certain cases, since the presence of undesired field configurations can give rise to resonances which appear as large reflections in the transmission line. As is mentioned in Chap. 6, this requirement of impedance match is imposed by the sensitivity of most microwave oscillators to their load impedances and by the effect that large standing waves may have on the operation or power-handling capacity of other transmission-line components. The power lost through reflection at a mismatched component is usually so small as to be a secondary consideration. Second, special precautions are frequently necessary to minimize the r-f leakage from these components in order to prevent interference with receiving equipment or, when systems have very high power, to prevent damage from sparking to the moving mechanical parts of the unit such as the bearings.

A mechanical consideration that affects most of the designs for motional joints is that of pressurization, discussed to some extent in Chap. 3. It is sometimes desirable to operate a microwave transmission line under considerable pressure or to maintain sea-level pressures at high altitudes to reduce the likelihood of breakdown at high powers. In systems designed for ship installation or for operation in the tropics or other regions having high humidity, the transmission line is kept dry by the introduction of dry air at a pressure slightly greater

than atmospheric. Therefore, it has become standard practice to provide for pressurization in the design of nearly all microwave transmission-line components. In terms of the type of motion for which they are designed, motional joints may be classified as (1) rotary joints, and (2) other types of motional joints. Each category includes designs for both waveguide and coaxial line.

Rotary Joints.—Rotary joints provide for continuous rotation in either direction about one axis. This requires field configurations with symmetry about the axis of rotation. In practice either the *TEM*-mode (dominant coaxial mode) or the *TM*₀₁-mode in round waveguide is used. A round-waveguide rotary joint using a circularly polarized *TE*₁₁-mode has been developed experimentally. In systems where the coaxial mode is used throughout, the electrical problem is relatively simple. More frequently, however, the transmission line consists of rectangular waveguide carrying the *TE*₁₀-mode, so that transitions to a symmetrical mode are required for the rotary joint. The transition problems have been treated in Chap. 6.

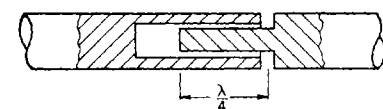
Other Types of Motional Joints.—There is often need for joints that provide for translational displacements that are small compared with a wavelength or for rotations of considerably less than 360°; these usually do not involve a change of mode. Such joints include vibrational or alignment joints, which allow very small translational and rotational displacements in any direction or about any axis; "swivel" joints, which permit rotation through fairly large angles about the longitudinal axis of the transmission line; hinge joints, for small angular displacements about either of the transverse axes; and universal joints for angular displacements about both transverse axes simultaneously. Most of these devices have been designed for rectangular waveguide although a few have been built for coaxial line. The function of the vibration or alignment joint is sometimes accomplished through the use of flexible waveguide or coaxial cable (see Chap. 5). These require considerable space, however, and are not to be recommended for applications involving continuous motion.

MOTIONAL JOINTS IN COAXIAL LINE

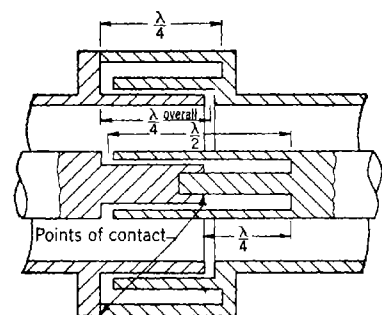
BY F. L. NIEMANN

7-1. General Design Considerations for Coaxial Rotary Joints.—Since the field configurations for the *TEM*- or dominant mode in coaxial line are functions of the radius only, they are suitable for a continuous rotary motion about the axis of the line. Impedance-matching is therefore quite simple, and the chief problems in the design of such a joint are mechanical in nature. The major electrical requirement is

that there be a low impedance in series with the line at the point of discontinuity where there is relative motion between the rotating and fixed parts. An impedance minimum (and therefore a voltage minimum) is necessary in order to prevent burning of contacts, to minimize leakage, and to match the discontinuity. For low-speed joints operating at low powers, a well-designed mechanical "wiping" contact on both inner and outer conductor is satisfactory. A more desirable arrangement that allows high speeds of rotation and operates well at high powers is the following. As small a gap as it is convenient to make mechanically is left between the moving and the fixed parts of the conductor.



(a)



(b)

FIG. 7-1.—Coaxial chokes in rotary joints.

Figure 7-1a the choke section consists of a quarter wavelength of coaxial line terminated in an open circuit, the fields being rapidly attenuated in the region beyond the coaxial section. This places a low impedance at the discontinuity between the two parts of the conductor. This arrangement is applicable only to the center conductor, since, in the case of the outer conductor, the chokes must be designed to come outside the conductor, and a perfect open circuit is not possible. Figure 7-1b shows chokes of slightly different constructions on both inner and outer conductors. These chokes consist of half-wavelength sections terminated by short circuits. This arrangement also places a low impedance across the gap. Each half-wavelength section consists of two quarter-wavelength sections, one of which has several times the impedance of the other. As is shown in Chap. 2, this greatly reduces the frequency sensitivity of the choke; well-made junctions of this kind have almost unmeasurable reflections over as much as a 30 per cent band. Further, these chokes are so designed that the short circuit occurs just a quarter-wavelength from the point of contact. This places a high impedance and, therefore, a current minimum in this region. This design has a further advantage over the quarter-wavelength section in that the center

¹The theory of r-f chokes is discussed in Chap. 2.

conductors of the two members may be joined in a bearing and thereby be more rigidly supported.

In practice, the use of these chokes results in a completely satisfactory impedance match for a rotary joint. However, in certain units used at high powers, leakage sufficient to cause damage to the bearings has occurred through these chokes. The elimination of this effect by the use of an absorbing material will be discussed later.

7-2. Examples of Rotary Joint Construction.—The chief differences among the various ways of constructing coaxial rotary joints are mechani-

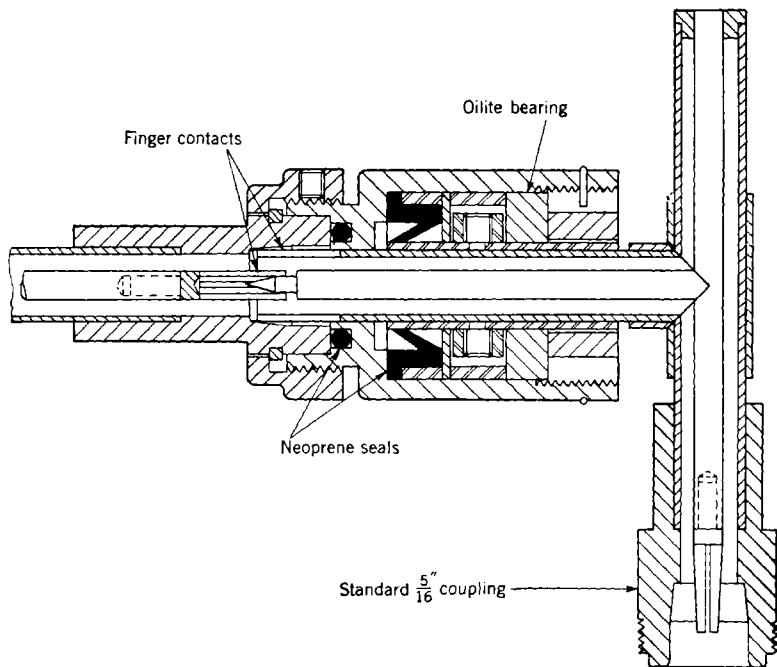


FIG. 7-2.—10-cm rotary joint for $\frac{5}{16}$ -in. line.

cal in nature and are determined by the speed of rotation, temperature, loading, and pressure difference under which the joint is to be operated. The final solutions to some of the problems involved have not been obtained; the several examples presented here are representative of designs developed during the last few years at various stages of progress in microwave engineering. Most of them could be improved by the utilization of later developments, particularly in the technique of low-temperature high-speed pressure seals. Also, in certain cases the designs were intended for applications not requiring high-speed or low-tempera-

ture operation, and the units could be simplified by the use of sleeve bearings and neoprene seals. For speeds greater than a few hundred revolutions per minute, or for heavy loading, or both, ball bearings are necessary. If, in addition, the joint is to be operated over a wide range of temperatures and pressures, as in the case of aircraft installations, a Sealol type of pressurizing seal is more successful.

Figure 7-2 shows a design for a 10-cm rotary joint in $\frac{5}{16}$ -in. coaxial line. This rotary joint is designed for fairly low speeds, of 60 rpm or less, and both the inner and outer conductors are made of beryllium-copper or phosphor-bronze and slotted to form "fingers" which, under tension, provide a good mechanical wiping contact. A sleeve bearing and a neoprene- or rubber-lip seal are satisfactory for the conditions under which this unit is designed to operate. The particular applica-

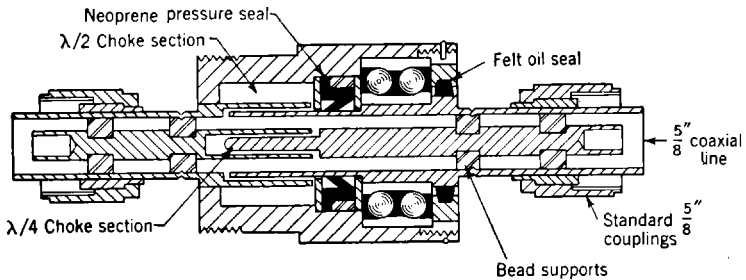


FIG. 7-3.—10-cm bead-supported rotary joint for $\frac{5}{8}$ -in. line.

tion for which this was designed required a right-angle connection so that the center conductor is supported by a right-angle quarter-wavelength stub. It could equally well be supported by "straight through" stubs or by means of beads if the power rating is not a limiting factor. If a special low-temperature neoprene is used in the pressurizing seal, the unit should be satisfactory at temperatures down to about -20°C . However, since this rotary joint was designed for low-power and low-speed applications, pressurization was incorporated chiefly as a means to keep out dirt and moisture. The unit has had only limited application.

A later design of a 10-cm rotary joint is shown in Fig. 7-3. This is for a bead-supported $\frac{5}{8}$ -in. coaxial line and incorporates coaxial chokes at the discontinuity. A quarter-wavelength, open-circuited section is used on the center conductor and a two-section, half-wavelength, short-circuited choke coupling on the outer conductor. It should be noted that the close spacing desirable in these couplings requires a very accurate alignment of the bearings. If low-temperature neoprene is used in the seal, this unit should be satisfactory for speeds of 300 rpm or less and should be effectively pressurized at temperatures down to

-20°C . In both these specifications the seal is the limiting factor. Use of the Sealol type should permit operation at speeds of several thousand revolutions per minute and at temperatures considerably lower than -20°C .

In this design, as in most others, it is desirable to have the seal come between the choke sections and the bearings. This arrangement prevents the leakage of oil or grease into the chokes and helps to shield the bearings from any radiation that may leak through the chokes. In certain high-power applications, it is necessary to take further precautions to prevent damage to the bearings from r-f arcing.

In the design for a $\frac{7}{8}$ -in. stub-supported coaxial rotary joint shown in Fig. 7.4, the two-section half-wavelength broadband choke is used on

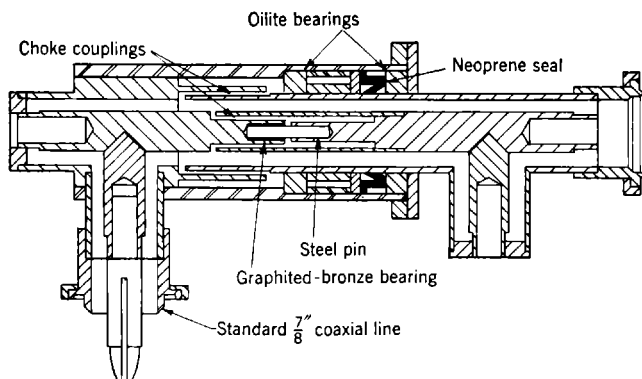


FIG. 7.4.— $\frac{7}{8}$ -in. medium-speed rotary joint for 10 cm.

both the inner and the outer conductor. This allows the inner conductor to be supported at the discontinuity by means of the steel pin turning in a graphited-bronze (Morganite) bearing. Because it has sleeve bearings and a low-temperature-neoprene seal, this joint should probably not be operated at more than two or three hundred revolutions per minute nor at less than -20°C for continuous service. It has, however, been run satisfactorily at 600 rpm and at room temperature for 50 hr. In this design one of the Oilite bearings is between the choke and the seal. This arrangement is undesirable, in general, but has given no trouble in a number of different applications; it should be satisfactory provided that the joint is not operated at too high a power or at speeds of rotation at which the Oilite becomes overheated and exudes oil which can affect the operation of the choke sections. Two versions of this design differing only in the direction of the input line are pictured in Fig. 7.5.

A coaxial rotary joint, also in $\frac{7}{8}$ -in. line, designed expressly for high

speeds, heavy loading, and low temperatures is shown in Fig. 7-6. In addition to the half-wavelength choke sections and the graphited-bronze bearing on the inner conductor, it has two large ball-type main bearings, a Sealol pressurizing seal, and a balanced double-stub support on the rotor. This unit is designed for 3000 rpm and for temperatures down to -50°C .

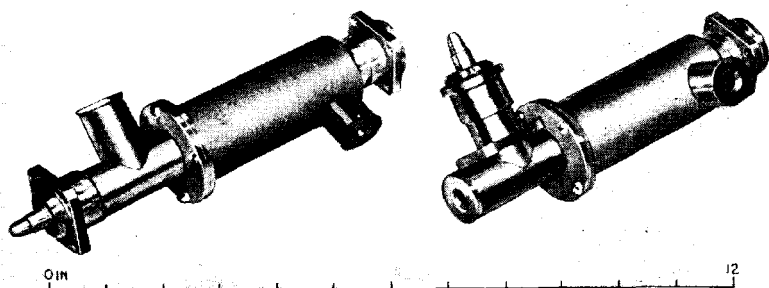


FIG. 7-5.— $\frac{7}{8}$ -in. coaxial stub-supported rotary joint.

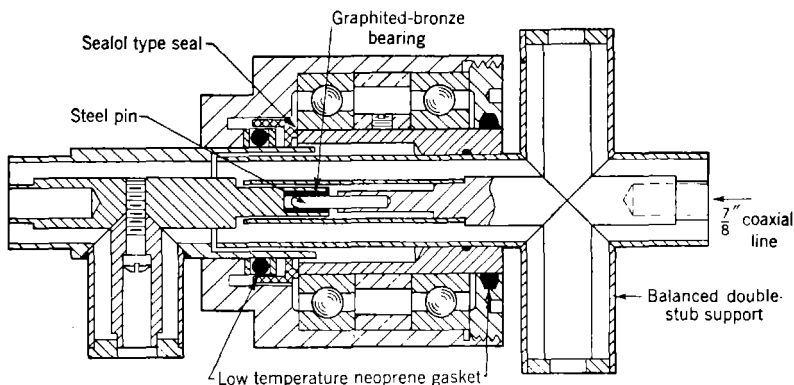


FIG. 7-6.—High-speed pressurized coaxial rotary joint for 10 cm.

These examples, chosen as typical of a large number of slightly different modifications, are all for 10-cm wavelengths. They can, of course, be adapted to both longer and shorter wavelength bands; models have been designed for wavelengths as long as 25 cm and as short as 3 cm. However, at the short wavelengths, machining tolerances become almost prohibitively small, and for the 3-cm and 1-cm bands, coaxial rotary joints have been replaced almost entirely by the $T.M_{01}$ -mode rotary joint.

There has been little reference to the power-handling capacity of these

joints because they are usually capable of transmitting at least as much power as the coaxial line itself can support. The power-handling capacity of the coaxial line is limited by the bead supports or by the coaxial transformers on the broadband stub supports (see Chap. 4). When the coaxial mode is utilized for a rotary joint in a high-power system having a waveguide transmission line, however, the coaxial section and its transitions to waveguide are frequently a limiting factor in the power rating of the system. This problem is to be discussed in a later section.

A similar consideration applies to the bandwidth of these joints in terms of the allowable impedance mismatch. As has been mentioned, the match provided by the two-section, half-wavelength, coaxial chokes is very good (the voltage standing-wave ratio is less than 1.05 if the choke sections are properly made) over a band which is probably somewhat wider than that for which a broadband stub support is as well matched. Bead supports in coaxial line usually constitute even more of a limiting factor in terms of match and bandwidth than do the stub supports.

A possible type of rotary-joint construction developed by the Naval Research Laboratory, which is not limited by chokes or by stub or bead supports in the frequency band over which it is usable, is shown in Fig. 7-7. It consists of a dielectric-filled coaxial line with a tapered contact that provides a long leakage path between the dielectric sections. The dielectric used is du Pont Poly F-1114, polytetrafluorethylene, called "Teflon." This has very good bearing properties and is highly resistant to chemical action. The contact is lubricated with Ignition Sealing Compound, which has a dielectric constant approximately the same as that of Teflon and has good high-voltage insulating properties. Spring-finger contacts are used on the inner and outer conductors. This type of joint should be usable at any frequency up to the cutoff frequency of the second coaxial mode. In a dielectric-filled line this, of course, occurs at a lower frequency than in an air-filled line of the same over-all dimensions. However, at microwave frequencies the power loss in the dielectric becomes appreciable. Furthermore, because of the dielectric and the mechanical contacts, such a joint is limited to low speeds and low average powers.

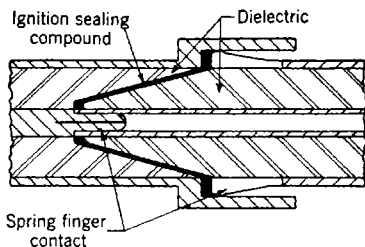


FIG. 7-7.—Contact-type dielectric-filled rotary joint.

7-3. Other Coaxial Motional Joints.—It is difficult mechanically to provide for relative motion between sections of coaxial line other than motion about the axis of the line, as in rotary joints. Various methods

have been proposed and some actually used experimentally with a certain amount of success. Since waveguide joints for these motions are considerably simpler and usually more satisfactory than coaxial joints, little use has been made of coaxial line for this purpose. In systems using coaxial line throughout, however, it is not always convenient to use a waveguide motional joint.

An example of a coaxial universal joint for small angular displacements is shown in Fig. 7-8. It is capable of about $\pm 3^\circ$ angular displacement about both transverse axes simultaneously. It was used in a "conical scan" antenna for an accurate direction-finding radar system. The desired beam scan with fixed polarization was obtained by an off-center nutating motion of the antenna feed. The conventional

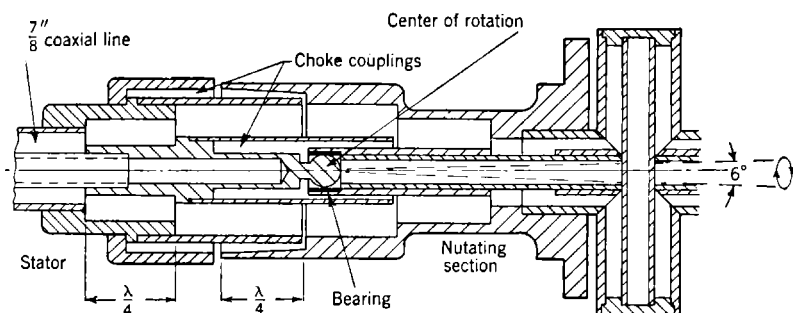
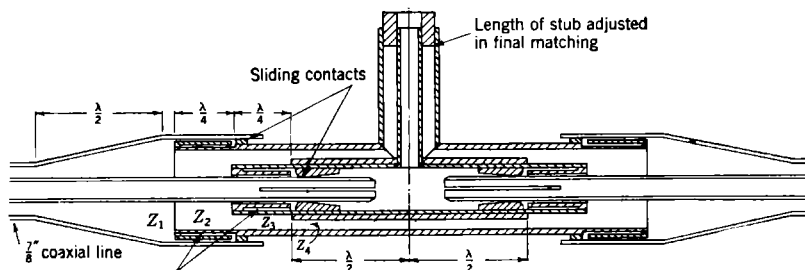


FIG. 7-8.—Coaxial universal joint for small displacements.

chokes are slightly modified to allow for the small angular displacement. The dimensions of the coaxial line are increased to facilitate the mechanical construction, but the line impedance is maintained at very nearly 50 ohms throughout. The two step discontinuities in diameter introduce approximately the same susceptance and are placed a quarter wavelength apart so that reflections from them cancel at the design wavelength. The discontinuities at the gap between moving parts in the inner and outer conductors are also a quarter wavelength apart for the same reason. Since this unit was designed to be operated at fairly high speeds (1800 rpm), a balanced double-stub support for the center conductor is used on the rotor. This design should be satisfactory for powers at which it is safe to operate $\frac{7}{8}$ -in. stub-supported coaxial line. However, because of the comparatively large susceptive discontinuities occurring at the changes in the size of the line, this motional joint is probably well matched for a rather narrow band, probably not more than 5 per cent for a voltage standing-wave ratio of less than 1.1.

A somewhat more complicated motional joint that provides for small displacements in all degrees of freedom, translational and rotational,

is shown in Fig. 7-9. The mechanical design, although simple, creates some interesting impedance-matching problems. Chokes are used at all points of contact, so that good electrical contact between moving parts is not essential. In order to make this construction feasible in a unit designed for use with $\frac{7}{8}$ -in. coaxial line, a coaxial line of larger size is used in regions of contact. However, in order to allow the desired longitudinal motion, the size of the inner conductor in these sections cannot be changed; therefore, several sections of coaxial line having different impedances are necessary. To provide for impedance-matching over a useful band, a half-wavelength taper in the outer conductor is used between the standard $\frac{7}{8}$ -in. line and the largest coaxial section.



"Folded" Choke couplings

FIG. 7-9.—Coaxial motional joint for small translational and rotational displacements. The four different impedances— Z_1 , Z_2 , Z_3 , and Z_4 —are designed to have approximately the relationship

$$\left(\frac{Z_2}{Z_1}\right)^2 = \frac{Z_3}{Z_2} = \left(\frac{Z_4}{Z_3}\right)^2,$$

or

$$2 \log \frac{Z_2}{Z_1} = \log \frac{Z_3}{Z_2} = 2 \log \frac{Z_4}{Z_3};$$

that is, the logarithmic increment between Z_3 and Z_2 is twice that between Z_2 and Z_1 or between Z_4 and Z_3 . As discussed by Slater¹ and in Chap. 6 of this book, this is the condition for broadband matching with two quarter-wavelength transformer sections.

The line section of impedance Z_1 is made large enough so that the choke sections on the inner conductor can be machined with reasonable ease. The susceptive discontinuity between Z_2 and Z_3 is also made twice that between Z_1 and Z_2 or between Z_3 and Z_4 , which are made approximately equal. Because of the quarter-wavelength spacings, reflections from the first and last of these discontinuities add and are canceled by that from the center discontinuity. Actually, Z_4 is some-

¹ J. C. Slater, *Microwave Transmission*, McGraw-Hill, New York, 1942, p. 57.

what different from the value that would be given by the relation previously stated. It is adjusted so that the reflections from the Z_4 -to- Z_3 discontinuity on either half of the unit (which will add since they are a wavelength apart) are canceled over an appreciable band by the reflection from the stub support for the inner-conductor section. The variation of the voltage standing-wave ratio with wavelength can be given a final adjustment in design by varying the position of the short-circuiting plug in the stub support.

Although the development of this joint for production or system use has never been completed, initial results indicate that it should be possible to build such a device having a VSWR of less than 1.2 over about a 10 per cent band. With properly rounded edges on the coaxial transformers, the unit should be capable of carrying as much power as can safely be used with $\frac{7}{8}$ -in. stub-supported coaxial line.

WAVEGUIDE ROTARY JOINTS

By F. E. EHLERS

If a section of waveguide transmission line must be rotated about an axis with respect to another section, as in scanners for radar equipment, some sort of round-waveguide section may be used. It is necessary that the round-waveguide section should be one that propagates a symmetrical mode (such as the TM_{01} -mode or circular polarization in the TE_{11} -mode), or one that has some means of rotating the polarization of the TE_{11} -mode.

7.4. Resonances in Rotary Joints.—The most satisfactory method of obtaining a waveguide rotary joint is by the use of the TM_{01} -mode.

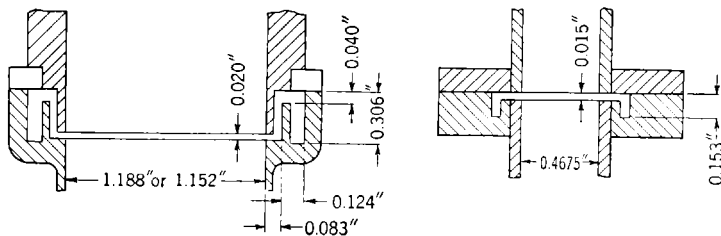


Fig. 7-10.—Choke sections in round waveguide for TM_{01} -mode. These designs are for wavelengths of 3.3 cm and 1.25 cm.

This may be done by using two TM_{01} - TE_{10} -mode transitions and a choke section in the round waveguide as shown in Fig. 7-10. The details of designing a choke for a broad wavelength band will not be treated here for they have been covered in Chap. 2. Since the coaxial sections in the choke will be excited by a symmetric field, they must be computed on the basis of the principal coaxial TEM -mode.

The difficulties of making a transition from a rectangular waveguide that produces a pure TM_{01} -mode in the round waveguide were discussed at considerable length in Chap. 6. The design of several transitions was described in which as little as one-half of 1 per cent of the energy is propagated in the TE_{11} -mode. With this small amount of energy in the TE -mode there will be very little variation in the reflection from the rotary joint and no variation in the output power with rotation. However, if the transitions should excite as much as 1 per cent of power in the TE_{11} -mode, variations in the input voltage standing-wave ratio of about ± 0.02 with rotation may be encountered. The amount of this variation will depend on two things: the relative amount of TE_{11} -mode in the round-waveguide section, and the variation with angle of polarization of the impedance of the transition to the TE_{11} -mode in the round waveguide. When the right-angle transition from rectangular to round waveguide is used, only one polarization of the TE -mode is propagated in the round waveguide, and that is one in which the electric vector is parallel to the rectangular-waveguide axis. Therefore, energy in the TE -mode in the round waveguide, which is polarized at 90° to the rectangular-waveguide axis, will be totally reflected from the transition. If there is any energy in the TE -mode with a polarization parallel to the rectangular-waveguide axis, a small fraction of this will be propagated in the rectangular waveguide. As the joint is rotated, then, different amounts of energy will be propagated in the rectangular waveguide and cause variations of the input voltage standing-wave ratio and of the output power. Some variation will also occur in the input voltage standing-wave ratio if the electrical length of the round-waveguide section for the TE_{11} -mode changes with angle of rotation, thereby introducing a varying reactance to the transmission line.

Even with as little as one-half per cent of TE_{11} -mode in the round waveguide, resonances may be obtained in the round-waveguide section if its equivalent electrical length is equal to an integral number of half wavelengths in the TE_{11} -mode. The theory of these resonances has been worked out.¹ The following relation gives the condition for resonance in the round-waveguide section:

$$\frac{l}{\lambda_p} = \frac{n}{2} + \frac{\cos^{-1} [\cos (\eta + \gamma) \cos^2 \theta + \cos (\eta - \gamma) \sin^2 \theta]}{4\pi} \quad (1)$$

In this equation, l is the length of the cylindrical waveguide measured between corresponding points in the two mode transformers whose position is specified below; λ_p is the wavelength in the TE_{11} -mode; θ is the angle of rotation; and n is an integer. The total shifts in phase

¹ H. K. Farr, "Theory of TM_{01} -Mode Rotary Joints," RL Report No. 993, Jan. 15, 1946. Also Vol. 21, Chap. 10, of the Series.

of the position of the minimum of the TE_{11} -wave with angle of rotation for the two transitions are, respectively, η and γ . The values of η and γ may be obtained experimentally. If the TE_{11} -mode is polarized parallel to an axis of symmetry, then all the energy that is reflected back will be in that polarization. For a right-angle transition from rectangular to round waveguide, this axis of symmetry is along the middle of the rectangular waveguide. Since no energy can be excited in the polarization at 90° to this axis of symmetry, any energy of that polarization in the round waveguide will be totally reflected without change of polarization. If the TE_{11} -wave, which is oriented differently from one of these polarizations, is reflected from a transition, then the reflected wave consists of two polarizations that are parallel and perpendicular, respectively, to the axis of symmetry. The phase difference in radians between the positions of the minima for these two polarizations in one of the transitions is η , and γ is the value for the other transition of the rotary joint. Then η and γ may be computed from the relations

$$\left. \begin{aligned} \eta &= \frac{2\pi x_1}{\lambda_g}, \\ \gamma &= \frac{2\pi x_2}{\lambda_g}; \end{aligned} \right\} \quad (2)$$

each x is the distance between the position of the minimum in the round waveguide for the TE_{11} -polarization parallel to the axis of symmetry and the minimum for that polarization which is perpendicular to the axis of symmetry; and λ_g is the wavelength for the TE_{11} -mode.

If there is no shift in phase between these two polarizations, there is no variation with rotation, and the resonant condition is

$$\frac{l}{\lambda_{g_1}} = \frac{n}{2};$$

and for the next higher resonant wavelength,

$$\frac{l}{\lambda_{g_2}} = \frac{n-1}{2}.$$

Calculating the bandwidth between resonant wavelengths, we have

$$\begin{aligned} \Delta\lambda_g &= \lambda_{g_2} - \lambda_{g_1} \\ \Delta\lambda_g &= \left(\frac{2}{n-1} - \frac{2}{n} \right) l = \frac{\lambda_{g_1}}{n-1}. \end{aligned}$$

As the number of half wavelengths in the round waveguide, and therefore the length of the waveguide, is increased, the bandwidth between resonances is decreased. In general, it is best to use a short rotary joint in order to obtain as broad a band as possible. If the rotary joint is made

less than one-half wavelength, there is some coupling between the two transitions of the asymmetrical fields near the junctions of the rectangular and round waveguides. This coupling will cause a variation in the input impedance of the joint with rotation.

A further limitation of the bandwidth between resonances is produced by the difference in phase between the reflections from the transitions of the two polarizations that are parallel and perpendicular to the axes of symmetry of the transitions. Figure 7-11 is a plot of resonant

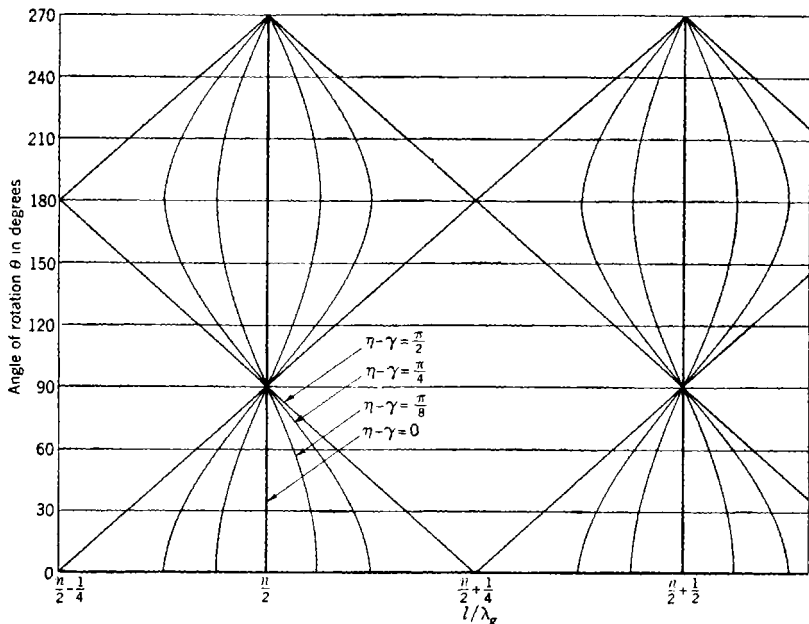


FIG. 7-11.—Plot of resonant wavelengths for several values of η with identical transitions.

wavelength for different values of η when the two transitions are identical and, therefore, $\eta = \gamma$. From the graph we see that, when η is equal to $\pi/2$, or the phase difference is a quarter wavelength, there is no band that is free of resonances. For η equal to zero, there is no spreading of the resonances with rotation but, as the value of η is increased, this spreading increases. Therefore, in the design of TM_{01} -transitions for rotary joints, every effort should be made to minimize the phase shift between the two polarizations.

Some interesting phenomena may be observed in these resonances. From Fig. 7-11, we see that if $\eta = \gamma$, the two pairs of resonances come together at 90° and reach their maximum spread at 0° and 180° . However, if the two transitions are different—that is, $\eta \neq \gamma$ —these two

resonances do not come together (see Fig. 7.12). As $\eta - \gamma$ becomes larger, the spread of resonances at 90° and 270° increases. If $\eta = 0$, there is no variation of these resonances with angle of rotation, but there are two fixed resonances that differ in fractions of a guide wavelength by $\gamma/2\pi$. Now, if η be fixed and γ varied, some improvement is made on the total spread of resonances if γ is made as small as possible. Therefore, if it is possible to improve the phase difference for one transition, an improvement will be obtained in the complete rotary joint.

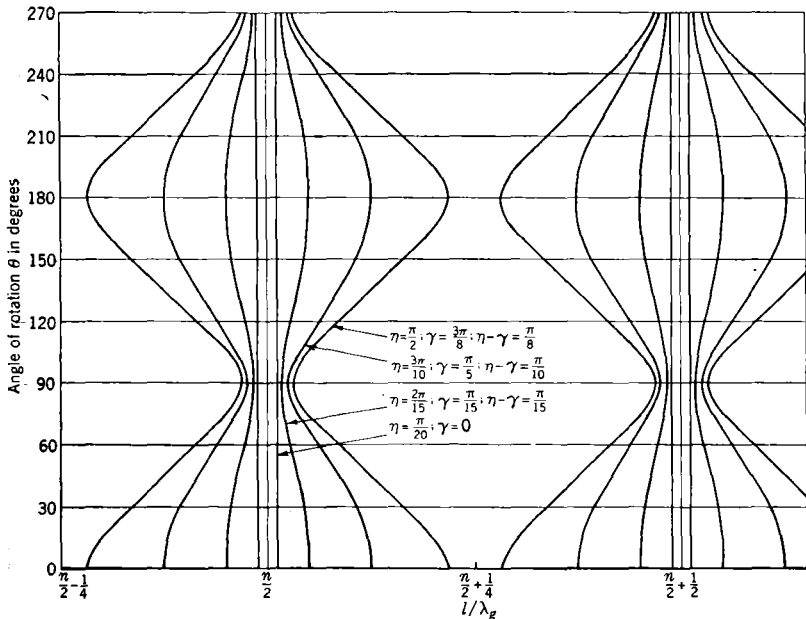


FIG. 7.12.—Resonant wavelengths with transitions with unequal values η and γ .

These deductions from the theoretical formula have been taken into account in the actual design of rotary joints.

7.5. Rotary Joints Using Transitions with the Compound TE - TM -stub.—Complete studies have been made on the resonances in rotary joints composed of the three types of the TM_{01} -transitions discussed in Chap. 6. One of these is the transition which uses a compound TE - and TM -mode round-waveguide stub that supports the TE_{11} -mode. For this transition, the change in phase of the reflection coefficient for the TE_{11} -mode with varying polarization is very small. Thus, there is little spreading of the resonances with rotation. It was found that for the ± 1 per cent band centered at 3.20 cm, resonances occurred when the distances measured between the centers of the rectangular waveguides

were equal to an integral number of half wavelengths (see Fig. 7-13). Permissible lengths which cover the band from 3.17- to 3.23-cm wavelength were determined experimentally and given in Table 7-1. A

TABLE 7-1.—PERMITTED LENGTHS L OF ROTARY JOINT

2.44- 3.90 cm	12.81-13.92 cm
4.51- 5.90	14.88-15.93
6.58- 7.91	16.96-17.93
8.66- 9.91	19.03-19.94
10.73-11.92	21.11-21.94

general empirical formula for the resonant lengths that must be avoided is given by

$$1.90 + 2.005n < L < 2.44 + 2.075n,$$

where L is the distance in centimeters between the centers of the rectangular waveguides, n is a whole number, and 2.005 and 2.075 are half the waveguide wavelengths in the TE_{11} -mode for a waveguide with an inner diameter of $1\frac{3}{16}$ in. at 3.17 and 3.23 cm respectively. For $n = 22$ or larger, the resonant regions begin to overlap at the edges of the ± 1 per cent band. For this reason a length $L = 40$ cm is the upper limit for a rotary joint that will perform well over a band from 3.17 to 3.23 cm. Within the range of the lengths listed above, the input voltage standing-wave ratio should vary less than ± 0.01 with rotation. The variation is least for the lengths halfway between the resonant lengths; and to eliminate the possibility of high standing-wave ratios near resonance, the extremes of the permitted lengths should be avoided.

Since each one of these transitions of the rotary joint will have a voltage standing-wave ratio of 1.1 at the extremes of the band from 3.17 to 3.23 cm, the input voltage standing-wave ratio of the complete rotary joint will vary from 1.2 to perfect match depending on the spacing

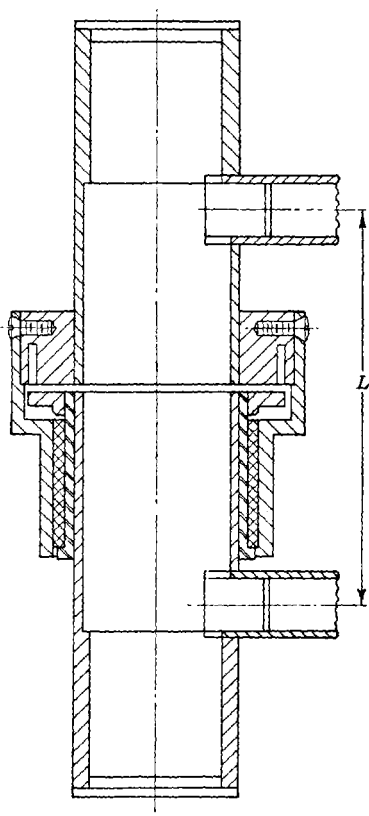


FIG. 7-13.—Assembly of rotary joint and E_o -transformers.

of the two transitions. It is possible to choose the length L so that, with the change of impedance with wavelength, the two transitions will cancel each other at the center of the band. The empirical formula for L that gives this cancellation is

$$L = 5.0 + 2.75n, \quad (3)$$

where 2.75 cm is equal to a half wavelength in the TM_{01} -mode for this waveguide at 3.20 cm.

For small values of L satisfying Eq. (3), this cancellation is very good; for long lengths, the phase change with wavelength is so large that there is little advantage in using this relation. It must be remembered that the primary restriction on the length L is the necessity of avoiding resonances in the TE_{11} -mode. Within the range of permitted lengths, L may be chosen to satisfy Eq. (3) as nearly as possible.

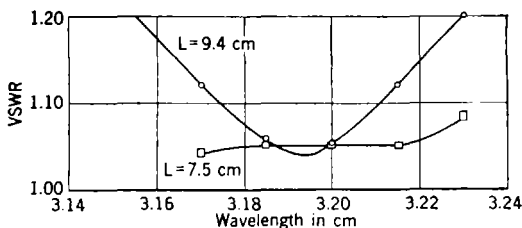


FIG. 7-14.—Voltage standing-wave ratio of TM_{01} -rotary joint with compound TE - TM -stub.

The input voltage standing-wave ratio for two typical completed rotary joints as a function of wavelength is shown in Fig. 7-14. The curve for $L = 7.5$ approximately satisfies Eq. (3). For the length of 9.40 cm, however, the reflections from the two transitions add at 3.23 cm. This represents about the worst mismatch that can be expected for any value of L .

7-6. Resonances in the High-power Rotary Joint.—This rotary joint consists of two transitions of the type shown in Fig. 6-79, Sec. 6-22. In this transition, a round short-circuiting plug is used in the rectangular waveguide and all sharp corners are rounded to increase the power-handling capacity. Because of these rounded surfaces, the transition must be manufactured by the processes of die-casting or electroforming. This transition contains no mode filters in the round waveguide; and consequently, there is little spread of the resonances with rotation. In Fig. 7-15 the resonant wavelengths are plotted against the total length of the round waveguide measured between the bottom surfaces of the rectangular waveguides. The shaded region indicates the total spread with rotation of the resonances. This spread is practically independent

of frequency. To find the limits of a resonance-free band of a rotary joint of a given length from Fig. 7-15, one should follow along a vertical line at the given length at the bottom of the chart and read from the vertical scale the upper resonant wavelength on the lower resonant region and the lower resonant wavelength on the upper resonant region. It is a safe policy to operate 0.02 cm in wavelength from each resonance to allow for mechanical tolerances and to avoid possible high standing-wave ratios near resonance.

A number of lengths of this rotary joint may be chosen which cover the complete band from 3.13- to 3.36-cm wavelength without resonances. But since the ratio of the TE -mode to TM -mode power is more than one-half per cent for wavelengths greater than 3.29 cm, there will be variations in the voltage standing-wave ratio with rotation. For a ratio of TE -mode to TM -mode of 1 per cent, the input voltage standing-wave ratio will vary about ± 0.025 ; and for a load matched to 1.3 in voltage, the shift in the position of the minimum in the input rectangular waveguide will be about 0.03 waveguide wavelengths. The variation in the output power will be about 1 per cent. If a rotary joint is designed to cover a narrow band centered at 3.30 cm, there will be less variation with rotation if a length is chosen that is midway between the resonant lengths.

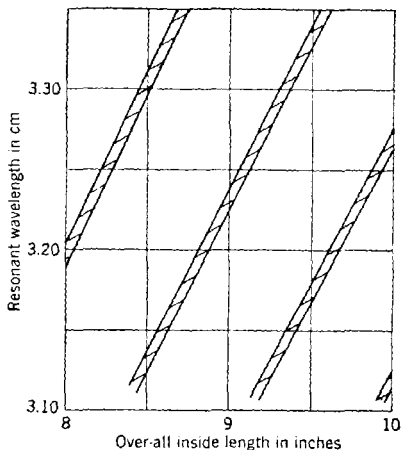


FIG. 7-15.—Resonant wavelength vs. over-all length for die-cast high-power rotary joint.

7-7. Resonances in the TE_{11} -mode for the Filter-ring Type of Rotary Joint.—The introduction of the filter ring in the TM_{01} -mode transition shown in Fig. 6-87 and discussed in Sec. 6-22 complicates the phenomenon of resonances in the rotary joint. The stub-supported resonant ring will transmit as much as 50 per cent of the TE_{11} -power incident on it if the polarization of the E -vector is in the direction of the stubs, as compared to 1 per cent of that polarization when it occurs 90° to it. Consequently, rotating the joint will tune the resonances. For that wavelength for which the ring is a half wavelength from the bottom, the resonances will be nearly constant with rotation. As the wavelength is increased or decreased from this point, the dependence of resonance on angle of rotation increases.

Experimental curves of resonance (Fig. 7-16) as a function of length indicate that the resonance is practically independent of rotation at 3.1 cm. However, with increasing wavelength, the width of the resonant region increases. The two outer resonances of the shaded region for a given length occur when the angle between the two transitions is 0° or 180° . As the second transition is rotated from this position, the outer resonances move in together and become nearly coincident at the 90° or 270° positions. At 3.5 cm it is impossible to space the transitions so

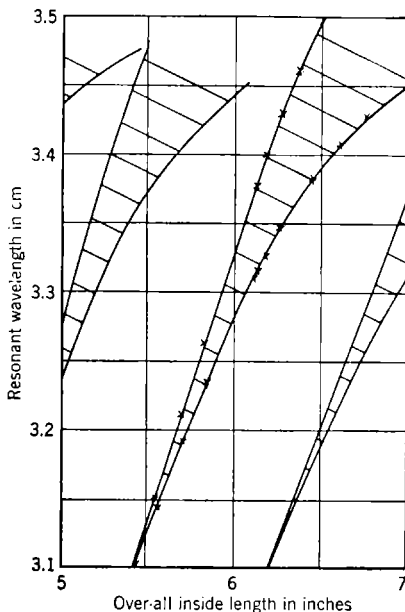


FIG. 7-16 — Resonant wavelength vs. over-all length for *H*-ring transition.

that resonance will not occur, since the electrical distance of the ring from the bottom is approaching one-quarter of a guide wavelength.

To avoid changing standing-wave ratio with rotation, the shortest rotary joint that is recommended for these transitions is one having $3\frac{3}{4}$ in. between the bottom surfaces of the transitions. This variation is probably caused by the interference of the fringing fields near the ring struts and is avoided when the transitions are sufficiently far apart. The largest band that can be obtained by a rotary joint from two of these transitions is 3.13 to 3.37 cm with a length of 3.789 in.

In Chap. 6 several techniques of matching this type of transition are discussed. The chart of resonant wavelengths in Fig. 7-16 may be used for all of these techniques since there is little or no effect on the resonances in the round-waveguide section.

7.8. Rotary Joint Using TE_{11} -mode Filter-ring Type of Transitions with TE_{11} -absorbers.—As we have seen in the previous discussion, the necessity for avoiding troublesome resonances in the TE_{11} -mode imposes considerable limitation on the selection of lengths for rotating joints. If the round-waveguide section is made longer, the band between resonances is shortened. However, if some means of coupling the TE_{11} -power out of the round waveguide into an absorbing load is used, resonances may be eliminated and a rotary joint may be made any length. The bandwidth of such a rotary joint will be limited only by the match of the transitions and the purity of the TM_{01} -mode. This coupling may be done with four longitudinal slots spaced by 90° around the pipe. The currents in the waveguide for the TE_{11} -mode of one given polarization at two places on the round waveguide 180° apart (on the round guide) flow transverse to the slots, and therefore power is transmitted through them. (See Fig. 6-73 in the Introduction of Sec. 6-20.) Four slots are spaced by 90° around the waveguide in order to absorb all polarizations of the TE_{11} -mode. As the currents in the TM_{01} -mode are longitudinal everywhere, these slots have little effect on them.

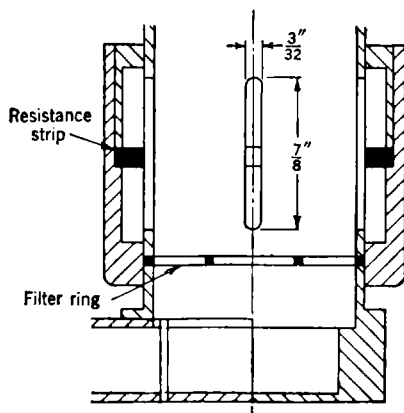


FIG. 7-17a.—Single-mode absorber.

In designing TE_{11} -mode absorbers, considerable care must be taken so that no appreciable amount of the TM_{01} -power is coupled into the absorber. Consequently, the use of wide slots must be avoided, and these slots must be located in the round waveguide so that a maximum amount of the TE_{11} -mode is coupled into them. This maximum coupling occurs when the center of the slots is placed at the voltage maximum, which is an odd integral number of quarter-guide wavelengths in the TE_{11} -mode away from the position of the short circuit of the transition. If there is considerable difference between the short circuit for the polarization aligned along the axis of the rectangular waveguide and for the short circuit of the polarization perpendicular to it, then some means must be provided so that a satisfactory match is obtained for both polarizations.

In the design of an absorber for the filter-ring type of transition, considerable difficulty was encountered with variation in the position of the short circuit with rotation of the polarization. In this design the

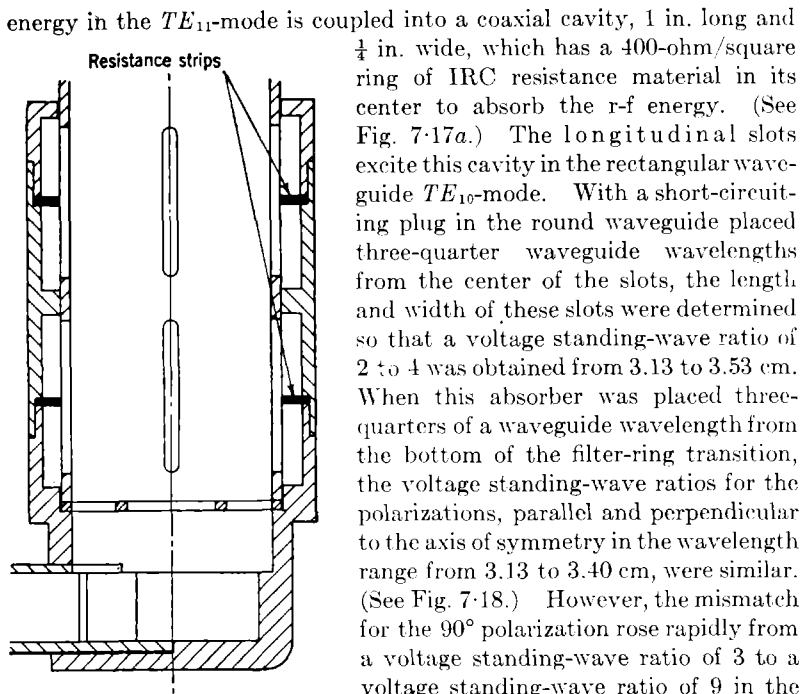


FIG. 7-17b.—Double-mode absorber.

absorber on only one of the transitions of a rotary joint will eliminate reso-

energy in the TE_{11} -mode is coupled into a coaxial cavity, 1 in. long and $\frac{1}{4}$ in. wide, which has a 400-ohm/square ring of IRC resistance material in its center to absorb the r-f energy. (See Fig. 7-17a.) The longitudinal slots excite this cavity in the rectangular waveguide TE_{10} -mode. With a short-circuiting plug in the round waveguide placed three-quarter waveguide wavelengths from the center of the slots, the length and width of these slots were determined so that a voltage standing-wave ratio of 2 to 4 was obtained from 3.13 to 3.53 cm. When this absorber was placed three-quarters of a waveguide wavelength from the bottom of the filter-ring transition, the voltage standing-wave ratios for the polarizations, parallel and perpendicular to the axis of symmetry in the wavelength range from 3.13 to 3.40 cm, were similar. (See Fig. 7-18.) However, the mismatch for the 90° polarization rose rapidly from a voltage standing-wave ratio of 3 to a voltage standing-wave ratio of 9 in the range from 3.4 to 3.53 cm. A single mode

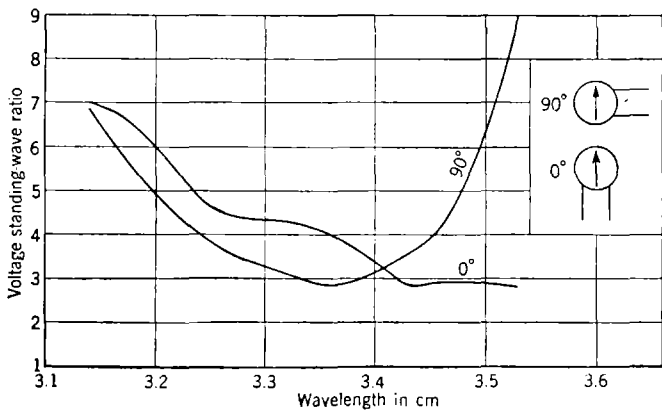


FIG. 7-18.—VSWR for TE_{11} -mode absorbers for filter-ring transitions.

nances from 3.13 to 3.4 cm. Apparently for this type of rotary joint, the

TE_{11} -mode absorber need not be so efficient to eliminate resonances at the low wavelengths as at the high wavelengths. If an absorber is used with each transition, or if two absorbers are combined, as shown in Fig. 7-17b, rotary joints of any length will cover the entire band from 3.13 to 3.53 cm without resonances.

7-9. Rotary Joints for 1.25-cm Wavelength.—Since bends in $\frac{1}{2}$ -by $\frac{1}{4}$ -in. waveguide occupy so little space, only one length for the rotary joint, consisting of two transitions described in Fig. 6-75, Sec. 6-21, has been used. This length is 2.110 in., measured between bottom surfaces

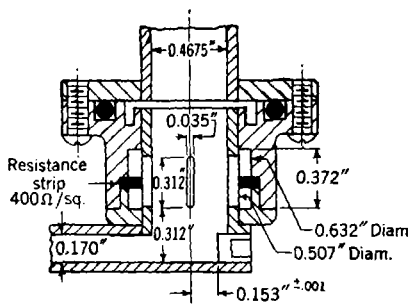


FIG. 7-19.—Transition of rotary joint with plug for 1.25 cm.

of the transition; and the resonances occur at wavelengths of 1.21 and 1.30 cm. This is considerably outside the usable band for the transition. However, to eliminate some of the bends in rectangular waveguide, a long rotary joint was designed using TE_{11} -mode absorbers. The dimensions for this absorber were obtained from scaling the dimensions of the design described in the preceding paragraphs. From 40 to 60 per cent of the energy in the TE_{11} -mode is dissipated in a single-mode absorber; and one absorber is required with each transition to eliminate the resonances completely. This rotary joint will function from 1.23 to 1.26 cm with a maximum variation in the voltage standing-wave ratio of ± 0.03 and a maximum variation of 2 per cent in the transmitted power. The introduction of the slots near the junction of the rectangular and round waveguides increases the voltage standing-wave ratio of the transition, and the short-circuiting plug has to be readjusted in order to obtain a match. This change in the short-circuiting plug increases the amount of TE_{11} -mode excited in the round waveguide over the original design in Fig. 6-75, Sec. 6-21; and the absorber is not sufficiently well matched for the TE_{11} -mode to eliminate the rotational variation. The dimensions for the transition of this rotary joint are shown in Fig. 7-19.

7-10. Analysis of the Resonances in Rotary Joints Composed of Transitions with Diametric Fins in the Round Waveguide.—In Sec. 6-22,

Fig. 6-93 shows a sketch of a transition with a diametric fin to suppress the TE_{11} -mode in the round waveguide. This fin will totally reflect all the energy in the polarization of the TE_{11} -mode that is aligned parallel to it. The polarization which is 90° to this fin will be readily transmitted, since the electric vector is perpendicular to its surface, and will be reflected from the bottom of the rectangular waveguide. Because this fin is rather long, the difference in phase between the positions of the short circuit for these two polarizations will be about one or two wavelengths. With transitions of this type, it may be possible to adjust the fin so that η and γ in Eq. (1) are equal to zero at one wavelength; but with changes in wavelength, the values of η and γ will increase rapidly. Consequently, in order to obtain a broad band with this transition, a TE_{11} -mode absorber may have to be used to eliminate resonances.

The straight-on transitions that use a dividing fin, such as in Fig. 6-100 in Sec. 6-23, will have the same difficulty since the fin is practically no obstruction to the transverse polarization of the TE_{11} -mode. The addition of a mica or dielectric-supported ring will eliminate this difficulty as well as a TE_{11} -mode absorber, since the energy of all polarizations is reflected from the resonant ring in the same phase. This resonant ring must be placed so that resonances do not occur between the ring and the fin or between the ring and the base of the transition. For transitions that use dielectric-supported resonant rings, the resonance occurs when the spacing between the rings is approximately equal to an integral number of half-guide wavelengths. The distance between these rings is selected as an odd integral number of quarter-guide wavelengths at the center of the wavelength band to obtain the largest possible range free of resonances on either side of this center wavelength.

7-11. Rotary Joint Using Circular Polarization.—In Sec. 6-18 various methods of obtaining circular polarization in the TE_{11} -mode were dis-

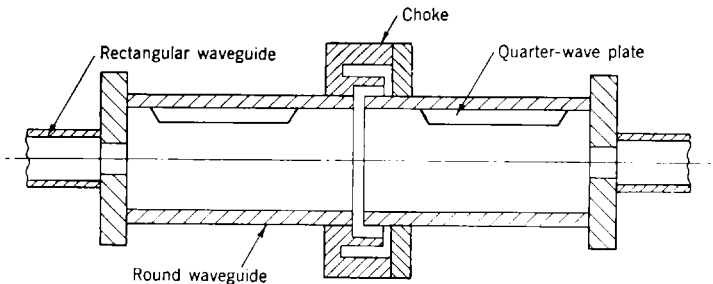


Fig. 7-20.—Rotary joint with circular polarization.

cussed. Two transitions from rectangular to round waveguide which transform all of the energy in the rectangular waveguide into a circular-

polarized wave may be combined as in Fig. 7-20 to make a rotary joint. Since the wave propagated in the round-waveguide section is symmetric there will be no variation in the output power with rotation. This wave at a given reference point x_1 in the round waveguide at the output transition has the form

$$E_r = Ee^{j(\omega t - \beta x_1 + \phi)}.$$

If there is a mismatch in the transition, part of this wave will be reflected back to this same point with some definite phase change. Now if the output transition is rotated through an angle θ , the amplitude of the wave at the same instant with respect to the output transition is

$$E_r = Ee^{j(\omega t - \beta x_1 + \phi + \theta)}.$$

For constant ϕ about an axis of the output transition, the equivalent line length added to the round waveguide is θ radians. From this, the total phase shift in the position of the minimum for the standing wave is equal to θ radians; and the input admittance for the rotary joint will make two complete revolutions around a Smith admittance diagram for every revolution of the output transition. Consequently, the transitions and load in the output rectangular waveguide will have to be perfectly matched if variation of the input admittance and "pulling" of the oscillator is to be avoided.

7-12. Resonance in a Circular-polarization Rotary Joint.—Because of the frequency sensitivity of a quarter-wave plate, it is not possible to design a transition to the circular-polarized TE_{11} -mode over a broad band without some of the energy in the round waveguide being propagated in a plane-polarized wave. If the angle of the output transition is such that the plane-polarized wave is not affected by the 45° quarter-wave plate, it can be resolved into two components, each at 45° to the plane wave. One of these components will be propagated into the rectangular waveguide, the other one will be reflected back into the round-waveguide section. For other orientations of the output transition, this plane-polarized wave will be converted into an elliptically polarized wave in passing through the quarter-wave plate of the output transition. Some of the components of the elliptically polarized wave will be reflected back into the round waveguide. This reflected wave may in turn be reflected from the other end; and if the electrical length between the two transitions for this reflected wave is equal to an integral number of half wavelengths, resonances will occur that will absorb and reflect a large amount of the energy. These resonances may be eliminated by using a transition from rectangular to round waveguide which will present a match to all polarizations of the TE_{11} -wave. In the transition of Fig. 6-58, Sec. 6-17, the TE_{11} -polarization excited through the

quarter-wavelength transformer will not be propagated in the shunt rectangular waveguide. But if an incident TE_{11} -wave of any other polarization is propagated in the round waveguide, it can be resolved into two components—one which will be propagated through the quarter-wavelength transformer and down the main transmission line, and another which will be coupled into the shunt rectangular waveguide. If a quarter-wave plate is combined with this type of transition and two such combinations are used to make a rotary joint, then no resonances can occur, since any plane wave in the round waveguide will be matched regardless of its polarization. The elimination of these resonances makes it unnecessary to determine specific lengths to avoid resonances. There

are two other transitions that have this property of being matched to all polarizations. These are the transitions with the two shunt rectangular arms spaced at 90° shown in Fig. 6-57, Sec. 6-17, and the turnstile transition shown in Figs. 6-66 and 6-67 in Sec. 6-18.

7-13. Rotary Joints Using a TE_{11} -mode Polarization Rotator.—In the same manner that a quarter-wave plate will set up circular polarization, a half-wave plate may be used to rotate the polarization of the TE_{11} -mode.

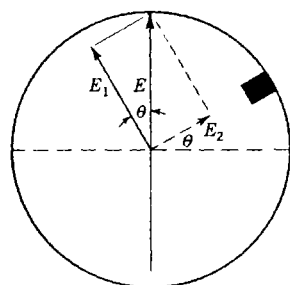


FIG. 7-21.—Resolution of modes.

The radial electric vector E_r of a TE_{11} -wave may be resolved into two components at right angles; thus,

$$E_r = [E_1 \sin \phi + E_2 \cos \phi] e^{j(\omega t - \beta x)}. \quad (4)$$

Since the amplitude of the input wave is constant, then

$$E = \sqrt{E_1^2 + E_2^2}.$$

If θ is defined as the angle which the E_1 component above makes with the resulting wave E , then from Fig. 7-21,

$$E_r = E [\sin \phi \cos \theta + \sin \theta \cos \phi] e^{j(\omega t - \beta x)},$$

or

$$E_r = E \sin (\phi + \theta) e^{j(\omega t - \beta x)}. \quad (5)$$

Now if a half-wavelength difference in phase is introduced between the two components, then

$$\begin{aligned} E_r &= E [\sin \phi \cos \theta - \sin \theta \cos \phi] e^{j(\omega t - \beta x)}, \\ E_r &= E \sin (\phi - \theta) e^{j(\omega t - \beta x)}. \end{aligned} \quad (6)$$

The maximum radial vector is at the angle for which the sine function is equal to 1; thus, the angle of the maximum vector for the incident wave is

$$\phi = \frac{\pi}{2} - \theta,$$

and for the output wave,

$$\phi = \frac{\pi}{2} + \theta.$$

If the polarization of the input wave is fixed and the half-wave plate is rotated, the output polarization is rotated through twice the angle of the half-wave plate. We can make use of this property in the construction of a rotary joint in the round waveguide. If we rotate the output transition through twice the angle of the section containing the half-wave plate, then the polarization of the input TE_{11} -mode will be rotated correctly to be transmitted through the output transition.

The same techniques may be employed in designing a half-wave plate as in designing the quarter-wave plates in Figs. 6-61, 6-62 and 6-63 in Sec. 6-18. The same step may be used to match the ends of the plate, and the length may be extended to obtain a half-wavelength difference in phase between the two components of the incident wave.

The length for the half-wave plate may be calculated from the formula

$$4\pi \left(\frac{l_t}{\lambda_{t_1}} - \frac{l_t}{\lambda_{t_2}} \right) + 2\pi \left(\frac{l}{\lambda_1} - \frac{l}{\lambda_2} \right) = \pi. \quad (7)$$

In this equation, l_t is the length of the step-matching transformers, and l is the remaining length of the half-wave plate; λ_{t_1} and λ_{t_2} are the wave-

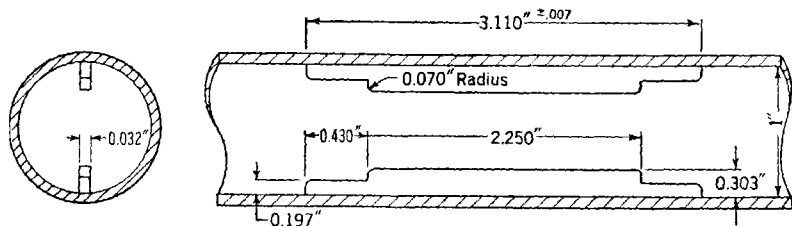


Fig. 7-22.—Half-wave plate for a wavelength of 3.40 cm.

guide wavelengths in the matching transformer for the components E_1 and E_2 in Eq. (4); and λ_1 and λ_2 are the corresponding waveguide wavelengths in the remaining length of the half-wave plate. To make the plate shorter, two fins may be used to obtain the half-wavelength phase shift. Figure 7-22 shows the dimensions of such a half-wave plate in a round waveguide with an inner diameter of 1.000 in. for a wavelength of 3.40 cm.

Let us consider the broadband possibilities of a rotary joint using a polarization rotator. Over an appreciable pass band, the phase shift will not always be an exact half wavelength because of the frequency sensitivity of the half-wave plate. If we define δ as the difference in

phase shift from a half wavelength, then the TE_{11} -wave, after going through the half-wave plate, will be

$$E_r = E(\sin \phi \cos \theta - \sin \theta \cos \phi e^{j\delta})e^{j(\omega t - \beta x)},$$

$$E_r = E(\sin \phi \cos \theta - \sin \theta \cos \phi \cos \delta - j \sin \theta \cos \phi \sin \delta)e^{j(\omega t - \beta x)}. \quad (8)$$

If

$$(E \sin \phi \cos \theta \cos \delta - E \sin \theta \cos \phi \cos \delta)e^{j(\omega t - \beta x)} = 0$$

is added to Eq. (8) and the terms are regrouped, the result is

$$E_r = [E \cos \delta \sin (\phi - \theta)e^{j(\omega t - \beta x)} + (1 - \cos \delta)E \sin \phi \cos \theta \cos \delta - jE \sin \theta \cos \phi \sin \delta]e^{j(\omega t - \beta x)}. \quad (9)$$

From Eq. (9), it may be seen that if the phase shift is not equal to a half wavelength, the resulting wave consists of one part that is rotated

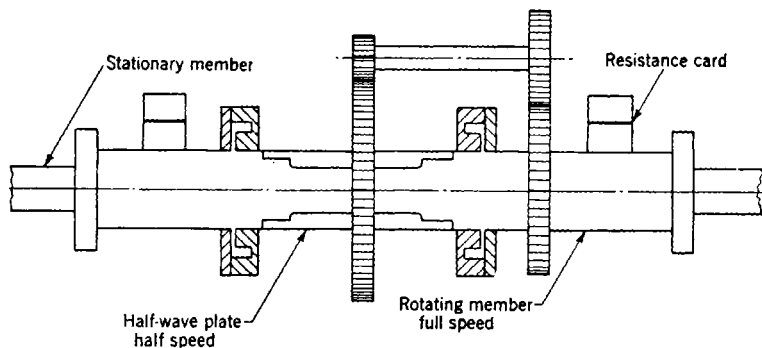


FIG. 7-23.—Rotary joint employing a half-wave plate.

correctly to be transmitted through the output transition and another part that is an elliptically polarized wave. The magnitude of the components of this elliptically polarized wave will vary with the angle of rotation. If θ is zero, all the incident wave will be transmitted; but for θ greater than zero, some components of this elliptical wave will be reflected from the two ends of the rotary joint. These reflected waves will set up resonances if the electrical length is equivalent to an integral number of half wavelengths in the guide. These resonances may be eliminated in the same way as in the circularly polarized rotary joint—that is, by using transitions from rectangular to round waveguide which are matched to all polarizations. Figure 7-23 shows a sketch of a rotary joint using that type of transition. This rotary joint is superior to the type employing circular polarization because the phase of the reflected wave from a mismatched load does not vary with rotation.

MISCELLANEOUS WAVEGUIDE MOTIONAL JOINTS

By F. T. WORRELL

In addition to rotary joints, joints that allow other kinds of motion have been developed. These are the swivel joint, the hinge joint, and the universal joint. The first allows a limited twisting of one piece of waveguide relative to another about their common axis. The second allows oscillation of one piece of waveguide relative to another about an axis perpendicular to the longitudinal axis of the two waveguides and lying in either the *E*-plane or the *H*-plane. This is sometimes called a "nod" joint. The universal joint allows both possible displacements of the hinge joint to be made simultaneously, so that the moving waveguide can move anywhere within a cone whose axis is the axis of the fixed waveguide and whose apex is at a point on the axis between the two pieces of waveguide.

7-14. Swivel Joints.—The simplest swivel joint, good only for small angles of twist, consists of two pieces of waveguide connected by a choke-to-flange junction in which the choke and flange are free to rotate with respect to each other about the common longitudinal axis of the two waveguides. A schematic drawing of such a joint is shown in Fig. 7-24. The standing-wave ratio for a 3-cm joint of this design, at various wavelengths and at various angles of twist, is shown in Fig. 7-25. This joint consists of the choke illustrated in Fig. 4-45(b2) and listed in Table 4-8 which is separated 0.020 in. from a flange of the same diameter. Figure 7-26 gives the performance of a similar 10-cm joint using the choke of Fig. 4-45a, listed in Table 4-8, separated 0.020 in.

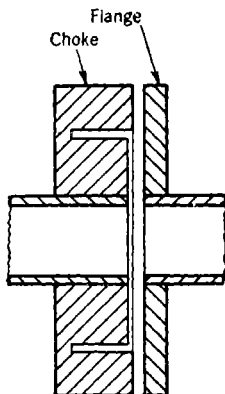


Fig. 7-24. —Simple swivel joint.

The performance of the simple joint can be improved if, instead of using a single junction, two such junctions separated by a section of waveguide a quarter wavelength long are used, as shown in Fig. 7-27. This design has two advantages over the simple one. First, for a given total angle of twist, the twist per junction is reduced by a factor of 2. Second, reflections that are not too large will cancel, since the two junctions are separated by a quarter wavelength of line. It would therefore be expected that the allowable twist would be more than twice that of the simple joint. The standing-wave ratio of the improved 3-cm model for various wavelengths and angles of twist is shown in Fig. 7-28. It should be noted that whereas the simple model can be twisted only up to 10° before the voltage standing-wave ratio rises above 1.10, the

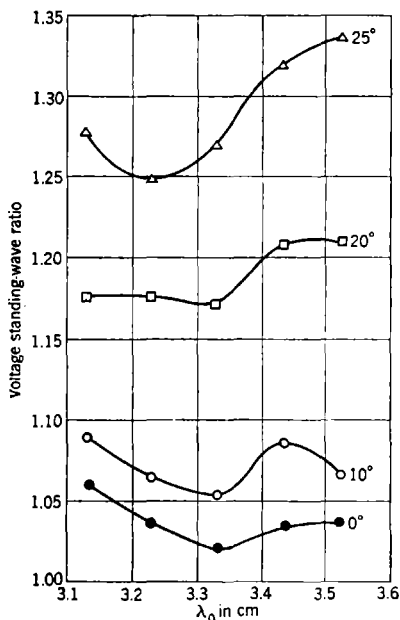


FIG. 7-25.—Standing-wave ratio for a 3-cm band choke-flange joint for various angles of twist.

further increasing the amount that the joint may be twisted. Here again the twist per junction is reduced for any given total twist. The performance of the 3-cm four-junction joint is shown in Fig. 7-31.

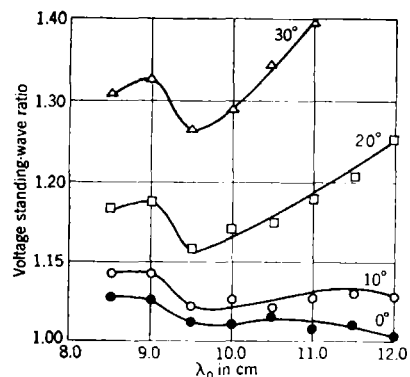


FIG. 7-26.—Standing-wave ratio for 10-cm band choke-flange joint for various angles of twist.

second model can be twisted more than 30° under the same restrictions. The performance of the improved 10-cm model is shown in Fig. 7-29.

In many cases the two-junction model would be sufficiently good. However, a still better 3-cm model has been designed which will twist up to 60°. The limitation in the twisting of this joint is in the mechanical design; as far as electrical performance is concerned, the joint could twist a greater amount. This swivel joint, which is shown in Fig. 7-30, consists essentially of two of the two-junction joints separated by a half wavelength. It can be seen that the resulting distance between centers of the pairs of junctions is $3/4\lambda_g$; therefore small residual mismatches in the two pairs of junctions cancel, thus

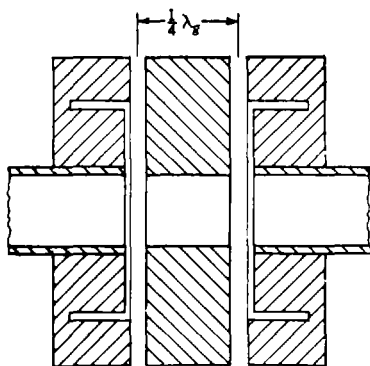


FIG. 7-27.—Two-junction swivel joint.

It is interesting to inspect the performance curves to find the cause of this improvement. In Figs. 7-32 and 7-33 the voltage standing-wave ratio is plotted as a function of angle for various wavelengths for the two- and four-junction joints, respectively. These curves show that at a wavelength of 3.5 cm the impedance match of the two-junction joint changes rapidly at the end of its useful range of twisting (40°). At this same wavelength the four-junction joint can be twisted only twice as much. This indicates that the standing-wave ratio becomes so large that the addition of the extra pair of junctions does not help much in decreasing it, and therefore, that the improvement is entirely the result of having half the twist per junction for the same amount of total twist in the four-junction joint as against the two-junction joint. However, at a wavelength of 3.2 cm, the two-junction

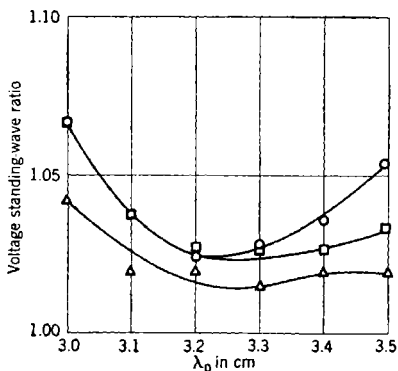


FIG. 7-28.—Performance of a 3-cm band two-junction swivel joint. Triangles represent 10° twist, squares 20° , and circles 30° .

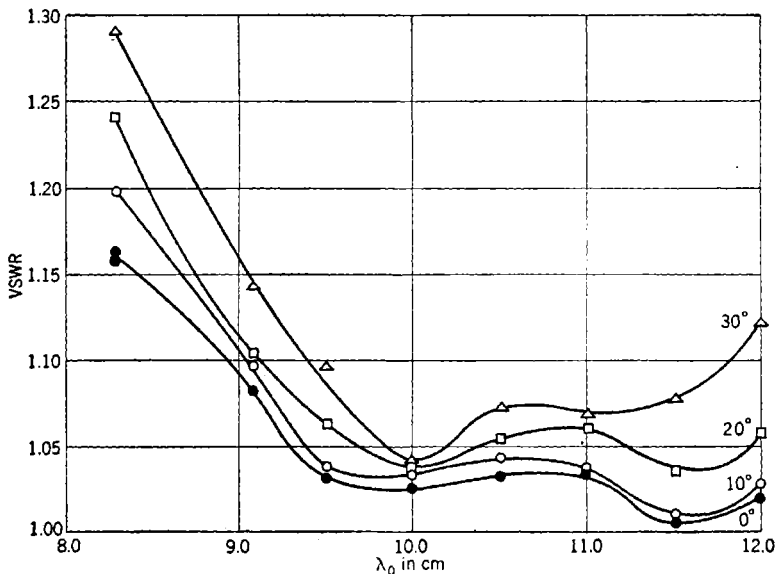


FIG. 7-29.—Voltage standing-wave ratio vs. λ_0 for different angles of twist of 10-cm swivel joint.

joint is deteriorating at a slow rate at the position of maximum twist, so the addition of the two extra junctions allows more than twice the twist to be given.

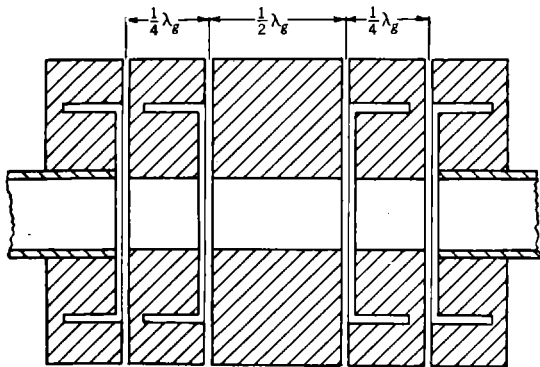


FIG. 7-30.—Four-junction swivel joint.

The constructional details of the four-junction 3-cm swivel joint are shown in Fig. 7-34. The individual sections are mounted in ball-bearing races. The twisting motion is transmitted by three wires running the length of the joint. Each wire is fastened to each section by a ball-and-

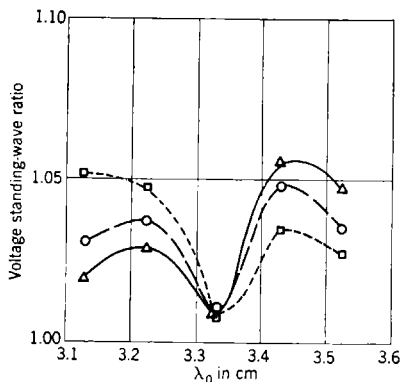


FIG. 7-31.—VSWR vs. λ_0 for a 3-cm band four-junction swivel joint for several angles of twist. Triangles represent 10° twist, circles 20°, and squares 30°.

socket joint, and the point of fastening is chosen so that when one end of the joint is twisted each of the four sections is twisted, relative to the adjacent section, by one-quarter of the total amount. This design seems to be sufficiently sturdy. One sample has been tested by twisting through $\pm 60^\circ$ at a rate of 1 cps; the test was stopped at the end of 3.5 million cycles, at which time the electrical characteristics of the joint were still unchanged from the original values, and the mechanism was still operating.

Some trouble was experienced with resonances in the 10-cm swivel joint. At short wavelengths these resonances appeared only at large angles of twist; at long wavelengths these appeared at very small angles. The resonances apparently are not caused by reflections from the housing; at least efforts to remove the resonances by altering the housing design produced no results. The cause

of the resonances is not definitely known but it may be the excitation of the TE_{21} -mode in the region between the choke and flange. This mode is not excited normally but could be excited when the choke and flange are twisted with respect to one another. If this were the case, the trouble

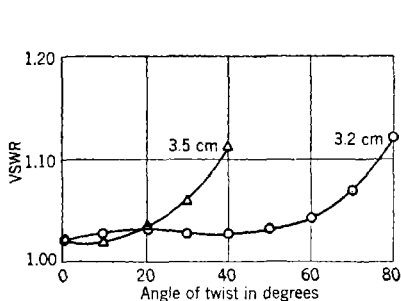


FIG. 7-32.—VSWR as a function of angle of twist for two wavelengths for two-junction swivel joint.

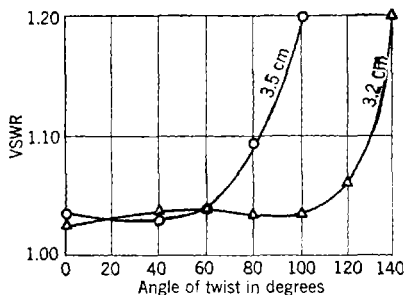


FIG. 7-33.—VSWR as a function of angle of twist for two wavelengths for four-junction swivel joint.

might be eliminated by inserting thin partitions in the choke ditch as shown in Fig. 7-35. Such a partition imposes the requirement that the field across the choke ditch be zero at the partition, which would suppress the TE_{21} -mode.

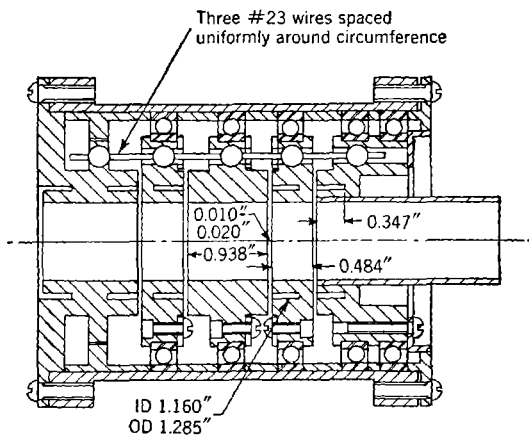


FIG. 7-34.—Construction of the 3-cm four-junction swivel joint.

High-power tests indicate that the 3-cm joint will stand at least 200-kw peak power at 1- μ sec pulse length, 500 pps. Except at points of resonance over restricted regions the 10-cm joint will handle at least 1.1 Mw at 1- μ sec pulse length, 420 pps. At these resonant points, which were mentioned in the preceding paragraph, breakdown appears

to occur between choke and flange at considerably lower power levels than when the resonance is absent.

The swivel joint has an advantage over the rotary joint in that it has fewer critical dimensions and is easier to construct. It has the disadvantage of being bulkier and heavier.

7-15. Hinge Joints.—A simple hinge joint can be made by mounting two pieces

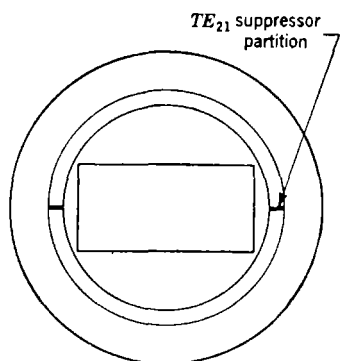


FIG. 7-35.—Choke with TE_{21} -mode suppressor partitions.

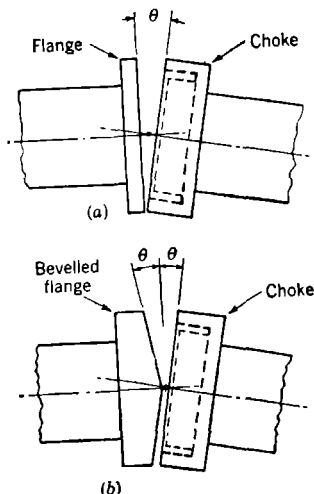


FIG. 7-36.—Simple hinge joints.

of waveguide, one with a choke, the other with a flange, in a housing which allows them to move as indicated in Fig. 7-36a. If an ordinary flange is used, it is necessary to have the choke-flange separation large in order to allow oscillations of more than a few degrees. The flange is therefore beveled from the edge to the center, as shown in Fig. 7-36b. This beveling allows a smaller

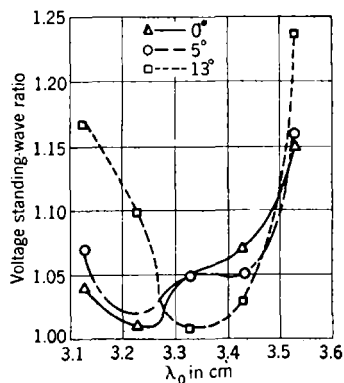


FIG. 7-37.—Performance of E -plane hinge joint for three different hinge angles.

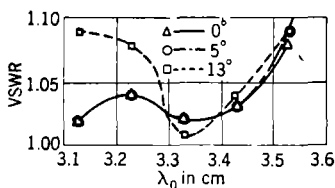


FIG. 7-38.—Performance of H -plane hinge joint for three different hinge angles.

choke-flange separation, and therefore an improved performance of the joint results. In the H -plane hinge joint the design is complete at this

point. A 3-cm model has been made which will oscillate through an angle of $\pm 13^\circ$. An *E*-plane joint of this design has resonances; to remedy this trouble, the choke ditch has been plugged, as described in the discussion

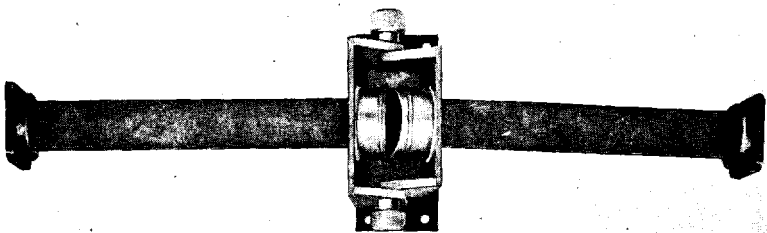
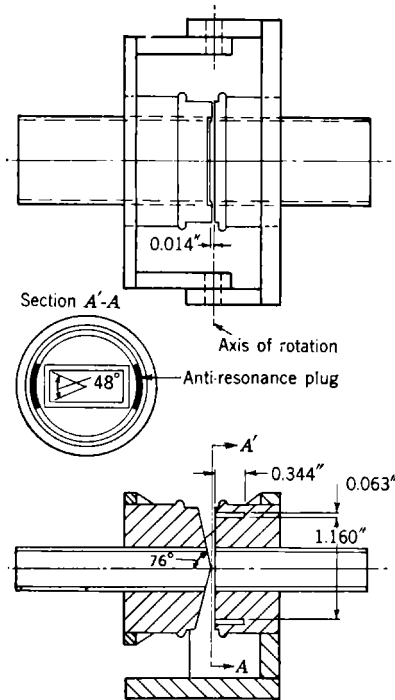


FIG. 7-39.—*E*-plane 3-cm hinge joint.

of open choke-flange junctions in Sec. 5-20. The loss and voltage standing-wave ratio of the 3-cm *E*-plane and *H*-plane joints as a function of angle at various wavelengths are shown in Figs. 7-37 and 7-38. The complete joints are shown in Figs. 7-39 and 7-40.

High-power tests show that, except as noted below, both the *E*-plane and *H*-plane 3-cm hinge joints will handle 200 kw, at 1 μ sec and 500 pps, without sparking. However, when the choke-flange separation becomes

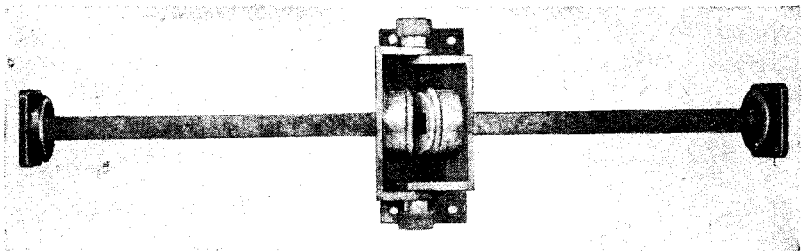
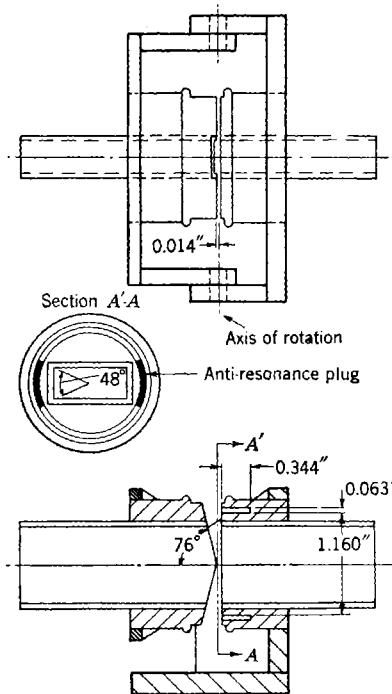


FIG. 7-40.—*H*-plane 3-cm hinge joint.

less than 0.010 in. in the *H*-plane joint, sparking occurs between the choke and flange. When the *E*-plane joint is turned so that the choke and flange touch at one edge, sparking occurs across the choke ditch on the other side.

As one might expect, there is an appreciable amount of loss from

either type of hinge joint in the region of maximum displacement. This is not large enough to be serious from the standpoint of loss of transmitted power but may be serious if there are any sensitive detectors near by. It may also become serious if the housing around the joint is

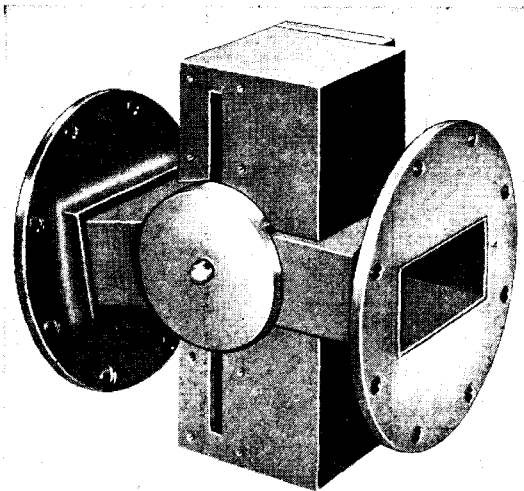
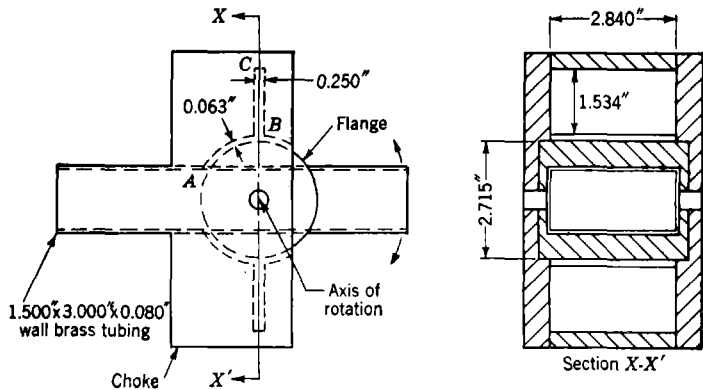


FIG. 7-41.—Rectangular-choke hinge joint. One side-plate has been removed in the photograph.

incorrectly designed. If the design is such that some of the leakage power is reflected back into the joint, there may be a resonance between the housing and some part of the joint.

In an effort to make a hinge joint with less leakage, the design shown in Fig. 7-41 has been tried. This design is based upon a modification

of a British choke.¹ The "flange" in this joint is the inner cylinder, whose axis is the axis of rotation of the hinge joint. The choke consists essentially of a T-stub, one-half wavelength deep, of the same width as the waveguide but of smaller height. The stub is folded along the line ABC , where AB and BC are each a quarter wavelength. Inspection of the figure will show that as the joint is displaced from the neutral position, there is no widening gap to allow leakage, as in the other type of hinge joint. However, the distance from the waveguide wall to the

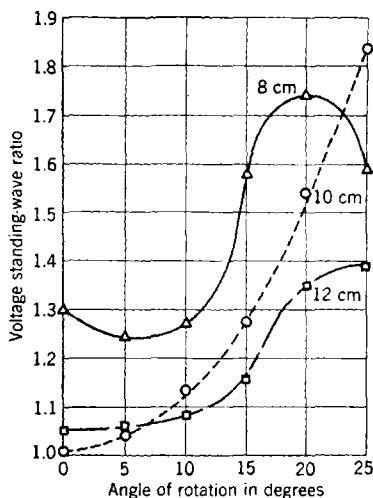


FIG. 7-42.—Performance of rectangular-choke hinge joint at three wavelengths.

bottom of the choke ditch gets farther and farther from the correct value as the joint is bent. This causes an appreciable mismatch.

In Fig. 7-42 is shown a set of performance curves for a 10-cm model of this joint. The joint does not appear promising although it could doubtless be improved; it has not yet been tested for resonances or power-handling capacity.

7-16. Universal Joints.—The universal joint is so named because its mechanical arrangement is like that of the common universal joint used in machines. The simplest electrical arrangement of such a joint has a standard rigid-line choke coupling on each piece of waveguide. The chokes are placed a small distance apart, so that the joint can move in a cone of limited angle. Since the rigid-line choke couplings are not designed to be used with a gap between them, the simple joint must be modified to make it satisfactory. The modifications are those to be

¹ See Sec. 4-10 for description of this choke.

expected from previous discussions of other joints. (1) The surface of each choke is rounded in the shape of a cone, so that the two couplings can be used closer together; (2) the choke ditch is made wider, to approximate more closely the low-impedance-high-impedance condition; (3)

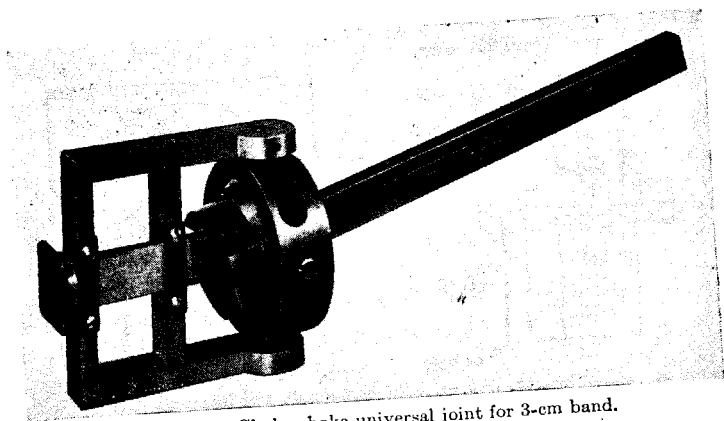
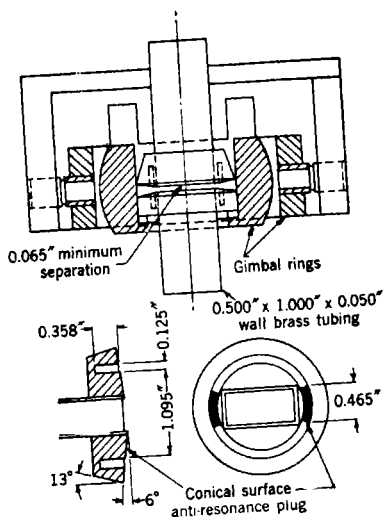


FIG. 7-43.—Choke-choke universal joint for 3-cm band.

the depth of the ditch is changed so that the r-f leakage is a minimum; (4) the diameter of the ditch is altered to that which gives the optimum standing-wave ratio; (5) the ditch is plugged in order to remove resonances from the joint. The final design is shown in Fig. 7-43.

This joint was designed to operate over a wavelength range from 3.1 to 3.5 cm. In Fig. 7-44 is shown the voltage standing-wave ratio as a function of wavelength for various positions of the joint. The joint has been tested at powers up to 100 kw, 1- μ sec pulse width, 500 pps,

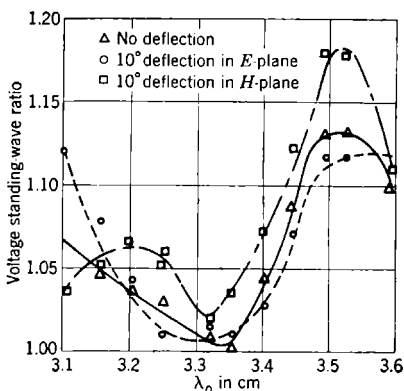


FIG. 7-44.—Performance of 3-cm band universal joint in three angular positions.

without breakdown. This joint has appreciable losses at large angles just as hinge joints have. The losses are considerable in that, if there is some reflection from the housing, it appears as an appreciable mismatch at the joint. In one instance, the change in the housing from the original design made the performance of the joint worse. For this

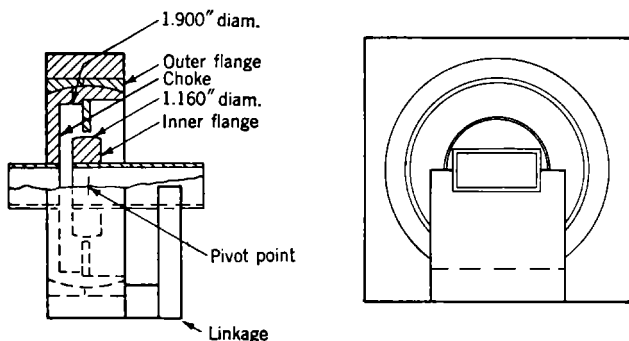


FIG. 7-45.—Radial-choke universal joint.

reason, the housing should be designed with care, in order to avoid resonances.

Some work has been done with another type of universal joint which, it is hoped, will be satisfactory over greater angles and will allow less r-f leakage. The design of this joint is illustrated in Fig. 7-45.

A radial choke is used rather than the more conventional folded choke. The moving waveguide ends in a flange, the outer surface of which is in the shape of a sphere. This rides in a housing of the same shape. The break between these two parts is at the same distance from the rectangular waveguide as the ditch of a conventional choke would be and is, therefore, at a current minimum. This design feature removes the need for a mechanical contact between the two parts. The inner flange is connected by an external linkage to another ball-and-socket joint which forms the bearing for the assembly, holding the two waveguides in a definite position relative to one another. Since this spherical surface is the supporting bearing, the inner flange does not touch the

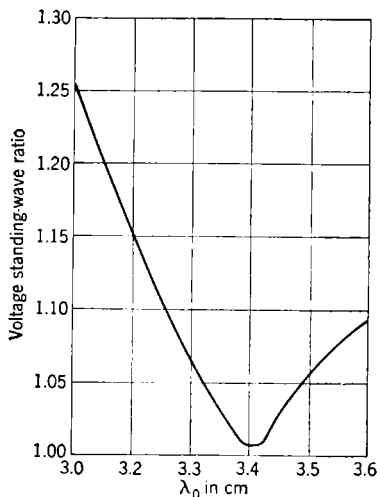


FIG. 7-46.—Reflections from radial-choke universal joint.

choke but, instead, clears it by a small amount, thus preventing a variable contact from affecting the operation of the joint. The radial choke is designed to have a good low-impedance-high-impedance ratio by making the first quarter-wave section small in height, and the second section greater in height. This joint does not give so much trouble with r-f leakage as the conventional one.

Unfortunately, not enough work has been done on this joint to prove its worth. Resonances are present, which could presumably be removed by some sort of plugging scheme. If the resonances were removed, the joint might be quite satisfactory. It might be possible to get a larger angle of motion with this joint than with the conventional type. The variation of the standing-wave ratio with wavelength for the straight-through position of the joint is shown in Fig. 7-46.

MOTIONAL JOINTS COMBINING COAXIAL LINE AND WAVEGUIDE

BY F. L. NIEMAN

7-17. General Considerations.—As discussed in the introduction to this chapter, the design of a motional joint capable of continuous rotation for a microwave transmission line requires the use of a symmetrical field configuration. This may be the dominant coaxial mode (*TEM*-mode), or either the symmetrical *TM*₀₁-mode or a circularly-polarized *TE*₁₁-mode in round waveguide. When rectangular tubing is used for the waveguide transmission line, as is generally the case in modern microwave systems, transitions from the *TE*₁₀-mode in rectangular waveguide to one of the symmetrical modes in coaxial line or round waveguide are necessary. The problem of designing well-matched transitions for this purpose is discussed in Chap. 6. Where such transitions are used to provide a symmetrical field for a rotary joint it is usually desirable and sometimes advantageous to design the unit so that it may include the transitions.

Rotary joints in round waveguide for use with rectangular-waveguide transmission lines are discussed in Secs. 7-4 through 7-13. In these, the propagation of several possible modes and resonances due to the proximity of the two mode-exciting transitions and the possibility of using a circularly polarized asymmetrical mode, all present many new problems. However, most of these problems do not arise in the design of waveguide rotary joints using the coaxial mode. Asymmetrical fields excited by the transition discontinuity are attenuated to a negligible value in a very short distance so that joints of this type are almost never short enough to give rise to resonance effects between transitions. Thus, the chief requirement for a useful rotary joint with combined coaxial line and waveguide is the design of a well-matched transition from coaxial line to waveguide. The only further requirement placed upon the mechanical design of the joint is that it should not allow variation in the transition characteristics during rotation. Any of the types of transition from coaxial line to waveguide described in Chap. 6 may be used in the design of a coaxial rotary joint for a waveguide line. Some examples of different transitions applied to this type of rotary joint are given in the following paragraphs. The details of mechanical construction such as the types and arrangements of bearings and pressure seals will be discussed only in so far as they differ from those for the coaxial rotary joints treated in Secs. 7-1 through 7-3.

7-18. Rotary Joints with Cross-transition from Coaxial Line to Waveguide.—The first coaxial-line-to-waveguide transition developed, and therefore the first applied to rotary joints, was that in which the coaxial line crosses the waveguide as shown in Fig. 6-8a. A discussion

of the matching of this type of transition by variation of the lengths of the coaxial and waveguide short-circuited sections is given in Chap. 6 together with specific examples. A possible arrangement using this transition in the design of a rotary joint (as developed for 3-cm wavelengths by the Sperry Gyroscope Company) is shown in Fig. 7-47. The coaxial chokes and mechanical details are similar to those for the coaxial rotary joints. This joint and transition have had but limited application since they are rather frequency-sensitive compared with other types. Although the ball in the transition region does effect a slight improvement in the bandwidth, such transitions have standing-wave ratios less than the desired limit of about 1.1 over a frequency band of only a few per cent.

7-19. Rotary Joints with Probe Transitions.

7-19. Rotary Joints with Probe Transitions.—A design, also for 3-cm wavelengths, of a coaxial rotary joint between waveguides with probe transitions from coaxial line to waveguide is shown in Fig. 7-48. Seal and bearing details are not given. This type of transition (see Sec. 6-9), and therefore this rotary joint, if properly constructed, provides a good impedance match (voltage standing-wave ratio of less than 1.2) over a frequency band of about 10 per cent in width. In practice, the

advantage of the broad band obtained from the probe transition is somewhat offset by the fact that the electrical characteristics of the transition are sensitive to the probe depth and centering. These dimensions are difficult to hold accurately in stub-supported assemblies. In the rotary-joint application, the problem is complicated further by the relative motion between one waveguide section and its exciting probe. If the assembly is not properly centered a variation of the impedance with rotation occurs. However, this type of joint requires no coaxial chokes

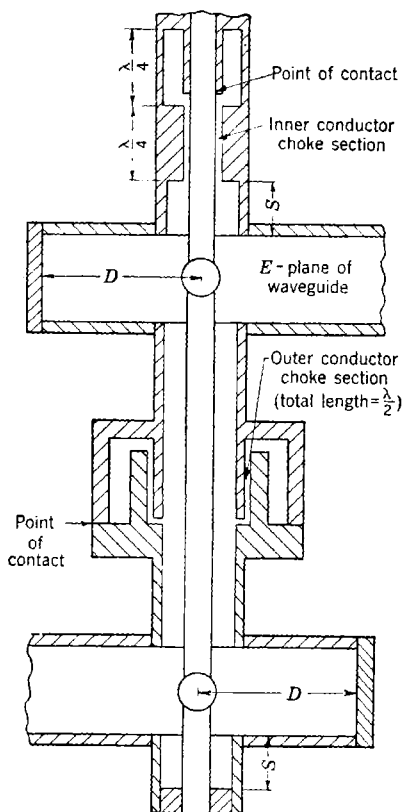


Fig. 7-47. —3-cm waveguide rotary joint using coaxial mode with cross transition.

on the center conductor, a fact which greatly facilitates mechanical construction, particularly for the small dimensions necessarily used at 3-cm wavelengths.

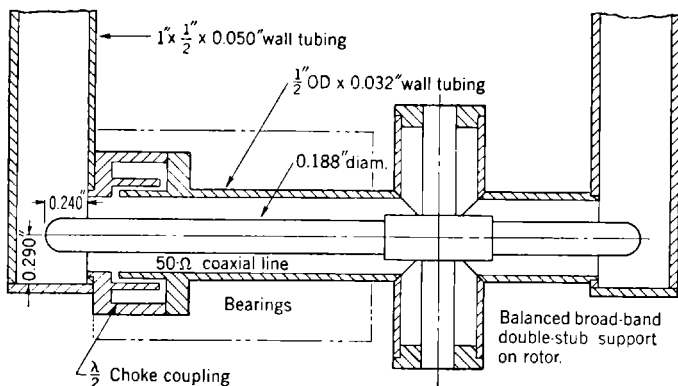


FIG. 7-48.—Waveguide rotary joint with probe transition for 3.2-cm wavelength.

7-20. Rotary Joints with Combinations of Transitions.—Two rotary joints for 3-cm wavelengths having probe transitions combined with a loop-coupling or a crossbar transition have been developed at the Bell

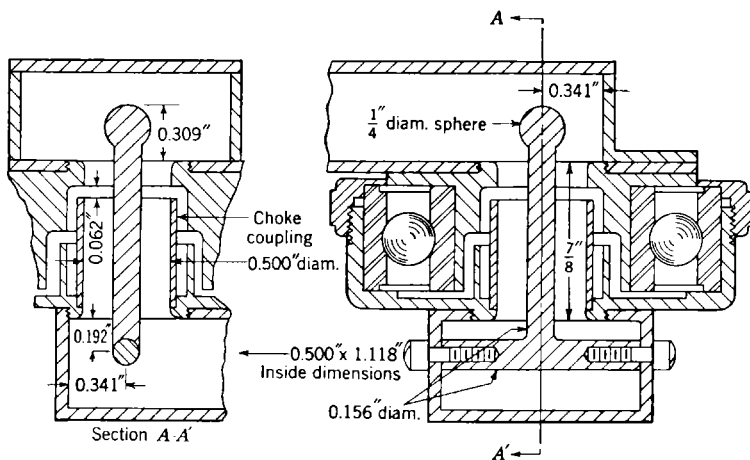


FIG. 7-49.—3-cm coaxial rotary joint between waveguides with probe and crossbar transitions.

Telephone Laboratories. Both these designs eliminate the stub support for the coaxial center conductor, which allows a shorter and more compact design. One of these, shown in Fig. 7-49, uses a probe transition

on one end and a crossbar transition on the other.¹ The design and characteristics of this crossbar transition are discussed in Sec. 6-9. The impedance match of the probe transition as a function of frequency is slightly better than that of the crossbar transition. The combination in this rotary joint introduces a voltage standing-wave ratio of less than 1.1 for a frequency band of about 12 per cent. Different lengths of coaxial line between transitions were tried, and it was found that those with lengths of $\frac{5}{8}$ in. or more between the inner wall surfaces of the waveguides gave no variation of impedance with rotation, indicating that the higher asymmetrical coaxial modes are either not strongly excited or are damped to negligible values in a very short length of coaxial-line.

A similar joint using an "in line" loop- or magnetic-coupling transition between the coaxial line and the waveguide in place of the crossbar transition is shown in Fig. 7-50.² This arrangement permits the rotation of one waveguide section about an axis perpendicular to the axis of the other, an arrangement that is advantageous in certain applications. The probe transition in this design is identical with that in the unit just described except that the matching parameters, the waveguide end-plate distance, and the probe depth have all been adjusted to give a match over a slightly different wavelength band. The bandwidth and the excellence of match are essentially the same. However, the loop-coupling transition is considerably more frequency-sensitive than is the crossbar type. The combination has a bandwidth of about 5 per cent for a voltage standing-wave ratio of less than 1.1.

In this design, an improved technique is used in eliminating the effects of the discontinuity in the coaxial line. First, each coaxial choke consists of two quarter-wavelength sections of different impedance, an arrangement that increases the wavelength range over which the chokes are effective. Second, a section of lossy dielectric is provided between the choke and the bearing to attenuate further any power leaking from the coaxial line. This is sometimes necessary on joints used in high-power systems to prevent leakage that can cause interference with receiving components and even damage to the bearing itself.

Joints of both designs have been tested and found satisfactory at voltages corresponding to pulse powers of 100 kw at atmospheric pressure. Since this much power was not available for 3-cm wavelengths at the time, the equivalent power was obtained by the introduction of standing waves in the transmission line of which the joint is a part (see Chap. 4). Further tests at pressures reduced sufficiently to cause breakdown showed

¹ C. F. Edwards, "Preliminary Report on a Wave Guide Rotating Joint," BTL Memorandum 43-160-120, July 30, 1943.

² C. F. Edwards, "An X-band Rotating Joint Between Perpendicular Waveguides," BTL Memorandum 44-160-71, March 30, 1944.

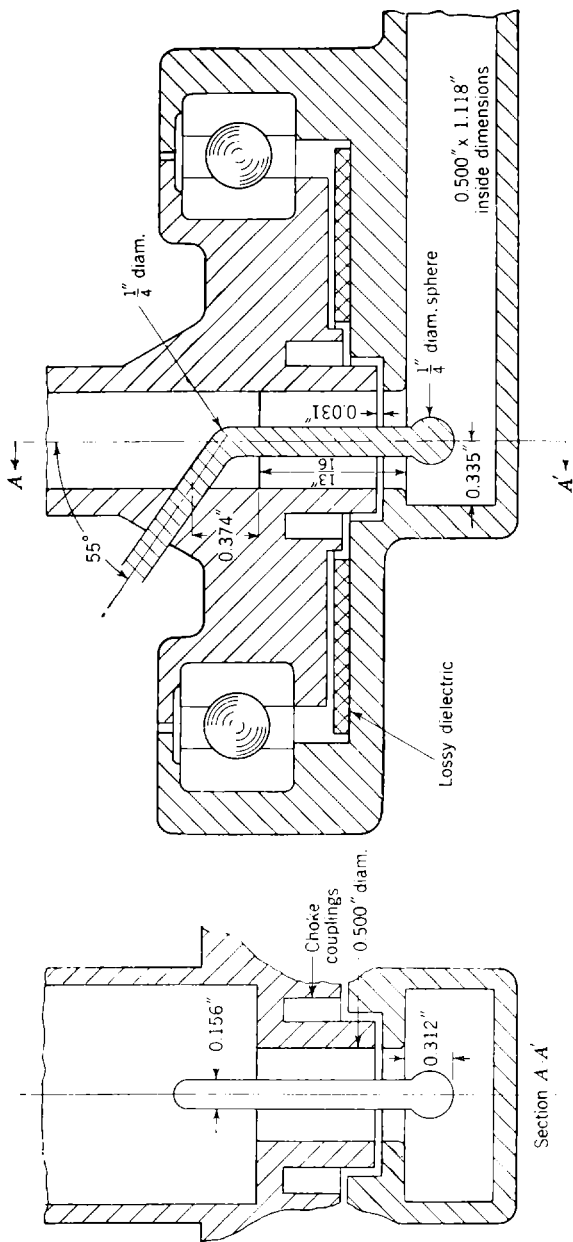


Fig. 7-50.—3-cm coaxial rotary joint between perpendicular waveguides.

that, in each joint, failure is most likely to occur in the waveguide at the probe. In each case, breakdown occurred at about the same values of pulse power and pressure indicating that the joints should be rated at the same power, which is probably not greatly in excess of 100 kw.

It is worth noting, since data for comparisons are given in Chap. 6, that the bandwidths obtained in these units are not necessarily to be expected at other wavelengths when the various standard sizes of waveguide and coaxial line are used. For example, the bandwidths obtained for the crossbar and loop-coupling transitions in these rotary joints are somewhat larger than those which result from similar matching techniques applied to the same type of transition at 10-cm wavelengths using standard 1½-in. by 3-in. by 0.080-in. wall waveguide and one of the standard 50-ohm coaxial lines. The reason for this is that the sizes of coaxial line and waveguide for these 3-cm transitions are larger relative to the wavelength than are those for the standard 10-cm waveguide and coaxial lines. This makes for the decreased frequency sensitivity of the 3-cm units in two ways. First, since the impedance of the guide is slightly less and the impedance of the coaxial line is considerably greater than for the 10-cm transitions, the discontinuity between these is appreciably less, thus reducing its frequency sensitivity. Second, the 3-cm units operate at frequencies farther from the cutoff frequency; that is, the ratio of the guide wavelength to the cutoff wavelength is less. Consequently, the variation of the guide wavelength, and therefore the electrical dimensions of the transitions, with frequency is less (see Secs. 2-15 and 6-9). These are, of course, relative considerations based upon the electrical properties of the transition as a function of its geometrical configuration and do not alter the fact that a microwave component is more sensitive to changes in dimension at shorter wavelengths than at longer ones. One-thousandth of an inch at 10 cm is still 1 mil at 3 cm, but it is a larger fraction of a wavelength, and the construction tolerances are correspondingly less.

7-21. High-power Rotary Joints with Doorknob Transitions.—Transitions from coaxial line to waveguide designed to carry pulse powers up to the limit of the coaxial line are discussed in Sec. 6-9. In the most successful of these, the center conductor of the coaxial line terminates on the opposite side of the guide from the junction (for a right-angle transition) in a knob which is of the proper size and shape to permit impedance-matching and which has a "streamlined" or rounded contour to minimize the likelihood of breakdown. These have had their greatest application in rotary joints at the 8- to 11-cm wavelengths for two reasons. First, the need for such a high-power joint arose because there was, at the time, proportionately more power available at these wavelengths than at shorter ones. Second, coaxial rotary joints or those with

combined coaxial line and waveguide were used almost exclusively at these wavelengths since the sizes of the round waveguide required result in rather large and unwieldy units. Further, very satisfactory round-waveguide rotary joints had been developed for the 1.25- and 3-cm wavelength bands (see Secs. 7-4 through 7-13).

The two units to be described here have been used, to a considerable extent, in radar systems designed to operate at pulse powers up to 1 Mw. No breakdown trouble has been experienced, and there are indications that properly constructed units of these designs should be usable at pulse powers up to nearly 1.5 Mw in well-matched transmission lines (see Chap. 4). These joints, if well made, introduce reflections of 1.2 or less in voltage standing-wave ratio for a 10 to 12 per cent band. As discussed in Sec. 6-9, the electrical properties of the doorknob transition are critical as to variations in dimensions; and considerable care is required in the assembly of these joints in order to achieve the quality of match just stated. Data on the match as a function of wavelength for preliminary production models of one design will be given later.

The first of the two designs used most extensively is shown in Fig. 7-51.¹ It is designed for $1\frac{1}{4}$ -in. coaxial line and utilizes a hemispherically shaped doorknob with a built-in choke section to provide for relative motion between the center conductor and the doorknob at either end. It operates at 8- to 9-cm wavelengths. The capacity or choke couplings on the outer conductor are of the standard type for coaxial rotary joints. On both the inner and the outer conductor these choke sections follow the conventional principle for broadband choke couplings, having, in series, two quarter-wavelength sections of different impedances. However, because of space limitations, the second (larger impedance) section for the center-conductor coupling at the doorknob is a so-called "disk resonator" in which an equivalent quarter wavelength—that is, the distance from the short circuit to a voltage maximum—is somewhat longer than one-quarter of the free-space wavelength (see Sec. 4-8).

This design is an example of symmetrical construction in which choke couplings are provided for both the inner and outer conductors at both ends of the joint, which makes it possible to remove separately either transition and the coaxial center conductor. This is a desirable feature in many installations but not necessarily an essential one either mechanically or electrically.

In joints operating at pulse powers of 1 Mw it has been found that the coaxial choke couplings allow sufficient leakage to cause actual burning of the bearing surfaces. This is particularly true of the choke sections on the center conductor where the field strength is greatest. No difficulty has, as yet, been experienced with the choke sections and

¹ Mechanical design by the Raytheon Manufacturing Co.

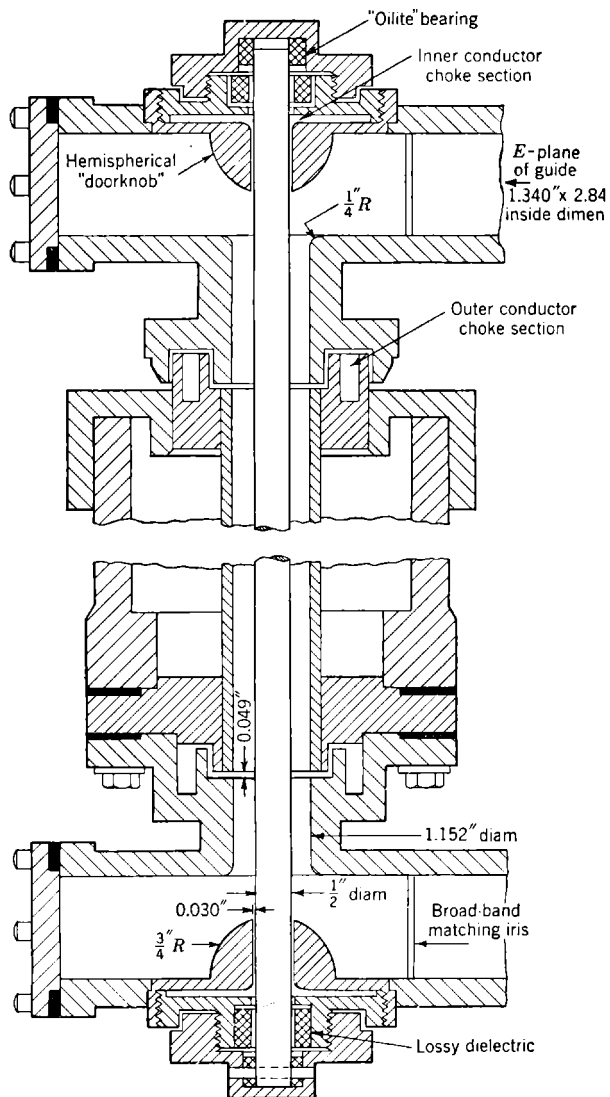


FIG. 7 51.— $1\frac{1}{4}$ -in. coaxial rotary joint between waveguides for 8 to 9 cm.

bearings for the outer conductor, in joints operating at these powers.

To prevent this highly undesirable effect a section of lossy dielectric, consisting of a specially prepared, finely powdered iron (such as poly-iron) in either a ceramic or phenolic-resin base, is placed between the choke coupling and the bearing. Bushings $\frac{1}{2}$ in. long and $\frac{1}{4}$ in. thick with $\frac{1}{32}$ -in. spacing between the rotating conductor and the bushing provide adequate protection from leakage.

A design for a pressurized, high-power, $1\frac{1}{2}$ -in. coaxial rotary joint between waveguides operating at 10- to 11-cm wavelengths is shown in Fig. 7-52 and a model is pictured in Fig. 7-53. Designed for airborne operation, it has a pulse-power breakdown rating of 1500 kw at atmospheric pressure and of 3000 kw at 25-lb pressure on a matched line. These ratings are for a 1- μ sec pulse at 500 cps repetition rate. The general design for this joint is the same as that for the one just discussed except that it has capacity couplings at only one end and uses a different shape of doorknob. Since this doorknob is larger (for the longer wavelengths) than that in the previous design, it has been possible to build the choke coupling for the center conductor entirely within the doorknob in the form of a folded coaxial line.

Figure 7-52 also shows a proposed method for using the center conductor of this coaxial rotary joint to carry a second concentric coaxial line. This may be used

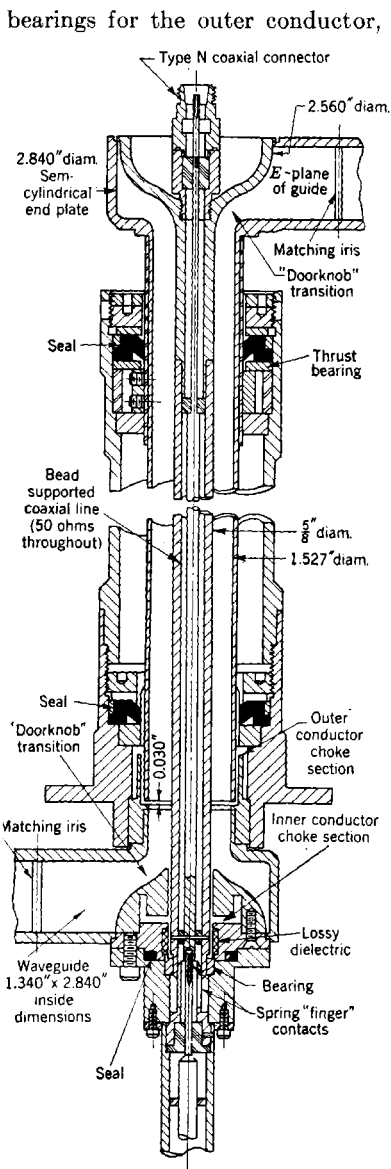


FIG. 7-52.—Diagram of 10-cm, $1\frac{1}{2}$ -in. coaxial rotary joint between waveguides.

with a second antenna for a separate receiving system or low-power radar

interrogation system, for example. The use of a single rotating scanner mechanism for two systems is a very great advantage in many installations.

The voltage standing-wave ratio as a function of wavelength averaged for several of the first production models of this design is shown in Fig.

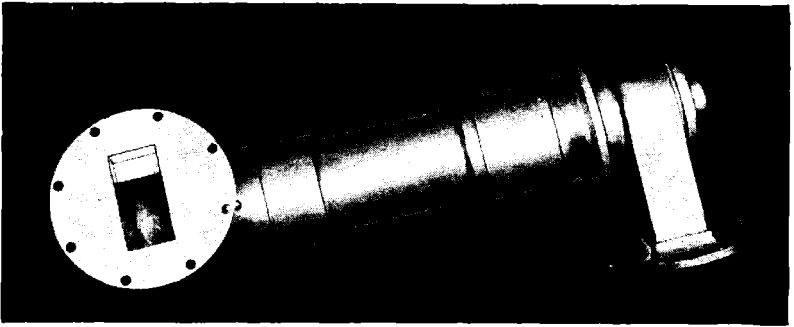


FIG. 7-53.—Photograph of 10-cm, $1\frac{5}{8}$ -in. coaxial rotary joint between waveguides.

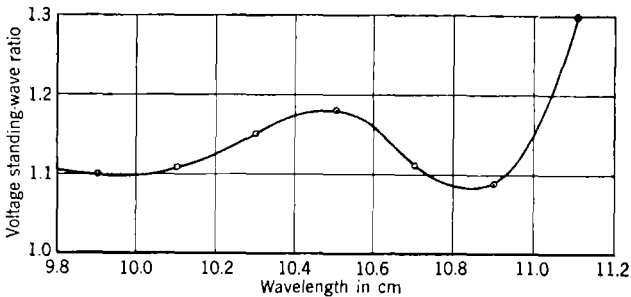


FIG. 7-54.—VSWR vs. wavelength for $1\frac{5}{8}$ -in. coaxial rotary joint with doorknob transition.

7-54. These results are within tolerable limits but it should be possible to improve upon them as the accuracy of production techniques increases. Within the limits of measurement (voltage standing-wave ratios of 1.01) these joints exhibit no change of impedance with rotation.

CHAPTER 8

TUNERS, POWER DIVIDERS, AND SWITCHES

BY G. L. RAGAN AND F. L. NIEMANN¹

TUNERS (VARIABLE IMPEDANCE TRANSFORMERS)

APPLICATIONS AND GENERAL PRINCIPLES

8-1. Applications.—Variable impedance transformers are used to alter the impedance at points on the input side of the lines in which they are inserted. A transformer of a general type, frequently referred to as a “tuner” or as an “impedance matcher,” is capable of altering both the magnitude and the phase of the standing-wave pattern in the input line. A less general but very important type, commonly referred to as a “phase shifter” or “line stretcher,” does not alter the magnitude of the standing wave existing in the line in which it is inserted but acts simply as a line section of variable length, thus shifting the phase of the input standing-wave pattern.

It may be found helpful to classify the various tuners according to their functions, which are:

1. That of introducing a prescribed impedance at some reference point in the input line with the output line terminated in its characteristic impedance.
2. The inverse function, frequently referred to as “matching a line,” of causing no standing wave to appear on the input line when the output line is terminated in an arbitrary impedance.
3. The function of causing a prescribed impedance to appear in the input line when the output line is terminated in an impedance other than the characteristic impedance of the line.

A number of legitimate applications of variable impedance transformers will be found, especially in connection with laboratory test and design work. The use of such circuits is not to be considered, however, as an easy substitute for careful design of matched circuits. It was pointed out in Sec. 2-14 that a matched transmission line is an aid in achieving broad bandwidth, low line losses, high power-handling capacity, and transmitter-tube stability. If the matched condition is maintained all along the line, these objectives will be more fully realized

¹ Sections 8-10 through 8-15 by F. L. Niemann.

than if an attempt is made to match a poorly designed line by means of a variable impedance transformer.

When used as a supplement to a carefully made line, an impedance transformer, especially one of the phase-shifter type, may be required in order to achieve oscillator stability. The use of a phase shifter is especially recommended in connection with long transmission lines, and it is of paramount importance if the oscillator is to be tuned to a particular frequency. The reasons behind this requirement are discussed in Vol. 6.

Unless the use of a variable impedance transformer is demanded by the transmitting tube for the reasons indicated in the preceding paragraph, it is considered unwise to include one in an engineered r-f system. Usually the improvement in performance is too small to justify the effort expended in obtaining proper adjustment and in making the frequent readjustments required. For this reason, the adjustment is apt to be poorly made or readjustment neglected, with the result that on the average the performance of the system is worse with the variable transformer in place than it would be without it.

The principal applications of variable impedance transformers are (1) in test work in the laboratory in which it is desired to achieve some required impedance accurately and (2) in engineered r-f systems in those instances where their use is demanded in order to achieve stable transmitter operation or operation at a prescribed frequency.

8.2. General Principles; Use of Impedance Charts.—In general any obstacle inserted into a uniform transmission line in which a pure traveling wave exists will cause part of the power in this traveling wave to be reflected back toward the generator, thus setting up a standing wave in the input line. The impedance at any chosen point in the input line is thereby altered, and the new impedance may be determined, by means of the relationships developed in Chap. 2, from a knowledge of the magnitude and phase of the standing-wave ratio at that point. Although the magnitude and phase of the wave transmitted past the obstacle will bear a new relationship to those of the incident wave, it is not possible for the obstacle to set up in the output line a wave traveling back toward the generator, that is, toward itself. Therefore, the impedance at all points in the output line remains equal to the characteristic impedance of the line. Thus the insertion of the obstacle has resulted in an impedance transformation.

It is convenient to represent the effect on the impedance at some chosen reference point in the input line by means of an impedance (or admittance) chart. The type of chart found best suited to most discussions of impedance tuners is the Smith chart, Fig. 2-29. An analysis of the effect of inserting a thin wire or screw through a small hole in

the center of the broad face of a rectangular waveguide affords a good example of the use of such a chart. It is found (Vol. 10 of the Series) that the admittance in the waveguide at the position of the screw starts from the center of the chart, for zero insertion of the screw, and moves continuously out along the semicircle C of Fig. 8-1 as the screw is inserted. This semicircle $Y = 1 + jB$ is the locus of input admittances to which the screw may transform the output admittance $Y = 1 + j0$. The semicircle C represents the admittance at the screw and at positions an

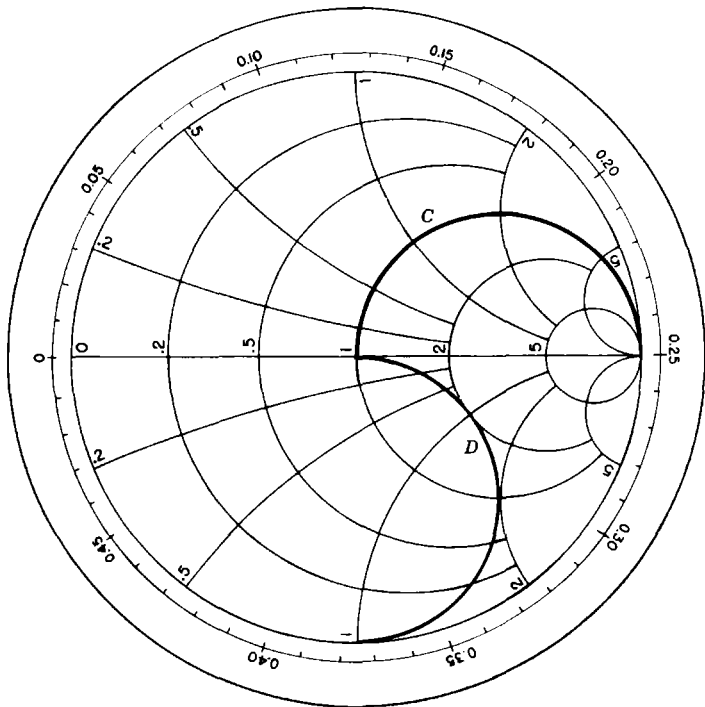


FIG. 8-1.—Admittance contours for screw in waveguide.

integral number of half wavelengths toward the generator from the screw. If some other point in the waveguide is chosen as the reference point, the corresponding contour of admittances may be obtained simply by rotating the semicircle C through the appropriate angular distance on the chart. For example, if it is desired to represent the admittance contour at a point in the waveguide which is one-eighth wavelength toward the generator from the screw, a 90° clockwise rotation of the semicircle C to the position D is required.

The representation on a Smith chart of such a transformation of an

admittance contour along the line is facilitated by the use of a tracing-paper overlay, as indicated by Fig. 2-30. The tracing paper is pivoted at the center of the chart, the index at the zero of the wavelength scale is marked, and the given admittance contour C is drawn. The paper is then rotated so that the index indicates the proper distance in wavelengths. The new position of the given contour with respect to the chart beneath represents the admittance at the point indicated on the wavelength scale. The Smith chart may, of course, be used as an impedance chart in exactly the same way. In addition, if at any time it is desired to convert from impedance to admittance, or vice versa, a simple half turn of the tracing paper produces the desired result. These features of the Smith chart make it ideally suited to discussions of variable impedance transformers.

A circuit provided with a single variable parameter (in the given example, the circuit was a screw in a waveguide) is capable of accomplishing a certain degree of impedance (or admittance) transformation; that is, at any chosen position in the input line, a certain admittance contour may be described. In order to be able to introduce, at any given point, impedances other than those on this contour, one or more additional variable elements are needed. One of the most effective ways of supplying this need, and one that is extremely easy to evaluate on a Smith chart, is to vary the position of the screw along the line. This may be accomplished, in a manner described more fully in Sec. 8-10, by inserting the screw through a longitudinal slot in the waveguide. If the screw is first inserted, for example, at a point one wavelength from the reference point in the input line, the admittance contour C of Fig. 8-1 may be obtained. At a screw insertion corresponding to any point on this contour the screw may be moved along the line by any distance, a half wavelength of motion corresponding to a complete rotation of the tracing paper. Thus the curve C sweeps over the entire area of the chart, indicating the fact that a sliding-screw tuner is capable of introducing any admittance into a matched line.

The sliding-screw tuner has been discussed at some length in order to illustrate the general method of predicting the area of the admittance chart which may be presented to the input line by a given variable impedance transformer when the output line is matched. It is also of interest to know what region of output-line impedances may be transformed by a tuner into a matched input line. If the tuner is reversed in the line, so that the reference point formerly on the input side is on the output side, the problem is easily solved. Of course if the tuner is symmetrical with regard to input and output ends, as most are, it is not necessary to carry out an actual reversal of the circuit. It is easily shown that the region of output-line impedances (referred to the refer-

ence point now in the output line) that may be matched by the reversed tuner is the complex conjugate of the region covered by the tuner in its original position with output line matched.

It is somewhat more convenient to treat a tuner in the matched-output condition and then take the complex conjugate of the resulting region if this tuning characteristic is desired. The complex conjugate of a region plotted on tracing paper in the manner described may be obtained by merely turning the sheet over, keeping the real axis in the same position before and after turning. The merits of a tuner are usually judged on the basis of the maximum standing-wave ratio, occurring in any phase in the output line, which can be tuned to $r = 1$ in the input line. It does not seem worth while to transform to the conjugate region, therefore, since the maximum standing-wave ratio is the same as in the region originally obtained. In the examples presented in the following sections the admittance (or impedance) region plotted will be that which may be obtained at the indicated reference point in the input line.

There remains the more general problem of transforming an output impedance differing from the characteristic impedance of the line into a prescribed input impedance. Since this problem involves a double set of variables, it is more difficult to analyze than those previously discussed.

COAXIAL LINE TUNERS

8-3. Short-circuiting Plungers.—In order to prepare the way for a discussion of coaxial-stub tuners, it is first necessary to discuss means of achieving a perfectly reflecting termination of variable phase. Such a device has other applications as well, one of which will be discussed in Sec. 8-18. It has become common practice to refer to such a reflecting termination as a short-circuiting plunger although a complete reflection of any phase will suffice, and the effective position of the short circuit in a given design is usually dependent on the operating wavelength.

The obvious approach to the problem is to insert into the line a tightly fitting metal plunger of the type sketched in Fig. 8-2a. It is very difficult, and in fact impractical, to obtain a plunger which moves with sufficient ease and at the same time makes good contact with the conductors. This consideration is extremely important, since a poor contact presents an undesirable series resistance to the currents flowing between the coaxial conductors, and leads to power loss and to erratic behavior.

The use of metallic fingers, indicated by Fig. 8-2b, offers a very effective means of reducing the contact resistance. At the same time, the current flowing in the line at the point of sliding contact is reduced to zero since the tips of the fingers are a quarter wavelength from the current maximum which occurs at the short-circuited end of the coaxial

cavity formed by the plunger. The fingers should be made of a springy metal such as beryllium copper, phosphor bronze, or spring brass. They should be given an initial deformation in order that the restoring force maintains pressure at the contacts when they are inserted into the coaxial line. It is essential to provide good contact since the current is zero only at the exact wavelength for which the plunger cavity is a quarter wavelength long. For reasonably broad bands the current is still considerably smaller than that in the plain plunger of Fig. 8-2a to

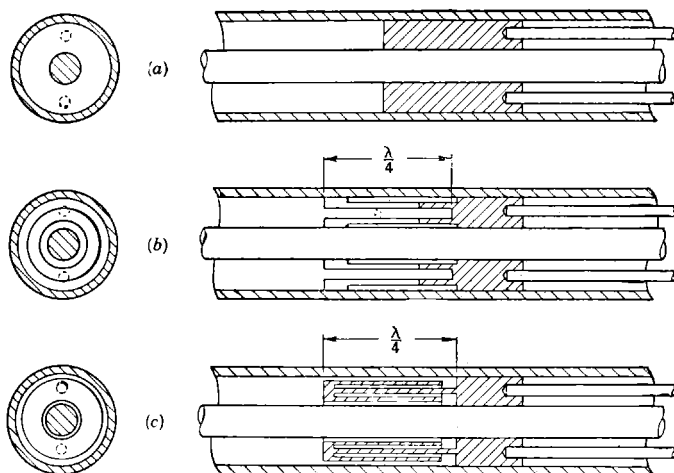


FIG. 8-2.—Coaxial short-circuiting plungers. (a) Plain-contact type. (b) Quarter-wavelength-finger type. (c) Capacity-coupled type.

which it is related by the cosine of the electrical angle of the plunger cavity.

Another method of reducing the current flowing in the sliding contact is shown in Fig. 8-2c. The principle involved is that of the folded half-wavelength capacity or choke coupling discussed in Sec. 2-17. Separate half-wavelength sections are used to couple from the plunger to the outer conductor and from the plunger to the inner conductor. In each case the sliding contact comes at the low-current point in the folded-line section. The principles of design discussed in Sec. 2-17 apply here as well. The important points to remember are these:

1. The impedance of the two capacity-coupling sections formed between the coaxial-line conductors and the plunger should be as low as is practical. This means that the clearance between this part of the plunger and coaxial-line conductors should be made as small as is consistent with the requirement that the plunger

must not come into actual contact with the coaxial-line conductors at any point along these capacity-coupling sections.

2. The impedance of the folded-choke sections contained within the plunger should be made as large as possible.
3. The resistance at the sliding contacts should be made as small as possible.

Of the three types of plungers illustrated by Fig. 8-2, that of Fig. 8-2c modified in the manner indicated in Figs. 8-3 and 8-4 has been found

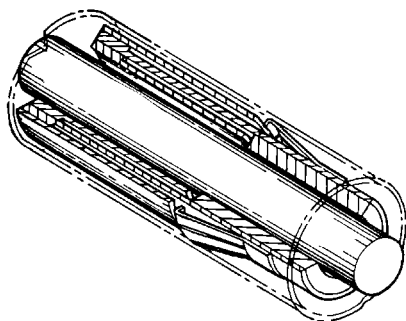


FIG. 8-3.—Capacity-coupled, short-circuiting plunger.

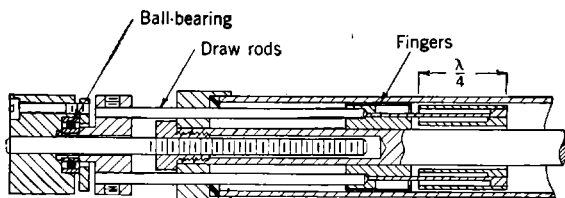


FIG. 8-4.—Capacity-coupled, short-circuiting plunger.

to be best for most purposes. Its principal advantages over the other types are found to be these.

1. It presents a more nearly perfect reflection of power (that is, its losses are lower).
2. It is necessary to make only one short set of fingers, and the contact provided by them need not be extremely good since the alternation of high and low impedances in the coupling section reduces the importance of the contact resistance (see Sec. 2-17).
3. The alignment of the outer and inner conductors of the coaxial line into which the plunger is inserted need not be especially good, since the one set of fingers can be made very flexible and the clearance between the plunger and the outer conductor can be large enough to permit considerable misalignment of the conductors.

4. Although this plunger has approximately the same over-all length as the plunger of Fig. 8-2*b*, it presents a short circuit at its input end whereas the simple plunger with fingers presents an open circuit. This feature of the choke plunger permits the design of a more compact stub tuner as will be shown in Sec. 8-7.
5. When the three designs are considered from the point of view of ease of manufacture, especially in the light of the second and third points of this enumeration, most manufacturers would find the plunger of Figs. 8-3 and 8-4 easier to make.

In certain applications the fingers shown in Figs. 8-3 and 8-4 may be omitted entirely, and manufacture is thus made still simpler. If this is done, however, one must consider the impedance presented at the plunger by the section of line behind the plunger, through which the rods moving the plunger extend. This impedance appears in series with the high impedance of the folded choke, and for certain plunger positions the combination will become resonant resulting in large losses and anomalous behavior of the impedance at the input end of the plunger. The coupling to this section of line behind the plunger may be reduced by adding to the plunger, in the region where the fingers are omitted, a metal sleeve having an outer diameter nearly equal to the inner diameter of the outer conductor. The resonance will thus be sharpened; that is, it will be noticeable over a smaller range of plunger positions. If the wavelength range used and plunger motion required are small enough, the length of the line behind the plunger may be chosen to avoid trouble due to the resonance.

As a matter of fact, there is a very slight, but noticeable, coupling to the line behind the plunger even when the construction indicated in Figs. 8-3 and 8-4 is used. For a plunger of this type used in a $\frac{7}{8}$ -in. coaxial line at a wavelength of 10 cm, it was found that an extremely sharp resonance occurs at certain plunger positions. In this particular example, all metal parts were gold-plated. The input standing-wave ratio was measured as a function of plunger position. For one sharply defined position, the input SWR dropped to about 36 db, while for all other positions it was about 45 db. It was found possible to remove all signs of this resonance by introducing some absorbing material into the line behind the plunger. Any absorbing material that presents a fair match to the characteristic impedance of the line should be satisfactory for such a purpose. One arrangement that was found to give good results was to place a thin washer of polyiron¹ material against the metal end cap through which the rods that move the plunger extend.

¹ A washer, 0.1 in. thick, made of the H. L. Crowley Co.'s D-1 material was used.

8-4. The Sliding Series Stub Tuner.—A tuner of this type is in theory one of the simplest of coaxial-line tuners, yet it is capable of canceling standing waves of any magnitude or phase. It has been described by M. S. Glass¹ whose design is presented in Fig. 8-5. The plunger in the stub may be moved through a distance of half a wavelength or more, and the whole outer assembly including the stub may be moved through a similar distance. The details concerning the contacts between this assembly and the outer conductor of the line and the effect of the increased outer-conductor diameter in the region of the stub will not be considered in the preliminary discussion.

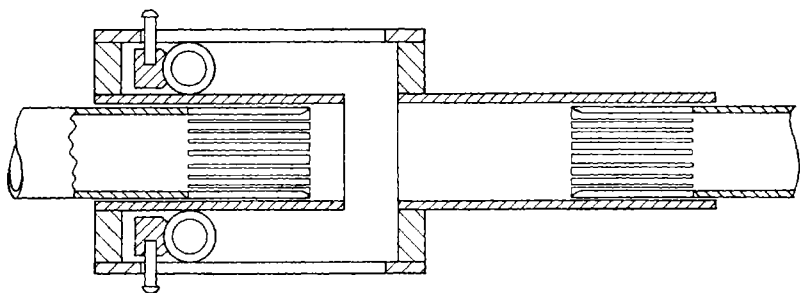


FIG. 8-5.—Sliding series stub tuner.

The discussion of Sec. 8-2 in connection with a sliding-screw tuner applies also to the sliding-stub tuner, with slight modification. Whereas the screw inserted into a waveguide behaves as a shunt susceptance, the stub of Fig. 8-5 acts as a series reactance. Unlike the screw, which for reasonable lengths acts only capacitively, the stub may add reactance of either a capacitive or an inductive nature. The impedance in the line at the point where the series stub joins it is $Z = 1 \pm jX$, as indicated by the circle *C* of Fig. 8-6. Since the distance between any chosen reference point in the input line and the stub position may be varied by at least half a wavelength, the circle *C* may be rotated through 360° and may thus cover the whole impedance plane. It is therefore obvious that this tuner can introduce standing waves of any phase and amplitude when its output line is matched. By the arguments of Sec. 8-2, it may also tune out a standing wave of any phase and amplitude, and it may match any output impedance to any input impedance.

The plunger used in the stub is one that was not described in the preceding section dealing with coaxial-line plungers. A coiled spring that fills the space between outer and inner conductors is used. It is,

¹ M. S. Glass, "A Variable Series Reactance for Coaxial Lines," BTL Report Mn-42-140-51, Sept. 12, 1942.

in its free state, somewhat larger and is therefore under a compressional strain, which leads to low contact resistance.

The contacts between the outer conductor and the sliding assembly are of the finger type discussed in the preceding section. In this case, however, the full line current flows in the contacts; hence the need for low-resistance contacts is obvious. The construction of fingers that will give the required quality of contact and maintain it in service appears to offer a serious problem. Perhaps a capacitance-coupling scheme such as that used in the coaxial phase shifter (to be described in Sec. 8-7) would prove more suitable. One disadvantage of such a change, however, is that a larger change of outer diameter results.

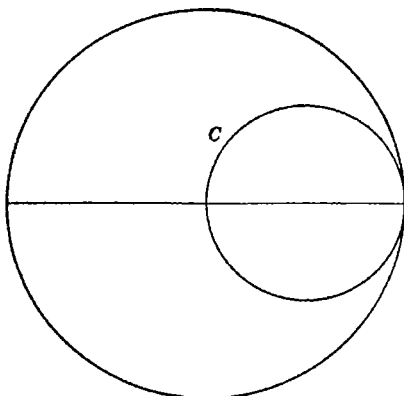


FIG. 8-6.—Impedance diagram for sliding-stub tuner.

The effect of the change in outer diameter is twofold: the characteristic impedance in that part of the line is increased, and an effective shunt capacitance is introduced at each end because of the well-known junction effect. The characteristic impedance could be restored to equality with that of the line by the proper increase of the diameter of the inner conductor, and the junction capacitance could probably be well compensated in the manner suggested by Fig. 6-5*d*. In the original design the higher-impedance line is made an integral number of half wavelengths long; thus when the stub is in its null position (zero added reactance) the line section gives the one-to-one transformation ratio characteristic of lines an integral number of half wavelengths long.

Although one or more of the refinements mentioned may be worth while in contributing to the ease of adjustment of the tuner, none of them is really required for tuning any output impedance to any input impedance. This statement may be checked by considering a half-wavelength section of the high-impedance line, which also contains the

stub, as the actual variable transformer, and the remaining end portions containing junctions as output and input transformers. Obviously any output impedance transformed through the output transformer is still a general impedance. And any required input impedance may be obtained by presenting the appropriate impedance to the input transformer.

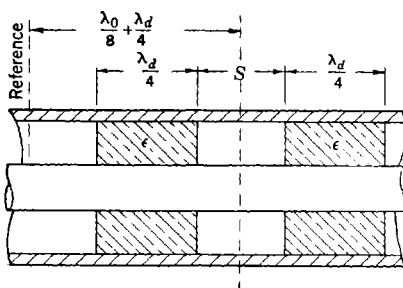


FIG. 8-7.—Double-slug tuner with dielectric slugs.

8-5. Slug Tuners.—Tuners of this type have some very desirable characteristics, both from the standpoint of use and from that of fabrication. The tuner shown in Fig. 8-7 is particularly easy to analyze and has been found satisfactory for applications in which the power level is not excessive and the required tuning range is only moderately large.

Each dielectric bead, commonly referred to as a “slug,” acts as a quarter-wavelength transformer of impedance $Z_T = Z_0/\sqrt{k_e}$, introducing a VSWR of magnitude k_e . The slugs may be moved along the line by

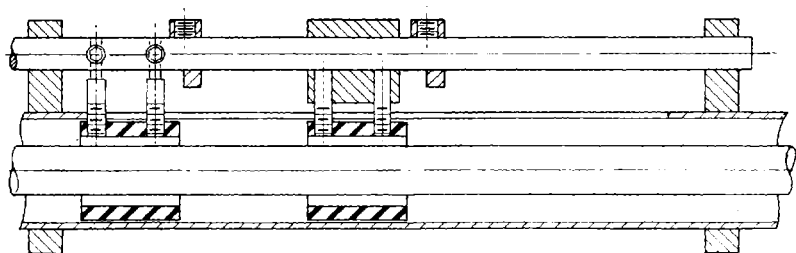


FIG. 8-8.—Double-slug tuner for small standing waves.

means of dielectric handles extending through a longitudinal slot in the outer conductor, as indicated in the design shown in Fig. 8-8. As the spacing S between the slugs is varied, the standing-wave ratio introduced by the pair varies from unity to a maximum value equal to k_e^2 , the product of the individual values of VSWR, as indicated by Items 6a and 6b of Table 2-2. The standing-wave ratio is a maximum for $S = \lambda_0/4$ and is equal to unity when $S = 0$, when the two slugs join to form a single half-wavelength section of line.

The magnitude of the standing-wave ratio as a function of the angular separation $360^\circ(S/\lambda)$ is given in Fig. 8-9 for slugs of several dielectrics. When the separation is $S = \lambda_0/4$, the maximum standing-wave voltage ratio $r = k_e^2$, is introduced. Assuming the generator to be on the left in Fig. 8-6 and assuming the output line to be matched, the input end of the left-hand slug is at the reference point indicated. The input impedance at this point is real and equal to $1/k_e^2$, as indicated in the impedance plot of Fig. 8-10, which gives the impedance at the reference point for slugs of dielectric constant 2.56 (polystyrene). By means of an impedance chart or by application of the transmission-line equation, Eq. (2-41), it may be shown that, for other values of S , the impedances are those indicated in Fig. 8-10.

It is evident from the impedance chart that there is little change in the phase of the standing waves introduced as S is varied if the center of the combination is kept at a fixed point in the line. The phase shift δ of the minimum of the standing-wave pattern from the reference point is plotted as a function of the angular separation $360^\circ(S/\lambda)$ in Fig. 8-11. The voltage minimum is shifted slightly toward the load from the reference point.

One method of changing the separation of the slugs without

moving the center point can be seen from Fig. 8-12. The two slugs are fastened to the small blocks that are moved along the slot by the oppositely pitched threads of the upper screw. Turning this screw gives control over the magnitude of the VSWR introduced. The phase of the standing wave may be varied by turning the lower screw that moves the whole slug assembly. This adjustment has the effect of rotating the impedance contour of Fig. 8-10, sweeping out the entire shaded area of the impedance diagram. Any impedance within this area may be introduced when the load is matched, and any load whose impedance lies in this area can be matched to the input line.

The screw arrangement just described is found to be too slow for work involving large adjustments. For such applications the mechanical

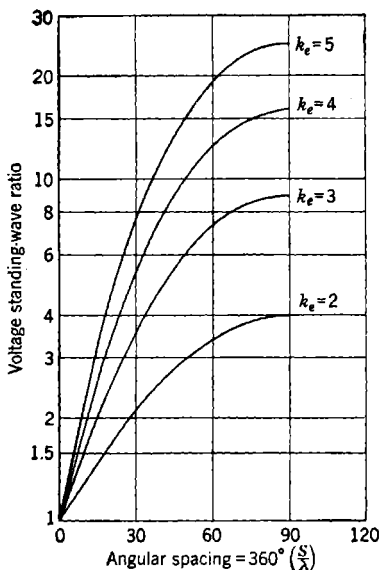


FIG. 8-9.—Standing-wave ratio of double-slug tuner of Fig. 8-7 for values of $K_e = 2, 3, 4, 5$.

arrangement of Fig. 8-13 is preferable. The whole assembly is moved along by means of a fast-motion rack-and-pinion drive.

The slug tuner in this form has been found to be extremely useful for introducing known impedances to magnetrons for the purpose of studying their load-impedance characteristics. The fact that the magnitude and phase of the standing wave may be separately varied makes it easy to obtain a uniform coverage of the impedance chart. For this

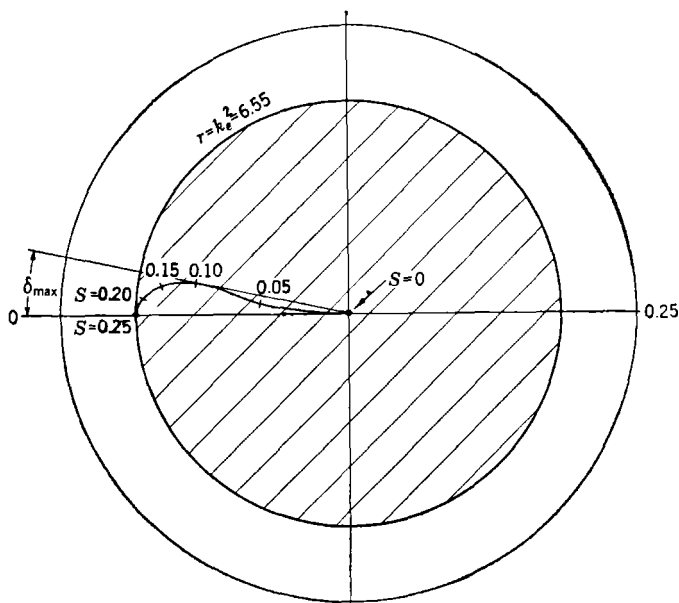


FIG. 8-10.—Impedance of dielectric slug tuner of Fig. 8-7, $K_e = 2.56$. S is measured in wavelengths.

application it is desirable to be able to introduce high values of VSWR, the usual requirement being about $r = 10$. This requires a high value of dielectric constant or the use of metallic slugs partly filling the line. Since the power levels are high, the metallic slugs, which give better high-power performance, are used.

Each slug is suspended from a separate carriage by means of two mica sheets projecting through two longitudinal slots cut in the sides of the outer conductor. The two carriages are connected by means of a metal strip that is fastened to the top surface of the carriage on the left. A screw projects upward from the carriage on the right through a slot in the strip. By tightening a wing nut on this screw, the strip is fastened to the right-hand carriage with the carriages at the desired separation.

The two carriages then move together with this separation, as the pinion gear is turned by the crank shown.

A larger drawing of the metal slug used appears in Fig. 8-13. It was designed for use in the $1\frac{1}{2}$ -in. line at a wavelength of about 10 cm, and a tuner using a pair of such slugs should be able to introduce a VSWR of

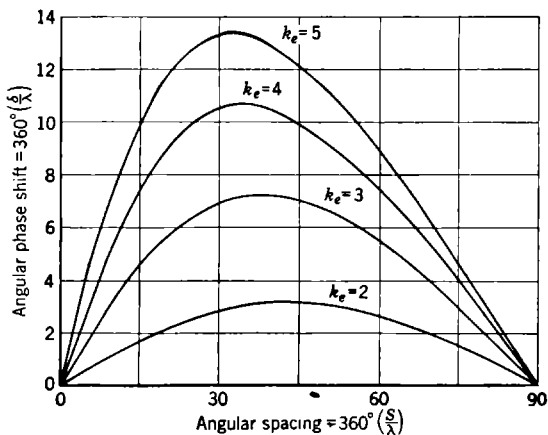


FIG. 8-11.—Phase shift of double-slug tuner for values of $K_e = 2, 3, 4, 5$.

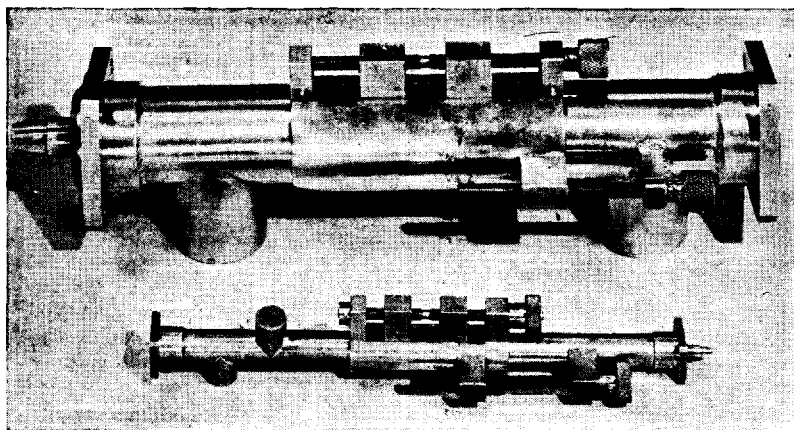


FIG. 8-12.—Double-slug tuners.

about 10. In order to avoid breakdown it is important that all corners be rounded. Slugs should be made of aluminum so that they will be light and therefore easy to support.

A few words should be included concerning the behavior of metal slugs in regard to impedance. If little or no space is left between the

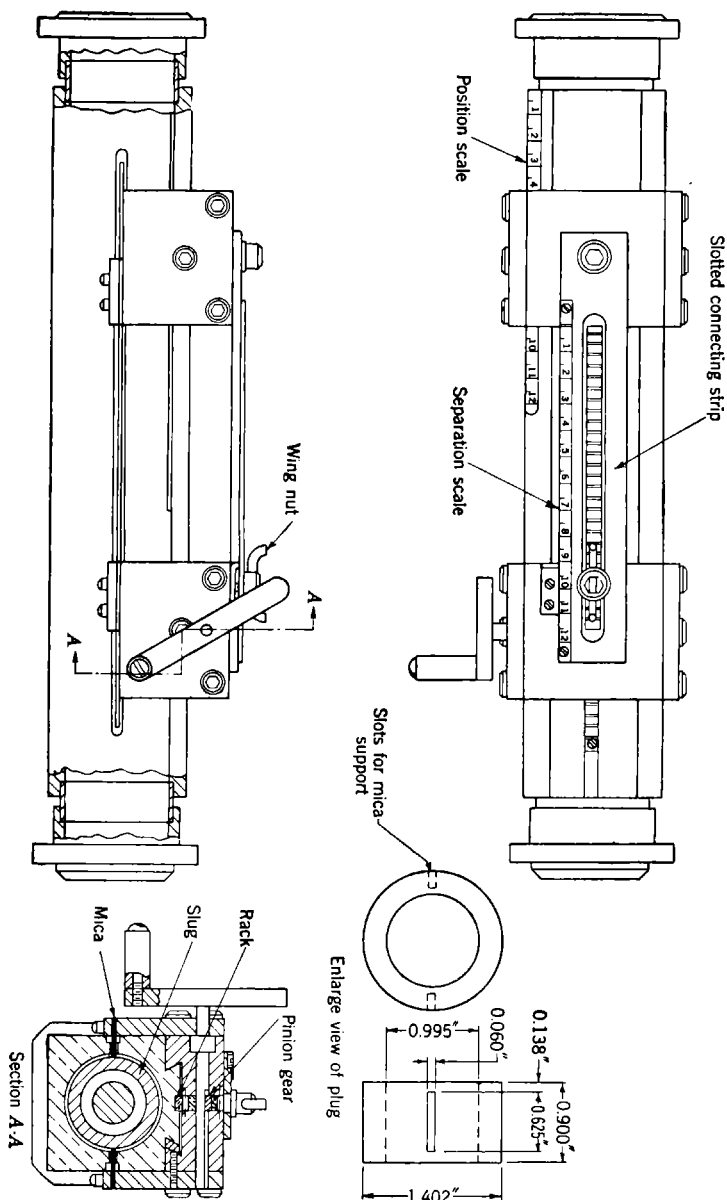


FIG. 8-13.—Double-slug tuner for $1\frac{5}{8}$ -in. coaxial line.

slug and the outer conductor, the metal slug is simply a transformer of the type shown in Fig. 4-35c. The characteristic impedance of the transformer section containing a metal slug of outer radius b' and inner radius a' is desired. If the original line has an impedance Z_0 , the transformer impedance may be shown to be

$$Z_T = Z_0 - Z'_0, \quad (1)$$

where Z'_0 is given by

$$Z'_0 = 138 \log_{10} \frac{b'}{a'}. \quad (2)$$

There are, of course, shunt-capacitance effects at the end of the transformer sections, but since these are a quarter wavelength apart, a certain amount of compensation results.

Neglecting shunt-capacitance effects, the behavior of any slug tuner having transformers of impedance Z_T is exactly the same as that of a tuner having dielectric slugs of the same characteristic impedance and electrical length. Therefore Figs. 8-9, 8-10, and 8-11 apply to quarter-wave slugs in general, provided that Z_T and k_e are related to the characteristic impedance of the line by

$$\frac{Z_T}{Z_0} = \frac{1}{\sqrt{k_e}}. \quad (3)$$

Slugs of other forms and other methods of support have also been used. One design calls for a dielectric sleeve filling the space between the slug and the outer conductor. This design is mechanically more rugged but is subject to greater breakdown trouble. A type of slug which is extremely useful when the introduction or removal of low standing waves is desired is that of Fig. 8-8. The dielectric does not completely fill the line but takes the form of a sleeve fitting against the outer conductor. The characteristic impedance of a dielectric transformer of inner radius c fitting against the outer conductor of a line whose radii are b and a is

$$Z_T = 138 \sqrt{\left(\frac{\log_{10} \frac{b}{c}}{k_e} + \log_{10} \frac{c}{a} \right) \log_{10} \frac{b}{a}}. \quad (4)$$

This equation is a modification of Eq. (5-3). The wavelength in the transformer section is smaller than that in the main line by the factor Z_T/Z_0 ; therefore the physical length of the slug should be shortened accordingly.

The particular slug tuner shown in Fig. 8-8 is designed for operation at wavelengths of 9 to 11 cm, the slug lengths being somewhat shorter than a quarter wavelength at 9 cm. At any wavelength in this band,

unity VSWR is obtained when the slugs are slightly separated. There is less tendency for sparking to occur at high power levels if the slugs are not allowed to touch. The maximum VSWR that may be introduced is slightly greater than 1.5 at all wavelengths. This relatively low value was the maximum required for the particular application for which the tuner was designed. It was desired to introduce a standard VSWR of 1.50 which could be varied through all phases in order to test the "pulling figure" of magnetron oscillators.¹ It was also necessary to be able to restore with ease the matched condition in order to obtain a standard for comparison. Both conditions are easily obtained with the simple mechanical design evolved. One slug is attached by dielectric pins to a rod that parallels the axis of the line. The other slug is attached to a metal block that slides on the same rod. Stops on the rod at either side of the second slug may be set in such positions that they define the minimum and maximum slug separations corresponding to $r = 1$ and $r = 1.50$ for a given wavelength. The whole assembly may be moved as a unit along the line to vary the phase of the standing wave.

Usually it is desirable to use a slug tuner that will give a maximum VSWR only slightly in excess of that likely to be needed in practice. If a tuner capable of excessive tuning is used the adjustments become more critical than necessary and nothing is gained. In addition, larger standing waves and hence larger voltage gradients are introduced into the line by the tuner of larger range, a factor that may cause breakdown. The added difficulty of adjustment is easily seen by noting that in Fig. 8-9 the rate of change of VSWR with separation is higher for the slugs of higher dielectric constant.

There are indications that the use of two slots, as in the design of Fig. 8-13, leads to more slot radiation than does the use of one slot, as in the designs of Fig. 8-12. The difference is greater than that resulting from the larger open area of the two slots, and it appears to be caused by a greater freedom of propagation of higher modes in the double-slot line. For this reason, it seems desirable to use a single slot, rather than double slots, even though the single slot may need to be several times as wide in order to provide sufficient support for the slug. A slight modification of the designs shown in Fig. 8-12 should permit single-slot construction. Support by means of dielectric pins such as those used in Fig. 8-8 is suggested.

8-6. Stub Tuners.—Coaxial-line transformers utilizing one or more branch lines of variable length have long been popular. A schematic diagram of such a tuner having three branch lines or stubs is presented in Fig. 8-14. A practical design of a double-stub tuner is illustrated in

¹ See Fig. 2-45 and accompanying text, Sec. 2-14.

Fig. 8-15. The stubs contain short-circuiting plungers like those of Fig. 8-4. The physical arrangement of the lines is seen to be quite different from the conventional arrangement of Fig. 8-14. The two plungers are mounted in a straight section of coaxial line which is slightly larger and slightly heavier in construction than the input and output sections of line. This construction affords better alignment of the coaxial conductors in the stubs.

The admittance diagrams showing the performance of a double-stub tuner in which the spacing between the stubs is a quarter wavelength are given in Fig. 8-16. Diagram *a* gives the admittance at the stub nearest the matched load. A coaxial-line stub is capable of introducing

a shunt susceptance of either positive or negative sign. Thus any admittance lying on the circle *D*, for which the conductance is $G = 1$, may be introduced at the output stub when the line beyond it is terminated in a perfect match, point *d*. In diagram *b* the admittance at the next stub a quarter wavelength toward the generator is indicated. The

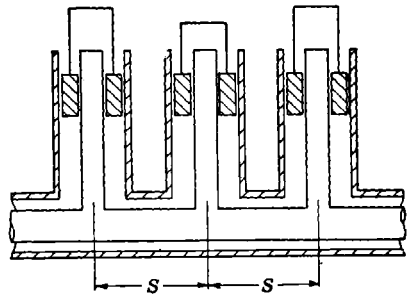


FIG. 8-14.—Triple-stub tuner.

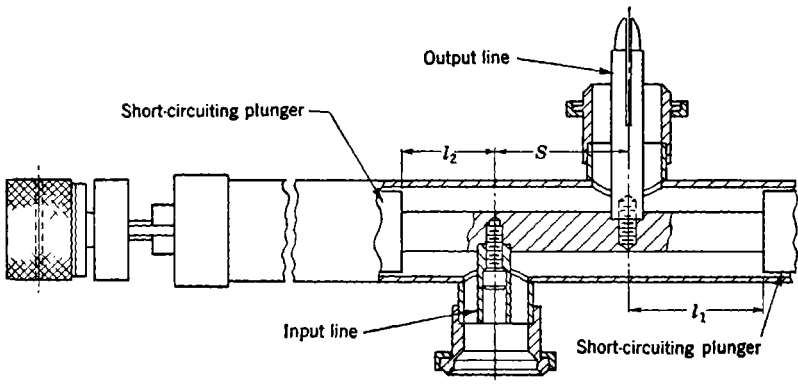


FIG. 8-15.—Double-stub tuner.

transformation of the circle *D* on which a typical point *e* is indicated is easily accomplished on the Smith chart. Transformation through a quarter wavelength of line entails simply a rotation through 180° about the center of the chart, point *d*. This rotation is easily accomplished by the use of tracing paper in the manner described in Sec. 8-2. Any

admittance lying on the dashed circle D may be presented to the second stub. The typical point e may be transformed by means of the second stub along the circle F . Circle F is one of the family of constant-conductance circles of the Smith chart, and it may be traversed by adding pure susceptances by means of the stub. The addition of susceptances to the point d gives the circle E of unit conductance. There is no point on circle D which has a conductance greater than unity, hence there is no way of presenting, at the input side of the second stub, any admittance within the circle E corresponding to conductances greater than one. Any point on the chart which does not lie within this area may be obtained by the combination of two stubs spaced a quarter wavelength

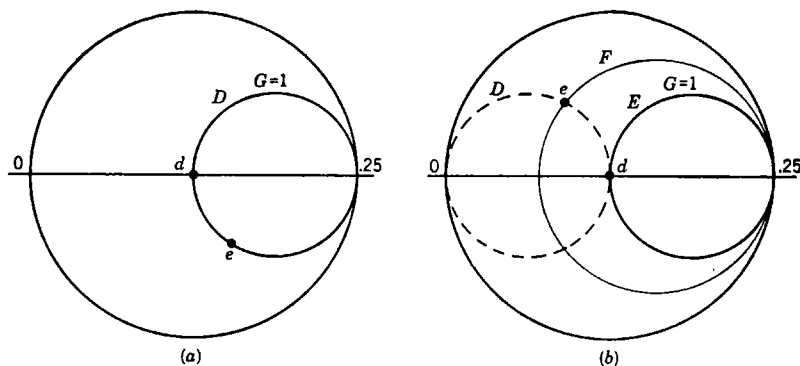


FIG. 8-16.—Admittance of double-stub tuner, $\frac{1}{4}\lambda$ -spacing: (a) at output stub; (b) at next stub, $\frac{1}{4}\lambda$ away.

apart. It is, therefore, clear that standing waves of very large magnitude may be obtained in some phases, but that a standing wave larger than unity cannot be introduced in a phase along the real axis to the right of point d .

If a third stub is added, a quarter wavelength toward the load from the first, a triple-stub tuner such as that of Fig. 8-14 is formed. The two stubs nearest the load may now be used to present, on the input side of the middle stub, any admittance that does not lie within the unit conductance circle of Fig. 8-16b. This region transforms at the stub nearest the generator to the region inside the circle D of the same diagram. Thus the two stubs nearest the load may introduce at the input stub any admittance exterior to the circle D . The middle stub and the input stub may introduce at the same point any admittance exterior to the circle E , as shown in the preceding paragraph. Since these unattainable regions are mutually exclusive it is clear that the three-stub tuner with quarter-wavelength spacing is capable of introducing standing waves of any phase and magnitude.

The admittance diagrams corresponding to two stubs spaced three-eighths of a wavelength apart are given in Fig. 8-17. As in the preceding figure, diagram *a* represents the admittance obtainable at the stub nearest the load. Typical points *c*, *d*, *e*, *f* on this circle of unit conductance are indicated. In diagram *b*, transformation through three-eighths wavelength results in the new position of circle *D* and its typical points. Circles *E*, *F*, and *G* indicate the transformations of these points which may be effected by the second stub. The maximum conductance obtainable, $G = 2$, encloses a region that is not obtainable by a double-

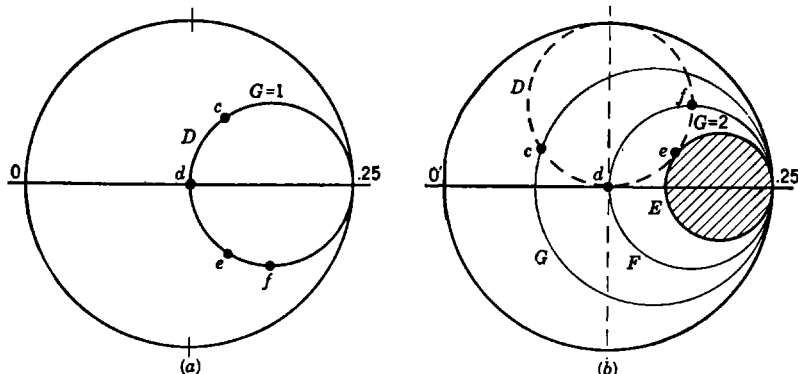


Fig. 8-17.—Admittance of double-stub tuner, $\frac{3}{8}\lambda$ -spacing: (a) at output stub; (b) at input stub, $\frac{3}{8}\lambda$ away.

stub tuner of this type. The standing-wave ratio associated with admittances lying within this region, however, are all equal to or greater than $r = 2$. Therefore, any standing-wave voltage ratio of magnitude less than or equal to two is certainly obtainable in all phases.

The method of analysis indicated by Figs. 8-16 and 8-17 may be extended to other stub spacings. For any stub spacing there will be a circle of maximum obtainable conductance which will define the region of the admittance chart which is not available by means of the double-stub tuner with this spacing. The value of this maximum conductance is given as a function of stub spacing in Fig. 8-18.

On the basis of Fig. 8-18 it might seem advisable to choose a stub spacing of approximately one-half wavelength, and an angular spacing of approximately 180° . It will be found, however, that if such spacing is used it will become necessary to introduce extremely large susceptances in order to tune out standing waves of only moderate amplitudes if the phase of this standing wave is unfavorable. The same disadvantage exists in the case of quarter-wavelength spacing. In addition, the procedure to be followed in tuning out a mismatch with spacings approximating either quarter-wavelength or half-wavelength values is very

difficult. On the other hand, the procedure required for spacings of an odd number of eighth wavelengths is relatively simple. A comparison of the procedures involved is given in Fig. 8-19. It is assumed that in

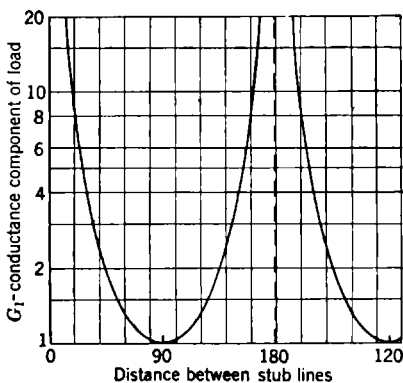


FIG. 8-18.—Maximum conductance obtainable by double-stub tuner.

both cases shown in Fig. 8-19 the stubs are originally in their null or zero-susceptance position. Both diagrams *a* and *b* represent the admittance at the input stub. The admittance at this stub is originally that indicated by point 0. The effect on this admittance of adjusting the output stub is represented by motion along the circle *D*. If diagram *a* is rotated through 180° and diagram *b* through 90° clockwise, it will be clear that the circle *D* represents the effect of the output stub. The point *a* on this circle represents the proper transformation required of the output stub. The input stub may then transform the point *a* along the circle *E* to the point *b* representing the matched input condition. If the effectiveness of the tuning adjustment is judged from the magnitude of the input standing-wave ratio, it will be found that minimum

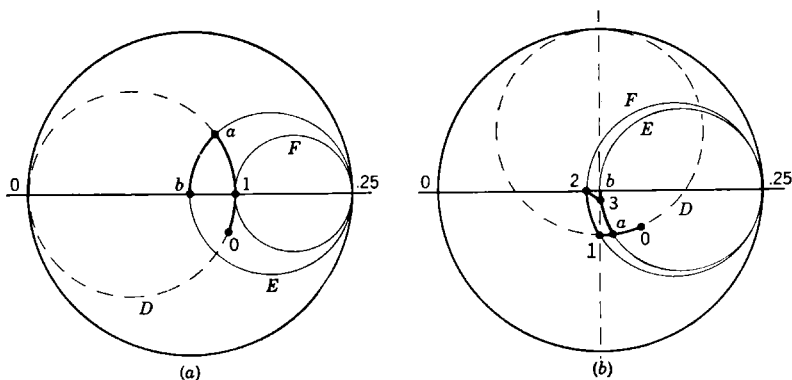


FIG. 8-19.—Tuning out a mismatch: (a) with $\frac{1}{4}\lambda$ -spaced stubs; (b) with $\frac{3}{8}\lambda$ -spaced stubs.

input VSWR occurs at the point 1 on the circle *D*. That is, the point 1 represents the closest approach to the center of the diagram. The admittance point 1 is transformed by the input stub along the circle *F*. In the case of the quarter-wavelength spacing, diagram *a*, this leads to

no reduction in input VSWR. In the case of three-eighths-wavelength spacing, the admittance point 2 on circle F represents the minimum VSWR obtainable by adjustment of the input stub. If the input stub is left in this position and the output stub is readjusted, it can be shown that the resulting input admittance moves from the point 2 along a circle whose closest approach to perfect match is indicated by the point 3. It is evident that a process involving successive reduction of the input standing-wave ratio is occurring and that the approach toward perfect match is rapidly achieved. This procedure is in marked contrast to the unsatisfactory termination of the equivalent procedure indicated in diagram a . The first adjustment leads to the admittance point 1 which cannot be improved by further adjustments. In order to obtain the matched condition with stubs spaced a quarter wavelength apart, it is necessary to proceed by guess work, since the process of successive reduction of input standing-wave ratio leads to an impasse.

The difficulty just described constitutes one forceful argument in favor of a stub spacing of one-eighth or three-eighths wavelength over a spacing of a quarter wavelength. Another disadvantage of the quarter-wavelength spacing is that three stubs are required. It is difficult, first of all, to decide which pair of adjacent stubs represents the proper combination for tuning out a given load admittance. In regard to spacings approximating one-half wavelength, it has already been mentioned that extremely high susceptances are sometimes required in order to match standing-wave ratios of moderate magnitude if the phase happens to be wrong. In view of these considerations, it is felt that a spacing of an odd number of eighth wavelengths represents the most practical value if its inherent limitation of $r \leq 2$ can be tolerated.

A method of increasing the tuning range of a double-stub tuner with any spacing is to use an additional section of line which may be inserted or removed at will. One method of accomplishing this objective is to make the tuner reversible and have the length of line different on output and input sides. This arrangement requires the use of an adapter or couplings of the same polarity attached to the input and output lines. The practical value of this suggestion is doubtful since it requires uncoupling and reversing the tuner if the required tuning is not accomplished in the original position. If the output and input lines differ in length by a quarter wavelength, it is easily shown that all phases and magnitudes of standing-wave ratio are obtainable. Usually, a change of length of less than a quarter wavelength will suffice. The minimum length required for various stub spacings has been studied by Smith.¹

Another method of increasing the tuning range of a given double-

¹ P. H. Smith, "Two Stub Transmission Line Impedance Matching Circuits," BTL MM-43-170-14, Aug. 19, 1943.

stub tuner is to decrease the characteristic impedance of the line between the stubs. For example, Smith gives curves that show that if the characteristic impedance of the line between stubs is 0.7 times that of the main line, the tuning range of a double-stub tuner with one-eighth- or three-eighths-wavelength spacing is increased from $r = 2$ to $r = 4$. Similarly, the tuning range of a double-stub tuner with quarter-wavelength spacing is increased from $r = 1$ to $r = 2$ by the same change of line impedance. The effect of such a design change on the ease of tuning, discussed in connection with Fig. 8-19, has not been investigated. Before attempting this modification, it would be advisable to study the possible results of the change.

8-7. Phase Shifter.—Variable impedance transformers of this type, popularly known as “line stretchers,” are required in transmission-line assemblies more frequently than any of the other transformers. They are needed in order to obtain stability of operation of microwave magnetrons when the line length is excessive or when the frequency of a tunable magnetron is changed. If the impedance presented to the magnetron falls within the unstable region shown on the Rieke diagrams of Fig. 2-45, the situation may be remedied by means of a change of line length between the magnetron and the load. The effect of this change of line length, which may be accomplished by means of a line stretcher, corresponds, on the impedance chart, to a rotation, about the center of the chart, of the impedance presented to the magnetron. In this way the load impedance is easily transformed into a region of stability. As the frequency of a tunable magnetron is changed, the load impedance presented to the magnetron also changes. If the line is long, there will be an especially rapid shift in the phase of the VSWR at the magnetron, since the line length in terms of wavelengths varies rapidly with change of wavelength in a long line. The load impedance at the desired operating frequency is often found to be in an unstable region, but readjustment of the phase shifter will result in stable operation.

One of the most satisfactory designs of phase shifter for coaxial lines is that shown in Figs. 8-20 and 8-21. It operates in much the same way as the slide of a trombone. The input line (lower left) and output line (lower right) are standard $\frac{1}{8}$ -in. coaxial lines. The H-shaped line section at the top corresponds to the slide of the trombone. The sliding and stationary line sections are coupled by means of capacitance-coupling sections of the folded half-wavelength type illustrated by Fig. 2-53a.

In order to make possible the construction of a capacitance-coupling unit of this type, the outer conductor of the sliding section is increased to $1\frac{1}{4}$ -in. OD, and the center conductor is reduced to $\frac{1}{4}$ -in. diameter. In addition, it is necessary to increase the diameter of the center conductor in the $\frac{7}{8}$ -in. line sections. The impedance in the sliding section is

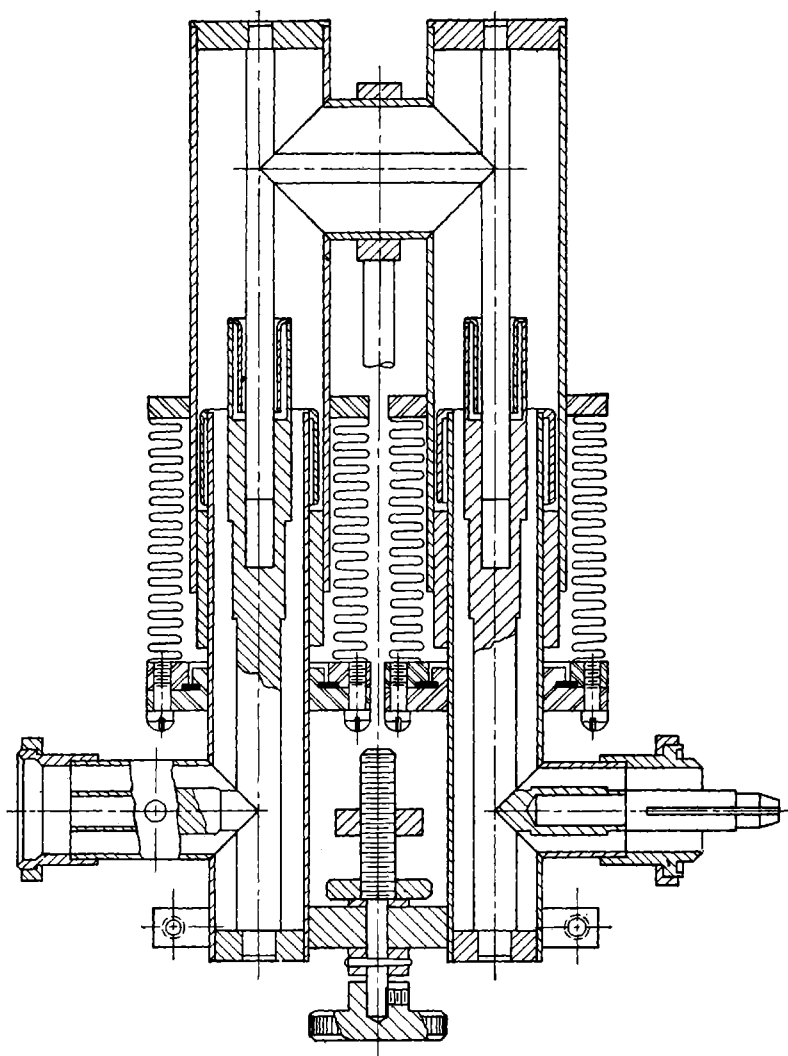


FIG. 8-20.—Cross-section view of coaxial phase shifter.

91.8 ohms, which is matched to the 46.4-ohm impedance of the $\frac{7}{8}$ -in. line by means of three transformers, each a quarter wavelength long. The characteristic impedances of the transformer sections are, proceeding in order from the 46.4-ohm line, 37.8, 29.1, and 50.1 ohms. The frequency sensitivity of the combination of transformers plus the two capacitance-

coupling sections is about the same as that of the $\frac{7}{8}$ -in. stub angle used. Each unit is best matched at a wavelength of 9.1 cm, and each separately gives a VSWR of about 1.05 at $\lambda = 8.8$ cm and $\lambda = 9.4$ cm. By judicious choice of the spacing between stub angle and transformer section, the resultant VSWR of the combination remains below 1.05 from $\lambda = 8.8$ to $\lambda = 9.8$ cm. This example illustrates one broadbanding technique discussed in Sec. 2-16.

Neither of the stub angles of the slide section is matched, when taken separately. The stub length is chosen to give the minimum mismatch

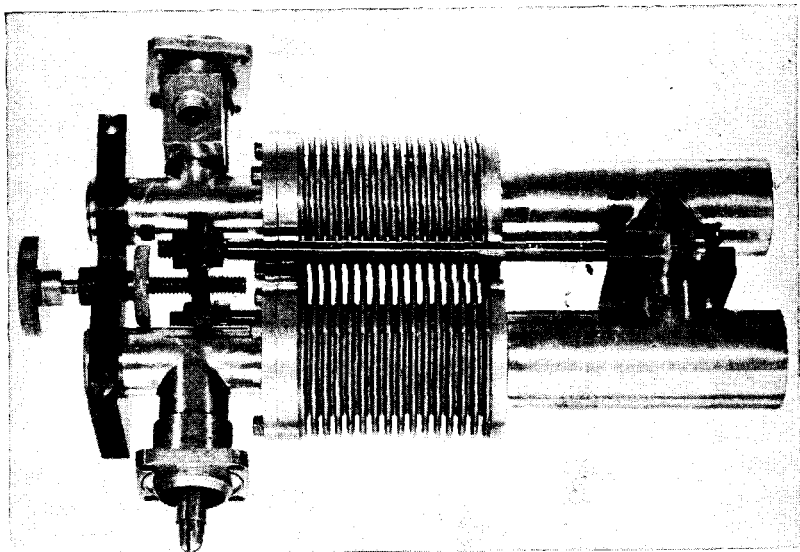


FIG. 8-21.—Photograph of the phase shifter of Fig. 8-20.

obtainable at a wavelength of 9.4 cm, the value of VSWR being about 1.38. The two stubs are spaced to obtain cancellation of their mismatches at a wavelength of 9.4 cm. The resulting combination of two stubs, in the H-shaped form shown, gives a VSWR of 1.05 at wavelengths of about 9.1 and 9.7 cm. If the two stubs were combined in a π -shaped structure (stubs projecting left and right instead of upward) the frequency sensitivity of the combination would be greater. It would be greater also if one stub projected upward and the other to the right or left.

The bellows surrounding the sliding joint is for the purpose of rendering the device airtight, while permitting adjustment of the slide. A lengthening of the line of a full half wavelength is permitted for wavelengths up to about 10 cm.

The design shown is recommended only for wavelengths between 9.0

and 9.6 cm. Outside this range the standing-wave ratio becomes excessive and the length of the capacitance-coupling sections deviates too far from a quarter wavelength. Tests indicate that the line power must be about 500 kw at a wavelength of 9.4 cm to cause breakdown in air at atmospheric pressure. Each of a group of 52 units manufactured was tested for match at all slide positions at a wavelength of 9.4 cm. The maximum VSWR observed for any position of the 52 units was $r = 1.35$, and for half of the units the highest figure was $r = 1.16$.

Several other designs for coaxial phase shifters have been proposed. Most of these use the trombone-slide principle, but employ slotted-finger contacts instead of the capacitance coupling used in the design just

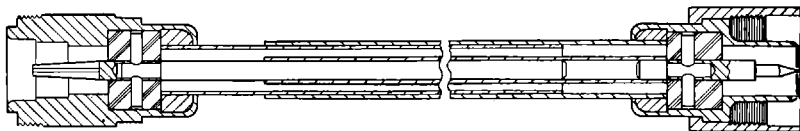


FIG. 8-22.—Type N line stretcher

described. None of these has proved to be very easy to manufacture or very satisfactory in performance.

A line stretcher of a simple type which is literally all the name implies, is illustrated in Fig. 8-22. It is intended for use at low power levels in lines, usually flexible cables, equipped with type N connectors. Unfortunately, the impedance is not matched through the unit; hence, in addition to a shift of phase, a mismatch is introduced.

WAVEGUIDE TUNERS

8-8. Short-circuiting Plungers.—A variable-position short circuit is frequently needed in waveguides, just as in coaxial lines. Short circuits find numerous applications in experimental laboratory work as well as in circuits such as stub tuners and variable power dividers.

Short-circuiting plungers for circular waveguide may be made as shown in Fig. 8-23. This proposed design, which has not, to the author's knowledge, been tried, uses a folded half-wavelength capacitance-coupling scheme similar to that used in coaxial-line plungers. The two quarter-wavelength sections of the plunger are actually coaxial lines, but because of the asymmetrical excitation by the waveguide currents they operate in the second coaxial mode, the TE_{10} -mode of Fig. 2-22. The wavelength λ_{10} in this mode may be calculated by the methods of Chap. 2. The wavelength will of course be different in the two sections, the respective values being denoted by λ'_{10} and λ''_{10} in Fig. 8-23. The practice of alternating low and high characteristic impedances, discussed in Sec. 2-17, leads to good performance over a broad band of wave-

lengths. The sliding contact comes at a current node, as in the coaxial counterpart. It may be found desirable here, as for the coaxial plunger, to improve the contact by using short slotted fingers.

A limitation on the use of slotted fingers in waveguides operating in the lowest mode or in coaxial lines in which the second mode exists should be borne in mind; namely, that the currents are not wholly longitudinal, as they are in coaxial lines excited in the lowest or *TEM*-mode or in round waveguide excited in the second or *TM*₀₁-mode. Some transverse components of current are interrupted by longitudinal slots and good performance is therefore not to be expected. For this reason, a quarter-wavelength plunger with slotted fingers, similar to the coaxial plunger of Fig. 8-2b, is not recommended.

A plunger of the type used in the double-stub tuner of Fig. 8-26 has been found to give satisfactory performance in laboratory test work

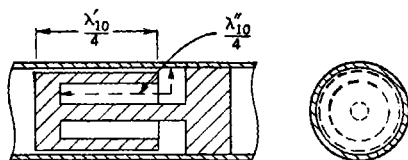


FIG. 8-23.—Short-circuiting plunger for round waveguide.

at low power levels. It is extremely easy to make, especially at very short wavelengths where the plunger is small. The alternation of low and high impedances makes the attainment of low contact resistance less important than it would be in a plain cylindrical plunger relying solely on low contact resistance. It may be shown that the current in the contact is reduced below that in the main waveguide by the factor Z_{01}/Z_{02} by the alternation of the low characteristic impedance Z_{01} and the high characteristic impedance Z_{02} . Plunger losses are reduced by the square of this ratio compared with those in a plain cylindrical plunger having the same contact resistance. The contact resistance of the plunger of Fig. 8-23 plays a still smaller role in plunger losses and contributes, in principle, zero loss at midband.

The problem of designing a plunger for rectangular waveguide is not so straightforward, in theory, as that of designing one for round waveguide. A very practical and satisfactory design has been evolved, however, and it is shown in Fig. 8-24. The large hollow cavity within the plunger forms a section of waveguide one-quarter of a guide wavelength long. Therefore the input impedance, along the slots adjacent to the contacts of the sliding block, is infinite and the current in the contacts is zero. This infinite impedance is transformed, by the quarter-wavelength line of low impedance formed between the plunger and the wave-

guide walls, to zero at the input end of the plunger. It is difficult to visualize the action of this low-impedance line formed between closely spaced coaxial tubes of rectangular cross section. At the input end this line is excited only along the broad waveguide surfaces, and at its output end it is short-circuited along the narrow waveguide surfaces, and coupled through a slot to infinite impedance along the broad surfaces. In practice, however, a plunger of this type has been found to perform very satisfactorily. The r-f loss in such a plunger terminating a waveguide has been observed to be about the same as that in one wavelength of waveguide. This is about what might be expected from the conductor losses in the walls of the line sections composing the plunger; therefore the sliding contacts cannot contribute much to the loss.

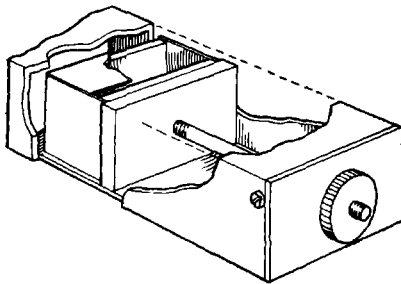


FIG. 8-24.—Plunger-type choke for a waveguide $1\frac{1}{2}$ by 3 in. by 0.080-in. wall.

In earlier designs, a thick metal sheet parallel to the broad surfaces of the waveguide divided the high-impedance cavity into two separate waveguide sections. Each section was coupled separately through one of the two slots to the outer low-impedance line. It was reasoned that if this plate were made as thin as possible, the impedance of each of the sections would be a maximum. It was then argued that the fields and currents are such that the presence of the plate is not needed; consequently the plate was omitted in later designs.

Quarter-wavelength sections with slotted fingers similar to the coaxial plunger of Fig. 8-2b have also been used. They are found¹ to be inferior to plungers of the capacity-coupled type.

8-9. Waveguide Stub Tuners.—Although stub tuners were frequently used early in the development of microwave circuits, they are now seldom employed. This is due partly to the development of tuners of alternative types which are more convenient to use and partly to the general trend toward the elimination of tuners from r-f lines such as those used in radar sets. It seems probable, however, that of all the

¹ C. G. Montgomery and D. D. Montgomery, "Losses and Reflections Introduced by Joints and Plungers in 3-cm Waveguides," RL Report No. 164, Oct. 15, 1942.

types of tuners used in waveguides, the stub tuner is least likely to break down under high-power service. This would seem to be its chief advantage.

A double-stub tuner of one type used in rectangular waveguide is illustrated in Fig. 8-25. The branch sections of waveguide, containing movable short-circuiting plungers like those of Fig. 8-24, are attached to the broad surfaces of the waveguide, forming a configuration frequently

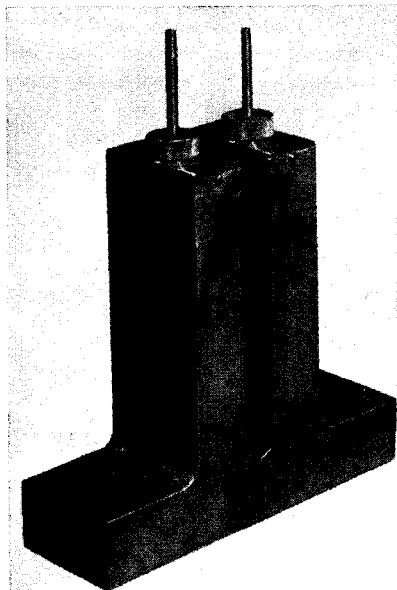


FIG. 8-25.—Double-stub tuner in rectangular waveguide.

termed an “*E*-plane T-junction.” In the equivalent circuit of such a junction the branch section appears in series with the main waveguide. The rounding of the angle formed between branch line and main waveguide, apparent in the figure, has the purpose of avoiding the high electric fields that would otherwise occur along this junction line.

An alternative method of coupling the branch line to the main waveguide is by means of an *H*-plane T-junction connection, which is made by joining the branch line to the narrow surface of the waveguide. The equivalent circuit of the *H*-plane T-junction consists of an effective shunt connection between branch line and main waveguide. The principal advantage of the *H*-plane connection is that it is not necessary to

round the angle along the junction line since there is no electric field at this point in the waveguide junction.

Because it is connected in shunt, the *H*-plane stub has exactly the same effect as the coaxial-line stub discussed in Sec. 8-6. In fact, the entire analysis of the performance of multiple-stub tuners of various spacings is the same in the two cases. A spacing of an odd number of eighth wavelengths is most frequently used in waveguide double-stub tuners, just as it was in coaxial lines. If the stubs are placed on opposite sides of the waveguide, spacings as small as one-eighth wavelength may be used, although the distortions of the fields in the vicinity of the junctions may cause some peculiarities in tuning behavior. If the stubs are placed on the same side, as they usually are for ease of adjustment,

a considerably greater minimum spacing is required. The spacing in terms of wavelengths varies much more rapidly with wavelength in this case, and the band in which good tuning characteristics are obtained is therefore narrower.

The analysis of the tuning characteristics of a stub tuner using the E -plane connection of Fig. 8-25 is like that given in connection with coaxial stubs, with the following simple modifications. The admittance diagrams of Sec. 8-3 must all be considered as impedance diagrams, and the words impedance, resistance, and reactance must be substituted for admittance, conductance, and susceptance throughout the discussion. The VSWR limitations are unchanged. The minimum spacing possible for stubs placed on the same side of the waveguide is obviously smaller for E -plane stubs than for H -plane stubs.

An interesting design, which has been found useful for tuners used at a wavelength of 1.25 cm, is illustrated by Fig. 8-26. The series branches in this instance consist of round waveguides. The performance is similar to that of the E -plane stub tuner of Fig. 8-25. The plunger shown has already been discussed in Sec. 8-8. It is felt that a plunger of the type indicated in Fig. 8-23 would be preferable. The design as shown has, however, given satisfactory performance. It may be worth while to point out the possibility of the occurrence of a resonant condition for some settings of the plunger. Only one of the two mutually perpendicular polarizations that may exist in the round waveguide is strongly excited. It is possible that a slight coupling to the other polarization might lead to a resonance for certain plunger positions. The resonance would presumably be so sharp that it would seldom be encountered, and a slight change of plunger position would then eliminate the trouble.

8-10. Variable-position, Single-screw Tuner.—A very simple and convenient device for low-power impedance tuning in rectangular wave-

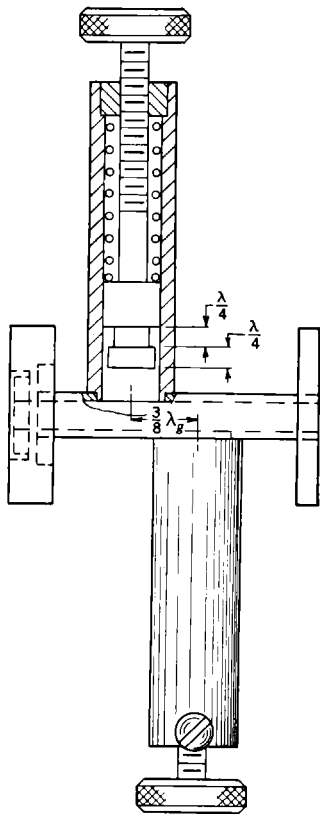


FIG. 8-26 — Double-stub tuner using round-waveguide stubs.

guide is shown in Fig. 8-27. This tuner consists of a small screw projecting through a slot into the center of the wide side of the guide parallel to the electric field in the region of maximum field intensity. Such an obstacle appears in the line as a nearly pure shunt susceptance, capacitive for insertions smaller than about one-quarter wavelength in free space and inductive for insertions greater than this resonant length. At the resonant length the susceptance is nearly infinite.

The normalized admittance at the screw, when the tuner is followed by a matched line, is $1 + jb$ for insertions less than the resonant length, where b is the shunt capacitive susceptance relative to the characteristic admittance of the line. The magnitude of this admittance is $\sqrt{1 + b^2}$ which can have any value from unity to very large values. If the slot

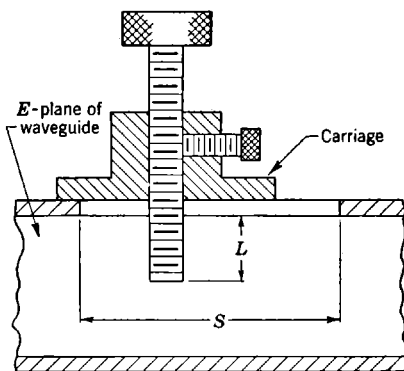


FIG. 8-27.—Single-screw tuner.

is of such a length that the position of the screw can be varied by at least one-half the guide wavelength, this admittance is obtainable in all possible phases. Conversely, an admittance of any magnitude and phase can be tuned to unity, or matched, by adjusting the tuner in such a way that its reflection just cancels that from the admittance to be tuned.

In terms of the quantities actually observed in an impedance or admittance measurement, it is possible with this tuner to introduce a reflection of any phase or magnitude (standing-wave ratio). The reflection coefficient is a useful concept to use in a discussion of impedance tuning since the standing-wave voltage ratio and the phase of the reflection coefficient are the quantities usually measured and those that uniquely determine the impedance at a given reference plane in the waveguide. The actual value of the normalized impedance associated with a given reflection is easily obtained by the use of a Smith impedance chart (see Sec. 2-11) by plotting the voltage standing-wave ratio and the electrical distance (the phase angle of the reflection coefficient) from

a voltage maximum (or minimum for the admittance) to the desired reference plane. Since many waveguide tuners involve elements that behave as shunt susceptances, reference to a Smith chart in this discussion will usually imply its use as an admittance plot.

The statement that a screw inserted parallel to the electric field appears as a shunt capacitance can now be clarified by reference to such an admittance plot. If the admittance obtained from measurements of the standing-wave ratio and distance, in guide wavelengths, from a minimum to the plane of the screw is plotted as a function of depth of insertion of the screw, for a given wavelength, the plot will lie along the circle of unity conductance on the upper half (positive-susceptance side) of the Smith-chart admittance diagram. This behavior is characteristic of screws with diameters small compared with a guide wavelength except when the standing-wave ratio is large (that is, for large screw insertions) and losses in the tuner become appreciable and result in a change in conductance.

As the screw approaches a free-space quarter-wavelength insertion it becomes resonant and presents a nearly infinite shunt admittance or a nearly infinite reflection limited only by losses in the tuner. Thus, since the insertion can be adjusted for nearly any magnitude of reflection and this reflection presented in any phase by varying the position of the screw along the line, nearly any admittance can be presented or matched with this device.

Practically, of course, this tuner is limited in the magnitude of the admittance that it can tune by the fact that the adjustment becomes very critical for large insertions of the screw. As the screw approaches a quarter-wavelength insertion the rate of increase in reflection with insertion increases very rapidly. Furthermore, losses, not only in the screw itself but in the power coupled out of the slot by the screw, become appreciable for large insertions, and therefore the contact between the screw carriage and the waveguide becomes important. This effect makes it difficult to obtain or reproduce the desired phase of a large reflection by adjusting the position of the tuner. Figure 8-28 shows an improved design for a single-screw tuner in which a folded half-wavelength coaxial choke section is used to create a low impedance in the region of contact between the screw holder and the surface of the waveguide and, thereby, to minimize the effect of variations in contact as the carriage is moved along the guide. This design has been found to be advantageous for accurate work even when the reflections to be tuned are comparatively small (VSWR of 1.2 or less, for example). When it is desired to achieve the degree of match represented by a standing-wave voltage ratio of less than 1.01, contact effects can greatly hamper the facility of adjustment and reproducibility of results.

Impedance tuning of this type is ideally suited to impedance measurements in microwave systems, since these measurements are most frequently made in terms of the magnitude and phase of a reflection. The variable-position single-screw tuner offers a means of adjusting these two quantities in a relatively independent manner. The magnitude of the reflection from the screw is completely independent of the phase; that is, it depends only upon the insertion and does not vary with changes in position of the tuner. However, it is evident from the Smith-chart admittance plot of a variable shunt susceptance that the phase of the reflection is approximately independent of the magnitude only for small values of susceptance along the circle of unity conductance. For a

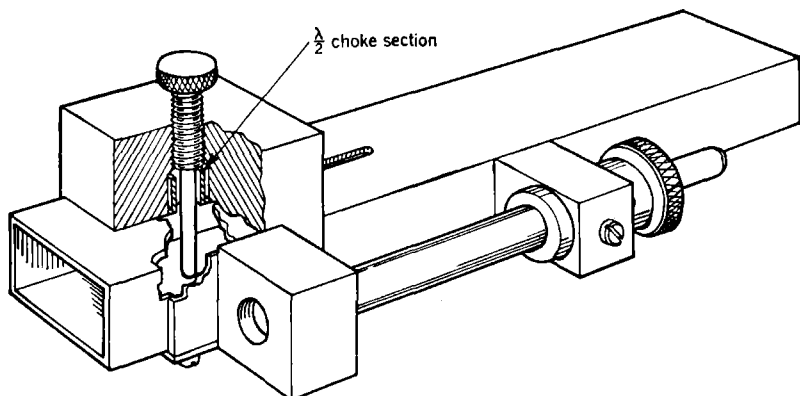


FIG. 8-28.—Sliding-screw tuner.

fixed position of the screw the rate of change of the reflection phase angle with insertion is small for insertions and increases with the insertion. As the insertion increases from zero to a quarter wavelength, the phase of reflection changes by an eighth guide wavelength—a change of 90° in the phase angle of the reflection coefficient.

The fact that these two parameters are approximately independent, for small standing waves, makes this method of tuning quite convenient for impedance measurements of certain kinds. For example, the reflection from a small mismatch frequently has a negligible variation in magnitude over a fairly broad wavelength band. Such a mismatch, tuned out at one wavelength by means of the screw tuner, can then be tuned quickly at other wavelengths by a single adjustment of the position of the screw along the guide.

The use of the sliding-screw tuner is not limited by the wavelength range over which it is desired to tune impedances except in so far as the waveguide itself is limited. If the slot length S (Fig. 8-27) is sufficiently large to allow a variation in the position of the screw of one-half a guide

wavelength for the longest wavelength to be used, then all phases of reflection are possible at any wavelength. If the screw length is long enough to permit an insertion L equal to one-quarter wavelength in free space at the longest wavelength, then reflections of any magnitude are possible within the limitations set by losses in the tuner at large insertions. Because of its simplicity and versatility, the single-screw tuner has been used almost exclusively in low-level impedance measurements of waveguide components. Since there is seldom need to tune extremely large standing waves with great accuracy, this tuner is entirely adequate for most applications.

8-11. Single-slug Tuner.—Probably the most stringent limitation on the application of the single-screw tuner to waveguide lines is that of its

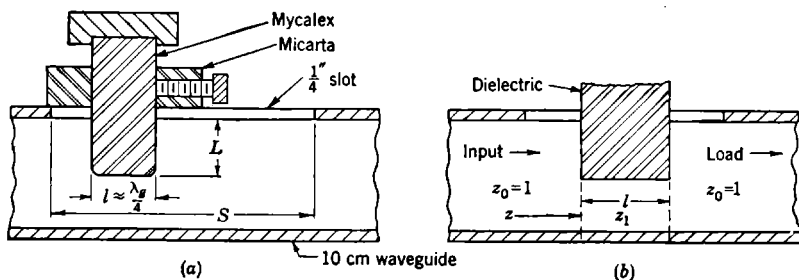


FIG. 8-29.—High-power single-slug tuner.

low power-handling capacity. The slot must be made comparatively narrow in order to minimize leakage and reflections, and the screw must be, accordingly, of small diameter. In order to maximize the tuning range, however, the screw must be inserted in the region of maximum field strength, or at the center of the guide. For these reasons there are always high field intensities at the screw, and the use of this tuner is therefore usually limited to the test bench or to low-power systems where only small standing waves are to be tuned.

A similar tuner, in which a thin slab of dielectric replaces the screw, has been used successfully at high powers and for standing-wave ratios of two or three in voltage. This tuner, shown in Fig. 8-29a, is often referred to as a "single-slug" tuner.

The effect of such an element in a transmission line may be studied by considering the element to be a series section of line of variable characteristic impedance which may also be varied in position. If the characteristic impedance of the waveguide is taken as unity as indicated in Fig. 8-29b, and if z_1 is the normalized characteristic impedance of the waveguide in the region of the dielectric, then the normalized input impedance at the slug is (assuming a lossless line, or real z_1)

$$z = z_1 \left(\frac{1 + jz_1 \tan \beta l}{z_1 + j \tan \beta l} \right), \quad (5)$$

where $\beta = 2\pi/\lambda g$, and λg is the guide wavelength in the region of the dielectric. For a thin slug this wavelength is found to be very nearly the usual guide wavelength; the experimental determination of the wavelength will be described later. Equation (5) also assumes negligible discontinuity capacitances at each end of the dielectric strip. This is a good approximation for strips having a thickness small compared with the width of the waveguide. From Eq. (5) it is seen that the reflection coefficient appearing on the input side of the slug is

$$\Gamma = \frac{z - 1}{z + 1} = \frac{j(z_1^2 - 1)}{\frac{2z_1}{\tan \beta l} + j(z_1^2 + 1)}, \quad (6)$$

and its magnitude is

$$|\Gamma| = \frac{(z_1^2 - 1)}{\left[\frac{4z_1^2}{\tan^2 \beta l} + (z_1^2 + 1)^2 \right]^{1/2}}$$

The quantity $|\Gamma|$, considered as a function of l , has its maximum value when the first term in the denominator vanishes, or when $\beta l = \pi/2$ or $l = \lambda_g/4$. This gives

$$|\Gamma|_{\max} = \frac{z_1^2 - 1}{z_1^2 + 1}.$$

Then, for a length l equivalent to a quarter of a guide wavelength, the standing-wave voltage ratio is

$$r = \frac{1 + |\Gamma|_{\max}}{1 - |\Gamma|_{\max}} = z_1^2 \quad (7)$$

and depends only on the insertion, if z_1 is real. It should be noted that if r is defined as always greater than unity then $r = 1/z_1^2$, if z_1 is less than one. Furthermore, it is seen from Eq. (6) that if z_1 is real and l is an equivalent quarter wavelength the reflection coefficient is real and depends only on z_1 , which means that the phase of the reflection is independent of the magnitude. This holds for all insertions, within the approximations that z_1 is real and that λ_g in the region of the dielectric does not vary appreciably with insertion. This slug tuner differs from the single-screw tuner in that the phase of reflection from the screw is not independent of the insertion for large reflections.

From Eq. (5) it is seen that, as l approaches an equivalent half wavelength in guide, the normalized input impedance approaches unity and there is no reflection. This suggests a simple method for determining equivalent electrical lengths in the region of the dielectric. A

strip of the dielectric to be used is inserted in the guide and its length trimmed until a minimum reflection is measured. This length is an equivalent half wavelength and, to a good approximation, half this length is an equivalent quarter wavelength. These electrical lengths are, of course, functions of the wavelength.

For the Mycalex¹ dielectric used in the high-power tuner shown in Fig. 8-29a, these lengths were found to be very nearly the usual values for waveguide without the dielectric. Mycalex, a fused mixture of powdered mica and soft glass, is used because of its good high-voltage properties, low loss, and high dielectric constant that makes it possible to obtain sizable reflections from strips necessarily limited in thickness by the slot width. For example, a quarter-wavelength strip of $\frac{3}{16}$ -in. thickness produces a standing-wave voltage ratio of about 4 for full insertion at 10-cm wavelengths. In experimental work the slugs can be coated with ignition sealing compound² which serves both to improve the high-voltage breakdown characteristics and to lubricate the transverse motion of the slug in its Micarta carriage.

It is difficult to give an unambiguous statement of the power rating of such a tuner. Breakdown phenomena are erratic and the factors affecting them are not well understood. This is particularly true for pulsed operation in which transient effects and the multiple harmonics produced by some oscillators contribute to the general confusion of results. The power rating of the tuner just described depends, among other things, upon the insertion required to introduce a given reflection and this, in turn, depends upon the wavelength. Furthermore, proper techniques of tuning can increase considerably the useful power limit of the tuner. That is, a tuner that is just "safe" for all phases of a given reflection at a given pulse power may be used at considerably higher powers or larger reflections (insertions) if the insertion is made in small steps, each accompanied by an adjustment in position to determine the proper phase for matching. It will be shown that, if the normalized characteristic impedance in the region of the slug is less than unity, as it is for a low-loss dielectric when the guide is operated in the TE_{10} -mode, the voltage across the line in the region of the tuner is always equal to or less than the voltage across the matched portion of the line. The "voltage across the line" at any point is that relative to the voltage across a matched line, and is calculated from the normalized impedance at the point.

This condition on the voltage holds, if the tuner is properly used, for either of two cases: (1) when the tuner is followed by a matched line and is being used to present a desired input impedance, or (2) when

¹ GE Mycalex 1364 recommended.

² Dow Corning Corp., Ignition Sealing Compound 4.

the tuner is used to tune out a mismatched load impedance that follows it in the line. For matching a load impedance, the tuner is adjusted in such a way that the normalized input impedance of the combination of tuner and load is unity. It will be shown that, for a given power delivered to the load, the voltage across the line in the region of the tuner is never greater than that across a matched line in Case (1) for any position of the tuner; this is also true in Case (2) when the tuner is adjusted to match the load impedance.

This statement can be justified in the following way. For Case (1), in which the tuner is followed by a matched load, the normalized output impedance of the tuner is unity. This is the condition expressed in Eq. (5), which reduces to

$$z = z_1^2$$

for $l = \lambda g/4$, where z is the normalized input impedance and z_1 is the normalized characteristic impedance in the tuner section (see Fig. 8-29a). If z_1 is less than unity, the impedance along the tuner decreases from unity at the output end to z_1^2 at the input end. For a constant power, the voltage across the line decreases from V_0 , the voltage across the matched line at the output end to $V_0 z_1$ at the input end of the tuner section.

For Case (2), in which the tuner is used to match a load impedance different from unity, the general transmission-line equation is

$$z = z_1 \left(\frac{z_R + jz_1 \tan \beta l}{z_1 + jz_R \tan \beta l} \right),$$

where z_R is the normalized impedance at the output end of the tuner and depends on the impedance of the load. The input impedance z is the transformation of z_R through the line of characteristic impedance z_1 and length l . This impedance reduces to

$$z = \frac{z_1^2}{z_R}$$

for $l = \lambda g/4$. If the tuner is adjusted for match, the normalized input impedance is unity or

$$z_R = z_1^2.$$

Then, if z_1 is less than unity, the impedance along the tuner decreases from unity at the input end to $z_R = z_1^2$ at the output end. Similarly the voltage decreases from V_0 to $V_0 z_1$.

It should be remembered that the conditions just described hold in Case (2) only when the tuner is adjusted for match. When the tuner is being used to match another impedance there are possible positions of the tuner where the voltage across the line is considerably greater than

V_0 because of the standing waves. The result obtained indicates the proper method of tuning to be used at high powers. The proper phase for match is determined at small insertions of the tuner by the usual standing-wave-measurement technique. Then, as has been shown for this tuner, the proper insertion may be made without appreciable variation of the phase and the slug will automatically be at a position of lowest voltage.

The voltage across the line mentioned in this discussion may be considered as the voltage that would occur across an empty guide if the same conditions of impedance were established by other means. The actual voltages occurring across the gap between the slug and the opposite side of the guide are, of course, considerably different from the voltage across the line. It seems reasonable, however, to assume that this "gap voltage" is least where the voltage across the line is least. It has been shown that, with proper tuning technique, this gap voltage need never be greater than it is in regions where the voltage across the line is that for the matched condition.

In view of the many factors affecting the power rating of a tuner of this type, it must suffice to give an example of conditions under which these tuners have been used satisfactorily. Both single and double¹ Mycalex-slug tuners have been used in standard 10-cm waveguide to introduce standing-wave ratios up to 2 or 3 in voltage for pulse powers up to 800 kw, with a pulse width of 1 μ sec, and a repetition rate of 400 cps, at atmospheric pressure, and with 10-cm magnetrons of the 4-J series. Methods for estimating extrapolations to other conditions are discussed in Chap. 4.

A slug tuner can, of course, be made with slugs of other dielectrics or of metal. Few other dielectrics, however, have as good high-voltage properties as Mycalex for the same high dielectric constant. Little is gained by the use of dielectrics in a low-power tuner since all dielectric tuners are limited in the maximum amount of reflection obtainable, and are therefore considerably less satisfactory for low-power work than the single-screw tuner. This analysis of the quarter-wavelength-slug tuner, however, suggests that the use of a thin metal slug would result in a low-power tuner having some advantages over the single-screw type. One of the chief advantages would be that a larger reflection would be introduced by a thin metal slug than by a small screw of the same thickness for the same insertion. Conversely, the same reflection could be obtained with less insertion. This effect would make a metal-slug tuner more useful than the single-screw tuner for tuning large reflections since it would be less critical to adjust. Such a tuner, however, has not been developed since it has seldom been necessary to tune large standing

¹ Double-slug tuners are discussed in Sec. 8-12.

waves with great accuracy, and the single-screw tuner has proved adequate for most low-power work.

8-12. Waveguide Double-slug Tuners.—Since a dielectric slug is limited in the amount of reflection that it can introduce, such elements

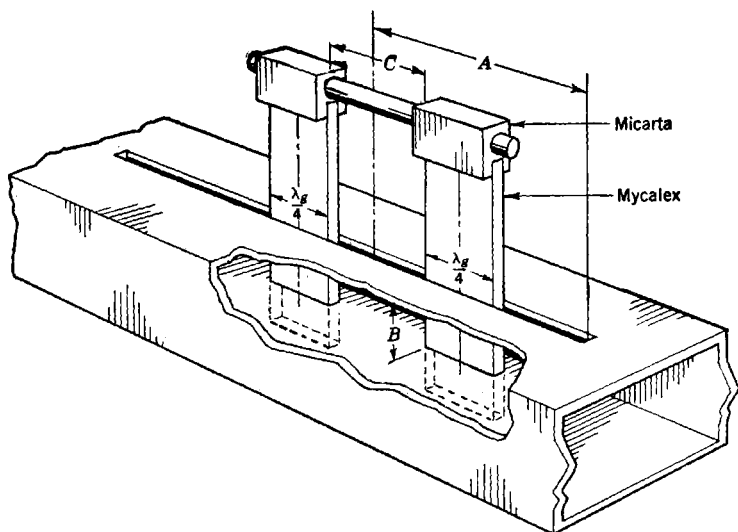


FIG. 8-30.—Mycalex double-slug tuner for waveguide.

may be used in pairs, as shown in Fig. 8-30, to increase the tuning range. The maximum reflection from two slugs $\lambda_g/4$ in length occurs when the

separation C is $\lambda_g/4$ where λ_g is the guide wavelength. The normalized impedances at different points in the tuner section are given in Fig. 8-31. These impedances are obtained by application of the usual transmission-line equation as discussed in Sec. 8-11. If z_1 is the normalized characteristic impedance in the region of the dielectric, then the combination, when followed by a matched line, has an input impedance z_1^4 as

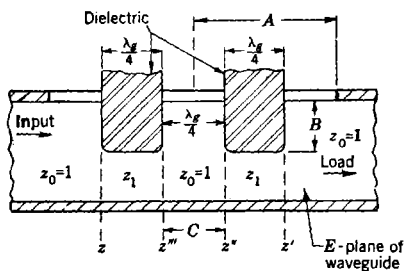


FIG. 8-31.—Normalized impedances in waveguide double-slug tuner. $z' = 1$, $z'' = z_1^2$, $z''' = 1/z_1^2$, $z = z_1^4$.

compared with z_1^2 for a single element.

Tuning is accomplished in either of two ways: (1) by varying the depth of insertion B and the position along the line A of the two slugs together without changing their separation C , or (2) by varying the sepa-

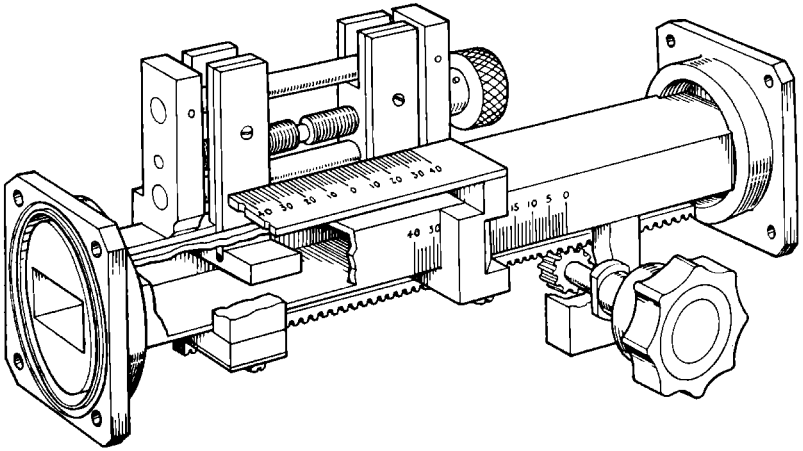
ration of the slugs for a given insertion and varying the position of the tuner. In the first method the variations in the phase and in the magnitude of the reflection are independent, as in the case of the single-slug tuner. It can be shown that, in the second method, if the separation C of the elements O is varied in such a way as to keep the position A of the center of the tuner constant, there is very little change in the phase of the reflection. Since the normalized input impedance of the tuner followed by a matched line is unity for a separation of the slugs equal to zero or an integral number of half wavelengths in the guide, impedances varying from unity to z_1^4 are obtainable by this method for a given depth of insertion. The impedance z_1 , of course, depends upon the insertion. It is usually more convenient mechanically, with a tuner of this type, to use the first method of tuning. The additional adjustment on the separation of the slugs, however, is of advantage when the tuner is used over a wide wavelength band. This adjustment may be used to maximize the reflection obtainable with a given insertion at different wavelengths.

The power rating of a single Mycalex-slug tuner was discussed in the previous section. The double-slug tuner may be used at slightly higher pulse powers than the single-slug tuner for the same standing-wave ratio because the double-slug type requires less insertion for the same magnitude of reflection. As has been shown, the maximum standing-wave voltage ratio obtainable is equal to $1/z_1^4$ for the double-slug tuner, as compared with $1/z_1^2$ for the single-slug type, where z_1 is the normalized impedance for a given insertion in the region of the dielectric and the standing-wave ratio is defined as greater than unity.

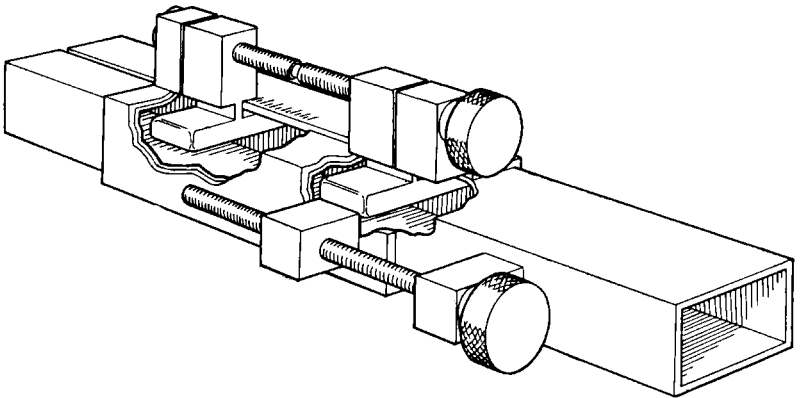
The advantage, however, is not so great as might be expected from the difference in the insertion required for a given reflection. This statement may be justified qualitatively for the double-slug tuner as follows. If the normalized characteristic impedance z_1 in Fig. 8-31 is less than unity, then for a quarter-wavelength separation the output end of the first slug is at the position of an impedance maximum (and, therefore, a voltage maximum) because of the reflection from the second slug. At this point the voltage across the line, as defined in the last section, is V_0/z_1 which is greater than V_0 , the voltage across the matched line. Thus the voltage across the line is not equal to or less than V_0 everywhere in this tuner as it was shown to be for the single-slug tuner. However, double-slug tuners of this type using Mycalex slugs have been used at 10-cm wavelengths, at pulse powers up to nearly a megawatt, to tune standing-wave voltage ratios of about two under the conditions given in the last section and using the tuning technique described there.

Another form of high-power slug tuner in which the variation in the magnitude of the reflection is obtained by changing the slug separation

is illustrated in Fig. 8-32*a* and *b*. Both dielectric and metal slugs have been used in this design. For most applications the faster motion afforded by the version of Fig. 8-32*b* is preferred. The maximum reflec-



(a)



(b)

FIG. 8-32.—Perspectives of double-slug tuner of type indicated in Fig. 8-33; (a) slow motion; (b) fast motion.

tion occurs when the slugs are separated by a quarter of the guide wavelength. For this condition the standing-wave voltage ratio, by the relations given in the last section, Eq. (7), is

$$r = \frac{1}{z_1^4} = \left(\frac{Z_0}{Z_1} \right)^4,$$

where Z_1 is the characteristic impedance in the region of the slug and Z_0 is the characteristic impedance of the waveguide. The general expression¹ for the impedance of a rectangular waveguide operated in the TE_{10} -mode is

$$Z = \sqrt{\frac{\mu \lambda_g b}{\epsilon \lambda_0 a}}$$

where ϵ and μ are the electric and magnetic inductive capacities, λ_g and λ_0 are the guide and free-space wavelengths, and b and a are the inside guide dimensions as indicated in Fig. 8-33. Then for metal slugs where the thickness of the slug is $b - b'$, the maximum standing-wave voltage ratio is given by

$$r = \left(\frac{Z_0}{Z_1}\right)^4 = \left(\frac{b}{a} \cdot \frac{a}{b'}\right)^4 = \left(\frac{b}{b'}\right)^4.$$

This equation is valid if the slug extends across nearly the full width of the guide, since the guide wavelength is then the same in the tuner as it is elsewhere in the guide. The proper size of metal slug for a desired mismatch is given by this expression. A similar calculation for dielectric slugs is more complicated.

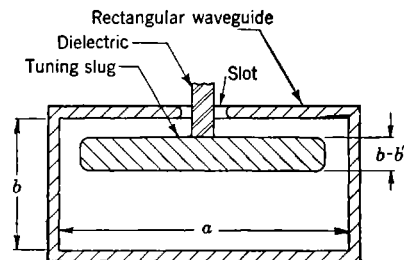


FIG. 8-33.—Dimensions for calculation of impedance of slug tuner.

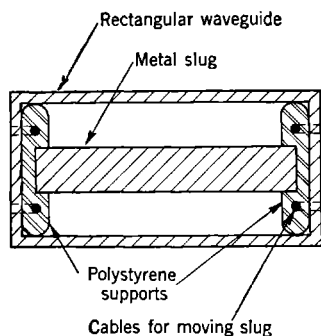


FIG. 8-34.—High-power tuning slug in waveguide.

This simple analysis neglects the discontinuity capacitance at each end of the slug. The neglect of this capacitance is warranted not only because these effects are small even for a slug that fills about one-third of the guide, but also because these effects occur a quarter of a guide wavelength apart for each slug. The reflection caused by the end effect at one end of a slug is of nearly the proper phase to cancel that from the other end.

Dielectric slugs have been used in tuners of this type, but since a dielectric slug must have considerably greater thickness than a metal slug in order to introduce the same reflection, it has no advantage over the metal slug in terms of power-handling capacity. The most satisfactory design for a double-slug tuner for high power is shown in Fig. 8-34. It consists of metal slugs held by polystyrene supports at each side of

¹ J. C. Slater, "Microwave Transmission," McGraw-Hill, New York, 1942, p. 185.

the guide where the field intensities are low. This design eliminates the slot that frequently contributes to breakdown phenomena at high powers.

Motion of the slugs in this design is effected by means of small cables that enter from the side of the guide. Such a tuner has proved to be fairly satisfactory electrically but difficult to construct in such a way as to provide for the proper motion of the slugs. This tuner has, at best, about the same power rating as the Mycalex double-slug tuner previously described which is considerably simpler to construct and use.

8-13. Fixed-position, Capacitive-screw Tuners.—The theory of tuning with fixed-position, variable susceptances is discussed in Sec. 8-6. In particular it can be shown that impedances of all phases and magnitudes can be tuned with various combinations of three or more capacitive screws spaced one-quarter or one-eighth of a guide wavelength apart. Two screws capable of adding infinite susceptance, placed one-eighth of a guide wavelength apart, can, theoretically, tune all possible reflections for which the voltage standing-wave ratio is less than two at the frequency for which their separation is adjusted. At other frequencies the maximum reflection tunable in all phases is less. In addition to this limitation, the double capacitive-screw tuner has the disadvantage that, for certain phases of impedance, tuning a very small mismatch requires large insertions of one or both screws. Furthermore, the tuning is not direct; that is, for many phases of mismatch to be tuned, the resulting standing-wave ratio observed varies in a complicated manner as the screws are inserted. The combined reflection of tuner and mismatch may become considerably larger than that of the mismatch alone as the screws are inserted. Since it is usually desirable to be able to tune a mismatch by observing only the magnitude of the reflection (standing-wave ratio) without regard to its phase, this anomalous variation makes it difficult to find the proper insertions of the screws for match.

More complete tuning is obtained by the use of at least three screws with one-eighth- or one-quarter-wavelength spacing, as shown in Fig. 8-35. Four screws with one-eighth-wavelength spacing are sometimes used. Tuning with such combinations of three or more screws is more direct, for some phases of mismatch, and these tuners are usable over broad wavelength bands. Usually, no more than two of the screws are necessary to tune a given mismatch and, provided that the proper pair is used, tuning can be accomplished with a minimum of insertion. Thus adjustment becomes less critical and the losses in the screws are minimized.

These advantages are largely offset by the problem of determining just what combination of screws will give the most desirable tuning. This problem arises from the fact that with these tuners many imped-

ances are tunable with more than one pair of screws or with a great many different settings of three screws. Moreover, some impedances that can be tuned exactly with one pair of screws can be very nearly tuned with another. The tuning of a given reflection without reference to its phase, therefore, becomes a rather tedious process, and a knowledge of the properties of the tuners is required to determine whether or not a given setting that matches the reflection is the most desirable one. Complicated rules have been developed for tuning with multiple fixed-position susceptances. These rules serve chiefly to indicate that other methods of tuning should be used whenever possible.

There is seldom the necessity to tune large reflections at high powers. At low powers, the single sliding-screw tuner (Sec. 8-10) is almost com-

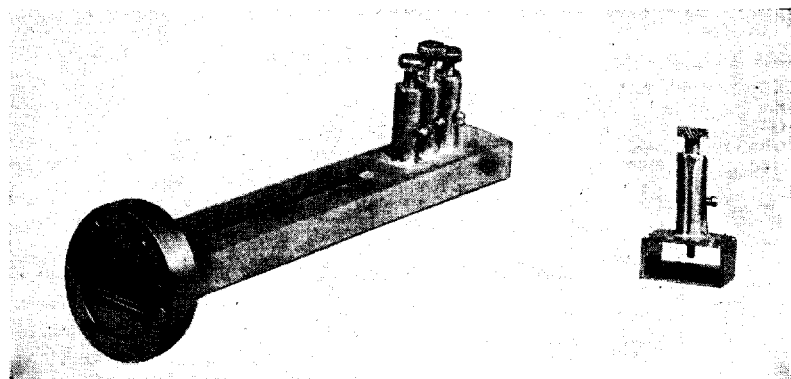


FIG. 8-35.—Waveguide capacitive-screw tuners.

pletely satisfactory for a waveguide tuner and is simple to use. For limited reflections at high powers, the dielectric-slug tuners (Secs. 8-11 and 8-12) or general-susceptance screws next to be discussed (Secs. 8-14 and 8-15) are adequate and considerably less complicated than the capacitive-screw tuners.

8-14. General-susceptance Screws.—The complexity of tuning with fixed-position capacitive screws led to the development of general-susceptance screws, that is, fixed-position screws that are capable of introducing either inductive or capacitive shunt susceptance at very nearly constant phase. A pair of such screws spaced one-eighth of a guide wavelength apart form a tuner that combines many desirable features (although not the range) of the double-stub tuner with the mechanical simplicity of a screw tuner. In addition, a tuner of this type has no slot leakage as have the variable-position waveguide tuners. Furthermore, because larger screws may be used, the depth of insertion for a given reflection is less and the breakdown power is correspondingly

greater than for the sliding-screw or metal-slug tuners. (Secs. 8-10 through 8-12).

The chief limitation of general-susceptance screw tuners is that the amount of inductive susceptance obtainable even with a large screw is comparatively small. Thus the maximum reflection tunable in all phases is limited if no more than two screws are to be used. The use of more than two tuning screws is undesirable because of the added complexity of tuning discussed in Secs. 8-6 and 8-13. There is, however, wide application for a simple and accurate impedance-tuning device which can match all phases of a limited reflection over a 15 or 20 per cent band, which has negligible r-f leakage, and which can handle appreciable power.

A simple and convenient device for obtaining, with a single screw, a susceptance that can be made either capacitive or slightly inductive and that is variable both in phase and in magnitude has been developed at the Bell Telephone Laboratories.¹ This tuner consists of a large-

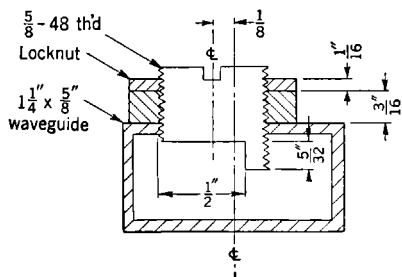


FIG. 8-36.—Single asymmetrical screw for 3-cm band.

diameter screw offset from the center of the guide and having a small projection beyond the end of the screw as shown in Fig. 8-36. If the screw is effectively one-quarter of a guide wavelength in diameter, this projection behaves as a lumped capacitive susceptance which "scans" through one-quarter wavelength in phase and changes gradually in magnitude with rotation of the screw. If this device is followed by a matched line, the shunt admittance at some fixed reference plane on the input side will appear to vary from a pure capacitive susceptance to a pure inductive susceptance of nearly the same magnitude if the pitch of the screw thread is sufficiently small. The admittance as a function of insertion of the screw shown in Fig. 8-36, at a wavelength of 3.33 cm, is plotted in Fig. 8-37. The conjugates of these admittances may be matched with this tuner.

A tuner of this design has the appreciable advantage of providing approximate tuning over a limited range of impedances with a single control. Such simplification is seldom a step in the wrong direction. This tuner has certain properties, however, that should be noted in connection with experimental applications. The exactness with which an arbitrary impedance may be tuned is determined by the change in the

¹ P. H. Smith, "The Asymmetrical Waveguide Tuning Plug," BTL Report, MM 44-170-59, Dec. 8, 1944.

magnitude of the reflection introduced between scans. This change, of course, depends upon the pitch of the screw thread, which, in turn, is limited by the diameter of the screw. The diameter of the screw is a function of the wavelength, since it must be effectively equal to a quarter wavelength, and it is limited by the size of the guide. Furthermore, it may be seen from Fig. 8-37 that successive scans of the imped-

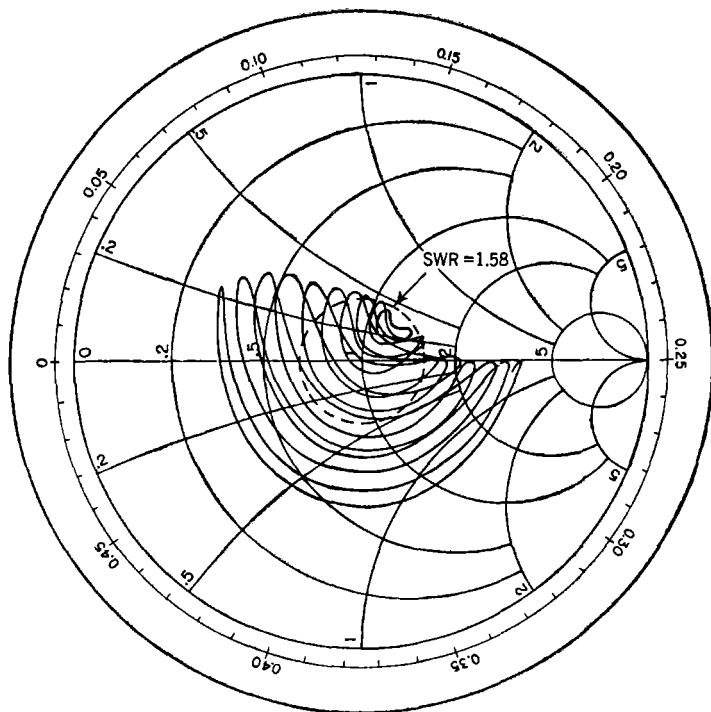


FIG. 8-37.—Admittance of asymmetrical screw shown in Fig. 8-36; variation with screw rotation.

ance phase are usually not adjacent curves in terms of the magnitude of reflection introduced. This effect is to be expected since the projection on the screw moves transversely as well as longitudinally in the guide with rotation of the screw. Thus on alternate half turns of the screw, the projection is near the side of the guide, where the reflection is considerably less than that occurring when it is near the center. Finally, the shunt susceptance of the rest of the screw is superimposed on the admittance of the projection. Since the former is fixed while the latter varies in phase by approximately plus or minus one-eighth wavelength

from the center of the screw, the phase angle between the reflections from each of these sources varies from 0 to $\pm 90^\circ$, approximately.

Because of all these effects, the standing-wave ratio observed in tuning a mismatch is a complicated function of the insertion. In tuning without reference to the phase of the mismatch, it is not always readily evident that an improvement is being effected or that a given minimum reflection is the best possible match that may be obtained. If properly used, however, this tuner is capable of matching an admittance of any phase within the circle indicated (VSWR of 1.4 or less) to a standing-wave voltage ratio of 1.2 or less; for some phases considerably larger reflections may be matched to the same degree.

Another method of obtaining capacitive and inductive susceptance with a single screw utilizes the fact that, just as a screw projecting into

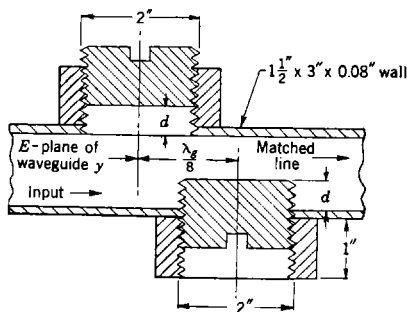


FIG. 8-38.—Double-screw tuner for 10-cm wavelength.

the guide parallel to the electric field appears as a shunt capacitive susceptance, so the same screw retracted into its boss, leaving a cavity, behaves somewhat as a lumped inductive susceptance that varies with the length of the cylindrical cavity so obtained. A tuner for mismatches corresponding to a standing-wave voltage ratio of about 1.15, which uses two such screws 1 in. in diameter, spaced one-eighth of a guide wavelength apart, is described in Sec. 6-8. This tuner is used to provide a small adjustment on the admittance of a broadband matching iris in the waveguide sections of a transition from coaxial line to waveguide. A greater maximum inductive susceptance may be obtained by the use of screws of larger diameter (2 in.) as shown in Fig. 8-38. An admittance plot for this tuner is shown in Fig. 8-39. The admittance at the center of the input screw is plotted for each screw separately; that is, one screw is varied with the other set flush with the inside of the guide. It is found that there is little interaction between the screws when both are used simultaneously even for fairly large insertions and for screw diameters considerably greater than $\lambda_g/8$. Consequently, the

admittances that can be produced are obtained by combining the admittances of the two screws. For example, the admittance represented by point A in Fig. 8-39 is obtained with an insertion of slightly less than 0.05 in. of the input screw and a retraction of 0.40 in. of the output screw.

It is seen from Fig. 8-39 that the variation of admittance with retraction of the screw departs appreciably from the circle of unity conductance.

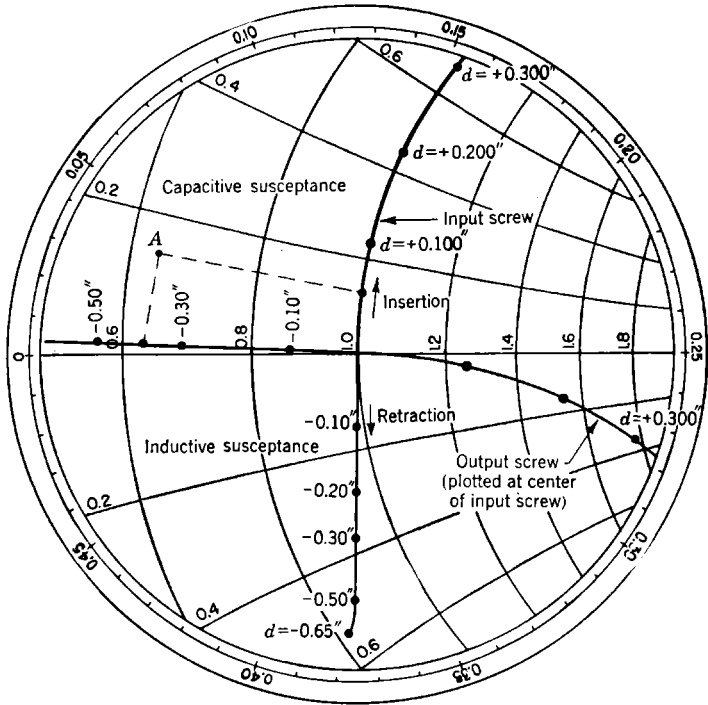


FIG. 8-39.—Admittance as a function of screw setting for two 2-in. diameter general-susceptance screws.

ance on which the plot of a pure shunt inductive susceptance should fall. It will be shown later that, provided this deviation is not too great, it is somewhat advantageous. This effect can increase the maximum reflection that can be tuned in all phases by a pair of these screws at a given wavelength, or can increase the wavelength range over which a given reflection can be tuned in all phases for a fixed screw separation. The factors determining the proper size and spacing of screws for optimum broadband tuning will be discussed here and in the next section in so far

as they have been investigated experimentally in the development of a double-screw tuner for 10-cm waveguide.

A screw inserted in the center of the guide, parallel to the electric field, gives nearly an infinite shunt capacitive susceptance for an insertion of a free-space quarter wavelength only if the screw diameter is small compared with the guide wavelength. As discussed in Sec. 8-10, however, a screw of this type requires considerable insertion to produce

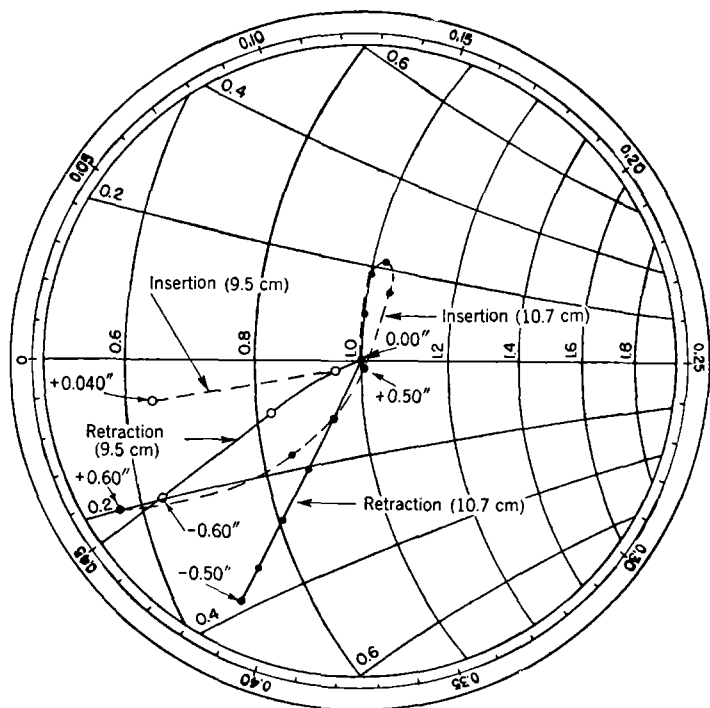


FIG. 8-40.—Admittance as a function of screw setting at 9.5 and 10.7 cm for $2\frac{1}{2}$ -in. diameter general-susceptance screw.

a usable effect and, consequently, has a low power-handling capacity. It is desirable to obtain a given susceptance with a minimum insertion, which is done by increasing the diameter of the screw. This limits the maximum susceptance obtainable, however, and if the screw is too large the resulting plot of admittance as a function of insertion is quite different from a simple variation in shunt susceptance. This effect is to be expected, since a sufficiently large screw will behave as a length of line having a characteristic impedance and guide wavelength that vary with the insertion of the screw. At some insertion the screw may appear as

a half-wavelength section of line and give no reflection. Such an effect is shown in Fig. 8-40 which is a plot of admittance as a function of screw setting for a 2.5-in. diameter screw. This screw provides very little capacitive susceptance at 10.7 cm and none at 9.5 cm. Furthermore, the plots for both inductive and capacitive settings of the screw appear to be anything but a simple variation in shunt susceptance.

As expected, the effect for a given screw size is more pronounced at short wavelengths. Figure 8-41 is a plot at various wavelengths of standing-wave voltage ratio as a function of insertion for a screw 2 in.

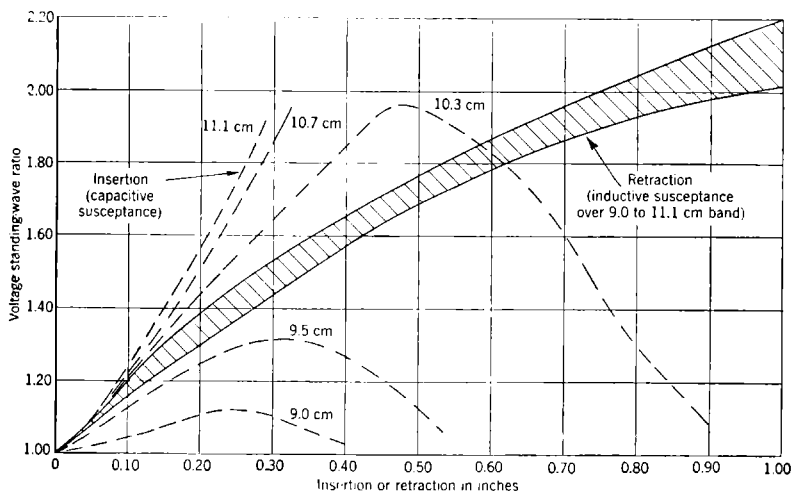


FIG. 8-41.—Voltage standing-wave ratio as a function of screw setting for 2-in. diameter screw at different wavelengths.

in diameter. A similar result, although one not so pronounced, is obtained with a 1.5-in. screw in the 8- to 11-cm region. A 1-in. diameter screw, however, is found to be quite satisfactory over this wavelength range for standing-wave ratios up to 3 in voltage. It shows a comparatively small variation of reflection with frequency for a given insertion as shown in Fig. 8-42. The shaded area represents the spread in curves of standing-wave voltage ratio as a function of insertion at five different wavelengths between 8.1 and 11.1 cm.

Also plotted to the same scale in Fig. 8-42 is the almost negligible inductive susceptance produced by retracting the 1-in. screw into its boss. From this curve it is readily evident that a much larger screw is necessary to provide a usable amount of inductive susceptance. A compound screw of the type shown in Fig. 8-43, Sec. 8-15 is necessary to provide a usable amount of either inductive or capacitive susceptance with the same screw.

Although a larger screw will give a greater inductive susceptance,

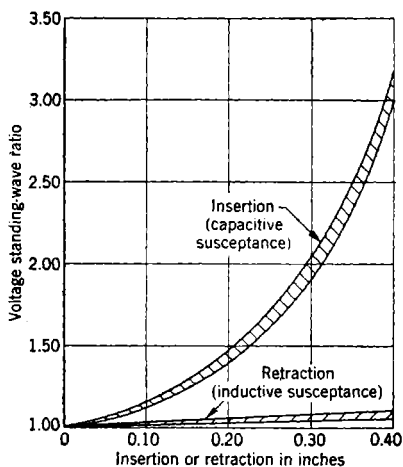


FIG. 8-42.—Voltage standing-wave ratio as a function of screw setting for 1-in. diameter screw in waveguide; spread over 8.1- to 11.1-cm band.

one-eighth guide wavelength apart. Tuning with two screws is least complicated when one screw tunes the conductance component of a given

there are factors that limit the size of screw that can be used over a desired wavelength range. It is shown in Fig. 8-40 that, as the wavelength decreases, the plot of admittance as a function of retraction departs considerably from a purely susceptive variation. Data for different screw diameters indicate that this effect becomes more marked as the ratio of screw diameter to guide wavelength increases. The resulting characteristics are undesirable in two ways. First, they limit the magnitude of inductive susceptance that may be obtained. Second, they affect the "orthogonality" of tuning as shown in Fig.

8-39 for a pair of screws spaced

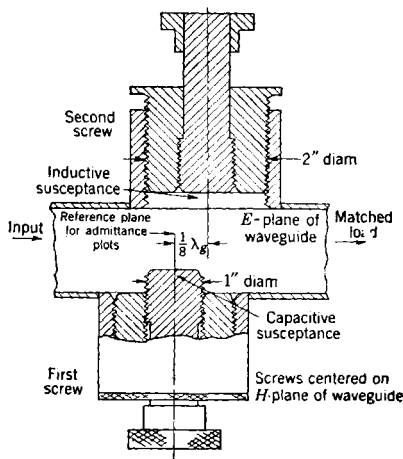


FIG. 8-43.—Tuning screws for adjusting match of transitions.

admittance and the other, the susceptance component. Departures from this characteristic make tuning without reference to the phase of the

mismatch a more complicated procedure as in the case of the capacitive screws discussed in Secs. 8-6 and 8-13.

This effect on the admittance as a function of retraction for the inductive screw is to be expected. In large-diameter cavities at sufficiently short wavelengths, appreciable propagation of the lowest round-waveguide or TE_{11} -mode is possible. In this case the discontinuity becomes a short-circuited section of line of small but finite length which appears in the waveguide as a series reactance as well as a shunt susceptance. Since the whole effect is distributed over a large fraction of a guide wavelength it can hardly be treated as a single lumped susceptance. Experimentally, it has been found that the shunt admittance of a retractable screw 2 in. in diameter is very nearly a pure susceptance in the wavelength range 9 to 11 cm. This result is shown in Fig. 8-41. A screw of this size has been used successfully in a double-screw tuner for standing waves up to 2 in voltage over this wavelength range.

All effects described here probably can be analyzed and the optimum screw sizes calculated for a desired tuning range from the theory of waveguide discontinuities. In the interest of obtaining quickly the design for a useful tuner, however, the theory is left for more leisurely application.

8-15. A Waveguide Double-screw Tuner.—As discussed in the last section it is possible to tune a limited reflection in all phases by use of two general-susceptance tuning screws centered in the wide side of the guide. Such a tuner for 10 cm using the compound screws described in Sec. 8-14 is shown in Fig. 8-43. A plot of admittance as a function of setting of each screw separately would be similar to that shown in Fig. 8-39 where the admittance is referred to the plane of the input screw. The tuner is followed by a matched load. The compound screws will give a greater susceptance variation over a wide band than may be obtained with the simple screw tuner whose tuning is illustrated in Fig. 8-39. The relative sizes of the inductive and capacitive section of the compound screw were determined experimentally for the 9- to 11-cm band as described in the last section. It remains to discuss the tuning range, over a broad wavelength band, of a pair of these compound screws with a fixed separation, that is, one-eighth guide wavelength for only one wavelength in the band. The best separation for maximum tuning range over a given band may also be determined.

In Sec. 8-6 it was shown that two susceptive elements capable of adding infinite inductive and capacitive shunt susceptance and which are spaced an eighth wavelength along a transmission line can tune reflections of any phase for which the standing-wave voltage ratio is no larger than two. That is, all admittances except those lying within the circle of normalized conductance 2 on a Smith chart may be presented

or their conjugates matched with such a tuner. This condition holds theoretically only for the wavelength at which the tuning elements are an eighth of the line wavelength apart. At other wavelengths the maximum reflection that may be tuned in *all* phases is smaller than that for which the standing-wave ratio is 2 in voltage.

Very nearly the same result is obtained with general-susceptance screws that introduce only limited inductive and capacitive suscept-

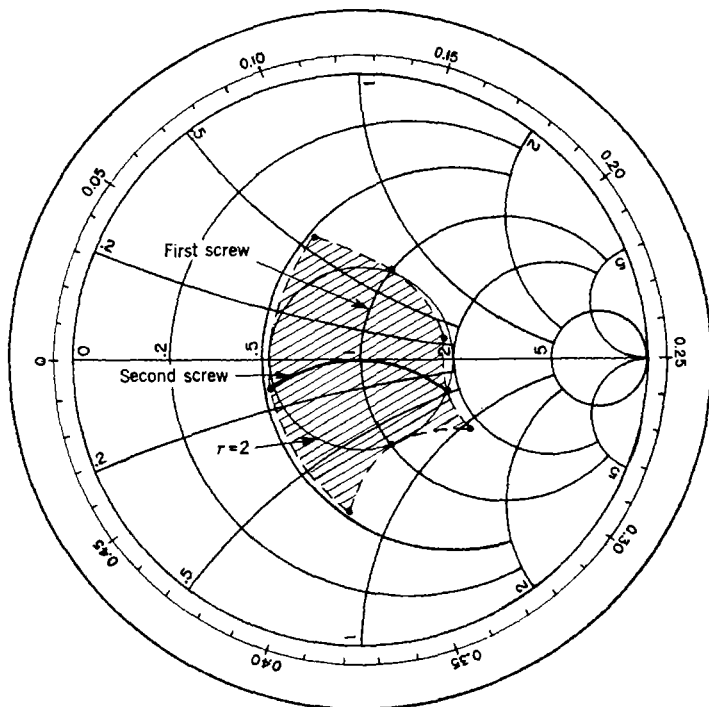


FIG. 8-44.—Theoretical tuning range at midband of double-screw tuner with $\lambda_0/8$ spacing; admittance plotted at input screw.

ances. Figure 8-44 is a plot of the theoretical tuning range of two screws with $\lambda_0/8$ spacing which can introduce ± 0.7 unit of susceptance. Much larger capacitive susceptances are obtainable with actual screws but this 0.7 unit of inductive susceptance is about the limit that can be obtained with a 2-in. diameter screw at 10 cm. As indicated in Fig. 8-43, the admittance is referred to the center of the first or input screw and the device is assumed to be followed by a matched load. The conjugates of all admittances within the shaded area may be matched with such a tuner at the wavelength for which the separation is $\lambda_0/8$. The

maximum reflection that may be tuned in all phases is that represented by a standing-wave voltage ratio of about 1.9.

Assuming that the screws can add the same maximum susceptance at all wavelengths in a given band, the tuning range over the band may be predicted as shown in Fig. 8-45. This plot shows the tunable regions of admittance at 9.0 cm (broken curve) and at 11.0 cm (solid curve)

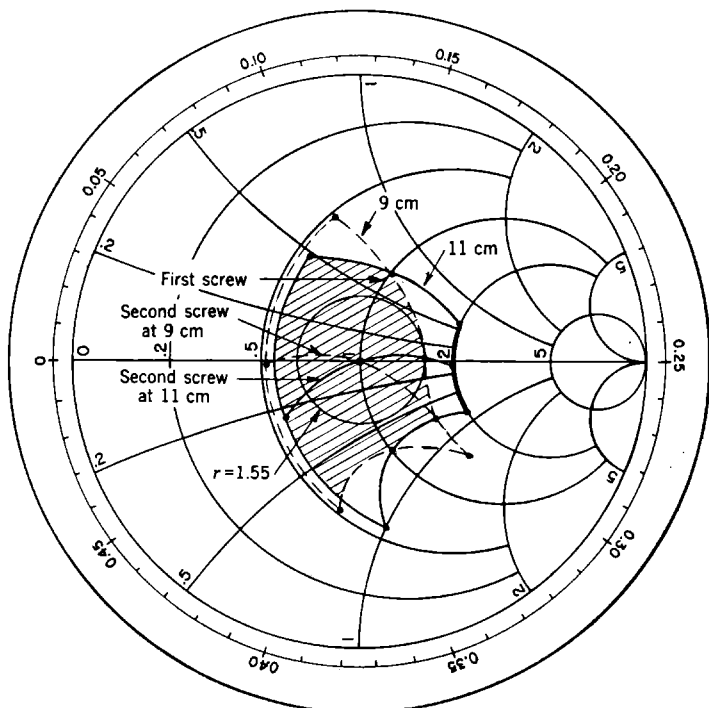


FIG. 8-45.—Theoretical tuning at 9 and 11 cm of double-screw tuner with $\lambda_g/8$ spacing at 10 cm; admittance plotted at input screw.

of a tuner for which the screw separation is $\lambda_g/8$ at 10 cm. Only the region enclosed by both curves is tunable over this 20 per cent band. The maximum reflection that can be tuned in all phases over the band is that for which the standing-wave voltage ratio is 1.55. It is limited by the range of the tuner at 9.0 cm. This effect suggests that the proper spacing for maximum tuning over the band should be $\lambda_g/8$ not at mid-band (10 cm) but at a shorter wavelength. Figure 8-46 shows the effect of using a screw separation that is one-eighth guide wavelength at 9.0 cm. The maximum reflection tunable in all phases over the band is now that for which the standing-wave ratio is 1.75 in voltage. It is limited on

the low-conductance side of the plot by the range of the tuner at 11.0 cm, therefore, the best spacing appears to be one-eighth guide wavelength at a somewhat longer wavelength than 9.0 cm. Usually, the exact spacing for a maximum tuning range over a given band will depend upon the bandwidth and the guide wavelengths involved.

A comparison of the tuning ranges at 9 and 11 cm for the two different spacings of Figs. 8-45 and 8-46 shows, however, that the range of

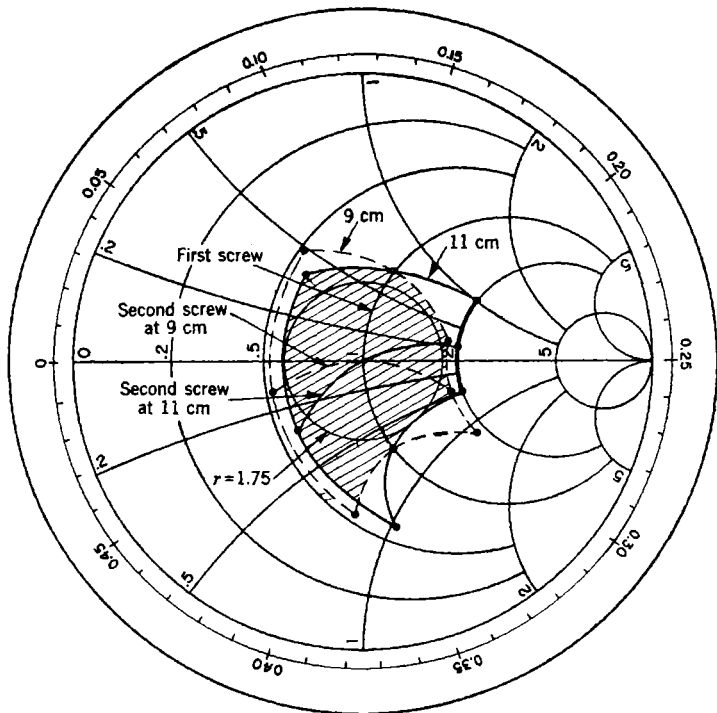


FIG. 8-46.— Theoretical tuning at 9 and 11 cm of double-screw tuner with $\lambda_g/8$ spacing at 9 cm; admittance plotted at input screw.

tuning at 11 cm is considerably less affected by changes in screw spacing than that at 9 cm; hence, little improvement is effected by increasing the separation from $\lambda_g/8$ at 9 cm. Thus, to a very good approximation the spacing required for a maximum tuning range over a given band is an eighth wavelength for the shortest wavelength at which tuning is desired.

Except at the shortest wavelengths the experimental results obtained with actual tuners show somewhat better coverage than that predicted in the preceding analysis. The compound screws described here can add very large capacitive susceptances, but the maximum inductive

susceptance obtainable is about that assumed in the previous discussion. The shunt admittance added by these screws in a retracted position, however, is not a pure inductive susceptance. The plot of admittance as a function of screw setting at a given wavelength departs from the curve of unity conductance, as shown in Fig. 8-39, in such a way that it increases the maximum reflection that may be tuned in all phases.

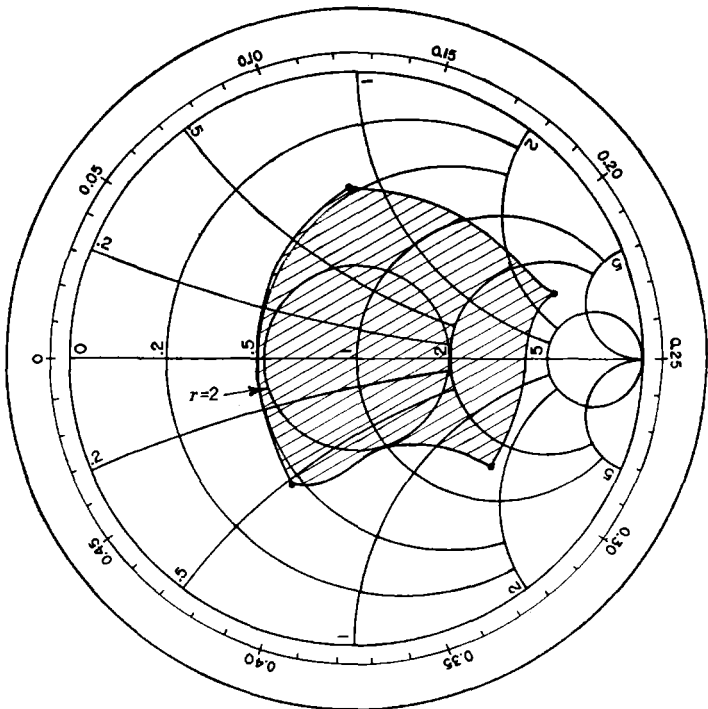


FIG. 8-47.—Experimental tuning at 10.3 cm of double-screw tuner with $\lambda_g/8$ spacing at 10.3 cm wavelength; admittance plotted at input screw.

Figure 8-47 is the plot of tuning range for an experimental double-screw tuner of the type described in this section and gives the tuning range at 10.3 cm for a screw spacing that is $\lambda_g/8$ at this wavelength. It is seen that reflections equivalent to a standing-wave voltage ratio of 2 are tunable in all phases, although neither screw can introduce separately more than 0.7 unit of inductive susceptance.

A plot of the same type at 9 cm for a screw spacing of $\lambda_g/8$ at 9 cm is given in Fig. 8-48. Here, the tuning range is limited to reflections in all phases for which the standing-wave ratio is 1.71 or less in voltage. The reasons for this reduced range have not been thoroughly analyzed,

but the effect is probably due to interactions between screws. In the last section several suggestions are given as to why such effects can occur at the shorter wavelengths.

Figure 8-49 shows the tuning range at 11.1 cm of the same tuner ($\lambda_g/8$ spacing between screws at 9.0 cm). This plot demonstrates the conclusion, given in the previous analysis, that the spacing between

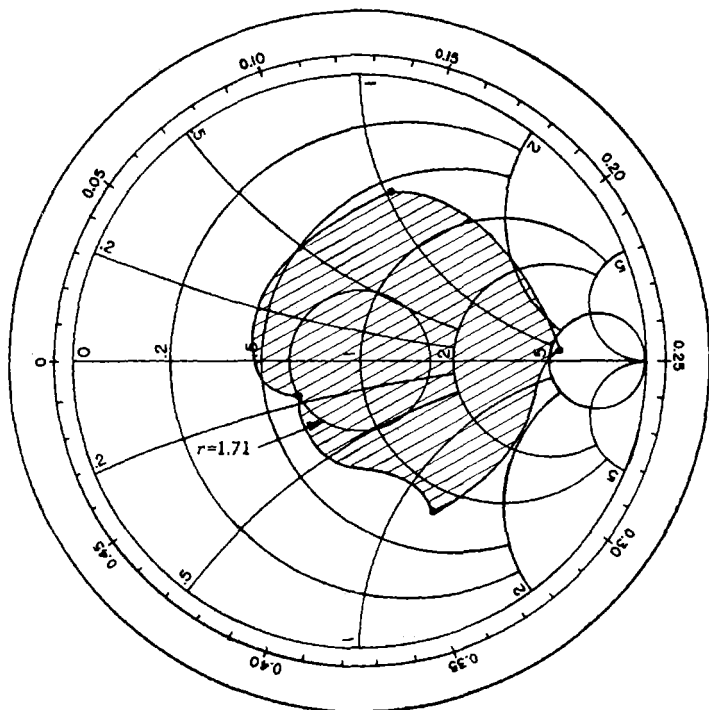


FIG. 8-48.—Experimental tuning at 9 cm of double-screw tuner with $\lambda_g/8$ spacing for 9 cm; admittance plotted at input screw.

screws should, usually, be one-eighth guide wavelength for the shortest wavelength at which the tuner is to be used. For a reasonable bandwidth (about 20 per cent) this spacing allows the maximum of tuning at the shortest wavelength and does not appreciably affect the tuning range at the long-wavelength end of the band which usually is greater than the range at the short-wavelength end. The tuner described here will tune in any phase reflections for which the voltage standing-wave ratio is 2 or less from about 9.5 cm to more than 11.1 cm. For certain phases, very large reflections may be tuned since these screws can introduce very large capacitive susceptance.

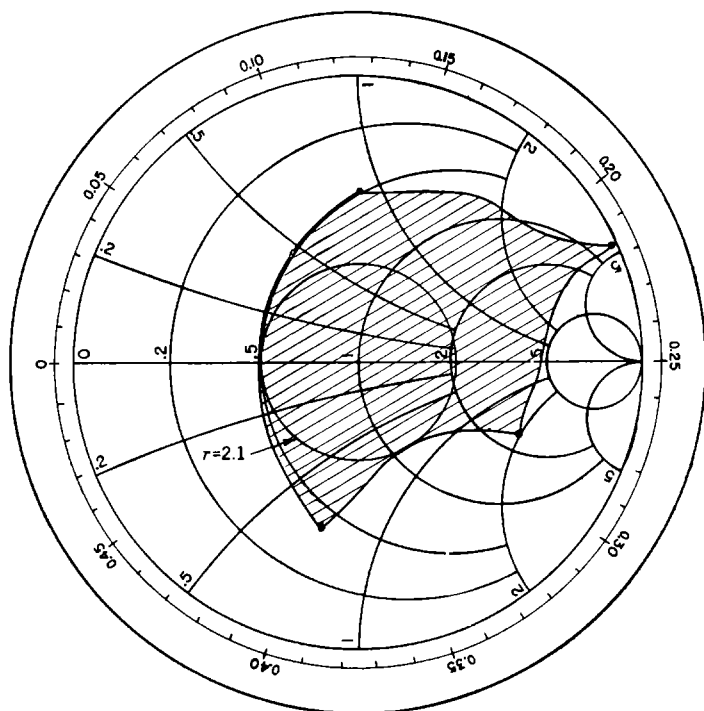


FIG. 8-49.—Experimental tuning at 11.1 cm of double-screw tuner with $\lambda_g/8$ spacing for 9 cm; admittance plotted at input screw.

8-16. Phase Shifters.—The importance of phase shifters in certain applications has been emphasized in Sec. 8-7. Two simple and effective forms of waveguide phase shifters that have found favor are illustrated by Figs. 8-50 and 8-51.

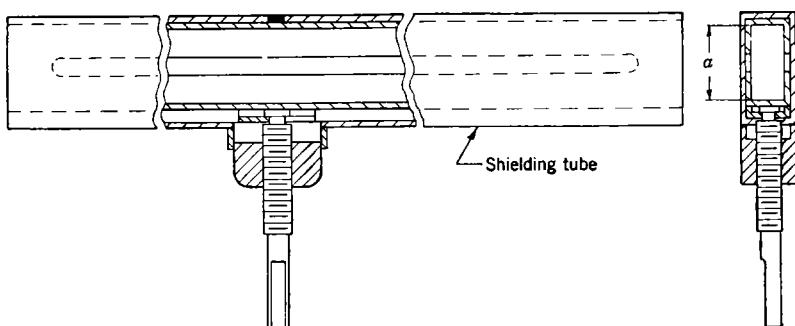


FIG. 8-50.—Slotted-waveguide phase shifter.

These two models operate on entirely different principles. The simpler principle is that underlying the version shown in Fig. 8-50. Long longitudinal slots are cut along the center of the two broad surfaces of a rectangular waveguide, each slot being very similar to those used in connection with standing-wave measurements. Since there are no transverse currents interrupted by these slots, they do not radiate appreciably. If desired, any slight amount of radiation may be suppressed by the outer section of rectangular tubing indicated in Fig. 8-50. When the clamp indicated in the figure is tightened, the larger dimension a of the wave-

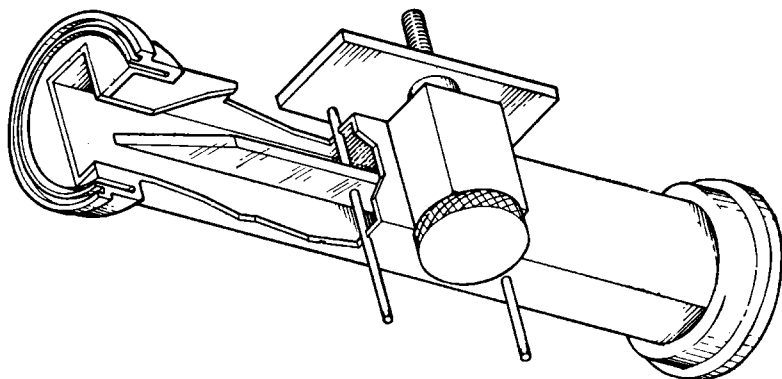


FIG. 8-51.—Dielectric phase shifter.

guide cross section is reduced, resulting in a reduction in the cutoff wavelength and an increase in guide wavelength. The relations are

$$\lambda_c = 2a, \quad (8)$$

$$\lambda_g = \frac{\lambda_0}{\sqrt{1 - \left(\frac{\lambda_0}{\lambda_c}\right)^2}} \quad (9)$$

The change in the dimension a is distributed over a long section of line that functions as an impedance-matching taper. As the guide wavelength is increased, the effective electrical length of the whole waveguide section is decreased, thus effecting a shift in phase.

In the phase shifter of Fig. 8-51, the change in guide wavelength is brought about by moving a long dielectric slab laterally across the interior of the waveguide. The effect on guide wavelength of such a slab has been calculated (Vol. 10) theoretically for the case in which the slab extends all the way from the top to the bottom wall of the waveguide. It seems to be easier to determine experimentally the change in guide wavelength caused by motion of the modified slab indicated in Fig. 8-52. Qualitatively, it is easy to see that the effect of the dielectric should be

much greater when it is in the region of the high electric fields present at the center of the waveguide than when it is in the weak fields near the side walls. The length of the slab must be great enough to give a complete half-wavelength change in equivalent length as the slab is moved from center position to the side wall.

The slab is supported by means of either two or three rods, spaced in such a way that cancelation of reflections is achieved. Two rods of equal diameter spaced three-quarters of a wavelength apart have been used. The wavelength to be used is the effective wavelength for an average position of the slab at the midband frequency. Alternatively, three rods with quarter-wavelength spacing may be used. The center rod should produce twice as much reflection

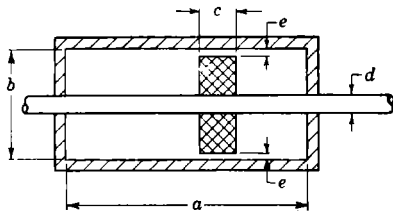


FIG. 8-52.—Section view of dielectric phase shifter.

the central rod should have a diameter $\sqrt{2}$ times that of the others. For small rods, the reflection coefficient is proportional to d^2 , consequently the central rod should have a diameter $\sqrt{2}$ times that of the others.

The ends of the dielectric slab are tapered in the manner indicated in Fig. 8-51, the length of the taper being half a wavelength. The wavelength to be used here is something like the mean between the normal guide wavelength and that in the section containing the slab in an average

position. The double taper shown in Fig. 8-53 was found also to give good results. It was expected that a broader band would result from this arrangement, but its superiority over the single taper has not been established.

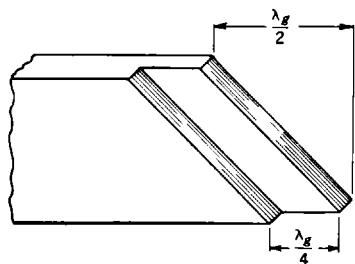


FIG. 8-53.—Double tapered dielectric slab.

The dielectric that has been found to be most satisfactory for the slab material is polystyrene or one of the new materials of high softening temperature and the same dielectric constant

stant. The plastic materials have the advantages of being easy to machine and unlikely to break in use. They have, however, the defect of being likely to suffer permanent damage if a spark is permitted to occur in the vicinity. Materials such as Mycalex, polyglas, or glass of various types are not damaged by sparking, but they are difficult to machine and subject to breakage. It is explained in the next paragraph that there is a maximum permissible thickness of slab which decreases as the dielectric constant

of the slab material is increased. Since glasses in general have high dielectric constants, glass slabs must be made thin; hence, they are fragile. It is possible that either Mycalex or polyglas might offer a good compromise in regard to machinability, ruggedness, and arc resistance.

If the dielectric slab is made too thick, or if the width a of the waveguide is too large, more than one waveguide mode may be propagated. It has been observed that when this situation exists certain positions of the slab lead to a resonant condition. The resonance occurs when the effective length of guide section supporting the higher mode has a critical value of approximately half a wavelength. High values of dissipative loss and high values of input standing-wave voltage ratio result, and voltage breakdown is likely to occur. The waveguide normally used at wavelengths near 1.25 cm is so wide ($a = 0.420$ in.) relative to the wavelengths used that it is subject to this difficulty. In the construction of phase shifters, the width is decreased, by means of a half-wavelength taper, to the value indicated in Table 8-1.

The dimensions and performance characteristics of dielectric phase shifters designed for three wavelength regions are given in Table 8-1.

TABLE 8-1.—DIMENSIONS OF POLYSTYRENE ($k_r = 2.56$) PHASE SHIFTERS
(Wavelength range for $r < 1.10$)

	Symbol and units	Model I $\lambda = 1.23$ to 1.27 cm	Model II $\lambda = 3.13$ to 3.53 cm	Model III $\lambda = 8.5$ to 11.6 cm
Waveguide dimensions.....	a , in.	0.350	0.900	2.840
	b , in.	0.170	0.400	1.340
Slab thickness.....	c , in.	0.075	0.188	0.500
Clearance gap.....	e , in.	0.020	0.044	0.170
Slab length, including tapers.....	in.	2	5	15
Diameter of two rods.....	d , in.	0.030	0.041	0.124
Diameters of central rod, if used..	d , in.	0.042	0.058
Rod spacing.....	in.	0.173	0.470	4.426
Dielectric taper length.....	in.	0.346	0.940	2.050
Breakdown power.....	kw	70	200	1000

POWER DIVIDERS

COAXIAL POWER DIVIDERS

8-17. Fixed Coaxial Power Dividers.—When it is desired to send half the power into each of two loads, a circuit of the type illustrated in Fig. 8-54 may be used. A modification, giving an unequal division of the power, is presented in Fig. 8-56. Several alternative circuits have been devised, but the ones given here have proved to be most satisfactory.

The operation of the circuit of Fig. 8-54 is good over a broad band, as

shown qualitatively by the following analysis. It may be reasoned that the two loads and the stub are effectively in parallel at the junction point. Each of the two loads presents the characteristic admittance Y_0 of the line at the junction point, giving a total load admittance at that point of $2Y_0$. At midband wavelength, the stub length is adjusted to be effectively a quarter wavelength, consequently it adds zero susceptance. The

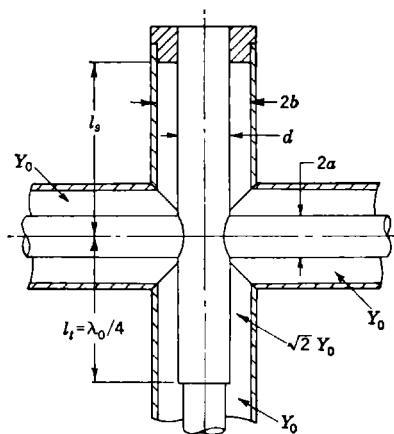


FIG. 8-54.—Power divider for equal division of power.

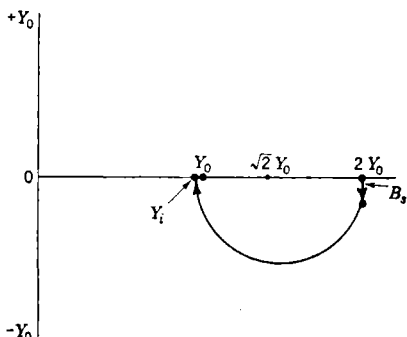


FIG. 8-55.—Admittance transformations in power divider of Fig. 8-54.

enlargement of the conductor of the quarter-wavelength section of the input line, a continuation of the center conductor of the stub, is chosen to give a characteristic admittance $\sqrt{2} Y_0$. This section acts as an admittance transformer, matching the load admittance $2Y_0$ to the characteristic admittance Y_0 of the input line.

At a wavelength longer than the midband wavelength, the stub is too short and adds an inductive (negative) susceptance B_s to the load

admittance $2Y_0$, as indicated in Fig. 8-55. This is desirable, however, since at this wavelength the transformer section is also too short. The combined action of stub and transformer leads to an input admittance Y_i that is very close to Y_0 even at wavelengths longer than the midband wavelength, as indicated in Fig. 8-55. Similarly, for shorter wavelengths, the stub adds a positive susceptance that combines with the transformer, now too long, to give a good match in the input line.

It is easily shown that for small departures from midband wavelength, the susceptance added by the stub is quantitatively equal to that required to produce the compensation indicated in Fig. 8-55. For larger departures from midband wavelength, compensation is no longer exact, but it is still good. The dimensions given in Table 8-2 were found to give a VSWR below 1.1 for the wavelength range 9 to 11 cm. All dimensions

TABLE 8-2.—DIMENSIONS OF POWER DIVIDERS OF FIG. 8-54

Dimension	Standard line size	
	$\frac{5}{8}$ in.	$\frac{7}{8}$ in.
Stub length l_s	1.220	1.107
Conductor diameter d	0.325	0.468
Transformer length l_t	1.110	1.000

except the stub length are calculated according to the simple theory outlined above. The stub length is then adjusted to give minimum input VSWR at midband wavelength.

The principle of operation of the power divider of Fig. 8-56 is similar to that of the model shown in Fig. 8-54. In order to obtain unequal power division, quarter-wavelength transformers are inserted in the two load lines. The characteristic admittances of the transformer sections are chosen to give the admittances Y_1 and Y_2 , satisfying the relations

$$Y_1 + Y_2 = 2Y_0, \quad (10)$$

$$\frac{Y_1}{Y_2} = \frac{P_1}{P_2}. \quad (11)$$

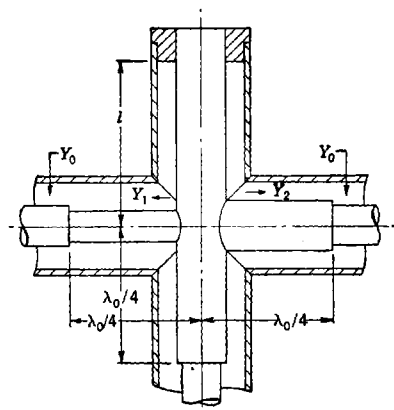


FIG. 8-56.—Power divider for unequal division of power.

be equal to $2Y_0$ just as in the simpler model of Fig. 8-54. The same char-

Equation (10) requires the total load admittance at the junction to

characteristic admittance, $\sqrt{2} Y_0$, is then used for the stub and the input transformer whose action, including compensation for wavelength change, is just as before. Equation (11) enables the circuit to be designed to obtain any desired ratio between the powers P_1 and P_2 going to the two loads. At midband wavelength both Y_1 and Y_2 are pure conductances, and they are in parallel and subject to the same rms voltage V . The powers P_1 and P_2 going to the two loads are then $V^2 Y_1$ and $V^2 Y_2$, and Eq. (11) follows.

As the wavelength is varied, Y_1 and Y_2 take on susceptive components; but their conductive components remain almost constant for wavelength variations that are not too large, and the power-division ratio remains almost constant. The constancy of the conductance component of admittance at the input side of a quarter-wavelength transformer is easily demonstrated with the aid of an admittance chart or by means of the admittance-transformation equation. It is found also that the signs of the susceptance components of Y_1 and Y_2 are opposite; consequently, there is a tendency for them to cancel each other. Quantitatively, the cancellation is good when Y_1 and Y_2 are nearly equal, but the susceptance component of the larger admittance Y_2 is always larger. This situation leads to a greater frequency sensitivity than that of the simple circuit of Fig. 8-54. It is possible to obtain accurate compensation of the frequency sensitivities of the stub, output transformers, and input transformer by suitable modification of the design. It is necessary to decrease the characteristic admittance of the stub and input transformer by the proper amount and make the appropriate change on the right side of Eq. (10). In the limit, as Y_1 approaches zero, a right-angle stub with a half-wavelength broadbanding transformer will result. By theory, the characteristic admittance of stub and transformers is, in this case, $1.22 Y_0$, which may be compared with $1.41 Y_0$ in the case of Fig. 8-54.

8-18. Variable Power Divider.—The purpose of this device is to vary at will the ratio between the power delivered to two output lines. At the same time, the input impedance remains matched; therefore, no power is reflected by the circuit. The theory outlined below applies equally well for transmission lines of various types. Both coaxial and waveguide versions have been made and found to operate essentially as expected.

Such power dividers are used to divide a given input power in any proportion desired between two operating loads (for example, two antennas) or, with a "dummy" load connected to one arm, to achieve an attenuator that has a minimum insertion loss of zero and is well matched at all attenuations. Although such an attenuator follows a calculable law closely, it is rather sensitive to slight frequency changes and hence not especially suitable for precision work.

The principle of operation may be understood by considering the

model indicated schematically in Fig. 8-57. The conditions prevailing for three different stub lengths will be discussed.

(1) $l_c = \frac{1}{2}\lambda$, hence $l_d = \frac{1}{4}\lambda$. In this case, stub *C* presents a short circuit ($Z_c = 0$ or $Y_c = \infty$) across the junction *ACE*. This prevents the passage of power into output line *A*. Since this short circuit occurs $\frac{1}{4}\lambda$

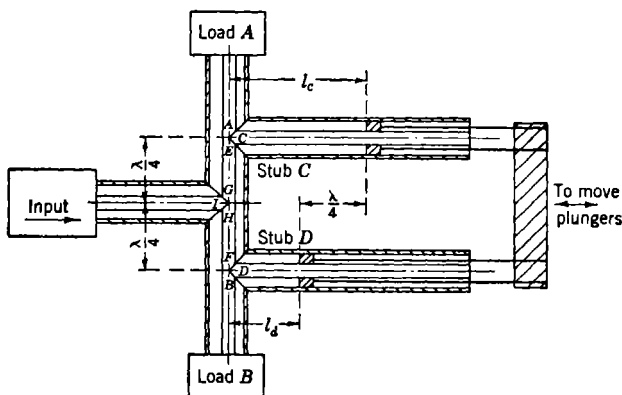


FIG. 8-57.—Variable power divider.

from the input junction *GHI*, it presents an open circuit across this junction ($Z_c = \infty$ or $Y_c = 0$). Thus the output branch *G* acts as a quarter-wavelength stub support, allowing free passage of power from input line *I* into the other branch *H*. This branch *H* is matched since the stub *D* ($\frac{1}{4}\lambda$ long) acts as a normal stub support and permits free passage of power into the matched load *B*. Thus the input line *I* is matched, all the power is delivered to load *B* and none to *A*.

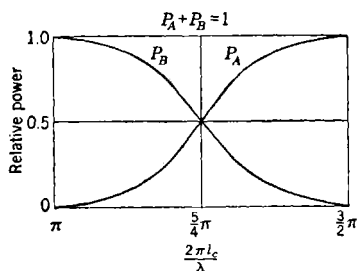


FIG. 8-58.—Division of power vs. stub length for the power divider of Fig. 8-57.

(2) $l_c = \frac{3}{4}\lambda$, hence $l_d = \frac{1}{2}\lambda$. Now the stub *D* short-circuits the load *B*, while the stub *C* allows free passage into load *A*, since it acts as if it were a quarter-wavelength stub support. Thus all the power is now delivered to load *A*, none to *B*, and the input line *I* is matched.

(3) $l_c = \frac{5}{8}\lambda$, hence $l_d = \frac{3}{8}\lambda$. Stub *D* is now capacitive and stub *C* is inductive. These stub susceptances are added in shunt with the loads *A* and *B*. At the input junction *GHI*, the admittances at *E* and *F* have been transformed by the quarter-wavelength sections *EG* and *FH* in such a way that the inductive effect of one branch

is exactly compensated by the capacitive effect of the other, and the conductances add to give exactly the characteristic admittance of the coaxial line. Hence the admittance at the input line I exactly matches the line. The power divides equally between output lines A and B , as indicated by Fig. 8-58.

Application of the transmission-line equation shows that, for all values of l_c , the admittance at the input line I exactly matches the line. The fraction of the available power delivered to output line A and to output line B may be calculated from the equations

$$\left. \begin{aligned} P_A &= \sin^2 \left(\frac{2\pi l_c}{\lambda} \right) \\ P_B &= \sin^2 \left(\frac{2\pi l_d}{\lambda} \right) \\ P_B &= \cos^2 \left(\frac{2\pi l_c}{\lambda} \right) \end{aligned} \right\} \quad (12)$$

These quantities are plotted in Fig. 8-58.

It should be realized, however, that a power divider of this type presents a matched impedance in the input line only when the line is the branch so indicated in Fig. 8-57. If power is fed in through one of the other branches, say branch A , and branch B and the branch indicated as the input line are terminated in matched loads, the impedance looking in at

A will not, in general, be matched. For the setting of the stubs that would normally give complete transmission into load A , the impedance looking in the reversed direction will be matched. For other settings of the plungers, a certain amount of mismatch will occur. The percentage of the power in the incident wave which is coupled through from one branch to another is the same regardless of which branch is used as the input one. It is not true, however, that the input impedances or standing-wave voltage ratios in the two cases are equal. In the first

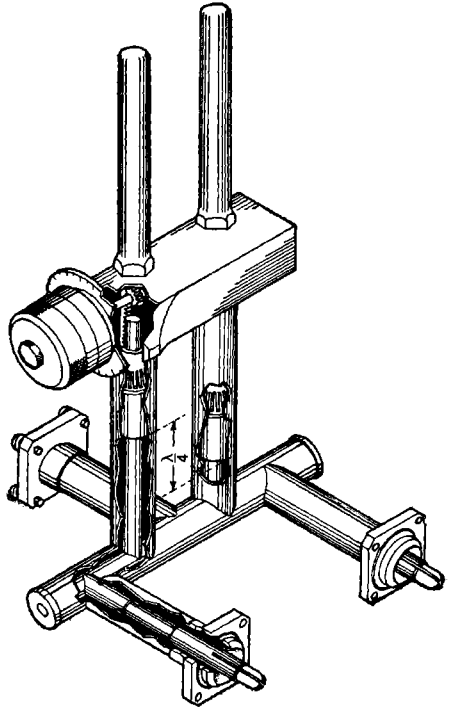


FIG. 8-59.—Coaxial power divider for $\frac{7}{8}$ -in. line.

case all the power of the incident wave not transmitted to load *A* is dissipated in load *B*, but in the reversed arrangement, the power not dissipated in the branch *I* is partly reflected back along branch *A* and partly dissipated in load *B*.

The actual form of the final circuit is that shown in Fig. 8-59. The input line is shown in the rear and the two output lines are shown in the foreground. The right-angle stubs in the two output lines are like those of Fig. 4-31, including undercut transformers. An identical undercut transformer occurs in the input line. The two plungers are moved by pinioned gears attached to a common shaft.

It was found necessary in order to obtain an improvement in impedance-matching to alter the length of the two stubs in the input and output branches. The VSWR finally obtained was about 1.1 at the design wavelength of 9.1 cm. Power levels of about 500 kw were required to cause breakdown.

The effectiveness of a variable-length stub in short-circuiting either one of the output lines is limited by the conductivity of the metals and the losses in the plunger. It was found that the maximum attenuation obtainable at either output line was limited to about 45 db.

WAVEGUIDE POWER DIVIDERS

8-19. Fixed Power Divider.¹—Fixed waveguide power dividers of two types have been developed, the Y and the T, so-called because of their shape. The principle of operation of the Y-shaped power divider is simple. A rectangular waveguide carrying power in the TE_{10} -mode is illustrated in Fig. 8-60*a*; a thin conducting plate may be inserted across the waveguide, perpendicular to the electric field, as in Fig. 8-60*b*. The introduction of this plate does not change the fields inside the waveguide, nor does it change the currents in the walls; consequently, the input impedance relations undergo no change when the partition is put in. Since the field is uniform in the *y*-direction, the voltage across the waveguide will be divided between the two branch waveguides in the ratio of $V_2/V_1 = Eb_2/Eb_1 = b_2/b_1$. In addition, the currents in the two branches are equal to each other and to the currents in the main waveguide. The two branches are, therefore, in series with the main waveguide, and the power transmitted through the two branch waveguides will be in the ratio of their heights. This waveguide circuit is then a power divider.

This power divider in its simplest form would not be convenient, since

¹ Contributions to Secs. 8-19 and 8-20 were made by F. T. Worrell.

each branch, having a height less than the height of the waveguide, has an impedance different from the impedance of the main waveguide. This simple version should be modified by tapering each branch into a waveguide of standard size, as shown in Fig. 8-60c. In practice, it is found convenient to have the two branch waveguides separated from one

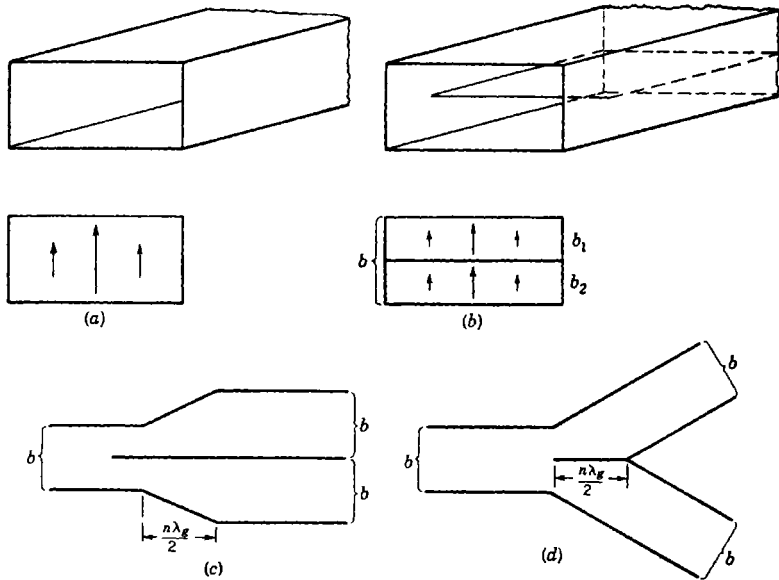


FIG. 8-60.—Development of Y-type power divider.

another, rather than joined by a common wall, and a further modification that results in the Y-shaped power divider is made as in Fig. 8-60d.

Models have been designed, as indicated in Fig. 8-61 and Table 8-3, for the 3-cm and 10-cm regions. All are for an equal division of power, although models can be designed for some other ratio of power division, if desired. It should be noted that the critical dimensions in each

TABLE 8-3.—DESIGN PARAMETERS FOR THE POWER DIVIDERS OF FIG. 8-61

Band for VSWR = 1.07	<i>a</i> , in.	<i>b</i> , in.	<i>c</i> , in.	<i>d</i> , in.	<i>e</i> , in.	θ
10.0-11.1	2.840	1.340	0.562	$\frac{1}{2}$	0.080	11° 31'
8.5-11.5	2.840	1.340	0.9375	$\frac{7}{16}$	0.080	7° 6'
3.1- 3.4	0.900	0.400	0.200	$\frac{3}{4}$	0.050	13° 14'
3.1- 3.4	0.900	0.400	0.230	$\frac{1}{4}$	0.050	7° 3'

case are the angle of the Y, which determines the length of the taper, and the position of the leading edge of the vane. These dimensions were both determined experimentally. The 10-cm model has been tested on high power; it did not break down at the maximum available power of 1.1 Mw.

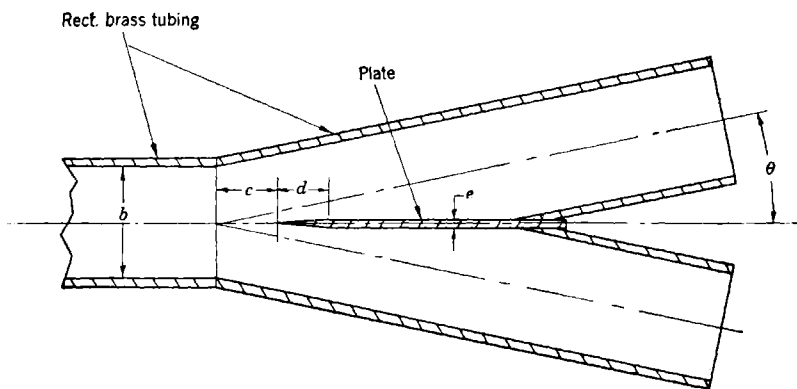


FIG. 8-61.—Waveguide power divider, fixed Y-type.

It is probable that a power divider of this type will handle almost as much power as the waveguide itself.

Another possible form of fixed power divider makes use of a series-branching T-junction, as in Fig. 8-62. If power is fed into arm A, it will divide equally between arms B and C. If the three branches are all waveguides of the same size, however, there will be a considerable mis-

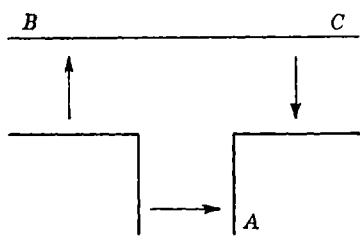


FIG. 8-62.—A T-type power divider. Arrows represent electric fields.

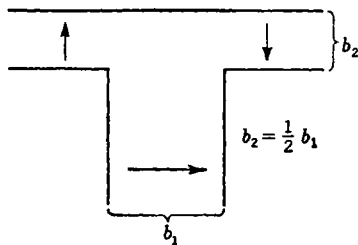


FIG. 8-63.—Power divider, modified T-type. Arrows represent electric fields.

match consisting, in part, of the mismatch due to the junction effect, and, in part, of the mismatch due to the load of impedance $2Z_0$ terminating a waveguide of impedance Z_0 . In practice it has been found difficult to match such a power divider over any reasonably large wavelength band. There are a number of ways in which this frequency sensitivity could be reduced. One way that might succeed would be to use the T of Fig. 8-63, a series-branching T, in which the output branches are half the height

of the input branch, with, therefore, half the characteristic impedance. Then, only the junction effect would be left to match. Again, the height of the output branches could be set at some other value found experimentally, to correct partially the junction effect. In either case, the output branches would have to be tapered up to full size, and the result would not be a particularly simple arrangement. In addition, because of the sharp corners, it probably could not handle as much power as the Y-type.

The power divider just discussed used a series-branching, or *E*-plane T. An *H*-plane T might be used, but it would probably be more frequency-sensitive than the *E*-plane T. It would have the advantage, however, of handling higher powers.

If the geometric arrangement of the T is preferable to that of the Y, the latter can be modified to get a T that is almost as compact as a simple T, and that has the broadband characteristics of the Y. This design is

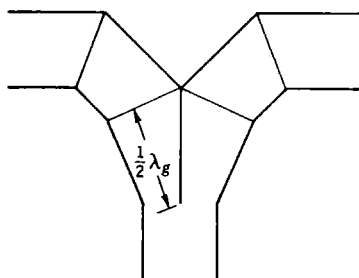


FIG. 8-64.—A Y-type power divider with T-shape.

illustrated in Fig. 8-64. It can be seen that this design uses a Y-type power divider the branches of which have mitered angles placed as close as possible to the divider. A dimensioned drawing is shown in Fig. 8-65. The input VSWR is below 1.1 over the wavelength band 3.15 cm to 3.65 cm. This power divider has been tested at pulse powers up to 225 kw, 1- μ sec pulse duration, 1000 pps, without breakdown.

8-20. Variable Power Dividers.

A simple variable power divider can be made using a Y-junction with the dividing partition hinged at one end as shown in Fig. 8-66. Such a power divider should be

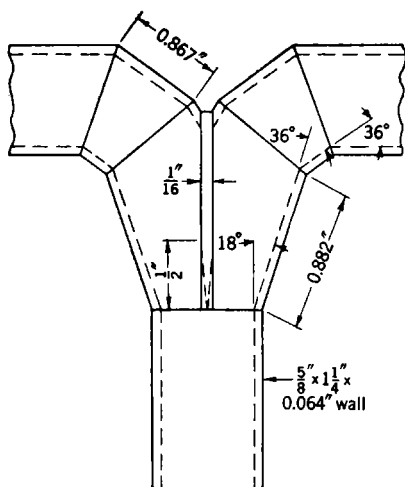


FIG. 8-65.—Power divider for use at wavelengths between 3.15 cm and 3.65 cm.

well matched over a broad band, since it is derived from a broadband fixed power divider. The power divides between the two output branches in the ratio of the heights b_1 and b_2 , just as in the related fixed power divider of Sec. 8-19. Some work was done on such a power divider, but it was not

carried through to completion. A model designed for a wavelength of 10.5 cm was tested at various wavelengths and found to have a maximum standing-wave voltage ratio of about 1.25 for all adjustments over the band from 8.2 to 11.5 cm. This model was not well constructed; as a result the data are not particularly meaningful. Better performance could probably be obtained from a well-built model. One troublesome feature was the design of a capacitance joint to connect the moving partition to the waveguide walls. The joint on the one model that was made gave trouble with r-f leakage and was not considered satisfactory.

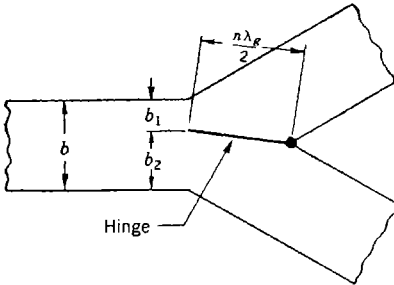


FIG. 8-66.—A Y-junction variable power divider with hinged partition.

version of the coaxial-line power divider. An idealized model of such a power divider is shown in Fig. 8-67. Power enters arm *A*, arms *B* and *C* are connected to the two loads between which the power is to be divided. Arms *D* and *E*, each a quarter guide wavelength from *A*, have plungers riding in them. The plungers are ganged and are set a quarter guide wavelength apart vertically.

As was shown in the discussion of the coaxial-line power divider, if the T-junctions are all ideal the power divider will be matched at all settings of the ganged plungers. But the waveguide T-junctions are not ideal; hence an equivalent circuit (Vol. 10) including a junction effect must be used in the analysis. Therefore, as the plunger in arm *D* is moved, instead of an impedance of $1 + j \tan \beta l$ being seen at the junction of arm *D* with the main line, an impedance that differs from this

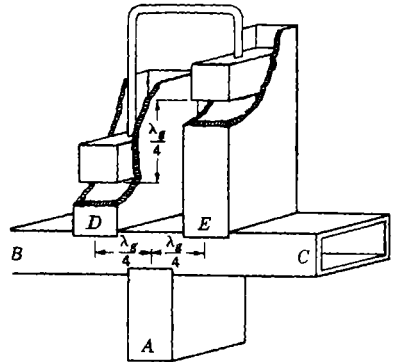


FIG. 8-67.—Waveguide variable power divider.

value is seen because of the effect of the junction. A similar effect occurs at arm *E*. Thus, as the ganged plungers are moved, the impedance seen looking into the power divider will vary approximately as shown in Curve *a* of Fig. 8-68. This circle will close on itself when the plungers have moved a quarter wavelength from their starting position, since the

power divider then looks the same as in the beginning. The center of the curve is displaced from the center of the chart, since the junction of *A* with the main line also is nonideal. If, then, a matching iris is placed in the input arm, the impedance of the power divider as a function of plunger position will be a circle about the center of the chart.

This nonideal behavior can be compensated by putting in a matching element that makes the junction behave like an ideal one. The matching

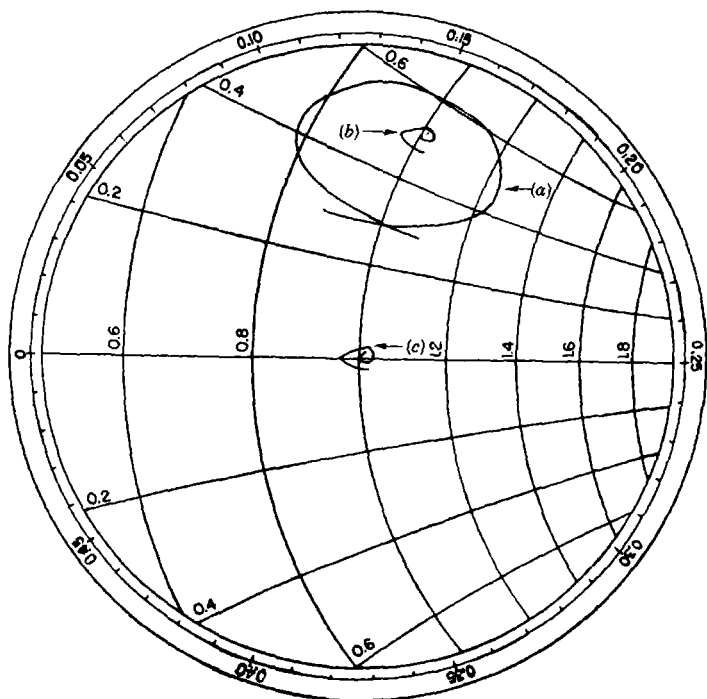


FIG. 8-68.—Input admittance of power divider as plungers are moved. Reference point is $0.16 \lambda_p$ on input side of junction and $\lambda = 3.2$ cm. (a) no irises in stubs; (b) irises in stubs; (c) iris also in input.

iris that is used is the same one used in matching a series-branching T. When this iris was used in arms *D* and *E*, the impedance of the power divider no longer varied as Curve *a* of Fig. 8-68 but was fairly constant as in Curve *b*. Since the junction of *A* with the main guide is nonideal, a matching iris is required there also. When this iris is inserted, Curve *c* of Fig. 8-68 results.

This power divider is frequency-sensitive, as might be expected from the design which includes several rather long stubs. One power divider has been designed for a wavelength of 3.20 cm. In the wavelength band

from 3.17 to 3.23 cm, the maximum standing-wave voltage ratio is 1.20. The power-division ratio is limited by the loss in the stubs and the plungers; the maximum ratio obtainable with this divider is about 35 db.

This basic design of power divider for waveguide has been modified, as was the coaxial-line version, by putting a gas switch on one of the plunger arms. The tube is arranged to be ineffective at high-power levels, allowing the power divider to attenuate the transmitted signal. At low power, the switching tube is effective in reducing the attenuation of the low-level signal. An additional problem arose in the design of this model. It was discovered, when making standing-wave measurements on the first experimental model, that the plot of standing-wave ratio as a function of plunger position was a circle that closed only after a plunger motion of one-half wavelength. This effect was similar to that caused by the plungers being improperly set relative to one another. Since the plungers had been set accurately a quarter wavelength apart, the trouble was thought to be caused by an abnormally large phase shift introduced by the T-junction to which the gas switch was attached. This was found to be the case; and, when the distance between the plungers was changed to compensate for this effect, the performance was the same as in the simple power divider.

SWITCHES

8-21. Coaxial-line Switches.—The variable power divider described in Sec. 8-18 may be used as a coaxial-line switch by moving the pair of short-circuiting plungers between the two positions corresponding to full power transmission first into one load and then into the other. Such a switch would carry about as much power as the normal stub-supported line of which it is composed, and it would be well matched even during the switching process.

For certain applications it is desired to have a switch that is more compact, lighter in weight, simpler to build, and faster in switching. In many of these applications the problem is simplified by the fact that the switch is not required to operate at high power levels, and usually the mismatch during switching is of no consequence.

A switch that possesses all these desirable characteristics, but which is limited to low power levels and is not matched during switching, is shown in Fig. 8-69. It was designed for use at wavelengths around 10 cm, but there is nothing in the design which makes it unsuitable for other wavelengths. The switch was designed for laboratory test work, so it is equipped with type-N connectors, the connector most frequently used on coaxial test cables. Switching is accomplished by shifting the connection of the center conductor from one output line to the other. The center conductor of the input line is pressed, by an internal spring,

against the movable section of the center conductor; thus good electrical contact is maintained. The center-conductor section is moved by means

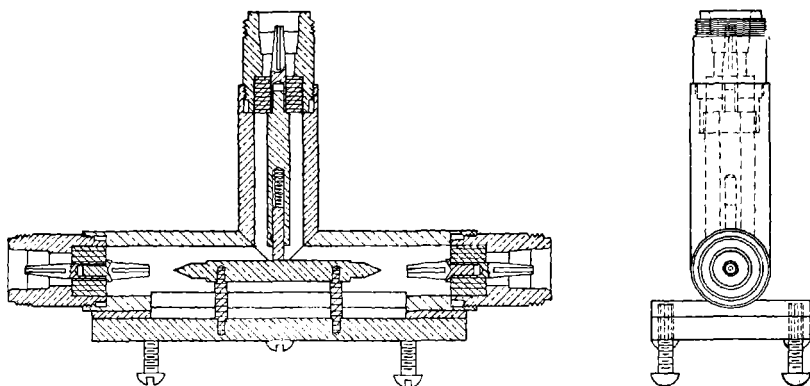


FIG. 8-69.—R-f switch, shown in OFF position. The horizontal pin in the center may be slid right or left to complete the circuit to either one of the two output lines.

of dielectric pins attached, through a slot, to an external carriage moving on ways. Each end of this section is fitted with a pin that plugs alternately into one or the other of the slotted-finger receptacles in the two output lines.

The number of switches of this type which have been made is insufficient to give an accurate figure for the input VSWR that can be expected in production. Indications are that the value is probably about 1.5 at a wavelength of 10 cm. Although this figure is acceptable for many applications, it is not very good. The high mismatch is probably caused by a combination of connector mismatches and mismatch at the right angle formed at the center of the switch.

A switch of another type suitable for similar applications is that of Fig. 8-70. The design represents a variation on a switch developed at Radio Research Laboratory at Harvard, which is a six-way switch, type number M2415. Type-N

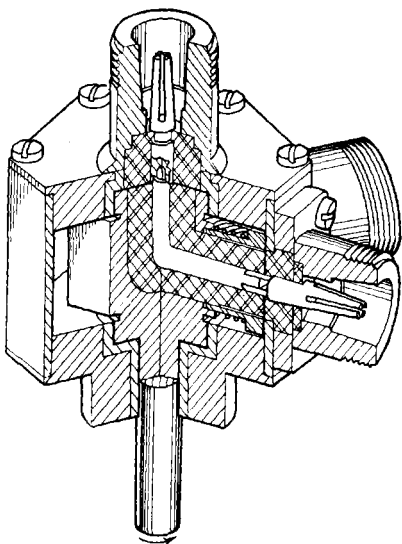


FIG. 8-70.—Type-N switch with two output lines. Rotation of the shaft transfers the connection from one to another of the two output lines at the right.

connectors are again used, but the principle of operation is different. The input line is at the top of the figure, coaxial with the hexagonal block forming the body of the switch. The coaxial-line elbow inside the body is rotated by means of the shaft indicated in the lower part of the figure. The upper end of the elbow is connected to the input line, but the output end may be rotated to either of the two output lines shown. With the hexagonal block, as many as six output lines could be used. The center conductor of the elbow makes contact with the input line by means of a slotted tip inserted into a hole in the input center conductor. The connection to the center conductor of the output line is made by a projecting blade that is squeezed between two open fingers of the center conductor of the output line. The outer conductor of the elbow makes contact by a rotating machined fit. Contact with the output lines is furnished by a coaxial sleeve that is pressed, by the spring shown, against the cylindrical inner surface of the hollow body. One end of the sleeve is rounded to fit this cylindrical surface, and the other end is slotted to form fingers that contact the outer conductor of the main part of the elbow. Of course, it is necessary to allow for the passage of the two fingers of the center conductor of the output line as the elbow is rotated. This is accomplished by cutting a wide horizontal slot through the end of the sleeve and through the end of the dielectric filling the line within the sleeve.

The first group of switches made according to this design gave an average VSWR of about 1.5 to 2.0. It was felt that this was partly caused by mismatches in the connectors and in the elbow angle, but principally by the relatively large cutaway section for allowing passage of the center conductor of the output line. As an expedient, the impedance transformation resulting from drilling away a large part of the dielectric within the entire length of the elbow section was tried. Four holes of 0.120-in. diameter were drilled parallel to the center conductor, removing most of the dielectric material. It was found that this transformation decreased the VSWR to an acceptable value. A switch of this type, mounted on a box containing a relay, is shown on the left in Fig. 8-72.

Two other modifications were found also to be desirable:

1. Trouble was experienced from "freezing" of the metallic contacts in the rotating machined fit at the input end of the elbow, so the closeness of the fit was relaxed and a thin washer of poly-F dielectric was inserted as a spacer. This material is ideal for the purpose, being tough yet smooth and slippery. The low capacitance across the washer gives adequate coupling of the outer conductors.
2. The coupling to the outer conductor of the output lines was also made capacitive by removing the spring and soldering the sleeve in place to leave a gap of from 0.005 to 0.010 in. between the sleeve

and the cylindrical inner surface of the body. Actually, the sleeve was rebuilt, omitting the slotted fingers and increasing the diameter of the output end to give maximum coupling capacity. Five switches, incorporating these two modifications and having the holes drilled in the dielectric, gave a VSWR below 1.2 at a wavelength of 10 cm and below 1.3 at 9 cm and 11 cm. Operation was satisfactory from -50° to $+75^{\circ}\text{C}$.

Neither of these switches is capable of the extremely fast switching that is sometimes required. It is frequently desired, in certain rapid-scanning devices, to switch alternately between two antennas at rates measured in hundreds or thousands of switching cycles per minute.

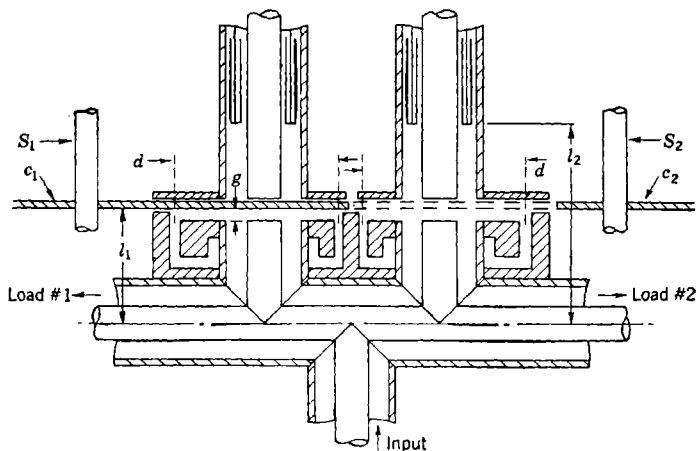


FIG. 8-71.—Proposed high-speed coaxial switch.

The power levels required are also beyond the capabilities of the two switches just described. Attempts have been made to design a coaxial-line switch capable of fulfilling these requirements, but none of these efforts has met with any noteworthy success. It may be remarked, however, that these unsuccessful attempts were made some time ago and it may be that a determined attack on the problem using present knowledge and techniques would prove more fruitful.

One of the more promising early switches bore a resemblance to the variable power divider that was developed somewhat later. A combination of some of the principles of this early switch with the power divider of Fig. 8-57 is represented schematically in Fig. 8-71. The two stub branches are cut to permit the two "choppers" c_1 and c_2 to short-circuit the line giving a stub length l_1 , equivalent to a quarter wavelength.

A radial capacitance-coupling section is used on the outer conductor. The choke sections would have to be folded under as indicated in order to make them a full quarter wavelength long for suppressing leakage of power. The diameter d is made as large as possible in order to get maximum capacity in the coupling. Unfortunately, there is not sufficient room for a full quarter wavelength of radial line. The gap g is made as small as is practical—perhaps 0.010 in. or less. Looking at the stub on the left, appreciable capacitive reactance will appear in the capacitance couplings of both inner and outer conductors. This may be compensated by proper adjustment of l_1 in design. The capacitive reactance is

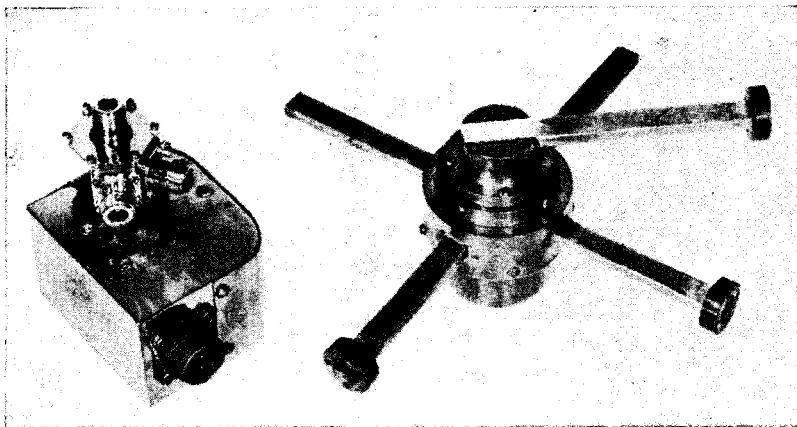


FIG. 8-72.—R-f switches.

still larger in both conductors when the copper sheet is removed, as on the right. This reactance is not serious, since it is in series with a very high reactance caused by the short-circuiting plunger, about a quarter wavelength away. Any slight effect may be compensated by adjustment of l_2 .

The action of the switch is as follows: The two chopper sheets c_1 and c_2 are essentially half disks mounted on shafts S_1 and S_2 . The shafts are rotated in synchronism in such a way that when one stub is short-circuited by its chopper the other is not. In the condition shown, the left stub is short-circuited and acts as a quarter-wavelength stub, allowing power to go past it to the load on the left. The right stub is short-circuited by the movable plunger at a length l_2 equivalent to a half wavelength. Just as in the power divider, this short-circuits the right load cutting off its power. Since this short circuit appears a quarter wavelength from the input junction, the input power is permitted to flow out to the left load.

The original switch was essentially of this type, but the upper lines containing plungers were omitted. Trouble was experienced with breakdown at moderate power levels, hence rounding of sharp corners is advisable. Care must be exercised to ascertain that both loads are never short-circuited at the same time. That is, the choppers should be slightly more than half a disk with the result that during switching, power is delivered to both loads for an instant, and the condition in which neither load can dissipate the input power is avoided.

If such a switch does not give satisfactory performance, recourse may be had to the use of a waveguide switch. This alternative would involve transitions from coaxial lines to waveguide, but it is probable that the simplicity and high-power capabilities of waveguide switches would more than compensate for the necessity of using transitions.

8-22. Waveguide Switches.¹—The simple T-switch is basically a T-junction such as the one shown in Fig. 8-62 with the input line at A,

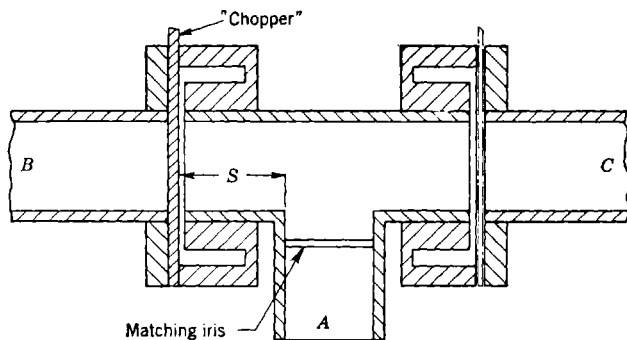


FIG. 8-73.—A T-type waveguide switch.

and the two loads between which power is to be switched at B and C. Some mechanical arrangement is used that alternately puts a short circuit in branch B, sending power into C, and then in branch C, sending power into B. The short circuits are so located that reflectionless transmission occurs around the corner when the T-switch is properly matched by an iris in A.

Several such switches have been designed at 3 and 10 cm for switching power from one antenna to another. One design is shown in Fig. 8-73. In this model there are, in the output branches, two choke-flange junctions with the choke on the input side of the junction separated from the flange just enough to allow a metal "chopper" plate to move in and out. The length S of the short-circuited branch and the dimensions of the input matching iris may be determined by experiment or may

¹ Contributions to Sec. 8-22 were made by F. T. Worrell.

be taken from data reported elsewhere (Vol. 10). The two choppers are mounted in such a way that when one is between its choke and flange the other one is removed from its choke and flange; thus power is allowed to go through the open junction. The choppers may be sections of disks mounted on a common shaft. They should short-circuit the respective branches somewhat less than 180° of rotation in order to avoid both loads being cut off at the same time. An alternative design differs from this version in having the corners of the junction rounded to reduce the likelihood of power breakdown.

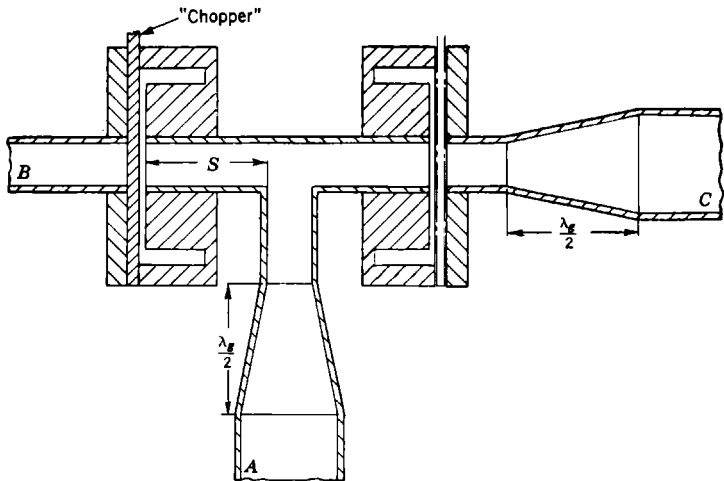


FIG. 8-74.—Modified T-type waveguide switch.

The British have also made a switch of this type. It differs in that the waveguide narrows down in the switch, as shown in Fig. 8-74, and uses a British choke like the one discussed in Sec. 4-10. The chopper consists of sector disks with 36° sectors. Since the waveguide height is so small, the switching can be done rapidly; as a matter of fact, this switch was designed to switch power from one antenna to another and back on alternate pulses.

A waveguide switch that will switch power into any one of three circuits is presented in Fig. 8-75. The power applied to *A* may be switched into *B*, *C*, or *D*. Short-circuiting is accomplished by means of resonant rings, one in each output branch. The matching irises, required for matching around the corner into branch *B* or *C*, are inserted in these branches rather than in the input line where they would affect straight-through transmission into branch *D*.

This switch is of interest because it is the only one of American design

to use resonant rings as the short-circuit devices. The ring used is shown in Fig. 8-76. The shape of the ring, which is different from the simple rectangular resonant ring normally used in rectangular waveguide, is such that the impedance of the ring is relatively insensitive to frequency changes. A ring is desired which will be as good a short circuit as possible over a large frequency band when its plane is perpendicular to the longitudinal axis of the waveguide. Actually, a small amount of power leaks past the ring. The amount of power leaking past the ring is 61 db down from incident power level at midband wavelength, 9.1 cm and 30 db down at the edges of a 7 per cent band. The rings are made of $\frac{3}{32}$ -in. duraluminum stock, and all edges are rounded to reduce tendency to spark. They are rotated by motors with stopping pins inserted in the mount. Switching may be accomplished in about 0.03 sec. In the switching cycle, the new branch is opened before the old one is closed to avoid complete reflection of input power. The VSWR during switching has a maximum value of about 2.7. Sparking occurs at an undetermined point, probably in the resonant ring, at a power of about 200 kw.

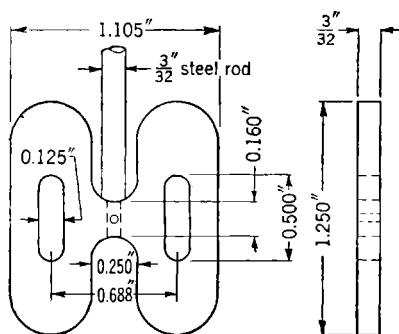


FIG. 8-76.—Detail of resonant ring.

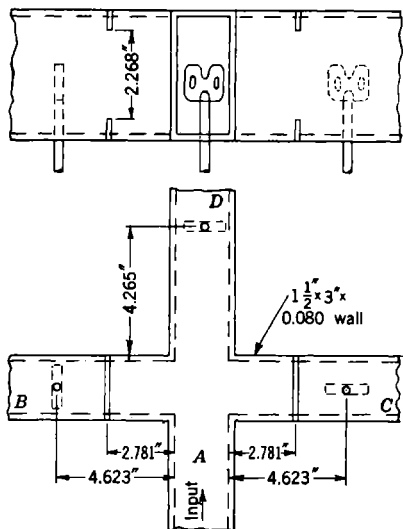


FIG. 8-75.—Views of three-way switch.

The VSWR during switching has a maximum value of about 2.7. Sparking occurs at an undetermined point, probably in the resonant ring, at a power of about 200 kw.

A special two-way switch has been designed for switching 3.2-cm power alternately into the two ends of a linear antenna array. In Fig. 8-77 is a schematic diagram showing the switch that was developed cooperatively by Radiation Laboratory and Bell Telephone Laboratory.¹ When the

switch is in the position shown, power coming in arm C is switched to B, then through the antenna, from which most, but not all, goes

¹ Drawings and data on final design supplied by C. N. Nebel of BTL.

out into space. The power that is not radiated, amounting to some 10 per cent, comes back in arm *A* and into an absorbing load in arm *D*. When the switch is thrown the other way, the power goes into *A*, through the antenna, back into *B*, and then into the load at *D*. The ratio of the power delivered into branches *A* and *B* (i.e., the discrimination factor for

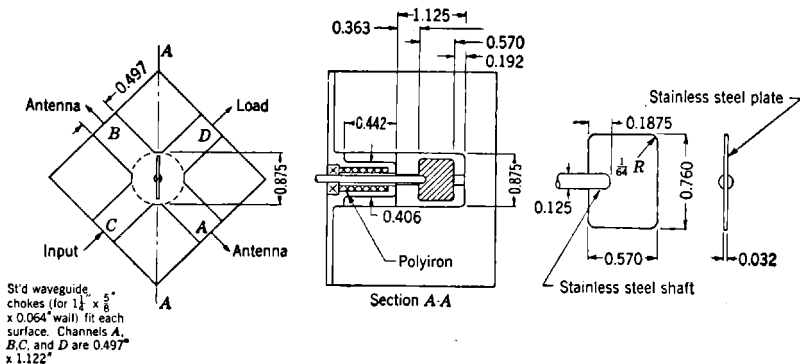


FIG. 8-77.—Two-way r-f switch.

one switch position) is about 40 to 50 db, on the average. The VSWR observed on one representative switch was below 1.02 over the frequency range 9320 to 9400 Mc/sec, rising to 1.04 at 9430 Mc/sec. Transmission loss through the switch was about 0.1 db. At a pressure corresponding to an altitude of 50,000 ft, breakdown occurred at about 50 kw pulse power on the average.

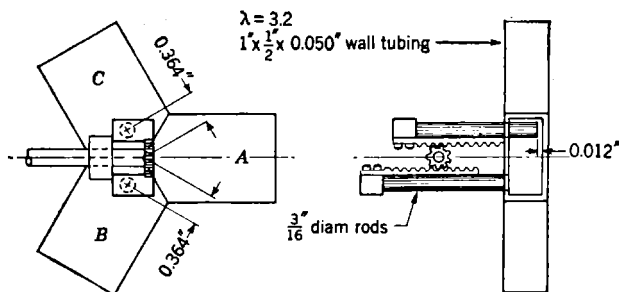


FIG. 8-78.—A Y-switch with short-circuiting pins.

Junctions that are Y-shaped with 120° between arms have been found to have properties that make them desirable for switching applications. In particular, if a short circuit is placed close to the junction in one output branch, power will be transmitted around the corner into the other branch with only a small reflection over a broad band of wavelengths. This property has been used to advantage in the switch shown in Fig.

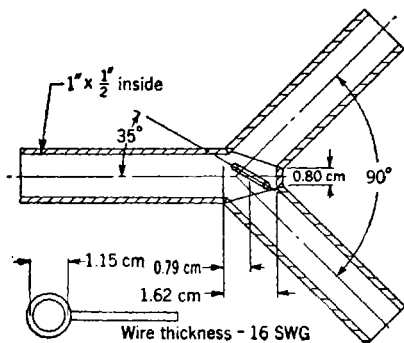


FIG. 8-79.—A Y-switch with resonant ring.

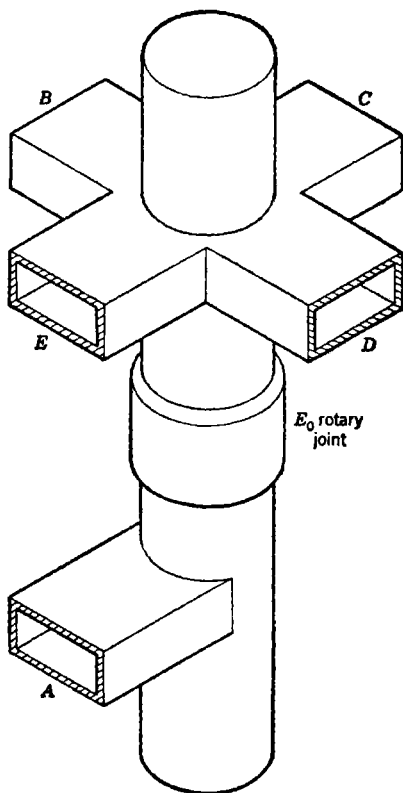


FIG. 8-80.—Schematic diagram of rotary switch.

8-78. The short circuit is provided by a rod that is inserted to within 0.012 in. of the bottom of the waveguide. The power leaking past this rod is 55 db below that transmitted into the other branch. Breakdown occurred at about 10 kw pulse power when the switch was operated while the power was applied.

A Y-switch using a resonant ring has been designed by the British.¹ This switch, which is shown in Fig. 8-79, is designed for a wavelength

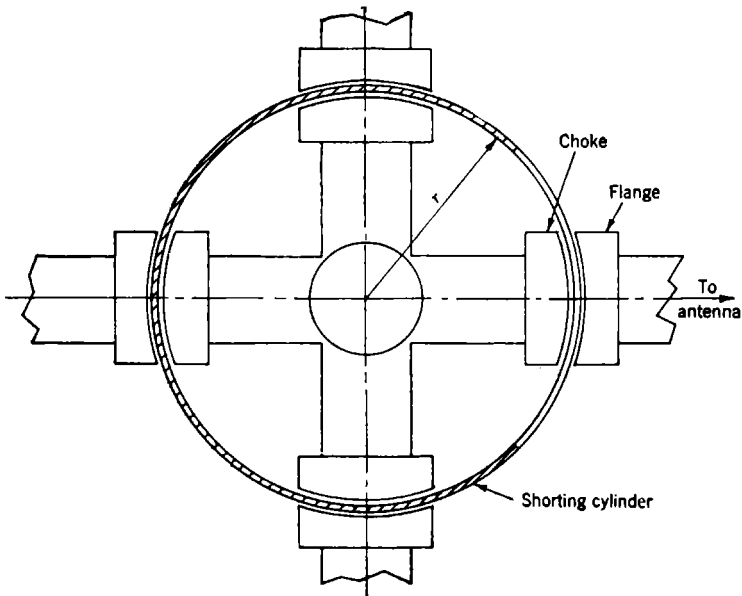


FIG. 8-81.—Switching system for rotary switch.

of 3.2 cm, and uses the British waveguide 1- by $\frac{1}{2}$ -in. ID. The standing-wave voltage ratio is less than 1.06 over a band whose total width is 6 per cent. The discrimination between the two output branches is better than 25 db over this band. The switch has transmitted 20 kw at pressures down to 5 in. of mercury.

A switch of a different type is that operating on a rotary principle. One such switch that has been developed is based on a 3-cm E_0 -mode rotary joint. A schematic drawing of such a switch is shown in Fig. 8-80. Power is introduced at *A* through a standard E_0 -transition into the rotary section. The transition back to rectangular waveguide has four branches, *B*, *C*, *D*, and *E*. In the application for which this switch was designed each of these four arms was fastened to a horn antenna feed. As the

¹ W. D. Allen, "Resonant Rings and Ring Switches in Waveguides," TRE Report G-10/R137/WDA, Feb. 19, 1943.

joint rotated, each feed in turn swept past the throat of a folded horn antenna. The switching arrangement, not shown in this figure, short-circuited the three arms which were not transmitting power into the antenna.

The switching system is shown in Fig. 8-81. Each arm is broken at a certain place by an open choke-flange coupling in which the faces of the choke and flange are cut to a radius r . Fitting in between these open junctions is a stationary metal cylinder with an aperture. As the switch rotates, each arm in succession will carry power to the antenna while the others are short-circuited. The radius of the cylinder is so chosen that power is transmitted through the switch with minimum reflection. The chokes in the open junction are standard chokes that have been turned down as indicated to get a well-matched open junction. The aperture in the cylinder must be chosen carefully to afford the smallest possible impedance variation during switching. The aperture found to be best is 105° .

The standing-wave ratio during switching is fairly low, a VSWR of slightly over 2, and the change in standing-wave ratio takes place in such a way that the phase is fairly constant. This is found to be desirable to avoid excessive frequency-pulling of the magnetron. A switch of this type performs well over a relatively narrow band of wavelengths, a total band width of about 1 per cent being all that may be expected. Powers of about 100 kw may be used.

A switch of this type, designed for a wavelength of 1.25 cm, is shown on the right in Fig. 8-72.

CHAPTER 9

THE THEORY OF MICROWAVE FILTERS

BY R. M. FANO AND A. W. LAWSON

Filters are passive networks which selectively transmit waves of different frequencies. The design of such networks consists in the appropriate choice and arrangement of circuit components to obtain specified frequency characteristics. Methods for designing networks consisting of inductances, capacitances, and resistances have been highly developed. When microwave components are used, however, the existing low-frequency methods of design are no longer directly applicable. The proper solution of the design problem at ultrahigh frequencies would be the development of a new design method which would use microwave components as building blocks. The development of such a design method, however, presents mathematical difficulties which have not yet been overcome. Under these circumstances, it is natural to inquire whether microwave components could be used to approximate the behavior of lumped elements over a limited frequency band. If so, it would then be possible to obtain microwave filters from low-frequency filters by the simple process of substituting for the lumped elements the corresponding microwave components. Fortunately, such a design procedure is feasible in most practical cases, and a variety of microwave filters have been successfully designed in this manner.

In the light of the foregoing discussion, the subject of microwave filter design can be divided into two parts; namely, the design of lumped-element filters with prescribed electrical characteristics, and the transformation of these filters into microwave structures having approximately the same characteristics over a specified range of frequencies.

The present chapter deals with the first part of the problem, that is, the design of lumped-element filters. Since a complete treatment of this subject would require at least an entire volume, this chapter represents a compromise. The authors have tried to present enough basic material to permit the reader not familiar with network theory to understand and profitably apply the simpler methods of design. On the other hand, it has been considered worth while to include more refined design procedures developed in recent years because they are not presented in any book available at this time. A good understanding of these procedures, however, requires a certain familiarity with network theory,

which for the sake of brevity is not discussed here. For a detailed discussion of this subject, the reader is referred to Vol. 2, *Communication Networks*, by E. A. Guillemin, and to *Network Analysis and Feedback Amplifiers*, by H. W. Bode.¹ In this connection, it should be pointed out that some network theorems, as for example the reciprocity theorem, apply to microwave networks as well as to lumped-element networks. Other theorems, however, have been proved only in the case of lumped elements although they are generally believed to apply to microwave networks also. For a discussion of the extension of network theorems to distributed-constant systems, the reader is referred to Vol. 8, Chap. 5, of this series.

Chapter 10 deals with the approximate transformation of lumped-element structures into microwave structures and with the realization of microwave filters in practical forms. Since filters are needed at microwave frequencies for the same purposes and reasons as at lower frequencies, the transformation of lumped-element structures provides an adequate variety of filter characteristics. However, one important practical difference exists. At low frequencies, low-noise amplifiers may be used to supply power lost in dissipative filters; at microwave frequencies, no satisfactory amplifiers have been built to date. Consequently, dissipative filters have not been studied, and all the filters described below provide frequency discrimination by selective reflection; any resistive loss is purely incidental and represents an unavoidable design hazard.

MATHEMATICAL REPRESENTATION OF TWO-TERMINAL-PAIR NETWORKS

9-1. Parameters Specifying Two-terminal-pair Networks.—The simplest type of filter consists of a network with a pair of input terminals and a pair of output terminals. It is customary to refer to such a network as a four-terminal network or a two-terminal-pair network. Filters with more than two pairs of terminals can be designed by properly connecting a number of filters of the simplest type. It seems appropriate, therefore, to focus our attention on two-terminal-pair networks and, in particular, on the mathematical representation of their external characteristics.

A two-terminal-pair network is illustrated schematically in Fig. 9-1 as a box with two pairs of terminals. The network inside the box is assumed to be linear and passive but may be completely arbitrary in



FIG. 9-1.—A two-terminal-pair network.

¹ See, for example, references 5 and 1 of the bibliography at the end of the chapter. Numeral superscripts in the text refer to the corresponding numbered reference of the bibliography.

all other respects. The external behavior of the network can thus be expressed by means of any two linear relations involving the variables V_1 , V_2 , I_1 , I_2 . Six pairs of such relations can be written expressing any two of these variables as functions of the other two. Only three of these six pairs, however, are sufficiently important in practice to deserve special attention.

The first pair of relations is obtained by expressing the voltages V_1 and V_2 as functions of the currents I_1 and I_2 .

$$\left. \begin{aligned} V_1 &= Z_{11}I_1 + Z_{12}I_2, \\ V_2 &= Z_{21}I_1 + Z_{22}I_2. \end{aligned} \right\} \quad (1)$$

One usually refers to the coefficients Z_{11} , Z_{12} , Z_{21} , Z_{22} as the "open-circuit impedances." In fact, if the output terminals are open-circuited, that is, if $I_2 = 0$, one obtains

$$Z_{11} = \left(\frac{V_1}{I_1} \right)_{I_2=0}, \quad Z_{21} = \left(\frac{V_2}{I_1} \right)_{I_2=0}. \quad (2)$$

Similarly one obtains for $I_1 = 0$,

$$Z_{22} = \left(\frac{V_2}{I_2} \right)_{I_1=0}, \quad Z_{12} = \left(\frac{V_1}{I_2} \right)_{I_1=0}. \quad (3)$$

According to the reciprocity theorem, which states that if, in any linear passive network, the positions of a voltage source V and an ammeter measuring a current I are interchanged, the ratio V/I remains the same, the two open-circuit transfer impedances Z_{12} and Z_{21} defined above are always equal. Consequently, an arbitrary two-terminal-pair network is completely specified by only three open-circuit impedances.

The second pair of linear relations can be obtained by expressing the currents I_1 and I_2 as functions of the voltages V_1 and V_2 as follows:

$$\left. \begin{aligned} I_1 &= Y_{11}V_1 + Y_{12}V_2, \\ I_2 &= Y_{21}V_1 + Y_{22}V_2. \end{aligned} \right\} \quad (4)$$

The coefficients Y_{11} , Y_{12} , Y_{21} , Y_{22} are called the "short-circuit admittances" because they can be defined as follows:

$$Y_{11} = \left(\frac{I_1}{V_1} \right)_{V_2=0}, \quad Y_{21} = \left(\frac{I_2}{V_1} \right)_{V_2=0}. \quad (5)$$

$$Y_{12} = \left(\frac{I_1}{V_2} \right)_{V_1=0}, \quad Y_{22} = \left(\frac{I_2}{V_2} \right)_{V_1=0}. \quad (6)$$

As in the previous case, the short-circuit transfer admittances Y_{12} and Y_{21} are always equal because of the reciprocity theorem. Therefore, as one would expect, three short-circuit admittances are sufficient to specify any arbitrary two-terminal-pair network.

By solving the pair of Eqs. (4) for V_1 and V_2 and comparing the results with the pair of Eqs. (1), the following identifications can be made:

$$\left. \begin{aligned} Z_{11} &= \frac{Y_{22}}{\det Y}, & Z_{22} &= \frac{Y_{11}}{\det Y}, \\ Z_{12} &= Z_{21} = -\frac{Y_{12}}{\det Y}, \end{aligned} \right\} \quad (7)$$

where $\det Y$ is the value of the determinant

$$\det Y = \begin{vmatrix} Y_{11} & Y_{12} \\ Y_{21} & Y_{22} \end{vmatrix} = Y_{11}Y_{22} - Y_{12}^2. \quad (8)$$

Following the opposite procedure, one obtains

$$\left. \begin{aligned} Y_{11} &= \frac{Z_{22}}{\det Z}, & Y_{22} &= \frac{Z_{11}}{\det Z}, \\ Y_{12} &= Y_{21} = -\frac{Z_{12}}{\det Z}, \end{aligned} \right\} \quad (9)$$

where $\det Z$ is the value of the determinant

$$\det Z = \begin{vmatrix} Z_{11} & Z_{12} \\ Z_{21} & Z_{22} \end{vmatrix} = Z_{11}Z_{22} - Z_{12}^2. \quad (10)$$

From these equations, one obtains

$$\det Z = 1/\det Y. \quad (11)$$

The third pair of linear relations expresses the variables at the input terminals V_1 , I_1 , as functions of the variables at the output terminals V_2 , I_2 ,

$$\left. \begin{aligned} V_1 &= \mathfrak{A}V_2 - \mathfrak{B}I_2, \\ I_1 &= \mathfrak{C}V_2 - \mathfrak{D}I_2. \end{aligned} \right\} \quad (12)$$

The coefficients \mathfrak{A} , \mathfrak{B} , \mathfrak{C} , \mathfrak{D} are called the "general circuit parameters" and can be defined as follows:

$$\left. \begin{aligned} \mathfrak{A} &= \left(\frac{V_1}{V_2} \right)_{I_2=0}, & \mathfrak{B} &= -\left(\frac{V_1}{I_2} \right)_{V_2=0}, \\ \mathfrak{C} &= \left(\frac{I_1}{V_2} \right)_{I_2=0}, & \mathfrak{D} &= -\left(\frac{I_1}{I_2} \right)_{V_2=0}. \end{aligned} \right\} \quad (13)$$

\mathfrak{A} and \mathfrak{D} are dimensionless transfer ratios, whereas \mathfrak{B} and \mathfrak{C} have, respectively, the dimensions of impedance and of admittance. These circuit parameters are related to the open-circuit impedances and to the short-circuit admittances as follows:

$$Z_{11} = \frac{\alpha}{\mathfrak{C}}, \quad Z_{12} = \frac{1}{\mathfrak{C}}, \quad Z_{22} = \frac{\mathfrak{D}}{\mathfrak{C}}, \quad (14)$$

$$Y_{11} = \frac{\mathfrak{D}}{\mathfrak{B}}, \quad Y_{12} = -\frac{1}{\mathfrak{B}}, \quad Y_{22} = \frac{\alpha}{\mathfrak{B}}, \quad (15)$$

$$\det Y = \frac{1}{\det Z} = \frac{\mathfrak{C}}{\mathfrak{B}}, \quad (16)$$

$$\left. \begin{aligned} \alpha &= -\frac{Y_{22}}{Y_{12}} = \frac{Z_{11}}{Z_{12}}, & \mathfrak{B} &= -\frac{1}{Y_{12}} = \frac{\det Z}{Z_{12}}, \\ \mathfrak{C} &= -\frac{\det Y}{Y_{12}} = \frac{1}{Z_{12}}, & \mathfrak{D} &= -\frac{Y_{11}}{Y_{12}} = \frac{Z_{22}}{Z_{12}}, \end{aligned} \right\} \quad (17)$$

where

$$\begin{vmatrix} \alpha & \mathfrak{B} \\ \mathfrak{C} & \mathfrak{D} \end{vmatrix} = \alpha\mathfrak{D} - \mathfrak{B}\mathfrak{C} = 1. \quad (18)$$

The last relation states that only three of the four circuit parameters are independent, as one would expect as a result of the reciprocity theorem.

In the particular case of symmetrical networks, that is, of networks whose input and output terminals cannot be distinguished by means of external measurements, the parameters necessary to specify a two-terminal-pair network reduce to two. One has, in fact,

$$Y_{11} = Y_{22}, \quad Z_{11} = Z_{22}, \quad \alpha = \mathfrak{D}. \quad (19)$$

Reciprocal impedance networks represent another special case in which the number of independent parameters is two. These networks are characterized by the property

$$\mathfrak{B} = \mathfrak{C} \quad (20)$$

from which one obtains, using Eqs. (16) and (17),

$$\left. \begin{aligned} \det Y = \det Z = 1, & \quad Z_{12} = -Y_{12}, \\ Y_{11} = Z_{22}, & \quad Z_{11} = Y_{22}. \end{aligned} \right\} \quad (21)$$

It will be seen later that most practical filters are either symmetrical networks, or reciprocal impedance networks.

9.2. The Use of Matrices in Circuit Analysis.—The linear relations between the current and voltage variables of a two-terminal-pair network can be written in matrix form as follows:

$$\begin{pmatrix} V_1 \\ V_2 \end{pmatrix} = \begin{pmatrix} Z_{11} & Z_{12} \\ Z_{21} & Z_{22} \end{pmatrix} \times \begin{pmatrix} I_1 \\ I_2 \end{pmatrix}, \quad (22)$$

$$\begin{pmatrix} I_1 \\ I_2 \end{pmatrix} = \begin{pmatrix} Y_{11} & Y_{12} \\ Y_{21} & Y_{22} \end{pmatrix} \times \begin{pmatrix} V_1 \\ V_2 \end{pmatrix}, \quad (23)$$

$$\begin{pmatrix} V_1 \\ I_1 \end{pmatrix} = \begin{pmatrix} \alpha & \mathfrak{B} \\ \mathfrak{C} & \mathfrak{D} \end{pmatrix} \times \begin{pmatrix} V_2 \\ -I_2 \end{pmatrix}. \quad (24)$$

These three matrix equations may be considered as shorthand representations of the three pairs of relations, Eqs. (1), (4), and (12). Such representations are very convenient when a number of two-terminal-pair networks are to be connected in series, parallel, or cascade.

For the convenience of the reader not familiar with matrix algebra, four fundamental operations on four-element matrices are defined below

$$\mathbf{A} + \mathbf{B} = \begin{pmatrix} A_{11} & A_{12} \\ A_{21} & A_{22} \end{pmatrix} + \begin{pmatrix} B_{11} & B_{12} \\ B_{21} & B_{22} \end{pmatrix} = \begin{pmatrix} A_{11} + B_{11} & A_{12} + B_{12} \\ A_{21} + B_{21} & A_{22} + B_{22} \end{pmatrix}, \quad (25)$$

$$\begin{aligned} \mathbf{A} \times \mathbf{B} &= \begin{pmatrix} A_{11} & A_{12} \\ A_{21} & A_{22} \end{pmatrix} \times \begin{pmatrix} B_{11} & B_{12} \\ B_{21} & B_{22} \end{pmatrix} \\ &= \begin{pmatrix} A_{11}B_{11} + A_{12}B_{21} & A_{11}B_{12} + A_{12}B_{22} \\ A_{21}B_{11} + A_{22}B_{21} & A_{21}B_{12} + A_{22}B_{22} \end{pmatrix}, \end{aligned} \quad (26)$$

$$k\mathbf{A} = k \begin{pmatrix} A_{11} & A_{12} \\ A_{21} & A_{22} \end{pmatrix} = \begin{pmatrix} kA_{11} & kA_{12} \\ kA_{21} & kA_{22} \end{pmatrix}, \quad (27)$$

$$\mathbf{A}^{-1} = \begin{pmatrix} A_{11} & A_{12} \\ A_{21} & A_{22} \end{pmatrix}^{-1} = \begin{pmatrix} \frac{A_{22}}{\det \mathbf{A}} & \frac{-A_{21}}{\det \mathbf{A}} \\ \frac{-A_{12}}{\det \mathbf{A}} & \frac{A_{11}}{\det \mathbf{A}} \end{pmatrix}, \quad (28)$$

$$\det \mathbf{A} = \begin{vmatrix} A_{11} & A_{12} \\ A_{21} & A_{22} \end{vmatrix} = A_{11}A_{22} - A_{12}A_{21}. \quad (29)$$

The reader will notice that

$$\mathbf{A} \times \mathbf{B} \neq \mathbf{B} \times \mathbf{A}. \quad (30)$$

A matrix consisting of a single column may be considered as a square matrix in which the elements of the second column are equal to zero. The reader can convince himself that, on the basis of the above definitions, Eqs. (22), (23), and (24) are identical to the pairs of linear relations Eqs. (1), (4), and (12).

Suppose now one wishes to study the behavior of two networks connected in parallel as shown in Fig. 9-2. One obtains for the currents I_1 and I_2

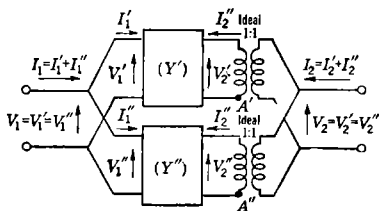


FIG. 9-2.—A parallel combination of two-terminal-pair networks.

$$\left. \begin{aligned} I_1 &= I_1' + I_1'' = (Y_{11}'V_1' + Y_{12}'V_2') + (Y_{11}''V_1'' + Y_{12}''V_2'') \\ &= (Y_{11}' + Y_{11}'')V_1 + (Y_{12}' + Y_{12}'')V_2, \\ I_2 &= I_2' + I_2'' = (Y_{21}'V_1' + Y_{22}'V_2') + (Y_{21}''V_1'' + Y_{22}''V_2'') \\ &= (Y_{21}' + Y_{21}'')V_1 + (Y_{22}' + Y_{22}'')V_2. \end{aligned} \right\} \quad (31)$$

This pair of equations can be written in matrix form as follows:

$$\begin{aligned} \begin{pmatrix} I_1 \\ I_2 \end{pmatrix} &= \begin{pmatrix} I'_1 \\ I'_2 \end{pmatrix} + \begin{pmatrix} I''_1 \\ I''_2 \end{pmatrix} = \begin{pmatrix} Y'_{11} & Y'_{12} \\ Y'_{21} & Y'_{22} \end{pmatrix} \times \begin{pmatrix} V'_1 \\ V'_2 \end{pmatrix} + \begin{pmatrix} Y''_{11} & Y''_{12} \\ Y''_{21} & Y''_{22} \end{pmatrix} \times \begin{pmatrix} V''_1 \\ V''_2 \end{pmatrix} \\ &= \left\{ \begin{pmatrix} Y'_{11} & Y'_{12} \\ Y'_{21} & Y'_{22} \end{pmatrix} + \begin{pmatrix} Y''_{11} & Y''_{12} \\ Y''_{21} & Y''_{22} \end{pmatrix} \right\} \times \begin{pmatrix} V_1 \\ V_2 \end{pmatrix}. \quad (32) \end{aligned}$$

It follows that the matrix of the parallel combination of the two networks is simply

$$Y = Y' + Y''. \quad (33)$$

The simplicity of this last equation places in evidence the advantages of matrix algebra. The ideal transformers of Fig. 9-2 can be eliminated if the points A' and A'' are at the same potential and can, therefore, be tied together without changing the behavior of the system. This

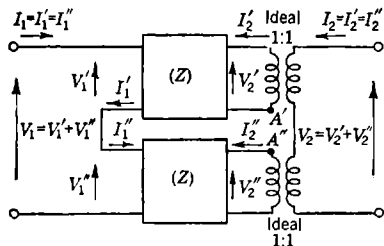


FIG. 9-3.—A series combination of two-terminal-pair networks.

is the case in most practical networks because the input and output terminals are usually connected by a ground wire.

Figure 9-3 illustrates two networks connected in series. In this case one finds that the Z -matrix of the whole network is the sum of the corresponding matrices of the two component networks.

$$Z = Z' + Z''. \quad (34)$$

In this case also, the ideal transformers can be eliminated if the points A' and A'' are at the same potential and can, therefore, be tied together without modifying the behavior of the system. As pointed out before, this elimination is possible in most practical cases.

The third and most important type of network combination is the cascade connection illustrated in Fig. 9-4. The pair of relations between the input and output variables can be written in matrix form as follows:

$$\begin{pmatrix} V_1 \\ I_1 \end{pmatrix} = \begin{pmatrix} \alpha' & \beta' \\ \epsilon' & \mathcal{D}' \end{pmatrix} \times \begin{pmatrix} V_2' \\ -I_2' \end{pmatrix} = \begin{pmatrix} \alpha' & \beta' \\ \epsilon' & \mathcal{D}' \end{pmatrix} \times \begin{pmatrix} \alpha'' & \beta'' \\ \epsilon'' & \mathcal{D}'' \end{pmatrix} \times \begin{pmatrix} V_2 \\ -I_2 \end{pmatrix}. \quad (35)$$

The matrix of the whole network is, therefore, equal to the product of the matrices of the two component networks, namely,

$$\begin{pmatrix} \alpha & \beta \\ \epsilon & \mathcal{D} \end{pmatrix} = \begin{pmatrix} \alpha' & \beta' \\ \epsilon' & \mathcal{D}' \end{pmatrix} \times \begin{pmatrix} \alpha'' & \beta'' \\ \epsilon'' & \mathcal{D}'' \end{pmatrix}. \quad (36)$$

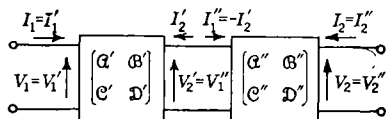
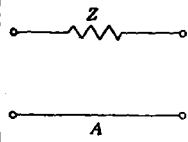
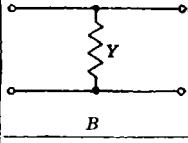
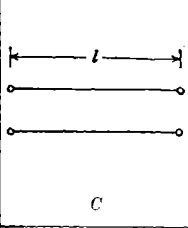
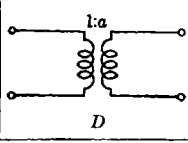


FIG. 9-4.—Cascade connection of two-terminal-pair networks.

The above results can be generalized to any desired number of networks. In the particular case of a cascade connection, the $(\alpha\beta\gamma\delta)$ matrix of the whole network is simply the product of the corresponding matrices of the component networks. It is noteworthy that the multiplications must be performed in the proper order because the commutative law does not apply to products of matrices, as was pointed out in Eq. (30).

For the convenience of the reader, a number of basic networks are shown in Tables 9-1 and 9-2, together with the matrices by which they are most simply represented.

TABLE 9-1.—SIMPLE COMPONENTS AND THEIR CORRESPONDING MATRICES

Component	Circuit	$\alpha\beta\gamma\delta$ Matrix
Series impedance		$\begin{pmatrix} 1 & Z \\ 0 & 1 \end{pmatrix}$
Shunt admittance		$\begin{pmatrix} 1 & 0 \\ Y & 1 \end{pmatrix}$
Section of line		$\begin{pmatrix} \cosh \gamma l & Z_0 \sinh \gamma \\ \frac{\sinh \gamma l}{Z_0} & \cosh \gamma l \end{pmatrix}$ $Z_0 =$ Characteristic impedance $\gamma =$ Propagation function
Ideal transformer		$\begin{pmatrix} 1 & 0 \\ a & a \end{pmatrix}$

9-3. Determination of Input Impedance and Insertion Loss.—The matrices discussed above specify the behavior of a two-terminal-pair network independently of the characteristics of the generator and of the load that are connected to the input and output terminals. In many cases, on the other hand, one is interested specifically in the behavior

TABLE 9-2.—SIMPLE STRUCTURES AND THEIR CORRESPONDING MATRICES

Structure	Circuit	Matrix
T-section		$[z] = \begin{pmatrix} Z_a + Z_c & Z_c \\ Z_c & Z_b + Z_c \end{pmatrix}$
π -section		$[y] = \begin{pmatrix} Y_a + Y_c & -Y_c \\ -Y_c & Y_b + Y_c \end{pmatrix}$
Symmetrical lattice		$[z] = \begin{pmatrix} \frac{Z_b + Z_a}{2} & \frac{Z_b - Z_a}{2} \\ \frac{Z_b - Z_a}{2} & \frac{Z_b + Z_a}{2} \end{pmatrix}$ $[y] = \begin{pmatrix} \frac{Y_b + Y_a}{2} & \frac{Y_b - Y_a}{2} \\ \frac{Y_b - Y_a}{2} & \frac{Y_b + Y_a}{2} \end{pmatrix}$

of the network when it is inserted between a given generator and a given load. Two functions are particularly useful in this connection, namely, the input impedance Z of the network when a load impedance Z_L is connected to the output terminals, and the voltage insertion ratio, which will be defined later. To compute the input impedance let the network be specified by the parameters α , β , ϵ , \mathcal{D} , and let α' , β' , ϵ' , \mathcal{D}' be the corresponding parameters of the cascade connection of the network and the load impedance Z_L as shown in Fig. 9-5. One obtains then



FIG. 9-5.—Two-terminal-pair network terminated in a load Z_L .

$$\begin{pmatrix} \alpha' & \beta' \\ \epsilon' & \mathcal{D}' \end{pmatrix} = \begin{pmatrix} \alpha & \beta \\ \epsilon & \mathcal{D} \end{pmatrix} \times \begin{pmatrix} 1 & 0 \\ \frac{1}{Z_L} & 1 \end{pmatrix} = \begin{pmatrix} \alpha + \frac{\beta}{Z_L} & \beta \\ \epsilon + \frac{\mathcal{D}}{Z_L} & \mathcal{D} \end{pmatrix}. \quad (37)$$

At this point one observes that the driving-point impedance Z is the same as the open-circuit impedance of the cascade connection to which

Eq. (37) applies. Therefore, Z can be expressed in terms of α' and β' by means of Eq. (14). One has then

$$Z = \frac{\alpha Z_L + \beta}{\epsilon Z_L + \mathcal{D}} = \frac{\alpha}{\epsilon} \frac{Z_L + \frac{\beta}{\alpha}}{Z_L + \frac{\mathcal{D}}{\epsilon}} \quad (38)$$

Another convenient expression for Z can be obtained by substituting for the ratios α/ϵ , β/α , and \mathcal{D}/ϵ by means of Eqs. (14) and (15)

$$Z = Z_{11} \frac{Z_L + \frac{1}{Y_{22}}}{Z_L + Z_{22}} \quad (39)$$

It is interesting to note that this equation contains only driving-point impedances and admittances and, moreover, that one could multiply all the impedances measured at the output terminals by a constant k without changing the ratio Z/Z_{11} . In other words, the ratio Z/Z_{11} depends only on the relative values of the impedances measured at the output terminals. This fact is of primary importance in connection with waveguide networks, as is shown in Sec. 10-6.

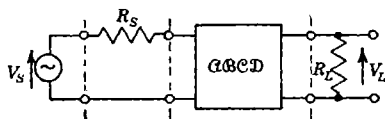


FIG. 9-6.—Two-terminal-pair network inserted between a generator and a load.

The voltage insertion ratio is the function most commonly used to describe the over-all behavior of a filter when it is inserted between a specified generator and a specified load. It will be defined below, in a manner somewhat unconventional, for the particular case of practical importance in which both the load impedance and the generator impedance are pure resistances. With reference to Fig. 9-6, let V'_L be the voltage across the load resistance R_L when the filter is removed and the generator is matched to the load by means of an appropriate transformer in order to maximize the load power. The voltage insertion ratio is defined as the ratio of V'_L to the voltage V_L measured across R_L when the filter is inserted between the generator and the load. One obtains for the voltage V'_L

$$V'_L = \frac{1}{2} V_s \sqrt{\frac{R_L}{R_s}} \quad (40)$$

The voltage V_L can be determined in terms of the general network parameters in the following manner. Let α' , β' , ϵ' , \mathcal{D}' be the elements of the matrix representing the cascade connection of the generator

resistance, the filter, and the load as illustrated in Fig. 9-6. This matrix can be computed as follows:

$$\begin{aligned} \begin{pmatrix} \alpha' & \beta' \\ \epsilon' & \mathfrak{D}' \end{pmatrix} &= \begin{pmatrix} 1 & R_s \\ 0 & 1 \end{pmatrix} \times \begin{pmatrix} \alpha & \beta \\ \epsilon & \mathfrak{D} \end{pmatrix} \times \begin{pmatrix} 0 & 1 \\ \frac{1}{R_L} & 1 \end{pmatrix} \\ &= \begin{pmatrix} \left(\alpha + \frac{\beta}{R_L} + R_s \epsilon + R_s \mathfrak{D} \right) & (\beta + R_s \mathfrak{D}) \\ \left(\epsilon + \frac{\mathfrak{D}}{R_L} \right) & \mathfrak{D} \end{pmatrix}. \end{aligned} \quad (41)$$

One observes then that the ratio V_s/V_L is, by definition, equal to α' ; that is,

$$\frac{V_s}{V_L} = \alpha + \frac{\beta}{R_L} + R_s \epsilon + \frac{R_s}{R_L} \mathfrak{D}. \quad (42)$$

It follows that the insertion ratio is given by

$$\frac{V'_L}{V_L} = \frac{1}{2} \left[\left(\sqrt{\frac{R_L}{R_s}} \alpha + \sqrt{\frac{R_s}{R_L}} \mathfrak{D} \right) + \left(\frac{\beta}{\sqrt{R_s R_L}} + \sqrt{R_s R_L} \epsilon \right) \right]. \quad (43)$$

If the filter is nondissipative, that is, if it contains only reactive elements, α and \mathfrak{D} are real quantities but β and ϵ are imaginary. This property can be derived from Eqs. (17) by observing that the open-circuit impedances and the short-circuit admittances are imaginary in the case of reactive networks.

If one is concerned only with the frequency discrimination properties of a filter irrespective of its transient behavior, the phase of the ratio V'_L/V_L is immaterial. It is customary to refer to the square of the magnitude of the insertion ratio as the "power-loss ratio." In fact, if P_0 is the maximum power available from the generator and P_L is the power delivered to R_L when the filter is inserted between the generator and the load, one obtains

$$\frac{P_0}{P_L} = \left| \frac{V'_L}{V_L} \right|^2. \quad (44)$$

The reciprocal of this ratio, that is, P_L/P_0 , is called the "power-transmission ratio." The *insertion loss* L , on the other hand, is the value in decibels of P_0/P_L , that is,

$$L = 10 \log_{10} \frac{P_0}{P_L} = 20 \log_{10} \left| \frac{V'_L}{V_L} \right|. \quad (45)$$

This definition of the insertion loss differs from the one made in many textbooks in that the power delivered to the load is normalized

with respect to the power available from the generator rather than to the power that would be delivered to the load if the load were connected directly to the generator. Of course, the two definitions coincide if the load resistance is equal to the source resistance.

In the particular case of nondissipative networks, which is the most important case in practice, the expression for the power-loss ratio, given by Eqs. (43) and (44), can be transformed into a more convenient form in the following manner. Since the first term of Eq. (43) is real, whereas the second term is imaginary, using Eq. (18) one obtains for the power-loss ratio

$$\begin{aligned} \frac{P_0}{P_L} &= \frac{1}{4} \left[\left(\frac{R_L}{R_s} \mathcal{G}^2 + \frac{R_s}{R_L} \mathcal{D}^2 + 2\mathcal{G}\mathcal{D} \right) - \left(\frac{\mathcal{B}^2}{R_s R_L} + R_s R_L \mathcal{C}^2 + 2\mathcal{B}\mathcal{C} \right) \right] \\ &= 1 + \frac{1}{4} \left[\left(\sqrt{\frac{R_L}{R_s}} \mathcal{G} - \sqrt{\frac{R_s}{R_L}} \mathcal{D} \right)^2 - \left(\frac{\mathcal{B}}{\sqrt{R_s R_L}} - \sqrt{R_s R_L} \mathcal{C} \right)^2 \right]. \end{aligned} \quad (46)$$

The advantage of this last expression is that it simplifies readily in the case of a symmetrical network ($R_L = R_s$, $\mathcal{G} = \mathcal{D}$) and in the case of a reciprocal impedance network ($R_L R_s = 1$, $\mathcal{B} = \mathcal{C}$).

9.4. Wave Matrices and Accumulative Mismatches.—Before leaving the subject of the mathematical representation of two-terminal-pair networks it is well to discuss, to some extent, two matrices which are particularly useful in connection with transmission-line systems. Figure 9-7 illustrates a network terminated in two arbitrary nondissipative transmission lines. Let I_1 be defined as the square root of the product of the voltage and the current of an incident wave at the input terminals of the network. In other words, the magnitude of I_1 is equal to the square root of the power carried by the incident wave, and the phase of I_1 is equal to the phase of the voltage. Similarly, let R_1 be defined as the square root of the product of the voltage and the current of the reflected wave at the input terminals. I_2 and R_2 represent the incident and reflected waves at the output terminal as indicated in Fig. 9-7. The variables I_1 , R_1 , I_2 , R_2 may be considered as normalized voltages.

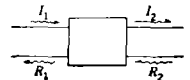


FIG. 9-7.—Network terminated in lossless lines.

Matrices that relate these four variables may be defined as in the case of terminal voltages and currents. For instance, one may write the following matrix equations,

$$\begin{pmatrix} R_1 \\ I_2 \end{pmatrix} = \begin{pmatrix} \Gamma_1 & T_2 \\ T_1 & \Gamma_2 \end{pmatrix} \times \begin{pmatrix} I_1 \\ R_2 \end{pmatrix}, \quad (47)$$

$$\begin{pmatrix} I_1 \\ R_1 \end{pmatrix} = \begin{pmatrix} A_{11} & A_{12} \\ A_{21} & A_{22} \end{pmatrix} \times \begin{pmatrix} I_2 \\ R_2 \end{pmatrix}. \quad (48)$$

The elements of the two matrices thus defined can be determined as follows:

$$\left. \begin{aligned} \Gamma_1 &= \left(\frac{R_1}{I_1} \right)_{R_2=0} & \Gamma_2 &= \left(\frac{I_2}{R_2} \right)_{I_1=0} \\ T_1 &= \left(\frac{I_2}{I_1} \right)_{R_2=0} & T_2 &= \left(\frac{R_1}{R_2} \right)_{I_1=0} \end{aligned} \right\}, \quad (49)$$

$$\left. \begin{aligned} A_{11} &= \left(\frac{I_1}{I_2} \right)_{R_2=0} & A_{12} &= \left(\frac{I_1}{R_2} \right)_{I_2=0} \\ A_{21} &= \left(\frac{R_1}{I_2} \right)_{R_2=0} & A_{22} &= \left(\frac{R_1}{R_2} \right)_{I_2=0} \end{aligned} \right\}, \quad (50)$$

where Γ_1 and Γ_2 are the reflection coefficients at the input and output terminals, respectively, when the line on the other side of the network is properly terminated, and T_1 and T_2 are the transmission coefficients measured under the same conditions. Because of the reciprocity theorem one has

$$T_1 = T_2 = T. \quad (51)$$

The parameters defined by Eq. (50) are related to Γ_1 , Γ_2 , and T as follows:

$$\left. \begin{aligned} A_{11} &= \frac{1}{T}, & A_{12} &= -\frac{\Gamma_2}{T}, \\ A_{21} &= \frac{\Gamma_1}{T}, & A_{22} &= T - \frac{\Gamma_1 \Gamma_2}{T} \end{aligned} \right\} \quad (52)$$

It follows that

$$A_{11}A_{22} - A_{12}A_{21} = 1. \quad (53)$$

The reader will observe that the parameter $A_{11} = 1/T$ is the voltage insertion ratio defined above and, therefore, $|A_{11}|^2$ is the power-loss ratio. If the network is nondissipative, the power transmitted through the network must equal the incident power minus the reflected power. It follows that, if the output line is properly terminated, one has

$$|T|^2 = 1 - |\Gamma_1|^2. \quad (54)$$

Similarly, if the direction of power flow is reversed and the input line is properly terminated, one has

$$|T|^2 = 1 - |\Gamma_2|^2. \quad (55)$$

It follows that the magnitudes of the reflection coefficients for the input and the output terminals are equal; that is,

$$|\Gamma_1| = |\Gamma_2| = |\Gamma|. \quad (56)$$

The VSWR measured in either line when the opposite line is properly

terminated is then given by

$$r = \frac{1 + |\Gamma|}{1 - |\Gamma|}. \quad (57)$$

The \mathbf{A} -matrix has properties similar to the (α , β , ϵ , \mathcal{D})-matrix, that is, the \mathbf{A} -matrix of a cascade connection of a number of networks is equal to the product of the \mathbf{A} -matrices of the component networks. One must observe, however, that this method of analysis can be used only if the transmission lines that are joined in the process of cascading the networks have the same characteristic impedance. If this is not the case, the junctions of transmission lines of different characteristic impedances must be considered as separate networks.

An illustration of the use of \mathbf{A} -matrices is the following problem. Let \mathbf{A}' and \mathbf{A}'' be the matrices of two nondissipative networks, and r' and r'' be the magnitude of the VSWR in the input lines of the two networks when their output lines are properly terminated. If the two networks are connected in cascade as shown in Fig. 9-8, the magnitude r of the VSWR in the input line will depend on the angular length θ of the line joining the two networks. It is desired to determine the maximum and minimum values of r that can be obtained by varying θ . The \mathbf{A}_θ -matrix of the section of line of length θ is found to be

$$\mathbf{A}_\theta = \begin{pmatrix} e^{j\theta} & 0 \\ 0 & e^{-j\theta} \end{pmatrix}. \quad (58)$$

Therefore, the matrix of the whole system is

$$\begin{aligned} \mathbf{A} &= \begin{pmatrix} A'_{11} & A'_{12} \\ A'_{21} & A'_{22} \end{pmatrix} \times \begin{pmatrix} e^{j\theta} & 0 \\ 0 & e^{-j\theta} \end{pmatrix} \times \begin{pmatrix} A''_{11} & A''_{12} \\ A''_{21} & A''_{22} \end{pmatrix} \\ &= \begin{pmatrix} A'_{11} & A'_{12} \\ A'_{21} & A'_{22} \end{pmatrix} \times \begin{pmatrix} A''_{11} e^{j\theta} & A''_{12} e^{j\theta} \\ A''_{21} e^{-j\theta} & A''_{22} e^{-j\theta} \end{pmatrix}. \end{aligned} \quad (59)$$

At this point one observes that the maximum and minimum values of r must correspond, respectively, to the minimum and maximum values of the magnitude of the transmission coefficient T of the whole network since no power is lost in the network. The value of A_{11} , that is, of $1/T$, is easily obtained from Eq. (59) as follows:

$$\begin{aligned} A_{11} &= 1/T = A'_{11}A''_{11}e^{j\theta} + A'_{12}A''_{21}e^{-j\theta} \\ &= \frac{e^{j\theta}}{T' T''} (1 - \Gamma'_1 \Gamma''_2 e^{-j\theta}). \end{aligned} \quad (60)$$

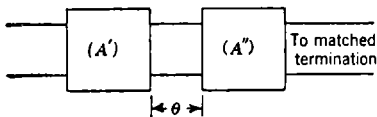


FIG. 9-8.—Two networks connected in cascade by a transmission line.

The maximum and minimum values of the magnitude of T are evidently given by

$$\frac{1}{|T|_{\min}} = \frac{1 + |\Gamma'_2||\Gamma''_1|}{|T'||T''|} = \frac{1 + |\Gamma'_2||\Gamma''_1|}{\sqrt{(1 - |\Gamma'_2|^2)(1 - |\Gamma''_1|^2)}}, \quad (61)$$

$$\frac{1}{|T|_{\max}} = \frac{1 - |\Gamma'_2||\Gamma''_1|}{|T'||T''|} = \frac{1 - |\Gamma'_2||\Gamma''_1|}{\sqrt{(1 - |\Gamma'_2|^2)(1 - |\Gamma''_1|^2)}}. \quad (62)$$

One has, then, for the minimum and maximum values of the magnitude of the reflection coefficient,

$$|\Gamma|_{\min} = \sqrt{1 - |T|_{\max}^2} = \left| \frac{|\Gamma'_1| - |\Gamma'_2|}{1 - |\Gamma'_1||\Gamma'_2|} \right|, \quad (63)$$

$$|\Gamma|_{\max} = \sqrt{1 - |T|_{\min}^2} = \left| \frac{|\Gamma'_1| + |\Gamma'_2|}{1 + |\Gamma'_1||\Gamma'_2|} \right|. \quad (64)$$

Finally, by means of Eq. (57), one obtains for the maximum and minimum values of the VSWR in the input line

$$r_{\max} = r'r'', \quad (65)$$

and

$$r_{\min} = \begin{cases} \frac{r'}{r''} & \text{for } r' > r'' \\ \frac{r''}{r'} & \text{for } r'' > r' \end{cases}. \quad (66)$$

IMAGE PARAMETERS

9-5. Image Impedance and Propagation Functions.—The so-called "image" parameters of a network play a very important part in the conventional design of filters. It is desirable, therefore, to review briefly their definitions and to discuss some of their properties.

The image parameters of a two-terminal-pair network are the *image impedances* of the two pairs of terminals and the *propagation function*. The two image impedances Z_{11} and Z_{12} may be defined as follows: with reference to Fig. 9-9, Z_{11} is the impedance which would be measured between terminals 1 and 1', if an impedance equal to Z_{12} were connected to terminals 2 and 2'; conversely, Z_{12} is the impedance which would be measured between terminal 2 and 2' if an impedance equal to Z_{11} were connected to terminals 1 and 1'.

The propagation function specifies the transmission properties of the network when the source and load impedances are equal to the image impedances. With reference to Fig. 9-9, suppose a voltage source is

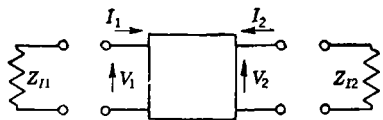


FIG. 9-9.—Two-terminal-pair network terminated in its image impedance.

placed in series with Z_{11} . The ratio V_1/V_2 may be expressed in terms of the propagation function γ as follows:

$$\frac{V_1}{V_2} = \sqrt{\frac{Z_{11}}{Z_{12}}} e^\gamma. \quad (67)$$

The factor $\sqrt{Z_{11}/Z_{12}}$ represents the transformer action of the network and becomes unity in the case of a symmetrical network. If the voltage source is placed in series with Z_{12} , the voltage ratio becomes

$$\frac{V_2}{V_1} = \sqrt{\frac{Z_{12}}{Z_{11}}} e^\gamma. \quad (68)$$

The consistency of Eqs. (67) and (68) follows from the reciprocity theorem. The propagation function is, in general, a complex quantity

$$\gamma = \alpha + j\beta.$$

The real part α is called the "attenuation function," and the imaginary part β is called the "phase function."

The image parameters are related to the circuit constants \mathfrak{A} , \mathfrak{B} , \mathfrak{C} , \mathfrak{D} , defined in Sec. 9-1, as follows:

$$Z_{11} = \sqrt{\mathfrak{A}\mathfrak{B}/\mathfrak{C}\mathfrak{D}}, \quad Z_{12} = \sqrt{\mathfrak{D}\mathfrak{B}/\mathfrak{C}\mathfrak{A}}, \quad (69)$$

$$\cosh^2 \gamma = \mathfrak{A}\mathfrak{D}, \quad \sinh^2 \gamma = \mathfrak{B}\mathfrak{C}. \quad (70)$$

Two other quantities, namely, the open-circuit and short-circuit impedances of a network, are often useful in the computation of the image parameters. These are defined in the following manner. Let Z_{oc1} and Z_{sc1} be, respectively, the impedances measured between terminals 1 and 1' when terminals 2 and 2' are open-circuited and short-circuited. Let Z_{oc2} and Z_{sc2} be the corresponding impedances measured between terminals 2 and 2'. It can be shown that the image parameters are given by the following equations:

$$Z_{11} = \sqrt{Z_{oc1}Z_{sc1}}, \quad (71)$$

$$Z_{12} = \sqrt{Z_{oc2}Z_{sc2}}, \quad (72)$$

$$\gamma = \tanh^{-1} \sqrt{\frac{Z_{sc1}}{Z_{oc1}}} = \tanh^{-1} \sqrt{\frac{Z_{sc2}}{Z_{oc2}}}, \quad (73)$$

which may be written alternatively as

$$\gamma = \frac{1}{2} \ln \frac{1 + \sqrt{Z_{sc1}/Z_{oc1}}}{1 - \sqrt{Z_{sc1}/Z_{oc1}}} = \frac{1}{2} \ln \frac{1 + \sqrt{Z_{sc2}/Z_{oc2}}}{1 - \sqrt{Z_{sc2}/Z_{oc2}}}. \quad (74)$$

In the case of geometrically symmetrical networks, the image parameters can be expressed in terms of the open-circuit and short-circuit

impedances of half the network. Special consideration must be given here to the meaning of open circuit and short circuit since the terminals involved may be more than two. With reference to Fig. 9-10, Z_{och} is determined by separating the two halves of the network at the geometric plane of symmetry and then short-circuiting the terminals resulting from any pair of wires which cross each other on that plane, leaving all the other terminals disconnected.

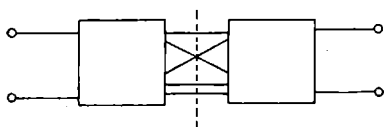


FIG. 9-10.—Bisection of a symmetrical network.

Conversely, Z_{sch} is determined by tying together all the terminals at the geometric plane of symmetry except the ones that were short-circuited before. In terms of these impedances, Bartlett's bisection theorem, as extended by Brune,³ states that the image impedance (obviously $Z_{i1} = Z_{i2} = Z_I$) and the propagation function are given by

$$Z_I = \sqrt{Z_{och}Z_{sch}} \quad (75)$$

$$\gamma = 2 \tanh^{-1} \sqrt{\frac{Z_{sch}}{Z_{och}}} \pm j\pi = \ln 1 + \frac{\sqrt{Z_{sch}/Z_{och}}}{1 - \sqrt{Z_{sch}/Z_{och}}} \pm j\pi. \quad (76)$$

Equations (75) and (76) are extremely useful in connection with symmetrical networks because they save a considerable amount of labor in the computation of the image parameters. Moreover, as will be shown later, they form the basis of a classical method of filter design.

Two networks connected in cascade as shown in Fig. 9-11 will now be considered. It is assumed that $Z_{i2} = Z_{i3}$. The image impedances for terminals 1 and 4 of the cascade connection are, respectively, Z_{i1} and Z_{i4} , that is, the image impedances for the same terminals of the two networks, considered separately. In fact, if an impedance equal to Z_{i4} is connected to terminals 4, the network 3-4 will load the network 1-2 with an impedance equal to Z_{i3} , which by assumption is equal to Z_{i2} .

Consequently, the input impedance measured at terminals 1 will be equal to Z_{i1} as required by the definition of image impedance. Similarly, if an impedance equal to Z_{i1} is connected to terminals 1, the impedance measured at terminals 4 will be equal to Z_{i4} . The propagation function of the cascade combination is then by definition

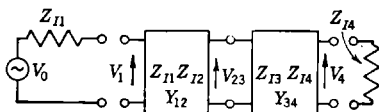


FIG. 9-11.—Two-terminal-pair networks connected in cascade and terminated in image impedances.

$$\gamma = \ln \left[\frac{V_1}{V_4} \sqrt{\frac{Z_{i4}}{Z_{i1}}} \right] = \ln \left[\frac{V_1}{V_{23}} \sqrt{\frac{Z_{i2}}{Z_{i1}}} \right] + \ln \left[\frac{V_{23}}{V_4} \sqrt{\frac{Z_{i4}}{Z_{i3}}} \right]. \quad (77)$$

Both networks are separately terminated in the proper image impedances

when Z_{14} is connected to terminals 4. It follows that

$$\gamma_{12} = \ln \left[\frac{V_1}{V_{23}} \sqrt{\frac{Z_{12}}{Z_{11}}} \right]; \quad \gamma_{34} = \ln \left[\frac{V_{23}}{V_4} \sqrt{\frac{Z_{14}}{Z_{13}}} \right] \quad (78)$$

and consequently,

$$\gamma = \gamma_{12} + \gamma_{34}. \quad (79)$$

In other words, the propagation function of the two networks in cascade is equal to the sum of the propagation functions of the two networks. These results can be generalized for a cascade connection of any number n of networks in which the image impedances are matched at every junction. The propagation function of the cascade connection will be equal to the sum of the propagation functions of the individual networks, and the two image impedances will be equal to Z_{11} and Z_{12n} .

9-6. Behavior of Image Parameters of Reactive Networks.—The properties of the image parameters of nondissipative networks will now be considered in more detail. In such networks the impedances Z_{oc1} , Z_{oc2} , Z_{sc1} , Z_{sc2} become purely imaginary, and if X_{oc1} , X_{oc2} , X_{sc1} , X_{sc2} are the corresponding reactances, the expressions for the image parameters become

$$Z_{11} = \sqrt{-X_{oc1}X_{sc1}}, \quad Z_{12} = \sqrt{-X_{oc2}X_{sc2}},$$

$$\gamma = \frac{1}{2} \ln \frac{1 + \sqrt{X_{sc}/X_{oc}}}{1 - \sqrt{X_{sc}/X_{oc}}}. \quad (80)$$

It follows that both image impedances are real and γ is purely imaginary when $(X_{sc2}/X_{oc2}) = (X_{sc1}/X_{oc1}) < 0$. The band of frequencies in which this condition is satisfied is called the "pass band," since the attenuation α is identically zero. Conversely, when $(X_{sc1}/X_{oc1}) = (X_{sc2}/X_{oc2}) > 0$, both image impedances become purely imaginary and γ becomes

$$\gamma = \alpha + jk \frac{\pi}{2}, \quad (81)$$

where k is an integer. The band of frequencies in which $\alpha \neq 0$ is called the "attenuation band." The sign of the ratio $X_{sc1}/X_{oc1} = X_{sc2}/X_{oc2}$ must change, by definition, at each end of a pass band. But, according to Foster's reactance theorem, the slope of any reactance function is always positive. It follows that one of the two reactances (X_{sc} or X_{oc}) must be either zero or infinite whenever the ratio $X_{sc1}/X_{oc1} = X_{sc2}/X_{oc2}$ changes sign. This must be true, of course, for both pairs of terminals. Conversely, a pole or a zero of either reactance marks the limit of a pass band unless both reactances are critical, that is, both change sign at the same frequency. It follows also that the image impedances become either zero or infinite at the ends of any pass band. The attenuation α

becomes infinite when $X_{sc}/X_{oc} = 1$. However, the image impedances are noncritical when α is infinite, unless both reactances are, independently, critical.

The propagation function has been shown to have very useful properties in connection with the design of filters. The actual transmission characteristics of a filter, however, are represented correctly by the propagation function only when the source and load impedances are equal to the image impedances. In practice, the source and load impedances are pure resistances and, consequently, do not properly terminate the filter at all frequencies. Let R_L and R_S be the source and load resistances, respectively. The power-loss ratio is given in terms of α , \mathfrak{B} , \mathfrak{C} , \mathfrak{D} by Eq. (46) which is rewritten below.

$$\frac{P_0}{P_L} = 1 + \frac{1}{4} \left\{ \left[\sqrt{\frac{\alpha R_L}{\mathfrak{D} R_S}} - \sqrt{\frac{\mathfrak{D} R_S}{\alpha R_L}} \right]^2 \alpha \mathfrak{D} - \left[\sqrt{\frac{\mathfrak{B}}{R_S R_L \mathfrak{C}}} - \sqrt{\frac{R_S R_L \mathfrak{C}}{\mathfrak{B}}} \right]^2 \mathfrak{B} \mathfrak{C} \right\}. \quad (82)$$

When the image parameters are introduced, by means of Eqs. (69) and (70), this equation becomes

$$\frac{P_0}{P_L} = 1 + \frac{1}{4} \left\{ \left[\sqrt{\frac{Z_{I1} R_L}{R_S Z_{I2}}} - \sqrt{\frac{Z_{I2} R_S}{R_L Z_{I1}}} \right]^2 \cosh^2 \gamma - \left[\sqrt{\frac{Z_{I1} Z_{I2}}{R_S R_L}} - \sqrt{\frac{R_S R_L}{Z_{I1} Z_{I2}}} \right]^2 \sinh^2 \gamma \right\}. \quad (83)$$

It will be noticed that the image impedances and the terminating resistances appear in this equation only as Z_{I1}/R_S and Z_{I2}/R_L . Therefore, it is possible in all cases to normalize the image impedances with respect to the corresponding terminating resistances. This is equivalent to saying that both terminations can be made equal to unity without loss of generality. Physically speaking, this is done by changing the impedance level of the whole network and by using, if necessary, an ideal transformer. It will be sufficient, therefore, from now on to consider only networks terminated in 1-ohm resistances.

Two groups of networks are particularly important; symmetrical networks for which, according to Eqs. (19) and (69), $Z_{I1} = Z_{I2}$, and networks with reciprocal image impedances for which, according to Eqs. (20) and (69), $Z_{I1} = 1/Z_{I2}$. In the case of symmetrical networks with 1-ohm terminations, Eq. (83) reduces to

$$\frac{P_0}{P_L} = 1 - \frac{1}{4} \left[Z_1 - \frac{1}{Z_1} \right]^2 \sinh^2 \gamma. \quad (84)$$

In the pass band, γ is a pure imaginary $j\beta$, and Z_1 is real. Therefore, Eq. (84) becomes

$$\frac{P_0}{P_L}(\beta) = 1 + \frac{1}{4} \left[Z_I - \frac{1}{Z_I} \right]^2 \sin^2 \beta. \quad (85)$$

Z_I is finite over the whole pass band but becomes either zero or infinite at the cutoff frequencies. The function β must have a positive slope and must equal an integer times π at the cutoff frequencies. In fact it can be shown that, in the case of a symmetrical network, Z_{sc} cannot vanish while Z_{oc} is finite, and Z_{oc} cannot become infinite while Z_{sc} is finite. It follows that the power ratio oscillates between unity and the value $1 + \frac{1}{4} \left[Z_I - \frac{1}{Z_I} \right]^2$. The maxima occur approximately when $\sin^2 \beta = 1$, that is, when β is equal to an odd integer times $\pi/2$. At the cutoff points, $\left(Z_I - \frac{1}{Z_I} \right)^2$ becomes infinite and $\sin \beta$ vanishes. The limit of the product can be found by substituting in Eq. (85) the values of Z_I and $\sin \beta$ expressed as functions of Z_{oc} and Z_{sc} . This limit is always finite.

In the attenuation band, Z_I is imaginary and β is equal to an integer times π . Therefore, Eq. (84) reduces to

$$\frac{P_0}{P_L}(\alpha) = 1 + \frac{1}{4} \left[|Z_I| + \frac{1}{|Z_I|} \right]^2 \sinh^2 \alpha. \quad (86)$$

The limit of this expression at the cutoff, that is, when α approaches zero and $|Z_I| + \frac{1}{|Z_I|}$ approaches infinity, must be equal to the value obtained when approaching the cutoff from the pass band. The power ratio is never less than, and, for large values of α , is approximately equal to

$$\frac{P_0}{P_L}(\alpha) \approx \frac{1}{16} \left[|Z_I| + \frac{1}{|Z_I|} \right]^2 e^{2\alpha}. \quad (87)$$

The minimum value of $\left[|Z_I| + \frac{1}{|Z_I|} \right]^2$ is 4. Therefore, the power ratio is never smaller than

$$\frac{P_0}{P_L}(\alpha) \Big|_{\min} = \frac{e^{2\alpha}}{4}. \quad (88)$$

The common statement of this fact is that the insertion loss is never more than 6 db below the attenuation function.

Networks of the second group have image impedances reciprocal to each other. Let $Z_I = Z_{I1} = 1/Z_{I2}$. Equation (83) is simplified to

$$\frac{P_0}{P_L} = 1 + \frac{1}{4} \left[Z_I - \frac{1}{Z_I} \right]^2 \cosh^2 \gamma. \quad (89)$$

In the pass band, γ is imaginary and Z_l is real, as in the previous case. Therefore, this equation reduces to

$$\frac{P_0}{P_L}(\beta) = 1 + \frac{1}{4} \left[Z_l - \frac{1}{Z_l} \right]^2 \cos^2 \beta. \quad (90)$$

It can be shown that, when $Z_{l1} = 1/Z_{l2}$, Z_{oc} cannot vanish while Z_{sc} is finite and Z_{sc} cannot become infinite while Z_{oc} is finite. This situation is exactly opposite to that encountered in the case of symmetrical networks. It follows from Eq. (80) that, at the cutoff points, β must be given by

$$\beta = \frac{\pi}{2} + n\pi, \quad (91)$$

that is, $\cos \beta$ vanishes at both ends of the pass band. At these points $[Z_l - 1/Z_l]$ becomes infinite but, as in the previous case, the limit of the product of the two factors is finite. Again the power ratio oscillates between unity and the value $1 + \frac{1}{4}[Z_l - 1/Z_l]^2$, the maxima occurring approximately when $\cos^2 \beta = 1$.

In the attenuation band, β is a constant equal to the value at the cutoff given by Eq. (91), and Z_l is imaginary. Therefore, Eq. (89) reduces to

$$\frac{P_0}{P_L}(\alpha) = 1 + \frac{1}{4} \left[|Z_l| + \frac{1}{|Z_l|} \right]^2 \sinh^2 \alpha. \quad (92)$$

Since this equation is identical to Eq. (86), no further discussion is required.

NORMALIZATION OF FILTER DESIGNS

The particular values of the components used in a final filter design depend on the electrical specifications which include, among other things, the desired values of the terminating impedances and the width of the pass band. To avoid unnecessary duplication in computation, it is desirable to "normalize" designs so that, by slight alterations, a single basic design may be made to satisfy a variety of given specifications.

First, a procedure will be developed by which a filter design appropriate for 1-ohm terminations may be adapted for use with any pair of terminating impedances. In principle, such a procedure is always applicable but may in certain instances lead to practical problems requiring special handling. Fortunately, such cases are the exception rather than the rule. Second, certain frequency transformations that normalize the frequency dependence of most practical filters will be discussed. The first and simplest transformation reduces the design of all low-pass filters to the design of prototypes with cutoff frequencies of 1 radian/sec. More complex transformations will then be introduced which permit

the design of a whole class of high-pass, bandpass, and band-elimination filters from these low-pass prototypes. The use of such transformations reduces considerably the amount of algebraic manipulation and numerical computation required to yield final data and eliminates the necessity for redundant expositions in the remainder of the chapter. It should be realized, however, that the filters generated from a basic low-pass filter by such transformations of variables do not always afford the most advantageous design for a given problem. Except for rather special applications, however, such filters are quite satisfactory and are widely used.

9-7. Impedance Normalization.—The normalization with respect to the terminating impedances does not present any difficulty when the terminating impedances are equal. It is evident that the insertion loss of a filter remains unchanged when all the impedances of the system, the

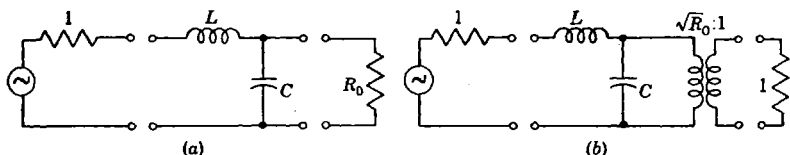


FIG. 9-12.—Impedance-level transformations in a low-pass filter.

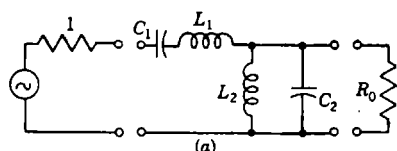
source and load impedances included, are multiplied by the same constant. Therefore, a filter designed to operate between 1-ohm terminations can be modified to operate between R -ohm terminations by simply multiplying all the inductances and the resistances by R and dividing all the capacitances by R . In the case in which the terminating impedances are not equal, the basic design can still be used, but the impedance level of one side of the filter must be changed. In theory this can be done very easily by means of an ideal transformer, but in practice the behavior of an ideal transformer can be only approximated. In many practical cases, however, the ideal transformer can be lumped with other elements of the network. In other words, the network can be modified so that the proper change of impedance level is produced at the most convenient place between the input terminals and the output terminals.

A similar procedure must be followed when the basic design requires terminating impedances different from each other, whereas the specified impedances are equal. By way of illustration, consider Figs. 9-12a and 9-13a, which show the simplest basic designs for a low-pass filter and a bandpass filter, respectively. In the case of the low-pass filter, the basic design can be modified to operate between equal terminations only by means of a transformer (Fig. 9-12b). Therefore, the original frequency response cannot be reproduced exactly since all practical transformers are frequency-sensitive. The bandpass filter, on the contrary, can be

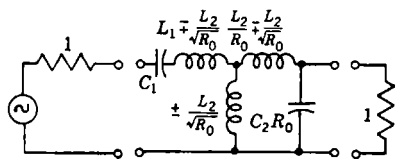
transformed very easily as shown in Fig. 9-13*b* and *c* without any change of frequency behavior. Even in this case, however, the transformation is possible only if the coupled coils are practically realizable, that is, if

$$\frac{L_1 L_2}{R_0} > \frac{L_2^2}{R_0} L_1 > L_2. \quad (93)$$

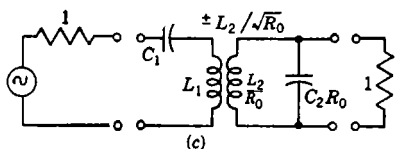
It turns out that this condition is satisfied whenever the band of the filter is greater than 1 radian/sec, that is, in all practical cases. For a further discussion of such changes of impedance level, the reader is referred to



(a)



(b)



(c)

FIG. 9-13.—Impedance-level transformations in a bandpass filter.

a source and a load. The insertion loss, $L(\omega)$, of the network is proportional to the logarithm of the magnitude of a real function of the variable $j\omega$; thus

$$L(\omega) = 20 \log_{10} |f(j\omega)|. \quad (94)$$

But $f(-j\omega)$ is the conjugate of $f(j\omega)$ since the function (not the value of the function) is real. It follows that

$$L(\omega) = 20 \log_{10} |f(j\omega)| = 20 \log_{10} |f(-j\omega)| = L(-\omega). \quad (95)$$

In words, the insertion loss is always an even function of the frequency.

Consider now the change of variable

$$\omega = k\omega', \quad (96)$$

where k is a positive constant. This substitution is obviously equivalent to a change of the frequency scale. The variable $k\omega'$ enters in the func-

standard texts on network theory. It must be pointed out, however, that there is no straightforward procedure which leads in all cases to the desired result, and that the success of a network manipulation of this type depends to a certain extent on the ingenuity of the designer.

9-8. Pass-band Normalization.

Normalization with respect to the pass band and to the attenuation band reduces most practical filters to basic low-pass structures. From the mathematical point of view, such normalization consists simply of a change of variable. To study this question, consider first an arbitrary two-terminal-pair network connected between

tion $L(k\omega')$ always in the combinations $Lk\omega'$, $Ck\omega'$, and $Mk\omega'$, and in those combinations only. Therefore, if ω' is considered as a real frequency, the function $L(k\omega')$ is the insertion loss of a network obtained from the original one by multiplying all self-inductances, mutual inductances, and capacitances by the constant k . In particular, given the design of a low-pass or high-pass filter whose cutoff frequency is 1 radian/sec, the cutoff frequency can be altered to an arbitrary value ω_c by merely dividing the values of all the reactive elements by ω_c .

Consider now another change of variable, namely,

$$\omega = -k/\omega'. \quad (97)$$

This substitution has the effect of interchanging the origin with the point at infinity, and the positive axis with the negative axis. For instance,

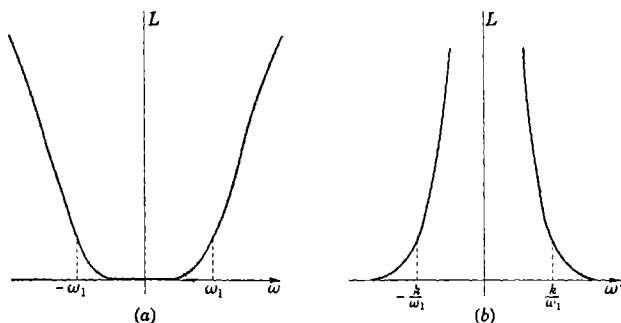


FIG. 9-14.—Insertion loss of a low-pass and a high-pass filter.

the insertion loss of a low-pass filter shown in Fig. 9-14a is transformed into the function shown in Fig. 9-14b, which is obviously the insertion loss of a high-pass filter. When ω' is a real frequency, the change of variable of Eq. (97) transforms any inductive reactance ωL into a capacitive reactance $-kL/\omega'$ and any capacitive reactance $-1/\omega_c$ into an inductive reactance ω'/kC . Therefore, the function $L(-k/\omega_c')$ shown in Fig. 9-14b is the insertion loss of a network obtained from the original one by substituting for any inductance L a capacitance $C' = 1/kL$ and for any capacitance C an inductance $L' = 1/kC$.

The presence of any mutual inductance in the original network would lead to difficulties, since there is no such thing as a mutual capacitance which can be substituted for a mutual inductance. A mutual inductance M can produce an inductive mutual reactance ωM between two loops of a network without requiring any electrical connection between the loops (Fig. 9-15a). In order to introduce a capacitive mutual reactance in the same manner, it is necessary to use an ideal transformer as shown in Fig. 9-15b. The equivalent mutual capacitance of the coupling circuit

of Fig. 9-15*b* is equal to aC . As in the case of impedance transformations, the presence of an ideal transformer is very important from the construction point of view, but is immaterial as far as the theoretical work involved in the process of normalization is concerned.

The transformation just described can be used to design a high-pass filter from a low-pass filter. If the constant k is made equal to the cutoff frequency of the low-pass filter, the high-pass filter will have the same cutoff frequency. Conversely, any high-pass filter can be reduced to a low-pass filter by the reverse transformation. By combining the transformations defined by Eqs. (96) and (97), any high-pass or low-pass filter can be derived from a low-pass filter with a cutoff frequency of

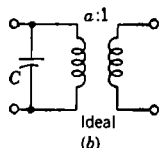
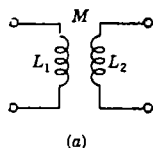


FIG. 9-15.—Mutual inductance and effective mutual capacitance.

1 radian/sec by uniform changes of the elements, regardless of the complexity of the structure.

Finally, consider the change of variable

$$\omega = k\omega'_0 \left(\frac{\omega'}{\omega'_0} - \frac{\omega'_0}{\omega'} \right), \quad (98)$$

where both ω'_0 and k are positive constants. This substitution transforms an even function of ω into an even function of ω' which has a geometric symmetry with respect to the points $\omega' = \omega'_0$ and $\omega' = -\omega'_0$. In fact, the points ω_1 and $-\omega_1$ are transformed into the two pairs of points

$$\left. \begin{aligned} \omega'_1 &= -\frac{\omega_1}{2k} + \sqrt{\frac{\omega_1^2}{4k^2} + (\omega'_0)^2} \\ \omega'_2 &= \frac{\omega_1}{2k} + \sqrt{\frac{\omega_1^2}{4k^2} + (\omega'_0)^2} \end{aligned} \right\}, \quad (99)$$

$$\left. \begin{aligned} -\omega'_1 &= \frac{\omega_1}{2k} - \sqrt{\frac{\omega_1^2}{4k^2} + (\omega'_0)^2} \\ -\omega'_2 &= -\frac{\omega_1}{2k} - \sqrt{\frac{\omega_1^2}{4k^2} + (\omega'_0)^2} \end{aligned} \right\}. \quad (100)$$

The product of the points of each pair is

$$\omega'_1\omega'_2 = (\omega'_0)^2, \quad (101)$$

which reveals the geometric symmetry involved in the transformation. The difference between the points of each pair is

$$\omega' = \omega'_2 - \omega'_1 = \omega_1/k. \quad (102)$$

It follows that an insertion loss function $L(\omega)$ such as the one shown in Fig. 9-14*a* for a low-pass filter is transformed into the function of ω' shown in Fig. 9-16, which is obviously that of a bandpass filter.

The change of variable of Eq. (98) transforms any inductive reactance ωL_1 into a reactance

$$X = kL_1\omega'_0 \left(\frac{\omega'}{\omega'_0} - \frac{\omega'_0}{\omega'} \right). \quad (103)$$

This function is easily recognized as the reactance of the series-tuned circuit of Fig. 9-17a, in which

$$L'_1 = kL_1, \quad C'_1 = \frac{1}{L'_1(\omega'_0)^2} = \frac{1}{kL_1(\omega'_0)^2}. \quad (104)$$

Similarly any capacitive susceptance ωC_2 is transformed into a susceptance,

$$B = kC_2\omega'_0 \left(\frac{\omega'}{\omega'_0} - \frac{\omega'_0}{\omega'} \right), \quad (105)$$

which may be recognized as the susceptance of the parallel-tuned circuit of Fig. 9-17b, in which

$$C'_2 = kC_2, \quad L'_2 = \frac{1}{C'_2(\omega'_0)^2}. \quad (106)$$

In order to represent the coupling reactance

$$X_m = kM\omega'_0 \left(\frac{\omega'}{\omega'_0} - \frac{\omega'_0}{\omega'} \right) \quad (107)$$

resulting from a mutual inductance M , it is again necessary to use an ideal transformer, as shown in Fig. 9-17c, in which

$$aL'_m = kM, \quad C'_m = 1/L'_m(\omega'_0)^2. \quad (108)$$

By the use of Eq. (98), a low-pass filter with a cutoff frequency of 1 radian/sec is transformed into a bandpass filter with a bandwidth w equal

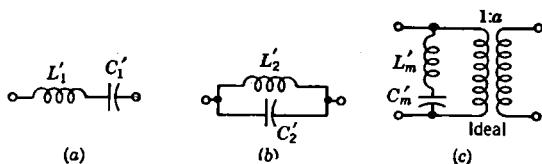


FIG. 9-17.—Resonant elements.

to $1/k$. Therefore, the design of a bandpass filter with mean frequency ω'_0 can be obtained simply by substituting for any inductance L_1 a series-tuned circuit with elements

$$L'_1 = L_1/w', \quad C'_1 = 1/L'_1(\omega'_0)^2; \quad (109)$$

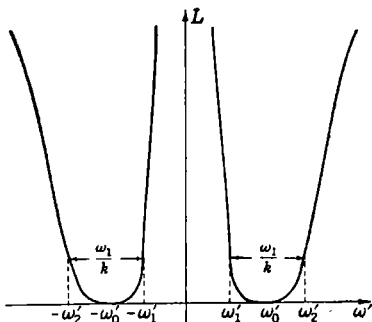


FIG. 9-16.—Insertion loss of a bandpass filter.

for any capacitance C_2 , a parallel-tuned circuit with elements

$$C'_2 = C_2/w', \quad L'_2 = 1/C'_2(\omega'_0)^2; \quad (110)$$

and for any mutual inductance M , a circuit such as the one of Fig. 9-17c in which

$$aL'_m = M/w, \quad C'_m = 1/L'_m(\omega'_0)^2. \quad (111)$$

The converse, however, is not in general true. Only a bandpass filter whose insertion loss has the proper geometric symmetry about the mean frequency can be reduced to a low-pass filter. The transformation of Eq. (98) can also be applied to a high-pass filter having an insertion loss such as the one plotted in Fig. 9-14b. The result would be, evidently, a band-elimination filter whose insertion-ratio curve would look like the one shown in Fig. 9-18. The mechanism of the transformation and the equations relating the parameters are the same as in the case of the bandpass filter.

By combining the changes of variable of Eqs. (96) and (98), it is possible to obtain a band-elimination filter from a low-pass filter. As in the previous case, the converse is not true.

REACTIVE NETWORKS WITH SPECIFIED IMAGE PARAMETERS

9.9. Designs Based on Lattice Structures.—The symmetrical lattice shown in Fig. 9-19 is, for two reasons, a very useful structure in filter design. First of all, it is the most general symmetrical network. In the second place, it lends itself to a simple synthesis procedure based on prescribed image parameters. Both properties become evident when Bartlett's bisection theorem is applied to the lattice structure. The open-circuit and short-circuit impedances of half the network are simply

$$Z_{och} = Z_b, \quad Z_{sch} = Z_a. \quad (112)$$

Since Z_a and Z_b can be any two physically realizable impedances, it is evident that any symmetrical network can be reduced to a symmetrical lattice. Moreover, the image impedance is specified by the product $Z_a Z_b$, whereas the propagation function is specified by the ratio Z_a/Z_b . It follows that the two image parameters can be specified independently,

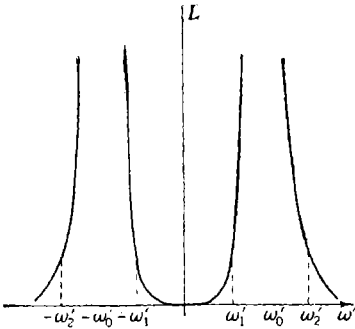


FIG. 9-18.—Insertion loss of a band-rejection filter.

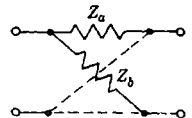


FIG. 9-19.—Symmetrical lattice.

and the two impedances Z_a and Z_b can be found from them without difficulty. In the case of nondissipative networks, Z_a and Z_b are reactances and can be realized in Foster form, in either Cauey form, or in any convenient combination of them.

The design problems for nondissipative filters will now be considered in more detail. It has been shown previously that Z_{oc} and Z_{sc} must have opposite signs in the pass band and the same sign in the attenuation band. The same is true for Z_{och} and Z_{sch} since Eqs. (75) and (76) have the same forms as Eqs. (71), (72), (73), and (74). It follows that either Z_a or Z_b (not both) must be critical at the cutoff frequency. Moreover, the poles and zeros of Z_a and Z_b must coincide in the attenuation band, whereas in the pass band the poles of Z_a must coincide with the zeros of Z_b and vice versa. A possible distribution of poles and zeros for a low-pass filter is shown in Fig. 9-20.

According to Foster's reactance theorem, a reactance is specified, except for a constant multiplier, by the locations of its poles and zeros. For instance, Z_a and Z_b can be written, for the case of Fig. 9-20, as follows:

$$Z_a = \frac{k_a j \omega (\omega_2^2 - \omega^2)}{(\omega_a^2 - \omega^2)}, \quad (113)$$

$$Z_b = \frac{k_b (\omega_a^2 - \omega^2) (\omega_2^2 - \omega^2)}{j \omega (\omega_1^2 - \omega^2)}. \quad (114)$$

The image impedance is then

$$Z_I = \sqrt{Z_a Z_b} = \sqrt{k_a k_b} \frac{\omega_2^2 - \omega^2}{\sqrt{\omega_1^2 - \omega^2}}. \quad (115)$$

The ratio $\sqrt{Z_a/Z_b}$ which determines the propagation function is

$$\sqrt{\frac{Z_a}{Z_b}} = \sqrt{\frac{k_a}{k_b}} \frac{j \omega \sqrt{\omega_1^2 - \omega^2}}{\omega_a^2 - \omega^2}. \quad (116)$$

It will be noticed that Z_I depends on the cutoff frequency ω_1 and on the other critical frequency ω_2 but not on ω_a . On the contrary, $\sqrt{Z_a/Z_b}$ depends on ω_1 and ω_a but not on ω_2 . This fact may be generalized in the following manner. The image impedance depends on the critical frequencies located in the attenuation band (cutoff frequency included) and not on the critical frequencies located inside the pass band. The ratio $\sqrt{Z_a/Z_b}$, on the other hand, depends on the critical frequencies located in the pass band (cutoff frequency included) and not on those

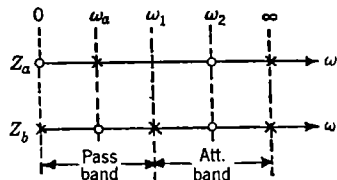


FIG. 9-20.—Distribution of poles and zeros in the impedance functions of a low-pass filter.

located in the attenuation band. This makes even more evident the fact that the image-impedance function and the propagation function can be specified independently.

Equation (85) shows that the power ratio in the pass band is unity when Z_I is equal to unity (for 1-ohm terminations). Therefore, the image-impedance function must be selected so that unity is approximated over the pass band in the best possible way. The larger the number of critical frequencies in the attenuation band, the closer the function may be made to approximate unity. However, the number of elements required in the filter also increases with the number of critical frequencies. Consequently, in general, some compromise must be made between performance and practicability.

The attenuation function α becomes infinite when $\sqrt{Z_a/Z_b} = 1$. Consequently, to obtain high off-band attenuation, the function $\sqrt{Z_a/Z_b}$ must be selected so that unity is approximated in the best possible way. The approximation may be improved by increasing the number of critical frequencies in the pass band but only, as before, at the expense of increased circuit complexity. The procedure for determining the location of the critical frequencies that yield the best approximation will not be discussed here.⁵

The symmetrical lattice is very useful for the basic design of filters, but is quite impractical as a final filter structure. For instance, the tolerances on the values of the elements are very strict, and the balanced form of the structure leads to difficulties in grounding the network. It is therefore necessary, once the basic design has been made, to develop the lattice into a more convenient structure—an unbalanced ladder, for example. This operation depends to a large extent on the ingenuity of the designer and, moreover, cannot always be performed since the lattice is a more general structure than the ladder. The lattice development will not be completely discussed here. Two basic steps, however, are sufficiently important to deserve attention.

In the network of Fig. 9-21a, the open-circuit and short-circuit impedances of half the network are

$$\left. \begin{aligned} Z_{och} &= Z + Z_b \\ Z_{sch} &= Z + Z_a \end{aligned} \right\} \quad (117)$$

These impedances, on the other hand, form the arms of the lattice of Fig. 9-21b. The network of Fig. 9-21a is thus equivalent to the lattice of Fig. 9-21b. It follows that, if the arms of a lattice contain a common series impedance, this impedance can be taken out of the lattice as shown in Fig. 9-21a.

The dual operation is shown in Figs. 9-21c and d. The open-circuit and short-circuit admittances of half the network of Fig. 9-21c are

$$\left. \begin{aligned} Y_{och} &= Y + Y_b \\ Y_{sch} &= Y + Y_a \end{aligned} \right\} \quad (118)$$

Again, these admittances form the arms of the lattice of Fig. 9-21*d*, and the two networks are thus equivalent. It follows that if the arms of a lattice contain a common parallel admittance, this admittance can be taken out and placed in shunt to both pairs of terminals. Both methods of lattice development can be used in succession to take out common poles and zeros of the two impedances Z_a and Z_b .

Another method of developing a lattice is based on the fact that the propagation function of a filter is entirely specified by the cutoff frequencies and by the locations of the infinite peaks of attenuation. The infinite peaks of attenuation can be divided among a number of lattices all having the same image impedance. These lattices, when placed in

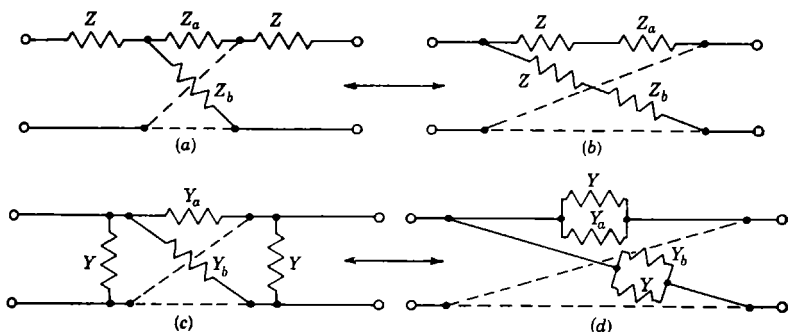


FIG. 9-21.—Two equivalent lattice structures and their duals.

cascade, are equivalent to the original lattice since their combination has the same propagation function. The resulting lattices are then separately developed into more convenient structures.

9-10. Constant- k Filters.—The method of design based on constant- k and m -derived structures was the first to be developed and because of its simplicity is still widely used when the design requirements are not too strict. For this reason, it will be discussed here in some detail. These designs will be treated as particular cases of the lattice structure. Although the meaning of conventional expressions such as “constant k ” and “ m -derivation” will be partially lost by such an approach, other more important concepts will be made clearer than they would be if the traditional derivations were followed. The discussion will be limited to low-pass filters designed to operate between 1-ohm resistances. All the other types of filters can be derived from these basic designs by means of the transformations described in Secs. 9-7 and 9-8.

Consider the simplest possible type of filter, that is, one with no

critical frequency other than that which separates the pass band from the attenuation band. There are two sets of reactance functions which may be used for Z_a and Z_b . These functions are plotted in Fig. 9-22. The two functions of each set have opposite signs from $\omega = 0$ to $\omega = 1$, and the same sign from $\omega = 1$ to $\omega = \infty$. The cutoff frequency is, therefore, 1 radian/sec, and the filter is of the low-pass type. The image impedance and the ratio $\sqrt{Z_a/Z_b}$ are, for the functions of Fig. 9-22a,

$$Z_l = \sqrt{Z_a Z_b} = \sqrt{L_a L_b} \sqrt{1 - \omega^2}, \quad \sqrt{\frac{Z_a}{Z_b}} = \sqrt{\frac{L_a}{L_b}} \frac{j\omega}{\sqrt{1 - \omega^2}} \quad (119)$$

and, for the function of Fig. 9-22b,

$$Z_l = \sqrt{Z_a Z_b} = \frac{1}{\sqrt{C_a C_b} \sqrt{1 - \omega^2}}, \quad \sqrt{\frac{Z_a}{Z_b}} = \sqrt{\frac{C_b}{C_a}} \frac{j\omega}{\sqrt{1 - \omega^2}} \quad (120)$$

It is evident that the functions corresponding to Fig. 9-22b are the reciprocals of the functions corresponding to Fig. 9-22a. Therefore, it is not necessary to carry further the design for the case of Fig. 9-22b. The final network for this case will be the dual of the network resulting from the functions of Fig. 9-22a.

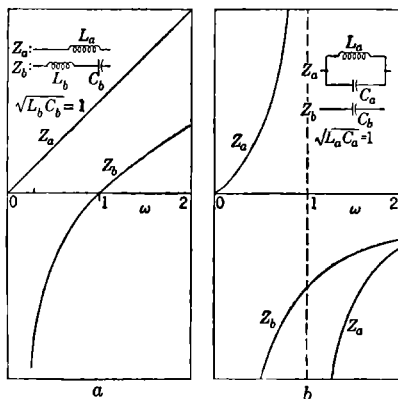


FIG. 9-22.—Behavior of Z_a and Z_l for two simple filters.

The product $L_a L_b$ is fixed by making the image impedance equal to unity at zero frequency. The ratio $\sqrt{L_a/L_b}$ specifies the location of the peak of infinite attenuation, since $\alpha = \infty$ for $\sqrt{Z_a/Z_b} = 1$. If $\alpha = \infty$ at $\omega = \infty$, it follows that

$$L_a = L_b = 1. \quad (121)$$

This means that the functions Z_a and Z_b of Fig. 9-22a are tangent at infinity where their slope is equal to unity. The resulting lattice is

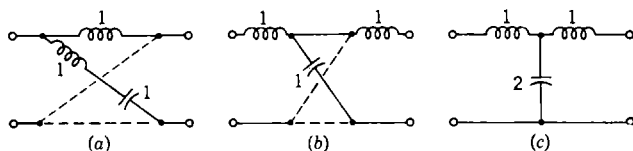


FIG. 9-23.—Transformation of lattice in Fig. 9-22a to an equivalent ladder structure.

shown in Fig. 9-23a. This lattice can be developed following the method described in Figs. 9-21 and 9-22. First of all, the inductance is taken

out; the remaining capacitances in the *b*-arms of the lattice are in parallel and can be lumped together. These steps are shown in Figs. 9-23*b* and *c*. The dual network resulting from the functions of Fig. 9-22*b* is shown in Fig. 9-24. The propagation function for both filters is given by

$$\gamma = 2 \tanh^{-1} \frac{j\omega}{\sqrt{1 - \omega^2}} = \ln \frac{1 + \frac{j\omega}{\sqrt{1 - \omega^2}}}{1 - \frac{j\omega}{\sqrt{1 - \omega^2}}} \quad (122)$$

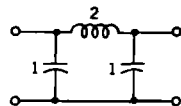


FIG. 9-24.—Ladder equivalent of lattice structure shown in Fig. 9-22*b*.

The image impedance for the filter of Fig. 9-23 is

$$W_{1k} = \sqrt{1 - \omega^2}, \quad (123)$$

and for the filter of Fig. 9-24 the image impedance is

$$W_{2k} = -\frac{1}{\sqrt{1 - \omega^2}} \quad (124)$$

Plots of these functions are shown in Figs. 9-25*a* and 9-25*b*. It will be noticed that the half sections obtained by bisecting the filters of Figs.

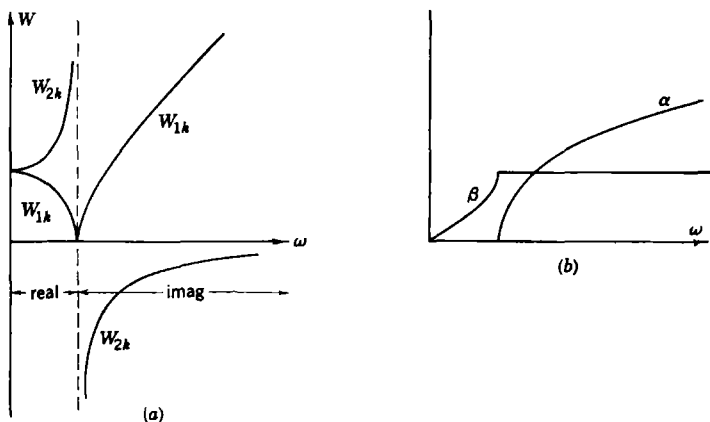


Fig. 9-25.—Image parameters for structures shown in Figs. 9-23 and 9-24.

9-23*c* and 9-24 are identical. It follows that the image parameters of the nonsymmetrical filter shown in Fig. 9-26, are

$$W_{1k} = \sqrt{1 - \omega^2}, \quad (125)$$

$$W_{2k} = \frac{1}{\sqrt{1 - \omega^2}}, \quad (126)$$

$$\gamma_{k/2} = \tanh^{-1} \frac{j\omega}{\sqrt{1 - \omega^2}} = \frac{1}{2} \ln \frac{1 + \frac{j\omega}{\sqrt{1 - \omega^2}}}{1 - \frac{j\omega}{\sqrt{1 - \omega^2}}} \quad (127)$$

The power-loss ratio for the filter of Fig. 9-23c can be computed by substituting Eqs. (122) and (123) in Eq. (84), after noting that

$$\sinh^2 \gamma_k = 4 \frac{\tanh^2 \frac{\gamma_k}{2}}{\left(1 - \tanh^2 \frac{\gamma_k}{2}\right)^2} = -4\omega^2(1 - \omega^2). \quad (128)$$

Thus, after some algebraic manipulation, one finds

$$\frac{P_0}{P_L} = 1 + \omega^6. \quad (129)$$

The same expression is found for the filter of Fig. 9-24.

The power ratio for the half section of Fig. 9-26 is found by substituting Eqs. (125) and (127) in Eq. (89) and noting that

$$\cosh^2 \frac{\gamma_k}{2} = \frac{1}{1 - \tanh^2 \frac{\gamma_k}{2}} = 1 - \omega^2. \quad (130)$$

The final expression reduces to

$$\frac{P_0}{P_L} = 1 + \frac{1}{4} \omega^4. \quad (131)$$

The filters of Figs. 9-23c, 9-24, and 9-26 are usually referred to as "constant- k " structures. The name originates from the fact that the ratio k of the impedances of the series branch to the impedance of the shunt branch is a constant independent of frequency.

The filters of Figs. 9-23c and 9-24. **9-11. m -derived Filters.**—The physical meaning of the well-known process of m -derivation becomes evident when the operation is performed on a lattice structure such as the one of Fig. 9-27a. The impedance Z_a is multiplied by a positive constant m , while the impedance Z_b is divided by the same constant, as shown in Fig. 9-27b. The image impedance which depends on the product of the two new impedances $Z'_a = mZ_a$ and $Z'_b = Z_b/m$ remains unchanged. The cutoff frequency also remains unchanged. The ratio Z_a/Z_b , on the contrary, is multiplied by m^2 :

$$Z'_a/Z'_b = m^2(Z_a/Z_b). \quad (132)$$

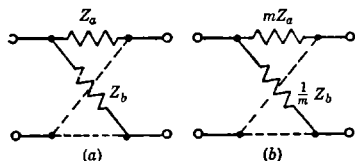


FIG. 9-27.—Illustration of m -derivation of a lattice structure.

It follows that the ratio Z'_a/Z'_b can be made equal to unity at any desired frequency in the attenuation band by properly adjusting the value of m .

In other words, since $\alpha = \infty$ for $Z'_a/Z'_b = 1$, a peak of infinite attenuation can be produced at any desired frequency in the attenuation band.

Application of this process of *m*-derivation to the lattice of Fig. 9-23*a* leads to the lattice of Fig. 9-28*a* which can be developed into the T-section of Fig. 9-28*b*. In this particular case, *m* must be smaller than unity since Z_a is larger than Z_b . The functions Z'_a and Z'_b are plotted in Fig. 9-29. The peak of infinite attenuation occurs at a frequency ω_∞ given by the solution of the equation

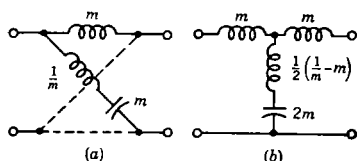


FIG. 9-28.—Two equivalent forms for *m*-derivation of lattice in Fig. 9-23*a*.

$$\frac{Z'_a}{Z'_b} = m^2 \frac{\omega_\infty}{\sqrt{\omega_\infty^2 - 1}} = 1, \tag{133}$$

which yields

$$\omega_\infty = \sqrt{\frac{1}{1 - m^2}}. \tag{134}$$

The attenuation for $\omega = \infty$ becomes

$$\alpha_k(\infty) = 2 \tanh^{-1} m = \ln \frac{1 + m}{1 - m}. \tag{135}$$

The propagation function $\gamma_{km} = \alpha + j\beta$ is plotted in Fig. 9-30.

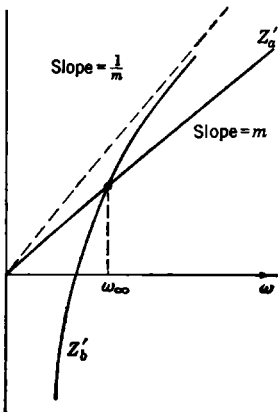


FIG. 9-29.— Z'_a and Z'_b for the *m*-derived section shown in Fig. 9-28.

The process of *m*-derivation may also be applied to the filter of Fig. 9-24. The resulting network shown in Fig. 9-31 is the dual of the network of Fig. 9-28*b*. The image impedance of this filter is still given by Eq. (124) and its propagation function is the

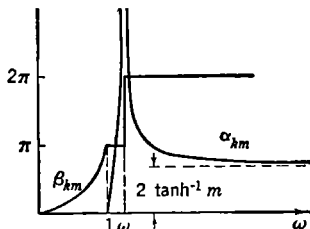


FIG. 9-30.—Propagation function of an *m*-derived section.

same as for the filter of Fig. 9-28*b*. The power-loss ratio turns out to be, for both types of *m*-derived filters,

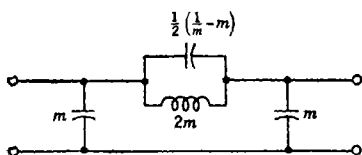


FIG. 9-31.—Dual of network shown in Fig. 9-28b developed by m -derived filter shown in Fig. 9-24.

$$\frac{P_0}{P_L} = 1 + \frac{m^2 \omega^6}{1 - (1 - m^2) \omega^2}. \quad (136)$$

It is interesting to note that the ratio at the cutoff frequency ($\omega = 1$) is still equal to 2 as for the original filters of Figs. 9-23c and 9-24.

The process of m -derivation is traditionally performed directly on the T- and π -structures as shown in Fig. 9-32a and b. The lattices of Fig. 9-27 can be developed into the T- and π -structures of Fig. 9-32, provided the following identifications are made:

$$Z_a = \frac{Z_1}{2} = \frac{1}{\frac{Y_1}{2} + 2Y_2}, \quad (137)$$

$$Z_b = \frac{Z_1}{2} + 2Z_2 = \frac{2}{Y_1}. \quad (138)$$

It is seen that in the nonsymmetrical filters shown in Fig. 9-33 and obtained by bisecting the m -derived filters of Figs. 9-28b and 9-31, the image impedances W_{1k} are still equal to the image impedances of the

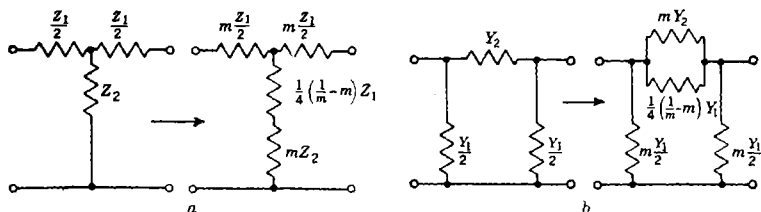


FIG. 9-32.—Traditional method of performing m -derivation on a T- or π -structure.

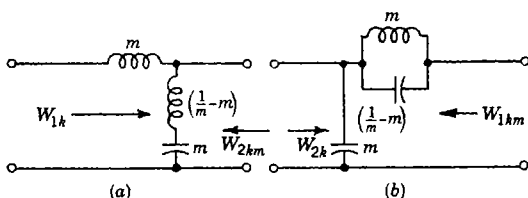


FIG. 9-33.—Two derived half sections corresponding to filters shown in Figs. 9-28b and 9-31.

original constant- k structures, and the propagation function $\gamma_{k,m/2}$ is half of the propagation function of the m -derived filters. The image impedances W_{2km} and W_{1km} are

$$W_{2km} = \frac{1 - \omega^2(1 - \omega^2)}{\sqrt{1 - \omega^2}} = W_{2k}[1 - \omega^2(1 - \omega^2)], \quad (139)$$

$$W_{1km} = \frac{\sqrt{1 - \omega^2}}{1 - \omega^2(1 - m^2)} = \frac{W_{1k}}{1 - (1 - m^2)\omega^2} \quad (140)$$

It follows that if two identical half sections are connected in cascade as shown in Figs. 9-34*a* and *b*, the resulting symmetrical filters will have image impedances equal to W_{2km} and W_{1km} , respectively, and propagation functions equal to γ_{km} as for the *m*-derived filters.

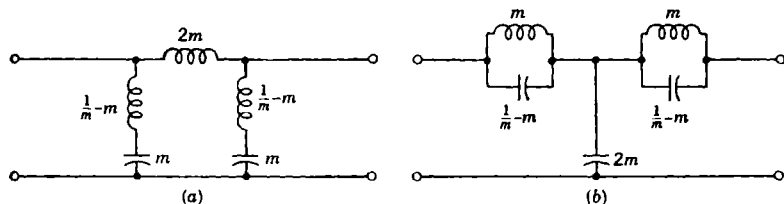


FIG. 9-34.—Arrangements at *m*-derived half sections with improved image impedances.

The two image impedances W_{1km} and W_{2km} are plotted in Fig. 9-35. It is evident that these functions approximate unity better over the pass band than do W_{1k} and W_{2k} . The process of *m*-derivation and bisection can be carried further by using the structures of Fig. 9-34 as starting points. The resulting structures can be again *m*-derived and bisected, and so on. This procedure leads to filters whose image impedances approximate unity to a better and better degree, over the pass band, and whose propagation functions have more and more peaks of infinite attenuation.

It must be pointed out, however, that the image impedance and the propagation function cannot be specified independently. In practice, image impedances resulting from more than one, or at most two, *m*-derivations are used very seldom. As far as the propagation function is concerned, the desired number of infinite peaks of attenuation is obtained by cascading *m*-derived sections having different values of ω_∞ . These sections have simple constant-*k* image impedances. If *m*-derived impedance is desired for the whole network, one section is bisected and the two half sections are placed at the two ends of the network as shown in Fig. 9-36. The propagation function for this network is the sum of the propagation constants of the individual sections. The image impedance

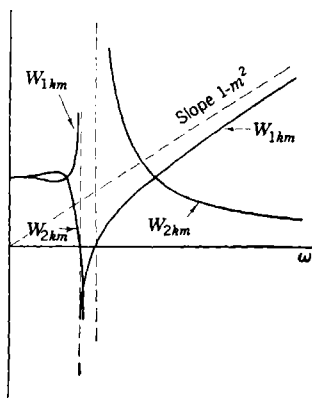


FIG. 9-35.—Image impedances of sections shown in Fig. 9-34.

of the whole network is equal to W_{2km} . The image impedances of the individual sections at the four junctions are all equal to W_{1k} . If the image impedance and the propagation function have to be specified entirely independently, the lattice method of design must be used. This is particularly true when the required image impedance is not a simple function.

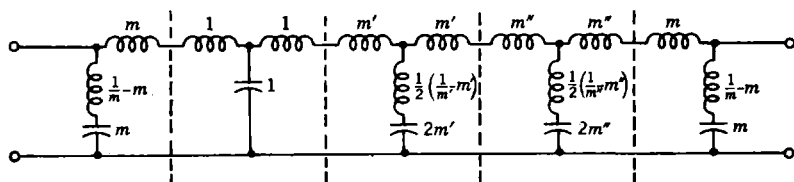


Fig. 9-36.—Cascade of m -derived sections terminated in half sections.

9.12. Limitations on the Use of Image Parameters.—The image-parameter method of design fails when the design specifications are so strict that the effect of mismatched terminations cannot be neglected. In order to estimate the order of magnitude of such effects, the power ratio in the pass band must be considered. This quantity, given by Eq. (85), depends on the product of $(Z_I - 1/Z_I)^2$ and $\sin^2 \beta$. The quantity $(Z_I - 1/Z_I)^2$ becomes infinite at the cutoff while $\sin^2 \beta$ becomes zero. It has already been pointed out that the limit of the product of these two quantities is finite at the cutoff. In other words, the large value of $(Z_I - 1/Z_I)^2$ is balanced by the small value of $\sin^2 \beta$. However, if β changes so fast that $\sin^2 \beta$ becomes unity one or more times while $(Z_I - 1/Z_I)^2$ is still large, sizable peaks of insertion loss will result.

For a given image-impedance function and a given pass band, the tolerance on the loss depends primarily on the total change of β in the pass band, assuming for the moment that the rate of change of β is fairly constant. In fact, the larger the number of frequencies at which $\sin^2 \beta$ becomes equal to one, the closer one of these frequencies will be to a cutoff point. The number n of these frequencies is equal to one plus the number of poles and zeros of $\sqrt{Z_a/Z_b}$ inside the pass band, (the cutoff points and the points $\omega = 0$ and $\omega = \infty$ excluded), since β becomes equal to an integral multiple of π every time $\sqrt{Z_a/Z_b}$ vanishes or becomes infinite. On the other hand, these poles and zeros are the parameters controlling the behavior of α in the attenuation band. For instance, the number of infinite peaks of attenuation, that is, the number of roots of the equation $\sqrt{Z_a/Z_b} = 1$ corresponding to real positive values of ω , can be at most equal to n . It follows that a large change of β is unavoidable when α has to be very large in the attenuation band.

When the behavior of the propagation function is considered in more detail, it is found that the rate of change of β in the vicinity of a cutoff

frequency is usually larger than its average value over the pass band. This is particularly true when the attenuation rises steeply on the other side of the cutoff. This fact makes the situation even worse as far as the tolerance in the pass band is concerned.

It may be concluded that, for a given image impedance, the tolerance in the pass band limits the attenuation in the rejection band and vice versa. In particular, there is an upper limit to the number of m -derived sections with a specified image impedance that can be placed in cascade if the loss in the pass band has to be kept within a specified tolerance. This tolerance can be improved by a better choice of image impedance but only at the expense of added complexity in the sections. A special case will be considered more quantitatively because of its practical importance in the microwave field; it is a filter composed of n identical sections in cascade. Let Z_l and β_0 be, respectively, the image impedance and the phase function of one section. The power ratio in the pass band is, for n sections,

$$\frac{P_0}{P_L} = 1 + \frac{1}{4} \left(Z_l - \frac{1}{Z_l} \right)^2 \sin^2 n\beta_0 = 1 + \epsilon_n^2, \quad (141)$$

where

$$\epsilon_n^2 \equiv \frac{P_0}{P_L} - 1. \quad (142)$$

Then the ratio of this quantity for n sections to the corresponding quantity for one section is given by

$$\frac{\epsilon_n^2}{\epsilon_1^2} = \frac{\sin^2 n\beta_0}{\sin^2 \beta_0}. \quad (143)$$

Plots of ϵ_n/ϵ_1 for $n = 3, 5,$ and 10 are shown in Fig. 9-37.

Let the sections be, for instance, of the constant- k low-pass type. The power ratio for one section is given by Eq. (129). The quantity ϵ_1^2 is then

$$\epsilon_1^2 = \omega^6. \quad (144)$$

The phase function β_0 is given by Eq. (122)

$$\beta_0 = 2 \tan^{-1} \frac{\omega}{\sqrt{1 - \omega^2}} = 2 \sin^{-1} \omega. \quad (145)$$

Plots of $\epsilon_n^2/\epsilon_1^2$ for $n = 3, 10,$ and ∞ are shown in Fig. 9-38. Figure 9-39 shows the insertion loss, in decibels, for $n = 1, 10,$ and ∞ . It is evident from these curves that the pass-band tolerance becomes progressively worse as n is increased.

The analysis of filters consisting of several sections in cascade has been carried out for the particular case of symmetrical sections. The

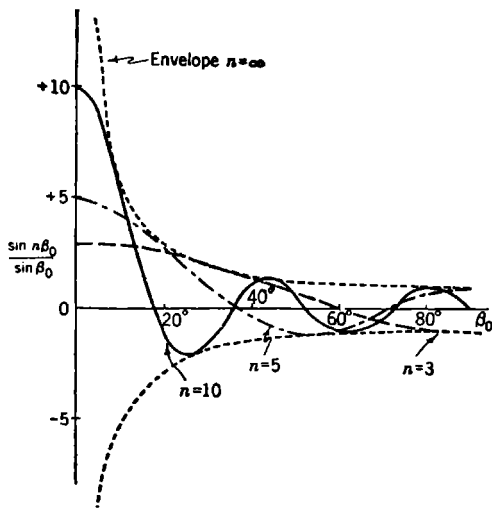


FIG. 9-37.—Plot of function $\frac{\sin n\beta_0}{\sin \beta_0}$.

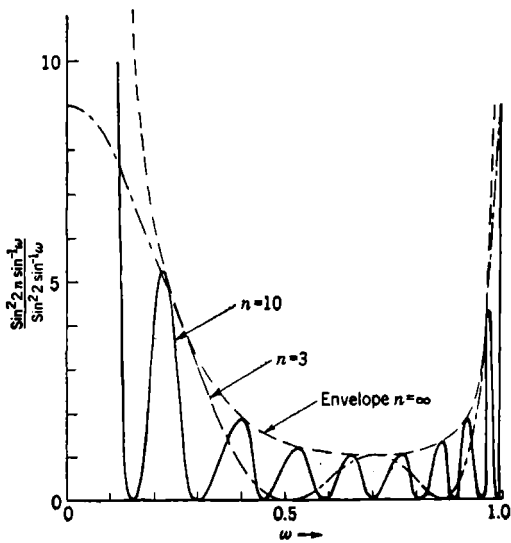


FIG. 9-38.—Plot of function $\frac{\sin^2(2n \sin^{-1} \omega)}{\sin^2(2 \sin^{-1} \omega)}$.

results, however, can be extended to the case of nonsymmetrical sections, provided the image impedances for any two pairs of terminals which are joined together are identical. The case of nonsymmetrical sections, however, is not sufficiently important to deserve a detailed analysis.

It is evident from the preceding discussion that, for a given image impedance, bandpass tolerances smaller than several decibels will be difficult to obtain by the image-parameter method if high attenuation in the stop band is required. Such a tolerance is not objectionable in many low-frequency filters in which the tolerance is usually determined by the maximum allowable distortion of the signal, and very seldom by loss considerations. Unfortunately, the situation is otherwise in the case of microwave filters. In the first place, no satisfactory microwave amplifiers have been developed as yet, and consequently any reflection

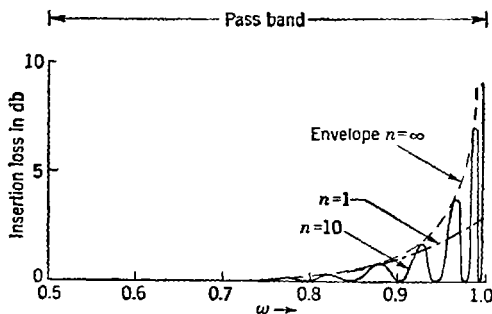


FIG. 9-39.—Insertion loss for a cascade of constant- k low-pass sections.

losses in the pass band of a receiver filter are equivalent to a decrease in receiver sensitivity. Secondly, in microwave systems, and particularly in radar systems, it is often necessary to limit the frequency spectrum of the high-power transmitter. It turns out that the magnetron, which is the only high-power oscillator available at present, does not operate satisfactorily if the power reflected by the load is too large. In general, the power reflected must be less than $\frac{1}{16}$ of the incident power, corresponding to a voltage standing-wave ratio of less than 1.5. Moreover, since allowance must be made for small reflections in other components of the transmitting system, it is desirable to use filters that, in the pass band, produce a VSWR smaller than 1.2, or in other words, that reflect less than about 1 per cent of the power. This means that, neglecting the effect of dissipation, the insertion loss should be less than 0.04 db in the pass band. The problem is made even more complex by the effect of incidental dissipation; the input VSWR or the input reflection coefficient, rather than the insertion loss, must then be kept within a specified tolerance. Such bandpass tolerances can be achieved with the image-

parameter method only by using an image impedance that approximates unity sufficiently well within the pass band. Thus as the tolerance becomes stricter, one is forced to use more and more complex sections to achieve the required image-impedance function. In principle, such a procedure may always be carried out; but as the sections become more involved, one encounters practical problems of manufacturability, particularly in the case of microwave filters, where mechanical design is complicated by the distributed nature of the components. Even then it is apparent that the components have not been used in the most efficient manner, since the design procedures based on the image-parameter method do not lead to uniformly distributed tolerances in insertion loss over the pass band. Of course, one may attempt to achieve a more uniform tolerance by cut-and-try manipulation of the basic design, but such a procedure is very tedious and often fruitless. Consequently, in the case of strict design requirements, when reflection losses can no longer be neglected, a method for directly synthesizing a network having a prescribed insertion loss becomes necessary. Such a method is described in the succeeding sections.

REACTIVE NETWORKS WITH SPECIFIED INSERTION LOSS

A design procedure⁴ which does not suffer from the drawbacks of the image-parameter method has been developed for nondissipative networks by S. Darlington* of the Bell Telephone Laboratories. This method permits the determination of the elements of a reactive network from a knowledge of its insertion loss for specified resistive terminations. In the following discussion each termination, that is, the load resistance and source resistance, is assumed to be equal to 1 ohm. This assumption does not limit the generality of the results since either termination can be made independently equal to any desired value by means of appropriate changes of impedance level.

9-13. Physical Realizability of Insertion-loss Functions.—The first question to be considered is the physical realizability of the insertion-loss function. It is evident that not every function of frequency can be the insertion loss of an actual network. Therefore, it is necessary to determine what restrictions must be imposed on a function of frequency in order to guarantee the existence of a network with such an insertion loss. The following analysis is limited to linear passive networks consisting of lumped elements only.

First will be considered the conditions of physical realizability for a two-terminal-impedance function. It can be shown that any impedance (not necessarily reactive) must be a real function $Z(j\omega)$ of the imaginary

* The following discussion of Darlington's method, which diverges somewhat from the original presentation, is due to E. A. Guillemin.

variable $j\omega$, and that this function is the ratio of two finite polynomials. A considerable amount of information about this function can be obtained by studying its behavior over the whole complex plane instead of on the imaginary axis only. Therefore, let p be a complex variable,

$$p = \sigma + j\omega. \quad (146)$$

The function $Z(p)$, which coincides with the physical impedance for $\sigma = 0$, is a real function of the complex variable p . Since $Z(p)$ is the ratio of two finite polynomials, it is a rational meromorphic function.

By making use of the fact that the network is passive, it can be shown that $Z(p)$ must be a positive real function (p.r.); that is, it must satisfy the condition

$$\operatorname{Re} [Z(p)] \geq 0, \quad \text{for } \sigma \geq 0. \quad (147)$$

Several properties of $Z(p)$ can be derived from this condition. The most important of these properties is that $Z(p)$ has no poles or zeros in the right half of the complex plane. In other words, the roots of the two polynomials of which $Z(p)$ is the ratio have nonpositive real parts.

Brune² showed that the p.r. condition is sufficient as well as necessary. In other words, any rational meromorphic function which satisfies Condition (147) is necessarily the impedance of a physical network. Brune proved this theorem by developing a method of determining the elements of a two-terminal-pair network having the prescribed impedance. Darlington⁴ gave a different proof of this theorem and, at the same time, showed that any dissipative impedance can be realized by means of a nondissipative two-terminal-pair network terminated in a pure resistance. This second theorem forms the basis of the new direct method of filter design, by permitting the determination of a nondissipative filter having any given input impedance when a pure resistance is connected to the output terminals. This output resistance can always be made equal to 1 ohm by means of an ideal transformer.

The input impedance, however, is not a convenient function to specify in the case of a filter. It is necessary, therefore, to develop a method of obtaining the input impedance from the insertion loss and, at the same time, to derive the conditions of physical realizability for the insertion loss from the conditions that must be satisfied by the input impedance. This problem has to be solved before the synthesis procedure can be discussed.

In the network of Fig. 9-40, the voltage reflection coefficient $\Gamma(p)$ at the input terminals is given by the well-known expression

$$\Gamma(p) = \frac{Z(p) - 1'}{Z(p) + 1'} \quad (148)$$

where $Z(p)$ is the input impedance of the nondissipative network terminated in a 1-ohm resistance. The right half of the Z -plane becomes, in the Γ -plane, according to Eq. (148), the region inside a circle of unit radius centered at the origin. In other words, the absolute value of $\Gamma(p)$ is smaller than unity when the real part of $Z(p)$ is positive. The imaginary axis of the Z -plane transforms into the circle of unit radius in the Γ -plane. Consequently,

$$|\Gamma(p)| \leq 1 \quad \text{for } \text{Re} [Z(p)] \geq 0. \quad (149)$$

Since $Z(p)$ is a positive real function, this inequality becomes

$$|\Gamma(p)| \leq 1 \quad \text{for } \sigma \geq 0. \quad (150)$$

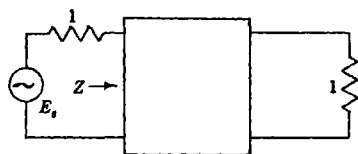


FIG. 9-40.—Two-terminal-pair network with input impedance Z .

Conversely, if the absolute value of $\Gamma(p)$ is smaller than or equal to one, the real part of $Z(p)$ must be positive or zero. It follows that if Eq. (150) is satisfied by an arbitrary function $\Gamma(p)$, the corresponding function $Z(p)$

is necessarily positive real. Of course, $\Gamma(p)$ must be a rational meromorphic function in order that $Z(p)$ may be the impedance of a lumped-element network.

It can be shown that if a function of a complex variable is regular in a region S , its absolute value at any point of S is smaller than or equal to the maximum absolute value over the boundary of S . This theorem can be applied to the function $\Gamma(p)$ which must be regular for $\sigma \geq 0$. Let S be the entire right half of the p -plane. Then, if the absolute value of $\Gamma(p)$ is smaller than or equal to one over the boundary of S , that is, if

$$|\Gamma(j\omega)| \leq 1, \quad (151)$$

then

$$|\Gamma(p)| \leq 1, \quad \text{for } \sigma \geq 0. \quad (152)$$

To summarize, if $\Gamma(p)$ is a rational meromorphic function which is regular in the right half of the p -plane and satisfies Eq. (151), then the function $Z(p)$ defined by Eq. (148) is positive real and consequently is a physically realizable impedance.

The fact that Eq. (151) has to be satisfied is physically obvious, since the fraction of the incident power which is reflected at the input to the network at real frequencies, $|\Gamma(j\omega)|^2$, cannot be larger than 1. Equation (151), however, is a necessary but not a sufficient condition, since $\Gamma(p)$ must also be regular in the right half of the plane.

The power-loss ratio is defined as the ratio of the power available from the source to the power delivered to the load. Since the two-terminal-pair network of Fig. 9-40 is nondissipative, the power reaching

the load is the difference between the power incident from the source and the power reflected. It follows that the power-loss ratio is

$$\frac{P_0}{P_L} = \frac{1}{1 - |\Gamma(j\omega)|^2} \geq 1. \quad (153)$$

The insertion loss for equal terminations is simply

$$L = 10 \log_{10} \frac{P_0}{P_L}. \quad (154)$$

Since $\Gamma(j\omega)$ is a real function of $j\omega$, the square of its magnitude must be an even real function of ω , that is, a real function of ω^2 :

$$|\Gamma(j\omega)|^2 = \Gamma(j\omega) \cdot \Gamma(-j\omega). \quad (155)$$

Moreover, $\Gamma(p)$ is a rational meromorphic function of p , and must satisfy Eq. (151). It follows that $|\Gamma(j\omega)|^2$ must be of the form

$$|\Gamma(j\omega)|^2 = \frac{M(\omega^2)}{N(\omega^2) + M(\omega^2)}. \quad (156)$$

The polynomials $M(\omega^2)$ and $N(\omega^2)$ must be real and nonnegative for all real, nonnegative values of ω^2 . In terms of these quantities, the power-loss ratio becomes simply

$$\frac{P_0}{P_L} = \frac{N(\omega^2) + M(\omega^2)}{N(\omega^2)} = 1 + \frac{M(\omega^2)}{N(\omega^2)}. \quad (157)$$

It will be shown later that $N(\omega^2)$ must be the square of either an even or an odd polynomial in ω . This condition, however, can be satisfied without imposing any further restriction on the function representing the power-loss ratio. In fact, it is sufficient to multiply both the numerator and the denominator of Eq. (157) by all the root factors of $N(\omega^2)$ that have odd multiplicity. It follows that no loss of generality results from rewriting Eqs. (156) and (157) as follows:

$$\frac{P_0}{P_L} = \frac{P(\omega^2) + Q^2(\omega)}{Q^2(\omega)} = 1 + \frac{P(\omega^2)}{Q^2(\omega)}, \quad (158)$$

and

$$|\Gamma(j\omega)|^2 = \frac{P(\omega^2)}{P(\omega^2) + Q^2(\omega)} = \frac{1}{1 + \frac{Q^2(\omega)}{P(\omega^2)}}. \quad (159)$$

The even polynomials $P(\omega^2)$ and $Q^2(\omega)$ must be real and nonnegative for all real values of ω .

9.14. Determination of Input Impedance from a Prescribed Insertion Loss.—It remains to be shown that for any function of the type represented in Eq. (159) it is possible to find a function $\Gamma(p)$ which is regular

in the right half of the p -plane. In other words, it must be shown that the conditions imposed on $|\Gamma(j\omega)|^2$ are sufficient, as well as necessary, for the determination of $\Gamma(p)$. This proof will consist of giving a method for obtaining from $|\Gamma(j\omega)|^2$ a function $\Gamma(p)$ which is regular in the right half of the p -plane.⁶ Let

$$\Gamma(p) = \frac{u_1 + v_1}{u_2 + v_2}, \quad (160)$$

where u_1, u_2 are even functions of p , that is, polynomials with even powers of p , and v_1, v_2 are odd functions, that is, polynomials with odd powers of p . It follows from Eq. (159) that

$$|\Gamma(j\omega)|^2 = \left[\frac{u_1^2 - v_1^2}{u_2^2 - v_2^2} \right]_{p=j\omega} = \left[\frac{(u_1 + v_1)(u_1 - v_1)}{(u_2 + v_2)(u_2 - v_2)} \right]_{p=j\omega} = \frac{P(\omega^2)}{P(\omega^2) + Q^2(\omega)}. \quad (161)$$

By substituting $-p^2$ for ω^2 in $P(\omega^2)$ and $Q^2(\omega)$, the following two equations are obtained

$$P(-p^2) = (u_1 + v_1)(u_1 - v_1), \quad (162)$$

$$P(-p^2) + Q^2(-jp) = (u_2 + v_2)(u_2 - v_2). \quad (163)$$

It should be noticed that, for $p = j\omega$, $(u_1 - v_1)$ and $(u_2 - v_2)$ are conjugates of $(u_1 + v_1)$ and $(u_2 + v_2)$, respectively.

First, the function $u_2 + v_2$ will be determined. The polynomial of Eq. (163) can be expanded in a product of root factors as follows:

$$P(-p^2) + Q^2(-jp) = k(p^2 - p_1^2)(p^2 - p_2^2) \cdots (p^2 - p_n^2), \quad (164)$$

where k is a real constant and p_1^2, p_2^2, p_n^2 are the roots of the polynomial in the variable p^2 . The roots p_v^2 can be either real or complex. If they are complex, they must be present in conjugate pairs p_v^2 and $(p_v^2)^*$, since the coefficients of the polynomial are real. Any pair of conjugate roots results in two root factors which can be expanded as follows:

$$[p^2 - p_v^2][p^2 - (p_v^2)^*] = [(p - p_v)(p - p_v^*)][(p + p_v)(p + p_v^*)]. \quad (165)$$

The location in the complex plane of the four p -roots resulting from the pair of conjugate p^2 -roots is shown in Fig. 9-41. On the imaginary axis, that is, for $p = j\omega$, the product $(p - p_v)(p - p_v^*)$ is the conjugate of the product $(p + p_v)(p + p_v^*)$. In fact, these products can be developed as follows:

$$\begin{aligned} (p - p_v)(p - p_v^*) &= [-\sigma_v + j(\omega - \omega_v)][-\sigma_v + j(\omega + \omega_v)] \\ &= [\sigma_v^2 - (\omega^2 - \omega_v^2)] - j2\omega\sigma_v, \end{aligned} \quad (166)$$

and

$$\begin{aligned} (p + p_v)(p + p_v^*) &= [\sigma_v + j(\omega + \omega_v)][\sigma_v + j(\omega - \omega_v)] \\ &= [\sigma_v^2 - (\omega^2 - \omega_v^2)] + j2\omega\sigma_v. \end{aligned} \quad (167)$$

Therefore, the right-hand side of Eq. (165) can be split into two parts, as indicated by the square brackets, which are conjugate on the imaginary axis. The product of these two parts is thus real and positive for $p = j\omega$. Any double real p^2 -root is a degenerate case of a pair of conjugate roots to which Eqs. (166) and (167) are applicable. It follows that the corresponding root factor

$$[p^2 - p_v^2]^2 = [(p - p_v)(p + p_v)]^2 \quad (168)$$

is nonnegative for $p = j\omega$.

Any negative real root, $p_v^2 = (j\omega_v)^2$, must be of even multiplicity. In fact, if the root were simple, the factor $[-\omega^2 + \omega_v^2]$ would be negative for $\omega^2 > \omega_v^2$ and positive for $\omega^2 < \omega_v^2$; and thus violate the assumption that $P(\omega^2) + Q^2(\omega)$ is nonnegative for nonnegative values of ω^2 .

Any nonnegative real root $p_v^2 = \sigma_v^2$ of odd multiplicity results in a factor $(p^2 - \sigma_v^2)$ which is negative or zero for $p = j\omega$. Since

$$P(\omega^2) + Q^2(\omega)$$

is nonnegative by assumption, the total number of nonnegative real roots of odd multiplicity must be even; otherwise the constant k of Eq. (164) must be negative. Since $(p^2 - \sigma_v^2)$ is negative, it is obviously impossible to express it as the product of two conjugate root factors. However, it is possible to associate a minus sign with all such roots provided a minus sign is also associated with k when the number of such roots is odd. Any such factor can then be expanded into a product of two factors which are conjugate for $p = j\omega$

$$-(p^2 - \sigma_v^2) = [-(p - \sigma_v)][p + \sigma_v]. \quad (169)$$

This product is, of course, real and nonnegative for $p = j\omega$.

It can be concluded that Eq. (164) can be written as the product of two groups of factors that are conjugate on the imaginary axis of the p -plane. Because of this property, the two groups can be identified with the two polynomials $(u_2 + v_2)$ and $(u_2 - v_2)$. Each polynomial contains, as a multiplier, the constant \sqrt{k} if k is positive, or $\sqrt{-k}$ if k is negative. The two conjugate factors resulting from any pair of conjugate p_v^2 roots (double real roots included) or from any single nonnegative real root can be placed arbitrarily in either polynomial. However, all the zeros of the polynomial $(u_2 + v_2)$ must be in the left half plane since the function $\Gamma(p)$ must be regular in the right half plane and on the imaginary axis. Therefore, all the factors $(p \pm p_v)$ in which the real part of $(\pm p_v)$ is negative must be placed in the polynomial $(u_2 + v_2)$, and all the other

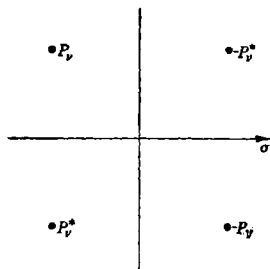


FIG. 9-41.—A quadruplet of conjugate roots.

factors, in which the real part of $(\pm p_*)$ is positive, are placed in the polynomial $(u_2 - v_2)$. The real part of the p_* can never be zero; that is, there cannot be any negative real root $p_*^2 = -\omega_*^2$, for then

$$P(\omega^2) + Q^2(\omega)$$

would vanish and $|\Gamma(j\omega)|^2$ would become infinite for $\omega = \omega_*$, contrary to the assumption made at the beginning of this discussion.

Equations (165), (168), and (169) ensure that the separation of the two polynomials can be performed. Therefore, the polynomial $(u_2 + v_2)$ in the variable p can be determined in all cases from the polynomial $P(\omega^2) + Q^2(\omega)$ by following the procedure outlined above. This procedure does not present any difficulty once the p_*^2 roots of

$$P(-p^2) + Q^2(-jp)$$

are known. The polynomial $(u_1 + v_1)$ can be determined in the same manner from the function $P(\omega^2)$. In this case, however, the zeros of $(u_1 + v_1)$ can be anywhere in the p -plane. It follows that the polynomials $(u_1 + v_1)$ and $(u_2 + v_2)$ can be separated in more than one way, and, therefore, the result is not unique. In most practical cases, however, all the zeros of $P(\omega^2)$ occur for real nonnegative values of ω^2 , that is, the real part of all p_* -roots is zero, and, therefore, the polynomial $(u_1 + v_1)$ is unique.

9-15. Specification of a Network with a Prescribed Input Impedance.—It may be concluded that a physically realizable function $\Gamma(p)$ can be obtained in all cases from a power-loss function P_0/P_L which satisfies the necessary conditions discussed before. It follows that these conditions are sufficient as well as necessary. The requirement on the regularity of $\Gamma(p)$ is automatically satisfied when the polynomial

$$(u_2 + v_2)$$

is properly determined. The input impedance of the nondissipative network of Fig. 9-40 can be found readily from $\Gamma(p)$ by means of the equation

$$Z(p) = \frac{1 + \Gamma(p)}{1 - \Gamma(p)} = \frac{(u_2 + v_2) + (u_1 + v_1)}{(u_2 + v_2) - (u_1 + v_1)} = \frac{(u_1 + u_2) + (v_1 + v_2)}{(u_2 - u_1) + (v_2 - v_1)} \quad (170)$$

For convenience, let

$$m_1 = u_2 + u_1 \quad n_1 = v_2 + v_1 \quad (171)$$

$$m_2 = u_2 - u_1 \quad n_2 = v_2 - v_1 \quad (172)$$

so that $Z(p)$ can be written as

$$Z(p) = \frac{m_1 + n_1}{m_2 + n_2} \quad (173)$$

At this juncture, further development depends on whether $Q(\omega)$ is even or odd. If it is assumed for the moment that $Q(\omega) = Q(-p^2)$ is an even function, the input impedance can be expressed in terms of the open-circuit and short-circuit impedances of the nondissipative network as

$$Z(p) = Z_{oc1} \frac{Z_{sc2} + 1}{Z_{oc2} + 1} = \frac{m_1 + n_1}{m_2 + n_2} = \frac{m_1 \frac{n_1}{n_2} + 1}{\frac{m_2}{n_2} + 1}. \quad (174)$$

This equation leads to the identifications

$$Z_{oc1} = \frac{m_1}{n_2} = \frac{u_2 + u_1}{v_2 - v_1}, \quad (175)$$

$$Z_{sc2} = \frac{n_1}{m_1} = \frac{v_2 + v_1}{u_2 + u_1}, \quad (176)$$

$$Z_{oc2} = \frac{m_2}{n_2} = \frac{u_2 - u_1}{v_2 - v_1}. \quad (177)$$

The three open-circuit impedances Z_{11} , Z_{12} , Z_{22} and the three short-circuit admittances Y_{11} , Y_{12} , Y_{22} can be obtained without difficulty from Eqs. (175), (176), and (177). Thus,

$$Z_{11} = \frac{m_1}{n_2} = \frac{u_2 + u_1}{v_2 - v_1}, \quad Z_{22} = \frac{m_2}{n_2} = \frac{u_2 - u_1}{v_2 - v_1}, \quad (178)$$

$$Z_{12} = \frac{\sqrt{m_1 m_2 - n_1 n_2}}{n_2} = \frac{\sqrt{(u_2^2 - u_1^2) - (v_2^2 - v_1^2)}}{v_2 - v_1} = \frac{Q(-p^2)}{v_2 - v_1}, \quad (179)$$

$$Y_{11} = \frac{m_2}{n_1} = \frac{u_2 - u_1}{v_2 + v_1}, \quad Y_{22} = \frac{m_1}{n_1} = \frac{u_2 + u_1}{v_2 + v_1}, \quad (180)$$

$$-Y_{12} = \frac{\sqrt{m_1 m_2 - n_1 n_2}}{n_1} = \frac{\sqrt{(u_2^2 - u_1^2) - (v_2^2 - v_1^2)}}{v_2 + v_1} = \frac{Q(-p^2)}{v_2 + v_1}. \quad (181)$$

It remains to be shown that the impedances and admittances defined above are separately physically realizable, and that they collectively satisfy the conditions of physical realizability for a two-terminal-pair reactive network. It can be shown by means of function theory that the ratio of the even part of either polynomial forming $Z(p)$ to the odd part of either polynomial behaves exactly like a reactance function. This property results from the fact that $Z(p)$ is a positive real function. It follows that all the driving-point impedances and admittances defined by Eqs. (175) to (181), inclusive, are physically realizable. The poles of the transfer impedance Z_{12} and of the transfer admittance Y_{12} coincide with poles of Z_{11} and Z_{22} and with the poles of Y_{11} and Y_{22} , respectively. This property together with the fact that both numerators are even polynomials guarantees the physical realizability of Z_{12} and Y_{12} . It

can be shown also that the residues k_{11} , k_{22} , k_{12} of Z_{11} , Z_{22} , Z_{12} for any one of their common poles satisfy identically the equation

$$k_{11}k_{22} - k_{12}^2 = 0. \quad (182)$$

This equation guarantees the physical realizability of the two-terminal-pair reactive network defined by Z_{11} , Z_{22} , and Z_{12} . The same equation is satisfied by the residues of Y_{11} , Y_{22} , and Y_{12} .

It was pointed out, in connection with Eq. (157), that the polynomial $N(\omega^2)$ had to be the square of either an even or an odd polynomial $Q(\omega)$. Equations (179) and (181) justify this requirement since $\sqrt{N(\omega^2)}$ appears in the numerators of Z_{12} and Y_{12} . Now Z_{12} and Y_{12} have been shown to be physically realizable if $Q(\omega)$ is an even polynomial, but this is not true if $Q(\omega)$ is an odd polynomial. In fact, the ratio of two odd polynomials is an even function and, therefore, cannot be physically realized as a transfer impedance or a transfer admittance. When $Q(\omega)$ is equal to $Q(-jp)$, an odd function, Eq. (174) may be manipulated in an alternative fashion to obtain

$$Z(p) = Z_{oc1} \frac{Z_{scs} + 1}{Z_{oc2} + 1} = \frac{m_1 + n_1}{m_2 + n_2} = \frac{n_1}{m_2} \frac{\frac{m_1}{n_1} + 1}{\frac{n_2}{m_2} + 1}. \quad (183)$$

The following identifications can be made:

$$Z_{oc1} = \frac{n_1}{m_2} = \frac{v_2 + v_1}{u_2 - u_1}, \quad (184)$$

$$Z_{sc2} = \frac{m_1}{n_1} = \frac{u_2 + u_1}{v_2 + v_1}, \quad (185)$$

$$Z_{oc2} = \frac{n_2}{m_2} = \frac{v_2 - v_1}{u_2 - u_1}. \quad (186)$$

Equations (178) to (181), inclusive, are then replaced by

$$Z_{11} = \frac{n_1}{m_2} = \frac{v_2 + v_1}{u_2 - u_1}, \quad Z_{22} = \frac{n_2}{m_2} = \frac{v_2 - v_1}{u_2 - u_1}, \quad (187)$$

$$Z_{12} = \frac{\sqrt{n_1 n_2 - m_1 m_2}}{m_2} = \frac{\sqrt{-Q^2(-jp)}}{u_2 - u_1} = \frac{jQ(-jp)}{u_2 - u_1}, \quad (188)$$

$$Y_{11} = \frac{n_2}{m_1} = \frac{v_2 - v_1}{u_2 + u_1}, \quad Y_{22} = \frac{n_1}{m_1} = \frac{v_2 + v_1}{u_2 + u_1}, \quad (189)$$

$$-Y_{12} = \frac{\sqrt{n_1 n_2 - m_1 m_2}}{m_1} = \frac{\sqrt{-Q^2(-jp)}}{u_2 + u_1} = \frac{jQ(-jp)}{u_2 + u_1}. \quad (190)$$

The numerators of Z_{12} and Y_{12} are odd functions of p . It should be noted that the imaginary unit results from the fact that $Q(-jp)$ is an even function of p multiplied by $-jp$. The denominators of Z_{12} and Y_{12} are even

functions of p . It follows that Z_{12} and Y_{12} are odd functions of p , and are, therefore, physically realizable. It can be shown that also in this case the residues of Z_{11} , Z_{22} , and Z_{12} at any common pole satisfy Eq. (182). The same is true for the residues of Y_{11} , Y_{22} , and Y_{12} . It follows that the nondissipative network defined by Eqs. (187) to (190) is physically realizable.

9-16. Summary of the Method of Designing Reactive Networks with Specified Insertion Loss.—The major steps in the design of a reactive network with specified insertion loss are summarized below for the convenience of the reader.

1. The input impedance $Z(p)$ must be a rational meromorphic function which is positive real.
2. In order to satisfy Condition (1), the reflection coefficient $\Gamma(p)$ must be a rational meromorphic function, regular in the right half plane and satisfying the inequality

$$|\Gamma(p)| \leq 1 \quad \text{for } \sigma \geq 0. \quad (191)$$

3. Condition (2) can always be satisfied if

$$\frac{P_0}{P_L} = 1 + \frac{M(\omega^2)}{N(\omega^2)}, \quad (192)$$

where the polynomials M and N are nonnegative for real values of ω .

4. If

$$N(\omega^2) = Q^2(\omega), \quad (193)$$

then by writing

$$\Gamma(p) = \frac{u_1 + v_1}{u_2 + v_2}, \quad (194)$$

where u_1 , u_2 are even and v_1 , v_2 are odd functions of p , it is possible to determine $(u_1 + v_1)$ and $(u_2 + v_2)$ from the roots of the polynomials $P(\omega^2) + Q^2(\omega)$ and $P(\omega^2)$, respectively.

5. Finally, from u_1 , v_1 , u_2 , v_2 it is always possible to determine at least one set of open-circuit impedances (or short-circuit admittances) specifying a two-terminal-pair reactive network having the prescribed power-loss ratio P_0/P_L . Succeeding sections will discuss the appropriate selection of the power-loss-ratio function and the synthesis of the two-terminal-pair reactive network specified above. These steps will complete the solution of the original synthesis problem.

SELECTION OF POWER-LOSS RATIOS

9-17. Selection of Polynomials $P(\omega^2)$ and $Q^2(\omega)$.—The selection of the polynomials $P(\omega^2)$ and $Q^2(\omega)$ depends on the purpose for which the

filter is designed. Moreover, practical considerations concerning the physical structure of the filter may place further requirements on the two polynomials. Microwave filters are designed, at present, to provide frequency discrimination without regard to transient response. It follows that the ratio P_L/P_0 must approximate unity in the pass band and zero in the attenuation band. Physical intuition tells one that the best function for this purpose is that for which all the minima in the pass band are equal and all the maxima in the attenuation band are equal. Moreover, it seems evident that there should be as many frequencies of zero loss ($P_L/P_0 = 1$) and infinite loss ($P_L/P_0 = 0$) as the degrees of the polynomials used permit. Since the zeros of $P(\omega^2)$ are evidently frequencies of zero loss and the zeros of $Q^2(\omega)$ are frequencies of infinite loss, it follows immediately that all the ω^2 roots of $P(\omega^2)$ and $Q^2(\omega)$ should be real and nonnegative. Fortunately it turns out, as will be shown later, that this condition guarantees that the network will be physically realizable in the convenient form of a ladder structure. The numbers of zeros of $P(\omega^2)$ and $Q^2(\omega)$, that is, the degrees of the polynomials, can be specified independently. Therefore, it seems logical to consider first the case of $Q^2(\omega) = 1$. The case of $P(\omega^2) = 1$ can be treated in a similar manner. If $Q^2(\omega) = 1$, the loss can be infinite only for $\omega = \infty$, when $P(\omega^2)$ becomes infinite. All the zeros of the polynomial $P(\omega^2)$, on the other hand, must be in the pass band and must be separated by equal maxima. These requirements can be met by using Tchebysheff polynomials of the first kind, properly modified for this purpose.

9-18. Tchebysheff Pass-band Behavior.—Consider the function

$$T_n(\omega) = \cos (n \cos^{-1} \omega) = \operatorname{Re} [(\omega + j \sqrt{1 - \omega^2})^n]. \quad (195)$$

This function oscillates between -1 and 1 as ω is increased from -1 to 1 . At the two ends of this band,

$$\left. \begin{aligned} T_n(1) &= 1, \\ T_n(-1) &= \begin{cases} -1 & \text{for } n \text{ odd.} \\ 1 & \text{for } n \text{ even.} \end{cases} \end{aligned} \right\} \quad (196)$$

The n zeros of $T_n(\omega)$ occur for $|\omega| < 1$. When $|\omega| > 1$, $\cos^{-1} \omega$ is imaginary, and the magnitude of $T_n(\omega)$ becomes larger than unity and, in fact, approaches infinity as the n th power of ω .

The right-hand side of Eq. (195) can be expanded in the form of a polynomial for integral values of n . The recurrence formula

$$T_{n+1} = 2\omega T_n - T_{n-1} \quad (197)$$

provides an alternate method of obtaining the same polynomials. Table 9-3 gives these polynomials for values of n from 1 to 8. The polynomials $T_3(\omega)$ and $T_4(\omega)$ are plotted in Fig. 9-42.

TABLE 9-3.—TCHEBYSHEFF POLYNOMIALS

$$T_1(\omega) = \omega.$$

$$T_2(\omega) = 2\omega^2 - 1.$$

$$T_3(\omega) = 4\omega^3 - 3\omega.$$

$$T_4(\omega) = 8\omega^4 - 8\omega^2 + 1.$$

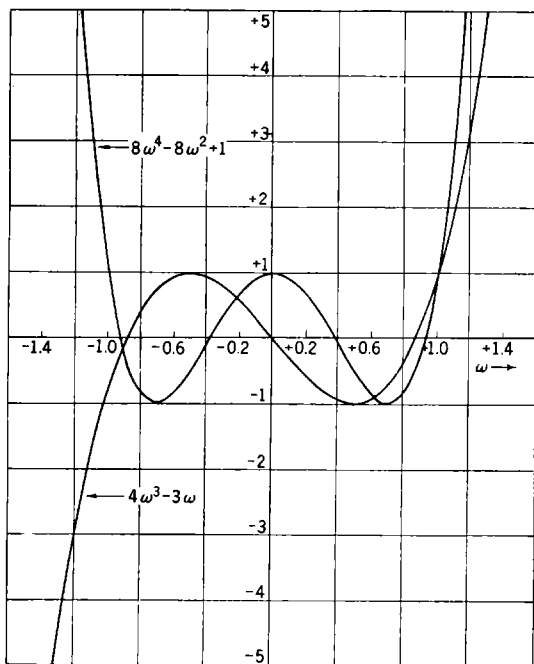
$$T_5(\omega) = 16\omega^5 - 20\omega^3 + 5\omega.$$

$$T_6(\omega) = 32\omega^6 - 48\omega^4 + 18\omega^2 - 1.$$

$$T_7(\omega) = 64\omega^7 - 112\omega^5 + 56\omega^3 - 7\omega.$$

$$T_8(\omega) = 128\omega^8 - 256\omega^6 + 160\omega^4 - 32\omega^2 + 1.$$

The $T_n(\omega)$ functions, when squared and multiplied by an arbitrary positive constant h^2 , provide polynomials suitable for use as $P(\omega^2)$ in the

FIG. 9-42.—Plots of the functions $T_3(\omega)$ and $T_4(\omega)$.

case of low-pass filters. In fact, $h^2 T_n^2(\omega)$ is an even polynomial whose value oscillates between zero and h^2 in the band $-1 < \omega < 1$. All the ω^2 roots are real and positive since they coincide with the n roots

$$T_n(\omega) = 0.$$

The power-loss ratio and the square of the magnitude of the reflection coefficient are then

$$\frac{P_0}{P_L} = 1 + P(\omega^2) = 1 + h^2 T_n^2(\omega), \quad (198)$$

$$|\Gamma(j\omega)|^2 = \frac{P(\omega^2)}{1 + P(\omega^2)} = \frac{h^2 T_n^2(\omega)}{1 + h^2 T_n^2(\omega)}. \quad (199)$$

The functions T_3^2 and T_4^2 are plotted in Fig. 9-43. The tolerance of the power-loss ratio P_0/P_L in the pass band is

$$\epsilon^2 = h^2. \quad (200)$$

For small values of h^2 , the maximum insertion loss in the pass band is approximately

$$L_{\max} \approx 4.23h^2. \quad (201)$$

For large values of ω , the power ratio approaches the asymptotic value

$$\left[\frac{P_0}{P_L} \right]_{\infty} \approx \frac{h^2}{4} (2\omega)^{2n}. \quad (202)$$

It follows that the ratio of this asymptotic value to the tolerance in the pass band is independent of h^2 since

$$\frac{1}{\epsilon^2} \left[\frac{P_0}{P_L} \right]_{\infty} = \frac{1}{4} (2\omega)^{2n}. \quad (203)$$

Thus, the tolerance in the pass band can be improved only at the expense of the loss in the attenuation band, or vice versa. The integer n may be considered as an over-all figure of merit of the filter. It can be shown that no polynomial $P(\omega^2)$ of $2n$ degree in ω can lead to a ratio

$$\frac{1}{\epsilon^2} \left[\frac{P_0}{P_L} \right]_{\infty}$$

larger than $\frac{1}{4}(2\omega)^{2n}$.

Once $P(\omega^2)$ is chosen, its zeros must be found together with the zeros of the polynomial $1 + P(\omega^2)$, as required by Eqs. (162) and (163). Fortunately, Eq. (195), which defines the function $T_n(\omega)$, permits a direct determination of these zeros. The double zeros of $h^2 T_n^2(\omega)$ occur for

$$n \cos^{-1} \omega = \left(\frac{\pi}{2} + m\pi \right) \quad (m = 0, 1, 2, \dots, n-1); \quad (204)$$

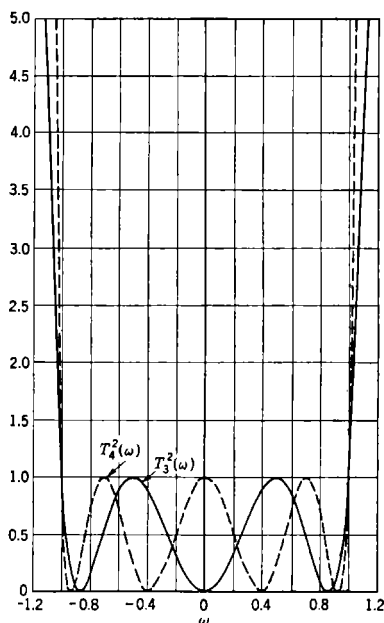


Fig. 9-43.—Plots of the functions $T_3^2(\omega)$ and $T_4^2(\omega)$.

that is, for

$$\omega = -jp = \cos \left(\frac{\pi}{2n} + \frac{m}{n} \pi \right). \quad (205)$$

The zeros of $1 + h^2 T_n^2(\omega)$ occur for

$$\cos (n \cos^{-1} \omega) = \pm j \frac{1}{h}; \quad (206)$$

that is, for

$$n \cos^{-1} \omega = \left(\frac{\pi}{2} + m\pi \right) - j \sinh^{-1} \left(\pm \frac{1}{h} \right) \quad (m = 0, 1, 2, \dots, n-1); \quad (207)$$

or

$$\omega = \cos \left[\left(\frac{\pi}{2n} + \frac{m}{n} \pi \right) - j \frac{1}{n} \sinh^{-1} \left(\pm \frac{1}{h} \right) \right]. \quad (208)$$

9-19. Tchebysheff Behavior in the Attenuation Band.—The case of $P(\omega^2) = 1$ can be treated in the same manner, and leads to Tchebysheff behavior in the attenuation band. The polynomial $hT_n(\omega)$ can be identified with $Q(\omega)$ so that the power ratio becomes

$$\frac{P_0}{P_L} = 1 + \frac{1}{Q^2(\omega)} = 1 + \frac{1}{h^2 T_n^2(\omega)}. \quad (209)$$

The corresponding expression for the square of the magnitude of the reflection coefficient is

$$|\Gamma(j\omega)|^2 = \frac{1}{1 + Q^2(\omega)} = \frac{1}{1 + h^2 T_n^2(\omega)}. \quad (210)$$

The function $h^2 T_n^2(\omega)$ is small for $|\omega| < 1$ and large for $|\omega| > 1$ so that the ratio P_0/P_L approximates unity at high frequencies. The filter having such a power-loss ratio is, therefore, of the high-pass type. The zeros of $T_n^2(\omega)$ yield peaks of infinite loss; P_0/P_L on the other hand approaches unity at high frequencies when $h^2 T_n^2(\omega)$ approaches infinity. The minima of P_0/P_L for $|\omega| < 1$ are all equal to the value of the ratio for $\omega = 1$.

$$\left[\frac{P_0}{P_L} \right]_{\omega=1} = 1 + \frac{1}{h^2} = 1 + \frac{1}{\epsilon^2}. \quad (211)$$

A low-pass filter may be derived from the high-pass filter by following the procedure discussed in Sec. 9-8, or by substituting $-1/\omega'$ for ω in Eq. (209) to obtain

$$\frac{P_0}{P_L} = 1 + \frac{1}{Q^2 \left(-\frac{1}{\omega'} \right)} = 1 + \frac{1}{h^2 T_n^2 \left(-\frac{1}{\omega'} \right)}. \quad (212)$$

Consider now the case in which both $P(\omega^2)$ and $Q^2(\omega)$ differ from unity, that is, the case in which there are several frequencies of infinite loss as well as several frequencies of perfect transmission. The desired type of behavior for the insertion loss is shown in Fig. 9-44. Consider the function

$$F(\omega^2) = \frac{P(\omega^2)}{Q^2(\omega)} = h^2 \frac{(\omega_1^2 - \omega^2)^2 (\omega_3^2 - \omega^2)^2 \cdots (\omega_{2n-1}^2 - \omega^2)^2}{(1 - \omega_1^2 \omega^2)^2 (1 - \omega_3^2 \omega^2)^2 \cdots (1 - \omega_{2n-1}^2 \omega^2)^2} \quad (213)$$

which satisfies the conditions of physical realizability for arbitrary positive real values of the ω_i^2 ; it can be shown that this function has the desired Tchebysheff behavior in the attenuation band as well as in the pass band if the ω_i^2 are chosen as follows:

$$\omega_i^2 = k \operatorname{sn}^2 \left(\frac{\nu K}{2n} \right), \quad (214)$$

where k is a positive real constant smaller than unity. The function $\operatorname{sn}(u)$ is the Jacobean elliptic function⁷ of modulus k defined by the two equations

$$\operatorname{sn}(u) = \sin \phi, \quad (215)$$

$$u = \int_0^\phi \frac{d\xi}{\sqrt{1 - k^2 \sin^2 \xi}}. \quad (216)$$

The constant K is the complete elliptic integral of modulus k defined by

$$K = \int_0^{\pi/2} \frac{d\xi}{\sqrt{1 - k^2 \sin^2 \xi}}. \quad (217)$$

The insertion loss corresponding to the function defined by Eq. (213) is sketched for $n = 2$ in Fig. 9-44a. The maxima in the pass band ($\omega < 1$) are equal to the value of the function for $\omega = \sqrt{k}$.

$$\epsilon_p^2 = F(k) = F(0) = h^2 [\omega_1 \omega_3 \cdots \omega_{2n-1}]^4. \quad (218)$$

The minima in the attenuation band are all equal to

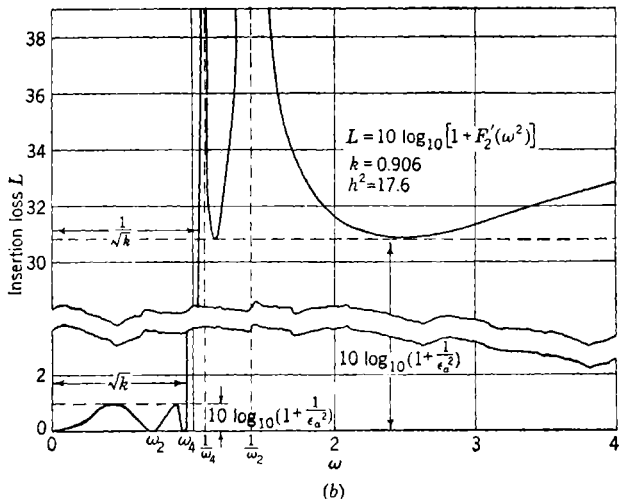
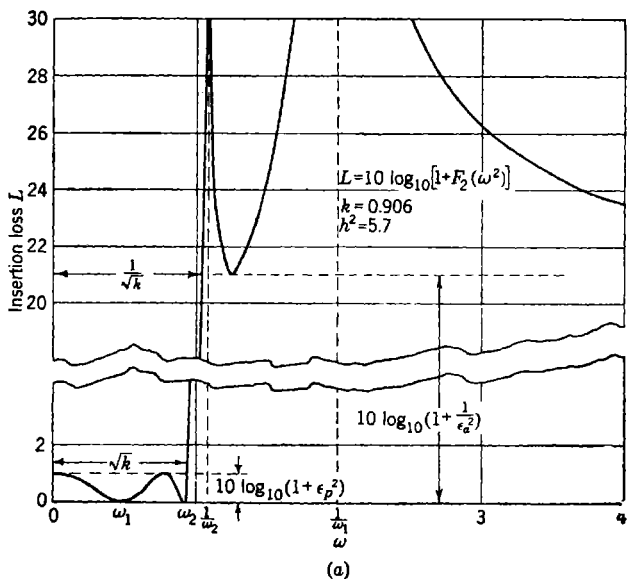
$$\frac{1}{\epsilon_a^2} = \frac{h^4}{\epsilon_p^2}, \quad (219)$$

since

$$\frac{1}{h^2} F(\omega^2) = \frac{h^2}{F(\omega^{-2})}. \quad (220)$$

It follows from Eqs. (218) and (219) that the product $\epsilon_a^2 \epsilon_p^2$ is fixed by the value of n , that is, by the degree of $P(\omega^2)$ and $Q^2(\omega)$. Thus,

$$\epsilon_a^2 \epsilon_p^2 = [\omega_1 \omega_3 \cdots \omega_{2n-1}]^4. \quad (221)$$


 FIG. 9-44.—Plots of the insertion-loss functions corresponding to $F(\omega^2)$ and $F'(\omega^2)$.

The value of k determines the width of the transition region between pass band and attenuation band. The width of this region is

$$\Delta\omega = \frac{1}{\sqrt{k}} - \sqrt{k} = \frac{1-k}{\sqrt{k}}. \quad (222)$$

Evidently, a large value of k results in a sharp cutoff. When k approaches unity, however, ω_c approaches k , and consequently the product $\epsilon_a^2 \epsilon_p^2$ also approaches unity. Since this product is a measure of the tolerance in both bands, it can be concluded that, for a given n , the rate of cutoff cannot be increased indefinitely except at the expense of increased tolerances. In addition to this theoretical limitation on the choice of k , there are certain practical limitations. First, the incidental dissipation is particularly effective in reducing the peaks of attenuation when such peaks are close to cutoff. In the second place, the adjustment of the filter elements is very critical when k is large. These factors should be taken into consideration in any practical design.

The function $F(\omega^2)$ whose corresponding insertion-loss function is sketched in Fig. 9-44a is the square of an even function of ω . On the other hand, the function $F'(\omega^2)$ that corresponds to the insertion-loss function sketched in Fig. 9-44b is the square of an odd function of ω . Let, then,

$$F'(\omega^2) = h^2 \frac{\omega^2(\omega_2^2 - \omega^2)^2(\omega_4^2 - \omega^2)^2 \cdots (\omega_{2n}^2 - \omega^2)^2}{(1 - \omega_2^2\omega^2)^2(1 - \omega_4^2\omega^2)^2 \cdots (1 - \omega_{2n}^2\omega^2)^2}. \quad (223)$$

This function is seen to satisfy the conditions of physical realizability. Tchebysheff behavior can be obtained by choosing the ω_p^2 as follows:

$$\omega_p^2 = k \operatorname{sn}^2 \frac{\nu K}{2n+1}. \quad (224)$$

Figure 9-44b is a sketch of the insertion loss corresponding to $F'(\omega^2)$ for $n = 2$.

The maximum values of $F'(\omega^2)$ for $|\omega| < 1$ are all equal to $F'(k)$ and are given by

$$\epsilon_p^2 = F'(k) = h^2 k [\omega_1 \omega_3 \omega_5 \cdots \omega_{2n-1}]^4, \quad (225)$$

since

$$\frac{\omega_p^2 - k^2}{1 - \omega_p^2 k} = k^2 \operatorname{sn}^4 \left[\frac{(2n+1-\nu)K}{2n+1} \right]. \quad (226)$$

The minimum values of $F'(\omega^2)$ for $|\omega| > 1$ are all equal to $F'(1/k)$ and are given by the expression

$$\frac{1}{\epsilon_a^2} = F' \left(\frac{1}{k} \right) = \frac{h^4}{F'(k)} = \frac{h^2}{k [\omega_1 \omega_3 \cdots \omega_{2n-1}]^4}. \quad (227)$$

It follows that the product $\varepsilon_j^2 \varepsilon_a^2$ is independent of h . Thus,

$$\varepsilon_j^2 \varepsilon_a^2 = k^2 [\omega_1 \omega_3 \omega_5 \cdots \omega_{2n-1}]^2. \quad (228)$$

Since the considerations on the value of k made in connection with $F(\omega^2)$ apply also to the case of $F'(\omega^2)$, no further discussion is required.

The zeros of the polynomial $P(\omega^2)$ are the ω_j^2 appearing in the numerators of $F(\omega^2)$ and $F'(\omega^2)$. The determination of the zeros of

$$P(\omega^2) + Q^2(\omega),$$

that is, of the roots of the equations

$$F(\omega^2) + 1 = 0, \quad F'(\omega^2) + 1 = 0 \quad (229)$$

does not present any serious difficulty. The procedure, however, involves the use of certain properties of elliptic functions which, for the sake of brevity, cannot be discussed here. The reader is referred to the original paper by Darlington⁴ or any standard treatise on elliptic functions.⁷

PHYSICAL REALIZATION OF SPECIFIED REACTIVE NETWORKS

9-20. Properties of Ladder Networks.—The next step in the design of a filter is the determination of a two-terminal-pair reactive network whose impedances Z_{11} , Z_{22} , and Z_{12} or admittances Y_{11} , Y_{22} , and Y_{12} are specified. Such a network can be obtained without difficulty in the form of a canonic T- or Π -structure.⁵ In practice, however, the branches of these structures are very difficult to construct, particularly in the case of microwave filters. Darlington⁴ of the Bell Telephone Laboratories has developed a general method of synthesis that permits the realization of the network in the form of a cascade of a number of sections, each of which corresponds to a pair of conjugate zeros of Z_{12} or Y_{12} . Such a cascade structure turns out to be satisfactory in most practical cases. Darlington's general method of synthesis, however, is not discussed here because most microwave filters fall in a special class for which the synthesis procedure is considerably simpler. In general, it is desired to have as many peaks of infinite loss as possible for a given number of elements. These finite frequencies at which the loss is infinite are the zeros of $Q(\omega)$ and, therefore, are also the zeros of Z_{12} and Y_{12} . Under these circumstances, that is, when the zeros of Z_{12} and Y_{12} occur for finite imaginary values of p , the filter can be realized as a simple ladder structure.

Consider the ladder structure shown in Fig. 9-45. Let Z'_{11} , Z'_{22} , Z'_{12} be its open circuit impedances. It can be shown that all the zeros of Z'_{12} are at real frequencies which coincide with the resonance frequencies of the shunt branches. Furthermore, Z'_{11} , Z'_{22} , and Z'_{12} have the same poles, at finite frequencies, and the residues at these poles satisfy the equation

$$k_{11}k_{22} - k_{12}^2 = 0. \quad (230)$$

This equation is also satisfied by the residues at the internal poles of Z_{11} , Z_{22} , and Z_{12} for the network to be synthesized. This fact does not mean that the internal poles of Z_{11} , Z_{22} , and Z_{12} must always coincide, for Eq. (230) can be satisfied if $k_{22} = k_{12} = 0$ while $k_{11} \neq 0$. However, if it is assumed for the moment that all the finite poles of Z_{11} , Z_{22} , and Z_{12} do coincide, and furthermore that it is possible to design a structure of the type shown in Fig. 9-45 for which $Z'_{11} = Z_{11}$ and the zeros of Z'_{12} coincide with the zeros of Z_{12} , it follows that Z_{12} and Z'_{12} must also have coincident poles, and, therefore, can differ only by a constant multiplier which can be made equal to unity by a proper choice of the value of a . If $Z_{11} = Z'_{11}$ and $Z_{12} = Z'_{12}$, the residues at the internal poles of Z'_{22} must be equal to the residues at the poles of Z_{22} since the residues for both sets of impedances satisfy Eq. (230). The elements C_{2n+1} and L_{2n+1} which control the behavior of Z'_{22} at infinity and at the origin can be adjusted to make $Z'_{22} = Z_{22}$ without changing Z'_{12} and Z'_{11} . The assumption that Z_{11} , Z_{22} , and Z_{12} have coincident poles at finite frequencies can now be

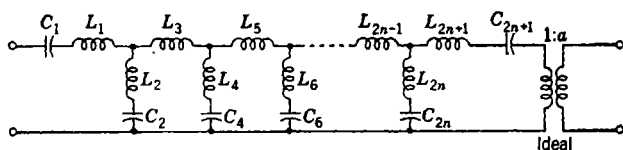


FIG. 9-45.—A simple ladder structure.

eliminated. In fact, all the terms of the partial fraction expansion of Z_{11} that correspond to poles not common to the other two impedances can be lumped together in any convenient form as a reactance in series with the input terminals. This series reactance does not change either Z_{22} or Z_{12} . The same procedure can be followed in the case of the poles of Z_{22} that are not common to Z_{11} and Z_{12} . In most practical cases, however, the original assumption concerning the poles of the Z 's is satisfied.

9-21. Determination of Ladder Elements.—The synthesis of the network has now been reduced to the problem of finding a ladder structure whose input impedance equals Z_{11} and whose shunt branches resonate at the zeros of Z_{12} . It can be shown that it is always possible to design such a ladder structure, provided the conditions assumed above are satisfied. Some of the series inductances may turn out to be negative. However, it is always possible to eliminate them by using coupled coils as shown in Fig. 9-46. Fortunately, in most practical cases, this situation does not arise. For further discussion of this point, the reader is referred to Darlington's original paper.⁴

The actual synthesis of Z_{11} can be performed in the following manner. Let $\pm\omega_2, \pm\omega_4, \pm\omega_6, \dots, \pm\omega_{2n}$ be the zeros of Z_{12} . Subtract from Z_{11}

a reactance equal to the value of Z_{11} for $\omega = \omega_2$. Use this reactance (realized in a manner consistent with the behavior of Z_{11} at $\omega = 0$ and $\omega = \infty$) as the first series branch of the ladder structure. The remainder $Z_{11}^{(1)}$ has zeros for $\omega = \pm\omega_2$. Subtract from the partial fraction expansion of $1/Z_{11}^{(1)}$ the term corresponding to the pair of poles at $\omega = \pm\omega_2$. This term is the admittance of the resonant branch L_2, C_2 . Let the inverse of the remainder be $Z_{11}^{(2)}$. Subtract from $Z_{11}^{(2)}$ the reactance $j\omega L_3$ so that the remainder $Z_{11}^{(3)}$ has a pair of zeros coincident with the pair of zeros $\pm\omega_4$ of Z_{12} . Eliminate these zeros by subtracting from the expansion of $1/Z_{11}^{(3)}$ the term corresponding to the poles at $\omega = \pm\omega_4$. The same operation is repeated on $Z_{11}^{(4)}$, the inverse of the remainder, and so on, until all the zeros of Z_{12} have been used. At this point, the synthesis of Z_{11} has been completed, and the remainder must be zero.

Some of the zeros of Z_{12} may occur for $\omega = \infty$. Since Z_{12} is an odd function of ω , the multiplicity of the zero at infinity must be odd. Let it be, for instance, $2m - 1$. In this case the ladder has m purely capacitive shunt branches. The same thing can be said about the zeros of Z_{12} for $\omega = 0$, except that in this case the shunt branches become purely inductive.

The special case in which all the zeros of Z_{12} occur at infinity is particularly important. If there are no internal zeros of Z_{12} , the polynomial $Q(\omega)$ must be a constant. The determination of the ladder structure reduces to a continuous fraction expansion of Z_{11} , that is, to a realization of Z_{11} in the well-known Cauer form

$$Z_{11} = pL_1 + \frac{1}{pC_2 + \frac{1}{pL_3 + \dots + \frac{1}{pC_n}}} \quad (231)$$

All the inductances in the shunt branches vanish and the capacitances C_1 and C_{n+1} are short-circuited. The inductance L_{n+1} is determined from the behavior at infinity of Z_{22} , and the ratio a of the ideal transformer from the constant multiplier of either Z_{12} or Z_{22} . In this case all the elements of the ladder are positive and no difficulty is encountered. Obviously the impedance Z_{22} can be expanded into a continued fraction instead of

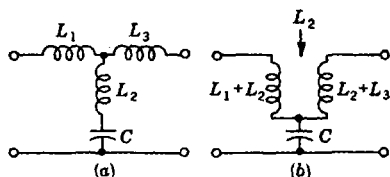


FIG. 9-46.—Elimination of negative inductances by use of coupled coils.

Z_{11} . The two expansions must lead to the same ladder, and, therefore, they provide a convenient method of checking the final results. It is also possible to expand into a continued fraction the input (or output) impedance of the network terminated in 1-ohm resistance. This method of synthesis must also lead to the same network obtained by expanding either Z_{11} or Z_{22} .

Most practical filters turn out to be of either the symmetrical or the reciprocal-impedance type. For a symmetrical filter $Z_{11} = Z_{22}$, $Y_{11} = Y_{22}$, whereas for a reciprocal impedance filter $Z_{11} = Y_{22}$, $Y_{11} = Z_{22}$. A symmetrical filter consists of two identical sections connected in cascade back-to-back. A reciprocal impedance filter, on the other hand, consists of two dual sections connected in cascade back-to-back. It is obvious that a priori knowledge of such properties facilitates the synthesis of the network.

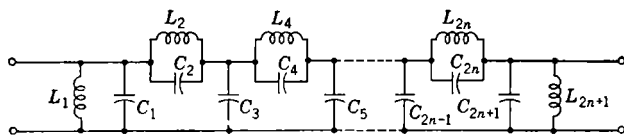


FIG. 9-47.—Dual of ladder structure shown in Fig. 9-45.

First will be considered the case where $Q(\omega)$ is an even polynomial. Equations (178) and (179) show that for a symmetrical network

$$m_1 = m_2, \quad n_1 = 0. \quad (232)$$

It follows from Eq. (162) that $P(\omega^2)$ must be the square of an odd function of ω . Reciprocal impedance networks are obtained, on the other hand, when

$$n_1 = n_2, \quad v_1 = 0; \quad (233)$$

$P(\omega^2)$ is then the square of an even function of ω . The attention of the reader is called to the fact that all the loss functions considered in Secs. 9-18 and 9-19 correspond to either symmetrical or reciprocal filters.

When $Q(\omega)$ is an odd polynomial, the situation is reversed. Symmetrical filters are obtained when $P(\omega^2)$ is the square of an even function, and reciprocal impedance filters are obtained when $P(\omega^2)$ is the square of an odd function.

The synthesis procedure discussed above is based on the open-circuit impedances Z_{11} , Z_{12} , and Z_{22} . It is evident that a dual procedure can be followed which is based on the short-circuit admittances Y_{11} , Y_{12} , and Y_{22} . The ladder structure resulting from this procedure is shown in Fig. 9-47. The details of the procedure can be obtained from the previous discussion by substituting admittance for impedance, short circuit for open circuit, series for shunt, capacitance for inductance, and vice versa. The zeros of Y_{12} , for instance, correspond to the resonance frequencies of

the series branches. Both procedures become identical when all the zeros of Z_{12} and Y_{12} occur at $\omega = \infty$, that is, when $Q(\omega)$ is a constant. In all other cases, one procedure is preferable to the other, but the resulting networks are not identical. Furthermore, in some cases, namely, in the case of reciprocal networks, it may be convenient to develop part of the network by one procedure, and the rest of the network by the other procedure. As a final remark, it should be pointed out that reciprocal networks, that is, networks for which $Y'_{11} = Z_{11}$, $Y'_{22} = Z_{22}$ and $Y'_{12} = Z_{12}$ have the same insertion loss when terminated in 1-ohm resistances.

EFFECT OF INCIDENTAL DISSIPATION ON FILTER CHARACTERISTICS

The methods of design discussed in the preceding sections are limited to nondissipative networks. In practice, since a small amount of dissipation is always present, the actual behavior of a filter differs somewhat from the behavior predicted theoretically on the assumption that the network is purely reactive. The two main effects of incidental dissipation are the introduction of a small but finite loss in the pass band and the rounding-off of the peaks of infinite loss in the attenuation band. The approximate effect of incidental dissipation can be computed without difficulty in most practical cases. In some cases it is even possible to modify the design of the network so that the incidental dissipation is taken into account, to a first approximation.

9.22. Analysis of Uniformly Dissipative Networks.—In most practical filters, the losses can be assumed to be uniformly distributed. In other words, if a series resistance R is associated with any inductance L and a shunt conductance G with any capacitance C , the ratios R/L and G/C are approximately equal for all elements. If the two ratios are equal, the computation of the effect of incidental dissipation is simplified by the substitution

$$\frac{R}{L} = \frac{G}{C} = \delta. \quad (234)$$

In terms of this quantity, the impedance of any dissipative inductance L and the admittance of any dissipative capacitance C become

$$Z_L = R + j\omega L = (\delta + j\omega)L, \quad (235)$$

$$Y_C = G + j\omega C = (\delta + j\omega)C. \quad (236)$$

If the complex variable $p = \sigma + j\omega$ is substituted for $j\omega$, these equations become

$$Z_L = (p + \delta)L, \quad (237)$$

$$Y_C = (p + \delta)C. \quad (238)$$

Consider any analytic function of the complex variable p characterizing the behavior of a nondissipative network, namely a driving-point

impedance $Z(p)$. If dissipation is introduced uniformly so that Eq. (234) is satisfied, the reactance of any inductance pL and the susceptance of any capacitance pC are given simply by Eq. (237) and Eq. (238), respectively. Since $Z(p)$ depends on p only through the reactances and the susceptances of the individual elements of the network, the impedance $Z_s(p)$ of the dissipative network can be obtained from $Z(p)$ by substituting $p + \delta$ for p . Thus,

$$Z_s(p) = Z(p + \delta). \quad (239)$$

It follows that the impedance of a uniformly dissipative network at any real frequencies ($p = j\omega$) is equal to the impedance of the nondissipative network at the complex frequency

$$p = \delta + j\omega. \quad (240)$$

To estimate $Z_s(j\omega)$, the function $Z(p + \delta)$ is expanded in a Taylor series about the point p as follows:

$$Z_s(p) = Z(p + \delta) = Z(p) + \frac{dZ}{dp} \delta + \frac{1}{2} \frac{d^2Z}{dp^2} \delta^2 + \dots \quad (241)$$

For $p = j\omega$, $Z(p)$ is a pure reactance;

$$Z(p) = jX(\omega). \quad (242)$$

Substituting Eq. (242) in Eq. (241), it is found that

$$Z_s(j\omega) = Z(\delta + j\omega) = jX(\omega) + \frac{dX(\omega)}{d\omega} \delta - j \frac{1}{2} \frac{d^2X(\omega)}{d\omega^2} \delta^2 + \dots \quad (243)$$

This Taylor series converges uniformly only within a circle centered at $j\omega$ (in the complex p -plane) whose radius equals the distance from $j\omega$ to the nearest singularity as shown in Fig. 9-48. In other words, the series cannot be used in the vicinity of a pole. However, this difficulty can be overcome easily by using the Taylor expansion of

$$Y_s(p) = Y(p + \delta) = \frac{1}{Z(p + \delta)}$$

which has a zero where $Z(p + \delta)$ has a pole. Then, for $p = j\omega$,

$$Y(p) = jB(\omega) \quad (244)$$

and consequently,

$$Y_s(j\omega) = Y(\delta + j\omega) = jB(\omega) + \frac{dB(\omega)}{d\omega} \delta - j \frac{1}{2} \frac{d^2B(\omega)}{d\omega^2} \delta^2 + \dots \quad (245)$$

When the Taylor series converges uniformly and $\delta \ll \omega$, the values of $Z_s(j\omega)$ and $Y_s(j\omega)$ are given to a good approximation by the first two or, at most, the first three terms of the series.

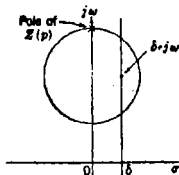


FIG. 9-48.—Circle of convergence for Taylor series approximating a dissipative impedance.

Consider now the case of dissipative networks for which the ratio R/L is the same for any L , and the ratio G/C is the same for any C but $\frac{R}{L} \neq \frac{G}{C}$. Let

$$\delta = \frac{1}{2} \left(\frac{R}{L} + \frac{G}{C} \right). \quad (246)$$

It can be shown that if

$$\frac{1}{2} \left| \frac{R}{\omega L} - \frac{G}{\omega C} \right| \ll 1, \quad (247)$$

the impedance of the dissipative network is still given, to a good approximation, by Eq. (239) and, therefore, by the Taylor series of Eq. (243). The same is true for the admittance or any other analytic function of the complex variable p . It should be noted, however, that power ratios and magnitudes of functions of p are not, in general, analytic functions of p .

9-23. Effect of Dissipation on Pass-band Characteristics.—Some of the most important applications of these formulas to the determination of the effects of incidental dissipation on the behavior of filters will now be discussed. First will be considered the case of filters designed by means of the image-parameter method. The propagation function $\gamma = \alpha + j\beta$ is imaginary in the pass band and is an analytic function of p . Equation (243) may be used directly to study the effect of incidental dissipation in the pass band by substituting $\beta(\omega)$ for $X(\omega)$ and, of course, $\gamma_s(j\omega)$ for $Z_s(j\omega)$. Then

$$\gamma_s(j\omega) = \gamma(\delta + j\omega) = j\beta(\omega) + \frac{d\beta(\omega)}{d\omega} \delta + \dots \quad (248)$$

In general, it is unnecessary to take into account the third term of the series. To a good approximation, then, the effect of incidental dissipation is to add an attenuation

$$\alpha_s = \frac{d\beta(\omega)}{d\omega} \delta \quad (249)$$

to the phase function $j\beta(\omega)$ of the nondissipative filter. It is interesting to note that α_s is proportional to the slope of the phase function. It follows that uniform attenuation in the pass band is obtained only when the phase function is linear.

The average attenuation in the pass band can be estimated from the total phase shift $\Delta\beta$ over the pass band and the corresponding bandwidth w . The average slope of the phase function is

$$\left[\frac{d\beta(\omega)}{d\omega} \right]_{\text{av}} = \frac{\Delta\beta}{w} \quad (250)$$

and the average attenuation is

$$(\alpha_s)_{\text{avg}} = \delta \frac{\Delta\beta}{w}. \quad (251)$$

Equation (74) shows that β increases by $\pi/2$ between a zero and a pole (or vice versa) of $\sqrt{Z_{sc}/Z_{oc}}$. On the other hand, the number of zeros and the number of poles must be equal to the number of roots of the equation $\sqrt{Z_{sc}/Z_{oc}} = 1$, that is, to the number of frequencies (real or complex) at which the attenuation becomes infinite. In the particular case of filters consisting of a cascade of n constant- k or m -derived sections, the total phase shift over the pass band is $2n\pi$, provided the pass band of a low-pass filter is taken equal to twice the cutoff frequency. Then, by Eq. (251)

$$(\alpha_s)_{\text{avg}} = \delta \frac{2\pi n}{w}. \quad (252)$$

In the case of bandpass filters consisting entirely of resonant LC -combinations tuned at the center frequency ω_0 , the quantity δ can be expressed in terms of the Q_0 of the resonant combinations as follows:

$$\delta = \frac{1}{2} \left(\frac{R}{L} + \frac{G}{C} \right) = \frac{1}{2} \omega_0 \left(\frac{R}{\omega_0 L} + \frac{G}{\omega_0 C} \right) = \frac{1}{2} \frac{\omega_0}{Q_0}. \quad (253)$$

Substitution for δ in Eq. (252) yields

$$(\alpha_s)_{\text{avg}} = \frac{n\pi \omega_0}{Q_0 w} \text{ nepers} = 8.686 \frac{n\pi \omega_0}{Q_0 w} \text{ db}. \quad (254)$$

In other words, the average attenuation is inversely proportional to Q_0 , and is directly proportional to the number n of sections and to the ratio of the mean frequency to the bandwidth.

9-24. Effect of Dissipation on Rejection-band Characteristics.—The effect of incidental dissipation on the propagation function γ in the attenuation band will now be considered. Since, in most cases, γ has poles at real frequencies (imaginary values of p), it is convenient to study the function $g = \sqrt{Z_{sc}/Z_{oc}}$ which is supposed to approximate unity for real frequencies in the attenuation band. This function may become infinite at a cutoff frequency, but this difficulty can be surmounted by considering instead the function $\sqrt{Z_{oc}/Z_{sc}}$ which has a zero where g has a pole.

If $g(p + \delta)$ is substituted for $Z(p + \delta)$ in Eq. (241), the expression for $\sqrt{Z_{sc}/Z_{oc}}$ becomes, in the presence of dissipation,

$$g_s(p) = g(p + \delta) = g(p) + \frac{dg(p)}{dp} \delta + \frac{1}{2} \frac{d^2g(p)}{dp^2} \delta^2 + \dots \quad (255)$$

Let

$$\left. \begin{aligned} g_s(j\omega) &= a + jb \\ g_s(j\omega) &= a_s + jb_s \end{aligned} \right\} \quad (256)$$

Since $g(p)$ is real for real frequencies in the attenuation band, the following expression may be written:

$$g_s(j\omega) = a_s + jb_s = g(\delta + j\omega) \\ = a(\omega) - j \frac{da(\omega)}{d\omega} \delta + \frac{1}{2} \frac{d^2a(\omega)}{d\omega^2} \delta^2 + \dots \quad (257)$$

At this juncture it is desirable to express the propagation function in the presence of dissipation in the form of Eq. (74), namely,

$$\gamma_s = \alpha_s + j\beta_s \approx \frac{1}{2} \ln \frac{(1 + a_s) + jb_s}{(1 - a_s) - jb_s} \quad (258)$$

Equating real parts of the preceding equation gives, for the attenuation α_s ,

$$\alpha_s \approx \frac{1}{4} \ln \frac{1 + a_s^2 + b_s^2 + 2a_s}{1 + a_s^2 + b_s^2 - 2a_s} - \frac{1}{4} \ln \frac{1 + \frac{2a_s}{1 + a_s^2 + b_s^2}}{1 - \frac{2a_s}{1 + a_s^2 + b_s^2}} \quad (259)$$

When no dissipation is present, the attenuation is

$$\alpha = \frac{1}{4} \ln \frac{1 + a^2}{1 - \frac{2a}{1 + a^2}} \quad (260)$$

If the following substitutions are made,

$$k = \frac{2a}{1 + a^2}, \quad k_s = \frac{2a_s}{1 + a_s^2 + b_s^2} \quad (261)$$

Eqs. (259) and (260) may be written in the same simple forms

$$\alpha_s = \frac{1}{4} \ln \frac{1 + k_s}{1 - k_s} \quad (262)$$

$$\alpha = \frac{1}{4} \ln \frac{1 + k}{1 - k} \quad (263)$$

When the dissipation is small, the following approximation can be used:

$$k_s = \frac{2a}{1 + a^2} \left\{ 1 + \left[\frac{1 - a^2}{2a(1 + a^2)} \frac{da^2}{d\omega^2} - \frac{1}{1 + a^2} \left(\frac{da}{d\omega} \right)^2 \right] \delta^2 \right\} \quad (264)$$

Since k_s is always smaller than unity for $\delta \neq 0$, it follows that the attenuation is never infinite when dissipation is present. When $\delta = 0$, α becomes infinite for $k = a = 1$. The corresponding k_s for the dissipative network is

$$[k_s]_{\infty} = 1 - \frac{1}{2} \left(\frac{da}{d\omega} \right)^2 \delta^2, \quad (265)$$

and the corresponding attenuation in the dissipative case is reduced to the approximate value

$$[\alpha_s]_\infty \approx \frac{1}{2} \ln \frac{2}{\left(\frac{da}{d\omega}\right)_\delta} \quad (266)$$

Further simplification is possible in the special case of an m -derived section of a filter. The function a is given by Eqs. (120) and (132).

$$\sqrt{\frac{Z'_a}{Z'_b}} = a = m \frac{\omega}{\sqrt{\omega^2 - 1}} \quad \text{for } \omega > 1. \quad (267)$$

Since Z'_a and Z'_b are the short-circuit and open-circuit impedances for half the network, it will be necessary to multiply the resulting attenuation by two in order to obtain the α_s for the whole network. It is found for the rate of change of a

$$\frac{da}{d\omega} = \frac{m}{(\omega^2 - 1)^{3/2}} \quad (268)$$

The peak of attenuation occurs for $a = 1$, that is, when

$$m = \frac{\sqrt{\omega^2 - 1}}{\omega} \quad (269)$$

At a frequency of infinite attenuation ω_∞ , Eq. (268) becomes

$$\left[\frac{da}{d\omega}\right]_\infty = \frac{1}{\omega_\infty(\omega_\infty^2 - 1)} \quad (270)$$

The attenuation for the whole m -derived section is twice the value given by Eq. (266), or

$$[\alpha_s]_\infty = \ln \frac{2\omega_\infty(\omega_\infty^2 - 1)}{\delta} \quad (271)$$

This equation shows that the maximum attenuation approaches zero when ω_∞ approaches the cutoff frequency, that is, unity. In other words, if the peak value of the attenuation must be larger than a given α_0 , ω_∞ must be larger than the value given by Eq. (271) for $[\alpha_s]_\infty = \alpha_0$.

The effect of incidental dissipation on loss arising from mismatched terminations is secondary in importance to the effect on the propagation function discussed above. It can be computed, if necessary, by following a procedure very similar to the one used in connection with propagation function. It must be pointed out, however, that, in general, there is no need of computing accurately the total effect of incidental dissipation since the image-parameter method of design leads to a loss function that is only roughly equal to the attenuation function. In other words, the

loss function is already so different from the design data that it would be a waste of time to compute accurately second-order corrections.

9-25. Correction for Uniform Dissipation.—The situation is quite different in the case of filters designed to have a specified insertion loss. Since in this case the loss of the ideal nondissipative filter is exactly equal to the specified function, it is desirable to compute more accurately the effect of incidental dissipation. Moreover, in this case it is worth while to make allowance in the original design for the effect of incidental dissipation, so that the dissipative filter will have a satisfactory loss function.

The general procedure discussed in the preceding pages may be applied to the voltage insertion ratio which is an analytic function of the complex variable p . It should be noted that the power-loss ratio P_0/P_L is the square of the magnitude of the voltage insertion ratio for $p = j\omega$. It follows from Eqs. (158) and (163) that the voltage insertion ratio ρ is given by

$$\rho(p) = \begin{cases} \frac{u_2 + v_2}{Q(-p^2)} & \text{for } Q(\omega) \text{ even,} \\ \frac{u_2 + v_2}{jQ(-jp)} & \text{for } Q(\omega) \text{ odd.} \end{cases} \quad (272)$$

The power insertion ratio of the dissipative filter is then

$$\left(\frac{P_0}{P_L}\right)_\delta = |\rho_\delta(p)|_{p=j\omega}^2 = |\rho(p + \delta)|_{p=j\omega}^2. \quad (273)$$

Since the computation involved is straightforward, no further discussion is required.

Darlington⁴ has developed a method for making allowance in the original design for the effect of incidental dissipation. This method is based on the following reasoning. It has been shown that the voltage insertion ratio $\rho_\delta(p)$ of a dissipative filter can be obtained by substituting $p + \delta$ for p in the expression for the insertion ratio $\rho(p)$ of the corresponding nondissipative filter. Consider now a nondissipative filter whose voltage insertion ratio is

$$\rho'(p) = \rho(p - \delta). \quad (274)$$

The ratio for the corresponding dissipative network is then

$$\rho'_\delta(p') = \rho(p + \delta - \delta) = \rho(p). \quad (275)$$

It follows that in order to obtain a filter whose insertion ratio is $\rho'_\delta(p) = \rho(p)$ it is sufficient to design a nondissipative filter with a pre-distorted ratio $\rho'(p) = \rho(p - \delta)$.

The new function $\rho(p - \delta)$ must satisfy the condition of physical realizability in order to be the voltage insertion ratio of a nondissipative

filter. Consequently, according to Sec. 9-13 and to Eq. (272), the zeros of $\rho(p - \delta)$ must have negative real parts. Moreover, the magnitude of $\rho(p - \delta)$ must not be smaller than unity at real frequencies, that is, for imaginary values of p . It follows that, assuming that $\rho(p)$ is physically realizable, δ must be smaller than the magnitude of the real part of any zero of $\rho(p)$. Moreover, $\rho(p - \delta)$ must be multiplied by a real constant equal to the reciprocal of the minimum value of $\rho'(j\omega) = \rho(j\omega - \delta)$ in order to make $\rho'(j\omega) \geq 1$. A final requirement on $\rho'(p)$ is that the polynomial $Q'(-jp) = Q[-j(p - \delta)]$ be either even or odd. In general, since this condition is not satisfied automatically, it is necessary to multiply both the numerator and the denominator of $\rho(p - \delta)$ by root factors of the type $(p + p_\nu)$, where p_ν is any zero of $Q[-j(p - \delta)]$ which does not come in a pair $p_\nu, -p_\nu$. These root factors have the effect of increasing considerably the number of elements of the network. Further analysis reveals, however, that a satisfactory solution can be obtained by using as a predistorted insertion ratio the function

$$\rho''(p) = \begin{cases} \frac{u_2(p - \delta) + v_2(p - \delta)}{Q(-p^2)} & \text{for } Q(-jp) \text{ even,} \\ \frac{u_2(p - \delta) + v_2(p - \delta)}{-jQ(-jp)} & \text{for } Q(-jp) \text{ odd.} \end{cases} \quad (276)$$

In other words, $(p - \delta)$ is substituted for p only in the numerator of $\rho(p)$. The voltage ratio for the dissipative network will then be

$$\rho'_\delta(p) = \begin{cases} \frac{u_2 + v_2}{Q[-(p + \delta)^2]} & \text{for } Q(-jp) \text{ even,} \\ \frac{u_2 + v_2}{Q[-j(p + \delta)]} & \text{for } Q(-jp) \text{ odd.} \end{cases} \quad (277)$$

This function is a good approximation of $\rho(p)$ except in the vicinity of the internal poles of $\rho(p)$, that is, of the zeros of $Q(-jp)$. The peaks of infinite loss of $\rho(p)$ are thus rounded off in the final dissipative network. In the particularly important case of $Q(\omega) = 1$, that is, when the loss in the attenuation band is a monotonic function, this difficulty does not arise.

Once the predistorted ratio $\rho'(p)$ has been determined, the polynomial $P'(\omega^2)$ is computed as follows:

$$P'(\omega^2) = |u'_2(j\omega) + v'_2(j\omega)|^2 = [Q'(\omega)]^2. \quad (278)$$

If the ratio $\rho''(p)$ is used, the polynomial $P''(\omega^2)$ is

$$P''(\omega^2) = |u_2(j\omega - \delta) + v_2(j\omega - \delta)|^2 - Q^2(\omega). \quad (279)$$

The filter is then designed following the procedure developed above for the nondissipative case.

The same predistortion procedure can be applied to the reflection coefficient $\Gamma(p)$ instead of to the voltage ratio $\rho(p)$. In this case $\Gamma'(p)$ becomes

$$\Gamma'(p) = \Gamma(p - \delta) = \frac{u_1(p - \delta) + v_1(p - \delta)}{u_2(p - \delta) + v_2(p - \delta)}. \quad (280)$$

The conditions of physical realizability lead to the requirement that δ must be smaller than the magnitude of the real part of any internal pole of $\Gamma(p)$. Furthermore, $\Gamma(p - \delta)$ must be multiplied by a real constant to meet the requirement

$$|\Gamma(j\omega - \delta)| \leq 1. \quad (281)$$

The polynomial

$$|Q'(\omega)|^2 = |u_2'(j\omega) + v_2'(j\omega)|^2 - |u_1'(j\omega) + v_1'(j\omega)|^2 \quad (282)$$

can be made a perfect square by multiplying both the numerator and the denominator of $\Gamma'(p)$ by the proper root factors, as in the previous case. The predistorted network is then designed following the original procedure for nondissipative networks.

It should be noted that it is not possible to predistort $\Gamma(p)$ and $\rho(p)$ independently. It follows that the predistortion procedure should be applied to $\Gamma(p)$ when strict tolerances are placed on the reflection coefficient, and to $\rho(p)$ when strict tolerances are placed on the insertion ratio.

EFFECT OF MISMATCHED TERMINATIONS ON FILTER CHARACTERISTICS

9-26. Superposition of Mismatches.—Before concluding the general discussion on the methods of filter design, it is worth while to consider the behavior of a filter when connected to the other components of a system. This question is very important because, although the filter is designed as a separate unit, it is the over-all behavior of the system including the filter that really matters. More specifically, the distortion of the loss characteristics of the filter arising from other components of the system must be tolerable, and conversely the design specifications for the filter must be consistent with the specifications for the other components of the system.

This last point is particularly important in view of the difficulties encountered in designing filters with very strict tolerances. For instance, the input voltage standing-wave ratio of a microwave system may be as large as the product of all the ratios for the individual components. Care must be taken, then, to divide the over-all VSWR among the components in proportion to the difficulty of design. It is often advisable to let the filter have a VSWR as high as the maximum VSWR of all the other components together.

Somewhat less important, but far from negligible, is the effect of

the other components of a system on the loss in the attenuation band of a filter. It will be shown later that the difference between the decibel loss of a filter and the decibel loss of the whole system may be as large as the sum of the VSWR's of the two terminations of the filter expressed in decibels. This fact points out that, if the loss of a system must be approximately equal over a certain band of frequencies to the loss of a filter that is part of the system, the other components must be reasonably well matched over the same band.

The characteristics of a filter have been computed on the assumption that both terminations are purely resistive and constant at all frequencies. In practice, this assumption is very seldom justified, particularly in the case of microwave filters. In this case both sides of the filter are connected to transmission lines or guides which would provide the proper resistive terminations for the filter if they were terminated in their characteristic impedances at the other ends. In practice, small reflections in the input and output lines are always present. Let r_s and r_L be the voltage standing-wave ratios of the input and output lines, when they are not connected to the filter.

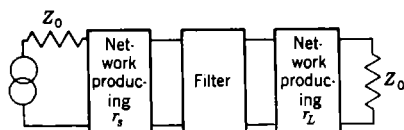


FIG. 9-49.—Filter with mismatched terminations.

The mismatches in the two lines may be considered as arising from mismatched reactive networks inserted in perfectly terminated lines. The equivalent network for the filter and its terminations is shown in Fig. 9-49. It is assumed in the following discussion that the filter is nondissipative. Let r_o be the VSWR produced by the filter in the input line when the output line is properly terminated, that is, when $r_L = 1$. When $r_L = 1$, the value of the VSWR in the input line, r'_o , depends on the phase of the reflection in the output line. It was shown in Sec. 9-4 that the maximum and minimum values of the r'_o are given by

$$[r'_o]_{\max} = r_o r_L, \quad (283)$$

$$[r'_o]_{\min} = \begin{cases} \frac{r_L}{r_o} & \text{for } r_L > r_o, \\ \frac{r_o}{r_L} & \text{for } r_L < r_o. \end{cases} \quad (284)$$

Equation (283) gives the maximum VSWR that may be present in the input line of a filter when the filter is not properly terminated at the output terminals. If other nondissipative components are inserted in the input line between the filter and the generator, the maximum VSWR in the output line of the generator will be

$$[r'_s]_{\max} = r_s [r'_o]_{\max} = r_s r_o r_L. \quad (285)$$

where r_s is the VSWR produced in the output line of the generator by the components preceding the filter when $r'_o = 1$, and is equal to the VSWR measured from the filter toward the generator when a matched termination is substituted for the generator. The minimum value of r'_s when $r_o > r_s r_L$, is

$$[r'_s]_{\min} = \frac{[r'_o]_{\min}}{r_s} = \frac{r_o}{r_s r_L}. \quad (286)$$

9-27. Accumulative Effect of Mismatches.—In general, r_s results from the reflections produced by a number n of components. Let r_{sk} be the VSWR on the input line of one of these components when its output line is properly terminated. Repeated application of Eq. (283) leads to the following expression for the maximum possible value of r_s :

$$[r_s]_{\max} = \prod_{k=1}^{k=n_s} r_{sk}. \quad (287)$$

Similarly the maximum possible value of r_L is

$$[r_L]_{\max} = \prod_{k=1}^{k=n_L} r_{Lk}, \quad (288)$$

where r_{Lk} is the VSWR of the k th of the n_L component on the load side of the filter. The maximum and minimum values of r'_s are obtained by substituting Eqs. (287) and (288) for r_s and r_L in Eqs. (285) and (286).

The magnitude of the reflection coefficient corresponding to r'_s is

$$|\Gamma'_s| = \frac{r'_s - 1}{r'_s + 1}. \quad (289)$$

Let P'_0 be the power available from the generator, that is, the power flowing in its output line when the line is properly terminated. Let P'_L be the power delivered to the load of the system. Since all the components are nondissipative, the ratio P'_0/P'_L , that is, the power-loss ratio for the whole system is given by

$$\frac{P'_0}{P'_L} = \frac{1}{1 - |\Gamma'_s|^2}. \quad (290)$$

The maximum value of this power ratio is found to be

$$\left(\frac{P'_0}{P'_L}\right)_{\max} = \frac{(r_s r_L r_o + 1)^2}{4r_s r_L r_o}. \quad (291)$$

Since

$$\frac{P_0}{P_L} = \frac{(r_o + 1)^2}{4r_o} \quad (292)$$

is the power-loss ratio of the filter alone when properly terminated,

improper terminations may increase the power-loss ratio of the system by the factor

$$\left(\frac{P_L}{P'_L}\right)_{\max} = \frac{(r_s r_L r_o + 1)^2}{r_s r_L (r_o + 1)^2} \quad (293)$$

If $r_o \gg 1$, that is, in the attenuation band of the filter, this factor becomes approximately

$$\left(\frac{P_L}{P'_L}\right)_{\max} \approx r_s r_L \quad (294)$$

Consider now the minimum value of P'_0/P'_L , when $r_o > r_L r_s$. This assumption limits the validity of the results to the attenuation band of the filter. However, it is only in the attenuation band that the minimum value of the loss is of any practical importance. Then

$$\left(\frac{P'_0}{P'_L}\right)_{\min} = \frac{(r_o + r_s r_L)^2}{4 r_o r_s r_L} \quad (295)$$

It follows that the improper terminations may decrease the power-loss ratio of the system by the factor

$$\left(\frac{P_L}{P'_L}\right)_{\min} = \frac{(r_o + r_s r_L)^2}{r_s r_L (r_o + 1)^2} \quad (296)$$

When $r_o \gg 1$, $r_o \gg r_s r_L$, that is, for large values of the loss, this factor reduces to

$$\left(\frac{P_L}{P'_L}\right)_{\min} = \frac{1}{r_s r_L} \quad (297)$$

This reduction of loss may be far from negligible. For instance, if $r_s = r_L = 2$ in the attenuation band of the filter, the loss of the system is 6 db lower than the loss of the filter alone when properly terminated. It follows that it is necessary to limit the VSWR of any component of a system that includes a filter not only over the pass band of the filter, but also over the portion of the attenuation band in which the minimum total loss of the system is specified.

BIBLIOGRAPHY

1. Bode, H. W., *Network Analysis and Feedback Amplifier Design*, Van Nostrand, New York, 1945.
2. Brune, O., "Synthesis of a Finite Two-Terminal Network Whose Driving-point Impedance is a Prescribed Function of Frequency," *J. Math. Phys.*, **10**, 3, 191 (1931).
3. Brune, O., "Note on Bartlett's Bisection Theorem for 4-Terminal Electrical Networks," *Phil. Mag.*, Ser. 7, **14**, 806 (1932).
4. Darlington, S., "Synthesis of Reactance 4-Poles," *J. Math. Phys.*, **18**, 257-353 (September 1939). Also, Bell Telephone System Monograph No. B-1186.
5. Guillemin, E. A., *Communication Networks*, **2**, Wiley, New York, 1935.
6. Gewertz, C. M., *Network Synthesis*, Williams and Wilkins, Baltimore, pp. 145, 224.
7. Hancock, H., *Theory of Elliptic Functions*, **1**, Wiley, New York, 1910.

CHAPTER 10

THE DESIGN OF MICROWAVE FILTERS

BY A. W. LAWSON AND R. M. FANO

A direct method of designing microwave filters has not yet been developed. In other words, no design procedure is available which leads directly to a structure physically realizable by means of microwave elements. Most microwave filters hitherto designed have been derived from lumped-element structures by approximating the behavior of inductances and capacitances by means of microwave elements, such as sections of lines, cavities, irises, etc. As will be seen, the lack of a direct synthesis procedure sets limitations on the design.

In addition to theoretical and practical limitations on filter design, the actual system applications often impose widely varying geometrical and physical requirements. These requirements are largely responsible for the ultimate appearance of any filter. Thus, two filters having exactly the same attenuation characteristics and circuit specifications may have radically different forms. For instance, one filter may be for a system using coaxial transmission line and another for a system using waveguide; alternatively, a cavity filter of reasonable dimensions at 10,000 Mc/sec may be prohibitively large at 100 Mc/sec for airborne systems; or again, a compact, rugged design suitable for low power levels may be completely inadequate in a system using higher power. For such reasons it appears impractical to discuss here all designs existing at the time of preparation of this manuscript. Rather, it appears desirable to describe typical examples as illustrations of the general methods of deriving microwave filters from lumped-element structures. These examples do not necessarily represent the most efficient designs or the ultimate, either practically or theoretically. In fact, a large number of the filters described below were designed, manufactured, and used before the theory involved was generally understood. In particular, some of the more elaborate methods of designing lumped-element filters will not be used in connection with any of these practical examples. This fact does not mean that such methods are not useful, but that, because of time limitations, the designer was forced to employ only techniques already available to him. Fortunately, however, these practical examples serve very well as illustrations of the methods of designing microwave filters.

In this chapter it will be shown how the simple ladder structures basic

to all methods of design discussed in the previous chapter are readily transformed into microwave structures. The relative values of the lumped elements, which depend on the method of design employed, are of no consequence in the transformation process. The discussion of practical microwave filters resulting from such transformations will be divided into four parts on the basis of the techniques used in approximating the behavior of lumped elements at microwave frequencies. The first part will deal with filters employing sections of lines alone or in combination with lumped inductances and capacitances. For practical reasons, filters of this type cannot be used when narrow pass bands (less than approximately 10 per cent) are required. The second part will deal with filters consisting of a cascade connection of direct-coupled cavities. The use of these filters is limited by the fact that the couplings between cavities become rather critical when the pass band is less than approximately 1 per cent. A design procedure suitable for narrow-band filters is presented in the third part. These filters take the form of chains of cavity resonators separated by quarter-wavelength sections of line. Filters with broader pass bands may be obtained by substituting resonant irises for the cavities. The fourth part will be devoted to miscellaneous types of filters some of which should be considered merely as suggestions for future developments.

FILTERS EMPLOYING TRANSMISSION LINES

10-1. The Frequency Behavior of Lines.—Before considering any practical filter structure, it is desirable to discuss in some detail the frequency behavior of a section of transmission line in order to determine under what conditions and to what extent it can be made to approximate the behavior of inductances and capacitances.

Let Z_0 be the characteristic impedance of a lossless line and l its length. If the section is short-circuited at the far end, the input impedance is

$$Z = jX = jZ_0 \tan \omega \frac{l}{c} \quad (1)$$

where ω is the angular frequency and c the velocity of light in the dielectric. The reactance function represented by this equation is plotted in Fig. 10-1. The reactance has an infinite number of poles and zeros at frequencies at which the length of the line is, respectively, an odd or even number of quarter wavelengths. The plot of the admittance of the line (Fig. 10-1b) is an identical curve displaced to the left by $\frac{\pi c}{2l}$. Thus,

$$Y = \frac{1}{Z} = jB = j \frac{1}{Z_0} \cot \omega \frac{l}{c} = -jY_0 \cot \omega \frac{l}{c} \quad (2)$$

Suppose now that the section of line is open-circuited at the far end. The input impedance becomes

$$Z = jX = -jZ_0 \cot \omega \frac{l}{c} \quad (3)$$

and the input admittance becomes

$$Y = jB = j \frac{1}{Z_0} \tan \omega \frac{l}{c} = jY_0 \tan \omega \frac{l}{c} \quad (4)$$

It will be noticed that Eq. (3) is identical in form with Eq. (2) whereas Eq. (4) is identical in form with Eq. (1). Therefore, Fig. 10-1a may be used also as a plot of Eq. (4) and Fig. 10-1b as a plot of Eq. (3).

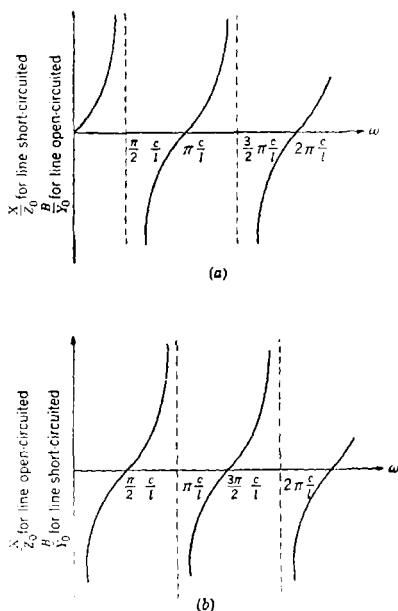


FIG. 10-1.—Frequency behavior of open-circuited and short-circuited lines.

It is interesting to compare these curves with the reactances and susceptances of an inductance, a capacitance, a series-tuned circuit, and a parallel-tuned circuit. The reactance of a simple inductance X_L and the susceptance of a condenser B_C are identical in form;

$$\begin{aligned} X_L &= \omega L \\ B_C &= \omega C. \end{aligned}$$

The plot of these functions is, evidently, a straight line of slope equal to L and C , respectively. The reactance of a series-tuned circuit and the susceptance of a parallel-tuned circuit are also identical in form.

$$X_s = \sqrt{\frac{L}{C}} \left(\frac{\omega}{\omega_0} - \frac{\omega_0}{\omega} \right) = L\omega_0 \left(\frac{\omega}{\omega_0} - \frac{\omega_0}{\omega} \right) \quad (5)$$

$$B_p = \sqrt{\frac{C}{L}} \left(\frac{\omega}{\omega_0} - \frac{\omega_0}{\omega} \right) = C\omega_0 \left(\frac{\omega}{\omega_0} - \frac{\omega_0}{\omega} \right) \quad (6)$$

where $\omega_0 = 1/\sqrt{LC}$ is the resonance frequency. These functions are plotted in Fig. 10·2.

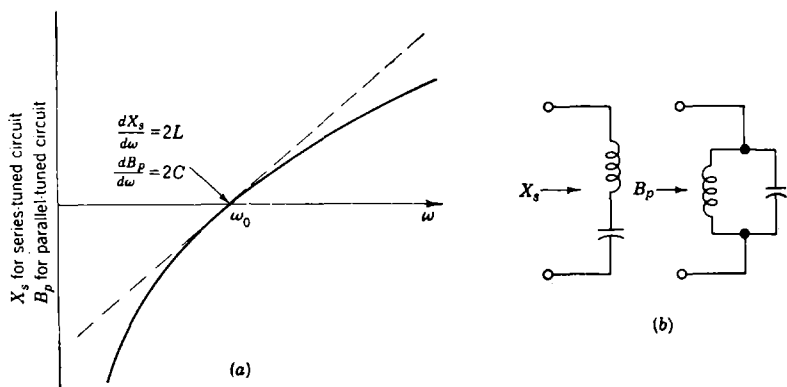


FIG. 10-2.—Frequency behavior of resonant circuits.

It will be noticed that the curve of Fig. 10·1a may be used to approximate a straight line in the vicinity of the origin. The slope of the curve at the origin is

$$\left(\frac{dX}{d\omega} \right)_{\omega=0} = Z_0 \frac{l}{c} \quad (7)$$

$$\left(\frac{dB}{d\omega} \right)_{\omega=0} = Y_0 \frac{l}{c} \quad (8)$$

Therefore, the frequency behavior of an inductance can be approximated by a section of short-circuited transmission line, provided the length of the section is much smaller than $(\pi/2)(c/\omega)$ at any frequency of interest. The slope given by Eq. (7) must be made equal to the inductance L , thus,

$$L = Z_0 \frac{l}{c} \quad (9)$$

This is done by adjusting Z_0 once the quantity l/c has been fixed to satisfy the required length of line.

A capacitance C can be simulated in a similar manner by means of an open-circuited section of transmission line. In this case, the slope of the susceptance function at the origin, as shown in Eq. (8), is made equal to C :

$$C = Y_0 \frac{l}{c} \quad (10)$$

The quantities Y_0 and l/c are adjusted to satisfy this equation while the length l is kept much smaller than the minimum value of $(\pi/2)(c/\omega)$.

Consider now the susceptance of a short-circuited line and the reactance of an open line (Fig. 10-1b) in the vicinity of a zero, that is, when the length of the line is close to an odd number of quarter wavelengths. In any one of these regions the function can be made to approximate the curve of Fig. 10-2. It follows that a short-circuited line can simulate a parallel-tuned circuit in a relatively small frequency band centered at the resonance frequency. Under the same conditions, an open line can simulate a series-tuned circuit. The line length is given in both cases by the expression

$$l = \frac{c}{\omega_0} \left(\frac{\pi}{2} + n\pi \right), \quad (11)$$

where n is any positive integer. The line admittance (or impedance) must be such that the slopes of the two curves are equal at the common zero. The slope of the susceptance function of a short-circuited line at a zero is

$$\left(\frac{dB}{d\omega} \right)_{\omega=\omega_0} = Y_0 \frac{l}{c} = \frac{Y_0}{\omega_0} \left(\frac{\pi}{2} + n\pi \right). \quad (12)$$

Similarly the slope of the reactance function of an open line at a zero is

$$\left(\frac{dX}{d\omega} \right)_{\omega=\omega_0} = Z_0 \frac{l}{c} = \frac{Z_0}{\omega_0} \left(\frac{\pi}{2} + n\pi \right). \quad (13)$$

The corresponding slopes for a parallel-tuned circuit and a series-tuned circuit are

$$\left(\frac{dB_p}{d\omega} \right)_{\omega=\omega_0} = 2C, \quad (14)$$

$$\left(\frac{dX_s}{d\omega} \right)_{\omega=\omega_0} = 2L. \quad (15)$$

It follows that, in the case of the parallel-tuned circuit, equivalence is obtained if

$$2C = \frac{Y_0}{\omega_0} \left(\frac{\pi}{2} + n\pi \right), \quad (16)$$

and in the case of the series-tuned circuit, if

$$2L = \frac{Z_0}{\omega_0} \left(\frac{\pi}{2} + n\pi \right). \quad (17)$$

The integer n should be as small as possible since, for a given tolerance, the width of the approximation band, in percentage of ω_0 , is inversely proportional to $2n + 1$. On the other hand, since the slope is directly

proportional to $(2n + 1)$, it may be necessary to make $n > 1$ in order to obtain a sufficiently large slope.

Series- and parallel-tuned circuits can be simulated also by means of a short-circuited line and an open line, respectively, of lengths equal to

$$l = n\pi \frac{c}{\omega_0}. \quad (18)$$

This equivalence results from the fact that the curve of Fig. 10-1a is identical to the curve of Fig. 10-1b, apart from a translation to the left of $\Delta\omega = (\pi/2)(c/l)$. The slope of the reactance function of a short-circuited line at one of its zeros is

$$\left(\frac{dX}{d\omega}\right)_{\omega=n\pi c/l} = Z_0 \frac{l}{c} = Z_0 \frac{n\pi}{\omega_0}. \quad (19)$$

Therefore, in order to approximate the behavior of a series-tuned circuit, the line impedance must satisfy the equation

$$2L = Z_0 \frac{n\pi}{\omega_0}. \quad (20)$$

Similarly, in the case of an open line approximating a parallel-tuned circuit, the line admittance must satisfy the equation

$$2C = Y_0 \frac{n\pi}{\omega_0}. \quad (21)$$

Compare a system in which all the reactive elements are equal lengths of line of arbitrary characteristic impedances with the network formed by the corresponding lumped elements. The impedance of each section of line can be obtained from the impedance of the corresponding lumped element (or elements) by means of a simple change of variable. In the case of simple inductances and capacitances, the change of variable is

$$\frac{c}{l} \tan \omega' \frac{l}{c} = \omega. \quad (22)$$

In the case of tuned circuits, the substitution is

$$-\frac{c}{l} \cot \omega' \frac{l}{c} = \frac{\omega_0}{2} \left(\frac{\omega}{\omega_0} - \frac{\omega_0}{\omega} \right) \quad (23)$$

if $\omega_0 = (\pi/2 + n\pi)(l/c)$, and

$$\frac{c}{l} \tan \omega' \frac{l}{c} = \frac{\omega_0}{2} \left(\frac{\omega}{\omega_0} - \frac{\omega_0}{\omega} \right) \quad (24)$$

if $\omega_0 = n\pi \frac{c}{l}$. Since, by assumption, the change of variable is the same

for all the elements of the system, any function describing the frequency behavior of the distributed-constant system can be obtained directly from the corresponding function for the lumped-element network by means of the same change of variable.

It is interesting to consider in more detail the physical significance of the change of variable. The substitution of Eq. (22), for instance, transforms the interval $-\infty$ to $+\infty$ in the ω domain into the interval $-(\pi/2)(c/l)$ to $+(\pi/2)(c/l)$ in the ω' domain. However, since ω' is a multivalued function of ω , the same interval in the ω domain is repeated an infinite number of times in the ω' domain in any interval $[\pi/2 + n\pi] - (c/l)$ to $[\pi/2 + (n + 1)\pi](c/l)$. To make this point clearer, consider the

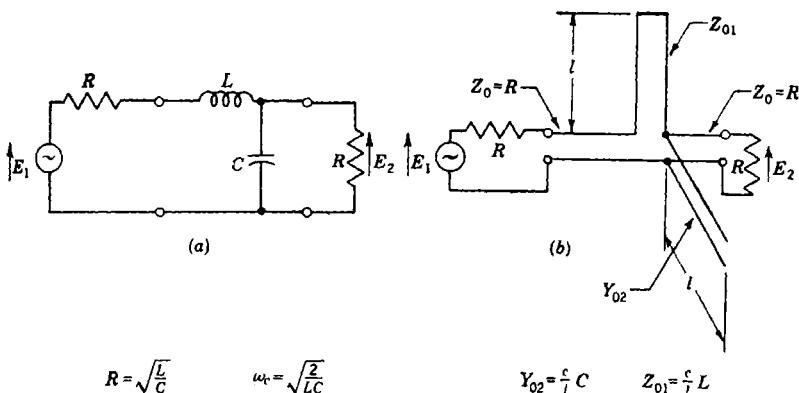


FIG. 10-3.—Transformation of a low-pass filter into its microwave equivalent.

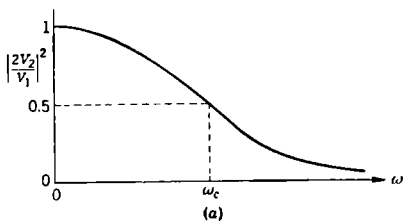
simple low-pass filter of Fig. 10-3a and the corresponding distributed-constant system of Fig. 10-3b. The power-loss ratio for the filter of Fig. 10-3a can be shown to be

$$\left| \frac{V_1}{2V_2} \right|^2 = 1 + \left(\frac{\omega}{\omega_c} \right)^4, \tag{25}$$

where ω_c is the half-power frequency. The loss ratio for the filter of Fig. 10-3b becomes then

$$\left| \frac{V_1}{2V_2} \right|^2 = 1 + \left[\frac{\tan \omega' \frac{l}{c}}{\tan \omega'_c \frac{l}{c}} \right]^4. \tag{26}$$

The reciprocals of these power ratios are plotted in Figs. 10-4a and 10-4b, respectively. Figure 10-4b shows that the structure of Fig. 10-3b is at the same time a low-pass and a bandpass filter. When it is considered as



a low-pass filter, its half-power frequency is

$$\omega'_c = \frac{c}{l} \tan^{-1} \omega_c \frac{l}{c} \quad (27)$$

When it is considered as a band-pass filter, its bandwidth is always equal to the expression

$$\omega' = 2\omega'_c = 2 \frac{c}{l} \tan^{-1} \omega_c \frac{l}{c} \quad (28)$$

whereas the mean frequencies are given by

$$\omega'_0 = n\pi \frac{c}{l} \quad (29)$$

The change of variable defined by Eq. (23) transforms the interval 0 to ∞ in the ω domain into the interval 0 to $\pi(c/l)$ in the ω' domain, or better, into any interval $n\pi(c/l)$ to $(n+1)\pi(c/l)$. Compare, for instance, the bandpass filter shown in Fig. 10-5a, which is derived from the low-pass filter of Fig. 10-3a, with the corresponding distributed-constant system shown in

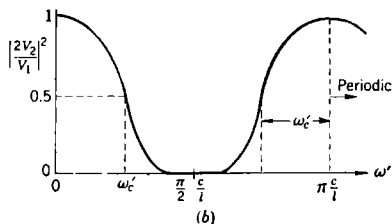


FIG. 10-4.—Power transmission ratios for structures of Figs. 10-3a and 10-3b, respectively.

Fig. 10-5a, which is derived from the low-pass filter of Fig. 10-3a, with the corresponding distributed-constant system shown in

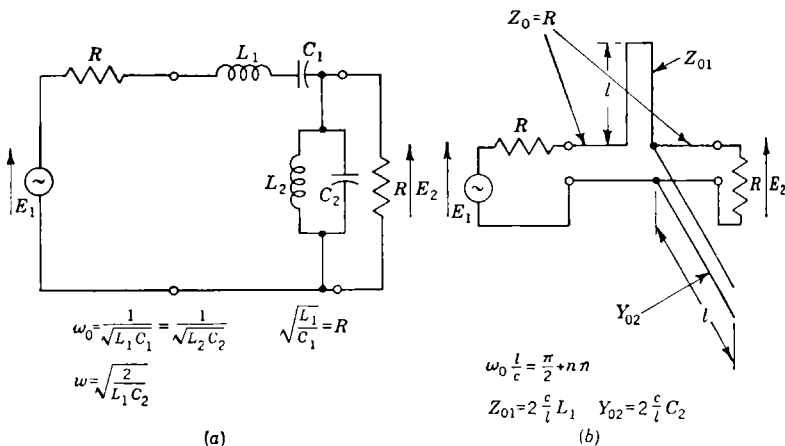


FIG. 10-5.—Transformation of a bandpass filter into its microwave equivalent.

Fig. 10-5b. The power-loss ratio for the lumped-element filter is found to be

$$\left| \frac{V_1}{2V_2} \right|^2 = 1 + \left[\frac{\omega_0}{w} \left(\frac{\omega}{\omega_0} - \frac{\omega_0}{\omega} \right) \right]^4. \quad (30)$$

On the other hand, the ratio for the structure of Fig. 10-5b is

$$\left| \frac{V_1}{2V_2} \right|^2 = 1 + \left[\frac{\cot \omega' \frac{l}{c}}{\cot \frac{w'l}{2c}} \right]^4. \quad (31)$$

The reciprocals of these power ratios are plotted respectively in Figs. 10-6a and 10-6b. It will be noticed that the curve of Fig. 10-6b is identical

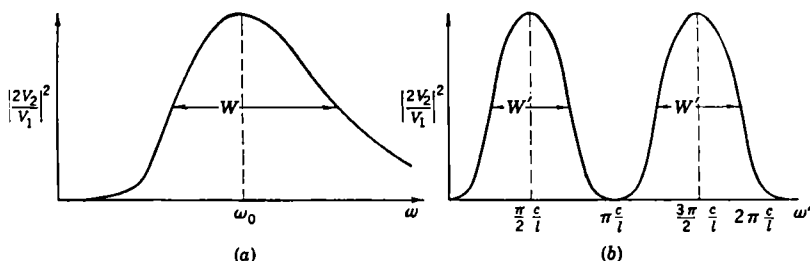


FIG. 10-6.—Power transmission ratios for structures of Figs. 10-5a and 10-5b, respectively.

to the curve of Fig. 10-4b but for a translation of $(\pi/2)(c/l)$. There is an infinite number of pass bands, all of which have a bandwidth equal to

$$w' = 2 \frac{c}{l} \cot^{-1} \frac{w l}{2c}. \quad (32)$$

The mean frequencies are given by the equation

$$\omega'_0 = \left(\frac{\pi}{2} + n\pi \right) \frac{c}{l}. \quad (33)$$

It is interesting to note that each pass band possesses arithmetic symmetry with respect to its mean frequency whereas in the case of Fig. 10-6a the symmetry is geometric.

The change of variable defined by Eq. (24) transforms the interval 0 to ∞ in the ω domain into the interval $\frac{\pi c}{2l}$ to $(\pi/2 + \pi)(c/l)$ in the ω' domain. However, since this interval is repeated an infinite number of times, the complete plot becomes identical to the plot of Fig. 10-4b. This similarity should not be surprising since the low-pass to bandpass transformation used to obtain the filter of Fig. 10-5a from the filter of Fig. 10-3a is mathematically equivalent to a change of variable of the type (see Sec. 9-8)

$$\omega = \frac{\omega'_0}{2} \left(\frac{\omega'}{\omega'_0} - \frac{\omega'_0}{\omega'} \right). \quad (34)$$

This change of variable combined with Eq. (22) leads to the substitution defined by Eq. (24).

Sections of lines may be used also as two-terminal-pair networks. Such elements may operate as integral parts of a filter, or merely as links. Here the correspondence between sections of lines and lumped elements is not so simple as in the previous cases. Two functions are required to describe the element since there are two symmetrical terminal pairs. These two functions may be chosen in several different ways, but the open-circuit and the short-circuit impedances of half the section, Z_{sch} , Z_{och} , are particularly convenient for reasons that will become evident later. Bartlett's bisection theorem already mentioned in Sec. 9-5 shows

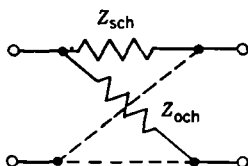


FIG. 10-7.—Symmetrical lattice structure.

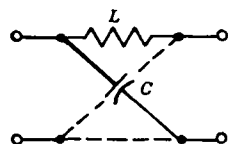


FIG. 10-8.—Low-frequency lattice equivalent of a section of line.

that the lattice structure of Fig. 10-7 is equivalent to the section of line under discussion. Let Z_0 be the characteristic impedance of the line and l its length. The short-circuit impedance of half the network is then

$$Z_{sch} = jZ_0 \tan \omega \frac{l}{2c}. \quad (35)$$

The open-circuit impedance is

$$Z_{och} = jZ_0 \cot \omega \frac{l}{2c}. \quad (36)$$

The Z_{sch} arm of the lattice is evidently a short-circuited line of characteristic impedance equal to Z_0 and length equal to $l/2$. Similarly, the Z_{och} arm is an open-circuited line having the same length and the same characteristic impedance. It follows that when $l/2$ is much smaller than a quarter wavelength, the section of line approximates the behavior of the lattice structure shown in Fig. 10-8. From Eqs. (7) and (8) the values of L and C are

$$L = Z_0 \frac{l}{2c} \quad (37)$$

$$C = Y_0 \frac{l}{2c}. \quad (38)$$

If l is made equal to an odd multiple of half wavelengths, the section of line may be used to simulate the behavior of the lattice structure

shown in Fig. 10-9. Both arms are tuned at a frequency ω_0 at which the line is an odd multiple of half wavelengths,

$$\omega_0 = \frac{1}{\sqrt{L_1 C_1}} = \frac{1}{\sqrt{L_2 C_2}} \quad (39)$$

$$= \left(\frac{\pi}{2} + n\pi \right) \frac{2c}{l}. \quad (40)$$

The values of L_1 and C_2 are given by Eqs. (20) and (21),

$$L_1 = \frac{Z_0}{2\omega_0} \left(\frac{\pi}{2} + n\pi \right) = \frac{Z_0 l}{4c} \quad (41)$$

$$C_2 = \frac{Y_0}{2\omega_0} \left(\frac{\pi}{2} + n\pi \right) = \frac{Y_0 l}{4c}. \quad (42)$$

If l is made approximately equal to an even multiple of half wavelengths, the lattice of Fig. 10-9 is transformed into the lattice shown in Fig. 10-10.

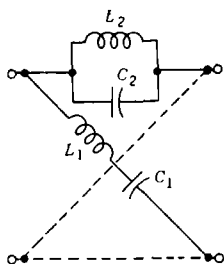


FIG. 10-9.—Lattice equivalent of line with odd number of half wavelengths.

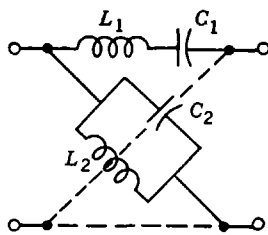


FIG. 10-10.—Lattice equivalent of line with even number of half wavelengths.

Notice that one lattice can be obtained from the other by interchanging the output terminals. In fact, Eqs. (20) and (21) show that

$$L_1 = \frac{Z_0}{2} \frac{n\pi}{\omega_0} = \frac{Z_0 l}{4c} \quad (43)$$

$$C_2 = \frac{Y_0}{2} \frac{n\pi}{\omega_0} = \frac{Y_0 l}{4c}. \quad (44)$$

10-2. Practical Limitations on the Use of Lines.—The technique of using sections of parallel wire or coaxial transmission line to approximate the behavior of lumped elements is relatively old.¹ The older filters, however, were designed to operate at relatively low frequencies. During the war, the range of operation of these filters was extended to frequencies as high as 3×10^9 cps. At higher frequencies, the dimensions of con-

¹ See, for example, the first reference listed in the bibliography at the end of the chapter. Numbered superscripts in the text refer to the corresponding numbered references of the bibliography.

ventional transmission lines become impractically small if the propagation of higher modes is to be prevented. This fact sets a limit to the range of application of filters employing sections of conventional transmission lines. It must be pointed out also that the stray effects due to geometrical discontinuities in a transmission line become rather important when the frequency of operation approaches the cutoff frequency of the TE_{11} -mode. For instance, it cannot be assumed that two lines having the same characteristic impedance but different dimensions can be joined without any reflection taking place. In practice, the stray effects become so important at frequencies of the order of 3×10^9 cps that filters cannot be designed by purely theoretical means. Although empirical adjustments of the elements can compensate to a certain extent for the stray effects, the actual characteristics of the filter are always somewhat different from the theoretical ones.

Another limitation to the field of application of filters using sections of lines is set by bandwidth considerations. Consider a prototype low-pass ladder structure with a cutoff frequency equal to 1 radian/sec and 1-ohm terminations. It turns out that in any structure of this type the inductances measured in henrys and the capacitances measured in farads have values of the order of magnitude of unity. Let this structure be transformed into a bandpass filter with a bandwidth w and a mean frequency ω_0 . Following the method discussed previously (see Sec. 9-8), each inductance becomes a series-tuned circuit whose reactance function at the mean frequency ω_0 has a slope of the order of magnitude of $2/w$. Similarly each capacitance becomes a parallel-tuned circuit whose susceptance function at the mean frequency ω_0 has a slope also of the order of magnitude of $2/w$. For these tuned circuits, let lines of length equal to an odd number $(2n + 1)$ of quarter wavelengths at the mean frequency ω_0 be substituted. The order of magnitude of the characteristic impedance of the open-circuited section of line which is substituted for any series-tuned circuit must be, according to Eq. (13),

$$Z_0 = \frac{4 \omega_0}{\pi w} \frac{1}{(2n + 1)}. \quad (45)$$

Similarly the order of magnitude of the characteristic admittance of the short-circuited section of line corresponding to any parallel-tuned circuit must also be, according to Eq. (12),

$$Y'_0 = \frac{4 \omega_0}{\pi w} \frac{1}{(2n + 1)} = \frac{1}{Z'_0}. \quad (46)$$

It follows that the ratio of the characteristic impedances of the two lines is

$$\frac{Z_0}{Z'_0} = \left(\frac{4 \omega_0}{\pi w} \frac{1}{2n + 1} \right)^2. \quad (47)$$

Note that the terminations of the filter are equal to 1 ohm, or in other words, that Z_0 and Z'_0 are normalized with respect to the terminating impedances.

The difficulties involved in obtaining narrow bands, that is, large ratios of Z_0/Z'_0 , are obvious when it is remembered that the characteristic impedance of a coaxial line is directly proportional to the natural logarithm of the ratio of the diameters of the two conductors and inversely proportional to the square root of the dielectric constant of the medium filling the line. Ratios of Z_0/Z'_0 as large as even 3 or 4 are difficult to obtain in practice without considerably increasing the losses of both lines. It follows that a large value of ω_0/w must be balanced by an almost equal value of $2n + 1$. Lines several wavelengths long are again impractical because of their inconvenient dimensions and their high losses. This bandwidth limitation may be circumvented by using loosely coupled cavity resonators instead of sections of lines. The techniques involved in this method of design will be discussed in Sec. 10-8. In practice, the upper limit for the ratio ω_0/w when sections of lines are used is about 10.

10-3. Filters Employing Lines as Two-terminal Elements.—It is of historical interest to note that, except for the simple resonant cavity,

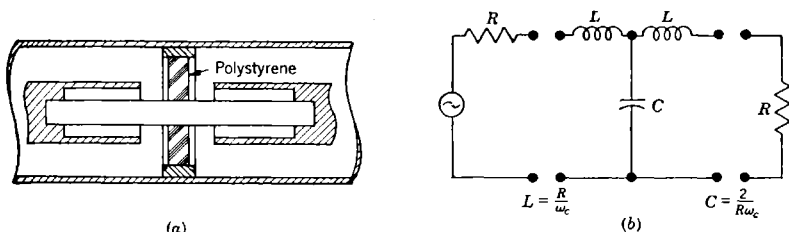


FIG. 10-11.—A low-pass filter with its lumped-element equivalent circuit.

low-pass filters were among the first to be required in the application of microwave techniques to radar. This circumstance arose from the fact that the efficient operation of crystal mixers requires the rejection of the third harmonic of the fundamental frequency to be received. Figure 10-11a illustrates the typical design of such a filter for a coaxial mixer input line. This filter, which consists of two reentrant line sections separated by a concentric condenser, is the coaxial embodiment of a simple constant- k prototype section whose equivalent lumped-constant analogue is represented schematically in Fig. 10-11b. This analogy obtains only at those frequencies for which the reentrant line sections are shorter than a quarter wavelength. At higher frequencies the reactances of the sections of line have poles and zeros that are not present in the lumped-element case and consequently the existence of spurious pass bands must be expected.

Let ω_c be the cutoff frequency of the lumped-element filter. The values of L and C given in Fig. 10-11b are obtained by properly transforming the prototype section of Fig. 9-23c. The characteristic impedance of the reentrant lines is given by Eq. (9),

$$Z_0 = L \frac{c}{l} = \frac{R c}{\omega_c l}. \quad (48)$$

The capacitance C may be assumed to be lumped if the width of the concentric condenser is small compared with l . Under these conditions the attenuation function behaves in the manner shown in

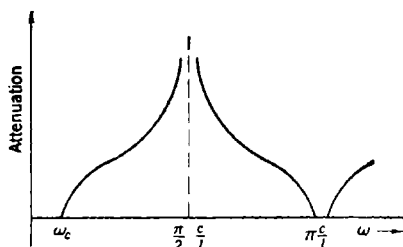


FIG. 10-12.—Attenuation characteristics of low-pass filter of Fig. 10-11a.

Fig. 10-12. The actual cutoff frequency ω'_c is somewhat smaller than ω_c because the reactance of the line is always larger than ωL . A peak of infinite attenuation occurs when the length l is a quarter wavelength. Since a spurious pass band appears when l is a half wavelength, the length should be made as small as possible.

The drawing of Fig. 10-11a is scaled to dimensions suitable for a $\frac{7}{8}$ -in., 46.2-ohm coaxial line. Polystyrene filler is used in the concentric condensers to shorten the filter and to add mechanical rigidity. The measured insertion loss for this filter is shown in Fig. 10-13.

The design formulas given above predict a cutoff frequency of 2860 Mc/sec; the actually observed value corresponding to 3-db insertion loss is 2440 Mc/sec. The discrepancy between the calculated and observed value arises in part from the approximation inherent in treating the sections of line as lumped inductances instead of as transmission lines; the remainder of the discrepancy may be accounted for by the extra fringing capacity neglected in the design formulas.

In practice, it is possible to compensate for such end effects by shaving down the length of the dielectric beads until the characteristic impedance of the filter matches the line.

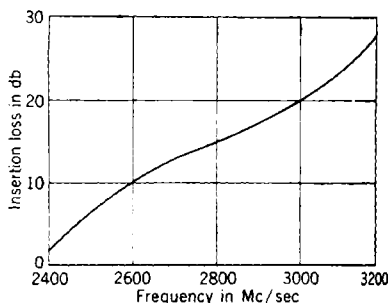


FIG. 10-13.—Rejection-band characteristics of filter of Fig. 10-11a.

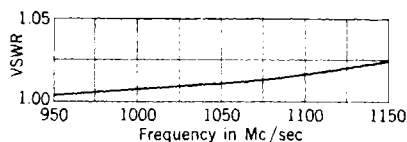


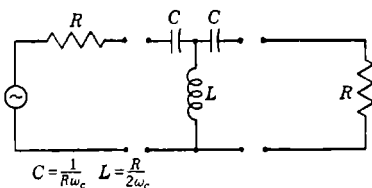
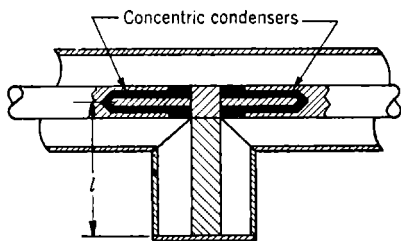
FIG. 10-14.—Bandpass characteristics of filter of Fig. 10-11a.

Under these circumstances, the standing-wave characteristics in the pass band are shown in Fig. 10-14.

A high-pass analogue⁵ of the harmonic filter described above is shown in Fig. 10-15 together with its equivalent lumped circuit. As in the case of the low-pass filter, a short-circuited line of length l is substituted for the lumped inductance L . The characteristic impedance of this line is again given by

$$Z_0 = L \frac{c}{l} \quad (49)$$

The two concentric condensers may be treated as lumped capacitances if their length is much smaller than l . Otherwise they should be considered as open-circuited lines. In the former case, a spurious pass band appears when the length of the short-circuited line becomes longer than a quarter wavelength. The attenuation, however, rises very slowly and hence the insertion loss may remain small until the length of the line approaches one-half wavelength.



$$C = \frac{1}{R\omega_c} \quad L = \frac{R}{2\omega_c}$$

Fig. 10-15.—High-pass microwave filter and its equivalent lumped circuit.

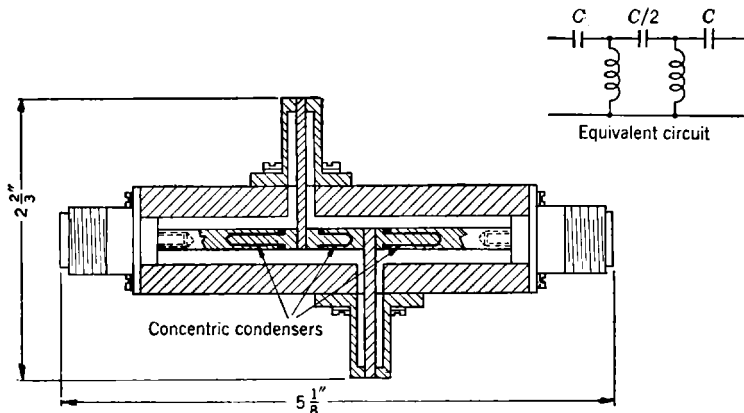


Fig. 10-16.—Two-section high-pass filter and equivalent circuit.

A two-section filter of this type is shown in Fig. 10-16. This drawing is scaled to dimensions suitable for a 50-ohm coaxial line. The filter was

intended to have a cutoff frequency of 900 Mc/sec; at this frequency the insertion loss should be, theoretically, equal to 7 db [see Eqs. (9-129) and (9-141)]. Actually, as seen from Fig. 10-17, which illustrates the experimentally determined insertion loss of the filter, the cutoff frequency is about 680 Mc/sec. As before, this large discrepancy is caused by the roughly approximate nature of the design equations. The insertion loss is less than 0.5 db over most of the frequency range from 800 Mc/sec to 4000 Mc/sec. There is, however, a small hump of about 1 db occurring at 2700 Mc/sec approximately, the frequency for which the coaxial stubs are a quarter wavelength long.

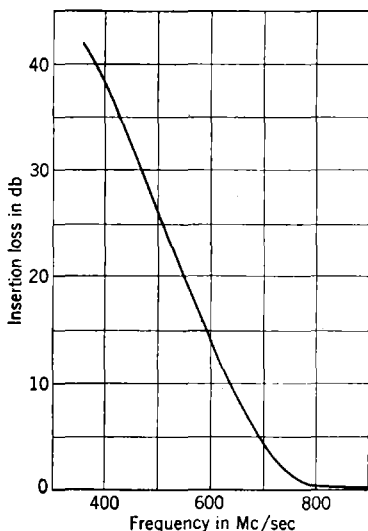


FIG. 10-17.—Rejection-band characteristics of high-pass filter shown in Fig. 10-16.

band of the filter, they may be considered as a convenient means of building resonant impedances. As in the case of m -derived structures, these filters may be designed to have very sharp cutoffs, at some cost in the attenuation farther from the pass band. Moreover, the use of half sections at the two ends of the filter, combined with a proper choice of their frequencies of infinite attenuation, results in improved bandpass characteristics.

Lumped-element structures are used as guides in the design of these filters. The values of the elements, however, must be determined without making any approximations concerning the frequency behavior of the lines. More specifically, in order to obtain satisfactory bandpass characteristics, it is necessary to plot families of image-impedance curves

The concentric condensers used in this filter are filled with Dilectene ($k_e = 3.5$) to provide mechanical rigidity and to reduce the over-all length of the filter. It will be noted that in the two-section filter, the center condenser is only one-half the size of the end condensers since it must be equal to two of the end condensers in series.

A group of filters that is somewhat analogous to the m -derived filters and suitable for the frequency range from 150 Mc/sec to 1000 Mc/sec has been developed. These filters are typified by the use of lumped elements in the series arms of the ladder structure and coaxial-line sections in the shunt arms. Since the coaxial lines are sufficiently long to be resonant near the pass

for various values of the design parameters. Attention must also be paid to the existence of superfluous pass bands arising from the repetitive dependence on frequency of the impedance of the coaxial lines.

It must be pointed out, however, that even when the above design procedure is followed, the neglect of the connecting-lead inductances and of the stray capacitances of the coils may result in small but appreciable differences between predicted and observed characteristics. Finally, the

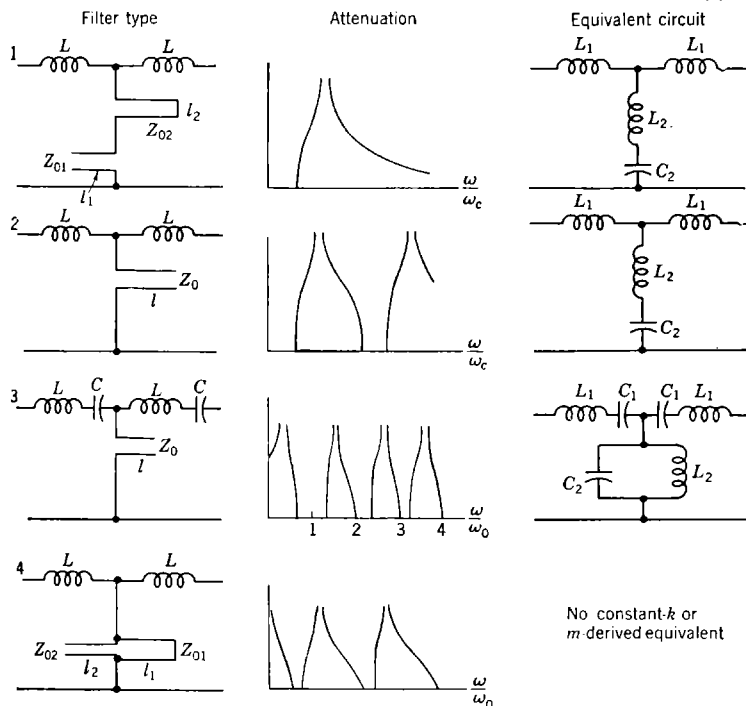


FIG. 10-18.—Four typical microwave filters employing lines as two-terminal elements.

incidental dissipation, which is not taken into account in the design, will smear the peaks of infinite attenuation and slightly increase the loss in the pass band.

The four types of filters that have been developed are schematically represented in Fig. 10-18 together with their attenuation functions. Type 1 is a low-pass filter obtained from a conventional *m*-derived section by substituting, in the shunt arm, a short-circuited line for the lumped inductance and an open-circuited line for the lumped capacitance. By properly transforming the prototype section of Fig. 9-28*b* to obtain a cutoff frequency ω_c and terminations equal to R , it is found for the lumped

element structure that

$$L_1 = \frac{mR}{\omega_c}, \quad C_2 = \frac{2m}{R\omega_c}, \quad L_2 = \frac{R}{2\omega_c} \left(\frac{1}{m} - m \right) \quad (50)$$

$$\omega_\infty = \frac{1}{\sqrt{L_2 C_2}} = \omega_c \frac{1}{\sqrt{1 - m^2}}.$$

It follows that the characteristic impedances of the two lines must be, according to Eqs. (9) and (10),

$$Z_{01} = \frac{l_1}{c} \frac{1}{C_2} = \frac{l_1}{c} \frac{R\omega_c}{2m} \quad (51)$$

$$Z_{02} = \frac{c}{l_2} \frac{R}{2\omega_c} \left(\frac{1}{m} - m \right). \quad (52)$$

If l_1 and l_2 are much smaller than one-quarter wavelength over the frequency band of interest, their actual values do not matter. If this is not the case, however, they must be selected in such a way that the actual cutoff frequency ω_c is kept unchanged. Consider the behaviors of Z_{och} and Z_{sch} , that is, of the open-circuit and short-circuit impedances of one-half the actual network. Since Z_{och} must vanish for $\omega = \omega_c$,

$$\cot \omega_c \frac{l_1}{c} - \frac{Z_{02}}{Z_{01}} \tan \omega_c \frac{l_2}{c} = \frac{\omega_c L_1}{2Z_{01}} = m^2 \frac{c}{\omega_c l_1}. \quad (53)$$

But from Eqs. (51) and (52) the following expression is obtained:

$$\frac{Z_{02}}{Z_{01}} = \frac{c^2}{l_1 l_2 \omega_c^2} (1 - m^2). \quad (54)$$

Equation (53) becomes, then,

$$\frac{\omega_c \frac{l_1}{c}}{\tan \omega_c \frac{l_1}{c}} - (1 - m^2) \frac{\tan \omega_c \frac{l_2}{c}}{\omega_c \frac{l_2}{c}} = m^2. \quad (55)$$

This equation may be solved for l_1 when l_2 is given or vice versa. Attention must be paid to the fact that the frequency at which l_2 becomes a quarter wavelength is the cutoff of a spurious pass band. Therefore, it is desirable to keep l_2 as small as possible. The constant m is usually made equal to 0.6 since for this value the image impedance of the half section (midshunt impedance) is reasonably constant over the pass band.

The peak of infinite attenuation occurs when $Z_{\text{och}} = Z_{\text{sch}}$, that is, when the impedance of the shunt arm is equal to zero. Therefore,

$$\tan \omega_\infty \frac{l_1}{c} \tan \omega_\infty \frac{l_2}{c} = \frac{Z_{01}}{Z_{02}} = \frac{l_1 l_2 \omega_c^2}{c^2 (1 - m^2)}. \quad (56)$$

It is interesting to note that ω_∞ depends on the product $l_1 l_2$. Equations (55) and (56) can be solved approximately by using the first two or three terms of the series expansions of the tangents. The propagation function of the filter is given by the expression

$$\gamma = 2 \tanh^{-1} \sqrt{\frac{Z'_{sch}}{Z_{och}}} = 2 \tanh^{-1} \left\{ 1 - \frac{2Z_{01} \omega_c}{\omega_c L_1 \omega} \left[\cot \left(\frac{\omega \omega_c l_1}{\omega_c c} \right) - \frac{Z_{02}}{Z_{01}} \tan \left(\frac{\omega \omega_c l_2}{\omega_c c} \right) \right] \right\}^{-1/2}. \quad (57)$$

The image impedance of the midshunt Π -section is

$$Z'_i = \sqrt{Z'_{och} Z'_{sch}} = 2Z_{01} \left[\cot \left(\frac{\omega \omega_c l_1}{\omega_c c} \right) - \frac{Z_{02}}{Z_{01}} \tan \left(\frac{\omega \omega_c l_2}{\omega_c c} \right) \right] \left\{ \frac{2Z_{01} \omega_c}{\omega_c L_1 \omega} \left[\cot \left(\frac{\omega \omega_c l_1}{\omega_c c} \right) - \frac{Z_{02}}{Z_{01}} \tan \left(\frac{\omega \omega_c l_2}{\omega_c c} \right) \right] - 1 \right\}^{-1/2}. \quad (58)$$

Filter No. 2 of Fig. 10-18 is derived from a conventional low-pass constant- k section by substituting open-circuited lines for the shunt capacitances. However, if the length l of the line has its quarter-wave resonance at a frequency ω_∞ slightly larger than the cutoff frequency ω_c , the frequency behavior of the filter becomes similar to the one of an m -derived section. The proper design procedure consists of making the cutoff frequency and the frequency of infinite attenuation of the actual filter coincide with ω_c and ω_∞ of the m -derived lumped-element section. The following expression is, then, obtained:

$$\omega_c \frac{l}{c} = \frac{\pi \omega_c}{2 \omega_\infty} \quad (59)$$

$$Z_0 = \frac{\omega_c L}{2} - \tan \omega_c \frac{l}{c} \quad (60)$$

The image impedance of the filter at zero frequency may be made equal to any desired value R , usually the impedance of the terminations. In this case,

$$(Z_{och} Z_{sch})_{\omega=0} = 2Z_0 \frac{c}{l} L = R^2. \quad (61)$$

Equations (59), (60), and (61) yield

$$\frac{Z_0}{R} = \frac{1}{2} \sqrt{\frac{\omega_c l}{c} \tan \omega_c \frac{l}{c}} = \frac{1}{2} \sqrt{\frac{\pi}{2} \frac{\omega_c}{\omega_\infty} \tan \frac{\pi}{2} \frac{\omega_c}{\omega_\infty}} \quad (62)$$

$$\frac{L}{R} = \frac{1}{\omega_c} \sqrt{\frac{\omega_c l / c}{\tan \omega_c l / c}} = \frac{1}{\omega_c} \sqrt{\frac{\pi}{2} \frac{\omega_c}{\omega_\infty} \cot \frac{\pi}{2} \frac{\omega_c}{\omega_\infty}} \quad (63)$$

where, for the m -derived section, the ratio ω_c/ω_∞ is equal to $\sqrt{1-m^2}$. In the case of lumped-element sections, m must be made equal to approxi-

mately 0.6 in order to obtain a well-behaved image impedance for the midshunt half section. In the present case a somewhat smaller value of m , approximately 0.55, may be used. The first spurious pass band starts at the frequency at which l becomes equal to one-half wavelength, that is, at a frequency equal to $2\omega_0$. For this filter, the propagation function is given by

$$\gamma = 2 \tanh^{-1} \sqrt{\frac{Z_{\text{sch}}^-}{Z_{\text{sch}}^+}} = 2 \tanh^{-1} \left[1 - \frac{2Z_0}{\omega_c L} \frac{\omega_c}{\omega} \cot \left(\frac{\omega}{\omega_c} \frac{\omega_c l}{c} \right) \right]^{-1/2}, \quad (64)$$

and the image impedance of the midshunt Π -section is

$$Z'_l = \sqrt{Z_{\text{sch}}^+ Z_{\text{sch}}^-} = 2Z_0 \cot \left(\frac{\omega}{\omega_c} \frac{\omega_c l}{c} \right) \left[\frac{2Z_0}{\omega_0 L} \frac{\omega_c}{\omega} \cot \left(\frac{\omega}{\omega_c} \frac{\omega_c l}{c} \right) - 1 \right]^{-1/2}. \quad (65)$$

Filter No. 3 is derived from a bandpass constant- k section by substituting for the tuned circuit in the shunt arm an open-circuited section of line resonating at the mean frequency ω_0 . By properly transforming the prototype low-pass structure into a bandpass filter with a mean frequency ω_0 , a bandwidth w , and terminations equal to R , the following expressions are obtained for the lumped elements

$$L_1 = \frac{R}{w}, \quad C_2 = \frac{2}{Rw}, \quad \omega_0 = \frac{1}{\sqrt{L_1 C_1}} = \frac{1}{\sqrt{L_2 C_2}}. \quad (66)$$

The length of the line is given, obviously, by

$$\frac{\omega_0 l}{c} = \pi. \quad (67)$$

The characteristic impedance of the line must be, according to Eqs. (16) and (66),

$$Z_0 = \frac{\pi}{2C_2 \omega_0} = R \frac{\pi w}{4 \omega_0}. \quad (68)$$

If ω_0/w is relatively small the actual bandwidth of the filter becomes somewhat smaller than w and can be computed as the difference between the frequencies at which Z_{sch} is equal to zero.

Peaks of infinite attenuation occur at the frequencies for which l is one-quarter and three-quarters wavelength. In spite of this fact, the filter can hardly be considered of the m -derived type since these frequencies are determined entirely by the mean frequency ω_0 , being equal to $\omega_0/2$ and $\frac{3}{2}\omega_0$. However, the image impedance of the midshunt Π -section is somewhat flatter than the image impedance of the corresponding lumped-element section, although its behavior cannot be adjusted independently of ω_0 and w . This image impedance is

$$Z'_l = \sqrt{Z'_{ocb} Z'_{sch}} = 2Z_0 \cot \left(\pi \frac{\omega}{\omega_0} \right) \left[\frac{2Z_0 \omega_0 \cot \pi \frac{\omega}{\omega_0}}{\omega_0 L \omega \left[1 - \left(\frac{\omega_0}{\omega} \right)^2 \right]} - 1 \right]^{-1/2} \quad (69)$$

The propagation function is, similarly,

$$\gamma = 2 \tanh^{-1} \sqrt{\frac{Z'_{sch}}{Z'_{ocb}}} = 2 \tanh^{-1} \left[1 - \frac{2Z_0 \omega_0 \cot \pi \frac{\omega}{\omega_0}}{\omega_0 L \omega \left[1 - \left(\frac{\omega_0}{\omega} \right)^2 \right]} \right]^{-1/2} \quad (70)$$

Spurious pass bands start at frequencies equal to $2\omega_0$, $3\omega_0$, $4\omega_0$, etc.

Filter No. 4 is derived from a lumped-element structure which is not of any conventional type. It has bandpass characteristics without any superfluous low-pass band. Its main advantage is that there are no condensers in the series arms. This fact makes it particularly suitable for use at high power levels. For design data on this filter, the reader is referred to the original report by Mode and Nosker.⁷

The filter of Fig. 10-19 will be examined in detail to illustrate the practical design procedure. This filter is intended to operate between 50-ohm terminations, to have a pass band from 220 to 260 Mc/sec, and rejection bands from 165 to 215 Mc/sec and from 275 to 375 Mc/sec. In order to obtain such characteristics, a Type 2 low-pass filter is used in tandem with a Type 3 bandpass filter. The sharp cutoff of the low-pass filter is used to eliminate the high-frequency portion of the pass band of the Type 3 filter where the image impedance is varying rapidly with frequency. Furthermore, the Type 2 filter increases the amount of attenuation obtainable per section far from the pass band. The resulting filter is composed of five coaxial lines making up the bandpass filter and five coaxial lines composing the low-pass filter. The two sets of lines

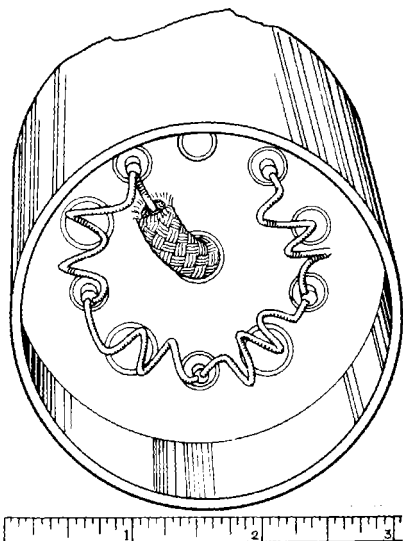


Fig. 10-19.—Filter composed of five sections of Type 2 and five sections of Type 3.

form a fascies which is bound in a cylindrical tube 21 by 3 in. OD. The lines are interconnected by a centrally located coaxial line.

The schematic diagram for the low-pass unit is shown in Fig. 10-20. The filter consists of four Π -sections. The A lines are made from a pipe $\frac{3}{8}$ in. in diameter with $\frac{1}{16}$ -in. inner conductors. These lines have a characteristic impedance of 111 ohms and are 8 in. in length. The B lines are made from $\frac{3}{8}$ -in. tubing with center conductors $\frac{5}{32}$ in. in diameter. Their characteristic impedance is 55.5 ohms and their length is also 8 in.

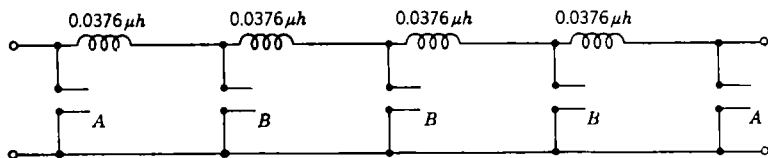


FIG. 10-20.—Low-pass unit of filter shown in Fig. 10-19.

The schematic diagram for the bandpass unit is shown in Fig. 10-21. The filter consists of four Π -sections. The A lines are $\frac{5}{16}$ -in. ID tubings with $\frac{3}{32}$ -in. OD center conductors. In this case $Z_0 = 139$ ohms. The lines are $13\frac{3}{8}$ in. long. The B lines, having a characteristic impedance of 69.5 ohms, are obtained from $\frac{7}{16}$ -in. ID tubing and $\frac{1}{8}$ -in. OD rods. Their length is equal to that of the A lines.

The theoretical curve for the attenuation function and the experimental curve for the insertion loss of this filter are compared in Fig. 10-22. It is not unusual to encounter 10 per cent discrepancies between theoretical and experimental results if allowance is not made for junction effects.

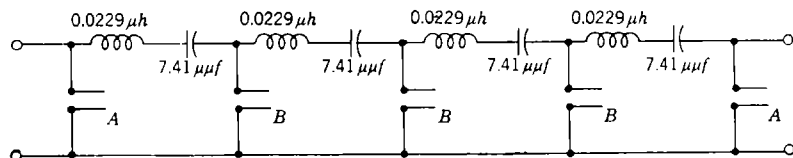


FIG. 10-21.—Bandpass unit of filter shown in Fig. 10-19.

10-4. Filters Employing Lines as Four-terminal Elements.—A number of other filters employing sections of lines have been developed. A comprehensive survey including the types shown in Fig. 10-23 can be found in a report by P. Richards.³ Reference should also be made to a much earlier survey by Mason and Sykes.¹ Four of these filters will be analyzed in some detail as illustrations of the design technique.

Some of the sections shown in Fig. 10-23 make use of lines as two-terminal-pair networks. These sections are used in some cases in combinations with sections of different types to provide mechanical

spacing. In other cases they are used to suppress undesired pass bands resulting from the periodicity of transmission-line impedances. The resulting filters cannot be analyzed by means of the image parameters of the individual sections because the image impedances of different sections are not, in general, equal. In such a case, the advantages of the image-parameter method of analysis disappear, and instead of computing the image parameters of the whole filter it is often just as easy to compute the elements of the $\mathcal{A}\mathcal{B}\mathcal{C}\mathcal{D}$ matrix (see Sec. 9-1) by multiplying the corres-

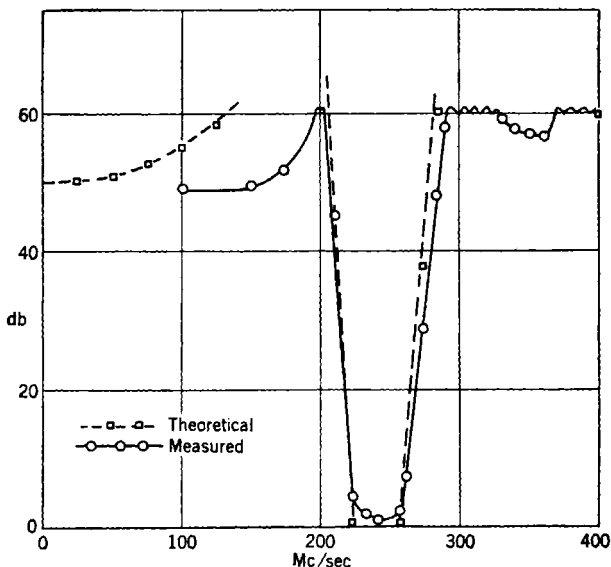


FIG. 10-22.—Comparison of observed insertion loss and computed attenuation characteristic of filter shown in Fig. 10-19.

ponding matrices of the individual sections. The insertion loss of the filter can be found readily from this matrix as shown in Sec. 9-3. A rough estimate of the attenuation function of the whole filter can sometimes, but not always, be obtained simply by adding the attenuation functions of the individual sections. The warning is necessary, however, that this method, which is correct when matched conditions exist at the junctions of different sections, may be misleading when mismatches are present. It may happen, for instance, that the whole filter has a pass band where the individual sections have an attenuation band. The physical meaning of this phenomenon is that the reflection from one section may cancel partially or totally the reflection from another section. Because of these considerations, the parameters $\mathcal{A}\mathcal{B}\mathcal{C}\mathcal{D}$ for the individual sections will be

given together with the design formulas although they are not used in the following discussion.

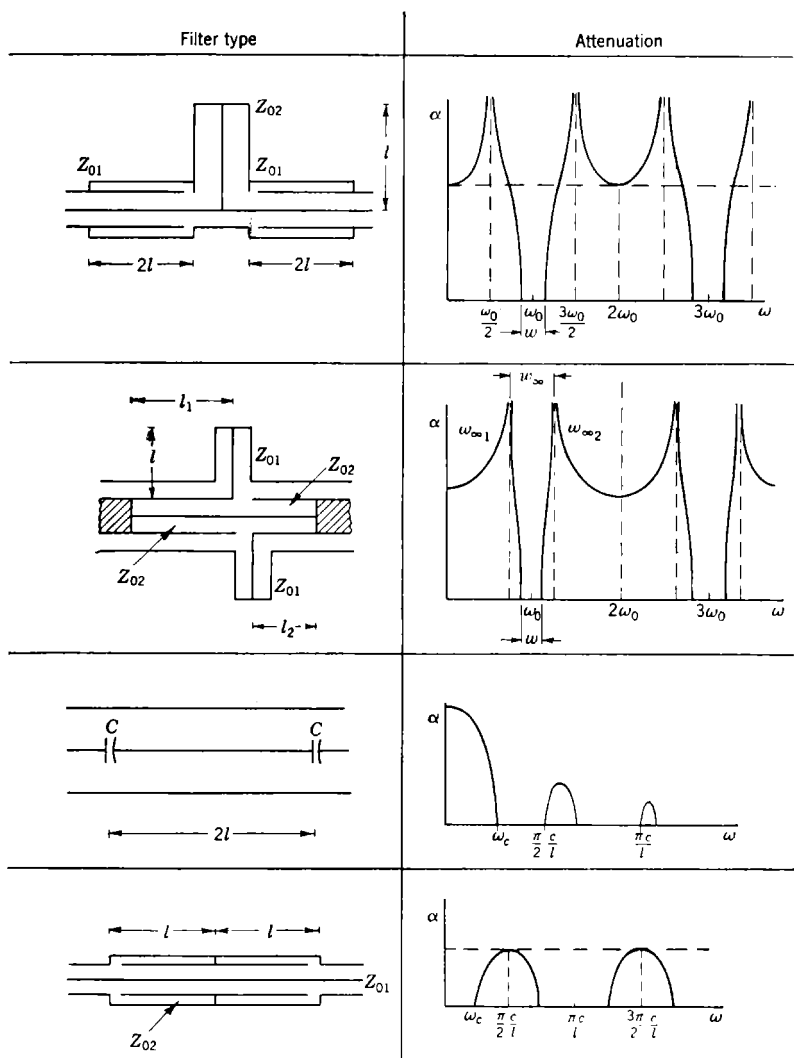


FIG. 10-23.—Four filter types and their attenuation characteristics.

Filter No. 1 (T-section) is derived from the constant- k bandpass section of Fig. 10-24. Let w be the bandwidth and ω_0 the mean frequency. A short-circuited line of characteristic impedance Z_{01} and

length $2l$ is substituted for the series arm, and a short-circuited line of characteristic impedance Z_{02} is substituted for the shunt arm. The length l is given by the expression

$$\frac{\omega_0 l}{c} = \frac{\pi}{2}. \quad (71)$$

With reference to Fig. 10-24a and using Eqs. (16) and (20), it is found for Z_{01} and Z_{02} that

$$Z_{01} = \frac{2R}{\pi} \frac{\omega_0}{w}, \quad Z_{02} = \frac{R\pi}{8} \frac{w}{\omega_0}. \quad (72)$$

The ratio of the characteristic impedances is then

$$\frac{Z_{01}}{Z_{02}} = \left(\frac{4}{\pi} \frac{\omega_0}{w} \right)^2. \quad (73)$$

These design equations are satisfactory when the ratio w/ω_0 is much smaller than $\frac{1}{2}$. If this is not the case, the actual bandwidth will be appreciably smaller. The proper design equations may be found by computing the cutoff frequencies of the filter as the frequencies for which Z_{och} is equal to zero. After proper manipulations, the following expression is obtained:

$$\frac{Z_{01}}{Z_{02}} = \cot^2 \left(\frac{\pi w}{4 \omega_0} \right) - 1 = 2 \left[\sec \left(\frac{\pi w}{2 \omega_0} \right) - 1 \right]^{-1}. \quad (74)$$

Furthermore, imposing the condition

$$Z_{och} Z_{sch} = R^2$$

at the mean frequency ω_0 yields the equation

$$Z_{01} Z_{02} = \left(\frac{R}{2} \right)^2. \quad (75)$$

Equations (74) and (75) together with Eq. (71) provide all the necessary design equations. It must be added, however, that because the impedance of the line in the series arms

becomes infinite for $\omega = \omega_0/2$ and $\omega = \frac{3}{2}\omega_0$, there is a peak of infinite attenuation on each side of the pass band. However, since the locations of these peaks obviously cannot be controlled, the filter can hardly be considered to be of the m -derived type. The propagation function is

$$\gamma = 2 \tanh^{-1} \sqrt{\frac{Z_{sch}}{Z_{och}}} = 2 \tanh^{-1} \left[1 + \frac{Z_2}{Z_1} \left(1 - \tan^2 \frac{\pi \omega}{2 \omega_0} \right) \right]^{-1/2}. \quad (76)$$

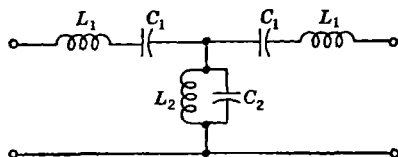


FIG. 10-24.—Constant- k bandpass section.

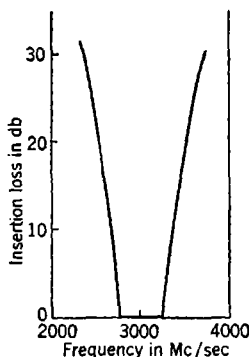


FIG. 10-25.—Insertion loss of filter Type 1 shown in Fig. 10-23.

TABLE 10-1.—MATRIX ELEMENTS FOR FILTER SECTION OF FIG. 10-23

	T	II	L
a	$1 + \frac{Z_{01}}{Z_{02}} \left(1 + \sec \pi \frac{\omega}{\omega_0} \right)$	$1 + \frac{Z_{01}}{Z_{02}} \left(1 + \sec \pi \frac{\omega}{\omega_0} \right)$	$1 + \frac{1}{2} \frac{Z_{01}}{Z_{02}} \left(1 + \sec \pi \frac{\omega}{\omega_0} \right)$
b	$j2Z_{01} \tan \pi \frac{\omega}{\omega_0} \left[1 + \frac{1}{2} \frac{Z_{01}}{Z_{02}} \left(1 + \sec \pi \frac{\omega}{\omega_0} \right) \right]$	$j2Z_{01} \tan \pi \frac{\omega}{\omega_0}$	$jZ_{01} \tan \pi \frac{\omega}{\omega_0}$
c	$-j \frac{1}{Z_{02}} \cot \pi \frac{\omega}{2\omega_0}$	$-j \frac{1}{Z_{02}} \cot \pi \frac{\omega}{2\omega_0} \left[1 + \frac{1}{2} \frac{Z_{01}}{Z_{02}} \left(1 + \sec \pi \frac{\omega}{\omega_0} \right) \right]$	$-j \frac{1}{2Z_{02}} \cot \pi \frac{\omega}{2\omega_0}$
d	a	a	1

An experimental curve is reproduced in Fig. 10-25 showing the insertion loss of one L-section, that is of one half of the filter shown in Fig. 10-24. Table 10-1 gives the matrix components for Filter No. 1 (T-section) and for the II- and L-sections derived from it.

Filter No. 2 in Fig. 10-23 is obtained from the m -derived II-section shown in Fig. 10-26a. The series arm of the section is transformed into a series combination of two resonant circuits tuned to the frequencies of infinite attenuation ω_{∞_1} and ω_{∞_2} , as shown in Fig. 10-26b. These two frequencies occur on opposite sides of the pass band. Two short-circuited lines of length

$$l = \frac{\pi c}{2\omega_0} \quad (77)$$

are substituted for the shunt arm. The characteristic impedance of these lines must be

$$Z_{01} = \frac{1}{2C_1} \frac{l}{c} = \frac{R\pi w}{4m \omega_0} \quad (78)$$

In the series arm two short-circuited lines of length l_1 and l_2 are substituted for the two resonant circuits. Then,

$$l_1 = \frac{\pi c}{2\omega_{\infty_1}}; \quad l_2 = \frac{\pi c}{2\omega_{\infty_2}} \quad (79)$$

For filters with a reasonably narrow band the following approximation can be made:

$$l_1 + l_2 = 2l. \quad (80)$$

It follows that the two lines must have the same characteristic impedance Z_{02} , since for $\omega = \omega_0$ the sum of their impedances must be equal to zero.

The quantity Z_{02} can be found by equating the slope of the reactance of the shunt arm at the mean frequency to $2L_2$, that is, to the corresponding value for the lumped network. Thus, it is required that

$$Z_{02} \left[\frac{d}{d\omega} \left(\tan \omega \frac{l_1}{c} + \tan \omega \frac{l_2}{c} \right) \right]_{\omega=\omega_0} = \frac{\frac{\pi}{\omega_0} Z_{02}}{\sin^2 \frac{\pi}{4} \frac{\omega_\infty}{\omega_0}} = 2L_2 \quad (81)$$

where $\omega_\infty = \omega_{\infty_2} - \omega_{\infty_1}$; whence it follows that

$$Z_{02} = \frac{2\omega_0}{\pi} L_2 \sin^2 \frac{\pi}{4} \frac{\omega_\infty}{\omega_0} = \frac{4mR}{\pi} \frac{\omega_0}{w} \sin^2 \frac{\pi}{4} \frac{\omega_\infty}{\omega_0}. \quad (82)$$

For small values of ω_∞/ω_0 this equation reduces to

$$Z_{02} = mR \frac{\pi}{4} \frac{w}{\omega_0} \left(\frac{\omega_\infty}{w} \right)^2 = R \frac{\pi}{4} \frac{m}{1 - m^2} \frac{w}{\omega_0}. \quad (83)$$

Equations (77), (78), (79), (80), and (83) form a complete set of design equations in the case of narrow-band filters. For larger values of w/ω_0

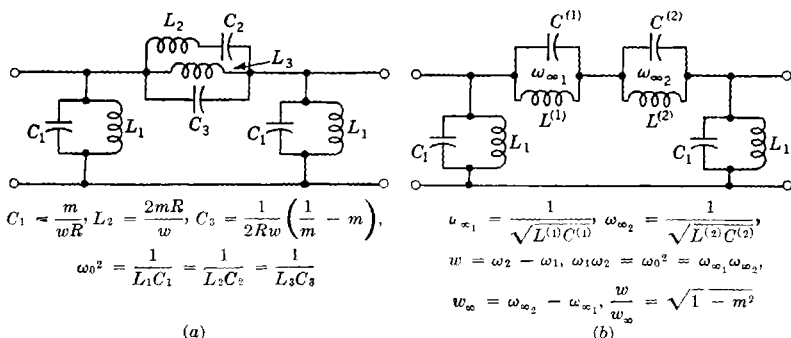


FIG. 10-26.—Two equivalent forms of m -derived bandpass filter.

the same equations may be used, but some disagreements must be expected between actual and predicted characteristics.

The components of the $\alpha\beta\gamma\delta$ matrix are

$$\alpha = 1 + \frac{Z_{02}}{Z_{01}} \frac{\tan \omega \frac{l_1}{c} + \tan \omega \frac{l_2}{c}}{\tan \omega \frac{l}{c}} = \mathcal{D},$$

$$\beta = jZ_{02} \left(\tan \omega \frac{l}{c} + \tan \omega \frac{l_2}{c} \right),$$

$$\gamma = -j \frac{2Z_{01} \tan \omega \frac{l}{c} + Z_{02} \left(\tan \omega \frac{l_1}{c} + \tan \omega \frac{l_2}{c} \right)}{Z_{01} Z_{02} \tan \frac{\omega l}{c} \left(\tan \omega \frac{l_1}{c} + \tan \omega \frac{l_2}{c} \right)}$$

Spurious pass bands are centered at frequencies $3\omega_0$, $5\omega_0$, etc. The characteristics of the filter, however, are not periodic functions of ω . For instance, the difference between the frequencies of infinite attenuation bracketing the pass band centered at $3\omega_0$ is $\frac{2}{3}\omega_0$. For further discussion of filters of this type, the reader is referred to the original paper by Richards.³

The measured insertion loss for a filter of this type is compared in

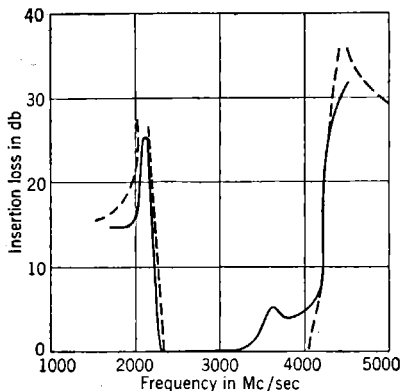


FIG. 10-27.—Insertion loss of filter Type 2 shown in Fig. 10-23.

Fig. 10-27 with the predicted attenuation function; except for the anomalous bump in the pass band the agreement is good. Part of the discrepancy, particularly near the frequencies of infinite attenuation, is caused by incidental dissipation. The bump in the pass band is inexplicable, unless it arises from spurious effects introduced by the test procedure.

Filter No. 3 may be considered as a high-pass filter derived from the lumped-element structure in Fig. 10-28. The cutoff frequency for this filter coincides with the zero of Z_{sch} , that is, with the resonance frequency of L_1 and C . The image impedance for $\omega = \infty$ is made equal to the terminating resistance R . The design equations are then

$$\omega_c^2 = \frac{1}{L_1 C} \quad (84)$$

$$R^2 = L_1 \frac{C_1 + C}{C_1 C} \quad (85)$$

A section of a line of characteristic impedance Z_0 and length $2l$ is then substituted for the lattice. From Eqs. (37) and (38) it is found that

$$L_1 = Z_0 \frac{l}{c}; \quad C_1 = \frac{1}{Z_0} \frac{l}{c} \quad (86)$$

Equations (84), (85), and (86) then yield, for $\omega_c l/c \ll 1$,

$$Z_0 = R \quad (87)$$

$$\omega_c C = \frac{1}{R} \frac{c}{\omega_c l} \quad (88)$$

The length l is arbitrary but must be made short compared with a quarter

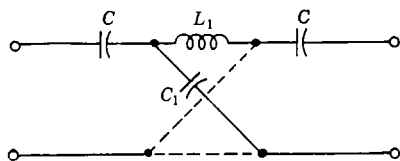


FIG. 10-28.—Equivalent circuit for filter Type 3 shown in Fig. 10-23.

wavelength over the frequency band of interest. When this condition is satisfied, the behavior of the actual filter approximates closely the behavior of the lumped-element network. On the other hand, if this condition is not satisfied, the behavior of Z_{oc} and Z_{sc} must be examined for the actual filter. It is easy to show that the exact value of the cutoff frequency ω_c is given by the expression

$$Z_0 \omega_c C \tan \omega_c \frac{l}{c} = 1 \quad \text{for } \omega_c \frac{l}{c} < \frac{\pi}{2}. \quad (89)$$

The impedance Z_0 can still be made equal to the terminating impedance R , since it is well known that under these conditions there is always a frequency at which the reflections arising from the two condensers cancel each other and perfect transmission results.

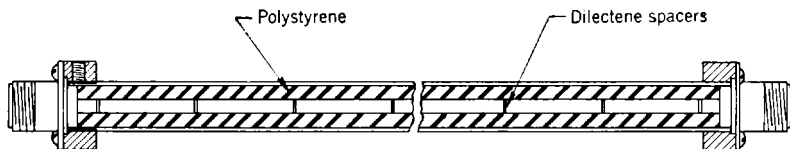


FIG. 10-29.—A practical form of filter Type 3 shown in Fig. 10-23.

Spurious attenuation bands appear between the frequencies at which l becomes equal to an integral number n of quarter wavelengths and the frequencies at which Eq. (89) is satisfied for $(n - 1) \frac{\pi}{2} < \frac{\omega_c l}{c} < n \frac{\pi}{2}$. It follows that this filter may be used also as a bandpass filter.

For the components of the $\mathcal{A}\mathcal{B}\mathcal{C}\mathcal{D}$ matrix it is found that

$$\left. \begin{aligned} \mathcal{A} &= \frac{1}{\omega C Z_0} \sin \frac{2\omega l}{c} + \cos \frac{2\omega l}{c}, \\ \mathcal{B} &= j \left[Z_0 \left(1 - \frac{1}{\omega^2 C^2 Z_0^2} \right) \sin \frac{2\omega l}{c} - \frac{2}{\omega C} \cos \frac{2\omega l}{c} \right] \\ \mathcal{C} &= j \frac{1}{Z_0} \sin \frac{2\omega l}{c}, \\ \mathcal{D} &= \frac{1}{\omega C Z_0} \sin \frac{2\omega l}{c} + \cos \frac{2\omega l}{c}. \end{aligned} \right\} \quad (90)$$

A practical design for a filter of this type is shown in Fig. 10-29. It consists of a coaxial line with polystyrene filler between the inner and outer conductors. The inner conductor is broken periodically and the sections thus formed are spaced with Dilectene washers to form series capacitances. The capacitances of the first and last condensers are equal to C whereas the capacitances of the other seven condensers are equal to $C/2$. The filter consists, thus, of eight prototype sections. The experimentally determined insertion loss for this filter is shown in Fig. 10-30.

Filter No. 4 in Fig. 10-23 may be derived from the low-pass filter shown in Fig. 10-31. The cutoff frequency ω_c of this filter coincides with the zero of Z_{och} , that is, with the resonance frequency of L_2 and C_1 . The zero-frequency image impedance is made equal to the terminating resistance R . Under these conditions, the design equations are

$$\omega_c^2 = \frac{1}{L_2 C_1} \quad (91)$$

$$R^2 = \frac{L_1 + L_2}{C_1} \quad (92)$$

Note that the attenuation never becomes infinite; however, the image impedance, and consequently the insertion loss, become infinite for $\omega = \infty$.

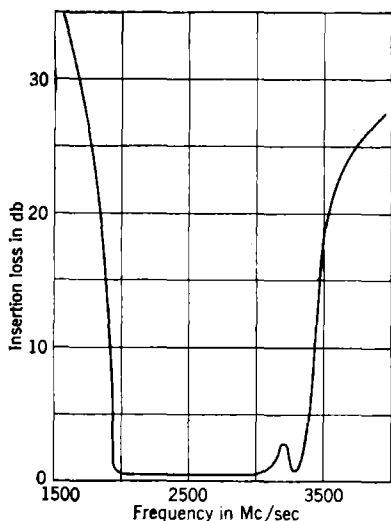


FIG. 10-30.—Insertion loss of filter shown in Fig. 10-29.

However, if $\omega_c l/c$ is small compared with unity, that is, if l is much smaller than one-quarter wavelength for $\omega = \omega_c$, the design can be simplified by letting $Z_{01} = R$. This will change the loss in the pass band somewhat; as a matter of fact, it will tend to improve the characteristics of the filter since perfect transmission will be obtained not only at zero frequency but also at the frequency for which the image impedance is equal to R .

Note that all the lumped elements have been effectively replaced by sections of line of equal length l . It follows, according to the discussion in Sec. 10-1, that the frequency characteristics of the microwave filter

The corresponding microwave filter is designed by substituting a line of characteristic impedance Z_{01} , and of length $2l$ for the lattice, and a short-circuited line of characteristic impedance Z_{02} and of length l for the series inductance. Then

$$\begin{aligned} L_1 &= Z_{01} \frac{l}{c}, & C_1 &= \frac{1}{Z_{01}} \frac{l}{c}, \\ L_2 &= Z_{02} \frac{l}{c} \end{aligned} \quad (93)$$

or

$$\begin{aligned} Z_{01} &= \sqrt{\frac{L_1}{C_1}}, \\ \frac{Z_{02}}{Z_{01}} &= \left(\frac{\omega_c l}{c}\right)^2. \end{aligned}$$

According to Eq. (92), the result is

$$R^2 = Z_{01}(Z_{01} + Z_{02}).$$

can be obtained without any approximations from the corresponding functions for the lumped-element filter by simply substituting $\tan \omega' \frac{l}{c}$

for ω . Thus the resulting functions have a period equal to $\pi \frac{c}{l}$, as shown

in Fig. 10-23. The components of the $\alpha\beta\epsilon\delta$ matrix can be obtained from Eq. (90) by substituting Z_{01}

for Z_0 and $Z_{02} \tan \frac{\omega l}{2}$ for $-\frac{1}{\omega C}$.

Other types of filters, similar to the one discussed above, can be designed without difficulty. For further discussion of these filters, the reader is referred to the original report by Richards.³

10-5. Waveguide Filters.—It may be noted that no waveguide filter has been described up to this point. Theoretically speaking, the behavior of hollow-pipe waveguides is so similar to the behavior of conventional transmission lines that one might expect to find waveguide filters analogous to the broadband filters discussed in the preceding section. No such filters, however, have ever been built for a number of reasons.

First of all, a waveguide is intrinsically a high-pass filter. Low-pass filters are thus excluded, and the need for any high-pass filter other than a simple section of guide is rather improbable. The characteristics of guides as high-pass filters are discussed below. In the second place, it would be rather difficult to design filters employing sections of waveguides as elements because of the junction effects. These junction effects, which in general can be minimized in the case of conventional transmission lines, become of paramount importance in the case of waveguides. It follows that not only does any theoretical design become worthless, but even the mathematical analysis of a given system becomes impossible to perform. In the case of narrow-band filters, however, the difficulties arising from the use of waveguides are easily overcome, as will be shown later.

In view of this situation, it is fortunate, indeed, that waveguide filters very seldom require a broad pass band. TR switches are the only broadband filters ever built. Even in this case, the design procedure for narrow-band filters is applicable. The fact that broadband filters are seldom needed becomes clear when one considers that the absolute frequency band required to transmit a given intelligence is independent of the frequency of the carrier. It follows immediately that the same intelligence that requires, for instance, a 10 per cent band at 300 Mc/sec will require only a 1 per cent band at 3000 Mc/sec.

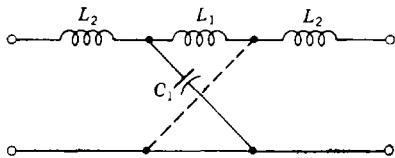


FIG. 10-31.—Equivalent circuit for filter Type 4 shown in Fig. 10-23.

It seems worth while to discuss the behavior of waveguides as high-pass filters in more detail. Below a certain critical frequency, an exciting field in a waveguide will die out exponentially according to the law $E = E_0 e^{-\alpha x}$ where E_0 is the amplitude of the field at the point of excitation and x is the distance from this point to the point of measurement. The threshold frequency for this phenomenon is known as the "cutoff frequency" and depends on the geometry of the waveguide and the particular mode excited.

In the following discussion, attention will be confined to the damping of dominant modes in rectangular and circular waveguide.

The attenuation function is given in all cases by

$$\alpha = 8.69 \sqrt{\left(\frac{2\pi}{\lambda_c}\right)^2 - \left(\frac{2\pi}{\lambda}\right)^2} \text{ db/meter}$$

where λ and λ_c are, respectively, the free-space wavelength and the cutoff wavelength in meters. It should be recalled that this attenuation is not a consequence of

dissipation of a traveling wave, but is attenuation by reflection just as in the case of nondissipative filters.

It is clear from the foregoing equation that the maximum obtainable attenuation is $54.6/\lambda_c$ db/meter. For the TE_{10} -mode in rectangular waveguide $\lambda_c = 2a$, where a is the wide dimension of the guide; for the TE_{11} -mode in circular waveguide, $\lambda_c = 3.41r$, where r is the radius of the guide.

Figure 10-32 gives a normalized plot of the attenuation function as a function of λ_c/λ . It is apparent from this graph that any device that alters λ_c will change the cutoff frequency. Thus, for instance, a variable cutoff high-pass filter can be obtained by placing in the guide a thin, longitudinal dielectric or metallic slab which can be moved across the waveguide. A method of obtaining the same result by means of a variable-width guide has been described by Wadey.⁴

The insertion loss of a section of guide differs from the total attenuation of the section and depends on the source and load impedances just as in the case of conventional filters. Tapers are used in most cases to

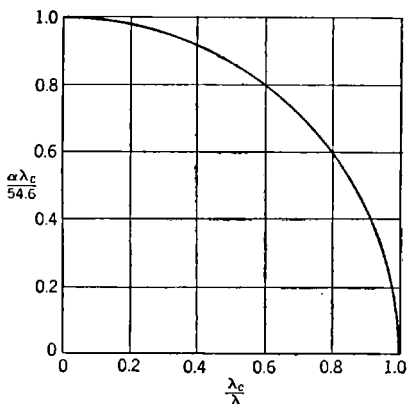


FIG. 10-32.—Attenuation below cutoff in a waveguide.

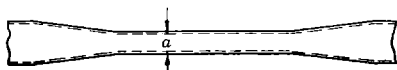


FIG. 10-33.—High-pass filter constructed from a tapered rectangular waveguide.

match the input and output guides to the attenuating section as shown in Fig. 10·33. However, a perfect match can never be obtained because the guide wavelength approaches infinity when the frequency approaches

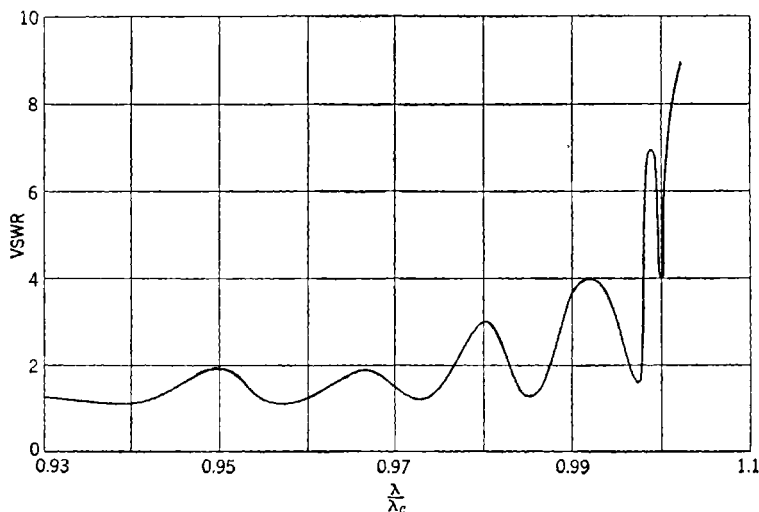


FIG. 10·34.—Behavior of tapered waveguide near cutoff frequency.

its cutoff value. Figure 10·34 gives typical data on a filter section of this type.

FILTERS EMPLOYING DIRECT-COUPLED CAVITY RESONATORS

It has been pointed out that the use of lines in filter design is limited by the values of characteristic impedances obtainable in practice. More specifically, it is not practical to build narrow-band filters employing lines, inductances, and capacitance, exclusively. A similar situation arises also in connection with lumped-element filters because of practical limitations on the size of the elements. In the latter case, the difficulty is overcome by transforming the network, usually a ladder structure, into a cascade of resonant circuits loosely coupled through mutual inductances. As an example, consider the bandpass section of the constant- k type shown in Fig. 10·35a. This filter is designed for a mean frequency ω_0 , a bandwidth w , and terminating impedances equal to R . With reference to the design equations given in Fig. 10·35a, it is obviously difficult to build inductances and capacitances of the widely different sizes required for a 1 per cent bandwidth, that is, for a ratio ω_0/w equal to 100.

To circumvent this difficulty the network is transformed into the

equivalent structure shown in Fig. 10-35*b*. The reader who is not familiar with the details of this transformation procedure is referred to Chap. 4, Sec. 6, of *Communications Networks* by E. A. Guillemin. The equivalence of the two structures as two-terminal-pair networks can be checked without difficulty, however, by computing the impedances Z_{och} and Z_{sch} . In the transformed network, all the inductances have the same value, and the ratio C_3/C_1 is only 2. If L_1 is still too large, the impedance level of the whole network may be changed by means of ideal transformers or, in practice, by means of two suitable matching networks. This method of designing narrow-band lumped-element filters leads to a solution of the analogous problem in the case of microwave filters. Cavity resonators are known to behave, in the vicinity of a resonance frequency, like simple resonant circuits. It follows that a possible microwave realization of a narrow-band filter will consist of a number of cavity

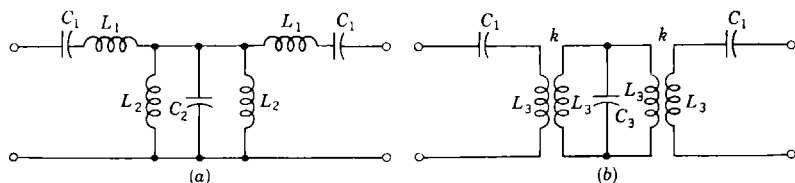


FIG. 10-35.—A prototype constant- k bandpass filter transformed into a more practical equivalent form.

resonators coupled to one another in such a way that they form a chain. For this reason, cavity filters will now be discussed. Initially, however, there will be a digression for the discussion of the properties of cavities as network elements.

10-6. Cavity Resonators as Circuit Elements.—Any cavity resonator is inherently a very complex network. It has an infinite number of natural frequencies of oscillation and, moreover, it may oscillate in more than one mode at any given natural frequency. The present section is concerned, particularly, with the external characteristics of cavities, that is, with their behavior as circuit elements. In view of this fact, one must consider a cavity together with the elements that couple it to the rest of the network. Under these conditions the frequency behavior of a cavity can be represented by means of any convenient set of three independent functions of frequency. The three open-circuit reactances X_{11} , X_{12} , X_{22} are particularly suitable for this purpose because they lead directly to a convenient form of equivalent circuit. These reactances are measured at the terminals of the cavity. No difficulty arises when the terminals consist of coaxial lines operated in the dominant *TEM*-mode. In the case of waveguide terminals, however, doubt may exist

concerning the exact meaning of impedance. This question deserves some attention before an analysis of cavities is given.

Impedance, when defined in the conventional manner as the ratio of voltage to current, loses its meaning in connection with waveguides because of the lack of terminals at which these quantities can be measured. It turns out, however, that the ratio of the transverse component of the electric field to the transverse component of the magnetic field is constant over any cross section of a waveguide and has the physical dimensions of an impedance. This ratio can be substituted, for most practical purposes, for the impedance as defined in the conventional manner. In particular, this ratio has the same functional properties with respect to frequency as regular impedance functions, that is, it obeys the same restrictions and follows the same theorems.

The only limitations to such a concept of impedance is that two such impedances cannot be compared when they are measured in different guides. This limitation, however, has no practical importance since such a situation never arises. In fact, the behavior of a network depends only on the relative values of the impedances measured at the same pair of terminals and never on the relative values of impedances measured at different pairs of terminals. A proof of this fact for the case of a two-terminal-pair network is given in Sec. 9-3. For further discussion of the physical meaning of waveguide impedance the reader is referred to Vol. 8.

According to the above definition of impedance, the characteristic impedance of a waveguide becomes the ratio of the transverse component of the electric field to the transverse component of the magnetic field for matched conditions, that is, when no standing wave is present in the guide. This ratio, which is also called the "wave impedance," can be expressed in the case of *TE*-modes as follows:

$$Z_0 = \sqrt{\frac{\mu}{\epsilon}} \frac{1}{\sqrt{1 - \left(\frac{\omega_c}{\omega}\right)^2}}, \quad (94)$$

where ω_c is the cutoff frequency of the guide.

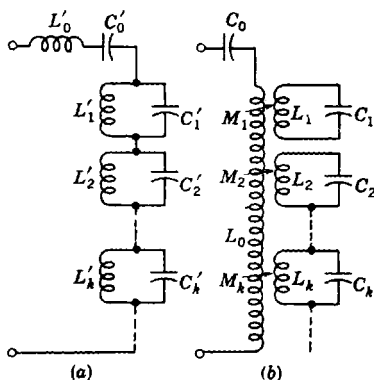


FIG. 10-36.—Equivalent circuits of a cavity resonator.

It is common practice in transmission-line work to normalize any impedance with respect to the characteristic impedance of the line in which such impedance is measured. The same practice is followed in the case of waveguides. It should be remembered, however, that since in this case the characteristic impedance is an irrational function of frequency, the normalized impedance does not have the same functional behavior as regular impedance functions.

The foregoing considerations on the meaning of impedance in waveguides permit the discussion of the frequency behavior of cavities without any limitation on the type of terminals. Consider first the case of a cavity with a single input line. Foster's reactance theorem^{19,20} states that the input reactance $X(\omega)$ of any two-terminal reactive network can be represented in the form shown in Fig. 10-36a. When this theorem is applied to a lossless cavity, each tuned circuit of the equivalent network corresponds to one of the resonance frequencies of the cavity, that is, one of the frequencies at which the input reactance becomes infinite.

The reactance of the cavity can then be written

$$X(\omega) = \omega L'_0 - \frac{1}{\omega C'_0} + \sum_{k=1}^{\infty} \frac{\omega}{C'_k(\omega_k^2 - \omega^2)}. \quad (95)$$

The values of the parameters are given by the expression

$$C'_k = \frac{1}{2} \left[\frac{dB(\omega)}{d\omega} \right]_{\omega=\omega_k}, \quad C'_0 = \left[\frac{dB(\omega)}{d\omega} \right]_{\omega=0}, \quad (96)$$

$$L'_0 = \left[\frac{d \left(X(\omega) - \frac{1}{\omega C'_0} \right)}{d\omega} \right]_{\omega=0} - \sum_{k=1}^{\infty} L'_k, \quad (97)$$

$$L'_k = \frac{1}{C'_k \omega_k^2}, \quad (98)$$

where $B(\omega)$ is the input susceptance of the cavity.

Another form of equivalent network is shown in Fig. 10-36b. The reactance $X(\omega)$ can be written in terms of the parameters of this network as follows:

$$X(\omega) = \omega L_0 - \frac{1}{\omega C_0} + \sum_{k=1}^{\infty} \frac{\omega^3 M_k^2}{L_k(\omega_k^2 - \omega^2)} = \omega L_0 - \frac{1}{\omega C_0} + \sum_{k=1}^{\infty} \left(\frac{\omega}{\omega_k} \right)^2 \frac{\omega}{C'_k(\omega_k^2 - \omega^2)}, \quad (99)$$

where

$$L_0 = L'_0 + \sum_{k=1}^{\infty} L'_k = \left[\frac{d \left(X(\omega) - \frac{1}{\omega C_0} \right)}{d\omega} \right], \tag{100}$$

$$\frac{L_k}{M_k^2} = \omega_k^2 C'_k = \frac{\omega_k^2}{2} \left[\frac{dB(\omega)}{d\omega} \right]_{\omega=\omega_k}, \tag{101}$$

$$C_k = \frac{1}{\omega_k^2 L_k}; \quad C'_0 = C'_0 = \left[\frac{dB(\omega)}{d\omega} \right]_{\omega=0} \tag{102}$$

The k th term of the summation of Eq. (99) is the reactance of the k th resonant loop reflected in the primary loop through the mutual inductance M_k . It is physically clear that, given any arbitrary value ω' of ω , at any frequency $\omega < \omega'$, the terms of the summation for which $\omega_k^2 \gg \omega'^2$ can be neglected. In fact, under these conditions the resonant loop is approximately an open circuit, and therefore the reactance reflected in the primary loop is negligible. For this reason, Eq. (99) and the corresponding network of Fig. 10-36b are preferable, in the case of distributed-constant systems, to Eq. (95) and the corresponding network of Fig. 10-36a. For a mathematical discussion of this question and of the convergence of the infinite summations of Eqs. (95) and (99), the reader is referred to the original paper by S. Schelkunoff,¹⁵ and to Vol. 8.

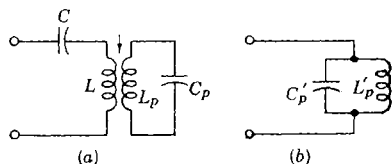


FIG. 10-37. Approximate circuits of a cavity resonator.

In most practical cases it is the behavior of a cavity in the vicinity of a resonance frequency ω_p , that is, of a pole of $X(\omega)$ that is of interest. By "vicinity" is meant a frequency band that is centered at ω_p and has a width small compared with ω_p and with the difference between ω_p and the adjacent resonance frequencies. Under these conditions all the terms of the summations in Eq. (99) either are negligible compared with the p th term or behave approximately like negative inductive reactances. The equivalent network reduces then to the one shown in Fig. 10-37a in which

$$C = C_0 \tag{103}$$

$$L = L_0 - \sum_{k=1}^{p-1} \frac{M_k^2}{L_k \omega_k^2} \tag{104}$$

If one step further is taken by neglecting the reactances of C and L and the variation of ω/ω_k , the equivalent network of Fig. 10-37b is obtained; its reactance is simply the p th term of the summation in Eq. (95).

Consider now the case of a cavity with input and output couplings. The cavity becomes then a two-terminal-pair network with an infinite number of natural modes of oscillation, that is, an infinite number of frequencies at which the open-circuit reactances X_{11} , X_{12} , X_{22} become infinite. If no dissipation is present, the extension of Foster's reactance theorem¹⁹ to the case of two-terminal-pair networks leads to the following expressions for the open-circuit reactances of a cavity:*

$$\left. \begin{aligned} X_{11}(\omega) &= \omega L_{10} - \frac{1}{\omega C_{10}} + \sum_{k=1}^{\infty} \frac{\omega^3 M_{1k}^2}{L_k(\omega_k^2 - \omega^2)}, \\ X_{22}(\omega) &= \omega L_{20} - \frac{1}{\omega C_{20}} + \sum_{k=1}^{\infty} \frac{\omega^3 M_{2k}^2}{L_k(\omega_k^2 - \omega^2)}, \\ X_{12}(\omega) &= \omega M_0 - \frac{1}{\omega C_{m0}} + \sum_{k=1}^{\infty} \frac{\omega^3 M_{1k} M_{2k}}{L_k(\omega_k^2 - \omega^2)}. \end{aligned} \right\} \quad (105)$$

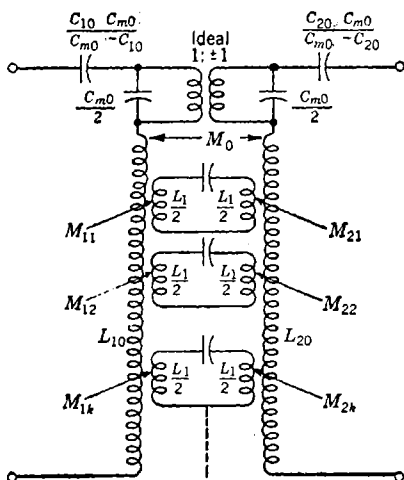


Fig. 10-38.—Equivalent circuit of a cavity with two pairs of terminals.

(101), and (102), namely,

The corresponding equivalent circuit is shown in Fig. 10-38. Each resonant loop is tuned to a natural frequency of the cavity and corresponds to one term in each of the summations of Eq. (105). The mutual inductance M_0 represents direct inductive coupling between the input and output terminals. The two capacitances $C_m/2$ together with the ideal transformer represent direct capacitive coupling between the input and output terminals.

The values of the elements in the equivalent network of Fig. 10-38 are given by equations similar in form to Eqs. (100),

* This analysis is based on the assumption either that only one mode of oscillation is associated with any resonance frequency of the cavity or, if several modes have the same resonance frequency, that these degenerate modes are coupled symmetrically to the input and output terminals. The case of degenerate modes asymmetrically coupled to the terminal can be considered as the limiting case of normal modes with almost equal resonance frequencies. This case, however, is rare since asymmetric couplings eliminate, in general, any preexistent degeneracy of modes.

$$\frac{L_k}{M_{1k}^2} = \frac{\omega_k^2}{2} \left(\frac{dB_{11}(\omega)}{d\omega} \right)_{\omega=\omega_k}, \quad (106)$$

$$\frac{L_k}{M_{2k}^2} = \frac{\omega_k^2}{2} \left(\frac{dB_{22}(\omega)}{d\omega} \right)_{\omega=\omega_k}, \quad (107)$$

$$\frac{L_k}{M_{1k}M_{2k}} = \frac{\omega_k^2}{2} \left(\frac{dB_{12}(\omega)}{d\omega} \right)_{\omega=\omega_k}, \quad (108)$$

$$C_{10} = \left(\frac{dB_{11}(\omega)}{d\omega} \right)_{\omega=0}, \quad L_{10} = \left[\frac{d \left(X_{11}(\omega) - \frac{1}{\omega C_{01}} \right)}{d\omega} \right]_{\omega=0}, \quad (109)$$

$$C_{20} = \left(\frac{dB_{22}(\omega)}{d\omega} \right)_{\omega=0}, \quad L_{20} = \left[\frac{d \left(X_{22}(\omega) - \frac{1}{\omega C_{02}} \right)}{d\omega} \right]_{\omega=0}, \quad (110)$$

$$C_{m0} = \left(\frac{dB_{12}(\omega)}{d\omega} \right)_{\omega=0}, \quad M_0 = \left[\frac{d \left(X_{12}(\omega) - \frac{1}{\omega C_{m0}} \right)}{d\omega} \right]_{\omega=0}, \quad (111)$$

where $B_{11} = -\frac{1}{X_{11}}$, $B_{22} = -\frac{1}{X_{22}}$, $B_{12} = -\frac{1}{X_{12}}$ are the open-circuit susceptances. As in the case of a cavity with a single pair of terminals, given any arbitrary value ω' of ω , for $\omega < \omega'$, the terms of the summations for which $\omega_k^2 \gg (\omega')^2$ can be neglected. Similarly, in the vicinity of any resonance frequency ω_p , the equivalent network reduces to the one shown in Fig. 10-39a. The parameters L_1 , C_1 , L_2 , C_2 are given by equations similar to Eqs. (103) and (104), whereas M and C_m are given by the expression

$$\left. \begin{aligned} M &= M_0 - \sum_{k=1}^{p-1} \frac{M_{1k}M_{2k}}{L_k} \\ C_m &= C_{m0}. \end{aligned} \right\} \quad (112)$$

If a further simplification is made by neglecting the reactances of L_1 , C_1 , L_2 , C_2 , M , and C_m , the equivalent circuit shown in Fig. 10-39b is obtained. The ideal transformer produces the required change of impedance level if the network is not symmetrical. The values of the elements are given by

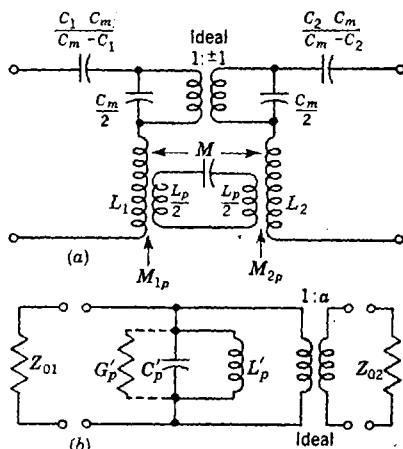


FIG. 10-39.—Approximate equivalent circuits of a cavity with two pairs of terminals.

$$C'_p = \frac{1}{\omega_p^2} \frac{L_p}{M_{1p}^2} = \frac{1}{2} \left(\frac{dB_{11}(\omega)}{d\omega} \right)_{\omega=\omega_p}, \quad L'_p = \frac{1}{\omega_p^2 C'_p} \quad (113)$$

$$a = \frac{M_{2p}}{M_{1p}} = \left(\frac{dB_{11}(\omega)}{d\omega} \right)_{\omega=\omega_p} \left(\frac{dB_{12}(\omega)}{d\omega} \right)_{\omega=\omega_p}^{-1} \quad (114)$$

The effect of incidental dissipation can be taken into account, to a first approximation, by inserting a series resistance R_k in every resonant loop of the equivalent circuit of Fig. 10-38. The value of R_k is usually expressed in terms of the Q of the cavity at the frequency ω_k by the relation

$$\frac{\omega_k L_k}{R_k} = Q_k, \quad (115)$$

where Q_k is defined as 2π times the ratio of the energy stored to the energy dissipated per cycle when the cavity oscillates at the k th natural frequency. The quantity Q_k can also be expressed in terms of the frequency behavior of the open-circuit impedances Z_{11} , Z_{22} , and Z_{12} . Let w_k be the difference between the frequencies on both sides of ω_k at which the square of the magnitude of any one of the three open-circuit impedances becomes one-half of its maximum value; then

$$Q_k = \frac{\omega_k}{w_k}. \quad (116)$$

It should be noted, however, that this equation is correct only if w_k is small compared with the difference between ω_k and the nearest resonance frequency of the cavity.

Dissipation is taken into account in the equivalent circuit of Fig. 10-39*b* by means of a shunt conductance G'_p given by

$$\frac{\omega_p C'_p}{G'_p} = Q_p. \quad (117)$$

It is common practice in dealing with a cavity resonator to express the elements of the equivalent circuits in a normalized form by means of the so-called "loaded Q 's." Let Z_{01} and Z_{02} be the characteristic impedances of the input and output lines respectively. The quantity $(Q_p)_{L1}$ is defined as the Q of the cavity at the frequency ω_p when a resistance equal to Z_{01} is connected to the input terminal. With reference to the equivalent circuit of Fig. 10-39*b*, which is exactly correct for $\omega = \omega_p$,

$$(Q_p)_{L1} = \omega_p C'_p Z_{01} = \frac{\omega_p Z_{01}}{2} \left[\frac{dB_{11}(\omega)}{d\omega} \right]_{\omega=\omega_p} = \frac{Z_{01}}{\omega_p} \frac{L_p}{M_{1p}^2}. \quad (118)$$

$(Q_p)_{L2}$ is defined similarly as the Q of the cavity when a resistance equal to Z_{02} is connected to the output terminals. In this case

$$(Q_p)_{L2} = \omega_p C_p' \frac{Z_{02}}{a^2} = \frac{\omega_p Z_{02}}{2} \left[\frac{dB_{22}(\omega)}{d\omega} \right]_{\omega=\omega_p} = \frac{Z_{02}}{\omega_p} \frac{L_p}{M_{2p}^2}. \quad (119)$$

It follows that the Q of the cavity, when loaded on both sides, becomes

$$(Q_p)_L = \omega_p C_p' \frac{Z_{01} Z_{02}}{a^2 Z_{01} + Z_{02}} = \frac{(Q_p)_{L1} (Q_p)_{L2}}{(Q_p)_{L1} + (Q_p)_{L2}}. \quad (120)$$

Note that in defining these loaded Q 's it has been assumed implicitly that there is no dissipation inside the cavity. If the loaded Q 's were determined experimentally, instead of $(Q_p)_{L1}$, $(Q_p)_{L2}$ the following values would be obtained:

$$(Q'_p)_{L1} = \frac{Q_p (Q_p)_{L1}}{Q_p + (Q_p)_{L1}} \quad (121)$$

$$(Q'_p)_{L2} = \frac{Q_p (Q_p)_{L2}}{Q_p + (Q_p)_{L2}}. \quad (122)$$

In conclusion, the behavior of a cavity in the vicinity of a resonance frequency ω_0 is determined by three parameters, namely, Q_0 , Q_{L1} and Q_{L2} . The subscript p has been dropped since from now on the behavior of cavities in the vicinity of only one resonance frequency will be considered.

10-7. Design of Cavity Resonators.—Of all the various types described, only the simple cylindrical cavity, the reentrant cylindrical cavity, and the rectangular cavity need be considered. These types satisfy, in general, the size and weight requirements imposed on filters and can be manufactured by simple processes.

The unloaded Q of a cavity is determined by the volume-to-surface ratio of the cavity, the mode excited, and the resistivity of the surface. In designing simple resonant cavities for filters, it is desirable, if possible, to have only one resonance frequency lying within the frequency range of interest. In general, this procedure sets an upper limit on the size of the cavity and consequently on the Q_0 of the cavity for a given surface material. In some cases a compromise must be effected, since to reduce the dissipative loss in the filter to a minimum, Q_0 should be as large as possible.

For quantitative illustration, consider the use of a symmetrical cavity as a selective transmission device. Let the input and output lines be properly terminated in their characteristic impedance Z_0 . An approximate equivalent circuit for the system is shown in Fig. 10-40a. The voltage source E_s in series with the line impedance Z_0 is transformed into an equivalent current source shunted by Z_0 as shown in Fig. 10-40b. The ratio of the power delivered to the load to the power available from the source behaves with frequency as a simple resonance curve, as shown in Fig. 10-41. The ratio of the mean frequency ω_0 to the difference w between the two half-power frequencies is, by definition, equal to Q'_L ,

the Q of the dissipative cavity when loaded on both sides by Z_0 . If Q_0 is the unloaded Q of a symmetrical cavity, for the insertion loss L at resonance

$$L = 20 \log_{10} \left(1 + \frac{Q_L}{Q_0} \right). \quad (123)$$

In view of the relation between Q_L and bandwidth, it is clear that losses are more important in narrow-band filters.

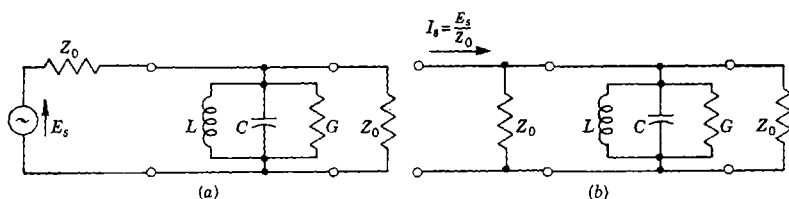


FIG. 10-40.—Two equivalent circuits of a cavity loaded on both sides.

From the foregoing discussion, it is evident that to change the effective bandwidth of a cavity, the coupling to the cavity must be altered. The exact manner in which this may be done depends on the type of coupling used, which in turn is largely dependent on system requirements.

In many cases, it is convenient to make a cavity resonator by placing two irises in a section of rectangular waveguide. This procedure has the advantage of permitting the theoretical calculation of the size of

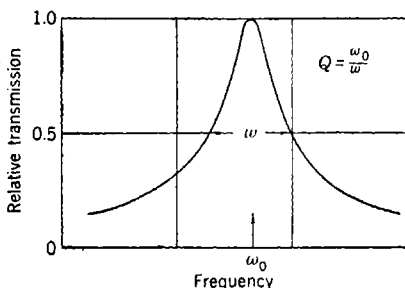


FIG. 10-41.—A simple resonance curve.

irises required for a given loaded Q . In waveguides, inductive irises are almost always used as couplings. These are superior to capacitive irises from the point of view of both loss and power-handling capacity. Even more important, perhaps, is the fact that for a given amount of coupling, the opening for an inductive iris is always bigger than for the corresponding capacitive iris, and

hence the inductive iris is easier to make. For instance, a normalized susceptance of 10 in a 1- by $\frac{1}{2}$ -in. waveguide requires a gap size in a capacitive iris of 0.004 in. whereas the opening in a symmetrical inductive iris with the same susceptance is approximately 0.25 in. For similar mechanical reasons, the symmetrical inductive iris is preferred to the asymmetrical iris. Moreover, the second mode excited by a symmetrical iris in a rectangular guide is the TE_{30} -mode whereas the asymmetrical iris excites the TE_{20} -mode also.

It is possible to calculate by simple formulas, as shown below, the normalized susceptance required for a rectangular cavity with a given loaded Q . From the normalized susceptance the size of the inductive iris required may be calculated. It is important to take into account the thickness of the iris since this has an appreciable effect on the normalized susceptance and hence on the loaded Q . Figure 10-42 shows a theoretical curve of the loaded Q as a function of iris size when zero iris thickness is assumed, and a similar experimental curve for irises $\frac{1}{32}$ in. thick in a 1- by $\frac{1}{2}$ -in. guide.

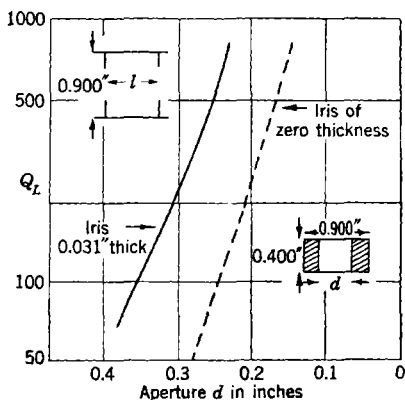


FIG. 10-42.—Loaded Q as a function of iris size for rectangular cavity in 1- by $\frac{1}{2}$ -in. guide.

If the cavity is made of rectangular

waveguide with completely closed ends, the resonance frequency occurs when the length of the cavity is equal to $\lambda_g/2$. When the coupling irises are introduced, however, the length of the cavity must be reduced to maintain the same resonance frequency. For stronger couplings, that is, larger iris openings, the shortening required is correspondingly greater. Figure 10-43 shows this relation for cavities made from 1- by $\frac{1}{2}$ -in. rectangular waveguide using $\frac{1}{32}$ -in. inductive irises. It is obviously impossible to build a cavity whose resonance frequency is exactly equal to a specified value. Therefore, it is considered good practice to make the distance between the irises slightly shorter than required and to provide a capacitive tuning screw which can be used to tune the cavity over a 10 per cent frequency band. If the screw is placed at the center of the cavity where the currents are a minimum, it introduces only a slight additional loss.

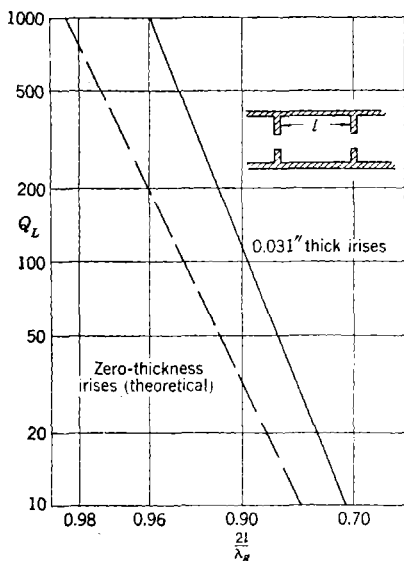


FIG. 10-43.—Foreshortening of rectangular waveguide cavity as function of loaded Q .

The final form of such a cavity constructed from 1- by $\frac{1}{2}$ -in. rectangular waveguide and designed to resonate at 3.3 cm is shown in Fig. 10·44.

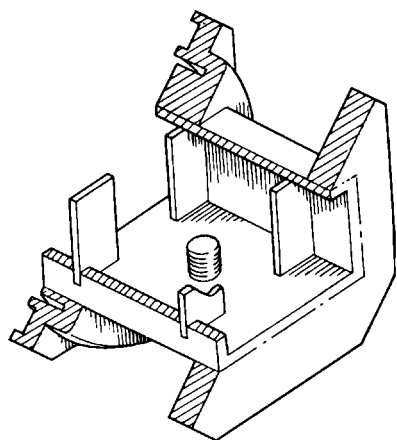


FIG. 10·44.—Rectangular cavity resonator.

In order to illustrate the general remarks made above it appears worth while to give the design calculations for this cavity as an example of the required procedure. Furthermore, these calculations will offer the opportunity of pointing out the effects of certain approximations currently made in the design of cavities.

The arrangement of two inductive irises in a rectangular waveguide and its equivalent circuit are shown schematically in Fig. 10·45*a* and Fig. 10·45*b*. Let b be the normalized susceptance of either iris.

The length l of the section of guide

can be determined by making the open-circuit input susceptance (not normalized) equal to zero for $\omega = \omega_0$. For B_{11}

$$B_{11} = \sqrt{\frac{\epsilon}{\mu}} \sqrt{1 - \left(\frac{\omega_c}{\omega}\right)^2} \left[b + \frac{b + \tan\left(\frac{l}{c} \sqrt{\omega^2 - \omega_c^2}\right)}{1 - b \tan\left(\frac{l}{c} \sqrt{\omega^2 - \omega_c^2}\right)} \right] \quad (124)$$

Therefore, the proper length l is given by the expression

$$\tan \frac{l}{c} \sqrt{\omega_0^2 - \omega_c^2} = \frac{2b_0}{b_0^2 - 1} \quad (125)$$

where b_0 is the value of b for $\omega = \omega_0$. To determine the loaded Q 's of the cavity, the slope of B_{11} for $\omega = \omega_0$ must first be computed. If Q_L is larger than 100; it is reasonable to neglect the frequency variation of b . On the basis of this assumption, from Eqs. (124) and (125) there is obtained the equation

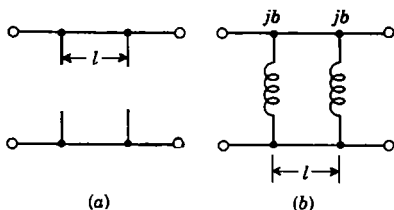


FIG. 10·45.—A simple rectangular cavity in waveguide and its transmission-line equivalent.

$$\left(\frac{dB_{11}}{d\omega}\right)_{\omega=\omega_0} = \sqrt{\frac{\epsilon}{\mu}} \frac{b_0^2 + 1}{\sqrt{\omega^2 - \omega_c^2}} \tan^{-1} \frac{2b_0}{b_0^2 - 1} \quad (126)$$

The loaded Q of the cavity is then, from Eq. (120),

$$Q_L = \frac{b_0^2 + 1}{4 \left[1 - \left(\frac{\omega_c}{\omega_0} \right)^2 \right]} \tan^{-1} \frac{2b_0}{b_0^2 - 1}. \quad (127)$$

For large values of b_0 this equation becomes approximately

$$Q_L = \frac{\pi}{4} \frac{b_0^2}{1 - \left(\frac{\omega_c}{\omega_0} \right)^2}. \quad (128)$$

Thus, to a first approximation, Q_L varies quadratically with b_0 .

The design of an inductive iris for a given b_0 is straightforward. For an infinitely thin symmetrical iris there is the approximate relation

$$b_0 = -2 \frac{\omega_c}{\omega_0} \frac{1}{\sqrt{1 - \left(\frac{\omega_c}{\omega} \right)^2}} \cot^2 \frac{\pi d}{2a} \quad (129)$$

where d is the opening of the iris and a is the width of the guide. Substitution of Eq. (129) in Eq. (128) yields

$$Q_L = \frac{\pi}{\left(\frac{\omega_0}{\omega_c} - \frac{\omega_c}{\omega_0} \right)^2} \cot^4 \frac{\pi d}{2a}. \quad (130)$$

Thus, for sufficiently small values of d/a , Q_L is proportional to d^{-4} . This relation reveals how critical are the iris dimensions for large values of Q_L . Equation (128), on the other hand, points to the necessity of correcting Eq. (129) to take into account the thickness of the irises.

The amount of loss at resonance may be calculated from Eq. (123). For instance, a cavity with a Q_0 of 10,000 and a loaded Q_L of 100 has a loss at resonance of only 0.08 db; but if Q_L is increased to 500, the corresponding loss is 0.42 db.

It is interesting to compare the above results with the insertion loss computed from the elements of the $\alpha\beta\mathcal{C}\mathcal{D}$ matrix of the system. For the matrix elements

$$\left. \begin{aligned} \alpha &= \mathcal{D} = \cos \theta - b_0 \sin \theta, \\ \beta &= j \sin \theta, \\ \mathcal{C} &= j[(1 - b_0^2) \sin \theta + 2b_0 \cos \theta] \end{aligned} \right\} \quad (131)$$

where

$$\theta = \frac{l}{c} \sqrt{\omega^2 - \omega_c^2}. \quad (132)$$

Consequently, it is found that for the insertion loss

$$L = 10 \log_{10} \left[1 + \frac{b_0^2}{4} (2 \cos \theta - b_0 \sin \theta)^2 \right]. \quad (133)$$

Since perfect transmission is obtained for

$$\tan \theta = \frac{2}{b_0}, \quad (134)$$

the proper value of l is given by

$$\tan \frac{l}{c} \sqrt{\omega_0^2 - \omega_c^2} = \frac{2}{b_0}. \quad (135)$$

The apparent disagreement between this equation and Eq. (125) results from the implicit assumption that perfect transmission through the cavity occurs at the resonance frequency ω_0 as the equivalent circuit of Fig. 10-39b would indicate. This equivalent circuit, however, neglects, in our case, the reactances $\omega_0 L_1 = \omega_0 L_2 = -Z_0/b_0$ (see Fig. 10-32b). It can be shown that these reactances shift the frequency of perfect transmission from ω_0 to

$$\omega'_0 = \omega_0 \left[1 - \frac{b_0}{2Q_L(1 + b_0^2)} \right]. \quad (136)$$

The bandwidth w' between the half-power points of the transmission curve becomes

$$w' = \frac{w'_0}{Q_L} \frac{b_0^2}{1 + b_0^2}. \quad (137)$$

For large values of b_0 these corrections are evidently negligible and Eqs. (125), and (135) lead to identical results for any practical purposes.

Consider now a rectangular cavity asymmetrically loaded. Let b_1 and b_2 be the normalized susceptances of the input and output irises respectively, and l the distance between the two irises. For B_{11} and B_{22}

$$B_{11} = \sqrt{\frac{\epsilon}{\mu}} \sqrt{1 - \left(\frac{\omega_0}{\omega}\right)^2} \left[b_1 + \frac{b_2 + \tan\left(\frac{l}{c} \sqrt{\omega^2 - \omega_c^2}\right)}{1 - b_2 \tan\left(\frac{l}{c} \sqrt{\omega^2 - \omega_c^2}\right)} \right], \quad (138)$$

$$B_{22} = \sqrt{\frac{\epsilon}{\mu}} \sqrt{1 - \left(\frac{\omega_0}{\omega}\right)^2} \left[b_2 + \frac{b_1 + \tan\left(\frac{l}{c} \sqrt{\omega^2 - \omega_c^2}\right)}{1 - b_1 \tan\left(\frac{l}{c} \sqrt{\omega^2 - \omega_c^2}\right)} \right]. \quad (139)$$

For $\omega = \omega_0$ both B_{11} and B_{22} must vanish. It follows that the proper length of the cavity is given by

$$\tan \frac{l}{c} \sqrt{\omega_0^2 - \omega_c^2} = \frac{b_1 + b_2}{b_1 b_2 - 1}. \quad (140)$$

The slopes of B_{11} and B_{22} at their common zero are given by

$$\left(\frac{dB_{11}}{d\omega}\right)_{\omega=\omega_0} = \sqrt{\frac{\epsilon}{\mu}} \frac{b_1^2 - 1}{\sqrt{\omega_0^2 - \omega_c^2}} \tan^{-1} \frac{b_1 + b_2}{b_1 b_2 - 1} \quad (141)$$

$$\left(\frac{dB_{22}}{d\omega}\right)_{\omega=\omega_0} = \left(\frac{dB_{11}}{d\omega}\right)_{\omega=\omega_0} \frac{b_2^2 + 1}{b_1^2 + 1} \quad (142)$$

The loaded Q 's of the cavity are then

$$Q_{L1} = \frac{b_1^2 + 1}{2 \left[1 - \left(\frac{\omega_c}{\omega_0}\right)^2 \right]} \tan^{-1} \frac{b_1 + b_2}{b_1 b_2 - 1} \quad (143)$$

$$Q_{L2} = Q_{L1} \frac{b_2^2 + 1}{b_1^2 + 1} \quad (144)$$

These equations can be further simplified for large values of b_1 and b_2 as in the case of symmetrical cavities.

A design procedure similar to the one just described can be followed when a circular waveguide is used instead of a rectangular waveguide. In this case circular irises are recommended.

In some cases it is desirable to use other types of cavities with rectangular waveguide feeds. Irises are still used as coupling elements although theoretical design is usually impossible since the field distribution is not, in general, the same on the two sides of an iris, and the correct coupling must be determined empirically. For obvious reasons of a mechanical nature, circular irises are preferred to inductive irises. An example of the use of circular irises is shown in Fig. 10-62.

To connect a cavity to a coaxial line, three types of coupling devices may be used, namely, loops, probes, and irises. These three methods of coupling are illustrated schematically in Fig. 10-46. The cavities shown in this figure are of the reentrant cylindrical type. They may be considered, roughly, as sections of coaxial lines short-circuited at one end and loaded with a capacitance at the other end. From the point of view of reproducibility, the iris and probe couplings are to be preferred. However, the loop coupling presents considerable advantages when the coupling has to be adjusted after assembly. In fact, the coupling can be varied very easily by rotating the plane of the loop with respect to the cavity.

The introduction of the coupling elements in a cavity alters the resonance frequency by a small but unpredictable amount. For this reason, as in waveguides, it is general practice to provide a method for tuning the cavity to the desired frequency after assembly. This tuning can be accomplished in reentrant cavities by making the length of the center conductor adjustable. A cavity with loop couplings and adjustable-screw tuning is shown in Fig. 10-47. This cavity can be tuned over

more than a 10 per cent band at about 3000 Mc/sec. Its Q_0 is about 5000 and the loaded Q with the loop size shown is about 500. The resulting transmission loss at resonance is about 0.5 db.

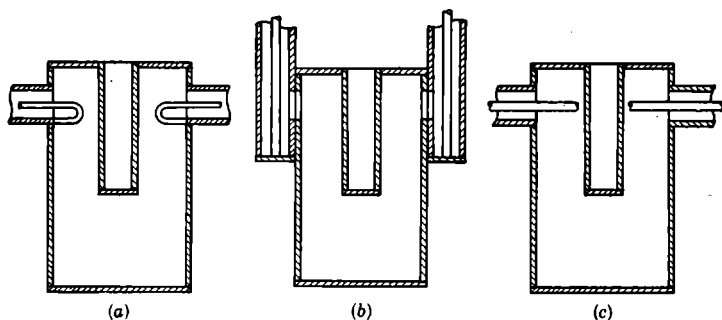


FIG. 10-46.—Alternative couplings to a reentrant cylindrical cavity.

The main disadvantages of a cavity resonator are its size and weight. In many cases where a loaded Q of less than 30 to 40 is sufficient, it is possible, by replacing cavities with resonant irises, to reduce the weight and space required. These irises behave like parallel-tuned circuits in shunt to the line and, therefore, may be considered as combinations of

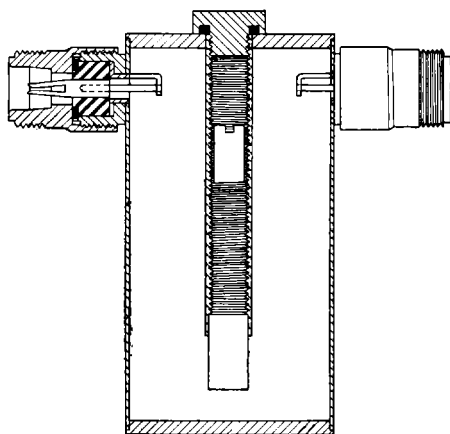


FIG. 10-47.—A reentrant cylindrical cavity resonator with loop couplings and provision for tuning.

inductive and capacitive irises. Several types of such irises may be used, the most common of which are illustrated schematically in Fig. 10-48.

The saving in space and weight associated with the use of a resonant iris results from the fact that the waveguide is used to store the energy associated with the iris, while still performing its function as link to other

components of the system. However, since the ratio of the effective volume to the surface is always smaller for an iris than for a cavity with the same loaded Q , the dissipative losses in the iris will always be greater. Thus, the use of resonant irises is restricted to values of loaded Q sufficiently small to keep the transmission loss within reasonable limits. On the other hand, the design of cavities becomes rather difficult when small loaded Q 's of the order of magnitude of 50 are desired because the coupling element becomes a major portion of the cavity. It follows that resonant irises are complements to cavities rather than substitutes for them. Their application in the design of broadband waveguide filters will make this fact more evident.

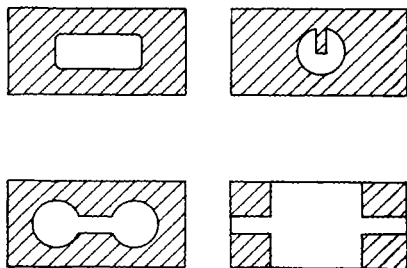


FIG. 10-48.—Simple resonant irises.

10-8. Theory of Direct-coupled Cavities.—In many applications, a simple resonant cavity does not provide sufficient off-band attenuation for a given maximum insertion loss in the pass band. Consequently, it is appropriate to inquire how more satisfactory characteristics may be obtained by using a chain of cavities directly coupled to one another. It has been pointed out previously that such a system resembles the well-known lumped-element structure characteristic of narrow-band filters. The following analysis will show that microwave filters consisting of a chain of cavities all tuned to the same frequency can actually be derived without difficulty from corresponding lumped-element filters.

Each cavity in a chain can be represented in the vicinity of its resonance frequency ω_0 by an equivalent circuit of the type shown in Fig. 10-39*a*. For simplicity, any direct coupling between input and output terminals will be neglected. Furthermore, since narrow-band filters are under consideration, the frequency dependence of all nonresonant reactances such as those resulting from mutual inductances will be neglected. It follows that the actual nature of such a nonresonant reactance is immaterial. For the sake of simplicity, these reactances will be indicated schematically as inductances.

On the basis of the above assumptions, the equivalent circuit for a chain of cavities takes the form shown in Fig. 10-49*a*. The reactance X_k is the coupling reactance $\omega_0 M_k$ between the k th cavity and the preceding one. X_s and X_L are the reactances of the input and output loops respectively. All elements of the network are normalized with respect to the terminating resistances, or, in other words, the network is designed to operate between 1-ohm terminations.

$$+ \frac{1}{\frac{ZX_1^2 X_3^2 \cdots X_{n-1}^2}{X_2^2 X_4^2 \cdots X_n^2}} + \frac{1}{(1 + jX_L) \frac{X_2^2 X_4^2 \cdots X_n^2}{X_1^2 X_3^2 \cdots X_{n+1}^2}}$$

If n is odd, the last terms of this equation become

$$+ \frac{1}{\frac{ZX_1^2 X_3^2 \cdots X_{n-2}^2}{X_2^2 X_4^2 \cdots X_{n-1}^2}} + \frac{1}{\frac{ZX_2^2 X_4^2 \cdots X_{n-1}^2}{X_1^2 X_3^2 \cdots X_n^2}} + \frac{1}{(1 + jX_L) \frac{X_1^2 X_3^2 \cdots X_n^2}{X_2^2 X_4^2 \cdots X_{n+1}^2}} \quad (148)$$

Consider now the prototype low-pass ladder structure shown in Fig. 10-49b; its cutoff frequency is 1 radian/sec. The input impedance Z'_1 of this filter terminated in a resistance R can also be expressed in the form of a continuous fraction. To avoid confusion with the ω used in connection with the bandpass filter, let ω' represent the frequency. For the impedance Z'_1

$$Z'_1 = \frac{1}{j\omega' C_1 + \frac{1}{j\omega' L_2 + \frac{1}{j\omega' C_3 + \cdots + \frac{1}{j\omega' C_{n-1} + \frac{1}{j\omega' L_n + R}}}}} \quad (149)$$

If the last element of the ladder of Fig. 10-49b were a condenser, that is, if the total number n of elements were odd, the last terms of Eq. (149) would become

$$+ \frac{1}{j\omega' L_{n-1} + \frac{1}{j\omega' C_n + \frac{1}{R}}} \quad (150)$$

It has been shown in Sec. 9-8 that a prototype low-pass filter with a 1-radian/sec cutoff frequency can always be transformed into a bandpass filter by means of the change of variable

$$\omega' = \frac{\omega_0}{w} \left(\frac{\omega}{\omega_0} - \frac{\omega_0}{\omega} \right), \quad (151)$$

where ω_0 is the mean frequency of the bandpass filter and w is its bandwidth. If this change of variable is introduced in Eqs. (149) and (150), the reactances and susceptances appearing in the continuous fraction expansion of Z'_1 are transformed as follows:

$$j\omega' L_{2k} \rightarrow j \frac{L_{2k}}{w} \omega_0 \left(\frac{\omega}{\omega_0} - \frac{\omega_0}{\omega} \right) \quad (152)$$

$$j\omega' C_{2k+1} \rightarrow j \frac{C_{2k+1}}{w} \omega_0 \left(\frac{\omega}{\omega_0} - \frac{\omega_0}{\omega} \right), \quad (153)$$

where k is any positive integer. With reference to Eq. (145), these reactances and susceptances can be identified with those appearing in the continuous-fraction expansion for the input impedance of the chain of cavities. This identification yields the relations

$$\frac{L_{2k}}{w} = L \frac{X_1^2 X_3^2 \cdots X_{2k-1}^2}{X_2^2 X_4^2 \cdots X_{2k}^2} \quad (154)$$

$$\frac{C_{2k+1}}{w} = L \frac{X_2^2 X_4^2 \cdots X_{2k}^2}{X_1^2 X_3^2 \cdots X_{2k+1}^2} \quad (155)$$

These two equations yield the following expressions for the coupling reactances:

$$X_1^2 = \frac{L}{C_1} w \quad (156)$$

$$X_{2k}^2 = \frac{L_2}{L_{2k} C_{2k-1}} w^2 = X_1^2 \frac{C_1^2}{L_{2k} C_{2k-1}} \quad (157)$$

$$X_{2k+1}^2 = \frac{L_2}{L_{2k} C_{2k+1}} w^2 = X_1^2 \frac{C_1^2}{L_{2k} C_{2k+1}} \quad (158)$$

If for the moment the reactance X_L is neglected, the output-coupling reactance X_{n-1} is given by

$$\left. \begin{aligned} X_{n+1}^2 &= \frac{LR}{L_n} w = X_1^2 \frac{C_1}{L_n} R && \text{for } n \text{ even} \\ X_{n+1}^2 &= \frac{L}{RC_n} w = X_1^2 \frac{C_1}{C_n} \frac{1}{R} && \text{for } n \text{ odd.} \end{aligned} \right\} \quad (159)$$

The reactances X_s and X_L of Fig. 10-49a do not correspond to any elements of the prototype structure of Fig. 10-49b. They may be considered as stray reactances whose presence, however, is unavoidable. It will be seen, on the other hand, that since X_s and X_L are of the order of magnitude of $\sqrt{w/\omega_0}$, they are very small in the case of narrow-band filters.

The determination of the effects of these stray reactances on the characteristics of the filter presents the same problem as the determination of the effects of mismatched terminations, which has been discussed in Sec. 9-27. It is found that because of the presence of X_s and X_L , the VSWR in the input line is multiplied or divided by a factor equal, at most, to the product of the VSWR's produced by the two stray reactances if they were placed separately in a properly terminated line. If both X_s and X_L are small compared with unity, the maximum value of this factor is equal, approximately, to $1 + X_s + X_L$. It follows that

the resulting distortion of the insertion-loss curve is usually negligible in the attenuation band. In the pass band, on the other hand, the increase of VSWR may not be tolerable. The reflections arising from X_s and X_L , however, can usually be eliminated over a sufficiently broad band by inserting equal and opposite reflections in the manner discussed in Sec. 2-15.

The method of design described above applies to any filter of the type shown in Fig. 10-49. The values of the lumped elements in the prototype structure can be determined by following any one of the design procedures discussed in Chap. 9. The fact that the first element of the network of Fig. 10-49b is a shunt capacitance does not limit the generality of the method of design; any similar filter whose first element is a series inductance can be transformed into its dual whose first element is then a shunt

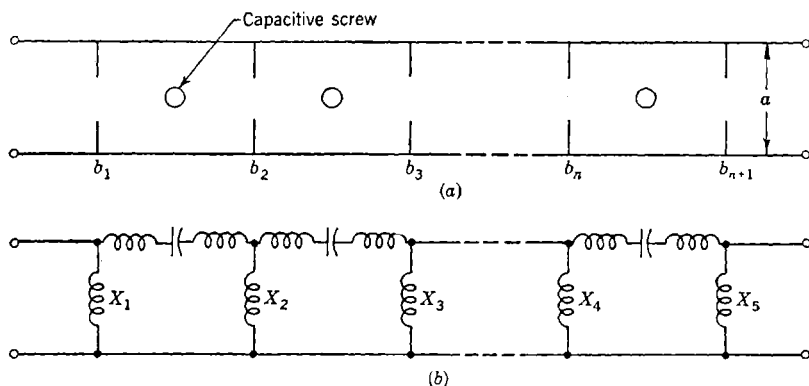


Fig. 10-50.—Chain of direct-coupled resonant cavities and equivalent circuit.

capacitance, as explained in Sec. 9-7. The power-transmission characteristics are not changed by such a transformation because dual networks have the same insertion loss.

The main limitation on the low-pass characteristics that can be obtained with a structure of the type shown in Fig. 10-49b is that no peak of infinite attenuation can exist at finite frequencies. Such a limitation, of course, applies also to the characteristics of the corresponding microwave filter but only in the frequency band in which the cavities can be considered as simple resonant circuits. It is likely that a similar method can be found for designing direct-coupled cavity filters with infinite peaks of attenuation near the pass band. However, no filter of this type has ever been designed.

A chain of direct-coupled cavities can be built by properly spacing inductive irises in a section of rectangular waveguide, as shown schematically in Fig. 10-50a. The values of the normalized susceptances b_1 , b_2 ,

... , b_n , b_{n+1} can be computed from Eqs. (156) to (159) inclusive with the help of Eqs. (106), (107), (141) and (142). If ω_0/w is larger than 100, to a good approximation

$$|b_1| = \left\{ \frac{2}{\pi} C_1 \frac{\omega_0}{\omega} \left[1 - \left(\frac{\omega_c}{\omega_0} \right)^2 \right] \right\}^{1/2}, \quad (160)$$

$$|b_{2k}| = b_1^2 \sqrt{\frac{L_{2k} C_{2k-1}}{C_1}}, \quad (161)$$

$$|b_{2k+1}| = b_1^2 \sqrt{\frac{L_{2k} C_{2k+1}}{C_1}}, \quad (162)$$

$$b_{n+1} = \left\{ \begin{array}{ll} b_1 \sqrt{\frac{L_n}{RC_1}} & \text{for } n \text{ even} \\ b_1 \sqrt{\frac{RC_n}{C_1}} & \text{for } n \text{ odd.} \end{array} \right\} \quad (163)$$

The lengths of the cavities are computed by means of Eq. (140). In practice, however, the irises are uniformly spaced and the cavities thus

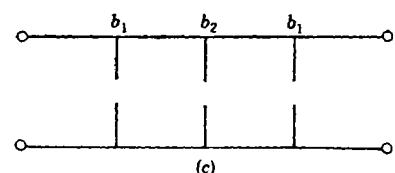
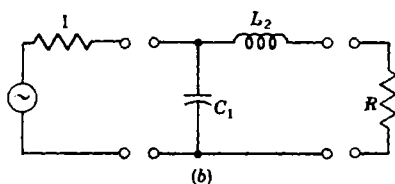
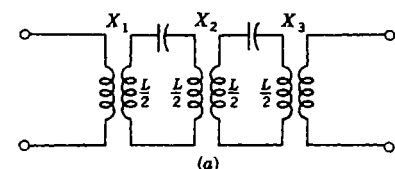


FIG. 10-51.—Two direct-coupled cavities, their equivalent circuit and the corresponding prototype structure.

formed are tuned separately to the frequency ω_0 by means of capacitive screws. An equivalent circuit for this chain of cavities is shown in Fig. 10-50b. This circuit is obtained from Fig. 10-49a by transforming the coupled coils into T-networks of inductances. This transformation places in evidence the fact, already clear from the above discussion, that the reactances of the irises are just the coupling reactances shown in Fig. 10-49a.

The design procedure discussed above is not limited, of course, to rectangular cavities. However, when other types of cavities are used, the dimensions of the coupling irises must be determined experimentally since no design equations are available.

10-9. Filters Employing Direct-coupled Cavities.—The simplest type of cavity filter consists, of course, of two direct-coupled cavities. The equivalent circuit shown in Fig. 10-51a is of the familiar double-tuned type. By varying the cou-

pling between the resonant loops in this circuit, the well-known transmission curves plotted in Fig. 10-52 may be obtained.

The two-cavity filter may be derived from the prototype structure shown in Fig. 10-51b. If

$$L_1 = C_2 = R = 1,$$

this structure becomes identical to the constant- k half section discussed in Sec. 9-10. The power ratio for this half section was found to be

$$\frac{P_0}{P_L} = 1 + \omega^4. \quad (164)$$

The condition $L_1 = C_2 = R = 1$ corresponds, then, to critical coupling.

If rectangular cavities are used, the irises can be designed theoretically, as explained above. With reference to Fig. 10-51c from Eqs. (160) and (151),

$$|b_1| = \sqrt{\frac{2}{\pi} \frac{\omega_0}{w} \left[1 - \left(\frac{\omega_c}{\omega_0} \right)^2 \right]}, \quad (165)$$

$$|b_2| = b_1^2. \quad (166)$$

A filter of this type has been designed and built by Fox. The dimensions of the filter are given in Fig. 10-53 for a mean frequency equal to 3000

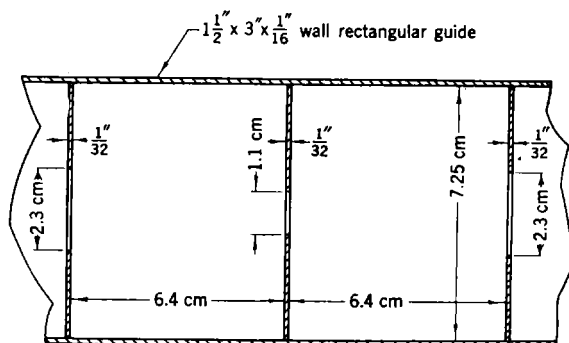


FIG. 10-53.—A bandpass filter consisting of two rectangular cavities, direct-coupled. (After Fox.)

Mc/sec and a bandwidth equal, approximately, to 1 per cent. Apart from a midband loss (due to dissipation) of 0.6 db, the general behavior of the filter follows the theoretical curve so closely that no useful purpose is served by reproducing the experimental curve.

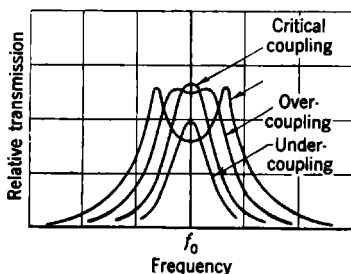


FIG. 10-52.—Effect of coupling on transmission through double-tuned circuits.

A different example of critical cavity coupling is afforded by the design of Cork and Clark¹² illustrated in Fig. 10-54. This filter is an engineered version of two reentrant cavities with iris couplings and coaxial terminals. In order to obtain a ratio ω_0/w between 85 and 105, it was found necessary to open the input iris until it extended the full height of the cavity. Likewise, to obtain critical coupling, the coupling iris also had to be extended the full height of the cavity. The consequent shape with reentrant cylindrical cavities was so grotesque that the rectangular shape shown in the final design was adapted to facilitate manufacture. Figure 10-55 shows the rough form of the filter for both cylindrical and rectangular shapes and illustrates the development. For practical reasons, it was also found desirable to bend the inner conductor of the input and output lines through 90°. These couplings thus appear more like loops than irises in the final design.

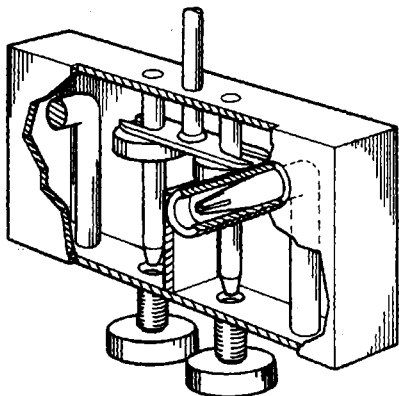


FIG. 10-54.—Tunable bandpass filter consisting of two direct-coupled reentrant cavities. (After Cork and Clark.)

This filter was designed to have a resonant frequency adjustable from 950 to 1150 Mc/sec with a constant bandwidth over the range of adjustment. In order to accomplish this, it was necessary to provide a mechanism for ganged tuning the cavities. Of the various possibilities, metal-slug tuning was selected because of its freedom from sliding metal contacts and because of the linearity of tuning with displacement

of the slugs, which is illustrated in Fig. 10-56. A dielectric bridge serves to couple the tuning slugs and permits ganged tuning. The introduction of the slugs increases the dissipation in the cavities, but the extra loss is not excessive when the cavities are loaded sufficiently and may be minimized by proper design of the slugs. In order to adjust the cavities to the same resonance frequency initially, trimmer screws are provided.

As the cavities are tuned over the band from 950 to 1150 Mc/sec, it is found that the condition of critical coupling is not maintained. The cavities appear overcoupled at the high-frequency end and undercoupled at the low-frequency end. In order to compensate for this variation, the metal diaphragm was introduced. The resulting pass bands at the middle and at the edges of the tuning range are shown in Fig. 10-57.

The empirical design of such a filter by "bench" testing is an undertaking of no mean proportions. Many of the distances are very critical.

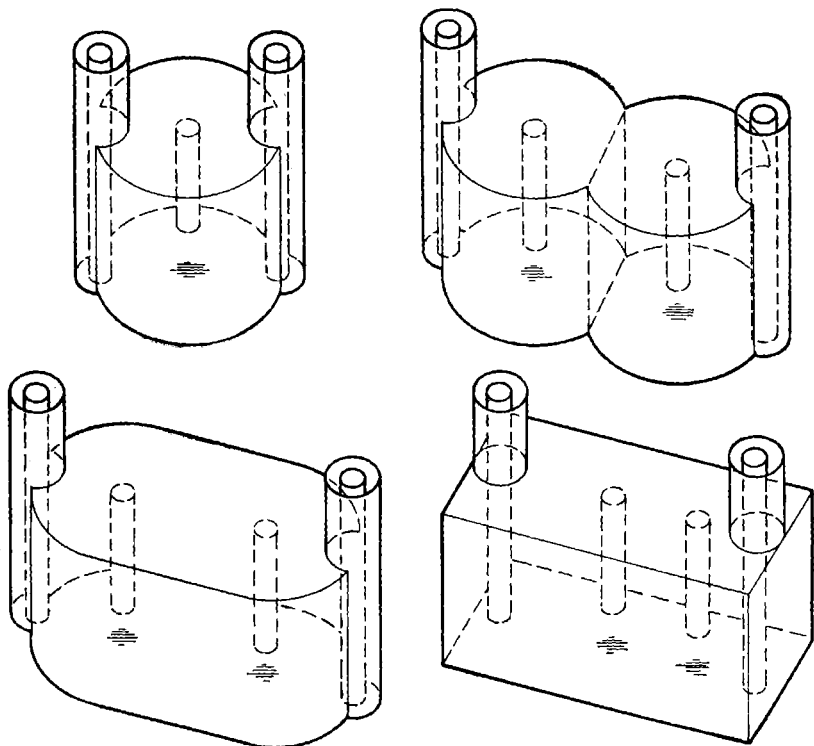


FIG. 10-55.—Successive stages in the development of the filter shown in Fig. 10-54.

For instance, it is evident from the plot of the input loaded Q of either cavity (Q_{L1}) against the separation of the input line and the cavity center line shown in Fig. 10-58 that a change in this distance of only 0.04 cm produces a change in Q_{L1} of about 10. The distance between cavity center lines is almost as critical. Thus, a change of 0.1 cm between cavity center lines alters the bandwidth by approximately 10 per cent. Other distances are much less critical. For instance, there is very little dependence of loaded Q on the length of the input and output irises. However, as in all coupled resonant circuits, the tuning of the

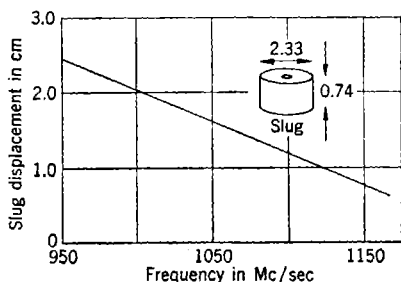


FIG. 10-56.—Resonant frequency of re-entrant cavity shown in Fig. 10-54 as a function of slug position.

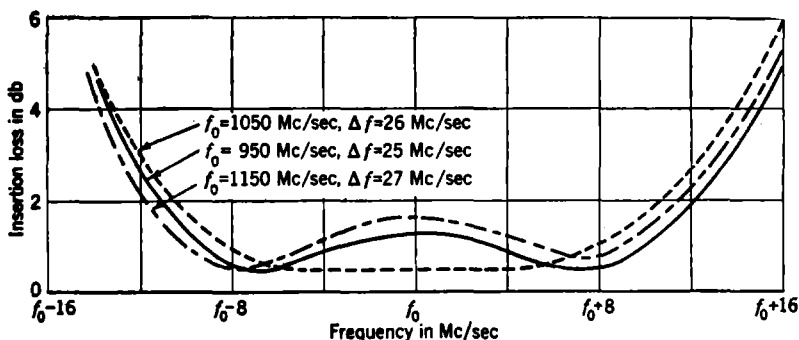


FIG. 10-57.—Bandpass characteristics of filter shown in Fig. 10-54 for various values of the mean frequency.

cavities is critical. For instance, if the trimmer screw is advanced by 0.011 in. in one cavity, the center of the filter pass band is shifted by 5 Mc/sec.

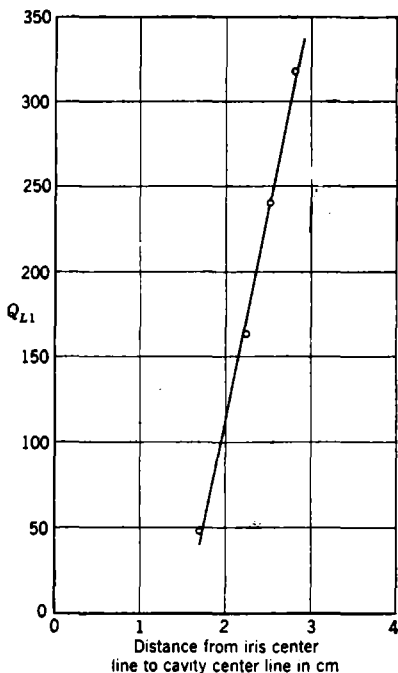


FIG. 10-58.—Dependence of Q_{L1} of the cavity shown in Fig. 10-54 on coupling.

In addition to the difficulties of manufacture imposed by close tolerances, other production problems are created by assembly requirements. Thus, it was decided to make the dielectric bridge from steatite, whose distortion temperature exceeds 1000°C, so that silver solder might be used in the final assembly. However, steatite is very hard and results in considerable wear on the cavity center conductor unless it is chromium-plated. Fortunately, in this case, the chromium does not introduce an excessive amount of loss since the pass band is relatively broad.

In actual practice, this filter is used as a duplexer by substituting a TR tube for one of the trimmer screws. The transmitter power and the local oscillator signal are applied to opposite ends of the filter through additional irises which are omitted from the drawing in the interests of simplicity. The two coaxial terminals are connected

to the antenna and mixer, respectively. Consequently, the desirable filter feature is high image rejection. Table 10-2 gives the attenuations observed for image frequencies 120 Mc/sec away from various signal frequencies in the tuning range. This filter has been described in somewhat greater detail than some of the others because it is one of the few filters that to date have been engineered for quantity production.

TABLE 10-2.—IMAGE REJECTION OF DIRECT-COUPLED FILTER

Signal frequency, Mc/sec	Image frequency, Mc/sec	Insertion loss, db
950	830	..
....	1070	48
1050	930	39
....	1170	52
1150	1030	38
....	1270	> 50

The two filters described above are adjusted for critical coupling. This adjustment, however, does not yield maximum bandwidth for given loss tolerances in the pass band and given sharpness of cutoff. The optimum design for frequency discrimination corresponds to overcoupling. The amount of overcoupling required depends on the tolerance allowed in the pass band. This question can best be investigated by studying the behavior of the power-loss ratio for the prototype low-pass structure of Fig. 10-51*b* for arbitrary values of R and C_1 . The value of L_2 cannot be specified independently if the cavity filter must be symmetrical. In fact, Eq. (159) yields for $X_1^2 = X_{n+1}^2$,

$$L_2 = RC_1. \quad (167)$$

When RC_1 is substituted for L_2 in the expression for the power ratio,

$$\frac{P_0}{P_L} = 1 + \frac{(1-R)^2}{4R} \left[\frac{C_1^2 R}{1-R} \omega^2 - 1 \right]^2. \quad (168)$$

This equation can be identified with Eq. (198) of Sec. 9-18 in which the Tchebysheff polynomial is $T_2(\omega)$. Since the coefficient of ω^2 must be equal to 2, the following relation must be satisfied by R and C_2 ,

$$C_1^2 = \frac{2(1-R)}{R}. \quad (169)$$

The tolerance of the power ratio in the pass band is then

$$\epsilon^2 = h^2 = \frac{(1-R)^2}{4R}. \quad (170)$$

Eqs. (167), (169), and (170) thus permit the design of a low-pass filter having a cutoff frequency equal to one radian/sec and a specified tolerance of ϵ^2 . The cutoff frequency is defined, in this case, as the maximum frequency at which the power ratio is within the specified tolerance. Since, as pointed out in Sec. 9-18, Tchebysheff polynomials yield maximum sharpness of cutoff for a given tolerance and a given cutoff frequency, an optimum design has been obtained.

For critical coupling, that is, for monotonic behavior of the ratio P_0/P_L , R must be equal to 1. Equation (168) becomes then

$$\frac{P_0}{P_L} = 1 + \frac{C_1^4}{4} \omega^4. \quad (171)$$

The tolerance for unity cutoff frequency is

$$\epsilon^2 = \frac{C_1^4}{4}. \quad (172)$$

It follows that for the same bandpass tolerance and the same bandwidth, the off-band insertion loss for an overcoupled filter is 6 db larger than for a critically coupled filter. Once the values of the elements of the prototype section are determined, the microwave filter can be designed by following the procedure discussed above.

The actual insertion loss of a two-cavity filter will depart from the predicted behavior because of dissipation in the cavities. The effect of dissipation is a distortion of the characteristics as well as a finite loss over the whole pass band. Nothing can be done, of course, about the loss. However, it can be shown that it is possible to correct approximately for distortion of the characteristics by substituting for C_1 , L_2 , R the values C'_1 , L'_2 , R' defined by

$$C'_1 = \frac{C_1}{(1 + \delta C_1)} \quad L'_1 = L_1(1 + \delta C_1) \quad R' = R(1 + \delta C_1)^2. \quad (173)$$

The loss factor δ depends on the unloaded Q_0 of the two cavities and on the ratio ω_0/w as follows:

$$\delta = \frac{1}{Q_0} \frac{\omega_0}{w}. \quad (174)$$

If these corrections are made, the actual power ratio will be equal to the theoretical power ratio in the absence of dissipation multiplied by the factor $(1 + \delta C_1)^2$. In other words, the final effect of dissipation will be a constant loss L_d given by the expression

$$L_d = 20 \log_{10} (1 + \delta C_1) \approx 8.7 \frac{\omega_0}{w} \frac{C_1}{Q_0}. \quad (175)$$

The design of direct-coupled cavity filters is straightforward. There are, however, several practical considerations that limit the usefulness of such filters. First of all, the tolerances on the dimensions of the coupling irises set a practical limit to the ratio ω_0/w . For instance, in rectangular cavities the susceptance of each coupling iris is about $(1/\pi)(\omega_0/w)$. It follows from Eq. (129) that in the case of a 1-by $\frac{1}{2}$ -in. rectangular waveguide for $\omega_0/w = 300$, a change of 0.005 in. in the opening of the iris would correspond approximately to a 10 per cent change of bandwidth. It is evident that such a tolerance in the dimensions of the irises would result in a considerable distortion of the characteristics of the filter.

A second practical difficulty arises from the fact that the individual cavities cannot be separately tested and adjusted before assembly. The lineup procedure after assembly becomes very complex if more than two or three cavities are used. These difficulties may be overcome through careful construction, but the manufacturing cost will be correspondingly high. A method of designing cavity filters that circumvents most of the limitations noted above is discussed in Sec. 10-11.

In the preceding sections, the direct coupling of modes in separate cavities has been considered. Before leaving the subject of direct coupling, it is worth while to consider the possibility of utilizing several modes in a single cavity. The next section is devoted to this topic.

10-10. Cavities Excited in More Than One Mode.—The reader will recall that a cavity resonator is inherently a complex reactive network as the equivalent circuit of Fig. 10-38 indicates. Therefore, the possibility of approximating the behavior of a complex lumped-element filter by means of a single-cavity resonator may be considered. Such a method of design would result obviously in a considerable saving of space and weight. Although very little research has been done up to the present along this line, it seems worth while to indicate a method of attack that may lead to useful results. A type of cavity that, alone, behaves like a two-cavity filter will also be described. An experimental model of such a cavity has been built by the authors and the results of the test are reported below.

According to Foster's reactance theorem, any two-terminal-pair reactive network can be represented in the form shown in Fig. 10-38 with the possible addition of arbitrary reactances in series with the input terminals. It can be shown, however, that most practical filters, and, in particular, the ones that have the optimum Tchebysheff behavior discussed in Secs. 9-18 and 9-19, do not require these additional series reactances. It follows that if the resonance frequencies of a cavity and the coupling to the different modes are successfully adjusted to coincide with the corresponding quantities for a lumped-element filter, the behavior of the filter will be approximated by the cavity over a limited frequency band.

As an illustration of this statement, consider the equivalent circuit of

the two-cavity filter shown in Fig. 10-59a. This circuit can be transformed into either one of the normal forms shown in Figs. 10-59b and 10-59c. The two normal frequencies ω_1 and ω_2 can be expressed in terms of ω_0 and the coupling coefficient $k = M/L$, as follows:

$$\omega_1 = \frac{\omega_0}{1+k}, \quad \omega_2 = \frac{\omega_0}{1-k} \quad (176)$$

Note that one of the mutual inductances of Fig. 10-59b is negative. This negative mutual inductance corresponds to the ideal transformer (Fig.

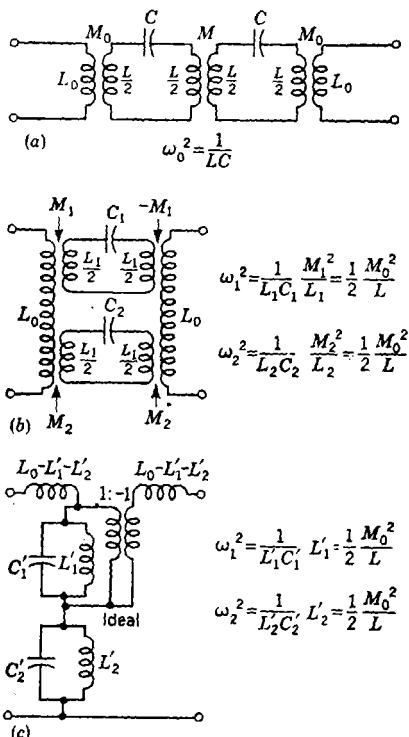


FIG. 10-59.—Three equivalent forms of a double-tuned filter.

10-59c) which produces a 180° phase shift. If the ideal transformer were missing, the insertion loss of the filter would be infinite for $\omega = \omega_0$ because the reactance of the shunt arm of the T would vanish at that frequency.

Consider now a cavity consisting of a section of square guide closed at both ends. Such a cavity has two independent modes of resonance at the frequency for which the length of the cavity equals one-half the guide wavelength for the TE_{10} -mode. The lines of electric field and mag-

netic field for these two modes are shown in Figs. 10-60*a* and 10-60*b*. The resonance frequency of one mode can be changed with respect to the frequency of the other mode by deforming the square into a rectangle or, more simply, by inserting a capacitive screw as shown in Fig. 10-60*c*. Thus the resonance frequencies of the two modes can be adjusted to coincide with ω_1 and ω_2 in Fig. 10-59. The two modes are then equally coupled to the input and output coaxial lines by means of loops lying in the diagonal planes of the guide at 90° with respect to each other. Such an arrangement provides equal couplings for the two modes, together with the 180° phase shift required by the network of Fig. 10-59*b*. In fact, the magnetic fluxes of the two modes linking the loop shown in Fig. 10-60*d* are equal in both magnitude and phase for one orientation of the loop, but they are opposite in phase for the other orientation as shown in Fig. 10-60*e*. The self-inductances of the loops are represented by the two inductances L_0 in Fig. 10-59*b*. In conclusion, if the presence of other modes of resonance is neglected, the cavity is equivalent to the network of Fig. 10-59*b* and, therefore, to the network of Fig. 10-59*a*.

The equivalence of the cavity to the original network of Fig. 10-59*a* can be seen more directly in the following manner. The independent modes of oscillation of the cavity, before the introduction of the screw, can be chosen in an infinite number of ways as arbitrary linear combinations of the particular modes shown in Figs. 10-60*a* and 10-60*b*. For instance, modes that may be considered as independent are those having the field configurations shown in Figs. 10-60*f* and 10-60*g*. The mode of Fig. 10-60*f* is coupled to the loop shown in Fig. 10-60*d* but not to the loop shown in Fig. 10-60*e*. Vice versa, the mode of Fig. 10-60*g* is coupled to the loop of Fig. 10-60*e* and not to the loop of Fig. 10-60*d*. It follows that no transmission can take place if the loops are normal to each other. However, if the two modes are coupled to each other inside the cavity by any convenient device, the cavity becomes equivalent to the network of Fig. 10-59*a* and power will be transmitted from one loop to the other. The screw shown in Fig. 10-60*c*, for instance, can be used to couple the two modes so that the two methods of design lead to the same result. It

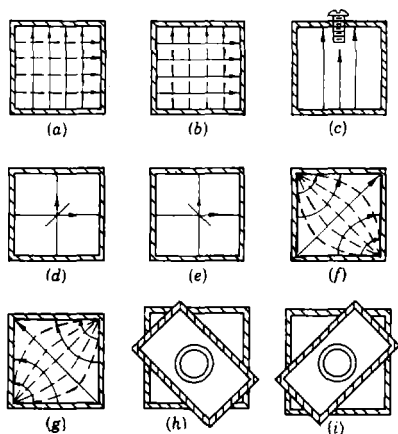


FIG. 10-60.—Illustration of the operation of a rectangular cavity behaving as a double-tuned filter.

is evident from this discussion and from Eq. (176) that the coupling coefficient k depends on the length of the screw. It follows that by adjusting the screw transmission, curves of the types shown in Fig. 10-52 may be obtained. In this process, however, the length of the cavity must be readjusted if the mean frequency ω_0 is to be kept constant. Loop coupling is not essential to the design. Iris coupling can also be used as shown in Figs. 10-60*h* and 10-60*i*.

A cavity of the same type can be designed using a section of circular waveguide. The configurations of the two independent modes for this case are shown in Figs. 10-61*a* and 10-61*b*. The input and output waveguides are coupled through the cylindrical surface although the end plates could be used just as well for this purpose. The operation of this

cavity is very similar to the operation of the cavity discussed above, as indicated schematically in Fig. 10-61. An experimental model of a cavity of this type is shown in Fig. 10-62. Figure 10-63 is a plot of the insertion loss as a function of frequency for such a filter. It will be observed that the stray direct coupling between the irises, which has been neglected in the above analysis, limits the ultimate off-band insertion loss that is obtainable to 35 to 40 db. This effect becomes progressively more important as the bandwidth of the filter is increased by opening the iris holes. One would expect the direct coupling to be smaller for the same bandwidth when the input and output guides are connected to the end plates. This fact, however, has not been checked experimentally. The adjustment of the bandwidth and of the coupling screw must be done experimentally but the apparatus described below make such adjustments relatively simple. In actual practice, it has been found desirable to provide two additional tuning screws symmetrically inserted into the cavity along

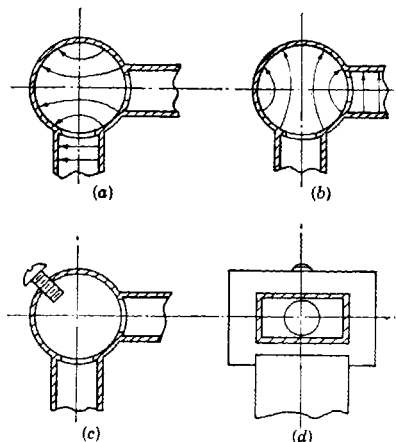


FIG. 10-61.—Illustration of the operation of a cylindrical cavity behaving as a double-tuned filter.

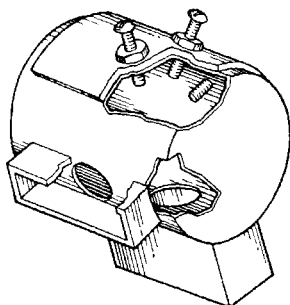


FIG. 10-62.—A cylindrical cavity that behaves as a double-tuned filter.

radii at 45° to the coupling screw to permit the tuning of both modes to the same desired frequency. This procedure is necessary, in general, unless the cavity has perfect symmetry about the plane of the coupling screw, a condition impossible to achieve in practice.

It is possible to couple two such cavities with a quarter wavelength of transmission line, as explained in the next section, and obtain characteristics equivalent to those for four quarter-wavelength-coupled cavities with single resonances. The advantage of this type of filter from the standpoint of weight and space is obvious.

In principle, a cavity that has three independent modes of oscillation successively excited may be designed. However, to date this has not been accomplished, according to the best information of the authors. It should be remarked that in extending the principle of multiresonance, spurious modes excited at frequencies near the pass band must be avoided.

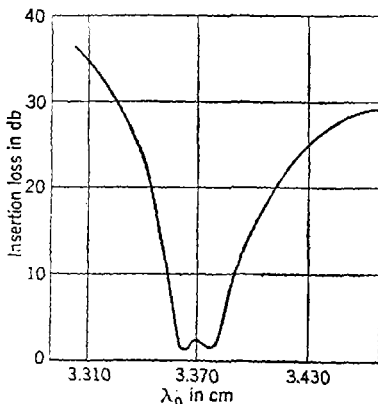


Fig. 10-63.—Insertion loss of filter shown in Fig. 10-62.

FILTERS EMPLOYING QUARTER-WAVELENGTH COUPLINGS

The difficulties of manufacturing and adjusting filters employing direct-coupled cavities become increasingly serious as the pass band becomes narrower. However, a method of cavity coupling which circumvents these difficulties has been developed and will be described below. This method is by no means limited to narrow-band applications but may be used advantageously in certain broadband designs.

10-11. Theory of Quarter-wavelength Coupling.—The method of coupling discussed in this section is based on the impedance-transforming properties of quarter-wavelength lines. In order to understand this transformation property, consider a quarter-wavelength line terminated in a normalized impedance Z . The normalized input impedance of such a line is

$$Z' = \frac{Z + j \tan \frac{\pi}{2}}{1 + jZ \tan \frac{\pi}{2}} = \frac{1}{Z} \quad (177)$$

It follows that the circuit of Fig. 10.64a is equivalent to the circuit of Fig.

10-64*b* if the normalized impedance Z' is equal numerically to the normalized admittance Y and if both lines in Fig. 10-64*a* are one-quarter of a wavelength long. In fact, the two networks have the same open-circuit and short-circuit impedances.

Consider now the ladder structure of Fig. 10-65*a*. This structure can be transformed as shown in Fig. 10-65*b* where Y_2, Y_4, Y_6 , etc. are equal, respectively, to Z'_2, Z'_4, Z'_6 , etc. The two networks are exactly equivalent at the frequency for which the coupling lines are one-quarter wavelength long. All the sections of line must, of course, have unity characteristic impedance, that is, the admittances and impedances of the elements must be normalized. However, if the frequency band of interest is small compared with the mean frequency, as in the case of narrow-band filters, the frequency dependence of the electrical length of the lines may be neglected to a first approximation.

Let Y_1, Y_3, Y_5, \dots of Fig. 10-65*a* be the normalized admittances of parallel-tuned circuits resonating at the frequency ω_0 , and Z'_2, Z'_4, Z'_6 be the normalized impedances of series-tuned circuits also resonating at the frequency ω_0 . A filter of this type, shown in Fig. 10-66*a*, can be derived from the prototype low-pass structure of Fig. 10-49*b* by following the procedure described in Sec. 9-8.

The corresponding filter employing $\lambda_g/4$ couplings is shown in Fig. 10-66*b*. The Q 's of the parallel-tuned circuits, when loaded on both sides by the characteristic impedances of the adjacent lines, are given by

$$(Q_L)_{2k+1} = \frac{1}{2} C_{2k+1} \frac{\omega_0}{w} \quad (178)$$

where w is the bandwidth between the two frequencies corresponding to the point $\omega = 1$ in the frequency response of the prototype structure.

Since a symmetrically loaded transmission cavity has been found to be approximately equivalent to a shunt-tuned circuit, whose loaded Q is given by Eq. (178), a simple microwave realization of the structure of

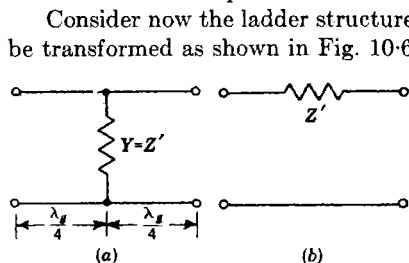


FIG. 10-64.—Illustration of the impedance-transforming properties of $\lambda_g/4$ lines.

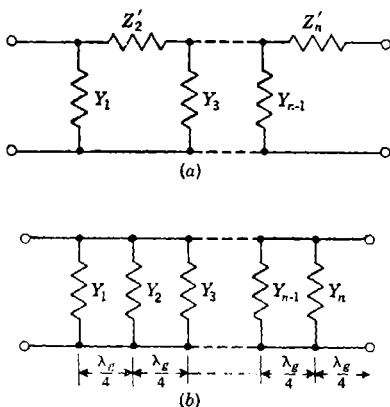


FIG. 10-65.—Equivalent ladder structures.

Fig. 10-66*b* is obtained in the form of a chain of cavities coupled by quarter-wavelength lines. The only difficulty may arise from the fact that the terminating resistance R is not in general equal to the characteristic

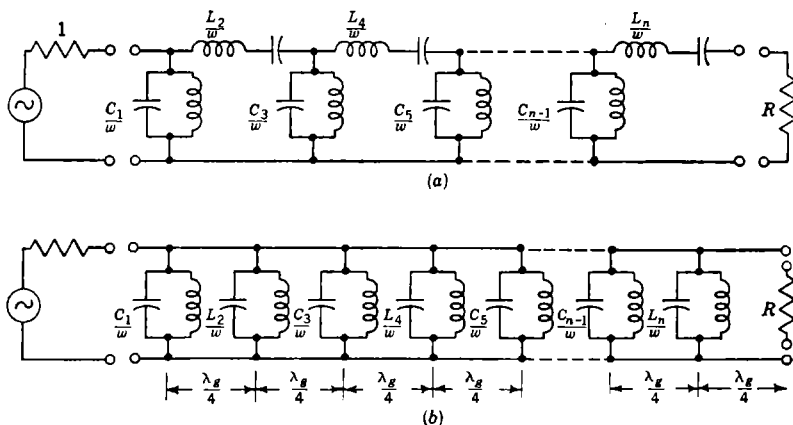


FIG. 10-66.—A bandpass filter and its $\lambda_g/4$ -coupled equivalent.

impedance of the output line, that is, $R \neq 1$. In this case, the last element of the network is transformed as shown in Fig. 10-67. Because of the transforming property of the quarter-wavelength line, a conductance $G' = R$ can be substituted, as shown in Fig. 10-67*b*, for the last section of line of Fig. 10-67*a* terminated by the resistance R . The conductance G' is then transformed into a properly terminated line of unity characteristic impedance preceded by an ideal transformer of ratio 1 to \sqrt{R} , as shown in Fig. 10-67*c*. The last tuned circuit together with the ideal transformer is then identified with an asymmetrically loaded cavity, as shown in Fig. 10-39*b*, for $Z_{01} = Z_{02} = 1$ and $a = \sqrt{R}$. The input and output loaded Q 's of the cavity are then, respectively,

$$\left. \begin{aligned} (Q_{L1})_n &= L_n \frac{\omega_0}{w}, \\ (Q_{L2})_n &= \frac{L_n \omega_0}{R w}. \end{aligned} \right\} \quad (179)$$

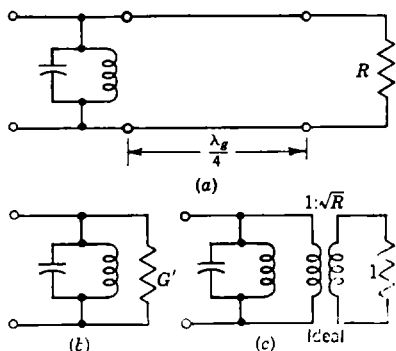


FIG. 10-67.—Change of impedance level at the output terminals of the structure shown in Fig. 10-66*b*.

The Q of the cavity loaded on both sides then becomes

$$(Q_L)_n = \frac{L_n}{1 + R} \frac{\omega_0}{w}. \quad (180)$$

If the last element of the structure of Fig. 10-49b is a shunt-tuned circuit, the last quarter-wavelength section of line will be missing from the structure of Fig. 10-66b. In this case

$$(Q_{L2})_n = RC_n \frac{\omega_0}{w}, \quad (181)$$

$$(Q_L)_n = \frac{RC}{1 + R} \frac{\omega_0}{w}.$$

Changes of impedance level similar to the one just described can be performed at other points in the structure.

The method of design based on the use of quarter-wavelength couplings is not limited to cavity filters. For instance, resonant irises can be used to approximate the behavior of the parallel-tuned circuits in Fig. 10-66b. However, since resonant irises have relatively low Q_0 's, they are not used in connection with narrow-band filters. On the other hand, in the case of bandwidths of a few per cent, the use of resonant irises instead of cavities results in a considerable saving of space and weight. Some examples of filters employing resonant irises will be described later. The design procedure for such filters is the same as for cavity filters. It must be pointed out, however, that only structures for which the terminating resistance R is equal to unity can be physically realized by means of resonant irises. In fact, no change of impedance level can be performed in this case since resonant irises are inherently symmetrical.

The advantages of quarter-wavelength coupling over direct coupling are evident from the above discussion. In the first place, the tolerances on the dimensions of the cavity couplings are considerably relieved. For instance, in the case of rectangular cavities that are quarter-wavelength-coupled by rectangular guides of the same dimensions as the cavities, the irises have susceptances approximately equal to

$$\left(\frac{1}{\pi} \frac{\omega_0}{w} \right)^{1/2},$$

that is, to the square root of the value required if the cavities were directly coupled. In the second place, the quarter-wavelength lines provide a simple way of mechanically connecting the individual cavities. Since these coupling lines are not resonant, an electrical connection made at any point in the line will not interfere with the filter operation, provided this connection satisfies reasonable specifications on voltage standing-wave ratio and loss. The connection should also be sufficiently

far from the cavity couplings to prevent interference with their operation. Each cavity can then be built, adjusted, and tested as a separate unit, so that only minor readjustments are necessary when the cavities are assembled into a filter. The advantages of this adjustment and test procedure for quantity production are obvious.

The construction problems can be further simplified by making all the cavities identical. Such a design is not optimum in the sense that better filter characteristics could be obtained with the same number of cavities, but very often the resulting simplicity of construction is worth the loss of performance. The power-loss ratio of a filter consisting of n identical cavities (or resonant irises) can be computed by means of Eqs. (141) and (143) of Sec. 9-12. In fact, the structure of Fig. 10-66 can be considered as a cascade combination of n identical sections when all the tuned circuits are equal and the terminating resistance is equal to one. Each of these sections consists of a quarter-wavelength line of characteristic impedance equal to one, shunted at its midpoint by a tuned circuit. Let the normalized susceptance of the tuned circuit be

$$B = 2x \quad (182)$$

where

$$x = Q_L \left(\frac{\omega}{\omega_0} - \frac{\omega_0}{\omega} \right) \approx 2Q_L \frac{\omega - \omega_0}{\omega_0} \quad (183)$$

is a frequency variable normalized with respect to the resonance frequency ω_0 and the loaded Q . In terms of this variable, the power-loss ratio for one section is

$$\frac{P_0}{P_L} = 1 + x^2, \quad (184)$$

and the propagation function is

$$\gamma_0 = \cosh^{-1}(-x). \quad (185)$$

It follows that the power-loss ratio for n sections is given by

$$\left(\frac{P_0}{P_L} \right)_n = 1 + x^2 \frac{\sin^2 [n \cos^{-1}(-x)]}{\sin^2 [\cos^{-1}(-x)]} = 1 + x^2 U_n^2(-x) = 1 + x^2 U_n^2(x). \quad (186)$$

The function $U_n(x)$ is the Tchebysheff polynomial of the second kind and of the order n . The polynomials corresponding to $n = 1, 2, 3, 4$ are given below.

$$\left. \begin{aligned} U_1(x) &= 1 \\ U_2(x) &= 2x \\ U_3(x) &= 4x^2 - 1 \\ U_4(x) &= 8x^3 - 4x. \end{aligned} \right\} \quad (187)$$

The recurrence formula for these polynomials is

$$U_{n+1} = 2xU_n - U_{n-1}. \quad (188)$$

Note that the validity of Eq. (186) is not limited to the case in which the shunt branches are tuned circuits. In this circuit B can be any susceptance, provided, of course, that the proper expression for x is used.

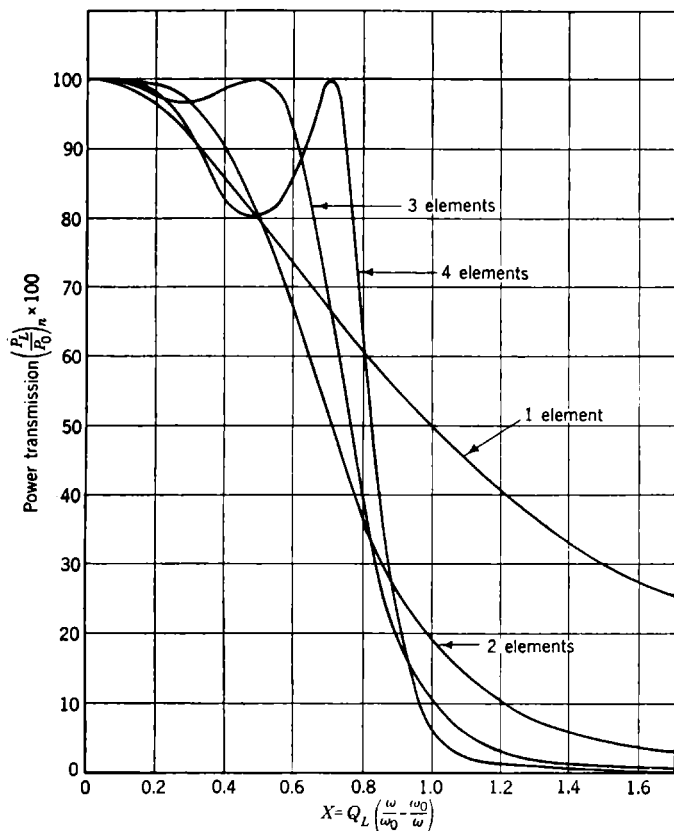


FIG. 10-68.—Power-transmission curve for n quarter-wavelength-coupled resonant elements.

Plots of the percentage transmission, that is, of $(P_L/P_0)_n$, are shown in Fig. 10-68 for $n = 1, 2, 3, 4$. These curves show that the bandpass tolerance increases with n ; consequently, values of n larger than 4 are seldom used. For large values of x , the off-band insertion loss becomes approximately

$$L_n \approx 6(n - 1) + 20n \log_{10} x. \quad (189)$$

The application of these formulas to the design of practical filters will be discussed in the succeeding section.

10-12. Filters Employing $\lambda_g/4$ -coupled Cavities.—Because of the construction advantages mentioned above, $\lambda_g/4$ -coupled cavities are becoming increasingly popular. The applications are scattered throughout the frequency range from 200 to 10,000 Mc/sec, using both waveguide and coaxial couplings. Typical examples will be described, one of them in detail. The actual behavior of these filters deviates so little from the predicted behavior that it does not appear worth while to give complete experimental data in all cases.

The filter that will be discussed most completely consists of a number of reentrant cylindrical cavities of the type illustrated in Fig. 10-47, separated by quarter-wavelength coaxial lines. The lines are loop-coupled to the cavities so that the effective locations of the input terminals of the cavities must be determined experimentally. This determination can be performed, with the help of a standing-wave detector, by finding the position of the voltage zero in the input line when the cavity is detuned. Under these conditions the input terminals of the cavity are effectively short-circuited. It follows that their location must be an integral number of half wavelengths from the position of any voltage zero. This experimental determination may be done in such a way that the equivalent line length of whatever fittings are used to connect the cavity to the coaxial lines is included. The effective length of the coupling lines is often made equal to three or five quarter wavelengths to provide additional mechanical spacing. These longer lines are, of course, more frequency-sensitive, but their frequency behavior can still be neglected in most practical cases.

Because of incidental dissipation, perfect transmission is never obtained. The minimum insertion loss of n identical cavities quarter-wavelength-spaced is very nearly n times the minimum loss of one cavity. Dissipation tends also to smooth out the curve of the insertion loss in the pass band. For instance, the experimental curves for the insertion loss plotted in Fig. 10-69, which are in good agreement with the corresponding theoretical curves in the attenuation band, show no appreciable wiggles in the pass band.

The fact that type N couplings may be used in practice to link the cavities to the transmission lines mechanically would indicate that the tolerance on the effective length of coupling lines is extremely liberal. This contention was experimentally substantiated by inserting a line stretcher between two cavities and observing the effect on the transmission curve of the filter. The resulting characteristics observed for various line lengths in the case of a two-cavity filter are presented in Fig. 10-70. It will be noted that a variation of $\pm\lambda_g/20$ in the length

of the coupling line is tolerable for most purposes. As the length of the coupling line approaches half wavelength, the transmission curve becomes

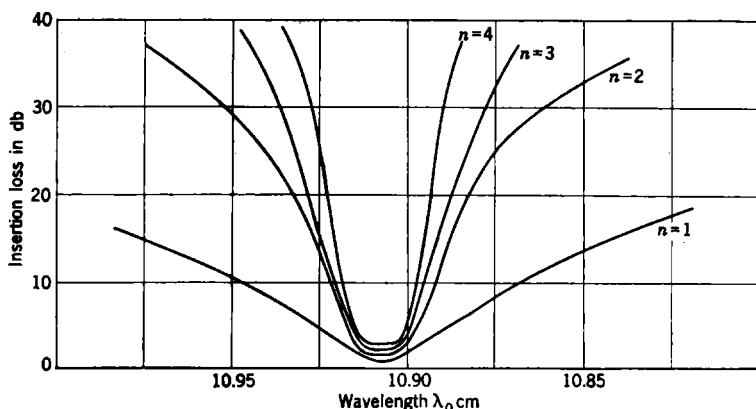


FIG. 10-69.—Observed insertion loss of n quarter-wavelength-coupled cavities of the type shown in Fig. 10-47.

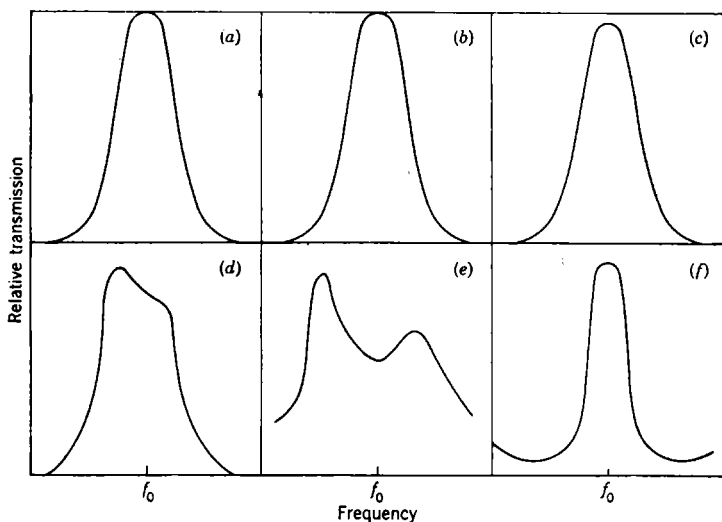


FIG. 10-70.—Effect of improper spacing between two identical cavities. Curves a, b, c, d, e, and f refer to spacings of $\lambda_g/4$, $1.2 \lambda_g/4$, $1.4 \lambda_g/4$, $1.6 \lambda_g/4$, $1.8 \lambda_g/4$, and $\lambda_g/2$, respectively.

lopsided and a double hump appears. These two humps separate more and more until finally, at exactly half-wavelength spacing, three symmetrically arranged humps appear. It should be remarked that this

experiment justifies the assumption made above in neglecting the frequency behavior of the coupling lines for narrow-band filters.

When the length of the coupling line is held fixed at a quarter wavelength, it is found, as one would expect, that the angular position of the coupling loop in the cavity is not critical. Transmission curves for various orientations of the loops are shown in Fig. 10-71. This method of varying the coupling provides a feasible method of adjusting the bandwidth over a limited range. Thus a rotation of the loops through 45° from the position of maximum coupling should reduce the bandwidth by a factor of 2. Since the loaded Q is doubled in this process, an increased midband loss as actually observed is to be expected. Roughly speaking, the loaded Q of a cavity varies inversely as the square of the area of the coupling loop. Consequently, when the bandwidth is critical, the loop size must be held to a close tolerance.

The theory of quarter-wavelength-coupled cavities assumes that all the cavities are tuned to the same frequency. This adjustment is perhaps the most critical in the construction of such a filter. Figure 10-72 shows the effect of detuning one of the cavities in a two-cavity

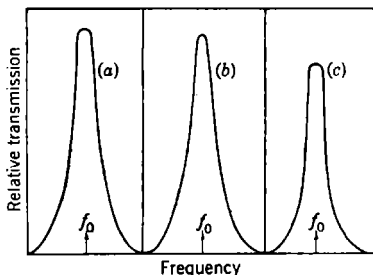


FIG. 10-71.—Effect of loop orientation on transmission through two $\lambda_g/4$ -coupled cavities. Curve *a* shows all loops oriented for maximum coupling; Curve *b* shows one loop of coupling line rotated off 30° ; and Curve *c* shows all loops rotated off 45° and thus reducing loaded Q of each cavity by a factor of approximately 2.

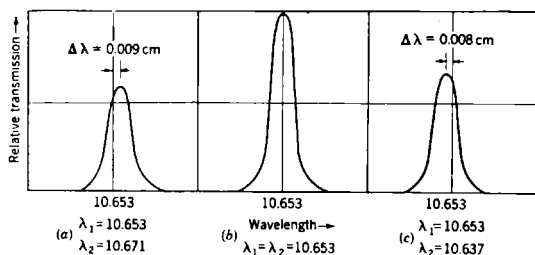


FIG. 10-72.—Effect of detuning of transmission through two $\lambda_g/4$ -coupled cavities.

filter by an amount equal to the bandwidth of a cavity. As might be expected, the minimum loss is greatly increased and the center of the pass band is shifted. Of course, the higher the loaded Q , the more critical the adjustments are. Fortunately, the accurate adjustment of a cavity to a given frequency by means of a tuning screw is not a difficult procedure.

Before progressing to a discussion of other types of quarter-wave-length-coupled filters, it is interesting to investigate the characteristics that can be obtained if the tuning of the cavities is varied and the length of the coupling lines readjusted to optimum values. Unfortunately, no simple method of theoretical analysis is available to handle the general

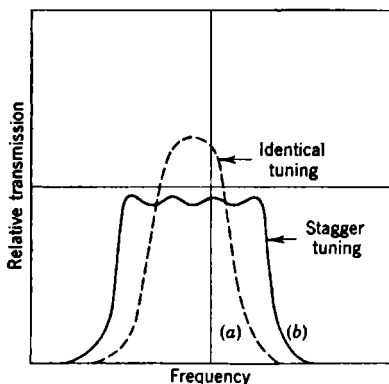


FIG. 10-73.—Observed transmission through four $\lambda_g/4$ -coupled cavities, stagger-tuned.

case. Figure 10-73, however, presents an observed transmission curve which illustrates how the bandwidth may be expanded at some cost in minimum transmission loss. This curve is included mainly to satisfy the curiosity since, in general, more satisfactory transmission curves can be achieved in other ways.

Filters similar to those just described have been constructed at both 200 and 300 Mc/sec. At these frequencies, reentrant cavities using uniform center conductors become inordinately large. If the required loaded Q is not too high,

$$\omega_0 \approx \frac{1}{\sqrt{LC}} \quad (190)$$

it is customary to foreshorten the cavity by increasing the capacity between the reentrant line and the end wall of the cavity. In the extreme case, the cavity appears as in Fig. 10-74 and may be regarded as composed of an inductive line L and a lumped capacity C . Increasing the capacity decreases the length of line required to produce a certain resonant frequency since

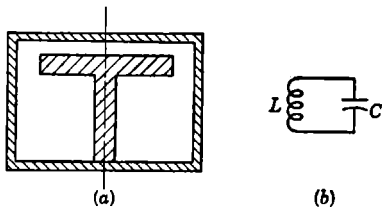


FIG. 10-74.—A reentrant cylindrical cavity foreshortened by the use of capacity loading and its equivalent circuit.

Even if the capacity is estimated from the electrostatic capacity of the parallel plate combination without regard for fringing and the inductance is treated as the lumped equivalent of a short section of concentric line, the frequency estimated by the familiar equation given above is accurate to 10 per cent.

The sketch of Fig. 10-75 is scaled to dimensions suitable for a loaded Q of about 30 and a resonance frequency adjustable from 190 to 220 Mc/sec. The condenser plates are made unequal to increase the linearity of tuning with displacement and to increase the displacement required for a given

frequency change. Type N fittings are suitable for input and output connections to either coaxial line or cable. The center conductor of the coaxial line is usually run straight through the cavity and is connected to the cavity center conductor. Such coupling obviously constitutes a loop and thus the loaded Q may be changed by varying the distance h of the wire from the bottom of the cavity since Q_L is roughly inversely proportional to h^2 . As in the previous case, the effective location of the input terminals of the cavity must be determined experimentally. In a typical application of these cavities, the distance for effective quarter-wavelength coupling between successive cavity center lines is only $5\frac{7}{8}$ in., only slightly larger than the diameter of the cavities used, namely, $4\frac{1}{4}$ in.

The introduction of lumped capacities in the cavity considerably decreases the unloaded Q because of the increased surface area. However, for a loaded Q of 30, the minimum transmission loss for the cavity just described is only 0.2 db. The tandem arrangement of three cavities of this type is not unusual. A similar cavity used

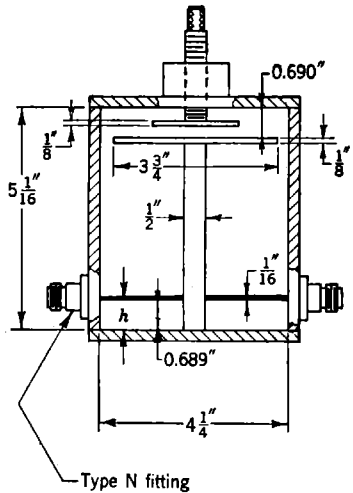


FIG. 10-75.—A practical structure for a capacity-loaded cavity with loop coupling.

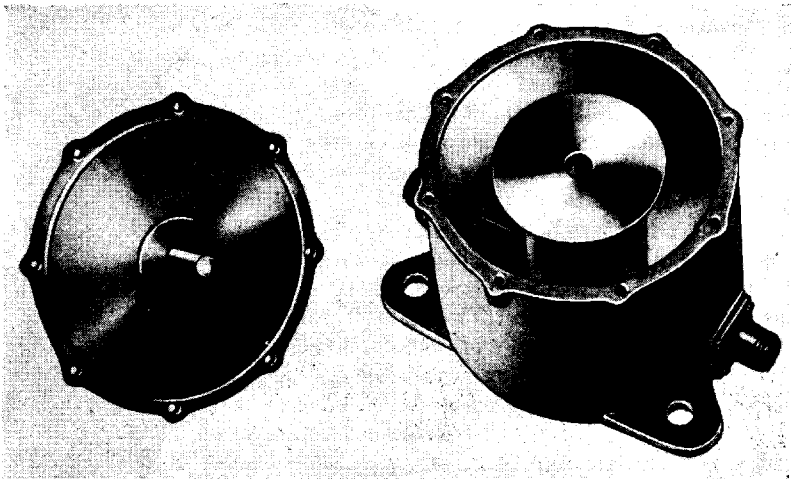


FIG. 10-76.—Production model of capacity-loaded cavity used at 300 Mc/sec.

at 300 Mc/sec has been produced on a fairly large scale in the form shown in Fig. 10-76.

A practical procedure for the design of high- Q , quarter-wavelength-coupled filters in waveguide is illustrated in Fig. 10-77. Each cavity of the type shown in Fig. 10-44 has a section of waveguide, one-eighth of a guide wavelength long at the resonance frequency, extending past each iris. Choke and flange connectors are alternately attached to the ends. Thus, when several cavities are connected in cascade, the cavities are effectively spaced by quarter wavelengths. As pointed out above, the choke and flange electrical connection does not disturb the operation of the filter.

Such filters have been extensively investigated. Line stretchers have been inserted between cavities and the effect of the connecting line length observed. The results differ in no way from those presented above for the case of reentrant cavities. As many as four cavities with a loaded

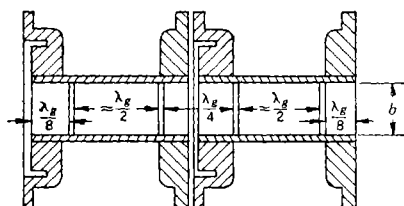


Fig. 10-77.—Practical form of filter composed of $\lambda_g/4$ -coupled, waveguide cavities.

Q of 130 and a resonance wavelength of 3.3 cm have been successfully coupled. The observed characteristics in no case differ from the expected behavior by more than an amount accounted for by dissipation. The midband loss due to dissipation was about 0.4 db per cavity for the particular type of cavities used. Since the

detailed design of rectangular cavities with given loaded Q and ω_0 has been considered in Sec. 10-7, no further discussion is required here.

10-13. Filters Employing Quarter-wavelength-coupled Resonant Irises.—A discussion of practical quarter-wavelength-coupled filters would not be complete without a description of the special type employing resonant irises. In fact, this type of filter was built before quarter-wavelength-coupled cavities were contemplated. The use of resonant irises is indicated in all cases where the loaded Q is sufficiently low, about 40, and space is at a premium. The reasons for using resonant irises instead of cavities have been discussed in Sec. 10-7.

One of the outstanding uses of this type of filter, 9 and 10, is in the construction of broadband TR tubes, illustrated in Fig. 10-78. These tubes have been designed and manufactured for operation at both 3000 and 10,000 Mc/sec. Their properties are fully discussed in Vol. 14, Chap. 3, to which the reader should refer for a detailed discussion. However, for the sake of completeness it seems worth while to mention a few of their electrical features. The tubes generally contain four or five resonant irises. Two of these irises are ovoid windows which serve

to seal the tubes; the others are of the dumbbell-slot variety. The loaded Q of all the elements is usually equal to about 4. Since the loaded Q is very low, its value is not critical. Moreover, the tolerance on the

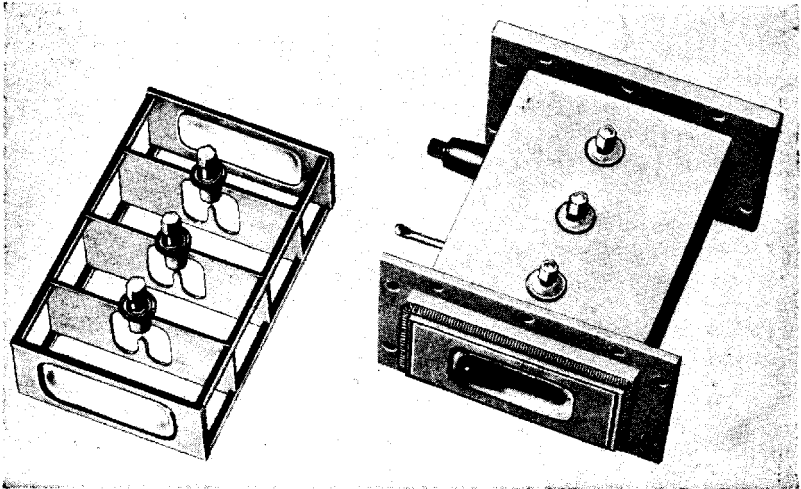


FIG. 10-78.—A broadband TR tube illustrating quarter-wavelength coupling of resonant irises.

tuning is so large that fixed-tuned irises may be used and, therefore, no adjustment is required after assembly. A typical curve illustrating the input voltage standing-wave ratio for such a tube is shown in Fig. 10-79.

When a filter with a narrower band is desired, it is no longer feasible to use resonant irises of the dumbbell-slot type. In fact an iris with a loaded Q of 30 and a resonance frequency of 2880 Mc/sec for use in a $1\frac{1}{2}$ -by 3-in. waveguide has a capacitive gap of only 0.004 in. The required tolerances in Q_L and ω_0 are such that a tuning screw must be provided. However, since the total range of the tuning screw must be less than 0.004 in., this adjustment is extremely critical. An iris suitable for narrow-band filters is the simple circular opening shown in Figs.

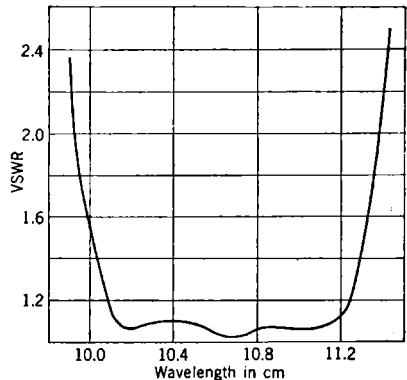


FIG. 10-79.—VSWR characteristics of the TR tube shown in Fig. 10-78.

10-80a and 10-80b. This iris resonates when the periphery of the opening

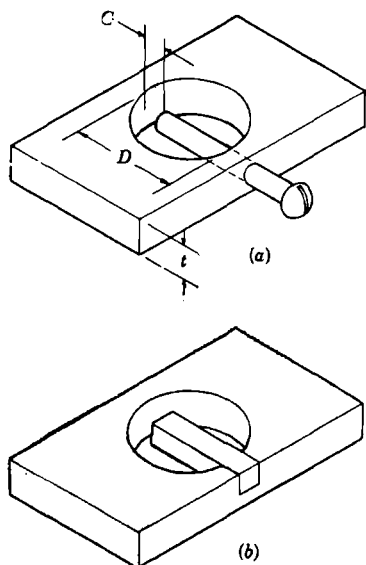


FIG. 10-80.—Irises suitable for narrow-band filters.

The transmission characteristics plotted in Fig. 10-83 reveal a loss of about 0.5 db.

Several remarks should be made concerning the construction of n -iris filters. In general, the losses are found to be appreciable in silver-plated brass irises unless the silver is burnished. In fact, plain brass has been found superior to unburnished silver plating. Some care must be exercised in soldering the tuning screws after final adjustment to ensure that such soldering does not itself alter the tuning adjustment. The actual lineup procedure for a multi-iris filter of this type will be discussed in Sec. 10-22.

10-14. Refined Theory of Quarter-wavelength Coupling.—It is perhaps worth while to review the simplifying assumptions made in the previous analysis of quarter-wavelength-cou-

pling is approximately equal to half a wavelength. The voltage standing-wave ratio for an iris of this type is plotted in Fig. 10-81. Such an iris may be machined to a very close tolerance and, moreover, may be tuned over a reasonable range with a capacitive screw. Since the capacitive screw is only a trimmer and carries a small fraction of the current at resonance, it does not introduce so much dissipation as a tuning screw in a dumbbell-slot iris of the same loaded Q . Furthermore, the tuning rate of a screw in a circular iris is considerably slower than that of a screw in an iris of the dumbbell-slot type. For instance, the gap width in a circular iris corresponding to a 0.004-in. gap in the dumbbell slot is 0.075 in. A filter of this type⁸ employing three resonant irises is shown in Fig. 10-82.

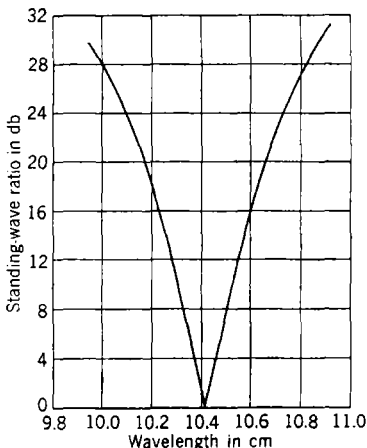


FIG. 10-81.—VSWR characteristics of a typical resonant iris of the type shown in Fig. 10-80.

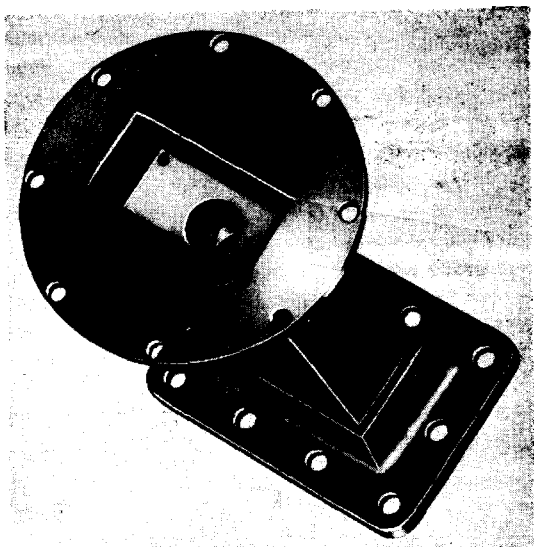


FIG. 10-82.—Narrow-band filter employing $\lambda_0/4$ -coupled resonant irises.

pled filters. The first assumption concerns the frequency sensitivity of the coupling sections. No theoretical investigation has yet been made of the distortion caused by this frequency dependence in the general case of unequal cavities or resonant irises. However, in the case of identical elements, it is possible to develop a simple expression for the power-loss ratio which takes into account the frequency dependence of the electrical length of the lines.

Let $\theta(\omega)$ be the angular length of a coupling section. At the mean frequency ω_0 this angular length is, by definition, equal to $\pi/2$. Proceeding as in the case of constant angular length, for the propagation function of one section, if the characteristic impedance of the lines is unity,

$$\gamma_0 = \cosh^{-1} \left(\cos \theta - \frac{B}{2} \sin \theta \right) \tag{191}$$

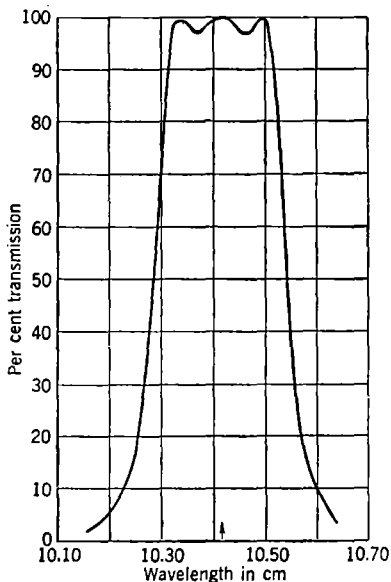


FIG. 10-83.—Characteristics of filter shown in Fig. 10-82.

where B is the susceptance of the resonant elements. The power-loss ratio for one section is still given by Eq. (184),

$$\frac{P_0}{P_L} = 1 + \frac{B^2}{4}. \quad (192)$$

The power-loss ratio for n sections is, therefore,

$$\left(\frac{P_0}{P_L}\right)_n = 1 + \frac{B^2 \sin^2 [n \cos^{-1}(y)]}{4 \sin^2 [\cos^{-1}(y)]} = 1 + \frac{B^2}{4} U_n^2(y) \quad (193)$$

where

$$y = \frac{B}{2} \sin \theta - \cos \theta. \quad (194)$$

$U_n(y)$ is the Tchebysheff polynomial of the second kind appearing in Eq. (186).

In order to compute the power-loss ratio, both B and θ must be expressed as functions of the frequency ω , as follows:

$$B = 2Q_L \left(\frac{\omega}{\omega_0} - \frac{\omega_0}{\omega} \right) \quad (195)$$

$$\theta = \frac{\pi \omega}{2 \omega_0} \sqrt{1 - \left(\frac{\omega_c}{\omega} \right)^2}; \quad (196)$$

Q_L is the loaded Q of the resonant element and ω_c is the cutoff frequency of the guide used as coupling line. Note that $\omega_c = 0$ when a coaxial line is used.

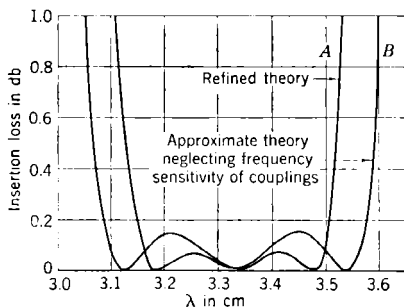


Fig. 10-84.—Effect of the frequency sensitivity of coupling lines on characteristics of a filter consisting of three elements, $\lambda_0/4$ -coupled.

Curve A in Fig. 10-84 is a plot of the insertion loss obtained from Eq. (193) for a filter consisting of three resonant irises with $Q_L = 4$, quarter-wavelength-spaced in a 1- by $\frac{1}{2}$ -in. rectangular guide. Curve B , on the other hand, is a plot of the insertion loss as obtained from Eq. (186) which neglects the frequency dependence of the sections of guide. The pass band of Curve B is approximately 40 per cent larger than the pass band of Curve A . Moreover, the

tolerance in decibels for Curve B is twice as large as for Curve A .

A simple formula for the ratio of the two bandwidths can be derived from Eq. (193). For this purpose it may be assumed that both B and θ

are proportional to the frequency difference $\Delta\omega = \omega - \omega_0$; hence Eqs. (189) and (190) reduce to

$$B = 4Q_L \frac{\Delta\omega}{\omega_0} \quad (197)$$

$$\theta = \frac{\pi}{2} \left[1 + \frac{\Delta\omega}{\omega_0} \frac{1}{1 - \left(\frac{\omega_c}{\omega_0}\right)^2} \right]. \quad (198)$$

Equation (194) can be simplified for values of θ near $\pi/2$ by means of the following approximations:

$$\begin{aligned} \sin \theta &\approx 1, \\ \cos \theta &\approx \frac{\pi}{2} - \theta. \end{aligned}$$

Then, for the variable y ,

$$y \approx 2Q_L \frac{\Delta\omega}{\omega_0} \left\{ 1 + \frac{\pi}{4} \frac{1}{Q_L \left[1 - \left(\frac{\omega_c}{\omega_0}\right)^2 \right]} \right\}. \quad (199)$$

It is convenient to introduce again the normalized frequency variable

$$x = 2Q_L \frac{\Delta\omega}{\omega_0} \quad (200)$$

already defined in Eq. (183). The ratio y/x is a constant

$$k = 1 + \frac{\pi}{4} \frac{1}{Q_L \left[1 - \left(\frac{\omega_c}{\omega_0}\right)^2 \right]}. \quad (201)$$

Substituting for y and B in Eq. (193) by means of Eqs. (195), (199), (200), and (201),

$$\left(\frac{P_0}{P_L} \right)_n = 1 + x^2 U_n^2(kx). \quad (202)$$

Equation (202) is identical to Eq. (186) but for the fact that the variable of the Tchebysheff polynomial is multiplied by k . Let w_θ be the width of the pass band between the outer zeros of $U_n^2(kx)$, and $w_{\pi/2}$ be the corresponding bandwidth for $\theta = \pi/2$, that is, the width between the outer zeros of $U_n^2(x)$. It is evident that

$$\frac{w_{\pi/2}}{w_\theta} = k \geq 1. \quad (203)$$

In the case of Fig. 10-84, that is, for $Q_L = 4$ and $\omega_c/\omega_0 = 0.73$, k is equal to 1.42. Equation (202) shows also that the frequency dependence of θ reduces the bandpass loss. In fact, x^2 is inversely proportional to k^2 for any given value of U_n^2 .

The percentage error in bandwidth, which results from assuming that θ is independent of frequency, is inversely proportional to Q_L and becomes approximately 3 per cent for $Q_L = 50$. Therefore, such an assumption is quite reasonable in the case of narrow-band filters.

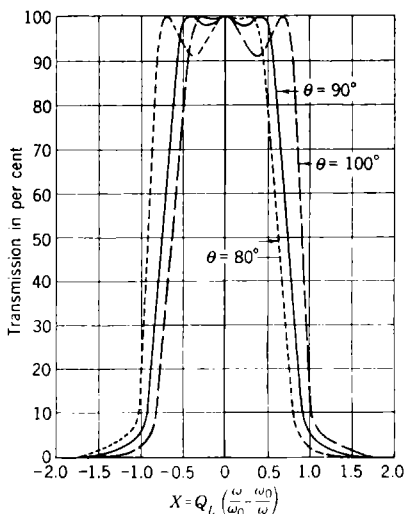


FIG. 10-85.—Effect of improper length of coupling line.

Equations (193) and (194) can also be used to study the effect of making the length of the coupling lines different from a quarter wavelength at the mean frequency ω_0 . It is clear that when $\theta(\omega_0) \neq \pi/2$ the frequency characteristics of the filter are not symmetrical with respect to ω_0 . The curves of Fig. 10-85 represent the percentage transmission obtained from Eq. (193) for $n = 3$ and for three different constant values of $\theta(\omega_0)$.

The second important assumption involved in the analysis of quarter-wavelength-coupled filters concerns the representation of cavity resonators as simple parallel resonant circuits. Figures 10-39a and 10-39b show that in using such a representation the series reactances of the input and output loops are neglected as well as the direct coupling between input and output terminals. The direct coupling is actually negligible in well-designed cavities. The series reactances, on the contrary, may have an appreciable effect on the bandpass characteristics of the filter.

To investigate this phenomenon, consider the section of a quarter-wavelength-coupled filter shown in Fig. 10-86, in which the two series reactances are equal to X_0 . In the case of rectangular cavities, X_0 is of the order of magnitude of $1/\sqrt{Q_L}$ [see Eq. (128)]. It follows that in computing Z_{sch} for the section of Fig. 10-86 X_0 may be neglected whenever $X_0 B \ll 1$. This condition is satisfied over the pass band when Q_L is larger than about 100. On the other hand, for Z_{sch}

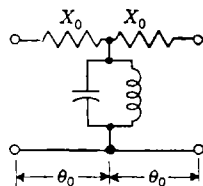


FIG. 10-86.—Section of $\lambda_0/4$ -coupled filter with series reactances.

$$Z_{sch} = j \frac{X_0 + \tan \frac{\theta_0}{2}}{1 - X_0 \tan \frac{\theta_0}{2}} \quad (204)$$

In this equation the presence of X_0 may be corrected for by making θ equal to the value for which $Z_{\text{in}} = j$, that is, approximately

$$\theta_0 = \frac{\pi}{2} - 2X_0. \tag{205}$$

Note that this correction is made automatically if the effective location of the terminals of the cavity is determined experimentally in accordance with the procedure outlined in Sec. 10-12.

As an illustration of the effect of the reactances X_0 , the filter shown schematically in Fig. 10-87 will be considered. This filter consists of four irises placed in a waveguide in such a way that two cavities separated by a quarter-wavelength section of guide are formed. According to our method of design, this filter behaves like a critically coupled, doubly tuned circuit when all the irises are equal. Overcoupling and undercoupling can be obtained by varying the ratio ρ of the susceptance of the two inner irises to the susceptance of the two outer irises. To find the frequencies of perfect transmission, one must solve the equation $\mathfrak{B} - \mathfrak{C} = 0$, as indicated by Eq. (46), Sec. 9-3, where in this case,

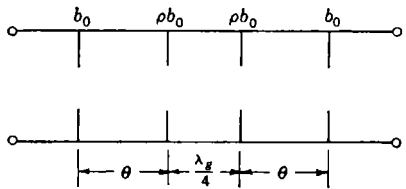


FIG. 10-87.—Two rectangular cavities, $\lambda_g/4$ -coupled.

To find the frequencies of perfect transmission, one must solve the equation $\mathfrak{B} - \mathfrak{C} = 0$, as indicated by Eq. (46), Sec. 9-3, where in this case,

$$\mathfrak{B} = (\cos \theta - b_0 \sin \theta)^2 - \sin^2 \theta \tag{206}$$

$$\mathfrak{C} = -(b_0 \rho \cos \theta + \sin \theta + b_0 \cos \theta - b_0^2 \rho \sin \theta)^2 + (\cos \theta - b_0 \sin \theta)^2 \tag{207}$$

where b_0 is the normalized susceptance of the outer irises and θ is the angular length of each cavity. The particular case of critical coupling occurs when the two θ roots of the equation $\mathfrak{B} - \mathfrak{C} = 0$ coincide. Such degenerate roots are found for a value of ρ , given by

$$\rho^4 = 1 + \frac{1}{b_0^2} \tag{208}$$

or, for $b > 10$, by

$$\rho \approx 1 + \frac{1}{b_0^2}. \tag{209}$$

Note that in this case the series reactance X_0 is equal to $-\frac{1}{b_0}$. Since critical coupling is obtained when $\rho > 1$, the two cavities are effectively undercoupled when all the irises are equal. It follows that the stray series reactances have the effect of decreasing the coupling between the two cavities. However, if the loaded Q of the cavities is about 100, this effect is of the order of magnitude of only 1 per cent.

In the narrow-band extreme, the elements of a quarter-wavelength-coupled filter may no longer be considered "dissipationless." In the theoretical section, methods for computing the effect of incidental dissipation and for correcting the design formulas have been discussed. However, in many cases the work involved in such corrections and the changes required in mechanical design do not pay sufficient dividends in improved performance to justify this procedure. It is common practice to accept such deviations from the predicted performance without compensating for them since, in many cases, the deviations are of minor importance. By way of illustration, Fig. 10-88 is included to show the

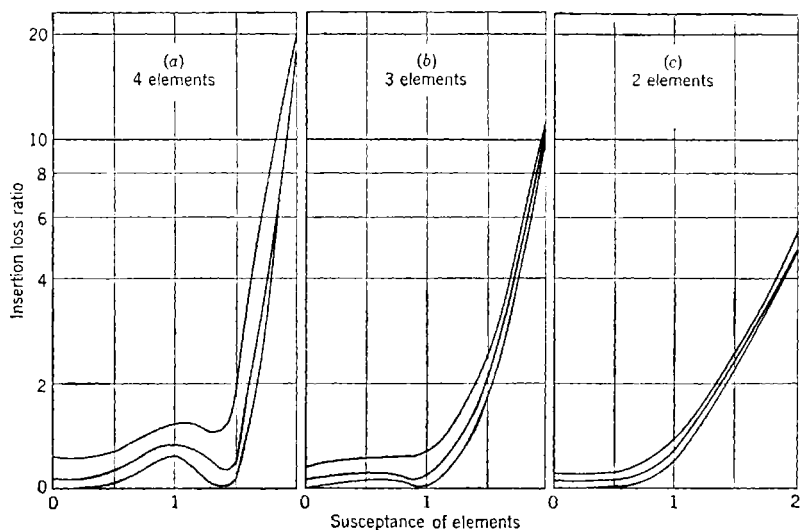


FIG. 10-88.—Effect of incidental dissipation on $\lambda_g/4$ -coupled resonant elements. Curves correspond to values of $g = 0, 0.02, \text{ and } 0.05$.

effect of a varying degree of dissipation on the characteristics of filters with two, three, and four identical resonant elements. The parameter used to measure the dissipation is the ratio of the loaded to the unloaded Q of the elements.

10-15. Quarter-wavelength-coupled Filters with Tchebysheff Characteristics.—Most of the quarter-wavelength-coupled filters that have actually been designed and built make use of identical cavities. However, in such a design, as pointed out before, the mechanical simplicity is achieved at the cost of electrical performance. For this reason, it is perhaps worth while to investigate this matter in some detail by comparing the optimum loss characteristics of the general structure shown in Fig. 10-66 with the characteristics of filters employing identical cavities. This structure can be derived from the prototype low-pass structure of

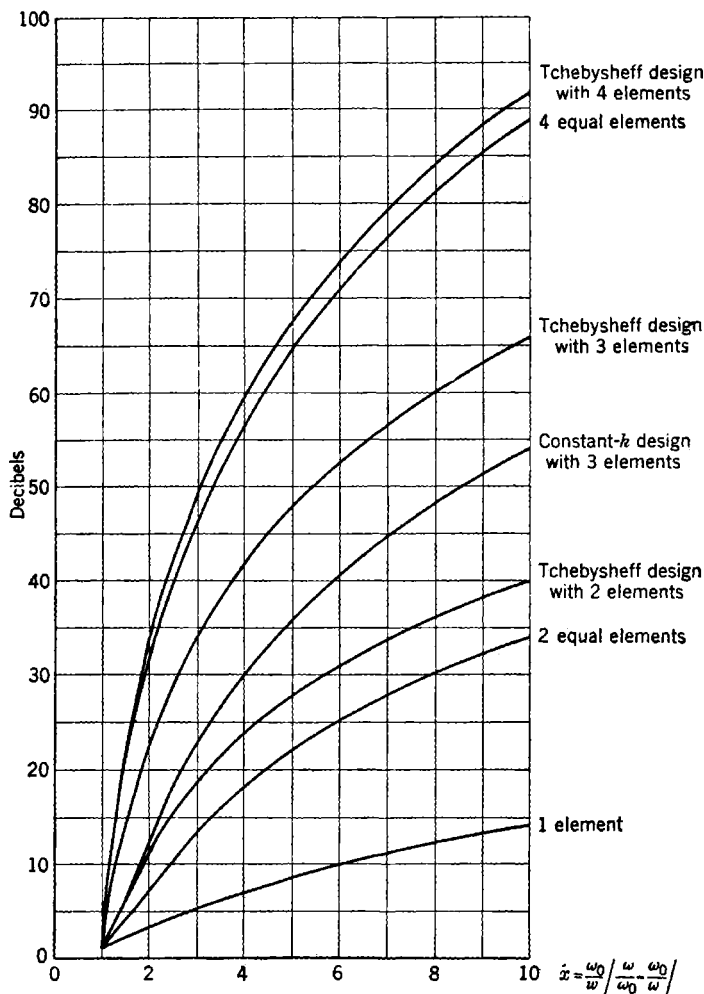


FIG. 10-89.—Off-band insertion loss for various filters having a bandpass tolerance of 1 db ($\epsilon^2 = 0.25$).

Fig. 10-49b, for which the optimum behavior of the power-loss ratio is of the form (see Sec. 9-18)

$$\frac{P_0}{P_L} = 1 + \epsilon^2 T_n^2(\omega) \quad (210)$$

where T_n is a Tchebysheff polynomial of the first kind, n is the number of elements, and ϵ^2 is the bandpass tolerance. It will be recalled that all

the maxima of this function and its value for $\omega = 1$ are equal to $1 + \epsilon^2$. The method of network synthesis that yields filters with prescribed power-loss ratios has been discussed in Chap. 9.

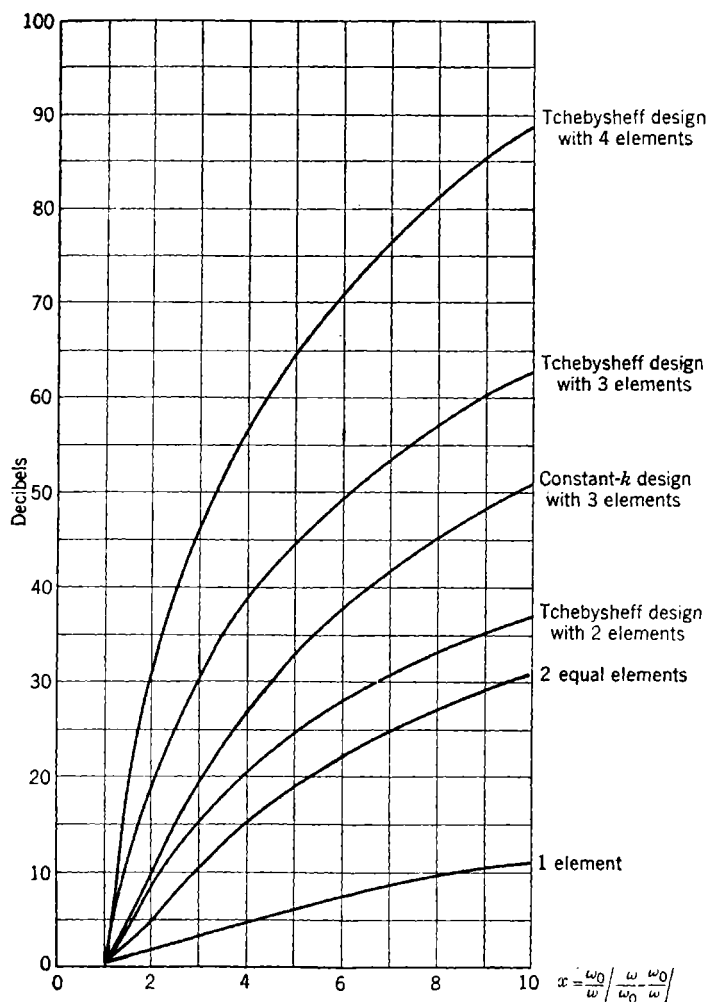


FIG. 10-90.—Off-band insertion loss for various filters having a bandpass tolerance of 0.5 db ($\epsilon^2 = 0.125$).

A quarter-wavelength-coupled filter consisting of two identical cavities can be derived from the prototype low-pass structure of Fig. 10-49*b* in which the inductance, the capacitance, and both terminating

resistances are equal to unity. This type of design which corresponds to critical coupling has already been discussed in Sec. 10-9 in connection with directly coupled cavity filters. It was found there that by over-coupling the two cavities, that is, by deriving the filter from a prototype structure having a power ratio of the optimum form, the off-band loss could be increased by 6 db, while maintaining the same bandwidth and the same bandpass tolerance. Design equations for this prototype structure are presented in the same section, together with a method of compensating for the effect of incidental dissipation. Plots of the off-band insertion loss of two element filters are shown in Figs. 10-89, 10-90, and 10-91 for different values of the bandpass tolerance.

In the case of three identical, quarter-wavelength-coupled cavities, the power-loss ratio is of the optimum form, but the tolerance ϵ^2 , which is equal to $\frac{1}{27}$, cannot be changed. In fact, it can be shown that Eq. (186) for $n = 3$ can be rewritten in the form

$$\left(\frac{P_0}{P_L}\right)_3 = 1 + \frac{1}{27} T_3^2(x') \quad (211)$$

by means of the change of variable

$$x' = \sqrt{3} x. \quad (212)$$

This transformation is merely a normalization of the independent variable which makes the power ratio equal to $1 + \frac{1}{27}$ for $x' = 1$.

In this connection, it is interesting to note that if the same transformation is applied to Eq. (202), which takes into account the frequency dependence of the coupling lines,

$$\left(\frac{P_0}{P_L}\right)_3 = 1 + \frac{1}{27k^2} T_3^2(kx'). \quad (213)$$

This equation shows very clearly that the frequency dependence of the coupling lines reduces the bandwidth by a factor equal to k . Moreover, it shows that the bandpass tolerance is reduced by the factor k^2 , a fact which is not evident in Eq. (202). In the particular case of Fig. 10-84, k is equal to 1.42 and the maximum loss in the pass band is thus reduced by 0.8 db.

The value of $\frac{1}{27}$ for ϵ^2 in Eq. (211) corresponds to a maximum loss in the pass band equal to 0.16 db which is satisfactory in most practical cases. However, if a different tolerance is desired, the loaded Q of the middle resonant element has to be different from the loaded Q of the outer resonant elements. The relation between the ratio of the loaded Q 's and the tolerance can be determined from the frequency behavior of the prototype structure of Fig. 10-92. The power-loss ratio of this structure

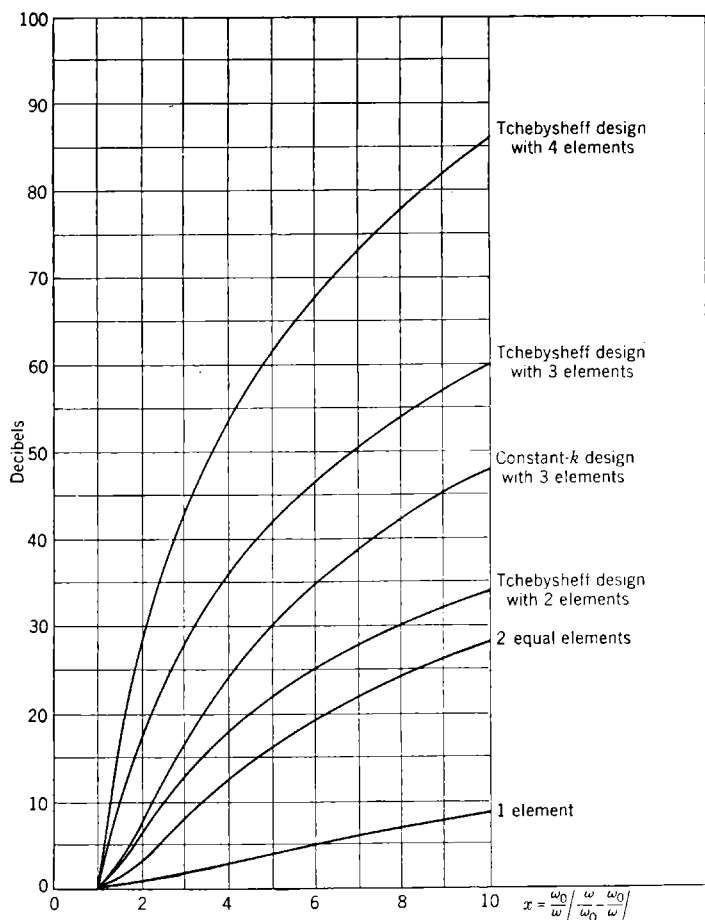


FIG. 10-91.—Insertion loss for various filters having a bandpass tolerance of 0.25 db ($\epsilon^2 = 0.0625$).

is found to be

$$\left(\frac{P_0}{P_L}\right)_{n=3} = 1 + \frac{L^2 C^4}{64} \omega^2 \left[4\omega^2 - 4\left(\frac{2}{LC} - \frac{1}{C^2}\right)^2 \right]. \quad (214)$$

This equation can be identified with Eq. (210) for $n = 3$, in which $T_3(\omega)$ is given by

$$T_3(\omega) = \omega(4\omega^2 - 3); \quad (215)$$

therefore the following conditions must be satisfied for optimum frequency response:

$$4 \left(\frac{2}{LC} - \frac{1}{C^2} \right) = 3 \tag{216}$$

$$\frac{L^2 C^4}{64} = \epsilon^2. \tag{217}$$

From these conditions the following two design equations can be derived:

$$L = \frac{8C}{3C^2 + 4} \tag{218}$$

$$\epsilon = \frac{L}{8C^2} = \frac{C^3}{3C^3 + 4}. \tag{219}$$

In transforming the low-pass structure to a bandpass structure, the pass band of the filter is defined as the frequency band in which the power ratio is smaller than, or equal to $1 + \epsilon^2$.

If w is the width of this band, one obtains for the loaded Q of the outer resonant element [see Eq. (120)]

$$Q_L = \frac{1}{2} C \frac{\omega_0}{w} \tag{220}$$

and the ratio of the loaded Q of the inner element to the loaded Q of the outer element becomes

$$r = \frac{L}{C}. \tag{221}$$

That this ratio becomes unity for $\epsilon^2 = \frac{1}{2} r$ can be checked.

Curves of the off-band insertion loss for different values of the maximum bandpass loss are plotted in Figs. 10-89, 10-90, and 10-91. The insertion loss for a filter derived from a constant- k low-pass section is also plotted in the same figures for the same values of bandpass loss. For a constant- k section the ratio r is equal to 2 and the transmission ratio has no maxima in the pass band other than the one at the mean frequency ω_0 .

In the case of a filter consisting of four identical resonant elements, the maximum value of the power-loss ratio is found to be 1.25. This value corresponds to a loss of approximately 1 db and a tolerance $\epsilon^2 = \frac{1}{4}$. The curve of the off-band insertion loss for this filter is compared in Fig. 10-89 with the corresponding curve for a four-element filter of optimum design which has the same bandwidth and the same bandpass loss. It can be seen that far from the pass band the filter of optimum design has a loss 2.65 db larger than the loss of the filter with equal elements. Since such a difference is negligible, the simple design with equal elements is quite satisfactory if a bandpass loss of 1 db is per-

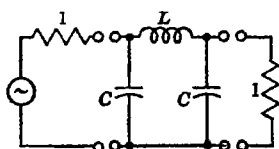


FIG. 10-92.—Three-element prototype low-pass structure.

mitted. If a different tolerance is desired, however, the filter must be designed following the procedure discussed in Chap. 9.

The off-band insertion loss of the filters discussed above is, in all cases, a monotonic function which increases with the frequency deviation from the center of the pass band. The rate of cutoff, for a given bandpass tolerance, is determined by the number n of resonant elements. More

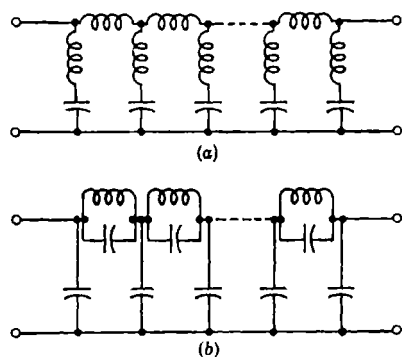


FIG. 10-93.—Prototype low-pass structures of the m -derived type.

precisely, in the case of optimum design sufficiently far from the pass band, the insertion loss in decibels is proportional to n . It follows that extremely sharp cut-offs require large numbers of resonant elements. In the case of lumped-element filters, this difficulty is circumvented by using filters of the m -derived type, that is, filters derived from prototype structures such as the ones shown in Fig. 10-93. These structures can be designed in a number of

ways, for instance, by cascading a number of actual m -derived sections, or by means of the direct synthesis procedure discussed in Chap. 9. The insertion loss of a low-pass filter of this type has a number of infinite peaks which coincide with the resonance frequencies of the branches of the ladder. These resonance frequencies can be placed in the vicinity of the pass band to increase the sharpness of the cutoff. The optimum design for filters of this type is discussed in Sec. 9-19.

Low-pass structures of the types shown in Fig. 10-93 can be transformed into quarter-wavelength-coupled filters by following the same procedure used in the case of the structure of Fig. 10-49b. The only difficulty encountered concerns the transformation of the resonant branches into microwave elements. Consider, then, one of the resonant branches of the structure of Fig. 10-93a which is assumed to have a cutoff frequency ω_c equal to 1. This branch, shown in Fig. 10-94a, resonates at the frequency

$$\omega_\infty = \frac{1}{\sqrt{LC}} \quad (222)$$

When the low-pass structure is transformed into a bandpass filter with a

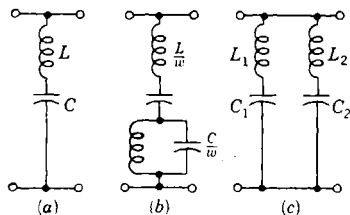


FIG. 10-94.—Transformation of resonant branches.

bandwidth w and a mean frequency ω_0 , the resonant branch is transformed into the network shown in Fig. 10-94b. Both tuned circuits resonate at the frequency ω_0 . This network cannot be realized directly at microwaves. Therefore, it is further transformed into the network of Fig. 10-94c by applying Foster's reactance theorem. The resonance frequencies ω_{∞_1} and ω_{∞_2} of the two series-tuned circuits are given by the following equations:

$$\omega_{\infty_1} \omega_{\infty_2} = \omega_0^2 \quad (223)$$

$$\omega_{\infty_2} - \omega_{\infty_1} = w_{\infty} = \omega_{\infty} w. \quad (224)$$

For large values of ω_0/w the following expressions are approximately true:

$$\omega_{\infty_2} \approx \omega_0 + \frac{w_{\infty}}{2} \quad (225)$$

$$\omega_{\infty_1} \approx \omega_0 - \frac{w_{\infty}}{2}. \quad (226)$$

The network of Fig. 10-94c places in evidence the fact that ω_{∞_1} and ω_{∞_2} are the frequencies at which the insertion loss of the bandpass filter becomes infinite. The values of L_1 and L_2 can be determined by requiring that the sum of the susceptances of the tuned circuits shall vanish at the frequency ω_0 and shall have, at the same frequency, a slope equal to $2 \frac{C}{w}$. Then

$$\frac{L_1}{L_2} = \frac{\omega_{\infty_2}}{\omega_{\infty_1}} \quad (227)$$

$$\frac{L_1 L_2}{L_1 + L_2} = \frac{L}{w}. \quad (228)$$

In the case of narrow-band filters, these equations yield approximately

$$L_1 = L_2 = 2 \frac{L}{w}. \quad (229)$$

The network of Fig. 10-94 can be approximated in a number of

ways by means of microwave elements. In the case of coaxial-line filters with a relatively broad band, two simple stubs in shunt with the main line may be used. When the ratio ω_0/w is so large that stubs become impractical, cavities quarter-wavelength-coupled to the main line as shown in Fig. 10-95a may be used. The Q of the cavity when loaded by the characteristic impedance of the coupling line is related to L by the approximate equation

$$Q_{L1} \approx 2L \frac{\omega_0}{w}. \quad (230)$$

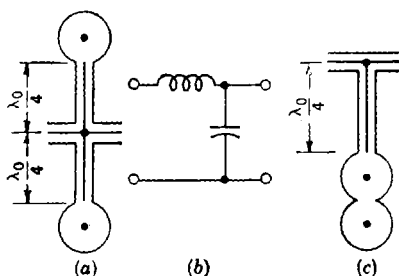


FIG. 10-95.—Microwave realizations of the resonant branches shown in Fig. 10-94.

Figure 10-96 illustrates the microwave realization of a bandpass m -derived section. A similar arrangement of cavities can be used in the case of waveguide filters.

An entirely different approach to the problem of transforming the branch of Fig. 10-94a into microwave elements is illustrated in Figs. 10-95b and 10-95c. The branch is considered as a separate filter whose

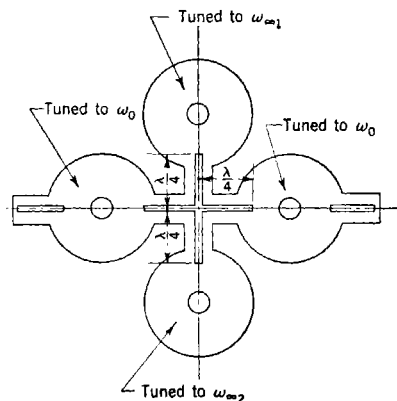


FIG. 10-96.—Microwave realization of an m -derived section.

output terminals are open-circuited. The transformation into the structure of Fig. 10-95c can be performed exactly as in the case of a direct-coupled, two-cavity filter. Both cavities are tuned to the frequency ω_0 , and the bandwidth w_∞ between the frequencies of infinite loss is controlled by the coupling between the two cavities. A similar arrangement can be used, of course, in the case of waveguide filters.

All the filters discussed in the preceding sections are of the bandpass type. Band-rejection

filters are seldom used, but can be designed in the same manner. A lumped-element bandpass filter can always be transformed into a band-rejection filter by substituting series-tuned circuits for parallel-tuned circuits and vice versa in accordance with the procedure discussed in Sec. 9-8. For instance, the structure of Fig. 10-66b would be transformed into the structure of Fig. 10-97. The L 's in Fig. 10-97 are

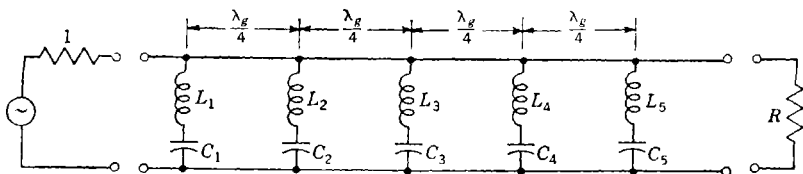


FIG. 10-97.—A band-rejection structure.

made equal numerically to the C 's in Fig. 10-66b, for coupling lines of unity characteristic impedance, and vice versa. Let the power-loss ratio of the bandpass filter be

$$\left(\frac{P_0}{\bar{P}_L}\right)_{\text{B.P.}} = 1 + f(x^2) \quad (231)$$

where

$$x = \frac{\omega_0}{w} \left(\frac{\omega}{\omega_0} - \frac{\omega_0}{\omega} \right). \quad (232)$$

The power-loss ratio of the band-elimination filter obtained from the bandpass filter as explained above is given then by

$$\left(\frac{P_0}{P_L}\right)_{\text{B.F.}} = 1 + f\left(\frac{1}{x^2}\right). \quad (233)$$

This equation shows that the pass band and the rejection band have been

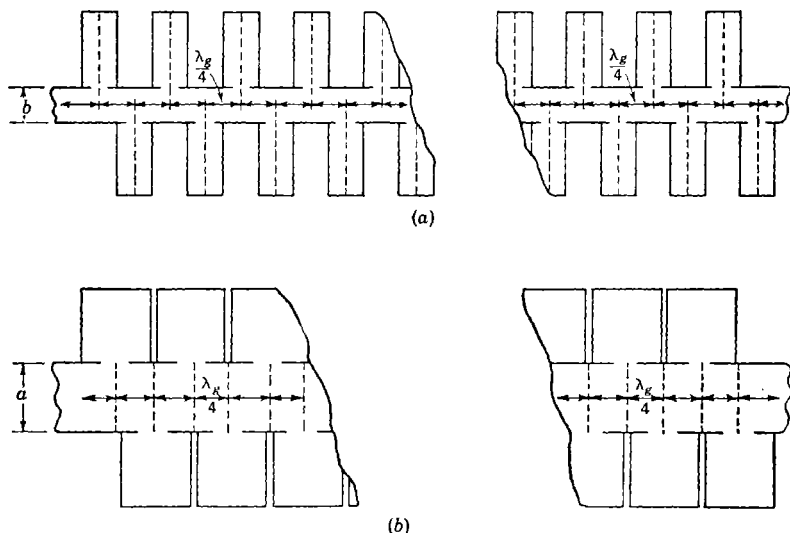


FIG. 10-98.—Two alternative microwave realizations of band-rejection structure.

interchanged in the frequency spectrum; thus the frequencies corresponding to $x = \pm 1$, that is, the two ends of the pass band are left fixed.

Microwave band-rejection filters can be designed without difficulty by using quarter-wavelength couplings as in the case of bandpass filters. Figure 10-98a illustrates a practical realization of a waveguide filter of this type. The cavities are placed in series with the guide and therefore they behave like parallel-tuned circuits in series with the line. However, this type of structure and the structure of Fig. 10-97 have the same insertion loss. This equivalence can be

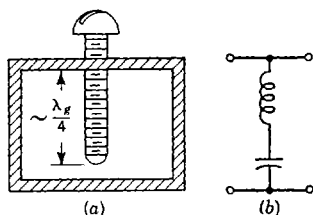


FIG. 10-99.—A series-resonant structure with its equivalent circuit.

be checked easily by simply adding quarter-wavelength sections at both ends of either structure. A structure more directly equivalent to the filter of Fig. 10-97 would consist of cavities coupled in shunt to the main guide, as shown in Fig. 10-98b. The input terminals of these cavities are effec-

tively spaced one-quarter wavelength from the guide since no reflection takes place in the guide when these terminals are short-circuited. In the case of coaxial-line filters, cavities quarter-wavelength-coupled to the main line, such as the ones shown in Fig. 10-96, may be used.

Transmission-resonant irises have their counterpart in the rejection-resonant irises which behave approximately like series-tuned circuits. Rejection irises can be obtained from transmission irises by the simple procedure of interchanging metal with hole. A very simple type of rejection iris is shown in Fig. 10-99 together with its equivalent circuit. Irises of this type can be quarter-wavelength-spaced in a guide to form a broadband rejection filter. The design procedure is the same as in the case of bandpass filters, apart from the transformation from bandpass to band-rejection filter already discussed above.

MISCELLANEOUS FILTERS

10-16. Lattice Networks.—Symmetrical lattice networks are extensively used in the process of designing lumped-element filters because

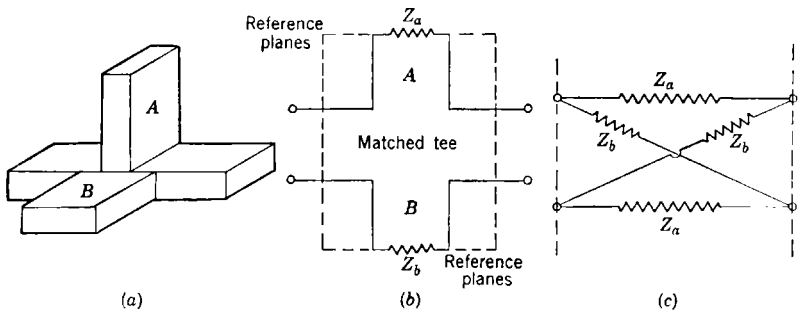


FIG. 10-100.—Simple waveguide magic T and its equivalent circuit.

they represent the most general form of symmetrical two-terminal-pair network. However, they are seldom used as final filter structures because they require extremely close tolerances on the values of the elements. The reader can be convinced of this fact by noting that proper operation of a lattice filter requires perfect coincidence of the critical frequencies of the series and shunt arms. Small differences between corresponding critical frequencies may produce considerable distortions of the frequency characteristics of the filter.

In spite of these practical considerations, it is of interest to inquire whether it is possible to simulate a lattice network by means of waveguides. An investigation of this question reveals that the simple magic T may be regarded as the nucleus of a lattice network. It will be recalled that a magic T in rectangular waveguide consists of an H -plane T and an

E-plane T formed at the same point of a waveguide, as shown in Fig. 10-100a. If, now, two of the arms of a properly matched magic T are terminated with impedances Z_a and Z_b , as schematically represented in Fig. 10-100b, the behavior of the resulting two-terminal-pair network may be represented by the lattice network of Fig. 10-100c.

As in the case of a lattice network, it is found that in a magic-T filter the impedances connected to the *A* and *B* arms must be held to very close tolerances. Moreover, the behavior of a magic T can be made to approximate the behavior of a simple lattice network only over a limited frequency range. For these reasons, magic-T filters are not, in general, feasible although they may present advantages in very special cases.

10-17. Mode Filters.—It is sometimes desirable to transmit energy through a waveguide or a coaxial line in a single preferred mode. For this purpose, structures have been designed that selectively propagate certain modes while reflecting others. Such devices are known as “mode filters.” These filters are outside the scope of this chapter but reference may be made to Chap. 7 for a detailed discussion of their application in rotary joints.

In certain special cases, however, mode filters may be used with advantage to provide frequency discrimination. Thus, if the two frequencies to be separated are extremely close together, it is often simpler to arrange to propagate the two frequencies in different modes and to utilize the difference in mode rather than the difference in frequency as the basis for discrimination. As an example, the simple case will be considered in which it is desired to separate two signals of slightly different frequencies received by the same antenna. If the antenna is designed to receive circularly polarized waves, it will accept waves of all possible polarizations. If the two waves to be received are plane-polarized at right angles, they may be transmitted through the same guide using different modes of propagation or different polarizations of the same mode. The two modes can then be separated by means of a mode filter. In this manner, it is possible to achieve without difficulty 20- to 30-db discrimination over a band of a few per cent. A filter that performs the same operation by frequency discrimination would become progressively more complex as the frequency difference between the two signals became smaller. Unfortunately, it is difficult by this method to extend this principle to obtain discrimination between more than two frequencies or to separate two signals of widely different frequencies.

10-18. Absorption Filters.—In some cases, in which it is desirable to attenuate a wide band of frequencies, the use of absorption filters is indicated. Such filters do not discriminate by reflection but by dissipation and, consequently, their use is limited to those cases where the attenuated frequencies are not to be utilized. Although substances, such as

ammonia, which have absorption bands in the microwave range are known, in general the application of absorption filters is limited to low-pass filters with gradual cutoffs. In these cases, it is possible to find suitable solid dielectric materials for which the loss functions vary as in Fig. 10-101. The dielectric may then be introduced into the transmission line or waveguide as a slug with suitable tapers to avoid reflections. For design information on dielectric materials, the reader is referred to a comprehensive report by A. von Hippel.²⁰

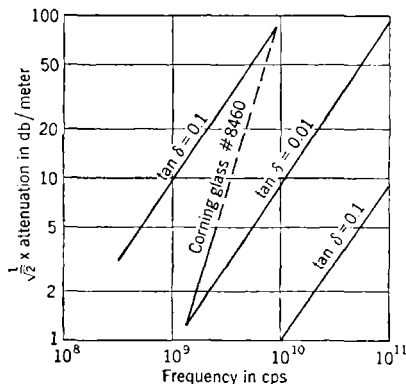


FIG. 10-101.—Attenuation as a function of frequency for dielectrics with constant loss angles, and for Corning Glass No. 6460.

pulses and detect subsequent echoes. Multiplexers permit the transmission of a number of signals from one station to another without the introduction of appreciable crosstalk and constitute, therefore, one of the main applications of filters.

It is obvious that microwave multiplexing requires a method of connecting channel filters across a transmission line or waveguide in such a way that the power in each signal is diverted to the appropriate branch with negligible loss. One such method, analogous in principle to that used in radar duplexing, has been experimentally tested by Fox¹⁴ and found to be very satisfactory. This multiplexer, schematically represented in Fig. 10-102, consists of n bandpass filters centered at the n frequencies of the signals to be separated. Each of these filters is connected in shunt to the main transmission line. For frequencies within a particular channel, the corresponding filter acts as a shunt impedance approximately equal to the characteristic impedance of the line; for such frequencies, the remaining filters appear as open circuits.

It follows from the above discussion that a signal of frequency ω_k within a particular channel is effectively aware of the presence of only one filter, namely, the one tuned to its own frequency. If the main guide is then short-circuited at the proper place, that is, approximately an odd number of quarter wavelengths from the center of the k th side branch,

the signal is reflected back into the main guide. For design information on dielectric materials, the reader is referred to a comprehensive report by A. von Hippel.²⁰

10-19. Multiplexers.—In the terminology of communication engineering, a multiplexer is a device for separating signals of different frequencies present in the same circuit and directing them into subsidiary circuits, or vice versa. Such a device is not to be confused with a duplexer as used in radar for electronic switching in systems designed to transmit

Multiplexers permit the transmission

the signal of frequency ω_k is matched into this branch without appreciable loss. The input iris of the last filter may be substituted for the end plate of the guide, as shown in Fig. 10-102, without modifying the behavior of the system. The branches containing all the other filters are then connected to the main guide at the proper distance from the input iris of the last filter as shown in Fig. 10-102. In the particular case considered, each filter consists of a simple cavity. However, more complex filters can be

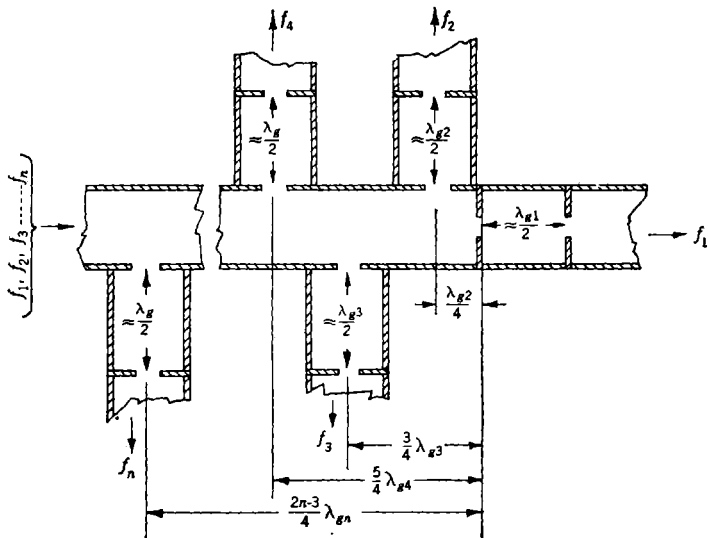


FIG. 10-102.—A multiplexer.

used if required by the frequency separation of the channels. Coaxial-line multiplexers similar to the waveguide multiplexer just described can be designed in a similar manner.

ASSEMBLY AND TEST PROCEDURES

10-20. Broadband Filters.—For broadband filters where the pass band is greater than 10 per cent in frequency, the mechanical tolerances are sufficiently loose, in general, to eliminate the necessity for adjustment after assembly. It suffices to check the insertion loss at several points in the pass band, for example, at the center and edges, to ensure that no gross mechanical error is present in the particular filter under test. The exact test procedure depends on the particular specifications, but usually does not present a major problem. For the measurement of insertion loss, an apparatus of the general type schematically represented in Fig. 10-103 is needed. When the generator is isolated from the filter

under test by an attenuating pad which reflects negligible power, and when a well-matched detector terminates the line, a comparison of the power reaching the detector with and without the filter interposed determines the insertion loss. It is wise to use a power monitor on the generator to ensure that the power output of the generator is unaltered by reflections from the filter since it is often not feasible to use sufficient

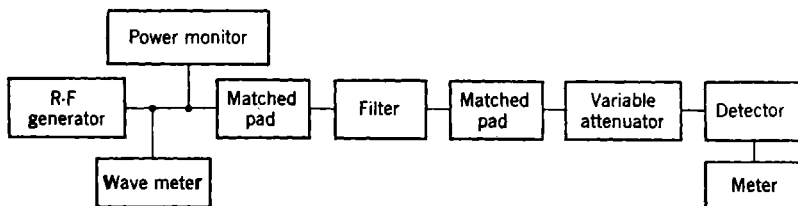


FIG. 10-103.—R-f bench for testing broadband filters.

padding to provide complete isolation. In this manner, it is possible to ascertain insertion losses up to about 60 db. For higher attenuations, extreme care must be exercised to avoid direct r-f leakage from the generator to the detector. In many cases, the available power from the generator is such that with 60 db of attenuation in the filter plus adequate padding, the power level is below the limit of sensitivity of the detector.

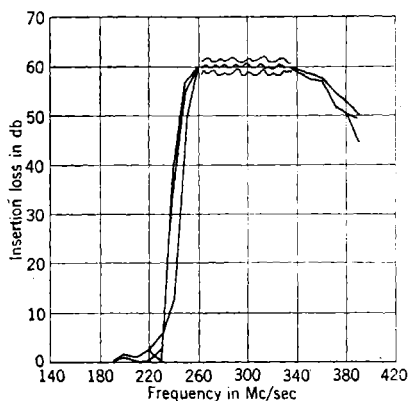


FIG. 10-104.—Insertion loss for three filters of the same type, illustrating reproducibility.

reproducibility of electrical characteristics including both manufacturing and test errors, curves for a number of Type 2 filters described in Sec. 10-3 are shown in Fig. 10-104.

10-21. Narrow-band Filters.—Point-by-point determination of insertion loss as a function of frequency is cumbersome but possible whenever

It should be recalled in the testing of broadband filters that spurious results are often introduced by the fact that the connectors to the filter are not sufficiently frequency-insensitive. For this reason, it is common practice to insert dummy connectors of the same type employed in the filter between the generator and load when the measurements are made with the filter removed. It must be realized, however, that this procedure does not determine the over-all insertion loss produced by the filter in actual practice.

As an example of the over-all

adjustments after assembly are not required. In narrow-band filters, where mechanical tolerances are close and compensating adjustments must be made after assembly, the point-by-point procedure becomes prohibitively expensive and other test and lineup procedures must be found. It is highly desirable in lining up multicavity filters, for instance, to be able to ascertain at a glance the effect of a small change of any one of the parameters of the system on the whole loss characteristic. In the

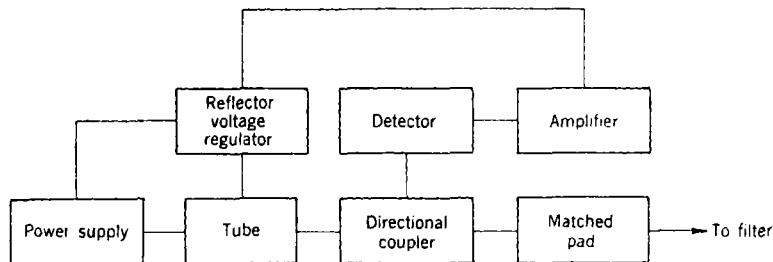


FIG. 10-105.—Schematic diagram of a volume control for a reflex oscillator.

case of narrow-band filters, it is possible to sweep a generator over the range of frequencies concerned and observe on a cathode-ray tube a frequency plot of the power transmitted by the filter to a detector. In order for the trace on the screen to represent sufficiently well the frequency characteristics of the filter alone, a scheme that keeps the output power of the generator constant over the frequency band of interest must be provided. A generator with such a volume control, used in conjunction with a frequency-insensitive detector, provides an adequate test system.

A circuit that maintains a constant output power from a reflex oscillator* is shown schematically in Fig. 10-105. A small fraction of the power carried by the wave traveling from the generator to the load is coupled into a detector by a directional coupler. The rectified voltage from the detector is

amplified and applied to the voltage regulator which controls the reflector voltage of the generator. Whenever possible, it is desirable to modulate the tube because high-gain d-c amplifiers are, in general, very trouble-

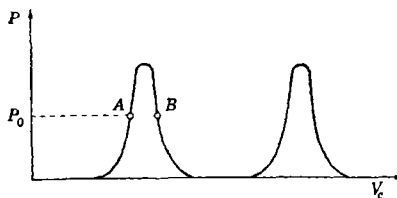


FIG. 10-106.—Power output of a reflex oscillator as a function of the reflector voltage.

* Most tunable generators are of the reflex type. In such oscillators, even if constant output is not required, the reflector voltage must track the resonance frequency of the cavity to maintain oscillations.

some. In this case, the output of the amplifier must be rectified before being fed into the voltage regulator.

Fig. 10-106 shows a typical plot of the output power of a reflex oscillator as a function of the reflector voltage for a given resonance frequency of the cavity. If the reflector voltage is initially adjusted for operation at the point *A*, any small change of the power coupled into the detector produces a large change of the reflector voltage, which in turn corrects the output power of the tube. This correction can be adjusted to have the proper sign for stable operation. The stability conditions can be expressed mathematically in the following manner. The reflector voltage V_r consists of two components V_0 and V_c . V_0 is independent of the output power of the tube and is manually adjusted, whereas V_c is a function of the output power specified by

$$V_c = f(P). \quad (234)$$

The tube characteristics can be expressed by

$$P = \phi(V_r, \omega) = \phi[(V_0 + V_c), \omega] \quad (235)$$

where ω is the resonance frequency of the cavity. The output power can be determined by substituting Eq. (234) for V_c in Eq. (235) and solving for P . Let P_0 be a value of the output power that can be obtained at any frequency within a specified band centered at ω_0 . V_0 can then be adjusted to the value for which Eqs. (234) and (235) are satisfied by $P = P_0$ and $\omega = \omega_0$. This condition of operation is stable if

$$\left(\frac{\partial \phi}{\partial V_c} \cdot \frac{dV_c}{dP} \right)_{P=P_0} < 0, \quad (236)$$

that is, if a positive increment of P in Eq. (234) corresponds to a negative increment of P in Eq. (235). If this condition is not satisfied at the point *A* in Fig. 10-106, it will certainly be satisfied at the point *B* and vice versa.

Suppose now it is desired to vary ω over the specified band centered at ω_0 while keeping the deviation of P from P_0 within a given magnitude ΔP_0 . Let ΔV_c be the maximum change of V_c required, according to Eq. (235), to keep P within these specified limits. This change of reflector voltage can always be obtained by means of the feedback circuit, provided the gain of the amplifier is sufficiently high. It follows that ΔP_0 can be made arbitrarily small. Note that the only restriction to be placed on the functions $f(P)$ and $\phi[(V_0 + V_c), \omega]$ is that they must satisfy Eq. (236) for all values of P considered.

The directional coupler and the detector have been implicitly assumed to be frequency-insensitive. This is not the case in practice, however; the minimum value of ΔP_0 is therefore actually limited by the frequency

behavior of the r-f components. In fact, the output voltage of the detector, rather than the output power of the tube, is the quantity that is kept constant. Detectors of the barretter type can be matched to a VSWR less than 1.2 over a 10 per cent band. The frequency behavior of the directional coupler is therefore the actual limiting factor.

The volume control scheme of Fig. 10-105 has been tried out in connection with a type 2K45 oscillator. This tube is thermally tuned by controlling the grid voltage of a triode, which is the heating element. The resonance frequency of the cavity can thus be swept over a 10 per cent band with a 14-sec period* by alternating the control grid voltage over a suitable range. Any convenient on-off circuit can be used for this purpose. The same circuit can also provide the required sweep voltage for the oscilloscope presentation mentioned above. The long period associated with thermal tuning requires the use of a long persistence screen.

The accuracy of the measurement of the insertion loss of a filter may be improved by the use of logarithmic amplifiers in comparing the incident power with the power transmitted through the filter. If the output voltages of two logarithmic amplifiers are proportional, respectively, to the logarithm of the incident power and to the logarithm of the transmitted power, their difference is by definition proportional to the insertion loss. This method of measurement can be used in connection with the sweep frequency oscillator described above. If the output voltages of the two amplifiers are connected directly to the vertical plates of the oscilloscope, the vertical deflection of the beam will be proportional to the insertion loss. A plot of the insertion loss as a function of frequency can thus be obtained.

A satisfactory type of logarithmic amplifier²¹ makes use of a special type of germanium crystal, in which the "cat whisker" is welded to the surface of the crystal. For these crystals the static voltage-current characteristics obey the logarithmic law

$$V = K \log I$$

sufficiently well over a range of currents as large as 1000 to 1. If a crystal of this type is used as the plate load of a pentode, the voltage across the crystal will be proportional to the logarithm of the grid voltage of the pentode. Appropriate current feedback must be used to counteract the effect of the nonlinearity of the tube characteristics that would otherwise limit the accuracy of the logarithmic response. Other stages of amplification of conventional design can be used before and after the stage in which the crystal is connected.

* When tubes with external cavities are available, mechanical tuning permits frequency modulation at audio rates.

Quarter-wavelength-coupled filters are lined up experimentally in the following manner. Each cavity is tuned separately to the correct frequency. The value of the loaded Q is checked at the same time. The cavities are then connected and the frequency response of the filter is observed on the screen of an oscilloscope in the manner described above. Small readjustments of the elements are then made to obtain optimum bandpass characteristics. In general, if a filter is aligned for optimum bandpass characteristics, the off-band insertion loss will behave as predicted. The loss in the pass band depends critically on the alignment, and with a swept generator it takes only a matter of minutes to adjust a four-cavity filter. Without a swept generator and the auxiliary detecting apparatus, such an adjustment may require days of tedious measurements.

The alignment of a doubly resonant cavity may be easily accomplished with the same apparatus in the following manner. With the coupling screw almost removed, the screws that independently tune the two modes are adjusted until the transmission curve consists of a single peak of maximum amplitude. The coupling screw is then adjusted until the dip between the two peaks is equal to the allowed bandpass tolerance. The whole curve is then shifted to the desired resonant frequency by tuning both modes with a movable end membrane or by readjusting both tuning screws simultaneously. A filter consisting of two direct-coupled cavities can be lined up in the same manner.

10-22. Quarter-wavelength-coupled Filters.—In certain cases, special lineup procedures, which do not require swept generators, are practical. As an example, a method of adjusting quarter-wavelength-coupled filters is described. The apparatus required is schematically illustrated in Fig. 10-107. A frequency-stabilized generator should be used in connection with narrow-band filters. The filter to be adjusted is inserted between two standing-wave detectors in a line that is perfectly terminated. Initially, the resonant elements (cavities or irises) are all detuned and the generator is adjusted to the desired resonant frequency. Under these circumstances a large standing wave exists in the first slotted section. The positions A and A' of two minima of the voltage standing wave are determined. The first iris is then tuned until one of the minima coincides with the point B , half way between A and A' , that is, until the standing-wave minima are shifted by $\lambda_g/4$. The second iris is now tuned until the minima shift back to their original positions, A and A' . Thus, successive irises are tuned by alternately adjusting the position of a standing-wave minimum to occur at A and B . The last iris, however, cannot be tuned by this procedure. It should be adjusted to the desired midband response, that is, in many cases, maximum output power. Note that in the case of lossy filters the adjustment for

maximum output power does not yield unity standing-wave ratio in the input line. After these adjustments are made, the filter is checked at the edges of the pass band to make sure that the over-all behavior of the filter is satisfactory.

The details of the adjustment and test procedure may vary from filter to filter. However, it cannot be overemphasized that ease of adjustment should be a prime consideration in the design of any filter. Moreover,

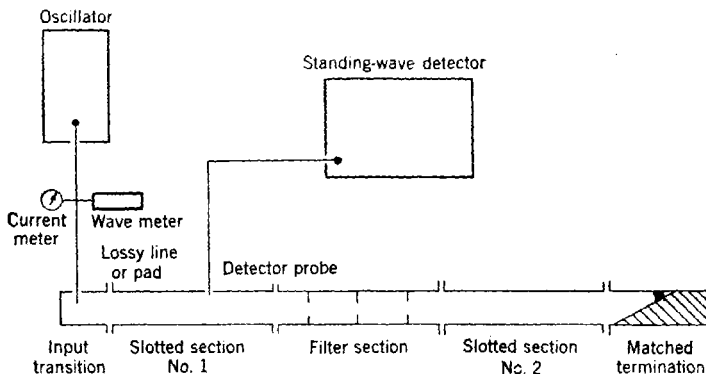


FIG. 10-107.—Test bench for $\lambda_g/4$ -coupled filters.

versatile test benches, including swept oscillators and logarithmic amplifiers, are of great help in laboratory work and become a virtual necessity in the case of quantity production of multielement filters.

BIBLIOGRAPHY

1. Mason and Sykes, "Use of Coaxial and Balanced Transmission Lines in Filters and Wide-band Transformers for High Radio Frequencies," *Bell Syst. Techn. J.*, **16**, 275 (1927).
2. P. I. Richards, "An Easily Constructed High-Pass Coaxial Filter," RRL Report No. 411-115A, March 9, 1945.
3. P. I. Richards, "Resonant-Section Coaxial Filters," RRL Report No. 411-115, Oct. 18, 1944.
4. W. G. Wadey, "A Variable Cut-off High Pass Filter (for use with AN/APR/5A)," RRL Report No. 411-161, March 14, 1945.
5. P. L. Harbury, "The M4601 and M4602 High Pass Filters," RRL Report No. 411-113, Nov. 5, 1944.
6. H. Goldstein, "Theory of Corrugated Transmission Lines and Waveguides," M.I.T. Thesis, RL Report No. 494, April 3, 1944.
7. D. E. Mode and L. W. Nosker, "R.F. Antenna Filters," RI. Report No. 952 (in process of publication).
8. H. Leiter, "A Microwave Bandpass Filter in Waveguide," RI. Report No. 814, Nov. 16, 1945.
9. M. D. Fiske, "A Broad Band TR-Switch," GE Report 10/18/43.

10. M. D. Fiske and Ann Warner, "Frequency Characteristics of Single and Multiple Tuned Circuits," GE Report, May 25, 1945.
11. P. Marcus, "The Interaction of Discontinuities on a Transmission Line," RL Report No. 930, Feb. 6, 1946.
12. M. Clark, Report No. CRG-56 "The Double-Tuned RF System. The TR Box," Dec. 19, 1944; Combined Research Group, Naval Research Laboratory.
13. A. Goldstein, NRL Report, C-F42-1/84 (312:AB), C-310-137A/45 (amc).
14. A. G. Fox, "Wave Guide Filters and Transformers," BTL Report MM-41-160-25, April 30, 1941.
15. P. I. Richards, "A Note on UHF Coupled Circuits," RRL Report No. 411-115C, March 20, 1945.
16. P. L. Harbury, RRL Report No. 411-113, Nov. 5, 1944.
17. P. S. Carter, R.C.A. Patent 2,397,313 (1944).
18. S. A. Schelkunoff, "Representation of Impedance Functions in Terms of Resonant Frequencies," *Proc. I.R.E.*, **32**, 83 (1944).
19. E. A. Guillemin, *Communications Networks*, Vol. II, Wiley, New York, 1935.
20. A. von Hippel, "Table of Dielectric Materials," Vol. 1, NDRC 14-237, Vol. 2, NDRC 14-425, M.I.T., Feb. 19, 1945.
21. H. Kallmann, "A Logarithmic Amplifier," *Electronics*, 1945.

Index

A

- A-c discharges, similarity for, principle of, 239
- Adapters, for coaxial connectors, 273
 - type N, 259, 261
- Admittance chart, 72
 - Smith, 67
 - use of, 94
- Admittances, short-circuit, 542
- Allen, W. D., 316, 538
- American Metal Hose Branch, American Brass Company, 274, 282
- Amplifiers, logarithmic, 713
- Angles, 170-182
- Army-Navy R-f Cable Coordinating Committee, 150, 243
- Army-Navy standard list of r-f cables, 269
- Assembly procedures, 709-714
- Attenuation, in actual coaxial line, 25
 - average, in pass band, 603
 - dielectric, 27, 50
 - in flexible cables, 245-247
 - of metals and alloys, 120
 - in plated conductors, 128
 - of standard cables, 268
- Attenuation band, 557
 - Tchebysheff behavior in, 593-597
- Attenuation function, 555

B

- Bandwidth, 96-99
- Barrow, W. L., 57
- Bartlett's bisection theorem, 556
- Bead, half-wavelength, 162
 - Teflon dielectric, 257
 - thin, 158
 - three-section, 165
 - undercut, 163
- Bead supports, 155-170

- Bell Telephone Laboratories, 418, 500, 535
- Bellows, Cook, 290
 - flexible, 288-291
- Beringer, E. R., 117
- Beryllium copper, 119
- Bode, H. W., 541, 612
- Brainerd, J. G., 10
- Breakdown, 106
 - of TM_{01} -transitions, 405
 - voltage (see Voltage breakdown)
- Breakdown field strength and pressure, relation between, 237
- Breakdown power, dependence of, on pulse width, 235
 - on repetition rate, 236
 - effect of radioactive cobalt on, 232
- Breckenridge, R. G., 136
- Broadband matching, with coaxial stubs, 332-335
 - with waveguide iris, 322-331.
- Brune, O., 556, 581, 612
- Bullet, 151
- Buttons and dents, capacitive, 215-217

C

- Cables, beaded, 243
 - coaxial (see Coaxial cables)
 - flexible, attenuation in, 245-247
 - high-power, 252
 - for low power, 248-252
 - connectors for, 256-259
 - r-f, Army-Navy standard list of, 269
 - solid dielectric, 243
 - standard, attenuation of, 268
- Capacity coupling, 100-114
- Carbide and Carbon Chemicals Corporation, 141
- Carter, P. S., 71, 716
- Casting, 138
 - centrifugal, 122

- Casting, die, 122
 - lost wax method of, 122
 - precision, 122
- Cavities, capacity-loaded, 687
 - direct-coupled, 661-666
 - chain of, 665
 - filters using, 666-673
 - dissipation in, 672
 - excited in more than one mode, 673-677
 - $\lambda_g/4$ -coupled, 683-688
 - rectangular, behaving as double-tuned filter, 675
 - reentrant cylindrical, 683
 - with two pairs of terminals, equivalent circuit of, 650
- Cavity resonators, as circuit elements, 646-653
 - design of, 653-661
 - direct-coupled, filters using, 645-677
 - equivalent circuits of, 647
 - insertion loss of, 654
 - rectangular, 656
 - reentrant cylindrical, 660
- Characteristics, distortion of, approximate correction for, 672
- Choke coupling, 100-114
 - design details for, 202
- Choke-flange couplings, circular-groove, 193-199
- Choke-flange junctions, open, 291-294
- Chromium copper, 119
- Chu, L. J., 57
- Circuit parameters, general, 543
- Clark, M., Jr., 318, 668, 716
- Clarke, H. F., 157, 227
- Coaxial cables, durability of, 254-256
 - flexible, 243-273
 - resonances in, 253
- Coaxial line, actual, attenuation in, 25
 - characteristic impedance of, 183
 - characteristics of, 150
 - couplings for, 150-155
 - factors in choice of dimensions of, 144-150
 - motional joints in, 407-416
 - tapers in, 305-311
 - transformer sections between, 311-314
 - transitions from, to waveguides, 314-361
 - matching techniques for, 317-336
- Coaxial line, transitions from one to another, 305-314
 - tubing for, 115-119
- Coaxial-line characteristics, 23-29
- Coaxial-line discontinuities, 184-188
- Coaxial-line switches, 528-533
- Coaxial-line tuners, 460-481
- Coaxial universal joint, 414
- Cohn, S. B., 57, 358
- Condon, E. U., 160
- Conductor attenuation, 50
- Conductor loss, 21, 26
 - minimum, 146, 147
- Conductors, metallic, at microwave frequencies, skin depth in, 127
 - plated, attenuation in, 128
- Connectors, assembling of, convention to be followed in, 153
 - for cables for low power, 256-259
 - coaxial, adapters for, 273
 - high-power, to rigid lines, 260-267
 - HN, 260
 - polarized, 151
 - Polyglas, 267
 - r-f cable, 270
 - Teflon, 259
 - type N, 256-259
 - unpolarized, 153
- Construction techniques, 120-124
- Contact losses, 108
- Contacts, sliding, 119
- Cook bellows, 290
- Cook Electric Company, 290
- Cork, B. B., 668
- Corrosion tests, 130-132
- Coupling, capacity, 100-114
 - choke (*see* Choke coupling)
- Coupling devices, 654, 659
- Coupling loop, 685
- Coupling sections, frequency sensitivity of, 691
- Coupling units, 288-303
- Couplings, choke-flange, circular-groove, 193-199
 - for coaxial line, 150-155
 - contact, 193
 - iris, 659
 - loop, 659
 - magnetic, 354
 - probe, 659
 - quarter-wavelength, 677-683

Couplings, quarter-wavelength, filters
 using, 677-706
 theory of, 690-696
 resonant-slot, 354
 sealing of, 140
 waveguide, 193-202

Crossbar transitions, 346-349
 Crowley, Henry L., 133, 463
 Current, longitudinal, 51
 Cutler, C. C., 282
 Cutoff frequency, 49

D

Darlington, S., 580, 581, 612
 Depth of penetration, 45
 Design factors, 95-100
 Design procedure, 82-100
 Dielectric attenuation, 27, 50
 Dielectric attenuation constant, 59
 Dielectric constant, complex, 28, 133
 Dielectric loss, 21
 Dielectric materials, 132-143
 characteristics of, 133-137
 Dielectric parts, construction of, 137-140
 Dielectric plugs, half-wavelength, 222
 Dielectrics, electrical properties of, 134, 135
 mechanical properties of, 134, 135
 Directional coupler, 229
 Dissipation, in cavities, 672
 effect of, on pass-band characteristics, 603
 on rejection-band characteristics, 604-607
 incidental, 601-609
 uniform, correction for, 607-609

Dixon, T. G., 129
 Dixon Crucible Company, 133
 Doorknob transitions, 349-353
 high-power rotary joints with, 451-455
 Dow Corning Corporation, 133, 143, 491
 Du Pont de Nemours, E. I., 125, 143, 286

E

Ebonol, 125
 Edson, W. A., 9, 12, 58, 383
 Edwards, C. F., 346, 449
 Ehlers, F. E., 383
 Electroforming, 121
 Electroplating, 124-132

Elliptic function, 594
 Enthone Company, 125

F

Fano, R. M., 357
 Farr, H. K., 417
 Fernico, 119
 Filter designs, normalization of, 560-566
 Filtering-ring transitions, 393
 Filters, absorption, 707
 band-rejection, 704
 broadband, 709, 710
 characteristics of, effect of degree of dissipation on, 696
 constant- k , 569-572
 using direct-coupled cavities, 666-673
 using direct-coupled cavity resonators, 645-677
 double-tuned, equivalent forms of, 674
 rectangular cavity behaving as, 675
 high-pass, waveguides as, 644
 using lines as four-terminal elements, 634-643
 using lines as two-terminal elements, 625-634
 m -derived, 572-576, 702
 mode, 707
 with n identical sections in cascade, 577
 narrow-band, 710-714
 quarter-wavelength-coupled, 714, 715
 using quarter-wavelength couplings, 677-706
 TE_{11} -mode, 388-400
 with transmission lines, 614-645
 waveguide, 643-645
 50-ohm line, 149
 Fin TE_{11} -mode filter, 397
 Finishes, 124-132
 nonmetallic, 124, 125
 Fiske, M. D., 715, 716
 Fox, A. G., 667, 716
 Frank, N. H., 211, 305, 332, 363
 Frequency behavior of transmission lines, 614-623
 Frequency sensitivity of coupling sections, 691
 Frequency stability, 83
 Fulton Sylphon Company, 288
 Fungus growth, protection against, 125

- G
- General Electric Company, 143, 214, 221, 352
- General Electric Mycalex, 491
- Gent, A. W., 309
- Gewertz, C. M., 612
- Glass, M. S., 464
- Goldstein, A., 716
- Goldstein, H., 282, 715
- Graton and Knight Company, 141
- Guide wavelength, 48
- Guided-wave concept, 36-40
- Guillemin, E. A., 10, 541, 580, 612, 716
- H
- Hancock, H., 612
- Hansen, W. W., 160
- Harbury, P. L., 715, 716
- Heins, A. E., 332
- Hinge joints, 438-442
- HN connectors, 260
- Hollingsworth, G. L., 349
- Holstein, T., 239
- I
- Ideal (lossless) line, 19, 23
- Image impedance, 554-557
- Image-impedance networks, reciprocal, 559
- Image parameters, of reactive networks, 557-561
- use of, limitations on, 576-580
- Impedance, 13-19
- characteristic, 12, 19-23, 41, 51
- of coaxial line, 183
- of eccentric line, 148
- effective, 52
- of free space, 58
- image (*see* Image impedance)
- input (*see* Input impedance)
- open-circuit, 542, 555
- short-circuit, 555
- wave (*see* Wave impedance)
- Impedance chart, rectangular, 72
- Smith, 60-67
- use of, 457-460
- Impedance-matching, 4, 59-100, 209-218
- reason for, 82
- Impedance-matching transformers, 90-95
- Impedance measurement, 18
- Impedance networks, reciprocal, 514
- Impedance normalization, 561
- Impedance transformers, variable, 456-516
- Input impedance, determination of, 583-586
- prescribed, network with, 586-589
- Insertion loss, 550
- of cavity resonators, 654
- specified, reactive networks with, 580-589
- Insertion-loss functions, physical realizability of, 580-583
- Iris, inductive, in waveguides, 78
- rejection, 706
- resonant, 660, 688-690
- waveguide, broadband matching with, 322-331
- J
- Jacketing materials, 247
- Jamieson, H. W., 184
- Joints, with polarization rotator, 430-432
- swivel, 433-438
- universal, 442-445
- K
- Kallman, H. E., 286, 716
- Kingsbury, S. M., 132
- Kohler, G., 10
- Kohlhaas, H. T., 155
- Kovar, 119
- Kuhn, S., 316
- L
- Ladder elements, determination of, 598-601
- Ladder networks, 597-601
- Lattice, symmetrical, 566
- Lattice networks, 706
- Lawson, J. L., 160
- Leiter, H., 715
- Line with small losses, 20
- Line stretcher, type N, 481

Loaded Q , 652
 Loss, conductor (*see* Conductor loss)
 dielectric, 21
 Loss length, 146
 Loss tangent, 29

M

Magic T, 706
 Magnetron, 83, 227
 Mansur, I., 157, 227
 Manufacturability, 95
 Marcus, P., 716
 Margenau, H., 239
 Mason, W. P., 173, 634
 Match, methods of achieving, 86
 Matching, narrow-band, 318-322
 Matching diaphragms, capacitive, 214,
 215
 inductive, 211-214
 Matrices, 544-547
 wave, 551-554
 Maxwell, E., 117
 Maxwell's equations, 3, 37
 Metal-hose, wound, 274-279
 Metallic materials, 115-124
 Metals and alloys, attenuation of, 120
 conductivity of, 120
 Microwave realizations of resonant
 branches, 703
 Microwave transmission circuits, 5
 Microwaves, useful properties of, 2
 Mismatched terminations, effect of,
 609-612
 Mismatches, accumulative, 551-554, 611
 measurement of, 85
 Mks units, rationalized, 8
 Mode, D. E., 633
 Mode purity, 99
 Modulator, 227
 Molding, compression, 138
 extrusion, 138
 transfer, 138
 Montgomery, C. C., 483
 Montgomery, D. D., 483
 Morgan Brush Company, 143
 Motional joints, 407
 in coaxial line, 407-416
 combining coaxial line and waveguide,
 446-455
 waveguide, 433-445

Multiplexers, 708
 Mycalex, General Electric, 491

N

Nebel, C. N., 535
 Networks, connected in cascade, 546
 connected in parallel, 545
 connected in series, 546
 ladder, 597-601
 lattice, 706
 with prescribed input impedance,
 586-589
 reactive, image parameters of, 557-
 561
 with specified insertion loss, 580-
 589
 reciprocal image impedance, 559
 reciprocal impedance, 544
 symmetrical, 544, 558
 two-terminal-pair, 541-554
 uniformly dissipative, 601-603
 Niemann, F. L., 353
 Nosker, L. W., 633

P

Pass band, 557
 average attenuation in, 603
 characteristics of, effect of dissipation
 on, 603
 Pass-band behavior, Tchebysheff, 590-
 593
 Pass-band normalization, 562-566
 Phase constant, 49
 Phase distortion, in broadband T-stub,
 176
 Phase function, 555
 Phase shifter, 478-481, 513-517
 dielectric, 514
 slotted-waveguide, 513
 Phase velocity, 12, 20, 42, 50
 Phosphor bronze, 119
 Pickering, W. H., 204
 Pierce, J. R., 196
 Pierce method for design of choke
 grooves, 198
 Pipe, elliptical, 57
 Plane wave in free space, 36
 Plate, quarter-wave, 371

- Plugs, dielectric, half-wavelength, 222
 T-shaped, three-quarters wavelength long, 223
- Plungers, short-circuiting, 460-463, 481-483
 capacity coupled, 462
 quarter-wavelength-finger, 461
- Polarization, circular, rotary-joint, 428
 in square waveguide, 378
 of TE_{11} -mode, 369-378
 elliptical, 54
- Polarization rotator, joints with, 430-432
- Polyglas, 132
- Polyglas connectors, 267
- Polyiron, 133, 463
- Polytechnic Institute of Brooklyn, 257
- Posin, D. Q., 157, 227
- Positive real function (*p r.*), 581
- Pound, R. V., 171, 173, 176
- Powder metallurgy, 123
- Power, reflection of, 29
 transmission of, 29
- Power-carrying capacity, maximum, 145, 147
- Power dividers, 516-528
 coaxial, 516-522
 fixed, 522-525
 fixed coaxial, 516-519
 variable, 519-522, 525-528
 waveguide, 522-528
- Power factor, 28
- Power-handling capabilities, 95
- Power-loss ratio, 550, 558
 selection of, 589-597
- Power-transmission ratio, 550
- Poynting vector, 41
- Pressurization problems, 139-143
- Preston TM_{01} -transition, 389
- Propagation factor, 13, 19-23
- Propagation function, 554-557
- Pulling figure, 84, 472
- Pulse width, dependence of breakdown power on, 235
- Q**
- Q , loaded, 652
 unloaded, 653
- R**
- Radiation losses, 108
- Radio Research Laboratory, 361
- Radioactive cobalt, effect of, on breakdown power, 232
- Radioactive cobalt chloride, 232
- Ragan, G. L., 227
- Ramo, S., 57, 129
- Raytheon Manufacturing Company, 452
- Reed, J., 159, 160
- Reflection coefficient, 13-19, 29, 63
 current, 15
 voltage, 15
- Reflection-coefficient chart, 60-67
- Reflex oscillator, volume control for, 711
- Reich, H. J., 10
- Rejection-band characteristics, effect of dissipation on, 604-607
- Resistance card load, 97
- Resonances, 99
 in high-power rotary joint, 422
 in rotary joints, 416-420
- Resonant aperture, 221
- Resonant ring, 391
- Resonators, cavity (*see* Cavity resonators)
- R-f cable connectors, 270
- R-f components of sample radar set, 6
- Richards, P. I., 634, 715, 716
- Rieke diagram, 83
- Robbins, Theo Eloise, 184
- Rotary-joint pressure seals, 141-143
- Rotary joints, 100-109, 407
 circular-polarization, 428
 resonance in, 429
 coaxial, 407-413
 coaxial chokes in, 408
 with combinations of transitions, 448-451
 with cross-transition from coaxial line to waveguide, 446
 filter-ring, TE_{11} -mode for, resonances in, 423
 high-power, with doorknob transitions, 451-455
 resonances in, 422
 with probe transitions, 447
 resonances in, 416-420
 with TE_{11} -mode filter-ring transitions
 with TE_{11} -absorbers, 425
 waveguide, 416-433

S

- Salisbury, W. W., 160
 Salt-spray test, 130
 Sarbacher, R. I., 9, 12, 58, 383
 Scaling, 87
 Schaevitz, H., 57
 Schaible, G. J., 247
 Schelkunoff, S. A., 9, 52, 716
 Schuster, N. A., 349
 Screws, general-susceptance, 499-507
 Sealol, 142
 Series branches, 100-114
 Sheets, thin, nonresonant, 218-220
 reflections from, 220
 in resonant mount, 220-222
 Shunt susceptance elements, 93
 Similitude, 87
 Skin depth, 26, 45
 in metallic conductors at microwave frequencies, 127
 Slater, J. C., 9, 53, 99, 116, 245, 313, 315, 316, 362, 415, 497
 Smith, P. H., 63, 500
 Smith admittance chart, 67
 Smith impedance chart, 60-67
 Soldering, 123
 hard, 123
 silver, 123
 soft, 123
 Sperry Gyroscope Company, 129, 189, 210, 307, 447
 Standing-wave ratio, 17, 63
 voltage, 17
 Standing waves, 13-19
 Stratton, J. C., 87
 Stub supports, 170-182
 Stub tuners, 472-478
 sliding series, 464-466
 waveguide, 483-485
 Stubs, coaxial. broadband matching with, 332-335
 right-angle, 176-179
 universal, 179
 dimensions for, 180
 Susceptance shunting matched line, 31
 Switches, 528-539
 coaxial-line, 528-533
 type N, 529
 waveguide, 533-539

- Swivel joints, 433-438
 Sykes, R. A., 634

T

- T-stub supports, simple, 170-173
 T-stubs, broadband, 173-176
 dimensions for, 175
 phase distortion in, 176
 Tapers in coaxial line, 305-311
 Tchebysheff behavior in attenuation band, 593-597
 Tchebysheff characteristics, 696-706
 Tchebysheff pass band behavior, 590-593
 Tchebysheff polynomials, 590
 TE -mode, 39
 TE_{10} -mode rectangular waveguide, 46-54
 TE_{11} -mode, circular polarization of, 369-378
 in cylindrical waveguide, determining percentage of, 381-388
 for filter-ring rotary joint, resonances in, 423
 TE_{11} -mode filters, 388-400
 Fin, 397
 Teflon, 143
 Teflon connectors, 259
 Teflon dielectric beads, 257
 Telecommunications Research Establishment, 352, 392
 Telegraphers' equation, 9-11
 TM -mode, 39
 Test equipment, 7
 Test procedures, 709-714
 Thermistor bridge, 229
 Titeflex, 116, 279-281
 Titeflex, Inc., 280
 TM -mode, 39
 TM_{01} -mode, transitions to, 379-381
 TM_{01} -transitions, breakdown of, 405
 Preston, 389
 straight-on, 400-403
 TR tubes, 688
 Tracing paper, 65
 Transformers, coaxial impedance, 182-184
 impedance-matching, 90-95
 quarter-wavelength, 90-92, 217
 variable impedance, 456-516
 Transmission-line charts, 59-82
 choice of, 75-82

- Transmission-line components, 5
 - Transmission-line equations, 32
 - Transmission-line theory, 9
 - Transmission lines, filters with, 614-645
 - frequency behavior of, 614-623
 - low-loss, relations in, 34
 - radial, voltage and current nodes in, 196, 197
 - relations in, 29-36
 - rigid, 144-242
 - sealing of, 140
 - use of, limitations on, 623-625
 - Tubing, for coaxial lines, 115-119
 - dimensional tolerances of, 117
 - silver-lined, 117
 - for waveguides, 115-119
 - Tuners, 456-516
 - capacitive-screw, 498
 - coaxial line, 460-481
 - double-screw, waveguide, 507-513
 - double-slug, waveguide, 494-498
 - single-screw, variable-position, 485-489
 - single-slug, 489-494
 - sliding-screw, 459
 - slug, 466-472
 - stub (*see* Stub tuners)
 - waveguide, 481-516
 - Tuning screw, capacitive, 216
 - Tunncliffe, P. R., 352
- U
- Uglove, K. M., 352
 - U. S. Graphite Company, 143
 - Units, 8
 - Universal joints, 442-445
 - Unloaded Q , 653
- V
- Velocity, group, 12
 - phase (*see* Phase velocity)
 - signal, 12
 - Voltage, effective, 51
 - Voltage breakdown, 84
 - at microwave frequencies, 227-242
 - Voltage insertion ratio, 549
 - Von Hippel, A., 132, 136, 716
 - VSWR introduced by junction between two waveguides, 118
- W
- Wadey, W. G., 644
 - Walker, R. M., 129, 222, 227
 - Wall surfaces, corrugated, 116
 - scratched, 116
 - Wallin, P. J., 309
 - Warner, A., 716
 - Washburne, B. P., 188
 - Water load, 229
 - Wave impedance, 41, 53, 647
 - of free space, 37
 - Waveguide bends, and twists, 207-209
 - Waveguide constants, 191
 - Waveguide corners, 203-207
 - Waveguide couplings, 193-202
 - Waveguide filters, 643-645
 - Waveguide mode, transitions with change in, 379-405
 - Waveguide motional joints, 433-445
 - Waveguide power dividers, 522-528
 - Waveguide rotary joints, 416-433
 - Waveguide stub tuners, 483-485
 - Waveguide switches, 533-539
 - Waveguides, common, characteristics of, 54-59
 - cylindrical, determining percentage of TE_{11} -mode in, 381-388
 - different, joining of, 53
 - dimensions for, choice of, 188-193
 - fields in, 39
 - flexible, wire-screen, 287
 - as high-pass filters, 644
 - inductive iris in, 78
 - lossless, 40
 - metal-hose, minimum bending radii of, 276
 - nonresonant flexible, 274-288
 - parallel-plate, 40-46
 - plastic, 285-287
 - plastic-filled, 285-287
 - rectangular, of different sizes, transition between, 361-364
 - TE_{10} -mode, 46-54
 - transition from, to cylindrical, 364-369
 - resonant flexible, 288-303
 - ridge, 358
 - screw in, 458

- Waveguides, seamless corrugated, 282-285
square, circular polarization in, 378
transitions from coaxial line to, 314-361
tubing for, 115-119
two, VSWR introduced by junction
 between, 118
 vertebral flexible, 294-303
- Wavelength, critical, 48
cutoff, 48
guide, 48
intrinsic, 42
- Wesson, L. G., 132
- Westinghouse Electric and Manufacturing Company, 141, 221
- Whinnery, J. R., 57, 129, 184
- Whitmer, R. M., 285
- Windows, pressurizing, 218-227
- Woodruff, L. F., 10, 71
- X
- X-pandotite Cement, 133
- Y
- Yunker, E. L., 302

